Macular Surgery

Current Practice and Trends

Andrew Chang
William F. Mieler
Masahito Ohji

Editors

Springer

Macular Surgery

Andrew Chang
William F. Mieler • Masahito Ohji
Editors

Macular Surgery

Current Practice and Trends

Springer

Editors
Andrew Chang
Sydney Retina Clinic and
Sydney Eye Hospital
Sydney
NSW
Australia

Masahito Ohji
Department of Ophthalmology
Shiga University of Medical Science
Shiga
Japan

William F. Mieler
Department of Ophthalmology
and Visual Sciences
The University of Illinois at Chicago
Chicago
IL
USA

Preface

Advances in technology have improved the safety, efficiency, and outcomes of macular surgery. Vitrectomy machines and cutters allow more efficient microincisional surgical approaches with safe removal of vitreous and membranes with ultra-high cutting rates. A wide suite of ergonomic disposable microsurgical instruments is available for surgeons to perform delicate surgical manoeuvres. Dyes identify tissue for accurate removal. Improved visualization during surgery with digital, 3D technology, and data connectivity leads to better surgical control. Intraoperative OCT can permit high-resolution cross-sectional imaging of delicate membranes and structures during surgery. The surgical setting, anesthesia and postoperative care of patients have resulted in more rapid healing and visual rehabilitation. The close relationship of anterior and posterior segment surgery is reflected in modern collaborative efforts with ophthalmic subspecialties.

This book will review the expanded indications for macular surgery, advances in vitrectomy technology including viewing systems, vitreous cutters, vitrectomy machines, and instrumentation. New innovations and techniques including prosthetic vision, gene stem cell therapy, and robotic surgery are promising.

It is personally pleasing that this book is a collaborative effort of retinal specialists from the Asia Pacific region, the United States, and Europe.

We are grateful to the pioneers, colleagues, trainees, and our patients in encouraging vitreoretinal surgery to evolve macular surgery. We hope each chapter of this book would contribute to further innovations in future.

Sydney, NSW, Australia	Andrew Chang
Chicago, IL, USA	William F. Mieler
Shiga, Japan	Masahito Ohji

Contents

Part IX   Ancillary Resources for Retinal Surgery

Part I

Macula Anatomy and Physiology

Anatomy and Histology of the Macula

1

Dao-Yi Yu, Stephen J. Cringle, Paula K. Yu, and Er-Ning Su

1.1 Introduction

As an optical organ, the eye has some unique features. Key structures in the light path must be largely transparent, such as the cornea, aqueous fluid, the lens and the vitreous humour. The retina itself must also be largely transparent as the light-sensitive region of the photoreceptors is in the deeper retinal layers. The eye must also maintain a positive pressure to maintain its shape. Survival and proper function of the neuronal cells within the retina, particularly in the macula, require a stable intraocular environment. Homeostasis of the intraocular environments depends on many specific mechanisms and many signal pathways. These mechanisms and pathways are dynamic and interacting and often require a delicate balance. It means that these mechanisms and pathways can only maintain their integrity if they are capable of adapting to change in the face of physiological challenges such as illumination conditions or other local or systemic conditions. In diseased situations, which may be caused by genetic and/or environmental changes, the macula cannot adapt to these pathological challenges and pathological changes can occur. The ratio-

nale for treatment is to attempt to restore normal conditions as much as possible. However, most diseases, including macular diseases, often involve multiple mechanisms and pathways, whilst the treatments usually can only address the major pathogenic factors. So naturally, macular and vitreous surgery are combined with a variety of intervention option such as application of anti-VEGF drugs, intra-vitreal steroids, laser retinal photocoagulation and release of vitreo-retinal traction. All these procedures cause unavoidable alterations of the intraocular environment. How to achieve the therapeutic benefits and restore structure and function using the available interventions is always a challenge for macular surgeons.

1.2 Definition of the Macula

The macula lutea is the region containing a high concentration of yellow pigment. The description of its size in the literature can be confusing and varies by up to a factor of 10, ranging from 0.5 mm to more than 5 mm in diameter [1–3]. The ophthalmoscopy and gross anatomic correlations are not clearly defined. It is more generally accepted that the macula is approximately 5.8 mm in diameter and located approximately two disc diameters temporal to the optic nerve head [1]. The macular region can be subdivided into the foveola, fovea, parafoveal and perifoveal

D.-Y. Yu (✉) · S. J. Cringle · P. K. Yu · E.-N. Su
Centre for Ophthalmology & Visual Science, Lions Eye Institute, The University of Western Australia, Perth, WA, Australia
e-mail: dyyu@lei.org.au; Steve@lei.org.au; PaulaYu@lei.org.au; erning@lei.org.au

areas, although the boundaries of these specialized regions are also not well defined [1]. Figure 1.1 describes the relationship between fundus appearance and a sagittal macular section. Both the fundus image and the optical coherence tomography (OCT) image were sampled from a young healthy subject. Subdivided areas on fundus image are matched with the OCT image. The foveola is the central 350 μm in the middle of the foveal avascular zone (FAZ) and includes the base of the foveal pit where there is a peak density of cone photoreceptors for high acuity vision. It is formed only by cone outer and inner segments, a tightly packed multiple deep layer of cone cell bodies and surrounding Muller glial cell processes. It is surrounded by terminal capillaries, on the slope of the pit. The next ring is the fovea, which extends 750 μm around the foveola. Ganglion cells distribution ranges from an absence of ganglion cells near the foveola to up to eight cells deep on the edge of the fovea. Cone density in the fovea is lower than in the foveola. The outer plexiform layer appears in the fovea. It contains a thick layer of long cone axons called the fibres of Henle and the synaptic pedicles of the foveolar cones. The third ring is the parafovea (500 μm wide), and the outermost ring is the perifovea (1500 μm wide), which extends almost to the optic disc. These are no distinct morphological boundaries between these zones. Rods are

Fig. 1.1 Fundus image and OCT image from a young healthy subject illustrating the relationship between fundus appearance and sagittal macular section. Subdivided areas on fundus image are matched with OCT image. (**a**) The foveola: central ~350 μm includes the base of the foveal pit. (**b**) The fovea: extends 750 μm around the foveola. (**c**) The parafovea: third ring ~500 μm wide and (**d**) The perifovea: the outermost ring ~1500 μm wide, extending almost to the optic disc [4]

absent in foveola, have a low density in the fovea, are more numerous in the parafovea and predominant in the perifovea. In the parafoveal region, the retina has maximum thickness, owing to the high density of neural elements.

1.3   Macular Cellular Structure

1.3.1   Fovea and Foveola

The fovea is located roughly 4.0 mm temporal and ~0.8 mm inferior to the centre of the optic disc as shown in Fig. 1.1a. In the central fovea, there is a small excavation in the internal surface of the retina (Fig. 1.1b).

The foveola is roughly 350 μm across and is formed entirely by cones. Cone cell bodies, outer and inner segments are tightly packed (Fig. 1.2), and surrounded by Muller cell processes. All other layers are displaced peripherally from the pit. The foveola is the region of highest cone density so foveolar cones are very thin and have the longest inner and outer segments in the retina.

The fovea is the next ring around the foveola with width of approximately 750 μm. There is a variation in depth of the excavation in normal eyes. The averaged depth is about 250 μm in the human eye. The foveal slope is formed by walls of the pit (Fig. 1.2). Multiple layers of ganglion cell bodies are found in the fovea. Cone density is lower than in the foveola, and the cones are thicker. Rods are present at low density in the fovea (Fig. 1.2). A thick outer plexiform layer can be seen in the fovea. It consists of aggregated horizontally oriented fibres (long cone axons) called the fibres of Henle. The synaptic pedicles of the foveolar cones are also in the fovea (Fig. 1.2). Capillaries appear in the inner retina and encircle the foveal slope, where they form the border of the FAZ about 400–500 μm wide.

Cone density peaks sharply in the foveola and drops rapidly into the periphery, reaching a 1:1 ratio of rod/cone at approximately 500 μm eccentricity. The ratio of total rods/cones is ~20:1 based on estimates of 92 million rods and 4.6 million cones in the adult human retina [5]. Red and green cones constitute around 90% of the
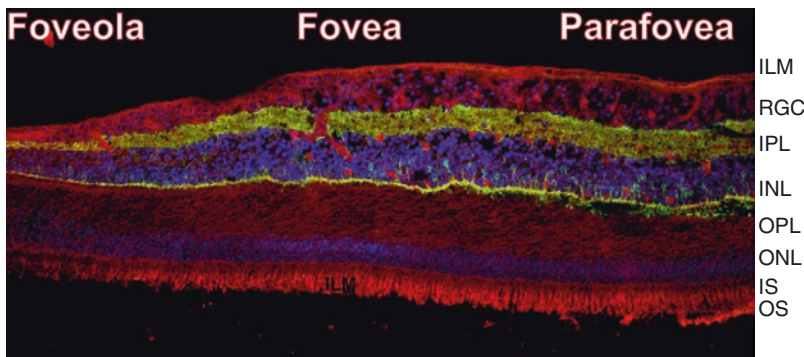
Fig. 1.2 Confocal image (8.05 μm total thickness projected) of a cryosection through the macula region of donor eye triple labelled for rod ON bipolar cells (anti-Goα, green), horizontal cells (anti-parvalbumin) and Lectin-TRITC (red) which is more strongly picked up by the Glycocalyx on the luminal side of vascular endothelial cells. The nuclei are count-stained using Hoechst (blue). In the foveola, multiple layers of cone nuclei are located in the outer nuclear layer (ONL) and the outer segments (OS) and inner segments (IS) are relatively thin. This section could be slightly off the centre of the foveola. In the fovea, the inner retina becomes thicker with multiple layers of retinal ganglion cells (RGC) layer, inner plexiform layer (IPL), inner nuclear layer (INL) and outer plexiform layer (OPL) in addition to the ONL, OS and IS. The foveal slope is clearly evidenced as part of the foveal pit. Cone nuclei in ONL are less than that in the foveola. However, the IS becomes thicker. Abundant fibres of Henle are found in the OPL. The cone pedicles seen in the fovea are the displaced pedicles of the foveolar cones during pit formation. In the parafovea, full thickness of the inner retina is present and the number of cones in the ONL is markedly reduced whilst number of rods is increased

cone population with blue cones the remaining 10%. Most humans have a ratio averaging two red cones/one green cone, but individuals can range from one red cone/eight green cones to nine red cones/one green cone and still have normal colour vision [6].

The functional integrity of our high visual acuity region (central 2 mm of retina) is dependent on approximately 90,000 cones [1, 6], which is roughly 2% of the total cone population and only 0.1% of the total photoreceptor population. The number of cones in the foveola is only 7000–10,000 [6]. It is very important to maintain the structural and functional integrity of the foveola and fovea throughout life.

1.3.2 Parafoveal Region

The parafoveal region has a width of about 0.5 mm (Figs. 1.1 and 1.2). It is characterized by the largest accumulation of nerve cells in the entire retina, especially those of the ganglion cell and inner nuclear layers and a thick outer plexiform layer, known as the fibres of Henle in this region. Rods are more numerous in the parafovea when compared within the fovea and foveola and cones are thicker and less numerous. There are four to five rows of nuclei seen in the outer nuclear layer, and in the outer part of this layer, they are mostly rod nuclei. The layer of fibres of Henle is still thick, and both rod spherules and cone pedicles appear here. The inner nuclear layer has more than ten rows of nuclei. The ganglion cell layer appears to have smaller and relatively uniform cell bodies forming multiple rows.

1.3.3 Perifoveal region

The perifoveal region measures 1.5 mm in width. Therefore, the entire macular area is 5.85 mm in diameter. In the perifovea, rods are the dominant photoreceptor and the retinal ganglion cells reduce their numbers towards the optic disc. The thickness of the ganglion cell layer is further reduced. The thickness of the outer nuclear layer is unchanged from that of the parafoveal region,

but the numbers of cones are reduced. Five to six rows of nuclei are seen in the outer nuclear layer. The outer plexiform layer is reduced to half the thickness of that in the perifoveal region. The inner nuclear layer is also reduced to the same thickness as in the peripheral retina, but the thickness of the inner plexiform layer is slightly increased.

1.4 Blood Supply of the Macula

The retina is supplied by both the retinal and choroidal circulations. An ophthalmic artery leads into the long and short posterior ciliary arteries feeding the choroidal/uveal circulation, and a central retinal artery and sometimes cilioretinal arteries feeds the retinal circulation. These two circulations possess significantly different properties and constraints. The visual image is focused on outer segments of the photoreceptors. The photoreceptor region is avascular to ensure optimal visual acuity with minimum optical interference from vascular structures. As a consequence, the photoreceptors' main source of nutrients, the choroidal circulation, lies totally outside the retina and supplies the photoreceptor layer with nutrients such as oxygen by diffusion [7–9]. The oxygen supply from the choroid is barely enough to prevent some regions of the outer retina from becoming hypoxic, which suggests that the high rate of blood flow through the choroid may be essential to maintain a sufficiently high oxygen level in the choriocapillaris to drive the oxygen diffusion process. The choroidal circulation possesses both sympathetic and parasympathetic innervation [10], presumably allowing systemic control of choroidal blood flow. However, there has been considerable disagreement as to whether the choroidal circulation is capable of functional regulation [11–15]. The retinal circulation is differently constrained in its design. Although it is responsible for feeding a high metabolic rate tissue, it must be anatomically sparse to minimize optical interference with the light path to the photoreceptors. A further unusual feature of the retinal circulation is that it has no autonomic innervation [16], so total reliance must be placed

on local vascular control mechanisms. These requirements result in a limited flow circulation, with a high arterio-venous oxygen tension difference. In most retinal regions, this circulation has at least two capillary networks, one feeding into the nerve fibre/ganglion cell layer and other feeding the middle retinal layers including the inner nuclear layer and plexiform layers. There is no controversy about the powerful regulatory ability of the retina circulation from both human and animal data [17]. Interestingly, we have demonstrated that the two major capillary layers have different regulatory capabilities showing that in the rat retina the oxygen level in the region supported by the superficial capillary layer is well regulated, whilst that of the deeper capillary layer is not [18]. This apparent vulnerability of the deep capillary bed area is an important observation as it provides a possible explanation for the high incidence of pathological involvement of the deep capillaries in retinal vascular disease [19, 20]. The feeder vessels to the eye may be also involved in the regulation of ocular blood flow and it is known that their vasoactive properties can vary significantly along their length [21–23]. This adds yet another dimension to the heterogeneity of vascular control mechanisms in the ocular vasculature.

There are also a number of competing or complementary mechanisms that are responsible for locally regulating the vessel tone. These local factors include bloodborne factors, tissue released factors and factors released from the autonomic system. They combine to ensure that the blood flow to the tissue is matched to the metabolic requirements. This integration of total blood flow is known to be achieved by the continuous and dynamic interplay between many regulatory factors, including factors emanating from the blood, the endothelial and smooth muscle cells of the vessel walls, the surrounding metabolizing tissue and the input pressure.

The vascular endothelium is a vital component of vascular regulation. It consists of a monolayer of thin squamous cells, which line the inside surface of blood vessels. One intracellular structure implicated in sensing external changes and mediating the output of the huge array of auto-coids known to change smooth muscle cell response is the cytoskeleton. The cytoskeleton gives the cell its shape as well as mediating the transmission of intracellular signalling. The response of the endothelium to shear stresses associated with local blood flow is another important mechanism for regulation of blood flow. The vascular endothelium in the retina is considered as the major component of blood–retinal barrier, which is a highly specialized structural, transport and biochemical barrier. It regulates the entry of compounds and cells between blood and retinal tissue, plays a fundamental role in retinal homeostasis and also forms a route of communication between circulating blood and underlying retinal tissues. Much of the structural barrier is due to the presence of tight junctions between the vascular endothelial cells. These junctions can be regulated, affected by disease states and can also be manipulated therapeutically.

1.4.1 Macula Blood Supply from the Retinal Circulation

Like most regions of the retina, the macula has dual supplies from both the retinal and choroidal circulations. However, there is a unique pattern of retinal vasculature in the macular area. Figure 1.3a shows a low magnification projected confocal image from the macula region of the left eye from a human donor eye [24]. The area imaged covers the foveola, fovea and parafovea regions indicated by three concentric circles superimposed on the vascular network. The microvasculature network distribution appears random; however, some common properties in topographic distributions can be identified in most normal subjects. An arteriole is easily differentiated from a venule by its thicker wall with stronger stain and a circular pattern of smooth muscle cells (Fig. 1.3b) [24]. It is also notable that the capillary free zone along the arteriole is less apparent around the macular region than that in the peripheral retina as previously reported [25]. There is a one-to-one relationship between a relatively large arteriole and a venule, the two being connected by a capillary plexus without
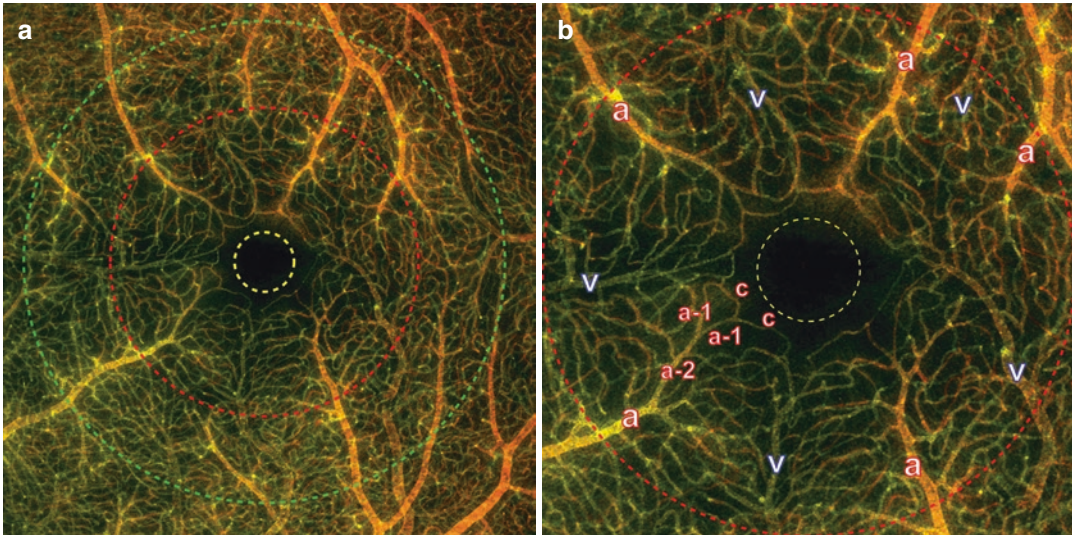
Fig. 1.3 Confocal images of retinal microvasculature at the macular region obtained from a donor eye after perfusion staining labelled for filamentous actin. The foveola, fovea and parafovea regions are indicated by three concentric circles (yellow, red and green, respectively). Capillary density in the foveal region is less than that in the parafoveal region.
A higher magnification image of the foveal region from figure (**a**) showing arterioles (**a**), venules (v) and the subsequent branching of the retinal arteriole into smaller arterioles (a-2 and a-1) and capillaries (**c**). Two capillaries (**c**) join together to form a first-order arteriole (a-1), and two a-1 arterioles join together to form a second-order arteriole (a-2). The capillaries branching off the retinal arterioles are predominantly in the superficial half of the image stack (red pseudocolour) before connecting to the capillaries draining towards the retinal venules lying in the deeper half of the stack (green pseudocolour). Foveolar area is located in the avascular region. Only a few pairs of arterioles and venules enter the foveal region [24]

shunt pathways that are present in other microcirculatory systems [1]. There are no arteriolar–venular shunts or connections between macular venules in the macular area. No evidence was found of a capillary arcade system as seen in peripheral retinal vessels suggesting that there is no bypass between the macular arterioles and venules or connections between pairs of arterioles or venules [26, 27]. Therefore the haemodynamics of the macular vasculature appears to be mainly determined by the branching structures. Numerous pairs (~9) of arterioles and venules are found in the macular area arranged in a radial pattern surrounding the foveola. Only a few arterioles (~3–4) enter the foveal region where they directly supply the terminal capillary ring (Fig. 1.3b). The avascular region is surrounded by terminal capillaries forming a terminal capillary ring which often has an irregular oval shape with a diameter of ~360 μm vertically and ~ 410 μm horizontally. In addition to these unique macular vascular patterns and distributions, the vascular tree distribution of individual vessel is also interesting. The topological description of vascular trees has been proposed by the Horton–Strahler and generation nomenclatures. The Horton–Strahler approach starts at the capillary level and proceeds centripetally. The order is increased if two segments of equal order join at a bifurcation. The generation (centrifugal) scheme starts from the most central vessel considered and proceeds to the capillary level, increasing the generation by one at every branch point. Figure 1.3b shows arterioles, venules and the subsequent branching of the retinal arteriole into smaller arterioles (a-2 and a-1) and capillaries (c). Two capillaries (c) join together to form a first-order arteriole (a-1), and two a-1 arterioles join together to form a second order arteriole (a-2). The capillaries branching off the retinal arterioles are predominantly in the superficial half of the image stack (red pseudocolour) before connecting to the capillaries draining towards the retinal venules lying in the deeper half of the

stack (green pseudocolour). The retinal arteriole traversed the parafoveal region before entering the foveal region (starting from top to the bottom of this image), and stop short of the foveola. It is also evident that there are many bifurcations from each arteriole or venule indicating that many generations are present in a short segment length. Some arterioles and venules only reach the parafoveal or perifoveal region. Higher order arterioles give off twigs of smaller branches of capillaries and arterioles which further bifurcate to form the capillary networks before converging to the venules. The number of vessel generations in the macular area imaged is ~12 and there are ~4 different orders of the vessel. A significant asymmetry exists between the order and generation counts of vessels in the macular region.

1.4.2 Macular Blood Supply from the Choroidal Circulation

The choroid is composed of various sized blood vessels surrounded by melanocytes, nerves and connective tissue. The macular choroid has an abundant blood supply and almost all temporal short posterior ciliary arteries supply the choroid in the macular region [28]. The macular choroid is much thicker than in other parts of the choroid. The choriocapillaris is thickest along with greatest density in the macular region [29]. Figure 1.4a shows a choroidal section from a human donor eye. The choroid can be divided into three parts from internal to external: (1) Bruch's membrane; (2) the vascular layers and (3) the suprachoroid (Fig. 1.4a). The inner boundary of the choroid is formed by Bruch's membrane, a thin layer derived in part from the retinal pigment epithelium and the choriocapillaris. Large- and medium-sized choroidal arteries and veins with increasing luminal diameters from internal to external can be found in the macular region. The innermost layer is capillaries (the choriocapillaris), the middle layer and the outer layer are medium-sized vessels and large vessels, respectively (Fig. 1.4a). Arterioles and venules join the choriocapillaris either obliquely or at right angles. There are no capillaries in the deeper lay-

ers of the choroidal stroma or the suprachoroidal lamellae. The melanocytes are mostly distributed in the outer layers of the choroid.

It is also important to appreciate that the posterior ciliary arteries and choroidal arteries are end arteries. Choroidal blood circulation has strictly segmental distribution without anastomoses between the adjacent segments at any level [28]. The border between the territories supplied by any two end arteries is called a watershed zone, in which actual perfusion flow could be relatively poor and vulnerable to ischemia. The location of the watershed zones is critical. Watershed regions between the posterior ciliary arteries could be crucial in ischemic disorders of the optic nerve head and the location of multiple watershed zones of the short posterior ciliary arteries in the macular choroid may play a role in macular ischemic lesions.

There is significant disagreement regarding the appearance and organization of the choroidal vasculature, particularly of the choriocapillaris. In fact, variation in the pattern of choroidal vasculature is great within different areas of the same eye and in eyes from different individuals. The choriocapillaris appears as a single layer of broad, wide capillaries lying in a plane just external to Bruch's membrane. Figure 1.4b shows a confocal image of choriocapillaris plane from a human donor eye. A high density of choriocapillaris is found in the macular region providing a large surface area for metabolic exchange. The capillaries appear as a continuous meshwork with irregular shape and sized channels separated by small columns or septa. These columns are formed by choroidal stroma tissues covered by endothelial cells.

The anatomy and function of the choroidal lobuli have been extensively studied; however, the controversy regarding the choroidal angioarchitecture is not yet settled. Fluorescein angiographic studies have shown that each terminal choroidal arteriole supplies an independent lobule of choriocapillaris, with the arteriole joining the segment in its centre and the draining venules lying around the periphery of this lobule. Each lobule of the choriocapillaris is an independent unit with no anastomosis with the adjacent
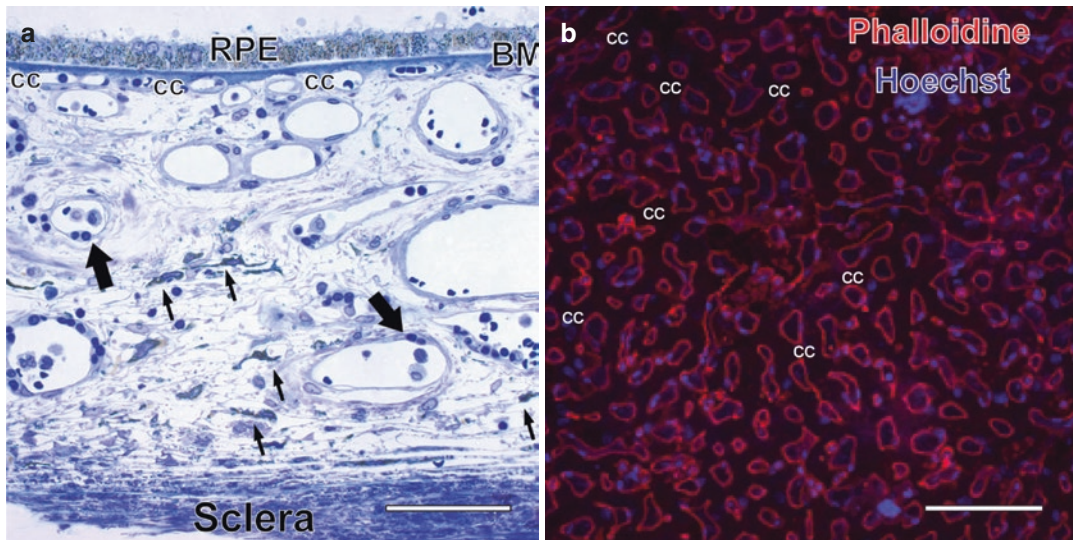
Fig. 1.4 Choroidal vasculature. (**a**) Histological section of the choroid from a human donor eye: The layers of medium and large choroidal vessels thicken the choroid in the macular region. The inner boundary of the choroid is formed by Bruch's membrane (BM), a thin layer which is derived in part from the retinal pigment epithelium (RPE) and the choriocapillaris (cc). Choriocapillaris only occupy a small proportion of the thickness of the choroid in the macular region. Outer choroid consists of multiple layered large- and medium-sized choroidal vessels (large arrows) surrounded by connective tissues and melanocytes (small arrows). Suprachoroidal space is located between the choroid and sclera. Scale bar = 100 μm. (**b**) Confocal image from the choriocapillaris from a human donor eye. The post-mortem eye was intravascularly perfused, fixed and stained with phalloidine (red for endothelium) and Hoechst (blue for nuclei). The choroidal stroma tissue is surrounded by endothelium appeared as numerous small columns. Choriocapillaris (cc) appear to be spaces between these islands. Scale bar = 100 μm [24, 25]

segments in vivo [28]. Reports from vascular casting and scanning electron microscopy studies have shown that collecting venules were found in the centre of 86% of the lobules as anatomic lobules, whilst a central feeding arteriole was observed in 14% as functional lobules [30].

Some histological features of the choriocapillaris are important [31]. The choriocapillaris in the macular region consists of a layer of fenestrated endothelial cells surrounded by a basement membrane similar to other regions of the choroid. The fenestrations are abundant and evenly distributed on the inner wall of the capillaries. The circular fenestrations are ~60–80 nm in diameter with a central thickening of 30 nm of cytoplasm permitting the passage of glucose and lipid-soluble molecules such as vitamin A to the RPE and retina. The nuclei of the endothelial cells are usually located on the external side of the capillaries. The cytoplasm of the choroidal side often contains mitochondria, endoplasmic reticulum, free ribonucleic particles and some pinocytotic vesicles. Pericytes are occasionally found in the external wall of the capillaries. There are some discontinuous tight junctions of the endothelial cells. Collagen from Bruch's membrane may extend down into the intervascular columns or septa which may help to hold the capillaries open.

1.5 Vitreal Anatomy and Its Relevance to the Macular Microenvironment

The vitreous has a gel-like structure which occupies four-fifths of the total eye volume. It is well known that it provides support for the ocular tissues and assists in the maintenance of the intraocular pressure and also acts as an optical medium to transmit the light to the retina. The roles of vitreous in providing a passageway for

metabolites utilized by the posterior lens and the retina are important in maintaining the homeostatic environment of the retina. These issues need to be considered following vitrectomy and other interventions that are extensively used in the management of retinal and macular diseases. These interventions unavoidably change the intraocular environment which could be beneficial or harmful in different circumstances.

1.5.1 Vitreal Anatomy and Biochemistry

Human vitreous volume is about 4 ml, containing 99% water. The viscosity of the gel-like vitreous varies regionally, being greater in the cortex than in the central part. Normal vitreous is many times more viscous than water (more than 300 times) [32]. A filtrate of the vitreous contains considerable hyaluronic acid and other colloidal material, but the viscosity is reduced to only ~twice that of water. The osmotic pressure of vitreous filtrate is close to that of the aqueous humour. The pH of normal vitreous is about 7.5.

The vitreous body has two distinct phases: the liquid vitreous humour and the solid residual protein. The residual protein is mainly collagen which is responsible for the gel-like state. There is a relatively high amount of collagen in the vitreous cortex, particularly in the vitreous base around the ora serrata. The liquid phase of vitreous humour contains a mucopolysaccharide called hyaluronic acid which is formed into long chains, arranged in a coil-like structure enclosing a relatively large amount of water.

The chemical composition of the vitreous humour is similar to that of the aqueous humour, except for the collagen and hyaluronic acid. In different parts of the vitreous concentration gradients of some substances are present. These substances may be utilized by the lens and retina. Glucose concentration in the vitreous is lower than plasma, but higher than in the aqueous. It is possible that glucose enters the vitreous mainly from the retina. Glucose level is higher in the anterior than in the posterior vitreous, as are sodium and potassium levels. The blood–vitreous

barrier plays a role in regulating the entrance of blood proteins into the vitreous.

Movement of substances through the vitreous is interesting. It has been demonstrated that many substances leaving the vitreous probably exit by more than one mechanism and pathway. Usually substances with large molecules reach a steady state slowly in the vitreous, probably because diffusion is a slow process and because of the special organization of the collagen and hyaluronic acid in the cortex, which may act as a molecular sieve. The concentration of soluble protein is higher in the vitreous cortex, a finding that suggests the origin of these proteins from the adjacent tissues. The content of the acidic glycoproteins amongst these soluble proteins is also very high.

The vitreous can be divided into five components, anterior hyaloid, posterior hyaloid, cortex, central vitreous and vitreous cells [1]. The collagen fibrils and their enclosed elements have been found in the anterior hyaloid and arranged in sheet-like aggregates parallel to the surface of the eye. The laminar appearance is greatest in the pars plana region, particularly in the peripheral portion, where the zonular fibres are observed. Slightly posterior to the vitreous base, the fibrils form very thin layers along the inner retina that gradually move away from the retina towards the central vitreous. Posterior to the equator the vitreous continues to be closely identified with the inner limiting membrane of the retina. Some vitreous fibrils insert into the basement membrane of the Muller and glial cells of the retina. The cortex is approximately 100 μm thick and includes the anterior and posterior hyaloid. It circumscribes the entire vitreous body, being formed by a condensation of collagen fibrils, cells, proteins and mucopolysaccharide in the interfibrillar spaces.

The vitreous has also been described as tract structures with their corresponding circular zonular ligaments [33]. Figure 1.5 illustrates the five major tracts in the normal vitreous. These tracts have their corresponding attached ligaments including: (1) the ora serrata and the preretinal tract, (2) the posterior epiciliary ligament and the posterior ciliary tract, (3) the anterior epiciliary
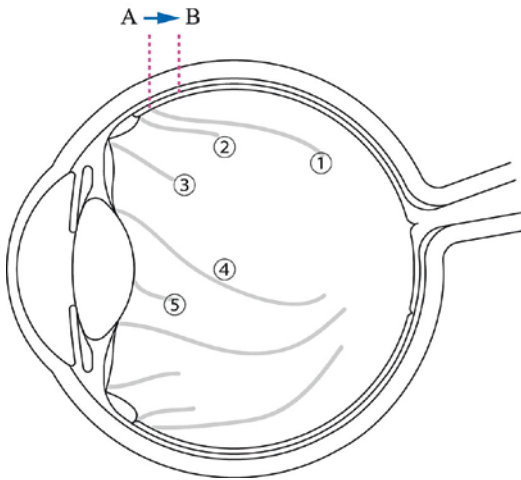
Fig. 1.5 The vitreous tracts in the normal vitreous. Five major tracts are shown in the schematic drawing: ① the preretinal tract, ② posterior ciliary tract, ③ the anterior ciliary tract, ④ the retrolental tract and ⑤ the area hyaloidea. The vitreous tracts are attached to their corresponding zonular ligaments. The vitreous base is located between the preretinal tract and posterior ciliary tract which is relatively invariable. However, the posterior vitreous base could be variable with age. In aged subjects, it may be moved from A towards B

Fig. 1.6 A schematic outline of major vitreous body attachments including (*1*) orbiculo-anterior zonular fibres to the lens; (*2*) orbiculo-posterior zonular fibres to the lens; (*3*) anterior vitreous face to the posterior lens capsule; (*4*) anterior extremity of canal of Cloquet; (*5*) vitreous base to mid pars plana (origin of vitreous face); (*6*) region of vitreous base; (*7*) region of diminishing adherence of vitreous base to the retinal surface; (*8*) vitreous–retinal attachments; (*9*) vitreous–retinal attachment in the fovea centralis; (*10*) attachment of posterior vitreous around the optic disc; (*11*) posterior extremity of canal of Cloquet (area Martegiani)

ligament and anterior ciliary tract, (4) the retrolental ligament and retrolental tract and (5) the area hyaloidea [33]. The vitreous base is the region in which the vitreous is solidly attached. It plays an important role in inducing clinical complications when iatrogenically affected during surgery or trauma. The vitreous base can be divided into two parts: anterior and posterior vitreous base. The anterior vitreous base is located from the ora serrata and preretinal tract to the posterior ciliary tract which is invariable, whilst the posterior vitreous base is variable and may only be identified after posterior vitreous detachment in elderly subjects. Different appearances of the vitreoretinal detachment can be caused by changes in vitreo-retinal adhesions.

In addition to attachment in the vitreous base, the vitreous is also attached to the retina in the peripapillary region through a narrow zone and several other locations shown in Fig. 1.6 [34]. With ageing, this attachment could be weaker. The cortex in the peripapillary attachment has more fibrils which are towards the basement membrane of the retinal Muller cells.

1.5.2 Vitreous and Its Interface with the Retina and Macula

It is well known that the vitreous plays an important role in maintaining the functional and structural stability of the retina and macula. Changes in vitreous properties either anteriorly or posteriorly can potentially cause problems for the retina and macula, which may or may not be evident clinically. However, we need to know how to predict and how to avoid the possible complications in the retina if possible.

The anterior vitreous membrane, particularly the thin vitreolenticular part, could be damaged during cataract surgery or trauma resulting in rhegmatogenous retinal detachment and/or cystoid macular oedema. Damage to the vitreolenticular barrier in the anterior vitreous may have repercussions on the vitreoretinal zone in the posterior vitreous and may cause either a volume shift or a chemical transfer. The volume shifting anteriorly may induce posterior vitreous detachment which exposes vitreoretinal adhesion. Chemical transfer may cause a movement of the substances between

the vitreous and the anterior chamber. It is undoubtedly true that the vitreous base – its posterior retinal part – plays the most important role in inducing clinical complications in the posterior segment when iatrogenically affected during surgery or trauma. This region of the eye is usually not visible without indentation. It is the most peripheral zone of the retina, the ora serrata, the posterior ciliary body and the vitreous base.

There are two types of posterior vitreous detachments: rhegmatogenous and non-rhegmatogenous vitreous detachment. Rhegmatogenous posterior vitreous detachment often occurs in the elderly and liquefied vitreous may pass through the hole into the retrovitreal space. During this process, retinal horseshoe holes may occur at the site of vitreoretinal adhesions. In a non-rhegmatogenous posterior vitreous detachment, volume transfer is a relatively slow process without hole formation, leading to a partial posterior vitreous detachment at least in the initial stage. It may induce cystoid macular oedema rather than a retinal hole. The consequence of the posterior vitreous detachment is that retina could be exposed to direct vitreous traction without stable vitreous cortex shielding. However, the traction affecting the retina and leading to the retinal detachment does not occur by the vitreous tract but by the posterior hyaloid membrane [31]. It is likely no further tearing will occur if complete posterior vitreous detachment is present.

1.6 Summary

This chapter mainly describes the anatomy and histology of the macula relevant to macular function. Macular cellular structure is highly dependent on the different regions, foveola, fovea, parafovea and perifovea. Blood supply from the retinal circulation and choroidal circulations is well matched to the demands of these regions but also determined by the functional requirements of high visual acuity. The human macula is very well structured in order to achieve the best vision. In addition, the vitreous has a very close relationship with the macula playing critical roles in stabilizing the microenvironment of the macula.

However, macular homeostasis depends on sophisticated specific arrangement of neuronal cells and blood supply. Knowledge of macular anatomy and histology is essential for understanding macular function and management of macular diseases.

References

1. Hogan MJ, Alvarado JA, Esperson Weddell J. Histology of the Human Eye. London: W.B. Saunders Company; 1971.
2. L'Esperance FA. Current diagnosis and management of chorioretinal diseases; 1977.
3. Thiel R. Atlas der Augenkrankheiten; 1948.
4. Chan G, Balaratnasingam C, Yu PK, Morgan WH, McAllister IL, Cringle SJ, et al. Quantitative morphometry of perifoveal capillary networks in the human retina. Invest Ophthalmol Vis Sci. 2012;53(9):5502–14.
5. Curcio CA, Sloan KA, Kalina RE, et al. Human photoreceptor topography. J Comp Neurol. 1990;292:497–523.
6. Hendrickson A. Fovea: primate. In: Encyclopedia of the eye, Elsevier; 2009.
7. Pournaras CJ, Riva CE, Tsacopoulos M, et al. Diffusion of O_2 in the retina of anesthetized miniature pigs in normoxia and hyperoxia. Exp Eye Res. 1989;49:347–60.
8. Yu D-Y, Cringle SJ. Oxygen distribution and consumption within the retina in vascularised and avascular retinas and in animal models of retinal disease. Prog Retina Eye Res. 2001;20:175–208.
9. Yu D-Y, Cringle SJ, Su E-N et al (2009) Retinal cellular metabolism and its regulation and control. In: Neurovascular medicine: pursuing cellular longevity for healthy aging. Oxford University Press, ISBN10: 0195326695, Kenneth Maiese.
10. Laties AM, Jacobowitz D. A comparative study of the autonomic innervation of the eye in monkey, cat, and rabbit. Anat Rec. 1966;156:383–9.
11. Alm A, Bill A. Blood flow and oxygen extraction in the cat uvea at normal and high intraocular pressure. Acta Physiol Scand. 1970;80:19–28.
12. Bill A. Autonomic nervous control of uveal blood flow. Acta Physiol Scand. 1962;56:70–81.
13. Friedman E. Choroidal blood flow. Pressure-flow relationships. Arch Ophthalmol. 1970;83:95–9.
14. Kiel JW, Shepherd AP. Autoregulation of Choroidal Blood Flow in the Rabbit. Invest Ophthalmol Vis Sci. 1992;33:2399–410.
15. Yu D-Y, Alder VA, Cringle SJ, et al. Choroidal blood flow measured in the dog eye in vivo and in vitro by local hydrogen clearance polarography: Validation of a technique and response to raised intraocular pressure. Exp Eye Res. 1988;46:289–303.

16. Laties AM. Central retinal artery innervation. Arch Ophthalmol. 1967;77:405–9.
17. Grunwald JE, Riva CE, Brucker AJ, et al. Altered retinal vascular response to 100% oxygen breathing in diabetes mellitus. Ophthalmology. 1984;91:1447–52.
18. Yu D-Y, Cringle SJ, Alder VA, et al. Intraretinal oxygen distribution in rats as a function of systemic blood pressure. Am J Phys. 1994;36:H2498–507.
19. Su EN, Alder VA, Yu DY, et al. Continued progression of retinopathy despite spontaneous recovery to normoglycemia in a long-term study of streptozotocin-induced diabetes in rats. Graefes Arch Clin Exp Ophthalmol. 2000;238:163–73.
20. Yanoff M, Fine BS. Ocular pathology. London: Mosby-Wolfe; 1996.
21. Yu D-Y, Alder VA, Su EN, et al. Relaxation effects of diltiazem, verapamil, and tolazoline on isolated cat ophthalmociliary artery. Exp Eye Res. 1992a;55:757–66.
22. Yu D-Y, Alder VA, Su EN, et al. Agonist response of human isolated posterior ciliary artery. Invest Ophthalmol Vis Sci. 1992b;33:48–54.
23. Yu D-Y, Su EN, Alder VA, et al. Pharmacological and mechanical heterogeneity of cat isolated ophthalmociliary artery. Exp Eye Res. 1992c;54:347–59.
24. Yu PK, Balaratnasingam C, Cringle SJ, et al. Microstructure and network organization of the microvasculature in the human macula. Invest Ophthalmol Vis Sci. 2010a;51:6735–43.
25. Yu PK, Balaratnasingam C, Morgan WH, et al. The structural relationship between the microvasculature, neurons and glia in the human retina. Invest Ophthalmol Vis Sci. 2010b;51:447–58.
26. Snodderly DM, Weinhaus RS. Retinal vasculature of the fovea of the squirrel monkey, *Saimiri sciureus:* Three-dimensional architecture, visual screening, and relationships to the neuronal layers. J Comp Neurol. 1990;297:145–63.
27. Spitznas M, Bornfeld N. The architecture of the most peripheral retinal vessels. Albrecht Von Graefes Arch Klin Exp Ophthalmol. 1977;203:217–29.
28. Hayreh SS. Physiological anatomy of the retinal vasculature. In: Encyclopedia of the eye. Elsevier Ltd.; 2010.
29. Weiter JJ, Ernest JT. Anatomy of the choroidal vasculature. Am J Ophthalmol. 1974;78:583–90.
30. Fryczkowski AW. Anatomical and functional choroidal lobuli. Int Ophthalmol. 1994;18:131–41.
31. Tasman W, Jaeger EA. Duane's clinical ophthalmology on CD-ROM; 2005.
32. Lee B, Litt M, Buchsbaum G. Rheology of the vitreous body Part I: Viscoelasticity of human vitreous. Biorheology. 1992;29:521–33.
33. Framme C, Wolf S. Retinal complications after damaging the vitreolenticular barrier. Ophthalmologica. 2012;227:20–33.
34. Fine BS, Yanoff M. Ocular histology. Hagerstowm, MD: Harper and Row; 1979.

Macular Physiology and Its Clinical Significance

Dao-Yi Yu, Stephen J. Cringle, Paula K. Yu, and Er-Ning Su

2.1 Introduction

Macular and vitreous surgeries may unavoidably alter the intraocular environment that could have therapeutic benefits for macular diseases but also cause potential problems. For example, when the gel-like vitreous is replaced with less viscous solutions such as saline after vitrectomy, the transport and distribution of all molecules, including oxygen and cytokines, can be changed [1].

Oxygen plays a critical role in influencing the intraocular environment in physiological, pathological, and postsurgical conditions. Oxygen is the only molecule serving as the primary biological oxidant [2]. Arguably, the retina has one of the highest energy demands per weight in the body. The energy is mostly used to reverse the ion influxes that underlie synaptic potentials and action potentials. If there is an inadequate supply of blood, glucose, and oxygen to a region of the retina, then neurons and glia become injured or die. To sustain neuronal function, the retina has evolved "neurovascular coupling" mechanisms to increase the flow of blood to regions in which neurons are active, a response termed functional

blood flow redistribution. Different information coding strategies and neural algorithms require different increases in blood flow, depending on the extent to which they consume energy. An understanding of the mechanisms that generate functional blood flow redistribution is a prerequisite for developing therapies to correct defects in blood flow control that occur after disorders such as retinal ischemia and diabetes [3]. In addition, oxygen is a major regulator which is a natural anti-VEGF factor [4] while hypoxia induces vascular endothelial growth factor (VEGF) and other growth factors.

For example, age-related macular degeneration (AMD) is often described as a multifactorial disease, and both ischemia and hypoxia have been implicated in the linking etiology and pathophysiology of AMD [5–7]. Choroidal ischemia is not the only contributor to retinal hypoxia found in AMD eyes, as some features of AMD such as confluent drusen, serous or hemorrhagic retinal detachment, retinal edema, and vitreoretinal adhesion may also interfere with retinal oxygen metabolism. Given the importance of the oxygen molecule in macular physiology and pathology, it is fortunate that vitreous and intraretinal oxygen levels can be quantitatively measured. Accumulated data from different animal species and some human studies provide valuable information for understanding the physiology of the vitreous and macula as well as the influence of surgical interventions. We will briefly describe

D.-Y. Yu (✉) · S. J. Cringle · P. K. Yu · E.-N. Su
Centre for Ophthalmology & Visual Science, Lions Eye Institute, The University of Western Australia, Perth, WA, Australia
e-mail: dyyu@lei.org.au; Steve@lei.org.au; PaulaYu@lei.org.au; erning@lei.org.au

the importance of retinal and macular energetics, and provide some detailed information on intraocular oxygen distribution including intraretinal and vitreous oxygen measurements. Intraretinal oxygen distribution in the macular area is very special due to the unique anatomic and histological structure of the macula. In order to better understand the oxygen distribution in the macula, we will first describe the intraretinal oxygen distribution in the more peripheral retina. Some features of the intraretinal oxygen distribution induced by common physiological and pathological conditions are also described. Possible consequences after vitreous and macular surgery will also be discussed.

2.2 Energy Demands of the Retina and Macula

Many ocular diseases with visual impairment stem from a defect of the retina. AMD is the leading cause of blindness in the Western world, and its prevalence is rising with the aging population [8]. Diabetic retinopathy remains the leading cause of preventable blindness in working adults [9]. Effective treatment of these visual impairments is limited because we lack detailed knowledge of the dysfunction underlying these disorders [10–13]. Accumulated information has made it possible to pursue a host of previously unanswerable questions [14]. Although multidisciplinary approaches are necessary, some common features for all retinal disorders may be more critical for linking multiple hypotheses. Retinal energetics could be a fundamentally important area, particularly for retinal and macular diseases [15].

2.2.1 High Oxygen Uptake of the Retina and Macula

All biochemical reactions involve energy exchange. The key energy-containing molecules of internal free energy within the cell are nucleo-tide triphosphates, such as adenosine triphosphate (ATP). Roughly 10^9 molecules of ATP are present in a typical cell at any instant. In many cells, all this ATP may be used up and replaced every 1-2 minutes [16]. ATP is produced by a series of chemical reactions and finally synthesized ~90% by oxidative phosphorylation in mitochondria and some by glycolysis in the cytosol.

The energetics in the retina and macula is more vulnerable than in most tissues. The retina is a thin sheet of brain-like tissue projected into the eye and has highly packed neurons, particularly in the macular area. The miracle of vision begins when the photoreceptors absorb light. Vision is the dominant sense in humans and other primates, with nearly 30% of our cortical surface representing information that is predominantly visual [17]. It is also estimated that 90% of our sense signals are from visual input. The photoreceptor must convert the energy of the absorbed photon into an electrochemical signal to be relayed to the visual cortex of the brain. The process of visual transduction involves a G-protein-mediated second messenger system, which ultimately controls membrane potential and neurotransmitter release. Furthermore, unlike other sense organs, the retina is not only sensing, but also performing a tremendous amount of processing of signals before transmission to the brain.

A large amount of energy is required to perform the normal function of the brain and retina. The high energy demand is mainly produced through the chemical process of oxidative phosphorylation in the mitochondria to produce adequate quantities of ATP. It is estimated that ~20% of the total oxygen consumption in the human body is consumed by the brain that constitutes only ~2% of the body weight [18] and oxygen consumption per tissue weight in the retina is higher than that in the brain [19]. As a consequence of unusual energy requirements, retinal cells are exquisitely sensitive to disturbances in the supply of their energy sources (oxygen and other substrates).

2.2.2 High Energy Demands and Limited Blood Supply in the Retina and Macula

The retina performs the vital task of transducing and encoding the visual input for later processing by the visual centers of the brain. The retina has the conflicting constraints of a high metabolic requirement, yet the transparency of the retina cannot be compromised by an overly rich vascular network on the inner retinal side. Therefore, only a limited blood supply can be provided by the retinal circulation. In addition, the photoreceptor layer itself is totally avascular, and oxygen supply is predominantly dependent on diffusion from the choroid. It is a challenge to maintain a delicate balance between the available oxygen supply and the consumption of oxygen within the retina. Such a delicate balance can only be achieved by precise regulatory mechanisms to match local blood flow with tissue demands in order to maintain retinal homeostasis. Disruption of these mechanisms can have severe consequences in the retina. This means that the retina is particularly vulnerable to a wide range of vascular diseases. In the Western world, 75% of blindness and visual loss are attributable to retinal diseases with a vascular component [20]. Such diseases include diabetic and hypertensive retinopathy, glaucoma, age-related macular degeneration, central and branch arterial occlusion, and venous occlusion. The underlying pathogeneses of these diseases remain poorly understood. Thus, we are not currently in a position to provide satisfactory procedures for early diagnosis and treatment. As oxidative metabolism is essential for supplying retinal energy and supporting function, retinal oxygenation and oxygen consumption provide important information that can be used to evaluate retinal energetics in healthy and diseased retinas.

2.2.3 Relevance of Intraocular Oxygen Distribution for Retinal Energetics

Intraocular oxygen distribution is remarkably nonuniform and contains important information regarding oxygen tension, oxygen supply from different circulations, oxygen diffusion and solubility properties, and oxygen consumption rates in specific retinal layers. In some intraretinal regions, the oxygen level is very low even under normal physiological conditions [21, 22]. It is fundamentally important to address how retinal cells and their compartments share the limited energy available responding to very active function under varying physiological and pathological conditions. Since oxygen cannot be "stored" in tissue, a constant and adequate supply must be guaranteed in order to preserve function. Oxygen supply to the retina is arguably more vulnerable to vascular deficiencies than in any other organ. It is very important to know how to achieve the delicate balance between high energy demands and limited blood supply. Consumption of free energy is fundamental to life [23]. It seems likely that the high energy demands and limited supply in the retina may require rapid redirection of energy sources when local energy demands change.

It is relatively easy to identify the high oxygen consumption region of the inner segments of the photoreceptors in the outer retina because the outer retina is an avascular region in which oxygen consumption can be determined using the mathematical models based on Fick's law of diffusion [24]. In contrast, the inner retina typically has vascular beds making it more difficult to determine the oxygen consumption in the inner retina. We performed a series of experiments involving changes in physiological conditions and/or occlusion of the retinal circulation to investigate oxygen consumption in the inner retinal layers [21, 22, 24–27]. It was demonstrated that two distinct regions of the inner retina, the inner and outer plexiform layers, have high oxygen consumption rates. There are abundant synapses located in the inner and outer plexiform layers. Interestingly, although the three distinct high oxygen consuming regions across the entire retina are rich in mitochondria, there are significant differences in the oxidative metabolism between the inner segments of the photoreceptors and the plexiform layers. For example, the oxygen consumption in the inner

segments can be significantly changed by dark and light adaptation, as well as some diseased situations such as retinal degeneration or laser-induced lesions, but it is not affected by increased oxygen availability [24, 26, 28–30]. However, the oxygen consumption in the plexiform layers is not affected by dark and light adaptation, or by loss of outer retinal input due to retinal degeneration, but it is increased dramatically in the presence of increased oxygen availability [21, 24, 25, 31].

2.3 Intraocular Oxygen Distribution

Maintenance of adequate oxygen supply to the retina is critical for retinal function. In species with vascularized retinas, such as man, monkey, and rat, oxygen is delivered to the retina via a combination of the choroidal vascular bed, which lies immediately behind the retina, and the retinal vasculature, which lies within the inner retina. The high-oxygen demands of the retina and the relatively sparse nature of the retinal vasculature are thought to contribute to the particular vulnerability of the retina to vascular disease. Oxygen supply to the retina is likely to be a critical factor. Much attention has therefore been directed at determining the intraretinal oxygen environment in healthy and diseased eyes.

In recent years, the understanding of the mechanisms of coupling between the neuronal activity and the vascular supply has improved significantly. The traditional concept that active neurons generate a metabolic signal, such as decreased oxygen level or a rise in carbon dioxide, triggering an increase in blood flow has been challenged. New ideas have been proposed that neurotransmitter-mediated signaling, particularly by glutamate, has a major role in regulating cerebral blood flow, mainly mediated by astrocytes. Glutamate-mediated signaling leads to the release of nitric oxide and arachidonic acid derivatives from neurons and astrocytes. However, these molecules can either increase or decrease blood flow, depending on the local oxygen concentration. In both new and traditional concepts, the

important role of oxygen in controlling blood flow has been established.

Measurements of oxygen levels within the retina have largely been restricted to animal studies in which oxygen-sensitive microelectrodes can be used to obtain high-resolution measurements of oxygen tension as a function of retinal depth. Such measurements can immediately identify which retinal layers are supplied with oxygen from the different vascular elements. Some oxygen measurements have also been performed in human eyes using a fiberoptic oxygen sensor [32] or large polarographic oxygen electrodes [33] during surgical procedures. Although these measurements do not have the same spatial resolution as microelectrode-based studies in animals, the data obtained from human eyes are valuable, particularly when combined with research findings for interpreting the pathogenesis of many clinical diseases including both the anterior segment and posterior pole. It is very important to understand the data from both clinical and research studies and to pay attention to differences in species and technical limitations.

It is important to consider oxygen gradients to define the oxygen sources and consumption zones rather than the oxygen level per se. In this chapter, we would like to summarize what is known about the intraocular oxygen distribution from animal and human studies.

2.3.1 Intraretinal Oxygen Distribution

2.3.1.1 Intraretinal Oxygen Distribution in Normoxia

Before describing macular oxygenation, it is necessary to review the intraretinal oxygen distribution in the less specialized area of the retina. An example of the measured intraretinal oxygen distribution in the vascularized retina of the adult rat is shown in Fig. 2.1 [21].

The rat retina is a convenient model to illustrate the heterogeneity of the intraretinal oxygen distribution. The heterogeneity of the intraretinal oxygen distribution is mainly induced by the layered nature of the oxygen sources (vasculature)
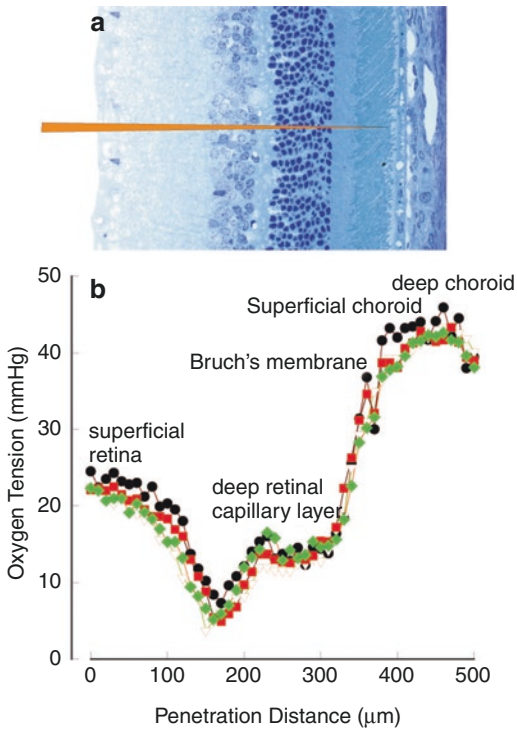
Fig. 2.1 Intraretinal oxygen distribution in rat. Histological section of a rat retina and schematic drawing of an oxygen-sensitive microelectrode (the tip size: ~1 μm) penetrating the retina.
Intraretinal oxygen profiles in the rat under normal physiological conditions. Oxygen tension is shown as a function of electrode track distance through the retina. The results from two sequential measurements which include both penetration and withdrawal data are shown. The intraretinal oxygen distribution reflects the relative oxygen sources and sinks within the retina and choroid [21]

and sinks (oxygen consuming cells). The rat retina is modestly thicker with relatively sparse vasculature when compared to the human and primate retina. The track distance is measured in micrometers from the internal limiting membrane, through to the deep choroid (450 μm) where the peak PO_2 occurs. At ~370 μm a discontinuity can be seen which is attributed to the penetration of Bruch's membrane. In these typical profiles, the oxygen tension in the innermost retina (~22 mmHg) decreased with retinal depth to reach a minimum PO_2 of ~5 mmHg at approximately 35% retinal depth. On further insertion, PO_2 values rose to a small secondary peak (~15 mmHg) between 60-70% retinal depth,

which corresponded well with the deep capillaries of the retinal circulation. Following this small peak, a plateau region was often seen prior to the steep rise in PO_2 to the choroid (42 mmHg). In examining the oxygen gradients in different regions, it is possible to determine which retinal layers receive their oxygen from the available oxygen sources. The deepest capillary layer lies within the outer plexiform layer. Between this deep capillary layer and the choroid, the outermost retinal layers are completely avascular. So, looking at the oxygen gradients, and remembering that oxygen can only flow "downhill" we can determine that the majority of the outer retinal oxygen supply is from the choroid. There is, however, a small contribution made by the deep retinal capillary layer. Between the two retinal capillary layers, the oxygen tension can fall to quite low values, but rarely approaching anoxic levels under normal physiological conditions.

2.3.1.2 Intraretinal Oxygen Distributions Under Light and Dark Adapted Conditions

The data presented are for light-adapted conditions. In the outer retina, the sudden change in oxygen gradient (at ~320 μm penetration depth) is due to the high oxygen consumption of the inner segments of the photoreceptors. The oxygen consumption of this region increases during dark adaptation, resulting in a significant fall in oxygen tension in this region as shown in Fig. 2.2 [1, 2]. But in the adult rat, the lowest oxygen tensions are still consistently found to occur in the inner retina between the two retinal capillary layers [30].

2.3.1.3 Intraretinal Oxygen Distribution in Graded Hyperoxia

Average intraretinal profile data in the hyperoxia trial are shown in Fig. 2.3 [26]. The rise in inner retinal oxygen tension is muted compared to that in the choroid, and the intraretinal minimum is preserved under all breathing conditions. The mean oxygen tension at the retinal surface under air breathing conditions was 19 mmHg, which then fell to a minimum (5 mmHg) within the
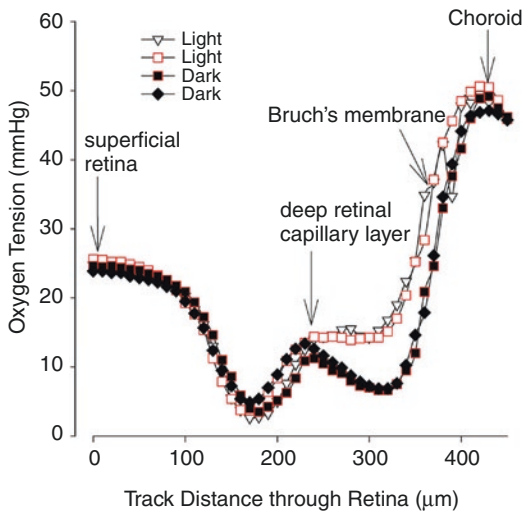
Fig. 2.2 Intraretinal oxygen distributions under light and dark adapted conditions.
Outer retinal oxygen level falls in the dark [24, 28]
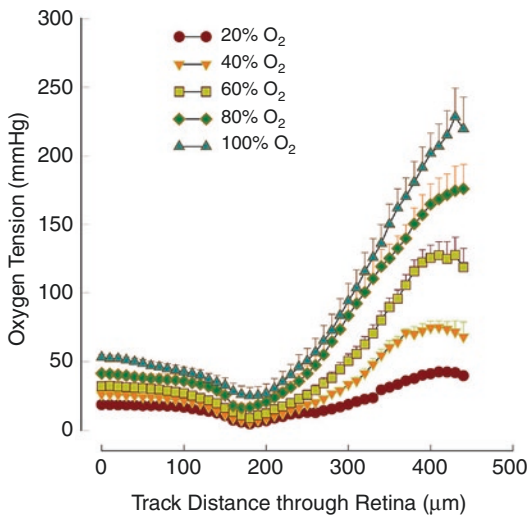
Fig. 2.3 Average intraretinal oxygen profiles in the rat following stepwise increases in oxygen ventilation level (20%, 40%, 60%, 80%, 100%). Oxygen tension is shown as a function of electrode track distance through the retina. Choroidal oxygen tension rises much more dramatically than that in the inner retinal layers. Even with 100% oxygen ventilation the presence of a minimum oxygen level within the inner retina, indicates the retinal circulation continues to provide net oxygen delivery to the retina [26]

inner plexiform layer before rising again through the plateau region to peak in the choroid at 42 mmHg. With 100% oxygen ventilation the

corresponding values are 53 mmHg at the retinal surface, 25 mmHg at the inner retinal minimum, and 228 mmHg at the peak choroidal oxygen tension. The oxygen gradients in the outermost retina are significantly increased during hyperoxic ventilation.

2.3.1.4 Intraretinal Oxygen Distribution and Consumption During Retinal Artery Occlusion and Graded Hyperoxia

The avascular nature of the outer retina, coupled with microelectrode-based measurements of intraretinal oxygen distribution, has allowed the high oxygen metabolism of the outer retina to be identified [22, 24, 31, 34]. However, the presence of retinal vasculature in the inner retina normally precludes such a simple analysis and this has led to the widely held, but mistaken view, that the oxygen requirements of the retina as a whole are dominated by the photoreceptors. An indication of the oxygen requirements of the inner retina can be gained by rendering the full thickness of retina "avascular' by occlusion of the retinal vasculature.

A typical intraretinal oxygen profile in the occluded region is shown in Fig. 2.4 [27]. Also shown for easy comparison is the measured profile prior to occlusion. It is evident that following retinal occlusion the choroid is now the only source of retinal oxygenation, and that under these air-breathing conditions the retinal occlusion renders much of the inner retina anoxic. Visual examination of the oxygen profile provides a guide to the local oxygen consumption since the intraretinal oxygen gradient changes most rapidly where the local oxygen consumption rate is the highest. The first major change of gradient at ~340 μm track distance corresponds to the inner segments of the photoreceptors. Whatever oxygen flows through this region is consumed by the outer plexiform layer (~260 μm track distance).

Averaged oxygen profiles from occluded retinas are shown in Fig. 2.5a for a range of increasing levels of inspired oxygen from 20 to 100% oxygen. With 20% oxygen ventilation the choroidal oxygen supply is sufficient to avoid any
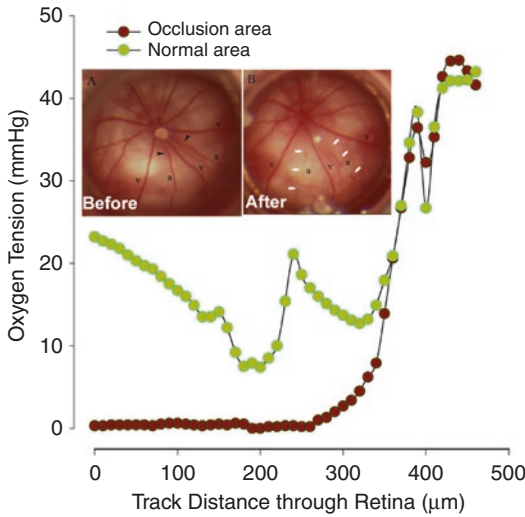
Fig. 2.4 Example of intraretinal oxygen distributions from retinal artery occlusion area and normal area with inserted fundus photographs of a rat retina (**a**) showing the radial distribution of retinal arteries (a) and veins (v) before the application of laser photocoagulation of the pair of the retinal arteries feeding the area in which intraretinal oxygen distributions were measured. Chosen sites for laser occlusion are marked by the black arrowheads. After laser (**b**) the arteries have either disappeared or have a stationary blood column indicating occlusion of blood flow (white arrows) [27]

anoxia in the outer retina where the dominant oxygen-consuming layer is the inner segments of the photoreceptors. However, any oxygen diffusing across the outer retina is consumed by the outer plexiform layer and anoxic regions are present in this and all the more proximal retinal layers. Choroidal oxygen level rises with each increment in the inspired oxygen level. This increase in choroidal oxygen level increases the range of choroidal delivered oxygen to include more of the inner retina with each elevation in choroidal PO_2. Thus, as choroidal oxygen tension increases the extent of inner retinal anoxia decreases. However, even with 100% oxygen ventilation, which produces an average choroidal PO_2 of almost 300 mmHg, the average oxygen tension in the innermost region of the inner retina is close to zero.

The potential for different levels of oxygen consumption in specific retinal layers is indicated by the uneven distribution of cytochrome oxidase

across the rat retina (Fig. 2.5c). Relatively dense layers of cytochrome oxidase staining are seen in the inner segments of the photoreceptors, the outer plexiform layer, and the inner plexiform layer.

The actual oxygen consumption rates of the individual retinal layers are calculated from a mathematical analysis of the individual oxygen profiles in each case. The average values for oxygen consumption are shown in Fig. 2.5b for each level of inspired oxygen ventilation. With 20% oxygen ventilation the oxygen consumption is dominated by the inner segments of the photoreceptors ($Q_2 = $ ~142 nL O_2/min/cm^2) and the outer plexiform layer ($Q_4 = $ ~ 91.0 nL O_2/min/cm^2), with the inner segments being the significantly larger consumer. With 40% oxygen ventilation almost all of the additional oxygen supplied by the choroid is consumed by the outer plexiform layer, which now has an oxygen consumption rate not significantly different from the inner segments. With 60% oxygen ventilation the oxygen consumption rate of the outer plexiform layer increases further but more oxygen is able to pass through to the more proximal retina and the oxygen uptake increases significantly in the deeper region of the inner plexiform layer (Q_6), but not significantly in the more superficial region of the inner plexiform layer (Q_7). With 80% oxygen ventilation there is no further increase in oxygen consumption in the outer plexiform layer but the oxygen consumption of the deeper region of the inner plexiform layer increased significantly. With 100% oxygen ventilation, only the oxygen consumption of the innermost retina (Q_8) increases significantly from the 80% oxygen ventilation level. Thus the general pattern is for oxygen consumption in the inner retinal layers to increase as more oxygen is available from the choroid. In contrast, the oxygen uptake of the outer retina (Q_2) showed no relationship to the inspired oxygen level.

The summed result of total inner and outer retinal oxygen consumption as a function of the inspired oxygen level is shown in Fig. 2.6. Inner retinal oxygen consumption is highly dependent on oxygen ventilation levels. With 20% oxygen ventilation outer retinal oxygen consumption
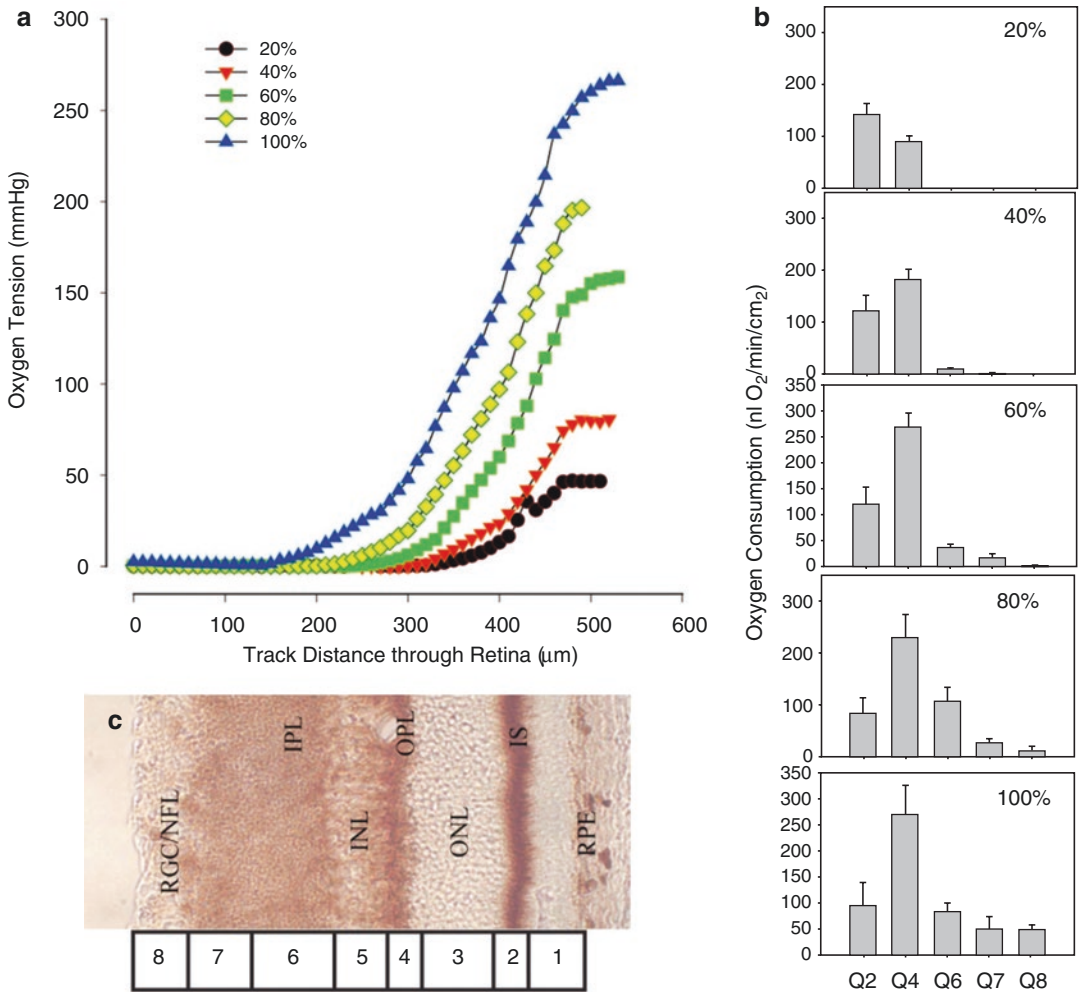
Fig. 2.5 The effect of increasing oxygen supply from the choroid to the retina.

The average intraretinal oxygen distribution in occluded retinas is shown for different levels of inspired oxygen (20, 40, 60, 80, and 100% oxygen). Each increment in inspired oxygen level allows the choroid to deliver more oxygen to the inner retina, however, even with 100% oxygen ventilation the average oxygen tension in the inner-most retina is close to zero.

The uneven distribution of cytochrome oxidase across the rat retina is shown. Relatively dense layers of cytochrome oxidase staining are seen in the inner segments of the photoreceptors, the outer plexiform layer, and the inner plexiform layer. A schematic of the starting position of each layer is also shown.

The result of applying the oxygen consumption model to each individual oxygen profile is shown in terms of oxygen consumption in each layer as a function of inspired oxygen percentage. As more oxygen is made available with hyperoxic ventilation the oxygen consumption of the inner retina increases and oxygen consumption is detected in the more proximal retinal layers [27]

($\sim$142 nL O_2/min/cm^2) is significantly higher than the total inner retinal oxygen consumption ($\sim$91.3 nL O_2/min/cm^2). At 40% inspired oxygen inner retinal oxygen consumption increases significantly and is not significantly different from outer retinal oxygen consumption. At 60% oxygen ventilation and above the total oxygen con-sumption of the inner retina is significantly greater than that of the outer retina. With 100% oxygen ventilation the average inner retinal oxygen consumption ($\sim$449 nL O_2/min/cm^2) is more than four times that of the outer retina ($\sim$95 nL O_2/min/cm^2). This observation of increased inner retinal oxygen consumption
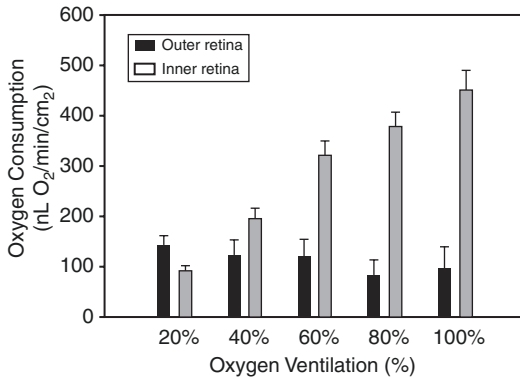
Fig. 2.6 The average oxygen consumption of the inner and outer retina as a function of inspired oxygen level. It is evident that with high levels of inspired oxygen the oxygen consumption of the inner retina becomes many times that of the outer retina [27].

with hyperoxia is also consistent with our studies in intact rat retinas [35].

2.3.2 Intraretinal Oxygen Distribution in the Macula

Many of the features apparent in the intraretinal oxygen distribution in the rat are present in larger species with vascularized retinas, such as the cat (Alder et al. 1983; [31]), pig (Pournaras et al. 1989; Tsacopoulos 1979) and primate [22, 34]. A general finding has been the existence of high oxygen tension in the region of the choriocapillaris/Bruch's membrane interface, steep oxygen gradients within the outermost retinal layers, and a minimum oxygen level within the retina, before a reversal of the oxygen gradient toward the innermost retina. At the very least, such information gives a picture of the relative oxygen level in the outer and inner halves of the retina. It also illustrates that oxygen measurements confined to the preretinal vitreous may not accurately reflect the oxygen status of the deeper retinal layers.

2.3.2.1 Macular Intraretinal Oxygen Distribution in Normoxia

The macula is a specific region anatomically and functionally. Information of the intraretinal oxygen distribution and consumption is important,

but can only be obtained from in vivo monkey experiments with highly precise measurements. Figure 2.7a shows the average data for oxygen tension as a function of penetration depth through the foveal region. Innermost retinal oxygen tension is about 6 mmHg, which decreased on penetration into the retina to reach a minimum of ~2 mmHg in the outer retina, before rising steeply to a peak of ~65 mmHg in the choroid. The small oxygen gradient in the inner retina indicates that there is some oxygen contribution to the outer retina from the vitreal side, but the large gradient in the outermost retina indicates that the dominant source of oxygen supply to this region of the retina is from the choroid. Although the oxygen gradient from the vitreous to the retina in this foveal region is small, it may well be significant in providing some oxygen supply from the vitreous to the avascular inner retina in this region. The lack of any local variation in the oxygen gradient in the inner retina reflects the lack of retinal capillaries in this region.

The average data for oxygen tension as a function of penetration depth through the parafoveal region of the retina is shown in Fig. 2.7b. There are some significant "bumps" present in the oxygen profile in the inner retinal layers of individual profiles indicating that in the parafovea area the oxygen contribution from the retinal capillary beds is evidenced. These "bumps" tend to be smoothed out by the averaging process across animals, but they are still evident in the averaged data. The average inner retinal surface oxygen tension is ~6 mmHg, which is not significantly different from equivalent locations in the foveal area, while the minimum oxygen tension in the outer retina is ~1 mmHg, which is significantly different from equivalent locations in the foveal area. The oxygen peak in the choroid is ~65 mmHg which is not significantly different from that in the fovea.

The average data for oxygen tension as a function of penetration depth through the inferior retina is shown in Fig. 2.7c. In the inferior retina, the oxygen contribution from the retinal capillary beds is also evident. The average inner retinal surface oxygen tension of ~14 mmHg and the minimum oxygen tension of ~6 mmHg in the
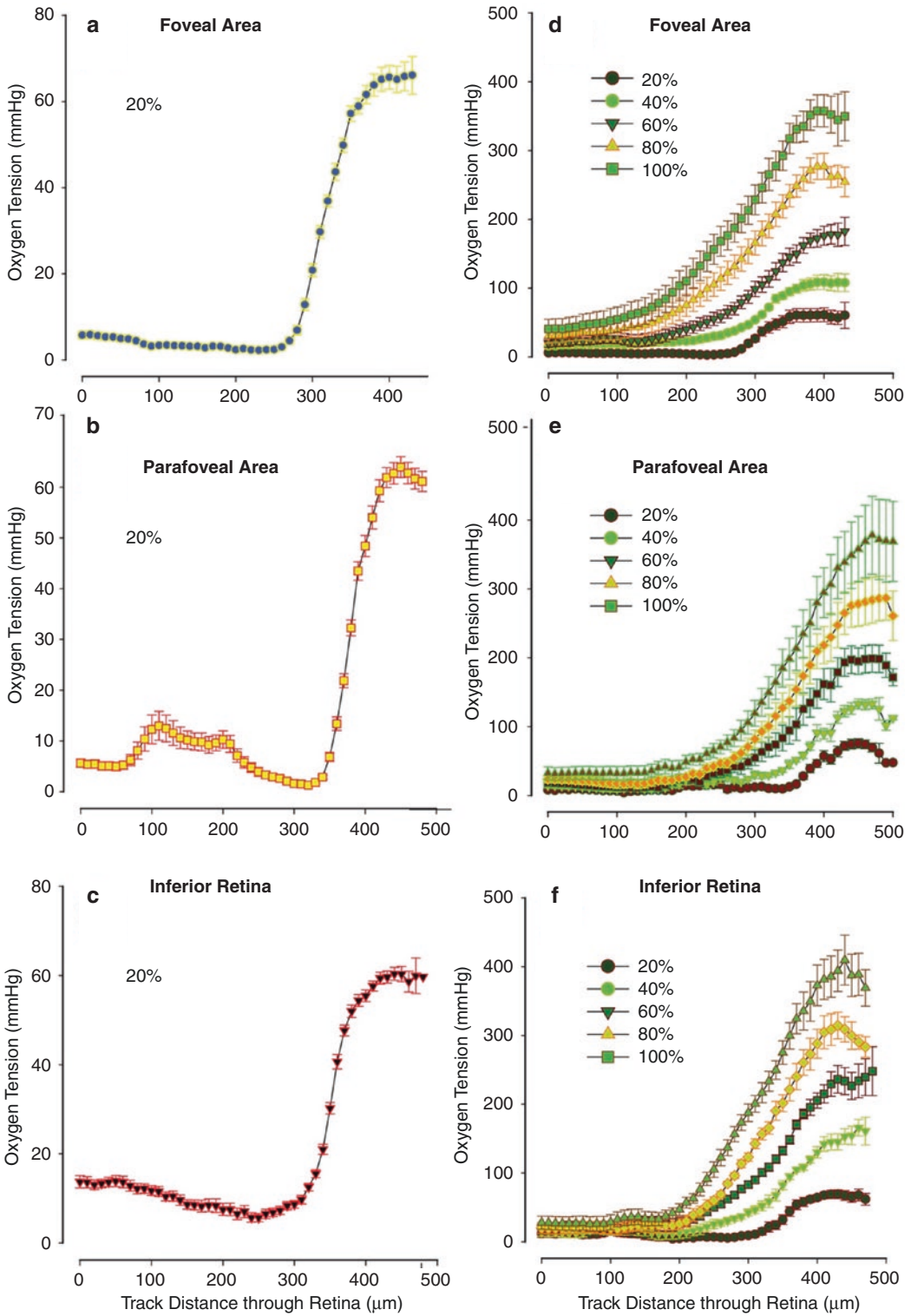
Fig. 2.7 Average intraretinal distribution as a function of track distance through the retina in the foveal area (top panel, **a** and **d**), parafoveal area (middle panel, **b** and **e**) and inferior retina (bottom panel, **c** and **f**) on 20% (left panels, **a**–**c**) and a range from 20 to 100% oxygen ventilation conditions (right panels, **d**–**f**) [22]

outer retina are both significantly higher than the corresponding locations in either the fovea or parafovea regions. The peak choroidal oxygen tension of ~60 mmHg in the inferior retina is not significantly different from that in the foveal and parafoveal areas.

2.3.2.2 Macular Intraretinal Oxygen Distribution in Graded Hyperoxia

It is of interest to know whether and how intraretinal oxygen distribution and consumption in the macula can be modulated. The stepwise increases in inspired oxygen percentage produced stepwise increases in systemic oxygen tension as expected, while pH and $PaCO_2$ are not significantly affected. The average response of intraretinal oxygen levels in the foveal area following stepwise systemic hyperoxia is shown in Fig. 2.7d. Each increase in the percentage of oxygen in the ventilation mixture creates a significant rise in choroidal oxygen tension, but a much smaller increase in inner retinal oxygen levels. Choroidal PO_2 increased from 60 mmHg at 20% oxygen ventilation to reach ~360 mmHg at 100% oxygen ventilation. The corresponding values at the surface of the inner retina are ~6 mmHg and ~41 mmHg for 20% and 100% oxygen ventilation respectively. At high levels of systemic hyperoxia, the shape of the intraretinal oxygen distribution indicates that there is a net gradient of oxygen from the retina to the vitreous. This reversal of the oxygen gradient at the retinal surface means that this region becomes a net source of vitreal oxygen.

The average response of intraretinal oxygen levels in the parafoveal area and inferior retina following stepwise systemic hyperoxia are shown in Fig. 2.7e, f. Each increase in the percentage of oxygen in the ventilation mixture induces a significant rise in choroidal oxygen tension reaching ~380 mmHg in the parafovea and 410 mmHg in the inferior retina at 100% oxygen ventilation. These choroidal values are not significantly different than in the foveal region. The oxygen levels in the innermost retina in the parafovea during 100% oxygen ventilation (32 mmHg) are not significantly different from that seen in the foveal area. The oxygen level of the innermost retina in the inferior retina during 100% oxygen ventilation (~20 mmHg) is lower than in the foveal or parafoveal areas. The oxygen gradients at the retinal surface are very flat during systemic hyperoxia in the parafoveal and inferior retina, indicating very little oxygen flux to the vitreous in these regions under hyperoxic conditions.

2.3.2.3 Oxygen Consumption in the Macula

The average oxygen consumption rates for the outer retina in each location can be calculated [22]. The outer retinal oxygen consumption was higher in the parafoveal area than in the foveal or inferior retina. There was no significant difference between outer retinal oxygen consumption in the foveal and inferior retina. In the subset of oxygen profiles measured under different levels of inspired oxygen, the three-layer oxygen consumption analysis reveals that outer retinal oxygen consumption did not change significantly with an inspired oxygen level in any of the three retinal locations tested.

In the special case of the completely avascular foveal area, the five-layer oxygen consumption model for the full thickness of the foveal profiles is applied and the average fitted curves for each oxygen ventilation condition. The arbitrary boundary (150 μm) is settled between the outermost retina and the remaining innermost retina. The oxygen consumption rates of the inner and outer regions of the fovea as a function of inspired oxygen percentage are shown in Fig. 2.8. Under normoxic conditions, the oxygen consumption of the inner region of the foveal area is only a small proportion of the total retinal oxygen consumption. However, the oxygen consumption of the innermost retina increased as a function of inspired oxygen percentage, becoming significantly greater at 60% oxygen and above. With 80% and 100% oxygen ventilation inner retinal oxygen consumption was not significantly different from outer retinal oxygen consumption. The total oxygen consumption of the foveal area approximately doubles during 100% oxygen ventilation.
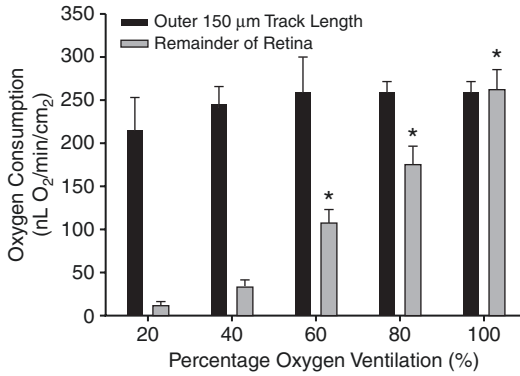
Fig. 2.8 Average oxygen consumption rates of the inner and outer regions of the foveal area at each oxygen ventilation level [22]

Fig. 2.9 Typical vitreal oxygen profiles measured as a function of distance from the retina starting at a retinal artery (red), vein (yellow), and intervascular location (blue) in a normal rat [21]

Such information from a "human like" macula such as in the monkey retina is particularly attractive for the study of the metabolic requirements of these specialized areas of the retina. Oxygen tension in the retina mainly depends on both supply and consumption. Both too little, and too much oxygen can be damaging to the retina. While retinal hypoxia plays a major role in ischemic retinal diseases, retinal hyperoxia is damaging to the developing human retina, as evidenced by the sight-threatening consequences of oxygen supplementation in premature infants [36]. The ability of the retina to cope with variations in the oxygen environment may be an important component of retinal homeostasis. The primate retina must also cope with a marked degree of spatial variation in photoreceptor density and type [37], which very likely requires individual photoreceptors to have different oxygen demands based on the local oxygen availability and the needs of its neighbors.

2.3.3 Vitreous Oxygen Distribution

The dominant oxygen sources in the eye are from vascularized structures such as the retina, ciliary body, and iris. A large volume of intraocular components, such as the lens, aqueous, and vitreous is avascular tissue. Oxygen supply to the avascular intraocular components is totally dependent on oxygen diffusion. Relatively low oxygen tension in the vitreous, lens and aqueous humor have been demonstrated. Intraocular oxygen distribution is not uniform and significant oxygen gradients are present. Tight regulation of the intraocular environment is critical for homeostasis and functional integration of the eye. Figure 2.9 shows typical vitreous oxygen profiles from the surface of the retina through the vitreous in rats. There is a significant gradient from a retinal artery; particularly within 200 μm from the surface of the retina. Much shallower gradients are seen close to retinal veins or intervascular areas.

It has been reported that the oxygen tension in the surface of the retina is higher than that in the posterior, central, and anterior vitreous in human and rabbit eyes [38]. Vitreal oxygen tension is reduced during retinal detachment [33, 38]. Oxygen tension in the anterior chamber is normally higher than that in vitreous as seen in both human and animal studies [1, 39]. Figure 2.10 shows the intraocular oxygen distribution in vitreous and aqueous humor in the human eye demonstrating that relatively low values of oxygen tension with oxygen gradients present in these intraocular components.
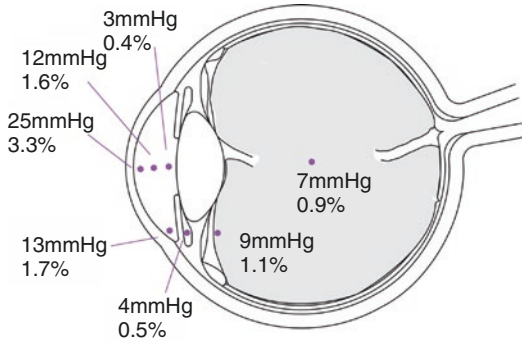
Fig. 2.10 Intraocular oxygen distribution in the human eye (measured oxygen tension and percentage). Data from Holekamp et al. [39]

2.4 Intraocular Oxygen Distribution After Vitrectomy

Potential changes in intraocular oxygen distribution after vitrectomy and macular surgery have been addressed over the past decades [1, 40–43]. Recent work [32, 39, 44] on measurements of oxygen tension in the human eye provides valuable information that has improved our knowledge and understanding possible causes of surgical outcomes of vitrectomy. It is important to integrate the information from both experimental animal work and clinical studies.

2.4.1 Increased Oxygen Tension in the Mid Vitreous and Adjacent to the Lens After Vitrectomy

It is generally agreed that the intraocular oxygen environment is altered after vitrectomy. Vitreous oxygen tension has been measured before, immediately after, and at longer times after vitrectomy clinically [39]. Immediately after vitrectomy, oxygen tension in the fluid-filled eye was significantly increased from 7 mmHg to 76 mmHg in the mid vitreous and from 9 to 70 mmHg adjacent to the posterior lens. In the longer term after vitrectomy, sustained increases in vitreal and anterior chamber oxygen levels have been

Fig. 2.11 Schematic drawing showing oxygen tension (percentage) in different locations long term after vitrectomy. Data from Holekamp et al. [39]

reported (Fig. 2.11), which is believed to be a possible mechanism for nuclear cataract formation after vitrectomy [39].

Increased retinal oxygen supply following pan-retinal photocoagulation and vitrectomy and lensectomy has been reported [42]. Some experimental studies also support clinical findings of increased vitreous oxygen tension after vitrectomy [45].

Possible mechanisms of increased vitreous oxygen tension after vitrectomy could be (1) Increased oxygen transport by diffusion or convection when the vitreous gel is replaced with less viscous saline after vitrectomy [1], and (2) Reduced oxygen consumption of vitreous gel after vitrectomy [44, 46].

2.4.2 Increased Oxygen Transport by Diffusion or Convection Could Improve Macular Oxygenation

Understanding the consequences of vitrectomy in terms of increased vitreous oxygenation is important. After vitrectomy, oxygen transport to the macula and other ischemic retinal areas could be improved resulting in significant benefits particularly for ischemic areas of the retina. We have demonstrated that the choroidal

circulation is not able to supply oxygen to the inner retina of vascularized retinas such as humans, monkeys, and rats (Fig. 2.4) [25, 27]. Our experimental studies in the monkeys suggest that improved oxygen transport in the vitreous could be particularly beneficial for macular oxygenation. Firstly, unlike other areas of the retina, the foveal area lacks retinal blood vessels and some of the oxygen supply to the inner retina in this region is from the vitreous (Fig. 2.7a). Increases in choroidal oxygen tension can only slightly raise the oxygen tension in the inner retina (Fig. 2.7d). This means that preretinal oxygen tension may be critical in the foveal area in both normal and diseased conditions. Secondly, in the parafoveal area, the retina is relatively thick with numerous neuronal cells and the highest level of oxygen consumption. Although retinal blood vessels are present in normal conditions the parafoveal area may be more vulnerable to ischemic diseases due to the high functional activity and energy demands. Additional oxygen supply from the vitreous after vitrectomy may, therefore, be beneficial. Thirdly, preretinal oxygen tension outside of the macula area even in intervascular regions (Fig. 2.7d) is higher than that in the macular area. Increased oxygen transport by diffusion or convection from outside of the macular area to the macular area could improve macular oxygenation.

There is some clinical evidence supporting the notion that vitrectomy is beneficial in diabetic macular edema in addition to the benefits of the release of vitreoretinal traction [47, 48]. Vitrectomy is believed to be critical in reducing macular edema in branch retinal vein occlusion [49] and sheathotomy may or may not have an additional effect [50]. It has also been reported that vitrectomy reduces macular edema in central retinal vein occlusion [51].

2.4.3 Molecular Transport After Vitrectomy

Stefansson has emphasized that after vitrectomy and vitreous gel are replaced with saline, transport of all molecules is facilitated including oxygen [1]. One critical molecule is vascular endothelial growth factor (VEGF), which is a major stimulus for retinal neovascularization. VEGF production is mainly controlled by oxygen tension.

Figure 2.12 shows possible differences in molecules transport before and after vitrectomy. In fact, oxygen diffuses from the perfused area to the ischemic area in the vitrectomized eye, resulting in improving hypoxia and reducing VEGF production in the ischemic area. VEGF is also cleared away from the retina at a faster rate. Such
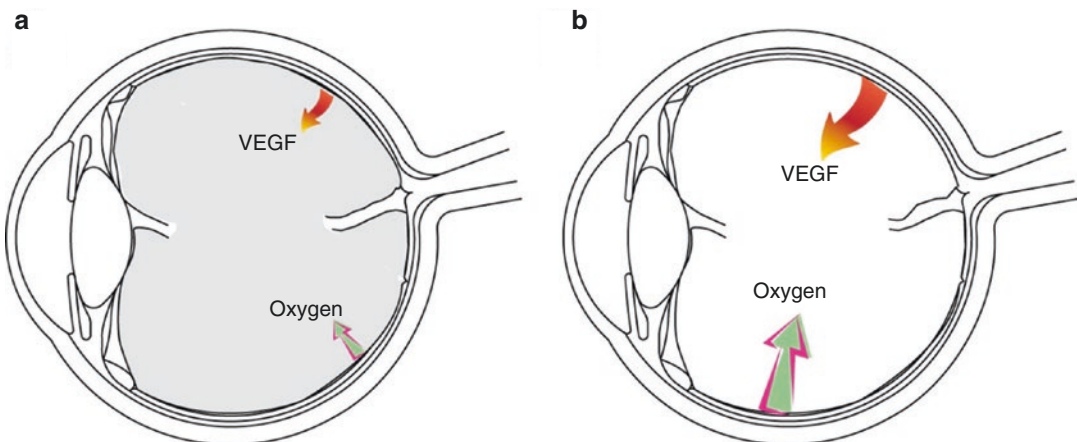
Fig. 2.12 Schematic drawings illustrating VEGF and oxygen diffusion and convection before (**a**) and after (**b**) vitrectomy.

All molecules including VEGF and oxygen have relatively low transport rate in the presence of the normal vitreous gel, however, much faster transport rate after vitrectomy

mechanisms could help to reduce VEGF levels in the retina, and inhibit neovascularization and edema. Posterior vitreous adhesion or detachment can influence such processes. Molecules produced in the retina, such as VEGF, may be cleared into the vitreous cavity if vitreous becomes more fluid after vitrectomy and/or posterior vitreous detachment.

It would be interesting to know the effects of clearance of molecules from the retina into the vitreous cavity after vitrectomy in a variety of eye diseases. The clearance of VEGF and other cytokines from ischemic retina could reduce retinal edema and neovascularization. However, there is a potential problem in stimulating iris neovascularization if oxygen is transported faster down a concentration gradient from the anterior to the posterior segment, while VEGF moves in the opposite direction, making the anterior segment less oxygenated and with more VEGF. It is also possible that oxygen tension adjacent to the lens could be one of the causes for nuclear cataract formation as Holekamp and Beebe have suggested [39].

Modern vitreoretinal surgery involves a variety of treatments in addition to vitrectomy, such as photocoagulation, anti-VEGF drugs, intravitreal steroids, and release of vitreoretinal traction. All these options can alter the effects of vitrectomy on the outcome. It is expected that the transport of anti-VEGF drugs can be faster in vitrectomized eyes. These anti-VEGF drugs have additional vasoactive effects on the retinal vessels [52].

2.5 Summary

Survival and function of retinal neurons depend on a homeostatic intraocular microenvironment. The homeostasis is maintained by a delicate balance between metabolic demands and tissue perfusion. Many pathological changes can induce changes in the intraocular microenvironment. For example, retinal ischemia can change intraretinal and intraocular oxygen distribution. The vitreous humor influences the transport of molecules including oxygen and cytokines within the vitre-

ous cavity. These properties can be altered due to aging, diseases, and surgical interventions, such as vitrectomy, or natural aging processes such as vitreal detachment and liquefaction. Therapeutic interventions including surgical, pharmacological, and/or lasers may have applications in stabilizing and restoring vision. However, any intervention, such as vitrectomy and other surgical procedures, unavoidably changes the intraocular microenvironment. A better understanding of the potential consequences could significantly improve our clinical management in order to achieve the best possible therapeutic outcomes.

References

1. Stefansson E. Physiology of vitreous surgery. Graefes Arch Clin Exp Ophthalmol. 2009;247:147–63.
2. Vanderkooi JM, Erecinska M, Silver IA. Oxygen in mammalian tissue: methods of measurement and affinities of various reactions. Am J Phys. 1991;260:C1131–50.
3. Attwell D, Buchan AM, Charpak S, et al. Glial and neuronal control of brain blood flow. Nature. 2010;468:232–43.
4. Vinores SA, Xiao WH, Aslam S, et al. Implication of the hypoxia response element of the Vegf promoter in mouse models of retinal and choroidal neovascularization, but not retinal vascular development. J Cell Physiol. 2006;206:749–58.
5. Feigl B. Age-related maculopathy—linking aetiology and pathophysiological changes to the ischaemia hypothesis. Prog Retin Eye Res. 2009;28:63–86.
6. Nickla DL, Wallman J. The multifunctional choroid. Prog Retin Eye Res. 2010;29:144–68.
7. Stefansson E, Geirsdottir A, Sigurdsson H. Metabolic physiology in age related macular degeneration. Prog Retin Eye Res. 2011;30:72–80.
8. Coleman HR, Chan CC, Ferris FL III, et al. Age-related macular degeneration. Lancet. 2008;372:1835–45.
9. Klein R, Klein BEK, Moss SE. The wisconsin epidemiological study of diabetic retinopathy: a review. Diab./Metab Rev. 1989;5:559–70.
10. Ambati J, Ambati BK, Yoo SH, et al. Age-related macular degeneration: etiology, pathogenesis, and therapeutic strategies. Surv Ophthalmol. 2003;48:257–93.
11. Mohamed Q, Gillies MC, Wong TY. Management of diabetic retinopathy: a systematic review. J Am Med Assoc. 2007;298:902–16.
12. Schmidt-Erfurth UM, Pruente C. Management of neovascular age-related macular degeneration. Prog Retin Eye Res. 2007;26:437–51.
13. Yu DY, Cringle SJ, Su EN, et al. Pathogenesis and intervention strategies in diabetic retinopathy. Clin Exp Ophthalmol. 2001;29:164–6.

14. Rattner A, Nathans J. Macular degeneration: recent advances and therapeutic opportunities. Nature. 2006;7:860–72.

15. Yu D-Y, Cringle SJ, Yu PK, et al. Retinal energetics: its critical role in retinal physiology and pathology. Expert Rev Ophthalmol. 2011;6:395–9.

16. Alberts B, Johnson A, Lewis J, et al. Molecular biology of the cell. UK: Garland Science, Taylor and Francis Group; 2002.

17. Chalupa LM, Werner JS. The visual neurosciences. Cambridge: MIT Press; 2004.

18. Coyle JT, Puttfarcken P. Oxidative stress, glutamate, and neurodegenerative disorders. Science. 1993;262:689–95.

19. Ames A, Li YY. Energy requirements of glutamatergic pathways in rabbit retina. J Neurosci. 1992;12:4234–42.

20. Cooper RL. Blind registrations in Western Australia: a five-year study. Aust N Z J Ophthalmol. 1990;18:421–6.

21. Yu D-Y, Cringle SJ, Alder VA, et al. Intraretinal oxygen distribution in rats as a function of systemic blood pressure. Am J Phys. 1994;36:H2498–507.

22. Yu D-Y, Cringle SJ, Su E-N. Intraretinal oxygen distribution in the monkey retina and the response to systemic hyperoxia. Invest Ophthalmol Vis Sci. 2005a;46:4728–33.

23. Sperelakis N. Cell physiology sourcebook a molecular approach. 3rd ed: Elsevier; 2001.

24. Cringle SJ, Yu D-Y, Yu PK, et al. Intraretinal oxygen consumption in the rat in vivo [published erratum appears in Invest Ophthalmol Vis Sci 2003 Jan;44(1)]. Invest Ophthalmol Vis Sci. 2002;43:1922–7.

25. Yu D-Y, Cringle SJ. Oxygen distribution and consumption within the retina in vascularised and avascular retinas and in animal models of retinal disease. Prog Retina Eye Res. 2001;20:175–208.

26. Yu D-Y, Cringle SJ, Alder VA, et al. Intraretinal oxygen distribution in the rat with graded systemic hyperoxia and hypercapnia. Invest Ophthalmol Vis Sci. 1999;40:2082–7.

27. Yu DY, Cringle SJ, Yu PK, et al. Intraretinal oxygen distribution and consumption during retinal artery occlusion and graded hyperoxic ventilation in the rat. Invest Ophthalmol Vis Sci. 2007;48:2290–6.

28. Yu D-Y, Cringle SJ. Outer retinal anoxia during dark adaptation is not a general property of mammalian retinas. Comp Biochem Physiol. 2002;132:47–52.

29. Yu D-Y, Cringle SJ, Su E-N, et al. Laser induced changes in intraretinal oxygen distribution in pigmented rabbits. Invest Ophthalmol Vis Sci. 2005b;46:988–99.

30. Yu D-Y, Cringle SJ, Su EN, et al. Retinal oxygen distribution in a rat model of retinal ischemia. Invest Ophthalmol Vis Sci. 2000;41:S19.

31. Linsenmeier RA. Effects of light and darkness on oxygen distribution and consumption in the cat retina. J Gen Physiol. 1986;88:521–42.

32. Siegfried CJ, Shui YB, Holekamp NM, et al. Oxygen distribution in the human eye: relevance to the etiology of open-angle glaucoma after vitrectomy. Invest Ophthalmol Vis Sci. 2010;51:5731–8.

33. Maeda N, Tano Y. Intraocular oxygen tension in eyes with proliferative diabetic retinopathy. Graefes Arch Clin Exp Ophthalmol. 1996;234:s66–9.

34. Ahmed J, Braun RD, Dunn R, et al. Oxygen distribution in the Macaque retina. Invest Ophthalmol Vis Sci. 1993;34:516–21.

35. Cringle SJ, Yu D-Y. A multi-layer model of retinal oxygen supply and consumption helps explain the muted rise in inner retinal PO_2 during systemic hyperoxia. Comp Biochem Physiol. 2002;132:61–6.

36. Cringle SJ, Yu D-Y. Oxygen supply and consumption in the retina: Implications for studies of retinopathy of prematurity. Documenta Ophthalmol. 2010;120:99–109.

37. Hoang QV, Linsenmeier RA, Chung CK, et al. Photoreceptor inner segments in monkey and human retina: mitochondrial density, optics, and regional variation. Vis Neurosci. 2002;19:395–407.

38. Sakaue H, Negi A, Honda Y. Comparative study of vitreous oxygen tension in human and rabbit eyes. Invest Ophthalmol Vis Sci. 1989;30:1933–7.

39. Holekamp NM, Shui YB, Beebe DC. Vitrectomy surgery increases oxygen exposure to the lens: a possible mechanism for nuclear cataract formation. Am J Ophthalmol. 2005;139:302–10.

40. Stefansson E. The therapeutic effects of retinal laser treatment and vitrectomy. A theory based on oxygen and vascular physiology. Acta Ophthalmol Scand. 2001;79:435–40.

41. Stefansson E, Hatchell DL. Vitrectomy prevents retinal hypoxia in branch retinal vein occlusion. Invest Ophthalmol Vis Sci. 1990;31:284–9.

42. Stefansson E, Landers MB, Wolbarsht ML. Increased retinal oxygen supply following pan-retinal photocoagulation and vitrectomy and lensectomy. Trans Am Ophthalmol Soc. 1981;LXXIX:307–34.

43. Stefansson E, Landers MB, Wolbarsht ML. Vitrectomy, lensectomy, and ocular oxygenation. Retina. 1982;2:159–66.

44. Holekamp NM, Shui Y-B, Beebe DC. Regulation of intraocular oxygen by the vitreous gel. In: Dartt DA, Besharse J, Dana R, editors. Encyclopedia of the eye: Academic Press; 2010.

45. Barbazetto IA, Liang J, Chang S, et al. Oxygen tension in the rabbit lens and vitreous before and after vitrectomy. Exp Eye Res. 2004;78:917–24.

46. Shui YB, Holekamp NM, Kramer BC, et al. The gel state of the vitreous and ascorbate-dependent oxygen consumption: relationship to the etiology of nuclear cataracts. Arch Ophthalmol. 2009;127:475–82.

47. Kaiser PK, Riemann CD, Sears JE, et al. Macular traction detachment and diabetic macular edema associated with posterior hyaloidal traction. Am J Ophthalmol. 2001;131:44–9.

48. Lewis H, Abrams GW, Blumenkranz MS, et al. Vitrectomy for diabetic macular traction and edema associated with posterior hyaloidal traction. Ophthalmology. 1992;99:753–9.

49. Charbonnel J, Glacet-Bernard A, Korobelnik JF, et al. Management of branch retinal vein occlusion with vitrectomy and arteriovenous adventitial sheathotomy, the possible role of surgical posterior vitreous detachment. Graefes Arch Clin Exp Ophthalmol. 2004;242:223–8.

50. Kumagai K, Furukawa M, Ogino N, et al. Long-term outcomes of vitrectomy with or without arteriovenous sheathotomy in branch retinal vein occlusion. Retina. 2007;27:49–54.

51. Hvarfner C, Larsson J. Vitrectomy for non-ischaemic macular oedema in retinal vein occlusion. Acta Ophthalmol Scand. 2006;84:812–4.

52. Su EN, Cringle SJ, McAllister IL, et al. An experimental study of VEGF induced changes in vasoactivity in pig retinal arterioles and the influence of an anti-VEGF agent. BMC Ophthalmol. 2012;12:10.

Part II

Diagnostic Modalities

Angiography Using Fluorescein and Indocyanine Green Dye

3

Simon K. H. Szeto and Timothy Y. Y. Lai

3.1 Introduction

Fundus fluorescein angiography (FA) and indocyanine green angiography (ICGA) are commonly performed ophthalmic investigations in the assessment of various vitreoretinal and macular conditions, in particular, for diseases affecting the retinal or choroidal circulation. The most common indications of FA and ICGA include the evaluation of age-related macular degeneration (AMD), polypoidal choroidal vasculopathy (PCV), and retinal vascular occlusions.

Recently, the use of optical coherence tomography angiography (OCTA), a noninvasive method to detect flow in the retinal and choroidal vasculature without the use of exogenous dye, can be used to evaluate retinal microvasculature. OCTA has been used to detect choroidal neovascularization in patients with neovascular AMD and for quantifying foveal avascular zone (FAZ)

and area of retinal non-perfusion in retinal microvasculature in patients with diabetic retinopathy and retinal venous occlusion [1–5]. Despite these advances in OCTA, FA and ICGA are dynamic imaging modalities that remain very valuable tools and are still the current gold standards in detecting leakage from various retinal or choroidal lesions, which cannot be replaced by OCTA at the present stage.

3.2 Equipment for FA and ICGA

3.2.1 Flash-Based System

Flash-based fundus camera is the conventional imaging method to obtain FA and ICGA. Common commercially available systems include Topcon, Canon, and Carl Zeiss fundus cameras. The flash-based fundus camera uses an electronic flash tube combined with filters of various wavelengths to transmit a blue–green light to excite the fluorescein sodium dye or an infrared light to excite the indocyanine green dye in order to cause fluorescent of the dye. The reflected fluorescent light will then pass through filters that block all visible wavelengths except the specific color of the wavelength of interest.

S. K. H. Szeto
Hong Kong Eye Hospital, Department of Ophthalmology & Visual Sciences, The Chinese University of Hong Kong, Kowloon, Hong Kong, China

T. Y. Y. Lai (✉)
Hong Kong Eye Hospital, Department of Ophthalmology & Visual Sciences, The Chinese University of Hong Kong, Kowloon, Hong Kong, China

2010 Retina and Macula Centre, Kowloon, Hong Kong
e-mail: tyylai@cuhk.edu.hk

3.2.2 Confocal Scanning Laser Ophthalmoscopy Systems

FA and ICGA can also be taken using a confocal scanning laser ophthalmoscope (cSLO) such as Heidelberg and Optos systems. CSLO makes use of a diode laser to scan the retina and the reflected light is detected by an image detector at a focal plane conjugate to retina to produce a digital image. Compared with conventional flash-based system, cSLO system has the potential to produce images with higher contrast and finer details. This is because cSLO has a higher signal to noise ratio and it blocks out of unfocused or scattered light. With the use of two lasers scanning at different wavelengths, cSLO can allow simultaneous FA and ICGA image acquisitions. The Heidelberg Spectralis system (Heidelberg Engineering, Heidelberg, Germany) also allows the performance of multimodal imaging and spectral-domain optical coherence tomography (SD-OCT) can be performed simultaneously to allow point-to-point correlation of the images.

In addition to the standard 35–50° images, cSLO also enables ultra-widefield (UWF) images to be obtained. For instance, up to 200° of retina can be captured in one picture with the Optos Daytona system. Ultra-widefield angiography can also be taken with the Heidelberg HRA system using the UWF 102° noncontact interchangeable lens or the 150° Staurenghi contact lens. UWF images have the potential benefit of identifying peripheral retinal lesions such as retinal non-perfusion in diabetic retinopathy, which is a risk factor for disease progression [6]. Previous study has demonstrated that more retinal pathological changes and peripheral retinal non-perfusion can be identified in patients with diabetic retinopathy using UWF angiography compared to conventional seven-field imaging [7].

3.3 Fluorescein Angiography (FA)

3.3.1 Basics of FA

FA can be used to assess a large variety of retinal conditions and is the standard diagnostic tool for evaluating retinal vascular integrity, choroidal neovascularization (CNV), capillary dropout or non-perfusion, and leakage. FA requires the injection of sodium fluorescein ($C_{20}H_{10}Na_2O_5$), which is an orange-colored water-soluble dye with a molecular weight of 376 g/mol. As a fluorescent molecule, fluorescein sodium is stimulated by blue light with peak absorption wavelength at 490 nm and yellow light will be emitted with peak wavelength at 530 nm. The image can be captured with a fundus camera with a set of blue excitation filter and a green barrier filter. Following intravenous injection, approximately 30% of the dye remains as free serum unbound fluorescein which is observed in fluorescence. Sodium fluorescein is metabolized by the liver and is excreted through the kidneys.

3.3.2 Interpretation of FA

3.3.2.1 Normal Fluorescence

Normal fluorescence can be observed in retinal vasculature in normal circumstances because fluorescein sodium cannot cross the blood–retinal barrier of the retinal vascular endothelium. There are different phases observed during normal FA, in which various extent of fluorescence will be observed depending on the timing from the start of the dye injection.

	Phase	Time from dye injection
1	Filling of posterior ciliary arteries	9 s
2	Pre-arterial phase with background choroidal fluorescence	10 s
3	Arterial phase	10–15 s
4	Arteriovenous phase	15–30 s
5	Venous phase	30–60 s
6	Recirculation phase	1–5 min
7	Late phase	>5 min

3.3.2.2 Hyperfluorescence in FA

Hyperfluorescence may be observed in various chorioretinal diseases when the normally impermeable blood–retinal barrier has been disrupted, and fluorescein dye will then leak though the retinal vessels. Causes of hyperfluorescence are listed below:

Cause	Conditions
RPE window defect	RPE atrophy, photoreceptor degeneration, macular hole, congenital depigmentation
Pooling of dye	Central serous chorioretinopathy, RPE detachment
Staining of tissue by dye	Scar, drusen, sclera, lamina cribrosa
Leakage of dye	Cystoid macula edema, central serous chorioretinopathy, vasculitis, choroidal neovascularization, retinal neovascularization

3.3.2.3 Hypofluorescence in FA

A background level of fluorescence is observed in normal retina due to staining of the Bruch's membrane with fluorescein dye. Hypofluorescence is observed when the background level of fluorescence is reduced by certain retinal diseases.

Causes of hypofluorescence are listed below:

Cause	Conditions
Blocked fluorescence	Hemorrhage, pigments, exudates
Filing defect	Occlusion of arterioles or venules in the retina or choroid
Loss of tissue	Chorioretinal atrophy in myopic degeneration or chorioretinal degeneration

3.3.3 Contraindication of FA

In general, fluorescein angiography is a safe procedure. Skin and urine discoloration are common side effects but they might be frightening to patients who are unaware of these side effects. Mild allergic reactions such as nausea and pruritis may develop in some patients. More severe life-threatening allergy such as angioedema, bronchospasm with compromised airway, and anaphylactic shocks are rare but are documented potential complications. Therefore, resuscitation trolley should be available in premises where FA is performed.

FA is contraindicated in patients with known allergy to fluorescein sodium and severe renal impairment (since fluorescein sodium is excreted via the kidneys). Fluorescein sodium can cross the placenta and has an FDA Pregnancy Category C rating; hence, pregnancy is a relative contraindication to FA. In a retrospective review of 105 pregnant women who had undergone FA, it has been reported that no higher rate of birth anomalies or complications was observed following FA procedures [8]. Nonetheless, the risk–benefit of performing FA in pregnant women should be seriously considered and FA should not be performed unless it is totally necessary for the management of the patient.

3.4 Indocyanine Green Angiography (ICGA)

3.4.1 Basics of ICGA

Indocyanine green angiography (ICGA) makes use of tricarbocyanine dye ($C_{43}H_{47}N_2NaO_6S_2$), which is a water-soluble compound with a molecular weight of 775 g/mol and contains 5% iodine. ICG dye is 98% plasma protein bound (as compared to 70–85% plasma protein bound for sodium fluorescein), hence the amount of fluorescence emitted during ICGA is much lower compared to FA since only 2% of ICG dye remain free in the serum. In ICGA, ICG is stimulated by an infrared light with a peak absorption wavelength at 780–800 nm and a higher wavelength of infrared light at 830 nm is emitted. Fundus camera with digital capturing system is required to capture the very dim invisible light emitted by ICGA which is in the infrared region. ICG dye is excreted by the liver into the bile without being metabolized.

3.4.2 Interpretation of ICGA

ICGA is an excellent tool to visualize the choroidal vasculature, which is poorly visualized with FA. ICGA can be used to visualize choroidal vasculature due to two reasons. Firstly, ICG molecules remain in the choroidal vasculature because they are highly protein bound and hence do not leak through the fenestrated endothelial cells of the choriocapillaris. Secondly, the infrared emitted by ICG molecules penetrates the retinal pig-

ment epithelial (RPE) cells and associated fluid and exudates better. ICGA is generally more tolerable by patients because it is less photophobic due to the infrared stimulating light.

3.4.2.1 Normal Fluorescence in ICGA

The early phase of ICGA occurs during the first minute after dye injection, filling of large choroidal vessels and retinal arteries occur during this phase. The mid phase occurs after 1–15 min, filling of retinal arteries and veins and fading of choroidal vessels occur during this phase. The late phase occurs after 15 min and can be taken up to 30–40 min. No details of the choroidal or retinal vessels will be seen in this phase and CNV may appear as a hyperfluorescent lesion.

3.4.2.2 Hyperfluorescence in ICGA

Retinal or choroidal diseases which cause localized accumulation or leakage of ICG dye in the retina or choroid will cause hyperfluorescence. Causes of hyperfluorescence are listed in the table below:

Cause	Conditions
Leakage of ICG dye from disc	Vogt–Koyanagi–Harada disease or other forms of chorioretinitis
Leakage of ICG dye from choroid or choroidal neovascularization	Choroidal neovascularization, polypoidal choroidal vasculopathy, choroidal hemangioma, central serous chorioretinopathy
Leakage of ICG dye from retina	Retinal artery microaneurysm

3.4.2.3 Hypofluorescence in ICGA

Hypofluorescence may be observed in ICGA when there is blockage of fluorescence, filling defect, or loss of choroidal tissue. The causes of hypofluorescence in ICGA are summarized in the table below:

Cause	Conditions
Blocked fluorescence	RPE detachment, hemorrhage, pigments, exudates
Filling defect	Choroidal ischemia

Cause	Conditions
Loss of tissue	Chorioretinal atrophy in age-related macular degeneration, myopic degeneration or chorioretinal degeneration

3.4.3 Contraindication of ICGA

ICGA is generally a safe investigation. The contraindications of ICGA include known allergy to iodine, hepatic failure, renal failure with concurrent use of metformin (in which patients may develop lactic acidosis), and pregnancy. Mild adverse reactions may be experienced and should be warned to patients. These include stool discoloration, nausea, vomiting, and pruritis. More severe side effects include syncope, dyspnea, and anaphylaxis, but are rare.

3.5 Applications of FA and ICGA in Macular Surgery

3.5.1 Macular Hole

Macular holes are common vitreoretinal conditions and OCT is the diagnostic tool of choice for the evaluation of macular holes. Sometimes, macular hole may mimic a macular hemorrhage in fundus examination. In FA, macular hole appears as a localized area of focal early hyperfluorescence due to RPE window defect (Fig. 3.1). However, the presence or absence of focal hyperfluorescence is not reliable in differentiating full thickness (stages 2, 3, or 4) from partial-thickness macular hole (stage 1). In some cases, FA findings may precede the development of symptoms in patients with early stages of macular hole [9].

3.5.2 Epiretinal Membrane/ Vitreomacular Adhesion

Epiretinal membranes (ERM) are made up of glial and fibrocellular proliferative membrane which develop following partial or complete pos-
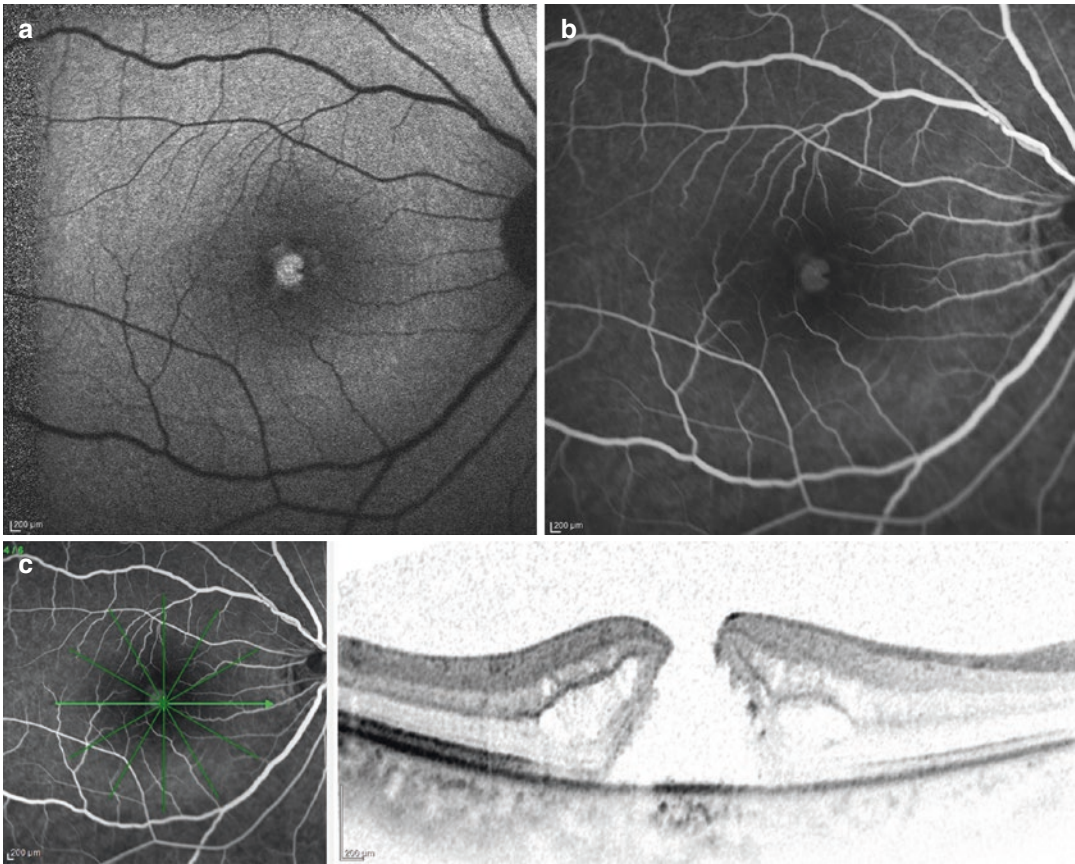
Fig. 3.1 (**a**) Fundus autofluorescence image of the right eye of a patient with full-thickness macular hole showing increased autofluorescence at the site of the macular hole. (**b**) Mid-phase fluorescein angiography showing central hyperfluorescence due to transmission defect. (**c**) Spectral-domain optical coherence tomography showing full-thickness macular hole

terior vitreous detachment. The contracture of ERM may cause secondary alteration of the macular vasculature including change in the size of the foveal avascular zone (FAZ), macular vascular distortion (such as vascular straightening), and fluorescein dye leakage.

In patients with ERM, FA can identify the degree of changes in retinal vasculature, which may correlate with the macular structural changes and visual functions (Fig. 3.2). It has been shown that the contracture of FAZ diameters was negatively correlated with central macular thickness (CMT) of optical coherence tomography (OCT), while the grades of macular vascular distortion and macular vascular leakage were positively correlated with CMT [10]. In addition, the extent of vascular distortion graded on FA also correlated with the severity of metamorphopsia. Due to the noninvasiveness of OCT, OCT is the most commonly used investigation for evaluating ERM. OCT provides quantitative measurements in the retinal thickness and whole macular volume, a higher CMT generally correlates with worse visual acuity [11]. However, there was no correlation between OCT findings and the subjective severity of metamorphopsia. In addition, OCT is unable to identify secondary vascular changes associated with the ERM. Therefore, FA may still be a useful tool in the evaluation of patients with ERM and it might be useful in elucidating the pathophysiology underlying ERM development.
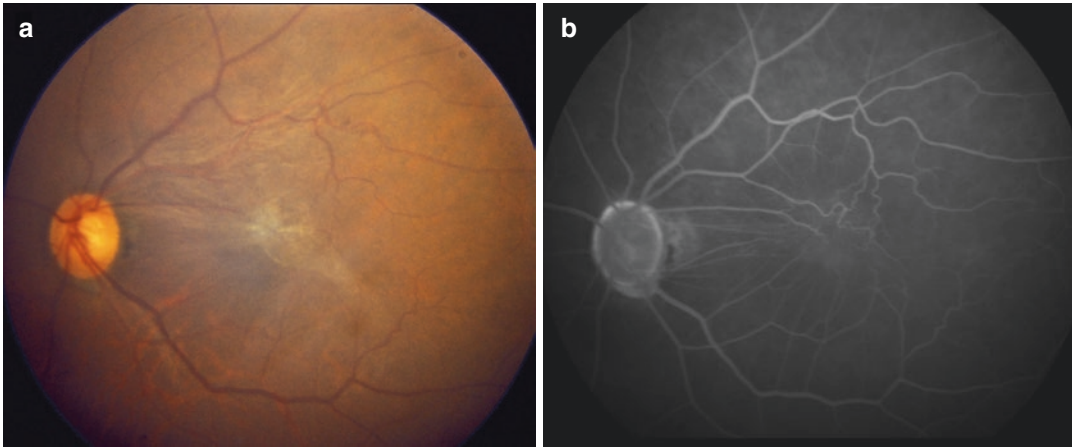
Fig. 3.2 (**a**) Fundus photo of the left eye of a patient with epiretinal membrane showing distortion of the macula. (**b**) Late-phase fluorescein angiography showing reduc-tion in the size of foveal avascular zone with distortion of the retinal vasculature and mild fluorescein leakage at the central macula

3.5.3 Pathologic Myopia

Pathologic myopia is associated with increased risk of developing a number of retinal conditions, including dome-shaped macula, myopic CNV, myopic foveoschisis, and myopic macular hole.

Dome-shaped macula (DSM) occurs in approximately 10% of patients with pathologic myopia associated with posterior staphyloma. Various vision-threatening complications such as myopic CNV and serous retinal detachment without CNV can develop in patients with DSM. It has been demonstrated that serous retinal detachment in dome-shaped macula was associated with pinpoint leakage on FA and punctate hyperfluorescent spots and oval hypofluorescent spot on late-phase ICGA. It was postulated that the punctate hyperfluorescent spots on ICGA correlate with choroidal abnormality that may cause secondary anatomical changes in RPE that present as PED and punctate leakage on FA, with serous retinal detachment developing as the end result [12].

Myopic CNV is one of the most common causes of visual loss in patients with pathologic myopia. It is sometimes difficult to diagnose clinically due to underlying chorioretinal atrophy, pigmentary changes, and visibility of large choroidal or scleral vessels that are commonly associated with pathologic myopia. FA and OCT are valuable diagnostic tools in the assessment of myopic CNV. Myopic CNV presents as early hyperfluorescence with progressive increase in intensity and size in late phase, while subretinal hemorrhage may present as hypofluorescence due to blocked fluorescence on FA. It has been shown that FA has a higher repeatability and reproducibility in diagnosing myopic CNV than OCT [13].

Eyes with high myopia may also develop various forms of myopic traction maculopathy (MTM), including myopic foveoschisis, and myopic macular hole with or without retinal detachment. FA and ICGA have been used to evaluate the choroidal circulatory changes in patients undergoing macular buckle surgery for treatment of MTM and results have revealed no evidence of choroidal blood flow alteration [14]. Myopic CNV can also coexist in eyes with MTM and FA will be useful to evaluate the activity of myopic CNV and determine the treatment outcome (Fig. 3.3) [15].

3.5.4 Diabetic Retinopathy

Traditionally, FA can be used to detect leakage from neovascularization in proliferative diabetic retinopathy and to differentiate neovascularization from intraretinal microabnormalities (IRMA). In addition, presence of FA leakage from microaneurysms may guide the application
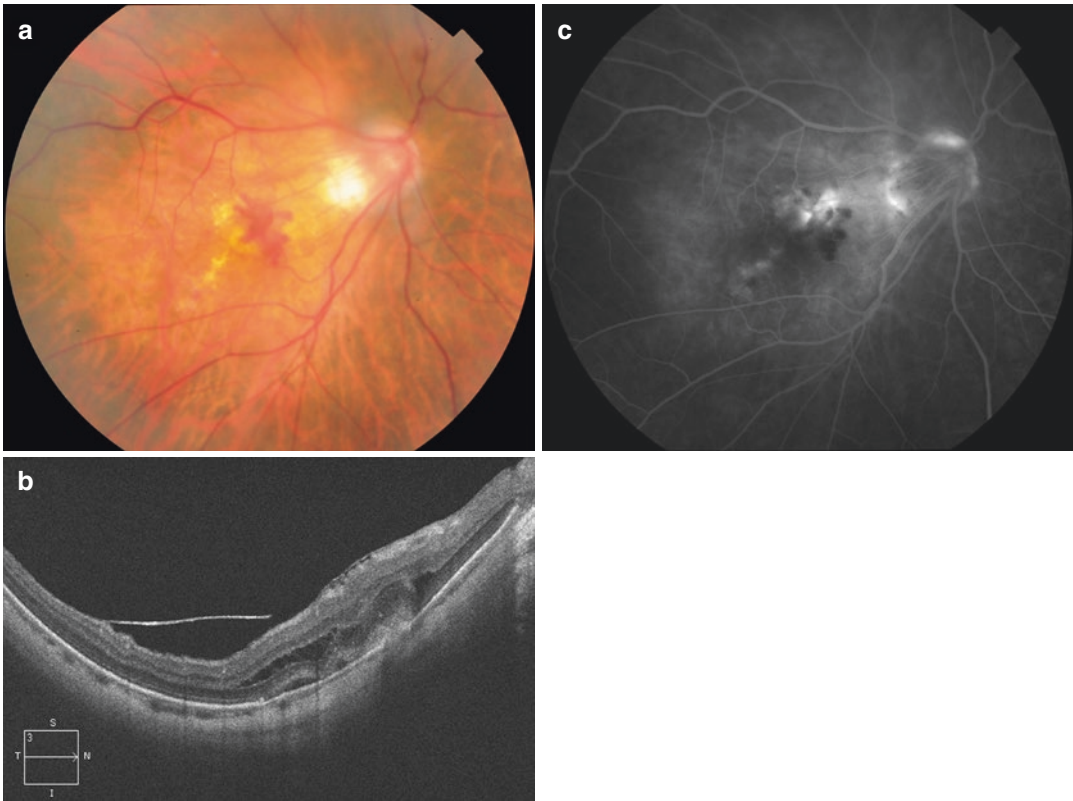
Fig. 3.3 (**a**) Fundus photo of the right eye of a patient with pathologic myopia with macular hemorrhage and macular atrophy. (**b**) Optical coherence tomography scan of the macula showing epiretinal membrane and myopic traction maculopathy associated with subretinal hyperre-flective material due to subretinal hemorrhage. (**c**) Mid-phase fluorescein angiography showing leakage due to myopic choroidal neovascularization and associated blocked fluorescence due to hemorrhage

of focal laser photocoagulation for the treatment of diabetic macular edema.

FA may also assist the planning of vitreoretinal surgery in patients with proliferative diabetic retinopathy. More accurate delineation of avascular peripheral retinal area may allow more precise application of laser photocoagulation, which might be more effective in preventing iris neovascularization and subsequent neovascular glaucoma.

It has been reported that intraoperative FA of the peripheral retina taken with endoscope during pars plana vitrectomy may aid intraoperative evaluation and treatment of proliferative diabetic retinopathy. Extreme peripheral retina can be visualized with intraoperative FA and allows the identification of anterior hyaloidal fibrovascular proliferation, which is associated with a higher risk of postoperative rubeosis iridis and will require more extensive laser pan-retinal photocoagulation (PRP) treatment [16].

With the advent of ultrawide field imaging, ultrawide field FA (UWF-FA) imaging of the peripheral retina is also now possible (Fig. 3.4). Peripheral retinal ischemia is associated with higher risk of progression to proliferative diabetic retinopathy [6]. UWF-FA may increase the diagnosis rate of peripheral retinal ischemia and hence allow earlier treatment with laser PRP and arranging closer monitoring of the patients.

3.5.5 Retinal Vascular Occlusions

In retinal vein occlusion, FA can delineate ischemic retinal area, which is a significant prognostic factor in predicting the risk of secondary macular edema and retinal neovascularization
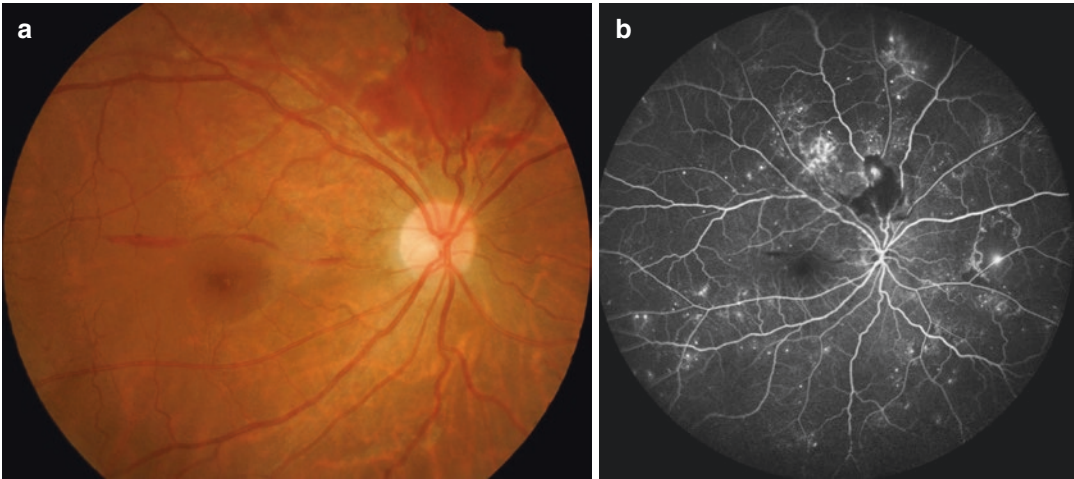
Fig. 3.4 (**a**) Fundus photo of the right eye showing pre-retinal hemorrhage and retinal neovascularization due to proliferative diabetic retinopathy. (**b**) Mid-phase ultra-widefield fluorescein angiography showing multiple pin-point hyperfluorescence due to microaneurysms, leakage superior to the optic disc due to retinal neovascularization and hypofluorescence in the superior retina due to retinal ischemia with capillary dropout

[17]. In retinal artery occlusion, delayed filling of the affected vessels and reduced arterial caliber can be observed along the vessels involved [18]. With the development of novel surgical treatment options for retinal vein and artery occlusion like endovascular cannulation of the affected vessel with or without tissue plasminogen activator (tPA) injection [19, 20], FA can be used to confirm the reperfusion of the ischemic area after treatment.

3.5.6   Uveitis

In uveitis, cystoid macular edema (CME) is one of the major causes of visual loss, which would appear on FA as progressive hyperfluorescence in a petaloid pattern [21]. FA is also an important tool in diagnosing retinal vasculitis, which may manifest with vascular wall staining, extravascular leakage, retinal ischemia, and retinal neovascularization. These findings on FA, in particular retinal ischemia, have important prognostic implications and may affect the management of uveitis. For example, early PRP treatment can be performed in cases with retinal ischemia to prevent formation of retinal neovas-cularization and more intense treatment such as immuno-suppressive agents or biologics might be required to control the uveitis. The introduction of UWF-FA has allowed visualization of peripheral retina and increased the diagnosis of retinal vascular pathology in patients with retinal vasculitis [22].

3.5.7   Coats' Disease

Coats' disease is a retinal vascular disorder characterized with the formation of telangiectactic vessels and microaneurysms, which leads to retinal and subretinal exudation with serous retinal detachment. In advanced cases, complications such as neovascular glaucoma and possibly phthisis bulbi may develop. FA can be used to guide the application of laser photocoagulation in patients with Coat's disease by visualizing leakage sites and ischemic areas [23].

3.5.8   Retinal Transplantation

It had been proposed that autologous transplantation of RPE in addition to excision of CNV

membrane may restore vision in patients with neo-vascular AMD due to subfoveal CNV. Preoperative and postoperative FA and ICGA can be performed in order to confirm revascularization and reperfusion of the RPE transplant [24].

References

1. Jia Y, Bailey ST, Wilson DJ, Tan O, Klein ML, Flaxel CJ, et al. Quantitative optical coherence tomography angiography of choroidal neovascularization in age-related macular degeneration. Ophthalmology. 2014;121:1435–44.

2. Ishibazawa A, Nagaoka T, Takahashi A, Omae T, Sogawa K, Yokota H, et al. Optical coherence tomography angiography in diabetic retinopathy: a prospective pilot study. Am J Ophthalmol. 2015;160:35–44.

3. Kashani AH, Lee SY, Moshfeghi A, Durbin MK, Puliafito CA. Optical coherence tomography angiography of retinal venous occlusion. Retina. 2015;35:2323–31.

4. Samara WA, Say EA, Khoo CT, Higgins TP, Magrath G, Ferenczy S, et al. Correlation of foveal avascular zone size with foveal morphology in normal eyes using optical coherence tomography angiography. Retina. 2015;35:2188–95.

5. Agemy SA, Scripsema NK, Shah CM, Chui T, Garcia PM, Lee JG, et al. Retinal vascular perfusion density mapping using optical coherence tomography angiography in normal and diabetic retinopathy patients. Retina. 2015;35:2353–63.

6. Silva PS, Cavallerano JD, Haddad NM, Kwak H, Dyer KH, Omar AF, et al. Peripheral lesions Identified on ultrawide field imaging predict increased risk of diabetic retinopathy progression over 4 years. Ophthalmology. 2015;122:949–56.

7. Wessel MM, Aaker GD, Parlitsis G, Cho M, D'Amico DJ, Kiss S. Ultra-wide-field angiography improves the detection and classification of diabetic retinopathy. Retina. 2012;32:785–91.

8. Halperin LS, Olk RJ, Soubrane G, Coscas G. Safety of fluorescein angiography during pregnancy. Am J Ophthalmol. 1990;109:563–6.

9. Gass JD. Idiopathic senile macular hole. Its early stages and pathogenesis. Arch Ophthalmol. 1988;106:629–39.

10. Liu J, Qian Y, Yang S, Yan L, Wany Y, Gao M, et al. Pathophysiological correlations between fundus fluorescein angiography and optical coherence tomography results in patients with idiopathic epiretinal membranes. Exp Ther Med. 2017;14:5785–92.

11. Michalewski J, Michalewski Z, Cisiecki S, Nawrocki J. Morphologically functional correlations of macular pathology connected with epiretinal membrane studied by spectral optical coherence tomography (SOCT). Greaefes Arch Clin Exp Ophthalmol. 2007;245:1623–31.

12. Viola F, Dell'Arti L, Benatti E, Invernizzi A, Mapelli C, Ferrar F, et al. Choroidal findings in dome-shaped macula in highly myopic eyes: a longitudinal study. Am J Ophthalmol. 2015;159:44–52.

13. Chhablani J, Deepa MJ, Tyagi M, Narayanan R, Kozak I. Fluorescein angiography and optical coherence tomography in myopic choroidal neovascularization. Eye (Lond). 2015;29:519–24.

14. Parolini B, Frisina R, Pinackatt S, Gasparotti R, Gatti E, Baldi A, et al. Indication and results of a new L-shaped macular buckle to support a posterior staphyloma in high myopia. Retina. 2015;35:2469–82.

15. Iacono P, Battaglia Parodi M, Iuliano L, Bandello F. How vitreomacular interface modifies the efficacy of anti-VEGF therapy for choroidal neovascularization. Retina. 2018;38:84–90.

16. Terasaki H, Miyake Y, Awaya S. Fluorescein angiography of peripheral retina and pars plana during vitrectomy for proliferative diabetic retinopathy. Am J Ophthalmol. 1997;123:370–6.

17. Jaulim A, Ahmed B, Khanam T, Chatziralli IP, et al. Branch retinal vein occlusion epidemiology, pathogenesis, risk factors, clinical features, diagnosis, and complications. An update of the literature. Retina. 2013;33:901–10.

18. Varma DD, Cugati S, Lee AW, Chen CS. A review of central retinal artery occlusion: clinical presentation and management. Eye (Lond). 2013;27:688–97.

19. Kadonosono K, Yamane S, Arakawa A, Inoue M, Yamakawa T, Uchio E, et al. Endovascular cannulation with a microneedle for central retinal vein occlusion. JAMA Ophthalmol. 2013;131:783–6.

20. Kadonosono K, Yamane S, Inoue M, Yamakawa T, Uchio E. Intra-arterial arterial cannulation using a microneedle for central retinal artery occlusion. Sci Rep. 2018;8:1360.

21. Antcliff RJ, Stanford MR, Chauhan DS, Graham EM, Spalton DJ, Shilling JS, et al. Comparison between optical coherence tomography and fundus fluorescein angiography for the detection of cystoid macular edema in patients with uveitis. Ophthalmology. 2000;107:593–9.

22. Jones NP, Sala-Puigdollers A, Stanga PE. Ultra-widefield fundus fluorescein angiography in the diagnosis and management of retinal vasculitis. Eye (Lond). 2017;31:1546–9.

23. Angora C, Lepore F, Molle F, Paliara MM, De Santis R, Orazi L, et al. Fluorescein angiography in the management of Coats' disease laser treatment. Invest Ophthalmol Vis Sci. 2007;48:4166.

24. Maclaren RE, Uppal GS, Balaggan KS, Tufail A, Munro PM, Milliken AB, et al. Autologous transplantation of the retinal pigment epithelium and choroid in the treatment of neovascular age-related macular degeneration. Ophthalmology. 2007;114:561–70.

Optical Coherence Tomography Angiography in Macular Disorders

4

Colin S. Tan, Louis W. Lim, and Srini Vas R. Sadda

4.1 Introduction

Advances in ocular imaging technology, particularly imaging of the retina and choroid, have revolutionized the practice of ophthalmology in recent years. In addition to color fundus photos and fluorescein and indocyanine green angiography [1–3], newer imaging modalities such as optical coherence tomography (OCT), widefield imaging [4–7] and multicolor imaging have assumed increasingly important roles in the diagnosis, monitoring, and management of various retinal diseases. Optical coherence tomography angiography (OCTA) is a novel and exciting technology that has revolutionized the practice of ophthalmology in the few years since its intro-

duction in commercial imaging devices. This chapter describes OCTA technology, discusses its applications among common retinal conditions, and reviews its strengths and limitations.

4.2 Principles of OCTA

OCTA is a noninvasive imaging modality that utilizes OCT technology to produce en face images of the retinal, subretinal, and choroidal vasculature (Figs. 4.1, 4.2, and 4.3).

Due to the improvements in scanning speed, OCTA devices are able to rapidly acquire repeated B-scans at the same location of the eye. Variations between B-scans are the result of moving objects such as blood flow, while stationary objects will appear similar at different time points. Thus, these repeated B-scans allow for blood flow to be detected in the form of changes in signal amplitude and/or phase. Repeated B-scan images at a particular retinal location are compared to each other using algorithms to generate a motion contrast image. Volumetric data of the retina are then produced by repeating these B-scans at different locations on the retina—typically in a raster scan pattern. The volumetric data produced can be segmented at different layers of the retina and choroid, thereby producing vascular flow maps at the desired retinal vascular layer (superficial, intermediate, or deep capillary plexus), the choriocapillaris, and the choroid.

C. S. Tan (✉)
National Healthcare Group Eye Institute, Tan Tock Seng Hospital, Singapore, Singapore

Fundus Image Reading Center, National Healthcare Group Eye Institute, Singapore, Singapore

Duke-NUS Medical School, Singapore, Singapore

Lee Kong Chian School of Medicine, Nanyang Technological University, Singapore, Singapore

L. W. Lim
National Healthcare Group Eye Institute, Tan Tock Seng Hospital, Singapore, Singapore

S. V. R. Sadda
Doheny Eye Institute, University of California Los Angeles, Los Angeles, CA, USA
e-mail: ssadda@doheny.org
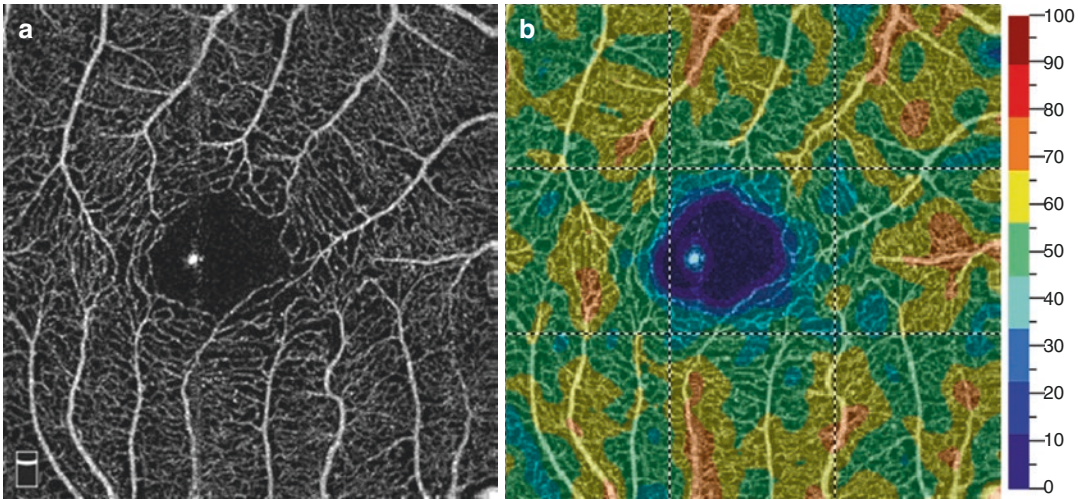
Fig. 4.1 OCTA of a normal eye. (**a**) 3 × 3 mm OCTA can. (**b**) Vessel density map of the same eye, showing the variations in vessel density, which are color-coded
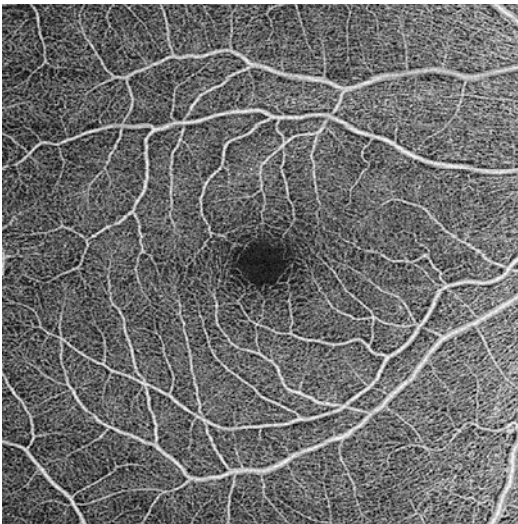
Fig. 4.2 6 × 6 mm OCTA scan of a normal eye
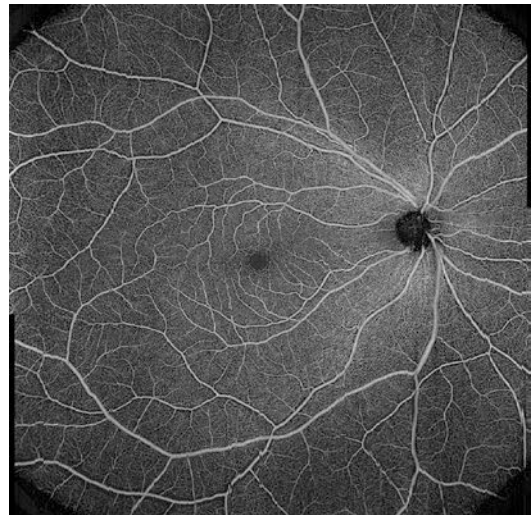
Fig. 4.3 15 × 15 mm OCTA scan of a normal eye, showing OCTA of the peripheral retina

These images can also be viewed cross-sectionally, allowing the reader to confirm the spatial location of any pathology which is seen on the en face images.

Various algorithms are used by different OCTA devices to calculate motion contrast. These algorithms detect motion perpendicular to the direction of the OCT beam using signal amplitude, signal phase, or both. Examples of algorithms include split spectrum amplitude decorrelation (SSADA), which uses OCT signal amplitude. SSADA was first demonstrated by Jia et al. [8] to improve image quality by reducing machine sensitivity to bulk eye motions as well as improving signal to noise ratio. SSADA generates a flow signal by measuring the speckle decorrelations between consecutive B-scans. The full OCT spectrum is split into multiple narrowband spectra, where decorrelation is calculated for each band before being averaged and combined to get the final flow signal. In this case, noise from bulk motion in the axial dimension is reduced without compromising flow signal from

the transverse dimension (retinal and choroidal flow). The downside of splitting the spectrum, however, is a reduction in axial resolution.

Other algorithms with clinical applications include speckle variance, phase variance, optical microangiography (OMAG), and correlation mapping [9, 10].

Speckle variance works to detect intensity (speckle) changes in OCT images [11–13]. Speckles are discrete areas of constructive interferences. When reflected off a moving object, the produced speckle will change more rapidly over time. Conversely, speckles reflected off stationary objects will not vary much with time. By measuring the amount of reflection at each voxel, the values of successive images measured at two different time points can be compared pixel by pixel. Large changes would typically correspond to the motion of erythrocytes in blood vessels [9, 14].

Another method for detecting motion contrast is to assess for phase variance or changes in the phase of the light waves. Moving erythrocytes will induce a variation in the phase of light reflected from one instant to the next, allowing for this to be measured. For moving erythrocytes, the variance will be much higher than in areas of no motion that show low variance from residual motion and Brownian movement.

OMAG uses both intensity and phase changes of the OCT signal to contrast blood for information [15]. OMAG improves differentiation between normal tissue and erythrocyte flow by modifying OCT hardware to introduce an externally imposed phase variation [9, 15, 16]. This helps counter the issue of bulk eye motion that phase-based detection was very sensitive to. OMAG has been implemented by the CIRRUS HD-OCT 5000 system with AngioPlex OCT angiography.

4.3   Advantages and Disadvantages of OCTA

Traditional methods of imaging vascular flow include dye-based angiography such as fluorescein angiography (FA) [17] and indocyanine green angiography (ICGA), [1–3] which require the injection of fluorescent dyes prior to imaging.

FA and ICGA have been used in ophthalmology for decades and continue to play important roles in clinical practice. However, these imaging modalities have some limitations and disadvantages. Firstly, they are invasive and require intravenous access. They are contraindicated among patients with allergies to the dyes, and while these allergies are uncommon, the drugs may sometimes result in severe allergic reactions or even anaphylaxis. They are also time-consuming, requiring up to 45 minutes for the complete investigation, in order to visualize the different phases of the angiograms. FA and ICGA do not allow differentiation of vessels from different layers of the retina and choroid, respectively. Instead, the en face angiogram is a composite image of vessels from different vascular layers. This is especially evident in flash angiograms, where the choroid appears as a mass of overlapping vessels. While confocal scanning laser ophthalmoscopy, which is employed in devices such as the Heidelberg Spectralis, partially overcomes this by limiting light reflection from a specific tissue plane, it is still not possible to have depth resolution using these devices. Finally, the devices and/or drugs required for these investigations are not available in some centers or populations, thus limiting their applicability.

OCTA overcomes many of the limitations inherent in dye-based angiography. Firstly, OCTA is noninvasive, painless, and does not require contact with the patient. It does not require intravenous dye injection, hence eliminating the risk of allergic reactions. It is also much faster, taking a few minutes to perform, and hence more efficient in busy clinics. These advantages allow OCTA to be performed more frequently in patients, which makes it more suitable for close monitoring of patients. OCTA also provides depth resolution of the various vascular layers, which is unavailable with dye-based angiography. Moreover, it is possible to display both en face and cross-sectional images, allowing for flow within specific retinal and choroidal layers to be visualized and correlated with structural abnormalities. OCTA images are also not obscured by dye leakages seen in FA or ICGA and underlying diseased vessels can potentially be visualized.

However, OCTA does have several important limitations. OCTA is not able to demonstrate leakage from vessels. Unlike FA and ICGA, which demonstrate dynamic filling of the blood vessels, OCTA is a static image and the direction of blood flow cannot be determined using this modality alone. OCTA image data are dependent on the underlying OCTA instruments used. Algorithms may vary, and different machines have different protocols and processing methods, which may affect the appearance of the OCTA image. Hence, care is required when interpreting and comparing images from different machines. OCTA images can also be subject to different types of artifacts, leading to misinterpretation. These artifacts may be due to both technical and clinical factors and are discussed in detail in a subsequent section.

4.4   OCTA Vessel Density

OCTA en face images can be viewed qualitatively for the presence of abnormalities and can be further processed to produce quantitative, objective data on the vascular parameters. Objective metrics that have been described in reports include vessel density (Fig. 4.1b), vessel length density (skeletonized density), blood flow index, and fractal dimension.

Vessel density is defined as the percentage of the en face image that is occupied by retinal vessels [18]. Vessel density allows objective, quantitative measurements which facilitate comparison of OCTA scans and can potentially be used in further clinical trials.

Vessel density has been shown in several studies to vary with different physiological parameters. In a study by Wang et al. [19] that analyzed 105 normal patients, vessel density was shown to decrease with age. There were also gender differences, with the male sex correlating with higher densities of the superficial retinal plexus and the female sex correlating with higher densities of the deep retinal plexus. In another study by Mo et al. [20], macular, choriocapillaris, and radial peripapillary capillary densities (RPC) were measured and compared between groups of emmetropes, high myopes, and pathological myopes. Compared with the first two, pathological myopes had significantly decreased macular and RPC vessel densities. There was also a negative correlation seen between axial length and superficial, deep retinal, and RPC vessel densities.

Vessel density also has the potential for clinicians to differentiate between normal and pathological eyes. Superficial and deep retinal vessel densities have been shown to decrease in diabetic eyes even without retinopathy compared to healthy subjects [21]. In another study by Durbin et al. [22] comparing normal and diabetic subjects, vessel density measured in the superficial retinal layer had a high area under the receiver-operating characteristic curve; suggesting that it is an efficacious method for differentiating eyes with and without diabetic retinopathy. In this study, vessel density also correlated negatively with best-corrected visual acuity and severity of diabetic retinopathy.

Several studies have shown good reproducibility (inter and intraobserver) with the use of vessel density as a metric assuming the same machine, quantification algorithm, and angiocube size are used. In a study by Lei et al. [23], eyes from both healthy participants and patients with retinal diseases were examined with three different software versions of the same model of OCTA device (Cirrus HD-OCT model 5000; Carl Zeiss Meditec, Inc). Both vessel length density and perfusion density of the superficial retinal vasculature were shown to be obtained using high levels of repeatability and reproducibility. In this particular study, within each device (repeatability), the coefficient of variation (CV) ranged from 2.2 to 5.9% and 2.4 to 5.9% for vessel length density and perfusion density respectively, while the intraclass correlation coefficient (ICC) ranged from 0.82 to 0.98 and 0.83 to 0.95 for vessel length density and perfusion density, respectively. Among the three different software versions (reproducibility), the CV in all groups was less than 6%,

with the ICC ranging from 0.62 to 0.95. It is important to note, however, that vessel density measurements can vary significantly among various machines. Various OCTA devices use proprietary software with heterogeneous algorithms to binarize the OCTA images and calculate vessel density. Aside from using these machines to calculate vessel density, most studies export and post-process OCTA angiograms with different thresholding methods. This includes the use of the ImageJ algorithm and Otsu's algorithm [24–26].

4.5   Artifacts on OCTA

An important limitation of OCTA is the presence of artifacts. Artifacts may be a result of a multitude of factors, ranging from how the image data is being acquired, processed, and displayed, to the intrinsic properties of the eye being imaged. Artifacts are also common. In a study done by Falavarjani et al., at least one type of artifacts was seen in 89.4% of eyes imaged using OCTA [27]. These included banding, segmentation, and motion artifacts most commonly (89.4%, 61.4%, and 49.1%, respectively), as well as others such as unmasking, blink, vessel doubling, and out-of-window artifacts.

4.5.1   Low Signal Strength

Signal strength is influenced by the signal to noise ratio and are commonly influenced by pathologies as well as ocular factors. Low signals lead to difficulty in visualizing the smaller vessels of the eye that correspondingly produce smaller signals. Media opacities in the anterior segment, such as cataracts or corneal scars, may decrease the OCT signal. Other factors that decrease signal-to-noise ratio include dry eyes or incorrect position of the machine. In such situations, reimaging after lubrication or repositioning the patient may improve signal strength in some instances. Loss of signal strength may be global or focal. Global losses of signal strength include

dense cataracts and vitreous hemorrhages. Focal losses of signal strength are due to focal opacities such as prominent vitreous floaters that obscure visualization of both the underlying retina and choroid or subretinal hemorrhage that obscures visualization of the underlying choroid.

While measures such as lubrication and repositioning may increase signal strength, approaches to reduce noise are often manufacturer specific.

4.5.2   Motion Artifacts

Eye movement during imaging is an important source of artifacts and can come from bulk eye movements, small saccades, or movement within the eye. For the latter, positional changes of the retina are often in the axial direction due to choroidal pulsation or intraocular pressure fluctuations.

Bulk eye movement often produces obvious shearing or gaps in en face images. In many machines, bulk eye movements are accounted for by active eye tracking. This works by measuring the position of the eye, with corrective measures taking place if the motion of the eye be greater than a selected threshold.

An approach to deal with artifacts from eye saccades and movement is a software-based approach developed by Kraus et al. [28]. This includes obtaining two OCT volumes from the same region—one in the horizontal and one in the vertical direction. These represent the same retinal structures but the effects of eye movements on these scans will be different and complementary.

Software-based methods work by estimating the amount of eye motion for each A-scan, translating the A-scan and then comparing the volumes. This software approach is intensive due to the number of A-scans needed. It should also be noted that while being able to correct movement artifacts, this software approach introduces artifacts on its own, such as loss of detail, vessel-doubling, image stretching, and quilting.

Other methods of account for eye movement would be to rescan portions affected by movement

with the rescanned image being stitched into the original image.

Software registration and correction complement active eye tracking and correct for some error that is not picked up by eye tracking. A study done by Camino et al. showed that a combination of eye tracking and software motion correction has been shown to reduce artifacts associated with software motion correction alone [29].

4.5.3 Projection Artifacts

During the imaging process, the OCT beam passes through overlying retinal structures to reach deeper layers. As it passes through the retina, the OCT beam may be reflected, absorbed, refracted, or scattered by these overlying structures leading to projection artifacts. For example, light may have varying fluctuations as it passes through flowing erythrocytes. These deeper structures may be illuminated by this fluctuating light even though these structures are stationary. Hence, a false impression of blood flow in these stationary structures may be given should they be deep to a blood vessel. The result of this would be the false detection of superficial vessels in the deeper layers of the retina. As such, it is no surprise that projection artifacts are seen in almost all images visualizing vessels at the level of the RPE. Several approaches to reduce projection artifacts have been investigated. One of the simplest would be to subtract the en face image of the superficial capillary plexus from the deeper layer.

4.5.4 Masking Defects

Masking defects arise from a process known as masking or thresholding. Masking describes the removal of OCTA data from structures with low signal or high amount of noise. This is important as areas with low signal can have the false appearance of flow due to random fluctuations of noise. However, this process of removing low signal results from the OCTA images makes it difficult to image flow deep in the choroid—an area of low signal especially if the RPE and choriocapillaris are intact. Hence, choroidal vessels underlying areas of intact RPE have little reflectivity and conversely, deep choroidal vessels can be visible in areas of RPE atrophy.

4.5.5 Segmentation Artifacts

In order to create en face images of the eye, different layers of the retina are selected, before summing up the vessel projected in these layers. Parameters such as reflectivity, texture, or continuity can be used to differentiate these layers, but are often less effective in pathological eyes that have distorted anatomy. Moreover, layer thickness varies from eye to eye and may be thinner, thicker, or even absent. In patients with pathological or high myopia, the presence of staphyloma may also lead to segmentation errors due to altered curvature. Incorrect segmentation can be identified and corrected by viewing the OCT B-scan images. However, this often is time-consuming and may be impractical to do for every imaged eye.

4.6 OCTA of the Normal Retinal Vasculature

Histological studies suggest three layers of capillary plexuses in the human retina—superficial vascular (SVP), intermediate capillary (ICP), and deep capillary plexuses (DCP) [30, 31]. While early OCTA studies describe only major vascular plexuses (superficial and deep vascular complexes), novel algorithms such as the 3-D projection artifact removal (PAR) may improve visualization of all the three capillary plexuses, in particular the ICP [32].

In a study done by Hirano et al. [33] eyes from 22 normal participants were examined using a full-spectrum, probabilistic OCTA, with and without 3-D PAR. In the study, en face

OCTA images of different vascular layers were described. Images of the SVP showed a centripetal branching pattern that terminated in a capillary ring around the foveal avascular zone. Comparing the ICP and DCP, DCP images reviewed vascular loops that were configured around a central point—much like a vortex. This central point is postulated by the authors to represent a vertical interconnecting vessel. This vortex-like configuration of vessels was not seen with the ICP.

4.7   OCTA of AMD

Optical coherence tomography angiography (OCTA) has become a useful tool in the management of age-related macular degeneration (AMD). The features detected on OCTA depend on the severity and spectrum of the disease. In addition to its roles in diagnosis and follow-up of nAMD, OCTA may also provide insights into the natural history and pathophysiology of the disease.

4.7.1   Non-Neovascular AMD

Non-neovascular or dry AMD is characterized by the presence of drusen which are yellow deposits located beneath the retinal pigment epithelium.

OCTA is useful in dry AMD to detect the presence of subclinical neovascularization in asymptomatic patients. This has been reported in up to 30% of patients with intermediate AMD [34]. These patients with subclinical CNV had an approximately 15 times greater risk of progressing to exudation compared to those without [35, 36].

The retinal pigment epithelium overlying the drusen may be highly reflective, which may cause projection artifacts from the overlying retinal vessels and giving the pseudo appearance of neovascularization [37]. As AMD progresses, OCTA shows measurable changes in signal void sizes in the choriocapillaris [37].

4.7.2   OCTA of the Choriocapillaris

OCTA is useful in imaging the choriocapillaris, where the dynamic nature of blood flow within the choriocapillaris allows detection of flow. By segmenting the RPE plus Bruch's membrane and projecting several micrometers below the RPE, a resultant en face OCTA image of the choriocapillaris is generated, which appears as a granular pattern of bright and dark areas [38–40]. Regions without flow signal (i.e., dark areas) are known as flow voids [37] and may represent either atrophic choriocapillaris vessels, vessels with a very slow flow rate that is slower than the device's sensitivity or may represent areas of shadowing arising from attenuation of OCT signal [41–43].

In healthy eyes, the number of flow voids increased with age and also with decreasing distance from the fovea [44–46]. Spaide described an increased number of choriocapillaris flow voids in normal eyes imaged with SD-OCTA with increasing age and a history of hypertension [45]. Utilizing SS-OCTA and a validated novel algorithm [47], Zheng et al. reported a positive correlation between decades of age and percentage of choriocapillaris flow deficits (FD%) which was consistent across the central and peripheral macula ($r > 0.50$ and $p < 0.001$ in all areas). The FD% increase was found to be the greatest in the central 1-mm circular area centered on the macula and smallest in the 2.5-mm rim in the peripheral retina [46].

Among eyes with geographic atrophy, flow voids were significantly increased compared with age-matched controls [48]. Additionally, Rinella et al. reported that the number of flow voids in the periphery of the atrophic regions (within 2° of GA) was found to be significantly greater compared to areas away (outside 2° of GA) [48]. Flow voids were also reported to be significantly increased in eyes with choroidal neovascularization (CNV) compared to age-similar normal controls. (20.56 ± 4.95, 95% CI: 17.64–23.49 vs. 10.95 ± 2.08, 95% CI: 9.73–12.18, respectively; $P = 0.0001$) which also correlated positively with CNV lesion area ($r = 0.84$; 95% CI: 0.49–0.96; $P = 0.001$) [42].

4.7.3   Exudative AMD

For many decades, the diagnosis and classification of exudative AMD have been made using fluorescein angiography (FA). However, FA is associated with some disadvantages, such as its invasive nature and the potential for allergic reactions caused by fluorescein dye. OCTA overcomes these limitations. It has been reported to be able to show between 75 and 90% of the flow patterns as seen on FA [49, 50].

4.7.3.1 Type 1 CNV

OCTA has been reported to detect between 67 and 100% of type 1 choroidal neovascularizations [50–52]. There is better visualization of the vascular structures in Type 1 CNV on OCTA compared to FA because there is less masking from the overlying retina pigment epithelium and the absence of obscuration from dye leakage [53].

On cross-sectional OCTA, intrinsic flow is seen within the pigment epithelial detachment in the sub-RPE space. On the corresponding en face OCTA, CNV lesions can be visualized as a well-defined network or tangle of vessels lying between the RPE and the Bruch's membrane [54]. Trunk vessels may be present. The choriocapillaris in the region beneath and around the CNV may show some signs of loss. Chronic CNV lesions may also exhibit a network of tiny capillaries around the CNV border with a lack of mature dilated feeder vessels [55].

4.7.3.2 Type 2 CNV

On cross-sectional OCTA, an active type 2 CNV lesion is seen as subretinal hyperreflective material above the RPE with intrinsic flow signals (Fig. 4.4). Hyperflow patterns detected (often described as glomerulus or medusa shaped) are associated with a thicker main vessel branch connected to the deeper choroid. In some cases, this high flow signal may cause a projection artifact onto the deeper choriocapillaris layer. A dark halo may be seen around the lesion and this was postulated to correspond to masking from surrounding blood, exudation, or subretinal fibrosis [56, 57].

On the corresponding en face scans, type 2 CNV is seen as a network of vessels in the normally avascular outer retina [58] These vascular networks often have a lacy pattern with uniform intensity but variable caliber. The CNV lesions detected on OCTA correlate closely with the area of leakage on FFA and are generally more distinct compared to ICGA [59]. Similar to type 1 CNV, the choriocapillaris surrounding the CNV may show some signs of loss and trunk vessels may be present.

An added benefit of OCTA is the identification of both the superficial subretinal type 2 component and the deeper sub-RPE type 1 component by varying the depth of segmentation.

4.7.3.3 Type 3 CNV

Cross-sectional OCTA of type 3 CNV showed two patterns of flow: [60].
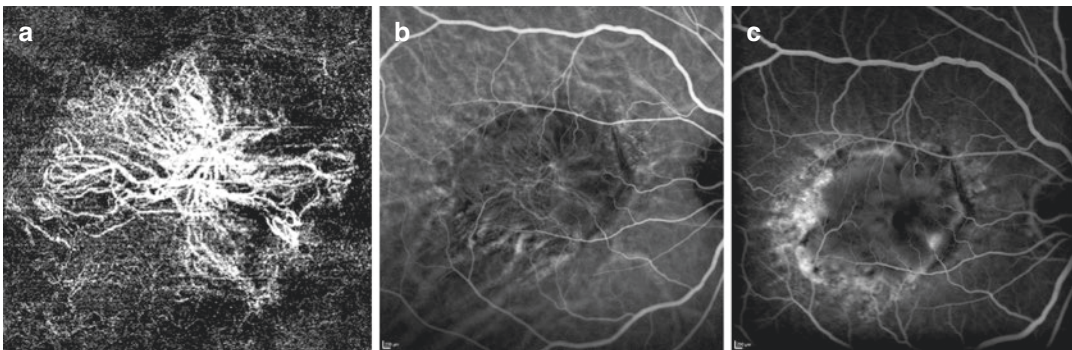
Fig. 4.4 Neovascular age-related macular degeneration. (**a**) OCTA demonstrating the CNV lesion. (**b**) Indocyanine green angiogram at 3 min, showing the CNV vessels. The overlying retinal vessels as well as the large choroidal vessels are visible. (**c**) Fluorescein angiogram showing occult leakage

1. Discrete intraretinal flow signal or
2. Linear flow signal extending from the intra-retinal areas through to the RPE band

The en face OCTA shows a discrete bright tuft of microvessels with high flow extending from the middle retinal layers or deep capillary plexuses into the deep retina and, occasionally, past the RPE [60]. As the type 3 CNV develops over time, these vessels anastomose with the deep retinal capillary plexuses and extend into the outer retina and eventually into the sub-RPE space [60]

4.7.4   Sensitivity and Specificity

Compared with FA, OCTA has a sensitivity of 50–100% and a specificity of 79–91% [51, 61, 62]. In some studies where when structural OCT was used together with OCTA data, the sensitivity increased to 87% [61].

4.7.5   Use of OCTA in Management of AMD

4.7.5.1 Active or Inactive MNV
Since OCTA may detect incidental findings of neovascularization in patients who are asymptomatic and appear clinically to have non-neovascular AMD, it is imperative to determine if treatment is indicated. There are some reports on characteristics of the CNV lesion on OCTA, as well as correlating with structural OCT, which can help clinicians determine the activity levels of such lesions and the need for treatment. Examples of such features include:

Active CNV:
1. Presence of fine vessels at the edge of the neovascularization.
2. Peri-lesional dark halo.
3. Extensive vascularity.
4. Appearance of anastomoses and loops,
5. Well-defined shape (lacy wheel or sea-fan shaped) [63].

Inactive CNV:
1. Large vessels which have the appearance of a "dead tree" [63].
2. Paucity of fine branching vessels [63].
3. Absence of anastomoses, loops, and peripheral arcades.
4. Paucivascular fibrotic scar.

4.7.5.2 Monitoring of Treatment Efficacy
OCTA provides both quantitative and qualitative evaluation of MNV and hence is an useful and powerful tool for monitoring and follow-up of MNV.

Following treatment with anti-VEGF agents, neovascularization has been shown to decrease in size as well as density due to the loss of finer vessels along the border and within the CNV [64, 65]. This regression is maximal around 1–2 weeks following treatment [64].

Chronic CNV lesions may show little anatomical response to anti-VEGF and the lesion area and vessel density may remain unchanged. These may eventually develop a pruned tree appearance, which is an indicator of inactivity [54].

4.7.6   Limitations and Pitfalls in Diagnosing MNV on OCTA

Projection artifacts from the superficial retinal vasculature can give the erroneous appearance of neovascularization in a normal eye [66]. Other retinal elevations such as drusen, serous, and drusenoid pigment epithelial detachments as well as scars can also affect the segmentation of retinal layers and give the false appearance of neovascularization.

In patients with macular atrophy and loss of the choriocapillaris, the larger choroidal vessels may appear within the choriocapillaris slab. These may appear similar to neovascularization.

This illustrates that it is important to assess the OCT B-scan to correlate the presence of flow with the appearance of the en face image. It is also useful to perform careful mapping of the vessels as well as confirming the location of these

vessels beneath the Bruch's membrane. This will help to differentiate the normal vessels from neovascularization.

4.8 OCTA of Polypoidal Choroidal Vasculopathy (PCV)

Polypoidal choroidal vasculopathy (PCV) is characterized by the presence of polypoidal lesions together with a branching vascular network (BVN) that supplies these lesions. This condition occurs more commonly among some populations, such as Asians [67, 68]. Currently, ICGA is the gold standard for diagnosing PCV [1, 3, 69, 70], although color fundus photography, multicolor

imaging, and FA [6, 7] can identify features which are suggestive of PCV. OCTA provides a complementary diagnostic tool to ICGA in diagnosing PCV with the sensitivity of OCTA in detecting PCV ranging from 39.5 to 43.9% and the specificity varying from 79.1 to 87.1% [68, 71].

4.8.1 Polypoidal Lesions

The polypoidal lesions exhibit variability in their flow characteristics and structure, with some appearing as hyperflow round structures (Fig. 4.5) with a hypointense halo and up to 75% appearing as hypoflow round structures. Hyperflow lesions tended to be less pulsatile and to have a thicker subfoveal choroid. The round structures were
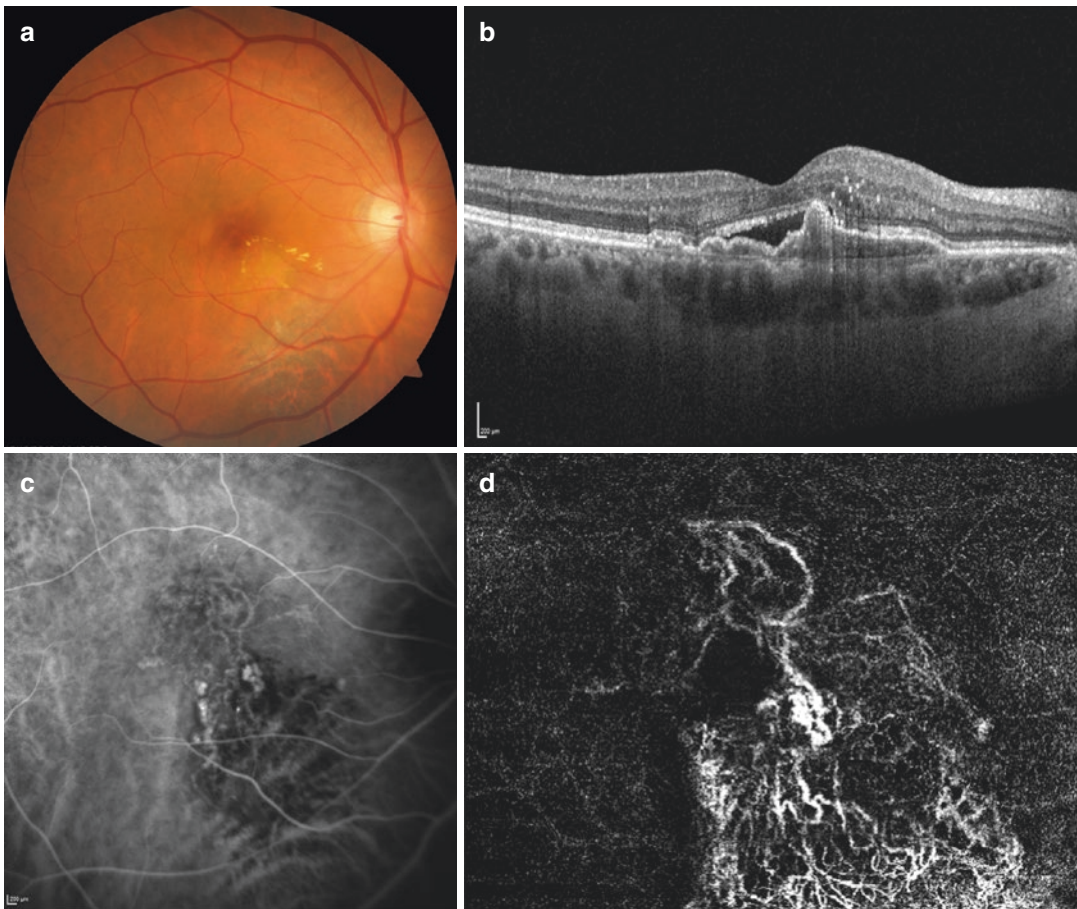
Fig. 4.5 Polypoidal choroidal vasculopathy (PCV). (**a**) Color fundus photograph, showing mottling and thinning of the retina inferiorly. (**b**) OCT B-scan showing elevation of the retinal pigment epithelium, corresponding to the pol-

ypoidal lesion. Subretinal fluid is observed. (**c**) Indocyanine green angiogram showing polypoidal lesions and the associated branching vascular network. (**d**) OCTA illustrating the polypoidal lesion and branching vascular network

typically situated at the termini of the vascular network. These polypoidal structures were mainly above the Bruch's membrane within the dome of the RPE detachment, with the choroidal stalks extending deeper in the choroid layer.

However, OCTA is only able to detect 17–85% of polyps compared to ICGA. It is believed that the absence of lesions on OCTA may be related to slow or turbulent flow within the polypoidal lesions.

In contrast to the BVN, the rate of polyp progression was highly variable ranging from 17 to 85% [72–75].

4.8.2   Branching Vascular Membranes (BVNs)

The BVN is detected using OCTA in between 77.8 and 100% of eyes with PCV. It is visualized as a hyperflow lesion, located between the RPE and Bruch's membrane [73, 76]. This vascular net was variable in size but correlated closely with the location and shape seen on the ICGA. Often, en face OCTA of the BVN showed networks of vessels in much more detail than ICGA.

In one study, 70.9% of the PCV cases (22/31) had clear or obvious BVNs and that this feature was the most sensitive to make an accurate diagnosis (sensitivity 97.5%). The sensitivity increased from 69.5 to 90% after OCTA [77].

Following treatment with anti-VEGF and PDT, reduction in flow within the PCV complexes in most eyes is expected. However, despite significant improvement in exudation, the vascular network may remain unchanged. Early recurrence of PCV may be detected on OCTA via changes in the appearance of the vascular network as well as the presence of persistent flow signals within the vascular network.

4.9   OCTA of Retinal Vascular Diseases

4.9.1   Diabetic Retinopathy

The prevalence of diabetes mellitus is increasing in many parts of the world and, with it, the fre-

quency of ocular complications such as diabetic retinopathy and diabetic macular edema. Previously, FA was required to assess the presence and extent of retinal non-perfusion and to neovascularization at the disc and elsewhere. Due to the requirement for venous access and the use of intravenous dye injections, this investigation could not be performed frequently. In contrast, the convenience of OCTA allows more frequent reviews of eyes with diabetic eye disease and also provides new insights due to the ability to segment different vascular plexuses in the retina.

OCTA is able to detect microaneurysms [78–81], which is the hallmark of diabetic retinopathy. Unlike FA, where microaneurysms typically appear as round dots, OCTA can differentiate various shapes in microaneurysms, including solid round lesions, round lesions with dark centers, or fusiform lesions [81]. It is important, however, to note that there is incomplete agreement between FA and OCTA in terms of the number and locations of microaneurysms. Studies have reported that a greater number of microaneurysms are detected using FA compared to OCTA and it has been suggested that the histology of microaneurysms could potentially result in turbulent or slower blood flow, the velocity of which is below the slowest detectable flow using current OCTA devices [79, 80]. Parravano et al. reported varying detection rates of microaneurysms on OCTA depending on their internal reflectivity on spectral-domain OCT. They found that microaneurysms with hyporeflectivity on OCT had a lower detection rate on OCTA, compared to those with moderate or hyperreflectivity [82].

Retinal neovascularization at the optic disc or elsewhere can be detected using OCTA [79, 80, 83]. By setting the segmentation of the OCTA slab above the internal limiting membrane, blood flow through these new vessels can be detected. OCTA is advantageous in that it is not affected by leakage, unlike FA where leakage from the neovascularization can obscure image details in later phases of the angiogram.

Another feature in eyes with diabetic retinopathy which can be detected using OCTA are looping vessels with increased caliber adjacent to areas of impaired capillary perfusion [78, 81]. In

some cases, these are consistent with clinically defined intraretinal microvascular abnormalities, which is a feature of more advanced diabetic retinopathy [81]. Other features, such as dilated capillary segments [78] and clustered or tortuous capillaries [78], also illustrate the underlying features associated with retinal vascular diseases.

Since diabetes mellitus affects the microvasculature in the eye, it is not surprising that eyes with diabetic retinopathy will manifest with areas of retinal non-perfusion and capillary dropout (Fig. 4.6). These can be identified using both FA and OCTA, however, OCTA has the additional advantage of being able to resolve different vascular plexuses in the retina, thus illustrating the areas of non-perfusion in the superficial, intermediate, and deep capillary plexuses [78–81, 83, 84]. Studies have reported that the area of retinal non-perfusion differs between the superficial and deep retinal plexuses [80, 85, 86]. The area of retinal non-perfusion increases with the severity of diabetic retinopathy [84, 87]. Besides the reduction in blood flow in the retinal circulation, studies have also reported regionals of flow impairment in the choriocapillaris among patients with non-proliferative and proliferative diabetic retinopathy [78].

Changes occur at the foveal avascular zone (FAZ) in diabetics, with both more irregularity of the FAZ and enlargement of this region. OCTA of normal eyes demonstrates a range of FAZ sizes and circularity (the extent to which the FAZ resembles a perfect circle) [88]. Using OCTA, increasing irregularity of the FAZ has been identified in eyes of diabetics, with gaps and interruptions of the capillary networks [85, 89, 90]. The size of the FAZ is larger among eyes with diabetic retinopathy compared to those without [83, 86, 91, 92]. This difference appears to be more pronounced in the deep capillary plexus [89, 90].
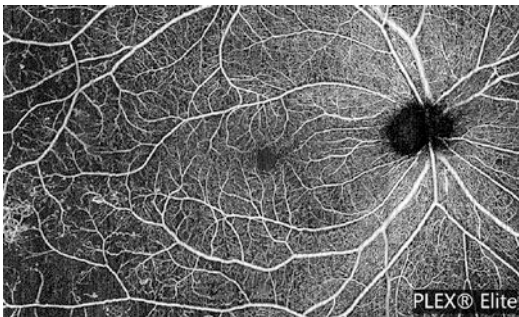
Retinal vessel density is a measure of the amount of flow within a region of an OCTA scan. Studies comparing eyes of diabetics with normal controls have reported that eyes of diabetics have reduced vessel densities compared to normal controls [21, 79, 86, 87]. This reduction is evident even among eyes of diabetics with no clinical features of diabetic retinopathy and becomes more severe as the severity of diabetic retinopathy worsens [87]. The reduction in vessel density with diabetic retinopathy is observed in both the superficial and deep capillary plexuses [21, 83, 86, 87]. Local reductions in vascular density of the deep capillary plexus have been shown to correlate with regions of disorganization of the retinal inner layers (DRIL), which are demonstrated on OCT B-scans [37, 93].

Changes in vessel density may serve as useful biomarkers for early detection of diabetic retinopathy and to indicate the potential for progression. Studies have reported significant correlations between systolic blood pressure and ocular perfusion pressure and the vessel density in the deep retinal plexus in patients with non-proliferative diabetic retinopathy [21].

An important consideration when using OCTA to assess for features of diabetic retinopathy is that the disease can occur throughout the retina and may not be localized in a specific region. Hence, the field of view of the OCTA scan is an important consideration. Investigators have reported that a wider field of view on the OCTA was useful for detecting the full extent of vascular changes as well as capillary non-perfusion [83]. This is especially important when considering that studies of ultra-widefield FA in patients with retinal vascular diseases have identified significant regions of retinal non-perfusion in the peripheral retina [4, 5].

Fig. 4.6 Diabetic retinopathy. OCTA of the superficial retinal plexus, showing capillary dropout which is more severe in the temporal periphery

4.9.2   Diabetic Macular Edema

Although the features of diabetic macular edema (DME) are seen on structural OCT, studies have described some findings on OCTA associated with this condition. Microaneurysms are associated with DME and occur with higher density in the deep capillary plexus compared to the superficial capillary plexus ($1.71/mm^2$ vs. $0.17/mm^2$, $P < 0.001$) [94].

OCTA scans also show dark regions devoid of flow signal which correspond to the presence of intraretinal cysts [37, 81, 85, 95]. These are usually oval or oblong in shape, with smooth borders and do not follow the distribution of the surrounding capillaries [95]. It is believed that these may result from spaces with low perfusion, blockage of signal from the vessels caused by the presence of intraretinal fluid or due to displacement of the retinal vessels caused by the edema [95].

Intraretinal cysts and fluid may also manifest with extravascular signals, which are seen on en face OCTA images. "Suspended scattering particles in motion (SSPiM)" is a relatively novel imaging feature of retinal vascular diseases, including DME, which are detected on OCTA [96]. SSPiM represents an extravascular OCTA signal which is related to varying degrees of hyperreflective material seen on structural OCT. It is believed that these are due to Brownian motion of particles within the intraretinal fluid, which appears as flow on OCTA B-scans [96].

Eyes with both diabetic retinopathy and DME have been reported to have significantly lower vascular flow density in the deep capillary plexus compared to eyes with diabetic retinopathy but no DME (13.23% vs. 20.75%, $p < 0.001$) [97]. In contrast, there was no statistically significant difference in vascular flow density in the superficial layer. Following treatment with anti-VEGF agents, patients with poor treatment response showed lower vessel density, more microaneurysms, and a larger FAZ in the deep capillary plexus compared to those who responded favorably [97].

4.9.3   Retinal Vein Occlusion

Among patients with retinal vein occlusion, OCTA is useful in detecting the extent of vascular non-perfusion, which occurs in both the superficial and deep capillary plexuses (Fig. 4.7) [98, 99]. Similar to diabetic retinopathy, the FAZ may be enlarged in both the superficial and deep vascular plexuses [99].

OCTA also detects evidence of capillary changes [98, 100], such as dilation, pruning,
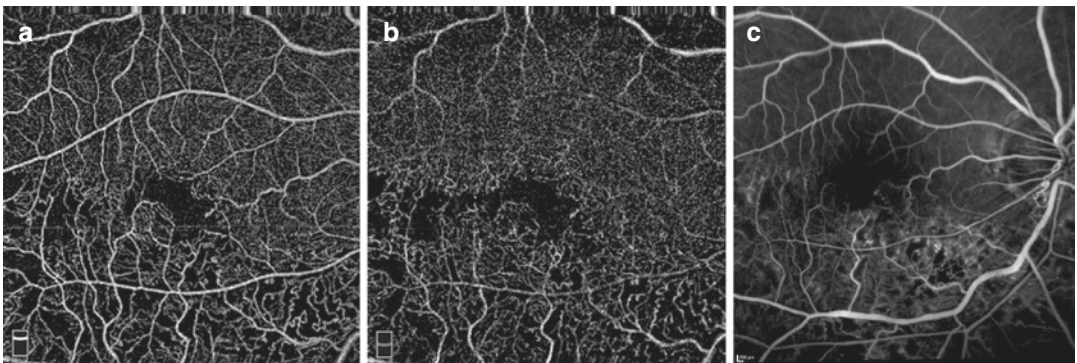
Fig. 4.7 Branch retinal vein occlusion. (**a**) OCTA of the superficial retinal plexus, showing capillary dropout inferiorly. The foveal avascular zone outline is irregular. (**b**) OCTA of the deep retinal plexus, showing the capillary dropout affecting the inferior retina. (**c**) Fluorescein angiogram, illustrating the capillary dropout in the retina. The FAZ is less well demarcated compared to the OCTA

telangiectasia, and vascular dilation, as well as the presence of shunt vessels [98] and retinal neovascularization [100]. Among patients with retinal vein occlusion, cystoid spaces occur more commonly in the deep compared to the superficial retinal plexus [101].

Paracentral acute middle maculopathy (PAMM) refers to band-like hyper-reflective lesions which are mostly confined to the inner nuclear layer visualized on SD-OCT. [102] Initially described by Sarraf et al. as a variant of acute macular neuroretinopathy [102], it is now understood to be a clinical finding associated with ischemia or infarction of the deep vascular complex (intermediate and deep retinal capillary plexus) [103]. PAMM has been reported to be associated with a large spectrum of retinal vascular disorders and systemic conditions [103–107]. Bakhoum et al. described a distinct progression of PAMM pattern progression on SD-OCT, pointing toward an ischemic cascade occurring in the parafoveal region in eyes with retinal vascular occlusion. The authors found that the ischemia occurred in the parafoveal macula, initially developing at the venular pole of the deep capillary plexus (manifesting as perivenular fern-like PAMM in the INL), which progresses laterally through the INL (manifesting as globular PAMM in the INL), and then anteriorly into the inner retina at the level of the superficial capillary plexus (SCP), with worsening visual acuity in each stage [108]. This anterior progression of ischemia implies a serial organization of the retinal capillary plexuses [109].

Unlike fluorescein angiography, OCTA's ability to produce detailed, high-resolution images of the retinal vasculature segmented by layer [37] has allowed for the correlation of PAMM with attenuation and pruning of the DCP visualized on the OCTA in multiple studies [67, 103, 104, 106, 110, 111]. While no study has reproduced Bakhoum et al.'s findings of a distinct PAMM ischemic cascade on OCTA, a recent study by Maltsev et al. described a tendency for resolved PAMM lesions, defined as INL thinning with OPL elevation, to localize paravascularly in majority of BRVO and CRVO patients [112].

4.9.4 Retinal Artery Occlusion

In patients with retinal artery occlusion, OCTA is useful in detecting the presence of macular ischemia and vascular flow changes, which may occur in both the superficial and deep capillary plexuses. These typically correspond to regions of delayed perfusion seen on FA [113]. In some eyes, perfusion of the deep capillary plexus may be maintained in areas of persistent ischemia in the superficial plexus [113]. In addition, there may be attenuation of the radial peripapillary capillaries, which correspond to thinning of the retinal nerve fiber layer [113].

4.10 OCTA in Inflammatory Conditions and Inherited Retinal Dystrophies

OCTA has been shown to be useful for evaluating the choroidal and retinal blood flow among patients with inherited retinal dystrophies and inflammation, including Stargardt disease, retinitis pigmentosa, Best vitelliform macular dystrophy, and choroideremia [114]. Areas of hypoperfusion and vascular insufficiency are well demonstrated in these conditions.

In addition, OCTA can detect neovascularization occurring in diseases of the retina and choroid, including inherited retinal dystrophies and inflammatory conditions [115–118]. The CNV lesions more clearly seen on OCTA compared to other imaging modalities such as FA [114]. In a study of ten eyes with multifocal choroiditis, OCTA identified all CNV lesions [115]. Active CNV lesions were found to have well-circumscribed margins, interlacing shapes, and a surrounding dark ring. In contrast, inactive CN lesions had poorly circumscribed margins, tangled shapes, and a "dead tree" appearance, with the surrounding dark ring appearing less frequently [115].

In patients with Stargardt disease, decreased vessel densities in the superficial and deep retinal plexuses, and the choriocapillaris, have

been demonstrated using OCTA. In addition, the superficial FAZ was found to be larger than normal controls [114, 119]. In a study of consecutive patients with Stargardt disease, quantitative parameters such as vessel density, vessel tortuosity, vessel dispersion, and vessel rarefaction were significantly worse than normal controls [120]. A study comparing OCTA of patients with Stargardt disease and AMD found greater areas of rarefaction of the choriocapillaris flow signal in Stargardt disease compared to AMD [121].

Different patterns of choroidal hypoperfusion were reported on OCTA among patients with white dot syndromes [122]. For patients with presumed ocular histoplasmosis syndrome and multiple evanescent white dot syndrome, choroidal hypoperfusion correlated well with clinical pathology. In contrast, regions of choroidal hypoperfusion were more widespread in both acute posterior multifocal placoid pigment epitheliopathy (APMPPE) and birdshot chorioretinopathy. One study reported that the resolution of choroidal hypoperfusion in APMPPE preceded the resolution of photoreceptor abnormality and visual recovery [123]. This suggests that the pathophysiology of APMPPE likely involves a primary hypoperfusion of the inner choroid with resultant RPE and photoreceptor abnormality and vision loss [123].

In Best vitelliform macular dystrophy, OCTA was shown to be superior to FA in detecting CNV because of masking of the CNV on FA by the vitelliform material [124]. In addition, the majority of patients had abnormal FAZ in the superficial and deep FAZ with patchy loss of vascularity in both retinal plexuses [124].

4.11   Conclusion

OCTA has changed the practice of ophthalmology, especially in the diagnosis, monitoring, and management of retinal diseases. Its noninvasive nature, rapid scanning time, and ability to segment different vascular layers have proved invaluable to understanding the pathophysiology of retinal diseases. It is important, however, to understand the current limitations and pitfalls of this modality.

References

1. Tan CS, Ngo WK, Chen JP, et al. EVEREST study report 2: imaging and grading protocol, and baseline characteristics of a randomised controlled trial of polypoidal choroidal vasculopathy. Br J Ophthalmol. 2015;99:624–8.
2. Tan CS, Ngo WK, Lim LW, et al. EVEREST study report 3: diagnostic challenges of polypoidal choroidal vasculopathy. Lessons learnt from screening failures in the EVEREST study. Graefes Arch Clin Exp Ophthalmol. 2016;254:1923–30.
3. Tan CS, Ngo WK, Lim LW, Lim TH. A novel classification of the vascular patterns of polypoidal choroidal vasculopathy and its relation to clinical outcomes. Br J Ophthalmol. 2014;98:1528–33.
4. Singer M, Tan CS, Bell D, Sadda SR. Area of peripheral retinal nonperfusion and treatment response in branch and central retinal vein occlusion. Retina. 2014;34:1736–42.
5. Tan CS, Chew MC, van Hemert J, et al. Measuring the precise area of peripheral retinal non-perfusion using ultra-widefield imaging and its correlation with the ischaemic index. Br J Ophthalmol. 2016;100:235–9.
6. Tan CS, Ting DS, Lim LW. Multicolor fundus imaging of polypoidal choroidal vasculopathy. Ophthalmol Retin. 2019;3(5):400–9. https://doi.org/10.1016/j.oret.2019.01.009.
7. Tan CS, Ting DS, Lim LW. Multicolour imaging for the detection of polypoidal choroidal vasculopathy and age-related macular degeneration. Clin Exp Ophthalmol. 2019;47:621–30.
8. Jia Y, Tan O, Tokayer J, et al. Split-spectrum amplitude-decorrelation angiography with optical coherence tomography. Opt Express. 2012;20:4710.
9. Chen C-L, Wang RK. Optical coherence tomography based angiography [Invited]. Biomed Opt Express. 2017;8:1056.

10. McNamara PM, Subhash HM, Leahy MJ. In vivo full-field en face correlation mapping optical coherence tomography. J Biomed Opt. 2013;18:126008.

11. Conroy L, DaCosta RS, Vitkin IA. Quantifying tissue microvasculature with speckle variance optical coherence tomography. Opt Lett. 2012;37:3180.

12. Mahmud MS, Cadotte DW, Vuong B, et al. Review of speckle and phase variance optical coherence tomography to visualize microvascular networks. J Biomed Opt. 2013;18:50901.

13. Mariampillai A, Leung MKK, Jarvi M, et al. Optimized speckle variance OCT imaging of microvasculature. Opt Lett. 2010;35:1257.

14. Spaide RF, Fujimoto JG, Waheed NK, et al. Optical coherence tomography angiography. Prog Retin Eye Res. 2018;64:1–55.

15. Wang RK, Jacques SL, Ma Z, et al. Three dimensional optical angiography. Opt Express. 2007;15:4083.

16. Huang Y, Zhang Q, Thorell MR, et al. Swept-source OCT angiography of the retinal vasculature using intensity differentiation-based optical microangiography algorithms. Ophthalmic Surg Lasers Imaging Retin. 2014;45:382–9.

17. Tan CS, Ngo WK, Lim LW, et al. EVEREST study report 4: Fluorescein angiography features predictive of polypoidal choroidal vasculopathy. Clin Exp Ophthalmol. 2019;47:614–20.

18. Rabiolo A, Gelormini F, Sacconi R, et al. Comparison of methods to quantify macular and peripapillary vessel density in optical coherence tomography angiography. PLoS One. 2018;13:e0205773.

19. Wang Q, Chan S, Yang JY, et al. Vascular density in retina and choriocapillaris as measured by optical coherence tomography angiography. Am J Ophthalmol. 2016;168:95–109.

20. Mo J, Duan A, Chan S, et al. Vascular flow density in pathological myopia: an optical coherence tomography angiography study. BMJ Open. 2017;7:e013571.

21. Dimitrova G, Chihara E, Takahashi H, et al. Quantitative retinal optical coherence tomography angiography in patients with diabetes without diabetic retinopathy. Invest Opthalmology Vis Sci. 2017;58:190.

22. Durbin MK, An L, Shemonski ND, et al. Quantification of retinal microvascular density in optical coherence tomographic angiography images in diabetic retinopathy. JAMA Ophthalmol. 2017;135:370–6.

23. Lei J, Durbin MK, Shi Y, et al. Repeatability and reproducibility of superficial macular retinal vessel density measurements using optical coherence tomography angiography en face images. JAMA Ophthalmol. 2017;135:1092.

24. Devarajan K, Di Lee W, Ong HS, et al. Vessel density and En-face segmentation of optical coherence tomography angiography to analyse corneal vascularisation in an animal model. Eye Vis. 2019;6:2.

25. Lauermann JL, Eter N, Alten F. Optical coherence tomography angiography offers new insights into choriocapillaris perfusion. Ophthalmologica. 2018;239:74–84.

26. Nicolò M, Rosa R, Musetti D, et al. Choroidal vascular flow area in central serous chorioretinopathy using swept-source optical coherence tomography angiography. Investig Ophthalmol Vis Sci. 2017;58:2002–10.

27. Ghasemi Falavarjani K, Al-Sheikh M, Akil H, Sadda SR. Image artefacts in swept-source optical coherence tomography angiography. Br J Ophthalmol. 2017;101:564–8.

28. Kraus MF, Potsaid B, Mayer MA, et al. Motion correction in optical coherence tomography volumes on a per A-scan basis using orthogonal scan patterns. Biomed Opt Express. 2012;3:1182.

29. Camino A, Zhang M, Gao SS, et al. Evaluation of artifact reduction in optical coherence tomography angiography with real-time tracking and motion correction technology. Biomed Opt Express. 2016;7:3905–15.

30. Henkind P. Radial peripapillary capillaries of the retina. I. Anatomy: human and comparative. Br J Ophthalmol. 1967;51:115–23.

31. Tan CSH, Cheong KX. Macular choroidal thicknesses in healthy adults—relationship with ocular and demographic factors. Investig Opthalmol Vis Sci. 2014;55:6452.

32. Garrity ST, Iafe NA, Phasukkijwatana N, et al. Quantitative analysis of three distinct retinal capillary plexuses in healthy eyes using optical coherence tomography angiography. Investig Ophthalmol Vis Sci. 2017;58:5548–55.

33. Hirano T, Chanwimol K, Weichsel J, et al. Distinct retinal capillary plexuses in normal eyes as observed in optical coherence tomography angiography axial profile analysis. Sci Rep. 2018;8:1–7.

34. Carnevali A, Cicinelli MV, Capuano V, et al. Optical coherence tomography angiography: a useful tool for diagnosis of treatment-naïve quiescent choroidal neovascularization. Am J Ophthalmol. 2016;169:189–98.

35. de Oliveira Dias JR, Zhang Q, Garcia JMB, et al. Natural history of subclinical neovascularization in nonexudative age-related macular degeneration using swept-source OCT Angiography. Ophthalmology. 2018;125(2) Elsevier Inc.:255–66.

36. Hanutsaha P, Guyer DR, Yannuzzi LA, et al. Indocyanine-green videoangiography of drusen as a possible predictive indicator of exudative maculopathy. Ophthalmology. 1998;105:1632–6.

37. Spaide RF. Volume-rendered optical coherence tomography of diabetic retinopathy pilot study. Am J Ophthalmol. 2015;160:1200–10.

38. Braaf B, Vermeer KA, Vienola KV, de Boer JF. Angiography of the retina and the choroid with phase-resolved OCT using interval-optimized backstitched B-scans. Opt Express. 2012;20:20516.

39. Choi WJ, Mohler KJ, Potsaid B, et al. Choriocapillaris and choroidal microvasculature

imaging with ultrahigh speed OCT angiography. PLoS One. 2013;8(12):e81499.

40. Sohrab M, Wu K, Fawzi AA. A Pilot study of morphometric analysis of choroidal vasculature in vivo, using en face optical coherence tomography. PLoS One. 2012;7:e48631.

41. Cole ED, Novais EA, Louzada RN, et al. Visualization of changes in the choriocapillaris, choroidal vessels, and retinal morphology after focal laser photocoagulation using OCT angiography. Investig Ophthalmol Vis Sci. 2016;57:OCT356–61.

42. Keiner CM, Zhou H, Zhang Q, et al. Quantifying choriocapillaris hypoperfusion in patients with choroidal neovascularization using swept-source OCT angiography. Clin Ophthalmol. 2019;13:1613–20.

43. Mullins RF, Johnson MN, Faidley EA, et al. Choriocapillaris vascular dropout related to density of drusen in human eyes with early age-related macular degeneration. Investig Ophthalmol Vis Sci. 2011;52:1606–12.

44. Nassisi M, Baghdasaryan E, Tepelus T, et al. Topographic distribution of choriocapillaris flow deficits in healthy eyes. PLoS One. 2018;13(11):e0207638.

45. Spaide RF. Choriocapillaris flow features follow a power law distribution: implications for characterization and mechanisms of disease progression. Am J Ophthalmol. 2016;170:58–67.

46. Zheng F, Zhang Q, Shi Y, et al. Age-dependent changes in the macular choriocapillaris of normal eyes imaged with swept-source optical coherence tomography angiography. Am J Ophthalmol. 2019;200:110–22.

47. Zhang Q, Zheng F, Motulsky EH, et al. A novel strategy for quantifying choriocapillaris flow voids using swept-source OCT angiography. Invest Ophthalmol Vis Sci. 2018;59:203–11.

48. Rinella NT, Zhou H, Zhang Q, et al. Quantifying choriocapillaris flow voids in patients with geographic atrophy using swept-source OCT angiography. Ophthalmic Surg Lasers Imaging Retin. 2019;50:E229–35.

49. Coscas F, Querques G, Forte R, et al. Combined fluorescein angiography and spectral-domain optical coherence tomography imaging of classic choroidal neovascularization secondary to age-related macular degeneration before and after intravitreal ranibizumab injections. Retina. 2012;32:1069–76.

50. Kuehlewein L, Bansal M, Lenis TL, et al. Optical coherence tomography angiography of Type 1 neovascularization in age-related macular degeneration. Am J Ophthalmol. 2015;160:739–48.e2

51. Inoue M, Jung JJ, Balaratnasingam C, et al. A comparison between optical coherence tomography angiography and fluorescein angiography for the imaging of type 1 neovascularization. Investig Ophthalmol Vis Sci. 2016;57:OCT314–23.

52. Veronese C, Maiolo C, Morara M, et al. Optical coherence tomography angiography to assess pigment epithelial detachment. Retina. 2016;36:645–50.

53. Malihi M, Jia Y, Gao SS, et al. Optical coherence tomographic angiography of choroidal neovascularization ill-defined with fluorescein angiography. Br J Ophthalmol. 2017;101:45–50.

54. Tan ACS, Tan GS, Denniston AK, et al. An overview of the clinical applications of optical coherence tomography angiography. Eye. 2018;32(2):262–86.

55. Xu D, Dávila JP, Rahimi M, et al. Long-term progression of Type 1 neovascularization in age-related macular degeneration using optical coherence tomography angiography. Am J Ophthalmol. 2018;187:10–20.

56. Dansingani KK, Tan ACS, Gilani F, et al. Subretinal hyperreflective material imaged with optical coherence tomography angiography. Am J Ophthalmol. 2016;169:235–48.

57. El Ameen A, Cohen SY, Semoun O, et al. Type 2 neovascularization secondary to age-related macular degeneration imaged by optical coherence tomography angiography. Retina. 2015;35:2212–8.

58. Souied EH, Miere A, Cohen SY, et al. Optical coherence tomography angiography of fibrosis in age-related macular degeneration. Dev Ophthalmol. 2016;56:86–90.

59. Cheung CMG, Lai TYY, Ruamviboonsuk P, et al. Polypoidal choroidal vasculopathy: definition, pathogenesis, diagnosis, and management. Ophthalmology. 2018;125:708–24.

60. Kuehlewein L, Dansingani KK, De Carlo TE, et al. Optical coherence tomography angiography of type 3 neovascularization secondary to age-related macular degeneration. Retina. 2015;35:2229–35.

61. Bonini Filho MA, De Carlo TE, Ferrara D, et al. Association of choroidal neovascularization and central serous chorioretinopathy with optical coherence tomography angiography. JAMA Ophthalmol. 2015;133:899–906.

62. de Carlo TE, Romano A, Waheed NK, Duker JS. A review of optical coherence tomography angiography (OCTA). Int J Retin Vitr. 2015;1:5.

63. Coscas GJ, Lupidi M, Coscas F, et al. Optical coherence tomography angiography versus traditional multimodal imaging in assessing the activity of exudative age-related macular degeneration: a new diagnostic challenge. Retina. 2015;35:2219–28.

64. Lumbroso B, Rispoli M, Savastano MC. Longitudinal optical coherence tomography-angiography study of type 2 naive choroidal neovascularization early response after treatment Optical Coherence Tomography View project. Artic Retin. 2015; https://doi.org/10.1097/IAE.0000000000000879.

65. Marques JP, Costa JF, Marques M, et al. Sequential morphological changes in the CNV net after intravitreal anti-VEGF evaluated with OCT angiography. Ophthalmic Res. 2016;55:145–51.

66. Bhutto I, Lutty G. Understanding age-related macular degeneration (AMD): relationships between the photoreceptor/retinal pigment epithelium/Bruch's membrane/choriocapillaris complex. Mol Asp Med. 2012;33:295–317.

67. Dansingani KK, Balaratnasingam C, Klufas MA, et al. Optical coherence tomography angiography of shallow irregular pigment epithelial detachments in pachychoroid spectrum disease. Am J Ophthalmol. 2015;160:1243–54.e2

68. De Carlo TE, Kokame GT, Kaneko KN, et al. Sensitivity and specificity of detecting polypoidal choroidal vasculopathy with en face optical coherence tomography and optical coherence tomography angiography. Retina. 2019;39:1343–52.

69. Tan CS, Hariprasad SM, Lim LW. New paradigms in polypoidal choroidal vasculopathy management: the impact of recent multicenter, randomized clinical trials. Ophthalmic Surg Lasers Imaging Retin. 2018;49:4–10.

70. Tan CS, Lim TH, Hariprasad SM. Current management of polypoidal choroidal vasculopathy. Ophthalmic Surg Lasers Imaging Retin. 2015;46:786–91.

71. Chi Y-T, Yang C-H, Cheng C-K. Optical coherence tomography angiography for assessment of the 3-dimensional structures of polypoidal choroidal vasculopathy. JAMA Ophthalmol. 2017;135:1310–6.

72. Kawamura A, Yuzawa M, Mori R, et al. Indocyanine green angiographic and optical coherence tomographic findings support classification of polypoidal choroidal vasculopathy into two types. Acta Ophthalmol. 2013;91:e474–81.

73. Srour M, Querques G, Semoun O, et al. Optical coherence tomography angiography characteristics of polypoidal choroidal vasculopathy. Br J Ophthalmol. 2016;100:1489–93.

74. Takayama K, Ito Y, Kaneko H, et al. Comparison of indocyanine green angiography and optical coherence tomographic angiography in polypoidal choroidal vasculopathy. Eye. 2017;31:45–52.

75. Tanaka K, Mori R, Kawamura A, et al. Comparison of OCT angiography and indocyanine green angiographic findings with subtypes of polypoidal choroidal vasculopathy. Br J Ophthalmol. 2017;101:51–5.

76. Cheung CMG, Yanagi Y, Akiba M, et al. Improved detection and diagnosis of polypoidal choroidal vasculopathy using a combination of optical coherence tomography and optical coherence tomography angiography. Retina. 2019;39:1655–63.

77. Huang Y-M, Hsieh M-H, Li A-F, Chen S-J. Sensitivity, specificity, and limitations of optical coherence tomography angiography in diagnosis of polypoidal choroidal vasculopathy. J Ophthalmol. 2017;2017:3479695.

78. Choi W, Waheed NK, Moult EM, et al. Ultrahigh speed swept source optical coherence tomography angiography of retinal and choriocapillaris alterations in diabetic patients with and without retinopathy. Retina. 2017;37:11–21.

79. Hwang TS, Jia Y, Gao SS, et al. Optical coherence tomography angiography features of diabetic retinopathy. Retina. 2015;35:2371–6.

80. Ishibazawa A, Nagaoka T, Takahashi A, et al. Optical coherence tomography angiography in diabetic retinopathy: a prospective pilot study. Am J Ophthalmol. 2015;160:35–44.e1

81. Matsunaga DR, Yi JJ, De Koo LO, et al. Optical coherence tomography angiography of diabetic retinopathy in human subjects. Ophthalmic Surg Lasers Imaging Retin. 2015;46:796–805.

82. Parravano M, De Geronimo D, Scarinci F, et al. Diabetic microaneurysms internal reflectivity on spectral-domain optical coherence tomography and optical coherence tomography angiography detection. Am J Ophthalmol. 2017;179:90–6.

83. de Carlo TE, Chin AT, Bonini Filho MA, et al. Detection of microvascular changes in eyes of patients with diabetes but not clinical diabetic retinopathy using optical coherence tomography angiography. Retina. 2015;35:2364–70.

84. Salz DA, De Carlo TE, Adhi M, et al. Select features of diabetic retinopathy on swept-source optical coherence tomographic angiography compared with fluorescein angiography and normal eyes. JAMA Ophthalmol. 2016;134:644–50.

85. Couturier A, Mané V, Bonnin S, et al. Capillary plexus anomalies in diabetic retinopathy on optical coherence tomography angiography. Retina. 2015;35:2384–91.

86. Hwang TS, Miao Z, Bhavsar K, et al. Visualization of 3 distinct retinal plexuses by projection-resolved optical coherence tomography angiography in diabetic retinopathy. JAMA Ophthalmol. 2016;134:1411–9.

87. Agemy SA, Scripsema NK, Shah CM, et al. Retinal vascular perfusion density mapping using optical coherence tomography angiography in normals and diabetic retinopathy patients. Retina. 2015;35:2353–63.

88. Tan CS, Lim LW, Chow VS, et al. Optical coherence tomography angiography evaluation of the parafoveal vasculature and its relationship with ocular factors. Invest Ophthalmol Vis Sci. 2016;57:224–34.

89. Di G, Weihong Y, Xiao Z, et al. A morphological study of the foveal avascular zone in patients with diabetes mellitus using optical coherence tomography angiography. Graefes Arch Clin Exp Ophthalmol. 2016;254:873–9.

90. Freiberg FJ, Pfau M, Wons J, et al. Optical coherence tomography angiography of the foveal avascular zone in diabetic retinopathy. Graefes Arch Clin Exp Ophthalmol. 2016;254:1051–8.

91. Takase N, Nozaki M, Kato A, et al. Enlargement of foveal avascular zone in diabetic eyes evaluated by en face optical coherence tomography angiography. Retina. 2015;35:2377–83.

92. Zhang M, Hwang TS, Dongye C, et al. Automated quantification of nonperfusion in three retinal plexuses using projection-resolved optical coherence tomography angiography in diabetic retinopathy. Invest Ophthalmol Vis Sci. 2016;57:5101–6.

93. Moein HR, Novais EA, Rebhun CB, et al. Optical coherence tomography angiography to detect macular capillary ischemia in patients with inner retinal

changes after resolved diabetic macular edema. Retina. 2018;38:2277–84.

94. Hasegawa N, Nozaki M, Takase N, et al. New insights into microaneurysms in the deep capillary plexus detected by optical coherence tomography angiography in diabetic macular edema. Invest Ophthalmol Vis Sci. 2016;57:OCT348–55.

95. de Carlo TE, Chin AT, Joseph T, et al. Distinguishing diabetic macular edema from capillary nonperfusion using optical coherence tomography angiography. Ophthalmic Surg Lasers Imaging Retina. 2016;47:108–14.

96. Kashani AH, Green KM, Kwon J, et al. Suspended scattering particles in motion: a novel feature of OCT angiography in exudative maculopathies. Ophthalmol Retin. 2018;2:694–702.

97. Lee J, Moon BG, Cho AR, Yoon YH. Optical coherence tomography angiography of DME and its association with anti-VEGF treatment response. Ophthalmology. 2016;123(11) Elsevier Inc.,:2368–75.

98. Kashani AH, Lee SY, Moshfeghi A, et al. Optical coherence tomography angiography of retinal venous occlusion. Retina. 2015;35:2323–31.

99. Rispoli M, Savastano MC, Lumbroso B. Capillary network anomalies in branch retinal vein occlusion on optical coherence tomography angiography. Retina. 2015;35:2332–8.

100. Nobre Cardoso J, Keane PA, Sim DA, et al. Systematic evaluation of optical coherence tomography angiography in retinal vein occlusion. Am J Ophthalmol. 2016;163:93–107.e6

101. Coscas F, Glacet-Bernard A, Miere A, et al. Optical coherence tomography angiography in retinal vein occlusion: evaluation of superficial and deep capillary plexa. Am J Ophthalmol. 2016;161:160–71.e2

102. Sarraf D, Rahimy E, Fawzi AA, et al. Paracentral acute middle maculopathy a new variant of acute macular neuroretinopathy associated with retinal capillary ischemia. JAMA Ophthalmol. 2013;131:1275–87.

103. Rahimy E, Kuehlewein L, Sadda SR, Sarraf D. Paracentral acute middle maculopathy what we knew then and what we know now. Retina. 2015;35:1921–30.

104. Nemiroff J, Kuehlewein L, Rahimy E, et al. Assessing deep retinal capillary ischemia in paracentral acute middle maculopathy by optical coherence tomography angiography. Am J Ophthalmol. 2016;162:121–32.e1

105. Phasukkijwatana N, Rahimi M, Iafe N, Sarraf D. Central retinal vein occlusion and paracentral acute middle maculopathy diagnosed with en face optical coherence tomography. Ophthalmic Surg Lasers Imaging Retin. 2016;47:862–4.

106. Sridhar J, Shahlaee A, Rahimy E, et al. Optical coherence tomography angiography and en face optical coherence tomography features of paracentral acute middle maculopathy. Am J Ophthalmol. 2015;160:1259–68.e2

107. Yu S, Pang CE, Gong Y, et al. The spectrum of superficial and deep capillary ischemia in retinal artery occlusion. Am J Ophthalmol. 2015;159:53–63. e1–2

108. Bakhoum MF, Freund KB, Dolz-Marco R, et al. Paracentral acute middle maculopathy and the ischemic cascade associated with retinal vascular occlusion. Am J Ophthalmol. 2018;195:143–53.

109. McLeod D, Beatty S. Evidence for an enduring ischaemic penumbra following central retinal artery occlusion, with implications for fibrinolytic therapy. Prog Retin Eye Res. 2015;49:82–119.

110. Christenbury JG, Klufas MA, Sauer TC, Sarraf D. OCT angiography of paracentral acute middle maculopathy associated with central retinal artery occlusion and deep capillary ischemia. Ophthalmic Surg Lasers Imaging Retin. 2015;46:579–81.

111. Khan MA, Rahimy E, Shahlaee A, et al. En face optical coherence tomography imaging of deep capillary plexus abnormalities in paracentral acute middle maculopathy. Ophthalmic Surg Lasers Imaging Retin. 2015;46:972–5.

112. Maltsev DS, Kulikov AN, Burnasheva MA, Chhablani J. Prevalence of resolved paracentral acute middle maculopathy lesions in fellow eyes of patients with unilateral retinal vein occlusion. Acta Ophthalmol. 2020;98:e22–8.

113. Bonini Filho MA, Adhi M, de Carlo TE, et al. Optical coherence tomography angiography in retinal artery occlusion. Retina. 2015;35:2339–46.

114. Dingerkus VLS, Munk MR, Brinkmann MP, et al. Optical coherence tomography angiography (OCTA) as a new diagnostic tool in uveitis. J Ophthalmic Inflamm Infect. 2019;9:10.

115. Dutheil C, Korobelnik JF, Delyfer MN, Rougier MB. Optical coherence tomography angiography and choroidal neovascularization in multifocal choroiditis: a descriptive study. Eur J Ophthalmol. 2018;28:614–21.

116. Patel RC, Gao SS, Zhang M, et al. Optical coherence tomography angiography of choroidal neovascularization in four inherited retinal dystrophies. Retina. 2016;36:2339–47.

117. Pichi F, Sarraf D, Arepalli S, et al. The application of optical coherence tomography angiography in uveitis and inflammatory eye diseases. Prog Retin Eye Res. 2017;59:178–201.

118. Türkcü FM, Şahin A, Yüksel H, et al. OCTA Imaging of choroidal neovascular membrane secondary to toxoplasma retinochoroiditis. Ophthalmic Surg Lasers Imaging Retina. 2017;48:509–11.

119. Battaglia Parodi M, Cicinelli MV, Rabiolo A, et al. Vascular abnormalities in patients with Stargardt disease assessed with optical coherence tomography angiography. Br J Ophthalmol. 2017;101:780–5.

120. Arrigo A, Romano F, Aragona E, et al. OCTA-Based identification of different vascular patterns in Stargardt disease. Transl Vis Sci Technol. 2019;8:26.

121. Müller PL, Pfau M, Möller PT, et al. Choroidal flow signal in late-onset stargardt disease and age-related macular degeneration: an OCT-angiography study. Invest Ophthalmol Vis Sci. 2018;59:AMD122–31.

122. Wang JC, Laíns I, Sobrin L, Miller JB. Distinguishing white dot syndromes with patterns of choroidal hypoperfusion on optical coherence tomography angiography. Ophthalmic Surg Lasers Imaging Retina. 2017;48:638–46.

123. Park SS, Thinda S, Kim DY, et al. Phase-variance optical coherence tomographic angiography imaging of choroidal perfusion changes associated with acute posterior multifocal placoid pigment epitheliopathy. JAMA Ophthalmol. 2016;134:943–5.

124. Ong SS, Patel TP, Singh MS. Optical coherence tomography angiography imaging in inherited retinal diseases. J Clin Med. 2019;8:2078.

Optical Coherence Tomography of the Vitreoretinal Interface

5

Wei Kiong Ngo and Colin S. Tan

5.1 Introduction

The advent of optical coherence tomography in the early 1990s [1] has revolutionised the field of ophthalmology and has given us images of the human eye which are of unprecedented detail and clarity. The cross-sectional images generated are analogous to histologic equivalents of living eye tissue. These scans give far superior details and information on the structures within the eye compared to what traditional biomicroscopy offers.

Optical coherence tomography imaging is especially useful in the diagnosis and management of vitreoretinal interface diseases. The relationship of the vitreous with regards to the retina, the presence of anomalous posterior vitreous detachment and the cross-sectional appearance of the retina are essential considerations in the man-

agement of vitreoretinal interface diseases. Such details are not easily appreciated on biomicroscopy. Serial scans on optical coherence tomography also allow monitoring of disease progression. Optical coherence tomography has since become gold standard in the diagnosis and evaluation of vitreoretinal interface diseases.

The use of optical coherence tomography for vitreoretinal interface disease still has limitations. Media opacity limits the scan signal strength and resolution, and focal disease may be missed if the interval distance between line scans is too large.

Enhanced depth imaging optical coherence tomography is a technique available on commercially available spectral-domain optical coherence tomography machines for the visualisation of deep retinal and/or choroidal structures [2]. Although this technique gives superior choroidal images, the vitreoretinal interface is best visualised on scans without enhanced depth imaging [3].

W. K. Ngo

National Healthcare Group Eye Institute, Tan Tock Seng Hospital, Singapore, Singapore

Fundus Image Reading Center, National Healthcare Group Eye Institute, Singapore, Singapore

C. S. Tan (✉)
National Healthcare Group Eye Institute, Tan Tock Seng Hospital, Singapore, Singapore

Fundus Image Reading Center, National Healthcare Group Eye Institute, Singapore, Singapore

Duke-NUS Medical School, Singapore, Singapore

Lee Kong Chian School of Medicine, Nanyang Technological University, Singapore, Singapore

5.2 Posterior Vitreous Detachment

The human vitreous gel is initially solid during infancy and in the early years of life [4–6]. Two factors result in posterior vitreous detachment, which typically occurs as one ages. First, liquefaction and syneresis of the vitreous gel occur.

Second, there is age-related weakening of the adhesions between the internal limiting membrane of the neurosensory retina and the cortical vitreous. With enough liquefaction of the vitreous gel and weakening of the vitreoretinal adhesions, liquid vitreous enters the retrohyaloid space. The liquid cleaves a plane and separates the cortical vitreous from the internal limiting membrane (Fig. 5.1). Subsequent collapse and pulling away of the vitreous gel from the retinal surface result in posterior vitreous detachment [4–6]. Occasionally, splitting between layers of the posterior vitreous cortex (vitreoschisis) results in a thin remnant layer of cortical vitreous still attached to the neurosensory retina [7].

Improvement in optical coherence tomography technology allowed high-resolution cross-sectional imaging of the vitreoretinal interface and gave us new understanding of the evolution of age-related posterior vitreous detachment. Using optical coherence tomography, Johnson [7] described the evolution and staged age-related posterior vitreous detachment:

- Stage 1: perifoveal posterior vitreous detachment with residual vitreofoveal adhesion (Fig. 5.2).
- Stage 2: macular posterior vitreous detachment no vitreofoveal adhesion.
- Stage 3: near-complete posterior vitreous detachment with only vitreopapillary adhesion remaining (Fig. 5.3).
- Stage 4: complete posterior vitreous detachment.

Fig. 5.1 Early posterior vitreous detachment occurring around the macula region
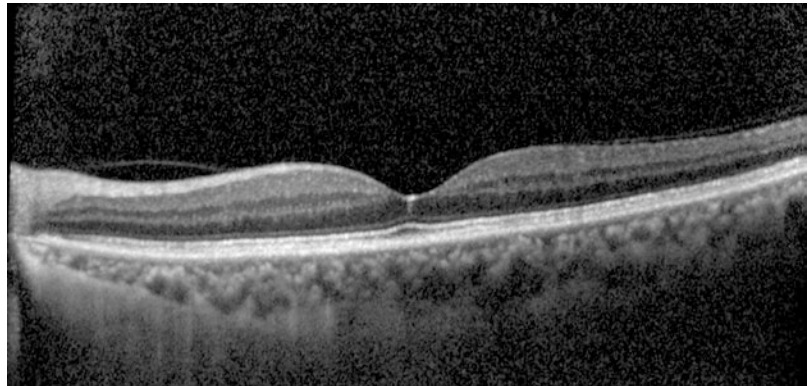
Fig. 5.2 Stage 1 PVD showing perifoveal PVD with residual vitreofoveal attachment of vitreous
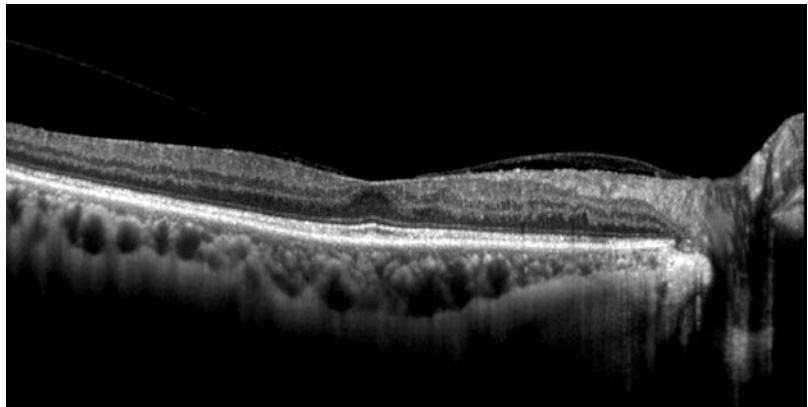
Fig. 5.3 Stage 3 PVD showing almost complete PVD with only vitreopapillary attachment remaining
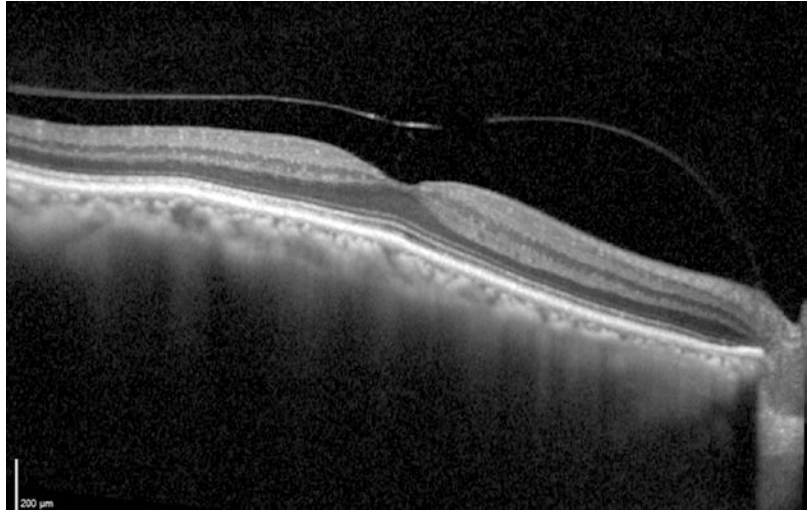
5.3   Anomalous Posterior Vitreous Detachment

As discussed earlier, two factors are implicated in age-related posterior vitreous detachment. Anomalous posterior vitreous detachment [8, 9] occurs when there is an imbalance of the two factors. Higher degree of liquefaction of the vitreous gel in relationship to the age-related weakening of the vitreoretinal adhesions results in anomalous posterior vitreous detachment and undue traction on the neurosensory retina. This is thought to be the underlying pathophysiological cause of various vitreomacular diseases which will be described later in the chapter [10].

5.4   Vitreomacular Adhesion

Incomplete separation of the cortical vitreous and resultant traction on the neurosensory retina/macula (anomalous posterior vitreous detachment) results in a spectrum of vitreomacular diseases [7–12].

The International Vitreomacular Traction Study (IVTS) Group [13] described the optical coherence tomography definition of vitreomacular adhesion. Vitreomacular adhesion is defined by an elevation of the cortical vitreous above the retinal surface, with remaining vitreous attached within an arbitrarily defined 3-mm radius around the fovea. An acute angle between the vitreous and the inner retinal surface is noted. The retina should display no change in contour or morphologic features on optical coherence tomography because of the vitreous adhesion.

Vitreomacular adhesion can be further subdivided based on the extent of the adhesion into *focal* (<1500 μm) (Fig. 5.4) or *broad* (>1500 μm). Finally, vitreomacular adhesions are referred to as *isolated* when there is no associated macular disease and *concurrent* when there is any associated macular disease such as age-related macular degeneration, diabetic macular oedema or retinal vein occlusion [14–17].

5.5   Vitreomacular Traction

Anomalous posterior vitreous detachment results in tractional forces on the neurosensory retina [7–12]. Prolonged traction results in anatomical changes in the normal contour of the foveal surface. When perifoveal posterior vitreous detachment is associated with abnormal anatomical changes of the retina, the eye is characterised as having vitreomacular traction [7, 8, 10, 18–20].

The IVTS Group [13] provided the optical coherence tomographic definition of vitreomacular traction. All the following criteria must be apparent on at least one optical coherence tomography B-scan image:

Fig. 5.4 Focal vitreomacular adhesion is shown here. The retina preserves its morphological appearance anatomically. The vitreous and the inner retinal surface forms an acute angle, differentiating it from early-stage PVD
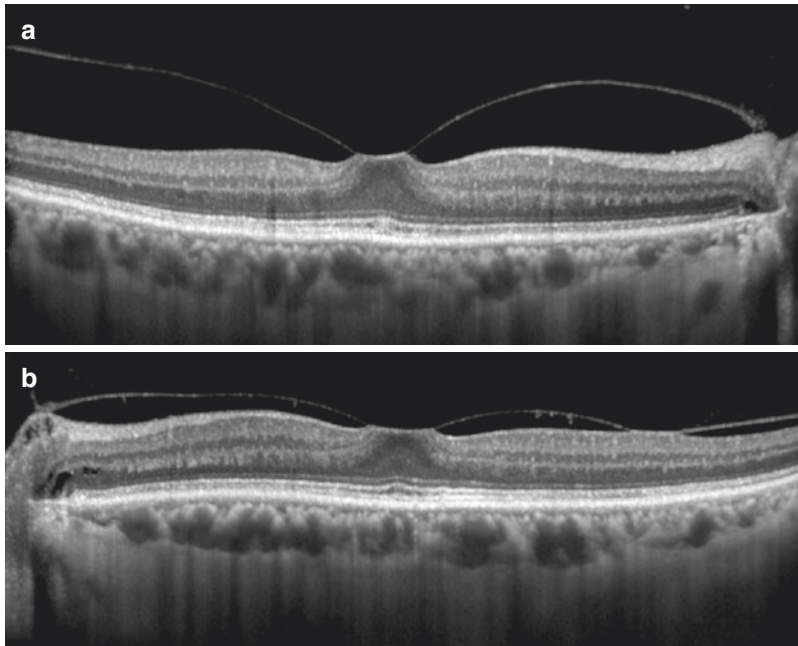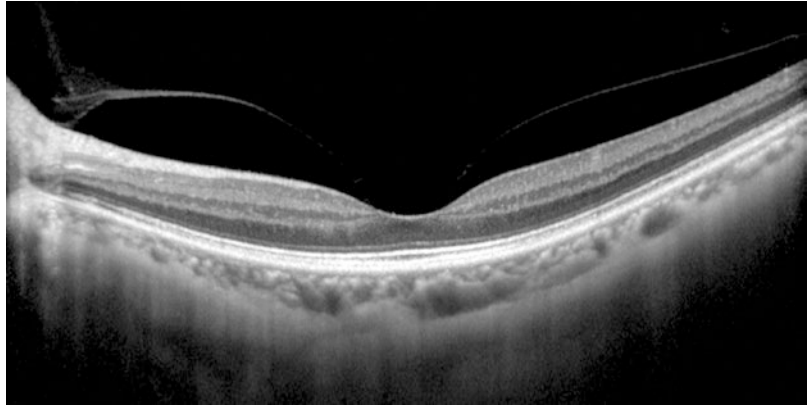
Fig. 5.5 (**a**) Focal vitreomacular traction with resultant elevation and distortion of the fovea contour. There is associated elevation of the inner retinal layers but the outer retinal layers are preserved. No intraretinal cystic changes are seen in this scan. (**b**) In this image, two separate areas of focal vitreomacular traction are seen, first at the fovea and the other temporal to the fovea. Again, there is elevation and disruption to the fovea contour. At both areas of traction, there is abnormal flattening of the inner retinal contour with slight elevation of the inner retinal layers

1. Perifoveal vitreous cortex detachment from the retinal surface.
2. Macular attachment of the vitreous cortex within a 3-mm radius around the fovea.
3. Association of attachment with distortion of the foveal surface, intraretinal structural changes, elevation of the fovea above the RPE, or a combination thereof, but no full-thickness interruption of all retinal layers.

Like vitreomacular adhesion, vitreomacular traction can be further classified as *focal* (<1500 μm) (Fig. 5.5a, b) or *broad* (>1500 μm) [13]. Focal traction at the fovea (vitreofoveal traction) results in elevation and distortion of the foveal contour with formation of pseudocysts. After release of the traction, the pseudocysts generally resolve over time with little residual visual deficit. Broad vitreomacular traction

Fig. 5.6 55° OCT segment showing vitreopapillary traction. Note the acute angle the vitreous makes with the edges of the optic disc and elevation of the retinal nerve fibre layer
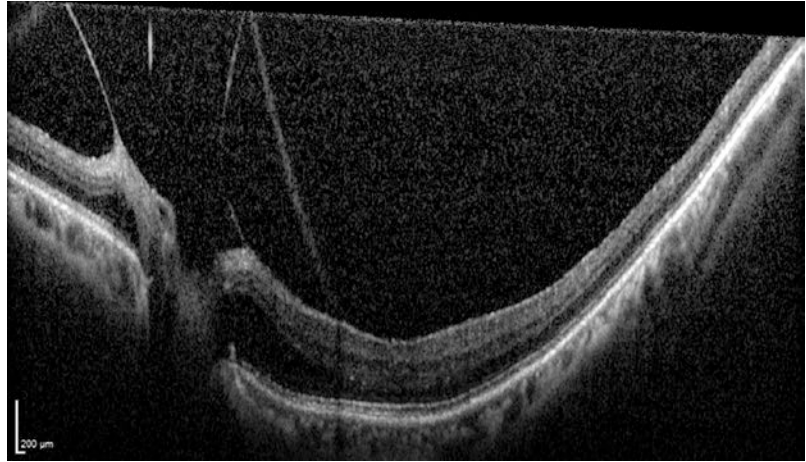
causes generalised macular thickening, macular schisis, cystoid macular oedema with resultant vascular leakage on fluorescein angiography [10, 13, 19, 20].

In addition, the vitreous may be adherent and cause traction to the margins of the optic disc, a condition referred to as vitreopapillary traction (Fig. 5.6). This may occur independently or coexist with vitreomacular or vitreofoveal traction.

5.6 Epiretinal Membrane

With progressive posterior vitreous detachment, residual vitreous tissue is often left on the inner retinal surface due to vitreoschisis. The residual vitreous may proliferate and form an epiretinal membrane. Epiretinal membranes are composed primarily of extracellular matrix (collagen, laminin, fibronectin, etc.) and cellular components (glial cells, retinal pigment epithelium, fibrocytes, etc.). With continual cellular proliferation and contracture, macular traction and stress on the underlying retina lead to distortion in the fovea architecture and cystoid macular oedema [21–23].

A clinical grading system was proposed by Gass to describe the different stages of the disease. In grade 0 (cellophane maculopathy), there is a translucent membrane with no underlying retinal distortion. In grade 1, the epiretinal membrane is associated with irregular wrinkling of the inner retina (Fig. 5.7a). In grade 2, there is an opaque membrane leading to obscuration of the retinal vessels and significant full-thickness retinal distortion. However, to date, there is no widely practised OCT classification of epiretinal membranes.

OCT has an exceptionally high sensitivity in identifying epiretinal membranes (Fig. 5.7b, c). Besides identifying the membrane, OCT also gives us additional information on the underlying retina. OCT can detect the presence of associated cystoid macular oedema (Fig. 5.8), macular pseudohole, lamellar hole or less commonly full-thickness macular hole. OCT also detects any disruption to the underlying retinal photoreceptor layers, which predicts visual prognosis with management [24–27]. These additional findings on OCT aid in our surgical decision-making.

5.7 Full-Thickness Macular Hole

A macular hole is a round, full-thickness defect of the retinal layers from the internal limiting membrane to the retinal pigment epithelium, usually at the fovea centre. It usually results from abnormal vitreofoveal tractional forces causing the formation and breakdown of cystoid spaces as well as elevation and breakdown of the retina tissue (Fig. 5.9a) [18]. Acute full thickness macula holes tend to have an hourglass shape due to the presence of intraretinal oedema at the edges
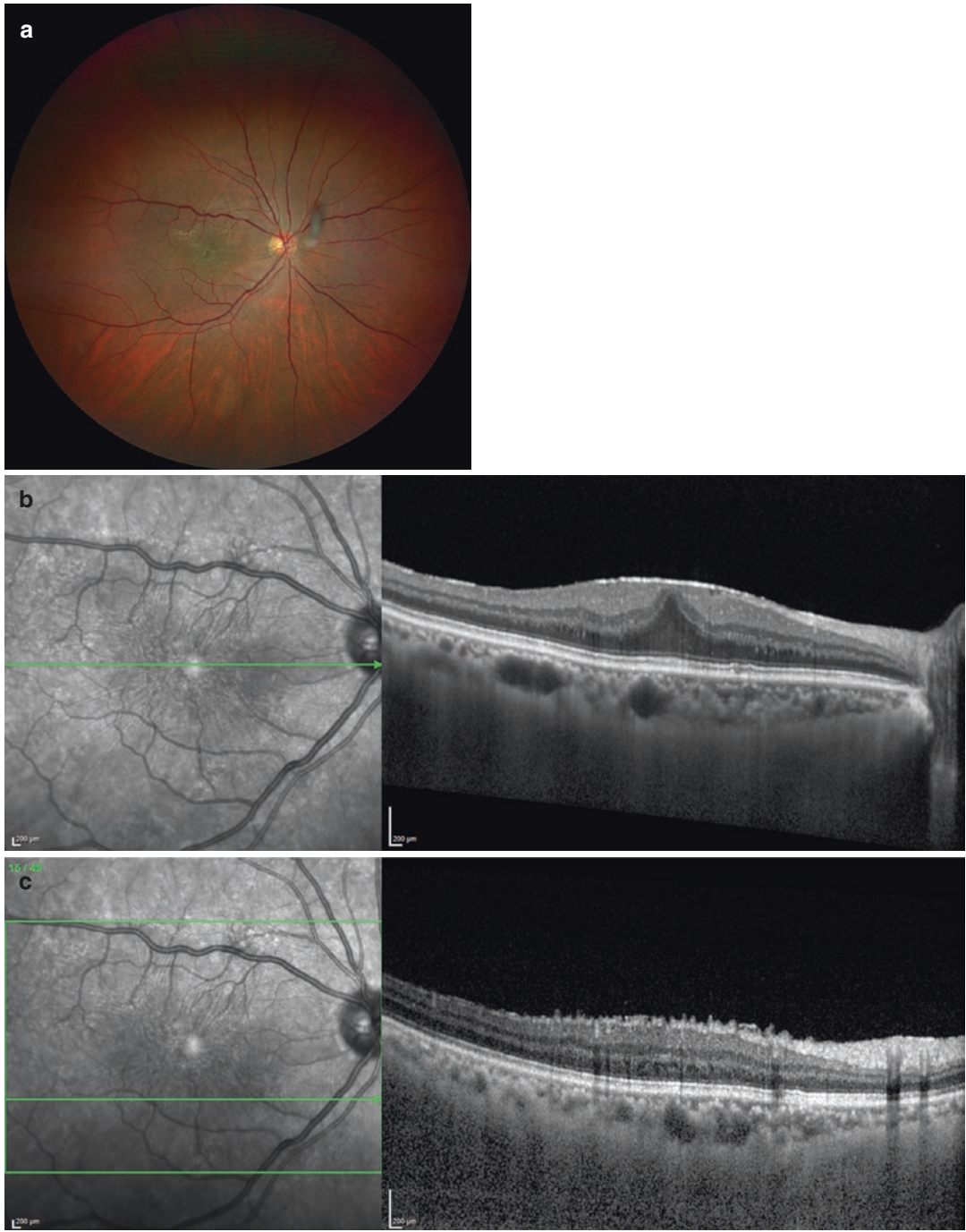
Fig. 5.7 (**a**) Fundus photograph showing an epiretinal membrane. Note the puckering of the retina caused by the membrane with resultant increase tortuosity of the fine retinal vessels. There is also the appearance of a macular pseudohole, which is difficult to differentiate from a lamellar hole or a full-thickness hole on biomicroscopy alone. (**b**) In the same patient, the infrared image clearly illustrates the retinal puckering caused by the dense epiretinal membrane. On the OCT image, the epiretinal membrane is seen as a dense hyperreflective line, which at times may obscure the inner limiting membrane. The fovea contour is lost and there is elevation of the inner retinal layers. (**c**) The off-centred OCT segment shows puckering of the retina associated with the epiretinal membrane. Instead of a smooth inner retinal surface, the surface is thrown into a series of jagged saw-tooth appearance

Fig. 5.8 Epiretinal membrane causing cystoid macular oedema. There is also disruption of the ellipsoid zone and may predict visual outcome after successful vitrectomy with epiretinal membrane peeling
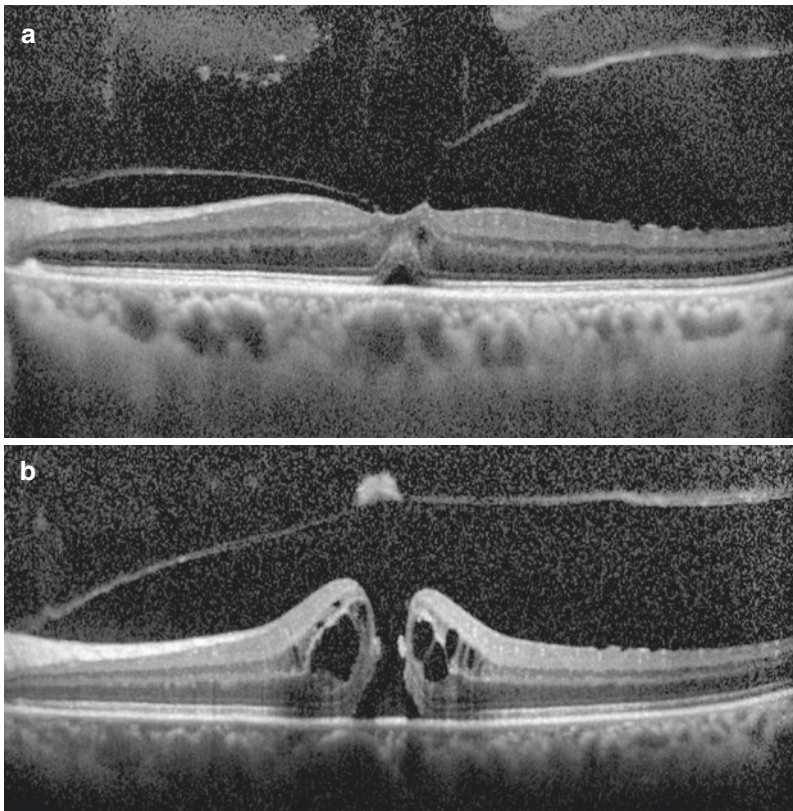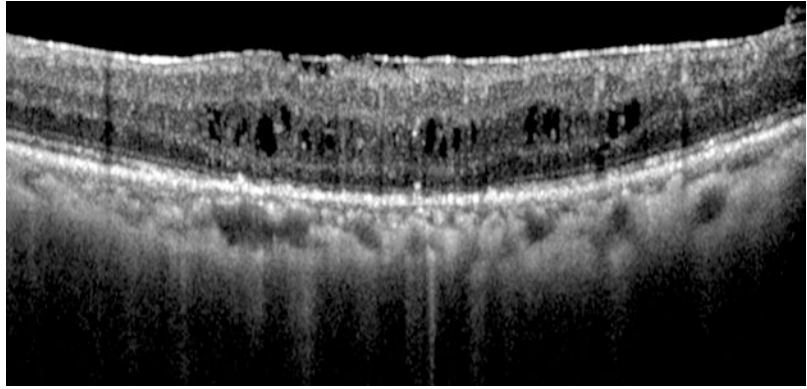
Fig. 5.9 (**a**) Vitreofoveal traction with resultant elevation and disruption of fovea contour. This is associated with retinal pseudocyst and elevation of the ellipsoid zone over the retinal pigment epithelium. (**b**) In the same patient above, a full-thickness macular hole results from continued traction. The hole assumes an hour-glass appearance with intra-retinal cysts and oedema around its margins. There is subsequently spontaneous release of the vitreofoveal traction. (**c**) Following spontaneous release of the vitreofoveal traction, there is spontaneous closure of the full thickness macular hole. (**d**) There is spontaneous bridging of the inner retina with reconstitution of the fovea contour. The ellipsoid zone here still shows disruption and elevation above the retinal pigment epithelium. (**e**) The normal anatomy of the fovea is restored when there is bridging of the ellipsoid zone and reattachment to the retinal pigment epithelium
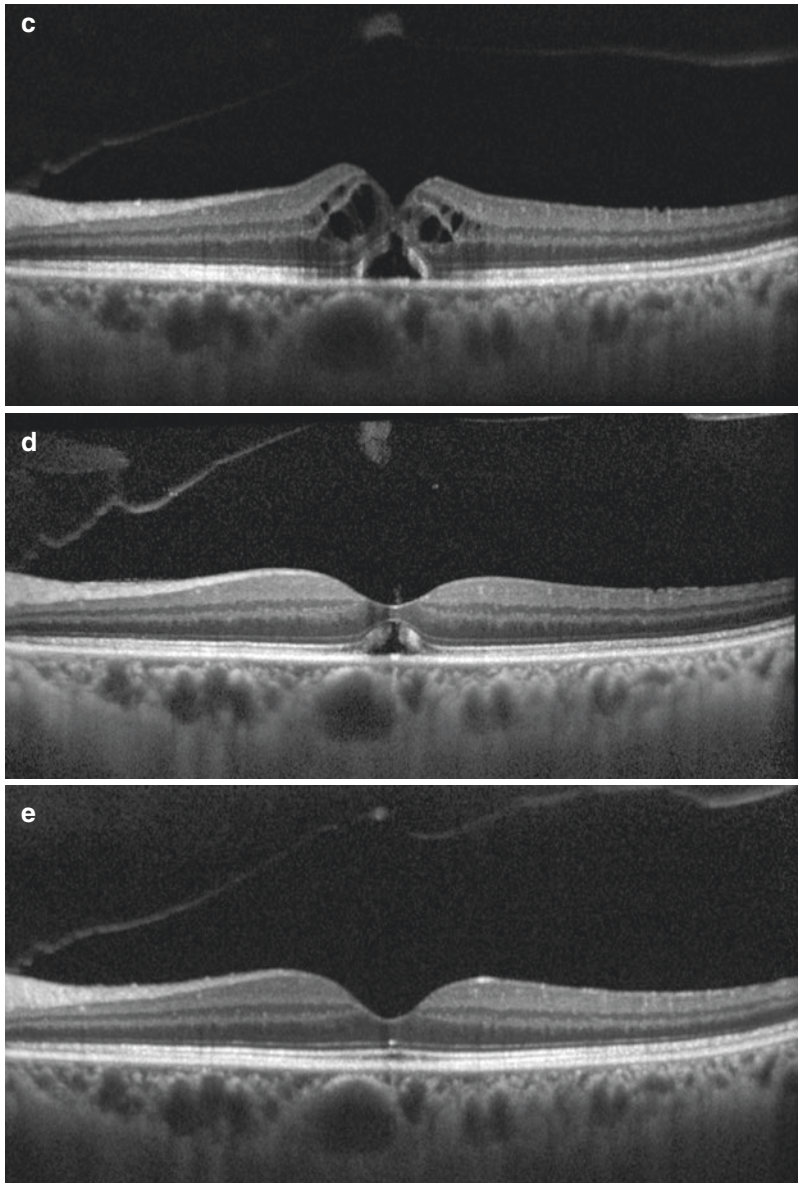
Fig. 5.9 (continued)

of the hole. The edges may also appear to be slightly elevated from the retinal pigment epithelium (Fig. 5.9–e). Over time, the oedema may resolve and the edges flatten back onto the retinal pigment epithelium to assume an inverted Y shape. Macular holes can also be associated with the presence of vitreomacular traction, epiretinal membrane and macular oedema [18, 28–30].

Traditionally, the Gass classification was based on clinical examination and divided the condition into four stages [31, 32]. However, OCT has replaced clinical examination as the gold standard for the diagnosis of macular holes and therefore an OCT-based anatomic classification system would be more informative for our understanding of the pathogenesis and progression of macular holes.

Fig. 5.10 Caliper showing the measurement of the aperture of the macular hole
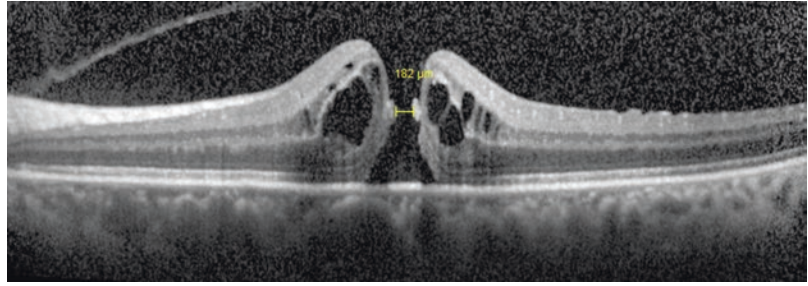
The International Vitreomacular Traction Study Group classification system [13] on macular holes is the most commonly used and has its basis on OCT-observed anatomical features (size of hole, presence or absence of vitreomacular traction) and aetiology (primary or secondary hole). This classification system also aims to predict prognosis in terms of successful hole closure after pharmacological vitreolysis or vitrectomy surgery.

The most important feature of this classification is the size of the hole. The size (or aperture) of the hole is the measurement horizontally (parallel to the retinal pigment epithelium) across the narrowest part of the hole, usually in the mid retinal layers using a caliper on the OCT-viewing software (Fig. 5.10). The size of the hole can be classified as *small* (aperture size of <250 μm), *medium* (aperture size between 250 and 400 μm) and *large* (aperture size more than 400 μm) at the time of diagnosis on OCT. The cut offs of the aperture sizes were derived from studies describing prognosis of macular holes of various sizes [13, 18, 28–30]. Small holes have the best prognosis with a possibility of spontaneous closures, very high rates (almost 100%) of closure with vitrectomy surgery and are most responsive to pharmacological vitreolysis. Medium holes show high rates of closure (>90%) after vitrectomy with or without inner limiting membrane peeling. Vitrectomy without inner limiting membrane peeling for large holes has lower rates of closure (approximately 75%) compared to vitrectomy with inner limiting membrane peeling (90–95%) [13, 18, 28–30].

Macular holes are secondarily categorised based on whether there is presence of vitreomacular traction (vitreous attachment to the edge of the hole). Pharmacological vitreolysis is only considered for macular holes with the presence of vitreomacular traction [20].

Lastly, macular holes may be sub-divided based on their aetiology. *Primary* holes are a result of anomalous posterior vitreous detachment and abnormal vitreofoveal traction forces. *Secondary* holes, on the other hand, result from other pathologies that do not have pre-existing or concurrent vitreofoveal traction. These secondary causes may include blunt trauma, surgical trauma, high myopia, macular schisis, macular telengectasis and lightning strikes. Comparatively, secondary holes usually have poorer prognosis.

5.8 Lamellar Macular Hole

A lamellar macular hole is a partial thickness defect of the retinal layers at the fovea centre. It is distinguished from a full-thickness macular hole by the preservation of the photoreceptor layer. Anatomically, on OCT, a lamellar macular hole classically presents as an irregular defect of the inner retinal layers at the fovea with or without actual tissue loss. There may also be the splitting (schisis) of intraretinal layers typically between the outer plexiform and outer nuclear layers (Fig. 5.11). On biomicroscopy, it appears as a round or oval, well-circumscribed reddish lesion. It is difficult to detect early lamellar macular hole using biomicroscopy alone (Fig. 5.12a) and the OCT has replaced biomicroscopy as the gold standard technique of choice in diagnosing lamellar macular hole (Fig. 5.12b) [13, 33].

The pathophysiology of lamellar macular hole is thought to be related to incomplete

Fig. 5.11 In a high myope, the lamellar macular hole is often accompanied by schisis of the outer nuclear and outer plexiform layers. There is also the presence of an epiretinal membrane. The thin choroid and highly concave inner retinal curvature are also typical of a highly myopic eye
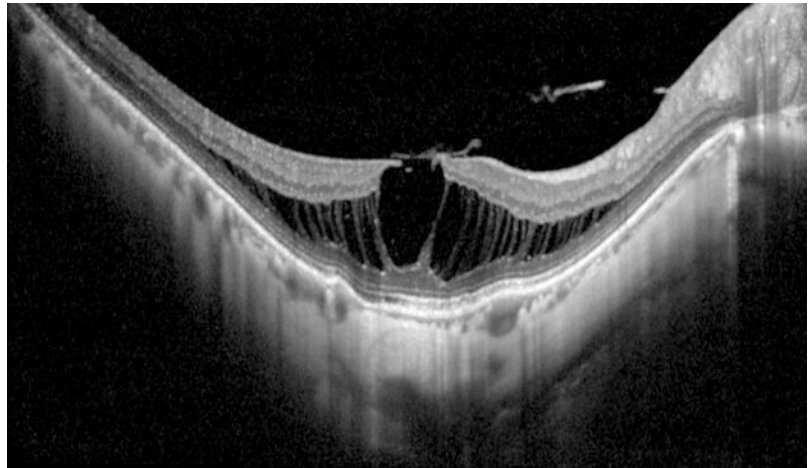
Fig. 5.12 (**a**) Fundus photo illustrates a lamellar macular hole in association with an epiretinal membrane with retinal pucker. On biomicroscopy, it is often difficult to detect a lamellar hole. (**b**) In the same patient, OCT clearly shows the presence of a lamellar macular hole with an associated epiretinal membrane. The lamellar hole is partial thickness and the ellipsoid zone and outer retinal layers are preserved
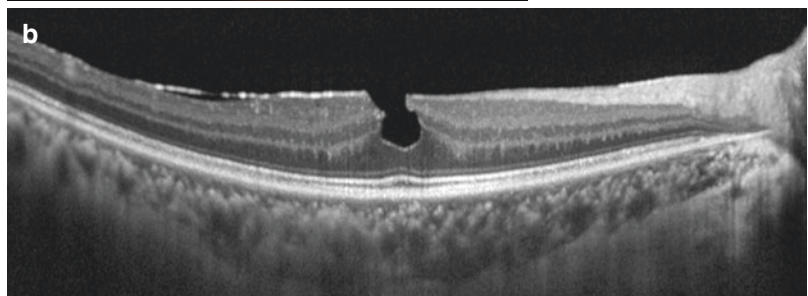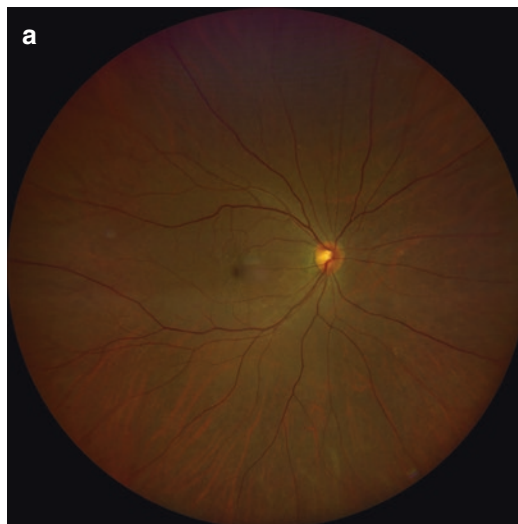
full-thickness macular hole formation, centripetal tractional forces from epiretinal membrane or the deroofing of fovea cysts. Lamellar macular holes usually progress slowly and most patients report mild or no symptoms directly resulting from it. A few patients may report mild metamor-

phopsia and limited central vision loss. However, tangential tractional forces on the lamellar macular hole have been known to result in rapid expansion in its width due to horizontal enlargement from the tractional forces (usually from an epiretinal membrane) (Fig. 5.13a) [33, 34]. Surgical

Fig. 5.13 (**a**) Preoperative OCT image of a patient presenting with epiretinal membrane with resultant tangential tractional force and lamellar hole. There are intraretinal cysts at the margins of the lamellar hole. There is preservation of the ellipsoid zone. An incidental area of chorioretinal atrophic scar is seen nasally. (**b**) At 1 month after a vitrectomy with epiretinal membrane peel, the lamellar macular hole is closed but there is residual intraretinal cysts and oedema
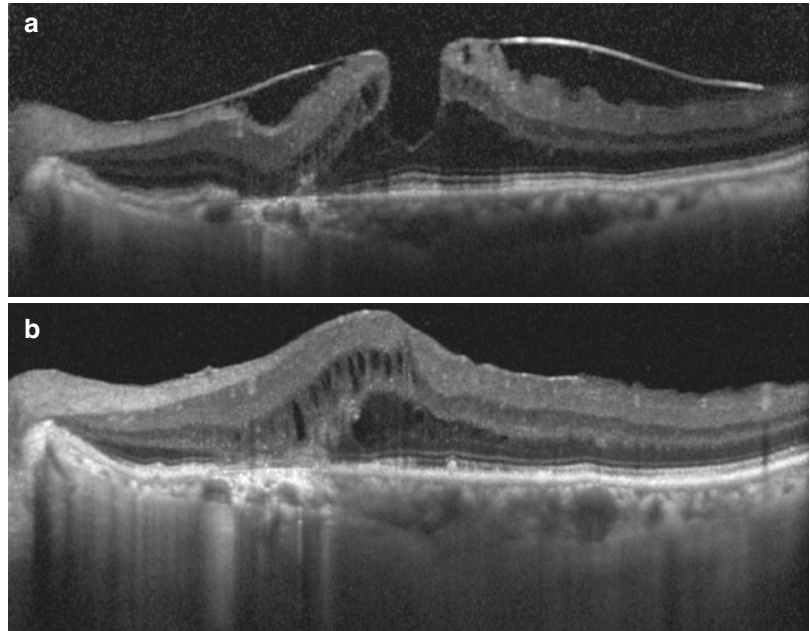
vitrectomy for lamellar macular hole remains controversial and careful patient selection is recommended (Fig. 5.13b) [35].

5.9   Macular Pseudohole

As the name suggests, a macular pseudohole appears as a well-demarcated round or oval reddish lesion at the fovea, very much similar in appearance to a full-thickness macular hole on slit-lamp biomicroscopy [13, 36, 37]. It is often difficult to differentiate on biomicroscopy alone and a pseudohole can result in a false-positive diagnosis of a full-thickness hole. Again, OCT has emerged as the gold standard tool in the diagnosis of a macular pseudohole.

OCT elucidates both the anatomy and the pathophysiology of a macular pseudohole. The presence of an epiretinal membrane on the macular surface distorts the fovea contour into a shape with steep slopes, results in altered light reflex when observing on slit-lamp biomicroscopy. The underlying retina is pulled towards the fovea centre, resulting in the invagination of perifoveal retina into a shape mimicking a hole. A macular pseudohole contains no loss of retinal tissue as observed on OCT (Fig. 5.14) [36, 37].

The macular pseudohole itself results in no visual symptoms. The associated epiretinal membrane, if severe, may result in metamorphopsia and decrease in central vision. If truly symptomatic, a vitrectomy surgery with epiretinal membrane peeling is the procedure of choice, leading to restoration of foveal anatomy and improvement in visual acuity.

5.10   Conclusion

OCT is useful in providing detailed anatomy of the retina at the fovea and elsewhere in the posterior pole. In addition to visualisation of the retina and choroid, it is also useful to visualise the vitreomacular interface and vitreous itself. The findings from OCT provide new insights into the pathophysiology of vitreomacular interface conditions. OCT is also helpful in identifying specific features present at the vitreomacular interface and can diagnose vitreomacular interface pathology more accurately for better management.
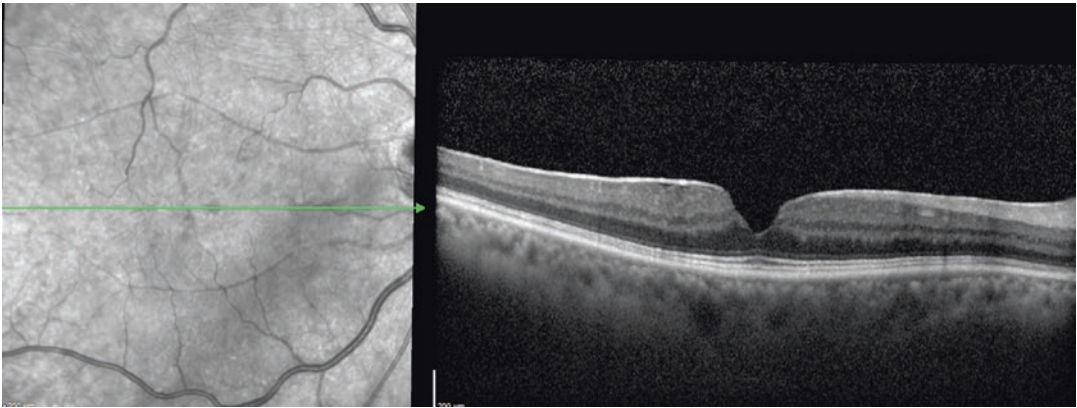
Fig. 5.14 On the infrared image, the epiretinal is seen with associated retinal striae. At the fovea centre, there is a well-demarcated, circular lesion which well resembles a full-thickness macular hole. On the segment of the OCT, however, illustrates that the epiretinal membrane has distorted the normal fovea contour, resulting in steeper fovea slopes resembling a hole on biomicroscopy. There is no actual loss of retinal tissue

References

1. Huang D, Swanson EA, Lin CP, Schuman JS, Stinson WG, Chang W, Hee MR, Flotte T, Gregory K, Puliafito CA, et al. Optical coherence tomography. Science (New York, NY). 1991;254(5035):1178–81.

2. Wong IY, Koizumi H, Lai WW. Enhanced depth imaging optical coherence tomography. Ophthalmic Surg Lasers Imaging. 2011;42(Suppl):S75–84.

3. Verner-Cole EA, Campbell JP, Hwang TS, Klein ML, Lauer AK, Choi D, Bailey ST. Retinal and choroidal imaging with 870-nm spectral-domain OCT compared with 1050-nm spectral-domain OCT, with and without enhanced depth imaging. Transl Vis Sci Technol. 2014;3(3):3.

4. de Smet MD, Gad Elkareem AM, Zwinderman AH. The vitreous, the retinal interface in ocular health and disease. Ophthalmologica Journal international d'ophtalmologie International journal of ophthalmology Zeitschrift fur Augenheilkunde. 2013;230(4):165–78.

5. Fincham GS, James S, Spickett C, Hollingshead M, Thrasivoulou C, Poulson AV, McNinch A, Richards A, Snead D, Limb GA, et al. Posterior vitreous detachment and the posterior hyaloid membrane. Ophthalmology. 2018;125(2):227–36.

6. Snead MP, Snead DR, Mahmood AS, Scott JD. Vitreous detachment and the posterior hyaloid membrane: a clinicopathological study. Eye (Lond). 1994;8(Pt 2):204–9.

7. Johnson MW. Posterior vitreous detachment: evolution and complications of its early stages. Am J Ophthalmol. 2010;149(3):371–82. e371

8. Sebag J. Anomalous posterior vitreous detachment: a unifying concept in vitreo-retinal disease. Graefe's Arch Clin Exp Ophthalmol. 2004;242(8):690–8.

9. Theodossiadis GP, Chatziralli IP, Sergentanis TN, Datseris I, Theodossiadis PG. Evolution of vitreomacular adhesion to acute vitreofoveal separation with special emphasis on a traction-induced foveal pathology. A prospective study of spectral-domain optical coherence tomography. Graefe's Arch Clin Exp Ophthalmol. 2015;253(9):1425–35.

10. Bottos JM, Elizalde J, Rodrigues EB, Maia M. Current concepts in vitreomacular traction syndrome. Curr Opin Ophthalmol. 2012;23(3):195–201.

11. Jackson TL, Nicod E, Simpson A, Angelis A, Grimaccia F, Kanavos P. Symptomatic vitreomacular adhesion. Retina (Philadelphia, PA). 2013;33(8):1503–11.

12. Stalmans P, Duker JS, Kaiser PK, Heier JS, Dugel PU, Gandorfer A, Sebag J, Haller JA. Oct-based interpretation of the vitreomacular interface and indications for pharmacologic vitreolysis. Retina (Philadelphia, PA). 2013;33(10):2003–11.

13. Duker JS, Kaiser PK, Binder S, de Smet MD, Gaudric A, Reichel E, Sadda SR, Sebag J, Spaide RF, Stalmans P. The International Vitreomacular Traction Study Group classification of vitreomacular adhesion, traction, and macular hole. Ophthalmology. 2013;120(12):2611–9.

14. Mojana F, Cheng L, Bartsch DU, Silva GA, Kozak I, Nigam N, Freeman WR. The role of abnormal vitreomacular adhesion in age-related macular degeneration: spectral optical coherence tomography and surgical results. Am J Ophthalmol. 2008;146(2):218–27.

15. Nesmith BL, Palacio AC, Schaal Y, Gupta A, Schaal S. Diabetes alters the magnitude of vit-

reomacular adhesion. Retina (Philadelphia, PA). 2017;37(4):749–52.

16. Krebs I, Brannath W, Glittenberg C, Zeiler F, Sebag J, Binder S. Posterior vitreomacular adhesion: a potential risk factor for exudative age-related macular degeneration? Am J Ophthalmol. 2007;144(5):741–6.

17. Schmidt JC, Mennel S, Meyer CH, Kroll P. Posterior vitreomacular adhesion: a potential risk factor for exudative age-related macular degeneration. Am J Ophthalmol. 2008;145(6):1107. author reply 1107–1108

18. Steel DH, Lotery AJ. Idiopathic vitreomacular traction and macular hole: a comprehensive review of pathophysiology, diagnosis, and treatment. Eye (London, England). 2013;27(Suppl 1):S1–21.

19. Khanani AM, Duker JS, Heier JS, Kaiser PK, Joondeph BC, Kozma P, Rosberger DF, MacCumber M, Boyer DS, Pieramici DJ. Ocriplasmin treatment leads to symptomatic vitreomacular adhesion/vitreomacular traction resolution in the real-world setting: The Phase IV ORBIT Study. Ophthalmol Retina. 2019;3(1):32–41.

20. Wan R, Hong T, Tariq Y, Chang A. Pharmacotherapy of vitreomacular traction. Curr Pharm Des. 2018;24(41):4874–81.

21. Bu SC, Kuijer R, Li XR, Hooymans JM, Los LI. Idiopathic epiretinal membrane. Retina (Philadelphia, PA). 2014;34(12):2317–35.

22. Carpineto P, Ciciarelli V, Borrelli E, Aharrh-Gnama A, Mastropasqua R. Epiretinal membrane in eyes with vitreomacular traction. Retina (Philadelphia, PA). 2019;39(6):1061–5.

23. Johnson MW. Important role of epiretinal membrane in tractional vitreomaculopathies. Retina (Philadelphia, PA). 2019;39(6):1031–2.

24. Garnavou-Xirou C, Xirou T, Gkizis I, Kabanarou SA, Dimitriou E, Theodossiadis P, Chatziralli I. The role of disorganization of retinal inner layers as predictive factor of postoperative outcome in patients with epiretinal membrane. Ophthalmic Res. 2019:1–5.

25. Takagi S, Kudo S, Yokota H, Akiba M, Mandai M, Hirami Y, Takahashi M, Kurimoto Y, Ishida M. Assessment of the deformation of the outer nuclear layer in the Epiretinal membrane using spectral-domain optical coherence tomography. BMC Ophthalmol. 2019;19(1):113.

26. Wilkins JR, Puliafito CA, Hee MR, Duker JS, Reichel E, Coker JG, Schuman JS, Swanson EA, Fujimoto JG. Characterization of epiretinal membranes using optical coherence tomography. Ophthalmology. 1996;103(12):2142–51.

27. Zur D, Iglicki M, Feldinger L, Schwartz S, Goldstein M, Loewenstein A, Barak A. Disorganization of retinal inner layers as a biomarker for idiopathic epiretinal membrane after macular surgery—The DREAM Study. Am J Ophthalmol. 2018;196:129–35.

28. Bikbova G, Oshitari T, Baba T, Yamamoto S, Mori K. Pathogenesis and management of macular hole: review of current advances. J Ophthalmol. 2019;2019:3467381.

29. Chen Q, Liu ZX. Idiopathic Macular Hole: A Comprehensive Review of Its Pathogenesis and of Advanced Studies on Metamorphopsia. J Ophthalmol. 2019;2019:7294952.

30. Singh SR, Hariprasad SM, Narayanan R. Current management of macular hole. Ophthalmic Surg Lasers Imaging Retina. 2019;50(2):61–8.

31. Gass JD. Idiopathic senile macular hole. Its early stages and pathogenesis. Arch Ophthalmol (Chicago, IL 1960). 1988;106(5):629–39.

32. Gass JD. Idiopathic senile macular hole: its early stages and pathogenesis. Retina (Philadelphia, Pa) 2003. 1988;23(6 Suppl):629–39.

33. Frisina R, Pilotto E, Midena E. Lamellar macular hole: state of the art. Ophthalmic Res. 2019;61(2):73–82.

34. Yang YS, Lee JS, Son G, Sohn J. Epiretinal proliferation associated with lamellar hole or macular hole: origin and surgical prognosis. Korean J Ophthalmol. 2019;33(2):142–9.

35. Haritoglou C, Tadayoni R, Hubschman JP. Lamellar macular hole surgery - current concepts, future prospects. Clin Ophthalmol (Auckland, NZ). 2019;13:143–6.

36. Chen JC, Lee LR. Clinical spectrum of lamellar macular defects including pseudoholes and pseudocysts defined by optical coherence tomography. Br J Ophthalmol. 2008;92(10):1342–6.

37. Fish RH, Anand R, Izbrand DJ. Macular pseudoholes. Clinical features and accuracy of diagnosis. Ophthalmology. 1992;99(11):1665–70.

Automated Analysis and Quantification of OCT Images

Sebastian M. Waldstein
and Ursula Schmidt-Erfurth

In retinal imaging, recent advances in hardware instrumentation have only partially been matched by improvements in analysis software. This is particularly true for OCT, where latest generation devices deliver thousands of images in three-dimensional data sets within seconds. Yet, despite the tremendous level of morphologic detail that modern OCTs are able to resolve, retinal surgeons are often left to manually analyze complex three-dimensional data, although modern image analysis methods already allow to interpret and quantify these data in an automated, reproducible manner. This chapter is intended to provide an overview of recent advances in the field of automated OCT analysis, a burgeoning research area that is likely to have a substantial impact on clinical practice in the upcoming near future.

6.1 Principles of Modern Image Analysis

In order to understand the possibilities, chances, and drawbacks associated with the automated analysis of retinal imaging data, the clinician needs to be aware of the basic technical principles of modern image analysis. Recently, a sig-

nificant paradigm shift has occurred from traditional image analysis methods to artificial intelligence approaches based on deep learning, which offers substantial advances, but carries inherent limitations [1]. The following paragraphs outline these basic principles.

6.1.1 Traditional Image Analysis

For many years, the automated analysis of medical imaging data was based on mathematical methods identifying prespecified patterns in images. For instance, an algorithm may try to interpret the transition from dark to bright areas of the image and vice versa as the boundaries between different retinal layers. In general, these image characteristics used by the software method need to be specifically encoded when developing the algorithm [2].

A popular example of this technical approach is the group of graph-theory based segmentation methods [3]. A graph is a mathematical structure used to model pairwise relations between objects. In the context of retinal image analysis, three-dimensional graph models can for instance be used to fit a set of surfaces into an OCT volume. Pre-specified cost functions are assigned trying to minimize cost when fitting the surfaces through the volume (e.g., by penalizing sharp turns of a surface, or too small or large distances between two surfaces). Based on this technology, accurate

S. M. Waldstein (✉) · U. Schmidt-Erfurth
Department of Ophthalmology, Medical University of Vienna, Vienna, Austria
e-mail: sebastian.waldstein@meduniwien.ac.at;
ursula.schmidt-erfurth@meduniwien.ac.at

and reproducible layer segmentation software algorithms have been developed, which are still in clinical use today. The main disadvantage of these methods is that they cannot deal with high variability in the image data. While they work successfully on, for example, normal appearing retina, they will frequently fail in heavily diseased cases because a priori encoded "rules" of the algorithm (e.g., that two boundaries maintain a certain distance) no longer hold true.

6.1.2 Machine Learning and Deep Learning

Advances in computer hardware, particularly in parallel computing, have driven the breakthrough of a new group of image analysis methods based on artificial intelligence in the recent decade. In medical image analysis, most artificial intelligence applications are based on so-called machine learning methods [4]. A specific subtype of machine learning is deep learning, which will be explained further below.

In machine learning, the computer algorithm is presented with a large set of data and associated outputs (e.g., images and a corresponding diagnosis or marking). An artificial intelligence algorithm is then trained to learn the association between the input and output in a purely data-driven way, that is, without relying on a priori encoded information. In classical machine learn-

ing, a set of features is first extracted from an image (including for instance, brightness and texture information or shape descriptors), because the image itself is too complex to serve as the input. The set of quantitative parameters is then fed into a machine learning classifier that matches features with the output. Of course, the classification part of the pipeline will only be successful if the predefined features capture the diagnostically relevant information in the image well (enough). This reliance on human expertise and domain knowledge to define the features represents the main disadvantage of the classical machine learning approach. However, once a functioning algorithm has been obtained, a major advantage is that these algorithms allow easy interpretation of the individual features that contributed to reaching a particular result, and thus allow transparent judgment of their decision-making process.

The current explosion of automated OCT analysis tools is boosted by the increasing popularity of so-called deep learning in medical imaging (Fig. 6.1). In this specific branch of artificial intelligence, the association between an image and a corresponding output is learned "end-to-end," without extracting features from the image beforehand. Deep learning methods are based on artificial neuronal networks that emulate human brain architecture. In the individual neuronal layers of the multilayer architecture of such a network, image characteristics are detected, which are then developed into increasingly abstract rep-

Fig. 6.1 Development of deep learning as a basic principle of medical image analysis. The bar graph shows a count of PubMed listings using the search term "deep learning" since the last 20 years. Since the early 2010s, the use of deep learning in research practice has increased exponentially

Search results for "deep learning" in PubMed
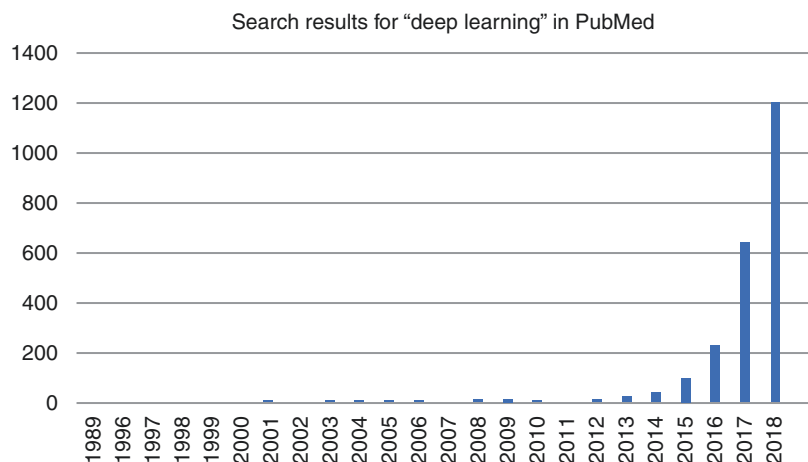
resentations as the information is propagated deeper into the network, resulting in high-level outputs (such as a diagnosis corresponding to an image). The application of these methods became broadly feasible because of (1) easier availability of high-performance computing infrastructure and (2) availability of enormous amounts of annotated natural images in publicly available databases (e.g., image net [5]), which allow pre-training of neuronal networks on general image data and subsequent application on smaller sets of ophthalmic imaging data. Nevertheless, these systems are still extremely data-hungry, as illustrated by a recent article, where an OCT algorithm trained on 15,000 scans was described as requiring much less data than usual [6].

The main advantage of deep learning is the extremely high accuracy that can be achieved, well surpassing traditional machine learning methods. Deep learning is capable to generalize and it can therefore effectively deal with complex, highly variable data. However, in addition to the fact that these methods require huge data sets (which are often expensive or simply not available) to be trained, an important downside is the difficulty to interpret the decision-making process of the algorithm. This "black box" phenomenon has been criticized in the medical community, as fully transparent procedures continue to be an important factor in medical practice [7].

6.2   Targets for Automated Analysis and Quantification

Retinal disease in general and vitreoretinal pathology in particular offer a wealth of potential biomarkers in OCT imaging that can be addressed by automated image analysis. In the following, we describe specific biomarkers where analysis tools are available and their clinical implication.

6.2.1   Automated Diagnosis and Screening

The simplest application of computerized image analysis in the context of retinal OCT lies in the field of automated image-based diagnosis. Similar to the available diagnostic tools for fundus images (which are for instance capable of diagnosing diabetic retinopathy on color photographs [8]), the software has been developed to automatically screen OCT volumes for particular diseases and to triage these into certain categories.

Researchers recently presented a validated algorithm pipeline based on deep learning that could automatically replicate diagnoses and referral decisions in a large-scale, real-world clinical data set of OCT volumes with an accuracy *en par* with retina specialists and exceeding experienced optometrists [6]. The system first detects a set of biomarkers in the OCT images, and subsequently uses the resulting tissue-segmentation maps to predict a diagnosis (normal, choroidal neovascularization, macular edema, macular hole, central serous retinopathy, vitreomacular traction, and geographic atrophy) together with a corresponding referral category (urgent, semi-urgent, routine, and observation only). Other developments addressing screening applications include the automated diagnosis of age-related macular degeneration [9], screening of OCT images for macular edema, macular hole or degenerative disease [10], and screening for disease activity in macular neovascularization [11]. Another recent application involved the automated determination of retreatment indication in the therapy of neovascular age-related macular degeneration [12].

6.2.2   Retinal Layers

The condition of the individual retinal layers and retinal thickness as a summary measure have been among the first targets for automated OCT quantification. Today, most OCT devices offer some degree of layer segmentation in their built-in analysis software. Regarding device-independent software, the Iowa Reference Algorithm is a publicly available, 11-surface layer segmentation method based on a graph-theoretic approach [3]. Due to its encoded a priori constraints, it is not suitable for application in

severely diseased retinas, and will for instance likely fail in a macular hole case. Other recently proposed layer segmentation algorithms have improved capabilities to work correctly in eyes with macular changes [13].

In eyes with vitreoretinal pathology, measuring individual retinal layer thicknesses may be worthwhile to enable a prognostic preoperative evaluation, as the thickness of the inner nuclear layer correlates with tangential retinal displacement and seems to be closely associated with postoperative metamorphopsia scores [14]. Furthermore, evaluation of the ectopia of inner retinal layers has been shown as an important negative prognostic factor in epiretinal membrane surgery [15].

6.2.3   Photoreceptor Changes

The integrity of the photoreceptor layers is an important biomarker in macular disease and particular in epiretinal membrane surgery and retinal detachment repair [16, 17]. Automated quantification of photoreceptor layer thickness and disruption has been attempted previously [3, 18–20]. It is important to note that current automated methods measuring the thickness and integrity of the outer retinal layers may be much less reliable in eyes with severe retinal changes.

6.2.4   Vitreomacular Interface

From the vitreoretinal surgeon's perspective, disappointingly little research has been invested into the quantification of vitreomacular interface changes per se. Using today's computer science methods, it would be well feasible to automatically quantify epiretinal membranes, vitreomacular adhesion and traction, and posterior vitreous detachment.

Automated detection and delineation of the posterior hyaloid interface have been developed previously [21]. A machine learning algorithm enabled reproducible segmentation of the vitreous boundary, resulting in vitreous-ILM distance maps (Fig. 6.2). These maps can be utilized to quickly judge the condition of the vitreomacular interface clinically or to group patients into different categories of partial posterior vitreous detachment (which represents a prognostic factor in intravitreal pharmacotherapy). Using these methods, it would also be possible to measure the degree of traction in eyes with vitreomacular traction syndrome, but thus far this has not been addressed systematically. A recently developed deep learning algorithm was capable of segment epiretinal membranes, although no data were provided on the reproducibility and accuracy of the method with regards to measuring changes at the vitreomacular interface [6].

6.2.5   Retinal Fluid

Many diseases of the vitreoretinal interface give rise to intraretinal changes imposing as intraretinal or subretinal fluid, including a retinoschitic appearance. Today, on a research level, several validated software methods are available to automatically identify retinal fluid, and quantify its amount and location [22–25]. The most extensively studied deep learning algorithm (Fig. 6.3) reproducibly measures intra- and subretinal fluid in two different OCT systems and is validated in eyes with macular degeneration, diabetic macular edema, and retinal vein occlusion [26]. It is likely that some of these fluid measurement algorithms will be integrated into commercially available OCT devices in the near future.

In clinical practice, the measurement of fluid offers several advantages over the simple measurement of retinal thickness that is often performed today. First, in contrast to retinal thickness, the amount of fluid offers some correlation with visual acuity and may serve as a prognostic factor in the therapy of macular disease [27]. However, the prognostic and functional role of fluid in retinal surgical disorders remains to be studied. Second, reproducible measurement of cystoid changes may enable more precise followup in patients with epiretinal membranes or vitreomacular traction, who are observed over sometimes extended periods of time. Third, retinal thickness as a summary measurement may
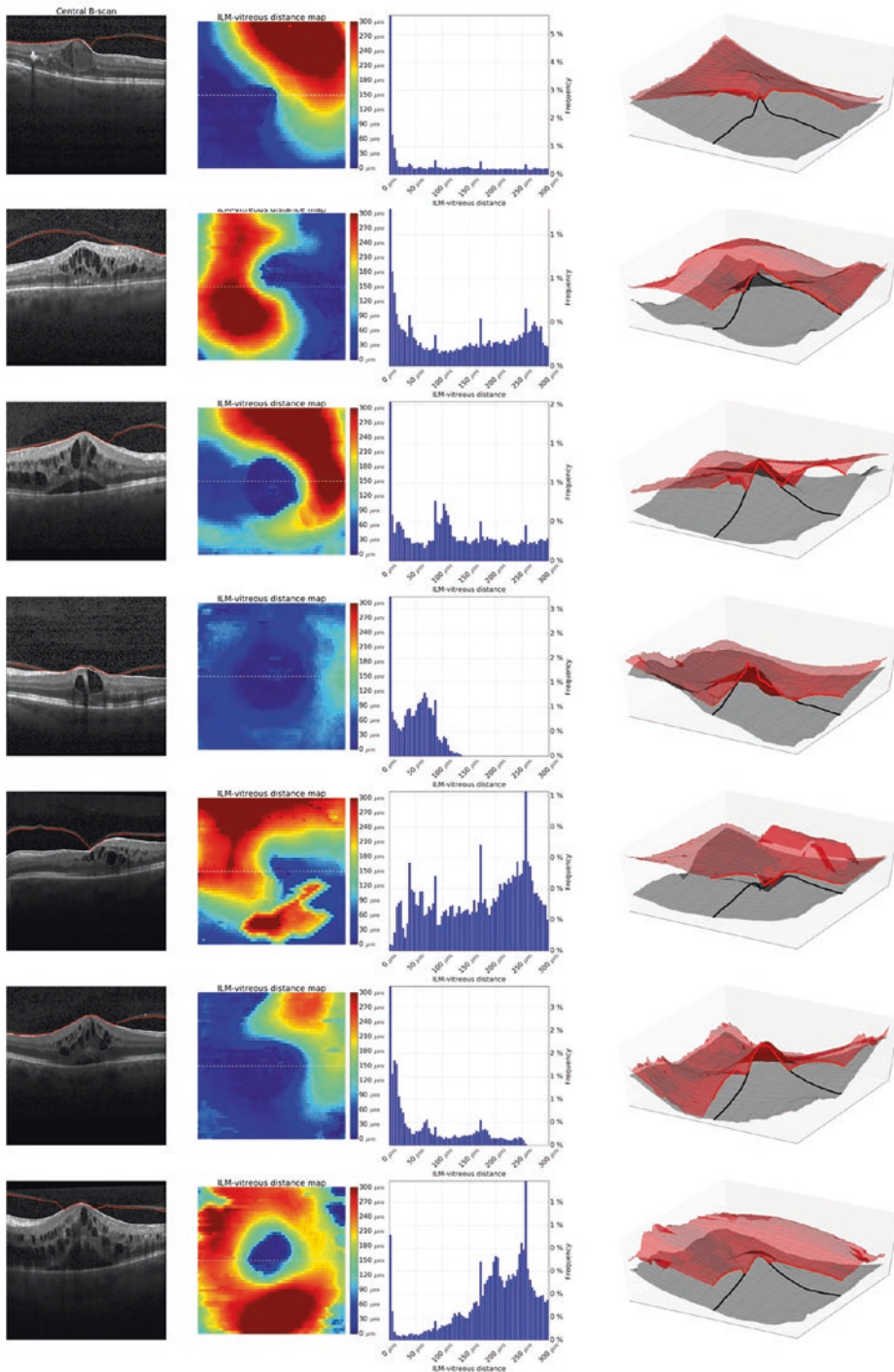
Fig. 6.2 Automated segmentation of the posterior vitreous boundary by machine learning. The left column shows original OCT slices with the hyaloid boundary segmented in red. The segmentation can be displayed in vitreous—internal limiting membrane distance maps (second column) or as three-dimensional renderings (right column). Figure reproduced under a Creative Commons Attribution 4.0 International License (https://creativecommons.org/licenses/by/4.0/), from: [21]
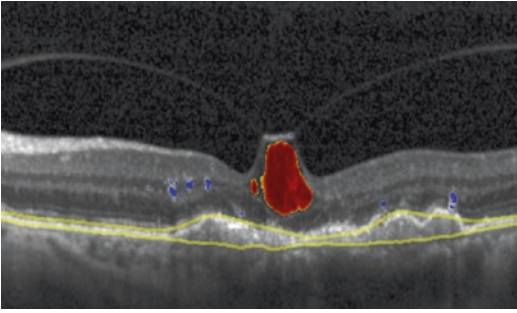
Fig. 6.3 Automated quantification of intraretinal changes in an eye with vitreomacular traction and concomitant age-related macular degeneration. Intraretinal cystoid fluid is marked in red. Automatically quantified hyperreflective foci are delineated in blue. These foci are an important risk factor for the development of retinal pigment epithelial atrophy

"mask" individual changes that occur at individual retinal sublevels, such as increasing vitreomacular traction causing serous retinal detachment as opposed to intraretinal fluid. In the context of macular degeneration, it has been proposed that intraretinal and subretinal fluid have opposite effects on visual function, in the sense that subretinal fluid confers a positive prognostic value [28]. Whether the same is true in vitreomacular interface disorders needs to be addressed in scientific studies. Nevertheless, there is definitely value in judging and measuring the different fluid compartments within the retina individually, and automated algorithms may offer significant workflow enhancement in clinical practice in this respect.

6.2.6 Changes of the Retinal Pigment Epithelium

Similar to retinal fluid, several automated methods are available to quantify changes at the level of the retinal pigment epithelium. These include soft drusen and pigment epithelial detachments, which are usually measured as the distance between the two surfaces, Bruch's membrane and the retinal pigment epithelium [20, 29]. This also allows subsequent automated diagnosis of pigment epithelium detachment type, including serous or fibrovascular [30].

Automated detection and quantification of reticular drusen (pseudodrusen) on OCT is currently still lacking. Furthermore, pigmentary atrophy (geographic atrophy) can be measured [31]. Drusen measurements are becoming important in clinical practice because drusen volume has been demonstrated as an important risk factor for the progression of age-related macular degeneration [32].

6.2.7 Hyperreflective Foci

Hyperreflective foci in the retina may represent migratory retinal pigment epithelium cells, activated inflammatory cells, and lipid exudation. It is possible to automatically quantify these foci using deep learning [33]. Similar to drusen, the number and volume of hyperreflective spots are a risk factor for advanced age-related macular degeneration [34].

6.3 Artificial Intelligence for Personalized Healthcare

The truly disruptive potential of automated OCT analysis in retina lies in the field of predictive medicine. Similar to personalized healthcare in oncology, where treatments can be individualized according to tumor genotype using next-generation sequencing, the analysis of retinal imaging data offers the opportunity to automatically derive prognostic information as well as individual treatment recommendations from OCT data.

Although these developments have not yet reached macular surgery, a few recent advances may be mentioned to inform the reader about the breakthrough nature of artificial intelligence in the retina. In the context of predictive medicine, several scenarios have been addressed in the recent past. This includes the prediction of therapeutic outcomes, treatment requirements, and future natural disease course.

Regarding the former, researchers have demonstrated that OCT image analysis enables precise prediction of future visual acuity outcomes

INITIATION PHASE   PRO RE NATA PHASE

M0   M1   M2 | M3   M23
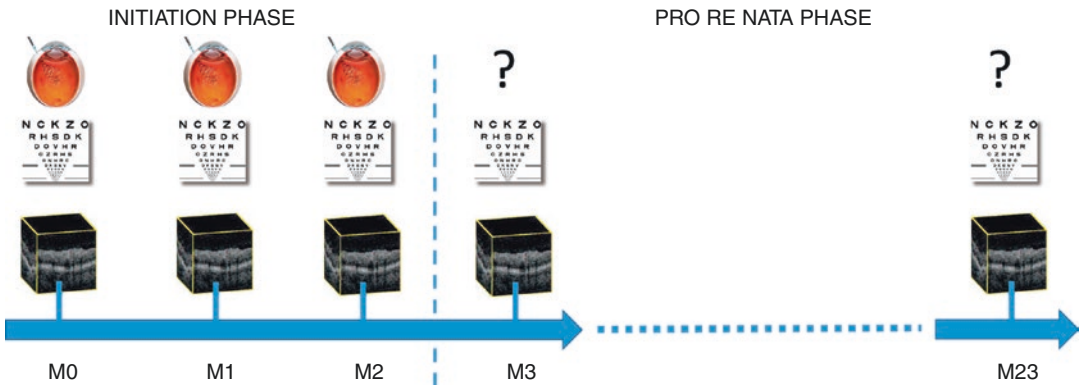
Fig. 6.4 Example of personalized healthcare using artificial intelligence-based analysis of retinal imaging data. A number of OCT volumes of a patient are used to predict the future treatment need in intravitreal therapy for age-related macular degeneration. The computer algorithm is trained on a large dataset giving hundreds of prior examples. Using these methods, the artificial intelligence tool reaches an accuracy of 70–77%, which is 50% more accurate than a retina specialist performing the task. Reprinted, with permission, from: [35]

in patients with age-related macular degeneration. Based on the analysis of OCT images and visual acuity data obtained from three consecutive anti-VEGF injections, it was possible to predict the final visual acuity of the patients after one year of therapy within an error margin of fewer than two lines of vision [27]. Similar results were shown in the therapy of diabetic macular edema and retinal vein occlusion.

Another relevant target for predictive analyses represents the future therapeutic requirement of anti-VEGF treatment (Fig. 6.4). Automated algorithms may allow to determine a priori, which patients will require a low, medium, or a high number of retreatments. Machine learning software achieved higher accuracy in predicting these categories than experienced retina specialists [35].

Lastly, artificial intelligence has been leveraged to predict the future natural disease course in eyes with early age-related macular degeneration. Automated software was not only able to foresee the growth behavior of drusen over time, but also to predict whether and when a patient would develop macular neovascularization or geographic atrophy. Machine learning additionally allowed insight into the pathophysiology of disease development by revealing the most important biomarkers for the individual progression pathways [34].

6.4 Future Perspective

A wealth of automated software for OCT image analysis and quantification has been developed in the last few years, boosted by recent advances in artificial intelligence and deep learning. While the majority of work is still at a proof-of-principle level, some software methods have already been validated on a large scale. The retina specialist will likely be able to take advantage of advanced analysis tools enabling precise and reproducible quantification of detailed morphologic changes in OCT within a mouse click in the next few years. Furthermore, ophthalmologists may be able to augment their practice by prognostic personalized healthcare tools, once these have been validated in clinical trials.

For further reading, a recent review article by the authors [36] may serve as a useful and comprehensive source of information.

References

1. Hinton G. Deep learning—a technology with the potential to transform health care. JAMA. 2018;320(11):1101–2.
2. Abramoff MD, Garvin MK, Sonka M. Retinal imaging and image analysis. IEEE Trans Med Imaging. 2010;3:169–208.

3. Garvin MK, Abramoff MD, Wu X, Russell SR, Burns TL, Sonka M. Automated 3-D intraretinal layer segmentation of macular spectral-domain optical coherence tomography images. IEEE Trans Med Imaging. 2009;28(9):1436–47.

4. Deo RC. Machine learning in medicine. Circulation. 2015;132(20):1920–30.

5. Deng J, Dong W, Socher R, Li L-J, Li K, Fei-Fei L. ImageNet: a large-scale hierarchical image database. IEEE Conference on Computer Vision and Pattern Recognition (CVPR): IEEE; 2009. pp. 248–55.

6. De Fauw J, Ledsam JR, Romera-Paredes B, Nikolov S, Tomasev N, Blackwell S, et al. Clinically applicable deep learning for diagnosis and referral in retinal disease. Nat Med. 2018;24(9):1342–50.

7. Castelvecchi D. Can we open the black box of AI? Nature. 2016;538(7623):20–3.

8. Abràmoff MD, Lavin PT, Birch M, Shah N, Folk JC. Pivotal trial of an autonomous AI-based diagnostic system for detection of diabetic retinopathy in primary care offices. NPJ Digital Med. 2018;1(1):39.

9. Venhuizen FG, van Ginneken B, van Asten F, van Grinsven M, Fauser S, Hoyng CB, et al. Automated staging of age-related macular degeneration using optical coherence tomography. Invest Ophthalmol Vis Sci. 2017;58(4):2318–28.

10. Liu Y-Y, Ishikawa H, Chen M, Wollstein G, Duker JS, Fujimoto JG, et al. Computerized macular pathology diagnosis in spectral domain optical coherence tomography scans based on multi-scale texture and shape features. Invest Ophthalmol Vis Sci. 2011;52(11):8316–22.

11. Chakravarthy U, Goldenberg D, Young G, Havilio M, Rafaeli O, Benyamini G, et al. Automated identification of lesion activity in neovascular age-related macular degeneration. Ophthalmology. 2016;123(8):1731–6.

12. Prahs P, Radeck V, Mayer C, Cvetkov Y, Cvetkova N, Helbig H, et al. OCT-based deep learning algorithm for the evaluation of treatment indication with anti-vascular endothelial growth factor medications. Graefes Arch Clin Exp Ophthalmol. 2018;256(1):91–8.

13. Montuoro A, Waldstein SM, Gerendas BS, Schmidt-Erfurth U, Bogunovic H. Joint retinal layer and fluid segmentation in OCT scans of eyes with severe macular edema using unsupervised representation and auto-context. Biomed Opt Express. 2017;8(3):1874–88.

14. Ichikawa Y, Imamura Y, Ishida M. Inner nuclear layer thickness, a biomarker of metamorphopsia in epiretinal membrane, correlates with tangential retinal displacement. Am J Ophthalmol. 2018;193:20–7.

15. Govetto A, Virgili G, Rodriguez FJ, Figueroa MS, Sarraf D, Hubschman JP. Functional and anatomical significance of the ectopic inner foveal layers in eyes with idiopathic epiretinal membranes: surgical results at 12 months. Retina. 2019;39(2):347–57.

16. Hosoda Y, Ooto S, Hangai M, Oishi A, Yoshimura N. Foveal photoreceptor deformation as a significant predictor of postoperative visual outcome in idiopathic epiretinal membrane surgery. Invest Ophthalmol Vis Sci. 2015;56(11):6387–93.

17. Gharbiya M, Grandinetti F, Scavella V, Cecere M, Esposito M, Segnalini A, et al. Correlation between spectral-domain optical coherence tomography findings and visual outcome after primary rhegmatogenous retinal detachment repair. Retina (Philadelphia, PA). 2012;32(1):43–53.

18. Wang Z, Camino A, Hagag AM, Wang J, Weleber RG, Yang P, et al. Automated detection of preserved photoreceptor on optical coherence tomography in choroideremia based on machine learning. J Biophotonics. 2018;11(5):e201700313.

19. Wang Z, Camino A, Zhang M, Wang J, Hwang TS, Wilson DJ, et al. Automated detection of photoreceptor disruption in mild diabetic retinopathy on volumetric optical coherence tomography. Biomed Opt Express. 2017;8(12):5384–98.

20. Zhang L, Sonka M, Folk JC, Russell SR, Abramoff MD. Quantifying disrupted outer retinal-subretinal layer in SD-OCT images in choroidal neovascularization. Invest Ophthalmol Vis Sci. 2014;55(4):2329–35.

21. Waldstein SM, Montuoro A, Podkowinski D, Philip AM, Gerendas BS, Bogunovic H, et al. Evaluating the impact of vitreomacular adhesion on anti-VEGF therapy for retinal vein occlusion using machine learning. Sci Rep. 2017;7(1):2928.

22. Breger A, Ehler M, Bogunovic H, Waldstein SM, Philip AM, Schmidt-Erfurth U, et al. Supervised learning and dimension reduction techniques for quantification of retinal fluid in optical coherence tomography images. Eye (Lond). 2017;31(8):1212–20.

23. Roy AG, Conjeti S, Karri SPK, Sheet D, Katouzian A, Wachinger C, et al. ReLayNet: retinal layer and fluid segmentation of macular optical coherence tomography using fully convolutional networks. Biomed Opt Express. 2017;8(8):3627–42.

24. Lee CS, Tyring AJ, Deruyter NP, Wu Y, Rokem A, Lee AY. Deep-learning based, automated segmentation of macular edema in optical coherence tomography. Biomed Opt Express. 2017;8(7):3440–8.

25. Venhuizen FG, Ginneken BV, Liefers B, Asten FV, Schreur V, Fauser S, et al. Deep learning approach for the detection and quantification of intraretinal cystoid fluid in multivendor optical coherence tomography. Biomed Opt Express. 2018;9:1545–69.

26. Schlegl T, Waldstein SM, Bogunovic H, Endstraßer F, Sadeghipour A, Philip A-M, et al. Fully automated detection and quantification of macular fluid in OCT using deep learning. Ophthalmology. 2018;125:549–58.

27. Schmidt-Erfurth U, Bogunovic H, Sadeghipour A, Schlegl T, Langs G, Gerendas BS, et al. Machine learning to analyze the prognostic value of current imaging biomarkers in neovascular age-related macular degeneration. Ophthalmol Retina. 2018;2(1):24–30.

28. Schmidt-Erfurth U, Waldstein SM. A paradigm shift in imaging biomarkers in neovascular age-related macular degeneration. Prog Retin Eye Res. 2016;50:1–24.

29. Chen Q, Leng T, Zheng L, Kutzscher L, Ma J, de Sisternes L, et al. Automated drusen segmentation and quantification in SD-OCT images. Med Image Anal. 2013;17(8):1058–72.
30. Lee SY, Stetson PF, Ruiz-Garcia H, Heussen FM, Sadda SR. Automated characterization of pigment epithelial detachment by optical coherence tomography. Invest Ophthalmol Vis Sci. 2012;53(1):164–70.
31. Ji Z, Chen Q, Niu S, Leng T, Rubin DL. Beyond retinal layers: a deep voting model for automated geographic atrophy segmentation in SD-OCT images. Transl Vis Sci Technol. 2018;7(1):1.
32. Abdelfattah NS, Zhang H, Boyer DS, Rosenfeld PJ, Feuer WJ, Gregori G, et al. Drusen volume as a predictor of disease progression in patients with late age-related macular degeneration in the fellow eye. Invest Ophthalmol Vis Sci. 2016;57(4):1839–46.
33. Schlegl T, Bogunovic H, Klimscha S, Seeboeck P, Sadeghipour A, Gerendas BS, et al. Fully Automated segmentation of hyperreflective foci in optical coherence tomography images. arXivorg. 2018:arXiv:1805.03278.
34. Schmidt-Erfurth U, Waldstein SM, Klimscha S, Sadeghipour A, Hu X, Gerendas BS, et al. Prediction of individual disease conversion in early AMD using artificial intelligence. Invest Ophthalmol Vis Sci. 2018;59(8):3199–208.
35. Bogunovic H, Waldstein SM, Schlegl T, Langs G, Sadeghipour A, Liu X, et al. Prediction of anti-VEGF treatment requirements in neovascular AMD using a machine learning approach. Invest Ophthalmol Vis Sci. 2017;58(7):3240–8.
36. Schmidt-Erfurth U, Sadeghipour A, Gerendas BS, Waldstein SM, Bogunovic H. Artificial intelligence in retina. Prog Retin Eye Res. 2018;67:1–29.

Artificial Intelligence in the Assessment of Macular Disorders

Paisan Ruamviboonsuk, Christopher Semturs,
Rajiv Raman, Variya Nganthavee,
and Peranut Chotcomwongse

The industrial revolution automated manual work, the information revolution automated mental work, the machine learning automated automation.

Pedro Domingos, a professor in machine learning from the University of Washington, wrote this sentence in his best-selling book: The Master Algorithm.

Artificial intelligence (AI) including machine learning (ML), a subfield of AI, and deep learning (DL), a subfield of ML, have recently been studied extensively for automated screening, classification, segmentation, quantification of biomarkers, prediction of treatment burden, prediction of disease outcome, and so on, for retinal and macular disorders. If the invention of film-based retinal cameras automated retinal examination, digital retinal images automated the film-based retinal images; then, AI would automate automation of the digital retinal images.

P. Ruamviboonsuk (✉) · V. Nganthavee
P. Chotcomwongse
Department of Ophthalmology, Rajavithi Hospital, Faculty of Medicine, Rangsit University, Bangkok, Thailand

C. Semturs
Google Health, Google, Mountain View, San Francisco, CA, USA

R. Raman
Shri Bhagwan Mahavir Vitreoretinal Services, Sankara Nethralaya, Chennai, Tamil Nadu, India

Algorithms, that is, a set of rules to be followed in problem-solving operations, of AI have already infiltrated our daily lives no matter we are aware of them or not, searching the internet, filtering emails, using face recognition, just to name a few. In medicine, AI has been used for cancer treatment recommendation [1], X-ray interpretation [2], finding tumor cells in pathological biopsies [3], and so on. Of these involvements of AI in our societies, involvements in medicine may have caused the most enthusiastic and controversial debates of all. How do we use AI in real-world practice? Would we believe in AI recommendation? Will doctors be replaced by AI?

Similar questions may be posted for the roles of AI in ophthalmology, one of the most image-rich fields in medicine. And of all subfields of ophthalmology, current managements of retinal and macular disorders are mostly depended on decisions from image interpretations. There is no doubt why AI has come into studies on retinal and macular disorders before other subfields in ophthalmology. Last year, Dr. Siddhartha Mukhergee, the Pulitzer Prize winner wrote about AI in general medicine in an article of a popular weekly news magazine. He named his article: "the algorithm is seeing you now." In ophthalmology, we may apply similar contexts about AI saying: "the algorithms are assessing your retina and macula now."

7.1 Artificial Intelligence, Machine Learning, and Deep Learning

What Are AI Algorithms
Software approaches to retinal image assessment in the 1990s were based on traditional software development paradigms: a human identifies what the program should do, implements the program (with basic instructions), and runs it on a given fundus image. That approach was very predictable but limited by human programmer capacity on improving sensitivity or specificity. The rise of AI technologies in the 2010s enabled to shift the paradigms.

AI is a broad field and often mislabeled in the media. It is important to understand the differences between AI and ML as listed below:

- Artificial intelligence (AI): Any kind of intelligence displayed by entities not being biological (not being humans or animals). For instance, a supercomputer being able to hold a rich conversation with a human. Or a virtual doctor where the patient cannot tell the difference to a human doctor, as seen in science fiction movies.
- Machine learning (ML): One approach toward creating AI. A computer learning the ability to fulfill a task by relying on a big set of examples to observe. For instance, recognizing a stop sign on the street or identifying the language of a text.

ML, in the 1990s, required prework by software developers to scope the problem in manage-

able computational complexity. For instance, a software developer would write the basic algorithm to identify "sharp edges" in a photo. Those subunits of a photo are then used as input for ML, to learn how to distinguish different street signs (e.g., stop sign vs. one-way-street sign). A variety of algorithms were developed for ML to fulfill the task, using representative names like "logistic regression" (putting "weights" on different input factors), "decision tree" (identify decision factors) or "random forest" (mix various decision trees).

In 2010, a new approach for ML evolved with the advancements in computing power and some breakthroughs in math: "Deep Learning" (DL). Rather than trying to make systems intelligent by telling them what to do, a DL network identifies itself what to look for, by observation. No handwritten code is required anymore to isolate the learning features upfront, the raw data (e.g., image or text) are provided as input.

So how does DL work? It can be easiest thought of as "learning by example." It can learn a task without being explicitly programmed on how to accomplish it. It happens to work particularly well on images. It learns what to look for in an image to accomplish a task and can apply that knowledge on new images to execute the task. The learned knowledge is often called a "deep neural network (DNN)," practically the "rules" on which decision weight to apply on which aspects of the input image.

For example, let's use DL for the task "identify images of planets." We have two images available for learning, one labeled as "planet" and the other one as "not planet":

(images from www.wikipedia.org)

DL acts like a toddler. It does not know what a planet is. It does not understand concepts like spheres, water, gas, nor does it know what a football field looks like. In our example, it just sees those two images, not knowing anything else about the world, and tries to identify what to look for to tell if an image is a planet image or not. To simplify a likely learning result, in this case, it could learn "colorful circle means planet image."

But will this work in all cases? Let's apply the learned DNN on another input, a soccer ball:

(image from www.wikipedia.org)

It will most likely misdiagnose this as a planet image—after all, it is a colorful circle. So clearly the learned model did not generalize well. Learning the DNN again based on the three images will help DL to pick up more details (e.g.,

"needs to be a circle, and mostly blue"), but it would most likely fail on the next challenge. Clearly, three images are not sufficient!

DL is very efficient in learning a task and it only requires images (and its label). But it requires lots of them, in the order of hundreds of thousands or even millions of images, and it also requires a diversity of images to succeed. For instance, training it based on 500,000 Earth images will most likely fail the first time it encounters an image of Mars. But with a good diverse data set, it will pick up all the features to reliably execute the desired task.

Getting Clean Input Data

Applying DL on fundus images works identical to the planet example above:

1. Get a lot of images.
2. Acquire clean and precise labels for the given task to learn.

Step 2 can be easy—for instance, metadata related to the image are clean and precise —for instance, for tasks like "how old is the patient?" or "which camera was used to take the fundus image?." But very often the task is more complicated!

For predictions by specialists (e.g., ophthalmologists), getting clean labels is a difficult problem. After all, the specialists don't always agree on a given diagnosis. For instance, look at this table for getting grades on diabetic retinopathy (DR):
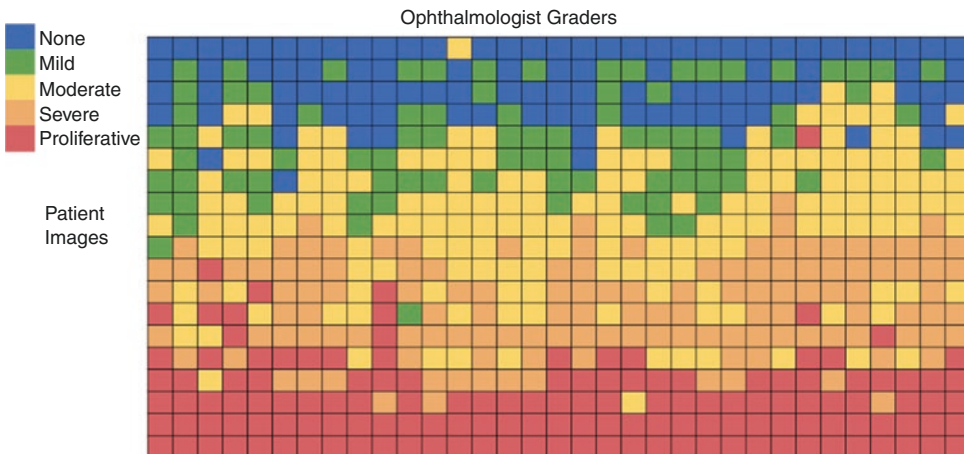
Consistency: intragrader ~65%, intergrader ~60%

Each column is the opinion of an ophthalmologist and each row is one image. DL would pick up very different features depending on which column is used as input. And if all of them are used, it would be a set of inconsistent labels, which just confuses DL, and most likely just produces inconsistent results.

Getting clean labels is crucial for DL. Methodologies like adjudication panels are required to ensure clean input labels in cases where a human's interpretation is required because no hard outcomes are available.

Make It Understandable and Trustworthy
The success of a DNN is often measured in traditional statistical terms (e.g., sensitivity and specificity on a test set of images). Quite often DL is referred to as a black box, the DNN itself is not really readable. However, it is often interesting to "understand" what features the DNN picked up, as a human "sanity check." The planet example above referred to concepts as "circles" and "color," but those are not the concepts the DNN is using internally, it uses weights and matrices. Ultimately, for a given task on an image, it applies "weights" on parts of the image deemed most useful for identifying an image. Those parts of the image can be highlighted using a heatmap:

This image above is an example from the study on predicting cardiovascular risk factors, [4] it is answering the question "does this person have high blood pressure." The heatmap confirms that the DNN mainly "looks" at the blood vessels, which sounds reasonable given the task. So in addition to sensitivity and specificity, examples like this increase our confidence that the DNN learned the "right" things and not a random correlation that would not generalize. When the heat map looks wrong, adding a more diverse set of cleanly labeled input images will help DL to pick up the right features.

Last, it is important to understand that a DNN can only answer the task it was trained for, based on similar images as it was in the training. For instance, if a DNN was trained for the DR grade purely on fundus images and it is presented an image of a soccer ball it might happily derive "this is a proliferative diabetic retinopathy (PDR) diagnosis"—simply because it is the closest based on the features it learned and matched to the soccer ball. Having that answer by a diagnosis product would erode trust very quickly, it is nonsensical! Therefore, when applying DNN in a real-world product most likely one needs to combine several tasks at once, like:
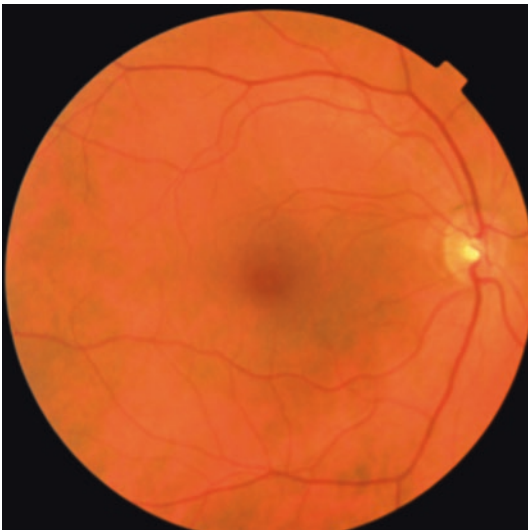
Image of retina
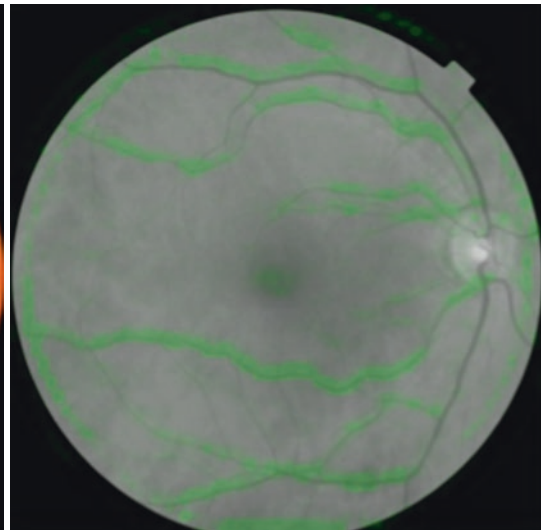
Blood pressure predictions
focus on blood vessels

- Is the image a fundus image?
- Is the image gradable (are the relevant features visible)?
- What is the DR grading based on the fundus image?

All of these tasks need to be answered and combined into one single answer via traditional software programming. For instance, if an image is identified to NOT be a fundus image, answering the DR question does not make any sense anymore.

Similar, untrained tasks cannot be answered. In our example above, since the task "detect retinal tumors in fundus image" was not trained, the question "does the patient have eye cancer" cannot be answered. Luckily DL can be used to also learn this task to answer that question, by getting many images with and without retinal tumors and labeling them cleanly.

Because DL does not "understand" the fundus image, sometimes errors might look odd or weird based on our human intuition. Ultimately, though, each classification error by a DNN can be fixed by providing more and diverse examples images to DL.

Getting more and clean data, combined with the advancements of computational power, will strictly improve the performance of DNN over time. Sometimes performing as good as human specialists (but more consistent during the day). Sometimes even better, in case it picks up new signals unknown before. Peng has demonstrated how a number of input images, and clean labels, drastically affect the performance of the DNN positively [5]. The performance of human specialists was matched. Peng has also shown how new signals can be detected via DL, given the fact that the labels are clean and available (in that specific example attributes of the patient, like age or smoking status) [4].

And that is the real advancement of DL: With an extensive and cleanly labeled data set for each task, everything is possible.

Early Algorithms for Automated Assessment of Retinal Disorders

Even before retinal images were available in digital format, attempts had been made to digitize film photographs for automated detection of common focal retinal abnormalities, such as microaneurysms, exudates, etc., including retinal diseases. Gardner et al. [6] trained a backpropagation artificial neural network (ANN), one of the primitive forms of AI, with 700×700-pixel images of fundi of 147 patients with DR and 32 images of normal subjects, to detect DR. These images were scanned from 60°, red-free, retinal film photographs. Using grading by retinal specialists as a reference standard, the network could recognize retinal structures, such as blood vessels, exudates, hemorrhages in 300 retinal images (DM = 200, controls = 100) with sensitivity from 73.8% to 93.1% and also the determination of DR from the whole image with a sensitivity of 88.4% and specificity of 83.5%. The performances of this ANN were comparable with other modalities for screening DR, such as Polaroid photographs, at the time. The limitation then was not only the unavailability of digital retinal images but also computing power. Training of the ANN sometimes required up to 5 days of computing [6].

The studies for automated detection of retinal diseases started to proliferate near the end of the 1990s when digital retinal cameras were available commercially and computing power increased dramatically year by year. Sinthanayothin et al. [7], used a few algorithms to analyze 112 digital retinal images to localize the optic discs (identifying variation in the intensity of adjacent pixels), blood vessels (multilayer perceptron neural network, for which the inputs were derived from a principal component analysis of the image), the foveas (matching correlation with characteristics typical of a fovea). Using these methods with the reading by an experienced ophthalmologist as standard for validation of 174 patches of retinal images, the investigators were able to achieve the sensitivity and specificity of 99.1% and 99.1% for detecting the optic discs, 83.3% and 91.0% for blood vessels, and 80.4% and 99.1% for foveas, respectively. This study laid the groundwork for many studies to come [7].

Usher et al. in 2003, further improved algorithms for classifying DR levels to identify

patients for referral to ophthalmologists. Retinal images, 45°, macula-centered, of 500 eyes from DR screening programs were used for training the AI algorithms whereas images of 773 eyes were used for validation. There were four main phases for processing images: (i) preprocessing; (ii) identification of normal structures; (iii) identification of candidate lesions; and (iv) extraction of candidate lesion features. Then, the images were classified in two phases comprising: (i) classification of each candidate lesion as a true lesion or noise using ANN; and (ii) classification of images and patients as normal or abnormal using mathematical rules. The optimal sensitivity and specificity for detection of any retinopathy on a per-patient basis, using grading by a diabetologist as standard, were 94.8% and 52.8% respectively [8].

This kind of model developed by combining various engineer-driven algorithms, each detected specific DR lesions, for automated detection of DR was validated by Abramnoff et al. in a real-world large patient data set in 2008. In this retrospective analysis of 5692 patients with diabetes whose retinal photographs with sufficient quality, taken from two visits with three types of cameras at 10 centers, were determined as a presence or absence of referable retinopathy by the model. Grading by retinal specialists was used as standard. Although both the area under the curve (AUC) of Receiving Operator Curve (ROC) and sensitivity was found to be the same and as high as 0.84, specificity was found at only 64%. Twenty-seven percent of false negatives in this study contained large hemorrhages and/or neovascularizations [9]. This plateau of high sensitivity but relatively low specificity, around 50%, was found across the algorithms for detecting DR in this era.

Even the winner from the "online challenge competition" for developing algorithms for detecting DR also had similar sensitivity and specificity [10].

The algorithms for the detection of retinal diseases were initially focused on screening DR because the screening had the potential to reduce the risk of visual loss in patients with diabetes by early detection of referrals to have timely treatments [11]. Unmet need for the screening was found in many rural areas where accessibility to eye care is limited [12]. The availability of compact commercial retinal cameras had made the screening accessible and cost-effective [13]. The screening in some resource settings, however, still requires personnel to interpret the images [14]. Automated detection, if proven to be with acceptable accuracy, might have come to play important roles to reduce the workload of the retinal image interpreters. The plateau performance, especially approximately 50% of specificity, of the automated algorithm in the era of 2000s to early 2010s might be the main reason why there was a reluctance in adopting the software in real-world screening.

The Turning Point of the Algorithms

Increasing computing power and availability of a huge number of retinal images in recent years have led to the successful training of deep convolutional neural network (DNN) to detect DR with significantly higher accuracy. Abramnoff et al. integrated DL into the existing version of the automated detection of DR in the device called IDx-DR X2.1. The investigators then analyzed the performance of the device for detection of referable and vision-threatening DR in public data sets of 872 subjects compared with the performance of the older version of the algorithm in terms of sensitivity, specificity, and accuracy, using retinal specialists grading as a reference standard. They found that the IDx-DR X2.1, although not significantly increased sensitivity (96.8%, $p = 0.615$), increased specificity significantly (87.0% with 95% CI: 84.2–89.4%), compared to the specificity (59.4% with 95% CI: 55.7–63.0%) of the older version [10].

The IDx-DR X2.1 has become the first device with integrated AI which was approved by the US FDA for DR screening. The DL algorithm, not resided within the device, is used with a cloud-based system. The approval was based on a study

of 900 patients with diabetes from 10 primary care units who had no treatments or other eye diseases at baseline and the algorithms were able to achieve a sensitivity for detecting DR at 87.4% and specificity at 89.5% whereas the mandatory sensitivity and specificity set for the FDA for approval was more than 85% and 82.5% respectively [15, 16].

The first large scale study on DL for DR was from Gulshan et al. A total of more than 128,000 retinal images of patients with diabetes from a public data set of the US and from three eye hospitals in India, graded by 54 US licensed ophthalmologists and ophthalmology senior residents were used as developmental data set of the DNN algorithms. The algorithms were then externally validated in the other two public data sets, EyePACS-1 and Messidor-2, containing a combination of more than 20,000 images. The other two groups of seven and eight ophthalmologists graded these images with adjudication as a reference standard. For detecting referable DR (moderate nonproliferative diabetic retinopathy [moderate NPDR] or worse), with the specificity set at 98%, the sensitivity was 90.3% and 98.5% for the two validation data sets respectively. On the other hand, with the sensitivity set at 97%, the specificity was 93.4% and 93.9% respectively. This was the best performance in terms of diagnostic accuracy that algorithms for automated detection of DR could ever achieve [17].

Subsequently, another DL system for DR was developed by Ting et al. The algorithms in this study not only detect DR but also detect possible glaucoma and referable age-related macular degeneration (AMD). The highlights of this study included a large development data set of more than 76,000 retinal images from Singapore and another large validation data set of slightly more than 40,000 images from multiple ethnicities. There was a variety of standards for images in these populations of multiple ethnicities, ranging from optometrists to retinal specialists. This study also tested the deployment of the algorithms in clinical settings. Similar to the study by

Gulshan et al., sensitivity and specificity for referable DR were very high at 90.5% and 91.6%. For sight-threatening DR, the sensitivity and specificity were 100% and 91.1% [18]. Therefore, according to these two large-scale studies, it seems that standard has been set for applying DL for screening DR: either sensitivity or specificity of an algorithm for detecting referable DR should not be less than 90%.

In another large-scale study of DNN for detecting DR, Gargeya et al. also developed a model from more than 70,000 retinal images; however, they validated the model with approximately 2000 images from public data sets with the existing grades of the images as reference standard without overreading by another group of specialists. The investigators in this study also achieved a sensitivity of 93% and specificity of 87% [19].

The DNN algorithm developed by Gulshan et al. has been further validated in another real-world nationwide screening program for DR [20]. This study has strength in having adjudication of image reading by international retinal specialists as a reference standard. In addition, the accuracy of the DNN was compared to human personnel who were actual graders in the screening program. This study may be the only study to date that contains a head-to-head comparison between DNN and human graders in an external validation data set. It was found that, from more than 25,000 images of patients with diabetes, the algorithm could achieve the overall sensitivity of 97% whereas the 13 graders (each from each health region of the country) could achieve the overall sensitivity of 74% for detecting moderate NPDR or worse ($p < 0.001$) whereas the overall specificity by the human graders was 98.2% and the algorithm was 95.7% ($p < 0.001$). However, the quadratic weighted Kappa was 0.776 by the human graders and 0.846 by the algorithm. This study suggested that DL tended to be much more sensitive but human graders tended to be slightly more specific for screening DR.

7.2 Application of AI in Macular Disorders

Retinal specialists have privileges in obtaining multimodal images of the macula, such as images in 2-D, 3-D, color, angiography, optical coherence tomography (OCT), and so on, for the best practice of patient care. These different image formats may serve different purposes for different disorders not only in clinical practice but also in research. Availability of these images is a treasure for studies of AI.

Images from OCT are replacing CFP for assessment of the macula in many circumstances. Interpretation of OCT images by retinal specialists is becoming routine for almost all patients with active macular disorders in each of their visits in retinal clinics. Workload of OCT interpretations could be a real burden in many busy retinal clinics. Even in a research setting, interpretation of OCT images sometimes requires subjective judgment and prone to bias. Automated assessor of OCT images should be useful in such situations. Although the automated assessor is provided within all commercial OCT devices, its application for detecting biomarkers is limited [21] and poor reproducibility could be found [22]. Automated interpretation of clinical OCT data represents another unmet need in retinal practice and research; these are the areas where AI was explored for augmentation in many studies.

Detection, Quantification, and Segmentation of Retinal Fluid on OCT
Early attempts for automated analysis of OCT images lied on automated segmentation of the normal retinal layers and automated segmentation and quantification of some common biomarkers, such as retinal fluid. These procedures of segmentation of biomarkers are important for quantification of longitudinal changes of disease activity at the macula but are tedious tasks and time-consuming for human experts [23]. In a study by Lee CS et al. a total of 934 manually segmented OCT images of AMD, diabetic macular edema (DME), or retinal vein occlusion (RVO), were designated as a training set for a DNN and another set of 355 images was used for

cross-validation. The investigators compared the Dice coefficients for the automated segmentation against manual segmentations performed by four independent clinicians. The mean Dice coefficient for human inter-rater reliability and DNN were 0.750 and 0.729 respectively, claiming a generally accepted value of the excellent agreement. No statistically significant difference was found between clinicians and the DNN ($p = 0.247$) [24].

In another study by Schlegl et al., the investigators also used DL approaches to quantify macular fluid in OCT images in three different macular disorders. The clinical data set consisted of 1200 OCT volumes of patients with neovascular AMD ($n = 400$), DME ($n = 400$), or RVO ($n = 400$). The volumes were acquired from two commercially available OCT devices, each with 600 OCT volumes. The newly designed, fully automated neural network based on DL in this study achieved optimal accuracy for the detection and quantification of the intraretinal cyst (IRC) for all three macular disorders with a mean accuracy (AUC) of 0.94 (range, 0.91–0.97), a mean precision of 0.91, and a mean recall of 0.84. The detection and measurement of subretinal fluid (SRF) were also highly accurate with an AUC of 0.92 (range, 0.86–0.98), a mean precision of 0.61, and a mean recall of 0.81, with superior performance in neovascular AMD and RVO compared with DME. The investigators confirmed a high linear correlation between automated and manual fluid localization and quantification, yielding an average Pearson's correlation coefficient of 0.90 for IRC and of 0.96 for SRF [25].

Prediction of Indication of Treatment with Anti-VEGF Based on OCT
Prahs et al. trained DNN to predict treatment indication of anti-vascular endothelial growth factor (anti-VEGF) as "Injection" or "No Injection" based on central retinal OCT B-scans. A total of 183,402 of the retinal scans of nonspecific macular disorders were cross-referenced with the electronic institutional intravitreal injection records to obtain data of intravitreal injection. If the injection was performed during the first 21 days after image acquisition, the corresponded images were assigned into the

"Injection" group, while the same amount of random OCT images without intravitreal injections was labeled as "No Injection." The images were then divided into a 9:1 ratio to training and test data sets.

After successful training, the DNN classifier predicted 16,166 of the 17,112 images in the test data set correctly as either "No Injection" or "Injection," representing an overall accuracy of 94.5%. In another validation set, 5115 of the 5358 images were classified correctly, representing an accuracy of 95.5%, a sensitivity of 90.1%, and a specificity of 96.2%. The AUC was 0.968 on a per B-scan image basis, and 0.988 by averaging over six B-scans per examination [26].

7.2.1 Diabetic Macular Edema

7.2.1.1 Application on Color Fundus Photographs

Screening of DME

DME, one of the leading causes of blindness in patients with diabetes, is included as one of the criteria for referable DR in general screening programs of DR. Although it is highly possible that the prevalence of DME based on grading of CFP may not be in concordance with the prevalence of DME derived from OCT [27], CFP should still be used for screening DME as long as OCT devices are not ubiquitous or made for screening purposes.

In the large scale validation of a DNN model for DR by Gulshan et al. mentioned previously, screening for DME, defined as the presence of hard exudates within 1 disc diameter from the foveal center, was also validated in two public data sets, the EyePACS-1 and the Messidor-2 with a combination of almost 10,000 fully gradable images, sensitivity, and specificity of 90.8% and 98.7% were achieved respectively. Adjudication of ophthalmologists for grading the images was set as reference standard for the validation for referable DR in this study [17].

The algorithm for detecting DME by Gulshan et al. was also validated externally in a nationwide screening program for DR with 24,332 CFP images of patients with diabetes in the study. The study design was similar to the validation for DR

described previously in this chapter. In short, the diagnostic accuracy of the algorithm was compared to that of the 13 actual graders, each from a health region of the country. A group of international retinal specialists graded DME on CFP by adjudication, using the same criteria as the algorithm as a reference standard. A total of 1756 DME images was found. The sensitivity for the regional graders for detecting referable DME was 0.613 (0.421–0.805 across the regions), and the specificity was 0.992 (0.973–0.999). For the DL algorithm, sensitivity was measured at 0.940 (0.847–1.000 across the regions) and specificity was measured at 0.982 (0.947–0.992) [20].

Figure 7.1 shows examples of cases where the DL algorithm agreed with the adjudication by retinal specialists, but not with the graders, and cases where the graders agreed with the adjudication, but not with the DL algorithm.

In another large-scale study on DL for screening DR from CFP by Ting et al. described previously, in which the algorithm was externally validated in multiethnic populations of slightly more than 40,000 retinal images, cases with DME was grouped within cases with referable DR without a separated report on DME and the sensitivity for detecting referable DR from 91.8 to 100% and specificity from 73.3 to 92.2% were found across the multiethnic populations.

It was found, however, that even in the hands of expert graders who grade CFP for detecting DME, the agreement was rather poor and inconsistent. The prevalence of DME, in different definitions, determined from using CFP was significantly different from that determined by using OCT devices [27]. Although DME determined from OCT is the gold standard for making diagnosis and monitoring treatments, OCT devices are usually available in referral centers whereas CFP from retinal cameras is more readily available for screening DME in ubiquitous primary care centers. Varadarajan et al. [28] attempted to develop algorithms for detecting DME according to OCT devices but using CFP from retinal cameras for analysis and making predictions. These algorithms were developed from more than 7000 retinal images which had corresponded data on center point thickness (CPT) of the fovea from OCT devices and were
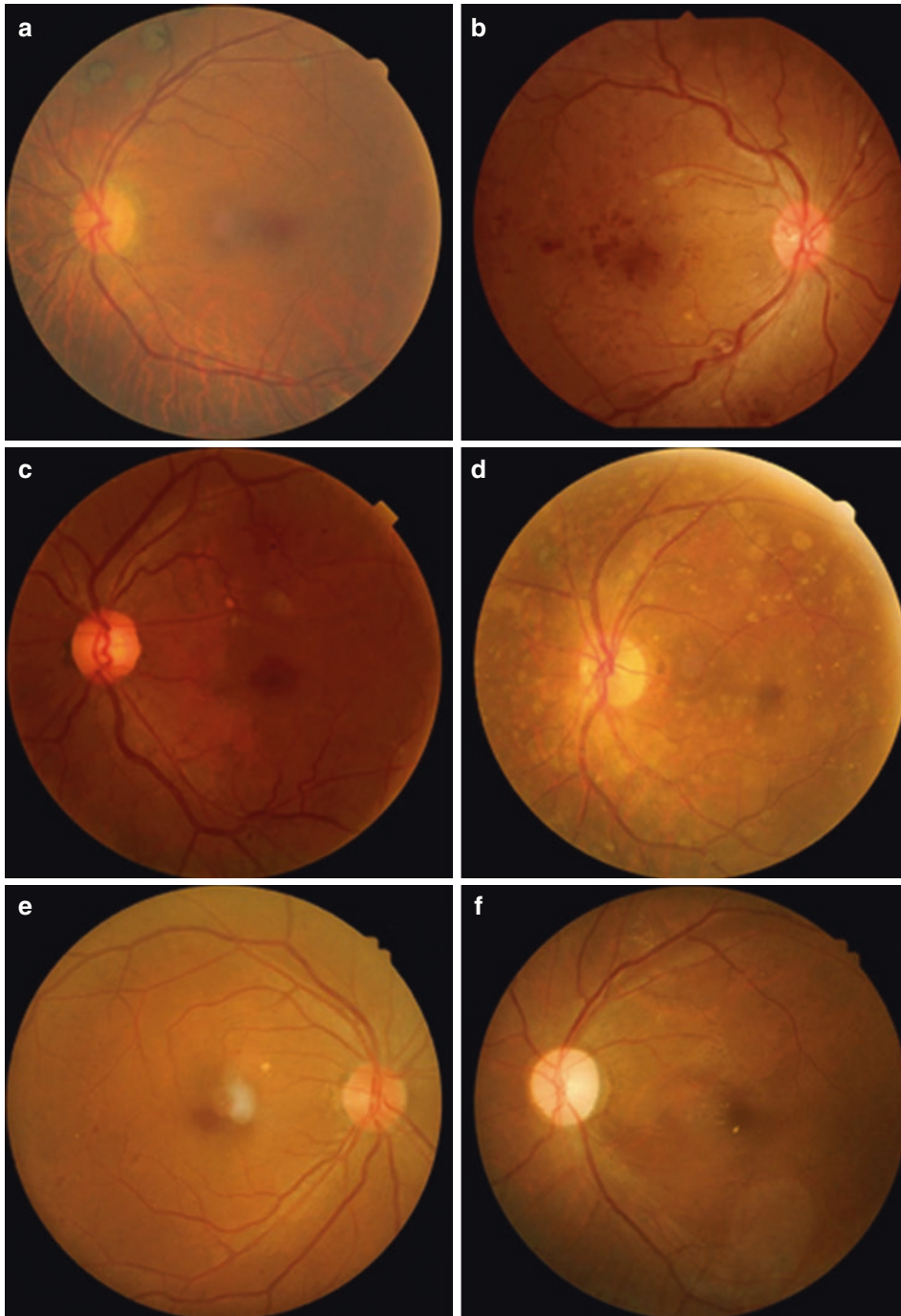
Fig. 7.1 Disagreement in detecting diabetic macular edema (DME) among deep learning (DL), human graders (HG), and adjudication by international retinal specialists (RS). (**a**) RS graded as DME from finding hard exudates within the macula (within 1 disc diameter from the foveal center) by magnification whereas DL and HG graded as no DME. (**b**) RS graded as no DME since intraretinal hemorrhages without hard exudates within the macular area are not counted as DME but HG and DL graded as DME. (**c**) DL graded as DME but HG and RS graded as no DME, note drusen, not hard exudates within the macula. (**d**) DL graded as no DME but HG and RS graded as DME, note asteroid hyalosis obscuring parts of the macula but hard exudates could still be seen within the macula. (**e**) HG graded as DME but DL and RS graded as no DME, note artifacts, and drusen in the middle of the photograph. (**f**) HG graded as no DME, but DL and RS graded as DME, note hard exudates at the foveal center

validated for the detection of Center-Involved (CI)-DME (CPT $\geq$ 250 μm) from CFP against the grading of retinal specialists. The algorithms were found to have AUC of 0.89 (95% CI: 0.87–0.91), which corresponds to a sensitivity of 85% at a specificity of 80%. In comparison, three retinal specialists had similar sensitivities (82–85%), but only half the specificity (45–50%, $p < 0.001$ for each comparison with the algorithms). The positive predictive value (PPV) of the algorithms was 61% (95% CI: 56–66%), approximately double the 36–38% by the retinal specialists. In addition to predicting CI-DME, the algorithms were able to detect the presence of intraretinal fluid with AUC of 0.81 (95% CI: 0.81–0.86) and subretinal fluid with AUC of 0.88 (95% CI: 0.85–0.91).

7.2.1.2 Application on OCT Images
Segmentation of Retinal Layers, Detection of Retinal Fluid in DME and Classifying DME
In a study by Roy et al., the investigators claimed to be the first to use a fully convolutional DL approach for automated segmentation of retinal layers and fluid. This end-to-end learning approach, without handcrafting of features to train the algorithms, was driven entirely by OCT images from eyes with DME of an SD-OCT public data set which was consisted of 110 annotated SD-OCT B-scan images obtained from 10 patients with DME (11 B-scans per patient). These 110 B-scans were annotated for the retinal layers and fluid regions by two expert clinicians. The investigators demonstrated that their model was superior to other state-of-the-art retinal layer segmentation methods [29].

Alsaih et al. also attempted to train ML models to classify DME based on OCT images. The data set consists of 32 OCT volumes (DME = 16, normal = 16). Each volume contains 128 B-scans with more than 3800 images being processed. All SD-OCT volumes are read and assessed by trained graders and identified as normal or DME cases based on evaluation of retinal thickening, hard exudates, intraretinal cystoid space formation, and SRF. They found that combined machine learning algorithms, local binary pattern (LBP) vectors while represented and classified using principal component analysis and a linear-support vector machine (SVM), gave the best results for classifying normal and DME leading to sensitivity and specificity of 87.5% and 87.5% respectively [30].

Predicting Visual Outcome for Anti-VEGF Treatment of DME
Gerendas et al. used a publicly available automated segmentation algorithm based on graph theory to perform segmentation to detect biomarkers in OCT images from Protocol T of DRCR.net clinical trial, which compared different anti-VEGFs for treatment of DME. They then used the markers as inputs in a random forest prediction path of ML to predict BCVA at baseline and after one year of the treatment. The data set from the trial comprised of 621 patients and 1863 OCT volumes. Of the 312 potential predictive factors at the three-time points (baseline, weeks 12, and 24), IRC in the outer nuclear layer within the 3-mm area from the foveal center was the best predictive value for BCVA at baseline. IRC and the total retinal thickness within the 3-mm area at weeks 12 and 24 were the best predictive values for BCVA after one year. The goodness of fit of the prediction model was $R^2 = 0.23$ ($p < 0.001$) [31].

7.2.2 Age-Related Macular Degeneration

7.2.2.1 Application on Color Fundus Photographs
Screening and Staging of AMD
Screening for AMD is different from screening for DR in some aspects. While screening for DR has a specific target population of patients with diabetes, to screen AMD in a population of patients who are between 40 and 90 years old may not be cost-effective [32]. Similar to DME, early and timely intervention of neovascular AMD with anti-VEGF was proven to improve vision in a significant number of patients (CATT 2016). While the modality of screening for DR and DME is settled on using CFP, the modality for early detection of AMD has still been explored in many possibilities, for example, hyperacuity perimetry [33]. Some investigators proposed that SD-OCT should be the first line for the screening

of DME [34]. However, no general consensus was reached on the modality for screening AMD.

Many studies have evaluated the roles of AI for detecting AMD using either CFP or OCT. The AI algorithms for detecting AMD on CFP, if proven to be accurate enough and well accepted, may practically be combined with algorithms for screening DR on CFP; screening for AMD can then be conducted at the same time as screening for DR in patients with diabetes [35]. A challenge for screening AMD would then lie on finding high-risk populations who were not diabetes. Deploying AI for screening AMD should, therefore, be studied in terms of targeted population, practicality, and also cost-effectiveness.

There were at least two published studies on the development of AI models for detecting AMD based on images of the macula from the large longitudinal clinical trial: Age-Related Eye Disease Study (AREDS). Grassman et al. developed AI algorithms from more than 120,000 CFP of more than 3000 participants in the AREDS to classify AMD according to AREDS severity scales. They used 86,770 images to train six different DNNs to classify AMD classes for the images. The class prediction from each network was then used to train a random forest classifier to further improve classification accuracy. The random forest ensemble classifier was then used to predict the nine-step AREDS severity scales of early to intermediate AMD, the three-step AREDS scales of late AMD, and a scale of ungradable images. The rest of the AREDS images was used for validation and testing. Finally, the model was validated in an independent external data set of 5555 fundus images from a population-based KORA: Cooperative Health Research in the Region of Augsburg Study, grading by a trained ophthalmologist was used as a reference standard.

The model was able to predict classes of AMD in the data set of AREDS with a quadratic weighted Kappa of 92% (95% CI, 89–92%) and overall accuracy of 63.3%. For the KORA data set, the model had the best performance in the subset of participants who were more than 55 years old with the prior exclusion of other retinopathies providing the increase of weighted and unweighted Kappa from 35% and 11% to be 50% and 63% respectively. Upon grouping the AREDS

scales into early or late AMD, the model had a sensitivity of 84.2% and specificity of 94.3% respectively [36].

Burlina et al. also used CFP from AREDS study to develop and train DNN to classify AMD [37]. In this study, they evaluated two models of DNN and found that a model, specifically trained to solve AMD classification problems, consistently outperformed another model that had a simpler training requirement. The two models, however, were required to grade AMD into two classes: non-referable (no or early AMD) and referable (intermediate and advanced AMD) with accuracy that ranged between 88.4% (SD, 0.5%) and 91.6% (SD, 0.1%), the AUC was between 0.94 and 0.96, and Kappa coefficient (K) was between 0.764 (SD, 0.010) and 0.829 (0.003) whereas the human grader in this study yielded an accuracy of 90.2 and K of 0.8. There was no external validation in this study.

Ting et al. in their large-scale study for validation of DL for screening referable and sight-threatening DR in multiethnic populations, also developed a DL model for screening referable AMD, defined as the presence of intermediate AMD and/or advanced AMD according to AREDS grading system. This DNN model for screening referable AMD was trained with 72,610 CFP including 38,185 images from a DR screening program, 2180 from two clinic-based studies of AMD, and the rest from an epidemiologic study of AMD. All these studies were conducted in Singapore and the validation data set was from Singapore with 35,948 images from the DR screening program in the years different from those in the developmental data sets. All AMD grades were assessed by retinal specialists as a reference standard. The AUC of 0.931 (95% CI, 0.928–0.935) was found with sensitivity of 93.2% (95% CI, 91.1–99.8%) and specificity of 88.7% (95% CI, 88.3–88.9%). There has not yet been external validation of this algorithm for detecting AMD [18].

7.2.2.2 Application on OCT Images
Detection and Quantification of Biomarkers in AMD
One of the limitations of OCT image studies has been the availability of various vendors, each

with its scan protocols, of the OCT devices in the market. Venhuizen et al. [38], in their study to develop DNN algorithms for intraretinal cyst segmentation and quantification of OCT images of patients with AMD, also assessed the generalizability of the proposed algorithms to multiple OCT vendors, namely: Heidelberg Spectralis, Zeiss Cirrus, Topcon 3D 2000, and Nidek RS3000. Performance of the algorithms based on images from the four devices, each from each vendor, against reference standard (i.e., the intersection of manual annotation of two human graders) provided Dice coefficients of 0.738 ± 0.159 whereas interobserver variability was 0.846 ± 0.049. Thus, the algorithms had the potential to be applied to OCT scans of any of these vendors without significant variability.

For non-exudative AMD, automated segmentation of the retinal layer would be a challenge due to the distortion of the outer retina caused by drusen. Fang et al. proposed that the labelings by DNN may not be precise enough to localize the retinal layer boundaries in non-exudative AMD. Therefore, they integrated graph theory and dynamic programming methods into the DNN-based probability maps to create the final boundaries of the retinal layer. They validated the proposed method on 60 volumes (2915 B-scans) from 20 eyes with non-exudative AMD and found that, in comparison with other automated software, the proposed method gave the best results for segmentation of majority of the retinal layers in terms of mean difference in pixels compared with manual segmentation by an expert grader [39].

For neovascular AMD, the graph search method was integrated into another DNN model for segmentation of IRC, SRF, and retinal pigment epithelium (RPE) in another study by Klimscha et al. [40] The investigators aimed to use the model to find spatial correspondence between the fluid and retinal pigment epithelial detachment (PED) in patients with active treatment-naive neovascular AMD. Automated image segmentation was successful in 1182 OCT volumes of the patients, yielding more than 61 million A-scans for analysis. The IRC-presenting A-scans showed SRF and PED in a median of 2.5 and 32.9% respectively. The SRF-presenting A-scans showed IRC and PED in 0.3% and 1.4%

respectively. Finally, the PED-presenting A-scans showed IRC and SRF in 5.2% and 2.0% respectively. Similar patterns were observed in the manually segmented subsets and via pixel-wise odds ratio analysis. Using the AI model, the investigators were able to find low spatial correspondence of SRF with IRC and PED but increased colocalization of IRC and PED in neovascular AMD.

In another study by Xu et al., the investigators proposed a dual-stage method of DNN for auto-segmentation of PED in polypoidal choroidal vasculopathy (PCV). The proposed DNN framework was quantitatively analyzed in 1800 B-scans of SD-OCT of 50 patients with PCV and then compared with other algorithms and segmentation by retinal specialists were reference standard. The dual-stage DNN outperformed other existing PED segmentation methods for all segmentation accuracy parameters, including true positive volume fraction (85.74 ± 8.69%), dice similarity coefficient (85.69 ± 8.08%), positive predictive value (86.02 ± 8.99%) and false-positive volume fraction (0.38 ± 0.18%). The investigators claimed that the model can be used for auto-segmentation of both serous and vascularized PED in PCV, with possibilities of applying in central serous chorioretinopathy (CSC), typical choroidal neovascularization (CNV) in AMD, and myopic CNV [41].

Measurement of choroidal thickness from enhanced-depth imaging OCT scans (EDI-OCT) is important in assisting the diagnosis and management of certain retinal disorders that may involve macula, such as CSC, and PCV. The measurement, however, often falls into variability in intra- and inter-reader agreement [42]. In a study by Chen et al., a total of 62 EDI-OCT retinal images from 32 patients with AMD were used for the development and validation of a DL model for auto-segmentation of boundaries of the choroid. Two images were acquired from each patient, the first image was of a retina with dry (atrophic) AMD from one eye, and the second image was of a retina with neovascular AMD from the other eye. Each EDI-OCT image was a 2-D cross-sectional slice centered on the fovea, manual segmentation of the choroid was performed by a trained rater and served as the ground

truth in validation. They found the average of the Dice overlap coefficients was 0.83 and the average Bruch's membrane boundary distance errors of the choroidal segmentation were only 5.07 pixels by the DL model. These were comparable with the graph cut method conventionally used in other studies [43].

Differentiate AMD from Normal Macula

Treders et al. conducted a study on DL to automatically differentiate neovascular AMD from healthy macula from OCT images. A total of 1112 cross-section SD-OCT images of patients with neovascular AMD and a healthy control group were used for training and validation of a DNN classifier which was pretrained with 1.2 million images from the public data set (ImageNet). The training was performed in 1012 images (AMD = 701, healthy = 311) and the internal validation was performed in the rest 100 untrained images (AMD = 50, healthy = 50). They defined an AMD testing score of 0.98 or higher as presumed AMD. After full training, they found the model could achieve the average AMD scores of 0.997 ± 0.003 in the AMD validation group and 0.9203 ± 0.085 in the healthy comparison group. The difference between the two groups was statistically significant ($p < 0.001$). The investigators highlighted the capability of using a small data set (approximately 1000 images) to train a DNN model pretrained with public images in ImageNet database to differentiate neovascular AMD from healthy macula with the acceptable performance [44].

In another model trained with a much larger data set for DNN to differentiate AMD from the normal macula, Lee et al. used International Classification of Diseases, ninth Revision (ICD-9) diagnosis codes of AMD, visual acuity, and history of intravitreal injection from electronic medical records (EMR) to classify patients with AMD and normal macula. The investigators carefully classified the patients according to these criteria to ensure that they most likely had either the macular pathology in both eyes or normal macula in both eyes. OCT images linked to the patients in each group were then retrieved to develop a convolutional neural network (CNN) classifier. The investigators successfully extracted 2.6 million OCT images of 43,328 macular OCT scans from 9285 patients from their database. After linking the macular OCT scans to the data from EMR, 48,312 images from 4392 normal OCT scans and 52,690 images from 4790 AMD OCT scans were selected. A total of 80,839 images (AMD = 41,074, normal = 39,765) were used for training and 20,163 images (AMD = 11,616, normal = 8547) were used for validation. They analyzed their results in three levels, at the level of an individual image, an area under the ROC curve of 92.78% with an accuracy of 87.63% was achieved. At the macula level, performed by grouping the images of the same macula and averaging the probabilities of each image, they achieved an area under the ROC curve of 93.83% with an accuracy of 88.98%. At a patient level, performed by averaging the probabilities of images from the same patient, they achieved the highest area under the ROC curve of 97.45% with an accuracy of 93.45% [45].

Assessment of AMD Disease Activity

In a study by Chakravarthy et al., a commercial ML and image recognition computational classifier, Notal OCT Analyzer (NOA) trained with 654 data sets of OCT scans, was validated for the detection of lesion activity of neovascular AMD. The activity was defined as the presence or absence of fluid (intraretinal fluid (IRF) or SRF or PED) in OCT scans of the patients and three retinal specialists graded these parameters as the reference standard. In the primary analysis of 142 OCT scans, the NOA showed a sensitivity of 92% (95% CI, 6%), a specificity of 91% (95% CI, 7%), and a diagnostic accuracy of 91% (95% CI, 7%) relative to the majority grading by the three retinal specialists. For the 121 scans where results from all the three retinal specialists were in concordant, the NOA showed a sensitivity of 94%, specificity of 89%, and an accuracy of 92%. On the other hand, for the 21 scans on which the three retinal specialists disagreed, the sensitivity of the NOA was lower at 83%, the specificity was higher at 100%, and the accuracy was not different at 92%. The NOA outcome was in concordance with the majority vote of the retinal specialists in 19 of 21 cases (90%).

In the second analysis, the investigators tested the use of NOA as an automated scoring and ranking tool of individual B-scans. On testing the subset of the OCT scans within the 121 scans that achieved consensus grading by all of the three retinal specialists, the average number of B-scans needed by any retinal specialist to identify the fluid was 1.08. On average, the three specialists could identify fluid in 95% of the scans by just reviewing a single B-scan with the highest score selected by the analyzer. The identification was increased to 99.5% of the scans when the specialists reviewed three scans with the highest scores selected by the analyzer, and 100% when they reviewed up to the six scans with the highest scores [46].

Prediction of Visual Outcome of AMD Treatment

To predict visual acuity of patients with neovascular AMD after treatment with anti-VEGF, Rohm et al. developed an AI model using 41 "real-world" clinical features, for example, visual acuity from EMR of a data warehouse, together with 124 measurement features from OCT, for example, central retinal thickness, of patients with neovascular AMD (653 patients with 738 eyes for 3-month prediction and 456 patients with 508 eyes for 12-month prediction) for training five different ML algorithms to predict visual acuity of these patients after three injections of anti-VEGF. The best machine learner in this study was the L1 regularized linear model Lasso. Based on data at 3 months, the difference between the prediction and the existing ground truth was between 0.14 logMAR (7 letters) root mean square error (RMSE) and 0.02 logMAR (19 letters) RMSE, whereas at 12 months the difference was between 0.2 logMAR (10 letters) RMSE and 0.26 logMAR (13 letters) RMSE [47].

In another study, Schmift-Erfurth et al. used extracted quantitative OCT biomarkers, for example, IRF, SRF, and PED together with best-corrected visual acuity (BCVA) measurements at baseline and months 1, 2, and 3 to train a random forests ML algorithm to predict BCVA at 12 months of 614 patients with neovascular AMD treated with anti-VEGF injections in a clinical trial "HARBOR." The model

could predict the corresponding BCVA from the extracted morphologic imaging biomarkers from OCT with an accuracy of $R^2 = 0.21$. The RMSE was 11.4 letters. IRF, especially the horizontal extension of fluid within 1-mm and 3-mm of the foveal center as well as IRF volume in the central 1 mm conveyed the highest predictive power of concomitant BCVA. For predicting visual outcomes, the accuracy of the model increased in a linear fashion each month, with the best prediction found at month 3, when the accuracy of $R^2 = 0.7$ with the RMSE of 8.6 letters. While the 12-month outcomes could be predicted from the baseline data with RMSE of 12.9 letters [48].

Interestingly, this RMSE for the 12-month prediction from Schmift-Erfurth et al. was accidentally in the similar range, 10–13 letters, of the prediction at 12 months found by Rohm et al. This occurred although the study by Rohm et al. was based on real-world data whereas the study by Schmift-Erfurth was based on data from a randomized controlled trial.

Prediction of Treatment Requirement in AMD

Bogunovic et al. conducted a post hoc analysis on data from the HARBOR trial using AI to predict treatment requirements on neovascular AMD. They also used 2-year data of patients in the pro re nata (PRN) arm of the study, these included demographic characteristics, BCVA, OCT images at baseline, month 1, and month 2, which were quantified for spatiotemporal features by automated segmentation of the retinal layer using graph-theoretic methods and automated segmentation of IRF and SRF using DNN, to train the random forest classifier for the prediction. Of the 317 eligible patients, during the PRN phase of the study (month 3–23), 71 patients were in the lower quartile of the number of injections, that is, received "low" requirements or no more than five injections, and 70 patients were in the upper quartile of the number of injections, that is, received "high" requirements or receiving 16 or higher injections in this study.

The AI model could predict the requirement of "low" and "high" number of anti-VEGF injections of the individual patients with neovascular

AMD, as in the HARBOR trial, with an area under the ROC curve of 0.7 and 0.77 respectively. A retinal specialist also performed grading by estimating the two categories of treatment requirements based on observing three volumetric OCT scans from the initial phase. For predicting the low requirement, the model had sensitivity and specificity of 58% and 71% respectively whereas the retinal specialist had a sensitivity of 41% and specificity of 84%. For predicting the high requirement, the model had sensitivity and specificity of 71% and 70% respectively whereas the retinal specialist had the sensitivity of 37% and specificity of 84%. The most relevant feature for the prediction was SRF volume in the central 3 mm from the fovea, with the highest predictive values at month 2 [49].

Prediction of Disease Conversion in AMD
The HARBOR trial also offered 614 fellow eyes with intermediate AMD of 1095 eyes with neovascular AMD to be studied for disease conversion in AMD. In the study by Schmidt-Erfurth et al. according to the gold standard grading of conversion to advanced AMD from the intermediate AMD eyes by two independent retinal specialists in the trial, 32% (159 of 495 eyes) of intermediate AMD eyes had conversions, 23.2% (114 of 495 eyes) to CNV and 9.4% (45 of 495 eyes) to geographic atrophy (GA) within 2 years. The investigators used a sparse Cox proportional hazards (CPH) model, commonly used for survival time analysis, which was regularized with the least absolute shrinkage and selection operator (LASSO) method of ML to develop two predictive models. One for estimating the risk of conversion into CNV, and the other for conversion into GA to predict disease conversion in AMD. The investigators had input extensive features into the models including imaging features, and nonimaging features. The imaging features were from OCT detected by automated image analysis of eight categories of outer retinal biomarkers, for example, drusen, pseudodrusen, outer nuclear layer volume, hyperreflective foci volume, and so on, with a total number of 34 quantitative features. The nonimaging features combined two categories, that is, three features of demographic data: age, gender, and smoking status, and 34 single nucleotide polymorphisms of genetic data.

Compared with the gold standard, the predictive models could differentiate converting versus non-converting eyes with an area under the ROC curve of 0.68 and 0.80 for CNV and GA, respectively. The two predictive models showed different hallmarks of the quantitative features for prediction, for CNV the markers were mostly drusen-centric, while for GA they were associated with neurosensory retina and age [50].

7.2.2.3 Application on Ultra-Wide-Field Images
Detection of AMD
The roles of ultra-wide-field (UWF) images in AMD or other macular disorders are still not clear since the major advantage of UWF is detecting disorders in the peripheral retina. It seems that AI may have roles in certain applications of UWF, such as assisting in automated detection of more cases of DR. However, since availability and generalizability of UWF are still limited, applying AI on UWF may be less appealing compared with CFP or OCT images.

In a study by Matsuba et al. a DNN model was developed from UWF images of an Optos device using 227 images of normal patients without retinal disease and 137 images of patients with neovascular AMD from the clinical ophthalmology database at a hospital in Japan. The investigators then divided images in each group as training (70%) and test (30%) data sets respectively. This yielded 253 training images (normal = 158, neovascular AMD = 95) and 111 test images (normal = 69, neovascular AMD = 42). Subsequently, the 253 training images were subjected to preprocessing, followed by amplification to 5000 images (normal = 4130, neovascular AMD = 870). The standard for neovascular AMD was based on the results of retinal examinations, OCT, and fundus angiography conducted by two independent retinal specialists. The DNN yielded an average AUC of 99.76% (95% CI, 99.75–99.76), with average sensitivity

of 100% (95% CI, 90.97–n/a) and specificity of 97.31% (95% CI, 93.84–99.12) [51].

In the second experiment, the investigators compared the diagnostic accuracy between the DNN and ophthalmologists. They prepared 111 images (normal = 69, neovascular AMD = 42) as the test data. Of these, 42 images were extracted from normal data using a random number generation method to yield 84 sheets comprising 50% of normal and 50% of neovascular AMD. A total of 84 sheets were used as test data. The correct answer rate, specificity, sensitivity, and also response times by DNN and six independent ophthalmologists were assessed. Of these 84 test images, the six ophthalmologists yielded an average correct answer rate of 81.9%, a sensitivity of 71.4%, and specificity of 92.5%. The average required time was 11 min 23.54 seconds. The DNN, on the other hand, yielded an average correct answer rate, sensitivity, and specificity of 100%, with a required time of 0 min, 26.29 s.

7.2.3 Macular Edema in Retinal Vein Occlusion

7.2.3.1 Application on OCT Images
Predicting Recurrence of Macular Edema (ME) and Visual Outcome After Treatment with Anti-VEGF in Retinal Vein Occlusions (RVO)
Vogl et al. proposed the ML approaches: sparse logistic regression and random forests-based extra trees (ET) to predict recurrence of ME in RVO after treatment with anti-VEGF. Both approaches could identify spatiotemporal signatures based on retinal thickness features measured in longitudinal 3-D SD-OCT imaging and predict the individual patient outcome as "Recurrence of ME" or "No Recurrence of ME" using these quantitative characteristics. These models were evaluated in 155 patients with ME associated with central retinal vein occlusion (CRVO) and 92 patients with branch retinal vein occlusion (BRVO). The patients received three monthly ranibizumab injections, then monthly

PRN with a follow-up period of a year. Data from the first 3 months of the patients provided better prediction than using data from only the first month. The AUC, sensitivity, and specificity for predicting recurrence of ME in BRVO were 0.83, 0.77, and 0.77, respectively; the same parameters for CRVO were 0.79, 0.67, and 0.79, respectively. The ET model performed slightly better than logistic regression [52].

Predicting Longitudinal Visual Acuity After Standard Anti-VEGF Injection in CRVO Patient
A study by Vogl et al. to predict visual outcome after treatment of ME in patients with CRVO may be a good illustration of how AI can be deployed in clinical research. This study used an AI model as a tool for assessment of biomarkers on SD-OCT, that is, IRF and SRF, incorporating data of measured BCVA as longitudinal, monthly, clinical variables in a statistical model of multivariable repeated-measure mixed-effects regression for the trajectory of BCVA over time. Using data from the CRYSTAL trial of anti-VEGF treatments for CRVO, the investigators were able to create a population-wide mixed model that could not only reveal the impact of fluid on BCVA but also be used for predicting the future VA of individual patients using initial BCVA and the fluid measurements as co-variables for the prediction. The impact of fluid on BCVA was highest for IRF in the central millimeter around the fovea, with -31.17 letters/mm^3 (95% CI, 39.70–23.32) [52].

7.2.4 Inherited Macular Disorders

7.2.4.1 Application on OCT Images
Segmentation of Ellipsoid Zone in Choroideremia and Retinitis Pigmentosa
Camino et al. used a segmentation method by a DNN model, consisting of sliding-window binary classification of en face OCT sections, to objectively quantify the preserved area of photoreceptor layer (seen as an ellipsoid zone in OCT B-scans) of two inherited retinal degenera-

tions (IRDs): choroideremia and retinitis pigmentosa. An excellent segmentation accuracy of approximately 90% was achieved for both IRDs compared with segmentation by a human expert. Due to the flexibility of this technique, the investigators claimed that this method has the potential to be extended to other IRDs in the future [53].

7.2.4.2 Application on Adaptive Optics Scanning Light Ophthalmoscope (AOSLO) Images

Quantify Cone Cells in Stargardt Disease
In another interesting study by Davidson et al. a robust DL framework of Multidimensional Recurrent Neural Network (MDRNN) was developed to automatically identify in vivo cone photoreceptors imaged by Adaptive Optics Scanning Light Ophthalmoscope (AOSLO) split detection. The investigators showed that the MDRNN achieved the average Dice score and respective standard deviation of 0.9431 ± 0.0482 (0.9628 ± 0.0252 for healthy and 09233 ± 0.0571 for Stargardt disease) which is the most robust, compared to other automated detection methods. Although AOSLO images are used rarely in clinical practice due to the requirement of manual counts on the visualized cone cells, this study showed a promising role of AI in advanced retinal imaging technology in that the visualized cone cells can be automatically detected and counted relatively accurately [54].

7.3 The Potential Application of AI for Macular Surgery

Studies on applying AI for macular or retinal surgery are still relatively uncommon compared to studies on applying AI for the medical retina. Surgical management involves many more complex steps of patient care, for example, preoperative evaluation, assessment of potential surgical outcome, intraoperative decision making, early detection of postoperative complications, and so on, which in many occasions are unique and may have different perspectives from medical man-

agement. Each of these steps contains a huge amount of multimodal data on which AI can be applied for augmentation. Due to inherited variability of many surgical retinal procedures, such as variable methods of macular hole closure surgery [55] or retinal reattachment surgery [56], cleaning surgical data to train AI algorithms effectively would be a real challenge. The true potential of AI in macular and retinal surgery remains to be seen and could be difficult to predict.

One of the first steps toward applying AI for macular or retinal surgery, however, may not be much different from recent studies in medical retina. For example, prediction of visual outcome after macular surgery by AI, in theory, maybe studied in the same way as a prediction of visual outcome after intravitreal injections by ML or DL models described previously. The AI models for this purpose can be developed and validated given that surgical procedures are employed in standardized fashions across the surgeries and outlier data, such as cases with complications, should be excluded from training the models. Therefore, the models should be applied for making predictions under the ideal condition of having no complication. A common, simple, straightforward macular surgery, such as epiretinal membrane peeling may be the most suitable macular surgery on which AI can be applied to predict visual outcome in this infancy stage. There is also an unmet need for membrane peeling procedure in that visual outcome in some cases are difficult to predict [57] and AI may be able to fill this gap.

A subfield of AI called "computer vision" [58] is able to utilize mathematical models to analyze surgical video streams as quantifiable features such as color, texture, and position to be used within a data set in which an AI model can learn to identify statistically meaningful events. In short, "computer vision" is a vision of computer which may have resulted in machines achieving human-level capabilities for object or scene recognition [59]. For example, in general surgery, real-time analysis of laparoscopic video has yielded 92.8% accuracy in the automated identification of the steps of sleeve gastrectomy and

noted missing or unexpected steps [60]. With 1-minute of high-definition surgical video estimated to contain 25 times the amount of data found in a high-resolution computed tomography image [61], the video could contain a wealth of actionable data [62, 63].

Similar scenarios may also be applied to macular or retinal surgery. In the future, in surgery for traction retinal detachment in PDR, for example, predictive video analysis algorithms may be able to provide preoperatively the probability of having iatrogenic breaks or may be able to warn surgeons if the break is about to occur intraoperatively. Before we are reaching these scenarios, however, AI could have played roles in augmentation of current advanced technology of retinal surgery, such as intraoperative OCT or robotic retinal surgery [64].

The most important of all issues related to applying AI in macular or retinal surgery should not be different from applying AI in the medical retina or other specialties in medicine. It is the role of physicians which is essential. Retinal specialists should have clinical insight that can guide data scientists and engineers to answer the right questions with the right data to fill the gap of unmet need in taking care of patients with retinal disorders. They should know the advantages, disadvantages, strengths, and weaknesses of AI. Retinal specialists should be active, not passive, in embracing AI.

7.4 Limitation of AI

Although the AI-based models have achieved high accuracy in many of the diseases in ophthalmology, the current challenge is the clinical validation and real-time deployment of these models in clinical practice. Most of the studies have utilized training sets from relatively homogenous populations [10, 18, 24, 25]. Diversifying the data set, in terms of ethnicities, and hardware to capture the images will address this challenge to some extent [65].

Also, the training and tuning data set often is subjected to many variables like the field of view, magnification, image quality, and artifacts. One of the challenges in the development of AI models in ophthalmology has been the lack of availability of large data for diseases that are not common (e.g., ophthalmic tumors) and also for diseases which are common but not routinely imaged (e.g., cataract). Likewise, diseases like retinopathy of prematurity and glaucoma, where the definition used are also variable across ophthalmologists, the development of an AI algorithm is a challenge. Some of the ophthalmic diseases need multiple instruments for establishing a diagnosis, (e.g., glaucoma), which also poses a challenge for developing an AI algorithm.

The computer term "GIGO" (Garbage in, Garbage out) also applies to AI. The software is unlikely to give accurate prediction if the training set of images given to the AI tool is too small or not representative of real patient populations. More evidence on methods of getting high-quality ground-truth labels is required. Krause et al. reported that adjudication grades by retina specialists were a more rigorous reference standard, especially to detect artifacts and missed microaneurysms in DR, than a majority decision and showed that by doing so the algorithm performance improved [66]. Almost all current systems of DL in ophthalmology are based on cross-sectional data. These algorithms are currently studied to handle the time factor, like the disease progression. This is an important area of research for future AI models.

Although many recent studies on AI using the DL system have boasted its powerful diagnostics excellence, few have demonstrated the power calculation which is important for the independent data set. Predetermining the required operating threshold on the training set, analysis such as sensitivity and specificity on the test set to evaluate the calibration of the algorithm is important, this should be calculated using the prevalence, type I, type 2 errors, precision, and confidence intervals, and so on.

DL models are often considered as "Black Boxes." In health care, it is not only the quantitative algorithmic performance but also the reason why the algorithms work which is important to

understand. These may not only help to convince the physician but also may help in modifying the classification system of disease. However, groups have been attempting to generate heat maps highlighting the regions of influence on the image which contributed to the algorithm conclusion [67, 68].

However, such maps are often challenging to interpret [69]. Sometimes, it may highlight an area, with no visible disease [70, 71]. A different approach has been used in the DL system developed by Moorfields Eye Hospital and DeepMind—in this system, the generation of an intermediate tissue representation by a segmentation network is used to highlight for the clinician (and quantify) the relevant areas of retinal pathology [72].

The AI-DR screening systems have been developed and validated using two-dimensional images and lack stereoscopic aspects, thus making identification of elevated lesion like retinal traction, vitreous traction, PED is often challenging. Using the information from multimodal imaging in future AI algorithms may potentially address this challenge. In addition, the medicolegal aspects and the regulatory approvals are different in various countries and settings, which also need to be addressed before its use in real clinical settings.

One of the most important challenges to the clinical adoption of AI-based technology is to understand how the patients entrust clinical care to machines. Keel S et al. studied the patient acceptability of the AI-DR screening model in an endocrinology outpatient setting and reported that 96% of participants were satisfied or very satisfied with the automated screening model [73]. However, this patient's acceptability for AI-based screening may vary in various countries and may pose challenges in its implementation. Over time it is important to understand the impact of AI on clinical care. If the AI systems gain widespread use, we will start identifying more people who need treatment. The health authorities have to plan for this anticipated increase in the volume of referrals in their health system. The summary of challenges and limitations are listed in the Table.

Challenges
1. Ethnicities of the different population around the globe
2. Nonavailability of longitudinal data set
3. The requirement of multiple instruments for disease diagnosis
Limitations
1. Lack of data for uncommon diseases (rare to be imaged and reported) and common diseases (not imaged regularly)
2. Difficulty in predetermining the required operating threshold on training data set
3. AI uses heat images for analyses might lead to the wrong diagnosis considered as "Black Boxes" of AI
4. Building up patient entrust
5. Medicolegal, ethical issues, and regulations

7.5 Outlook

For developing AI algorithms, DL enabled significant leaps when applied on imaging. Applying clear principles (lots of images, clean labels) enables AI to pick up the right signals and provide diagnosis, independent of the specific imaging technology, or the specific disorder being investigated. The approach works similarly on fundus or OCT images, on retinal disorders, macular disorders, or other diseases not directly related to the eye Selected studies on AI for macular disorders are listed in Tables 7.1, 7.2, and 7.3.

This technological advancement unlocks new approaches both in research and in the daily work in the clinic. In research, the big opportunity lies in collecting more imaging data where the labels do not require human interpretation. For instance, instead of asking specialists for their DR grading of a given fundus image, knowing which patients developed blindness 10 or 20 years later might help in picking up a novel or precise signals. It is likely that there are more subtle patterns to identify in current imaging technology.

AI, once approved for clinical use and adopted widely, will be at the fingertips of the doctor. The diagnosis of images can be assisted or delegated (e.g., to one or multiple competing AIs). Doctors will have the option of shifting their attention toward supervising the AI diagnosis or toward a

Table 7.1 Selected published studies on automated segmentation of retinal layers and biomarkers by AI

First author (year)	Disease	Image input	Algorithm	Output	Training dataset (n, Images)	Labelling training	Internal validation (n, Images)	Internal validation standard	External validation (n, Images)	External validation standard	Sensitivity	Specificity	Accuracy	AUC	Other statistics
Sinthanayothin (1999) [7]	DR	CFP	ANN and others	Optic disc, fovea, blood vessels	112	An ophthalmologist	NA	NA	174 patches of retinal images	An ophthalmologist	99.1, 83.3, 80.4 for optic disc, vessels, fovea detection, respectively	99.1, 91,99.1 for optic disc, vessels, fovea detection, respectively	NA	NA	NA
Usher (2003) [8]	DR	CFP	ANN	DR	500	A diabetologist	773	A diabetologist	NA	NA	94.8	52.8	NA	NA	NA
Lee (2017) [24]	Wet AMD, DME, RVO	OCT	DNN	Macular fluid	934	Clinicians trained by retinal specialists	355	Clinicians trained by	NA	NA	retinal specialists respectively NA	NA	NA	NA	Dice co-efficient 0.750, 0.729 in humans, and DLS, respectively
Schlegl (2018) [25]	Wet AMD, DME, RVO	OCT	DNN	Macular fluid	1200	Retinal specialists	Cross validation	Retinal specialists	NA	NA	NA	NA	NA	0.94,0.92 in IRF and SRF detection	Pearson''s correlation coefficient 0.9 and 0.96 for IRC and SRF quantification
Roy (2017) [29]	DME	SD-OCT	FCNN	Macular fluid	55	Clinicians	55	Clinicians	NA	NA	NA	NA	NA	NA	Dice overlap score 0.93
Alsaih (2017) [30]	DME	SD-OCT from SERI dataset	SVM, PCA	DME	3840	Trained graders	256	Trained graders	NA	NA	87.5	87.5	NA	NA	NA
Venhuizen (2018) [38]	AMD	SD-OCT	FCNN	IRC	3131	An human grader	540	An human grader	2487	An human grader	NA	NA	NA	NA	Dice co-efficient 0.786 ± 0.174 is
Fang (2017) [39]	Dry AMD	SD-OCT	CNN-GS	Eight retinal layers identification	171	An expert grader	2915	An expert grader	NA	NA	NA	NA	NA	NA	Compare mean difference in pixels of segmentation between difference models
Xu (2017) [41]	PCV	SD-OCT	Dual staged DNN	PED	1800	Retinal specialists	NA	NA	NA	NA	NA	NA	NA	NA	Dice co-efficient 85.69 ± 8.08%

(continued)

Table 7.1 (continued)

First author (year)	Disease	Image input	Algorithm	Output	Training dataset (n, Images)	Labelling training	Internal validation (n, Images)	Internal validation standard	External validation (n, Images)	External validation standard	Sensitivity	Specificity	Accuracy	AUC	Other statistics
Chen (2017) [43]	AMD	EDI-OCT	CNN	Choroidal thickness	50	A trained rater	12	A trained rater	NA	NA	NA	NA	NA	NA	Dice co-efficient 0.83
Chakravarthy (2016) [46]	Wet AMD	OCT	MLA	IRF, SRF, PED	654	Retinal specialists	NA	NA	142	Retinal specialists	92	91	91	0.97	NA
Matsuba (2018) [51]	AMD	UF-DPF	DNN	AMD	253	Retinal specialists	111	Retinal specialists	137	Ophthalmologists	100	97.31	NA	99.76	NA
Camino (2018) [53]	Choroideremia, RP	SD-OCT, enface images	SSADA, DNN	Photoreceptor loss in IRD	61,200	An expert grader	20,400	An expert grader	NA	NA	NA	NA	NA	NA	Jaccard similarity index = 0.912, 0.894 in Choroideremia, RP, respectively
Davidson (2018) [54]	Stargardt disease	AOSLO	MDRNN	Cone cell localization	176	Experienced clinical team members	14	Experienced clinical team members	96	Experienced clinical team members	NA	NA	0.9431	NA	Dice co-efficient 0.18 ± 1.47

AMD Age-related macular degeneration, *MDRNN* Multidimensional Recurrent Neural Network, *ANN* Artificial neural network, *MLA* machine learning algorithm, *AOSLO* Adaptive Optics Scanning Light Ophthalmoscopy, *MRM* mixed-effects regression model, *CNN* convolutional neural network, *CNN-GS* convolutional neural network with graph search methodology, *PCA* Principal component analysis, *CSC* Central serous chorioretinopathy, *PCV* polypoidal choroidal vasculopathy, *CFP* color fundus photograph, *RMSE* root mean square error, *DCNN* deep convolutional neural network, *RP* Retinitis pigmentosa, *DME* Diabetic macular edema, *RVO* Retinal vein occlusion, *DR* Diabetic retinopathy, *SSADA* Split spectrum amplitude–decorrelation algorithm, *FCNN* Fully conventional neural network, *UF-DFP* ultrawide field fundus imaging, *IRD* Inherited retinal degeneration, *SERI* Singapore eye research institute, *SVM* linear–support vector machine

Table 7.2 Selected published studies on automated classification of retinal and macular disorders by AI

First author (year)	Disease	Input	Algorithm	Output	Training dataset (n, Images)	Labelling training	Internal validation dataset (n, Images)	Internal validation standard	External validation dataset (n, Images)	External validation standard	Sensitivity	Specificity	Accuracy	AUC	Other statistics
Gardner (1996) [6]	DR	Digitized fundus image	ANN	Referable DR	179	A trained observer	NA	NA	301	Retinal specialists	88.4	83.5	NA	NA	NA
Abramoff (2008) [9]	DR	CFP	MLA	Referable DR	NA	NA	NA	NA	10,000	Retinal specialists	0.84	0.64	NA	0.84	NA
Gulshan (2016) [17]	DR	CFP	DNN	Referable DR	102,540	Ophthalmologists	25,635	Ophthalmologists	11,711	Ophthalmologists	90.3	98.1	NA	99.1	NA
Ting (2017) [18]	DR	CFP	DNN	Referable DR, vision threatening DR	76,370	Senior graders, retinal specialists	71,896	Senior graders, retinal specialists	40,752	Variety of graders	90.5; 100 for referable DR, visual threatening DR	91.6, 91.1 for referable DR, visual threatening DR	NA	0.936, 0.958 for referable DR, visual threatening DR	NA
	Referable AMD	CFP	DNN	Referable AMD	72,610	Senior graders,	35,948	Senior graders, retinal specialists	NA	NA	93.2	88.7	NA	0.931	NA
Gargeya (2017) [19]	DR	CFP	DNN	DR	60,137	Retinal specialists	15,000	Retinal specialists	2211	Existing grade of public dataset	93	87	NA	0.94	NA
Prahs (2018) [26]	AMD, RVO, DR, CSC	OCT	DNN	Requirement of antiVEGF injection	153,912	Treating clinicians	17,112	Treating clinicians	5358	Treating clinicians	90.1	96.2	95.5	0.988	NA
Grassmann (2018) [36]	AMD	CFP from ARDES study	DNN, Random forest	AREDS scoring level	86,770	A trained ophthalmologist	33,886	A trained ophthalmologist	5555	A trained ophthalmologist	82.2, 100 for intermediate and late AMD, respectively	97.1, 96.5 for intermediate and late AMD, respectively	83.1	NA	Unweighted and quadratic weighted kappa of 50.1% and 63.2%, respectively
Burlina (2017) [37]	AMD	CFP from ARDES study	DNN	AMD staging	53,920	Preexisting AREDS grade	13,480	Preexisting AREDS grade	NA	NA	85.7–87.2	93.4	88.4–91.6	0.94–0.96	Kappa 0.764–0.829

(continued)

Table 7.2 (continued)

First author (year)	Disease	Input	Algorithm	Output	Training dataset (n, Images)	Labelling training	Internal validation dataset (n, Images)	Internal validation standard	External validation dataset (n, Images)	External validation standard	Sensitivity	Specificity	Accuracy	AUC	Other statistics
Lee (2017) [24]	AMD	OCT, data from EMR	CNN	AMD	80,839	NA	20,163	NA	30	NA	92.64	93.69	87.63, 88.98, 93.45 for image, macular and patient level, respectively	92.78, 93.83, 97.45 for image, macular and patient level, respectively	NA
Treder (2018) [44]	AMD	SD-OCT	DNN	AMD	1012	NA	100	NA	NA	NA	92	96	100	NA	NA

AMD Age-related macular degeneration, *MDRNN* Multidimensional Recurrent Neural Network, *ANN* Artificial neural network, *MLA* machine learning algorithm, *AOSLO* Adaptive Optics Scanning Light Ophthalmoscopy, *MRM* mixed-effects regression model, *CNN* convolutional neural network, *CNN-GS* convolutional neural network with graph search methodology, *PCA* Principal component analysis, *CSC* Central serous chorioretinopathy, *PCV* polypoidal choroidal vasculopathy, *CFP* color fundus photograph, *RMSE* root mean square error, *DCNN* deep convolutional neural network, *RP* Retinitis pigmentosa, *DME* Diabetic macular edema, *RVO* Retinal vein occlusion, *DR* Diabetic retinopathy, *SSADA* Split spectrum amplitude–decorrelation algorithm, *FCNN* Fully conventional neural network, *UF-DFP* ultrawide field fundus imaging, *IRD* Inherited retinal degeneration

Table 7.3 Selected published studies on the prediction of treatment outcome of the macular disorder by AI

First author (year)	Disease	Input	Algorithm	Application	Output	Training dataset (n, Images)	Labelling training	Internal validation dataset (n, images)	Internal validation standard	Sensitivity	Specificity	AUC	Other statistics
Gerendas (2017) [31]	DME	SD-OCT from protocol T study, DRCR.net	MLA, Random forest	Segmentation Prediction	BCVA at baseline and one year	1863	NA	NA	NA	NA	NA	NA	$R^2 = 0.21/0.23$ at baseline and one year, respectively ($P < 0.001$)
Rohm (2018) [47]	Wet AMD with various anti-VEGF injection	OCT	MLA[a]	Prediction	VA at 3,12 months	653 patients	NA	NA	NA	NA	NA	NA	The difference between the prediction and ground truth was between 0.11 logMAR MAE/0.14 logMAR RMSE and 0.18 logMAR MAE/0.2 logMAR RMSE and 0.16 logMAR MAE/0.2 logMAR RMSE and 0.22 logMAR MAE/0.26 logMAR RMSE at 3, 12 months, respectively
Schmidt-Erfurth (2017) [48]	Wet AMD with ranibizumab injection	SD-OCT, BCVA from HARBOR study	MLA[b]	Prediction	BCVA at 12th month	2456	A retinal specialist	NA	NA	NA	NA	NA	$R^2 = 0.7$, RMSE 8.6 letters comparing with ground truth data
Bogunovic (2017) [49]	Wet AMD with ranibizumab injection	OCT, BCVA, demographic data from HARBOR study	MLA with forest classifier	Prediction	Low or high antiVEGF requirement[c]	285 patients	Preexisting HARBOR grade	32 Patients	Preexisting HARBOR grade	58, 70 in low and high requirement[c] comparing to a retinal specialist	71, 71 in low and high requirement[c] comparing to a retinal specialist	0.7, 0.77 in low and high requirement[c] comparing to a retinal specialist	NA
Schmidt-Erfurth (2018) [50]	AMD	SD-OCT, demographic data, genetic data from HARBOR study	MLA, CNN	Prediction	Advanced AMD conversion	445	Graders	50	Graders	0.8, 0.8 in CNV,GA comparing with ground truth data	0.46, 0.69 in CNV,GA comparing with ground truth data	0.68, 0.80 in CNV,GA comparing with ground truth data	NA

(continued)

Table 7.3 (continued)

First author (year)	Disease	Input	Algorithm	Application	Output	Training dataset (n, Images)	Labelling training	Internal validation dataset (n, images)	Internal validation standard	Sensitivity	Specificity	AUC	Other statistics
Vogl (2017) [52]	RVO with ranibizumab injection	SD-OCT	MLA[d]	Prediction	Recurrence of Macular edema at months 12	247 patients	NA	NA	NA	0.67, 0.77 in CRVO,BRVO comparing with ground truth data	0.79, 0.77 in CRVO,BRVO comparing with ground truth data	0.76, 0.83 in CRVO,BRVO comparing with ground truth data	Logistic regression 0.79, 0.78 in CRVO, BRVO
Vogl (2017) [52]	CRVO with ranibizumab injection	SD-OCT; BCVA from CRYSTAL study	MRM with quadratic growth term	Prediction	BCVA at months 12	193 patients	NA	NA	NA	NA	NA	NA	$R^2 = 0.658$

[a]AdaboostR2, Gradient boosting, Random Forest, Extremely Randomized Trees, Lasso

[b]CNN with graph theory with random forest regression

[c]Low requirement is defined as a patient with lower quartile of ranibizumab injection, corresponded to no more than 5 injections; the high requirement is defined as patient in upper quartile injection, correspond to $\geq$ 16 injections

[d]Logistic regression and random forests-based extra trees. *AMD* age-related macular degeneration, *MDRNN* Multidimensional Recurrent Neural Network, *ANN* artificial neural network, *MLA* machine learning algorithm, *AOSLO* Adaptive Optics Scanning Light Ophthalmoscopy, *MRM* mixed-effects regression model, *CNN* convolutional neural network, *CNN-GS* convolutional neural network with graph search methodology, *PCA* Principal component analysis, *CSC* Central serous chorioretinopathy, *PCV* polypoidal choroidal vasculopathy, *CFP* color fundus photograph, *RMSE* root mean square error, *DCNN* deep convolutional neural network, *RP* retinitis pigmentosa, *DME* diabetic macular edema, *RVO* retinal vein occlusion, *DR* diabetic retinopathy, *SSADA* split spectrum amplitude-decorrelation algorithm, *FCNN* fully conventional neural network, *UFDFP* ultra-wide field fundus imaging, *IRD* inherited retinal degeneration

more holistic view of the patient and a deepened direct patient–doctor connection. There will be demand for more research on which approach benefits the patient most. However, a general shift toward better caretaking and precise personalized diagnosis is very likely to happen one way or the other.

References

1. Doyle-Lindrud S. Watson will see you now: a super-computer to help clinicians make informed treatment decisions. Clin J Oncol Nurs. 2015;19(1):31–2.

2. Miotto R, Wang F, Wang S, Jiang X, Dudley JT. Deep learning for healthcare: review, opportunities and challenges. Bioinformatics. 2017;2016:1–11.

3. Litjens G, Sánchez CI, Timofeeva N, Hermsen M, Nagtegaal I, Kovacs I, et al. Deep learning as a tool for increased accuracy and efficiency of histopathological diagnosis. Sci Rep. 2016;6(1):1–11.

4. Peng L. Assessing cardiovascular risk factors with computer vision [Internet]. Google AI Blog. 2018 [cited 10 September 2018]. Available from: https://ai.googleblog.com/2018/02/assessing-cardiovascular-risk-factors.html

5. Peng L. Deep learning for detection of diabetic eye disease [Internet]. Google AI Blog. 2016 [cited 10 September 2018]. Available from: https://ai.googleblog.com/2016/11/deep-learning-for-detection-of-diabetic.html

6. Gardner GG, Keating D, Williamson TH, Elliott AT. Automatic detection of diabetic retinopathy using an artificial neural network: a screening tool. Br J Ophthalmol. 1996;80(11):940–4.

7. Sinthanayothin C, Boyce JF, Cook HL, Williamson TH. Automated localisation of the optic disc, fovea and retinal blood vessels from digital color fundus images. Br J Ophthalmol. 1999;83(4):902–10.

8. Usher D, Dumskyj M, Himaga M, Williamson TH, Nussey S, Boyce J. Automated detection of diabetic retinopathy in digital retinal images: a tool for diabetic retinopathy screening. Diabet Med. 2004;21(1):84–90.

9. Abràmoff MD, Niemeijer M, Suttorp-Schulten MSA, Viergever MA, Russell SR, Van Ginneken B. Evaluation of a system for automatic detection of diabetic retinopathy from color fundus photographs in a large population of patients with diabetes. Diabetes Care. 2008;31(8):2008.

10. Abràmoff MD, Lou Y, Erginay A, Clarida W, Amelon R, Folk JC, et al. Improved automated detection of diabetic retinopathy on a publicly available dataset through integration of deep learning. Invest Ophthalmol Vis Sci. 2016;57(13):5200–6.

11. American Diabetes Association. Diabetic retinopathy. Diabetes Care. 2002;25(Suppl):590–3.

12. Cummings DM, Morrissey S, Barondes MJ, Rogers L, Gustke S. Screening for diabetic retinopathy in rural areas: the potential of telemedicine. J Rural Health. 2001;17(1):25–31.

13. Kanjee R, Dookeran RI, Mathen MK, Stockl FA, Leicht R. Six-year prevalence and incidence of diabetic retinopathy and cost-effectiveness of tele-ophthalmology in Manitoba. Can J Ophthalmol. 2017;52(11):S15–8.

14. Ruamviboonsuk P, Teerasuwanajak K, Tiensuwan M, Yuttitham K. Interobserver agreement in the interpretation of single-field digital fundus images for diabetic retinopathy screening. Ophthalmology. 2006;113(5):826–32.

15. Augustin Terlinden, Patricia A. Deverka, Amine Aissaoui, Olivier Ethgen. Artificial intelligence (AI) and precision medicine: does the health economist need to adapt to the machine? ISPOR 23rd Annual International Meeting. 2018.

16. FDA permits marketing of artificial intelligence-based device to detect certain diabetes-related eye problems [Internet]. Fda.gov. 2018 [cited 6 September 2018]. Available from: https://www.fda.gov/NewsEvents/Newsroom/PressAnnouncements/ucm604357.htm.

17. Gulshan V, Peng L, Coram M, Stumpe MC, Wu D, Narayanaswamy A, et al. Development and validation of a deep learning algorithm for detection of diabetic retinopathy in retinal fundus photographs. JAMA. 2016;316(22):2402–10.

18. Ting DSW, Cheung CYL, Lim G, Tan GSW, Quang ND, Gan A, et al. Development and validation of a deep learning system for diabetic retinopathy and related eye diseases using retinal images from multiethnic populations with diabetes. JAMA. 2017;318(22):2211–23.

19. Gargeya R, Leng T. Automated identification of diabetic retinopathy using deep learning. Ophthalmology. 2017;124(7):962–9.

20. Raumviboonsuk P, Krause J, Chotcomwongse P, Sayres R, Raman R, Widner K, et al. Deep learning vs. human graders for classifying severity levels of diabetic retinopathy in a Real-World Nationwide Screening Program. NPJ Digit Med. 2019;2(25)

21. Schmidt-Erfurth U, Waldstein SM. A paradigm shift in imaging biomarkers in neovascular age-related macular degeneration. Prog Retin Eye Res. 2016;50:1–24.

22. Toth CA, DeCroos FC, Ying GS, Stinnett SS, Heydary CS, Burns R, Maguire M, Martin D, Jaffe GJ. Identification of fluid on optical coherence tomography by treating ophthalmologists versus a reading center in the comparison of age-related macular degeneration treatments trials. Retina. 2015;35(7):1303–13.

23. Srinivas S, Nittala MG, Hariri A, Pfau M, Gasperini J, Ip M, Sadda SR. Quantification of intraretinal hard exudates in eyes with diabetic retinopathy by Optical Coherence Tomography. Retina. 2018;38(2):231–6.

24. Lee CS, Tyring AJ, Deruyter NP, Wu Y, Rokem A, Lee AY. Deep-learning based, automated segmentation

of macular edema in optical coherence tomography. Biomed Opt Express. 2017;8(7):3440.

25. Schlegl T, Waldstein SM, Bogunovic H, Endstraßer F, Sadeghipour A, Philip AM, et al. Fully automated detection and quantification of macular fluid in OCT using deep learning. Ophthalmology. 2018;125(4):549–58.

26. Prahs P, Radeck V, Mayer C, Cvetkov Y, Cvetkova N, Helbig H, et al. OCT-based deep learning algorithm for the evaluation of treatment indication with anti-vascular endothelial growth factor medications. Graefes Arch Clin Exp Ophthalmol. 2018;256(1):1–8.

27. Wang YT, Tadarati M, Wolfson Y, Bressler SB, Bressler NM. Comparison of prevalence of diabetic macular edema based on monocular fundus photography vs optical coherence tomography. JAMA Ophthalmol. 2016;134(2):222–8.

28. Varadarajan A, Bavishi P, Raumviboonsuk P, Chotcomwongse P, Venugopalan S, Narayanaswamy A, et al. Predicting optical coherence tomography-derived diabetic macular edema grades from fundus photographs using deep learning. Nat Commun. 2020;11(1):130.

29. Roy AG, Conjeti S, Karri SPK, Sheet D, Katouzian A, Wachinger C, et al. ReLayNet: retinal layer and fluid segmentation of macular optical coherence tomography using fully convolutional network. Biomed Opt Express. 2017;8(8):111–8.

30. Alsaih K, Lemaitre G, Rastgoo M, Massich J, Sidibé D, Meriaudeau F. Machine learning techniques for diabetic macular edema (DME) classification on SD-OCT images. Biomed Eng Online. 2017;16(1):1–12.

31. Gerendas BS, Bogunovic H, Sadeghipour A, Schlegl T, Langs G, Waldstein SM, et al. Computational image analysis for prognosis determination in DME. Vis Res. 2017;139:204–10.

32. Tamura H, Goto R, Akune Y, Hiratsuka Y, Hiragi S. The clinical effectiveness and cost- effectiveness of screening for age-related macular degeneration in Japan: a Markov modeling Study. PLoS One. 2015;10(7):1–20.

33. Chew EY, Clemons TE, Bressler SB, Elman MJ, Danis RP, Domalpally A, Heier JS, Kim JE. Garfinkel RA; Appendix 1 for AREDS2-HOME Study Research Group. Randomized trial of the ForeseeHome monitoring device for early detection of neovascular age-related macular degeneration. The HOme Monitoring of the Eye (HOME) study design— HOME Study report number 1. Contemp Clin Trials. 2014;37(2):294–300.

34. Gualino V, Tadayoni R, Cohen SY, Erginay A, Fajnkuchen F, Haouchine B, et al. Optical coherence tomography, fluorescein angiography, and diagnosis of choroidal neovascularization in age-related macular degeneration. Retina. 2019;39(9):1664–71.

35. Chan CKW, Gangwani RA, Gangwani RA, McGhee SM, Lian JX, Wong DSH. Cost-effectiveness of screening for intermediate age-related macular degeneration during diabetic retinopathy screening. Ophthalmology. 2015;122(11):2278–85.

36. Grassmann F, Mengelkamp J, Brandl C, Harsch S, Zimmermann ME, Linkohr B, et al. A deep learning algorithm for prediction of age-related eye disease study severity scale for age-related macular degeneration from color fundus photography. Ophthalmology. 2018;125(9):1410–20.

37. Burlina PM, Joshi N, Pekala M, Pacheco KD, Freund DE, Bressler NM. Automated grading of age-related macular degeneration from color fundus images using deep convolutional neural networks. JAMA Ophthalmol. 2017;135(11):1170–6.

38. Venhuizen FG, van Ginneken B, Liefers B, van Asten F, Schreur V, Fauser S, et al. Deep learning approach for the detection and quantification of intraretinal cystoid fluid in multivendor optical coherence tomography. Biomed Opt Express. 2018;9(4):1545.

39. Fang L, Cunefare D, Wang C, Guymer RH, Li S, Farsiu S. Automatic segmentation of nine retinal layer boundaries in OCT images of non-exudative AMD patients using deep learning and graph search. Biomed Opt Express. 2017;8(5):2732.

40. Klimscha S, Waldstein SM, Schlegl T, Bogunović H, Sadeghipour A, Philip AM, et al. Spatial correspondence between intraretinal fluid, subretinal fluid, and pigment epithelial detachment in neovascular age-related macular degeneration. Invest Ophthalmol Vis Sci. 2017;58(10):4039–48.

41. Xu Y, Yan K, Kim J, Wang X, Li C, Su L, et al. Dual-stage deep learning framework for pigment epithelium detachment segmentation in polypoidal choroidal vasculopathy. Biomed Opt Express. 2017; 8(9):4061.

42. Ouyang Y, Heussen FM, Mokwa N, Walsh AC, Durbin MK, Keane PA, et al. Spatial Distribution of Posterior Pole Choroidal Thickness by Spectral Domain Optical Coherence Tomography. Invest Ophthalmol Vis Sci. 2011;52(9):7019–26.

43. Chen M, Wang J, Oguz I, VanderBeek BL, Gee JC. Automated segmentation of the choroid in EDI-OCT images with retinal pathology using convolution neural networks. Lect Notes Comput Sci 2017;10554 LNCS (2017):177–184.

44. Treder M, Lauermann JL, Eter N. Automated detection of exudative age-related macular degeneration in spectral domain optical coherence tomography using deep learning. Graefes Arch Clin Exp Ophthalmol. 2018;256(2):259–65.

45. Lee CS, Baughman DM, Lee AY. Deep Learning Is Effective for Classifying Normal versus Age-Related Macular Degeneration OCT Images. Ophthalmol Retina. 2017;1(4):322–27.

46. Chakravarthy U, Goldenberg D, Young G, Havilio M, Rafaeli O, Benyamini G, et al. Automated identification of lesion activity in neovascular age-related macular degeneration. Ophthalmology. 2016;123(8):1731–6.

47. Rohm M, Tresp V, Müller M, Kern C, Manakov I, Weiss M, et al. Predicting visual acuity by using

machine learning in patients treated for neovascular age-related macular degeneration. Ophthalmology. 2018;125(7):1028–36.

48. Schmidt-Erfurth U, Bogunovic H, Sadeghipour A, Schlegl T, Langs G, Gerendas BS, et al. Machine learning to analyze the prognostic value of current imaging biomarkers in neovascular age-related macular degeneration. Ophthalmology. 2017;124(1):24–30.

49. Bogunovic H, Waldstein SM, Schlegl T, Langs G, Sadeghipour A, Liu X, et al. Prediction of anti-VEGF treatment requirements in neovascular AMD using a machine learning approach. Invest Ophthalmol Vis Sci. 2017;58(7):3240–8.

50. Schmidt-Erfurth U, Waldstein SM, Klimscha S, Sadeghipour A, Hu X, Gerendas BS, et al. Prediction of individual disease conversion in early AMD using artificial intelligence. Investig Ophthalmol Vis Sci. 2018;59(8):3199–208.

51. Matsuba S, Tabuchi H, Ohsugi H, Enno H, Ishitobi N, Masumoto H, et al. Accuracy of ultra-wide-field fundus ophthalmoscopy-assisted deep learning, a machine-learning technology, for detecting age-related macular degeneration. Int Ophthalmol. 2018:1–7.

52. Vogl WD, Waldstein SM, Gerendas BS, Schmidt-Erfurth U, Langs G. Predicting macular edema recurrence from spatio-temporal signatures in optical coherence tomography images. IEEE Trans Med Imaging. 2017;36(9):1773–83.

53. Camino ACC, Ang ZHUOW, Ang JIEW, Ennesi MARKEP, Aul P, Ang Y, et al. Deep learning for the segmentation of preserved photoreceptors on en face optical coherence tomography in two inherited retinal diseases. Biomed Opt Express. 2018;9(7):1581–91.

54. Davidson B, Kalitzeos A, Carroll J, Dubra A, Ourselin S, Michaelides M, et al. Automatic cone photoreceptor localisation in healthy and Stargardt afflicted retinas using deep learning. Sci Rep. 2018;8(1):1–13.

55. Spiteri Cornish K, Lois N, Scott NW, Burr J, Cook J, Boachie C, Tadayoni R, la Cour M, Christensen U, Kwok AK. Vitrectomy with internal limiting membrane peeling versus no peeling for idiopathic full-thickness macular hole. Ophthalmology. 2014;121(3):649–55.

56. Kreissig I. Primary retinal detachment: a review of the development of techniques for repair in the past 80 years. Taiwan J Ophthalmol. 2016;6(4):161–9.

57. Scheerlinck LME, van der Valk R, van Leeuwen R. Predictive factors for postoperative visual acuity in idiopathic epiretinal membrane: a systematic review. Acta Ophthalmol. 2015;93(3):203–12.

58. Szeliski R. Computer vision. 1st ed. London: Springer; 2011.

59. Hashimoto DA, Rosman G, Rus D, Meireles OR. Artificial intelligence in surgery: promises and perils. Ann Surg. 2018;268(1):70–6.

60. Volkov M, Hashimoto D, Rosman G, Meireles ORD. Machine learning and coresets for automated real-time video segmentation of laparoscopic and robot-assisted surgery. IEEE Trans Med Imaging. 2017:754–9.

61. Natarajan P, Frenzel J, Smaltz D. Demystifying big data and machine learning for healthcare. 1st ed. Boca Raton: CRC Press; 2017.

62. Bonrath EM, Gordon LE, Grantcharov TP. Characterising "near miss" events in complex laparoscopic surgery through video analysis. BMJ Qual Saf. 2015;24(8):516–21.

63. Grenda TR, Pradarelli JC, Dimick JB. Using surgical video to improve technique and skill. Ann Surg. 2016;264(1):32–3.

64. De Smet MD, Naus GJL, Faridpooya K, Mura M. Robotic-assisted surgery in ophthalmology. Curr Opin Ophthalmol. 2018;29(3):248–53.

65. Ehteshami Bejnordi B, Veta M, Johannes van Diest P, et al. Diagnostic assessment of deep learning algorithms for detection of lymph node metastases in women with breast cancer. JAMA. 2017;318(22):2199–210.

66. Krause J, Gulshan V, Rahimy E, et al. Grader variability and the importance of reference standards for evaluating machine learning models for diabetic retinopathy. Ophthalmology. 2018;125(8):1264–72.

67. Fleck BW, Williams C, Juszczak E, et al. An international comparison of retinopathy of prematurity grading performance within the Benefits of Oxygen Saturation Targeting II trials. Eye. 2018;32(1):74–80.

68. Gilbert C, Rahi J, Eckstein M, O'Sullivan J, Foster A. Retinopathy of prematurity in middle-income countries. Lancet. 1997;350(9070):12–4.

69. Ramanishka V, Das A, Zhang J, Saen K. Top-down Visual Saliency Guided by Captions. 2018. [cited 10 September 2018]. Available from: https://arxiv.org/abs/1612.07360.

70. Lam C, Yu C, Huang L, Rubin D. Retinal lesion detection with deep learning using image patches. Invest Ophthalmol Vis Sci. 2018;59(1):590–6.

71. Quellec G, Charrière K, Boudi Y, Cochener B, Lamard M. Deep image mining for diabetic retinopathy screening. Med Image Anal. 2017;39:178–93.

72. De Fauw J, Ledsam JR, Romera-Paredes B, et al. Clinically applicable deep learning for diagnosis and referral in retinal disease. Nat Med. 2018;24(9):1342–50.

73. Campbell JP, Swan R, Jonas K, et al. Implementation and evaluation of a tele-education system for the diagnosis of ophthalmic disease by international trainees. AMIA Annu Symp Proc. 2015:366–75.

74. Maguire M, Martin D, Ying G, Jaffe G, Daniel E, Grunwald J, et al. 5-Year outcomes with Anti-VEGF treatment of neovascular Age-related Macular Degeneration (AMD): the comparison of AMD treatments trials. Ophthalmology. 2016;123(8):1751–61.

75. Boucher MC, Desroches G, Garcia-Salinas R, Kherani A, Maberley D, Olivier S, Oh M, Stockl F. Teleophthalmology screening for diabetic retinopathy through mobile imaging units within Canada. Can J Ophthalmol. 2008;43(6):658–68.

76. Takahashi H, Tampo H, Arai Y, Inoue Y, Kawashima H. Applying artificial intelligence to disease staging:

deep learning for improved staging of diabetic retinopathy. PLoS One. 2017;12(6):1–11.

77. Varadarajan A, Bavishi P, Raumviboonsuk P, Chotcomwongse P, Venugopalan S, Narayanaswamy A, et al. Predicting optical coherence tomography-derived diabetic macular edema grades from fundus photographs using deep learning. Nat Commun. 2020;11(1):130.

78. Vogl WD, Waldstein SM, Gerendas BS, Schlegl T, Schmidt-erfurth U. Analyzing and predicting visual acuity outcomes of anti- VEGF therapy by a longitudinal mixed effects model of imaging and clinical data. Invest Ophthalmol Vis Sci. 2018;58:4173–81.

79. Welikala RA, Foster PJ, Whincup PH, Rudnicka AR, Owen CG, Strachan DP, et al. Automated arteriole and venule classification using deep learning for retinal images from the UK Biobank cohort. Comput Biol Med. 2017;90(6):23–32.

Distortion and Scotoma Assessment in Surgical Macular Diseases

<div style="text-align:right">

8

</div>

Fred K. Chen

8.1 Introduction

Macular diseases are a major cause of irreversible blindness. For many of these diseases, the foveal centre is spared at the initial stage. As the disease progresses, the lesion spreads into the fovea to cause visual acuity loss. Treatment at this early stage, before visual acuity loss, can often prevent permanent loss of the high-quality foveal vision that is critical for daily tasks. In some patients, the disease has already progressed to cause permanent damage at the foveal centre. Reactivation or progression of macular disease at the edge of the lesion may not involve extrafoveal fixation locus located eccentric to the fovea. Hence visual acuity, served by these eccentric fixation loci, may not be affected during progression or recurrence of the disease in the late-stage either. Yet, most clinicians rely on the measurement of visual acuity alone for monitoring of all stages of macular diseases.

Some patients with the macular disease may present with a specific complaint of visual distortion or a blurry patch of vision somewhere in the central visual field but many will not because the disease affects their non-dominant eye. Even if the dominant eye is affected, the phenomenon of filling in of the visual field defect will lead to patient perception of visual features within the region of the blind spot through extrapolation of features surrounding the scotoma (e.g. the physiological blind spot). Therefore, we cannot rely on eliciting symptoms of distortion and scotoma alone for screening the presence of macula disease or its progression. It is essential that detailed qualitative and quantitative functional tests of the macula beyond the standard visual acuity measurement are performed in patients with macular diseases to identify perifoveal retinal dysfunction.

The purpose of this chapter is therefore to discuss current clinical tools for assessing macular function from a historical perspective. This is followed by a literature review of the use of specific clinical tools in common surgical macular diseases such as epiretinal membrane, vitreomacular traction (including the macular hole), and retinal detachment.

8.2 History of Macular Disease Symptomatology Documentation and Quantification

Recognition of the symptoms of macular disease evolved in parallel with technology to visualise the macula and treatment for maculopathy. Blurry central vision is not specific to macular pathology.

F. K. Chen (✉)
Centre for Ophthalmology and Visual Science (Incorporating Lions Eye Institute), Nedlands, WA, Australia
e-mail: fredchen@lei.org.au

The first symptom that was recognised as specific for retinal or macular pathology was visual distortion or metamorphopsia. Even back in 1764, Thomas Reid (1710–1796), a professor of moral philosophy at the University of Glasgow, described the relationship between his perception of macropsia (as a result of trying to look at the pathway of Venus through a telescope) and retinal contraction towards the centre of the retina due to the damage from light [1]. One hundred years later, Richard Forster (1825–1902), an ophthalmologist in Breslau, Germany, published the first medical illustration of visual distortion on a square grid of horizontal and vertical lines [1]. By the end of 1800s, several textbooks contained various types of parallel solid lines with a central fixation spot that were used to test and document the presence of metamorphopsia. George Berry, an eminent Scottish ophthalmologist also recognised an equally important early symptom of maculopathy: the relative scotoma, which could appear before or after onset of metamorphopsia. The scotoma was most noticeable at low contrast and it may disappear with increasing contrast [2]. Despite the well-established link between retinal disease and visual scotoma and metamorphopsia, it took another 100 years, into the mid-1900s, for printed test grids to be publicised widely in ophthalmology as a tool for detecting macular disease. Marc Amsler (1891–1968), a professor of ophthalmology at the University of Zurich, popularised the use of these macular grids after his work on various types of grid designs for almost 10 years. Frustrated by the observation that neither capimetry nor perimetry of his days was adequate in recording or detecting relative scotoma and metamorphopsia, he designed a series of seven types of macular grids (Fig. 8.1) [3, 4]. These consist of white lines or dots within a 10 cm × 10 cm square on black background except for charts 3 (red lines on black background) and 6 (black lines on white background). The commonly available version of black lines on white background was a modification of chart 1 of the Amsler grids [5]. Using a series of questions (Table 8.1), the examiner helps the patient to identify and draw regions of metamorphopsia and scotoma relative to the fixation point. Held at a distance of around 30 cm, the grid allows documentation of visual disturbance within the central 10° of the visual field (spanning 20° across central field).

The validity of the Amsler grid has been challenged over the years and several modifications of the grid have been developed to enhance its sensitivity in the detection of scotoma and to quantify metamorphopsia [6–10]. As mentioned in George Berry's book in 1889, relative scotoma is best detected using low contrast lines relative to the background (in dim light) [2]. This princi-
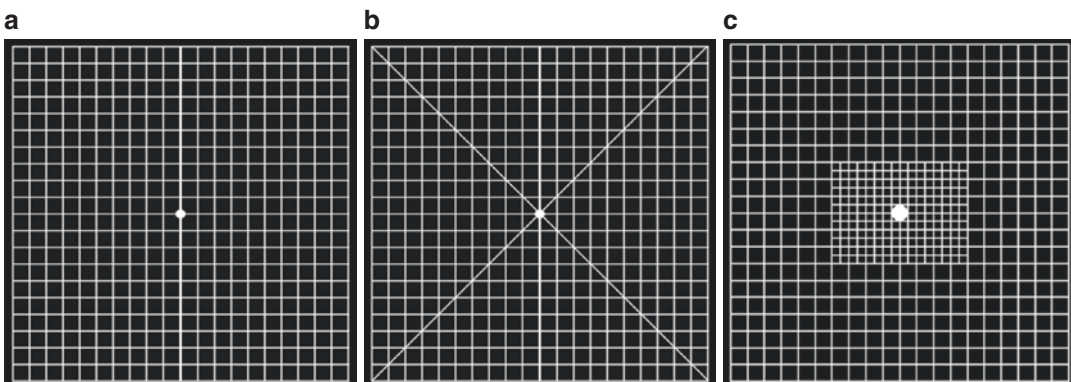
Fig. 8.1 Testing grids used to detect and localise distortion and scotoma as well as assess the severity of these symptoms. Chart 1 (**a**), 2 (**b**) and 7 (**c**) based on Amsler's original 7 tests grids. Held at 30 cm from the eye, the parallel lines subtend a visual angle of 1°. The central area of the smaller squares within grid #7 covers and area measuring 6° vertically and 8° horizontally

Table 8.1 An example of a modified questionnaire for Amsler grid #1, #2 and #7 testing

Amsler grid	Questions	Purpose
1	1. Are the lines of the grid straight and absolute parallel from beginning to end, especially close to the centre? 2. Are all the small squares regular and perfectly equal?	Testing for distortion
	3. Do you see the grid perfectly clear and without blurry spots everywhere? 4. Is the region around the central point as clear as the periphery of the grid? 5. In case there is a blurry spot: are the lines in the spot completely absent/interrupted or only attenuated?	Testing for scotoma
2	6. In which of the four quadrants do you see the distortion? 7. In which quadrant are the distortions the worst, the second worst and in which the least? Are they the same in certain quadrants?	Localising distortion
3	8. Do you see the distortions or blurry spots only within the area of the central grid with small squares or as well in the outer grid?	Localising scotoma

ple was adopted by Wall and Sadun in their development of the threshold Amsler grid in which the grid is visualised through a polarising filter that varied the perceived luminance contrast of the grid [8]. This design was later integrated into a computer-automated form which provides a stepped threshold Amsler grid test [11]. The scotoma plots at various contrasts are then reconstructed into three dimensions to allow visualisation of the shape, size, location, depth and slope of the central visual field defects [11]. Enhanced detection of scotoma in patients receiving hydroxychloroquine has been demonstrated using this computerised 3D threshold Amsler grid [12]. Several other modifications to the Amsler grid to provide quantitative measure of distortion were also reported. These included the use of additional grids with sinusoidal waves in the central portion of the grid with increasing

amplitude and frequency, in conjunction with the original Amsler grid (chart 1) so that unaffected fellow eye is used to grade the severity of distortion [13, 14]. Another modification is to use a grid with only seven horizontal and seven vertical lines so that patients can draw on the line using the unaffected fellow eye to illustrate the severity of distortion [15]. The total length of all the lines are added to provide a quantitative measure of distortion. Ugarte et al. developed a novel method for evaluation of dysmetropsia or disordered size perception, the New Aniseikonia test [16, 17]. In this test, the two eyes are dissociated by red and green filters, each viewing two half-moons of different sizes arranged in a series as a pair. Percentage of dysmetropsia is determined when subject indicates the pair of two half-moons are of equal size. All these types of tests require normal vision in fellow eye as control for documentation of metamorphopsia. Arndt et al. described the use of a scanning laser ophthalmoscope (SLO) to project an Amsler grid onto the retina and centred at the anatomic fovea [18]. Through a defined grid exploration strategy, the region of the grid affected by distortion can be plotted onto the retinal image. Hyperacuity measurement has also been investigated as an alternative to Amsler grid in detection of early lesions of age-related macular degeneration (AMD) [19–21]. Although preferential hyperacuity perimetry has greater sensitivity in detecting AMD lesions, it also has high false-positive rate compared to Amsler grid [22, 23]. More recently, Matsumoto developed the M-CHARTS (Fig. 8.2) to quantify severity of distortion along the horizontal and vertical meridian [24, 25]. This simple test has been used to quantify distortion in epiretinal membrane, full-thickness macular hole, macular degeneration, rhegmatogenous retinal detachment, branch retinal vein occlusion, and central serous retinopathy [24, 26–30]. Whilst the Amsler grid can be effective in identifying distortion in visual field, better clinical tool is clearly needed for the detection of macular scotoma.

Amsler may have abandoned the use of perimeter and capimeter for documenting scotoma arising from macular disease, these instruments continued to evolve. The Goldmann perimeter
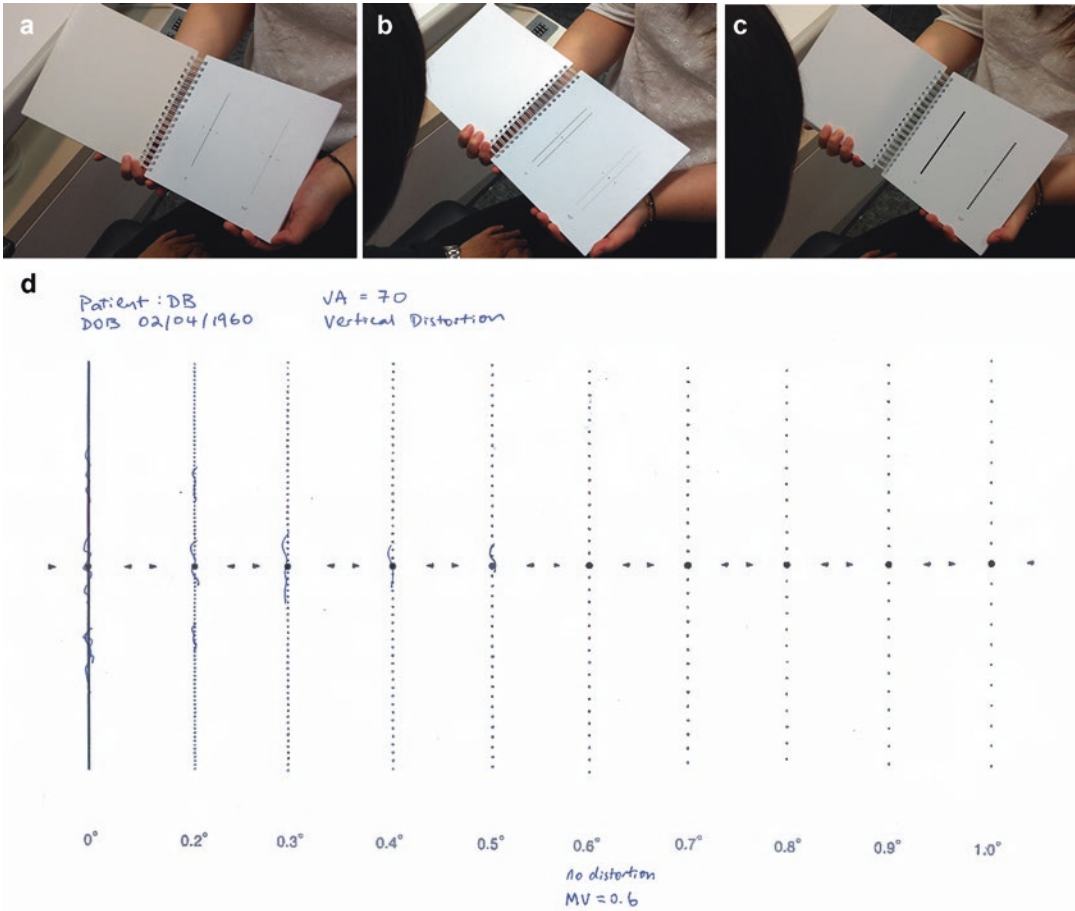
Fig. 8.2 Three types of M-CHARTS can be used to detect horizontal and vertical distortions. Type I (**a**) and II (**b**) charts can be used in patients with good visual acuity. Type 2 chart is designed for identifying distortion in patients with central scotoma and unable to fixate at the centre of the single solid line as used in type 1 charts. Type III (**c**) charts are used for patients with poor visual acuity. Example of a scoring sheet (**d**) with patient visualising misalignment of the dots at 0.5° separation but not at 0.6° separation; score is 0.6

was developed in 1945 and it was considered a versatile device allowing detailed mapping of scotoma using the kinetic technique. Static technique flourished during the 1980s with the release of several automated static perimeters. Specialised testing grids were designed to document macular diseases. However, even with the 10-2 grid, the test loci were separated by 2° of visual angle. The sparse testing grid may not allow small scotoma to be detected using a static method. As macular perimetry became more popular, developers explored the use of several other types of test stimuli that do not depend on

differential light sensitivity. For example, there were colour contrast, flicker contrast, short wave sensitive, motion detection and frequency-doubling technology used in visual field devices. Test stimuli were also arranged in the radial distribution in addition to the traditional Cartesian grid to improve sampling frequency within the central foveal region. Visual response to stimulation of particular regions in the macula is no longer limited to the patient's trigger response. Objective methods such as pupillary contraction, visual evoked potential and electroretinography were also used to determine the regional function
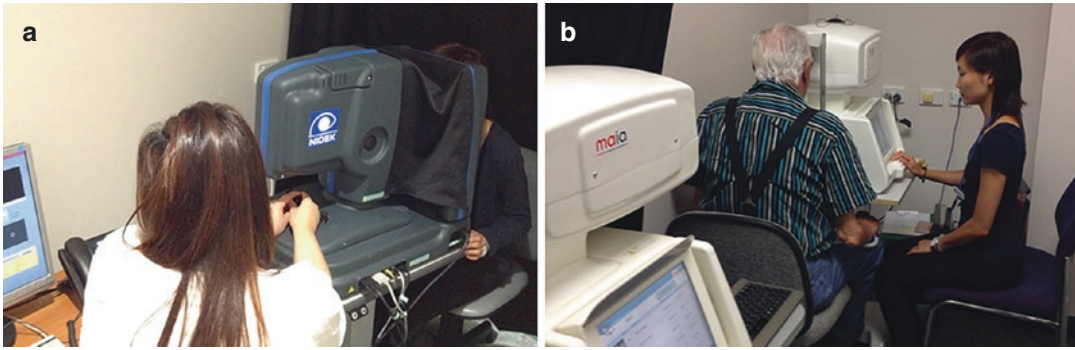
Fig. 8.3 Automated fundus-tracking perimeters. Nidek MP1 (**a**) uses liquid crystal display to project test stimulus and an infrared camera for continuous fundus monitoring. CenterVue Macular Integrity Assessment MAIA device (**b**) uses a scanning laser ophthalmoscope to monitor the fundus movement and project the test stimulus

of the macula through multifocal stimulation [31–33]. The main shortcoming of all these visual field assessment technique is the lack of eye tracking to enable continuous stimulus–fundus correlation during examination. This is particularly relevant in assessment of macular disease as fixation stability may be poor, location of preferred fixation locus may not be at the fovea and poor test–retest loci registration during follow-up assessment of the macula leading to large variability. Accurate fundus-tracking technology was made possible with the advent of scanning laser ophthalmoscope (SLO). The first fundus perimeter was developed in the 1980s but this traditional SLO-based device did not have automated fundus tracking capability [34]. In 2003, a new automated fundus-tracking perimeter, the Nidek MP1 (Fig. 8.3), using liquid crystal display for projection of test stimulus, became commercially available [35]. There were several advantages of the MP1 over the traditional SLO perimeter such as automation of eye tracking system and larger field of view [36]. More recently, two other companies reintroduced SLO-based microperimeters. CenterVue developed an SLO microperimeter (Fig. 8.3), which has incorporated the advantages of the MP1 system with the superior retinal image quality of the older SLO system [37]. OPKO Instrumentation (which became part of Optos plc from September 2011) also developed an SLO microperimeter which incorporates a spectral domain optical coherence tomography (SD OCT) [38].

In the following section, the most commonly used clinical tools for quantifying distortion and scotoma will be discussed. A review of the current literature relating to their use in specific surgical macular conditions will be used to illustrate the utility of these additional investigations in understanding the disease process and routine patient management.

8.3   Clinical Tests to Quantify Distortion

The most extensively studied method of quantifying metamorphopsia is the M-CHARTS [24, 25]. This chart consists of a solid straight line and a series of 19 dotted lines with increasing dot intervals from 0.2° to 2.0° in 0.1° steps of visual angle. The total length of the line subtends 20° of visual angle when held at 30 cm. A larger dot (diameter of 0.3°) at the centre of the line is used as fixation target. The patient is instructed to look at the fixation target and report presence or absence of distortion of the solid black line. In the absence of any distortion, the patient is assigned a score of 0.0. If distortion is present, the patient is instructed to look at the next dotted line with 0.2° separation between the dots. Each line is shown to the patient one after another until the patient is no longer

aware of misalignment between the dots. The smallest spacing between the dot that preclude visualisation of distortion is the assigned distortion score (range: 0.2–2.0 in 0.1 steps). The test is performed twice with the line orientated horizontally and then vertically (Fig. 8.2).

8.3.1 Epiretinal Membrane

Matsumoto et al. described increasing metamorphopsia scores with increasing severity of the epiretinal membrane [24]. The score from horizontal lines was consistently worse than the score from vertical lines. Severity of vertical retinal contraction induced by epiretinal membrane was correlated with worsening metamorphopsia score for horizontal line. Similarly, horizontal retinal contraction was correlated with vertical line metamorphopsia score [39]. Of the 29 eyes in this study, five eyes had already reached ceiling score of 2.0 at baseline and 15 had worsening of the metamorphopsia score over 3 years of monitoring. Three eyes had spontaneous improvement in the score [39]. Both of these studies showed poor correlation between metamorphopsia and visual acuity scores. Okamoto et al. investigated the relationship between foveal microarchitecture, visual acuity and metamorphopsia. They demonstrated significant correlation between visual acuity and ellipsoid zone integrity whilst metamorphopsia was correlated with inner nuclear layer thickness.

The effect of spontaneous and surgical peeling of epiretinal membrane on metamorphopsia score has also been investigated [21, 40, 41]. Improvement in both horizontal and vertical metamorphopsia scores were demonstrated after spontaneous peeling of epiretinal membrane. This also correlated with vertical and horizontal retinal movements respectively [41]. Kim et al. showed worsening of metamorphopsia score at 2 months after surgical peeling but statistically significant improvement in score from a mean of 0.32 at baseline to 0.23 post-operatively at 6 months [21]. In contrast, Kinoshita et al. showed consistent improvement in horizontal metamorphopsia score at 1, 3, 6, 9 and 12 months following surgical peeling. Vertical metamorphopsia score was lower

(better) than horizontal score at baseline (0.91 vs. 1.10) but improvement reached a plateau after 6 months (0.40) and thus remaining higher than horizontal metamorphopsia score at 12 months after surgery (0.39, vertical vs. 0.27; horizontal). The differential time courses in vertical and horizontal metamorphopsia scores were postulated to be due to greater vertical plasticity of the posterior retina and restricted horizontal displacement due to optic nerve head. Hence, to achieve satisfactory post-operative outcome in reducing metamorphopsia, Kinoshita et al. recommended that optimal surgical indication in relation to metamorphopsia outcome is a preoperative horizontal score of 0.5–1.7 and vertical score of 0.5–0.9. Subgroup analysis by Kim et al. also led to the recommendation that surgical peeling should be avoided in patients with visual acuity score of ≥70 letters and metamorphopsia score of <0.3 whereas the most significant improvement in distortion (0.54 decreased to 0.22) can be expected in those with good visual acuity (>70 letters) and at least moderate distortion (<0.3) [21]. Those with poor visual acuity (<70 letters) had good visual acuity improvement (12 letter gain) but limited reduction in metamorphopsia score even in eyes with distortion. Structure–function correlation in this study also suggested that inner nuclear layer thickness may be important in determining severity of distortion.

To date, studies involving M-CHARTS in the assessment of macular pucker have focused on the idiopathic epiretinal membrane. The utility of metamorphopsia score in predicting the surgical outcome of in regards to distortion in eyes with co-morbidity such as drusen, diabetic retinopathy, uveitis, retinal vein occlusion, retinal dystrophy and previous retinal tear or detachment remains to be investigated. Further work is also needed to correlate quality of life outcome with improvement in metamorphopsia scores after surgical intervention, taking ocular dominance into account.

8.3.2 Vitreomacular Traction

Distortion due to the full-thickness macular hole is typically described as a pin–cushion effect.

The M-CHARTS include a second set of plates specifically designed for patients with central scotoma due to conditions like the macular hole (Fig. 8.2). The two parallel solid or dotted lines are separated by 1° and fixation is directed towards a point in between the two lines. Similar to the single line test, there are also 19 pairs of dotted lines after solid continuous parallel lines. The dots are separated by 0.1° increments ranging from 0.2° to 2.0°.

Arimura et al. showed that the metamorphopsia score using the type II M-CHARTS was correlated with subretinal fluid cuff diameter [26]. Uei et al. reported 6 of 15 eyes (40%) undergoing repair of macular hole had resolution of metamorphopsia (score of ≤0.2) [42]. These eyes had significantly smaller size holes than those that had residual distortion. Reduction in metamorphopsia score (reduction >0.2) was achieved in 19 of 22 eyes (86%) reported by Arimura et al. [26]. In contrast, visual acuity improved by more than 2 lines in only 14 eyes (64%). Although time course in improvement of distortion has not been studied in detail, significant reduction in metamorphopsia score can be detected at 3 months following macular hole repair. This improvement in score correlated strongly with improved VFQ-25 composite score [43]. In this study the metamorphopsia score improved from 0.77 to 0.45 after vitrectomy. Kim et al. investigated the relationship between foveal remodelling and reduction in metamorphopsia score. They showed greater reduction in metamorphopsia score in eyes with preserved symmetry of the foveal architecture at 6 months. Eyes that had progressive asymmetric elongation of inter-outer plexiform layer gap of the fovea also had worse metamorphopsia score at 6 months.

There are many unanswered questions regarding distortion outcomes in the macular hole and vitreomacular traction surgery. More work is needed in examining the natural history of metamorphopsia scores in vitreomacular traction disorders before the formation of full-thickness macular holes and the effect of pharmacologic vitreolysis.

8.3.3 Retinal Detachment

Rhegmatogenous retinal detachment often presents with central visual distortion when the macula becomes involved. Residual or new distortion following successful repair of retinal detachment may be due to the development of epiretinal membrane, macular hole, macular oedema, persistent subretinal fluid, disruption of the ellipsoid zone and retinal translocation.

Okamoto et al. reported the presence of metamorphopsia in 39% of eyes that had undergone retinal detachment repair using the M-CHARTS. The prevalence was much lower for macula-on detachment as compared to macula-off detachment (13% vs. 68%). Amongst the 50 eyes that had post-operative distortion, 64% had no obvious abnormality on SD OCT. The remaining 36% had epiretinal membrane, cystoid macular oedema, macular hole, disrupted ellipsoid zone and subretinal fluid. In the eyes with apparent normal OCT features, the horizontal score was significantly higher (worse) than the vertical score (0.86 vs. 0.62). This may be due to vertical retinal displacement during reattachment.

Serous retinal detachment occurs in central serous retinopathy and choroidal neovascularisation. M-CHARTS have been used to quantify both of these conditions [28, 44, 45]. Nowomiejska et al. showed presence of metamorphopsia in 89% of patients with neovascular AMD and there was a significant reduction in horizontal but not vertical metamorphopsia score following one bevacizumab injection [44]. In central serous retinopathy, metamorphopsia was detected using the M-CHARTS in 15 of 33 eyes (45%). Eyes with visual distortion had higher prevalence of focal pigment epithelial detachment (40% vs. 6%). In another study, Fujita et al. reported 18 and 21 eyes of a total of 45 eyes had reduction in horizontal and vertical metamorphopsia scores respectively. The time course profile in horizontal and vertical scores varied depending on baseline visual acuity. In eyes with reduced visual acuity, there was no significant change in either vertical or horizontal scores and the former was consistently lower. In eyes with

normal visual acuity (logMAR ≤0.0) both horizontal and vertical scores declined significantly from around 0.5–0.6 to around 0.1. It is not apparent why the horizontal score is greater than vertical score in eyes with reduced visual acuity.

The dissociation between horizontal and vertical metamorphopsia scores in rhegmatogenous retinal detachment may be related to retinal rotation and vertical displacement. Similar findings in serous retinal detachment cannot be explained by retinal rotation. Further work using multimodal imaging is required to determine the underlying mechanism of metamorphopsia in central serous retinopathy.

8.4 Clinical Tests to Quantify Scotoma

There are three commercially available fundustracking perimeters: Nidek MP1 (Nidek Technologies, Padova, Italy), OptosOCT SLO (Optos, Dunfermline, Scotland, UK) and Macular Integrity Assessment, MAIA™ (CenterVue, Padova, Italy). The procedure for performing microperimetry is straight forward and similar between all three devices with the exception of the need for the operator to have skills in using a joystick for maintaining visualisation of the fundus for the Nidek MP1 and the OptosOCT SLO microperimeters. Although it is possible to perform microperimetry through an undilated pupil, the quality of the fundus image and tracking efficiency is improved if the pupil is fully dilated, especially when Nidek MP1S is used. These devices can autocorrect spherical refractive errors of over 10 Dioptres of hyperopia or myopia. The test is performed in a darkened room with the untested eye patched. Dark adaptation is not necessary but it is advisable that the patient perform microperimetry prior to any retinal imaging or examination to avoid excessive bleaching of photopigments. Patients should be given clear instructions on fixation during the test and be familiarised with the response trigger prior to starting the test. Testing algorithms can be modified to varying degrees. The most versatile instrument is the MP-1S that allows extensive user customisation of the testing algorithm including fixation target, stimulus size, duration and colour, pattern of testing grid and its relative position to imported OCT guided fundus landmark (e.g., foveal centre), dynamic testing and scotopic perimetry. The various subtle differences in instrument design are summarised in Table 8.2. Test re-test variability of all three devices in

Table 8.2 Specifications of three types of commercial microperimeters

Features	Nidek MP1	OptosOCT SLO	CenterVue MAIA
Fundus imaging	Infrared	SLO	SLO
Fundus image size	45°	29.7°	36°
Image resolution (pixels)	768×576	512×512	1024×1024
Fixation monitoring	Eye tracker	SLO	SLO
Fixation registration	25 Hz	4 or 8 Hz	24 Hz
Image registration	Automated or manual	Simultaneous SLO OCT	Simultaneous SLO
Background luminance (cd/m^2)	1.27	10	1.27
Brightest stimulus intensity (cd/m^2)	128 (assigned 0 dB)	125 (assigned 0 dB)	318 (assigned 0 dB)
Dimmest stimulus intensity (cd/m^2)	1.28	1.25	0.08
Stimulus attenuation	0–20 dB	0–20 dB	0–36 dB
Stimulus variation	Size I–V, variable duration, colour	Size I–V, variable duration	Size III, 200 ms fixed duration
Strategies	Static and dynamic	Static	Static
Scotopic microperimetry	Included	Not available	Not available
Biofeedback training	Included	Not available	Included
OCT imaging	Imported for grid centration	Included as simultaneous OCT	Not available

retinal sensitivity measurements has been examined. The results are summarised in Table 8.3. The duration of microperimetry can vary significantly, ranging from 3 minutes to over 20 minutes if a large number of test loci (> 60) is used in the test grid.

Table 8.3 References for normative values and test–retest variability

Key parameters	Nidek MP1	OptosOCT SLO	CenterVue MAIA
Normative value			
Authors	Midena et al. [46]	Sabates et al. [47]	Vujosevic et al. [37]
Number of subjects	190	169	200
Age range (years)	20–75	21–85	50–87
Average sensitivity	18.6–19.6 dB	16.8–17.9 dB	29–30 dB
Other studies		Anastasaki et al. [38]	
Intra session variability			
Authors	Chen et al. [48]	Anastasaki et al. [38]	Wu et al. [49]
Number of subjects	50	32	44
Number of sessions	2	2	3
CR for mean sensitivity	1.8	1–3 dB	1–2 dB
CR for point sensitivity	5.6	N/A	3–4 dB
Intra-class correlation	N/A	N/A	N/A
Other studies	Midena et al. [46]		
Inter session variability			
Authors	Weingessel et al. [50]	No report	No report
Number of subjects	35		
Number of sessions	2 (1 week apart)		
CR for mean sensitivity	1–2 dB		
CR for point sensitivity	N/A		
Intra-class correlation	0.94–1.00		

8.4.1 Epiretinal Membrane

Goto et al. used a scanning laser ophthalmoscope microperimeter to demonstrate reduced retinal sensitivity in eyes with idiopathic epiretinal membrane [51]. They also demonstrated that micro-scotoma recovered following membrane peel but could also be induced by surgical trauma and recurrence of epiretinal proliferation. More recently, the Nidek MP-1 has been used extensively to study the relationship between retinal sensitivity, best-corrected visual acuity, fixation stability, retinal thickness and integrity of the ellipsoid zone of the photoreceptor cells.

Richter-Mueksch et al. demonstrated an overall 2 dB increase in mean retinal sensitivity at 12 weeks after membrane peel by using a 41 stimuli test grid (covering an area of 8°) on the MP1. They also showed that 67% of eyes had a 1 dB increase in central macular sensitivity and the same proportion had a 2 line gain in visual acuity. Between 3 and 12 months following membrane peel, Cappello et al. demonstrated sustained improvement in overall retinal sensitivity. Most of the gain was observed by the first 3 months and driven by improvement in loci within the central 2° [52].

The mechanism of reduced retinal sensitivity in macular pucker was examined by Karacorlu et al. and Gorgun et al. in their structure–function correlation studies [53, 54]. They both found that reduced foveal sensitivity and visual acuity were correlated with a thicker retina. More detailed OCT study by Mayer et al. showed a correlation between depth of micro scotoma defect and the severity of ellipsoid zone disruption following membrane peel [55]. They postulated that functional recovery after membrane peel depends on the regeneration of the ellipsoid zone of the photoreceptor cells rather than a reduction in retinal thickness. Santarelli et al. also showed a significant inverse relationship between the extent of ellipsoid zone interruption length and mean retinal sensitivity [56]. Using a much larger test grid of 77 stimuli (covering an area of 20°), they showed a mere 1 dB improvement in overall mean retinal sensitivity and development of new micro scotoma outside the central 10°. They

postulated that the micro scotoma may arise from inner retinal damage during internal limiting membrane (ILM) peel or retinal pigment epithelium toxicity due to exposure to infracyanine green dye. The former hypothesis was supported by a comparative study of microperimetry response in those with and without ILM peeling during epiretinal membrane removal [57]. Ripandelli et al. showed that greater and faster recovery in the central 4° mean retinal sensitivity was observed at 3–12 months post-operatively in eyes without ILM peeling compared to eyes that had ILM peel during macular pucker surgery. Similarly, there was a greater number of dense micro scotoma (0 dB) within the central 12° retinal area in eyes that had ILM peel.

The traditional SLO and MP1 microperimeters have been used to demonstrate reduced retinal sensitivity related to the epiretinal membrane. Further structure–function correlation studies are required to determine the mechanism and natural history of reduced retinal sensitivity due to macular pucker. Both inner and outer retinal dysfunction may contribute to the loss of sensitivity but it remains to be determined if there are any imaging biomarkers that may predict reversibility of the scotomata. The feasibility and accuracy of follow-up microperimetry also require further study since it is not known whether remodelling of macular blood vessel architecture due to the progression of pucker or following its surgical removal will preclude exact test loci point-to-point registration between pre- and post-operative examination (Fig. 8.4). Microperimetry may also be a useful tool for exploring the mechanism of iatrogenic micro scotoma related to ILM peeling or vital dye used to stain ILM during epiretinal membrane peel. Multimodal image registration and analysis will help to further our understanding of idiopathic and secondary macular pucker pathophysiology [58].

8.4.2 Vitreomacular Traction

Sjaarda et al. used a traditional scanning laser ophthalmoscope microperimeter to demonstrate the presence of absolute scotoma within the area

of full-thickness macular hole and restoration of retinal sensitivity within the foveal centre following surgical closure of the hole [59]. Improvement was also noted in the region of relative scotoma surrounding the hole. Prior to the OCT era, SLO microperimeter was also useful in distinguishing between lamellar and full-thickness macular holes [60] and between different types of anatomical closure following macular hole repair [61].

Haritoglou et al. demonstrated the development of paracentral scotoma following uncomplicated macular hole surgery by using the traditional SLO microperimeter to map out foveal retinal sensitivity pre- and post-operatively. They hypothesised that surgical trauma from attempts to and complete ILM peeling as the cause. Other reports have also shown that 20–30% of patients develop these new perifoveal scotomas after successful macular hole repair [61–63]. Soon after the description of dissociated optic nerve fibre layer (DONFL) appearance after idiopathic ERM surgery by Tadayoni et al., the same appearance was noted following macular hole surgery (Figs. 8.4 and 8.5) [64, 65]. Microperimetry (traditional SLO and the MP1) was then used by at least three groups to determine if DONFL lesions represent damaged nerve fibre layers [66–68]. Although they could not demonstrate micro scotoma over the DONFL lesions, other groups have reported scotomata in the perifoveal region after successful macular hole closure related to either inner retinal damage by ILM peeling or neurotoxicity of the dye used to stain ILM [63, 69–71]. Tadayoni et al. used the OptosOCT SLO microperimeter (formerly OPKO/OTI combined OCT and microperimeter) to demonstrate that patients who had ILM peeling had lower overall retinal sensitivity, developed dense scotoma and had a greater number of the relative scotoma [69]. Beutel et al. used traditional SLO microperimeter to measure the potential retinal toxicity of indocyanine green versus trypan blue in ILM staining and they found no significant difference in the number of patients developing new scotomata after surgery with either dye [63]. Scupola et al. compared the impact of triamcinolone acetonide versus infracyanine green on macular retinal
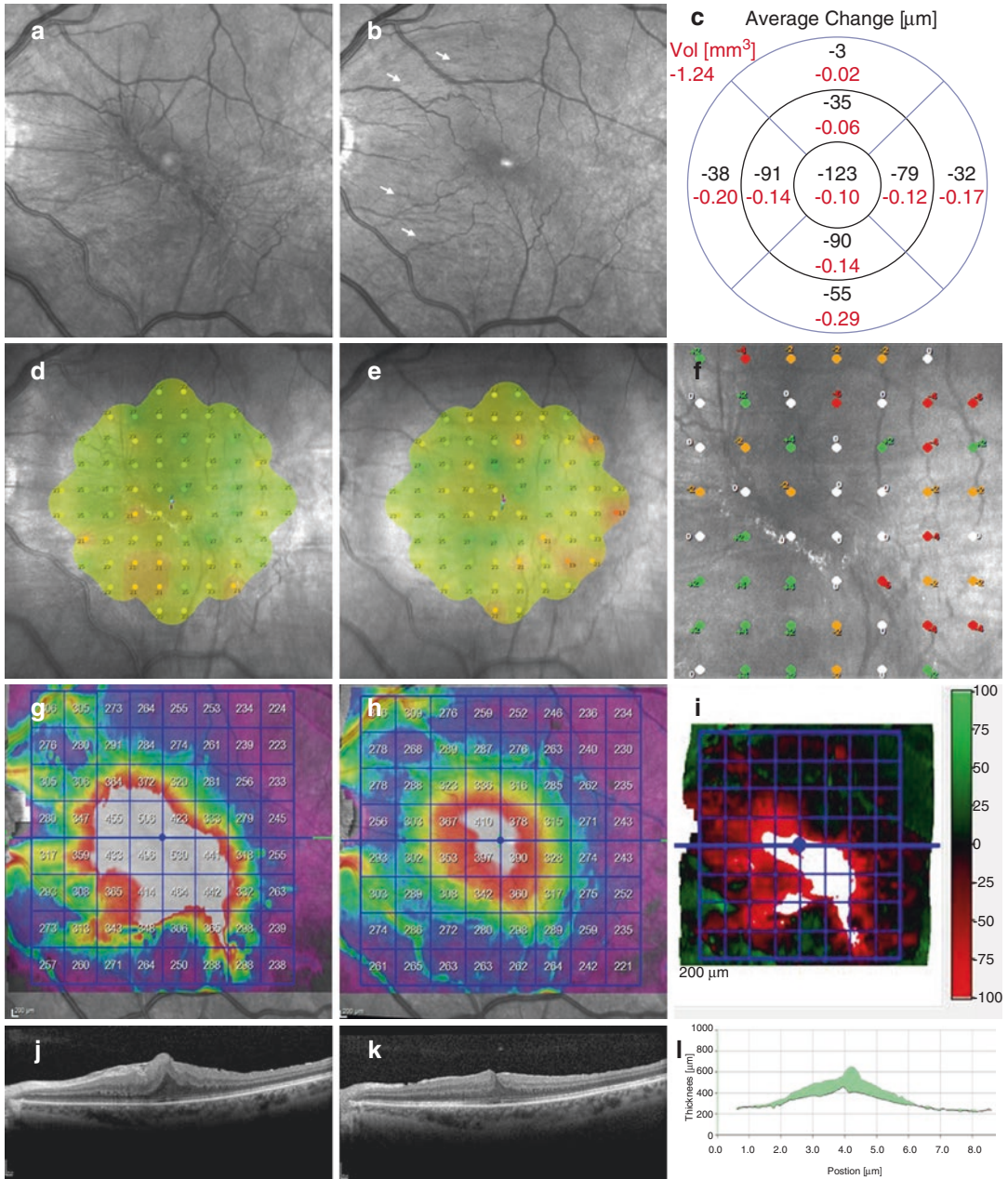
Fig. 8.4 A 62 year old female presented with progressive epiretinal membrane in the left eye. Her visual acuity was 70 ETDRS letters and the M-CHART vertical and horizontal scores were 0.6 and 0.7 respectively in the left eye. At 6 weeks post-operation, her visual acuity improved to 75 letters and vertical and horizontal scores were 0.4 and 1.0 respectively. Pre- (**a**) and 6-week post-operative (**b**) infrared reflectance images showing resolution of macular pucker and presence of dissociated optic nerve fibre layer after vitrectomy and internal limiting membrane peel (arrows). Central retinal thickness was reduced by 123 μm (**c**). Large grid (covering 20° of macula) MAIA microperimetry pre- (**d**) and 6 week post-operation (**e**) showed significant increase in retinal sensitivity in the inferonasal region of the macula (**f**). Heat map of retinal thickness pre- (**g**) and 6 week post-operation (H) showed most significant reduction in the foveal, and inferior-nasal perifoveal regions (**i**). Horizontal spectral domain optical coherence tomography pre- (**j**) and 6 week post-operation (**k**) showed reduction in retinal thickness (**l**)
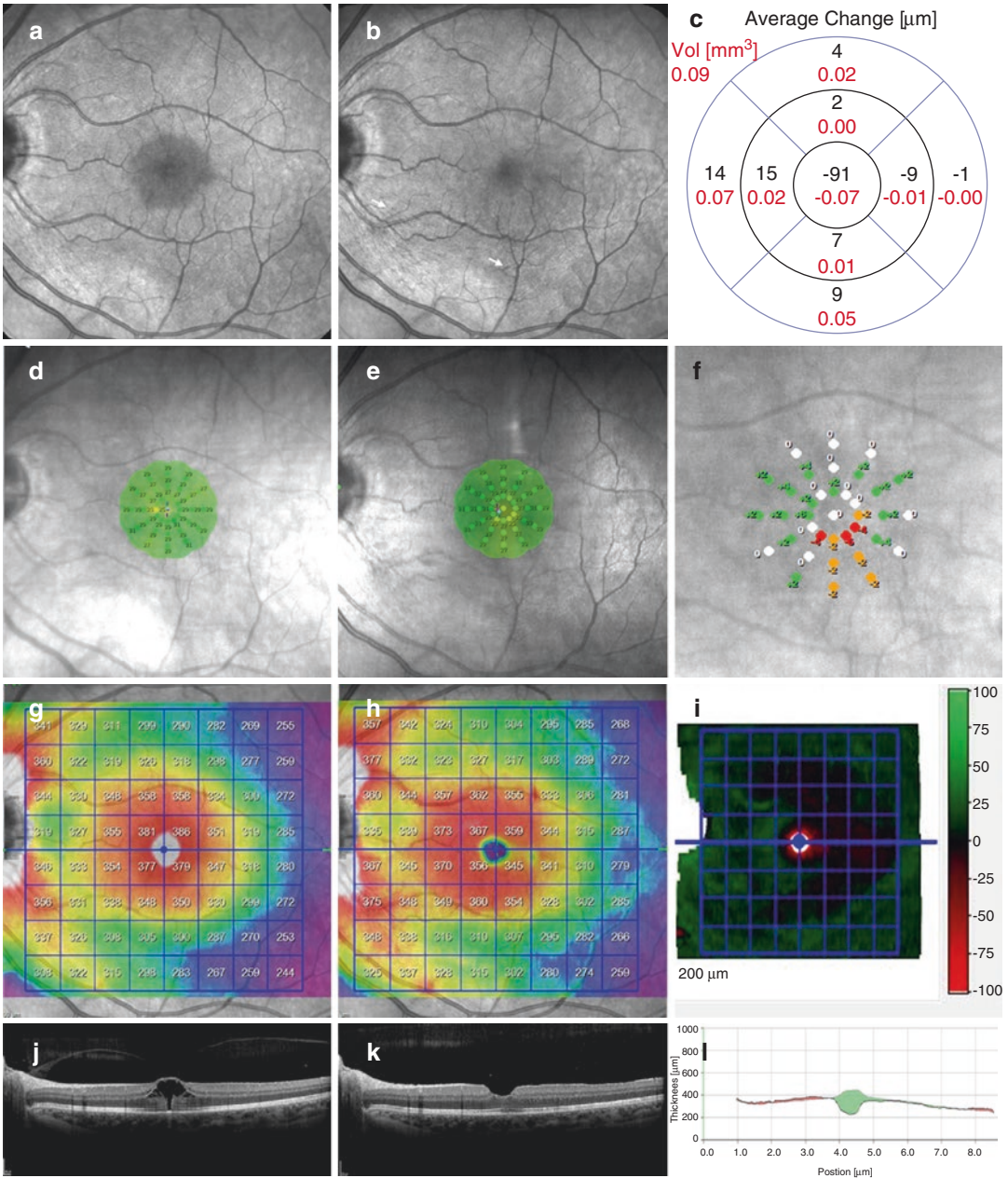
Fig. 8.5 A 57-year-old female presented with vitreomacular traction (stage Ib impending macular hole lesion) in the left eye. Her visual acuity was 63 ETDRS letters and the M-CHART vertical and horizontal scores were 0.2 and 0.0 respectively in the left eye. At 4 weeks post-operation, her visual acuity improved to 85 letters and vertical and horizontal scores were 0.2 and 0.3 respectively. Pre- (**a**) and 4-week post-operative (**b**) infrared reflectance images showing resolution of macular oedema surrounding the hole and presence of dissociated optic nerve fibre layer after vitrectomy and internal limiting membrane peel (arrows). Central retinal thickness was reduced by 91 μm (**c**). Small grid (covering central 6° of macula) MAIA microperimetry pre- (**d**) and 4 week post-operation (**e**) showed significant increase in retinal sensitivity at the loci immediately nasal to the fovea and new micro scotoma inferior to the fovea (**f**). Heat map of retinal thickness pre- (**g**) and 4 week post-operation (**h**) showed most significant reduction in the foveal, temporal perifoveal regions (**i**). Horizontal spectral domain optical coherence tomography pre- (**j**) and 4 week post-operation (**k**) showed reduction in retinal thickness associated with closure of outer retinal defect (**l**)

sensitivity using the MP1 and they found no significant difference between the groups [72]. Baba et al. demonstrated reduced thickness of ganglion cell complex (bounded by the internal limiting membrane and outer nuclear layer) but no change in outer retinal layer thickness in eyes that had undergone macular hole repair [70, 71]. They showed a positive correlation between the thickness of the ganglion cell complex layer and the overall macular retinal sensitivity at 6 months after hole repair [70]. In a subsequent study, they showed that the temporal perifoveal region had the greatest reduction in thickness of the ganglion cell complex and this region also had the lowest retinal sensitivity compared to the three remaining quadrants at 3 and 6 months after surgery [71]. They hypothesised that temporal perifoveal ganglion cell complex thinning is due to mechanical damage to the (more vulnerable temporal perifoveal) inner retina during ILM peeling and the remodelling of macular tissue to allow closure of the macular hole.

Several groups have also used microperimetry to study and predict foveal function recovery and its relationship to foveal photoreceptor cell integrity [73–75]. The OptosOCT SLO microperimeter was used by Chen et al. and Bonnabel et al. to demonstrate the importance of ellipsoid zone continuity in predicting good retinal sensitivity in the fovea after hole closure [74, 75]. Sun et al. showed that pre-operative retinal sensitivity and fixation stability may be predictive of post-operative visual acuity and restoration of the ellipsoid zone continuity [76]. Ooto et al. showed that reduced foveal sensitivity is related to a larger area of cone reflex loss on adaptive optics scanning laser ophthalmoscope [77].

Microperimetry in the macular hole is useful in demonstrating absolute scotoma within the hole, relative scotoma in the surrounding fluid cuff and normal retinal sensitivity outside this region (Fig. 8.5). It has contributed to our understanding of the functional consequences of various post-operative signs on detailed retinal imaging such as foveal outer retinal disturbance and temporal perifoveal inner retinal thinning (Fig. 8.5). The ability to restore foveal function is limited by pre-operative cone reserve and this

may be predicted by retinal sensitivity testing of the fluid cuff region. The development of new scotoma in the perifoveal region does not appear to correlate with the DONFL lesion (Fig. 8.5) but it may be related to thinning of a ganglion cell complex. More studies using microperimetry is need to explore the natural history of vitreomacular traction to determine the best time to intervene pharmacologically or surgically. Although ILM peeling might have a detrimental effect on perifoveal retinal function, it is not known if the ILM flap technique [78] or pharmacologic vitreolysis will avoid this complication [79].

8.4.3   Retinal Detachment

Vision recovery after reattachment of the retina in rhegmatogenous retinal detachment is often incomplete. In those presenting with macula still attached, the outcome for visual acuity and macular function is generally good whereas those with macula detached, variable recovery of vision has been attributed to the loss of foveal photoreceptor cells rather than inner retinal injury. Microperimetry has been used to determine the mechanism of incomplete retinal function recovery following repair of retinal detachment.

Smith et al. reported the microperimetry outcome using the MP1 in seven patients who had macula-off rhegmatogenous retinal detachment repair 3 or more months prior [80]. Although two of these had retinal sensitivity within the normal range (they also had normal visual acuity), five had reduced sensitivity in regions of the macula that correlated with disruption of the ellipsoid zone or persistent subretinal fluid. Rossetti et al. reported the MP1 outcome in six patients at 1, 3, 6, 12, 18 and 60+ months after scleral buckle for macula-off rhegmatogenous retinal detachment [81]. They demonstrated gradual improvement in macular sensitivity over the first six months and only a very slight improvement from 6 to 18 months. By 5 years, there was a slight but non-significant reduction in overall mean sensitivity. Amongst the six patients, two had <1 dB change between 18 and 60 months whereas four had a 2–10 dB decline in mean sensitivity despite

normalisation of the ellipsoid zone integrity. The authors did not report detailed structure–function correlation to explore the mechanism for such a large decline in macular sensitivity in these four patients. Lai et al. reported the MP1 outcome of 12 patients (5 macula-on and 7 macula-off rhegmatogenous retinal detachment) > 6 months after a successful repair [82]. All eyes with macula-on detachment had mean macular sensitivity of greater than 15 dB except for one patient with a sensitivity of 13.6 dB. None of these patients had an inner or outer retinal abnormality on spectral domain OCT and all had normal fundus autofluorescence signal in the macula. In contrast, only two of seven patients with macula-off detachment had normal autofluorescence signal and OCT features and they had a sensitivity of 13.4 and 15.6 dB. The remaining five patients had abnormal autofluorescence and OCT features with sensitivity values ranging from 0.9 to 10.8 dB. Delolme et al. examined the correlation between OCT and retinal sensitivity using the OptoOCT SLO microperimeter in 30 patients with successful macula-off retinal detachment repair 6 months prior. They showed that eyes with >1 lesion on OCT had significantly lower foveal and macular retinal sensitivity [83]. Sensitivity in the central 12° was associated with the presence of ellipsoid zone defect whereas sensitivity in the central 4° was correlated to thinner photoreceptor outer segment thickness.

Macular detachment and retinoschisis are all features of optic disc pit maculopathy, vitreomacular traction syndrome and pathologic myopia or posterior staphyloma. Microperimetry has been used to demonstrate mechanisms of visual loss in optic disc maculopathy (Fig. 8.6). Caverretta et al. showed reduced sensitivity using the MP1 in the region of macular schisis secondary to disc pit. Brar et al. showed reduced sensitivity using the MP1 in a region of the attached retina with loss of ellipsoid zone due to previous detachment secondary to disc pit. Chen et al. also used MP1 to demonstrate differential reversibility of retinal sensitivity loss in different types of retinoschisis associated with disc pit. Ripandelli et al. showed

that serial microperimetry (MP1) can detect the progression of myopic foveoschisis and lamellar hole formation in patients with posterior staphyloma even before visual acuity drops. They also showed significant differences in overall foveal retinal sensitivity between patients with foveoschisis, lamellar and full-thickness defects and macular detachment secondary to pathologic myopia. Ikuno et al. demonstrated a reduction of the scotoma size following vitrectomy and ILM peel in patients with myopic foveoschisis without the macular break using the traditional SLO microperimeter suggesting reversibility of retinal dysfunction in areas of retinoschisis and foveal detachment [84].

Submacular surgery to reconstruct retinal pigment epithelium (RPE) and macular translocation to re-establish photoreceptor–RPE contact have been performed in patients with massive submacular haemorrhage not amenable to anti-vascular endothelial growth factor therapy. Microperimetry has been used to document the restoration of macular function, photoreceptor rescue, and long term maintenance of photoreceptor cell survival by autologous equatorial or extramacular RPE [85–88]. Microperimetry has also been used to document rescue of retinal function following retina–RPE transplantation [89]. intravitreal bone marrow stem cell injection, [90] and subretinal gene therapy for the treatment of RPE-65 and REP-1 gene mutation associated retinal dystrophies [91, 92].

Microperimetry is useful in assessing patients with impaired vision after retinal detachment repair. Correlation of functional mapping with SD OCT features has demonstrated photoreceptor cell damage as the main reason for the incomplete recovery of retinal sensitivity. Further longitudinal studies are required to correlate cone mosaic, inner and outer retinal sublayer thickness and reflectivity maps with microperimetry to identify predictive imaging biomarkers for reversible visual loss and thus identify patients who may benefit from experimental neuroprotective therapy in enhancing visual recovery after detachment repair.
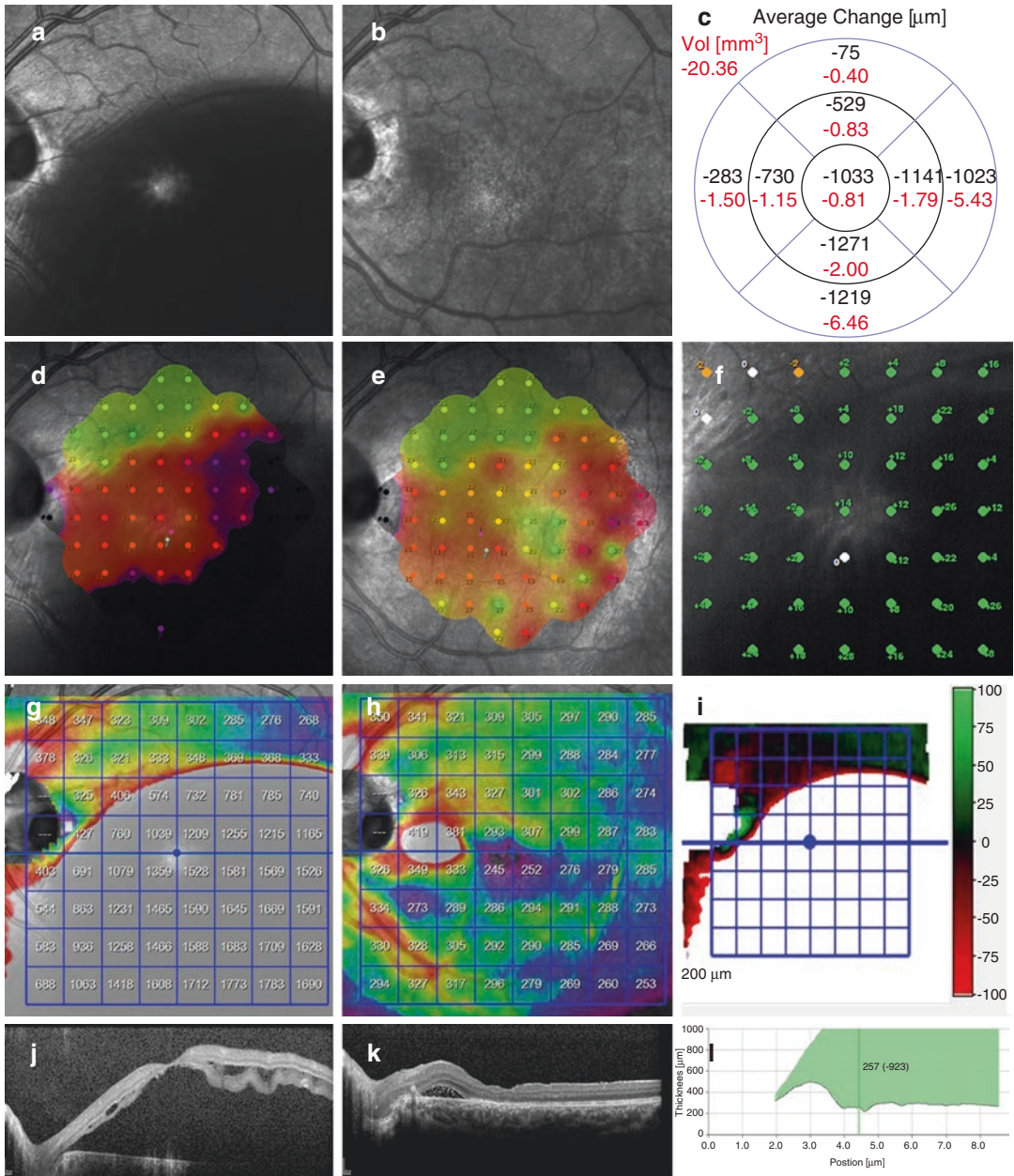
Fig. 8.6 A 24-year-old male presented with optic disc pit maculopathy in the left eye. His visual acuity was 36 ETDRS letters. At 6 months post-operation, his visual acuity improved to 56 letters. Pre- (**a**) and 6-month post-operative (**b**) infrared reflectance images showing resolution of submacular fluid. Central retinal thickness was reduced by 1033 μm (**c**). Large grid (covering central 20° of macula) MAIA microperimetry pre- (**d**) and 6 month post-operation (**e**) showed significant increase in retinal sensitivity in the inferior macular region where subretinal fluid had resolved (**f**). Heat map of retinal thickness pre- (**g**) and 6 month post-operation (**h**) showed significant thickness reduction in the foveal and inferior perifoveal regions (**i**). Horizontal spectral domain optical coherence tomography pre- (**j**) and 6 month post-operation (**k**) showed partial resolution in subretinal fluid (**l**)

Microperimetry is now an important clinical tool to assess the efficacy and potential adverse events in experimental treatments involving the subretinal delivery of cellular therapy and viral vectors. Its routine use to guide retreatment in novel laser therapy in drusen is yet to be determined [93, 94].

8.5 Conclusions

Visual acuity assessment alone cannot measure the impact of the macular disease in the perifoveal region and is unable to distinguish retinal dysfunction arising from the various layers of the retina. Assessment of visual distortion and retinal sensitivity in the central visual field using the M-CHARTS and a fundus-tracking perimeter can provide additional invaluable information to clarify the differential diagnoses and allow detailed monitoring of disease progression and treatment response. There are many other measures of macular function not mentioned in this chapter including contrast sensitivity, reading ability, colour discrimination, fixation stability and electrophysiology. Although many of these are also used as endpoint measures in clinical trials, a detailed discussion of these is beyond the scope of this chapter. The clinician assessing macular function needs to understand the basic principles, basis and limitation of these tests and choose the optimal combination of testing strategies based on clinical history, retinal imaging and current literature.

References

1. Marmor MF. A brief history of macular grids: from Thomas Reid to Edvard Munch and Marc Amsler. Surv Ophthalmol. 2000;44(4):343–53.
2. Berry GA. Diseases of the eye. Pentland: Edinburgh; 1889.
3. Amsler M. L'examen qualitatif de la fonction maculaire. Ophthalmol J Int d'ophtalmol. 1947;114:248–61.
4. Amsler M. Earliest symptoms of diseases of the macula. Brit J Ophthalmol. 1953;37(9):521–37.
5. Augustin AJ, Offermann I, Lutz J, Schmidt-Erfurth U, Tornambe P. Comparison of the original Amsler grid with the modified Amsler grid: result for patients with age-related macular degeneration. Retina. 2005;25(4):443–5.
6. Fine AM, Elman MJ, Ebert JE, Prestia PA, Starr JS, Fine SL. Earliest symptoms caused by neovascular membranes in the macula. Arch Ophthalmol. 1986;104(4):513–4.
7. Achard OA, Safran AB, Duret FC, Ragama E. Role of the completion phenomenon in the evaluation of Amsler grid results. Am J Ophthalmol. 1995;120(3):322–9.
8. Wall M, Sadun AA. Threshold Amsler grid testing. Cross-polarizing lenses enhance yield. Arch Ophthalmol. 1986;104(4):520–3.
9. Roy MS. Vision loss without Amsler grid abnormalities in macular subretinal neovascularization. Ophthalmol J Int d'ophtalmol. 1985;191(4):215–7.
10. Schuchard RA. Validity and interpretation of Amsler grid reports. Arch Ophthalmol. 1993;111(6):776–80.
11. Fink W, Sadun AA. Three-dimensional computer-automated threshold Amsler grid test. J Biomed Opt. 2004;9(1):149–53.
12. Almony A, Garg S, Peters RK, Mamet R, Tsong J, Shibuya B, Kitridou R, Sadun AA. Threshold Amsler grid as a screening tool for asymptomatic patients on hydroxychloroquine therapy. Brit J Ophthalmol. 2005;89(5):569–74.
13. Bouwens MD, Van Meurs JC. Sine Amsler Charts. a new method for the follow-up of metamorphopsia in patients undergoing macular pucker surgery. Graefe's Archive Clin Exp Ophthalmol. 2003;241(2):89–93.
14. Ugarte M, Shunmugam M, Laidlaw DA, Williamson TH. Morphision: a method for subjective evaluation of metamorphopsia in patients with unilateral macular pathology (i.e., full thickness macular hole and epiretinal membrane). Indian J Ophthalmol. 2013;61(11):653–8.
15. Shinoda K, Ishida S, Kawashima S, Matsuzaki T, Yamada K, Katsura H. A new method for quantification of metamorphopsia in patients with epiretinal membrane. Japanese J Ophthalmol. 2000;44(4):424–7.
16. Ugarte M, Williamson TH. Horizontal and vertical micropsia following macula-off rhegmatogenous retinal-detachment surgical repair. Graefes Arch Clin Exp Ophthalmol. 2006;244(11):1545–8.
17. Ugarte M, Williamson TH. Aniseikonia associated with epiretinal membranes. Brit J Ophthalmol. 2005;89(12):1576–80.
18. Arndt C, Rebollo O, Seguinet S, Debruyne P, Caputo G. Quantification of metamorphopsia in patients with epiretinal membranes before and after surgery. Graefes Arch Clin Exp Ophthalmol. 2007;245(8):1123–9.
19. Loewenstein A, Malach R, Goldstein M, Leibovitch I, Barak A, Baruch E, Alster Y, Rafaeli O, Avni I, Yassur Y. Replacing the Amsler grid: a new method for monitoring patients with age-related macular degeneration. Ophthalmology. 2003;110(5):966–70.
20. Lakshminarayanan V, Aziz S, Enoch JM. Quantification of metamorphopsia using hyperacuity techniques. Optometry Vis Sci. 1991;68(12):942–5.

21. Kim JH, Kang SW, Kong MG, Ha HS. Assessment of retinal layers and visual rehabilitation after epiretinal membrane removal. Graefes Arch Clin Exp Ophthalmol. 2013;251(4):1055–64.
22. Alster Y, Bressler NM, Bressler SB, Brimacombe JA, Crompton RM, Duh YJ, Gabel VP, Heier JS, Ip MS, Loewenstein A, et al. Preferential hyperacuity perimeter (PreView PHP) for detecting choroidal neovascularization study. Ophthalmology. 2005;112(10):1758–65.
23. Goldstein M, Loewenstein A, Barak A, Pollack A, Bukelman A, Katz H, Springer A, Schachat AP, Bressler NM, Bressler SB, et al. Results of a multicenter clinical trial to evaluate the preferential hyperacuity perimeter for detection of age-related macular degeneration. Retina. 2005;25(3):296–303.
24. Matsumoto C, Arimura E, Okuyama S, Takada S, Hashimoto S, Shimomura Y. Quantification of metamorphopsia in patients with epiretinal membranes. Invest Ophthalmol Vis Sci. 2003;44(9):4012–6.
25. Matsumoto C, Arimura E, Hashimoto S, Takada S, Okuyama S, Shimomura Y. A new method for quantification of mtamorphopsia using M-CHARTS [in Japanese]. Rinsho Ganka. 2000;54:373–7.
26. Arimura E, Matsumoto C, Okuyama S, Takada S, Hashimoto S, Shimomura Y. Quantification of metamorphopsia in a macular hole patient using M-CHARTS. Acta Ophthalmol Scand. 2007;85(1):55–9.
27. Arimura E, Matsumoto C, Nomoto H, Hashimoto S, Takada S, Okuyama S, Shimomura Y. Correlations between M-CHARTS and PHP findings and subjective perception of metamorphopsia in patients with macular diseases. Invest Ophthalmol Vis Sci. 2011;52(1):128–35.
28. Fujita K, Imamura Y, Shinoda K, Matsumoto CS, Mizutani Y, Mizota A, Yuzawa M. Quantification of metamorphopsia in chronic central serous chorioretinopathy after half-dose verteporfin photodynamic therapy. Retina. 2014;34(5):964–70.
29. Okamoto F, Sugiura Y, Okamoto Y, Hiraoka T, Oshika T. Metamorphopsia and optical coherence tomography findings after rhegmatogenous retinal detachment surgery. Am J Ophthalmol. 2014;157(1):214–20.e211
30. Nakagawa T, Harino S, Iwahashi Y. Quantification of metamorphopsia in the course of branch retinal vein occlusion with M-CHARTS. Nippon Ganka Gakkai Zasshi. 2007;111(4):331–5.
31. Bell A, James AC, Kolic M, Essex RW, Maddess T. Dichoptic multifocal pupillography reveals afferent visual field defects in early type 2 diabetes. Invest Ophthalmo Vis Sci. 2010;51(1):602–8.
32. Jiang L, Zhang H, Xie J, Jiao X, Zhou H, Ji H, Lai TY, Wang N. Application of multifocal visual evoked potentials in the assessment of visual dysfunction in macular diseases. Eye (Lond). 2011;25(10):1302–9.
33. Lai TY, Chan WM, Lai RY, Ngai JW, Li H, Lam DS. The clinical applications of multifocal electro-

retinography: a systematic review. Surv Ophthalmol. 2007;52(1):61–96.
34. Timberlake GT, Mainster MA, Webb RH, Hughes GW, Trempe CL. Retinal localization of scotomata by scanning laser ophthalmoscopy. Invest Ophthal Vis Sci. 1982;22(1):91–7.
35. Midena E, Radin PP, Pilotto E, Ghirlando A, Convento E, Varano M. Fixation pattern and macular sensitivity in eyes with subfoveal choroidal neovascularization secondary to age-related macular degeneration. A microperimetry study. Semin Ophthalmol. 2004;19(1-2):55–61.
36. Rohrschneider K, Springer C, Bultmann S, Volcker HE. Microperimetry--comparison between the micro perimeter 1 and scanning laser ophthalmoscope--fundus perimetry. Am J Ophthalmol. 2005;139(1):125–34.
37. Vujosevic S, Smolek MK, Lebow KA, Notaroberto N, Pallikaris A, Casciano M. Detection of macular function changes in early (AREDS 2) and intermediate (AREDS 3) age-related macular degeneration. Ophthalmol J Int d'ophthalmol. 2011;225(3):155–60.
38. Anastasakis A, McAnany JJ, Fishman GA, Seiple WH. Clinical value, normative retinal sensitivity values, and intrasession repeatability using a combined spectral domain optical coherence tomography/scanning laser ophthalmoscope microperimeter. Eye (Lond). 2011;25(2):245–51.
39. Arimura E, Matsumoto C, Okuyama S, Takada S, Hashimoto S, Shimomura Y. Retinal contraction and metamorphopsia scores in eyes with idiopathic epiretinal membrane. Invest Ophthalmol Vis Sci. 2005;46(8):2961–6.
40. Kinoshita T, Imaizumi H, Okushiba U, Miyamoto H, Ogino T, Mitamura Y. Time course of changes in metamorphopsia, visual acuity, and OCT parameters after successful epiretinal membrane surgery. Invest Ophthalmol Vis Sci. 2012;53(7):3592–7.
41. Nomoto H, Matsumoto C, Arimura E, Okuyama S, Takada S, Hashimoto S, Shimomura Y. Quantification of changes in metamorphopsia and retinal contraction in eyes with spontaneous separation of idiopathic epiretinal membrane. Eye (Lond). 2013;27(8):924–30.
42. Uei B, Lee Z, Shimada H, Yuzawa M. Preoperative factors for postoperative resolution of metamorphopsia in idiopathic macular hole surgery. Nippon Ganka Gakkai Zasshi. 2005;109(9):591–5.
43. Fukuda S, Okamoto F, Yuasa M, Kunikata T, Okamoto Y, Hiraoka T, Oshika T. Vision-related quality of life and visual function in patients undergoing vitrectomy, gas tamponade and cataract surgery for macular hole. Brit J Ophthalmol. 2009;93(12):1595–9.
44. Nowomiejska K, Oleszczuk A, Brzozowska A, Grzybowski A, Ksiazek K, Maciejewski R, Ksiazek P, Juenemann A, Rejdak R. M-charts as a tool for quantifying metamorphopsia in age-related macular degeneration treated with the bevacizumab injections. BMC Ophthalmol. 2013;13:13.

45. Bae SW, Chae JB. Assessment of metamorphopsia in patients with central serous chorioretinopathy. Indian J Ophthalmol. 2013;61(4):172–5.

46. Midena E, Vujosevic S, Cavarzeran F. Normal values for fundus perimetry with the microperimeter MP1. Ophthalmology. 2010;117(8):1571–6. e1571

47. Sabates FN, Vincent RD, Koulen P, Sabates NR, Gallimore G. Normative data set identifying properties of the macula across age groups: integration of visual function and retinal structure with microperimetry and spectral-domain optical coherence tomography. Retina. 2011;31(7):1294–302.

48. Chen FK, Patel PJ, Xing W, Bunce C, Egan C, Tufail AT, Coffey PJ, Rubin GS, Da Cruz L. Test-retest variability of microperimetry using the Nidek MP1 in patients with macular disease. Invest Ophthalmol Vis Sci. 2009;50(7):3464–72.

49. Wu Z, Ayton LN, Guymer RH, Luu CD. Intrasession test-retest variability of microperimetry in age-related macular degeneration. Invest Ophthalmol Vis Sci. 2013;54(12):7378–85.

50. Weingessel B, Sacu S, Vecsei-Marlovits PV, Weingessel A, Richter-Mueksch S, Schmidt-Erfurth U. Interexaminer and intraexaminer reliability of the microperimeter MP-1. Eye (Lond). 2009;23(5):1052–8.

51. Goto M, Nishimura A, Shirao Y. Scanning laser ophthalmoscopic microperimetry on idiopathic epiretinal membrane and vitreomacular traction syndrome. Japanese J Ophthalmol. 2001;45(1):115.

52. Cappello E, Virgili G, Tollot L, Del Borrello M, Menchini U, Zemella M. Reading ability and retinal sensitivity after surgery for macular hole and macular pucker. Retina. 2009;29(8):1111–8.

53. Karacorlu M, Ozdemir H, Senturk F, Karacorlu SA, Uysal O. Correlation of retinal sensitivity with visual acuity and macular thickness in eyes with idiopathic epimacular membrane. Int Ophthalmol. 2010;30(3):285–90.

54. Gorgun E, Yenerel NM, Dinc UA, Tatlipinar S, Kucumen RB, Kulacoglu DN, Ciftci F. Central retinal function assessment using microperimetry in patients with idiopathic epiretinal membrane. J Retina-Vitreous. 2010;18:263–8.

55. Mayer WJ, Vogel M, Neubauer A, Kernt M, Kampik A, Wolf A, Haritoglou C. Pars plana vitrectomy and internal limiting membrane peeling in epimacular membranes: correlation of function and morphology across the macula. Ophthalmol J Int d'ophtalmol. 2013;230(1):9–17.

56. Santarelli M, Veritti D, Dal Mas G, Lanzetta P. Functional and morphological changes after macular pucker surgery: an optical coherence tomography and microperimetric study. Ophthalmol J Int d'ophtalmol. 2014;232(4):200–6.

57. Ripandelli G, Scarinci F, Piaggi P, Guidi G, Pileri M, Cupo G, Sartini MS, Parisi V, Baldanzellu S, Giusti C, et al. Macular pucker: to peel or not to peel the internal limiting membrane? A microperimetric response. Retina. 2015;35(3):498–507.

58. Brue C, Saitta A, Nicolai M, Mariotti C, Giovannini A. Epiretinal membrane surgery for combined ham-

59. Sjaarda RN, Frank DA, Glaser BM, Thompson JT, Murphy RP. Resolution of an absolute scotoma and improvement of relative scotomata after successful macular hole surgery. Am J Ophthalmol. 1993;116(2):129–39.

60. Kakehashi A, Ishiko S, Konno S, Akiba J, Yoshida A. Differential diagnosis of macular breaks by microperimetry using the scanning laser ophthalmoscope. Japanese J Ophthalmol. 1996;40(1):116–22.

61. Hikichi T, Ishiko S, Takamiya A, Sato E, Mori F, Takahashi M, Yanagiya N, Akiba J, Yoshida A. Scanning laser ophthalmoscope correlations with biomicroscopic findings and foveal function after macular hole closure. Arch Ophthalmol. 2000;118(2):193–7.

62. Guez JE, Le Gargasson JF, Massin P, Rigaudiere F, Grall Y, Gaudric A. Functional assessment of macular hole surgery by scanning laser ophthalmoscopy. Ophthalmology. 1998;105(4):694–9.

63. Beutel J, Dahmen G, Ziegler A, Hoerauf H. Internal limiting membrane peeling with indocyanine green or trypan blue in macular hole surgery: a randomized trial. Arch Ophthalmol. 2007;125(3):326–32.

64. Tadayoni R, Paques M, Massin P, Mouki-Benani S, Mikol J, Gaudric A. Dissociated optic nerve fiber layer appearance of the fundus after idiopathic epiretinal membrane removal. Ophthalmology. 2001;108(12):2279–83.

65. Miura M, Elsner AE, Osako M, Iwasaki T, Okano T, Usui M. Dissociated optic nerve fiber layer appearance after internal limiting membrane peeling for idiopathic macular hole. Retina. 2003;23(4):561–3.

66. Mitamura Y, Ohtsuka K. Relationship of dissociated optic nerve fiber layer appearance to internal limiting membrane peeling. Ophthalmology. 2005;112(10):1766–70.

67. Ito Y, Terasaki H, Takahashi A, Yamakoshi T, Kondo M, Nakamura M. Dissociated optic nerve fiber layer appearance after internal limiting membrane peeling for idiopathic macular holes. Ophthalmology. 2005;112(8):1415–20.

68. Imai H, Ohta K. Microperimetric determination of retinal sensitivity in areas of dissociated optic nerve fiber layer following internal limiting membrane peeling. Japanese J Ophthalmol. 2010;54(5):435–40.

69. Tadayoni R, Svorenova I, Erginay A, Gaudric A, Massin P. Decreased retinal sensitivity after internal limiting membrane peeling for macular hole surgery. Brit J Ophthalmol. 2012;96(12):1513–6.

70. Baba T, Yamamoto S, Kimoto R, Oshitari T, Sato E. Reduction of thickness of ganglion cell complex after internal limiting membrane peeling during vitrectomy for idiopathic macular hole. Eye (Lond). 2012;26(9):1173–80.

71. Baba T, Sato E, Oshitari T, Yamamoto S. Regional reduction of ganglion cell complex after vitrectomy with internal limiting membrane peeling for idiopathic macular hole. J Ophthalmol. 2014;2014:372589.

artoma of the retina and retinal pigment epithelium: role of multimodal analysis. Clin Ophthalmol. 2013;7:179–84.

72. Scupola A, Mastrocola A, Sasso P, Fasciani R, Montrone L, Falsini B, Abed E. Assessment of retinal function before and after idiopathic macular hole surgery. Am J Ophthalmol. 2013;156(1):132–9. e131

73. Ozdemir H, Karacorlu M, Senturk F, Karacorlu SA, Uysal O. Retinal sensitivity and fixation changes 1 year after triamcinolone acetonide assisted internal limiting membrane peeling for macular hole surgery—a MP-1 microperimetric study. Acta Ophthalmol. 2010;88(6):e222–7.

74. Chen WC, Wang Y, Li XX. Morphologic and functional evaluation before and after successful macular hole surgery using spectral-domain optical coherence tomography combined with microperimetry. Retina. 2012;32(9):1733–42.

75. Bonnabel A, Bron AM, Isaico R, Dugas B, Nicot F, Creuzot-Garcher C. Long-term anatomical and functional outcomes of idiopathic macular hole surgery. The yield of spectral-domain OCT combined with microperimetry. Graefes Arch Clin Exp Ophthalmol. 2013;251(11):2505–11.

76. Sun Z, Gan D, Jiang C, Wang M, Sprecher A, Jiang AC, Xu G. Effect of preoperative retinal sensitivity and fixation on long-term prognosis for idiopathic macular holes. Graefes Arch Clin Exp Ophthalmol. 2012;250(11):1587–96.

77. Ooto S, Hangai M, Takayama K, Ueda-Arakawa N, Hanebuchi M, Yoshimura N. Photoreceptor damage and foveal sensitivity in surgically closed macular holes: an adaptive optics scanning laser ophthalmoscopy study. Am J Ophthalmol. 2012;154(1):174–86. e172

78. Michalewska Z, Michalewski J, Adelman RA, Nawrocki J. Inverted internal limiting membrane flap technique for large macular holes. Ophthalmology. 2010;117(10):2018–25.

79. Quezada Ruiz C, Pieramici DJ, Nasir M, Rabena M, Avery RL. Severe acute vision loss, dyschromatopsia, and changes in the ellipsoid zone on Sd-Oct associated with intravitreal ocriplasmin injection. Retinal Cases Brief Rep. 2015;9(2):145–8.

80. Smith AJ, Telander DG, Zawadzki RJ, Choi SS, Morse LS, Werner JS, Park SS. High-resolution Fourier-domain optical coherence tomography and microperimetric findings after macula-off retinal detachment repair. Ophthalmology. 2008;115(11):1923–9.

81. Rossetti A, Doro D, Manfre A, Midena E. Long-term follow-up with optical coherence tomography and microperimetry in eyes with metamorphopsia after macula-off retinal detachment repair. Eye (Lond). 2010;24(12):1808–13.

82. Lai WW, Leung GY, Chan CW, Yeung IY, Wong D. Simultaneous spectral domain OCT and fundus autofluorescence imaging of the macula and microperimetric correspondence after successful repair of rhegmatogenous retinal detachment. Brit J Ophthalmol. 2010;94(3):311–8.

83. Delolme MP, Dugas B, Nicot F, Muselier A, Bron AM, Creuzot-Garcher C. Anatomical and functional macular changes after rhegmatogenous reti-

nal detachment with macula off. Am J Ophthalmol. 2012;153(1):128–36.

84. Ikuno Y, Sayanagi K, Ohji M, Kamei M, Gomi F, Harino S, Fujikado T, Tano Y. Vitrectomy and internal limiting membrane peeling for myopic foveoschisis. Am J Ophthalmol. 2004;137(4):719–24.

85. Chen FK, Uppal GS, Rubin GS, Webster AR, Coffey PJ, Da Cruz L. Evidence of retinal function using microperimetry following autologous retinal pigment epithelium-choroid graft in macular dystrophy. Invest Ophthalmol Vis Sci. 2008;49(7):3143–50.

86. Chen FK, Patel PJ, Uppal GS, Rubin GS, Coffey PJ, Aylward GW, Da Cruz L. A comparison of macular translocation with patch graft in neovascular age-related macular degeneration. Invest Ophthalmol Vis Sci. 2009;50(4):1848–55.

87. Chen FK, Patel PJ, Uppal GS, Tufail A, Coffey PJ, Da Cruz L. Long-term outcomes following full macular translocation surgery in neovascular age-related macular degeneration. Brit J Ophthalmol. 2010;94(10):1337–43.

88. Chen FK, Patel PJ, Coffey PJ, Tufail A, Da Cruz L. Increased fundus autofluorescence associated with outer segment shortening in macular translocation model of neovascular age-related macular degeneration. Invest Ophthal Vis Sci. 2010;51(8):4207–12.

89. Radtke ND, Aramant RB, Petry HM, Green PT, Pidwell DJ, Seiler MJ. Vision improvement in retinal degeneration patients by implantation of retina together with retinal pigment epithelium. Am J Ophthal. 2008;146(2):172–82.

90. Park SS, Bauer G, Abedi M, Pontow S, Panorgias A, Jonnal RS, Zawadzki RJ, Werner JS, Nolta J. Intravitreal autologous bone marrow CD34+ cell therapy for ischemic and degenerative retinal disorders: preliminary Phase 1 clinical trial findings. Invest Ophthalmol Vis Sci. 2015;56(1):81–9.

91. Bainbridge JW, Smith AJ, Barker SS, Robbie S, Henderson R, Balaggan K, Viswanathan A, Holder GE, Stockman A, Tyler N, et al. Effect of gene therapy on visual function in Leber's congenital amaurosis. N Engl J Med. 2008;358(21):2231–9.

92. MacLaren RE, Groppe M, Barnard AR, Cottriall CL, Tolmachova T, Seymour L, Clark KR, During MJ, Cremers FP, Black GC, et al. Retinal gene therapy in patients with choroideremia: initial findings from a phase 1/2 clinical trial. Lancet. 2014;383(9923):1129–37.

93. Guymer RH, Brassington KH, Dimitrov P, Makeyeva G, Plunkett M, Xia W, Chauhan D, Vingrys A, Luu CD. Nanosecond-laser application in intermediate AMD: 12-month results of fundus appearance and macular function. Clin Exp Ophthalmol. 2014;42(5):466–79.

94. Jobling AI, Guymer RH, Vessey KA, Greferath U, Mills SA, Brassington KH, Luu CD, Aung KZ, Trogrlic L, Plunkett M, et al. Nanosecond laser therapy reverses pathologic and molecular changes in age-related macular degeneration without retinal damage. FASEB J. 2015;29(2):696–710.

Part III

Adjunctive Surgical Techniques

Trends in Microsurgical Instrumentation

9

Kazuhito Yoneda and Yusuke Oshima

9.1 Wide-Angle Viewing Systems (WAVs)

The use of WAVs in conjunction with wide-angle illumination, like a chandelier lighting, allows easier bimanual maneuvers because they can provide a view of all inside the ocular globe without eye rotation, eliminating concerns regarding fragility of small-gauge instruments.

These tools play a part in the more widespread use of small-gauge vitrectomy, especially with 27-g system, for a variety of vitreoretinal pathologies.

At the same time, recently a variety of WAVs has been newly developed or upgraded from previous version along with the recent widespread use of MIVS.

To obtain a sufficient view of the posterior segment, it is necessary to use a highly refractive lens (60D, 90D, 120D) which is placed in front of the lens of the surgical microscope comparable to indirect ophthalmoscopes. With regard to the noncontact type WAVs, the Oculus BIOM can be used with all microscopes, but the Resight viewing system can only be used with a Zeiss micro-

scope (Fig. 9.1), and the EIBOS viewing system can only be used with a Leica microscope. OULUS HD Disposable LenZ is one of the best indirect lens. Benefit from the OCULUS quality even if you don't use the OCULUS BIOM system. The new OCULUS HD Disposable LenZ is designed for single use on the ZEISS RESIGHT. The HD Disposable LenZ combines an extremely wide field of view with high-definition clarity. This makes it ideal for all stages of vitreoretinal surgery including macula viewing under high magnification. Every system offers excellent optical images with a variety of different magnifications and fields of view. There has been some useful improvement of WAVs. For example, Leica Proveo 8 has two impressive development. One is "FusionOptics" and another is "synchronized focus."

FusionOptics captures different information from each of the two beam paths, delivering high resolution to the left eye and depth of field to the right eye. It is possible to merge the visual information into a high-contrast, detailed image with an expanded area in focus. Not only does this enhance the surgical view, it enhances surgeon's workflow as refocusing is reduced during the surgery.

In regard to the synchronized focus, it is useful system for noncontact type WAV, the BIOM. Mount the BIOM 5 from OCULUS in a matter of seconds and swing into the beam path when needed. Synchronized focusing of the

K. Yoneda (✉)
Subarukai Eye Center, Higashiomi, Japan

Sakura Eye Clinic, Maizuru, Japan
e-mail: kazuyone@koto.kpu-m.ac.jp

Y. Oshima
Oshima Eye Clinic, Takatsuki, Japan

Fig. 9.1 Variety of noncontact type lens for WAVs 128D (yellow) and 60D (green) lens for Resight (Zeiss) Disposable lens (Oculus) for Resight (Zeiss). Each lens is suitable for Resight (Zeiss) and each has different features. 128D lens has a wide surgical field and fit to core to peripheral vitrectomy. On the other hand, the field of 60 D lens is narrow, but it has high resolution enough to perform a macular procedure such as membrane peeling
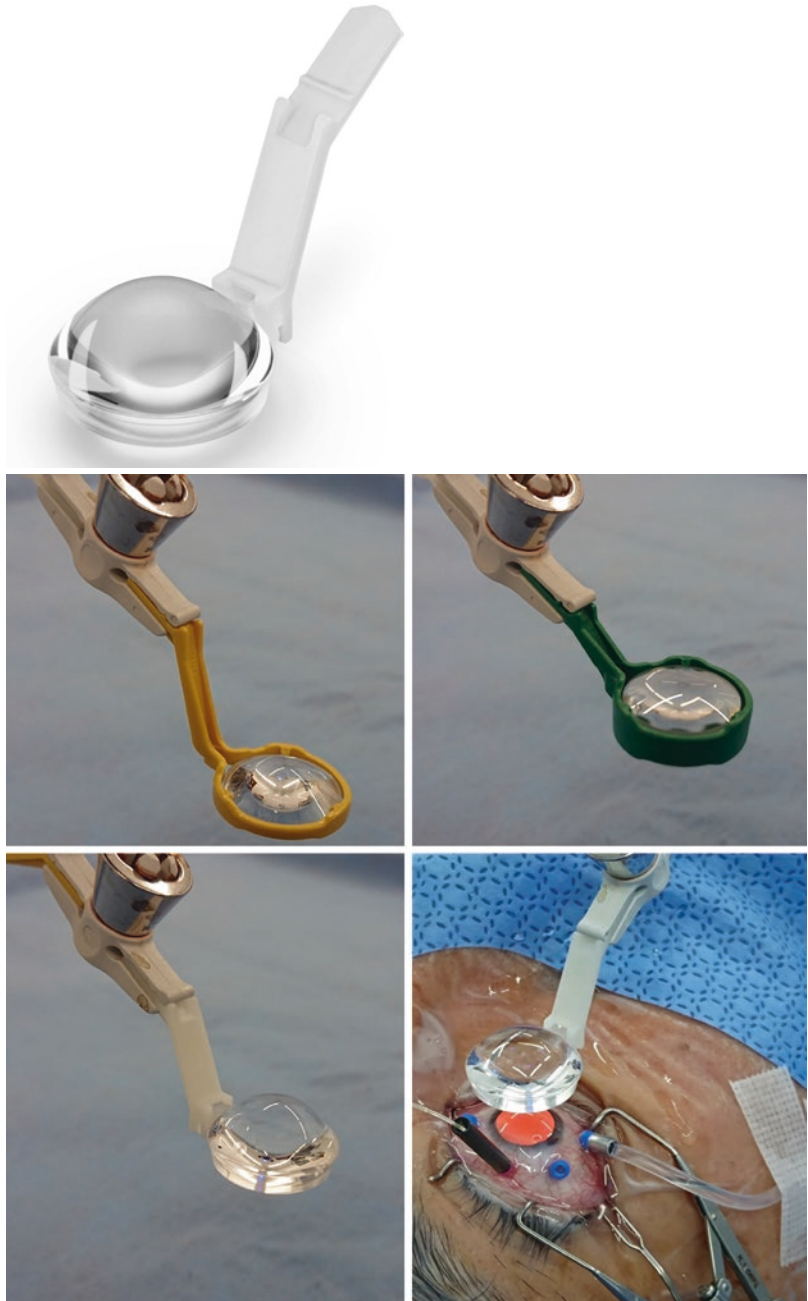
Fig. 9.2 BIOM 5 with synchronized focus
For contact-free, wide-angle observation of the fundus during vitreous surgery. Mount the BIOM 5 from OCULUS in a matter of seconds and swing into the beam path when needed. Synchronized focusing of the optics carrier and BIOM 5 means the front lens does not move vertically in relation to the eye

optics carrier and BIOM 5 means the front lens does not move vertically in relation to the eye (Fig. 9.2).

9.2 High-Speed Vitreous Cutter

Recent single-port vitreous cutters have a cut rate of 10,000 cuts/min. Additionally, the most recent vitreous cutter has two open cutting ports and a second cutting blade. DORC first developed this system and named twin duty cycle (TDC) cutter that has a cut rate of 16,000 cuts/min (Fig. 9.3). This new invention comprises two new features, such as the permanent flow and two cutting blades. The two cutting blades are able to cut two times during one movement and double the cutting efficiency. Moreover, this new type cutter has a continuous and even flow due to the two open cutting port and high duty cycle. This technology reduces vitreous traction, decreases surgical time, and increases safety and efficiency of surgery. Recently, Alcon also launched dual-blade cutter, HYPERVIT Dual Blade Vitrectomy Prove at 20,000 cuts/min.
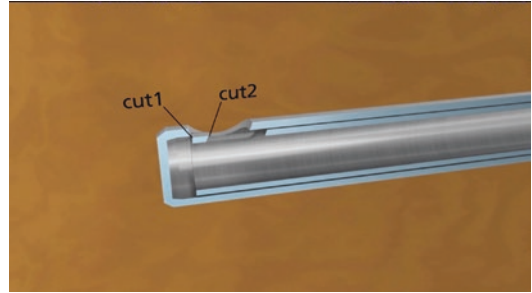
Fig. 9.3 High-speed vitreous cutter
This new invention comprises two new features, such as the permanent flow and two cutting blades. The two cutting blades are able to cut two times during one movement and double the cutting efficiency

9.3 Instruments for Macular Surgery

9.3.1 Finesse Sharkskin ILM forceps (Alcon) (Fig. 9.4)

Finesse Sharkskin ILM forceps have laser-ablated micro-surface and are designed to easily facilitate initiation of the ILM peel. Additionally, it has optimized grasping platform and angled tip closure to help mitigate membrane shredding.

9.3.2 Ultra-Peel Forceps (DORC) (Fig. 9.5)

Ultra-peel forceps were launched in 2018 and available in 25 g and 27 g. The ultra-peel forceps were designed specifically for surgeons working with dense, fibrotic, and adherent membranes where forceps are being used in close proximity to the retina and where the rounded tip design is designed to be atraumatic to the retina. Additionally, 27 g ultra-peel forceps were designed to deliver over 90% equivalent gripping area and a 50% improvement in grasping force when compared to the 23 g version.

Fig. 9.4 Finesse Sharkskin ILM forceps (Alcon)
Sharkskin ILM forceps have optimized grasping platform and angled tip closure to help mitigate membrane shredding

Fig. 9.5 Ultra-peel forceps (DORC)
Ultra-peel forceps are able to be used in close proximity to the retina and where the rounded tip design is designed to be atraumatic to the retina

9.3.3 Stiff DEX Forceps (Katalyst) (Fig. 9.6)

Stiff Dex forceps have 19 g telescoping stiffening sleeve and are 55 times stiffer than 27 g instruments. Retractable stiffening sleeve does not interfere with full length 32-mm shaft that does not deflate the eye and depress the eye wall even in the myopic eyes. This retractable stiffening sleeve technology is also useful for light pipe.

9.3.4 27ga Tano Diamond-Dusted Membrane Scraper (Synergetics) (Fig. 9.7)

The membrane scrapers (DDMS) offer an atraumatic means to locate the edge of the membrane. These single-use tools are ideal for removal of inner limiting membranes and epiretinal membranes.

Fig. 9.6 Stiff DEX Forceps (Katalyst) The forceps have 19 g telescoping stiffening sleeve and are 55 times stiffer than 27 g instruments Light pipe with stiffening sleeve
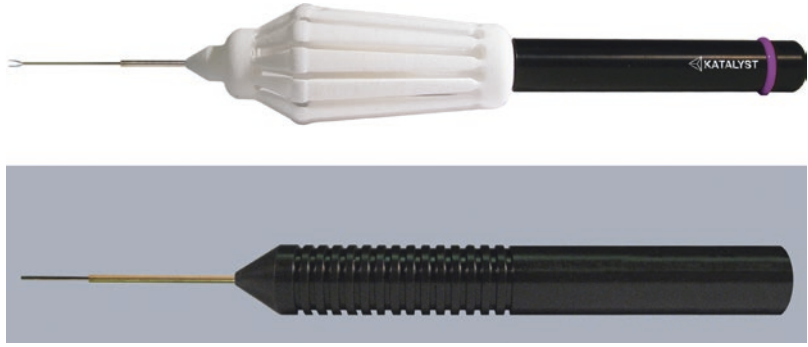
Fig. 9.7 27 ga Tano diamond-dusted membrane scraper (Synergetics) The membrane scrapers (DDMS) offer an atraumatic means to locate the edge of the membrane. These single-use tools are ideal for removal of inner limiting membranes and epiretinal membranes

The diamond-dusted soft silicone tip locates and pulls the edge of the membrane quickly and also paves the way for easy removal with your forceps. These DDMS products are available in several forms.

9.3.5 FINESSE Flex Loop (Alcon)
(Fig. 9.8)

FINESSE Flex Loop's nitinol loop was designed for consistency in creating an edge on the ILM/ERM without loss of particular matter such as retinal nerve fiber. The device has been designed with a retractable tip for an adjustable stiffness profile. It is possible to adjust the loop length that allows for variable bending stiffness and provides ease of insertion through valved and non-valved cannulas.

9.4 Synergetics™ 27 ga Oshima Vivid Chandelier

The 27 ga Oshima Vivid Chandelier is the most frequently used variant of the Synergetics brand chandeliers (Fig. 9.9).

Most importantly, this Chandelier provides full panoramic illumination with superior brightness. This brightness is enabled by a proprietary processing method of the resin.

Close to the end of the lighting fiber, there is a stoppage system, which includes the light blue rubber cap, which ensures the fiber positioning is maintained once the depth in the eye is established. This rubber cap can be pushed onto the cannula with a fiber insertion tool that is pre-mounted on the fiber.

9.5 Nano Cannula 25G/48G

Nano Cannula 25G/48G was developed to enable us to perform endovascular surgery (Fig. 9.10).

It is sharp and stiff enough to pierce microvessels. Some kind of solution can be injected into the vessel.

Fig. 9.8 FINESSE Flex
Loop (Alcon)
FINESSE Flex Loop's
nitinol loop was
designed for consistency
in creating an edge on
the ILM/ERM without
loss of particular matter
such as retinal nerve
fiber

Fig. 9.10 Nano cannula 25G/48G

Nano cannula 25G/48G was developed to enable us to perform endovascular surgery

It is sharp and stiff enough to pierce microvessels. Some kind of solution can be injected into the vessel
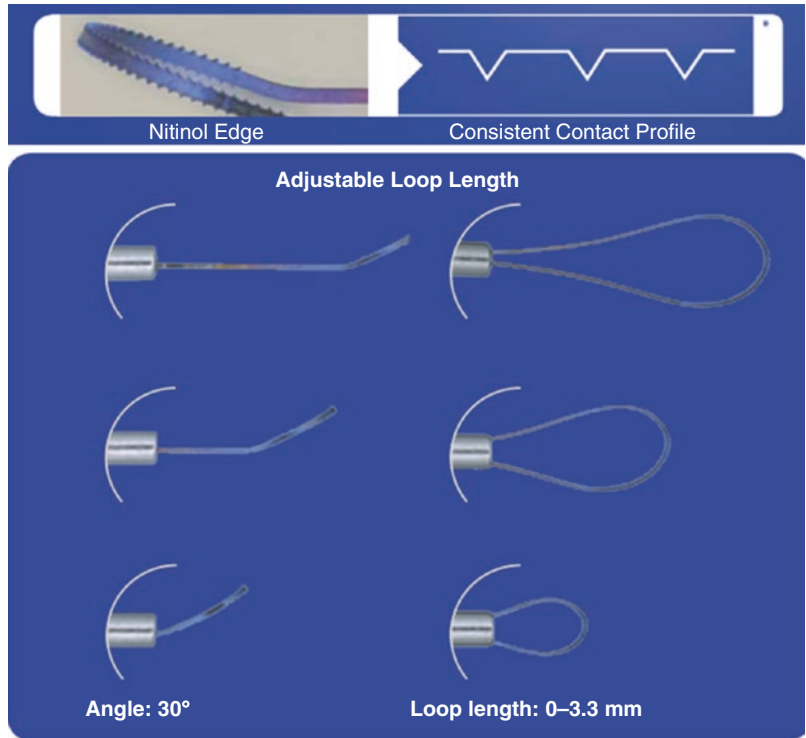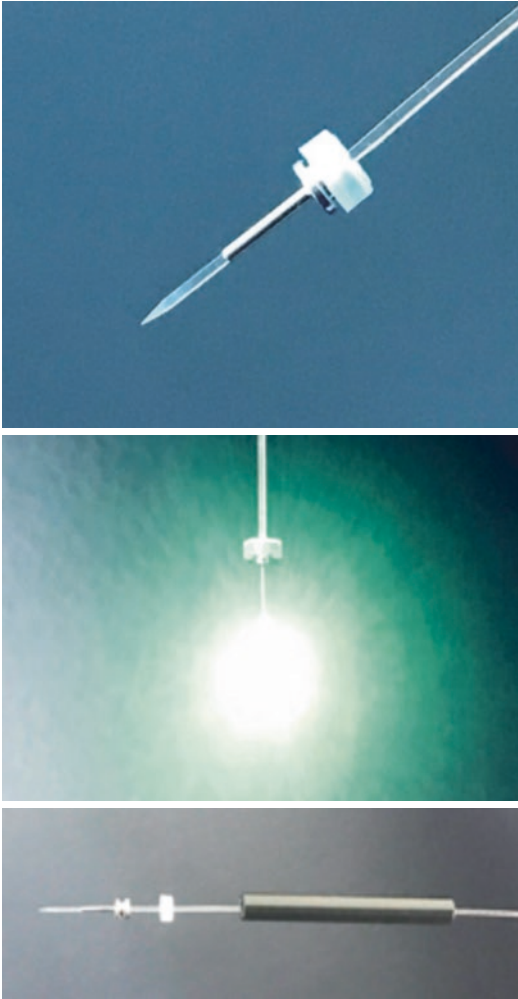
Fig. 9.9 Synergetics™ 27 ga Oshima Vivid Chandelier

This Chandelier provides full panoramic illumination with superior brightness. This brightness is enabled by a proprietary processing method of the resin

Staining Techniques of Internal Limiting Membrane and Vitreous During Vitreoretinal Surgery

10

Tzyy-Chang Ho

10.1 Introduction

Vitreoretinal surgery has grown rapidly in the past decade. New surgical techniques and adjuncts have decreased surgical time, increased precise understanding and localization of disease pathology, and increased surgical success rate. One of the innovative improvements vitreoretinal surgery has been the introduction of vital dyes to improve the visibility of retinal tissues and preretinal tissues [1, 2]. The term "chromovitrectomy" means the usage of vital dyes during surgery to assist in the identification of preretinal tissues and membranes [3]. The modern approach was first introduced in 2000 when the dye indocyanine green (ICG) was used to stain the very thin transparent internal limiting membrane (ILM) and it is currently still the most commonly used surgical dye in ophthalmology. However, over the past few years, controversial evidences have accumulated indicating that these dyes may have harmful effects. Following initial clinical experiences with ICG, clinical and experimental studies demonstrated signs of the retinal toxicity of ICG, which stimulated research on alternative dyes for chromovitrectomy. Other alternative biostains, including trypan blue (TB) or brilliant blue

(BriB) and patent blue (PB), have been added to the surgical list for chromovitrectomy [4]. This chapter presents the latest data on chromovitrectomy in terms of the biochemical properties, indications, and clinical experience with various vital dyes available for chromovitrectomy.

10.2 Biochemical Pharmacology

Vital staining means the coloration of living cells or tissues. The dyes used are organic molecules which contain chromophores. A chromophore refers to the part of a molecule responsible for its color [5]. The staining agents may be classified according to the chemical classification. Dyes used in chromovitrectomy can be classified as: (1) azo dyes; (2) arylmethane dyes; (3) cyanine dyes; (4) xanthene dyes; and (5) colored corticosteroids.

TB is an anionic hydrophilic azo dye which has a molecular weight of 960 Da. TB can kill trypanosomes, which are the parasites that cause sleeping sickness [6]. TB crosses the cell membranes of dead cells only, because of that stains dead tissues/cells blue. In ophthalmology, TB has in a preferential manner affinity for the epiretinal membrane (ERM) [7]. TB may be commercially available at a concentration of 0.15% for vitreoretinal surgery, called membrane blue (DORC International, Zuidland, Netherlands). Cyanine dyes have amphiphilic properties and thereby

T.-C. Ho (✉)
Department of Ophthalmology, National Taiwan University Hospital, College of Medicine, National Taiwan University, Taipei City, Taiwan
e-mail: hotchang@ntu.edu.tw

binds to both cellular and acellular elements in living tissues. ICG is a tricarbocyanine anionic vital dye with a molecular formula of $C_{43}H_{47}N_2NaO_6S_2$ and a molecular weight of 775 Da. The sterile hydrophilic powder represents a very useful contrast agent in angiography, allowing imaging of choroidal and retinal tissues [8]. For ophthalmology, ICG is commercially available under the names of ICG (Pulsion Medical Systems, Munich, Germany; 25- and 50-mg vials), ICV Indocianina Verde (Ophthalmos, São Paulo, Brazil; 5-, 25-, and 50-mg vials), Diagnogreen (Daiichi Pharmaceutical, Tokyo, Japan; 25-mg vial), and IC-Green (Akorn, Buffalo Grove, USA; 25-mg vial).

Infracyanine green (IfCG) is a green dye with a chemical formula and pharmacologic properties similar to those of ICG. However, IfCG has a clear advantage over ICG because it is synthesized without sodium iodine, as it is believed that iodine damages the cornea and retina [9]. On the other hand, iodide-free IfCG is not water-soluble and has to be dissolved in a 5% glucose solvent. It is commercially available under the brand name of Infracyanine (Laboratoires SERB, Paris, France; 25-mg vial).

Arylmethane dyes are stains which are formed by one carbon linked to benzene or naphthalene groups; they are commonly used in modern inks. BriB is a blue anionic arylmethane compound which has the chemical formula of $C_{47}H_{48}N_3S_2O_7$-Na and a molecular weight of 854 Da. This dye was reported to stain the ILM and to have no significant in vivo toxicity [10]. The dye gained acceptance for intraocular use under the brand name of Brilliant Peel (Geuder, Heidelberg, Germany) and it is provided in vials containing 2 mg/mL of the vital dye. Another example is Bromophenol blue (BroB) which is an acid–base indicator that has recently been proposed as a promising alternative biostain for vitrectomy because it has induced no damage in either in vitro or in vivo studies [11]. PB is a hydrophilic anionic triarylmethane dye with the chemical formula $C_{27}H_{31}N_2NaO_6S_2$ and a molecular weight of 582 Da. PB has been applied as an off-label agent in vitreoretinal surgery.

Xanthene is a yellow organic heterocyclic compound. Its chemical formula is C13H10O. Xanthene dyes tend to be fluorescent, yellow to pink to bluish red, brilliant dyes. Fluorescein is a xanthene fluorophore with the chemical structure $C_{20}H_{12}O_5$ and a molecular weight of 332 Da.

Corticosteroids are hormones produced naturally in the cortex of the adrenal gland, whose derivates may be synthetically produced to be used as drugs in the treatment of human diseases. Triamcinolone acetonide (TA) is a synthetic insoluble corticosteroid with the empirical formula $C_{24}H_{31}FO_6$ and a molecular weight of 434 Da. In intraocular surgery, TA has shown a good staining of the vitreous because of the physical crystal structures [12].

10.3   Light Source and Vital Dyes

In the modern era of vitreoretinal surgery, the interaction of light from endoillumination source and vital dye may increase or decrease the risk for toxicity. Light-induced retinal toxicity by the endoilluminator is dependent on factors such as the duration of use, type, power, and wavelength of light source [13]. Vital dyes have small chemical molecules that can pass through retinal tissues and may exacerbate retinal phototoxicity from light exposure [14]. Photosensitizing dyes could enhance phototoxicity by increasing levels of free radicals, creating a photoproduct that could be harmful to retinal cells and shifting light absorbance from one site of the retina to another [14]. In this regard, the dye on the retinal surface could increase the risk for phototoxicity to the neuroretina for light greater than 450 nm, which would not occur without dyes [15]. In addition, dyes that enter the subretinal space may have direct contact with and may exacerbate damages to the RPE after exposure to various wavelengths of light [16]. From a surgery perspective, among all light sources analyzed by Costa et al. [14], the greatest overlap was found with integrated laser pathway (Photon Xenon; Synergetics Photon) and halogen (Grieshaber GLS; GLS Corp.) and

the least overlap was found with mercury vapor lamp (Photon 2; Synergetics).

Recent usage of 3-D head-up digital surgery has the benefit of changing brightness, contrast, and color display on the monitor, which may decrease the usage of dye. The decreased endoillumination light intensity may also decrease the dye–light interaction and thus decrease the toxicity [17]. Real-time digital filtering can be used to highlight internal limiting membrane staining achieved during chromovitrectomy and digital gain manipulation can significantly reduce endoillumination requirements. Compared to traditional analog microscopes, the NGENUITY® by ALCON delivers up to 48% greater magnification, up to five times extended depth of field, and up to 42% finer depth resolution. The usage of staining time can be reduced and the light intensity can be reduced by 50–60%. And still has a good visibility of epiretinal membrane and internal limiting membrane.

10.4 Digital Filters in 3-D Visualization System

To be more specific, the ability to toggle color settings on the display monitor of the NGENUITY 3D Visualization System (Alcon) offers a novel mechanism for identifying different tissue during vitreoretinal surgery. Several situations in which digital filters offering on the platform combined with adjustments on other settings may aid in visualization. The red-free filter can be engaged to identify a hemorrhage, it may also help visualize a tissue plane during internal limiting membrane (ILM) peeling. Other tissues are more discernable with other color filters: epiretinal membrane is easier to visualize with a green filter, and vitreous may be more noticeable with a blue filter. In certain situations, the use of color filters can be extremely helpful:

- Extrascleral hemorrhage. Localizing the area for placing a port is greatly facilitated by use of the red-free filter.

- Dense vitreous hemorrhage. The presence of a hemorrhage results in a red hue being cast against an orange background, often making it difficult to distinguish the retina. Reducing the red in the display output therefore obscures the hemorrhage, permitting direct visualization of the retina.
- ILM peeling. Adjusting the hues to red-free and gains in the picture helps to highlight the ILM. In our surgeries, we have found that we can often find an edge and peel the membrane with very little dye.
- It is possible to turn hemorrhage from red to yellow so that you can see around the blood, see the tissue better, determine your depth, and ensure you are accomplishing your surgical goals overall.
- We also use a separate color channel for ILM peeling with ICG that creates a great view of the dye and the tissue. This allowed us to reduce the concentration of ICG dye that we use.
- Many surgeons like to turn down the red channel to make the image appear bluish. When the red reflex is diminished, you can see the clear vitreous better.
- Alteration to make the image appear somewhat red enhances visualization of indocyanine green stain; this allows the surgeon to dilute the stain at two to tenfold.
- Adjusting color gains to make the image look yellow–orange enhances the faint staining of brilliant blue G stain.

10.5 Dye Injection Techniques

The dye injection techniques are variable among surgeons.

1. There are different ways to protect the retinal pigment epithelial cells during dye injection in the vitreoretinal surgery: slow injection of the dye, placing substances over the macular hole, if apply, such as sodium hyaluronate [18] perflourocarbon liquids [19], autologous whole blood [20], or use of VINCE (vitreo-

retinal internal limiting membrane color enhancer), which enables selective painting of ILM that needs to be removed without staining perifoveal and peripheral retina [21].

2. The most common two ways in dye injection technique are: The "dry method" or "air-filled technique." This technique consists of removing the fluid in the vitreous cavity by a fluid–gas exchange before dye injection [21]. While the technique has the advantage of concentrating the dye in the posterior pole and avoiding contact at the posterior capsule of the lens, it may expose the retinal surface to a higher concentration of dye to the vitreoretinal interface [3].

3. Another way is the "wet method" or "fluid-filled technique." In this approach, the intravitreal fluid (usually balanced salt solution) is left inside the vitreous cavity, while the surgeon injects the dye. The amount of dye in contact with the retinal surface becomes much lower because it is immediately washed out by the fluid in the vitreous cavity [22]. Czajka et al. compared the two methods in a porcine model and concluded that the air-filled technique induces a higher incidence of RPE atrophy and outer retinal degeneration than the fluid-filled technique [23]. The wet method is more safer and faster during surgery than dry method.

4. In real-world practices, we found that dyes dissolved in 5% glucose water in a low concentration (e.g., 0.5 mg/mL as in the case of indocyanine green) can settle nicely over the macula without dispersion in the vitreous cavity. The volume injected can be lowered to as less as 0.1 mL and the procedure can be performed with a valved cannula in 25- or 27-gauge vitrectomy, which would have less turbulence during injection. Indocyanine green binds firmly and specifically to ILM and well-differentiated the boundary from epiretinal membrane, which makes the surgical planes of epiretinal membrane surgery clearly stratified.

10.6 Dyes Common Used in Clinical Practices

10.6.1 Triamcinolone Acetonide

Triamcinolone acetonide is a synthetic nonsoluble corticosteroid that can be used to stain the cortical vitreous or outline ILM. In its usual preparations, triamcinolone acetonide is composed of white crystals in an aqueous suspension. These crystals are responsible for its staining ability, as they bind avidly to acellular tissues such as vitreous and also deposit on the ILM. The duration that triamcinolone acetonide remains in the eye depends on the specific formulation, but studies have found that crystals can remain in the vitreous cavity for up to 40 days after instillation [24]. The half-life is around 18 days in nonvitrecomized eyes and 3 days in vitrectomized eyes. Application of triamcinolone acetonide typically consists of injecting 0.1–0.3 mL with a concentration of 40 mg/mL. Triamcinolone acetonide has been shown to be more effective in highlighting vitreous than trypan blue, infracyanine green, and fluorescein [25]. However, we found triamcinolone acetonide suspension very slippery, which hindered the surgery of ILM at the later stage of vitreoretinal surgery.

Triamcinolone acetonide, as a corticosteroid, has anti-inflammatory properties, and intravitreal injections are approved for the treatment of macular edema and uveitis. It has been speculated that usage of triamcinolone as a visualization tool may have the added benefit of decreasing postoperative inflammation and vitreoretinopathy. Triamcinolone acetonide has not been demonstrated to be toxic to the retina and remains a relatively safe option. There is a slightly increased risk in the development of cataracts and increased IOP with intravitreal triamcinolone use.

Commercial formulations of triamcinolone acetonide are available as Triesence (Alcon) and Kenalog (Bristol-Meyers). Triesence is preservative-free, while Kenalog contains benzyl alcohol as a preservative. Animal studies have suggested benzyl alcohol can have a toxic

effect on the neurosensory retina. Currently, only Triesence has FDA approval for intravitreal use. Usage of Kenalog for any indication intravitreally is considered off-label. The physical properties vary among different brands. To prevent slippery surface during ILM peeling, wash out needs to be performed after triamcinolone acetonide usage.

10.6.2 Trypan Blue

Subjective judgment of the tissue layers by the surgeon is necessary for using trypan blue. Trypan blue is a blue hydrophilic anionic azo dye that is generally used to stain ERMs but also weakly stains the vitreous and ILM. Trypan blue is unable to cross cell membranes in living cells and thus is only able to stain dead cells with compromised cell membranes. ERM contains a relatively high number of dead glial cells and thus has a high affinity for trypan blue. Due to its hydrophilicity, trypan blue also has a weak affinity for the ILM and vitreous. Trypan blue is seldom used to only stain the ILM or vitreous as other dyes (such as indocyanine green and corticosteroids) provide superior visualization [26].

Fluid–air exchange should first be performed to apply trypan blue for ERM staining to ensure the dye localizes to the macula. Afterward, 0.15% concentration can be injected into the posterior pole. Alternatively, a 3:1 mixture of 0.15% trypan blue to 10% glucose can be used to create a dense solution that does not require fluid–air exchange before injection.

Trypan blue is well tolerated by the retina at typical concentrations. At higher concentrations, histological analysis in few animals and in vitro studies have demonstrated mild retinal toxicity [27]. Trypan blue is FDA approved for intraocular injection. It is available as MembraneBlue (Dutch Ophthalmic Research Center) at a concentration of 0.15%. This should not be confused with VisionBlue (Dutch Ophthalmic Research Center), which is used to stain the anterior capsule. VisionBlue has a lower concentration of 0.06%, which may be inadequate for vitreoretinal procedures.

10.6.3 Brilliant Blue

Brilliant blue has a strong affinity for the ILM and is a blue anionic triarylmethane dye. Brilliant blue is commonly used for ILM peeling as it stains the ILM well without staining ERMs or vitreous. Adequate staining of the ILM can be achieved by applying brilliant blue at a concentration of 0.025% in an iso-osmolar solution toward the area of interest.

Retinal toxicity has not yet demonstrated in most in vitro and in vivo studies [28]. Atrophic changes of RPE have been reported when there is subretinal migration of the dye. Many studies seem to suggest a better safety profile for brilliant blue compared to indocyanine green [29]. Thus, brilliant blue may present a better option for ILM staining.

Brilliant blue is currently approved for use in Europe as Brilliant Peel (Fluoron). FDA approval is still awaiting. No FDA-approved commercial formulations are currently available in the United States and most part of the world, though compounding pharmacies can provide formulations.

10.6.4 Bromophenol Blue

Bromophenol blue has a high affinity for both ILM and ERM and is a blue triarylmethane dye. Bromophenol blue can be injected at a concentration of 0.13–0.2% and does not require fluid–gas exchange. In vitro studies have demonstrated low toxicity to the retina with significantly less toxic effects than indocyanine green. Studies in human subjects injected with intraocular bromophenol blue have also not shown any functional visual deficits as measured through perimetry and ERG [30].

Given the favorable safety profile, bromophenol blue is another dye that may be preferable to indocyanine green for ILM staining. It is currently approved for use in Europe and commercially available in a combined formulation with brilliant blue known as Brilliant Peel Dual Dye (Fluoron). It is not FDA-approved.

10.6.5 Patent Blue

Patent blue is being investigated as a potential stain for ERM and is a blue anionic triarylmethane dye. Like trypan blue, patent blue has moderate affinity for ERMs and a low affinity for the ILM [31]. Patent blue can be injected toward the area of interest in an iso-osmolar solution at 0.25% concentration or diluted in 0.25% glucose.

Most studies suggest that patent blue has a similar safety profile to trypan blue when used in the vitreous space. Animal studies have demonstrated low toxicity of patent blue when injected subretinally, and in vitro models have not shown any irreversible effect on retinal function [32]. Surgical case reports have not reported any postoperative visual field defects or grossly visible RPE changes. Patent blue is currently approved in Europe for capsular staining during cataract surgery under the brand name of Blueron® (Fluoron). Its use in vitreoretinal surgery is off-label and it does not yet have FDA approval.

10.6.6 Indocyanine Green and Infracyanine Green

ILM peel can be achieved after staining with ICG. The underlying retina remains unstained. Indocyanine green (ICG) is a green anionic cyanine dye that is useful for ILM staining. It has high affinity for components of the extracellular matrix present in the ILM such as collagen type IV and laminin. In porcine studies, ICG causes increased stiffness of the ILM when it is exposed to light, possibly due to alterations in collagen structure [33]. This stiffening may facilitate easier removal in one piece with less damage to underlying tissues. Various studies have shown improved ease of ILM removal and less trauma when ICG is applied before ILM peeling. ICG requires initial dilution in distilled water. If diluted initially in saline, the dye can precipitate. The diluted solution should then be subsequently diluted in balanced saline solution to create a less hypo-osmolar solution. In real-world practice, the ICG powder can be dissolved completely in 5% glucose water. We currently dilute it firstly with 10 mL 5% glucose water and then dilute again with 5 mL glucose water to make a 0.5 mg/mL concentration.

There are some concerns over ICG's toxicity when used intraocularly. A large-scale meta-analysis showed similar anatomical outcomes when using ICG versus no dye in ILM peels, but worse functional outcomes [34]. The authors implicated dye-induced toxicity as a possible culprit. Numerous animal studies have shown that ICG is toxic to chorioretinal cells when exposed to moderate to high concentrations. ICG has also been proposed to cause toxicity when applied and exposed to light through a photochemical mechanism. Studies performed in rabbits resulted in RPE changes and functional retinal damage when subretinal ICG injections were exposed to light [35]. The FDA has approved ICG for intravenous use in angiography, but not for intraocular use. Thus, its use in vitreoretinal surgery is currently off-label. However, in the case of myopic traction maculopathy, the toxicity is minimal due to the relative intact neurosensory retina [36]. Figure 10.1 shows the foveola nonpeeling (A) and fovea nonpeeling ILM surgery of myopic traction maculopathy. The ILM is peeled around the foveola or fovea to leave the central area, which releases the tangential traction all around but save the critical ILM over the foveola and fovea. Be aware that the "nonpeeling" denoting the flat margin after ILM surgery without curly or wrinkled margin. This is important because the wrinkled margin causes surface wrinkling and hinders visual function improvement.

Infracyanine green (IFCG) is very chemically and pharmacologically similar to indocyanine green. It is another green anionic cyanine dye like ICG. It primarily stains the ILM. The good part is that it does not contain sodium iodide unlike ICG (ICG contains 4–5% iodine in part as a byproduct of its synthesis and in part due to the presence of an iodine moiety on the molecule). Thus, it has the advantage of not requiring initial dilution in distilled water to avoid precipitation. It also avoids exposure of the retina to toxic iodide. More study is still needed to determine its toxicity.
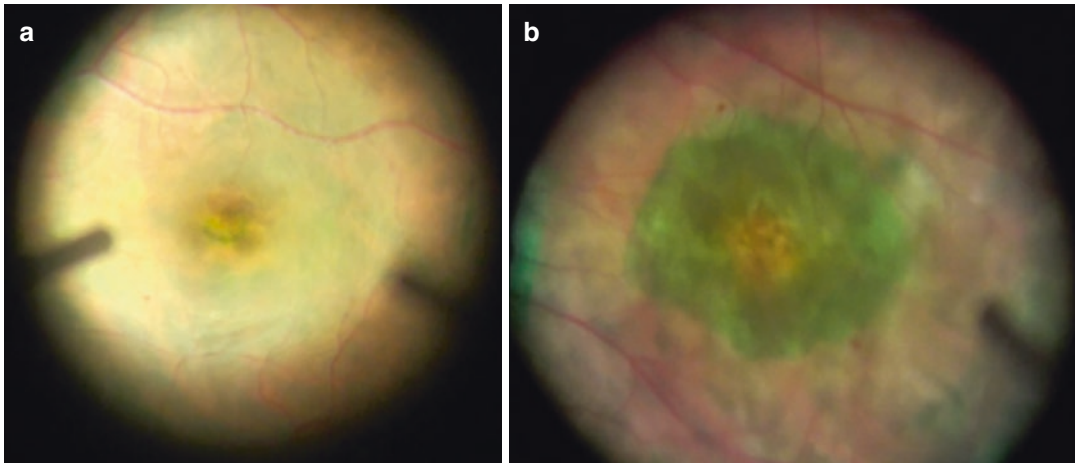
Fig. 10.1 Figure shows the foveola nonpeeling (**a**) and fovea nonpeeling (**b**) ILM surgery of myopic traction maculopathy. The ILM is peeled around the foveola or fovea to leave the central area, which releases the tangential traction all around but save the critical ILM over the foveola and fovea. The visual improvement is satisfactory to 0.8 and 1.0, respectively in **a** and **b**. The reason may be the intact neurosensory retina surface before dye staining. ICG was used and showed minimal toxicity in myopic traction maculopathy eyes

10.6.7 Sodium Fluorescein

Sodium fluorescein is a yellow fluorescent xanthene dye that has many ophthalmic applications including acting as a stain for the vitreous. Sodium fluorescein is highly hydrophilic and is well absorbed by the vitreous due to its high water content. Its benefits include its low toxicity and low cost. However, fluorescein is generally inferior to triamcinolone acetonide in its ability to highlight vitreous tissue and thus, is less commonly used [37].

FDA currently approved fluorescein for topical and intravenous use only and it is available in many commercial formulations. However intraocular use is off-label.

10.6.8 Toxicity and Complications

As with the injection of any intraocular substance, toxicity is a major concern. Toxicity may result from the pharmacologic effects of the dyes themselves or they may result from the vehicles and suspensions that dyes are delivered in. These vehicles can alter the osmolarity, pH, and ionic composition in the vitreous space to nonphysiologic levels that can induce toxic effects on the retina. Both hyperosmotic and hypo-osmotic solutions can induce toxicity when injected into the vitreous space. Hyperosmotic solutions have been shown to alter the cellular architecture of the retina and induce shrinkage of retinal layers. Animal studies in which eyes are injected with hyperosmotic solution leads to increased rates of retinal detachments and edema of the RPE. Hypo-osmotic solutions can be toxic to the retina as well. The mechanism is not completely understood but may be related to an influx of intracellular calcium and upregulation of enzymatic activity within RPE cells. Some of the toxicity attributed to ICG may be due to cases of injecting with a hypo-osmolar solution. Care should be taken to ensure that only iso-osmolar and pH-balanced dye solutions are injected intraocularly.

In addition to altering osmolarity and pH, vehicles for dyes can contain preservatives and additives that have their own deleterious effects. A frequently used commercial preparation of methylprednisolone acetate, Depo-Medrol (Pfizer), contains the preservative myristyl-γ-picolinium chloride. This preservative has been shown to be highly toxic to the retina. Animal studies in which eyes have been injected with myristyl-γ-picolinium chloride have shown a permanently decreased ERG response even

after many months [38]. Depo-Medrol only has FDA approval for periocular use as an anti-inflammatory agent, but does not have approval for intraocular use. Multiple case reports exist in which Depo-Medrol was unintentionally injected intraocularly or intentionally injected to stain vitreous by those unaware of its effects [39]. Retinal necrosis and various toxic sequelae were seen as a result of these instances. Given the toxic nature of myristyl-γ-picolinium chloride, Depo-Medrol and other formulations containing similar preservatives should never be used for intraocular staining.

Benzyl alcohol is another common preservative that is found in certain formulations of triamcinolone acetonide, including Kenalog. The data on the toxicity of benzyl alcohol at concentrations found in commercial formulations are still unclear. In animal studies comparing the effects of injecting triamcinolone acetonide formulations with benzyl alcohol (Kenalog) versus those without, severe retinal damage and histological disorganization of retinal layers were seen in the rabbit eyes injected with Kenalog. However, other animal studies have shown no observable toxic effects [40]. A small prospective study on human eyes did not find measurable signs of visual deterioration when Kenalog was injected intravitreally [37]. Until further data are obtained, it may be safer to use preservative-free formulations that are FDA-approved for intraocular use such as Triessence instead of those that contain preservative. Table summarized the characteristics of various staining dyes used in clinical practices (Adapted from Lu D, Brill D. EyeWiki Chromovitrectomy, American Academy of Ophthalmology 2019 [41] (Table 10.1).

Table 10.1 Characteristics of staining dyes used in vitreoretinal surgery

Dye	Suggested concentration	Stained tissue	Ocular toxicity
Triamcinolone acetonide	40 mg/mL (4%)	Vitreous and ILM	1. Increased risk of cataracts and glaucoma 2. Benzyl alcohol preservative in certain formulations can be toxic to retina
Trypan blue	1.5 mg/mL (0.15%)	High affinity for ERM. Low affinity for ILM	1. Relatively safe for intraocular use 2. Mild toxicity in some animal studies
Brilliant blue	0.25 mg/mL (0.025%)	ILM	1. Relatively safe for intraocular use 2. Mild RPE toxicity in animal studies when injected subretinally
Bromophenol blue	1.3 mg/mL (0.13%)	ILM and ERM	1. Relatively safe for intraocular use
Patent blue	2.4 mg/mL (0.24%)	Moderate affinity for ERM. Low affinity for ILM	1. Relatively safe for intraocular use 2. Similar toxicity to trypan blue
Indocyanine green	Dilute to <0.5 mg/mL	ILM	1. Potentially toxic at concentrations used in surgery 2. RPE changes and visual field defects have been noted in some studies
Infracyanine green	Dilute to <0.5 mg/mL	ILM	1. Potentially toxic at concentrations used in surgery 2. Potentially less toxic than ICG 3. RPE changes and visual field defects have been noted in some studies
Sodium fluorescein	Variable	Vitreous	1. Relatively safe for intraocular use

10.7 Summary and Future Considerations

In conclusion, for vitreoretinal surgery, vital dyes enable easier identification of the semitransparent preretinal membranes. Current recommendations for the application of dyes during vitreoretinal surgery indicate that indocyanine green, infracyanine green, brilliant blue, and bromophenol blue may be the best stains for the internal limiting membrane (ILM), while trypan blue may be preferred for staining the glial tissues like epiretinal membrane [42].

In regard to the toxicity issues in chromovitrectomy, a large number of experimental and clinical investigations in this challenging field with vital dyes have yielded some controversial results,but preliminary conclusions may be drawn at this time. Indocyanine green has been proven to be toxic to the retina, and brilliant blue showed a better safety profile and could protect against apoptosis, at least in vitro. Each vital dye injected intravitreally poses a rather dose-dependent toxicity to the retinal tissue. Furthermore, there is solid proof that light exposure, osmolarity, and existence of ions, for example, Na + and iodine, may apply further harm to the retina. Along these lines, general proposals for all vital dyes incorporate injection of a very low amount onto the retina, staying away from long macular exposure to endoillumination and expulsion of sodium and iodine from dye solutions. However, the role of vital dyes in effective vitreoretinal surgeries cannot be replaced by other maneuvers at this point. Our experience in foveola or fovea nonpeeling ILM surgery showed that if the neurosensory retina is intact before dye staining, the dye toxicity, even in the case of indocyanine green, tends to be minimal.

References

1. Burk SE, Da Mata AP, Snyder ME, Rosa RH Jr, Foster RE. Indocyanine green-assisted peeling of the retinal internal limiting membrane. Ophthalmology. 2000;107(11):2010–4.
2. Kadonosono K, Itoh N, Uchio E, Nakamura S, Ohno S. Staining of the internal limiting membrane in macular hole surgery. Arch Ophthalmol. 2000;118(8):1116–8.
3. Rodrigues EB, Meyer CH, Kroll P. Chromovitrectomy: a new field in vitreoretinal surgery. Graefes Arch Clin Exp Ophthalmol. 2005;243:291–3.
4. Rodrigues EB, Maia M, Meyer CH, et al. Vital dyes for chromovitrectomy. Curr Opin Ophthalmol. 2007;18:179–87.
5. IUPAC Gold Book Chromophore.
6. Chapter "Detection of caspase activation combined with other probes of apoptosis", Eurekah Bioscience Collection, NCBI bookshelf.
7. Li K, Wong D, Hiscott P, Stanga P, Groenewald C, McGalliard J. Trypan blue staining of internal limiting membrane and epiretinal membrane during vitrectomy: visual results and histopathological findings. Br J Ophthalmol. 2003;87(2):216–9.
8. Jackson TL, Hillenkamp J, Knight BC, et al. Safety testing of indocyanine green and trypan blue using retinal pigment epithelium and glial cell cultures. Invest Ophthalmol Vis Sci. 2004;45(8):2778–85.
9. Ullern M, Roman S, Dhalluin JF, et al. Contribution of intravitreal infracyanine green to macular hole and epimacular membrane surgery: preliminary study. J Fr Ophthalmol. 2002;25(9):915–20.
10. Enaida H, Hisatomi T, Goto Y, et al. Preclinical investigation of internal limiting membrane staining and peeling using intravitreal brilliant blue G. Retina. 2006;26(6):623–30.
11. Haritoglou C, Tadayoni R, May CA, et al. Short-term in vivo evaluation of novel vital dyes for intraocular surgery. Retina. 2006;26(6):673–8.
12. Al-Halafi AM. Chromovitrectomy: update. Saudi J Ophthalmol. 2013;27:271–6.
13. Narayanan R, Mungcal JK, Kenney MC, Seigel GM, Kuppermann BD. Toxicity of triamcinolone acetonide on retinal neurosensory and pigment epithelial cells. Invest Ophthalmol Vis Sci. 2006;47(2):722–8.
14. Costa Ede P, Rodrigues EB, Farah ME, Dib E, Penha F, Magalhães O Jr, et al. Vital dyes and light sources for chromovitrectomy: comparative assessment of osmolarity, pH, and spectrophotometry. Invest Ophthalmol Vis Sci. 2009;50(1):385–91.
15. Gorgels TG, van Norren D. Ultraviolet and green light cause different types of damage in rat retina. Invest Ophthalmol Vis Sci. 1995;36:851–63.
16. Yanagi Y, Inoue Y, Jang WD, Kadonosono K. A2e mediated phototoxic effects of endoilluminators. Br J Ophthalmol. 2006;90:229–32.
17. Kunikata H, Abe T, Nakazawa T. Heads-up macular surgery with a 27-gauge microincision vitrectomy system and minimal illumination. Case Rep Ophthalmol. 2016;7(3):265–9.
18. Yu SY, Damico FM, Viola F, D'Amico DJ, Young LH. Retinal toxicity of intravitreal triamcinolone acetonide: a morphological study. Retina. 2006;26(5):531–6.
19. Rodrigues EB, Meyer CH, Mennel S, Farah ME. Protecting the retinal pigment epithelium during macular hole surgery. Retina. 2007;27(7):958–70.

20. Chuang LH, Wang NK, Yeung L, Chen YP, Hwang YS, Wu WC, et al. Use of autologous whole blood during internal limiting membrane peeling and macular hole surgery is protective for indocyanine green toxicity. Cutan Ocul Toxicol. 2010;29(2):98–104.

21. Meyer CH, Rodrigues EB. A novel applicator for the selective painting of the pre-retinal structure during vitreoretinal surgery. Graefes Arch Clin Exp Ophthalmol. 2005;243:487–9.

22. Sorcinelli R. Surgical management of epiretinal membrane with indocyanine-green-assisted peeling. Ophthalmologica. 2003;217:107–10.

23. Czajka MP, McCuen BW, Cummings TJ, et al. Effects of indocyanine green on the retina and retinal pigment epithelium in a porcine model of retinal hole. Retina. 2004;24:275–82.

24. Beer PM, Bakri SJ, Singh RJ, Liu W, Peters GB 3rd, Miller M. Intraocular concentration and pharmacokinetics of triamcinolone acetonide after a single intravitreal injection. Ophthalmology. 2003;110(4):681–6.

25. Lee KL, Dean S, Guest S. A comparison of outcomes after indocyanine green and trypan blue assisted internal limiting membrane peeling during macular hole surgery. Br J Ophthalmol. 2005;89(4):420–4.

26. Stalmans P, Van Aken EH, Melles G, et al. Trypan blue not toxic for retinal pigment epithelium in vitro. Am J Ophthalmol. 2003;135(2):234–6.

27. Kwok AK, Yeung CK, Lai TY, et al. Effects of trypan blue on cell viability and gene expression in human retinal pigment epithelial cells. Br J Ophthalmol. 2004;88(12):1590–4.

28. Malerbi F, Maia M, Farah ME, et al. Subretinal Brilliant blue migration during epiretinal membrane peeling. BJO. 2009; Forthcoming

29. Balaiya S, et al. Comparative in vitro safety analysis of dyes for chromovitrectomy. Retina. 2011;31(6):1128–36. https://doi.org/10.1097/iae.0b013e3181fe543a.

30. Mennel S, Meyer CH, Tietjen A, et al. Patent blue: a novel vital dye in vitreoretinal surgery. Ophthalmologica. 2006;220(3):190–3.

31. Maia M, Penha F, Rodrigues EB, et al. Effects of subretinal injection of patent blue and Trypan blue in rabbits. Curr Eye Res. 2007;32(4):309–17.

32. Lüke C, et al. Effects of patent blue on human retinal function. Graefes Arch Clin Exp Ophthalmol. 2006;244(9):1188–90. https://doi.org/10.1007/s00417-005-0239-5.

33. Da Mata AP, Burk SE, Foster RE, et al. Long-term follow-up of indocyanine greenassisted peeling of the retinal internal limiting membrane during vitrectomy surgery for idiopathic macular hole repair. Ophthalmology. 2004;111(12):2246–53.

34. Maia M, Margalit E, Lakhanpal R, et al. Effects of intravitreal indocyanine green injection in rabbits. Retina. 2004;24(1):69–79.

35. Ullern M, Roman S, Dhalluin JF, et al. Contribution of intravitreal infracyanine green to macular hole and epimacular membrane surgery: preliminary study. J Fr Ophtalmol. 2002;25(9):915–20.

36. Ho TC, Yang CM, Huang JS, et al. Long-term outcome of foveolar internal limiting membrane nonpeeling for myopic traction maculopathy. Retina. 2014;34(9):1833–40. https://doi.org/10.1097/IAE.0000000000000149.

37. Negi A, Marmor MF. Experimental serous retinal detachment and focal pigment epithelial damage. Arch Ophthalmol. 1984;102:445–9.

38. Brill DA, et al. Methylprednisolone acetate (Depo-Medrol) injection during cataract surgery causing retinal necrosis. Ophthalmology. 2019;126(9):1332–3. https://doi.org/10.1016/j.ophtha.2019.03.034.

39. Yonekawa Y, et al. Retinal necrosis secondary to inadvertent intravitreal methylprednisolone acetate (Depo-Medrol) injection during Pars plana vitrectomy. Retinal Cases Brief Rep. 2009;3(4):336–9. https://doi.org/10.1097/icb.0b013e318173778d.

40. Dierks D, Lei B, Zhang K, et al. Electroretinographic effects of an intravitreal injection of triamcinolone in rabbit retina. Arch Ophthalmol. 2005;

41. Lu D, Brill D. EyeWiki chromovitrectomy, American Academy of Ophthalmology 2019.

42. Komur B. Book chapter: Advances in vitreoretinal surgery. 2019 edition Frontier in Ophthalmology and Ocular Imaging.

Viewing Systems in Vitreoretinal Surgery

11

Yuki Nakano and Kiyoshi Suzuma

11.1 Introduction

It is difficult to view the posterior segment of the eye, which contains the vitreous body and the retina, without some type of specialized device. This is because the cornea has a refractive power of +40D and the crystalline lens has a refractive power of +20D. Thus, when using only a microscope, the focal range is restricted to the region of the ora serrata.

To address these limitations, the inclusion of a corrective lens that neutralizes the cornea's refractive power is required in order to view the retina. In fact, examinations are typically done using a slit lamp, and examination of the vitreous body and retina is achieved by using contact and noncontact front lenses. There are mainly three types of enhancements that are applied when using a surgical microscope: (1) a contact front lens, (2) a contact wide-field (CWF) lens, and (3) a noncontact wide-angle lens. Each of these methods has unique characteristics. Method 1 is the oldest followed by 2, and 3 is the most recent method developed. Recently, noncontact CWF has become the most commonly used technique. When considering the techniques described above, it is relevant that the introduction costs increase from method 1 to 3, but the level of sur-

gical difficulty is reduced allowing the surgery to be performed more safely and within a shorter period of time. What follows is a discussion of the current trends associated with these three techniques.

11.1.1 Naked Eye (Gross Examination) and Microscope Only

It is possible to view the ora serrata even without a front lens. Confirmation of whether or not the tip of an infusion cannula has entered the vitreous body is easily done using the naked eye. It can be clearly viewed by turning off the microscope light and aiming a light guide diagonally from the opposite side. Even under microscopic view, the depression made in the sclera when the infusion cannula is pressed into it can be detected. Vitrectomy of the vitreous base can also be performed under direct observation. One hand holds the scleral depressor and applies firm pressure against the sclera while the other hand resects the vitreous body using a vitreous cutter. However, although the retina can be viewed under the microscope light, the vitreous body cannot. Thus, the microscope light is turned off and the use of slit illumination instead allows the vitreous body to be clearly observed (Fig. 11.1). Recently, it has been reported that favorable outcomes have been obtained when retinal peeling is performed, even

Y. Nakano (✉) · K. Suzuma
Faculty of Medicine, Department of Ophthalmology, Kagawa University, Kagawa, Japan
e-mail: nakano-y@med.kagawa-u.ac.jp
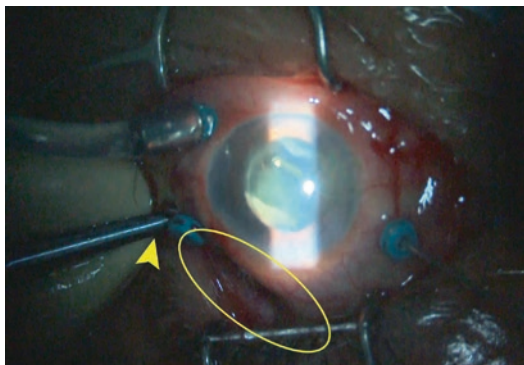
Fig. 11.1 Peripheral vitrectomy under direct view provided by slit illumination

without the use of scleral depression [1]. Thus, this portion of the procedure is no longer essential.

The inward bulge of the retina created by pressing against the sclera (oval) with a scleral depressor (arrowhead) can be viewed through the pupil.

With the microscopic illumination turned off and the slit light aimed at an angle of approximately 15° off perpendicular, so as to provide illumination from the opposite side (diagonally from the right), both the vitreous body and the retina are illuminated. Although the vitreous body cannot be seen when illuminated with diffuse light from the microscope, using slit light allows the vitreous body to be clearly viewed. Since this process is done under direct view, the vitreous base is not visible unless the sclera is depressed a considerable amount.

11.1.2 Direct Contact Lens

The contact surface of glass in direct contact lenses is designed to adhere perfectly to the corneal curvature. The characteristics of the lens are determined by the lens curve on the microscope side. There are three types: (1) the flat lens for normal use, (2) a magnifying lens with a convex surface, and (3) a wide-angle lens with a concave surface. These lenses are combined with a prism (e.g., no angle, 20°, 30°, or 45°). Although the lenses themselves are small and lightweight,

they are unstable when used alone so it is necessary to fix them to the cornea by using a lens mount (Fig. 11.2). The advantage of this approach is that the resolution is high and the cost is low. The only necessary instruments are the lens and the lens mount; therefore, the investment in an anterior segment surgical microscope can be kept to a minimum. The drawbacks are that the narrow field of vision must be covered by rotating the lens by using a prism. This limitation requires a high degree of expertise in order to perform surgery safely and swiftly, and, since a direct image is being viewed, if the pupil diameter is small then the field of view is even further restricted. The approaches described above are similar to those used in retinal photocoagulation, i.e., the three-mirror lens and the wide-angle indirect lens used with a slit lamp. These methods were commonly applied previously in the early stages of vitrectomy surgery, but today, since the application of micro-incision vitrectomy surgery (MIVS) has become widespread, the use of posterior pole view alone (which boasts a high degree of resolution), is typically applied, and as a result, the direct contact lens is less frequently needed. However, it is sometimes used in combination with a CWF lens system as discussed below.

When the microscope light is turned off, a direct view—as can be seen in the upper left—is obtained. The lens is fixed by either suturing the lens mount to the sclera or by using a non-suture eyelid speculum lens attachment that utilizes a silicon band, simplifying the procedure. This is shown in the upper right illustration.
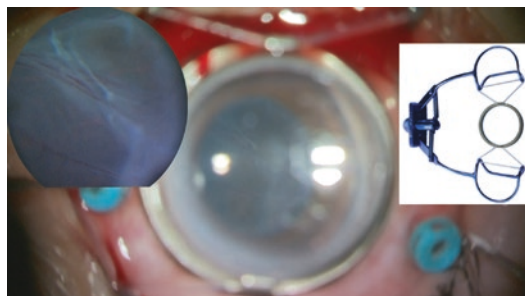
Fig. 11.2 Direct contact lens: posterior polar view of a HOYA HHV 20° prism meniscus lens in use

11.1.3 CWF Lens System

This is a technique in which a direct-contact inverted image lens of the type commonly employed in a slit lamp is used instead of the above-mentioned direct contact lens. A lens that is smaller than the type used in a slit lamp has been specifically developed for use in vitrectomy surgery and is currently on the market. However, depending on the specific type of lens it may be necessary for an assistant to hold it since it is difficult to perform the procedure alone with the use of a single lens (Fig. 11.3). Moreover, the assistant who holds the lens must have high expertise in this type of manipulation. In addition to the lens and lens mount, a prism inverter that converts the inverted image into a real image is required, and this presents an additional financial burden associated with the surgical technique. Since the X and Y axes of the microscope are inverted, some degree of familiarity with the technique is required. The merits include a large field of view and high resolution. The drawback is that it is difficult to tilt the eye. Tilting the eye also simultaneously tilts the lens, which in turn narrows the field of vision. Thus, surgery must be performed without tilting the eye. However, in fact, the eye can be moved slightly to dynamically shift the field of view. To do this, the surgeon tilts the eye while the assistant simultaneously tilts the lens in the opposite direction, allowing the narrowed field of view to return to normal. Clearly, this maneuver requires expert assistance because if excess force
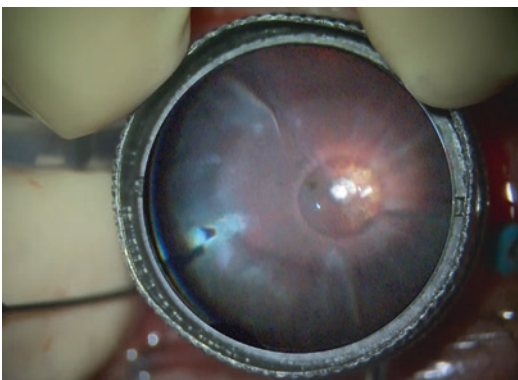
Fig. 11.3 Wide-angle field of view obtained using a CWF (MiniQuad manufactured by Volk)

is applied to the cornea, it can be adversely affected. An advantage of this technique is that it requires only a small initial investment and therefore is a good option for vitrectomy surgeries done in clinical facilities.

The CWF lens is placed on the lens mount and the assistant supports the lens (in the photo above, the assistant is using two fingers). When the microscope light is turned off, the field of view can be seen in the lens (The view shown in the lens above is the inset image of the same case and it is inverted). Since the surgical field is inverted, an inverter must be used to convert the image to the actual image.

11.1.4 Noncontact Wide-Angle Lens

The noncontact wide-angle lens is currently the most widely used viewing system for vitrectomy surgery. The basic principle is the same as the noncontact front lens of a slit lamp. The surgical microscope is fitted with a lens holder so that a floating lens can be utilized, removing the need to hold the lens. In many cases, a foot switch is used to adjust factors such as the distance from the cornea (the working distance) and the focus, making this system more difficult to operate than others. The commercially available systems consist of four types: (1) the Topcon OFFISS, (2) the Ocular BIOM, (3) the Volk MERLIN, and (4) the Zeiss Resight (Fig. 11.4). The OFFISS and the Resight have microscopes that were specifically designed by each manufacturer. The BIOM and MERLIN systems utilize third-party microscope attachments providing the user with a larger number of microscope options.

A floating lens system is attached to the main body of the microscope. This can be stored out of the way when not in use. It has an in-board inverter that is used to right inverted images, and in many cases, the system is coupled when the lens is extended. The OFFISS system is the only one that does not have a reduction lens mechanism. The Resight system is designed to allow two types of lenses to be attached. A rotating barrel allows switching between the lenses to be performed swiftly and easily.

Fig. 11.4 Non-contact wide-angle viewing systems

The front lens mainly consists of a peripheral view lens (120–130D) and a posterior polar view lens (40–60D). Some systems also have an equatorial view lens (80–90D) allowing different lenses to be used for different purposes. The peripheral view lens increases the working distance, which in turn narrows the field of view. By increasing the magnification power of the microscope, it can be utilized as a posterior pole view lens as well, but as a result, some resolution is lost.

The author has no experience using the MERLIN system; however, his impressions of the remaining three systems are as follows: The OFFISS system provides the largest field of view when using the peripheral view lens, and when the conditions are optimal, even the ora serrata can be viewed. The other systems have a slightly narrower field of view when using this lens, and as a result, it is difficult to view the ora serrata without the simultaneous use of scleral depression. However, the lens aperture plays a major role in determining the size of the field of view, and consequently, the instruments and palpebral fissure are liable to interfere with the lens, which in turn has a negative effect on operability. The OFFISS system has slightly poorer operability due to this phenomenon. Thus, when using this system on a case with poor viewing conditions,

application of a smaller lens may compensate for the difficulties in operability. The Resight and BIOM systems have smaller lenses and therefore have good operability.

There is no difference among the manufacturers in terms of the posterior polar view, but the early Resight reduction lens model had lens aberration, which had a negative effect on the view. The current model is the improved Version 2 which provides a clear view.

The noncontact, wide-angle lens system allows changes to be dynamically made in the field of view and resolution in accordance with all types of surgical environments. Important elements are: (1) the working distance (the distance between the posterior surface of the lens and the anterior surface of the cornea), (2) the tilt of the eyeball, (3) the condition of the cornea, and (4) the position of the IOL. Once a surgeon masters changing these factors, his or her surgical technique will improve.

The working distance is the most important factor related to field of view. Beginners find it difficult to maintain the proper distance using the foot switch. If the distance increases, the field of view narrows and the magnification decreases. By approaching very slowly, the proper distance can be obtained, and that is the point where the field of view and the magnification are at maxi-

mum. If one then moves closer, the magnification does not change but the peripheral view begins to distort, until finally, the lens contacts the cornea. It is important to remain fixed at the location where the magnification is at maximum.

The field of view can be dynamically shifted by tilting the eyeball in the direction the surgeon wants to view. Doing this shifts the corneal center which in turn vignettes the field of view. Thus, in order to restore the vignette view to a normal view, it is necessary to shift the *X*- and *Y*-axes of the microscope so as to tilt the device in the direction of the eyeball tilt. The *Z*-axis also shifts slightly, and so a shift in the retinal direction may also be necessary. This operation is the first step in smoothly controlling the field of view that the surgeon wants to obtain and it is difficult for inexperienced surgeons.

The cornea dries out when exposed to the air. Thus, it is necessary to frequently apply physiological saline or provide a coating using an ophthalmic viscosurgical device in order to protect the cornea. Problems with these methods include that the former requires frequent applications and that when using the latter it is difficult to apply the coating evenly since an uneven coating causes astigmatism. One solution is the application of a contact lens on the cornea. The use of a hard contact lens resolves the problem of corneal astigmatism in addition to providing protection to the cornea. It is therefore useful during posterior pole enlargement, which requires a particularly high degree of resolution.

The use of a lens with a prism that is placed directly onto the cornea allows the prism to shift the field of view, which in turn increases the field of view. It is advantageous to keep this in mind since it allows one to obtain a peripheral view in difficult cases such as when it is impossible to perform scleral indentation.

The pupil diameter and IOL affect the field of view. In general, the larger the pupil diameter, the larger the field of view, but this is only slightly advantageous during peripheral viewing. Nevertheless, since an IOL is closer to the vitreous body side than the pupil, it is vulnerable to the pupil effect, and the field of view can also be narrowed by the optical edge of the IOL or ante-

rior capsule contraction. In order to prevent this, the anterior chamber depth should be shallow and the IOL should be shifted toward the cornea. When simultaneously performing cataract surgery, a small amount of aqueous humor should be removed. Also, if the pupil diameter is small, misalignment of the corneal center and the horizontal center of the objective lens of the microscope will cause vignetting of the field of view which flattens the image and makes it difficult to obtain a 3D view. This is particularly marked when using a posterior-pole magnifying lens.

The unique drawbacks of the noncontact, wide-angle viewing system are lens clouding and contact between the lens and instruments. The OFFISS and BIOM systems have a metal ring around the edge of the lens, so condensation frequently occurs. This can be prevented by applying anti-clouding agent to the lens or using suction in the surgical field [2, 3]. Since air exhaled by the patient can enter the surgical field and become a cause of condensation, it is important to apply draping on the nose side of the surgical field. This is not much of a problem when using the Resight system since the edge of its lens is plastic. Lens contact is a problem because an instrument that strikes the lens when it is lifted or pointed upwards can shift the position of the lens. Several methods can be used to avoid this: (1) the lens can be positioned further away from the cornea but lost the field of view, (2) the use of round-type forceps can be avoided, and (3) the use of a trocar on the opposite side can be attempted.

11.2 Intraoperative Real-Time OCT

OCT imaging of the surgical field in real time can be performed through the intraoperative use of an external monitor or the half mirror of a microscope contact lens.

Currently, two types of microscope adapters are commercially available: The Rescan 700 (Zeiss) that is based on the OPMI Lumela 700 and the EnFocus, which is an additional attachment for Leica microscopes. At this writing, the resolution of the latter is clearly better

Fig. 11.5 Intraoperative real-time OCT image of a microscope field of view
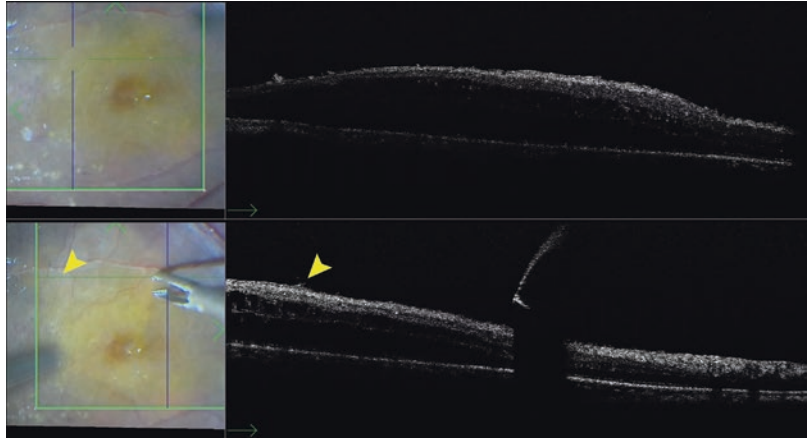
since the presence of an internal limiting membrane can be discerned after epiretinal membrane peeling when using this device (Fig. 11.5). The EnFocus allows the operator to obtain detailed data in the direction of the Z-axis, which is difficult to obtain when using a microscope field of view. This is useful when determining whether there is a retinal or macular hold or whether there is a preretinal membrane.

The devices in use are: Leica Proveo 8 + EnFocus + BIOM. A hard contact lens (HOYA HHV type Zd) was also used. The secondary macular epithelium is shown due to occlusion of retinal vein branch. Upper photo: Staining with brilliant blue G after epiretinal membrane peeling. The OCT image shows that a thin internal limiting membrane (ILM) remains. Lower photo: Same as shown in the upper photo. During ILM peeling, the ILM remains to the left of the arrowhead and the right of the shadow in the center. The shadow in the center of the photo is an acoustic shadow caused by the forceps.

11.3 Heads Up

Instead of viewing through the contact lens of a microscope, polarizing mirror eyeglasses can be worn and a 3D monitor can be used to ensure a three-dimensional view during surgery. For ophthalmologists, currently the Alcon NGENUITY is commercially available, and a large number of facilities have adopted this device. The contact lens of a conventional microscope is removed and this system is attached in its place. The image quality is 4 K (approximately 4000 × 2000 pixels), but there is a slight time lag. This is a new field, but in addition to Alcon, the Leica TrueVision 3D and other similar devices are also available. Their merits are: (1) surgery is possible even with small amounts of light, which is more comfortable for the patient and reduces photoretinal damage during surgery; (2) since the assistant is provided with an image that is of the same resolution as that provided to the surgeon, it is beneficial for surgical education; (3) image processing allows the contrast and color tone to be adjusted. The use of the high dynamic range (HDR) function allows dark fields of view to be brightened even when there is a marked difference between light and dark areas. Also, ILM peeling, which is dependent upon very fine differences in color tone, is made easier; (4) the three-dimensional view can be controlled, which is useful particularly when macular magnification is used; and (5) Chronic muscle fatigue that occurs when a specific body position is maintained—and particularly cervical spondylosis—can be avoided. Currently, these technologies are still under development and proficiency on new devices is required [4]. However, as these technologies are further developed, they may become standard in the future.

References

1. Tabandeh H, London NJS, Boyer DS, Flynn HW. Outcomes of small-gauge vitreoretinal surgery without scleral-depressed shaving of the vitreous base in the era of wide-angle viewing systems. Br J Ophthalmol. 2019;103(12):1765–8. https://doi.org/10.1136/bjophthalmol-2018-313626.

2. Uwaydat SH, Sims KW. Use of a urinary catheter to prevent fogging of the BIOM lens during vitrectomy. Can J Ophthalmol. 2016;51:e64–5.

3. Maeno T, Nagaoka T, Ubuka M, Hashimoto R, Masahara H. Antifogging device to prevent moisture condensation during vitrectomy with noncontact widefield viewing system. Retina. 2018;38:643–5.

4. Talcott KE, et al. Comparison of a three-dimensional heads-up display surgical platform with a standard operating microscope for macular surgery. Ophthalmol Retin. 2019;3:244–51.

Intraoperative OCT in Macular Surgery

12

Keiko Kataoka and Hiroko Terasaki

12.1 Introduction

In clinical settings, optical coherence tomography (OCT) is an indispensable tool for the diagnosis of anterior and fundus abnormalities and decision making in the management of ophthalmic diseases. OCT imaging provides live analysis of cross-sectional ocular tissues of the anterior and posterior segments. A conventional OCT is commonly used for preoperative and postoperative macular assessments for the surgical treatment of macular diseases, such as a macular hole or an epiretinal membrane (ERM); it is not used intraoperatively because of its large size and difficulty maintaining sterility in surgical fields. Intraoperative OCT (iOCT) resolves these concerns. To date, three types of iOCT have been developed: portable iOCT, which includes a handheld and microscope-mounted OCT [1–3], fiber-optic OCT probe [4, 5], and microscope-integrated iOCT (MIOCT). The fiber-optic OCT probe is limited to development stage in the field of ophthalmology [5]. This chapter introduces the current clinical usage of the MIOCT for the treatment of macular diseases in clinical cases.

12.1.1 Microscope-Integrated OCT

The microscope-integrated OCT (MIOCT) is now commercially available from Zeiss (Carl Zeiss Medic, Oberkochen, Germany), Leica (Leica Microsystems, Wetzlar, Germany), and Haag-Streit (Haag-Streit AG, Koeniz, Switzerland). The development of these three products was based on spectral-domain OCT. The specificity of MIOCT varies among different products and rapidly improves each year. The MIOCT introduced in this chapter has 840 nm wavelength, 5.5 μm axial resolution, and 27,000 A-scans (RESCAN 700, Carl Zeiss Medic). MIOCT uses the common optical pathway of a microscope. Thus, the surgeon can visualize the surgical field and real-time high-resolution OCT images simultaneously through the surgeon's microscope eyepieces. The current system does not facilitate mounting the iOCT images on an assistant surgeon's microscope eyepieces. However, MIOCT is compatible with 3-D heads-up surgery. The view of the surgical field and real-time OCT images can be recorded and shared with other surgical members through large monitors.

12.1.2 Procedures

RESCAN 700 MIOCT can be controlled by the surgeon with a foot pedal or by an operator with an external touch panel monitor (Fig. 12.1). The

K. Kataoka · H. Terasaki (✉)
Nagoya University Graduate School of Medicine,
Nagoya, Japan
e-mail: terasaki@med.nagoya-u.ac.jp
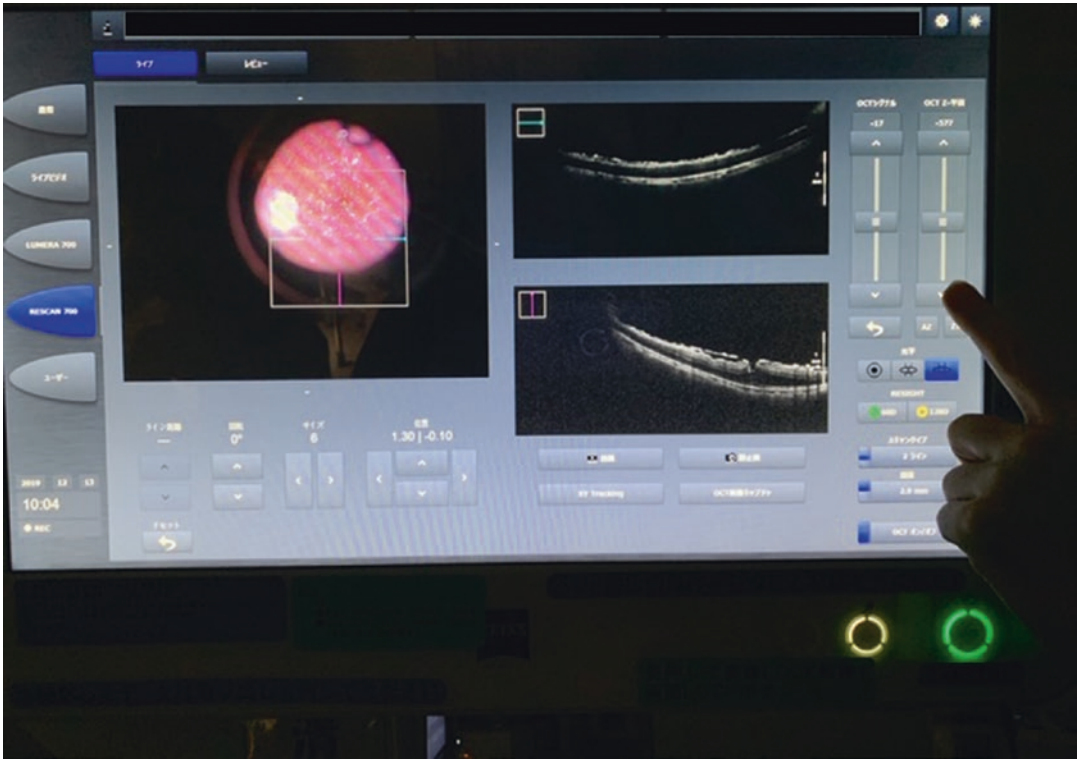
Fig. 12.1 The external display of microscope-integrated OCT controlled by a surgical assistant. The assistant changed the mode from anterior segment mode to poste-rior segment mode, switched the scanning line types, and adjusted the focus of the *Z*-axis

three modes are anterior segment mode, posterior segment mode with inverted images, and that with non-inverted images. RESCAN 700 can be used with a wide-angle viewing system (RESIGHT, Carl Zeiss Medic); thus, the power of the fixed lens (60 D or 128 D) can be chosen. The scan types of OCT contain one line, two cross-lines, or five lines; scan length ranges from 3 to 16 mm, which can be switched according to the surgeon's preference (Fig. 12.2). There is a line break in the middle of the lines to avoid cutting off a view of the surgical field. In addition, the A-scan depth can be chosen as 2.9 mm or 5.8 mm. For macular surgeries, 2.9 mm A-scan depth is generally used to assess the retina, while the 5.8 mm depth is used for anterior segment assessment. To obtain good OCT images, it is important to adjust the *Z*-axis in addition to the *X*–*Y* axis. The latest model has a *Z*-axis autofocus function and a *Z*-tracking function, which supports the *Z*-axis adjustment. Although iOCT images are beautifully mounted in the microscope eyepieces, the size of the view is relatively small for the assessment of small retinal structures, such as the presence of an inner limiting membrane (ILM) or a small macular hole. "Heads-up display," a new surgical viewing system, is now available to use together with iOCT (e.g., ARTEVO 800 from Carl Zeiss Medic). Therefore, the view of iOCT has become more surgeon-friendly during ocular surgeries [6]. While iOCT provides high-resolution OCT images (Fig. 12.3a), metallic surgical instruments cause light scattering and complete shadowing of
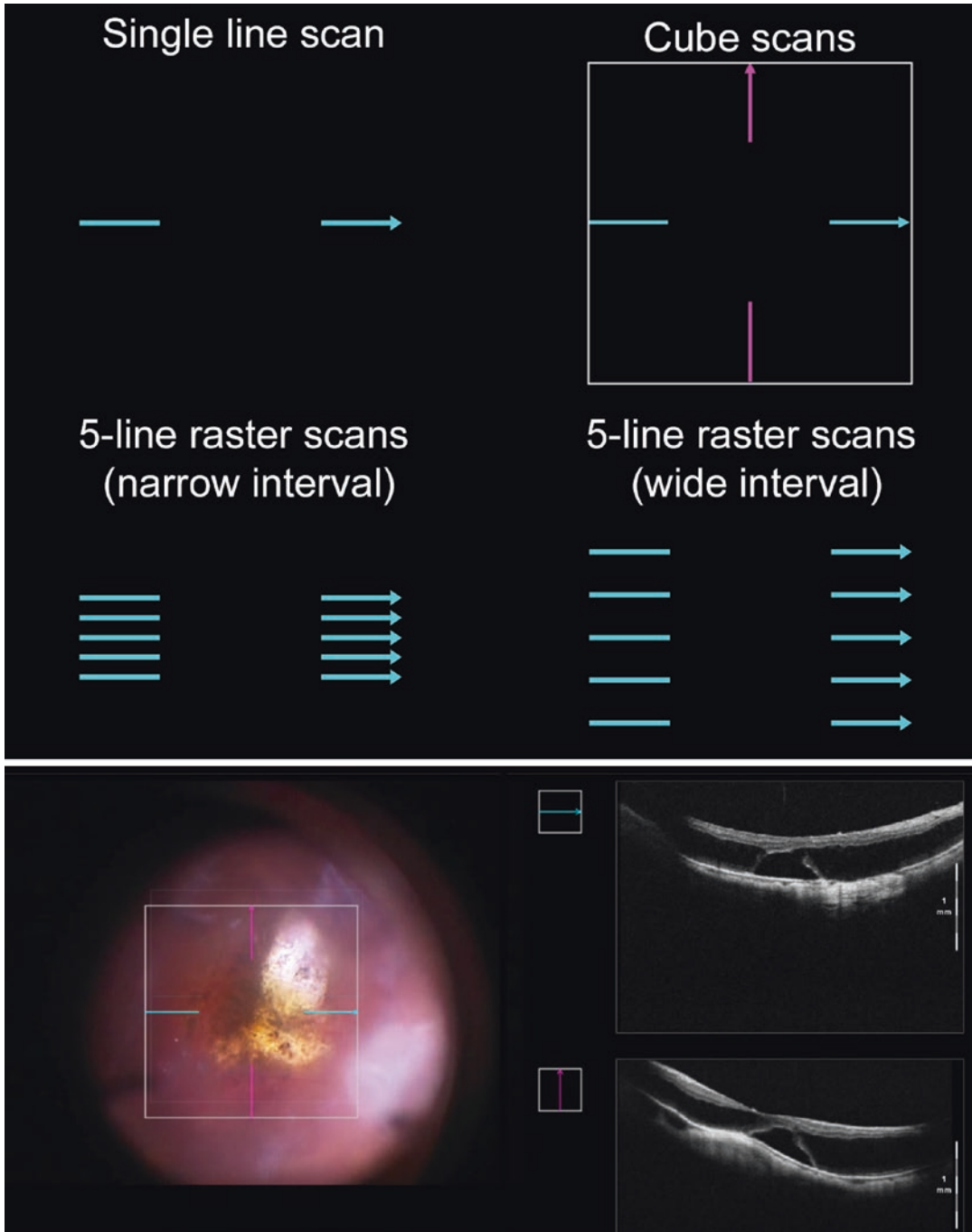
Fig. 12.2 Scanning mode types of microscope-integrated OCT. The upper row panel shows the scanning mode types in RESCAN 700 (Zeiss). Single line scans, cube scans (2 cross-lines), and 5-line raster scans can be chosen. In addition, the interval of 5-line raster scans can be changed. Note the line break in the middle of the lines to avoid cutting off a view of the surgical field. The middle panel shows a representative case of cube scans. The two cross-line scans show myopic retinoschisis with serous retinal detachment. The bottom panel shows 5-line raster scans. The OCT scan of the centerline was enlarged
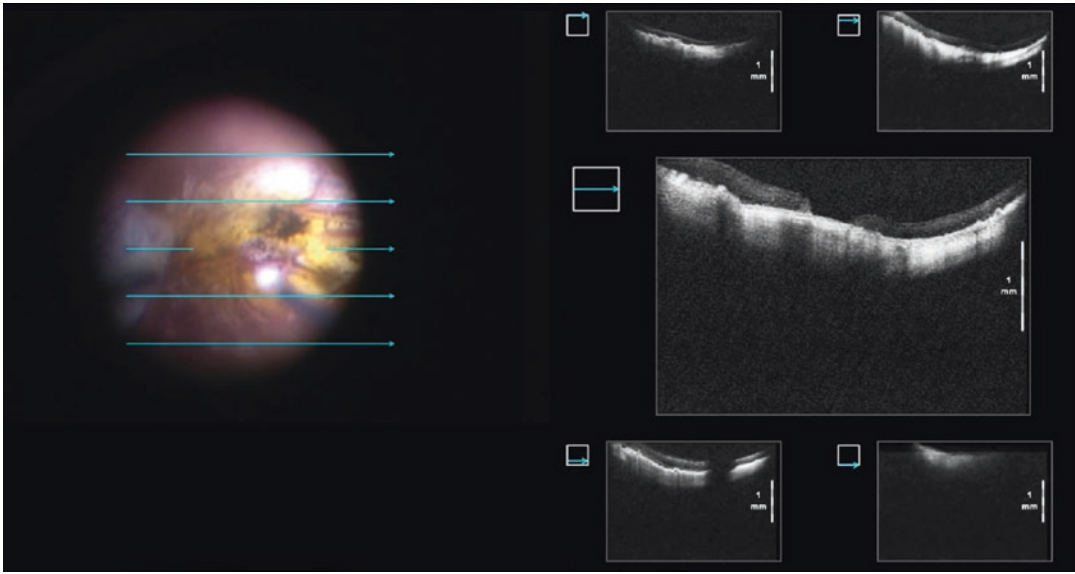
Fig. 12.2 (continued)
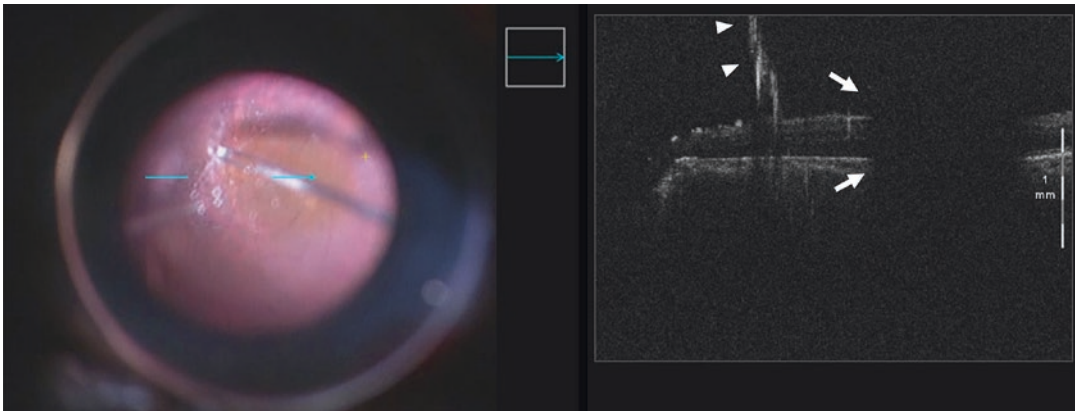
Fig. 12.3 Shadowing images from a metal surgical instrument. The microscope-integrated OCT captured the moment of posterior hyaloid membrane peeling with internal limiting membrane forceps (left side). The metal forceps completely blocked the OCT signal below the forceps (right side, arrows). The posterior hyaloid membrane was enhanced by triamcinolone acetonide particles (arrowheads)

the OCT images (Fig. 12.3b) [6, 7]. Surgical instruments made of semitransparent materials are now being developed for use with iOCT [6].

12.1.3　Indications for iOCT

iOCT is indicated in any vitreoretinal surgery; the criteria below comprise especially useful indications:

1. Assessment of the fovea during ERM/ILM peeling.

    Macular hole formation can occur unexpectedly during ERM/ILM peeling for eyes with ERM and vitreomacular traction, especially in highly myopic eyes. If iOCT reveals a macular hole formed during surgery, additional treatment can be performed, such as gas tamponade [8, 9]. Figure 12.4 shows a representative case of an eye with myopic macular schisis.
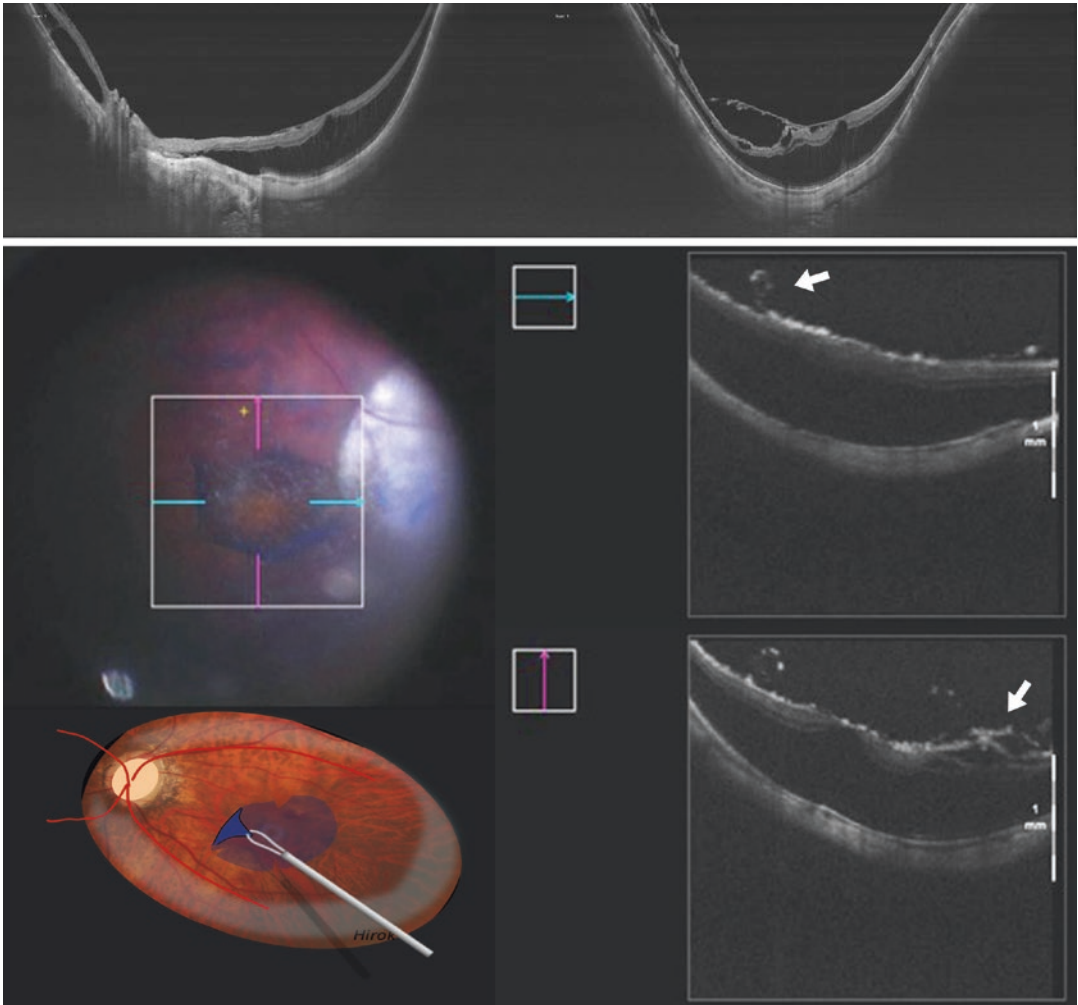
Fig. 12.4 A 55-year-old female presented with myopic macular schisis without macular hole or serous foveal detachment preoperatively (top panel). The lower panel shows the microscope-integrated OCT (MIOCT) images immediately after foveal sparing internal limiting membrane (ILM) peeling. The MIOCT images show that the ILM around the fovea remained (arrow), and no macular hole was formed during ILM peeling

The surgeon identified the residual ILM around the fovea and confirmed that neither a macular hole nor serous retinal detachment was formed immediately after fovea-sparing ILM peeling.

The Determination of Feasibility of Intraoperative Spectral-Domain Microscope Combined/Integrated OCT Visualization during En Face Retinal and Ophthalmic Surgery (DISCOVER) study was initiated in 2014 to assess the feasibility and usefulness of MIOCT. MIOCT found a residual membrane in 19.8% of the eyes, even though the surgeons thought the membranes were entirely peeled [10]. Furthermore, 40% of the eyes revealed complete membrane removal, although the surgeons thought that residual membrane remained. Thus, a detailed assessment with iOCT leads to precise surgical decision-making and prevents excess membrane peeling. Recently, the

inverted flap technique has been performed with ERM/ILM peeling for macular hole repair. It is important to confirm that the residual inverted membrane covers, or is inserted in, the macular hole. In such situations, iOCT is useful to identify the location of the ILM flap [11, 12]. Figures 12.5 and 12.6 illustrate a representative case of
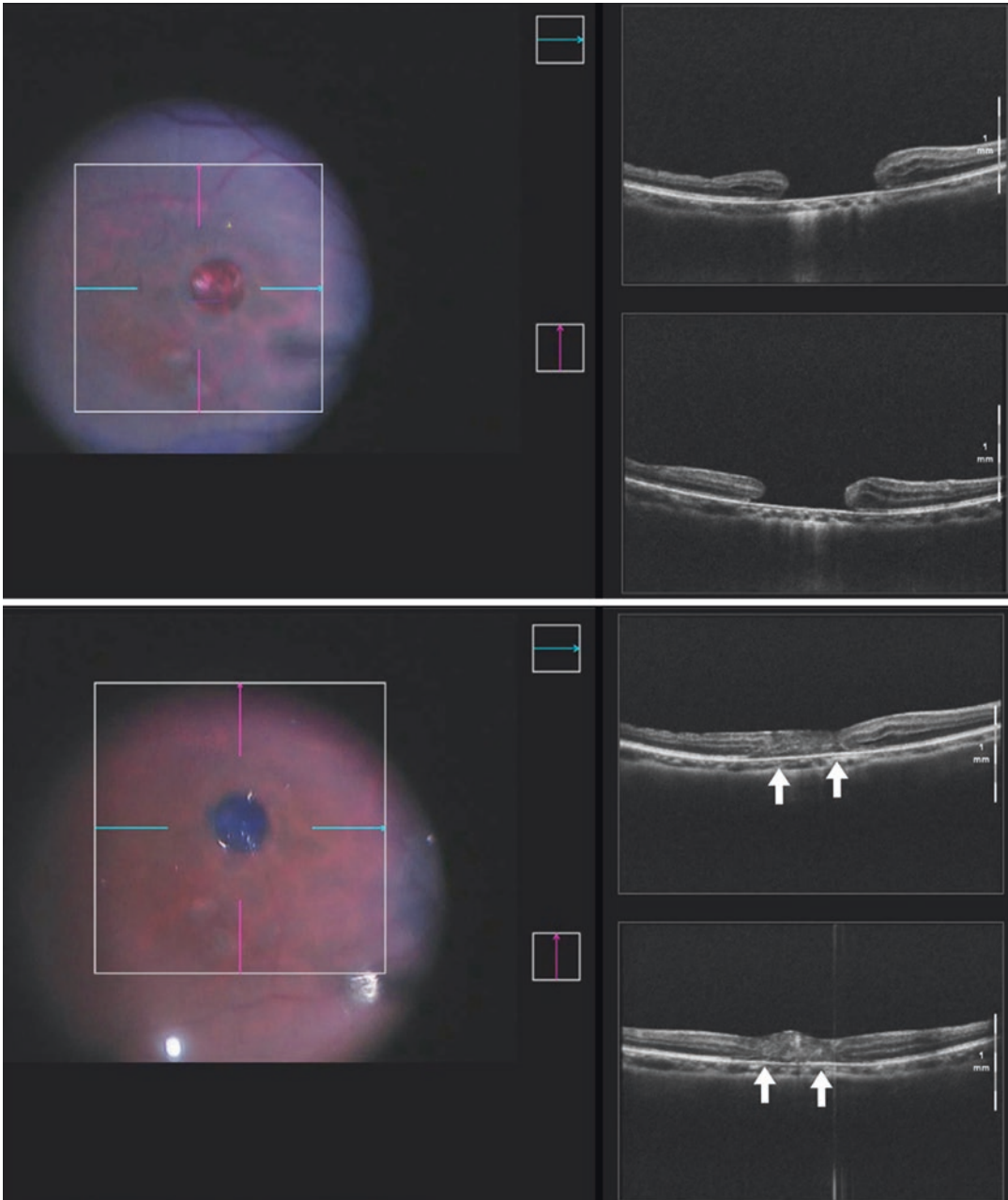
Fig. 12.5 A 44-year-old female presented with a recurrent macular hole, 9 months after the initial vitrectomy. Microscope-integrated OCT (MIOCT) images show a large macular hole during surgery (top panel); the internal limiting membrane (ILM) partially remained. Therefore, an inverted ILM flap was carefully inserted into the macular hole, which was identified on MIOCT images (middle panel, arrows). Subsequently, SF6 gas was injected as a tamponade material (bottom panel). The surface of gas was identified on MIOCT images (arrowhead). Note that the inserted ILM flap remained inside the macular hole (arrows)
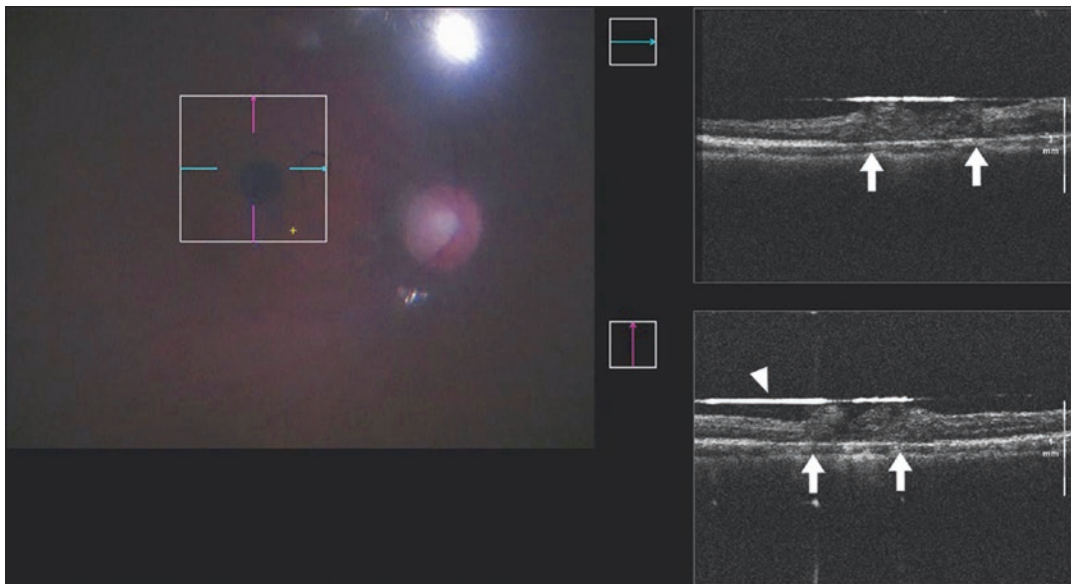
Fig. 12.5 (continued)

recurrent macular hole. The iOCT images revealed that the inverted ILM flap was inserted into the macular hole, and remained inside, after gas tamponade.

2. Three-dimensional assessment of proliferative tissue.

During surgeries for proliferative vitreoretinopathy, such as proliferative diabetic retinopathy (PDR), iOCT enables surgeons to differentiate a proliferative membrane from the underlying retina. The three-dimensional real-time structure information can lead to precise dissection of the proliferative membrane. Furthermore, iOCT enables identification of occult retinal breaks during PDR surgeries (Fig. 12.7) [10, 13].

3. Rhegmatogenous retinal detachment.

Assessment of the fovea during surgery for rhegmatogenous retinal detachment is necessary to identify foveal thinning and the macular hole to choose subsequent tamponade materials, even if retinal breaks were identified in the peripheral retina and no macular hole was observed preoperatively (Fig. 12.8) [14]. iOCT can also identify subretinal proliferative bands in eyes with proliferative vitreoretinopathy (Fig. 12.9).

4. Poor or invisible fundus before surgery.

The evaluation of retinal detachment, retinoschisis, macular edema, macular hole, and ERM is required to make surgical decisions regarding the application of tamponade and ILM peeling [13] when the ocular fundus is difficult to evaluate before surgery due to factors such as dense vitreous hemorrhage, vitreous opacity, or mature cataract. It is also useful in patients who cannot cooperate during preoperative OCT, such as infants and patients with psychiatric disorders.

5. Implantation, gene therapy, and chorioretinal biopsy.

In addition to the common clinical usage described above, iOCT has a potential role in new surgical techniques, such as the implantation of an artificial retina (Argus II retinal prosthesis system) [15, 16] and subretinal delivery of gene therapy agents [17]. During a chorioretinal biopsy, surgeons can obtain real-time feedback from the biopsy site, which facili-

Fig. 12.6 Preoperative (upper panel) and postoperative (lower panel) OCT images of the patient described in Fig. 12.5. The OCT image at 1-month post-surgery shows an inserted plug of inverted internal limiting membrane closing the macular hole (arrows)
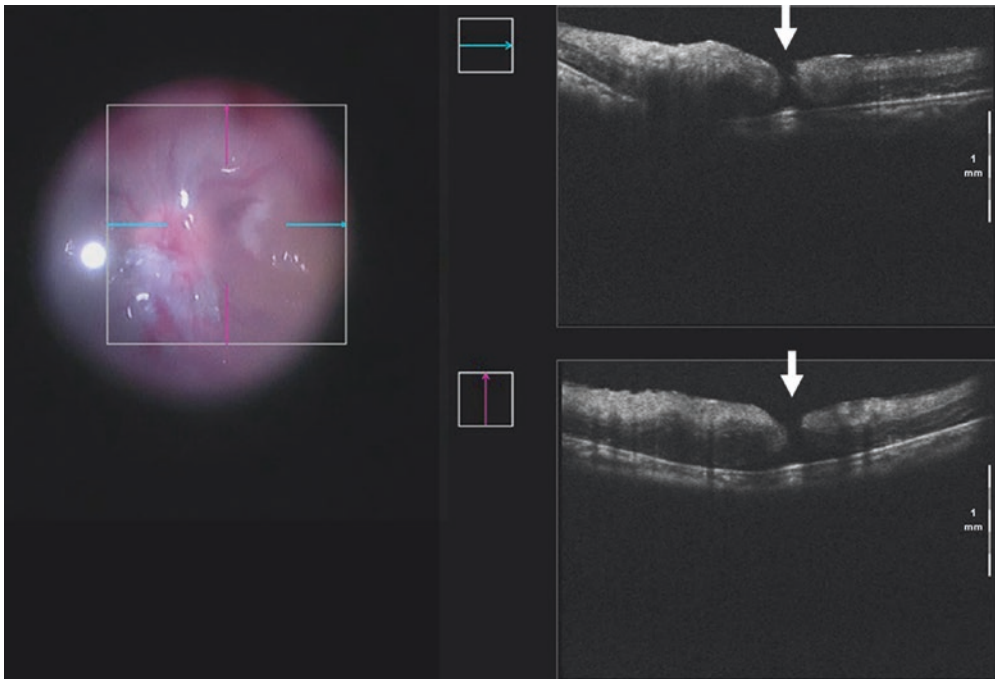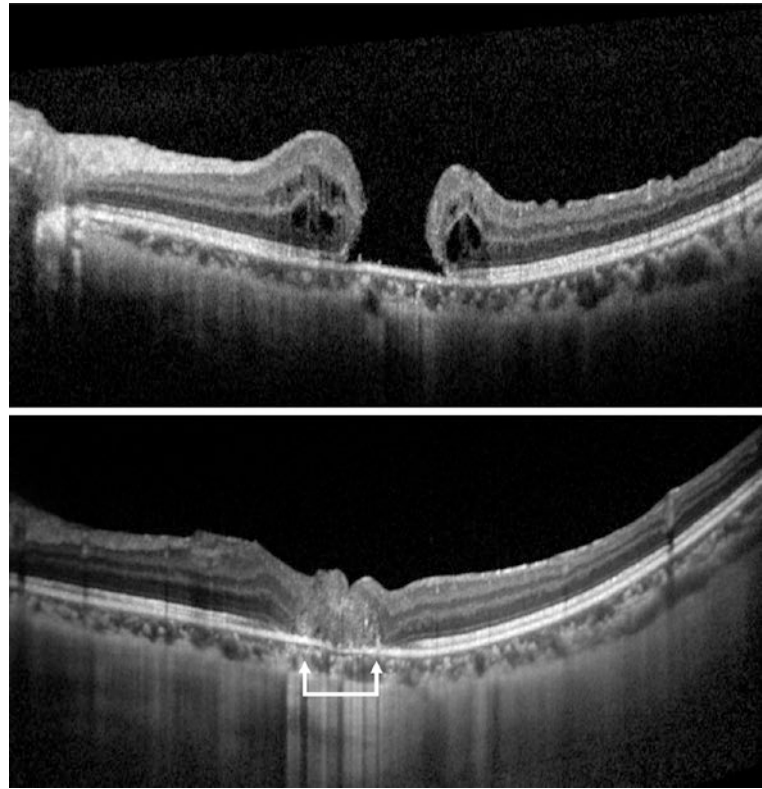
Fig. 12.7 A 34-year-old female presented with proliferative diabetic retinopathy. The left surgical view shows fibrovascular membranes expanding over the optic nerve. Microscope-integrated OCT revealed a paravascular retinal break near the fibrovascular membranes (arrows)
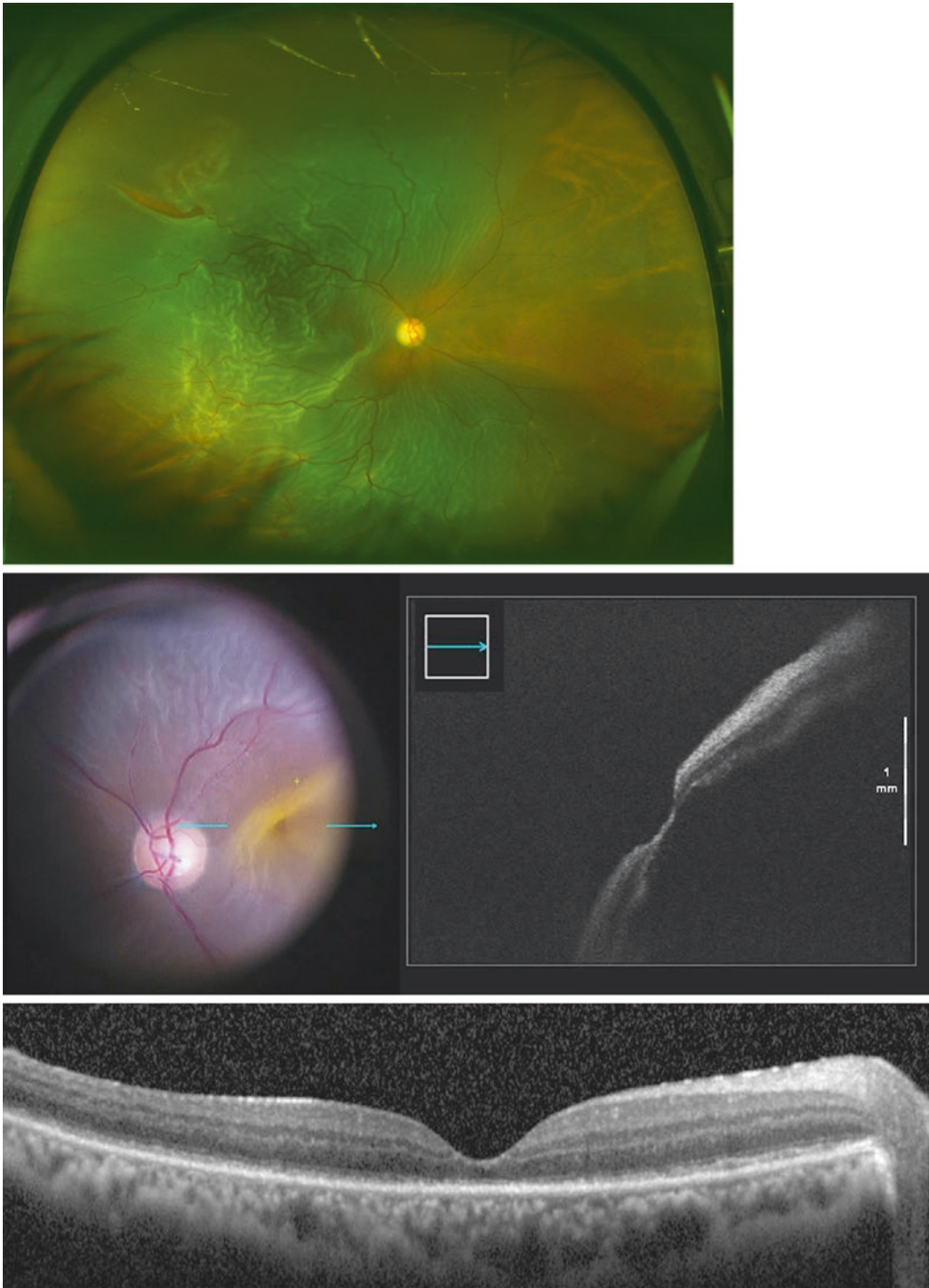
Fig. 12.8 A 56-year-old female presented with macula-off rhegmatogenous retinal detachment. The upper ultra-wide-field color fundus image shows retinal breaks in the periphery of the retina and bullous retinal detachment, including macular detachment. The middle panel shows the surgical view and the microscope-integrated OCT (MIOCT) image. The presence of a macular hole was difficult to assess on the surgical view; MIOCT revealed foveal thinning, but no macular hole. The lower panel shows an OCT image 2 weeks post-surgery. No macular hole was formed

Fig. 12.9 A 21-year-old
male with long-standing
retinal detachment
associated with atopic
dermatitis. The
ultra-widefield color
fundus image shows
grade C proliferative
vitreoretinopathy with a
circumferential
subretinal band (upper
panel). The microscope-
integrated OCT
identified the subretinal
band beneath the retina
(arrow)
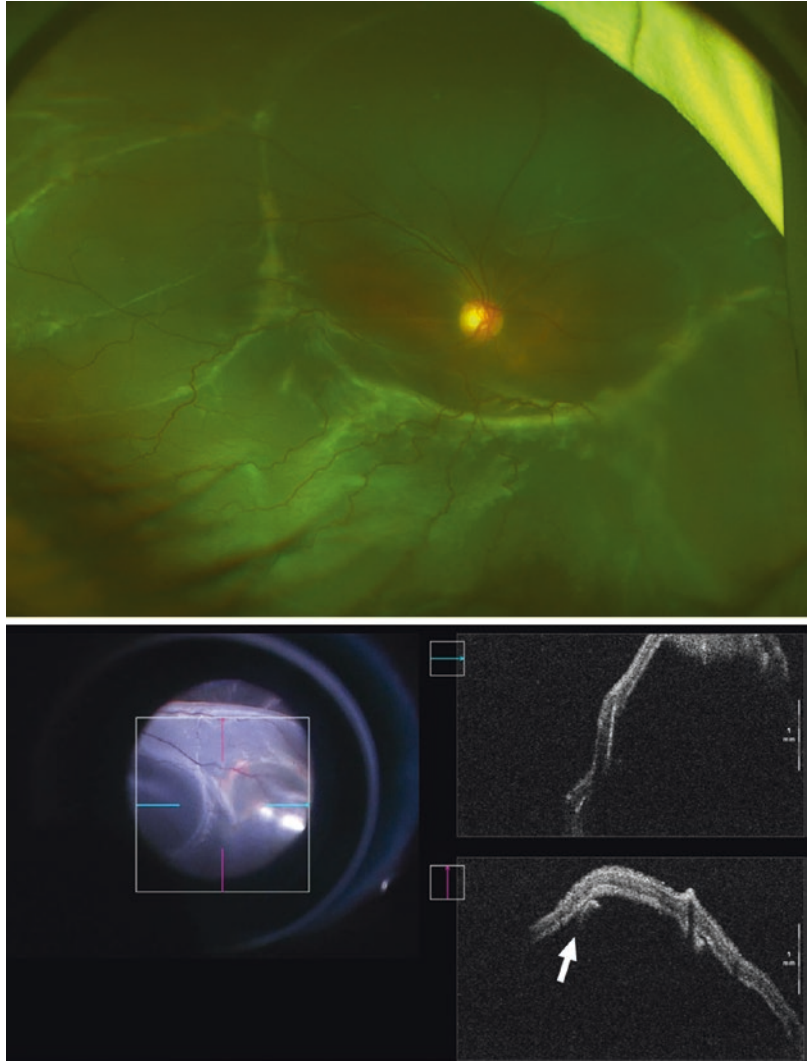
tates biopsy site selection. The structural infor-
mation provided by iOCT can assist in the
development of novel approaches and facili-
tates precise and safe surgical maneuvers [18].

12.2 Conclusion

Accurate visualization of an object is necessary
to understand it. With the advancement and
increasing popularity of MIOCT technology, sur-

geons can observe precise changes in tissue and
blood vessels during surgery. The latest prototype
MIOCT is based on swept-source OCT
(SS-MIOCT). It is reported to provide higher
resolution wide-field iOCT images with faster
acquisition [19]. Furthermore, SS-MIOCT has
been applied to MIOCT angiography [20] and
live volumetric imaging over time visualization,
called 4D MIOCT [21–23]. Thus, intraoperative
OCT is likely to become an essential tool for
macular surgery in the near future.

References

1. Tao YK, Ehlers JP, Toth CA, Izatt JA. Intraoperative spectral domain optical coherence tomography for vitreoretinal surgery. Opt Lett. 2010;35(20):3315–7.

2. Hahn P, Migacz J, O'Connell R, Maldonado RS, Izatt JA, Toth CA. The use of optical coherence tomography in intraoperative ophthalmic imaging. Ophthalmic Surg Lasers Imaging. 2011;42(Suppl):94.

3. Ehlers JP, Dupps WJ, Kaiser PK, Goshe J, Singh RP, Petkovsek D, et al. The Prospective Intraoperative and Perioperative Ophthalmic ImagiNg with Optical CoherEncE TomogRaphy (PIONEER) Study: 2-year results. almol. 2014;158(5):999–1007.

4. Han S, Sarunic MV, Wu J, Humayun M, Yang C. Handheld forward-imaging needle endoscope for ophthalmic optical coherence tomography inspection. J Biomed Opt. 2008;13(2):20505.

5. Asami T, Terasaki H, Ito Y, Sugita T, Kaneko H, Nishiyama J, et al. Development of a fiber-optic optical coherence tomography probe for intraocular use. Invest Ophthalmol Vis Sci. 2016;57(9):OCT568–OCT74.

6. Ehlers JP, Srivastava SK, Feiler D, Noonan AI, Rollins AM, Tao YK. Integrative advances for OCT-guided ophthalmic surgery and intraoperative OCT: microscope integration, surgical instrumentation, and heads-up display surgeon feedback. PLoS One. 2014;9(8):e105224.

7. Hahn P, Migacz J, O'Connell R, Izatt JA, Toth CA. Unprocessed real-time imaging of vitreoretinal surgical maneuvers using a microscope-integrated spectral-domain optical coherence tomography system. Graefes Arch Clin Exp Ophthalmol. 2013;251(1):213–20.

8. Bruyère E, Philippakis E, Dupas B, Nguyen-Kim P, Tadayoni R, Couturier A. Benefit of intraoperative optical coherence tomography for vitreomacular surgery in highly myopic eyes. Retina. 2018;38(10):2035–44.

9. Itoh Y, Inoue M, Kato Y, Koto T, Hirakata A. Alterations of foveal architecture during vitrectomy for myopic retinoschisis identified by intraoperative optical coherence tomography. Ophthalmologica. 2019;242(2):87–97.

10. Ehlers JP, Modi YS, Pecen PE, Goshe J, Dupps WJ, Rachitskaya A, et al. The DISCOVER study 3-year results: feasibility and usefulness of microscope-integrated intraoperative OCT during ophthalmic surgery. Ophthalmology. 2018;125(7):1014–27.

11. Lytvynchuk LM, Falkner-Radler CI, Krepler K, Glittenberg CG, Ahmed D, Petrovski G, et al. Dynamic intraoperative optical coherence tomography for inverted internal limiting membrane flap technique in large macular hole surgery. Graefes Arch Clin Exp Ophthalmol. 2019;257(8):1649–59.

12. Borrelli E, Palmieri M, Aharrh-Gnama A, Ciciarelli V, Mastropasqua R, Carpineto P. Intraoperative optical coherence tomography in the full-thickness macular hole surgery with internal limiting membrane inverted flap placement. Int Ophthalmol. 2019;39(4):929–34.

13. Khan M, Srivastava SK, Reese JL, Shwani Z, Ehlers JP. Intraoperative OCT-assisted surgery for proliferative diabetic retinopathy in the DISCOVER study. Ophthalmol Retina. 2018;2(5):411–7.

14. Ehlers JP, Ohr MP, Kaiser PK, Srivastava SK. Novel microarchitectural dynamics in rhegmatogenous retinal detachments identified with intraoperative optical coherence tomography. Retina. 2013;33(7):1428–34.

15. Seider M, Hahn P. Argus II retinal prosthesis malrotation and repositioning with intraoperative optical coherence tomography in a posterior staphyloma. Clin Ophthalmol. 2015;9:2213–6.

16. Rachitskaya AV, Yuan A, Marino MJ, Reese J, Ehlers JP. Intraoperative OCT imaging of the Argus II retinal prosthesis system. Ophthalmic Surg Lasers Imaging Retina. 2016;47(11):999–1003.

17. Gregori NZ, Lam BL, Davis JL. Intraoperative use of microscope-integrated optical coherence tomography for subretinal gene therapy delivery. Retina. 2019;39(Suppl 1):S9–S12.

18. Browne AW, Ehlers JP, Sharma S, Srivastava SK. Intraoperative optical coherence tomography–assisted chorioretinal biopsy in the DISCOVER study. Retina. 2017;37(11):2183–7.

19. Lu CD, Waheed NK, Witkin A, Baumal CR, Liu JJ, Potsaid B, et al. Microscope-integrated intraoperative ultrahigh-speed swept-source optical coherence tomography for widefield retinal and anterior segment imaging. Ophthalmic Surg Lasers Imaging Retina. 2018;49(2):94–102.

20. Chen X, Viehland C, Carrasco-Zevallos OM, Keller B, Vajzovic L, Izatt JA, et al. Microscope-integrated optical coherence tomography angiography in the operating room in young children with retinal vascular disease. JAMA Ophthalmol. 2017;135(5):483–6.

21. Gabr H, Chen X, Zevallos-Carrasco OM, Viehland C, Dandrige A, Sarin N, et al. Visualization from intraoperative swept-source microscope-integrated optical coherence tomography in vitrectomy for complications of proliferative diabetic retinopathy. Retina. 2018;38:S110–S20.

22. Carrasco-Zevallos OM, Keller B, Viehland C, Shen L, Waterman G, Todorich B, et al. Live volumetric (4D) visualization and guidance of in vivo human ophthalmic surgery with intraoperative optical coherence tomography. Sci Rep. 2016;6:31689.

23. Kolb JP, Draxinger W, Klee J, Pfeiffer T, Eibl M, Klein T, et al. Live video rate volumetric OCT imaging of the retina with multi-MHz A-scan rates. PLoS One. 2019;14(3):e0213144.

Heads-up Microscope Systems in Vitreoretinal Surgery

13

Ellie Bowditch, Kazuaki Kadonosono, and Andrew Chang

13.1 Synopsis

Advances in digitally assisted vitreoretinal surgery (DAVS) over the last 10 years have allowed vitreoretinal surgeons to operate using systems that incorporate three-dimensional (3-D) heads-up display with integrative camera–microscope and image processing tools to deliver technically advanced surgical visualisation platforms [1, 2]. Examples of 3-D digitally assisted heads-up endoscopic vitreoretinal surgery platforms that have been introduced over the past 2 years are the Ngenuity® 3-D visualisation system from

E. Bowditch
Sydney Institute of Vision Science,
Sydney, NSW, Australia

Sydney Retina Clinic & Day Surgery,
Sydney, NSW, Australia

K. Kadonosono
Department of Ophthalmology & Micro-Technology,
Medical School, Yokohama City University,
Yokohama, Japan
e-mail: kado@yokohama-cu.ac.jp

A. Chang (✉)
Sydney Institute of Vision Science,
Sydney, NSW, Australia

Sydney Retina Clinic & Day Surgery,
Sydney, NSW, Australia

University of Sydney, Sydney, NSW, Australia

Department of Ophthalmology, Sydney Hospital &
Sydney Eye Hospital, Sydney, NSW, Australia
e-mail: achang@sydneyretina.com.au

TrueVision Systems and Alcon and the Artevo® 800 3-D HD from Carl Zeiss Meditec [3]. These commercially available technologies can be integrated into other available visualisation systems to offer simultaneous viewing of intraoperative optical coherence tomography (iOCT), whilst software allows surgeons to track and customise data parameters in real time such as intraocular pressure, infusion pressure, laser power and flow rates on an overlay to the operating field shown on the heads-up monitor [4–6].

13.2 Heads-Up Surgical Displays

The general principle of heads-up surgical displays is the integration of three new technology components that are compatible adjuncts to a traditional operating microscope. The Ngenuity® and Artevo® 800 are DAVS platforms which enable high definition, heads-up display of the operating field during micro-ophthalmic vitreoretinal surgery. They consist of a HDR 3-D camera connected in the place of the eyepiece contact lens; the image is digitalised by an ultra-high speed image processor and displayed on a high definition, 3-D capable, 4 K (streaming at 3840 × 2160 pixels) OLED surgical monitor display. The result is an operating field that is visualised on the heads-up monitor by wearing polarised 3-D glasses. The image on the display

is that which would be seen by looking through the microscope eyepiece, with added digital enhancements provided by hardware components [3, 7, 8].

The quality of the 3D effect sensation is influenced by several factors such as the size and resolution of the monitor, the viewing angle and the distance between the surgeon and the display. Reports from users indicate surgeons can observe the vitreous cavity most clearly when seated approximately 1.5 m in front of the display (Fig. 13.1).

Benefits of a heads-up surgical display include simultaneous visualisation for both the surgeon and all participants within the operating suite allowing for an immersive operating experience compared to traditional operator-focused microscopy and physical flexibility within the theatre suite [9]. These platforms allow for surgical collaboration between all theatre personnel by displaying the operative field for fellows and other trainees as well as nursing staff to follow from multiple viewpoints in an operating theatre suite whilst still experiencing the same viewing angle as the surgeon. The shared display platform is a tool to facilitate communication and workflow improvements within the operating room for nursing staff as well as providing an educational platform for multiple trainees to view the operating field

[10]. An audience can be positioned away from the sterile field, which gives more space for the surgeon and assistant.

Heads-up surgical display may reduce the incidence of cervical spondylosis among surgeons and surgical trainees by changing the posture of the surgeon from looking down through a microscope eyepiece, to looking up to a display monitor [11]. Improved posture by using heads-up display may also reduce fatigue that is experienced through restrictive posturing when operating at a traditional operating microscope without digital viewing adjuncts [12].

13.3 Digitalisation of the Surgical Display

The digital features of image processing and manipulation provide a means to improve delineation of anatomical structures under high magnification such as internal limiting membranes (ILM), epiretinal membranes (ERM) and detached retina [13–15]. The ultra-high speed processor optimises the image by balancing light to mitigate glare and shadows, adding contrast and image sharpness to highlight natural colours which enables visualisation of the extended depth of field and peripheral operating field with clarity and resolution [2, 3, 5, 16]. As well as enhancing
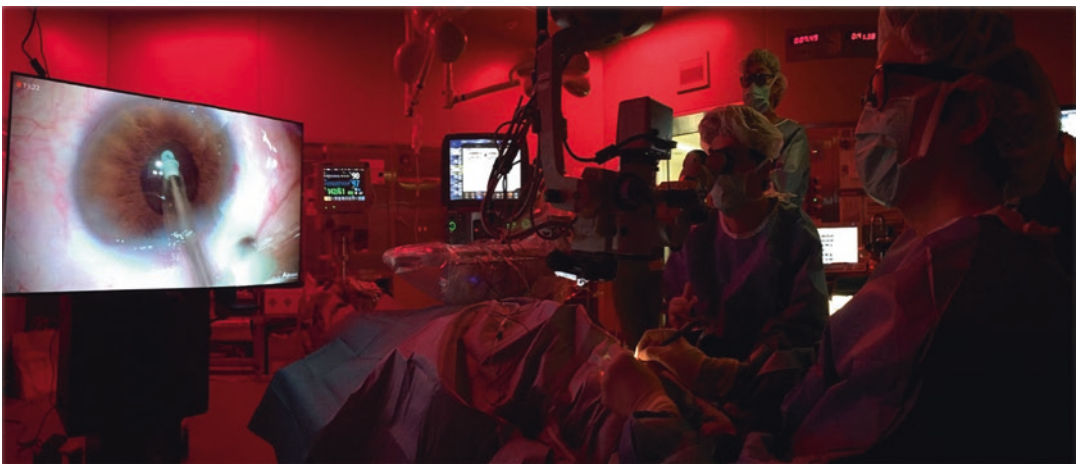
Fig. 13.1 A picture of an operating room. An Ngenuity® 3-D visualisation system is located 1.5 m ahead of a surgeon

the digital display, the image processor enables either 3-D or 2-D format streaming, plus multiple USB and cable connectivity with video recording [3]. Surgery can be recorded in 3-D allowing for subsequent viewing in a teaching setting. The recording files are also able to be converted to 2-D.

Digital enhancement reduces the amount of illumination required to recognise the contour of the ILM during peeling to approximately half of that which would be required if operating without digitally enhanced surgical displays [13, 15]. This feature allows surgery to be performed at lower illumination levels, providing more comfort for the patient and reducing the risk of retinal phototoxicity during surgery [17]. When staining epiretinal membranes, digital image enhancement has also enabled surgeons to decrease dye concentrations whilst maintaining functional definition of the retina [15]. Vitrectomy surgeries performed using digitally enhancing software have been quantitatively evaluated using algorithms recommended by the International Commission of Illumination. The algorithms are applied to assess the colour and contrast differences between two spots from snapshots obtained during ILM peeling. During analysis, two adjacent spots are selected during an ILM peel; the first lies inside the contour of the circular area which has been freed of ILM, whilst the second sits outside of the contour of the circular

area where the ILM is still adhered. The colour difference between the two spots increased with digital enhancement across all levels of illumination [15–18].

Digitally assisted vitreoretinal surgery (DAVS) provides higher resolution images and greater depth of field than a conventional operating microscope. This offers obvious advantages to surgeons requiring clear visualisation of the retina during delicate macular surgical procedures. In eyes with epiretinal membranes, for example, transparent membranes exhibit tortuosity of vessels and minor folds that can be difficult to distinguish from normal retina. DAVS also facilitates peeling of epiretinal membrane by enabling surgeons to easily differentiate topographic areas of retina with, and those without pre-retinal membranes (Fig. 13.2).

Generally speaking, the quality of digital images is influenced by five main factors—brightness, contrast, hue, gamma and saturation. It is important to adjust these digital parameters to obtain the maximum quality of images. Digital images obtained with default mode can be altered to match the needs of surgeons by changing image parameters (Fig. 13.2).

Depth of field (DOF) is the distance between the nearest and the farthest objects that are in acceptably sharp focus in an image. Vitrectomy requires good depth of field because the vitreous cavity is a small, three-dimensional space.

Fig. 13.2 An intraoperative picture of ERM as viewed with Ngenuity®. A membrane is clearly seen with high resolution. Digitalisation of the display enables fine-tuning using parameters displayed on the screen to achieve optimal live image enhancement
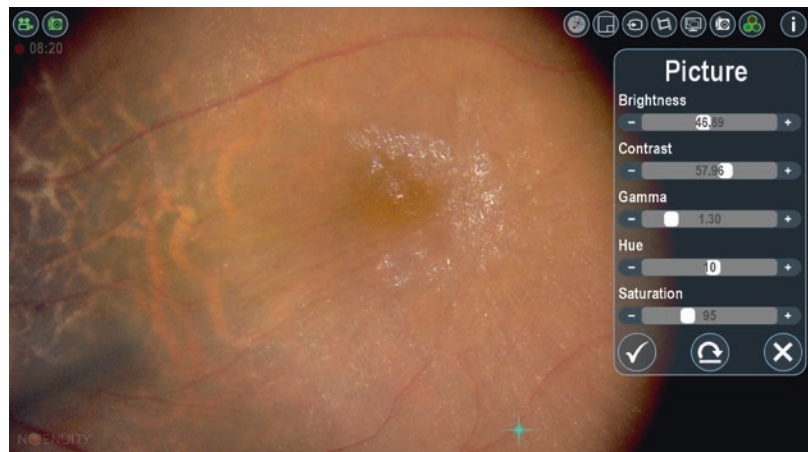
Fig. 13.3 An intraoperative picture of an eye with submacular haemorrhages. A vitrectomy cutter, an optic disc and retina are all seen clearly because Ngenuity® provides great depth of field
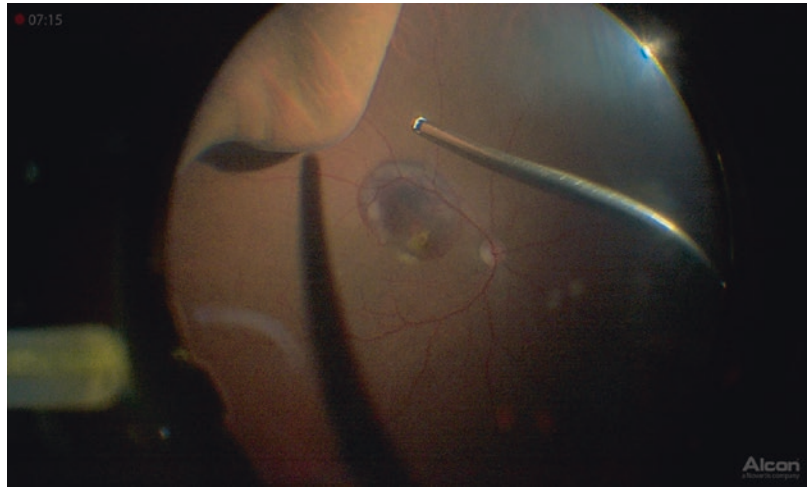
It is generally thought that compared to conventional operating microscopes, the improved DOF obtained in DAVS displays allows surgeons to more effectively perform vitrectomy, whilst also providing fundus images with better DOF. Fundus images obtained from DAVS allow sharp focus on all structures in view such as cutters, discs and the macula (Fig. 13.3).

Regarding the ILM, for example, the use of dyes such as indocyanine green (ICG), trypan blue and brilliant blue G (BBG), to help to differentiate the ILM is very common. Utilising changes in hue based on the colour circle allows surgeons to clarify images of the ILM stained with these dyes. If surgeons increase the level of hue during macular hole surgery with ICG, the image of the ILM gets much greener, facilitating peeling of the membrane as well as reducing photo-toxicity due to lower concentrations of dye (Fig. 13.4).

The HDR capabilities of the camera enable the surgeon to adjust the magnification whilst still maintaining a relatively wide field of view, without the need to adjust alignment of the lens or magnification of the microscope [19]. The HDR 3-D camera maintains a stereoscopic wide operative field of view with real depth perception and spatial dimension that is maintained in 3-D display by separating the delivery of visual information between right and left eyes [20]. The wide field of view platform allows awareness of positioning of intraocular instruments, their orientation and proximity to other ocular tissues that would otherwise not be visualised in the same operating field [21]. Digitalization of the view of the surgical field enables the variables of focus and parallax to become automatically corrected in a 3-D view to maintain accurate field of depth [22]. Surgical microscope integrated OCT (iOCT) offers the advantage for live assessment of retinal architecture during vitrectomy for many vitreoretinal pathologies including retinal detachment, vitreomacular traction syndrome, macula hole, submacular haemorrhage, pre-retinal membrane and proliferative vitreoretinopathy. iOCT is useful in differentiating pre-retinal/posterior hyaloid space haemorrhage from subretinal haemorrhage as shown in Fig. 13.5. In the case of epiretinal membrane and ILM peeling surgery, to facilitate adequate staining of the preretinal membrane or ILM, trypan blue (Membrane Blue™) can be injected over the posterior pole and allowed to stain the most superficial tissue. In the time given to allow for adequate staining of tissues after the injection of dye, the surgeon using iOCT can visualise the

Fig. 13.4 An image of ILM with different hue. An ILM (**a**) is enhanced to a greener image (**b**) when a surgeon increases the level of hue from 10° to 23°
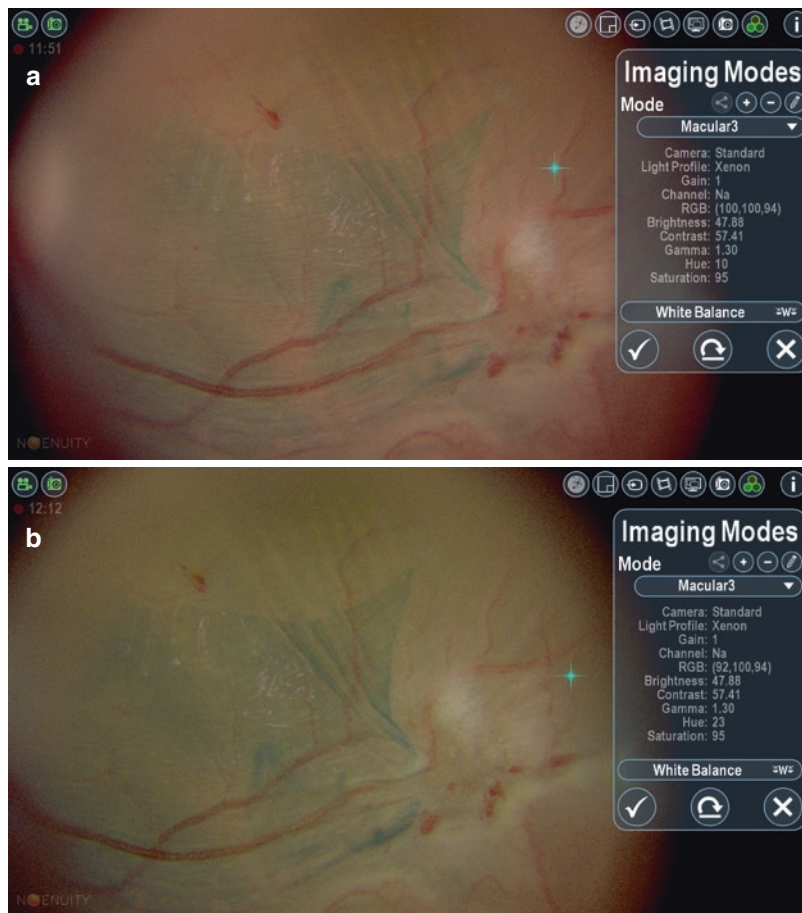
macula architecture through the dye that covers the macula with the same resolution as performing the iOCT through the infusion fluid in the vitreous space following posterior vitrectomy. During peeling, the iOCT can be 'locked' onto a specific region of the retina, such as directly over the fovea, or centered around a macula hole so that during membrane peeling where there is movement of the eye and of the instruments, iOCT displays the live stream of the tissue architecture at the selected location as it changes with tissue manipulation. This live iOCT offers the obvious benefit to the surgeon to confirm when enough peeling has been performed in the case of macula pucker where tangential traction is relieved to restore the foveal architecture, or when adequate tension has been relieved from the edges of a macula hole that would allow for opposition of the edges to enable successful hole closure.

13.4 Commercially Available Digital Heads-up Systems for Vitreoretinal Surgery

The Artevo 800 (Carl Zeiss Meditec) (Fig. 13.6) was introduced at the American Society of Cataract and Refractive Surgery in May 2019. This heads-up operating system is specific for vitreoretinal surgery and has cloud connectivity which allows users to access patient data remotely

Fig. 13.5 Zeiss Artevo® 800 integrated OCT (iOCT) display showing macula hole (**a**), submacular haemorrhage (**b**), epiretinal membrane under Membrane Blue dye (**c**)

and live stream from the operating room. The Artevo® 800 heads-up display system consists of a mobile display monitor that is mounted onto the hardware component of the DAVS platform that can be moved around the theatre. In integrating a DAVS platform to the vitreoretinal theatre suite, the heads-up display monitor is an additional equipment item that adds to the footprint require-ments of an operating room. The heads-up dis-play monitor is positioned 1.5 metres in front of the surgeon during surgery (Fig. 13.7).

The panoramic RUV800 Viewing System® (Leica Microsystems) can be added to the Leica M844 F40® operating microscope for wide-field posterior segment views, similar to that which would be achieved through an ultra-wide field
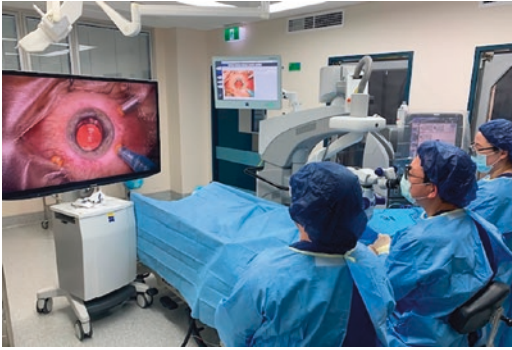
Fig. 13.6 Zeiss Artevo® 800 3-D HD (Carl Zeiss Meditec) configuration in an operating room

Fig. 13.7 The Artevo® 800 3-D HD (Carl Zeiss Meditec)

Fig. 13.8 Ngenuity® 3-D visualisation system (TrueVision Systems and Alcon)

camera. Leica Microsystems also have both 3-D and OCT software available for monitor display, but their operating microscopes are configured for a traditional heads down configuration for the surgeon.

The Ngenuity® 3-D visualisation system from Alcon (Fig. 13.8) was first introduced to

the vitreoretinal community at the American Society of Retina Specialists (ASRS) annual meeting in July 2018. The Ngenuity® system can be combined with other software such as Datafusion® and Constellation® vision systems which allow a data interface feedback on one screen during procedures [3]. The Ngenuity®

3-D visualisation system from Alcon is the most widely reviewed heads-up system available in the literature to date.

The Ngenuity® 3-D visualisation system has been reviewed across numerous international ophthalmology institutions, with clinical studies publishing user feedback comparing this DAVS heads-up experience with the traditional surgical microscope operator experience [2, 5, 7–9, 23]. The first 3-D surgery experience in the vitreoretinal ophthalmology field was published by Riemann at an American Academy of Ophthalmology Annual Meeting in 2010 [24]. Since then, clinical studies conducted at various ophthalmology institutions across America, Japan, Brazil, France, India and China have published both objective performance parameters and subjective feedback reviews from surgeons using 3-D visualisation for vitreoretinal surgery [2, 5, 7–10, 12, 13]. The data from these studies represent feedback from at least 269 surgical cases, although the number of vitreoretinal ophthalmologists at each centre who have experienced operating with the Ngenuity 3-D surgical viewing platform is unclear. In most studies to date, ophthalmologists show a preference for using the heads-up technique with enhanced digital processing over traditional operating microscopes without these newer technology adjuncts. The generally accepted main benefits described when using the Ngenuity® 3-D surgical viewing platform are advantages in image resolution, depth of field and stereopsis, image detail and ergonomics [6, 15, 19, 23].

13.5   Limitations

Concerns regarding heads-up surgical viewing platforms exist. The initial high cost for purchasing the system may be a barrier for some centres. Currently, the surgical microscope and the 3-D technology adjuncts need to be purchased separately, although most centres will already have a compatible operating microscope. With the addition of more equipment in the operating room, there needs to be enough space for the anaesthetics, nursing and surgical team to integrate around

the display monitor which is placed in the proximity of the dorsal end of the patients trolley, at a specific distance from the operating surgeon (1.5 metres) [3]. The assistant, positioned at a 90° angle to the heads-up monitor and to the surgeon, may find it difficult to turn their head in order to see the operating field without adjusting the orientation of their body to the monitor [6]. The addition of a large monitor to the operating theatre footprint may further confine already limited space in some operating rooms. It is unclear how much time would be required for a surgeon to up-skill or re-skill to operating in a heads-up configuration, and further to that, adjust to using a three-dimensional view. Most observational case series to date describe a learning curve associated with transitioning or expanding surgical repertoire to include operating using 3-D operating technology from using the surgical microscope [6, 10, 25]. There have been others, however, that subjectively describe an experienced surgeon who is able to master heads-up vitreoretinal surgery without any obvious obstacles, even without pre-surgery visualisation practice in 3-D [26].

Watching three-dimensional images is known to induce ocular and non-ocular symptoms, such as fatigue, nausea, headache and eye discomfort. This phenomena is referred to as '3-D asthenopia' and it can explain why in previous limited number of observational case series the surgeon and assistants described fatigue and ocular discomfort, particularly during laser photocoagulation [26]. 3-D visualisation has been observed to amplify the disturbance of opacity of the surgical media when operating in the posterior segment. Additionally, unclear images can be caused by adjustment of screen resolution and other automatic digital parameters that may be a barrier to the continuation of the case without interruption from the digitalised platform. Further disruptions to work flow may occur when a surgeon needs to switch from a heads-up view to the traditional eyepiece view during a case. The microscope eyepiece needs to be connected in place of the HDR camera and then the microscope needs to be adjusted to the new distance between the lens and the correct tissue plane. The time required to configure a 3-D heads up

system to an operating suite as well as educate all staff and provide training for surgeons adopting the new technology may be a barrier to some centres facilitating an introduction. Further to this, larger centres with multi-disciplinary use of theatre suites may find changing to heads-up viewing systems to be particularly cumbersome, especially when required to move equipment to suit different operating lists for other subspecialties not using the heads-up operating platforms. Published reviews and comprehensive data on vitreoretinal surgery experiences using these commercially available systems are lacking from several large ophthalmology institutes namely those from Australia and the United Kingdom. More research is required to study important variables including the length of procedure and theatre time as well as clinical outcomes for patients.

13.6   The Future

Heads-up surgical platforms are able to be used for cataract surgery and in glaucoma procedures to enable detailed visualisation of the iridocorneal angle which would not be otherwise available without iOCT; however, the system may have some latency particularly for faster movements [15]. It is expected that latency will become less obvious (currently 15 ms for Ngenuity®) as processors get faster and are able to show real-time visualisation. The potential for integration with other technology such as angiography and artificial intelligence warning systems would provide advantageous information for the surgeon. In the future the platform will become better customised for the colour profiles of laser photocoagulation, this will minimise the discomfort that is observed in three-dimensional visualisation.

Digitalised heads-up surgical viewing platforms serve as an adjunct to the traditional operating microscope and provide advantages particularly for ergonomics and visualisation of vitreoretinal microsurgery [7–9]. Whilst these technologies enhance visualisation for delicate, minimally invasive ophthalmic surgeries and provide functional advancements to the tradi-

tional operating microscope, they are relatively new to the vitreoretinal community so are not yet widespread among international ophthalmology institutes. Further randomised case–control studies with larger sample sizes and analysis of more objective variables should be carried out to establish the place for these technically advanced systems in the vitreoretinal surgical realm.

References

1. Eckardt C, Paulo EB. Heads-up surgery for vitreoretinal procedures: an experimental and clinical study. Retina. 2016;36(1):137–47.
2. Zhang T, Tang W, Gezhi X. Comparative analysis of three-dimensional heads-up vitrectomy and traditional microscopic vitrectomy for vitreoretinal diseases. Curr Eye Res. 2019;44(10):1080–6.
3. Alcon Data on File. Yin L, Sarangapani R. Assessment of visual attributes for NGENUITY® 3D Visualisation System 1.0 for digitally assisted vitreoretinal surgery. Alcon Modeling and Simulation. December 2017.
4. Ehlers JP. Intraoperative optical coherence tomography: past, present, and future. Eye (Lond). 2016;30(2):193–201.
5. Read SP, Fortun JA. Visualization of the retina and vitreous during vitreoretinal surgery: new technologies. Curr Opin Ophthalmol. 2017;28:238–41.
6. Ehlers JP, Uchida A, Srivastava SK. The integrative surgical theater: combining intraoperative optical coherence tomography and 3D digital visualization for vitreoretinal surgery in the DISCOVER study. Retina. 2018;38(Suppl 1):S88–96.
7. Talcott KE, Adam MK, Sioufi K, Aderman CM, Ali FS, Mellen PL, et al. Comparison of a three-dimensional heads-up display surgical platform with a standard operating microscope for macular surgery. Ophthalmol Retina. 2019;3(3):244–51.
8. Kumar A, Hasan N, Kakkar P, Mutha V, Karthikeya R, Sundar D, Ravani R. Comparison of clinical outcomes between "heads-up" 3D viewing system and conventional microscope in macular hole surgeries: a pilot study. Indian J Ophthalmol. 2018;66(12):1816–9.
9. Romano MR, Cennamo G, Comune C, et al. Evaluation of 3D heads-up vitrectomy: outcomes of psychometric skills testing and surgeon satisfaction. Eye. 2018;32:1093–8.
10. Berquet F, Henry A, Barbe C, Cheny T, Afriat M, Benyelles AK, et al. Comparing heads-up versus binocular microscope visualization systems in anterior and posterior segment surgeries: a retrospective study. Ophthalmologica. 2020; https://doi.org/10.1159/000507088.
11. Dhimitri KC, McGwin G Jr, McNeal SF, et al. Symptoms of musculoskeletal disorders in ophthalmologists. Am J Ophthalmol. 2005;139:179–81.

12. Freeman WR, Chen KC, Ho J, Chao DL, Ferreyra HA, Tripathi AB, et al. Resolution, depth of field, and physician satisfaction during digitally assisted vitreoretinal surgery. Retina. 2019;39(9):1768–71.

13. Kunikata H, Abe T, Nakazawa T. Heads-up macular surgery with a 27-gauge microincision vitrectomy system and minimal illumination. Case Rep Ophthalmol. 2016;7:265–9.

14. Matsumoto CS, Shibuya M, Makita J, Shoji T, Ohno H, Shinoda K, Matsumoto H. Heads-up 3D surgery under low light intensity conditions: new high-sensitivity HD camera for ophthalmology microscopes. J Ophthalmol Vol. 2019;2019:1. https://doi.org/10.1155/2019/5013463.

15. Akiyama K, Watanabe K, Fukui M, et al. Quantitative evaluation of digital-image enhancement during heads-up surgery. Sci Rep. 2019;9:15931.

16. Skinner C, Riemann CD. "Heads up" Digitally assisted surgical viewing for retinal detachment repair in a patient with severe Kyphosis. Retin Cases Brief Rep. 2018;12:257–9.

17. Adam MK, Thornton S, Regillo CD, Park C, Ho AC, Hsu J, et al. Minimal endoillumination levels and display luminous emittance during three-dimensional heads-up vitreoretinal surgery. Retina. 2017;37:1746–9.

18. Palacios RM, De Carvalho ACM, Maia M, Caiado RR, Camilo DAG, Farah ME. An experimental and clinical study on the initial experiences of Brazilian vitreoretinal surgeons with heads-up surgery. Graefes Arch Clin Exp Ophthalmol. 2019;257(3):473–83.

19. Bhadri PR, Rowley AP, Khurana RN, Deboer CM, Kerns RM, Chong LP, Humayun MS. Evaluation of a stereoscopic camera-based three-dimensional viewing workstation for ophthalmic surgery. Am J Ophthalmol. 2007;143:891–2.

20. Weinstock RJ, Donnenfeld ED. 3D visualization in ophthalmology. Cataract Refract Surg Today. 2008;38:S88. https://doi.org/10.1097/IAE.0000000000001999.

21. Coppola M, La Spina C, Rabiolo A, Querques G, Bandello F. Heads-up 3D vision system for retinal detachment surgery. Int J Retina Vitreous. 2017;3:46.

22. Chhaya N, Helmy O, Piri N, Palacio A, Schaal S. Comparison of 2D and 3D video displays for teaching vitreoretinal surgery. Retina. 2018;38:1556–61.

23. Brooks CC, Kitchens J, Stone TW, Riemann CD. Consolidation of imaging modalities utilizing digitally assisted visualization systems: the development of a surgical information handling cockpit. Clin Ophthalmol. 2020;14:557–69.

24. Riemann CD. Machine vision and vitrectomy: three-dimensional high-definition video for surgical visualization in the retina OR. Poster presented at: American Academy of Ophthalmology Annual Meeting; October 17, 2010; Chicago, IL.

25. Yonekawa Y. Seeing the world through 3-D glasses. Retina Today. 2016;28:31–4.

26. Zhang Z, Wang L, Wei Y, Fang D, Fan S, Zhang S. The preliminary experiences with three-dimensional heads-up display viewing system for vitreoretinal surgery under various status. Curr Eye Res. 2019;44(1):102–9.

Enzymatic Vitreolysis

14

Maxwell S. Stem, Bozho Todorich,
and George A. Williams

14.1 Introduction

Compared to the complex network of neurons, blood vessels, and glial cells in the retina, the boundary between the internal limiting membrane and the posterior vitreous cortex may, at first glance, seems dull or unexciting. However, understanding the anatomy and evolution of the vitreoretinal interface over time is fundamental to treating the myriad of patients whose visual complaints can be traced back to abnormalities at the boundary between the vitreous and the retina.

In 2013, the International Vitreomacular Traction Study Group provided optical coherence tomography (OCT)-based definitions of both normal and abnormal vitreoretinal anatomy [1]. Vitreomacular adhesion (VMA) is defined by a normal foveal configuration despite attachment(s) between the vitreous and the macula. Vitreomacular traction (VMT), on the other hand, is characterized by an abnormal posterior vitreous detachment (PVD) whereby vitreous remnants remain adherent to the macula and distort the normal foveal architecture. VMT can be described as focal if the vitreoretinal attachment is less than or equal to 1500 μm in diameter and broad if the diameter of the adhesion is greater than 1500 μm [1]. Full-thickness macular hole (FTMH) is defined as an interruption in all of the retinal layers at the fovea [1]. While VMA is generally asymptomatic and considered part of the normal process of vitreoretinal separation that occurs with aging, both VMT and FTMH are pathologic processes that can result in distorted or decreased vision.

Treatment of these conditions requires severing the vitreoretinal adhesions that are distorting the normal foveal architecture. Current management options include observation, pars plana vitrectomy (PPV), pharmacologic vitreolysis with ocriplasmin, or pneumatic vitreolysis with an intravitreal gas injection [2]. This chapter briefly reviews the normal anatomy of the vitreoretinal interface as well as the epidemiology of vitreoretinal interface disorders before discussing, in greater detail, the development and use of ocriplasmin to treat disorders such as VMT and FTMH.

14.2 Normal Anatomy of the Vitreomacular Interface

The vitreous gel undergoes significant changes in its composition in the time between conception and birth. At around month 1 of gestation, the

M. S. Stem · G. A. Williams (✉)
Oakland University William Beaumont School of
Medicine, Royal Oak, MI, USA
e-mail: George.Williams@beaumont.edu

B. Todorich
Pennsylvania Retina Specialists, P.C., Camp Hill,
PA, USA

space between the optic cup and the lens vesicle becomes filled with primary vitreous, which consists of an extensive network of vascular channels embedded in a matrix of fibrils and mesenchymal cells. The secondary vitreous begins to form shortly after the primary vitreous is established. It is composed of collagen fibrils and hyalocytes and continues to develop as the primary vitreous regresses. By approximately month 4 of gestation, the collagen fibrils of the secondary vitreous coalesce and form connections to the retina and optic nerve, more closely resembling the configuration of the vitreous found in a young child [3].

The adult human vitreous has an astoundingly different composition from the vitreous in utero or a newborn infant. In adults, vitreous accounts for approximately 80% of the volume of the eye and is composed of many collagen fibrils that run in an anterior–posterior direction, inserting anteriorly at the vitreous base and posteriorly at the vitreous cortex. The spaces between the collagen fibrils are filled mostly with water and to a smaller extent other molecules such as hyaluronan, chondroitin sulfate, and the protein opticin [4].

The anterior boundary of the retina is the internal limiting membrane, which is composed of footplates of Muller glial cells. The junction between the posterior vitreous cortex and the internal limiting membrane (ILM) is the vitreoretinal interface. The vitreous maintains adhesions to the retina through molecules such as laminin, fibronectin, and proteoglycans, which interact with the opticin in the vitreous gel to create bridges between the posterior vitreous cortex and the internal limiting membrane of the retina.

At birth and through young adulthood, the vitreous remains attached to the retina. It is most strongly attached to the retina at the vitreous base, but it also maintains strong adhesions at the fovea, the optic nerve, and the vascular arcades [5]. With time, the vitreous liquefies centrally and passes through small defects in the posterior cortex, leading to the development of fluid-filled pockets that directly overly the retina. As these pockets of liquefied vitreous coalesce over time, the connections between the posterior vitreous cortex and the internal limiting membrane are severed, resulting in a PVD [6].

Abnormal evolution of this normal aging process can result in vitreomacular disorders such as FTMH, epiretinal membrane (ERM) formation, and/or VMT [7].

14.3 Epidemiology of Vitreoretinal Disorders

Abnormalities of the vitreoretinal interface are a common problem faced by vitreoretinal surgeons, as evidenced by a retrospective multicenter study published in 2016. In this analysis of patients who had been evaluated in a retina clinic setting, 106 of the 719 subjects (15%) had evidence of either unilateral or bilateral VMA on OCT, and of the patients who had VMA, 28% exhibited foveal deformation characteristic of VMT [8]. Another recent population-based study evaluated approximately 2000 participants aged 63–102 years with spectral-domain (SD) OCT and found the prevalence of VMT to be 1.6% and the prevalence of FTMH to be 0.4% [9]. In a study of patients in a tertiary care setting in Spain, investigators found a slightly higher prevalence of these disorders; among the 2000 eyes that were evaluated, approximately 3.1% exhibited VMT whereas 1.9% had an FTMH [10]. Risk factors that are associated with the development of vitreomacular disorders include increasing age [9, 11], female sex [11], and myopia [12].

14.4 The Road to Ocriplasmin

The emergence of ocriplasmin as a means for pharmacologically inducing a PVD was driven primarily by two factors. First, since PPV was the standard of care for treatment of patients with VMT or FTMH, there was an impetus for a less invasive alternative that could achieve similar results while avoiding surgery. Second, the posterior vitreous cortex is very difficult to mechanically elevate in young patients undergoing vitreoretinal surgery, so the idea of a pharmacologic adjunct that could be used to create a clean plane of separation between the vitreous and the retina during PPV was very appealing.

By the 1990s, enzymes such as collagenase, dispase, nattokinase, hyaluronidase, and chondroitinase had been investigated for use as vitreolytic agents, but each of these potential treatments failed to progress into the clinical realm due to either insufficient efficacy or severe side effects [13]. In 1993, Verstraeten and colleagues demonstrated that a PVD could be induced in rabbit eyes via intravitreal injection of the serine–protease plasmin followed by vitrectomy [14]. Their results were later confirmed in 1999 when independent investigators showed that the combination of intravitreal plasmin and SF6 gas could achieve a PVD in the rabbit eye [15]. In the early 2000s, Gandorfer and colleagues published a series of papers demonstrating that intravitreal plasmin, in a dose-dependent fashion, could be used to separate the vitreous cortex from the ILM in either postmortem porcine [16] or human eyes [17] without the need for adjunct gas injection or vitrectomy. Shortly thereafter, these results were replicated by Li and colleagues, who also showed that the immunoreactivity of fibronectin and laminin at the vitreoretinal interface was reduced following injection of plasmin [18].

Despite these promising results with plasmin, the enzyme was also associated with significant drawbacks. A major hurdle was the lack of a commercially available product for clinical use [13]. To circumvent this problem in early studies, autologous plasminogen was harvested from patients via blood draw and purified with affinity chromatography. In one study evaluating the use of autologous plasmin as an adjunct to vitrectomy in four pediatric patients with traumatic macular holes, the authors reported a 100% closure rate [19]. While these early results were promising, the laborious and time-consuming process of purifying the autologous plasmin was the rate-limiting factor that prevented its widespread adoption into clinical practice. The second problem with autologous plasmin-assisted vitrectomy was its inherent instability. Plasmin is rapidly autolyzed and inactivated via binding to alpha-2 antiplasmin [13]. This led some investigators to explore whether plasminogen activators such as tissue plasminogen activator (tPA) or urokinase (UK) could be used to facilitate vitreoreti-

nal separation. One problem with this approach, however, is that plasminogen is not normally found in high abundance within the vitreous cavity [13]. Therefore, the investigators needed to either induce blood–retinal barrier breakdown with cryopexy [20] to achieve high enough intraocular concentrations of plasminogen or they had to concurrently inject plasminogen with an activator molecule in order to induce a PVD [21]. While the results from these studies were promising in that the investigators were able to achieve PVDs, the imprecise dosing inherent in this technique prevented its routine clinical use.

Given the shortcomings associated with plasmin, investigators next turned to a recombinant molecule called ocriplasmin, which was already being tested for use in patients with stroke or peripheral artery disease. Ocriplasmin is nothing more than the active site of plasmin and had several advantages over its larger parent molecule. First, it was commercially available and made using recombinant techniques, which helped to ensure its sterility for injection into the eye. Second, it is much more stable than plasmin and could be stored in a buffered solution [13]. In the early 2000s, Gandorfer and coworkers teamed with ThromboGenics, a company that was manufacturing and testing ocriplasmin for use in patients with stroke, to evaluate whether ocriplasmin could be used to induce a PVD [22]. Similar to their studies with plasmin, the investigators were able to show a dose–response relationship for ocriplasmin-induced PVDs in human postmortem eyes [23]. Animal experiments were also successful and histological analysis of the retinas after ocriplasmin injection did not reveal any evidence of alterations to retinal structure [23]. Based on these promising results, ocriplasmin had accumulated enough inertia to enter clinical testing.

14.5   Clinical Trials

Completed and ongoing clinical trials of ocriplasmin are summarized in a 2014 review article by Song and Smiddy [24]. This section reviews the major clinical trials that paved the way for

Food and Drug Administration (FDA) approval of ocriplasmin for use in patients with FTMH or VMT.

The first clinical study of microplasmin (ocriplasmin) for intravitreous injection (MIVI) was a phase II safety study, but it also gave an early indication of efficacy [25]. In this study, 60 patients were divided evenly into six different cohorts that received varying doses of ocriplasmin (25–125 μg) and had varying levels of drug "incubation" prior to vitrectomy (1 h–7 days). All of the patients had VMT or a stage II or III FTMH of less than 6 months duration and were already scheduled for vitrectomy. The highest rate of PVD (25%) was seen in patients with the longest incubation period (7 days). There were no major safety concerns and thus further MIVI studies were undertaken.

The MIVI-IIt study was a randomized, sham-controlled trial that compared different doses of ocriplasmin (or sham injection) for patients with VMA [26]. The primary end point was release of VMA on day 28 postinjection. Sixty participants were randomized to either 75, 125, or 175 μg of ocriplasmin or control vehicle. At day 28 postinjection, one patient in the sham cohort (8%) exhibited resolution of VMA. The highest rate of VMA release was observed in the ocriplasmin group that received the 125-μg injection (11 patients or 44%).

The MIVI-III study was a phase II randomized, double-masked, placebo-controlled trial that combined aspects of the previous two MIVI studies [27]. Subjects were again divided into four groups (25 μg, 75 μg, 125 μg of ocriplasmin or placebo), but the injections were administered 1 week prior to planned PPV. The primary endpoint was total PVD as assessed at the time of surgery. In the placebo group, 10% of participants had a PVD at the time of surgery compared to 31% in the group that received the injection of 125 μg of ocriplasmin.

Based on the favorable results from these prior studies, two pivotal clinical trials were undertaken to determine whether ocriplasmin could be used to treat VMT or FTMH [28]. These came to be known as the MIVI-TRUST (traction release without surgical treatment) tri-

als. In both of these phase III, double-masked, multicenter, placebo-controlled trials, a total of 652 eyes with VMT and/or FTMH were randomized to either a 125 μg injection of ocriplasmin or placebo. The primary end point was resolution of VMT on day 28 postinjection. Secondary endpoints assessed at day 28 postinjection included change in best-corrected visual acuity (BCVA) and proportion of participants who either experienced a total PVD, avoided vitrectomy, or had their FTMH closed. At postinjection day 28, significantly more eyes in the ocriplasmin group experienced resolution of VMT (26.5%) compared to the eyes in the placebo group (10.1%). This effect was maintained through month 6 of the study. Likewise, at day 28, total PVD was noted more frequently in eyes that received ocriplasmin (13.4%) versus those that received placebo (3.7%), and FTMH closed more often in ocriplasmin-treated eyes (40.6%) compared to placebo-treated eyes (10.6%) (Fig. 14.1). After 6 months, significantly fewer patients had undergone vitrectomy in the ocriplasmin group relative to the placebo group (17.7% vs. 26.6%, respectively). Finally, BCVA improved at least three lines in 12.3% of eyes injected with ocriplasmin compared to 6.4% of eyes injected with placebo. The results of the MIVI-TRUST study paved the way for FDA approval of ocriplasmin in October 2012 for the treatment of symptomatic VMA [29]. It became commercially available first in the United States at the end of January 2013 and then in Europe in March 2013.

Provided that not all patients who receive ocriplasmin will have release of their VMT or closure of their FTMH, a key question that arose is whether PPV following ocriplasmin use would yield similar anatomic and functional outcomes compared to primary PPV. To answer this question, Greven and colleagues assessed 51 eyes that underwent ocriplasmin injection prior to PPV and compared their outcomes with 22 eyes with VMT or FTMH that had a primary PPV [30]. The investigators found that visual improvement was similar between the groups at 3 and 6 months after surgery. Furthermore, 100% of eyes in the PPV-only group and 98% of eyes in the ocriplas-

Fig. 14.1 (**a**) This patient had a stage II macular hole associated with vitreomacular traction and visual acuity of 20/150. (**b**) 1 month after a single intravitreal injection of ocriplasmin the hole had closed and visual acuity was 20/40
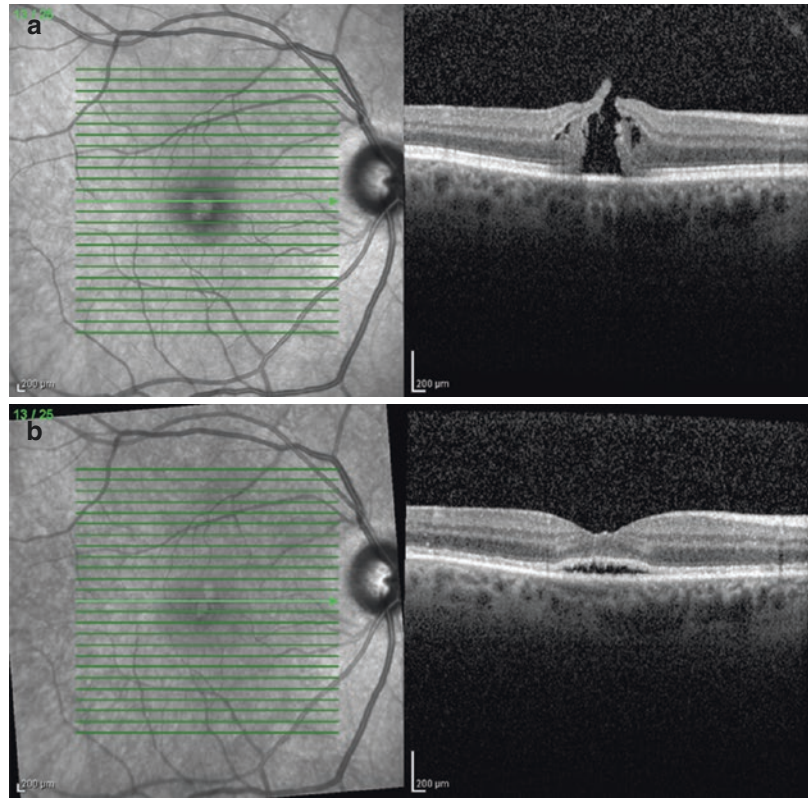
min–PPV group achieved release of VMT or closure of the FTMH, suggesting that eyes receiving ocriplasmin prior to PPV do just as well as eyes that undergo primary PPV for VMT or FTMH.

In addition to relieving VMT and closing FTMH, ocriplasmin may also be useful as a neoadjuvant to facilitate PVD induction during pediatric vitrectomy. A recent phase II clinical trial explored whether an intravitreal injection of 175 µg of ocriplasmin 30 or 60 min preoperatively was safe and effective compared to placebo for induction of PVD in pediatric patients scheduled for PPV [31]. The study included 24 eyes and excluded eyes with a history of ROP or significant media opacity. Among ocriplasmin-treated eyes, 50% (8/16) experienced a PVD either prior to vitrectomy or after suction was applied. Placebo-treated eyes showed a similar response rate, with 62.5% (5/8) meeting this end point [31]. One eye in the ocriplasmin group experienced lens subluxation. Although this study did not demonstrate an increased rate of PVD induction in response to ocriplasmin, the small sample size coupled with the heterogeneous nature of the complex pediatric vitreoretinal pathology precludes definitive conclusions regarding ocriplasmin efficacy during pediatric vitreoretinal surgery.

14.6 Identifying the Ideal Candidate for Enzymatic Vitreolysis

The MIVI-TRUST study identified several important patient-related factors that may contribute to successful resolution of VMT or closure of an FTMH after ocriplasmin injection. Additionally, post hoc analyses of the MIVI-TRUST data and meta-analyses of existing studies have been performed to ascertain which patients would be most likely to benefit from ocriplasmin injection.

In the MIVI-TRUST study, presence of an ERM or pseudophakic status was each associated with a lower likelihood of experiencing release of VMT [28]. Among all eyes treated with ocriplasmin, those with ERM exhibited resolution of VMT 8.7% of the time while 37.4% of eyes without an ERM had VMT release. This discrepancy was also noted in the placebo group, where resolution of VMT was noted in 1.5% of eyes with an ERM versus 14.3% of eyes without an ERM. Phakic eyes treated with ocriplasmin achieved VMT resolution in 34.2% of cases whereas pseudophakic eyes injected with ocriplasmin exhibited release of VMT in only 13.4% of cases.

Subsequent analyses of the data from the MIVI-TRUST study have revealed several important factors associated with successful release of VMT or closure of FTMH following ocriplasmin injection. In a post hoc subgroup analysis, Haller and colleagues showed that resolution of VMT 28 days post ocriplasmin injection was more frequent among patients less than 65 years old, eyes without ERM, phakic eyes, and eyes with focal VMT less than 1500 μm in diameter [32]. After 6 months, eyes with FTMH less than or equal to 250 μm in diameter were more likely to achieve closure following ocriplasmin injection (58.3%) than were eyes with FTMH greater than 250 μm in diameter (24.6%). A similar analysis by Dugel and colleagues also found that FTMH closure was more likely to occur on day 28 after ocriplasmin injection if the hole was less than 400 μm in diameter [33]. Among ocriplasmin-treated eyes at day 28 postinjection, they found that FTMH closed in 58.3% of eyes with FTMH ≤250 μm, 36.8% of eyes with holes between 250 and 400 μm in diameter, and zero eyes with FTMH >400 μm.

The anatomic success associated with either FTMH closure or release of VMT was shown to be associated with a concomitant improvement in visual acuity in another post hoc analysis of the MIVI-TRUST data. In this study by Gandorfer and colleagues, a substantial proportion of patients (42%) who achieved VMT resolution at day 28 exhibited at least a two-line gain in visual acuity at month 6 [34]. Similarly, 69% of patients whose FTMH closed by day 28 had at least a two-line gain in visual acuity by month 6. The patients treated with ocriplasmin also reported more satisfaction with their vision at month 6 compared to those treated with placebo as assessed by the National Eye Institute Visual Function Questionnaire [35].

A 2016 meta-analysis of ocriplasmin studies [36] reported results similar to those found in the post hoc analyses of the MIVI-TRUST data. Of the 194 abstracts that were screened, 19 eligible studies were included in the meta-analysis. Notably, age < 65 years, VMA diameter < 1500 μm, ERM absence, female gender, and phakic lens status were all associated with a higher rate of VMT resolution. Of these, VMA diameter < 1500 μm was the strongest predictor of VMT release. Regarding FTMH, size of the hole (<250 μm in diameter) was the only factor associated with an improved closure rate.

Taken together, the results of these studies suggest that the ideal ocriplasmin candidate is a young (<65 years old), phakic patient with symptomatic focal VMT (<1500 μm in diameter) who lacks an ERM. Patients with FTMH <250 μm are more likely to experience hole closure after ocriplasmin injection than are patients with larger diameter holes (Table 14.1).

14.7   Side Effects of Ocriplasmin

The pivotal MIVI-TRUST study provides insight into some of the side effects associated with intravitreal injection of ocriplasmin (Table 14.2)

Table 14.1 Patient factors that predict a favorable response to ocriplasmin use for either vitreomacular traction (VMT) or full-thickness macular hole (FTMH)

VMT	FTMH
• Phakic lens status	• Hole diameter < 250 μm
• Female gender • Age < 65 years • Vitreomacular adhesion < 1500 μm in diameter	
• Absence of epiretinal membrane	

Table 14.2 Summary of ocular AEs from the MIVI-TRUST [28] study that was significantly more likely to occur with ocriplasmin treatment than placebo

	Placebo (n = 187)	Ocriplasmin (n = 465)
Any ocular AE, n (%)	100 (53.5)	318 (68.4)
Visual impairment	3 (1.6)	25 (5.4)
Blurred vision	6 (3.2)	40 (8.6)
Injection-related eye pain	11 (5.9)	63 (13.5)
Vitreous floaters	14 (7.5)	78 (16.8)
Photopsias	5 (2.7)	55 (11.8)

[28]. Overall there were 318 adverse events (AEs) in the ocriplasmin treatment group (68.4%) versus 100 AEs in the placebo group (53.5%). Part of this discrepancy is due to the fact that eyes were randomized to ocriplasmin either 2:1 or 3:1, so many more eyes were injected with ocriplasmin than with vehicle alone. Nevertheless, a significantly higher percentage of ocriplasmin-treated eyes had AEs compared to placebo-treated eyes. Most of these AEs were associated with the visual phenomena that occur with PVD, such as vitreous floaters and photopsias, which were more common among eyes treated with ocriplasmin than those injected with placebo. Rates of retinal detachment and retinal tear were similar in the ocriplasmin and placebo groups. However, blurred vision was 2.7 times more likely to occur in ocriplasmin-treated eyes than in placebo-treated eyes, and visual impairment was likewise 3.4 times more likely to be experienced by those injected with ocriplasmin [28]. No cases of endophthalmitis were observed in any study eye.

After ocriplasmin gained FDA approval for the treatment of VMT in October 2012, retinal physicians began to notice that patients were experiencing side effects of the drug that were not typically associated with PVDs. In 2013, Freund and colleagues described a patient with an FTMH who was injected with ocriplasmin and subsequently developed worsening vision (from 20/100 at presentation to 20/400 1 week postinjection) [37]. Spectral-domain OCT (SD-OCT) revealed ellipsoid zone changes that were previously unrecognized. However, by 4 weeks postinjection, vision had improved to 20/50 and the ellipsoid zone changes on the SD-OCT had disappeared. Since this initial report, there have been numerous other case reports describing varying adverse effects following ocriplasmin injection, which some authors have described as acute ocriplasmin retinopathy [38]. Signs and symptoms of this condition may include reduction in visual acuity [37, 39–50], disruption of outer retinal signals on OCT [37, 39, 43–46, 48–53], emergence of subretinal fluid, [41, 42, 51, 53, 54] and reduced ERG responses [42, 49, 50, 54, 55].

In 2015, a more comprehensive review of the safety data from phase II and phase III studies of ocriplasmin was published [56]. The overall AE rate was comparable between placebo-treated patients (69.0%) and those injected with ocriplasmin (76.6%). Among the 1008 ocriplasmin-treated patients included in the analysis, nine experienced an acute, severe (greater than six line) transient decrease in vision that resolved in 100% of patients over a median time period of 2 weeks. Dyschromatopsia or changes in the ERG were reported in 18 patients or 1.8%. While these abnormalities usually resolved, a small number of patients (n = 4) had a persistently abnormal ERG with reduced a and b waves that persisted beyond postinjection month 6.

A comprehensive review of premarketing and post-marketing ocriplasmin safety data was published in 2015 and identified eight categories of adverse events associated with ocriplasmin use [57]. These included, "acute reduction in visual acuity attributable to either worsening macular pathology or development of subretinal fluid, electroretinogram changes, dyschromatopsia, retinal tears and detachments, lens subluxation and phacodonesis, impaired pupillary reflex, retinal vessel findings" and "ellipsoid zone (inner segment/outer segment) findings." The ellipsoid zone abnormalities were only reported in the post-marketing phase, which is due to the fact that the main ocriplasmin trials used time domain rather than spectral-domain OCTs for their analysis. Therefore, they likely did not have the image resolution necessary to appreciate the changes in the ellipsoid zone on OCT that was exhibited by a subset of eyes following ocriplasmin injection.

Among premarketing data, most patients who experienced a sudden decline in visual acuity recovered by month 6, although one patient had persistently decreased acuity despite resolution of VMA which persisted through postinjection month 6. In the post-marketing analysis, there were reports of 24 cases with profound vision loss (to at or below 20/200). Of these, 40% were reported to have resolved, 26% were ongoing, and 34% had an "unknown" resolution status.

14.8 Cost-Effectiveness Analysis

PPV has long been considered the gold standard treatment for patients with FTMH or VMT, and for good reason: it has a high success rate with relatively few complications [58]. However, some patients who are not good surgical candidates due to medical comorbidities or who prefer to avoid surgery may be better suited to therapy with an intravitreal injection that can be performed in the office. Ocriplasmin may be a viable alternative to surgery in such situations, but even after ocriplasmin injection, up to 20% of patients will still require PPV to ensure closure of an FTMH or release of VMT [59]. To obtain a better sense of the relative costs and benefits of primary PPV or ocriplasmin for the treatment of VMT or FTMH, Chang and colleagues performed a cost-effectiveness study that was published in 2014 [60]. Their models incorporated outcome data from important clinical studies for PPV [61] and ocriplasmin [28], and they obtained cost and reimbursement data from the Centers for Medicare and Medicaid Services (CMS). They found primary PPV to be more cost-effective than primary treatment with ocriplasmin. Specifically, in an ambulatory surgery center setting, primary PPV had an estimated cost per line of vision saved of 2368 dollars, whereas primary ocriplasmin injection carried a cost of 3666 dollars per line of vision saved.

Countries other than the United States have come to different conclusions about the relative cost-effectiveness of ocriplasmin. For example, the National Institute for Health and Care Excellence (NICE) guidelines, which inform practice patterns in the United Kingdom, state that ocriplasmin is cost-effective in patients with VMT who do not have an ERM or those with a stage II FTMH [62]. The Canadians drew similar conclusions regarding the use of ocriplasmin in special populations, and Spanish investigators have estimated that ocriplasmin use could save their national health service approximately one million Euros over 5 years [63].

14.9 Summary

The topography of the vitreomacular interface evolves over time, beginning with complete adherence between the vitreous and the retina in infancy and culminating in a complete PVD as the vitreous undergoes progressive liquefaction in later adulthood. Abnormal evolution of this process can lead to vitreoretinal disorders such as VMT and FTMH, resulting in decreased or distorted vision. These problems are commonly encountered by vitreoretinal surgeons and can be managed with observation, PPV, pharmacologic vitreolysis with ocriplasmin, or pneumatic vitreolysis.

Experiments performed on human cadaver eyes and animal eyes in the early 2000s demonstrated that plasmin was a promising agent that could be used to induce a PVD [17]. Due to the shortcomings of this larger molecule, such as rapid degradation and lack of commercial availability, attention was turned to recombinant ocriplasmin for use as a vitrectomy adjunct and to treat vitreoretinal disorders such as VMT and FTMH. In 2012, two phase III clinical trials demonstrated that intravitreal ocriplasmin was superior to intravitreal placebo in relieving VMT or closing FTMH <400 μm in diameter [28]. However, as more and more physicians began to use ocriplasmin after it achieved FDA approval in October 2012, it became apparent that the drug could cause severe vision loss that was, in most cases, transient in nature. Imaging with SD-OCT demonstrated changes in the ellipsoid zone following ocriplasmin injection, suggesting that its enzymatic activity was extending beyond the vit-

Table 14.3 Pros and cons of ocriplasmin use for VMT or FTMH

Pros	Cons
• Potential to avoid vitrectomy and all risks associated with surgery	• Some patients will still require vitrectomy despite treatment with ocriplasmin
• Less expensive than vitrectomy	• Long-term consequences of side effects unique to ocriplasmin such as visual loss, ERG changes, and EZ alterations are unknown
	• Less effective than vitrectomy for closing FTMH or relieving VMT

Abbreviations: *FTMH* full-thickness macular hole, *ERG* electroretinogram, *EZ* ellipsoid zone, *VMT* vitreomacular traction

reoretinal interface and into the retina itself [38]. While the vision loss and ellipsoid zone changes are usually transient, their long-term consequences on retinal structure and function have yet to be determined.

The decision to use ocriplasmin or proceed with PPV for patients with symptomatic VMA or FTMH is governed by multiple factors (Table 14.3). The cost of a single ocriplasmin dose is currently listed at $3950 [64]. In the MIVI-TRUST study, ocriplasmin had a 26.5% success rate in relieving symptomatic VMT and a 40.5% success rate of closing FTMH <400 μm in diameter [28]. The major therapeutic alternative to ocriplasmin, PPV, carries an estimated cost of $5800 (facility fee + professional fee) when performed at an ambulatory surgery center [60]. PPV is virtually always successful in relieving VMT and conservative estimates place the success rate for closure of FTMH following PPV at 76% [65]. Both ocriplasmin and PPV can have significant adverse effects; phakic patients who undergo PPV often develop visually significant cataracts within several years of their surgery. Endophthalmitis is a risk of both PPV and intravitreal injection of ocriplasmin. However, considering the risks of profound vision loss, ellipsoid zone changes, and ERG alterations associated with intravitreal ocriplasmin, its use is likely best reserved for patients who are both poor surgical candidates and ideal ocriplasmin

candidates. Characteristics that predict successful response to ocriplasmin include focal VMT less than 1500 μm in diameter, phakic lens status, lack of ERM, age < 65 years, and female gender [32, 36]. Patients with FTMH <250 μm in diameter are also much more likely to respond to ocriplasmin than are patients with larger holes. Patients with symptomatic VMA or FTMH who meet these criteria, understand the risks of intravitreal ocriplasmin, and who are unable to undergo vitrectomy would likely be good candidates for treatment with ocriplasmin.

The era of pharmacologic vitreolysis began with FDA approval of ocriplasmin in 2012. Without question, ocriplasmin has changed the vitreoretinal surgeon's approach to the patient with VMT or an FTMH. While ocriplasmin has been shown to be superior to placebo in treating patients with VMT or FTMH, its relatively low success rate compared to PPV precludes its use as a first-line therapy for all patients with VMT or FTMH. Moving forward, vitreolytic pharmacoagents will need to combine a low side effect profile with a very high success rate if they are to supplant PPV as the standard of care for patients with vitreomacular disorders.

Premarketing AEs associated with ocriplasmin also included ERG changes, dyschromatopsia, retinal tears and detachments, lens subluxation and phacodonesis, impaired pupillary reflex, and retinal vessel findings. Postmarketing AEs associated with ocriplasmin included all premarketing AEs plus EZ alterations on OCT [57]. Abbreviations: AEs, adverse events; ERG, electroretinogram; EZ, ellipsoid zone; MIVI-TRUST, microplasmin for intravitreous injection—traction release without surgical treatment; OCT, optical coherence tomography.

References

1. Stalmans P, Duker JS, Kaiser PK, Heier JS, Dugel PU, Gandorfer A, et al. Oct-based interpretation of the vitreomacular interface and indications for pharmacologic vitreolysis. Retina. 2013;33(10):2003–11.
2. Johnson MW. How should we release vitreomacular traction: surgically, pharmacologically, or pneumatically? Am J Ophthalmol. 2013;155(2):203–5. e1

3. Ophthalmology AAO. Fundamentals and principles of ophthalmology. Chalam KV, Ambati BK, Beaver HA, Grover S, Levine LM, Wells T, et al., editors. 2013.

4. Garcia-Layana A, Garcia-Arumi J, Ruiz-Moreno JM, Arias-Barquet L, Cabrera-Lopez F, Figueroa MS. A review of current management of vitreomacular traction and macular hole. J Ophthalmol. 2015;2015:809640.

5. Sebag J. Anatomy and pathology of the vitreo-retinal interface. Eye (Lond). 1992;6(Pt 6):541–52.

6. Steel DH, Lotery AJ. Idiopathic vitreomacular traction and macular hole: a comprehensive review of pathophysiology, diagnosis, and treatment. Eye (Lond). 2013;27(Suppl 1):S1–21.

7. Johnson MW. Perifoveal vitreous detachment and its macular complications. Trans Am Ophthalmol Soc. 2005;103:537–67.

8. Reichel E, Jaffe GJ, Sadda SR, Schuman S, Hariri AH, Skidmore K, et al. Prevalence of vitreomacular adhesion: an optical coherence tomography analysis in the retina clinic setting. Clin Ophthalmol. 2016;10:627–33.

9. Meuer SM, Myers CE, Klein BE, Swift MK, Huang Y, Gangaputra S, et al. The epidemiology of vitreoretinal interface abnormalities as detected by spectral-domain optical coherence tomography: the beaver dam eye study. Ophthalmology. 2015;122(4):787–95.

10. Flores-Moreno I, Arias-Barquet L, Vidal-Marti M, Munoz-Blanco A, Rubio-Caso MJ, Ruiz-Moreno JM, et al. The prevalence of vitreomacular interface pathology in a Spanish Tertiary Hospital. Ophthalmologica. 2016;235(3):179–83.

11. McCannel CA, Ensminger JL, Diehl NN, Hodge DN. Population-based incidence of macular holes. Ophthalmology. 2009;116(7):1366–9.

12. Coppe AM, Ripandelli G, Parisi V, Varano M, Stirpe M. Prevalence of asymptomatic macular holes in highly myopic eyes. Ophthalmology. 2005;112(12):2103–9.

13. Schneider EW, Johnson MW. Emerging nonsurgical methods for the treatment of vitreomacular adhesion: a review. Clin Ophthalmol. 2011;5:1151–65.

14. Verstraeten TC, Chapman C, Hartzer M, Winkler BS, Trese MT, Williams GA. Pharmacologic induction of posterior vitreous detachment in the rabbit. Arch Ophthalmol. 1993;111(6):849–54.

15. Hikichi T, Yanagiya N, Kado M, Akiba J, Yoshida A. Posterior vitreous detachment induced by injection of plasmin and sulfur hexafluoride in the rabbit vitreous. Retina. 1999;19(1):55–8.

16. Gandorfer A, Putz E, Welge-Lussen U, Gruterich M, Ulbig M, Kampik A. Ultrastructure of the vitreoretinal interface following plasmin assisted vitrectomy. Br J Ophthalmol. 2001;85(1):6–10.

17. Gandorfer A, Priglinger S, Schebitz K, Hoops J, Ulbig M, Ruckhofer J, et al. Vitreoretinal morphology of plasmin-treated human eyes. Am J Ophthalmol. 2002;133(1):156–9.

18. Li X, Shi X, Fan J. Posterior vitreous detachment with plasmin in the isolated human eye. Graefes Arch Clin Exp Ophthalmol. 2002;240(1):56–62.

19. Margherio AR, Margherio RR, Hartzer M, Trese MT, Williams GA, Ferrone PJ. Plasmin enzyme-assisted vitrectomy in traumatic pediatric macular holes. Ophthalmology. 1998;105(9):1617–20.

20. Hesse L, Nebeling B, Schroeder B, Heller G, Kroll P. Induction of posterior vitreous detachment in rabbits by intravitreal injection of tissue plasminogen activator following cryopexy. Exp Eye Res. 2000;70(1):31–9.

21. Unal M, Peyman GA. The efficacy of plasminogen-urokinase combination in inducing posterior vitreous detachment. Retina. 2000;20(1):69–75.

22. Gandorfer A. Microplasmin-assisted vitrectomy. Dev Ophthalmol. 2009;44:26–30.

23. Gandorfer A, Rohleder M, Sethi C, Eckle D, Welge-Lussen U, Kampik A, et al. Posterior vitreous detachment induced by microplasmin. Invest Ophthalmol Vis Sci. 2004;45(2):641–7.

24. Song SJ, Smiddy WE. Ocriplasmin for symptomatic vitreomacular adhesion: an evidence-based review of its potential. Core Evid. 2014;9:51–9.

25. de Smet MD, Gandorfer A, Stalmans P, Veckeneer M, Feron E, Pakola S, et al. Microplasmin intravitreal administration in patients with vitreomacular traction scheduled for vitrectomy: the MIVI I trial. Ophthalmology. 2009;116(7):1349–55, 55 e1–2

26. Stalmans P, Delaey C, de Smet MD, van Dijkman E, Pakola S. Intravitreal injection of microplasmin for treatment of vitreomacular adhesion: results of a prospective, randomized, sham-controlled phase II trial (the MIVI-IIT trial). Retina. 2010;30(7):1122–7.

27. Benz MS, Packo KH, Gonzalez V, Pakola S, Bezner D, Haller JA, et al. A placebo-controlled trial of microplasmin intravitreous injection to facilitate posterior vitreous detachment before vitrectomy. Ophthalmology. 2010;117(4):791–7.

28. Stalmans P, Benz MS, Gandorfer A, Kampik A, Girach A, Pakola S, et al. Enzymatic vitreolysis with ocriplasmin for vitreomacular traction and macular holes. N Engl J Med. 2012;367(7):606–15.

29. Weng CY, Fortun JA, Carvounis PE, Albini TA. Ocriplasmin and its role in the management of vitreoretinal interface disorders. Int Ophthalmol Clin. 2014;54(2):29–38.

30. Greven MA, Garg S, Chiu B, Shah SP, Wolfe J, Fine HF, et al. Vitrectomy after ocriplasmin for VitreOmacular adhesion or Macular hole (VAVOOM) study. Br J Ophthalmol. 2016;100(9):1211–5.

31. Drenser K, Girach A, Capone A Jr. A randomized, placebo-controlled study of intravitreal ocriplasmin in pediatric patients scheduled for vitrectomy. Retina. 2016;36(3):565–75.

32. Haller JA, Stalmans P, Benz MS, Gandorfer A, Pakola SJ, Girach A, et al. Efficacy of intravitreal ocriplasmin for treatment of vitreomacular adhesion: subgroup analyses from two randomized trials. Ophthalmology. 2015;122(1):117–22.

33. Dugel PU, Regillo C, Eliott D. Characterization of anatomic and visual function outcomes in patients with full-thickness macular hole in ocriplasmin phase 3 trials. Am J Ophthalmol. 2015;160(1):94–9. e1

34. Gandorfer A, Benz MS, Haller JA, Stalmans P, Pakola SJ, Girach A, et al. Association between anatomical resolution and functional outcomes in the MIVI-trust studies using ocriplasmin to treat symptomatic vitreomacular adhesion/vitreomacular traction, including when associated with macular hole. Retina. 2015;35(6):1151–7.

35. Varma R, Haller JA, Kaiser PK. Improvement in patient-reported visual function after ocriplasmin for vitreomacular adhesion: results of the microplasmin for intravitreous injection-traction release without surgical treatment (MIVI-TRUST) trials. JAMA Ophthalmol. 2015;133(9):997–1004.

36. Chatziralli I, Theodossiadis G, Xanthopoulou P, Miligkos M, Sivaprasad S, Theodossiadis P. Ocriplasmin use for vitreomacular traction and macular hole: a meta-analysis and comprehensive review on predictive factors for vitreous release and potential complications. Graefes Arch Clin Exp Ophthalmol. 2016;254:1247.

37. Freund KB, Shah SA, Shah VP. Correlation of transient vision loss with outer retinal disruption following intravitreal ocriplasmin. Eye (Lond). 2013;27(6):773–4.

38. Johnson MW, Fahim AT, Rao RC. Acute ocriplasmin retinopathy. Retina. 2015;35(6):1055–8.

39. Neffendorf JE, Lim LT, Gout II, El-Amir A. Widespread macular neurosensory detachment after ocriplasmin intravitreal injection. Retin Cases Brief Rep. 2016;10(4):354–6.

40. Gomez-Ulla F, Bande MF, Abraldes M. Acute loss of vision after an intravitreal injection ocriplasmin: a functional evolutionary study for 1-year follow-up. Doc Ophthalmol. 2015;131(3):231–5.

41. Luttrull JK. Chronic serous macular detachments and visual disturbance complicating consecutive cases of symptomatic vitreomacular adhesion with macular hole treated with ocriplasmin. Ophthalmic Surg Lasers Imaging Retina. 2015;46(9):976–8.

42. Hale BP, Au AK, Falk NS, Bhatnagar P, Beer PM. Flat electroretinography and acute visual loss after ocriplasmin injection for vitreomacular adhesion complicating macular schisis. Ophthalmic Surg Lasers Imaging Retina. 2015;46(8):888–92.

43. Quezada-Ruiz C, Pieramici DJ, Nasir M, Rabena M, Steinle N, Castellarin AA, et al. Outer retina reflectivity changes on sd-oct after intravitreal ocriplasmin for vitreomacular traction and macular hole. Retina. 2015;35(6):1144–50.

44. Quezada Ruiz C, Pieramici DJ, Nasir M, Rabena M, Avery RL. Severe acute vision loss, dyschromatopsia, and changes in the ellipsoid zone on sd-oct associated with intravitreal ocriplasmin injection. Retin Cases Brief Rep. 2015;9(2):145–8.

45. Reiss B, Smithen L, Mansour S. Transient vision loss after ocriplasmin injection. Retina. 2015;35(6):1107–10.

46. Reiss B, Smithen L, Mansour S. Acute vision loss after ocriplasmin use. Retin Cases Brief Rep. 2015;9(2):168–9.

47. DaCosta J, Younis S. Transient visual loss and delayed resolution of vitreomacular traction after intravitreal ocriplasmin. Drug Healthc Patient Saf. 2014;6:175–8.

48. Thanos A, Hernandez-Siman J, Marra KV, Arroyo JG. Reversible vision loss and outer retinal abnormalities after intravitreal ocriplasmin injection. Retin Cases Brief Rep. 2014;8(4):330–2.

49. Tibbetts MD, Reichel E, Witkin AJ. Vision loss after intravitreal ocriplasmin: correlation of spectral-domain optical coherence tomography and electroretinography. JAMA Ophthalmol. 2014;132(4):487–90.

50. Fahim AT, Khan NW, Johnson MW. Acute panretinal structural and functional abnormalities after intravitreous ocriplasmin injection. JAMA Ophthalmol. 2014;132(4):484–6.

51. Nudleman E, Franklin MS, Wolfe JD, Williams GA, Ruby AJ. Resolution of subretinal fluid and outer retinal changes in patients treated with ocriplasmin. Retina. 2016;36(4):738–43.

52. Barteselli G, Carini E, Invernizzi A, Ratiglia R, Viola F. Early panretinal abnormalities on fundus autofluorescence and spectral domain optical coherence tomography after intravitreal ocriplasmin. Acta Ophthalmol. 2016;94(2):e160–2.

53. Singh RP, Li A, Bedi R, Srivastava S, Sears JE, Ehlers JP, et al. Anatomical and visual outcomes following ocriplasmin treatment for symptomatic vitreomacular traction syndrome. Br J Ophthalmol. 2014;98(3):356–60.

54. Margo JA, Schocket LS, Klima K, Johnson MA. Persistent retinal changes after intravitreal ocriplasmin. Retin Cases Brief Rep. 2016;10(1):48–51.

55. Small KW, Shaya FS, La Fontaine M. Post-market experience with ocriplasmin including chronic electrophysiologic changes. Ophthalmic Surg Lasers Imaging Retina. 2015;46(9):956–62.

56. Kaiser PK, Kampik A, Kuppermann BD, Girach A, Rizzo S, Sergott RC. Safety profile of ocriplasmin for the pharmacologic treatment of symptomatic vitreomacular adhesion/traction. Retina. 2015;35(6):1111–27.

57. Hahn P, Chung MM, Flynn HW Jr, Huang SS, Kim JE, Mahmoud TH, et al. Safety profile of ocriplasmin for symptomatic vitreomacular adhesion: a comprehensive analysis of premarketing and postmarketing experiences. Retina. 2015;35(6):1128–34.

58. Park DW, Sipperley JO, Sneed SR, Dugel PU, Jacobsen J. Macular hole surgery with internal-limiting membrane peeling and intravitreous air. Ophthalmology. 1999;106(7):1392–7. discussion 7-8

59. Neffendorf JE, Kirthi V, Pringle E, Jackson TL. Ocriplasmin for symptomatic vitreomacular adhesion. Cochrane Database Syst Rev. 2017;10:CD011874.

60. Chang JS, Smiddy WE. Cost evaluation of surgical and pharmaceutical options in treatment for vitreomacular adhesions and macular holes. Ophthalmology. 2014;121(9):1720–6.

61. Spiteri Cornish K, Lois N, Scott NW, Burr J, Cook J, Boachie C, et al. Vitrectomy with internal limiting membrane peeling versus no peeling for idiopathic full-thickness macular hole. Ophthalmology. 2014;121(3):649–55.

62. Amoaku W, Cackett P, Tyagi A, Mahmood U, Nosek J, Mennie G, et al. Redesigning services for the management of vitreomacular traction and macular hole. Eye (Lond). 2014;28(Suppl 1):S1–10.

63. Garcia-Perez L, Abreu-Gonzalez R, Perez-Ramos J, Garcia-Perez S, Serrano-Aguilar P. Review of economic studies and budget impact analysis of ocriplasmin as a treatment of vitreomacular traction. Arch Soc Esp Oftalmol. 2016;91(6):257–64.

64. Ocriplasmin (Jetrea) (125 mcg Intravitreal Injection): for the treatment of symptomatic vitreomacular adhesion. CADTH Common Drug Reviews. Ottawa (ON). 2014.

65. Parravano M, Giansanti F, Eandi CM, Yap YC, Rizzo S, Virgili G. Vitrectomy for idiopathic macular hole. Cochrane Database Syst Rev. 2015;5:CD009080.

Part IV

Epiretinal Membrane and Macular Hole

Epiretinal Membrane Management

15

Rohit Goud Nallamasa and Jay Chhablani

15.1 Introduction

Epiretinal membrane (ERM) is also called macular pucker, cellophane maculopathy and surface wrinkling retinopathy. The mechanism of the formation of ERM is tissue damage and subsequent repair. Most of the patients are asymptomatic and have near-normal vision. If symptomatic, patients complain of metamorphopsia, diplopia and a decrease in vision. The cause for a decrease in vision is macular oedema, thick ERM at the fovea, full-thickness retinal fold, tabletop traction at the fovea and foveal ectopia caused by the ERM and stasis of axoplasmic flow (due to traction) [1–3].

15.1.1 Types of ERM

1. Idiopathic/primary—there is no antecedent ocular conditions or surgical procedures for the ERM formation.

2. Secondary—usually associated with other ocular conditions (diabetic retinopathy, retinal vein occlusions), post intraocular surgery, trauma.

15.1.2 Grades of ERM

Donald Gass had classified ERMs as

- Grade 0: Cellophane maculopathy (Fig. 15.1)
- Grade 1: Crinkled cellophane maculopathy (Fig. 15.2a, b)
- Grade 2: Macular pucker (Fig. 15.3a, b) [4]

Fig. 15.1 Left eye fundus photo of a 47-year-old male patient who was asymptomatic. On fundus evaluation, there was a fine membrane (arrow) with glistening light reflex with no retinal folds

R. G. Nallamasa
L V Prasad Eye Institute,
Visakhapatnam, Andhra Pradesh, India

Department of Ophthalmology, University of
Pittsburgh Medical Center, Pittsburgh, PA, USA

J. Chhablani (✉)
Department of Ophthalmology, University of
Pittsburgh Medical Center, Pittsburgh, PA, USA
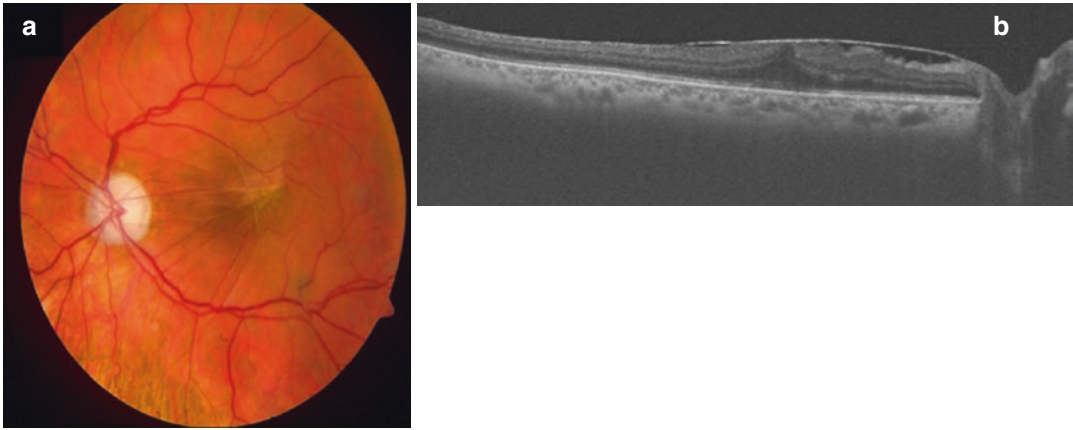
Fig. 15.2 Left eye fundus photo (**a**) of a 56-year-old male patient who was complaining of metamorphopsia and had visual acuity of 20/40. Fundus examination revealed an irregular light reflex, irregular and tortuous vessels at the macula and the temporal half of the epireti-nal membrane is opaque. Optical coherence tomography image (**b**) of the same patient showing epiretinal membrane with altered foveal contour and inner retinal folds nasal to the fovea
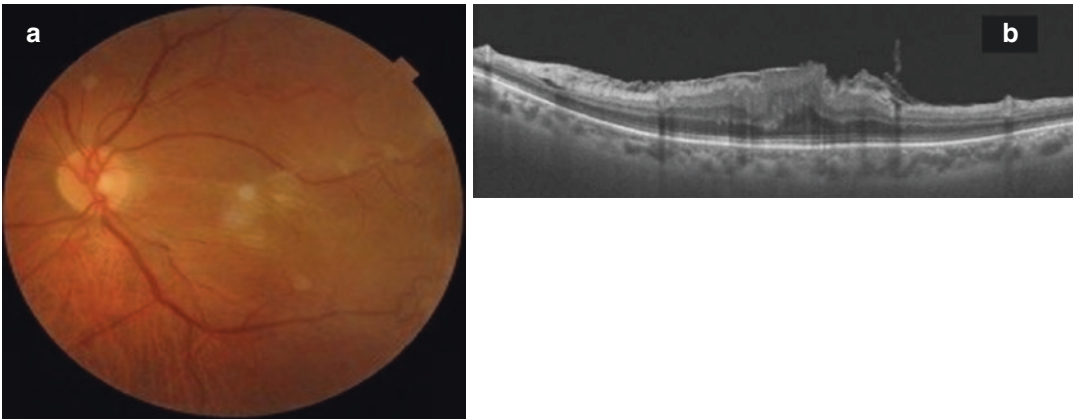
Fig. 15.3 Left eye fundus photo (**a**) of a 61-year-old female who was complaining of gross metamorphopsia and had visual acuity of 20/100, with thick ERM at macula with retinal folds. Optical coherence tomography image (**b**) showing distorted foveal contour with an epiretinal membrane, disorganised inner retinal folds at the fovea and normal outer retinal layers

Govetto et al. classified ERM on OCT

- Stage 1: The presence of foveal pit with well-defined retinal layers
- Stage 2: An absence of foveal pit with well-defined retinal layers
- Stage 3: An absence of foveal pit with well-defined retinal layers and the presence of ectopic inner foveal layers
- Stage 4: An absence of foveal pit with disrupted retinal layers and the presence of ectopic inner foveal layers [5]

15.1.3 Indications for Surgery

With the advancement of surgical instrumentation, the visual acuity threshold has reduced from 20/200 to 20/40. Most of the surgeons feel that

visual acuity 20/60 or worse is ideal for taking the patient for surgery but can intervene for surgery in patients with better vision if the patient is symptomatic (diplopia, metamorphopsia causing distress at work).

The surgeon should rule out the other causes for the decrease in vision like macular scar following trauma, choroidal neovascular membrane, macular hole, parafoveal telangiectasia and retinal vein occlusion (macular ischemia) before taking the patient for surgery.

Patients with poor visual acuity before surgery have poor visual gain after the surgery compared to those who had good visual acuity to start with. The thickness of ERM is also an important factor for determining the final visual outcome. Thin ERMs have good outcomes compared to the thick ones. Idiopathic ERMs usually take a much longer time for the patient to present with symptoms, it would be ideal to plan for surgery when there is marked reduction in vision [6–12].

Before the surgery, there should be a detailed counselling about the risks and benefits of the surgery with the patient. Documentation of visual change, change in distortion and progression on OCT (optical coherence tomography) scans are some of the preoperative requisites before ERM surgery. Correlation of clinical and imaging findings with the extent of ERM is very important before a surgical decision for ERM removal especially in eyes with good visual acuity. Cataract grading is important and the decision of combined procedure with cataract surgery needs to be discussed.

15.1.4 Surgical Procedure

Machemer developed the concept of membrane peeling in 1972 soon after he introduced vitrectomy. Originally, peeling was performed with a bent needle. O'Malley subsequently developed the concept of using a rounded, angulated instrument he called a pick to perform the peeling.

Detailed preoperative analysis of OCT high-definition scan as well as 3D volume scans helps to understand the extent of the membrane, vitreo-retinal interface relationship and also in planning the start of dissection.

Intraoperative, the centre of the membrane can be identified by visualising the direction of radial striae, the point of maximum elevation of the retina, the opaquest area in the membrane and relative movement of the membrane with respect to the retina during the sideward movement of the forceps. Vitrectomy, preferably 25 G vitrectomy (valve) should be used, as the intraocular pressure during the surgery is well controlled. Most of the surgeons prefer complete vitrectomy, but few authors did show leaving behind the anterior vitreous can be protective against the cataract progression.

Majority of idiopathic ERMs have a preexisting posterior vitreous detachment (PVD), in case the PVD is absent, PVD induction should be started from the disc with a high vacuum (depending on the gauge used for the vitrectomy) and move anteriorly under controlled retraction of the cutter. Intravitreal triamcinolone can aid in identifying the residual cortical vitreous and ensuring complete PVD. Previously a slit in the apparent centre of the ERM was made using the microvitreoretinal (MVR) blade or a sharp-tipped pic was used, this is not necessary with the Alcon 20-gauge or 25-gauge DSP forceps. [13, 14]

Visualisation with dyes—Indocyanine green (ICG), Trypan blue and Brilliant blue G (BBG) during vitrectomy has facilitated visualisation and peeling of the internal limiting membrane (ILM). ICG doesn't stain the ERM but stains the ILM, thereby peeling the ILM can confirm the complete ERM removal. Trypan blue and BBG stain both ILM and ERM. Double BBG staining assures the complete removal of ILM. [15, 16]

The raised end of the membrane is grasped with the forceps and peeling should be started in a centripetal fashion. Multiple peels and release method should be done while moving close to the fovea, to prevent inadvertent damage to the fovea. When close to the fovea the surgeon should always observe the fovea during the peeling process rather than focusing on the forceps to prevent tearing of fovea. Areas of stronger attachments to the ILM can be detected by noting fine fibres being lifted from the retinal surface

during the peeling process. After peeling the epiretinal membrane if striae are still prominent then ILM peeling with the 25-gauge DSP forceps should be performed to ensure complete ERM removal. Thin ERMs usually shred while peeling, for which it might require to restart the dissection of the membrane. The endpoint of membrane peeling is still debatable, but most of the surgeons feel that it should be done in the area between the arcades.

At the end of the surgery, it is important to look for any peripheral breaks or tears to prevent retinal detachment before the fluid air exchange. In case a break/tear is noted, laser or cryopexy should be done to prevent retinal detachment. Sclerotomies if leaking should be sutured with 7–0 or 8–0 absorbable sutures [17–21].

15.1.5 Post-op Recovery

ERM removal surgery does not require any post-surgery positioning unless an intraoperative complication has occurred. The macular fold starts unfolding from the post-operative day 1, but for a few cases, the folds tend to remain even after the ERM removal. Post-surgery visual recovery is usually slow. As previously mentioned, the pre-operative vision plays a major role in final visual acuity.

Natural course—Idiopathic ERMs tend to become stable after the initial growth and contraction. There are chances of spontaneous separation of ERM following PVD, which may result in improvement in vision.

Role of internal limiting membrane peel—Internal limiting membrane consists of the basement membrane of the Muller cells, composed of collagen fibres, glycosamine glycans, laminin and fibronectin. During embryogenesis, ILM plays an important role in the survival of retinal ganglion cells [22, 23]. ILM peel in ERM removal surgeries remains controversial. The removal of ILM should be considered in tractional maculopathies. Removal of ILM confirms the complete removal of the ERM. Ripandelli et al. had shown that mean retinal sensitivity in ILM not peeling group was earlier and better

than compared to the ILM peeling group, although there was no harmful effect on the final visual acuity. ILM peeling can cause nerve fibre layer damage, retinal oedema, retinal haemorrhage, electrophysiological changes and visual field changes [24].

15.1.6 Complications

Retinal tears—These can be posterior or anterior. Posterior tears are due to poor visualisation of the membranes or can be a result of aggressive multiple attempts to peel the membrane during surgery. These can be managed with or without laser, fluid–gas exchange and post-operative positioning. The anterior breaks can occur while moving the instruments in and out of the eye while stripping the vitreous from the base or during peripheral vitrectomy when the peripheral retina is cut. These need cryopexy or laser with a tamponade (gas/silicone oil if associated with retinal detachment).

Rhegmatogenous retinal detachment—This could primarily be due to overlooked retinal breaks or tears intraoperative, which could lead to a retinal detachment in the early post-operative period. In the late post-operative period, it could be due to the contraction of the uncut vitreous that gets incarcerated into the sclerotomies.

Cataract—It is the most common complication noted post-ERM removal surgery in phakic eyes. The type of cataract is usually nuclear sclerosis and the colour is subtle, greyish-green. A posterior subcapsular cataract is rare unless a lens touch might have occurred intraoperatively. Grading of cataract preoperative is very important and plan for combined cataract extraction with intraocular lens implantation with vitrectomy if there is a visually significant cataract. The visual gain post-ERM removal surgery is seen up to 6–9 months, then a gradual decrease in vision is noted as the progression of cataract, which warrants a cataract surgery for better vision.

Recurrence of ERM—This can occur in 0–5% of cases. Recurrent ERMs are usually thin and are not visually significant.

15.1.6.1 Other

Retinal toxicity—Phototoxicity could be due to endoilluminator or microscope illumination. Dye-related toxicity (ICG or sometimes BBG) can cause retinal pigment epithelium damage and visual field defects.

Cystoids macular oedema—The postoperative macular oedema thickness following ERM removal is known to affect the final visual outcome. A post-operative steroid injection can be considered for recurrent or persistent oedema. However, in regard to the use of there is a mixed opinion for the use of intraocular steroids at the end of the procedure for the reduction of the central macular thickness (CMT) and improving the final visual acuity, as controversial opinions still exists. There are studies that showed no difference in the final visual outcome with IVTA. Yonahawa et al. had used IVTA and intravitreal dexamethasone implant in ERM removal surgery, and at the end of 6 months found that there was an improvement in visual acuity and CMT, which were comparable in both the groups [25–27]. Overall, an early recovery of the foveal contour can be achieved by adding steroid at the end of the surgery, however, the final visual outcome does not change in the long term.

15.1.6.2 Endophthalmitis

Differential Diagnosis of ERM
Congenital hypertrophy of retina and retinal pigment epithelium (CHRRPE)—CHRRPE is a rare benign ocular tumour of the eye. It was first reported by Gass in 1973. On histology, the lesion has a disorganised amalgamation of retinal, glial, vascular and RPE cells. A most common location is peripapillary, macular and peripheral lesions. CHRRPE is diagnosed mainly by the clinical presentation, it has intralesional corkscrew vessels, retinal traction and ERM. OCT shows ERM with traction on the retinal layers that can involve all the layers of the retina. OCT angiography shows the distortion of retinal microvasculature within the lesion. Visual disturbance in these patients is due to the traction on the fovea or presence of subretinal fluid [28].

Tractional retinal detachment—Chronic tractional retinal detachment can be differentiated from uncomplicated ERM, with the presence of retinal haemorrhages and hard exudates.

15.1.7 Prognosticating Factors

Previous studies have shown that age, preoperative vision, duration of symptoms, OCT features and fundus autofluorescence help in determining the final visual outcome after visual outcome.

OCT—In addition to central macular thickness CMT, other features that are of clinical importance for predicting the final visual outcome post-surgery are IS/OS integrity and COST line (cone outer segment tips) integrity. The preoperative integrity of IS/OS determines the severity of metamorphopsia post-surgery, if the preoperative disruption was noted on the OCT, post-operative visual acuity was worse, compared to the intact group. COST line is also known as the Verhoeff membrane and is seen as a hyper-reflective line between the IS/OS junction and the RPE. Disruption of the COST line has shown to have poor visual acuity after surgery. The preoperative foveal contour, presence or absence of intraretinal cysts or macular pseudohole on OCT did not show any significant importance of the final visual outcome (Fig. 15.4a–d). Post-operative, due to ILM peeling, ganglion cell—inner plexiform complex thinning has been reported, which can explain poor retinal sensitivity on microperimetry or multifocal electroretinography [29–34]. Gradual recovery of foveal contour should be explained and needs to be followed up using OCT (Fig. 15.5).

Fundus auto fluorescence (FAF)—Normal FAF at the fovea is usually hypo autofluorescent. The pre- and post-operative analysis of the hypo AF area at the macula, when there was an increase in the hypo AF area involving the fovea and parafoveal area had poor visual acuity gain post-surgery [35].

Microperimetry—It gives the information on the foveal fixations and macular sensitivity and depth of central macular defects. Microperimetry can help in assessing the final visual outcome in
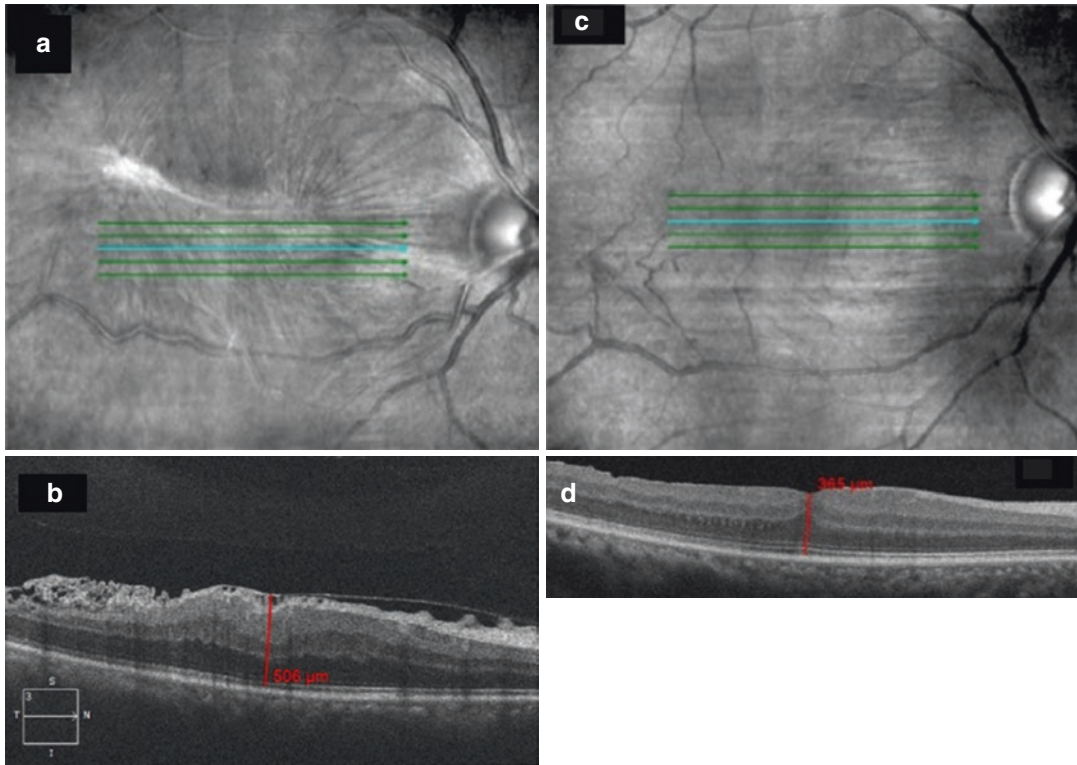
Fig. 15.4 (**a**) Right eye images of 53-year-old male patient who had a preoperative best-corrected visual acuity (BCVA) of 20/100. Red-free image showing retinal folds at the macula (**a**). Optical coherence tomography (**b**) (OCT) showed epiretinal membrane (ERM) with disorganised inner retinal layers, with focal attachments and fibrillations with an increased macular thickness (506 µm). At 1-month post-ERM removal surgery his BCVA improved to 20/40. At 1 month post-operative follow-up, red-free image (**c**) showed no retinal folds at the macula with corresponding OCT (**d**) showing minimal distorted foveal contour decrease in retinal oedema

a patient. Maarco et al. had conducted a study to find the changes in microperimetry readings preoperative and post-operative in idiopathic ERMs, and it was noted that there was an improvement in central 10° analysed area after surgery. Also, in this study, it was noted that the mean sensitivity and mean defect increased from 1 and 4 years follow-up period, illustrating significant dissociation between best-corrected visual acuity and retinal sensitivity. Ripandelli et al. had shown that the increase in micro scotomas in the macular area was more in the ILM peeling group compared to the ILM not peeling group.

Multifocal ERG (mfERG)—Kim et al. had shown that implicit time delay at baseline was a poor prognosticating factor. Terasaki et al. showed b-wave abnormalities after ILM peeling in their multifocal macular electroretinography study, suggesting that these findings are suggestive of the Müller cell damage [36].

Fluorescein angiography (FA)—FA could be useful in eyes with secondary ERMs to diagnose primary pathology and to evaluate foveal perfusion.

Multicolour imaging helps to visualise the early ERMs and demonstrates the extent of involvement (Fig. 15.6).

15.2 Recent Advances

15.2.1 Heads-Up Display

Heads-up display (HUD) is not new in the medical field. It had been used in neurosurgery and cardiopulmonary surgeries. It had been intro-
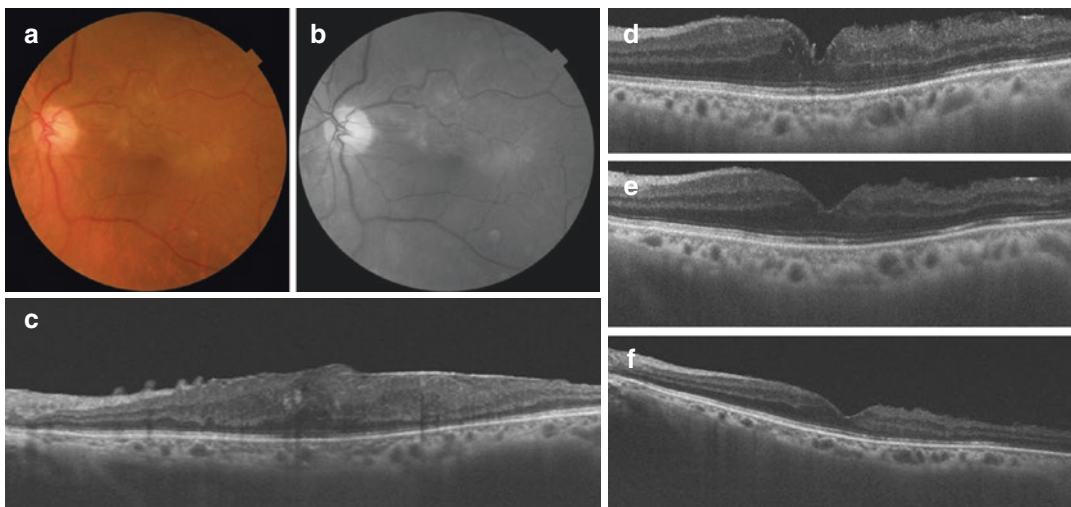
Fig. 15.5 A 72-year-old female complaints of DOV for 1 year in LE Her BCVA was 20/200 in LE (**a**) Colour fundus photo of LE showing greyish-white membrane at macula extending up to superior temporal arcade. (**b**) Red free image of LE showing distorted retinal vessels with a white reflection of membrane superior temporal. (**c**) Oct image of left eye showing epiretinal membrane with altered foveal contour, disorganised inner retinal layers with some amount retinal oedema. (**d**) 1-month post-ERM removal surgery BCVA in LE improved to 20/50, inner retinal architecture started to reappear. (**e**) At 6 months post-surgery still, some amount of macular oedema was noted with some amount of alteration in inner layer architecture temporal to the fovea. (**f**) 1-year post-surgery final BCVA was 20/30 with inner retinal layers returning to normal nasal to the fovea with few undulations temporal
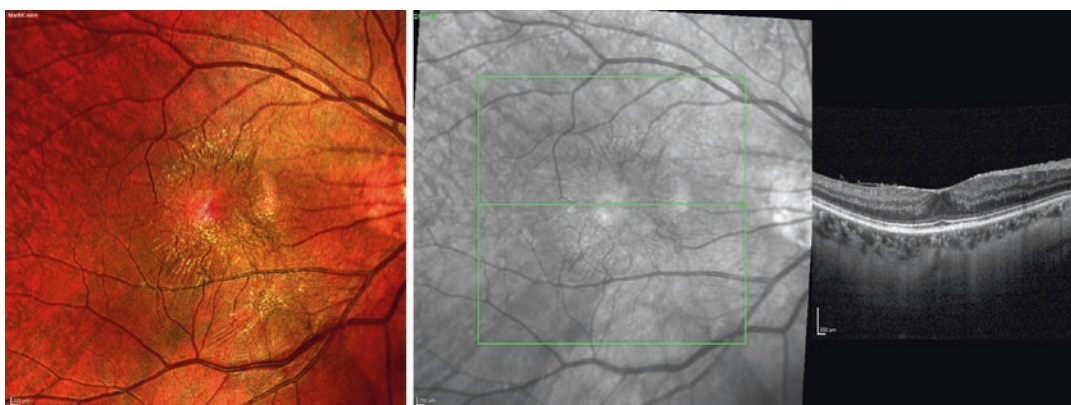
Fig. 15.6 A case of early epiretinal membrane (ERM) showing easy identification of ERM on multicolour imaging

duced in the field of ophthalmology recently. This enables surgeons to perform surgery by looking at OLED screen and wearing polarised 3D glasses [37, 38].

The surgeon screen distance should be minimum, approximately 3–4 feet, so that it enhances the depth of perception. Reduction of endoillumination as low as 10% with signal amplification and 3D HUD will reduce the risk of phototoxic-ity. With this new tool for macular surgeon high dynamic range (HDR), high magnification and frequent software update, it will be interesting to see if ILM peel would be possible with lower dye concentrations, thereby reducing the dye related toxicity on the retina. There are different filters in the system, with a blue filter on the peripheral vit-reous can be used to visualise better for complet-ing the vitrectomy. The yellow filter helps to

Fig. 15.7 Figure shows a screenshot during surgical removal of epiretinal membrane showing the intraoperative OCT
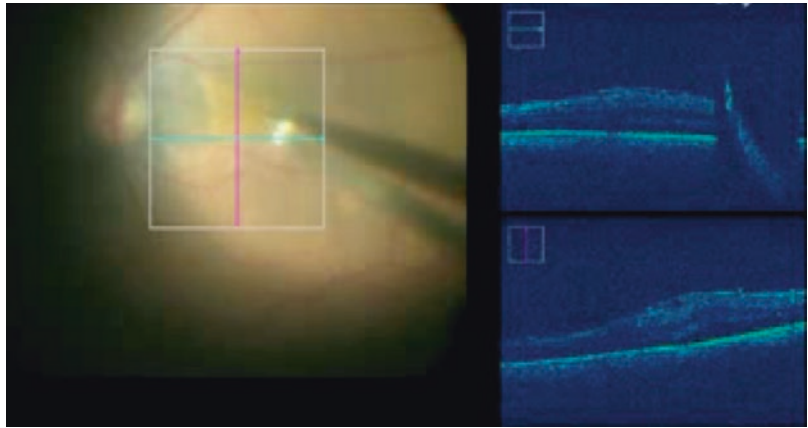
reduce the glare after the fluid–air exchange is done. The red-free filter has been noticed to help the digital suppression of haemorrhage in the vitreous cavity rephrase. Berrocal et al. had reported that the green channels in the system help in better visualisation of ERM during its removal. The added advantage being the magnification and HDR enables the surgeon to perform macular surgeries with the wide-field lens, instead of shifting to the macular lens for surgery [22, 39].

The advantages of HUD over the standard operating microscope (SOM) are better ergonomics, digital image processing and better visualisation that will reduce eye strain for the operating surgeon. Romano et al. had compared HUD and SOM and rated the subjective operating surgeon satisfaction (comfort, depth perception and teaching) higher with 3D HUD. Katherine et al. have reported less satisfaction and macular peel time was higher on 3D HUD compared to SOM, although the clinical outcomes were comparable in both the groups [40–42].

15.2.2 Intraoperative OCT

Intraoperative OCT to the standard operating microscope helps in a macular hole, ERM removal and rhegmatogenous retinal detachment surgery. This feature helps in identifying intraoperative changes on the retina that could not be picked up with the routine surgical procedure (Fig. 15.7). Renato et al. feel that incorporating this feature on to the heads-up system would have an added feature [40, 43–45].

References

1. Shea M. The surgical management of macular pucker. Can J Ophthalmol. 1979;2:110.
2. Wilkinson CP. Recurrent macular pucker. Am J Ophthalmol. 1979;88:1029.
3. Machemer R. A new concept for vitreous surgery: two instrument techniques in pars plana vitrectomy. Arch Ophthalmol. 1974;92:407–41.
4. Gass JDM. Macular dysfunction caused by epiretinal membrane contraction. In: Stereoscopic atlas of macular diseases: diagnosis and treatment, vol. 2. 4th ed. St. Louis, MO: Mosby; 1997. p. 938–50.
5. Govetto A, Lalane RA 3rd, Sarraf D, Figueroa MS, Hubschman JP. Insights into epiretinal membranes: presence of ectopic inner foveal layers and a new optical coherence tomography staging scheme. Am J Ophthalmol. 2017;175:99–113. https://doi.org/10.1016/j.ajo.2016.12.006.
6. Trese MT, Chandler DB, Machemer R. Macular pucker: prognostic criteria. Graefes Arch Clin Exp Ophthalmol. 1983;221:12–5.
7. Margherio RR, Cox MS, Trese MT, et al. Removal of epimacular membranes. Ophthalmology. 1985;92:1075–83.
8. McDonald HR, Verre WP, Aaberg TM. Surgical management of idiopathic epiretinal membranes. Ophthalmology. 1986;93:978–83.
9. de Bustros S, Thompson JT, Michels G, et al. Vitrectomy for idiopathic epiretinal membranes causing macular pucker. Br J Ophthalmol. 1988;72:692–5.
10. Rice TA, de Bustros S, Michels RG, et al. Prognostic factors in vitrectomy for epiretinal membranes of the macula. Ophthalmology. 1986;93:602–10.

11. Wong JG, Sachdev N, Beaumont PE, Chang AA. Visual outcomes following vitrectomy and peeling of epiretinal membrane. Clin Exp Ophthalmol. 2005;33:373–8.

12. Gribomont AC, Levi N. Prognosis of surgery in epimacular membranes after retinal break or rhegmatogenous retinal detachment. J Fr Ophtalmol. 2003;26:364–8.

13. Shimozono M, Oishi A, Hata M, Matsuki T, Ito S, Ishida K, et al. The significance of cone outer segment tips as a prognostic factor in epiretinal membrane surgery. Am J Ophthalmol. 2012;153:698–704.

14. Hahn P, Carrasco-Zevallos O, Cunefare D, Migacz J, Farsiu S, Izatt JA, et al. Intrasurgical human retinal imaging with manual instrument tracking using a microscope-integrated spectral-domain optical coherence tomography device. Transl Vis Sci Technol 2015;4:1. eCollection 2015.

15. Kwok AK, Lai TY, Li WW, et al. Indocyanine green-assisted internal limiting membrane removal in epiretinal membrane surgery: a clinical and histologic study. Am J Ophthalmol. 2004;138:194–9.

16. Park DW, Dugel PU, Garda J, et al. Macular pucker removal with and without internal limiting membrane peeling: pilot study. Ophthalmology. 2003;110:62–4.

17. Shimada H, Nakashizuka H, Hattori T, et al. Double staining with brilliant blue G and double peeling for epiretinal membranes. Ophthalmology. 2009;116:1370–6.

18. Schechet SA, DeVience E, Thompson JT. The effect of internal limiting membrane peeling on idiopathic epiretinal membrane surgery, with a review of the literature. Retina. 2017;37(5):873–80.

19. Hernandez F, Alpizar-Alvarez N, Wu L. Chromovitrectomy: an update. J Ophthalmic Vis Res. 2014;9:251–9.

20. Almony A, Nudleman E, Shah GK, et al. Techniques, rationale, and outcomes of internal limiting membrane peeling. Retina. 2012;32:877–91.

21. Mason JO 3rd, Feist RM, Albert MA Jr. Eccentric macular holes after vitrectomy with peeling of epimacular proliferation. Retina. 2007;27:45–8.

22. Donati G, Kapetanios AD, Pournaras CJ. Complications of surgery for epiretinal membranes. Graefes Arch Clin Exp Ophthalmol. 1998;236:739–46.

23. Mitchell P, Smith W, Chey T, et al. Prevalence and associations of epiretinal membranes. The blue mountain eye study. Aust Ophthalmol. 1997;104:1033–40.

24. Ripandelli G, Scarinci F, Piaggi P, et al. Macular pucker: to peel or not to peel the internal limiting membrane? A microperimetric response. Retina. 2015;35(3):498–507.

25. Lai CC, Wang NK, Wu WC, et al. The long-term anatomical and visual effect of intravitreal triamcinolone injection during vitrectomy for the treatment of idiopathic macular epiretinal membrane. Cutan Ocul Toxicol. 2011;30:292–7.

26. Ahn JH, Park HJ, Lee JE, Oum BS. Effect of intravitreal triamcinolone injection during vitrectomy for idiopathic epiretinal membrane. Retina. 2012;32:892–6.

27. Paspulati A, Punjabi OS, Theodoropoulou S, Singh RP. Triamcinolone acetonide as an adjuvant to membrane peeling surgery: a pilot study. Ophthalmic Surg Lasers Imaging Retina. 2013;44:41–5.

28. Chae B, Dhrami-Gavazi E, Dansingani KK, Freund KB, Lee W, Yannuzzi LA. Multimodal imaging of combined hamartoma of the retina and retinal pigment epithelium associated with an acquired vitelliform lesion. Int J Retina Vitreous. 2015;1:23. eCollection 2015. https://doi.org/10.1186/s40942-015-0023-6.

29. Okamoto F, Sugiura Y, Okamoto Y, Hiraoka T, Oshika T. Innernuclear layer thickness as a prognostic factor for metamorphopsia after epiretinal membrane surgery. Retina. 2015;35:2107.

30. Okamoto F, Sugiura Y, Okamoto Y, Hiraoka T, Oshika T. Timecourse of changes in aniseikonia and foveal microstructure after vitrectomy for epiretinal membrane. Ophthalmology. 2014;121:2255–60.

31. Pavlidis M, Georgalas I, Körber N. Determination of a new parameter, elevated epiretinal membrane, by en face OCTas a prognostic factor for pars plana vitrectomy and safer epiretinal membrane peeling. J Ophthalmol. 2015;838646

32. Bae SH, Kim D, Park TK, Han JR, Kim H, Nam W. Preferential hyperacuity perimeter and prognostic factors for metamorphopsia after idiopathic epiretinal membrane surgery. Am J Ophthalmol. 2013;155:109–17.e3.

33. Kinoshita T, Imaizumi H, Okushiba U, Miyamoto H, Ogino T, Mitamura Y. Time course of changes in metamorphopsia, visual acuity, and OCT parameters after successful epiretinal membrane surgery. Invest Ophthalmol Vis Sci. 2012;53:3592–7.

34. Falkner-Radler CI, Glittenberg C, Hagen S, Benesch T, Binder S. Spectral-domain optical coherence tomography for monitoring epiretinal membrane surgery. Ophthalmology. 2010;117:798–805.

35. Machado LM, Furlani BA, Navarro RM, Farah ME, Maia A, Magalhães O Jr, et al. Preoperative and intraoperative prognostic factors of epiretinal membranes using chromo vitrectomy and internal limiting membrane peeling. Ophthalmic Surg Lasers Imaging Retina. 2015;46:457–62.

36. Kim JH, Kim YM, Chung EJ, Lee SY, Koh HJ. Structural and functional predictors of visual outcome of epiretinal membrane surgery. Am J Ophthalmol. 2012;153:103–10.e1.

37. Austin JW. Evaluation of a "heads-up" display for cardiopulmonary bypass. J Extra Corpor Technol. 2000;32:49–53.

38. Eljamel MS. Frameless stereotactic neurosurgery: two steps towards the holy grail of surgical navigation. Stereotact Funct Neurosurg. 1999;72:125–8.

39. Charles S. Illumination and phototoxicity issues in vitreoretinal surgery. Retina. 2008;28:1–4.

40. Weinstock R. Operate with your head up. Cataract Refract Surg Today. 2011;66–74.

41. Zhou J, Xu HJ, Liang CZ, et al. A comparative study of distinct ocular symptoms after performing laparoscopic surgical tasks using a three-dimensional surgical imaging system and a conventional two-

dimensional surgical imaging system. J Endourol. 2015;29:816–20.

42. Dutra-Medeiros M, Nascimento J, Henriques J, et al. Three-dimensional headmounted display system for ophthalmic surgical procedures. Retina. 2017;37:1411–4.

43. Ehlers JP, Tam T, Kaiser PK, et al. Utility of intraoperative optical coherence tomography during vitrectomy surgery for vitreomacular traction syndrome. Retina. 2014;34(7):1341–6.

44. Wykoff CC, Berrocal AM, Schefler AC, et al. Intraoperative OCT of a full-thickness macular hole before and after internal limiting membrane peeling. Ophthalmic Surg Lasers Imaging. 2010;41(1):7–11.

45. Ehlers JP, Tao YK, Srivastava SK. The value of intraoperative OCT imaging in vitreoretinal surgery. Curr Opin Ophthalmol. 2014;25(3):221–7.

Structure and Function in Epiretinal Membrane Surgery

16

Andrew Chang and Ee Lin Ong

16.1 Background

Epiretinal membranes (ERM) are fibrocellular proliferations at the vitreomacular interface, with variable ramifications to one's vision through the membrane-induced mechanical distortion of the underlying neural tissues. With an estimated global prevalence of 7–11.8% in persons aged more than 50 years [1], ERMs are most commonly seen as congruent with normal aging, but also occur with higher frequency and accelerated progression in the context of other underlying retinal pathologies, such as diabetic retinopathy and uveitis [2, 3]. The natural history of ERM is highly variable, with a wide spectrum of symptoms, severity and clinical findings. While some patients remain completely asymptomatic, a significant proportion of patients are profoundly affected by metamorphopsia, loss of central vision and loss of binocularity [4, 5]. While the pathogenesis of ERM formation remains unclear, several hypotheses have postulated the internal limiting membrane (ILM) as a potential scaffold for deposition of the extracellular matrix, which occurs with glial cell hypertrophy at the time of posterior vitreous separation [3, 6].

Surgical pars plana vitrectomy (PPV) with mechanical membrane peeling has been the mainstay of surgical treatment of clinically significant ERM since 1978. The removal of delicate premacular tissue whilst minimizing trauma to the underlying retina involves considerable technical difficulty. Current literature on ERM surgery reports favourable anatomical and functional outcomes, with approximately 70–80% of patients benefiting from the improved vision and reduced metamorphopsia [4, 7, 8]. However, these are negated by complications such as cataract formation, retinal detachment and cystoid macula oedema; coupled with a relatively high recurrence rate of up to 10–21% after initial successful surgery [9, 10]. Modern vitreoretinal techniques have since evolved to include small-gauge vitrectomy, instrumentation and intraocular dyes to facilitate manipulation and visualization of retinal microstructures, resulting in surgery with reduced complications, expanding indications and improved visual outcomes.

A. Chang (✉)
Sydney Retina Clinic & Day Surgery, Sydney, Australia

Sydney Institute of Vision Science, Sydney, Australia

Retinal Unit, Sydney Eye Hospital, Sydney, Australia

Department of Ophthalmology, University of Sydney, Sydney, Australia
e-mail: achang@sydneyretina.com.au

E. L. Ong
Sydney Retina Clinic & Day Surgery, Sydney, Australia

Sydney Institute of Vision Science, Sydney, Australia

16.2 Preoperative Evaluation

16.2.1 Natural History and Symptom Progression

ERMs are amongst the most common conditions encountered by vitreoretinal specialists today [11, 12]. Patients typically present with symptoms such as metamorphopsia or blurring of central vision; while a significant proportion remains relatively asymptomatic, and are referred based on incidental findings on ophthalmic evaluation [4, 13]. Symptomatic ERMs are often found in the eyes with macular or peri-macular involvement. Distortion or monocular diplopia is commonly the most bothersome to patients, which impacts on visual function, particularly with binocular visual tasks such as reading and driving [14, 15]. Commonly, patients report closing one eye while reading, in order to eliminate distortion from the affected eye. Importantly, best-corrected visual acuity (BCVA) is often preserved at diagnosis, with previous reports suggesting that less than 5% of patients present with visual acuities of 20/200 or worse [16]. This is often followed by periods of relative stabilization in visual function, with limited progression over time. Accordingly, findings from a major population-based epidemiological study had observed worsening of visual acuity in only 28.6% of ERM patients over 5 years [1].

Many previous studies have attempted to describe the correlation between symptoms and structural changes caused by the ERM including photoreceptor dysfunction and retinal distortion [17–20]. In general terms, the extent of the visual effect of the disease is determined mainly by the degree of the induced retinal distortion, the position of the membrane in association to the macula, as well as its thickness and transparency [21, 22]. The decrease in VA can generally be attributed to the filtering effect of the ERM that prevents light from reaching the photoreceptors, the distortion of the retinal surface as well as macular oedema and the associated vitreoretinal traction due to incomplete PVD, if present. The distortion of the retinal surface due to ERM contraction, which in some cases can involve the entire retinal

thickness, is the primary cause for metamorphopsia, which is usually the leading and most disturbing symptom of the disease.

16.2.2 Clinical Examination

On slit-lamp fundus examination, the clinical appearance of ERMs can vary from thin, translucent cellophane-like membrane on the retinal surface, to thick and opaque preretinal fibrotic tissue that obscures the underlying retina. While the underlying neurosensory retina may often appear normal, contractile membranes can lead to retinal folds, distortion of the macular architecture, retinal vessel tortuosity, and even tractional dystopia of the fovea (Fig. 16.1). The normal foveal depression is often absent and other less common manifestations can arise such as cystoid spaces, lamellar macular hole, or even a full-thickness hole.

16.2.2.1 Structural and Functional Assessment of the Macula

In recent years, the advent of multimodal retinal imaging, image-enhancement techniques and methods for assessing retinal sensitivity such as microperimetry have facilitated a better understanding of the correlation between retinal microstructure and visual function. The introduction of this array of sophisticated ancillary tools to routine clinical practice has empowered clinicians and researchers alike to analyse the possible predictors of final visual outcomes, thus bringing an exciting new paradigm for patient evaluation and decision-making in vitreoretinal surgery for ERMs.

Assessing Structure
Macular morphologic abnormalities such as damage to the retinal layers and reduction in perifoveal circulation caused either by tractional forces generated by the ERM over time or intraoperative microtrauma, have been associated with decreased retinal sensitivity [17, 19, 23, 24].

Since Puliafito and colleagues [25] first described optical coherence tomography (OCT) imaging of the macula in 1995, OCT has evolved
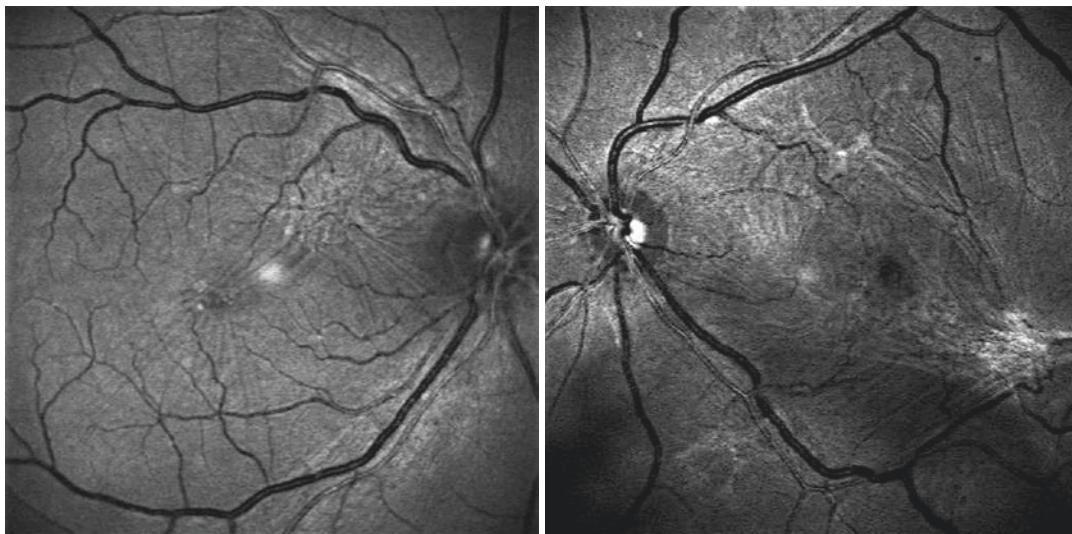
Fig. 16.1 Red-free clinical photographs showing the two distinct clinical phenotypes of epiretinal membranes: Cellophane maculopathy (right) and a more advanced pucker (left)

to become the gold standard for the diagnosis and management of most disorders affecting the vitreomacular interface. Spectral-domain optical coherence tomography (SD-OCT) is the most contemporary and advanced imaging modality, allowing non-invasive, cross-sectional visualization of retinal anatomy in high resolution. The addition of simultaneous real-time imaging with a confocal scanning laser ophthalmoscope (cSLO) not only enhances image quality with correction of fixation instability but also enables en-face imaging of the retinal layers for better location of pathology.

In OCT imaging, an ERM is typically demonstrated as a hyper-reflective band over the retinal surface, while wrinkling and distortion of the underlying neurosensory tissues are also easily visualized. Additionally, associated clinical entities, such as vitreomacular traction, macular oedema, loss of foveal pit and foveal tractional dystopia are also readily demonstrated. The tangential forces generated by the ERM contraction are able to induce neuron damage of the inner and outer retinal layers, associated with a reduction of the perifoveal circulation and changes in macular morphology (Fig. 16.2).

OCT angiography (OCTA) has recently replaced fundus fluorescein angiography (FFA)

in the pre- and post-operative evaluation of eyes with ERMs. Besides excluding other co-existing pathologies such as choroidal neovascularization and macular telangiectasis, its main utility lies in assessing the extent of retinal vasculature distortion and the detection of vascular leakage causing macula oedema. More recently, some reports have also described its use in evaluating foveal microarchitecture [26, 27], using surrogate imaging markers such as foveal vessel density (VD) and the foveal avascular zone (FAZ) which are indicative of the possible displacement of underlying capillaries by the ERM.

Lastly, fundus autofluorescence (FAF) imaging has also been useful in the detection of irreversible photoreceptor damage from ERMs, and a predictor of subsequent functional visual recovery post-operatively [28]. As photoreceptor cell loss causes decreased lipofuscin levels in the RPE, an increase in the area of foveal hypoautofluorescence on FAF imaging was shown to correlate negatively with post-operative visual outcome [29].

Assessing Function

Visual acuity (VA) is often inadequate in measuring post-operative visual performance based on its failure to correlate with patient satisfaction.
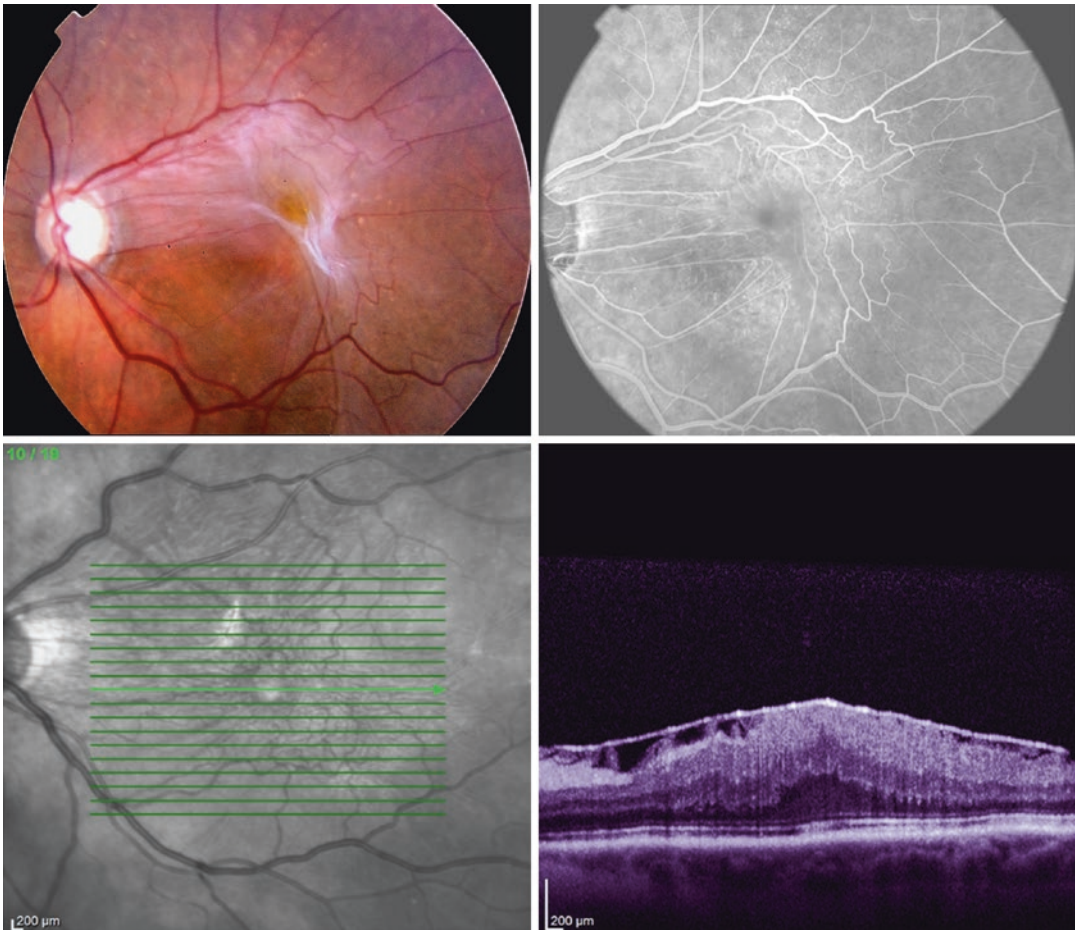
Fig. 16.2 Clinical photographs, fluorescein angiogram, infrared reflectance photograph and optical coherence tomography (OCT) scan of a thick epiretinal membrane causing tractional maculopathy

Its limitation lies in the disregard of paracentral or central microscotomata, which have shown to strongly affect patients' self-assessment of visual function [4, 30]. As the functioning of the central field is critical in day-to-day activities such as visual tasks involving contrast and colour sensitivity, reduced retinal sensitivity and the presence of paracentral microscotomata may cause visual discomfort despite good visual acuity, as reported by some patients after ERM surgery [31–34]. More recently, researchers have advocated for the inclusion of automated fundus-related microperimetry (MP), which involves the mapping of spatial light increment sensitivity and fixation re-establishment for a complete functional evaluation [24, 35, 36].

Evaluation of retinal sensitivity with MP under scotopic conditions is a rapid, safe, and non-invasive diagnostic procedure, and in recent years has been utilized as an adjunct to visual acuity measurements for optimal assessment of central macular function [37]. Microperimetry (MP) combines an anatomical and functional assessment of the retina by integrating viewing and projection systems in a single instrument. By simultaneously tracking the patient's fixation activity while mapping retinal sensitivity, MP overcomes fixation difficulties that commonly occur in patients with ERMs [38]. Apart from providing information on macular sensitivity, MP also allows assessment of foveal fixation stability and the depth of central macular defects. Thanks

to its auto-tracking software that corrects for involuntary eye movements, MP also allows surgeons to perform detailed comparative analysis pre- and post-surgery, enabling the monitoring of longitudinal outcomes in a reliable and reproducible fashion. Furthermore, microperimetry can detect subtle abnormalities, such as microscotoma that interfere with visual function but are not detected by assessment of visual acuity [39]. Since the release of the first microperimeter (the SLO101, Rodenstock), technological evolution has led to three commercially available models: the MP1 (Nidek), the OCT-SLO (Optos) and the MAIA system (Centervue) (Fig. 16.3).

The MP-1 microperimeter was the first to incorporate automated retinal tracking, which corrects for involuntary eye movements and enables the possibility of performing follow-up examinations [38]. Consisting of an infrared camera that creates a retinal image, stimuli are presented on an LCD screen within the instrument. The visual field is subsequently mapped and superimposed onto a retinal image. Test–retest variability has been shown to be relatively good in people with macular disease, with a reported mean sensitivity difference of 0.2 dB between two tests. The MP-1's advantage lies in its flexibility and ease-of-use, with many customizable aspects that include a wide array of visual field patterns and the ability to perform kinetic perimetry. However, mydriasis is usually required

for assessment with the MP-1, and the maximal target luminance of its stimulus is relatively dim compared to other cSLO-based devices (130 cd/m^2 compared to at least 200 cd/m^2 with the cSLO). Furthermore, it has a relatively limited dynamic range of only 2 log units, which makes microperimetry testing more susceptible to both floor and ceiling effects.

The OCT-SLO (Optos) integrates a spectral-domain OCT with a cSLO-based microperimeter. Since the optical pathways of both imaging modalities are coherent, the machine allows for the precise registration of the cSLO fundus image with the OCT structural image, resulting in en-face detection of pathology. With a similar dynamic stimulus range to the MP-1, the OCT-SLO can be performed without pupil dilation and a clearer retinal image is produced for retinal tracking during perimetry. The advantages of the OCT-SLO primarily lie in its ability to make direct structure/function comparisons underlying each microperimetric point. Function, in the form of retinal sensitivity, can be correlated to OCT features such as retinal thickness or the integrity of the photoreceptor layer. Additionally, the position of the preferred retinal locus (PRL) can be quantified in relation to the anatomic fovea.

The MAIA system [40] is the most advanced and consists of a near-infrared cSLO that incorporates a high frequency (25 Hz) eye tracker and an automated macular perimeter to determine

Fig. 16.3 The MP1 (Nidek), OCT-SLO (Optos) and MAIA system (Centervue) microperimetry systems

threshold sensitivity and fixation characteristics. Using an LED light as a stimulus, retinal image quality is high, and mydriasis is rarely required. The significant advantages of the MAIA microperimeter are its higher maximum target intensity and increased dynamic range of stimulus, with an attenuation range of 0–36 dB. However, the MAIA has fewer customizable options, with only two fixation targets and five grid patterns available. Moreover, stimuli can only be presented within the central 20° field, which is intended to remove the problem of aberrations and distortions of non-central targets reported on the MP-1.

16.2.3 Microperimetric Strategies in Evaluation of ERM

Microperimetry represents an important complementary tool for the monitoring of central macula function in the recovery period following vitrectomy surgery and ERM peeling. Its utility in macular surgery mainly lies in its ability to track and quantify functional improvements over time, while mapping sensitivity values to precise locations in the macula. Using microperimetry, iatrogenic post-operative damage to the macula can also be assessed. In theory, reduction in macular sensitivity (MS) can result from the combined effects of the optical density of the ERM (light filtering effect), together with the photoreceptor distortion caused by traction (Stiles–Crawford effect) [21, 41]. Retinal sensitivity is evaluated by studying the topographical point-to-point response to stimuli of incremental intensity, while fixation pattern (location and stability) has been shown to have significant ramifications on the quality of life, reading and near work. The temporal relationship between the restoration of these functional endpoints and related re-establishment of macular morphology in the post-operative period has also been studied [17, 36]. Overall, microperimetry-defined improvement in macular function has been shown to correspond well with improvements in visual acuity and decreased central macula thickness (CMT) after surgery.

The prognostic ability of microperimetry as a predictor of post-operative improvement in visual function has also been widely studied. Importantly, Mayer and colleagues highlighted the significance of the parafoveal retina by demonstrating a strong correlation between preoperative microperimetry-based sensitivity thresholds with improvements in visual acuity 12 months after surgery, an effect that was more pronounced in the parafoveal sectors. Interestingly, these results are consistent with the multifocal electroretinogram (mfERG)-based studies conducted by Kim et al., who reported that b-wave implicit times for responses from wider retinal eccentricities correlated stronger with post-operative visual acuity, as compared to responses obtained from the central 2° of retina.

16.2.3.1 Fixation Analysis

The parameters that evaluate fixation are assessed by tracking eye movements 25 times/s and by plotting the resulting distribution over the SLO image. Each movement is represented by a point in the distribution that constitutes the fixation pattern. All fixation positions during the examination are used by the instrument to calculate the fixation indexes P1 and P2, which represent the percentage of fixation points inside a circle of 2 and 4° of diameter from the total of fixation points, respectively. Subjects are classified as having stable fixation if P1 was more than 75%, relatively unstable fixation if P1 was less than 75% and P2 more than 75%, and unstable fixation if both P1 and P2 were below 75%.

The MAIA microperimeter also provides a more accurate estimation of the fixation pattern using the bivariate contour ellipse area (BCEA) [40]. By using two orthogonal diameters that describe the extent of the fixation points (in degrees), it calculates the area and orientation of an ellipse encompassing a given proportion (standardized to 63 and 95% in the MAIA) of the fixation points. Lower BCEA values define better fixation stability.

Lastly, the preferred retinal locus (PRL) or fixation location can also be determined by observation of the clustering of fixation points. The fixation location is divided into three

standard categories: central, paracentral and eccentric. If 50% of fixation points are within 0.5 mm of the foveal centre, fixation is classified as central. If 25% to 50% of the fixation points are within 0.5 mm of the foveal centre, fixation is classified as paracentral. Finally, if 25% of fixation points are within 0.5 mm of the foveal centre, fixation is classified as eccentric (Fig. 16.4).

16.2.3.2 Sensitivity Analysis

Mean retinal sensitivity threshold values (in decibels) are usually evaluated for the central 4° and 12° fields. If no threshold value is detected, the corresponding area is defined as an absolute scotoma. The total number of absolute scotoma locations in the central 4° and 12° areas are also taken into consideration.

Fig. 16.4 Fixation parameters obtained from a standard MAIA output from a typical eye with ERM. Eye movements during fixation are tracked by the system, after which the distribution is plotted and superimposed over an SLO image of the fundus. The fixation location (or preferred retinal locus) is described by the overall cluster of points (top). Ellipses are automatically generated on the image to encompass 63% and 95% of the fixation points; and its orthogonal diameters (area and orientation) are utilized to calculate BCEA values. Fixation indices P1 and P2 represent the percentage of fixation points within 2° and 4° diameter circles of the fovea. BCEA values and fixation indices are both markers of fixation stability
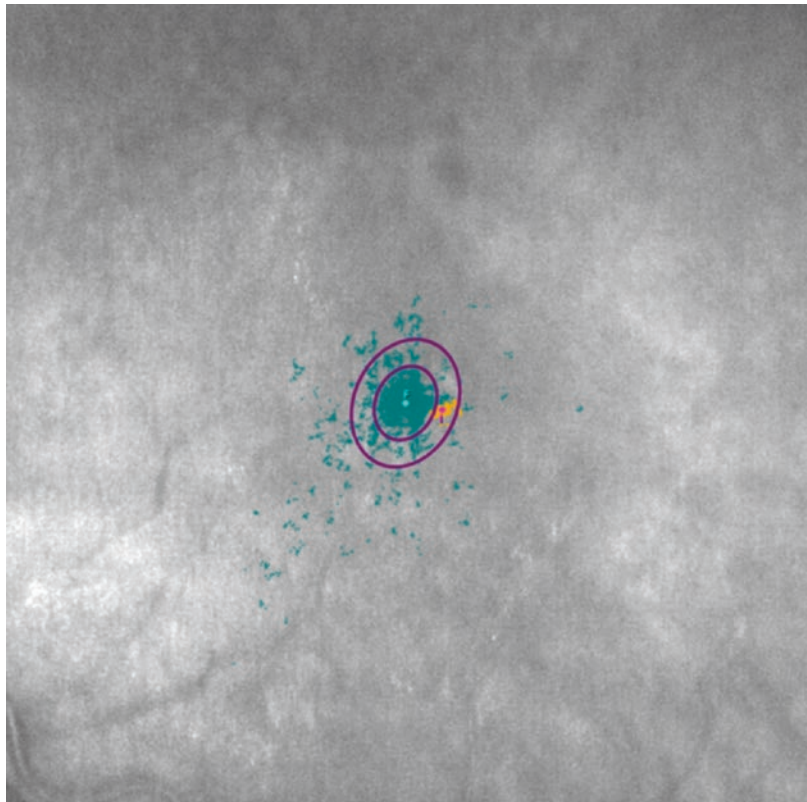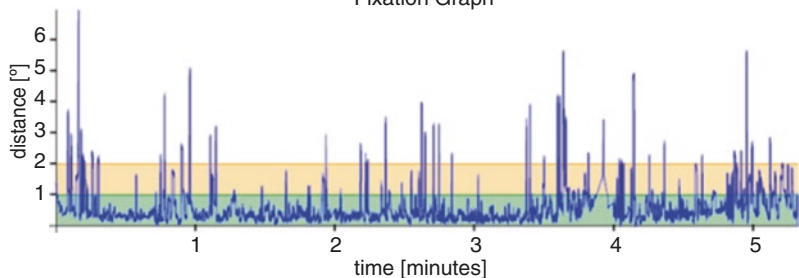
In addition to macula sensitivity values, an additional feature of the MAIA microperimeter analysis suite is the Macula Integrity Index (MII), which is a numerical value describing the likelihood that the patient's responses are normal or abnormal when compared to age-matched normative data. MII is calculated from age, average threshold value, measurements of points with threshold < 25 dB and all measured threshold values using a proprietary algorithm from the manufacturer (Fig. 16.5).
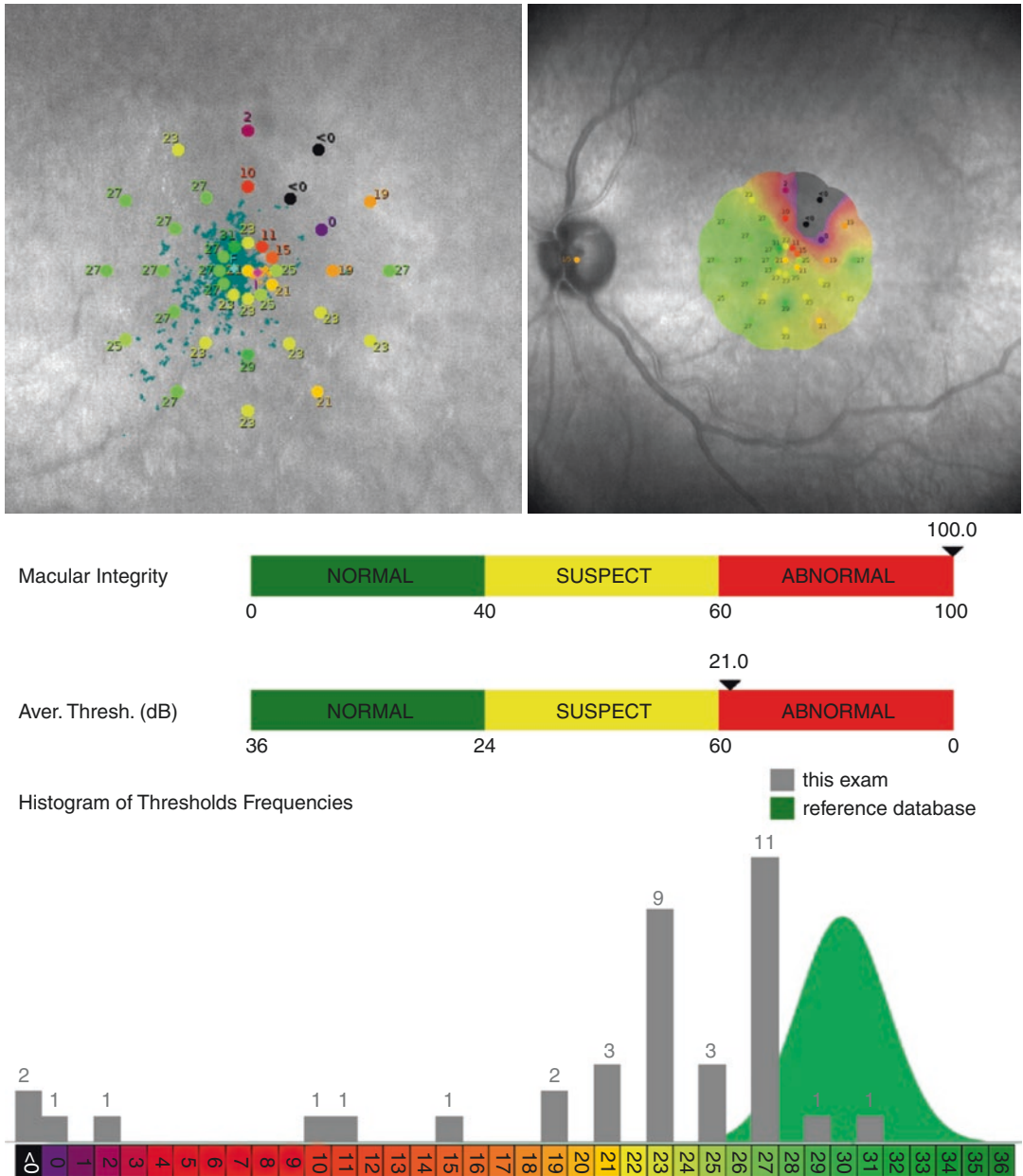
Fig. 16.5 Standard sensitivity output generated from the MAIA system of a typical eye with an ERM. The standard MAIA examination covers a 10° diameter area with 37 measurement points. Results are displayed in the MAIA sensitivity grid map (top right) and sensitivity plot (top right). Macular integrity and average threshold values are also reported. Threshold frequencies are compared to a histogram of reference database values on a decibel scale that is colour-coded according to MAIA normative studies, where "green" represents normal values, "yellow" suspect, "red" abnormal and "black" represents scotoma (bottom)

16.3   Surgical Considerations

The challenges of epiretinal membrane peeling include not only the knowledge of techniques in performing surgery but also the indication and timing in individual patients. Prediction of visual outcome is not only essential for weighing the benefits of surgery against the risk of complications but is also an important tool in patient counselling preoperatively. However, this is difficult as surgical indications have not been standardized. Management decisions and the clinical outcomes of surgery vary considerably amongst both patients and clinicians. With healthcare trends converging towards patient-centred and value-based medicine, patients are starting to take an active role and interest in the decision-making process regarding their health. As one of the prime movers of shared decision-making, elective eye surgery is no exception to this renewed paradigm; whereby both surgeons and patients share information, discuss options and come to an agreement on an appropriate treatment plan.

16.3.1 Surgery in Patients with Good Preoperative Visual Acuity

Visual acuity is only a surrogate marker for visual function. Yet, its traditional role as a principal factor in decision-making for ERM surgery remains unchanged, regardless of other more qualitative aspects of vision or the presence of debilitating symptoms, such as metamorphopsia or reduction in contrast sensitivity. Surgeons have conventionally adhered to traditional dogma of deferring surgery until an objective deterioration in VA occurs to justify the risk/benefit ratio of surgery. This was reflected in 2015's Preferences and Trends (PAT) poll survey by the American Society of Retinal Specialists (ASRS) [42]. When participants were asked how they would treat a 20/25 but symptomatic patient with an ERM, only 15.7% responded that they would offer surgical intervention, while a large proportion (81.3%) recommended observation. There is also an argument that if patients are starting with

such good vision, there is a ceiling effect of little potential for improvement in visual function. This attitude is further reinforced by the non-progressive natural history of the condition, with many patients being observed for years without requiring surgery [43, 44].

The main disadvantages of vitrectomy include the acceleration of cataract formation and increased risk of iatrogenic retinal breaks. Vitrectomy has been shown to increase the rate of cataract formation through unclear mechanisms, with a threefold increase noted in the rate of significant cataract formation in patients that have undergone vitrectomy after a follow-up period of only 6 months. In a single-centred randomized control trial, Kofod et al. [43] evaluated early versus deferred surgery for epiretinal membranes and found that, while early surgery resulted in excellent vision, patients in the deferred surgery group did not lose five letters of ETDRS vision. Thus, they deemed surgery deferral a safe clinical decision. Rouvas et al. [44] also recommended that non-tractional epiretinal membranes may be monitored safely over time if the patient is not a good surgical candidate. Furthermore, longitudinal studies [45] have reported accelerated thinning of retinal ganglion cell layer after vitrectomy surgery with ERM peeling. This is supported by electrophysiological studies [46] which found a reduction in macular function for up to 3 months after vitrectomy, thus confirming acute changes affecting retinal ganglion cells. However, based on modern retinal imaging modalities, neuronal healing and remodelling are believed to continue for up to 18 months following ERM peeling.

Instead, the majority of patients who undergo vitrectomy for removal of an ERM report improvement in symptoms, visual acuity and quality of life [14, 20]. Furthermore, data from several publications show that the people with the best visual acuity and minimal metamorphopsia following pars plana vitrectomy for ERMs are those with the best vision preoperatively [20, 47]. Other advocates for early surgery have also provided evidence that waiting too long may increase the risk of a worse overall outcome. Some investigators have reported that severe foveal dystopia in ERM may lead to capillary leakage and subse-

quent damage to retinal pigment epithelial cells and photoreceptors [47, 48]. Lo and colleagues [49] observed that the extent of tractional dystopia correlates with decreased VA. Such patients with extreme degrees of this dystopia may benefit from early intervention to prevent irreversible structural and functional changes.

Recent developments in surgical techniques and multimodal imaging have raised the possibility of earlier intervention in patients with good VA. Thompson first looked at surgical outcomes in patients with good starting vision in 2005 [50] and reported a mean improvement of at least 1 line in all patients (1.4 lines in those who started pseudophakic). Only 5% of the cohort were reported as having a 2 line or greater loss, which could not be attributed to cataract formation. This issue was re-examined by Rahman and Stephenson in 2013 [48], who found that 5% of patients had some degree of visual decline, while 67.2% noted significant improvement in visual functioning. More recently, a series of studies on patients with VA greater than 20/50 preoperatively reported that almost half of the patients improved the final VA by 1 Snellen line, and 25% kept their initial VA [51, 52]. Ten percent of patients lost VA with no specific defects observed on SD-OCT. Importantly, only one study reported subjective symptom improvement as a functional endpoint, even in the setting of unchanged BCVA. Lehpamer and Carvousnis [7] demonstrated an improvement in VA of about 1 line at 1 year, with 73% of patients experiencing improvement in visual symptoms. According to them, subjective visual improvement and/or a reduction in metamorphopsia should be the ultimate indicators for surgical success, even in the setting of unchanged BCVA.

16.3.1.1 Functional Indicators

Little is known about the outcomes of patients with very good starting visual potential prior to ERM surgery. Apart from visual acuity, early researchers have utilized patient-reported symptoms [44], Amsler grid distortion [29], contrast sensitivity [33] and quality of life questionnaires [14] as surrogate markers for assessing visual function caused by traction from ERMs. Overall,

the majority of patients who undergo vitrectomy for ERM removal have reported improvements in symptoms, visual acuity and quality of life [4, 31, 33].

Emerging literature has utilized microperimetry in combination with en-face OCT to better predict post-operative functional outcomes. In a prospective interventional case series of 73 patients, Romano and colleagues [53] analysed functional and morphological features in post-operative patients according to their degree of visual improvement at 6 months and attempted to prognosticate favourable functional outcomes with pre- and post-operative factors. Preoperatively, patients with deeper retinal changes, better BCVA and higher baseline sensitivity thresholds were found to significantly benefit more from vitrectomy and ERM peeling. Post-operative factors such as reduction of depth of retinal changes, the integrity of the ellipsoid zone, increment in macular sensitivity and the absence of intraretinal cysts were important predictors of improved functional outcomes [54].

16.3.1.2 Structural Indicators

Despite certain distinct features on clinical examination such as blunting of the foveal umbo, OCT remains the gold standard in the evaluation of tractional maculopathy caused by ERMs. Tractional effects of ERMs are typically responsible for patients' symptoms of visual loss and metamorphopsia, causing retinal thickening, wrinkling of the retinal surface and intraretinal schisis with cystic changes. Several studies have clearly demonstrated that central retinal thickness (CRT) on OCT imaging is increased in eyes with ERM, which correlates negatively with visual acuity [22, 55, 56]. More recently, further research into possible OCT parameters other than CRT for predicting post-operative outcomes has led to the evolution of biomarkers such as the integrities of different outer retinal layers including the IS/OS junction [20, 22, 57] (or ellipsoid zone), external limiting membrane (ELM) [19] and cone outer segment tips (COST) [20, 32]. The photoreceptor outer segment length (PROS), which measures the distance between the IS/OS junction and the RPE, has also been exten-

sively studied [15, 33, 58]. Of these, only IS/OS integrity was noted to have a variable association with post-operative VA and severity of metamorphopsia. In a prospective observational trial of 42 patients who underwent ERM surgery, Mayer et al. [19] reported that post-operative outer retinal changes correlated strongly with reduced retinal sensitivity measured by microperimetry, but not with central VA.

Nevertheless, vitreoretinal surgeons who advocate for early intervention have advised for the modification of benchmarks as to what qualifies as a successful visual outcome following epiretinal membrane surgery. Importantly, the majority of the studies done so far had reported on visual acuity improvement as opposed to final visual acuity in patients who have undergone epiretinal membrane peeling, which does not allow for the proper prediction of the likelihood of achieving excellent visual potential. Furthermore, only one study [7] had prospectively collected data on other measures of visual function such as metamorphopsia. Since it is now well-established that final visual acuity is heavily dependent on preoperative visual acuity, further guidance is needed from better-designed trials with more relevant endpoints, before a major shift is warranted towards early surgical intervention.

16.3.2 Internal Limiting Membrane (ILM) Peeling During ERM Removal

Incomplete removal of the ERM has been identified as a risk factor for recurrence [59] (Fig. 16.6). As a result, several investigators have advocated for concurrent peeling of the internal limiting membrane (ILM) to assure a more complete removal of the overlying ERM [10, 60, 61]. Along the same vein, the hypothesized role of the ILM as a scaffold along which the ERM can proliferate has also been supported by histopathological studies [62], which identified fibroblast cells on examination of residual ERM tissue. Although ILM peeling has generally been accepted as a fundamental step in macular hole repair, its role in surgery for ERM remains controversial.

Morris et al. [63] were the first to champion the intentional removal of the ILM during macular surgery. From their experience in demonstrating superior visual outcomes in more than 80% of eyes by peeling the ILM in eyes with haemorrhagic macular cysts secondary to Terson's syndrome, recommendations for the utility of this technique were extended by the authors to all cases of tractional maculopathy [64]. Park et al. [65] subsequently conducted the first pilot study comparing outcomes of eyes that underwent ERM peel with and without ILM removal, which yielded similar visual outcomes between both groups but with a lower recurrence rate in eyes that had undergone ILM peeling. Since then, many surgeons have advocated ILM peeling as a prophylactic measure to minimize ERM recurrence for two main reasons: (1) ILM removal may enable a more complete dissection of the ERM and (2) the ILM may act as a scaffold for ERM re-proliferation. Multiple retrospective studies and meta-analyses have supported this notion, coupled with the discovery of safer staining agents to aid visualization of the ILM during this manoeuvre. In a recent retrospective study of 251 consecutive patients undergoing vitrectomy and membrane peeling [60], 22.9% of eyes that solely underwent ERM peeling had clinical evidence of recurrent ERM formation 12 months after surgery, as compared to 1.8% which underwent concurrent ERM and ILM removal. Of these, 17 (12.1%) eyes required repeat vitrectomy, while none of the eyes with ILM removal required a second surgery. Only one randomized clinical trial [66] has been reported to date, which failed to show a reduced incidence of ERM recurrence in eyes that underwent surgery with ILM peeling after 12 months. However, this may have been confounded by the limited follow-up timeframe, and a longer observation period was generally recommended.

Despite its potential benefits, the purposeful removal of the ILM may have inherent deleterious effects to the underlying neural tissues of the retina. In recent years, a growing body of literature has reported complications such as nerve fibre layer damage [67], retinal hemorrhages [68], retinal thinning [56] and changes in
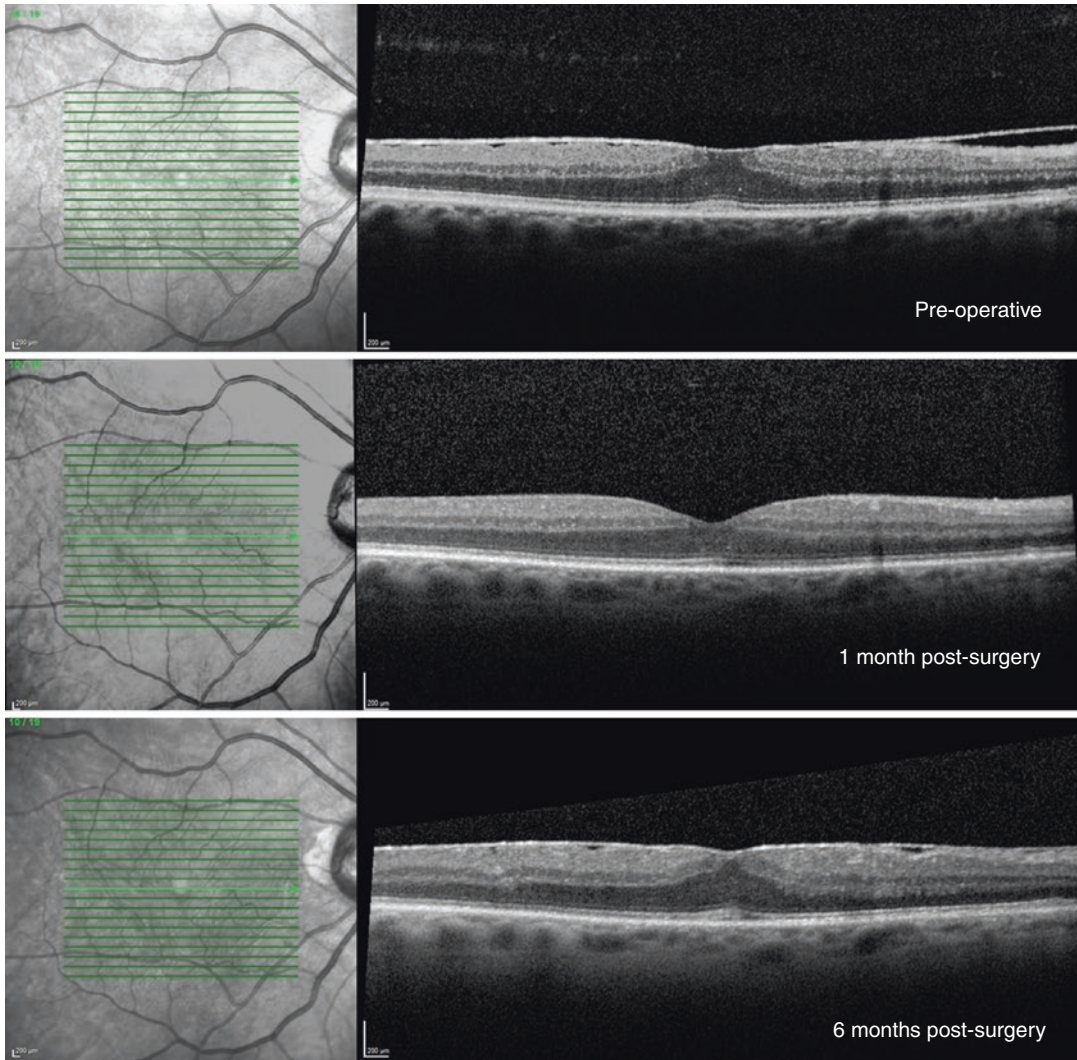
Fig. 16.6 Sequential OCT scans from a 71-year-old patient with ERM recurrence 6 months after the initial surgery. He was symptomatic on the initial presentation with a visual acuity of 6/12 (top). Vitrectomy was performed with separation of the hyaloid and ERM peeling, but with sparing of the ILM. OCT showed restoration of the foveal contour 1 month after surgery (middle). However, he presented 6 months post-operatively with worsening vision and distortion, and repeat OCT scan showed a recurrence of premacular fibrosis with underlying contracture of the ILM (bottom)

retinal sensitivity detected on electrophysiology [69] and microperimetry testing [24, 35] after ILM peeling. Moreover, recent reports have also illustrated the development of secondary eccentric or paracentral macula holes, with an occurrence rate of approximately 0.6–2.6% of macular surgeries that involved the removal of the ILM [70–74]. Although the mechanism of secondary hole formation remains unclear, these manifestations, coupled with functional changes in retinal sensitivity, are highly suggestive of iatrogenic microtrauma inadvertently caused by ILM peeling during surgery. Histopathologically, subclinical trauma to the inner retina in ILM peeling has been attributed to the damage of Muller cell endplates that are attached to the ILM, as explained by studies on the resultant ultrastructure of an enucleated human eye model

by Wolf and colleagues [75]. This has been thought to manifest as swelling of the arcuate nerve fibre layer in the initial 8–10 days post-operatively, which was observed to resolve by 2.5 months in a series of 102 eyes [67]. Structurally, additional studies have suggested that ILM peeling may further distort macular anatomy and cause thinning of central macular thickness post-operatively [76, 77].

In addition to structural and morphologic changes, post-operative functional deterioration has also been reported in patients who have undergone epiretinal membrane surgery with ILM peel, ranging from microscotomata on microperimetry testing to larger visual field defects seen on formal visual field perimetry [78]. (Fig. 16.7). Additionally, findings from Terasaki et al. [69] study on focal macular electroretinograms (mERGs) in post-vitrectomy

patients also demonstrated diminished b-wave amplitudes in the group of eyes that underwent ILM peeling—an effect which persisted even 6 months after surgery. In contrast, eyes that were spared ILM removal experienced significant recovery in b-wave amplitude to baseline soon after surgery. In all studies which assessed post-operative visual function by microperimetry, the sensitivity of the central 4° showed faster recovery and fewer absolute microscotomata in patients who did not undergo ILM peeling [24, 35, 36, 53]. A prospective multicentre clinical trial of 60 eyes conducted by Ripandelli and colleagues [35] used microperimetry to highlight that ILM peeling induced a higher number of microscotomata, as well as a slower recovery in retinal sensitivity. These findings have also been reflected in a small retrospective case series by Deltour et al. [24], collectively

Pre-operative   1 month post-surgery   3 months post-surgery   6 months post-surgery
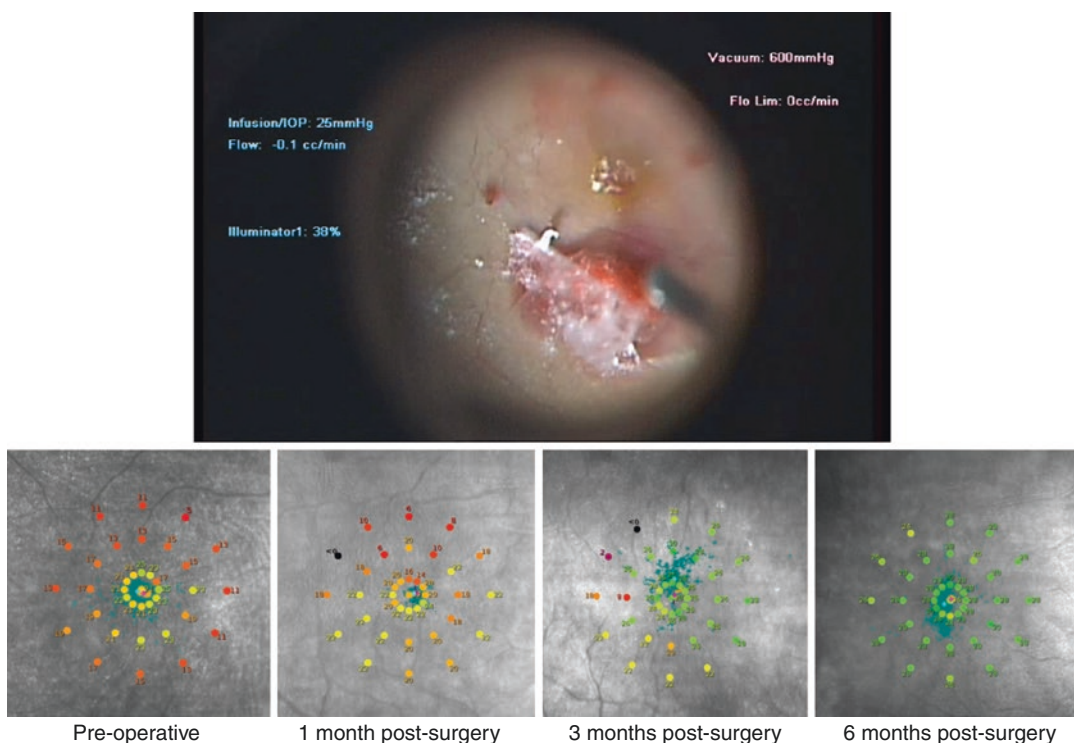
Fig. 16.7 Case example of a 76-year-old patient who experienced post-operative functional decline after epiretinal membrane surgery with ILM peel. Top: Still photograph from a surgical video recording of vitrectomy surgery showing intra-operative mechanical trauma induced by attempted peeling of the ERM and ILM complex with intraocular forceps. Bottom: Sequential MAIA microperimetry performed on the same patient demonstrating the presence of microscotomata within the central 4° and 10° fields with an associated visual disturbance at 1 and 3 months after surgery. Repeat microperimetry at 6 months showed complete resolution of microscotomata and normalization of macular perimetry threshold values

giving rise to the conclusion that theoretical microtrauma induced by retinal instrumentation whilst peeling the ILM may have resulted in microscotomata which were visually significant in number and density. However, there remains a paucity of prospective studies that performed both preoperative and post-operative microperimetry, thus rendering it unclear if microscotomata were due to preexisting disease, or sequelae of ILM peeling itself.

16.4 Conclusion

16.4.1 Implications for Practice

The prediction of visual outcome is essential for preoperative counselling and for considering the risks and benefits of surgery. Traditionally, due to the slow progression and variable symptomatology in ERMs, surgery is often delayed until symptoms become more pronounced. However, recent advancements in vitreoretinal surgical techniques, coupled with the ability to use multi-modal imaging and functional testing in the preoperative evaluation of patients with ERMs, give rise to the possibility of earlier surgical intervention in patients with ERMs to provide optimal visual outcomes. If early surgery is performed, complete and clean removal of the membrane is recommended, together with cautious and smooth peeling manoeuvres to minimize severe stretching of the underlying retina, trauma by forceps and subsequent structural retinal damage.

Evidence from current literature suggests that peeling of the ILM during ERM peel offers no additional benefit in terms of visual outcome. ILM peeling may theoretically reduce the recurrence rate, but many of these recurrences have not shown to need additional surgical intervention. Conversely, potential complications such as paracentral or eccentric macula holes, macular microscotomata, inner retinal dimpling, and ERG abnormalities have been associated with ILM peeling, and are highly suggestive of intraoperative retinal microtrauma which is potentially irreversible. As such, until further surgical

techniques or instrumentation becomes available to overcome potential complications from routine ILM removal routine ILM peeling in primary idiopathic ERM cases should be performed with caution.

16.4.2 Implications for Further Research

Visual acuity is often used in clinical trials as a surrogate marker for assessing functional outcomes post-macular surgery. Microperimetry testing allows for objective evaluation of macular function while systematically correlating its results with structural pathology seen on fundus photography and OCT imaging. However, there still remain little data in the published literature of its utility in the evaluation of visual function in the preoperative assessment of patients for macular surgery. Moreover, advancement in technology for improved vitreoretinal surgical outcomes requires validated clinical endpoints that are clinically meaningful, patient-relevant and accepted by regulatory agencies. This, therefore, necessitates development in the area of patient-reported outcomes, which can be translated into quantifiable values for a better understanding of surgical efficacy and cost-effectiveness by regulatory and funding authorities. Further research into these areas would be beneficial as an adjunct to visual acuity and microperimetry in the assessment of visual function.

References

1. Fraser-Bell S, Guzowski M, Rochtchina E, et al. Five-year cumulative incidence and progression of epiretinal membranes: the Blue Mountains Eye Study. Ophthalmology. 2003;110:34–40.
2. Mitchell P, Smith W, Chey T, et al. Prevalence and associations of epiretinal membranes: the Blue Mountains Eye Study, Australia. Ophthalmology. 1997;104:1033–40.
3. Mori K, Gehlbach PL, Sano A, et al. Comparison of epiretinal membranes of differing pathogenesis using optical coherence tomography. Retina. 2004;24:57–62.
4. Wong JG, Sachdev N, Beaumont PE, Chang AA. Visual outcomes following vitrectomy and peel-

ing of epiretinal membrane. Clin Exp Ophthalmol. 2005;33:373–8.

5. Arimura E, Matsumoto C, Nomoto H, et al. Correlations between M-CHARTS and PHP findings and subjective perception of metamorphopsia in patients with macular diseases. Investig Opthalmol Vis Sci. 2011;52:128.

6. Stevenson W, Prospero Ponce CM, Agarwal DR, et al. Epiretinal membrane: optical coherence tomography-based diagnosis and classification. Clin Ophthalmol. 2016;10:527–34.

7. Lehpamer BP, Carvounis PE. Pars plana vitrectomy for symptomatic epiretinal membranes in eyes with 20/50 or better preoperative visual acuity. Retina. 2015;35:1822.

8. Chang W-C, Lin C, Lee C-H, et al. Vitrectomy with or without internal limiting membrane peeling for idiopathic epiretinal membrane: a meta-analysis Mori K, ed. PLoS One. 2017;12:e0179105.

9. Donati G, Kapetanios AD, Pournaras CJ. Complications of surgery for epiretinal membranes. Graefes Arch Clin Exp Ophthalmol. 1998;236:739–46.

10. Kwok AK, Lai TY, Yuen KS. Epiretinal membrane surgery with or without internal limiting membrane peeling. Clin Exp Ophthalmol. 2005;33:379–85.

11. Gupta OP, Brown GC, Brown MM. A value-based medicine cost-utility analysis of idiopathic epiretinal membrane surgery. Am J Ophthalmol. 2008;145:923–928.e1.

12. Scott IU, Smiddy WE, Feuer W, Merikansky A. Vitreoretinal surgery outcomes: results of a patient satisfaction/functional status survey. Ophthalmology. 1998;105(5):795–803.

13. Ghazi-Nouri SMS. Visual function and quality of life following vitrectomy and epiretinal membrane peel surgery. Br J Ophthalmol. 2006;90:559–62.

14. Matsuoka Y, Tanito M, Takai Y, et al. Visual function and vision-related quality of life after vitrectomy for epiretinal membranes: a 12-month follow-up study. Investig Opthalmology Vis Sci. 2012;53:3054.

15. Chuang L-H, Wang N-K, Chen Y-P, et al. Comparison of visual outcomes after epiretinal membrane surgery. Taiwan J Ophthalmol. 2012;2:56–9.

16. Haivala DR, Parke DW. Macular epiretinal membranes. Albert Amp Jakobiecs Princ Amp Pract Ophthalmol. 2008:2073–81.

17. Richter-Mueksch S, Vécsei-Marlovits PV, Sacu SG, et al. Functional macular mapping in patients with vitreomacular pathologic features before and after surgery. Am J Ophthalmol. 2007;144:23–31.e1.

18. Miliatos I, Lindgren G. Epiretinal membrane surgery evaluated by subjective outcome. Acta Ophthalmol. 2017;95:52–9.

19. Mayer WJ, Fazekas C, Schumann R, et al. Functional and morphological correlations before and after video-documented 23-gauge pars plana vitrectomy with membrane and ILM peeling in patients with macular pucker. J Ophthalmol. 2015;2015:1–7.

20. Scheerlinck LME, Valk R, Leeuwen R. Predictive factors for postoperative visual acuity in idiopathic epiretinal membrane: a systematic review. Acta Ophthalmol. 2015;93:203–12.

21. Miller B. Epiretinal macular membranes: pathogenesis and treatment. Dev Ophthalmol. 1997 Jan 1;29:61–3.

22. Sheales MP, Kingston ZS, Essex RW. Associations between preoperative OCT parameters and visual outcome 3 months postoperatively in patients undergoing vitrectomy for idiopathic epiretinal membrane. Graefes Arch Clin Exp Ophthalmol. 2016;254:1909–17.

23. García-Fernández M, Castro Navarro J, González Castaño C, et al. Epiretinal membrane surgery: anatomic and functional outcomes. Arch Soc Esp Oftalmol Engl Ed. 2013;88:139–44.

24. Deltour J-B, Grimbert P, Masse H, et al. Detrimental effects of active internal limiting membrane peeling during epiretinal membrane surgery: microperimetric analysis. Retina. 2017;37:544–52.

25. Arevalo JF, editor. Retinal angiography and optical coherence tomography. New York: Springer Science & Business Media; 2008.

26. Chen H, Chi W, Cai X, et al. Macular microvasculature features before and after vitrectomy in idiopathic macular epiretinal membrane: an OCT angiography analysis. Eye Lond Engl. 2019;33:619–28.

27. Kim YJ, Kim S, Lee JY, et al. Macular capillary plexuses after epiretinal membrane surgery: an optical coherence tomography angiography study. Br J Ophthalmol. 2018;102:1086–91.

28. Reznicek L, Dabov S, Kayat B, et al. Scanning laser 'en face' retinal imaging of epiretinal membranes. Saudi J Ophthalmol. 2014;28:134–8.

29. Rodrigues IA, Lee EJ, Williamson TH. Measurement of retinal displacement and metamorphopsia after epiretinal membrane or macular hole surgery. Retina. 2016;36:695–702.

30. Mayer WJ, Vogel M, Neubauer A, et al. Pars Plana vitrectomy and internal limiting membrane peeling in epimacular membranes: correlation of function and morphology across the macula. Ophthalmologica. 2013;230:9–17.

31. Okamoto F, Okamoto Y, Hiraoka T, Oshika T. Effect of vitrectomy for epiretinal membrane on visual function and vision-related quality of life. Am J Ophthalmol. 2009;147:869–874.e1.

32. Okamoto F, Sugiura Y, Okamoto Y, et al. Stereopsis and optical coherence tomography findings after epiretinal membrane surgery. Retina. 2015;35:1415–21.

33. Sugiura Y, Okamoto F, Okamoto Y, et al. Contrast sensitivity and foveal microstructure following vitrectomy for epiretinal membrane. Investig Opthalmology Vis Sci. 2014;55:7594.

34. Jackson TL, Johnston RL, Donachie PHJ, et al. The Royal College of Ophthalmologists' National Ophthalmology Database Study of Vitreoretinal Surgery: Report 6, Diabetic Vitrectomy. JAMA Ophthalmol. 2016;134:79.

35. Ripandelli G, Scarinci F, Piaggi P, et al. Macular pucker: to peel or not to peel the internal limiting membrane? A microperimetric response. Retina. 2015;35:498–507.

36. Dal Vecchio M, Lavia C, Nassisi M, et al. Microperimetric assessment after epiretinal membrane surgery: 4-year follow-up. J Ophthalmol. 2016;2016:1–5.

37. Crossland M, Jackson ML, Seiple WH. Microperimetry: a review of fundus related perimetry. Optometry Rep. 2012;(1):2, e2.

38. Molina-Martín A, Pérez-Cambrodí RJ, Piñero DP. Current clinical application of microperimetry: a review. Semin Ophthalmol. 2018;33:620–8.

39. Centre for Ophthalmology and Visual Science (Lions Eye Institute), University of Western Australia, Wong EN, Department of Ophthalmology, Sir Charles Gairdner Hospital, et al. The use of microperimetry to detect functional progression in non-neovascular age-related macular degeneration: a systematic review. Asia-Pac J Ophthalmol. 2017;6:70–9.

40. Balasubramanian S, Uji A, Lei J, et al. Interdevice comparison of retinal sensitivity assessments in a healthy population: the CenterVue MAIA and the Nidek MP-3 microperimeters. Br J Ophthalmol. 2018;102:109–13.

41. Abdelhakim AH, Chen RWS. Macular surgery. In: Yiu G, editor. Vitreoretinal disorders. Singapore: Springer Singapore; 2018. p. 201–17. http://link.springer.com/10.1007/978-981-10-8545-1_8. Accessed 28 April 2019.

42. Anon. American Society of Retina Specialists. Preferences and Trends Survey (PAT). 2015. http://www.asrs.org/pat-survey.

43. Kofod M, Christensen UC, la Cour M. Deferral of surgery for epiretinal membranes: is it safe? Results of a randomised controlled trial. Br J Ophthalmol. 2015;100:688–92.

44. Rouvas A, Chatziralli I, Androu A, et al. Long-term anatomical and functional results in patients undergoing observation for idiopathic nontractional epiretinal membrane. Eur J Ophthalmol. 2015;26:273–8.

45. Lee S-B, Shin Y-I, Jo Y-J, Kim J-Y. Longitudinal changes in retinal nerve Fiber layer thickness after vitrectomy for epiretinal membrane. Investig Opthalmology Vis Sci. 2014;55:6607.

46. Shin M, Kim S, Park S, et al. Evaluation of macular function using pattern electroretinogram in idiopathic epiretinal membrane. Asia-Pac J Ophthalmol. 2015;4:267–72.

47. Wu XY. Relationship between the timing of vitreous surgery and prognosis after the open globe injuries. [Chinese]. Int Eye Sci. 2015;15:709–11.

48. Rahman R, Stephenson J. Early surgery for epiretinal membrane preserves more vision for patients. Eye. 2014;28:410–4.

49. Lo D, Heussen F, Ho H-K, et al. Structural and functional implications of severe foveal dystopia in epiretinal membranes. Retina Phila Pa. 2012;32:340–8.

50. Thompson JT. Epiretinal membrane removal in eyes with good visual acuities. Retina. 2005;25(7):875–82.

51. Chinskey ND, Shah GK. Epiretinal membrane peeling in patients with good preoperative vision. J Vitreoretin Dis. 2017;1:52–6.

52. Nakashizuka H. Short-term surgical outcomes of 25-gauge vitrectomy for epiretinal membrane with good visual acuity. J Clin Exp Ophthalmol. 2013;4:280. https://www.omicsonline.org/vitrectomy-for-epiretinal-membrane-with-good-visual-acuity-2155-9570.1000280.php?aid=15333. Accessed 3 July 2019

53. Romano MR, Cennamo G, Cesarano I, et al. Changes of tangential traction after macular peeling: correlation between *en-face* analysis and macular sensitivity. Curr Eye Res. 2017;42:780–8.

54. Laban KG, Scheerlinck LM, van Leeuwen R. Prognostic factors associated with visual outcome after pars plana vitrectomy with internal limiting membrane peeling for idiopathic epiretinal membrane. Ophthalmologica. 2015;234(3):119–26.

55. Spiteri Cornish K, Lois N, Scott N, et al. Vitrectomy with internal limiting membrane (ILM) peeling versus vitrectomy with no peeling for idiopathic full-thickness macular hole (FTMH) Cochrane Eyes and Vision Group, ed. Cochrane Database Syst Rev. 2013. http://doi.wiley.com/10.1002/14651858.CD009306.pub2. Accessed 28 April 2019.

56. Hisatomi T, Tachibana T, Notomi S, et al. Internal limiting membrane peeling-dependent retinal structural changes after vitrectomy in rhegmatogenous retinal detachment. Retina. 2018;38:471–9.

57. Suh MH, Seo JM, Park KH, Yu HG. Associations between macular findings by optical coherence tomography and visual outcomes after epiretinal membrane removal. Am J Ophthalmol. 2009;147:473–480.e3.

58. Hosoda Y, Ooto S, Hangai M, et al. Foveal photoreceptor deformation as a significant predictor of postoperative visual outcome in idiopathic epiretinal membrane surgery. Investig Opthalmology Vis Sci. 2015;56:6387.

59. Sandali O, El Sanharawi M, Basli E, et al. Epiretinal membrane recurrence: incidence, characteristics, evolution, and preventive and risk factors. Retina. 2013;33:2032–8.

60. Schechet SA, DeVience E, Thompson JT. The effect of internal limiting membrane peeling on idiopathic epiretinal membrane surgery, with a review of the literature. Retina. 2017;37:873–80.

61. Shimada H, Nakashizuka H, Hattori T, et al. Double staining with brilliant blue G and double peeling for epiretinal membranes. Ophthalmology. 2009;116:1370–6.

62. Beyazildiz Ö, Tirhiş MH, Hekimoğlu ER, et al. Histopathological analysis of internal limiting membrane surgically peeled from eyes with epiretinal membrane. Curr Eye Res. 2016;41:258–65.

63. Morris R, Kuhn F, Witherspoon CD. Hemorrhagic macular cysts. Ophthalmology. 1994;101:1.

64. Morris R, Kuhn F, Witherspoon CD, et al. Hemorrhagic macular cysts in Terson's syndrome and its implications for macular surgery. Dev Ophthalmol. 1997;29:44–54.

65. Park DW, Dugel PU, Garda J, et al. Macular pucker removal with and without internal limiting membrane peeling: pilot study. Ophthalmology. 2003;110:62–4.

66. Tranos P, Koukoula S, Charteris DG, et al. The role of internal limiting membrane peeling in epiretinal membrane surgery: a randomised controlled trial. Br J Ophthalmol. 2017;101:719–24.

67. Clark A, Balducci N, Pichi F, et al. Swelling of the arcuate nerve fiber layer after internal limiting membrane peeling. Retina. 2012;32:1608–13.

68. Hisatomi T, Notomi S, Tachibana T, et al. Ultrastructural changes of the vitreoretinal interface during long-term follow-up after removal of the internal limiting membrane. Am J Ophthalmol. 2014;158:550–556.e1.

69. Terasaki H, Miyake Y, Nomura R, et al. Focal macular ERGs in eyes after removal of macular ILM during macular hole surgery. Invest Ophthalmol Vis Sci. 2001;42:229–34.

70. Mason JO III, Feist RM, Albert MA Jr. Eccentric macular holes after vitrectomy with peeling of epimacular proliferation. Retina. 2007;27(1):45–8.

71. Sandali O, El Sanharawi M, Basli E, Lecuen N, Bonnel S, Borderie V, Laroche L, Monin C. Paracentral retinal holes occurring after macular surgery: incidence, clinical features, and evolution. Graefes Arch Clin Exp Ophthalmol. 2012;250(8):1137–42.

72. Enin MA, El-Toukhy HM, Swelam A. Non-foveal macular holes after PPV for macular pucker. Middle East Afr J Ophthalmol. 2010;17(3):254.

73. Brouzas D, Dettoraki M, Lavaris A, Kourvetaris D, Nomikarios N, Moschos MM. Postoperative eccentric macular holes after vitrectomy and internal limiting membrane peeling. Int Ophthalmol. 2017;37(3):643–8.

74. Rush RB, Simunovic MP, Aragon AV, Ysasaga JE. Postoperative macular hole formation after vitrectomy with internal limiting membrane peeling for the treatment of epiretinal membrane. Retina. 2014;34(5):890–6.

75. Wolf S, Schnurbusch U, Wiedemann P, et al. Peeling of the basal membrane in the human retina: ultrastructural effects. Ophthalmology. 2004;111:238–43.

76. Pichi F, Lembo A, Morara M, et al. Early and late inner retinal changes after inner limiting membrane peeling. Int Ophthalmol. 2014;34:437–46.

77. Lee JW, Kim IT. Outcomes of idiopathic macular epiretinal membrane removal with and without internal limiting membrane peeling: a comparative study. Jpn J Ophthalmol. 2010;54:129–34.

78. Uemura A, Kanda S, Sakamoto Y, Kita H. Visual field defects after uneventful vitrectomy for epiretinal membrane with indocyanine green–assisted internal limiting membrane peeling. Am J Ophthalmol. 2003;136:252–7.

Lamellar Macular Hole: Ultrastructural Analysis, Surgical Outcomes, and Visual Prognosis

17

Lawrence R. Lee, Corey Rowland, and Jennifer C. Chen

17.1 Introduction

Lamellar macular hole (LMH) is a unique and distinct clinical entity, defined as a partial thickness defect at the macula with an irregular foveal contour, an inner retinal defect, dehiscence between the inner and outer retina, an absence of a full-thickness foveal defect and intact photoreceptors [1]. LMH was originally described by Gass as a macular lesion that resulted from cystoid macular edema and on biomicroscopic examination, it typically appears as a round or irregular-shaped, well-circumscribed reddish lesion [2]. Clinical detection of LMH at an early stage can be difficult, however, the advent of high-resolution optical coherence tomography (OCT) imaging in recent times has transformed the understanding of in vivo retinal architecture and makes the diagnosis of LMH from other similar, yet distinct macular disorders, such as full-thickness macular holes (FTMH), macular pseudoholes (MPH), and vitreomacular traction (VMT) more definitive [1, 3–5]. In addition to distinguishing LMH from other vitreomacular disorders, OCT imaging reveals morphological features that can be used to categorize lamellar defects into subtypes of LMH and many studies have investigated how these morphological features and subtypes of LMH correlate with visual prognosis and outcomes of surgical intervention [4–10].

While OCT imaging provides unprecedented resolution, which facilitates detailed analyses of LMH morphology and OCT-based diagnostic criteria, there is a degree of heterogeneity over the definitions of LMH and MPH and the use of the two terminologies in the current literature [1, 5]. Both the terms, LMH and MPH, were initially coined on the basis of biomicroscopic observation and aimed at making differentiation from FTMH. They have now been suggested to be entirely different entities resulting from different underlying pathophysiological processes and in particular, MPH resulting from the centripetal contraction of an epiretinal membrane (ERM) should be differentiated from LMH which reflects an avulsion of the inner foveal tissue [4]. Research is now focused on reinterpreting the definitions of MPH and LMH based on OCT characterization and identifying precise, definitive morphological features that can be used to classify the two clinical entities. The difficulty lies with the observation that some cases of lamellar macular defects can present with mixed morphological features common to both entities. There is also a

L. R. Lee (✉) · C. Rowland
City Eye Centre, Brisbane, Australia

Department of Ophthalmology, University of Queensland, Royal Brisbane Hospital, Brisbane, Australia
e-mail: eye@cityeye.com.au

J. C. Chen
City Eye Centre, Brisbane, Australia
e-mail: jen@cityeye.com.au

myriad of terminologies used to describe the morphometric and morphological features of MPH and LMH as well as the types of ERM associated with these lamellar macular defects.

17.1.1 MPH Versus LMH Morphological Features

MPH has been classified as a lamellar macular defect characterized by a steepened foveal pit with straight, verticalized edges and it is an entity that can be clearly differentiated from LMH due to the clear-cut characteristic OCT profile. MPH has been postulated to result from the centripetal forces generated by the ERM, with the ERM having one epicenter of contraction around the foveal region [5]. Gaudric et al. further identified that when there are more than one ERM epicenters involved, eccentric to the foveal region, lamellar defects can exhibit stretched edges and an intraretinal split [5]. It was suggested that these types of macular defects should still be considered as a clinical spectrum of MPH rather than a different entity. However, an appraisal of the current literature would suggest that most authors have adopted the term LMH to define lamellar macular defects with an intraretinal split [1, 6, 9, 11, 12]. The contrary also occurs; sharply punched-out, partial-thickness macular defects with straight, verticalized edges, described as MPH by Gaudric et al. were referred to as LMH by Bottoni et al [5, 7]. There is indeed a discrepancy and a degree of overlap in the current literature over the definitions and use of terminologies of MPH and LMH.

17.1.2 Role of ERM in MPH and LMH Formation

There is however a general consensus that ERM is a common feature associated with both MPH and LMH and that ERM plays a significant contributing role in the formation of lamellar holes by exerting dynamic, tractional forces on the fovea. It has been observed that 50% of 92 eyes with lamellar macular defects in the study of Chen and Lee [6] had ERM; 62% of 29 eyes in the study of Haouchine et al. [4], 89% of 19 eyes in the study of Witkin et al. [1] and more recent studies, 100% cases of MPH and LMH were observed to be associated with ERM [5, 7–10]. The higher proportion of ERM identified in the latter studies may be attributed to the higher resolution of spectral-domain, ultrahigh-resolution OCT utilized.

17.1.3 Types of ERM

With the use of ultrahigh-resolution OCT, some studies were able to reveal differences in the type of ERM associated with lamellar holes and have focused on investigating how the variation in ERM appearances and composition may contribute to the formation of MPH and LMH subtypes [8, 9, 13]. Two types of ERM appearances have so far been identified: conventional (also described as thin, normal) and atypical (also described as dense, thick, or an epiretinal proliferation).

In conventional ERM, there is a tractional component resulting in the characteristic stretched, schisis-like intraretinal layers potentially being the underlying cause of the LMH defect. This is supported by histopathologic analysis and immunolabeling studies of the alpha-smooth muscle actin (α-SMA) which have revealed that α-SMA expression was more frequently demonstrated in conventional ERM, suggesting these membranes to have more contractility and exert tractional forces at the fovea, to a greater degree than the atypical, dense membranes [14].

Distinct from the tractional subtype, the atypical ERM appears to be dense, thickened, and non-contractile with a relatively firm adhesion at the edge of the hole and characterized by a corresponding mound on OCT [8, 13, 15]. The atypical ERM is often referred to as lamellar hole-associated epiretinal proliferation (LHEP) and follows the contour of the retinal surface without signs of traction on the intraretinal layers [15]. It has been suggested that the development of these types of LMH may be associated with a

slow, progressive, degenerative process resulting in loss of retinal tissue and the disruption of the ellipsoid layer [9]. The thickened epiretinal proliferation is also thought to be of a composition of native vitreous collagen resulting from the vitreous cortex remodeling process or glial tissue proliferation. Due to the differing morphological and histological properties, the types of ERM may contribute to different pathways of the underlying pathophysiological process in the formation of lamellar holes [8, 9, 13, 15].

It must be recognized that there may be other mechanisms underlying the pathogenesis of LMH. Haouchine et al. have previously identified foveal pseudocyst as a precursor to the development of both lamellar and macular hole formation and postulated that lamellar holes are caused by de-roofing of the pseudocyst with preservation of the foveal base [3]. LMH has also been considered as an aborted process from FTMH formation [16, 17].

Figure 17.1 shows the clinical spectrum of MPH and subtypes of LMH varying in different stages of severity or progression and highlights the morphological features on OCT of the differ-ent subtypes of lamellar macular defects. It must be noted that some cases of lamellar macular defects may present with mixed morphological OCT features and not all cases can be stratified into MPH, or either the LMH tractional or non-tractional subtypes. Natural history or progression may also result in one subtype of lamellar defects transitioning into the other.

17.1.4 MPH Versus LMH Morphometric Features

One established parameter of MPH and LMH that has been correlated with visual prognosis is the central or residual foveal thickness. This is the minimum thickness of the retina at the level of the foveal floor. It has been demonstrated in previous studies that LMH had reduced central foveal thickness compared to MPH [4, 6]. Furthermore, LMH with the atypical, thickened epiretinal proliferation has thinner central foveal thickness than LMH with conventional ERM and also a higher incidence of outer segment/inner segment (OS/IS) defect [7, 8, 10]. Findings
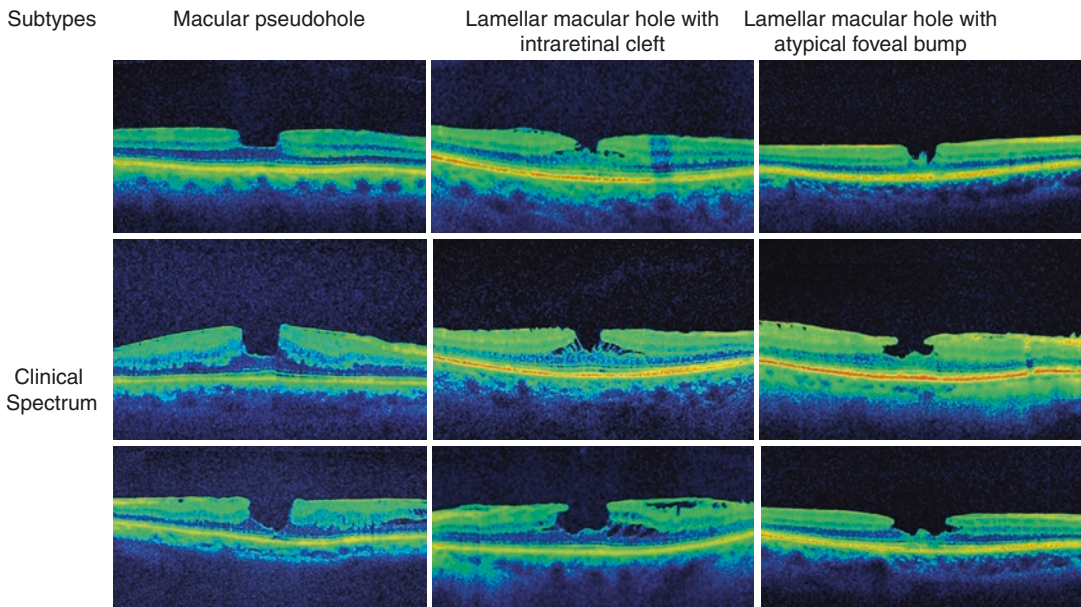
Fig. 17.1 Clinical spectrum showing varying degrees of severity of MPH and LMH subtypes and highlighting the distinct OCT morphological features of each category. Images were captured by Cirrus spectral-domain OCT device (Carl Zeiss Meditec, Dublin, California USA)

of thinner central foveal thickness and a disruption of the OS/IS junction or ellipsoidal zone were consistent with poorer visual acuity in LMH with thickened, atypical epiretinal proliferation [4, 7, 8].

Measurement of the defect diameter is another morphometric parameter used to correlate with visual function. LMH has been found to have wider base diameters than MPH, and LMH with the atypical, thickened epiretinal proliferation has larger diameters than LMH with conventional ERM [4, 6, 8]. However, lamellar defect diameter is a more variable factor as a measurement of the base diameter can refer to the inner diameter of the defect (maximum distance between the edges of the hole at the level of the internal limiting membrane (ILM)), the outer diameter (maximum distance at the base of the defect) or the maximal diameter of intraretinal cleft or cavitation.

In FTMH, the associated visual loss is said to result from the direct loss of foveal tissue and there is a suggestion that the thickness of cellular tissue between the base of the hole and the retinal pigment epithelium (RPE) layer is inversely proportional to the patients resulting visual acuity [18]. Given the current findings, it would be reasonable to postulate that the higher level of acuity of MPH is attributable to the smaller diameter and thicker central foveal tissue while the poor acuity of LMH is associated with the deeper/wider intraretinal split and thin foveal tissue respectively. Table 17.1 provides a summary of the nomenclature, OCT morphological features, possible underlying mechanisms and pathogenesis, ellipsoidal layer integrity, and visual prognosis of the different types of lamellar macular defects.

17.2 Association with Myopia

Studies have shown that high myopia is more prevalent in eyes with FTMH and LHEP than in eyes with FTMH and no LHEP [15]. Lai et al. found a prevalence of LHEP in highly myopic eyes at 66.2% with lamellar and FTMH [15]. The presence of this atypical ERM in those with high myopia

may be explained by the complex tractional forces and morphology that exist in myopia.

Lai et al. examined LHEP anatomical features on OCT and surgical findings in eyes with high myopia. The study found some unique morphological features of eyes with high myopia and LHEP. LHEP in highly myopic eyes tended to have a more broad extension (>1500 μm from the foveal center) than eyes without high myopia while LHEP-posterior hyaloid adhesion occurred more often in eyes without high myopia [15]. Highly myopic eyes frequently have a sheet of LHEP that is attached to or slightly elevated above the retinal surface. This membrane is part of the posterior hyaloid and can be traced to the mid periphery where it is connected to cortical vitreous. An ERM typically exists between the retinal surface and this posterior hyaloid membrane. Thus, LMH formation in those with high myopia frequently occurs in multiple layers of a preretinal membrane. Highly myopic eyes have complex tractional forces that lead to wider, deeper retinal defects, both of which are known LHEP risk factors. It is postulated that stronger tractional forces result in heightened stimulation for LHEP growth or the attached posterior hyaloid may be a better matrix for LHEP cellular proliferation than the typical ERM [15].

Studies on LMH in highly myopic eyes are limited and have mainly related to macular retinoschisis. FTMH in high myopia has poor outcomes with surgical closure and therefore it is important to understand the incidence of progression from LMH to FTMH in this subgroup of patients. A study by Tanaka et al. followed 24 highly myopic eyes with LMH for at least one year without intervention. It showed that 95.8% of the eyes showed no progression on OCT imaging [19]. In conjunction, there was no significant decrease in the best-corrected visual acuity (BCVA) over this one-year period [19]. Tanaka et al. suggest that LMHs in high myopia are relatively stable and surgery should only be considered if other findings suggest a differing course. 71% of the highly myopic eyes with LMH had an ERM, suggesting that ERM with traction could be integral in the pathogenesis of LMH in

Table 17.1 Summary of nomenclature, OCT morphological features, possible underlying mechanisms and pathogenesis, ellipsoidal layer integrity and visual prognosis of the different types of lamellar macular defects [5, 7–10, 13].

Subtypes	Macular pseudohole characterized with verticalized foveal edges	Lamellar macular hole characterized with an intraretinal cleft	Lamellar macular hole characterized with an atypical foveal bump
Nomenclature in the literature	• Macular pseudohole • Pseudomacular hole	• Lamellar hole associated with conventional ERM • Tractional LMH • ERM can also be termed C-ERM • Intraretinal splitting LMH	• Lamellar hole associated epiretinal proliferation (LHEP) • Non-tractional LMH • Degenerative LMH • ERM can also be termed A-ERM • V-shaped LMH
Morphological features on OCT	• Steepened foveal pit • Appearance of a sharply punched-out defect • May have either straight edges or stretched edges • Commonly associated with ERM	• Sharp-edged hyporeflective intraretinal split • More specifically schitic separation characterized by multiple, narrow hyperreflective tissue bridges crossing the wide hypo-reflective spaces between the outer plexiform and outer nuclear layers • The classical ERMs are thin and irregular, shown as hyperreflective lines above the inner retinal surface on OCT • The EMRs do not always have direct, uniform contact with the underling retina, suggesting a tractional component • "Moustache shape" defect • Intraretinal cystoid spaces may be present	• Round-edged hyporeflective intraretinal cavitation in the neurosensory retina • Presence of a retinal tissue "bump" in the foveal region is often observed • "Top hat shape" defect • Usually present with a wider diameter across the defect and a thinner residual foveal thickness compared to MPH or LMH with intraretinal cleft • Atypical ERMs—observed to be dense and thickened and presented as a homogenous pre-retinal line of medium reflectivity on the OCT • A direct, uniform contact between the medium reflective line and the underlying retina without evidence of traction • Intraretinal cystoid spaces are uncommon
Possible mechanisms	• Homogenous, centripetal contraction of ERM centered around the fovea, the epicenter	• Several epicenters of ERM centrifugal contraction resulting in stretched foveal edges and asymmetric intraretinal cleavage	• Chronic progressive degenerative mechanism resulting in loss of retinal tissue with a foveal "bump" of presumably spared tissue located at the base of the defect
Ellipsoid /ELM integrity	• Often presented with an intact ellipsoid layer	• Intact ellipsoid layer	• Early ellipsoid layer disruption
Visual prognosis	• Higher level of visual acuity compared to LMH, mostly likely due to the thicker central foveal thickness	• Poor visual function, potentially due to the wide intraretinal split	• Poor visual function, potentially due to thinner foveal thickness and ellipsoidal zone disruption

myopic eyes [19]. It is hypothesized that the contraction of the perifoveal complex of an epiretinal membrane and ILM with the existing anteroposterior vitreous traction is related to the pathogenesis of the LMH. The mechanism leading to LMH development may be similar between myopic and non-myopic eyes. Dell'Omo et al. also examined the natural history and morphologic characteristics of LMH in those with high myopia. Forty-four eyes of 44 patients were retrospectively analyzed using OCT, fundus autofluorescence (FAF), and BCVA [20]. The mean follow-up period for the cohort was 50.1 ± 28.9 months. It concluded that LMH in high myopia is frequently associated with ERM and LHEP, and demonstrates stability in BCVA and anatomical parameters over a long duration [20].

17.3 Prognosis

Studies about LMH and MPH report variable findings of the natural course and results after surgical interventions. Recommendation for surgical intervention in LMH and MPH remains controversial because of the clinical stability of these macular lesions over time. A study by Purtskhvanidze et al. examined this stability by providing morphological and functional data of foveal lesions with and without vitrectomy over a long follow-up [21]. Seventy-three patients were recruited for long-term follow-up for at least 5 years. Twenty-eight had LMH, 31 had MPH, and 14 had MPH with cleaved edges. Forty-six eyes were part of the observation group and 27 eyes underwent surgical intervention involving vitrectomy and membrane peeling. One of the main findings was that almost two-thirds of lamellar holes and pseudoholes remained stable without surgical intervention over a mean follow-up of 8.3 years [21]. LMHs tended to have worse visual function compared to MPHs and MPHs with cleaved edges; with a statistically significant median visual function loss of 0.1 logMAR over a mean of 9.3 years [21]. It also observed that spontaneous separation of a tractional epiretinal membrane with an improvement of the foveal contour is not uncommon in the long term [21].

Nava et al. evaluated the likelihood of LMH development in the fellow eyes of patients with unilateral LMH [22]. Thirty-five patients with diagnosed unilateral LMH were included. Their fellow eyes were retrospectively evaluated by BCVA, OCT, and FAF changes. This study concluded that the presence of a LMH in one eye does not significantly increase the risk of developing the same condition in the fellow eye after 4 years [22]. However, an ERM is often detected in the fellow eye [22].

17.4 Surgery

Surgical intervention for the treatment of LMH is indicated when there is potential for loss of vision and symptomatic changes such as distortion and scotoma formation. Intervention involves 3-port pars plana vitrectomy via small incisions (27, 25, and 23 gauge are common), with posterior hyaloid face peeling if attached and ERM staining with dye such as indocyanine green, MembraneBlue® (DORC), and Brilliant Peel® (Fluoron), or triamcinolone. This facilitates the safe peeling of the ERM and ILM, with microforceps and or diamond-dusted silicone Tano brush. Care should be taken to peel towards the LMH, to prevent tears and potential for FTMH formation. Frisina et al. had used a double inverted ERM and ILM flap (double flap) technique to treat idiopathic LMH with better functional recovery compared to the standard technique with reduced risk of subsequent FTMH development [23, 24].

In cases where the ERM and ILM are fused, they are removed together when the membranes are peeled. Hemorrhages often occur on the retinal surface, and this is a good sign indicating that the ILM has been peeled. Fluid air exchange is performed, and gas such as isovolumetric perfluoropropane (C_3F_8) and sulfur hexafluoride (SF_6) tamponade may be used, though it is not essential. As the LMH is not full thickness, the need for gas tamponade is contentious.

A paper by Holland et al. found excellent results in the surgical management of LMH [25]. The study included 89 eyes, of which 43% had

MPH, 28% had LMH, and 29% had foveal pseudocyst. This study found visual acuity improved in 71% of eyes [25]. The study concluded that the surgical indications for lamellar macular defect were poor vision and deep lamellar macular defect in the presence of an associated epiretinal membrane [25].

Patients with asymptomatic lamellar macular defects can be observed and monitored for progression at regular intervals. Surgical intervention would be recommended in eyes with a visual acuity of 20/40 or worse, whereby those with an acuity of 20/30 or more are best observed depending on patient symptomatology. Better prognosis with surgery occurs in patients who have a small LMH diameter, smaller preoperative base diameters, and better vision preoperatively, as well as thicker preoperative central macular thickness [25]. A study by Ko et al. was controversial and found no visual benefit after surgery in patients who had LMH associated with LHEP [26]. Choi found that LMH had a better prognosis in those who had highly reflective ERM compared to those with LHEP. Those with LHEP demonstrated a higher incidence of ellipsoid zone disruption, which has a resultant reduction in foveal function [27].

Lee et al. commented on the beneficial effect of surgery in those with LMH, with a 90% improvement in foveal appearance and good stability in vision improvement long-term over a mean follow-up of 3 years post-surgery [28]. Conversely, Purtskhvanidze et al. commented on the lack of statistical difference between an observation group and a vitrectomy group in patients with lamellar macular defects [21]. The study found that there was no difference in visual acuity between the observation group and the vitrectomy group irrespective of whether the patient had an LMH, MPH, or MPH with cleaved edges. Amongst the vitrectomy and observation groups, LMHs had worse visual outcomes compared to MPHs and cleaved MPHs at the end of follow-up. Purtskhvanidze et al. highlight the variable course and slow progression of these macular lesions. The study suggests as a reasonable approach, re-assessment after 6 months with OCT and visual function, for consideration of surgical intervention when the morphological changes progress and/or visual function decrease. In patients with obvious tractional ERM and reduced visual acuity, performing surgery earlier was considered an acceptable approach [21]. Figure 17.2 demonstrates an example of successful closure on OCT of a LMH with an intraretinal cleft, 1-week post vitrectomy with ERM peel, and air exchange.

17.5 Other Risks for FTMH

Few cases have been described in the literature on the development of FTMH after LMH surgical repair with vitrectomy. Medeiros et al. present a case of a patient who developed FTMH following surgical repair [29]. A 77-year-old man with symptomatic LMH underwent a standard 3-port vitrectomy, with separation and complete removal of the posterior hyaloid, epiretinal membrane peel, and air-fluid exchange with 20% SF_6 gas fill. Postoperatively, the patient maintained a face-down position for 5 days. On postoperative day 10, a FTMH had developed and was docu-
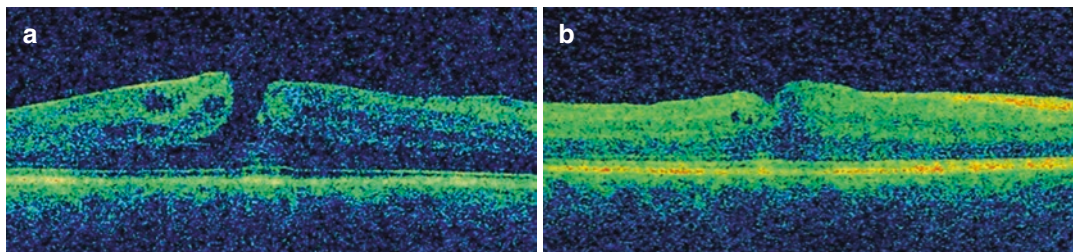
Fig. 17.2 LMH with an intraretinal cleft (**a**) demonstrating successful closure (**b**) one-week post vitrectomy with ERM peel and air exchange. Images were captured by Cirrus spectral-domain OCT device (Carl Zeiss Meditec, Dublin, California USA)

mented on OCT. Given the anatomically unsuccessful outcome, the patient underwent a second surgical procedure involving a widened ILM peel beyond the temporal vascular arcades and gas tamponade with 14% C_3F_8. The patient assumed a face-down position for an additional 5 days.

One month post the second vitrectomy, OCT revealed full anatomical closure of the macular hole. Six-months postoperatively, OCT showed the restoration of a normal foveal contour. FTMH formation after vitrectomy has been reported and the mechanism remains unknown. Several theories of pathophysiology addressing FTMH development post vitrectomy have been postulated, including tangential traction by remnant vitreous and ILM, or through ERM development [29]. Intrasurgical dynamics and anteroposterior mechanical forces may potentially induce vitreous traction at the fovea with subsequent FTMH formation [29]. Surgeons should be aware of these potential complications following LMH surgical repairs and take into account intraoperative vitreous dynamics.

17.6 Association with Ocriplasmin

Physiological liquefaction and contraction of the vitreous body result in disruption of the connection between the posterior hyaloid membrane and ILM of the retina. This process results in a posterior vitreous detachment (PVD). In the case of partial PVD, VMT can occur when a section of the posterior hyaloid face remains attached to the macula. This can subsequently lead to full-thickness or lamellar macular hole formation at the fovea. Pars plana vitrectomy continues to be the gold standard of care. Intravitreal ocriplasmin (Jetrea®), approved by the Food and Drug Administration (FDA) in 2012, provides a pharmacological alternative to the surgical release of symptomatic VMT [30]. Ocriplasmin is a low-molecular-weight recombinant molecule consisting of the catalytic domain of the human serine protease, plasmin. Plasmin can cleave glycoproteins that comprise the connection at the vitreoretinal interface, such as fibronectin and laminin. Ocriplasmin is injected intravitreally at a recom-

mended dose of 0.125 mg/0.1 ml to induce pharmacological vitreolysis and release of VMT. This treatment has been shown to successfully release VMT in only 31% of patients [30].

A case report by Chod et al. documented an association between ocriplasmin and the development of LMH [30]. A 76-year-old woman with asymptomatic VMT and impending macular hole underwent intravitreal ocriplasmin injection. The patient experienced a poor response to the initial injection and 7 months later, developed a LMH corresponding to the previous site of VMT. If intravitreal ocriplasmin injection fails to induce successful vitreomacular release, it may increase anteroposterior forces concentrated at the site of vitreofoveal adhesion. The forces may be great enough to overcome the intrinsic strength of the retinal tissue, resulting in LMH development [30].

References

1. Witkin AJ, Ko TH, Fujimoto JG, et al. Redefining lamellar holes and the vitreomacular interface: an ultrahigh-resolution optical coherence tomography study. Ophthalmology. 2006;113(3):388–97.
2. Gass JD. Lamellar macular hole: a complication of cystoid macular edema after cataract extraction: a clinicopathologic case report. Trans Am Ophthalmol Soc. 1975;73:231–50.
3. Haouchine B, Massin P, Gaudric A. Foveal pseudocyst as the first step in macular hole formation: a prospective study by optical coherence tomography. Ophthalmology. 2001;108(1):15–22.
4. Haouchine B, Massin P, Tadayoni R, et al. Diagnosis of macular pseudoholes and lamellar macular holes by optical coherence tomography. Am J Ophthalmol. 2004;138(5):732–9.
5. Gaudric A, Aloulou Y, Tadayoni R, Massin P. Macular Pseudoholes with lamellar cleavage of their edge remain Pseudoholes. Am J Ophthalmol. 2013;155(4):733–42.
6. Chen JC, Lee LR. Clinical spectrum of lamellar macular defects including pseudoholes and pseudocysts defined by optical coherence tomography. Br J Ophthalmol. 2008;92(10):1342–6.
7. Bottoni F, Deiro AP, Giani A, Orini C, Cigada M, Staurenghi G. The natural history of lamellar macular holes: a spectral domain optical coherence tomography study. Graefes Arch Clin Exp Ophthalmol. 2013;251(2):467–75.
8. Pang CE, Spaide RF, Freund KB. Comparing functional and morphologic characteristics of

lamellar macular holes with and without lamellar hole-associated epiretinal proliferation. Retina. 2015;35(4):720–6.

9. Govetto A, Dacquay Y, Farajzadeh M, et al. Lamellar macular hole: two distinct clinical entities? Am J Ophthalmol. 2016;164:99–109.

10. Zampedri E, Romanelli F, Semeraro F, Parolini B, Frisina R. Spectral-domain optical coherence tomography findings in idiopathic lamellar macular hole. Graefes Arch Clin Exp Ophthalmol. 2017;255(4):699–707.

11. Michalewski J, Michalewska Z, Dziegielewski K, Nawrocki J. Evolution from macular pseudohole to lamellar macular hole – spectral domain OCT study. Graefes Arch Clin Exp Ophthalmol. 2011;249(2):175–8.

12. Theodossiadis PG, Grigoropoulos VG, Emfietzoglou I, Nikolaidis P, Papathanasiou M, Theodossiadis GP. Spontaneous closure of lamellar macular holes studies by optical coherence tomography. Acta Ophthalmol. 2012;90(1):96–8.

13. Pang CE, Spaide RF, Freund BK. Epiretinal proliferation seen in association with lamellar macular holes: a distinct clinical entity. Retina. 2014;34(8):1513–23.

14. Parolini B, Schumann RG, Cereda MG, Haritoglou C, Pertile G. Lamellar macular holes: a clinicopathologic correlation of surgically excised epiretinal membranes. Invest Ophthalmol Vis Sci. 2011;52(12):9074–83.

15. Lai TT, Yang CM. Lamellar hole-associated epiretinal proliferation in lamellar macular hole and full-thickness macular hole in high myopia. Retina. 2018;38(7):1316–23.

16. Gaudric A, Haouchine B, Massin P, et al. Macular hole formation: new data provided by optical coherence tomography. Arch Ophthalmol. 1999;117(6):744–51.

17. Takahashi H, Kishi S. Tomographic features of a lamellar macular hole formation and a lamellar hole that progressed to a full-thickness macular hole. Am J Ophthalmol. 2000;130(5):677–9.

18. Tanner V, Chauhan DS, Jackson TL, et al. Optical coherence tomography of the vitreoretinal interface in macular hole formation. Br J Ophthalmol. 2001;85(9):1092–7.

19. Tanaka Y, Shimada N, Moriyama M, et al. Natural history of lamellar macular holes in highly myopic eyes. Am J Ophthalmol. 2011;152(1):96–9.

20. Dell'Omo R, Virgili G, Bottoni F, et al. Lamellar macular holes in the eyes with pathological myopia. Graefes Arch Clin Exp Ophthalmol. 2018;256(7):1281–90.

21. Purtskhvanidze K, Balken L, Hamann T, et al. Long-term follow-up of lamellar macular holes and pseudoholes over at least 5 years. Graefes Arch Clin Exp Ophthalmol. 2018;256(6):1067–78.

22. Nava U, Cereda MG, Bottoni F, et al. Long-term follow-up of fellow eye in patients with lamellar macular hole. Graefes Arch Clin Exp Ophthalmol. 2017;225(8):1485–92.

23. Frisina R, Pilotto E, Midena E. Lamellar macular hole: state of the art. Ophthalmic Res. 2019;61(2):73–82.

24. Frisina R, Parrozzani R, Pilotto E, Midena E. A double inverted flap surgical technique for the treatment of idiopathic lamellar macular hole associated with atypical epiretinal membrane. Ophthalmologica. 2019;8:1–10.

25. Holland L, Chen JC, Lee LR. Anatomical and functional outcomes of pars plana vitrectomy for lamellar macular defects. Asia Pac J Ophthalmol (Phila). 2015;4(3):134–9.

26. Ko J, Kim GA, Lee SC, et al. Surgical outcomes of lamellar macular holes with and without lamellar hole-associated epiretinal proliferation. Acta Ophthalmol. 2017;95(3):221–6.

27. Choi WS, Merlau DJ, Chang S. Vitrectomy for macular disorders associated with lamellar macular hole epiretinal proliferation. Retina. 2018;38(4):664–9.

28. Lee SJ, Jang SY, Moon D, Choi KS, Jung GY. Long-term surgical outcomes after vitrectomy for symptomatic lamellar macular holes. Retina. 2012;32(9):1743–8.

29. Dutra Medeiros M, Alkabes M, Nucci P, Branco J. Full-thickness macular hole after lamellar macular hole surgery: a case report. Eur J Ophthalmol. 2015;25(1):73–6.

30. Chod RB, Goodrich C, Saxena S, Akduman L. Lamellar macular hole after intravitreal ocriplasmin injection. BMJ Case Rep. 2015;2015:bcr2014207810.

Macular Hole Surgery: Current Approaches and Trends

18

Lawrence P. L. Iu and Ian Y. H. Wong

18.1 Introduction

Macular hole (MH) is a full-thickness defect in the neurosensory retina at the center of the macula. It was first described by Knapp in 1869 in a patient with ocular trauma [1]. Idiopathic MH without trauma is the most common form. The pathogenesis is related to an abnormal vitreomacular interface with a tractional force pulling on the fovea. The advent of optical coherence tomography (OCT) allows us to visualize how MH evolves in relation to the changes of the vitreoretinal interface.

18.2 Stages

In 1988, Gass JD postulated that the pathogenesis of MH is due to contraction of prefoveal vitreous cortex, which results in retinal dehiscence at the foveola followed by lateral displacement of the retinal photoreceptors [2]. Gass classified MH into four stages based on biomicroscopic findings [1, 2]. Stage 1A (Fig. 18.1) is an impending hole which appears as a yellow spot clinically. It occurs when the prefoveal vitreous cortex contracts and the foveolar retina detaches from the underlying retinal pigment epithelium. The yellow color was

L. P. L. Iu · I. Y. H. Wong (✉)
Department of Ophthalmology, LKS Faculty of Medicine, The University of Hong Kong, Pokfulam, Hong Kong
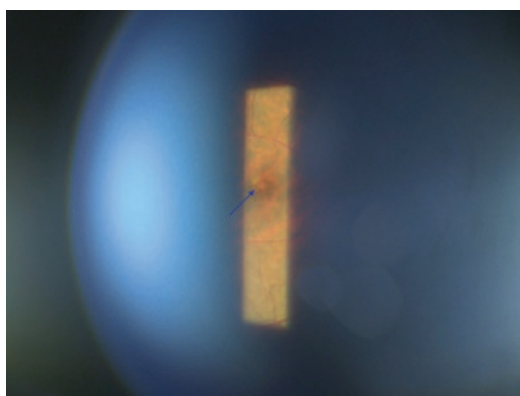
Fig. 18.1 Impending macular hole (stage 1A of Gass' classification). Slit-lamp biomicroscopic fundus photography showing a yellow spot at the fovea (arrow)

postulated to arise from intraretinal xanthophyll. Stage 1B is an impending or occult hole that appears as a yellow ring clinically. It occurs when the photoreceptors and xanthophyll of the foveolar retina retract laterally beneath the contracted prefoveal vitreous cortex. Stage 2 is full-thickness MH with a diameter of <400 μm. Stage 3 is full-thickness MH with a diameter ≥400 μm. Stage 4 is full-thickness MH with complete posterior vitreous detachment (PVD).

With the advent of OCT, we are able to evaluate the vitreoretinal interface and visualize the changes in early MH formation. The stages of MH based on OCT classification are as follows: Stage 0 MH (Fig. 18.2) has an abnormal vitreoretinal interface but the retinal architecture

Fig. 18.2 Stage 0 macular hole. Optical coherence tomography showing vitreomacular adhesion where the posterior hyaloid is detached in the perifoveal region but attached acutely at the fovea. There are no abnormal structural changes in the retina
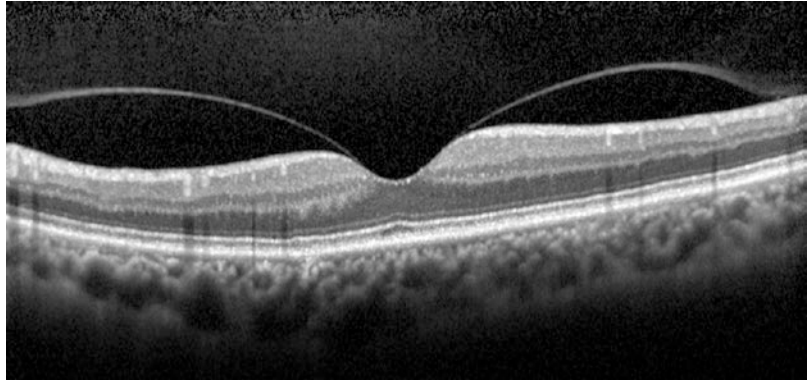
Fig. 18.3 Stage 1 macular hole. Optical coherence tomography showing vitreomacular traction at the fovea with foveolar detachment
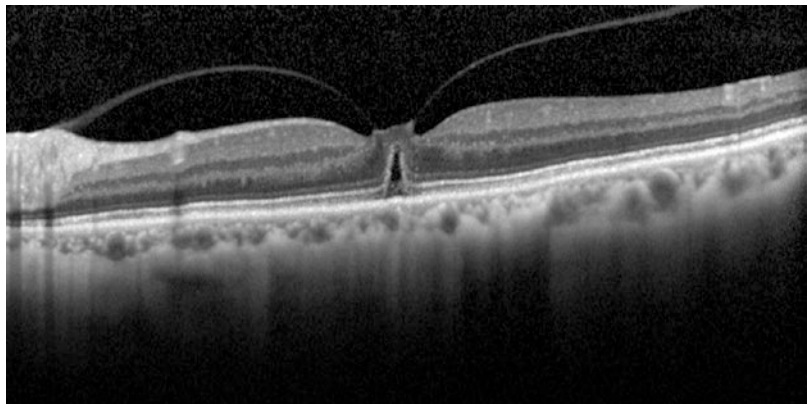
remains unaffected and normal [3]. The posterior hyaloid is detached in the perifoveal region but attached acutely at the fovea. There are no abnormal structural changes in the retina [3]. Stage 1 MH (Fig. 18.3) is characterized by the presence of foveolar detachment, foveal cyst formation, and/or inner foveal splitting due to the vitreoretinal traction at fovea [4, 5]. Stage 2 MH is characterized by a full-thickness MH with an incompletely separated operculum. The operculum is continuous with the posterior hyaloid and attaches to the edge of MH [6]. In stage 3 MH (Fig. 18.4), the operculum together with the posterior hyaloid is completely separated from the full-thickness MH, but the posterior hyaloid is still attached to the optic disc [6]. Stage 4 MH (Fig. 18.5) is a full-thickness MH with complete PVD [5].

In 2013, an expert panel of International Vitreomacular Traction Study Group proposed classification of MH based on (1) size, (2) status of vitreous, and (3) primary versus secondary [7]. Under this classification system, abnormal vitreoretinal interface with normal retinal architecture (i.e., OCT-stage 0 MH) is termed vitreomacular adhesion [7]. Abnormal vitreoretinal interface with retinal structural changes (i.e., OCT-stage 1 MH) is termed vitreomacular traction [7]. Full-thickness MH is defined as a foveal lesion with interruption of all retinal layers from the internal limiting membrane (ILM) to retinal pigment epithelium [7]. It is divided into small (<250 μm), medium (>250 μm and ≤400 μm) and large (>400 μm) based on the aperture size at the narrowest point [7].

Fig. 18.4 Stage 3 macular hole. Optical coherence tomography showing complete separation of all retinal layers. The posterior hyaloid and operculum are completely detached from the full-thickness macular hole
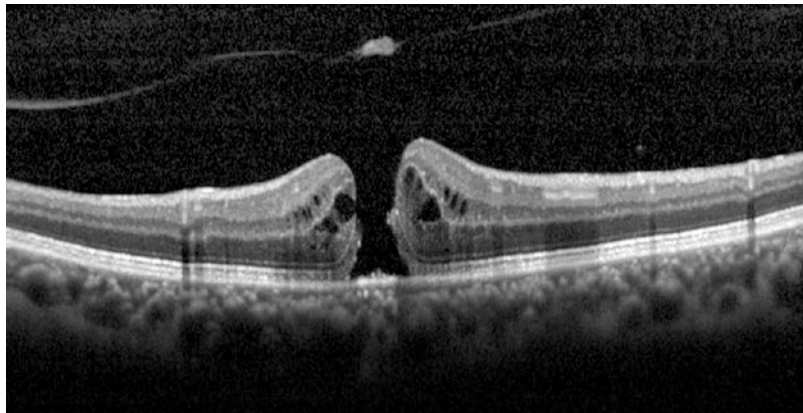
Fig. 18.5 Stage 4 macular hole. Optical coherence tomography showing a large macular hole with complete posterior vitreous detachment
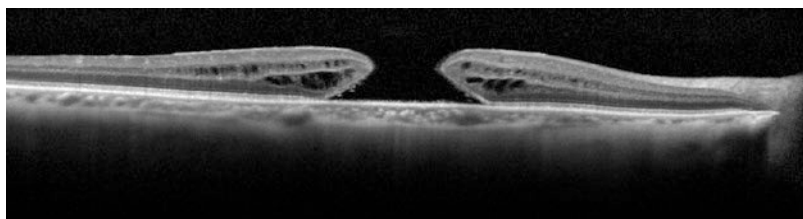
18.3 Epidemiology

Idiopathic MH affects mainly middle-aged and elderly patients and is more common in females [1, 8, 9]. The prevalence was reported to be 0.16% among people above the age of 40 years in the Beijing Eye Study [10], 0.11% in the Baltimore Eye Survey [11], and 0.45% in the Beaver Dam Eye Study [12]. In a study performed in the United States, the age-adjusted incidence of MH was 7.8 per 100,000 person-years with a female-to-male ratio of 3.3:1 [8]. In a study performed in Rogaland of Norway, the female-to-male ratio of MH was 2.2:1 [9].

Bilateral MH is not uncommon. McCannel CA et al. reported that bilateral involvement occurred in 11.7% of patients with MH [8]. A retrospective cohort study showed that 13% of patients with MH developed fellow eye involvement within 4 years [13]. The risk of fellow eye involvement appears to depend on whether PVD has occurred [14]. La Cour et al. suggested the risk is low of <2% if PVD is present [14] and the risk is 15.6% within 5 years if the vitreous is still attached [15].

18.4 Clinical Presentation

Patients usually present with subacute blurring or distortion of vision. Due to lateral displacement of photoreceptors, patients with early (≤6 months) and small MH have a pincushion type of image distortion, where para-axial images are bowed inward toward the center of fixation [14, 16].

Severity of visual impairment depends on the stage and chronicity of MH. In stage 1 MH, visual acuity (VA) is usually around 20/20–20/60 [14]. In stage 2 MH, VA is usually around 20/40–20/100 [14]. In stage 3 or stage 4 MH, VA is usually around 20/60–20/400 [14].

In a biomicroscopic examination, a well-defined full-thickness MH (Fig. 18.6) appears as a reddish lesion at the center of the macula due to the loss of neurosensory retinal tissue. There may be a surrounding cuff of subretinal fluid. Some yellow whitish dots may be present at the base of the hole. An overlying floating operculum may be seen. Watzke–Allen test is useful to confirm full-thickness MH. It is performed by shining a slit beam across the hole. The result is considered

positive if the patient reports the beam is broken or thinned at the center [17].

Amsler grid test may show a pincushion type of metamorphosia in early small MH, in which the para-axial straight lines are seen bowing inward toward the center of fixation [16]. In larger MH, Amsler grid test may show nonspecific metamorphosia [16] or central scotoma.

18.5 Investigation

Although slit-lamp biomicroscopy has been the standard of making a diagnosis for a long time, in recent years, OCT has become the standard in making and confirming the diagnosis after clinical assessment. It is extremely useful to confirm, to stage, and to differentiate it from other macular lesions such as foveal cysts, lamellar holes, and pseudoholes, as these may mimic MH at times on biomicroscopy. The OCT features in different stages of MH have been described in previous sections. In stage 3 or 4 MH (Fig. 18.7), OCT often reveals the presence of intraretinal cysts, retinal thickening, and elevation at the edge of MH in addition to complete separation of all retinal layers.

Fluorescein angiography (Fig. 18.8) shows early hyperfluorescence at MH due to transmission defect [1]. Since the advent of OCT, fluorescein angiography is rarely necessary for the management of MH.

Fundus autofluorescence imaging (Fig. 18.9) shows increased autofluorescence at the MH because the fluorophore of lipofuscin in retinal pigment epithelium becomes directly visualized without the hindrance of the overlying neurosensory retina [18]. Surrounding the increased auto-
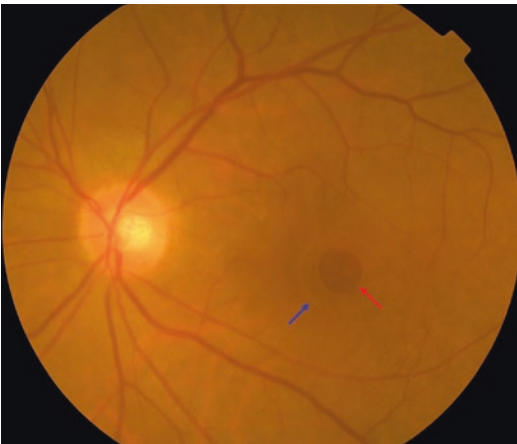
Fig. 18.6 Full-thickness macular hole. Fundus photography showing a full-thickness macular hole (red arrow) with a surrounding cuff of subretinal fluid (blue arrow) and some yellow whitish dots at the base of the hole

Fig. 18.8 Full-thickness macular hole. Fluorescein angiography showing hyperfluorescence in the early phase at the macular hole due to transmission defect (arrow)

Fig. 18.7 Full-thickness macular hole. Optical coherence tomography showing complete separation of all retinal layers, presence of intraretinal cysts, retinal thickening, and elevation at the edge of macular hole

fluorescence, there may be a ring of decreased autofluorescence corresponding to subretinal fluid cuff [19], and another ring of decreased autofluorescence corresponding to intraretinal cystic changes [18, 19].

18.6   Differential Diagnosis

18.6.1 Lamellar Macular Hole

Lamellar macular hole is a partial-thickness defect of the retina at the center of the macula. There is a loss of inner retinal tissue but the outer retina remains intact. Lamellar hole appears as an oval or

round reddish lesion in the fovea [7]. Unlike MH, lamellar hole does not have yellow whitish deposits at the base of the hole, cuff of subretinal fluid, or overlying operculum [1]. OCTs of the lamellar hole (Fig. 18.10) do not show complete separation of all retinal tissue; instead, there are irregular foveal contour, defect of the inner fovea, schitic changes at the edge of the hole, while the photoreceptor layer remains intact [7].

18.6.2 Pseudohole

Pseudohole is a lesion related to the centripetal contraction of an overlying epiretinal membrane (ERM) [20]. There is no loss of retinal tissue. However, the edge of the foveal pit becomes vertical following the contraction of the ERM [20]. Pseudohole appears as an oval or round reddish lesion in the fovea on slit-lamp biomicroscopy. On the OCT (Fig. 18.11), there are usually verti-

Fig. 18.9 Full-thickness macular hole. Fundus autofluorescence showing increased autofluorescence at the macula hole (arrow)
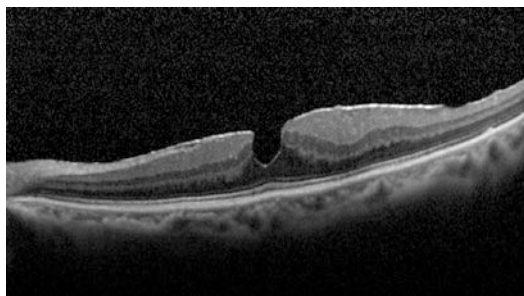
Fig. 18.11 Pseudohole. Optical coherence tomography showing vertical foveal edges, presence of an epiretinal membrane with a central opening and no loss of retinal tissue

Fig. 18.10 Lamellar hole. Optical coherence tomography showing the defect of inner retina, schitic change at the edge of the hole, and intact outer retinal layers

cal foveal edges, ERM with a central opening, normal, or near-normal central foveal thickness with no loss of retinal tissue [7].

18.7 Trend of Treatment: Pars Plana Vitrectomy and Internal Limiting Membrane Flap

MH was considered an untreatable condition until 1991 when Kelly and Wendel reported that vitrectomy, ERM peeling, gas tamponade, and postoperative strict facedown posture for at least 1 week was successful to treat idiopathic MH [21]. In their case series, 30 out of 52 patients (58%) achieved anatomical success after the operation [21]. The efficacy of PPV for MH was later confirmed in two large randomized controlled trials performed by the Vitrectomy for Macular Hole Study Group (VMHSG) [22, 23] and the Moorfields Macular Hole Study Group (MMHSG) [24]. VMHSG showed that after vitrectomy, stage 3 or 4 MH was closed in 69% and VA improved by at least two lines in 19% of eyes at 6 months [23]. MMHSG showed that after vitrectomy, MH was closed in 80% and 45% of eyes had VA of 20/40 or better at 24 months [24].

PPV serves several purposes in MH surgery. First, it allows the removal of vitreomacular traction, which is considered the etiology in MH formation. Second, PPV allows access to ERM and ILM so that the tangential tractional force on the macula can be relieved. Lastly, PPV creates space in the posterior segment so that gas tamponade can be performed. PPV, together with PVD induction, ERM removal, with or without ILM removal, gas tamponade, and postoperative facedown posture has become the standard of treatment for MH, with some modifications of technique to further improve the rate of surgical success.

In 1997, Eckardt et al. introduced the technique of *ILM peeling* to improve anatomical and functional success in MH surgery [25]. The ILM is the innermost layer of the retina and is considered the basement membrane of Muller cells, which contributes significantly to retinal rigidity

[26]. Removal of the ILM, therefore, improves retinal compliance and hence the chance of MH closure [26]. Studies showed that when ILM peeling had been performed, anatomical success was achieved in 92% to 100% of cases [27–30], whereas anatomical success was only 71% to 82% when no ILM peeling had been performed [28–30]. A meta-analysis of four randomized controlled trials showed that ILM peeling had significantly higher chances of MH closure than those without ILM peeling (odd ratio = 9.27, 95% confidence interval = 4.98 to 17.24), while the rates of intraoperative and postoperative complications were similar in both groups [31]. In addition to facilitating primary MH closure, ILM peeling also reduces the risk of postoperative ERM formation and MH reopening [26]. A meta-analysis of 50 publications on 5480 eyes showed that after 12 months, ILM peeling significantly reduced the MH reopening rate to 1%, compared with 7% without ILM peeling (odd ratio = 0.16, 95% confidence interval = 0.11–0.22) [32].

Despite PPV with ILM peeling, large chronic MH remains difficult to close. In a study of 24 eyes with chronic MH, 37.5% failed to close after a single operation [33]. In 2009, Michalewska et al. introduced the *inverted ILM flap* technique [34]. In this technique, a hinge of ILM flap at the edge of MH was left unpeeled during ILM peeling. The ILM flap is trimmed into an appropriate size with a vitreous cutter or vitreous scissors and is then inverted upside down to cover and fill the MH just before gas–fluid exchange [34]. Michalewska et al. showed with this technique the closure rate of large MH > 400 μm reached 98%, compared to 88% with PPV and conventional complete ILM peeling [34]. This technique is postulated to work by two mechanisms: (1) providing a scaffold for retinal tissue to approximate and (2) providing a flap that contains Muller cell fragments to induce glial cell proliferation. Subsequent studies show that this technique is promising in MH closure and visual improvement [35–37]. The inverted ILM flap technique has since become the trend for large MHs. The main difficulty lies in retaining the ILM flap in place during the later parts of the surgery, especially the gas–fluid exchange part. Different modifica-

tions of the technique have been suggested to improve the retention of the ILM flap on the macular surface, and to reduce the risk of iatrogenic retinal trauma and dissociated optic nerve fiber layer (DONFL). These include, but are not limited to techniques such as placing viscoelastic over the inverted ILM flap [38], covering the MH with several layers of inverted ILM flaps in a cabbage leave fashion [39], using heavy liquid for stabilization [40, 41], covering the MH instead of filling it [42], and creating temporal inverted ILM flap only to spare nasal ILM [43, 44].

Refractory and recurrent MH after previous vitrectomies remain major surgical challenges nowadays, especially when there is no ILM near the MH to enable the inverted ILM flap technique. Various procedures and adjuvant agents have been attempted to improve success rates for these cases, such as enlarging the area of ILM peel [45], perifoveal relaxing incisions to relax perifoveal tissue [46], temporal arcuate retinotomy [47], tapping of macular hole edges [48], outpatient gas–fluid exchange [49], autologous ILM transplantation [50], capsular flap transplantation [51], retinal free flap transplantation [52, 53], subretinal balanced salt solution injection to create macular detachment [54–57], macular plug with autologous serum [58], platelets concentrate [59], whole blood [59], or gluconated blood clumps [60]. However, most of these procedures were technically difficult to perform and were studied in small case series only. Therefore, they were not generally adopted [61]. There is still no universally agreed on consensus on the best approach [62]. Currently, the most straightforward approach for refractory or recurrent MH is to perform repeated PPV with enlargement of the ILM peel [62].

Another area of the controversy lies in the need and duration of postoperative facedown posture. Facedown posture is uncomfortable and is often associated with limited activities, back pain, and ulnar nerve palsy [62]. While strict facedown posture was considered necessary in Kelly and Wendel's pioneering case series in 1991, several studies suggested postoperative facedown posture was unnecessary and did not have any additional anatomical or functional benefits [63–65]. Two meta-analyses were performed

to evaluate the need for postoperative posture, but they concluded that evidence was insufficient due to large heterogeneity of studies regarding the duration of posture and surgical methods performed [66, 67]. The Positioning in Macular Hole Surgery (PIMS) study is a multicenter, randomized controlled trial currently underway to investigate the value of facedown posture after MH surgery [68, 69].

18.8   Conclusion

The management of idiopathic MH has evolved significantly since the past 30 years. There has been great improvement in the success rate of MH surgery due to a better understanding of disease pathogenesis and enhancement of surgical techniques, which evolve from ILM peeling to inverted ILM flap to facilitate MH closure. Various modifications in the technique have been attempted to improve the retention of the ILM flap on the macular surface and to reduce the risk of iatrogenic retinal trauma. Refractory and recurrent MH after previous vitrectomies remains major surgical challenges.

References

1. Ho AC, Guyer DR, Fine SL. Macular hole. Surv Ophthalmol. 1998;42(5):393–416.
2. Gass JD. Reappraisal of biomicroscopic classification of stages of development of a macular hole. Am J Ophthalmol. 1995;119(6):752–9.
3. Chan A, Duker JS, Schuman JS, Fujimoto JG. Stage 0 macular holes: observations by optical coherence tomography. Ophthalmology. 2004;111(11):2027–32.
4. Takahashi A, Yoshida A, Nagaoka T, et al. Macular hole formation in fellow eyes with a perifoveal posterior vitreous detachment of patients with a unilateral macular hole. Am J Ophthalmol. 2011;151(6):981–9.
5. Oh H. Idiopathic macular hole. Dev Ophthalmol. 2014;54:150–8.
6. Gaudric A, Haouchine B, Massin P, et al. Macular hole formation: new data provided by optical coherence tomography. Arch Ophthalmol. 1999;117(6):744–51.
7. Duker JS, Kaiser PK, Binder S, et al. The international vitreomacular traction study group classification of vitreomacular adhesion, traction, and macular hole. Ophthalmology. 2013;120(12):2611–9.

8. McCannel CA, Ensminger JL, Diehl NN, Hodge DN. Population-based incidence of macular holes. Ophthalmology. 2009;116(7):1366–9.

9. Forsaa VA, Lindtjorn B, Kvaloy JT, et al. Epidemiology and morphology of full-thickness macular holes. Acta Ophthalmol. 2018;96(4):397–404.

10. Wang S, Xu L, Jonas JB. Prevalence of full-thickness macular holes in urban and rural adult Chinese: the Beijing Eye Study. Am J Ophthalmol. 2006;141(3):589–91.

11. Rahmani B, Tielsch JM, Katz J, et al. The cause-specific prevalence of visual impairment in an urban population. The Baltimore Eye Survey. Ophthalmology. 1996;103(11):1721–6.

12. Meuer SM, Myers CE, Klein BE, et al. The epidemiology of vitreoretinal interface abnormalities as detected by spectral-domain optical coherence tomography: the beaver dam eye study. Ophthalmology. 2015;122(4):787–95.

13. Lewis ML, Cohen SM, Smiddy WE, Gass JD. Bilaterality of idiopathic macular holes. Graefes Arch Clin Exp Ophthalmol. 1996;234(4):241–5.

14. la Cour M, Friis J. Macular holes: classification, epidemiology, natural history and treatment. Acta Ophthalmol Scand. 2002;80(6):579–87.

15. Ezra E, Wells JA, Gray RH, et al. Incidence of idiopathic full-thickness macular holes in fellow eyes. A 5-year prospective natural history study. Ophthalmology. 1998;105(2):353–9.

16. Saito Y, Hirata Y, Hayashi A, et al. The visual performance and metamorphopsia of patients with macular holes. Arch Ophthalmol. 2000;118(1):41–6.

17. Tanner V, Williamson TH. Watzke-Allen slit beam test in macular holes confirmed by optical coherence tomography. Arch Ophthalmol. 2000;118(8):1059–63.

18. Teke MY, Cakar-Ozdal P, Sen E, et al. Fundus autofluorescence imaging of patients with idiopathic macular hole. Int J Ophthalmol. 2013;6(5):685–9.

19. Wakabayashi T, Ikuno Y, Sayanagi K, et al. Fundus autofluorescence related to retinal morphological and functional changes in idiopathic macular holes. Acta Ophthalmol. 2008;86(8):897–901.

20. Haouchine B, Massin P, Tadayoni R, et al. Diagnosis of macular pseudoholes and lamellar macular holes by optical coherence tomography. Am J Ophthalmol. 2004;138(5):732–9.

21. Kelly NE, Wendel RT. Vitreous surgery for idiopathic macular holes. Results of a pilot study. Arch Ophthalmol. 1991;109(5):654–9.

22. Kim JW, Freeman WR, Azen SP, et al. Prospective randomized trial of vitrectomy or observation for stage 2 macular holes. Vitrectomy for macular hole study group. Am J Ophthalmol. 1996;121(6):605–14.

23. Freeman WR, Azen SP, Kim JW, et al. Vitrectomy for the treatment of full-thickness stage 3 or 4 macular holes. Results of a multicentered randomized clinical trial. The vitrectomy for treatment of macular hole study group. Arch Ophthalmol. 1997;115(1):11–21.

24. Ezra E, Gregor ZJ. Surgery for idiopathic full-thickness macular hole: two-year results of a randomized clinical trial comparing natural history, vitrectomy, and vitrectomy plus autologous serum: Morfields Macular Hole Study Group Report no. 1. Arch Ophthalmol. 2004;122(2):224–36.

25. Eckardt C, Eckardt U, Groos S, et al. Removal of the internal limiting membrane in macular holes. Clinical and morphological findings. Ophthalmologe. 1997;94(8):545–51.

26. Chatziralli IP, Theodossiadis PG, Steel DHW. Internal limiting membrane peeling in macular hole surgery; why, when, and how? Retina. 2018;38(5):870–82.

27. Mester V, Kuhn F. Internal limiting membrane removal in the management of full-thickness macular holes. Am J Ophthalmol. 2000;129(6):769–77.

28. Olsen TW, Sternberg P Jr, Capone A Jr, et al. Macular hole surgery using thrombin-activated fibrinogen and selective removal of the internal limiting membrane. Retina. 1998;18(4):322–9.

29. Brooks HL Jr. Macular hole surgery with and without internal limiting membrane peeling. Ophthalmology. 2000;107(10):1939–48. discussion 48-9

30. Al-Abdulla NA, Thompson JT, Sjaarda RN. Results of macular hole surgery with and without epiretinal dissection or internal limiting membrane removal. Ophthalmology 2004;111(1):142–149.

31. Spiteri Cornish K, Lois N, Scott N, et al. Vitrectomy with internal limiting membrane (ILM) peeling versus vitrectomy with no peeling for idiopathic full-thickness macular hole (FTMH). Cochrane Database Syst Rev. 2013;(6):Cd009306.

32. Rahimy E, McCannel CA. Impact of internal limiting membrane peeling on macular hole reopening: a systematic review and meta-analysis. Retina. 2016;36(4):679–87.

33. Scott RA, Ezra E, West JF, Gregor ZJ. Visual and anatomical results of surgery for long standing macular holes. Br J Ophthalmol. 2000;84(2):150–3.

34. Michalewska Z, Michalewski J, Adelman RA, Nawrocki J. Inverted internal limiting membrane flap technique for large macular holes. Ophthalmology. 2010;117(10):2018–25.

35. Kuriyama S, Hayashi H, Jingami Y, et al. Efficacy of inverted internal limiting membrane flap technique for the treatment of macular hole in high myopia. Am J Ophthalmol. 2013;156(1):125–31.

36. Michalewska Z, Michalewski J, Dulczewska-Cichecka K, Nawrocki J. Inverted internal limiting membrane flap technique for surgical repair of myopic macular holes. Retina. 2014;34(4):664–9.

37. Olenik A, Rios J, Mateo C. Inverted internal limiting membrane flap technique for macular holes in high myopia with axial length >= 30 mm. Retina. 2016;36(9):1688–93.

38. Andrew N, Chan WO, Tan M, et al. Modification of the inverted internal limiting membrane flap technique for the treatment of chronic and large macular holes. Retina. 2016;36(4):834–7.

39. Aurora A, Seth A, Sanduja N. Cabbage leaf inverted flap ILM peeling for macular hole: a novel tech-

nique. Ophthalmic Surg Lasers Imaging Retina. 2017;48(10):830–2.

40. Shin MK, Park KH, Park SW, et al. Perfluoro-n-octane-assisted single-layered inverted internal limiting membrane flap technique for macular hole surgery. Retina. 2014;34(9):1905–10.

41. Pak KY, Park JY, Park SW, et al. Efficacy of the perfluoro-N-octane-assisted single-layered inverted internal limiting membrane flap technique for large macular holes. Ophthalmologica. 2017;238(3):133–8.

42. Rossi T, Gelso A, Costagliola C, et al. Macular hole closure patterns associated with different internal limiting membrane flap techniques. Graefes Arch Clin Exp Ophthalmol. 2017;255(6):1073–8.

43. Michalewska Z, Michalewski J, Dulczewska-Cichecka K, et al. Temporal inverted internal limiting membrane flap technique versus classic inverted internal limiting membrane flap technqiue: a comparative study. Retina. 2015;35(9):1844–50.

44. Takai Y, Tanito M, Sugihara K, et al. Temporal inverted internal limiting membrane flap technique for a macular hole patient unable to maintain postoperative prone positioning. Retin Cases Brief Rep. 2016;10(4):323–6.

45. D'Souza MJ, Chaudhary V, Devenyi R, et al. Re-operation of idiopathic full-thickness macular holes after initial surgery with internal limiting membrane peel. Br J Ophthalmol. 2011;95(11):1564–7.

46. Reis R, Ferreira N, Meireles A. Management of Stage IV macular holes: when standard surgery fails. Case Rep Ophthalmol. 2012;3(2):240–50.

47. Charles S, Randolph JC, Neekhra A, et al. Arcuate retinotomy for the repair of large macular holes. Ophthalmic Surg Lasers Imaging Retina. 2013;44(1):69–72.

48. Kumar A, Tinwala SI, Gogia V, Sehra SV. Tapping of macular hole edges: the outcomes of a novel technique for large macular holes. Asia Pac J Ophthalmol (Phila). 2013;2(5):305–9.

49. Rao X, Wang NK, Chen YP, et al. Outcomes of outpatient fluid-gas exchange for open macular hole after vitrectomy. Am J Ophthalmol. 2013;156(2):326–33.

50. Morizane Y, Shiraga F, Kimura S, et al. Autologous transplantation of the internal limiting membrane for refractory macular holes. Am J Ophthalmol. 2014;157(4):861–9.

51. Chen SN, Yang CM. Lens capsular flap transplantation in the management of refractory macular hole from multiple etiologies. Retina. 2016;36(1):163–70.

52. Liu PK, Chang YC, Wu WC. Management of refractory macular hole with blood and gas-assisted autologous neurosensory retinal free flap transplantation: a case report. BMC Ophthalmol. 2018;18(1):230.

53. Ding C, Li S, Zeng J. Autologous neurosensory retinal transplantation for unclosed and large macular holes. Ophthalmic Res. 2018:1–6.

54. Oliver A, Wojcik EJ. Macular detachment for treatment of persistent macular hole. Ophthalmic Surg Lasers Imaging. 2011;42(6):516–8.

55. Szigiato AA, Gilani F, Walsh MK, et al. Induction of macular detachment for the treatment of persistent or recurrent idiopathic macular holes. Retina. 2016;36(9):1694–8.

56. Claes CC. Internal repair of very large, myopic and recurrent macular holes by creation of a central retinal detachment and silicone oil tamponade. Retina. 2017;39:S72. https://doi.org/10.1097/IAE.0000000000001767. [Epub ahead of print].

57. Wong R, Howard C, Orobona GD. Retina expansion technique for macular hole apposition report 2: efficacy, closure rate, and risks of a macular detachment technique to close large full-thickness macular holes. Retina. 2018;38(4):660–3.

58. Ezra E, Aylward WG, Gregor ZJ. Membranectomy and autologous serum for the retreatment of full-thickness macular holes. Arch Ophthalmol. 1997;115(10):1276–80.

59. Purtskhvanidze K, Fruhsorger B, Bartsch S, et al. Persistent full-thickness idiopathic macular hole: anatomical and functional outcome of revitrectomy with autologous platelet concentrate or autologous whole blood. Ophthalmologica. 2018;239(1):19–26.

60. Chakrabarti M, Benjamin P, Chakrabarti K, Chakrabarti A. Closing macular holes with "macular plug" without gas tamponade and postoperative posturing. Retina. 2017;37(3):451–9.

61. Koo EB, Smiddy WE. Internal limiting membrane flap technique for macular holes: is it ready for prime time? Retina. 2018;38(5):865–9.

62. Tam ALC, Yan P, Gan NY, Lam WC. The current surgical management of large, recurrent, or persistent macular holes. Retina. 2018;38(7):1263–75.

63. Tornambe PE, Poliner LS, Grote K. Macular hole surgery without face-down positioning. A pilot study. Retina. 1997;17(3):179–85.

64. Tranos PG, Peter NM, Nath R, et al. Macular hole surgery without prone positioning. Eye (Lond). 2007;21(6):802–6.

65. Mittra RA, Kim JE, Han DP, Pollack JS. Sustained postoperative face-down positioning is unnecessary for successful macular hole surgery. Br J Ophthalmol. 2009;93(5):664–6.

66. Tatham A, Banerjee S. Face-down posturing after macular hole surgery: a meta-analysis. Br J Ophthalmol. 2010;94(5):626–31.

67. Solebo AL, Lange CA, Bunce C, Bainbridge JW. Face-down positioning or posturing after macular hole surgery. Cochrane Database Syst Rev. 2011;(12):Cd008228.

68. Pasu S, Bunce C, Hooper R, et al. PIMS (positioning in macular hole surgery) trial - a multicentre interventional comparative randomised controlled clinical trial comparing face-down positioning, with an inactive face-forward position on the outcome of surgery for large macular holes: study protocol for a randomised controlled trial. Trials. 2015;16:527.

69. Bell L, Hooper R, Bunce C, et al. Positioning in macular hole surgery (PIMS): statistical analysis plan for a randomised controlled trial. Trials. 2017;18(1):274.

Inverted Internal Limiting Membrane Flap for Full-Thickness Macular Hole

19

Jerzy Nawrocki, Zofia Nawrocka, and Zofia Michalewska

19.1 Introduction

Vitrectomy for macular hole (MH) became the treatment choice after the first publication on the topic by Kelly and Wendel in 1991 [1]. In their first paper, they reported MH closure in 58% of cases. At that time, reattached MH margins with visible bare pigment epithelium were considered as MH closure. They improved their results over the following 2 years to 73%, still defining surgical success as "the edges of the MH being attached to the underlying retinal pigment epithelium (RPE), with flattening of the cuff of retinal detachment (RD) around the hole" [2]. The results were based on ophthalmoscopic findings as optical coherence tomography (OCT) was not available in those days. They observed that large and old MHs closed very rarely and visual outcomes are worse in those eyes. The first huge improvement in anatomical results was associated with the introduction of an internal limiting membrane (ILM) peeling in MH surgery [3]. The development of optical coherence tomography as an everyday tool in ophthalmological practice has tremendously enhanced our knowledge of the etiopathogenesis and treatment of MH. Surgical success is now defined as either complete closure of the MH: types U, V, and irregular closure, or as flattening of the margins of the MH called "flat open."

The latter is associated with worse functional results and we, therefore, believe that this type of outcome should be considered a failed intervention and not a closure. (Examining the postoperative macula configuration with OCT, in 19% to 39% of cases, we see flat MH margins with bare retinal pigment epithelium, which are described variously in the literature as: flat open, W-type closure, flat closed MH, or type two closure) [4–6].

Initially, our surgical approach to an MH was vitrectomy, ILM peeling, and gas injection. Neither searching through the literature nor asking other surgeons gave us a solution for how to treat this condition whilst preventing the flat open postoperative configuration of the retina—which did not allow us to achieve our goal of visual acuity improvement. Thus, I (JN) decided to video all of my surgical interventions and to try to find a correlation with OCT images. In 2005, I operated on a large MH, in which traction had caused the inner retinal layers to split from the outer retinal layers. Whilst performing ILM peeling from the inner layers of the retina, I observed that some additional piece of tissue was removed. The case resulted in a flat open type of MH surgical outcome. My personal feeling was that if I had not removed that tissue, complete closure of the MH would probably have been achieved (see Figs. 19.1 and 19.2).

We later discussed what kind of tissue we might be able to use to improve the quality of MH closure. The obvious choice was ILM. In 2006, I performed my first surgeries with the inverted ILM

J. Nawrocki (✉) · Z. Nawrocka · Z. Michalewska
Gabinet Okulistyczny N&M, Łódź, Poland

Ophthalmic Clinic "Jasne Błonia", Łódź, Poland
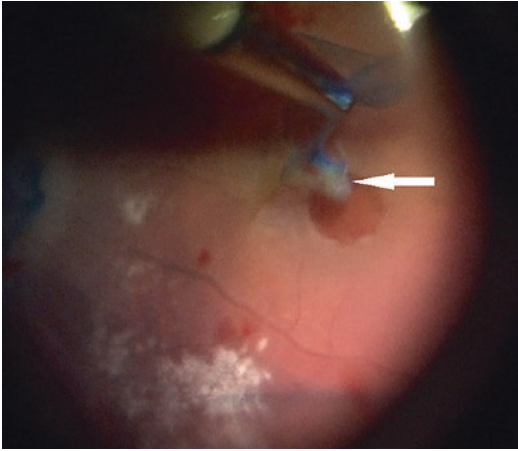
Fig. 19.1 ILM peeling from the torn inner layers of the retina. Please note that some whitish tissue is still present close to the center of the fovea (arrow)
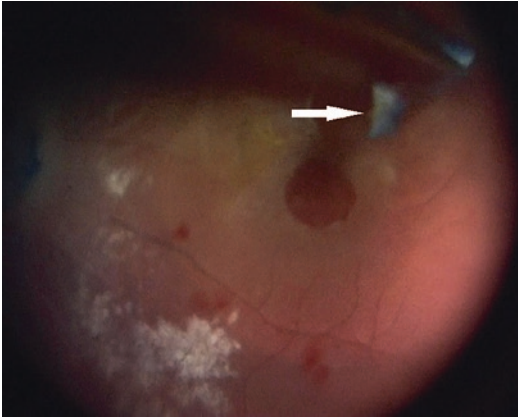
Fig. 19.2 ILM is peeled together with the whitish tissue, which is removed and is visible away from the retina

flap technique. From the very beginning, we had the feeling that the results seemed to be better but we waited until 2009 before we presented the method, just to confirm our primary results [7]. Subsequently, our video showing the technique was awarded at several annual meetings including the American Society of Retina Specialists, the European VitreoRetinal Society, and the German Ophthalmological Society. By that time, we had operated on more than 200 cases and we had some long-term observations for our comparative study of classical ILM peeling versus the inverted ILM flap technique, which we felt was ready for publication [8].

19.2   Mechanism of Action

ILM is the innermost layer of the retina, a thin, transparent membrane at the inner surface of the retina. Histopathological reports have confirmed its thickness to be 2.5–20 μm depending on the methods of histopathological tissue processing [9–11]. The ILM is thickest in the fovea and its thickness decreases toward the periphery. The vitreous side of ILM is smooth and the retinal side is rough with an appearance of mountains and ridges separated by valleys and crypts. The retinal side of the ILM is five times stiffer than the vitreal side [9].

Even if ILM itself has no contractile properties it was reported to act as a scaffold for the membranes to exert tangential traction on the fovea [12]. ILM cannot regrow [13]. However, as a base membrane, it has the properties to enable cell proliferation. In nonhuman primates, it was confirmed that healing of the ILM-debrided area occurred in the form of stretching and flattening of neighboring Müller cell processes in addition to reactive gliosis over the nerve fibers in the denuded area. Although histopathological examinations of eyes after successful vitrectomy with ILM peeling in humans are not available, Kase et al. have confirmed with histology examination that the membrane peeled and used for inverted ILM flap is ILM [14]. Thus, it might be extrapolated that after peeling just a fragment of the ILM and inverting it, so that it lies upside down on the macula, similar processes will occur and the cells additionally have a scaffold over the area of the MH to utilize.

Müller cells have a supportive role for neurons, they have a fundamental role in transmitting light through their funnel-like shape, similar to fiber optic plates [15]. Thus, gliosis after the inverted ILM flap technique may increase the amount of light falling on particular photoreceptors, which in turn might be responsible for increased visual acuity. Detailed visualization of the retina before and after vitrectomy with the inverted ILM flap technique has been presented [16]. Swept Source OCT enables us to show the changes in the anatomy of the retina confirming regeneration (Fig. 19.3).

Fig. 19.3 Swept Source OCT images. (**a**) Preoperative view of the macular hole. (**b**) 1-week postoperative image. The macular hole is closed with the inverted ILM flaps. (**c**) 5 months postoperatively some retinal tissue and photoreceptors are present and elevated above the retinal pigment epithelium. Small defects are visible in the photoreceptor layer. (**d**) 9 months postoperatively, complete recovery of the inner layers of the retina. Remnants of an ILM flap detached from the retina are visible in images **c** and **d**
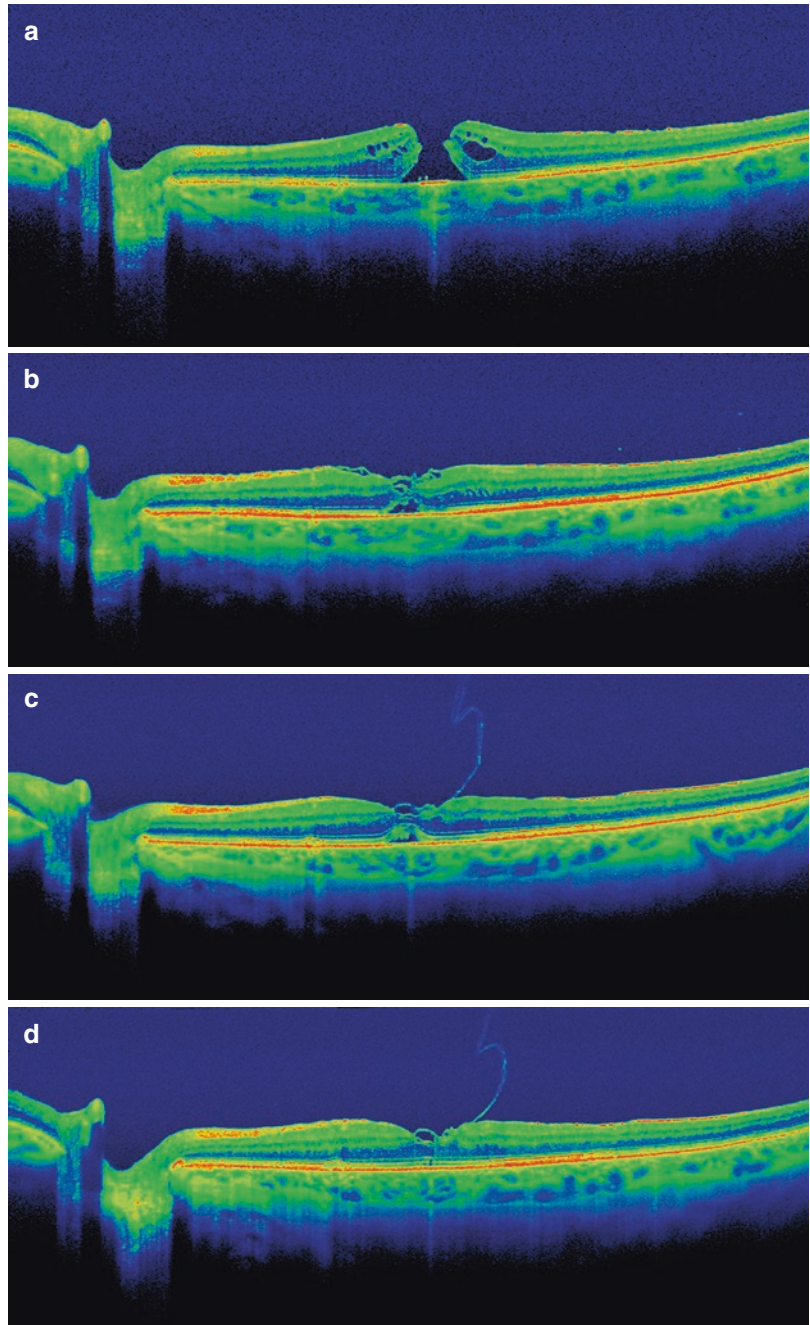
Retina regeneration has not been reported in humans. In zebrafish, it was reported that Müller glia undergoes dedifferentiation into multipotent progenitor cells. The progenitor cell can then divide and differentiate into a number of retinal cell types, including photoreceptor cells damaged during an earlier injury [17]. Experimental studies in human cell cultures have demonstrated that Müller cells may serve as stem cells for the adult retina and may be photoreceptor progenitors [18, 19] However, in mammals, there is a block disabling retinal regeneration [20].

Echoing our earlier 2010 paper, we have reported our observation of the MH filling with tissue during follow-up [21]. It seems that photoreceptor cells follow the gliosis and either reapproximate or regrow over time. It was previously suggested that ILM serves as a scaffold for gliosis [22].

Shiode et al. recently published the results of their investigation into the role of the inverted ILM flap in MH closure using an experimental MH model in monkeys. They confirmed that the ILM functioned as a scaffold for the migration and proliferation of Müller cells and that it may promote their activation [23].

Vieregge et al. conducted a 1-year follow-up study into retinal regeneration after the flap technique for MH repair. They observed complete anatomical closure in all 11 patients as well as microstructural regeneration and a decrease in ellipsoid zone defects. Compared to baseline, all patients showed a BCVA improvement of 1–4 lines [24].

19.3   Surgical Approach

During our original approach, core vitrectomy was performed, posterior hyaloid was detached and removed, and trypan blue staining (Membrane Blue, DORC, Rotterdam, Netherlands) was used for approximately 40 s to 1 min. ILM was peeled around the MH with Eckardt forceps (DORC, Rotterdam, Netherlands) at approximately 2 disc diameters but was not removed completely—the ILM was left attached to the margins of the MH. The peripheral part of the ILM was trimmed

with a vitreous cutter or vitreous scissors. (We were afraid at that time that leaving large pieces of ILM could increase the rate of postoperative epiretinal formation and so, by keeping the ILM flap as small as possible, we would lessen the chance of epiretinal membrane formation. Unfortunately, this maneuver may increase the chance of losing the flap.) The small remnants of the ILM were then massaged gently over the MH from all sides until the ILM was inverted, that is, turned upside down so that the surface normally facing the vitreous body now faced the retinal pigment epithelium but was still on the top of the retina, and the flaps were laying over the MH and covering it. (they were not introduced into the hole). The flap was then secured in place with fluid–air injection (Fig. 19.4). Patients were advised to stay for up to 3 days in a position where they could see the air bubble in the center of their visual field [8].

19.3.1 Modifications of the Original Technique

Since the introduction of the original inverted ILM flap technique, we and other authors have investigated modified approaches to most aspects
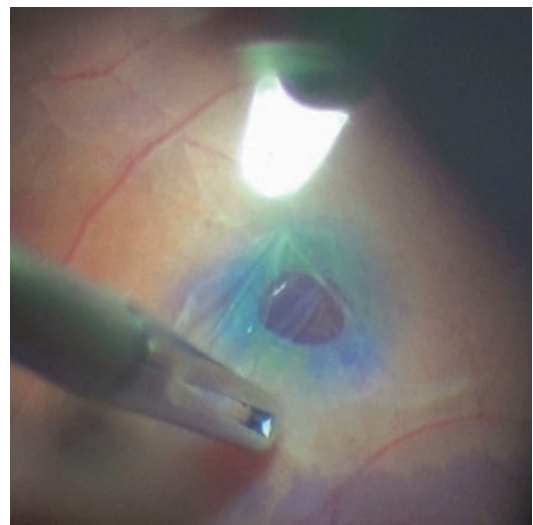
Fig. 19.4 The surgeon places the temporal ILM flap on the surface of the retina covering the macular hole

of the surgical intervention such as visualization, flap positioning: including laying the flap over the MH as in the original technique or "filling" the MH with the flap, using multiple flaps, transplanting a patch of ILM, and others. The literature dealing with many of these modifications are loosely grouped in the following subsections.

19.3.1.1 Visualization

Various authors have used different dyes to stain the ILM. Although some authors have been successful when using indocyanine green (ICG), Imai and Azumi have published a single case report showing that retinal pigment atrophy might occur if ICG is used during inverted flap surgery [25]. We believe that as the inverted ILM flap touches RPE and some ICG cytotoxicity to the RPE has been demonstrated, we should generally discourage its use when performing the technique and we prefer to use trypan blue. Mahalingam and Sambhav modified the surgical approach by using triamcinolone acetonide for better visualization in the induction of posterior vitreous detachment and Brilliant Blue dye for ILM peeling [26].

19.3.1.2 Peeling

A surgical approach may be performed with any kind of vitrectomy equipment including 20 g, 23 g, 25 g, and 27 g. Berrocal used the 27 g Finesse Flex Loop of Alcon's Constellation Vision System to break the ILM and remove it from around the macular, leaving a hinged flap to successfully close a large MH [27].

ILM peeling leads to dissociated optic nerve fiber layer (DONFL) as described by Tadayoni et al [28]. The role of this observation is still not completely understood. When using the original ILM flap technique, we had observed that during fluid–air exchange an ILM flap primarily positioned between the optic nerve and MH often returned to its original position. Considering these two facts, we proposed a modification of our original technique, which we call the "temporal inverted ILM flap technique" [29]. We refrain from peeling ILM in the area between the optic nerve and fovea. Instead, ILM is peeled only on the temporal side of the MH and put in inverted

fashion on the top of the retina, which causes less overall trauma to the nerve fibers. The results achieved showed no statistically significant differences between these techniques in either anatomical or functional results. However, in the temporal inverted ILM flap technique, DONFL is observed only on the temporal (peeled) side of the macular hole [16]. A similar idea came to Japanese authors who have published the successful results of their "hemi-inverted ILM flap technique" [30]. Belyi et al. suggest a similar method: "Surgical procedure was notable for an original ILM flap created in a way that resembles removing petals from a flower" [31]. The method implies that the ILM is peeled off all the way around the MH except for the foveolar area and one particular ILM fragment, which is only partially separated from the retina, from the periphery toward the MH, stopping at some 0.1–0.2 mm from its margin. This last fragment is then inverted to cover the MH. A recently published paper from Finn and Mahmoud describes what they call the "Retracting Door" technique [32]. In this interesting modification, the authors suggest peeling the taught ILM from the nasal side, over the hole to a point on the temporal side of the hole, and then laying it back down. The previously taught ILM has in effect "moved over" as it relaxes into the lower area behind the raised ridges of the hole's temporal edge so that the ILM is now relaxed and retracted and now covers the MH.

19.3.1.3 Flap Positioning and Tamponades

Chen and Yang suggest that lowering the perfusion pressure when inverting the flap might help to avoid dislocation of the flap during surgery [33].

Shin et al. used Brilliant Blue G for staining (BBG; Sigma Aldrich, St. Luis, MO, USA) and perfluoro-n-Octane liquid to secure the position of a specially prepared ILM flap in an inverted position. An ILM flap of about 1 disc diameter size was used to cover the MH from the superior margin [34]. Song et al. successfully used Viscoat (Alcon Laboratories, Fort Worth, TX, USA) as a glue to assist with the proper positioning of the

superior flap on the inferior part of the macula where ILM had been previously peeled in 15 cases of myopic MH [35]. To similarly stabilize the ILM flap, Sasaki et al. also used Viscoat and reported that the inverted ILM flap technique resulted in a 100% primary closure rate, 100% primary reattachment, and a significantly better 6-month BCVA when compared to ILM peeling for macular hole-associated RD in highly myopic eyes [36].

Andrew et al. presented a modification of the flap technique for chronic and large macular holes [37]. After vitrectomy and posterior hyaloid detachment, they peeled ILM at 2 disc diameters around the macular hole. "Care is taken to ensure that the ILM rhexis does not rupture while circumnavigating the hole and that small attachment connecting free ILM to the hole edge is preserved." The ILM flap is then folded into the MH bed to fill the defect completely and viscoelastic is injected over the ILM flap. Their technique allowed them to close all 24 chronic large macular holes and improve the mean visual acuity from 20/160 to 20/60.

Some authors prefer to harvest a flap of ILM from elsewhere and transplant this patch to cover of fill the MH. Hernandez-da Mota and Bejar-Cornejo inserted a "free" ILM flap into the MH, this time with the use of perfluorocarbon liquid (PFCL) [38]. Pires et al. harvested a fragment of the ILM and placed it into the hole for refractory MH [39]. They achieved closure in 11/12 eyes and mean visual acuity improvement from 20/400 to 20/160, however, less than 16.7% had visual acuity equal or above 20/63.

Joondeph published three cases of MH repair where he used either a flap or patch to successfully close the hole and suggested that the ILM can be gently tucked under the hole edge to help secure it [40]. Dai et al. used a free flap of ILM, carefully inserted into the MH, and trapped under the hole edges in 13 cases of large MH reoperation [41]. The mean preoperative base diameter was 1637.6 μm and successful closure was reported in 12 eyes. In one remaining case, the largest in the series, with a base diameter of 2092 μm, the patient had a history of vitrectomy for rhegmatogenous RD and the authors stated that the transplanted ILM flap moved away from the inside of the hole during the fluid–air exchange. The outcome was reported as a flat open closure (i.e., closed with bare RPE).

Recently Chakrabarti et al. performed a broad internal limiting membrane peel, inverted internal limiting flap repositioning, and used autologous gluconated blood clumps as a macular plug to close the MH [42]. One hundred percent MH closure was achieved in 26 eyes. Mean visual acuity improved from 6/60 to 6/18.

Many of the earlier papers show that some success may also be achieved if we introduce ILM into the hole. This is, however, somewhat in contradiction with the majority of papers and our own method concept, where the flap is placed on top of the hole. These approaches are often referred to as the "cover" (original) and the insertion (modified) methods with the latter commonly now being described as "filling" or "stuffing" the MH. Recently Park et al. presented a comparative study for large macular holes using internal limiting membrane insertion versus ILM flap technique [43]. The authors found that both methods may be effective for hole closure but the inverted ILM flap technique results in better recovery of photoreceptor layers and better visual acuity (0.773 vs. 0.527, $p = 0.006$) was achieved. Rossi et al. compared cover and fill techniques and found similar closure rates and postoperative vision at 3 months [44]. Again, they report better anatomical restoration and vision at 1 month in the "cover" group but found the "fill" technique more efficient in closing larger MHs.

Velez-Montoya et al. compared classical ILM peeling, inverted ILM flap, and free flap insertion for the treatment of large macular holes [45]. Although closure rates were similar in all three groups and all of the groups achieved ≈0.2 logMAR improvements in BCVA, the authors reported that a faster improvement in BCVA was achieved in the inverted flap technique group and only this group reached a statistically significant improvement ($p < 0.0007$ at the month 3 follow-up). A large cohort comparative study may prove useful if there is a difference in results between these two concepts similar to the ongoing study begun by Becker et al. [46]

Our own data in cases of repeated surgery may suggest that putting ILM on top of the retina may be less traumatic and lead to better results (Zofia Michalewska, Jerzy Nawrocki. Repeat surgery in failed primary vitrectomy for macular holes operated with the inverted ILM flap technique. Ophthalmic Surg Lasers Imaging Retina. In press.). However, in repeated cases after a failed classical approach as well as in difficult cases, for example in high myopia MH with RD, it may be very difficult to both create an ILM flap to place on the top of the retina and to keep it in position on the surface of the retina. Therefore, if using an autologous ILM transplant, it may be a good option to introduce the flap into the hole.

19.3.1.4   Patient Positioning

In cases when the patient cannot maintain a face-down position, it may be useful to use silicone oil as a tamponade agent [47]. Maneuvers with the inverted ILM flap are easier when using silicone oil and the surgeon can better confirm the position of the flap. Furthermore, the patient is not required to maintain a specific head position. Choi et al. used a superior inverted internal limiting flap to successfully close an FTMH and additionally suggest that with this method, strict facedown positioning may not be required [48]. Takai et al. used a temporal inverted ILM flap in such a case with success [49]. Chakrabarti's previously described autologous blood tamponade also seems to do away with the need for patient positing.

19.3.2 In Summary

Looking at the literature in regard to surgical approaches we can draw some basic conclusions, there is complete agreement that vitrectomy with posterior hyaloid detachment should be performed. Different stains may be used for better visualization of posterior vitreous or no staining at all. Most of the current discussions on the topic are directed to the question of where we should peel the ILM: Peel around the hole? Should we create a temporal or superior flap? Should we create more than one flap and multilayer them?

Cover or fill? We would like to focus on the fact that, if we succeed in covering the MH with ILM and securing it in place—we will close the MH. Each surgeon may decide to perform single or multilayer coverage of the MH according to her or his feelings and experience. We believe that it is probably better to put the flap on the top of the retina to cover the MH rather than introducing the flap into the hole. However, the latter may be easier to perform. The decision to use additional substances to help keep the flap in the position (viscoelastic, perfluorocarbon, etc.) should also be at the discretion of the surgeon. The number of papers presenting these various options is continuing to grow [50–63].

19.4   Indications

Shortly after the introduction of the inverted ILM flap technique for its primary indication, namely large, long-standing macular holes, new indications for the use of this technique were already being suggested. Some, such as using the technique to treat smaller idiopathic macular holes, are logical expansions of the technique and, in this case, have been found as effective as the more classical ILM peeling approach. The initial successes reported in the literature and at international ophthalmology meetings has also led surgeons to attempt more difficult MH cases such as myopic MH and rarer cases such as traumatic MH where their attempts have met with success. Other ideas have been explored by surgeons determined to find solutions to more challenging cases such as optic pit maculopathy.

19.4.1 Large Macular Holes

We selected large macular holes (i.e., those with a minimum diameter of at least 400 μm, not those with only large basal diameter) as our first indication for the inverted ILM flap technique because we knew that the results of the classical ILM peeling approach in this specific indication are not very encouraging and flat open MH is a frequently observed outcome. We decided to prepare

a prospective randomized clinical trial [8]. Group 1 comprised 51 eyes of 40 patients who were treated with standard pars plana vitrectomy ILM peeling and air, and Group 2 comprised 50 eyes of 46 patients where the inverted ILM flap technique was performed. Mean minimal hole diameters were 698 μm in Group 1 and 759 μm in Group 2. The results showed that in 43 eyes in Group 2, where the inverted ILM flap was left on the macular surface and covering the hole, 100% of macular holes were closed and no flat open appearance was observed. In Group 1, an 88% success rate, including 19% flat open macular holes, was achieved. Furthermore, functional results were statistically significantly better after 1 year in Group 2 (0.17 vs. 0.28 in Groups 1 and 2, respectively). This first paper also demonstrated that fovea contour shows filling with tissue and photoreceptor defects decrease over time. At that time, we were hesitant to refer to this as the regeneration of the foveal tissue. Good results using this technique for large macular holes were also achieved by Mahaligam and Sambhav and by Khodani et al. [26, 64]

At the ASRS meeting in Boston in 2017, Naresh Kanna presented a comparative study into the inverted ILM flap technique versus classical ILM peeling for large macular holes. He compared 28 cases of each method and reported closure in 89.3% of cases using the flap technique compared to 75% of cases where classical peeling was used.

Rizzo et al. conducted a very large comparative study in inverted flap intervention versus classical ILM peeling. They reported overall closure rates of 91.93% in an inverted flap group of 320 patients as opposed to 78.75% in the ILM peeling group of 300. BCVA improvements were statistically significant in the inverted flap cases with an MH diameter >400 μm [65]. In smaller MH cases, both techniques were equally successful.

Other authors have published papers reporting very encouraging results when using an inverted flap technique in relatively large comparison studies. Yamashita et al. compared surgical outcomes of ILM peeling to the inverted ILM flap technique for 165 cases of large macular holes from nine Japanese hospitals [66]. They found a medium–large MH closure rate of 95.2% (59/62) in the ILM peeling group and 100% (19/19) in the ILM flap group. In extra-large MH cases (> 550 μm), the closure rate was 88.4% (38/43) with ILM peeling and 100% (41/41) with the ILM flap technique. Additionally, Manasa et al. compared ILM peeling with the ILM flap technique in 100 cases of MH ≥ 600 μm [67]. They report type 1 closure in 34.04% of ILM peeling cases and in 62.79% of flap cases ($P = 0.02$). Two other papers have been published on the benefits of using the inverted flap technique in large, and especially very large, MH cases when compared to ILM peeling [68, 69].

We still do not know the limitations of our surgical attempts and at which size of MH we should give up. Probably the largest MH successfully treated with the flap technique to date, is that presented by Deshpande and Narayanan [70]. The basal diameter of the hole was 2845 μm and full closure was reported at the 2-week follow-up. Interestingly, Kubota et al. used the inverted ILM flap technique to attempt to close a 1.5 disc diameter idiopathic "horseshoe-like" macular tear with RD [71]. Although complete closure was not achieved, at the 1-month follow-up visit the tear was reduced to 0.5 disc diameter, VA improved and the retina around the tear was attached. It seems possible to us that the hole may continue to fill with tissue and improved results may yet follow.

19.4.2 Myopic Macular Hole with and without Retinal Detachment

Good results are also achieved in high myopia. Kuriyama et al. presented 10 cases with an axial length between 26.7 and 33.0 mm (Mean 29.5 mm) [72]. They used a variation of the flap technique for where they employed indocyanine green staining and 20% SF6 gas was finally added. Interestingly they did not peel the epiretinal membrane so as to remove it, but inverted it along with the ILM, which was not trimmed, and the macular holes were covered with larger

inverted flaps. By this time (2013) our group had already stopped trimming the ILM flap for two reasons: firstly, trimming increases the chances of losing the flap as it may be made too small to remain in place, and secondly, although we initially feared postoperative epiretinal membrane formation in the flap area, we had never seen this occur so trimming the flaps brought no additional benefit. Subsequently, our paper on myopic MH repair does not suggest trimming the ILM flaps [21]. We presented 19 eyes with myopic MH. Closure was achieved in all 19 eyes and visual acuity improved by a mean of 6 logMAR lines from the initial mean visual acuity of 1.2 logMAR to 0.56 logMAR at the 1-year follow-up. In Kuriyama's paper, seven eyes had either type 1 or 2 staphyloma. They achieved MH closure in three of four eyes with retinal detachment caused by MH and the fourth eye was healed after second surgery with silicone oil. MH was closed in five of six eyes without RD. Postoperative visual acuity improvement of more than two lines was achieved in 50% of eyes. The authors presented two cases with MH and myopic retinoschisis which were also successfully treated and suggest the usefulness of the method for myopic MH surrounded with retinoschisis. None of the closed macular holes showed flat open appearance after surgery. This finding was also confirmed by their subsequent paper in 2014 [73].

Wu reported a 100% first operation success rate in treating six highly myopic eyes with an axial length above 30 mm for MH by inserting the ILM flap into the holes [74]. Visual acuity improved from 1.21 log Mar to 1.08 logMAR after a mean follow-up of 8.5 months. In his concurrent ILM peeling group, the primary closure rate was 37.5% and visual acuity improved from 1.01 to 0.67 logMAR during the follow-up of 23.88 months.

A particularly interesting contribution to the discussion on the inverted ILM flap technique for MH in high myopia comes from Olenik et al. [75]. We learned from the paper of Suda et al. that macular holes do not close with the classical approach if the axial length of the eye is >30 mm [76]. Olenik et al. were the first authors to present their results of using the inverted ILM flap

technique in regard to this specific group of patients, additionally, all of their patients had staphyloma. In all 33 eyes, the macular holes were closed at the 1-month follow-up, and mean visual acuity improved from 0.59 logMAR to 0.4 logMAR. Dissociated optic nerve fiber layer was observed in 75% of cases. An additional aspect of this paper is that the above-cited group is famous for submacular plombage in this specific indication.

Garcia-Arumi performed a comparative study of high myopic eyes treated either by vitrectomy with ILM peeling or with the inverted ILM flap technique. He achieved a closure rate of 77% when performing ILM peeling and a closure rate of 100% when performing the inverted ILM flap technique. Visual acuity improvement was observed in both groups (Club Jules Gonin, Bordeaux, France, 2016). The comparative study by Rizzo and coworkers included a subgroup of myopes [65]. In patients with axial lengths ≥26 mm, they achieved closure in 88.4% of inverted flap cases as opposed to 38.9% in the ILM peeling group. BCVA improvements were statistically significant only in the inverted flap cases. They also reported success rates in patients affected by chorioretinal atrophy of 78% in ILM flap cases and 31.8% in ILM peeling cases. In a similar comparative study, Mete et al. concluded that using an inverted ILM flap seems preferable for all cases of myopic MH as the likelihood of surgical effectiveness was increased by 22.96 times when the inverted ILM flap technique was performed regardless of the hole diameter [77].

Xu et al. performed ILM peeling in 18 cases of moderately high myopia MH with RD and the ILM flap technique in 17 cases. The retina was reattached in all cases. The MH closed in 47.1% of cases where complete ILM peeling was performed and in 88.9% of cases where they performed the inverted ILM flap technique. Significant improvements in BCVA were reported for both groups but these were not statistically different between the groups [78].

Baba et al. compared the inverted flap technique with conventional ILM peeling in cases of RD associated with high myopic macular holes and found the flap technique to be more effective

for hole closure [79]. As confirmed by Kinoshita et al. over 20 months of follow-up [80].

In another comparative study of the inverted ILM flap technique and ILM peeling for MH with RD, Matsumura et al. found that the macular holes closed and retina was attached in 90% of cases using the ILM flap technique whereas only 33.3% of holes closed and only 50% of retinas were attached after using standard ILM peeling [81]. They also reported a significant improvement in BCVA in the flap group. In the one eye where both closure and reattachment were unsuccessful, they used the autologous ILM transplant first described by Morizane to successfully close the hole and reattach the retina in a subsequent surgery. Takahashi et al. confirmed a statistically better closure rate in their comparative study's flap group ($P = 0.006$) and found BCVA was significantly better in the flap group ($P = 0.04$) [82].

Chen and Yang presented a slightly different technique for myopic MH retinal detachment [33]. They peeled ILM from a larger area than most other authors and formed a ring-shaped ILM flap around the MH which was inserted into the MH with all free-floating ends of ILM carefully placed under the hole. Additional drainage retinotomy was performed in the temporal upper detached retina. This was treated with laser photocoagulation and a 20% C3F8 tamponade was used. Their comparative study reported that MH closure was statistically significantly more frequent (i.e., in all eyes) with the inverted ILM flap technique ($P < 0.001$). Mean visual acuity improved from 1.72 logMAR to 1.23 logMAR. (Chen has also modified the flap technique to create a very large semicircular flap for treating 17 highly myopic eyes [83]. The series included five eyes with foveoschisis, four with chronic MH, two with myopic choroidal neovascularization, and four with MH-associated RD. They achieved a 100% closure rate and a VA improvement from 1.26 ± 0.52 preoperatively to 0.69 ± 0.45 6 months postoperatively. In a later paper, Chen et al. compared the results of multiple free flap insertion in MH-associated RD in high myopia to traditional ILM peeling and found their flap technique better in terms of closure and visual outcomes [84].)

The aforementioned flap insertion study by Chen and Yang resulted in both interest and criticism in ophthalmology circles: Theodosiadis et al. felt that the introduction of ILM into the hole may enlarge the hole and that the different homogeneity of the ILM flap inserted into the hole and the surrounding neural structure does not help in transmitting nervous stimuli [85]. Inserting ILM tissue into the hole was also said to possibly create a column, which maintains a distance between the retinal pigment epithelium and retinal layers. Gosala and Manchikanty suggested that the introduction of ILM into the hole may enhance the reopening rate of macular holes due to unrelieved traction [86]. In response, Chen and Yang state that ILM left within the hole would pull the edge of the original MH centripetally and bring the neuronal tissue closer [87]. Looking at the results from both Chen and Yang and the paper from Andrew et al. we mentioned earlier, it appears that even if the introduction of ILM into the hole seems to be more traumatic when compared with the original technique (where ILM is placed on top of the retina) the procedure works and the patient benefits.

Another modified technique was used by Lai et al. in 27 cases of high myopic MH with RD where they filled the entire MH with an inverted internal limiting membrane flap and additionally used the patients' blood to keep the ILM flap in position [88]. The mean axial length was 29.37 mm and 25 of 27 eyes had staphyloma. They achieved retina reattachment in all 27 operated eyes and MH closure was achieved in all but one eye where a parafoveal hole was found.

Song et al. with the additional use of Viscoat, achieved closure "without foveal neurosensory defect" in 13 of 15 operated eyes [35]. However, in the remaining two eyes, what they describe as "macula hole closed with foveal neurosensory retinal defect" we equate with what we term a "flat open" MH. Seven of 15 eyes had an axial length above 30 mm. Mean postoperative visual acuity improved from 1.28 logMAR to 1.07 after 6 months of follow-up.

Okuda et al. presented that complete immediate retinal reattachment may not be necessary for MH closure [89]. In all three of their patients

with MH RD operated on using the ILM flap technique, the macular holes were successfully closed over the residual subretinal fluid. Furthermore, Lai states that three eyes with a closed hole showed persistent subretinal fluid (SRF) after gas absorption [88]. In two of these cases, the fluid absorbed completely during the follow-up period, but one eye exhibited persistent SRF, which was resolved progressively during the 12 months of follow-up.

Rizzo et al. have reported success rates in patients affected by chorioretinal atrophy of 78% in ILM flap cases and 31.8% in ILM peeling cases [65].

Tewari et al. reported on two cases of MH RD in Best vitelliform dystrophy [90]. BCVA, color fundus photographs, shortwave fundus autofluorescence, and swept-source optical coherence tomography were assessed. The inverted ILM flap technique led to type 1 closure of macular hole, resolution of retinal detachment, and improvement in vision in both patients: 20/400 to 20/60 at 12 months follow-up and 20/1200 to 20/80 in the second patient.

19.4.3 Uveitis

Hirano et al. modified the ILM flap technique to close an MH secondary to uveitis [91]. The authors used ICG for staining, peeled the ILM around the hole to create a bowl of ILM which they then halved and inverted over the hole. They used low molecular hyaluronic acid to stabilize the flap. The authors achieved closure of the MH but the ellipsoid zone remained defective and the patient's visual acuity remained 20/400.

19.4.4 Diabetic Macular Holes

The etiopathogenesis of MH in diabetic patients is complex. In proliferative diabetic retinopathy, they can occur due to tangential or anteroposterior traction as idiopathic macular holes do. They can also be iatrogenic after peeling for proliferative diabetic retinopathy. During the 2016 Club Jules Gonin Meeting in Bordeaux, France, Sheta

presented the results of his treatment of 26 cases of diabetic patients with macular holes, treated either with ILM peeling or with the inverted ILM flap technique. He concluded that the inverted ILM flap technique resulted in 100% closure, and ILM peeling in 77% closure.

Our experience of this topic shows that when we have an MH in a patient with diabetes or non-proliferative diabetic retinopathy, the treatment method and recovery are the same as with a regular MH. However, in cases with proliferative diabetic retinopathy, we observe that, even if the MH is closed with the ILM flap, some fluid may persist for several months under the fovea. This might be explained by the retinal pigment epithelium being ineffective or inefficient at the removal of the fluid. N.B. even if fluid persists under the fovea, the hole can be closed with the ILM flap [16]. Our observation may add to the information on the pathogenesis of diabetic MH due to proliferative diabetic retinopathy. Besides the tractional component, they may be also partially caused by decreased nutrition from the choroid and a malfunction of the retinal pigment epithelium's ability to remove the subretinal fluid.

19.4.5 Traumatic Macular Hole

Very little information exists regarding traumatic macular holes treated with the inverted ILM flap technique. Abou Shousha successfully used a flap inserted into the MH with a sulfur hexafluoride 20% tamponade in 12 large traumatic hole cases with basal diameters of 1300 to 2800 μm [92]. Macular hole closure was achieved in all 12 cases and visual acuity improved from 20/2000–20/200 to 20/400–20/50.

A similar technique of pushing the ILM into the MH has been described by Nuzzo et al. The MH was closed and the patient's visual acuity of the patient (a 7-year-old boy) improved from counting fingers to 20/100 [93].

Astir et al. presented a case of traumatic MH (899 μ min. linear diameter) with choroidal rupture and subretinal hemorrhage [94]. They positioned an ILM flap on the top of the retina and used a brush needle to help position the flap

during fluid–air exchange. Visual acuity improved from 5/60 to 6/18 at the 6-month follow-up.

Morizane et al. successfully used the technique of autologous ILM Flap for a series of persistent macular holes after vitrectomy with ILM peeling [95]. In one specific case: a traumatic MH with choroidal rupture and subretinal fibrosis, they achieved closure of the MH.

We have described a similar case of a traumatic hole with subretinal fibrosis treated primarily with the inverted ILM Flap technique with success [16]. Based on our experience with typical traumatic macular holes, the technique may be successfully used.

19.4.6 Age-Related Macular Degeneration and Macular Hole

Macular holes may coexist with both dry and wet age-related macular degeneration (AMD). In dry AMD cases with predominant signs of drusen, surgery may be performed with good results. Our previous paper presented one such case [8]. Drusen may be used as a topographical landmark to demonstrate the regeneration of retina tissue after vitrectomy with an inverted ILM flap. Our unpublished data show that in such cases, good anatomical and functional results are achievable.

Macular holes may also be associated with wet AMD due to decreased nutrition in the presence of subretinal neovascularization. We have not performed surgery in such cases because we believe that it would not lead to functional success [16]. It is, however, open to discussion whether doing the surgery and closing the MH followed by an anti-VEGF injection regime may lead to better results when compared to anti-VEGF injections alone.

19.4.7 Macular Hole Persistent After Retinal Detachment Surgeries

Recently we presented that the inverted ILM flap technique may be successfully used in cases of persistent MH after RD surgery with scleral buckle and vitrectomy [16]. Joondeph, Dai, and Chen have each discussed their successful experiences with persistent holes after retinal detachment using various modified ILM flap techniques [40, 41, 50].

19.4.8 Various Other Indications

The inverted ILM flap technique has been used by our group for MH with retinitis pigmentosa. Complete MH closure was achieved and visual acuity improved to 20/100 (Unpublished own results). And we have used it successfully in an eye with Coats disease (Unpublished own results).

Iwakawa et al. used an autologous ILM transplant enhanced by viscoelastic during second surgery in an eye with MH secondary to the rupture of a retinal arterial macroaneurysm [96]. 27 g vitrectomy was performed and, as ILM had been peeled during the first surgery, a free flap was used to close the hole. BCVA at the 6-month follow-up was 0.6.

19.5 Repeated Macular Hole Surgery after Inverted ILM Flap Techniques

At the time of writing this chapter, our data on repeated flap technique MH surgery has just been accepted for publication. (Zofia Michalewska, Jerzy Nawrocki. Repeat surgery in failed primary vitrectomy for macular holes operated with the inverted ILM flap technique. Ophthalmic Surg Lasers Imaging Retina. In press.) We presented our results at Vail Vitrectomy 2016 and they were compared with retina massage techniques used in cases of failure before the inverted ILM flap was devised. Much better anatomical and functional results were achieved when using the flap technique. The important observation during repeated surgery was that the inverted ILM flap was always detected off of the MH, on the surface of the retina. This finding suggests that failure of closure was caused by reapproximation of the flap to or toward its original position. Repeat surgery was

based on repositioning the flap on the MH/retina surface.

In rare cases where the temporal inverted ILM flap has failed to close the MH, a nasal ILM flap can be created during subsequent surgery as the ILM was not peeled from this side during the initial surgery. Where the original flap appears viable, repeated maneuvers can prove difficult and dislocation of the flap is very probable during fluid–air exchange. For this reason, the authors recommend using silicone oil for better control of the flap position at the end of surgery. Such surgery leads to complete closure of all macular holes and visual acuity improvement. The rate of improvement is lower when compared with primary successes but is still significant.

19.6 Repeated Macular Hole Surgery After Traditional ILM Peeling

Morizane et al. described a technique where they used Brilliant Blue G (Coomassie BBG 250 Sigma-Aldrich, St Louis, Missouri, USA) to identify where ILM was and was not already peeled off in previous surgery [95]. Then they peeled away a small piece of residual ILM approximately the same size as the MH and placed it inside the hole. It was secured in place with low molecular weight viscoelastic material (Opegan; Santen Pharmaceutical Co, Ltd., Osaka, Japan). After fluid–air exchange, 10% SF6 was used. Indication for surgery was: refractory MH (large: four eyes, posttraumatic: one eye, myopic foveoschisis: two eyes, proliferative diabetic retinopathy: one eye and foveoschisis after optic pit: two eyes). Macular hole was closed in 9/10 eyes. The mean best-corrected visual acuity improved from 0.99 to 0.57 log-MAR. The efficacy of this technique was also confirmed by other authors [97]. Guber et al. have reported the ability of the free flap technique to close MH after failed primary surgery [98]. And Gekka et al. have described their method of treatment of refractory MH [99]. They peeled the remaining ILM inferior from the MH to create a pedicle ILM flap. This ILM flap was

still attached in the upper part of MH and was used to cover it. In both operated eyes the MH was successfully closed.

The inverted ILM flap technique and its modifications seem to be successful in closing MH after a failed primary intervention but other authors are examining even greater modifications of the technique in order to resolve these difficult cases. Chen and Yang used a piece of the crystalline lens capsule to plug the MH in 20 cases of persistent MH [100]. A capsular flap was harvested from the posterior capsule in pseudophakic eyes. During combined cataract surgery in phakic eyes, the anterior capsule was stained with 0.125% ICG before transplantation, for better visualization, and the authors trapped the flaps under the edge of MH. The eyes where the anterior capsule was used had a significantly better closure rate but did not have a significantly better visual improvement. All 10 eyes with anterior capsular flap transplantation closed successfully. In the posterior capsular flap group, the hole was completely closed in five eyes, reduced in size in three eyes, and failed to close in two eyes. The authors found that the posterior capsule is not fibrotic and it tends to curl in a small roll instead of flat sheet and it is probably due to this that the flap was not large enough to cover the MH. Sometimes more than one flap was required. Both obtaining and manipulating the anterior flap were easier. Peng et al. have combined the lens capsular flap concept with autologous blood with successful results, even when harvesting the flap material from the fellow eye [101].

Grewal and Mahmoud have presented that during repeated surgery for failed MH closure, they could not find enough ILM for autologous transplant nor could they harvest lens capsule for MH closure [102, 103]. Therefore, they harvested a full-thickness neurosensory retinal free flap superior to the superotemporal arcade, which they used to cover the MH and secured in place with PFCL. Direct PFCL–silicone oil exchange was performed. The authors demonstrated not only MH closure but also improvement of visual acuity and improvement in microperimetry amplitudes.

During the Club Jules Gonin Meeting in Jersey in 2018, Rizzo reported that he has used an amniotic membrane for the treatment of refractory macular hole (unpublished data).

19.7 Inverted ILM Flap for Optic Pit Maculopathy

Different surgical approaches have been described for the treatment of optic pit maculopathy. In this subchapter, we discuss only the inverted ILM flap or similar techniques. Travassos et al. introduced an autologous scleral transplant [104]. They used a homogenous scleral tissue flap previously collected from the inferior nasal quadrant. The technique was used in three eyes with good results.

Mohammed and Pai described one case using the inverted ILM flap for the treatment of maculopathy associated with an optic pit [105]. They used a large ILM flap prepared in the center of the macula between the vascular arcades. The macular detachment regressed after 1 month and visual acuity improved from 6/60 to 6/24.

Between 2008 and 2014 we employed the inverted ILM flap technique in 8 cases (J. Nawrocki, Z. Michalewska unpublished data). Our surgical approach was vitrectomy, peeling of the ILM in a half distance between the border of the optic nerve and fovea. ILM was peeled in the direction of the optic nerve and left attached to the retina, inverted, and put on the top of the optic pit. In the area of ILM peeling, additional laser treatment was performed. Fluid–air exchange was performed to keep the flap in position. Membrane Blue or Membrane Blue Dual (DORC, Rotterdam, Netherlands.) staining was used. We initially achieved success in seven of eight operated eyes but after a few years of complete anatomical recovery two eyes had a recurrence. We submitted those cases to the 2014 EVRS Optic Pit Study but the statistical analysis did not confirm an advantage of this method against different vitrectomy approaches as the case series was too small [106]. In 2015 we decided to change the technique. The decision was prompted by failure in one case after two attempts and the pre-

viously mentioned recurrence in two cases. During repeated surgery, we found that similar to some rare failures in treating MH, the ILM had returned to its original position on the retina surface between the optic nerve and fovea. This was easy to detect after staining. In these cases, we once again peeled the previously created ILM flap, keeping it attached to the retina, but introduced the flap into the optic pit cave and secured it in place with fluid–air exchange. This led to immediate healing of the maculopathy associated with optic pit, observable at the first control after 1 week. The technique was described by us in 2016 [107]. A video of the technique is available at the EVRS web site: http://www.evrs.eu/managing-optic-pit-the-right-stuff. In 2015 and 2016 we operated on five optic pit maculopathy cases and one morning glory retinal detachment associated with an optic pit. Four of those cases were repeated surgeries and two were primary surgeries. To date, all of them have produced favorable results. D'Souza et al. have since reported good anatomical and functional results after plugging optic pit with a free flap of ILM [108]. Interestingly, Hara et al. used a small inverted ILM flap to successfully treat a case of retinal detachment associated with optic pit after two attempts (without using the flap technique) had failed and they believe that it might also be effective in treating optic pit maculopathy with retinoschisis [109].

19.8 Foveal Microstructure

Examination of foveal microstructure with Spectral Domain OCT (SD-OCT) or Swept Source OCT (SS-OCT) shows a recovery of the fovea during follow-up. Hayashi and Kuriyama have studied the subject in detail and they found reappearance of the IS/OS junction (ellipsoid zone) and ELM during 6 months' follow-up after inverted ILM flap surgery for MH [74]. They found that complete recovery of the IS/OS junction was not observed without the complete restoration of ELM. ELM recovery happens more frequently in large and myopic MH as compared to myopic MH retinal detachment.

Imai and Azumi presented a case where the expansion of submacular pigment epithelium atrophy was observed during follow-up [25]. Despite this observation, visual acuity improved in this case from 0.08 to 0.3 (with Landolt C).

Chen et al. have examined multifocal electroretinography (mfERG) after the inverted ILM flap technique for large macular holes [110]. They found improvement in mfERG and although it was not significantly correlated with best-corrected visual acuity it may be considered as a good supplement to evaluate postoperative functional recovery.

We have observed MH closed only by the inverted ILM flap itself, at the first follow-up visit approximately 1 week after surgery when using both the inverted flap technique and the temporal inverted flap technique [29]. This closure type, which we refer to as "flap closure", happens in larger MH cases and is the subject of our recent paper [111]. We reviewed 149 MH cases in which 56 had ILM flap surgery and 93 had temporal ILM flap surgery. We achieved anatomical success in 100% of the cases after the first surgery. We observed flap closure in 24 cases and these had a mean base diameter greater than that of the other MH closure types ($P < 0.001$). Although BCVA improved significantly in all cases, the group with flap closure improved less ($P < 0.001$). However, the improvement is still significantly better than cases with a flat open result and repeated surgery cases reported in the literature. The external limiting membrane regenerates slower than in other closure types but the number of patients with photoreceptor defects is similar. Regeneration of the retina layers is observed in all closure types during follow-up but an increased number of DONFL may be observed during follow-up in "flap closure" cases.

In a recently published paper, we examined retinal vasculature before and after temporal inverted flap surgery for FTMH using SS-OCT Angiography in 36 eyes [112]. The study shows that ILM peeling might lower the density of vessels below the peeled area and the postoperative area of the fovea avascular zone in the deep retina plexus corresponds to functional results.

19.9   Conclusion

The inverted ILM flap technique is of growing interest in the ophthalmic community with new and interesting papers now appearing in the literature and more than 20 videos are available on the Internet (Bing search. July 2018). Different modifications are being investigated and developed. It is difficult to switch from the habitual approach of ILM peeling and gas to the inverted ILM flap in routine cases. Therefore, most of the published literature are based on difficult, large, old, myopic macular holes, or reoperations, after conventional surgery have failed. If we encounter reoperations in case of failure and no preoperative selection of the patients with macular hole, we hope that the application of the described techniques can improve the overall results achieved with vitrectomy for macular hole.

According to the literature, in difficult cases, the inverted flap techniques improve both anatomical and functional results.

Whilst our own experience tells us that the inverted ILM flap techniques should be the method of choice in many situations, as with any new suggested procedure, large randomized control studies to prove the efficacy of the techniques, especially in regard to BCVA improvement, would be useful.

References

1. Kelly NE, Wendel RT. Vitreous surgery for idiopathic macular holes: results of a pilot study. Arch Ophthalmol. 1991;109:6549.
2. Wendel RT, Patel AC, Kelly NE, Salzano TC, et al. Vitreous surgery for macular holes. Ophthalmology. 1993;100(11):1671–6.
3. Eckardt C, Eckardt U, Groos S, Reale E. Entfernung der Membrana limitans interna bei Makulalöchern Klinische und morphologische Befunde. Ophthalmologe [Article in German]. 1997;94:545–51.
4. Michalewska Z, Michalewski J, Cisiecki S, Adelman RA, Nawrocki J. Correlation between foveal structure and visual outcome following macular hole surgery: a spectral optical coherence tomography study. Graefes Arch Clin Exp Ophthalmol. 2008;246:823–30.

5. Imai M, Iijima H, Gotoh T, Tsukara S. Optical coherence tomography of successfully repaired idiopathic macular holes. Am J Ophthalmol. 1999;128:621–7.

6. Kang SW, Ahn K, Ham DI. Types of macular hole closure and their clinical implications. Br J Ophthalmol. 2003;87:1015–9.

7. Michalewska Z, Michalewski J, Nawrocki J. Macular hole closure after vitrectomy: the inverted flap technique. Retina Today. 2009;73–3.

8. Michalewska Z, Michalewski J, Adelman RA, Nawrocki J. Inverted internal limiting membrane flap technique for large macular holes. Ophthalmology. 2010;117:2018–25.

9. Henrich PB, Monnier CA, Halfter W, Haritoglou C, et al. Nanoscale topographic and biomechanical studies of the human internal limiting membrane. Invest Ophthalmol Vis Sci. 2012;53(6):2561–70.

10. Fine BS, Tousimis AJ. The structure of the vitreous body and the suspensory ligaments of the lens. Arch Ophthalmol. 1961;65:95–110.

11. Foos RY. Vitreoretinal juncture; Topographical variations. Invest Ophthalmol. 1972;11(10):801–8.

12. Brooks HL Jr. Macular hole surgery with and without internal limiting membrane peeling. Ophthalmology. 2000;107:1939–49.

13. Nakamura T, Murata T, Hisatomi T, Enaida H, et al. Ultrastructure of the vitreoretinal interface following the removal of the internal limiting membrane using indocyanine green. Curr Eye Res. 2003;27(6):395–9.

14. Kase S, Saito W, Mori S, Saito M, et al. Clinical and histological evaluation of large macular hole surgery using the inverted internal limiting membrane flap technique. Clin Ophthalmol. 2017;11:9–14.

15. Franze K, Grosche J, Skatchkov SN, Schinkinger S, et al. Muller cells are living optical fibers in the vertebrate retina. Proc Natl Acad Sci U S A. 2007;104(20):8287–92.

16. Nawrocki J, Michalewska Z. SS-OCT for macular hole treated with the inverted internal limiting membrane flap technique. In: An atlas of SS-OCT. Springer: 2017. p. 97–113.

17. Bernardos RL, Barthel LK, Meyers JR, Raymond PA. Late-stage neuronal progenitors in the retina are radial Müller glia that function as retinal stem cells. J Neurosci. 2007;27(26):7028–40.

18. Bhatia B, Jayaram H, Singhal S, Jones MF, Limb GA. Differences between the neurogenic and proliferative abilities of Müller glia with stem cell characteristics and the ciliary epithelium from the adult human eye. Exp Eye Res. 2011;93(6):852–61.

19. Giannelli SG, Demontis GC, Pertile G, Rama P, Broccoli V. Adult human Müller glia cells are a highly efficient source of rod photoreceptors. Stem Cells. 2011;29(2):344–56.

20. Joly S, Pernet V, Samardzija M, Grimm C. Pax6-positive Müller glia cells express cell cycle markers but do not proliferate after photoreceptor injury in the mouse retina. Glia. 2011;59(7):1033–46.

21. Michalewska Z, Michalewski J, Dulczewska-Cichecka K, Nawrocki J. Inverted internal limiting membrane flap technique for surgical repair of myopic macular holes. Retina. 2014;34(4):664–9.

22. Ducournau D, Ducournau Y. A closer look at the ILM. Removal of the ILM induces a cellular response that allows retina to fight against edema. Retin Physician. 2008;6:4–15.

23. Shiode Y, Morizane Y, Matoba R, et al. The role of inverted internal limiting membrane flap in macular hole closure. Invest Ophthalmol Vis Sci. 2017;58:4847–55.

24. Vieregge M, Valmaggia C, Scholl HPN, Guber J. Microstructural retinal regeneration after internal limiting membrane flap surgery for repair of large macular holes: a 1-year follow-up study. Int Ophthalmol. 2018;39:1277. https://doi.org/10.1007/s10792-018-0941-z.

25. Imai H, Azumi A. The expansion of RPE atrophy after inverted ILM flap technique for a chronic large macular hole. Case Rep Ophthalmol. 2014;5(1):83–6.

26. Mahalingam P, Sambhav K. Surgical outcomes of inverted internal limiting membrane for large macular hole. Indian J Ophthalmol. 2013;61:601–3.

27. Berrocal MH. Inverted flap technique for large macular hole repair. Clinical Case Compendium, Supplement to Retina today July/Aug 2016.

28. Tadayoni R, Paques M, Massin P, Mouki-Benani S, Mikol J, Gaudric A. Dissociated optic nerve fiber layer appearance of the fundus after idiopathic epiretinal membrane removal. Ophthalmology. 2001;108:2279–83.

29. Michalewska Z, Michalewski J, Dulczewska-Cichecka K, Adelman RA, Nawrocki J. Temporal inverted internal limiting membrane flap technique versus classic inverted internal limiting membrane flap technique: a comparative study. Retina. 2015;35(9):1844–50.

30. Sakurai T, Kinishita T, Tano R, Fukuoka S, Takaoka G, Mano T. One-year outcome of macular hole treated by hemi-inverted internal limiting membrane flap technique. Jpn J Clin Ophthalmol. 2014;68(10):1449–53.

31. Belyi YA, Tereshchenko AV, Shkvorchenko DO, Erokhina EV, Shilov NM. Step-by-step creation of internal limiting membrane fragment for surgical treatment of large idiopathic macular holes. Vestn Oftalmol [Article in Russian]. 2016;132(1):23–30.

32. Finn AP, Mahmoud TH. Internal limiting membrane retracting door for myopic macular holes. Retina. 2017;39:S92–4. https://doi.org/10.1097/IAE.0000000000001787.

33. Chen SN, Yang CM. Inverted internal limiting membrane insertion for macular hole-associated retinal detachment in high myopia. Am J Ophthalmol. 2016;162:99–106.

34. Shin MK, Park KH, Park SW, Byon IS, Lee JE. Perfluoro-n-octane-assisted single-layered inverted internal limiting membrane flap technique for macular hole surgery. Retina. 2014;34(9):1905–10.

35. Song Z, Li M, Liu J, Hu X, Hu Z, Chen D. Viscoat assisted inverted internal limiting membrane flap technique for large macular holes associated with high myopia. J Ophthalmol. 2016;2016:8283062. https://doi.org/10.1155/2016/8283062.

36. Sasaki H, Shiono A, Kogo J, Yomoda R, Munemasa Y, Syoda M. Inverted internal limiting membrane flap technique as a useful procedure for macular hole-associated retinal detachment in highly myopic eyes. Eye (Lond). 2017;31(4):545–50.

37. Andrew NA, Chan WO, Tan M, Ebneyter A, Gilhotra JS. Modification of the inverted internal limiting membrane flap technique for the treatment of chronic and large macular holes. Retina. 2016;36(4):834–7.

38. Hernández-da Mota SE, Béjar-Cornejo F. Modified technique of autologous transplantation of internal limiting membrane for macular hole. Cir Cir [Article in Spanish]. 2016;84(6):454–8. https://doi.org/10.1016/j.circir.2016.03.010.

39. Pires J, Nadal J, Gomes NL. Internal limiting membrane translocation for refractory macular holes. Br J Ophthalmol. 2017;101(3):377–82. https://doi.org/10.1136/bjophthalmol-2015-308299.

40. Joondeph BC. Macular hole repair using an ILM patch. Retina Today July/Aug 2016.

41. Dai Y, Dong F, Zhang X, Yang Z. Internal limiting membrane transplantation for unclosed and large macular holes. Graefes Arch Clin Exp Ophthalmol. 2017;255(5):1047–8.

42. Chakrabarti M, Beniamin P, Chakrabarti K, Chakrabarti A. Closing macular holes with "macular plug" without gas tamponade and postoperative posturing. Retina. 2017;37(3):451–9.

43. Park JH, Lee SM, Park SW, et al. Comparative analysis of large macular hole surgeries using an internal limiting membrane: insertion technique versus inverted flap technique. Br J Ophthalmol. 2019;103(2):245–50. https://doi.org/10.1136/bjophthalmol-2017-311770.

44. Rossi T, Gelso A, Costagliola C, Trillo C, et al. Macular hole closure patterns associated with different internal limiting membrane flap techniques. Graefes Arch Clin Exp Ophthalmol. 2017;255:1073–8.

45. Velez-Montoya R, Ramirez-Estudillo JA, Sjoholm-Gomez de Liano C, Bejar-Cornejo F, et al. Inverted ILM flap, free ILM flap and conventional ILM peeling for large macular holes. Int J Retina Vitreous. 2018;4:8. https://doi.org/10.1186/s40942-018-0111-5. eCollection 2018

46. Becker MD, Hess JA, Michels S. Outcome of primary and secondary internal limiting membrane (ILM) transplantation, comparing pedicle with free ILM graft technique – first results of an ongoing retrospective single center case series. Bordeaux: Club Jules Gonin; 2016.

47. Michalewska Z, Nawrocki J. Macular hole surgery in a patient who cannot maintain facedown positioning case rep. Ophthalmology. 2013;4(1):1–6.

48. Choi SR, Kang JW, Jeon JH, et al. The efficacy of superior inverted internal limiting membrane flap technique for the treatment of full-thickness macular hole. Retina. 2018;38(1):192–7.

49. Takai Y, Tanito M, Sugihara K, Kodama T, Ohira A. Temporal inverted internal limiting membrane flap for a macular hole patient unable to maintain postoperative prone positioning. Retin Cases Brief Rep. 2016;10(4):323–6.

50. Chen SN, Yang CM. Double internal limiting membrane insertion for macular hole-associated retinal detachment. J Ophthalmol. 2017;2017:3236516. https://doi.org/10.1155/2017/3236516.

51. Aurora A, Seth A, Sanduja N. Cabbage leaf inverted flap ILM peeling for macular hole: a novel technique. Ophthalmic Surg Lasers Imaging Retina. 2017;48(10):830–2.

52. Ho TC, Ho A, Chen MS. Vitrectomy with a modified temporal inverted internal limiting membrane flap to reconstruct the foveolar architecture for macular hole retinal detachment in highly myopic eyes. Acta Ophthalmol. 2018;96(1):e46–53. https://doi.org/10.1111/aos.13514.

53. Chung CY, Wong DS, Li KK. Is it necessary to cover the macular hole with the inverted internal limiting membrane flap in macular hole surgery? A case report. BMC Ophthalmol. 2015;15:115.

54. Yamashiro K, Kinoshita-Nakano E, Ota T, Jingami Y, Nakata I, Hayashi H. Floating flap of internal limiting membrane in myopic macular hole surgery. Graefes Arch Clin Exp Ophthalmol. 2018;256(4):693–8.

55. Pak KY, Park JY, Park SW, Byon IS, Lee JE. Efficacy of the perfluoro-N-octane-assisted single-layered inverted internal limiting membrane flap technique for large macular holes. Ophthalmologica. 2017;238(3):133–8.

56. Ozdek S, Baskaran P, Karabas L, Neves PP. A modified perfluoro-n-octane-assisted autologous internal limiting membrane transplant for failed macular hole reintervention: a case series. Ophthalmic Surg Lasers Imaging Retina. 2017;48(5):416–20.

57. Casini G, Mura M, Figus M, Loiudice P, et al. Inverted internal limiting membrane flap technique for macular hole surgery without extra manipulation of the flap. Retina. 2017;37(11):2138–4458.

58. El-Baha SM, Abouhussein MA. Modified technique of internal limiting membrane staining in idiopathic macular hole surgery. Int Ophthalmol. 2019;39(3):557–62. https://doi.org/10.1007/s10792-018-0842-1.

59. Iovino C, Caminiti G, Miccoli M, Nasini F, Casini G, Peiretti E. Comparison of inverted flap and subretinal aspiration technique in full-thickness macular hole surgery: a randomized controlled study. Eur J Ophthalmol. 2017;18:324. https://doi.org/10.5301/ejo.5001040.

60. Nagesha CK, Prabu Baskaran P, Dhoble P. Inverted macular hole edges following an inverted internal limiting membrane transplantation surgery

for large macular hole. Indian J Ophthalmol. 2018;66(2):293–4.

61. Iwasaki M, Kinoshita T, Miyamoto H, Imaizumi H. Influence of inverted internal limiting membrane flap technique on the outer retinal layer structures after a large macular hole surgery. Retina. 2018;39:1470. https://doi.org/10.1097/IAE.0000000000002209.

62. Lyu WJ, Ji LB, Xiao Y, Fan YB, Cai XH. Treatment of refractory giant macular hole by vitrectomy with internal limiting membrane transplantation and autologous blood. Int J Ophthalmol. 2018;11(5):818–22. https://doi.org/10.18240/ijo.2018.05.17.

63. Hu Z, Ye X, Lv X, Liang K, et al. Non-inverted pedicle internal limiting membrane transposition for large macular holes. Eye (Lond). 2018;32:1512. https://doi.org/10.1038/s41433-018-0107-2.

64. Khodani M, Bansal P, Narayanan R, Chhablani J. Inverted internal limiting membrane flap technique for very large macular hole. Int J Ophthalmol. 2016;9(8):1230–2.

65. Rizzo S, Tartaro R, Barca F, Caprossi T, et al. Internal limiting membrane peeling versus inverted flap technique for treatment of full-thickness macular holes. A comparative study in a large series of patients. Retina. 2018;38(Suppl 1):S73–8. https://doi.org/10.1097/IAE.0000000000001985.

66. Yamashita T, Sakamoto T, Terasaki H, Iwasaki M, writing committee of Japan-Clinical Retina Research Team (J-CREST), et al. Best surgical technique and outcomes for large macular holes: retrospective multicentre study in Japan. Acta Ophthalmol. 2018;19:e904. https://doi.org/10.1111/aos.13795.

67. Manasa S, Kakkar P, Kumar A, Chandra P, Kumar V, Ravani R. Comparative evaluation of standard ILM peel with inverted ILM flap technique in large macular holes: a prospective, randomized study. Ophthalmic Surg Lasers Imaging Retina. 2018;49(4):236–40.

68. Gu C, Qiu Q. Inverted internal limiting membrane flap technique for large macular holes: a systematic review and single-arm meta-analysis. Graefes Arch Clin Exp Ophthalmol. 2018;256:1041–9.

69. Narayanan R, Singh SR, Taylor S, Berrocal MH, et al. Surgical outcomes after inverted limiting membrane flap versus conventional peeling for very large macular holes. Retina. 2018;39:1465. https://doi.org/10.1097/IAE.0000000000002186.

70. Deshpande R, Narayanan R. Surgical repair of a giant idiopathic macular hole by inverted internal limiting membrane flap. BMJ case Rep. 2015;2015:bcr2015210797.

71. Kubota M, Shibata T, Gunji H, Tsuneoka H. Idiopathic horseshoe-like macular tear: a case report. Int Med Case Rep J. 2016;9:219–2.

72. Kuriyama S, Hayashi H, Jingami Y, Kuramoto N, Akita J, Matsumoto M. Efficacy of inverted internal limiting membrane flap technique for the treatment of macular hole in high myopia. Am J Ophthalmol. 2013;156:125–31.

73. Hayashi H, Kuriyama S. Foveal microstructure in macular holes surgically closed by inverted internal limiting membrane flap technique. Retina. 2014;34(12):2444–50.

74. Wu TT, Kung YH, Chang CY, Chang SP. Surgical outcomes in eyes with extremely high myopia for macular hole without retinal detachment. Retina. 2017;38:2051. https://doi.org/10.1097/IAE.0000000000001806.

75. Oleñik A, Rios J, Mateo C. Inverted internal limiting membrane flap technique for macular holes in high myopia with axial length ≥30 mm. Retina. 2016;36(9):1688–93.

76. Suda K, Hangai M, Yoshimura N. Axial length and outcomes of macular hole surgery assessed by spectral – domain optical coherence tomography. Am J Ophthalmol. 2011;151:118–27.

77. Mete M, Alfano A, Guerriero M, Prigione G, et al. Inverted internal limiting membrane flap technique versus complete internal limiting membrane removal in myopic macular hole surgery: a comparative study. Retina. 2017;37(10):1923–30.

78. Xu CZ, Wu JH, He JW, Feng C. Observation of single-layered inverted internal limiting membrane flap technique for macular hole with retinal detachment in high myopia. Chin J Ophthalmol [Article in Chinese]. 2017;53:338–43.

79. Baba R, Wakabayashi Y, Umazume K, Ishikawa T, et al. Efficacy of the inverted internal limiting membrane flap technique with vitrectomy for retinal detachment associated with myopic macular holes. Retina. 2017;37(3):466–71.

80. Kinoshita T, Onoda Y, Maeno T. Long-term surgical outcomes of the inverted internal limiting membrane flap technique in highly myopic macular hole retinal detachment. Graefes Arch Clin Exp Ophthalmol. 2017;255(6):1101–6. https://doi.org/10.1007/s00417-017-3614-0.

81. Matsumura T, Takamura Y, Tomomatsu T, Arimura S, et al. Comparison of the Inverted internal limiting membrane flap technique and the internal limiting membrane peeling for macular hole with retinal detachment. PLoS One. 2016;11(10):e0165068. https://doi.org/10.1371/journal.pone.0165068.

82. Takahashi H, Inoue M, Koto T, Itoh Y, Hirota K, Hirakata A. Inverted internal limiting membrane flap technique for treatment of macular hole retinal detachment in highly myopic eyes. Retina. 2018;38(12):2317–26. https://doi.org/10.1097/IAE.0000000000001898.

83. Chen SN. Large semicircular inverted internal limiting membrane flap in the treatment of macular hole in high myopia. Graefes Arch Clin Exp Ophthalmol. 2017;255(12):2337–45.

84. Chen SN, Hsieh YT, Yang CM. Multiple free internal limiting membrane flap insertion in the treatment of macular hole-associated retinal detachment in high myopia. Ophthalmologica. 2018;6:1–7. https://doi.org/10.1159/000487337.

85. Theodosiadis G, Chatziralli I, Theodosiadis PG. Inverted internal limiting membrane insertion for macular hole – associated retinal detachment in high myopia. Am J Ophthalmol. 2016;165:206–7.

86. Gosala S, Manchikanty SM. Inverted internal limiting membrane insertion for macular hole – associated retinal detachment in high myopia. Am J Ophthalmol. 2016;166:210–1.

87. Chen SN, Yang CM. Inverted internal limiting membrane insertion for macular hole – associated retinal detachment in high myopia. Am J Ophthalmol. 2016;166:211.

88. Lai CC, Chen YP, Wang NK, Chuang LH, et al. Vitrectomy with internal limiting membrane repositioning and autologous blood for macular hole retinal detachment in highly myopic eyes. Ophthalmology. 2015;122(9):1889–98.

89. Okuda T, Higashide T, Kobayashi K, Ikuno Y, Sugiyama K. Macular hole closure over residual subretinal fluid by an inverted internal limiting membrane flap technique in patients with macular hole retinal detachment in high myopia. Retin Cases Brief Rep. 2016;10(2):140–4.

90. Tewari R, Kumar V, Ravani R, Dubey D, Chandra P, Kumar A. Macular hole-associated retinal detachment in best vitelliform dystrophy: series of two cases and literature review. Indian J Ophthalmol. 2018;66(5):708–11.

91. Hirano M, Morizane Y, Kawata T, Kimura S, et al. Case report: successful closure of a large macular hole secondary to uveitis using the inverted internal limiting membrane flap technique. BMC Ophthalmol. 2015;15:83.

92. Abou Shousha MA. Inverted internal limiting membrane flap for large traumatic macular holes. Medicine (Baltimore). 2016;95(3):e2523.

93. Nuzzo T, Patelli F, Esposito G, Colombo L, Rossetti L. Inverted ILM flap technique in a pediatric traumatic macular hole - a case report. J Vitreoretin Dis. 2017;1(5):338–40. https://doi.org/10.1177/2474126417714653. Epub 2017 June 30

94. Astir S, Shroff D, Gupta C, Shroff C. Inverted flap technique for a large traumatic macular hole with choroidal rupture and subretinal hemorrhage Oman. J Ophthalmol. 2018;11(1):68–70. https://doi.org/10.4103/0974-620X.226348.

95. Morizane Y, Shiraga F, Kimura S, Hosokawa M, et al. Autologous transplantation of the internal limiting membrane for refractory macular holes. Am J Ophthalmol. 2014;157:861–9.

96. Iwakawa Y, Imai H, Kaji H, Mori Y, et al. Autologous transplantation of the internal limiting membrane for refractory macular hole following ruptured retinal arterial macroaneurysm: a case report. Case Rep Ophthalmol. 2018;9:113–9.

97. De Novelli FJ, Preti RC, Ribeiro Monteiro ML, Pelayes DE, Junqueira Nóbrega M, Takahashi WY. Autologous internal limiting membrane fragment transplantation for large, chronic, and refractory macular holes. Ophthalmic Res. 2015;55(1):45–52.

98. Guber J, Lang C, Valmaggia C, et al. Internal limiting membrane flap techniques for the repair of large macular holes: a short-term follow-up of anatomical and functional outcomes. Klin Monatsbl Augenheilkd. 2017;234(4):493–6.

99. Gekka T, Watanabe A, Ohkuma Y, Arai K, et al. Pedicle internal limiting membrane transposition for refractory macular hole. Ophthalmic Surg Lasers Imaging Retina. 2015;46(10):1045–6.

100. Chen SN, Yang CM. Lens capsular flap transplantation in the management of refractory macular hole from multiple etiologies. Retina. 2016;36(1):163–70.

101. Peng J, Chen C, Jin H, Zhang H, Zhao P. Autologous lens capsular flap transplantation combined with autologous blood application in the management of refractory macular hole. Retina. 2017;38:2177. https://doi.org/10.1097/IAE.0000000000001830.

102. Grewal DS, Mahmoud TH. Autologous neurosensory retina free flap for closure of refractory myopic macular holes. JAMA Ophthalmol. 2016;134(2):229–30.

103. Grewal DS, Mahmoud TH, Fine HF. Management of challenging macular holes: current concepts and new surgical techniques. Ophthalmic Surg Lasers Imaging Retina. 2016;47(6):508–13.

104. Travassos AS, Regadas I, Alfaiate M, Silva ED, Proença R, Travassos A. Optic pit: novel surgical management of complicated cases. Retina. 2013;33(8):1708–14.

105. Mohammed OA, Pai A. Inverted autologous internal limiting membrane for management of optic disc pit with macular detachment. Middle East Afr J Ophthalmol. 2013;20(4):357–9.

106. European Vitreoretinal Society Optic Pit Study 2014. http://www.evrs.eu/op-study-connect/. Accessed 9 Aug 2016.

107. Nawrocki J, Bonińska K, Michalewska Z. Managing optic pit. The right stuff! Retina. 2016;36(12):2430–2.

108. D'Souza P, Babu U, Narendran V. Autologous free internal limiting membrane flap for optic nerve head pit with Maculopathy. Ophthalmic Surg Lasers Imaging Retina. 2017;48:350–3.

109. Hara R, Tsukahara Y, Simoyama T, Mori S. Refined internal limiting membrane inverted flap technique for intractable macular detachment with optic disc pit. Case Rep Ophthalmol. 2017;8:208–13.

110. Chen Z, Zhao C, Ye JJ, Wang XQ, Sui RF. Inverted internal limiting membrane flap technique for repair of large macular holes: a short-term follow-up of anatomical and functional outcomes. Chin Med J. 2016;129(5):511–7.

111. Bonińska K, Nawrocki J, Michalewska Z. Mechanism of "flap closure" after the inverted internal limiting membrane flap technique. Retina. 2017;38:2184. https://doi.org/10.1097/IAE.0000000000001861.

112. Michalewska Z, Nawrocki J. Swept-source optical coherence tomography angiography reveals internal limiting membrane peeling alters deep retinal vasculature. Retina. 2018;38:S154. https://doi.org/10.1097/IAE.0000000000002199.

Management of Macular Hole Retinal Detachment

20

An-Lun Wu, Kiet-Phang Ling, and Chi-Chun Lai

20.1 Introduction

Retinal detachment associated with macular hole (MHRD) is one of the most vision-threatening complications in highly myopic eyes, and it accounts for less than 1% of all cases [1], although some studies from Asian populations have reported higher incidence [2, 3]. Pathogenesis is not fully understood, although it is believed that MHRD in highly myopic eyes occurs due to three factors: anteroposterior vitreous traction on the posterior pole due to axial elongation or posterior staphyloma [4]; tangential traction on the macula from the contraction of the cortical vitreous and epiretinal membrane [5–7]; and reduced retinal adherence to the choroid due to retinal pigment epithelial (RPE) atrophy [4].

The different causes of MHRD have been described [8, 9]. One cause may be explained by the theory of mechanical stresses in the macula.

A.-L. Wu
Department of Ophthalmology, Chang Gung Memorial Hospital, Linkou, Taiwan

K.-P. Ling
Department of Ophthalmology, Sultanah Aminah Hospital, Johor, Malaysia

C.-C. Lai (✉)
Department of Ophthalmology, Chang Gung Memorial Hospital, Linkou, Taiwan

Department of Ophthalmology, Chang Gung Memorial Hospital, Keelung, Taiwan

Myopic foveoschisis is substantially a tractional disease before the development of MHRD (Fig. 20.1a). Although it can remain stable for years, the advancement of foveal detachment may occur over time once photoreceptors are separated from the RPE (Fig. 20.1b). At a later stage, premacular structures such as partially detached posterior hyaloid and epiretinal membrane (ERM), the rigidity of internal limiting membrane (ILM), and the retinal vascular traction may further cause tangential traction to the fovea and facilitate the development of MHRD (Fig. 20.1c, d). In addition, MHRD can develop after vitrectomy for pathologic myopic foveoschisis. In one study, secondary MHRD was reported in about 5.3% of the myopic foveoschisis cases [8]. Furthermore, they found that preoperative foveal detachment is a significant risk factor.

The classifications of MHRD have been described based on the extension of RD [10]. These are, briefly, classification of type 1 indicated RD within the macula, type 2 indicated RD beyond the macula, and type 3 indicated total RD.

20.2 Surgical Techniques

Surgical management of MHRD in highly myopic eyes poses a specific challenge for vitreoretinal surgeons. However, the two main surgical goals are achieving MH closure and retinal reattachment. Visual improvement is rare when these
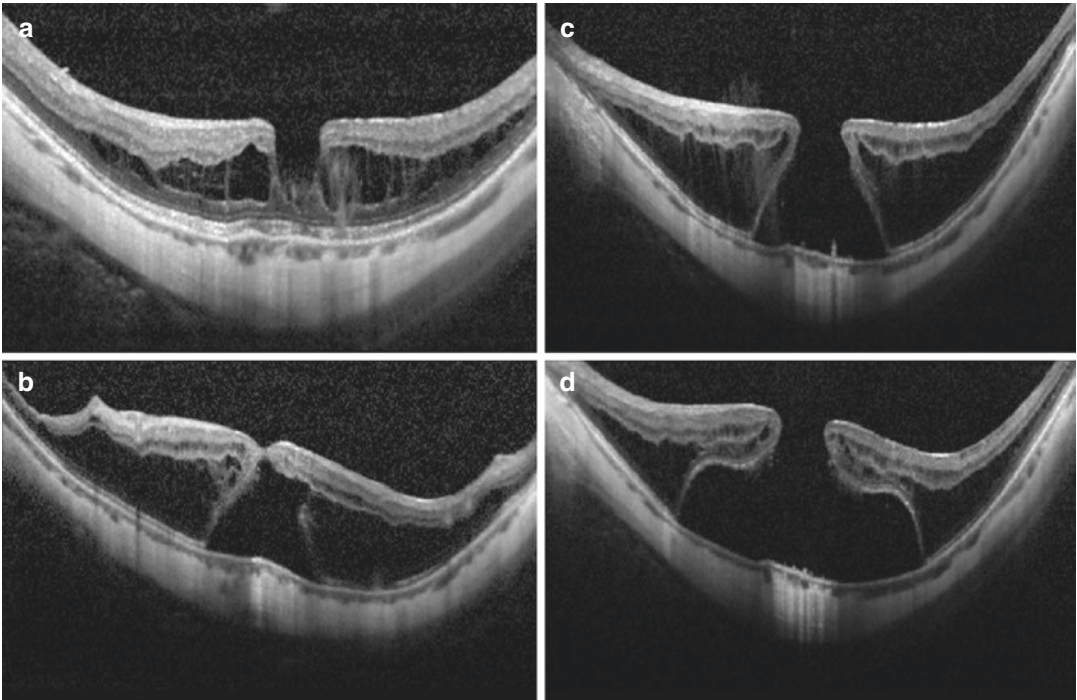
Fig. 20.1 Development of MHRD in highly myopic eyes. (**a**) The presence of posterior staphyloma with myopic foveoschisis in a highly myopic eye. (**b**) Foveal detachment occurred after foveoschisis had remained stable for years. (**c**) Foveal detachment enlarged horizontally and elevated vertically and consequent progression to the formation of a full-thickness macular hole. (**d**) Later development of MHRD

two goals are not attained. Various surgical approaches have been proposed to treat MHRD, including gas injection, macular buckling, vitrectomy with or without ILM peeling using gas or silicone oil as an internal tamponade, and combined vitrectomy with macular buckling or scleral imbrications [10, 11]. The history of the macular buckling technique treating in MHRD began in 1957 [12], which is designed to counteract the pulling effect of staphyloma. Since 1982 [13], vitrectomy has gained popularity and has become the most effective surgical approach for MHRD in recent years.

A search was carried out in the PubMed database of articles published from 2008 to 2017 (search terms: "macular hole retinal detachment," "macular hole associated retinal detachment," "MHRD," "macular buckling," and "vitrectomy") with the objective of presenting the number of published studies on different treatment modali-

ties for MHRD. During the past 10 years, there have been more than 29 clinical studies [11, 14–41] on the use of vitrectomy for MHRD, with an increasing number of reports in the last 5 years comparing it to the macular buckling procedure [16, 21, 34, 42–52] (Fig. 20.2).

20.2.1 Macular Buckling

Surgical management using the buckle technique in MHRD as a further specific myopic staphyloma-related complication and reshaping the posterior scleral wall seems to be reasonable treatments. Currently, macular buckling and scleral shortening techniques are able to change the concavity of the posterior part of the eye into a flat or even convex shape [12]. However, it was generally considered technically challenging probably because of the difficulties in achieving

Fig. 20.2 There has been an increase in the past 5 years in the number of clinical studies investigating the surgical approach of using vitrectomy for macular hole retinal detachment

20.2.2 Vitrectomy

Advances in surgical techniques have increased retinal reattachment and MH closure rates, making vitrectomy the primary procedure of choice for most surgeons. In recent years, successful outcomes have been reported with high rates of successful retinal attachment (from 95 to 100%) and MH closure (from 86 to 100%) following vitrectomy for MHRD [17, 18, 22, 25, 27, 31, 57]. The surgical goal is to release all retinal traction so as to reattach and to facilitate the closure of MH. The rigidity of the ILM has been considered an important factor. For this reason, vitrectomy combined with ILM peeling was believed to be a beneficial procedure for such patients.

the correct placement of the macular buckle [53]. In recent years, renewed interest and several new methods have been designed to overcome the difficulty, such as L-shaped buckle containing titanium stent [48], T-shaped buckling made of solid silicone [44], macular buckling with a three-armed adjustable silicone capsule [54], adjustable macular buckling device [55], and Gore-Tex vascular graft [52]. In addition, a 29-gauge chandelier light may be inserted into the indenting head of the buckle for optimal positioning [45].

A meta-analysis of the macular buckle technique for MHRD in myopic eyes involving a total of 16 studies (272 eyes) from the years 2000 to 2016 reported that the primary retinal reattachment rates ranged from 81.8 to 100% and MH closure rates ranged from 40 to 93.3% [12]. Concerning the functional outcome, the best-corrected visual acuity (BCVA) improvement rate ranged from 27.3 to 100% [16, 21, 34, 42–52]. They concluded that MH closure is a crucial step to successfully treating MHRD and improving functional outcomes [12].

One major concern for using macular buckling is that excessive compression possibly affects blood flow in the choroidal vasculature, leading to RPE changes [56]. Although the innovative technique using a suprachoroidal injection of long-acting hyaluronic acid may reduce the risk of secondary RPE atrophy [21], there may be some technical difficulties in correctly placing the injection and delivering an adequate volume in eyes with complex and deep staphyloma.

20.2.3 Removal of Cortical Vitreous and ERM

Detachment of the posterior hyaloid with complete removal of ERM is essential for successful retinal reattachment. Although a posterior vitreous detachment may appear to be present with a vitreous opacity resembling a Weiss ring, an adherent layer of vitreous frequently remains adherent to the retinal surface due to the schisis of the cortical vitreous [58, 59]. The use of intravitreal triamcinolone allows visualization of any remaining vitreous cortex [60]. Alternatively, a diamond-dusted scraper is useful in brushing
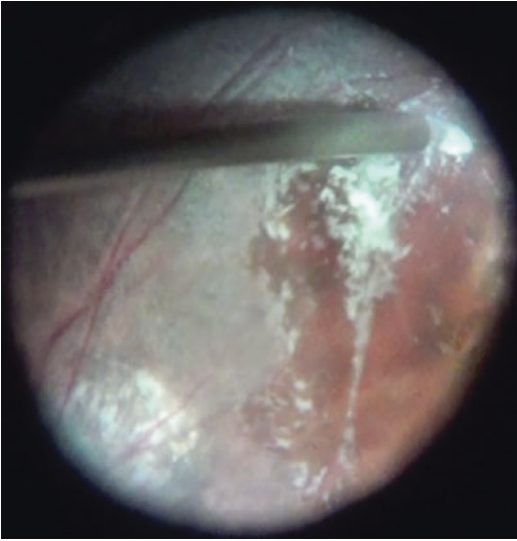
Fig. 20.3 Using a diamond-dusted scraper to separate the vitreous cortex from the retina after triamcinolone staining. Care should be taken to avoid an iatrogenic break in the thin and fragile retina in such eyes

strands of vitreous from the surface of the retina (Fig. 20.3). The thick premacular vitreous may be elevated and aspirated into the port using the vitreous cutter.

20.2.4 ILM Peeling

The rationale of ILM peeling could be used to remove premacular tractional elements (such as the vitreous cortex and epiretinal membrane), remove scaffold for cellular proliferation, and increase the flexibility of the retina to conform better to the posterior staphyloma [61]. Thus, the ILM peeling technique has nearly become the standard combined procedure, followed by vitrectomy, to manage MHRD. Although different ILM peeling methods have been attempted to achieve improved anatomic and functional outcomes, however, the best surgical approach remains controversial.

The inverted ILM flap technique was an alternative proposal to improve the success rates based on the mechanism that ILM may function as a scaffold for the proliferation and migration of Müller cells [62]. The concept was firstly pro-

posed by Michalewska et al. in larger MH to facilitate the healing process and has now been extended for use in treating MHRD [63]. There have been comparisons of the inverted ILM flap technique and ILM peeling for MHRD, but the results are contradictory [39, 57, 64]. In a meta-analysis review, the rate of retinal reattachment and MH closure after initial surgery was significantly higher after the inverted ILM flap technique than ILM peeling. However, there was no difference in postoperative BCVA between the two groups of eyes treated by different surgical strategies [65]. Because postoperative MH enlargement has been reported due to the imbalance between the retina and choroid–sclera complex [66], an inverted ILM insertion was designed to decrease the risk of the ILM flap reverting to the previous state and tearing off during surgery, especially during fluid–air exchange. In one direct comparison study [67], inverted ILM insertion showed a higher MH closure rate and the tendency of better postoperative BCVA in patients with MHRD as compared to conventional ILM peeling. However, full ILM tissue plugging in the fovea may interrupt retinal microstructure restoration, but it may also have cytotoxic effects on retinal neurons if there is persistent activation of glial cells, inducing excessive gliosis [68]. So, the adequate amount of inverted ILM tissue used for insertion needs to be further studied and determined for this procedure [69].

20.2.5 Macular Plug

Mechanism of MH closure treated with vitrectomy with inverted ILM peeling involves the stimulation of glial cell proliferation in the hole [62]. Adjuvant therapies have been used to accelerate the healing of the hole, including autologous serum, platelet concentrate, or blood, to enhance anatomic success [70, 71]. Lai et al. were the first to report the successful closure of MHRD using ILM repositioning and autologous blood clot (ABC) (Fig. 20.4) during vitrectomy [31]. ABC, in addition to being used as an adjuvant material, can act as a glue to increase stabil-
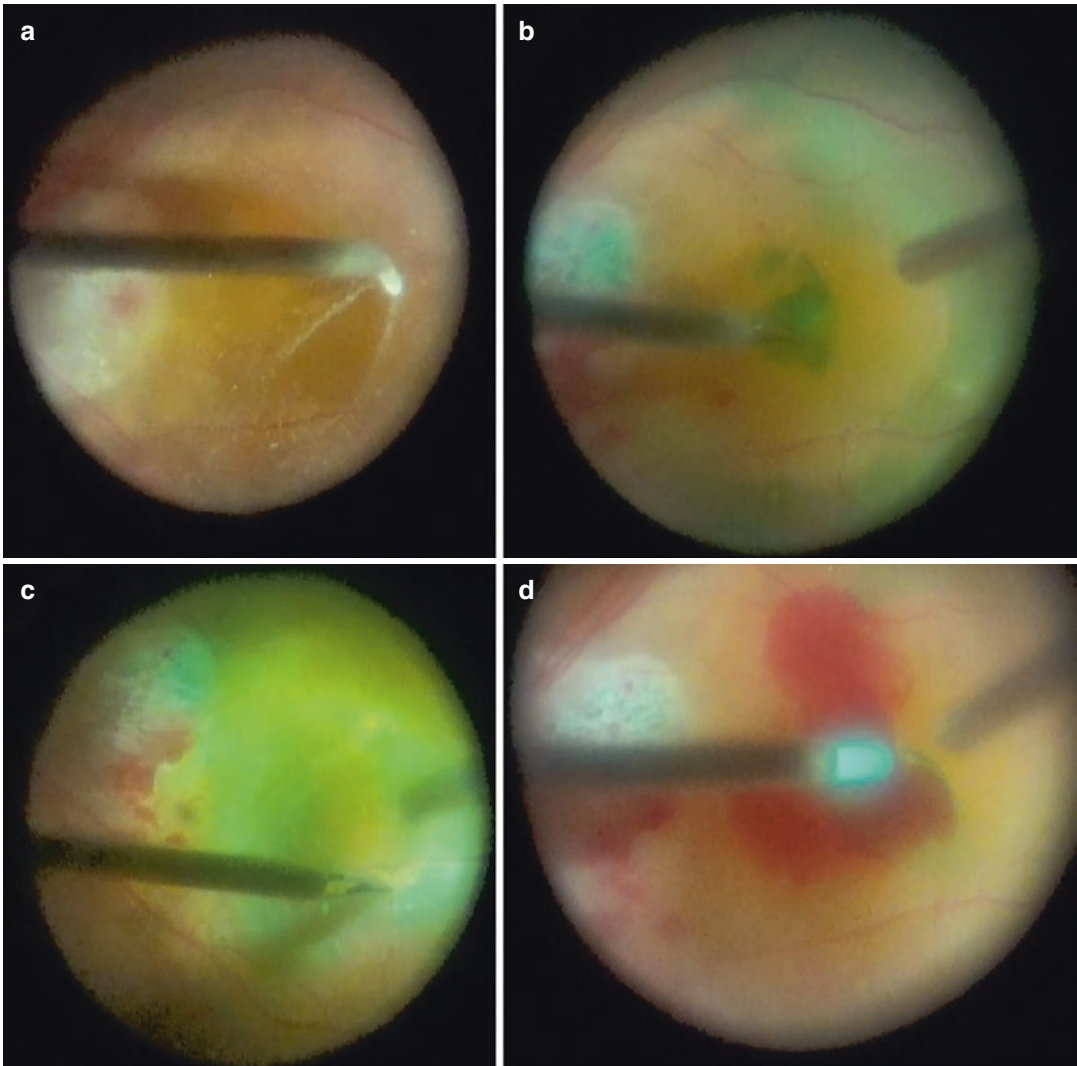
Fig. 20.4 The surgical procedure of macular hole retinal detachment repair through a vitrectomy combined with an inverted internal limiting membrane (ILM) repositioning and autologous blood clot. (**a**) After a vitrectomy, the posterior vitreous cortex was lifted by a diamond-dusted membrane scraper facilitated with diluted triamcinolone acetonide. (**b**) ILM lifting was assisted by staining with indocyanine green without intentional drainage of the subretinal fluid. (**c**) After the ILM was circumferentially lifted, the ILM flap remaining attached to the edge of the MH was inverted and placed into MH by forceps. (**d**) Fresh blood was used to cover the macula, and the repositioned ILM and autologous blood clot mixture became a macular plug that sealed the hole

ity and keep the repositioned ILM tissue in place, which reduces the risk of dislocation both intra-operatively and postoperatively. Therefore, remaining in a strictly prone position with gas tamponade was required for only 1 day. Furthermore, the mixture of ILM and ABC formed a macular plug that sealed the MH shortly after application, achieving 96% of primary reti-nal reattachment and 96% of MH closure rate (Fig. 20.5). It is of note that subretinal fluid was not intentionally drained to prevent the enlarged MH during the drainage maneuver and to reduce the risk of potential iatrogenic trauma to the reti-nal pigment epithelium and choroid at the fovea. Regarding toxicity issues due to blood products and fibrin degradation products used in this tech-
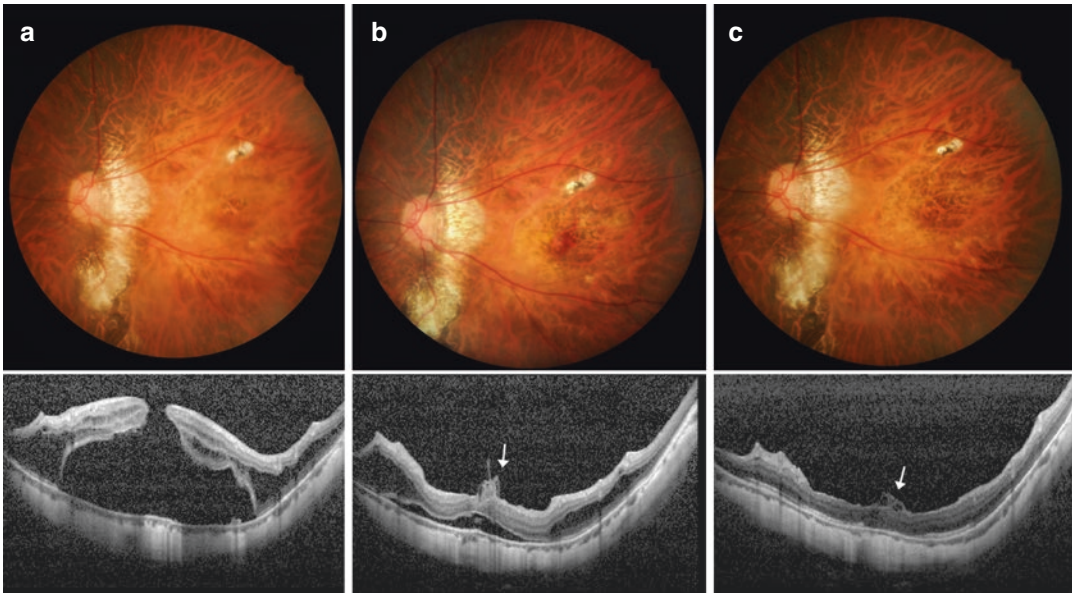
Fig. 20.5 Successful treatment using an inverted internal limiting membrane (ILM) repositioning and autologous blood clot technique in type 1 macular hole retinal detachment (MHRD). (**a**) Color fundus photograph and optical coherence tomography (OCT) image obtained before the surgery. The BCVA was 0.1. (**b**) Color fundus photograph and OCT obtained 5 days after surgery. Note that the blood clot remained and the hole was closed with repositioned ILM, though residual subretinal fluid was noted. (**c**) Color fundus photograph and OCT obtained 12 months after surgery. The BCVA improved to 0.4. Note that the retina is well attached and the macular hole remained closed. Arrows in (**b**) and (**c**) indicate the location of the repositioned ILM in the macular hole

nique, safety concerns are reduced because the repositioned ILM tissue barrier serves as a filler at the hole (Fig. 20.6).

20.2.6 Dyes

In the detached and mobile retina, it is difficult to visualize the ILM during surgery. The application of dyes and adjuvants can make MHRD surgeries safer and thus reduce the duration of surgery, decreasing the risk of mechanical trauma to the retina. However, chemical dyes can remain in the subretinal space after MHRD surgery and cause damage to retinal tissue, particularly the RPE and photoreceptors [72]. Furthermore, dyes can remain in the foveal area of preserved and stained ILMs for long periods of time and may have toxic effects on the retinal tissue [73]. Thus, the long-term safety of these dyes in chromovitrectomy for MHRD surgery has become an emerging issue. Indocyanine green (ICG) was the first dye to show good staining of the ILM, although the safety of this dye remains a major concern [72, 74, 75]. Several other dyes and staining materials, including trypan blue [76], brilliant blue G [77], triamcinolone acetonide [78], and blood [79] have subsequently been tested as alternatives. Nevertheless, their long-term iatrogenic effects have not been investigated.

Perfluoro-n-octane (PFO)-assisted ILM peeling in the presence of a detached retina could have some benefits (Fig. 20.7). One such benefit is that PFO can prevent the dye from gaining access to the subretinal space. During the procedure, a small amount of PFO is injected into the eye to cover the MH before applying the ILM staining. Another effect from PFO which could stabilize the retina and make it less mobile during ILM peeling, consequently reducing the possible mechanical microtrauma to the retina.
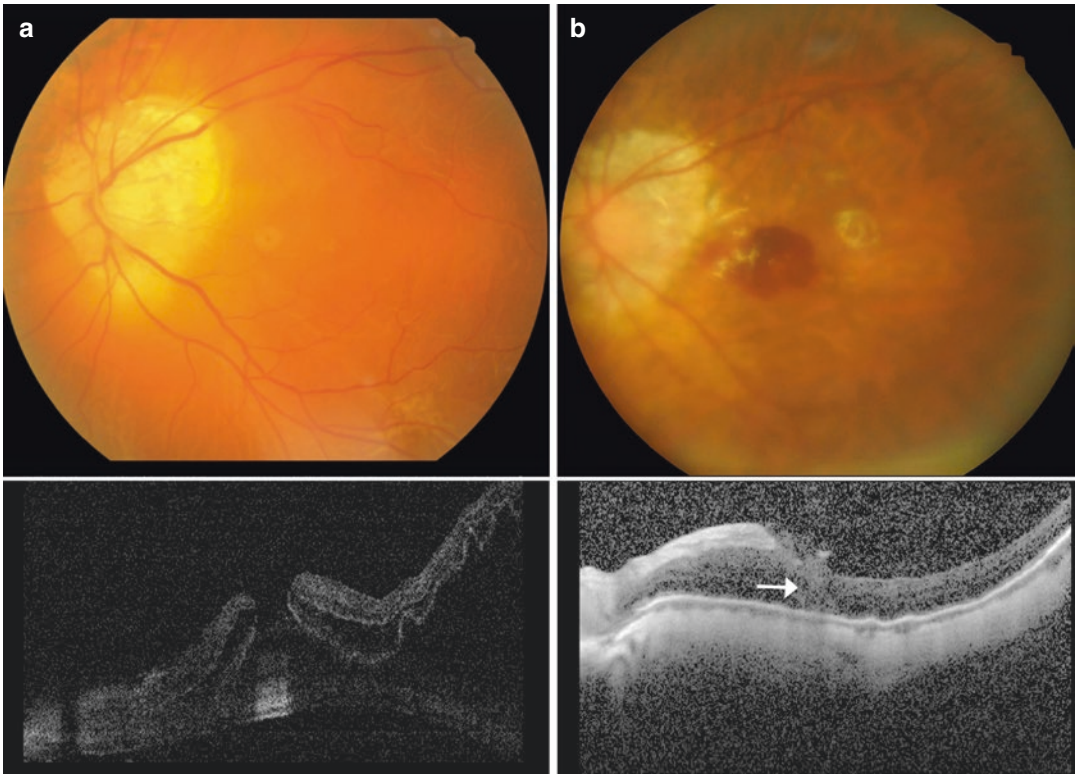
Fig. 20.6 Reattached retina with closed macular hole detected 1 day after the surgery in type 2 macular hole retinal detachment (MHRD) (**a**) Color fundus photograph and optical coherence tomography (OCT) image obtained before the surgery. (**b**) 1-day after the surgery using internal limiting membrane repositioning and autologous blood clot technique with silicone oil tamponade, the retina reattached well with closed hole confirmed by OCT. Note that the fovea hyperreflective signal (arrow) obtained from OCT indicate the blood clot located at about half of the retina depth
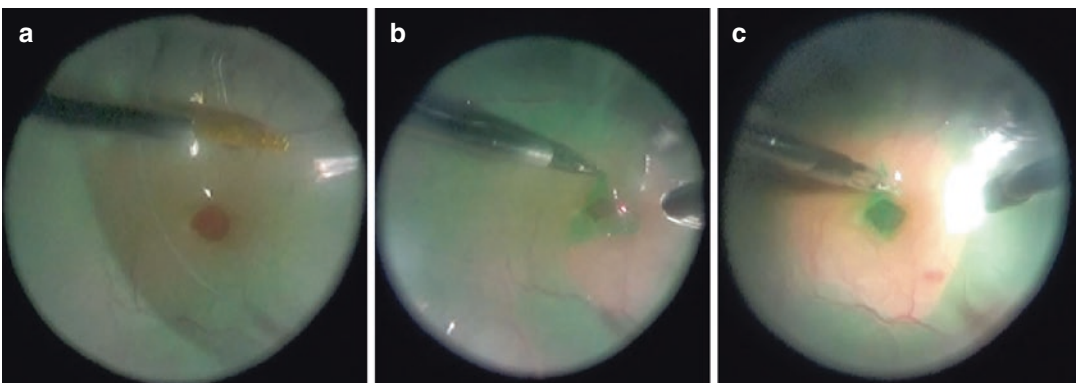
Fig. 20.7 The key steps of perfluoro-n-octane (PFO)-assisted internal limiting membrane (ILM) peeling technique in treating macular hole retinal detachment (**a**) A small amount of PFO bubble was introduced into the eye to protect the fovea followed by injection of indocyanine green dye. (**b**) PFO stabilizes the retina and makes it less mobile during ILM peeling. (**c**) Insertion of the ILM flap under PFO makes the manipulation easier to perform

20.3　Complications

The comparison of advantages, disadvantages, and potential complications using macular buckling and vitrectomy with ILM peeling in MHRD are summarized in Table 20.1. For the macular buckle, the main intraoperative complications include buckle malpositioning, perfora-

Table 20.1 Comparison of macular buckle and vitrectomy with ILM peeling in macular hole retinal detachment

	Macular buckling	Vitrectomy
Advantages	Address posterior staphyloma and relief anteroposterior traction	Direct relief of vitreous traction and tangential traction from ILM
	A reversible surgical technique	Enhance macular closure by ILM flap
	No need for postoperative facedown positioning	Enable drainage of subretinal fluid
Disadvantages	Technical difficulty	Internal tamponade of gas/silicone oil is required
	Change of macular surface shape	Potential light and dye toxicity
	Lack of buckling strength control	Unpleasant experience for the patient to remain in a prone position
	Unprecise alignment of the buckle under the fovea	Higher medical cost
Potential complications	Globe perforation	Iatrogenic breaks
	Vessel and nerve injury	Elevated intraocular pressure
	Subretinal/suprachoroidal hemorrhaging	Postoperative endophthalmitis
	Migration/exposure of buckle	Cataract progression
	Posterior RPE atrophy	Excessive gliosis

tion, vessel injury, and choroidal detachment or hemorrhaging. Late complications include buckle displacement, exposure, or retinal pigment epithelium changes due to circulatory disturbances [12]. The most common complication for vitrectomy is an increase in the rate of cataract development. Other potential complications include iatrogenic breaks, elevated intraocular pressure, and retinal re-detachment after surgery. Also, the macular hole may reopen after surgery. However, an understanding of the possible complications and new innovations in vitreous surgical instruments can facilitate safer surgeries. For example, long-shaft forceps were developed to use in ILM peeling in highly myopic eyes with axial lengths ranging from 27.89 to 29.9 mm [80]. Intraoperative OCT may also improve the identification and removal of premacular traction during the operation. It may guide vitreoretinal surgeons in their choice of whether and how to perform ILM peeling to minimize the risk of iatrogenic trauma to the macula.

20.4　Conclusions

MHRD represents one of the most challenging surgical diseases in ophthalmology. Although current treatments for MHRD improve primary anatomical success, functional outcomes should be a future goal. Further studies are required to identify a method to seal the MH and flatten the retina in a more physiological manner to improve the capability of restoring function.

References

1. Margheria RR, Schepens CL. Macular breaks. 1. Diagnosis, etiology, and observations. Am J Ophthalmol. 1972;74:219–32.
2. Wong TY, Ferreira A, Hughes R, et al. Epidemiology and disease burden of pathologic myopia and myopic choroidal neovascularization: an evidence-based systematic review. Am J Ophthalmol. 2014;157:9–25. e12.
3. Zhang CF, Hu C. High incidence of retinal detachment secondary to macular hole in a Chinese population. Am J Ophthalmol. 1982;94:817–9.

4. Morita H, Ideta H, Ito K, et al. Causative factors of retinal detachment in macular holes. Retina. 1991;11:281–4.

5. Oshima Y, Ikuno Y, Motokura M, et al. Complete epiretinal membrane separation in highly myopic eyes with retinal detachment resulting from a macular hole. Am J Ophthalmol. 1998;126:669–76.

6. Seike C, Kusaka S, Sakagami K, et al. Reopening of macular holes in highly myopic eyes with retinal detachments. Retina. 1997;17:2–6.

7. Stirpe M, Michels RG. Retinal detachment in highly myopic eyes due to macular holes and epiretinal traction. Retina. 1990;10:113–4.

8. Huang Y, Huang W, Ng DSC, et al. Risk factors for development of macular hole retinal detachment after pars Plana vitrectomy for pathologic myopic Foveoschisis. Retina. 2017;37:1049–54.

9. Sun CB, Liu Z, Xue AQ, et al. Natural evolution from macular retinoschisis to full-thickness macular hole in highly myopic eyes. Eye (Lond). 2010;24:1787–91.

10. Chen YP, Chen TL, Yang KR, et al. Treatment of retinal detachment resulting from posterior staphyloma-associated macular hole in highly myopic eyes. Retina. 2006;26:25–31.

11. Fujikawa M, Kawamura H, Kakinoki M, et al. Scleral imbrication combined with vitrectomy and gas tamponade for refractory macular hole retinal detachment associated with high myopia. Retina. 2014;34:2451–7.

12. Alkabes M, Mateo C. Macular buckle technique in myopic traction maculopathy: a 16-year review of the literature and a comparison with vitreous surgery. Graefes Arch Clin Exp Ophthalmol. 2018;256:863–77.

13. Gonvers M, Machemer R. A new approach to treating retinal detachment with macular hole. Am J Ophthalmol. 1982;94:468–72.

14. Ando Y, Hirakata A, Ohara A, et al. Vitrectomy and scleral imbrication in patients with myopic traction maculopathy and macular hole retinal detachment. Graefes Arch Clin Exp Ophthalmol. 2017;255:673–80.

15. Arias L, Caminal JM, Rubio MJ, et al. Autofluorescence and axial length as prognostic factors for outcomes of macular hole retinal detachment surgery in high myopia. Retina. 2015;35:423–8.

16. Bedda AM, Abdel Hadi AM, Abd Al Shafy MS. A comparative study between vitrectomy with internal tamponade and a new modified fiber optic illuminated ando plombe for cases of macular hole retinal detachment in myopic eyes. J Ophthalmol. 2015;2015:841925.

17. Chen SN, Yang CM. Inverted internal limiting membrane insertion for macular hole-associated retinal detachment in high myopia. Am J Ophthalmol. 2016;166:211.

18. Chen SN, Yang CM. Double internal limiting membrane insertion for macular hole-associated retinal detachment. J Ophthalmol. 2017;2017:3236516.

19. Chen Y, Shen L, Zhao S, et al. Internal limiting membrane peeling by 23-gauge endoscopy for mac-ular hole retinal detachment in a pathological myopic eye. Ophthalmic Surg Lasers Imaging Retina. 2017;48:179–82.

20. Cunningham MA, Tarantola RM, Folk JC, et al. Proliferative vitreoretinopathy may be a risk factor in combined macular hole retinal detachment cases. Retina. 2013;33:579–85.

21. El Rayes EN. Supra choroidal buckling in managing myopic vitreoretinal interface disorders: 1-year data. Retina. 2014;34:129–35.

22. Gao X, Guo J, Meng X, et al. A meta-analysis of vitrectomy with or without internal limiting membrane peeling for macular hole retinal detachment in the highly myopic eyes. BMC Ophthalmol. 2016;16:87.

23. Ghoraba HH, Elgouhary SM, Mansour HO. Silicone oil reinjection without macular buckling for treatment of recurrent myopic macular hole retinal detachment after silicone oil removal. J Ophthalmol. 2014a;2014:434272.

24. Ghoraba HH, Mansour HO, Elgouhary SM. Effect of 360 degrees episcleral band as adjunctive to pars plana vitrectomy and silicone oil tamponade in the management of myopic macular hole retinal detachment. Retina. 2014b;34:670–8.

25. Ho TC, Ho A, Chen MS. Vitrectomy with a modified temporal inverted limiting membrane flap to reconstruct the foveolar architecture for macular hole retinal detachment in highly myopic eyes. Acta Ophthalmol. 2018;96:e46–53.

26. Jeon HS, Byon IS, Park SW, et al. Extramacular drainage of subretinal fluid during vitrectomy for macular hole retinal detachment in high myopia. Retina. 2014;34:1096–102.

27. Kinoshita T, Onoda Y, Maeno T. Long-term surgical outcomes of the inverted internal limiting membrane flap technique in highly myopic macular hole retinal detachment. Graefes Arch Clin Exp Ophthalmol. 2017;255:1101–6.

28. Kobayashi W, Kunikata H, Abe T, et al. Retrospective comparison of 25- and 23-gauge microincision vitrectomy surgery and 20-gauge vitrectomy for the repair of macular hole retinal detachment. Asia Pac J Ophthalmol (Phila). 2014;3:331–6.

29. Kumar A, Kakkar P, Ravani RD, et al. Utility of microscope-integrated optical coherence tomography (MIOCT) in the treatment of myopic macular hole retinal detachment. BMJ Case Rep. 2017;2017:bcr-2016-217671.

30. Kumar A, Tinwala S, Gogia V, et al. Clinical presentation and surgical outcomes in primary myopic macular hole retinal detachment. Eur J Ophthalmol. 2012;22:450–5.

31. Lai CC, Chen YP, Wang NK, et al. Vitrectomy with internal limiting membrane repositioning and autologous blood for macular hole retinal detachment in highly myopic eyes. Ophthalmology. 2015;122:1889–98.

32. Laviers H, Zambarakji H. Management of macular hole retinal detachment and macular retinoschisis

secondary to pathological myopia: a national survey of UK practice patterns. Eye (Lond). 2013;27:1324.

33. Lee JE. Two-step surgery for retinal detachment caused by myopic macular hole. Clin Ophthalmol. 2012;6:1771–4.

34. Ma J, Li H, Ding X, et al. Effectiveness of combined macular buckle under direct vision and vitrectomy with ILM peeling in refractory macular hole retinal detachment with extreme high axial myopia: a 24-month comparative study. Br J Ophthalmol. 2017;101:1386–94.

35. Mancino R, Ciuffoletti E, Martucci A, et al. Anatomical and functional results of macular hole retinal detachment surgery in patients with high myopia and posterior staphyloma treated with perfluoro-propane gas or silicone oil. Retina. 2013;33:586–92.

36. Okuda T, Higashide T, Kobayashi K, et al. Macular hole closure over residual subretinal fluid by an inverted internal limiting membrane flap technique in patients with macular hole retinal detachment in high myopia. Retinal Cases Brief Rep. 2016;10:140–4.

37. Ortisi E, Avitabile T, Bonfiglio V. Surgical management of retinal detachment because of macular hole in highly myopic eyes. Retina. 2012;32:1704–18.

38. Otsuka K, Imai H, Shimoyama T, et al. Recurrence of macular hole retinal detachment after intravitreal ranibizumab injection for the treatment of choroidal neovascularization from the remaining macular hole edge. Case Rep Ophthalmol. 2012;3:424–7.

39. Sasaki H, Shiono A, Kogo J, et al. Inverted internal limiting membrane flap technique as a useful procedure for macular hole-associated retinal detachment in highly myopic eyes. Eye (Lond). 2017;31:545–50.

40. Takahashi H, Inoue M, Koto T, et al. Inverted internal limiting membrane flap technique for treatment of macular hole retinal detachment in highly myopic eyes. Retina. 2017:1.

41. Wei Y, Wang N, Zu Z, et al. Efficacy of vitrectomy with triamcinolone assistance versus internal limiting membrane peeling for highly myopic macular hole retinal detachment. Retina. 2013;33:1151–7.

42. Alkabes M, Bures-Jelstrup A, Salinas C, et al. Macular buckling for previously untreated and recurrent retinal detachment due to high myopic macular hole: a 12-month comparative study. Graefes Arch Clin Exp Ophthalmol. 2014;252:571–81.

43. Bedda AM, Abdel Hadi AM, Lolah M, et al. A new sutureless illuminated macular buckle designed for myopic macular hole retinal detachment. J Ophthalmol. 2017;2017:6742164.

44. Devin F, Tsui I, Morin B, et al. T-shaped scleral buckle for macular detachments in high myopes. Retina. 2011;31:177–80.

45. Forlini M, Szkaradek M, Rejdak R, et al. Modification of adjustable macular buckling with 29-G chandelier light for optimal positioning in highly myopic eyes with macular hole. Retinal Cases Brief Rep. 2017;11:249–54.

46. Mortada HA. A novel episcleral macular buckling: wire-strengthened sponge exoplant for recurrent

macular hole and retinal detachment in high myopic eyes. Med Hypothesis Discov Innov Ophthalmol. 2013;2:14–9.

47. Mura M, Iannetta D, Buschini E, et al. T-shaped macular buckling combined with 25G pars plana vitrectomy for macular hole, macular schisis, and macular detachment in highly myopic eyes. Br J Ophthalmol. 2017;101:383–8.

48. Parolini B, Frisina R, Pinackatt S, et al. Indications and results of a new L-shaped macular buckle to support a posterior staphyloma in high myopia. Retina. 2015;35:2469–82.

49. Qi Y, Duan AL, You QS, et al. Posterior scleral reinforcement and vitrectomy for myopic foveoschisis in extreme myopia. Retina. 2015;35:351–7.

50. Siam AL, El Maamoun TA, Ali MH. Macular buckling for myopic macular hole retinal detachment: a new approach. Retina. 2012;32:748–53.

51. Tian J, Tang LS, Guo XJ, et al. Episcleral macular buckling for posterior retinal detachment in silicone oil filled eyes associated with myopic macular hole. Int J Ophthalmol. 2013;6:165–8.

52. Wu PC, Sheu JJ, Chen YH, et al. Gore-tex vascular graft for macular buckling in high myopia eyes. Retina. 2017;37:1263–9.

53. Theodossiadis GP, Theodossiadis PG. The macular buckling procedure in the treatment of retinal detachment in highly myopic eyes with macular hole and posterior staphyloma: mean follow-up of 15 years. Retina. 2005;25:285–9.

54. Liu B, Ma W, Li Y, et al. Macular buckling using a three-armed silicone capsule for Foveoschisis associated with high myopia. Retina. 2016;36:1919–26.

55. Cacciamani A, Lazzeri S, Rossi T, et al. Adjustable macular buckling for full-thickness macular hole with foveoschisis in highly myopic eyes: long-term anatomical and functional results. Retina. 2016;36:709–16.

56. Mateo C, Bures-Jelstrup A. Macular buckling with Ando Plombe may increase choroidal thickness and mimic serous retinal detachment seen in the tilted disk syndrome. Retinal Cases Brief Rep. 2016;10:327–30.

57. Baba R, Wakabayashi Y, Umazume K, et al. Efficacy of the inverted internal limiting membrane flap technique with vitrectomy for retinal detachment associated with myopic macular holes. Retina. 2017;37:466–71.

58. Sakaguchi H, Ikuno Y, Choi JS, et al. Multiple components of epiretinal tissues detected by triamcinolone and indocyanine green in macular hole and retinal detachment as a result of high myopia. Am J Ophthalmol. 2004;138:1079–81.

59. Spaide RF, Fisher Y. Removal of adherent cortical vitreous plaques without removing the internal limiting membrane in the repair of macular detachments in highly myopic eyes. Retina. 2005;25:290–5.

60. Yamamoto N, Ozaki N, Murakami K. Triamcinolone acetonide facilitates removal of the epiretinal membrane and separation of the residual vitreous cortex in

highly myopic eyes with retinal detachment due to a macular hole. Ophthalmologica. 2004;218:248–56.

61. Almony A, Nudleman E, Shah GK, et al. Techniques, rationale, and outcomes of internal limiting membrane peeling. Retina. 2012;32:877–91.

62. Shiode Y, Morizane Y, Matoba R, et al. The role of inverted internal limiting membrane flap in macular hole closure. Invest Ophthalmol Vis Sci. 2017;58:4847–55.

63. Michalewska Z, Michalewski J, Adelman RA, et al. Inverted internal limiting membrane flap technique for large macular holes. Ophthalmology. 2010;117:2018–25.

64. Matsumura T, Takamura Y, Tomomatsu T, et al. Comparison of the inverted internal limiting membrane flap technique and the internal limiting membrane peeling for macular hole with retinal detachment. PLoS One. 2016;11:e0165068.

65. Yuan J, Zhang LL, Lu YJ, et al. Vitrectomy with internal limiting membrane peeling versus inverted internal limiting membrane flap technique for macular hole-induced retinal detachment: a systematic review of literature and meta-analysis. BMC Ophthalmol. 2017;17:219.

66. Ichibe M, Yoshizawa T, Murakami K, et al. Surgical management of retinal detachment associated with myopic macular hole: anatomic and functional status of the macula. Am J Ophthalmol. 2003;136:277–84.

67. Wakabayashi T, Ikuno Y, Shiraki N, et al. Inverted internal limiting membrane insertion versus standard internal limiting membrane peeling for macular hole retinal detachment in high myopia: one-year study. Graefes Arch Clin Exp Ophthalmol. 2018;256:1387.

68. Bringmann A, Iandiev I, Pannicke T, et al. Cellular signaling and factors involved in Muller cell gliosis: neuroprotective and detrimental effects. Prog Retin Eye Res. 2009;28:423–51.

69. Lai CC. ILM peeling in macular hole retinal detachment: insert or not? Graefes Arch Clin Exp Ophthalmol. 2018;256(8):1385–6.

70. Figueroa MS, Govetto A, Arriba-Palomero P. Short-term results of platelet-rich plasma as adjuvant to 23-G vitrectomy in the treatment of high myopic macular holes. Eur J Ophthalmol. 2016;26:491–6.

71. Purtskhvanidze K, Fruhsorger B, Bartsch S, et al. Persistent full-thickness idiopathic macular hole: anatomical and functional outcome of revitrectomy with autologous platelet concentrate or autologous whole blood. Ophthalmologica. 2018;239:19–26.

72. Horiguchi M, Nagata S, Yamamoto N, et al. Kinetics of indocyanine green dye after intraocular surgeries using indocyanine green staining. Arch Ophthalmol. 2003;121:327–31.

73. Chuang LH, Wu AL, Wang NK, et al. The intraocular staining potential of anthocyanins and their retinal biocompatibility: a preclinical study. Cutan Ocul Toxicol. 2018:1–22.

74. Grisanti S, Szurman P, Gelisken F, et al. Histological findings in experimental macular surgery with indocyanine green. Invest Ophthalmol Vis Sci. 2004;45:282–6.

75. Yamashita T, Uemura A, Kita H, et al. Long-term outcomes of visual field defects after indocyanine green-assisted macular hole surgery. Retina. 2008;28:1228–33.

76. Lee KL, Dean S, Guest S. A comparison of outcomes after indocyanine green and trypan blue assisted internal limiting membrane peeling during macular hole surgery. Br J Ophthalmol. 2005;89:420–4.

77. Ueno A, Hisatomi T, Enaida H, et al. Biocompatibility of brilliant blue G in a rat model of subretinal injection. Retina. 2007;27:499–504.

78. Shah GK, Rosenblatt BJ, Blinder KJ, et al. Triamcinolone-assisted internal limiting membrane peeling. Retina. 2005;25:972–5.

79. Lai CC, Hwang YS, Liu L, et al. Blood-assisted internal limiting membrane peeling for macular hole repair. Ophthalmology. 2009;116:1525–30.

80. Gao X, Ikuno Y, Nishida K. Long-shaft forceps for membrane peeling in highly myopic eyes. Retina. 2013;33:1475–6.

Part V

Myopic Maculopathy

Epidemiology of Myopic and Vitreomaculopathies

21

Chee Wai Wong, Beau J. Fenner, and Gemmy C. M. Cheung

21.1 Myopia

Myopia is a common ocular disorder. However, depending on the severity, its impact may range from mild distance vision impairment to permanent blindness [1]. In the past few decades, there has been a dramatic increase in the prevalence of myopia worldwide and the World Health Organization (WHO) has now identified myopia as an important global health problem [2]. The WHO now defines myopia as a condition in which the spherical equivalent objective refractive error is ≤ -0.50 D in either eye, while high myopia is ≤ -5.00 D in either eye [3].

21.1.1 Epidemiology and Economic Burden of Myopia in Different Populations

Uncorrected refractive error is the most common cause of avoidable visual impairment worldwide by a significant margin [4, 5]. Epidemiological studies indicate that myopia currently affects one in four of the world's population, with a predicted increase to one in two by the year 2050 [2]. High myopia, while less common than myopia, is following a similar trajectory (Fig. 21.1). The prevalence of myopia is highest in East Asia, with China, Japan, South Korea, and Singapore currently at approximately 50% prevalence among all age groups, while rates are lower in Africa, India, North and South America, Australia, and Europe, ranging from 5 to 30% [2, 6–8]. In virtually all geographic locations, however, current projections indicate dramatic increases in myopia prevalence in the coming decades, with East Asia and the Asia-Pacific regions expected to reach 66% by 2050 (Table 21.1). Even regions with a traditionally low prevalence of myopia such as Africa and Oceania are predicted to reach a prevalence of more than 20% in the next 30 years.

Development of myopia has been associated to varying degrees with living environment, lifestyle, socioeconomic factors, and genetic risk. Children living in urban environments have been reported to be more likely to have myopia compared to children from rural environments [7, 9, 10]. Less outdoor activity and more time spent indoors studying are also associated with longer axial length and myopia in school children [9, 11], although this effect varies significantly between studies [12–16]. A meta-analysis of seven observational studies that pooled odds ratios indicated that each additional hour spent outdoors conferred a 2% reduction in the odds ratio for myopia [17]. Work from animal studies has found that long-

C. W. Wong · B. J. Fenner · G. C. M. Cheung (✉)
Singapore National Eye Centre and Singapore Eye Research Institute, Singapore, Singapore
e-mail: wong.chee.wai@singhealth.com.sg;
beau.j.fenner@singhealth.com.sg;
gemmy.cheung.c.m@singhealth.com.sg

Fig. 21.1 Predicted global prevalence and total cases of myopia (−0.5 to −5.0 D) and high myopia (≤ −5.0 D). Data from Holden et al. [2]
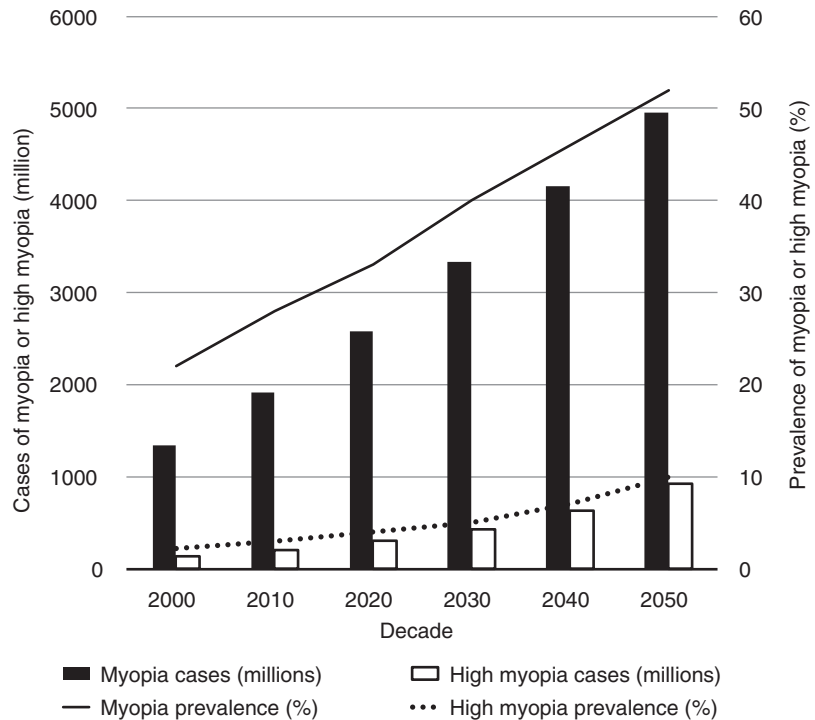
wavelength light (630 nm) promotes myopic progression [18], while high ambient lighting slows myopia development [19, 20].

Inherited risk also appears to play an important role in the development of myopia in children. Twin studies indicate that genetic factors contribute between 50 and 90% of the variability in refractive error [21–23], although genome-wide association studies (GWAS) focusing on single nucleotide polymorphisms explain only about 3% of this variation, with any particular myopia-associated gene mutation being present in at most 1–2% of myopes [24–26]. This "missing inheritance" may be due to the cumulative effects of multiple small effects and also epigenetic effects [27–31].

In 2012 the WHO estimated that the cost associated with lost productivity due to uncorrected refractive error was US$202 billion, or approximately 0.25% of world GDP [32]. This is substantial given that the economic burdens of cancer and cardiovascular disease respectively amounted to 1.5% [33] and 1.1% [34] of world GDP during the same period. Furthermore, health costs associated with myopia include both

the costs of refractive correction and specialist ophthalmic management such as vitreoretinal and glaucoma surgical interventions for myopia complications and public health costs that result from low vision [35]. The latter is more difficult to estimate and current projections may under-represent the true cost of myopia for modern society.

In the United States alone, the National Health and Nutrition Examination Survey (NHANES) calculated the direct cost of correcting myopic refractive errors at more than US$3.8 billion per year [36]. In Singapore, with a population of only 5.6 million but with a higher prevalence of myopia, the total direct and indirect costs of myopia were estimated at US$755 million per year [37], equating to 0.25% of national GDP. Similar studies from Japan showed an annual total cost of myopia of US$72 billion, or 1.7% of GDP [38].

An obvious sequela to increasing myopia prevalence is a concomitant rise in myopia-related vitreomaculopathies in the population, and this has been anticipated elsewhere [39]. To date, however, there are no epidemiological data that clearly establish an increase in the prevalence of

Table 21.1 Predicted prevalence of myopia in the WHO Global Burden of Disease regions between 2000 and 2050

Region	Predicted prevalence (%) over time					
	2000	2010	2020	2030	2040	2050
Andean Latin America	15.2	20.5	28.1	36.2	44.0	50.7
Asia-Pacific, high income	46.1	48.8	53.4	58.0	62.5	66.4
Australasia	19.7	27.3	36.0	43.8	50.2	55.1
Caribbean	15.7	21.0	29.0	37.4	45.0	51.7
Central Africa	5.1	7.0	9.8	14.1	20.4	27.9
Central Asia	11.2	17.0	24.3	32.9	41.1	47.4
Central Europe	20.5	27.1	34.6	41.8	48.9	54.1
Central Latin America	22.1	27.3	34.2	41.6	48.9	54.9
East Africa	3.2	4.9	8.4	12.3	17.1	22.7
East Asia	38.8	47.0	51.6	56.9	61.4	65.3
Eastern Europe	18.0	25.0	32.2	38.9	45.9	50.4
North Africa and Middle East	14.6	23.3	30.5	38.8	46.3	52.2
North America, high income	28.3	34.5	42.1	48.5	54.0	58.4
Oceania	5.0	6.7	9.1	12.5	17.4	23.8
South Asia	14.4	20.2	28.6	38.0	46.2	53.0
Southeast Asia	33.8	39.3	46.1	52.4	57.6	62.0
Southern Africa	5.1	8.0	12.1	17.5	23.4	30.2
Southern Latin America	15.6	22.9	32.4	40.7	47.7	53.4
Tropical Latin America	14.5	20.1	27.7	35.6	43.9	50.7
West Africa	5.2	7.0	9.6	13.6	19.7	26.8
Western Europe	21.9	28.5	36.7	44.5	51.0	56.2
Global	22.9	28.3	33.9	39.9	45.2	49.8

Data from Holden et al. [2]

these conditions. Given the currently low prevalence of pathological or degenerative myopia in most populations (0.9–3.1% in Asian and 1.2% in non-Asian populations) [39]; and the typically slow progression of these conditions [40], the full extent of this problem may take several more decades to surface.

21.2 Myopic Vitreomaculopathies

In highly myopic eyes, tractional forces at the vitreomacular interface within the macula are contributed by several factors. First, normal age-related changes of the vitreous (liquefaction) and at the vitreoretinal interface (weakening of vitreoretinal adhesion) occur concurrently in non-myopic eyes [41]. However, these normal processes do not typically occur in tandem in myopic eyes because liquefaction is accelerated and the vitreous destabilizes before vitreous adhesion to the retina is weakened, thus exposing the vitreoretinal interface to geographically differential anterior-posterior tractional forces, particularly at the macular where vitreoretinal adhesion is especially tenacious [42–45]. Second, outpouching of the posterior sclera in high myopes, termed posterior staphyloma, exerts tangential forces, while the more rigid inner limiting membrane and retinal vessels resist conformation to the steep scleral contour, pulling the retina inward [46]. These forces combine to produce pathologies such as myopic foveoschisis and myopic macular holes. Because of the aforementioned factors, vitreomaculopathies are particularly prevalent and confer significant morbidity in highly myopic individuals. Posterior staphylomata are common among high myopes, with prevalence ranging from 1 to 2% in low myopes to as much as 50–90% in eyes with more than −8 to −10 D of myopia [47–49]. Moreover, the appearance of posterior staphyloma is closely associated with aging, with recent epidemiological work from Japan indicating that the prevalence of posterior staphyloma approximately doubles every decade after the age of 50 years [50].

Although there are few population-based studies on the epidemiology of vitreomaculopathies in highly myopic individuals, a sense of the magnitude of the problem posed by this group of diseases can be gleaned from hospital-based studies. Ripandelli et al. reported on the prevalence of vitreomaculopathies in a retrospective, single-institution based series of 214 highly myopic eyes (axial length > 30 mm) of 116 patients with posterior staphyloma [51]. Vitreomaculopathies were present in 52.4% of eyes and most patients

(84.4%) showed bilateral involvement. The distribution (by eye) of vitreomaculopathies was as follows: epiretinal membranes (45.7%), schisis (25.2%), lamellar macular hole (LMH) (11.2%), full-thickness macular hole (FTMH) (8.4%), and foveal detachment with or without macular hole (9.3%). Over 5 years of follow-up, 15.4% of eyes with vitreomaculopathies required surgery ranging from 2% for ERM, 20% to 25% for schisis, LMH, and FTMH, and up to 50% for foveal detachment. In another hospital-based study, Henaine-Berra et al. reported on the prevalence of vitreomaculopathies in a cohort of 72 highly myopic (< −8 D) individuals (116 eyes) [52]. Overall, vitreomaculopathies were detected 22.4% of eyes and in 53.7% of eyes with posterior staphyloma. Foveoschisis was observed in 14.7%, vascular traction in 14.7%, ERM in 11.2%, and LMH in 1.72%. The large variation in prevalence estimates as reported in these two studies highlights the complexities of comparing between hospital-based studies with their inherent selection biases and differences in the definition of high myopia.

21.2.1 Posterior Vitreous Detachment

Posterior vitreous detachment (PVD) is an age-related physiologic process whereby the posterior vitreous cortex separates from the inner limiting membrane of the retina. As previously mentioned, physiologic PVD occurs with concurrent liquefaction of the vitreous gel and dehiscence of vitreoretinal adhesion [41]. Besides age, the onset of PVD is known to be earlier in eyes with higher refractive error [42, 44, 53]. In a large cohort of 224 eyes of 125 Japanese patients, PVD occurred earlier in highly myopic eyes, starting at 29 years and increased with age (23%, 29%, 44%, and 72% in the fourth through seventh decades, respectively, and 100% of patients aged 70 years or older). In contrast, none of the emmetropic eyes 39 years of age or younger had PVD, and the prevalence was lower in the corresponding age categories (8%, 23%,44%,74%, and 86% in the fifth through ninth decades, respectively)

[42]. In high myopes, prior to the development of a complete PVD, posterior hyaloid separation begins in the paramacular area, progressing to a perifoveal PVD and finally separates from the macula. Anomalous PVD frequently occurs in these eyes and is believed to play a significant role in the pathogenesis of various vitreoschisis (separation of vitreous layers) and vitreomacular traction. Even in the absence of vitreomaculopathies, PVD itself can decrease contrast sensitivity and degrade vision [54]. The reason for earlier anomalous PVD in high myopes is not clear. The concentrations of protein, collagen, and hyaluronic acid were found to be considerably lower in the vitreous of myopic patients compared with emmetropes, possibly predisposing to earlier degeneration of the vitreous gel [53]. The increased vitreous cavity volume may also play a role in the early development of vitreous degeneration.

Highly myopic patients with partial PVD around the macula and complete PVDs in high myopia were significantly younger (47.1 ± 14.1 and 61.2 ± 12.0 years, respectively) than emmetropic controls (59.0 ± 9.6 and 69.7 ± 6.6 years). Remnant vitreous cortex was found on the macula after complete PVD more commonly in high myopes (40.5%) than in emmetropes (8.7%). Interestingly, the posterior precortical vitreous pocket, a lesion that is involved in the development of idiopathic macular hole, was significantly larger in high myopia than in controls [55].

In addition to age and refractive error, the prevalence of complete PVD also varied depending on the underlying vitreoretinal disease. Complete PVD is common in eyes with retinal detachment and the epiretinal membrane (85 and 74.2%, respectively) but uncommon in myopic foveoschisis (14.3%). Complete PVD was also more common in a myopic macular hole with retinal detachment (42.9%) than in myopic macular hole without detachment (10%) [45].

21.2.2 Epiretinal Membranes

Epiretinal membrane (ERM) is a relatively common retinal pathology that can have a significant

impact on visual quality [56, 57]. ERMs may occur without any antecedent ocular conditions or surgical procedures, termed idiopathic or primary ERM, or can be secondary to other eye diseases (e.g., retinal vascular occlusion and diabetic retinopathy), or ocular surgery.

Few studies have evaluated the prevalence of epiretinal membrane in myopic individuals. Table 21.2 shows the population-based studies that have evaluated refractive error as a risk factor for ERM. With the exception of the Blue Mountains Eye Study [56] and the Singapore Malay Eye Study [58], these studies have found increasing myopic refraction or axial length to be significant risk factors for ERM. However, most of these studies have graded ERM using fundus photographs. Only the Handan and Jiangning eye studies use a combination of fundus photographs and OCT to diagnose ERM. Consequently, ERM may have been underdiagnosed in these studies, particularly among high myopes where the poorer retinal contrast may have complicated the accurate diagnosis of ERM. An ultrastructural study of epiretinal membranes in highly myopic eyes with macular hole retinal detachment revealed that these membranes are, in fact, the posterior cortical vitreous that is left behind after PVD (vitreous schisis) or represents the posterior wall of a posterior precortical vitreous pocket that progressively enlarges from the extensive vitreous liquefaction that is characteristic of highly myopic eyes [59].

21.2.3 Full-Thickness Macular Holes

A full-thickness macular hole (FTMH) is a defect in the fovea with separation of all neural retinal layers from the internal limiting membrane to the retinal pigment epithelium, causing a central scotoma and significant reduction in visual acuity [60]. FTMH is defined as primary when caused by vitreous traction, and secondary when due to other pathology [60]. Several large population-based studies have reported the prevalence of FTMH to range between 0 and 3.3 per 1000 individuals [56, 61–63]. The annual incidence of FTMH has been estimated to be between 4.1 and –7.8 per 100,000 individuals in two population-based studies [64, 65]. Age, history of cataract surgery, and female gender were significant risk factors for FTMH [62, 64–66].

Table 21.2 Population-based studies evaluating myopia as a risk factor for ERM

Study	Location	N	Age	Imaging	Myopia definition	ERM subtype	Odds ratio (95% confidence interval)
Blue Mountains Eye Study, 1997 [56]	Sydney	3490	≥49	Fundus photographs	–	Cellophane macular reflex	1.02–1.24 per diopter increase in spherical equivalent
Visual improvement project, 2005 [92]	Victoria	4314	>40	Fundus photographs	–	Premacular fibrosis	2.2 (1.0–4.6)
Singapore Malay Eye Study, 2008 [58]	Singapore	3265	40–80	Fundus photographs	SE < −0.5D	Any ERM	0.55 (0.37–0.82)
Handan Eye Study, 2009 [93]	He Bei, China	6565	>30	Fundu photographs and/or OCT	SE < −0.5D	Primary ERM	1.58 (1.12–2.23)
Singapore Indian Eye Study, 2012 [94]	Singapore	3328	40–80	Fundus photographs	SE < −0.5D	Primary ERM	1.14 (1.07–1.22)
Jiangning Eye Study, 2015 [95]	Shanghai	2005	>50	Fundus photographs and OCT	Axial length ≥ 25 mm	Primary ERM	2.21 (1.51–3.22)

Population-based data regarding myopia as a risk factor for FTMH is scarce. The 6-year incidence of FTMH in highly myopic individuals was 0.6 per 100,000 in a large population-based study conducted in Tasmania, Australia, compared to the overall incidence of 28.3 per 100,000. In a population-based study in South India, myopia (defined as the spherical equivalent of less than −0.5 D) was not found to be significantly associated with increased risk of FTMH (OR 1.12, 95% CI 0.15–8.24) [66]. Prevalence of FTMH in hospital-based cohorts of highly myopic eyes have been reported to range from 6.3 to 8.4% [51, 67]. Ripandelli et al. reported 8.4% of eyes with FTMH in a retrospective, single-institution based series of 214 highly myopic eyes (axial length > 30 mm) of 116 patients with posterior staphyloma [51]. Coppe et al reported a prevalence of 6.26% in a series of 383 eyes from 383 patients affected by very high myopia (between −14 and −32 D) [67], and Atta-Allah and coworkers observed FTMH in 8.4% of 472 eyes of 472 patients (> −6D) [68].

The pathogenesis of FTMH in high myopia is distinct from that of idiopathic macular hole and is contributed by several factors unique to highly myopic eyes. Posterior staphyloma is a recognized risk factor for FTMH [69]: axial elongation exerts anterior-posterior tractional forces from vitreomacular adhesion while the posterior bowing of the sclera creates an inward vector force due to the stiffness of the inner limiting membrane and retinal vasculature that resists conformation to the staphyloma configuration [46].

21.2.4 Macular Hole Retinal Detachment

Minoda reported in 1979 on a series of 441 consecutive cases of retinal detachment and within the 405 eyes with nontraumatic detachment, 36 (8.9%) were associated with a macular hole [70]. The incidence of the macular hole in highly myopic eyes was 24.4% and 9% in females and males respectively. Subsequently, Morita et al. studied 209 eyes with macular holes to determine what factors were associated with retinal detachment.

Of these, 104 eyes (49.8%) with macular hole also had a coexistent retinal detachment. The incidence of MHRD was 97.6% in myopia over −8.25 D, 67.7% in myopia between −8.0 and −3.25 D, and 1.1% in eyes under −3.0 D. Eyes with posterior staphyloma were more likely to develop MHRD (96% vs. 8.2%), as were eyes with chorioretinal atrophy (100% in widespread chorioretinal atrophy, 90.6% in spotty or lineal chorioretinal atrophy, 64.3% in the myopic tigroid fundus, and 0% in eyes without myopic tigroid or atrophy). The presence of PVD was not significantly associated with MHRD (56.4% in eyes with PVD vs. 51.9% in eyes without). Statistically significant factors associated with MHRD were refractive error, myopic chorioretinal change, and posterior staphyloma [71]. In a retrospective series of 52 consecutive eyes with macular hole and severe myopia (range −7 to −26 D), Akiba et al. reported the presence of MHRD in 71% of eyes, of which 73% had detachments localized within the posterior staphyloma cavity [72]. Posterior staphyloma was a strong risk factor for extensive retinal detachment in this study, observed in 95% of eyes with extensive retinal detachment. Zhang and colleagues analyzed 207 consecutive patients with retinal detachment and reported a prevalence of 10% for those with mild myopia (> −8 D) and 38% for those with severe (< −8 D) myopia. MHRD was more common in females than men (30% vs. 7%) and posterior staphyloma was observed in half of these cases [73]. Thus, posterior staphyloma appeared to be a consistent risk factor for MHRD. Dome-shaped macula (DSM), an anterior bulging of the macula caused by a relatively thicker subfoveal sclera compared to the perifoveal sclera, can be thought of as the converse of posterior staphyloma. DSM is not uncommon among highly myopic eyes. Gaucher et al. reported 15 eyes (10.7%) with DSM from a series of 140 myopic eyes (range −2 to −15 D) evaluated with OCT, and DSM was frequently associated with retinal pigment epithelium atrophy (100%) and foveal retinal detachment (63.3%) [74]. Liang et al. found the prevalence of DSM to be 20.1% (225 out of 1118 eyes) among highly myopic eyes of −8 D or more. On multivariate analysis, DSM

was found to be significantly associated with serous retinal detachment, foveal and extrafoveal schisis, but not with choroidal neovascularization [75].

Ohsugi et al. found that DSM was observed in more eyes with just FTMH as compared to that in eyes with MHRD (37.5% vs. 5.3%) [74]. These studies suggest that moderation of the steep posterior curvature from a posterior staphyloma may protect against retinal detachment in highly myopic eyes with FTMH. Decreased chorioretinal adhesion due to retinal pigment epithelium atrophy in highly myopic eyes may also contribute to a higher rate of retinal detachment following FTMH [71].

21.2.5 Lamellar Macular Holes

Lamellar macular hole (LMH) is a partial-thickness disturbance in foveal contour, sometimes associated with intraretinal splitting (schisis), typically between the outer plexiform and outer nuclear layers with the maintenance of an intact photoreceptor layer [60]. Studies on the epidemiology of the lamellar macular hole in myopic individuals are limited. Panozzo et al. reviewed 218 highly myopic eyes in 121 consecutive patients and reported that LMH was observed in only six eyes (4.8%) on OCT. [76] In another cohort of 72 patients with < −8 D of myopia, Henaine-Brerra found a prevalence of LMH of 14.65% [52].

Lamellar hole epiretinal proliferation (LHEP) is a recently recognized subtype of LMH in which a homogenous second membrane forms at the edge of the lamellar hole in addition to the conventional ERM associated with LMH [77]. In a clinic-based study of 43 highly myopic eyes with LHEP and 52 controls, Lai et al. observed that highly myopic subjects with LHEP (59.5 ± 11.6 years) tended to be slightly younger than non-highly myopic subjects with LHEP (64.3 ± 11.2 years). In addition, LHEP in high myopia was more extensive and more likely to have attachments to the posterior hyaloid [78].

21.2.6 Myopic Foveoschisis

Myopic foveoschisis (MF) refers to the splitting of retinal layers, presumably by the inability of the retinal layers to conform to the scleral contour due to the presence of a posterior staphyloma and taut internal limiting membrane, and may be associated with foveal retinal detachment [79]. Although MF is an important cause of visual loss in high myopes, it was difficult to diagnose on clinical examination and only received attention as a clinical entity with the advent of OCT. Takano and Kishi in 1999 first used time-domain OCT to characterize MF in 32 eyes of 19 consecutive patients with severe myopia (−8 to −31 D) and posterior staphyloma. They found that MF was a frequent occurrence in these eyes (11 eyes, 34%) and that eight eyes (72.7%) also had a concurrent foveal retinal detachment [80]. The retina was observed to split into a thick inner layer and a thin outer layer, suggesting that outer retinal schisis was the predominant form of MF in these eyes. Subsequently, in 2003, Baba et al. studied MF in 134 eyes of 78 patients with high myopia greater than eight dioptres with time-domain OCT. Of the 78 eyes with posterior staphyloma, OCT revealed foveal retinal detachment in seven eyes, and two out of these seven were found to have MF. None of the eyes in the group without posterior staphyloma were found to have either MF or foveal retinal detachment. In another time-domain OCT study, Panozzo et al. retrospectively reviewed 218 eyes in 121 patients with high myopia (range −8 to −26 D) and found that MF occurred in 25 (20%) eyes, with 17 of these eyes also found to have posterior staphyloma [76]. Wu et al. reviewed 124 eyes with high myopia (−6 D or worse) and found 10 eyes (8%) with foveoschisis (seven with foveoschisis of which three had concurrent foveal detachment) or foveal detachment without a macular hole (three eyes with foveal detachment only) on time-domain OCT. In the multivariate analysis, axial length > 31 mm, macular chorioretinal atrophy, and vitreoretinal interface factors (ERM and posterior vitreoschisis) were significantly associated with MF and/or foveal detachment [81].

In a prospective study using higher resolution spectral domain OCT by Henaine-Berra et al. [52], MF was identified in 17 (14.65%) of 116 eyes of 72 highly myopic patients (−8D or worse), and none of these eyes had foveal detachment. All 17 eyes had posterior staphyloma. Lichtwitz et al. used SD-OCT in a study of 87 eyes of 47 patients with −6 D or worse myopia and found 11% of eyes with MF but none of these eyes had foveal detachment. Again, posterior staphyloma was a significant risk factor for MF and other macular complications [82]. Finally, Itakura et al. studied 151 eyes of 151 highly myopic patients (−8 D or worse) with swept-source OCT and found 9.3% with MF and none of these eyes had foveal detachment [43].

Interestingly, visual acuity may be preserved in up to one-third of patients with MF [76]. This suggests that MF may be a slowly progressive condition that is asymptomatic in its early stages and that highly myopic individuals may benefit from OCT screening to detect the presence of MF before an irreversible visual loss occurs [83]. Shimada et al. studied the natural course of 207 highly myopic eyes (−8D or worse) of 168 consecutive patients with myopic retinoschisis over a mean duration of 36.2 ± 6.2 months, and classified the disease according to its location and extent: S0: no retinoschisis (32 eyes, 15.5%); S1: extrafoveal (56 eyes, 27.1%); S2: foveal (45 eyes, 21.7%); S3: both foveal and extrafoveal but not the entire macula (46 eyes, 22.2%); and S4: entire macula (28, 13.5%) [84]. Eight eyes (3.9%) experienced improvement, of which six had complete resolution of retinoschisis. Conversely, 26 eyes (11.6%) experienced the progression of retinoschisis, including the development of foveal retinal detachment in seven eyes. The eyes classified as S4 had a significantly greater risk for progression than any other group. Although most eyes with MF remain stable, eyes with extensive retinoschisis are more likely to progress. In a series of 50 eyes with MTM from Singapore 14 eyes (28%) had worsening visual acuity of ≥ 2 lines over a mean follow-up of 31.7 ± 7.7 months [85].

21.2.7 Paravascular Abnormalities

Various abnormalities have been observed on OCT at or around the retinal vessels in highly myopic eyes. These asymptomatic lesions include paravascular retinal cysts, vascular microfolds, and paravascular microholes [86–89]. Paravascular abnormalities are surprisingly common: Shimada and coworkers reported a high prevalence of paravascular retinal cysts (49.5%), vascular microfolds (44.6%), and paravascular retinal holes (26.8%) detected in highly myopic eyes (<−8D) on OCT. [86] Similarly, Li et al. found paravascular abnormalities in a high proportion of eyes with high myopia (<−6D), including paravascular microfolds in 82.9%, paravascular cysts in 71.7%, and paravascular lamellar holes in 28.9% [90].

Clinically, paravascular retinal cysts appear as spindle-shaped dark areas or fissure like lesions adjacent to blood vessels [91]. On OCT, cystoid spaces in the inner retina are seen adjacent to retinal blood vessels [87]. Vascular microfolds are observed on OCT as an inner retinal fold over a retinal blood vessel [89]. Paravascular cysts and vascular microfolds are postulated to arise due to the inability of retinal vessels to comply with the steep curvature of axially elongated myopic eyes, resulting in tenting traction of the inner retina over the retinal vessel. Paravascular cysts may be the first sign of mechanical stress and traction around retinal vessels in highly myopic eyes, and further progression of vitreoretinal traction in the proximity of these cysts may lead to the formation of paravascular retinal holes [86]. In addition, the presence of paravascular abnormalities may represent a risk factor for subsequent development of myopic retinoschisis [86, 90].

21.3   Conclusions

Myopia prevalence is rising and disease burden from myopia related vitreomaculopathies is expected to rise in tandem. Anomalous PVD coupled with changes in posterior eye wall shape

are believed to be key factors in the pathogenesis of various myopic vitreomaculopathies. There is still a lack of population-based epidemiological data on the prevalence and incidence of myopic vitreomaculopathies, in particular, longitudinal data on the progression rate of asymptomatic precursor lesions. These data are necessary to formulate screening strategies and assign appropriate resources to handle the burgeoning problem of myopia related visual loss.

References

1. Ohno-Matsui K, et al. Peri-dome choroidal deepening in highly myopic eyes with dome-shaped maculas. Am J Ophthalmol. 2017;183:134–40.
2. Holden BA, et al. Global prevalence of myopia and high myopia and temporal trends from 2000 through 2050. Ophthalmology. 2016;123(5):1036–42.
3. World Health Organization. The impact of myopia and high myopia — Report of the Joint World Health Organization-Brien Holden Vision Institute Global Scientific Meeting on Myopia. Sydney, Australia: World Health Organization, University of New South Wales; 2017.
4. Bourne RR, et al. Causes of vision loss worldwide, 1990-2010: a systematic analysis. Lancet Glob Health. 2013;1(6):e339–49.
5. Pascolini D, Mariotti SP. Global estimates of visual impairment: 2010. Br J Ophthalmol. 2012;96(5):614–8.
6. Saxena R, Vashist P, Menon V. Is myopia a public health problem in India? Indian J Community Med. 2013;38(2):83–5.
7. Rudnicka AR, et al. Global variations and time trends in the prevalence of childhood myopia, a systematic review and quantitative meta-analysis: implications for aetiology and early prevention. Br J Ophthalmol. 2016;100(7):882–90.
8. Keeffe JE, et al. Prevalence and causes of vision loss in south-east Asia and Oceania in 2015: magnitude, temporal trends and projections. Br J Ophthalmol. 2019;103(7):878–84.
9. Guo Y, et al. Outdoor activity and myopia among primary students in rural and urban regions of Beijing. Ophthalmology. 2013;120(2):277–83.
10. Ip JM, et al. Myopia and the urban environment: findings in a sample of 12-year-old Australian school children. Invest Ophthalmol Vis Sci. 2008;49(9):3858–63.
11. Guo Y, et al. Outdoor activity and myopia progression in 4-year follow-up of Chinese primary school children: the Beijing children eye study. PLoS One. 2017;12(4):e0175921.
12. Zadnik K, et al. Prediction of juvenile-onset myopia. JAMA Ophthalmol. 2015;133(6):683–9.
13. Jones LA, et al. Parental history of myopia, sports and outdoor activities, and future myopia. Invest Ophthalmol Vis Sci. 2007;48(8):3524–32.
14. French AN, et al. Risk factors for incident myopia in Australian schoolchildren: the Sydney adolescent vascular and eye study. Ophthalmology. 2013;120(10):2100–8.
15. O'Donoghue L, et al. Risk factors for childhood myopia: findings from the NICER study. Invest Ophthalmol Vis Sci. 2015;56(3):1524–30.
16. Hsu CC, et al. Prevalence and risk factors for myopia in second-grade primary school children in Taipei: a population-based study. J Chin Med Assoc. 2016;79(11):625–32.
17. Sherwin JC, et al. The association between time spent outdoors and myopia in children and adolescents: a systematic review and meta-analysis. Ophthalmology. 2012;119(10):2141–51.
18. Hung LF, et al. Narrow-band, long-wavelength lighting promotes hyperopia and retards vision-induced myopia in infant rhesus monkeys. Exp Eye Res. 2018;176:147–60.
19. Smith EL 3rd, Hung LF, Huang J. Protective effects of high ambient lighting on the development of form-deprivation myopia in rhesus monkeys. Invest Ophthalmol Vis Sci. 2012;53(1):421–8.
20. Zheng H, et al. The interactions between bright light and competing defocus during emmetropization in chicks. Invest Ophthalmol Vis Sci. 2018;59(7):2932–43.
21. Williams KM, Hysi P, Hammond CJ. Twin studies, genome-wide association studies and myopia genetics. Ann Eye Sci. 2017;2:69.
22. Chen Y, et al. What twin studies have taught us about myopia. Asia Pac J Ophthalmol (Phila). 2016;5(6):411–4.
23. Hammond CJ, et al. Genes and environment in refractive error: the twin eye study. Invest Ophthalmol Vis Sci. 2001;42(6):1232–6.
24. Feng CY, et al. Mutational screening of SLC39A5, LEPREL1 and LRPAP1 in a cohort of 187 high myopia patients. Sci Rep. 2017;7(1):1120.
25. Shi Y, et al. A genome-wide meta-analysis identifies two novel loci associated with high myopia in the Han Chinese population. Hum Mol Genet. 2013;22(11):2325–33.
26. Tedja MS, et al. Genome-wide association meta-analysis highlights light-induced signaling as a driver for refractive error. Nat Genet. 2018;50(6):834–48.
27. Wojciechowski R, Cheng CY. Involvement of multiple molecular pathways in the genetics of ocular refraction and myopia. Retina. 2018;38(1):91–101.
28. Hewitt AW, et al. Epigenetic effects on eye diseases. Expert Rev Ophthalmol. 2012;7(2):127–34.
29. Zhou X, et al. Experimental murine myopia induces collagen type Ialpha1 (COL1A1) DNA methylation and altered COL1A1 messenger RNA expression in sclera. Mol Vis. 2012;18:1312–24.
30. He S, et al. Review: epigenetic mechanisms in ocular disease. Mol Vis. 2013;19:665–74.

31. Fan Q, et al. Meta-analysis of gene-environment-wide association scans accounting for education level identifies additional loci for refractive error. Nat Commun. 2016;7:11008.

32. Fricke TR, et al. Global cost of correcting vision impairment from uncorrected refractive error. Bull World Health Organ. 2012;90:728–38.

33. Reboux G. Cancer overview. World Health Organization, Geneva, Switzerland; 2018.

34. Programme CA. The costs of CVD. World Heart Federation, Geneva, Switzerland; 2018.

35. Rose K, et al. The increasing prevalence of myopia: implications for Australia. Clin Exp Ophthalmol. 2001;29(3):116–20.

36. Vitale S, et al. Costs of refractive correction of distance vision impairment in the United States, 1999-2002. Ophthalmology. 2006;113(12):2163–70.

37. Zheng YF, et al. The economic cost of myopia in adults aged over 40 years in Singapore. Invest Ophthalmol Vis Sci. 2013;54(12):7532–7.

38. Roberts CB, et al. Economic cost of visual impairment in Japan. Arch Ophthalmol. 2010;128(6):766–71.

39. Wong YL, Saw SM. Epidemiology of pathologic myopia in Asia and worldwide. Asia Pac J Ophthalmol (Phila). 2016;5(6):394–402.

40. Yokoi T, et al. Peripapillary diffuse chorioretinal atrophy in children as a sign of eventual pathologic myopia in adults. Ophthalmology. 2016;123(8):1783–7.

41. Sebag J. Posterior Vitreous Detachment. Ophthalmology. 2018;125(9):1384–5.

42. Akiba J. Prevalence of posterior vitreous detachment in high myopia. Ophthalmology. 1993;100(9):1384–8.

43. Itakura H, et al. Vitreous changes in high myopia observed by swept-source optical coherence tomography. Invest Ophthalmol Vis Sci. 2014;55(3):1447–52.

44. Morita H, Funata M, Tokoro T. A clinical study of the development of posterior vitreous detachment in high myopia. Retina. 1995;15(2):117–24.

45. Philippakis E, et al. Posterior vitreous detachment in highly myopic eyes undergoing Vitrectomy. Retina. 2016;36(6):1070–5.

46. Ikuno Y, Gomi F, Tano Y. Potent retinal arteriolar traction as a possible cause of myopic foveoschisis. Am J Ophthalmol. 2005;139(3):462–7.

47. Vongphanit J, Mitchell P, Wang JJ. Prevalence and progression of myopic retinopathy in an older population. Ophthalmology. 2002;109(4):704–11.

48. Hsiang HW, et al. Clinical characteristics of posterior staphyloma in eyes with pathologic myopia. Am J Ophthalmol. 2008;146(1):102–10.

49. Liu HH, et al. Prevalence and progression of myopic retinopathy in Chinese adults: the Beijing eye study. Ophthalmology. 2010;117(9):1763–8.

50. Numa S, et al. Prevalence of posterior staphyloma and factors associated with its shape in the Japanese population. Sci Rep. 2018;8(1):4594.

51. Ripandelli G, et al. Macular vitreoretinal interface abnormalities in highly myopic eyes with posterior staphyloma: 5-year follow-up. Retina. 2012;32(8):1531–8.

52. Henaine-Berra A, et al. Prevalence of macular anatomic abnormalities in high myopia. Ophthalmic Surg Lasers Imaging Retina. 2013;44(2):140–4.

53. Berman ER, Michaelson IC. The chemical composition of the human vitreous body as related to age and myopia. Exp Eye Res. 1964;3:9–15.

54. Garcia GA, et al. Degradation of contrast sensitivity function following posterior vitreous detachment. Am J Ophthalmol. 2016;172:7–12.

55. Kishi S, Hagimura N, Shimizu K. The role of the premacular liquefied pocket and premacular vitreous cortex in idiopathic macular hole development. Am J Ophthalmol. 1996;122(5):622–8.

56. Mitchell P, et al. Prevalence and associations of epiretinal membranes. The Blue Mountains eye study, Australia. Ophthalmology. 1997;104(6):1033–40.

57. Klein R, et al. The epidemiology of epiretinal membranes. Trans Am Ophthalmol Soc. 1994;92:403–25. discussion 425-30

58. Kawasaki R, et al. Racial difference in the prevalence of epiretinal membrane between Caucasians and Asians. Br J Ophthalmol. 2008;92(10):1320–4.

59. Ishida S, et al. Macular hole retinal detachment in highly myopic eyes: ultrastructure of surgically removed epiretinal membrane and clinicopathologic correlation. Retina. 2000;20(2):176–83.

60. Duker JS, et al. The international Vitreomacular traction study group classification of vitreomacular adhesion, traction, and macular hole. Ophthalmology. 2013;120(12):2611–9.

61. Rahmani B, et al. The cause-specific prevalence of visual impairment in an urban population. The Baltimore eye survey. Ophthalmology. 1996;103(11):1721–6.

62. Wang S, Xu L, Jonas JB. Prevalence of full-thickness macular holes in urban and rural adult Chinese: the Beijing eye study. Am J Ophthalmol. 2006;141(3):589–91.

63. Liesenborghs I, et al. Prevalence of optical coherence tomography detected vitreomacular interface disorders: the Maastricht study. Acta Ophthalmol. 2018;96:729.

64. Darian-Smith E, et al. Tasmanian macular hole study: whole population-based incidence of full thickness macular hole. Clin Exp Ophthalmol. 2016;44(9):812–6.

65. McCannel CA, et al. Population-based incidence of macular holes. Ophthalmology. 2009;116(7):1366–9.

66. Sen P, et al. Prevalence of idiopathic macular hole in adult rural and urban south Indian population. Clin Exp Ophthalmol. 2008;36(3):257–60.

67. Coppe AM, et al. Prevalence of asymptomatic macular holes in highly myopic eyes. Ophthalmology. 2005;112(12):2103–9.

68. AttaAllah HR, Omar IAN, Abdelhalim AS. Assessment of posterior segment using spectral domain OCT in highly myopic eyes. Open Ophthalmol J. 2017;11:334–45.

69. Stirpe M, Michels RG. Retinal detachment in highly myopic eyes due to macular holes and epiretinal traction. Retina. 1990;10(2):113–4.

70. Minoda K. Retinal detachment due to macular hole among Japanese. Jpn J Ophthalmol. 1979;23:200.
71. Morita H, et al. Causative factors of retinal detachment in macular holes. Retina. 1991;11(3):281–4.
72. Akiba J, Konno S, Yoshida A. Retinal detachment associated with a macular hole in severely myopic eyes. Am J Ophthalmol. 1999;128(5):654–5.
73. Zhang CF, Hu C. High incidence of retinal detachment secondary to macular hole in a Chinese population. Am J Ophthalmol. 1982;94(6):817–9.
74. Gaucher D, et al. Dome-shaped macula in eyes with myopic posterior staphyloma. Am J Ophthalmol. 2008;145(5):909–14.
75. Liang IC, et al. Comparison of clinical features in highly myopic eyes with and without a dome-shaped macula. Ophthalmology. 2015;122(8):1591–600.
76. Panozzo G, Mercanti A. Optical coherence tomography findings in myopic traction maculopathy. Arch Ophthalmol. 2004;122(10):1455–60.
77. Pang CE, Spaide RF, Freund KB. Epiretinal proliferation seen in association with lamellar macular holes: a distinct clinical entity. Retina. 2014;34(8):1513–23.
78. Lai TT, Yang CM. Lamellar hole-associated epiretinal proliferation in lamellar macular hole and full-thickness macular hole in high myopia. Retina. 2018;38(7):1316–23.
79. Johnson MW. Myopic traction maculopathy: pathogenic mechanisms and surgical treatment. Retina. 2012;32(Suppl 2):S205–10.
80. Takano M, Kishi S. Foveal retinoschisis and retinal detachment in severely myopic eyes with posterior staphyloma. Am J Ophthalmol. 1999;128(4):472–6.
81. Wu PC, et al. Factors associated with foveoschisis and foveal detachment without macular hole in high myopia. Eye (Lond). 2009;23(2):356–61.
82. Lichtwitz O, et al. Prevalence of macular complications associated with high myopia by multimodal imaging. J Fr Ophtalmol. 2016;39(4):355–63.
83. Gohil R, et al. Myopic foveoschisis: a clinical review. Eye (Lond). 2015;29(5):593–601.
84. Shimada N, et al. Natural course of myopic traction maculopathy and factors associated with progression or resolution. Am J Ophthalmol. 2013;156(5):948–57. e1
85. Cheng C, et al. Myopic retinoschisis in Asians: structural features and determinants of visual acuity and prognostic factors for progression. Retina. 2016;36(4):717–26.
86. Shimada N, et al. Detection of paravascular lamellar holes and other paravascular abnormalities by optical coherence tomography in eyes with high myopia. Ophthalmology. 2008;115(4):708–17.
87. Ohno-Matsui K, et al. Detection of paravascular retinal cysts before using OCT in a highly myopic patient. Graefes Arch Clin Exp Ophthalmol. 2006;244(5):642–4.
88. Muraoka Y, et al. Paravascular inner retinal defect associated with high myopia or epiretinal membrane. JAMA Ophthalmol. 2015;133(4):413–20.
89. Sayanagi K, et al. Retinal vascular microfolds in highly myopic eyes. Am J Ophthalmol. 2005;139(4):658–63.
90. Li T, et al. Paravascular abnormalities observed by spectral domain optical coherence tomography are risk factors for retinoschisis in eyes with high myopia. Acta Ophthalmol. 2018;96(4):e515–23.
91. Komeima K, et al. Paravascular inner retinal cleavage in a highly myopic eye. Arch Ophthalmol. 2005;123(10):1449–50.
92. McCarty DJ, et al. Prevalence and associations of epiretinal membranes in the visual impairment project. Am J Ophthalmol. 2005;140(2):288–94.
93. Duan XR, et al. Prevalence and associations of epiretinal membranes in a rural Chinese adult population: the Handan eye study. Invest Ophthalmol Vis Sci. 2009;50(5):2018–23.
94. Koh V, et al. Prevalence and risk factors of epiretinal membrane in Asian Indians. Invest Ophthalmol Vis Sci. 2012;53(2):1018–22.
95. Ye H, et al. Prevalence and associations of epiretinal membrane in an elderly urban Chinese population in China: the Jiangning eye study. Br J Ophthalmol. 2015;99(12):1594–7.

Pathophysiology of Myopic Foveoschisis

22

Yasushi Ikuno

22.1 Introduction

Worldwide incidence rates of high myopia range from 1 to 5.5% and generally differ between ethnic groups, races, and countries [1–3]. However, the incidence is generally highest in Asian countries. Myopia is one of the major causes of visual impairment, especially in Europe and East Asia [5, 6], and its prevalence continues to increase [4]. Pathological myopia is defined as high myopia with any posterior myopia-specific pathology resulting from excess axial elongation. Its characteristic manifestation is the formation of staphyloma and it is associated with specific macular complications such as choroidal neovascularization and chorioretinal atrophy.

Myopic foveoschisis is very common in high myopia cases and occurs predominantly in middle-aged to older women. Reported risk factors include older age, longer axial length, a high degree of myopia, and the presence of chorioretinal atrophy [7]. Myopic foveoschisis, if untreated, can develop into a macular hole with retinal detachment. Both conditions are major macular diseases that require a vitrectomy, a surgery that

is challenging owing to atrophic and thin retinas, multiple and fragile membranes adhering to the retina, and the distant location of the fundus from the scleral entry site. Thus, it is critical to understand the background, pathogenesis, and clinical manifestations of myopic foveoschisis to make an informed decision regarding the choice and timing of the surgical maneuver.

It is well known that optical coherence tomography (OCT) can identify a variety of anomalies within a myopic fovea including lamellar holes and retinal cysts [8]. Myopic traction maculopathy (MTM) is a recently proposed term that includes various kinds of pathological macular traction conditions in high myopia [9]. The most frequent cause (58%) of macular damage in MTM was found to be retinoschisis, followed by retinal thickening, development of a lamellar hole, and shallow retinal detachment [9]. The present article aims to shed light on the pathogenesis and clinical manifestations of myopic foveoschisis, a precondition of subsequent macular hole formation with retinal detachment. Surgical indications and novel treatment strategies will be discussed in other chapters.

22.2 Pathogenesis

Myopic foveoschisis is characterized by retinoschisis and subsequent retinal detachment in individuals with high myopia. The formation of

Y. Ikuno (✉)
Ikuno Eye Center, Osaka, Japan

Department of Ophthalmology, Osaka University
Graduate School of Medicine, Osaka, Japan

Department of Ophthalmology, Kanazawa University
Graduate School of Medicine, Kanazawa, Japan
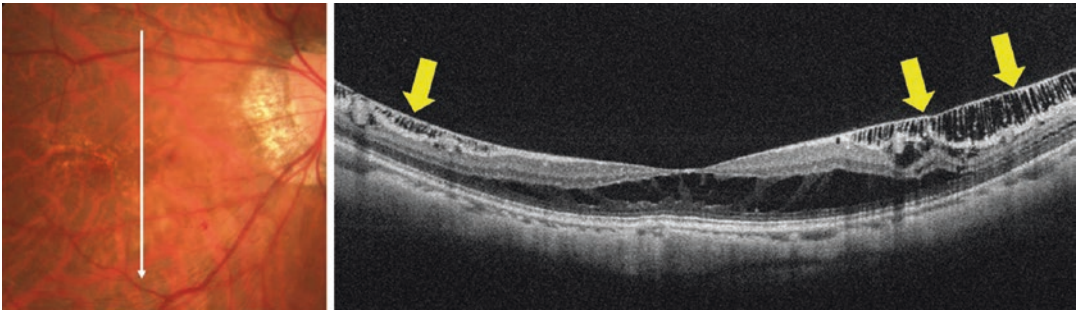
Fig. 22.1 Typical optical coherence tomography appearance of internal limiting membrane (ILM) detachment. The ILM layer is separated from the other retinal layers (yellow arrows). Retinal column, bridging the ILM and the neural retina, is often imaged as a thin line. The white arrow in the fundus photo shows the location of the optical coherence tomography scan

posterior staphyloma, a protrusion of the eyewall in the posterior fundus, is an important risk factor for myopic foveoschisis. Indeed, myopic foveoschisis has a higher prevalence in eyes with than without staphyloma [10]. Although myopic foveoschisis was first described by Phillips in the 1950s [11], the level of pathophysiological detail was lacking at the time given the absence of OCT. Almost 50 years later, a Japanese group documented the detailed macular architecture of highly myopic eyes and reported that it was so common as to be found in 10 of 32 highly myopic eyes [12].

Myopic foveoschisis results from one or several various components, such as the vitreous cortex, that can cause traction on the inner surface of the retina [13]. Retinal vitreous adhesion and vitreoschisis are frequently observed during vitrectomy with triamcinolone acetonide [14] or with swept-source OCT. [15] Epiretinal membranes (ERMs) are commonly present around the macula and can also generate retinal traction. Histological studies of the internal limiting membrane (ILM) excised intraoperatively have shown that the ERM adhering ILM surface was present in 70% of eyes with myopic foveoschisis, a percentage significantly higher than that observed in non-myopic macular holes (0%, $P < 0.05$) [16].

A rigid ILM and retinal vascular traction are pathological components that are unique to cases of high myopia, especially those with posterior staphyloma. Both are newly described elements of the pathogenesis of myopic foveoschisis that followed the advent of OCT. Indeed, ILM detachment from other retinal layers is often observed on OCT images of highly myopic eyes (Fig. 22.1) [17]. This is most frequently found in the region inferior to the macula, where the curve of the posterior staphyloma is the most pronounced. This indicates that the ILM is less flexible than the other retinal layers and that it exerts inward stress on them. Retinal vascular traction was initially postulated based on the discovery of retinal microfolds, which appear on OCT images as small peaks in the inner retina and are a typical finding after ILM peeling (Fig. 22.2) [18]. The retinal vessels, especially the retinal arterioles, are less flexible and cannot be stretched out as much as the other retinal components. Thus, myopic foveoschisis can be caused by multiple factors and can be regarded as a split between the flexible outer retina and the inflexible inner retinal parts.

22.3 Natural Course

The natural time course of myopic foveoschisis is still not yet completely understood, in part because there is large variability between individuals. Typically, although myopic foveoschisis starts with retinoschisis, it ultimately leads to the development of a macular hole via a focal retinal detachment. [13, 19] Studies have shown that 50–60% of myopic foveoschisis cases end up with a macular hole with or without retinal
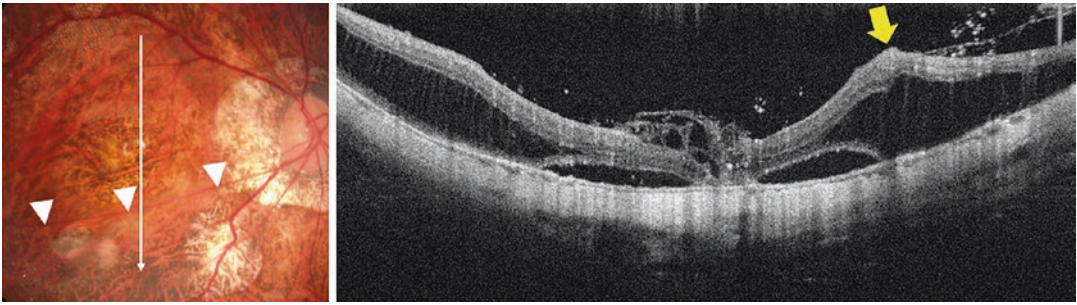
Fig. 22.2 Typical appearance of retinal vascular traction in highly myopic eyes. This vertical optical coherence tomography image shows a tent-like retinal elevation (yellow arrow). This is coincident with retinal arterioles in the fundus photo (white arrowheads) as a result of inflexibility. The white arrow in the fundus photo shows the location of the optical coherence tomography scan

detachment within the first 2–3 years [20, 21], thus putting them at a higher risk for extensive retinoschisis [22]. Histological studies of specimens obtained during vitrectomy have shown that the retinal detachment generally results from the tangential traction produced by the vitreous cortex and/or by thin ERMs adhering to the retinal surface [14, 16]. Two types of macular holes develop in cases of high myopia: one is a flat hole without retinoschisis, whereas the other is induced by the retinoschisis and is evidenced by OCT images [23]. The latter type exerts powerful traction and is highly likely to progress toward a retinal detachment. This progression can vary rapidly and a complete detachment can occur in as little as 1 or 2 weeks following the development of the macular hole. The flat hole type does not exert traction, is generally stable, and has a higher postoperative success rate compared with the retinoschisis hole type. The detailed clinical appearance of each type will be discussed below.

22.4 Clinical Manifestations and Diagnosis

Myopic foveoschisis can be characterized as a slight elevation of the posterior retina in the fundus of highly myopic eyes; however, it is difficult to diagnose without an OCT, particularly in cases of chorioretinal atrophy. The use of OCT and other imaging tools is essential for a complete assessment of the retinal status to ensure ade-

quate surgical decision-making and planning (i.e., to determine the presence/absence of retinoschisis and circumscribe the specific location of retinoschisis or retinal detachment). If the pigment epithelium OCT images reveal a high foveal detachment, there is an increased risk of rapid macular hole formation and surgery should be planned without delay (ideally within 1–2 months). However, if the patient presents with only retinoschisis without a foveal retinal detachment, the need for surgery is less urgent. Patients often complain of metamorphopsia during retinoschisis, whereas a central scotoma is often a sign that a macular hole has developed or that a retinal detachment has occurred.

22.5 Optical Coherence Tomographic Appearance

Retinoschisis can typically be found in multiple retinal layers in cases of myopic foveoschisis. The split retinal layers normally have a bridge between them, known as the column, which is presumed to consist of residual Müller cells as evidenced by histological analysis [24]. In cases with a very atrophic retina, it can be difficult to distinguish retinoschisis from a retinal detachment, and the presence of the column is an important clue for adequately diagnosing one or the other. Tracing a line around the ellipsoid zone is also useful for differentiating a retinal detachment from retinoschisis as shown in a previous

OCT study [25]. An ILM separation from the other retinal layers (i.e., an ILM detachment) can serve as an indicator of the tractional force placed on the ILM [17].

The tent-like peak of the inner retina, the retinal microvascular traction can be observed on the OCT image [18]. Because the retinal vessels are normally located in a horizontal direction around the macular area, there is an increased chance to observe the peak in a vertical cross section than a horizontal one. This traction component is also an important cause of paravacular microholes, which are specific to high myopia and are generally located along the vascular arcade [26, 27]. The ellipsoid zone of the photoreceptors can occasionally disappear in the area near the retinal detachment [28] (Fig. 22.3); however, this band of photoreceptors is typically well preserved in the area of retinoschisis, suggesting that the photoreceptor function is well preserved in this subtype. This defect of the outer retina was initially referred to as an "IS/OS defect in high myopia," [28] and is associated with a high risk of macular hole formation after surgery [29].

In cases of myopic foveoschisis, macular hole formation typically develops over three stages (Fig. 22.4) [13, 19]. The first stage is the development of retinoschisis in the absence of any retinal detachment. Subsequently, a retinal detachment (second stage) can eventually begin to form around the fovea several months (sometimes several years) later. This can then result in the development of macular hole (third and final stage),

where both a retinal detachment involving the fovea and signs of retinoschisis around the macula can be identified. This typically occurs when, after some time, the inner retina above the area of detachment further stretches and tears, producing a macular hole.

The edge of a macular hole provides valuable information for surgical treatment and predicted outcomes. As discussed earlier, there are two types of macular holes in highly myopic eyes based on OCT subtyping [23]. One is similar to an idiopathic macular hole (Fig. 22.5) where the edge of the hole is thickened by retinal cysts. There is no retinal detachment around the hole nor does this type usually induce a retinal detachment even after several months. The other type is characterized by retinoschisis surrounding the hole (Fig. 22.6). This type results from myopic foveoschisis and can be considered a transition phase between foveoschisis and the formation of a macular hole with a retinal detachment. The latter hole type typically progresses rapidly and is likely to complicate the retinal detachment because of underlying traction. The typical physical appearance of this type on an OCT image is characterized by a relatively high and rectilinear wall of the macular hole edge with an acute angle relative to the RPE line and by a sharp-angled edge of the top of the macular hole [23]. Therefore, an examination of the macular hole edge can provide critical information for both the differential diagnosis and vitreous surgery planning.
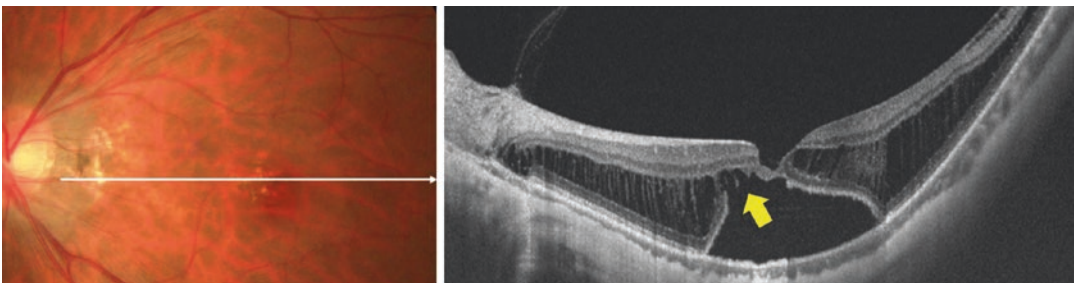
Fig. 22.3 Outer retinal defect in the area of retinal detachment in myopic foveoschisis. The retina is split and retinal detachment developed at the fovea. The outer retinal layers are missing in the area of detachment (yellow arrow). The white arrow in the fundus photo shows the location of the optical coherence tomography scan
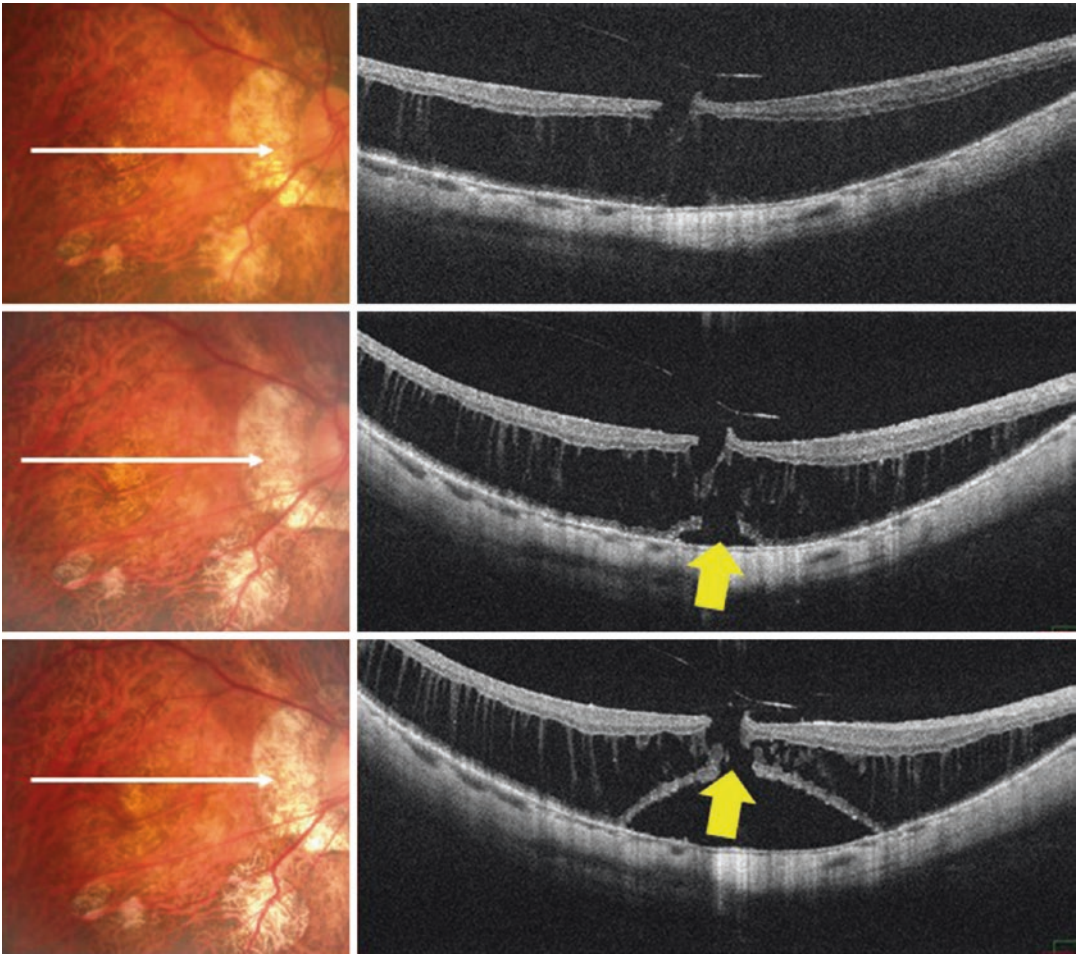
Fig. 22.4 Progress of myopic foveoschisis and optical coherence tomography images of each stage. Myopic foveoschisis starts with retinoschisis at the macula, but with no detachment yet (retinoschisis stage, top row). After several months, small retinal detachment (yellow arrow) is introduced by the traction of the fovea (foveal detachment stage, middle row). Finally, the foveal retina is torn and a small macular hole (yellow arrow) developed with retinal detachment (macular hole stage, bottom row). The white arrow in the fundus photo shows the location of the optical coherence tomography scan

22.6 Fundus Autofluorescence

In the atrophic fundus of myopic eyes, fundus autofluorescence helps distinguish the retinal detachment from the retinoschisis because of the loss of contact between the photoreceptors and the RPE results in hypo-autofluorescence. The hypofluorescent area indicates the retinal detachment and is a good indicator for monitoring its progression and the level of RPE damage [30]. Furthermore, macular hypofluorescence negatively predicts postoperative visual acuity [31].
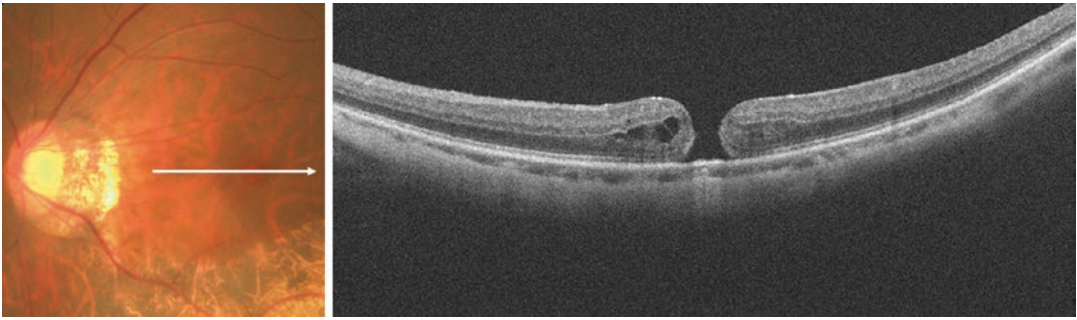
Fig. 22.5 Flat-type macular hole in highly myopic eyes. Similar to idiopathic holes in non-myopic eyes, the edge is flat and cystoid edema is observed. This type of macular hole is unlikely to progress to retinal detachment because of minimal traction. The white arrow in the fundus photo shows the location of the optical coherence tomography scan
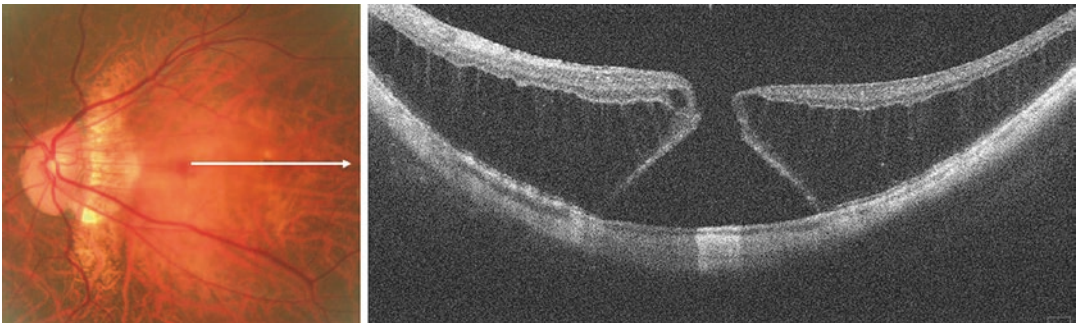
Fig. 22.6 Schisis-type macular hole. This is a result of foveal detachment type of myopic foveoschisis and high risk of retinal detachment due to the hole. The presence of retinoschisis indicates the tractional force elevates the retina at the edge of the hole. The white arrow in the fundus photo shows the location of the optical coherence tomography scan

22.7 Conclusions

Myopic foveoschisis is one of the retinal phenotypes resulting from various tractional components specific to high myopia. The pathogenesis includes vitreous traction, epiretinal membrane traction, ILM, and vascular inflexibility (especially arterioles). It normally begins as retinoschisis and can then progress into a foveal detachment and finally into a macular hole with retinal detachment. The use of OCT is essential for proper diagnosis. A variety of accompanying features such as ILM detachment, ERMs, and vascular traction indicates that myopic foveoschisis is indeed a tractional disease. Autofluorescence can also assist with assessing the extent of retinal detachment.

References

1. Katz J, Tielsch JM, Sommer A. Prevalence and risk factors for refractive errors in an adult inner city population. Invest Ophthalmol Vis Sci. 1997;38:334–40.
2. Xu L, Li J, Cui T, et al. Refractive error in urban and rural adult Chinese in Beijing. Ophthalmology. 2005;112:1676–83.
3. Sawada A, Tomidokoro A, Araie M, et al. Refractive errors in an elderly Japanese population: the Tajimi study. Ophthalmology. 2008;115:363–70.
4. Holden BA, Fricke TR, Wilson DA, Jong M, Naidoo KS, Sankaridurg P, Wong TY, Naduvilath TJ, Resnikoff S. Global prevalence of myopia and high myopia and temporal trends from 2000 through 2050. Ophthalmology. 2016;123:1036–42.

5. Klaver CC, Wolfs RC, Vingerling JR, et al. Age-specific prevalence and causes of blindness and visual impairment in an older population: the Rotterdam study. Arch Ophthalmol. 1998;116:653–8.

6. Iwase A, Araie M, Tomidokoro A, et al. Prevalence and causes of low vision and blindness in a Japanese adult population: the Tajimi study. Ophthalmology. 2006;113:1354–62.

7. Wu PC, Chen YJ, Chen YH, et al. Factors associated with foveoschisis and foveal detachment without macular hole in high myopia. Eye (Lond). 2009;23:356–61.

8. Benhamou N, Massin P, Haouchine B, et al. Macular retinoschisis in highly myopic eyes. Am J Ophthalmol. 2002;133:794–800.

9. Panozzo G, Mercanti A. Optical coherence tomography findings in myopic traction maculopathy. Arch Ophthalmol. 2004;122:1455–60.

10. Baba T, Ohno-Matsui K, Futagami S, et al. Prevalence and characteristics of foveal retinal detachment without macular hole in high myopia. Am J Ophthalmol. 2003;135:338–42.

11. Phillips CI. Retinal detachment at the posterior pole. Br J Ophthalmol. 1958;42:749–53.

12. Takano M, Kishi S. Foveal retinoschisis and retinal detachment in severely myopic eyes with posterior staphyloma. Am J Ophthalmol. 1999;128:472–6.

13. Ikuno Y. Pathogenesis and treatment of myopic foveoschisis. Nippon Ganka Gakkai Zasshi. 2006;110:855–63.

14. Sakaguchi H, Ikuno Y, Choi JS, et al. Multiple components of epiretinal tissues detected by triamcinolone and indocyanine green in macular hole and retinal detachment as a result of high myopia. Am J Ophthalmol. 2004;138:1079–81.

15. Itakura H, Kishi S, Li D, Nitta K, Akiyama H. Vitreous changes in high myopia observed by swept-source optical coherence tomography. Invest Ophthalmol Vis Sci. 2014;55:1447–52.

16. Bando H, Ikuno Y, Choi JS, et al. Ultrastructure of internal limiting membrane in myopic foveoschisis. Am J Ophthalmol. 2005;139:197–9.

17. Sayanagi K, Ikuno Y, Tano Y. Tractional internal limiting membrane detachment in highly myopic eyes. Am J Ophthalmol. 2006;142:850–2.

18. Ikuno Y, Gomi F, Tano Y. Potent retinal arteriolar traction as a possible cause of myopic foveoschisis. Am J Ophthalmol. 2005;139:462–7.

19. Ikuno Y, Sayanagi K, Soga K, Oshima Y, Ohji M, Tano Y. Foveal anatomical status and surgical results in vitrectomy for myopic foveoschisis. Jpn J Ophthalmol. 2008;52:269–76.

20. Shimada N, Ohno-Matsui K, Baba T, et al. Natural course of macular retinoschisis in highly myopic eyes without macular hole or retinal detachment. Am J Ophthalmol. 2006;142:497–500.

21. Gaucher D, Haouchine B, Tadayoni R, et al. Long-term follow-up of high myopic foveoschisis: natural course and surgical outcome. Am J Ophthalmol. 2007;143:455–62.

22. Shimada N, Tanaka Y, Tokoro T, Ohno-Matsui K. Natural course of myopic traction maculopathy and factors associated with progression or resolution. Am J Ophthalmol. 2013;156:948–57.

23. Jo Y, Ikuno Y, Nishida K. Retinoschisis: a predictive factor in vitrectomy for macular holes without retinal detachment in highly myopic eyes. Br J Ophthalmol. 2011;96:197–200.

24. Tang J, Rivers MB, Moshfeghi AA, et al. Pathology of macular foveoschisis associated with degenerative myopia. J Ophthalmol. 2010;2010:175613.

25. Ip M, Garza-Karren C, Duker JS, et al. Differentiation of degenerative retinoschisis from retinal detachment using optical coherence tomography. Ophthalmology. 1999;106:600–5.

26. Favre M. Trous parapapillaires comme cause du décollement de la rétine. Ophthalmologica (Basel). 1954;127:351–6.

27. Shimada N, Ohno-Matsui K, Nishimuta A, et al. Detection of paravascular lamellar holes and other paravascular abnormalities by optical coherence tomography in eyes with high myopia. Ophthalmology. 2008;115:708–17.

28. Sayanagi K, Ikuno Y, Soga K, et al. Photoreceptor inner and outer segment defects in myopic foveoschisis. Am J Ophthalmol. 2008;145:902–8.

29. Gao X, Ikuno Y, Fujimoto S, Nishida K. Risk factors for development of full-thickness macular holes after pars plana vitrectomy for myopic foveoschisis. Am J Ophthalmol. 2013;155:1021–1027.e1.

30. Sayanagi K, Ikuno Y, Tano Y. Different fundus autofluorescence patterns of retinoschisis and macular hole retinal detachment in high myopia. Am J Ophthalmol. 2007;144:299–301.

31. Arias L, Caminal JM, Rubio MJ, et al. Autofluorescence and axial length as prognostic factors for outcomes of macular hole retinal detachment surgery in high myopia. Retina. 2015;5:423–8.

Guidelines for the Treatment of Myopic Traction Maculopathy

23

Barbara Parolini, Michele Palmieri, Alessandro Finzi, Gianluca Besozzi, and Rino Frisina

23.1 Introduction

23.1.1 Pathologic Myopia

Myopia is one of the leading causes of visual loss, which can lead to potentially blinding ocular diseases [1, 2]. It is usually classified into two groups: non-pathologic and pathologic myopia (PM) [3]. PM is defined as a high refractive error (>−6.00D) or as an axial length >26.00 mm. However, the exact threshold between the two and the differentiation between myopia and pathologic myopia are yet to be established [4–6].

The disease is progressive and might present very early in childhood with a high risk of visual impairment due to pathological changes of sclera, choroid, retina, and optic nerve.

The prevalence of PM is 2%, although it differs in different areas of the world, being more common in Mediterranean area, Middle East countries, and East Asia [3–18]. Pi et al. [8] estimated a prevalence of pathological myopia-related visual impairment, in children, in China, of 0.10%.

Myopia is a multifactorial disease related to a complex interaction of hereditary and environmental factors. Based on studies in twins and in families with PM, autosomal dominant, recessive, and X-linked loci for PM have been identified in multiple chromosomes [19–37]. Finally, hours per year of sun, water hardness, levels of selenium, and the use of fluorinated water have been reported as possible environmental factors associated with PM [20, 21].

High myopia is associated with a progressive deformation of the scleral eyewall, which may be localized mainly at the posterior pole, leading to an anteroposterior elongation, but also in the lateral eyewall. Many consequences may develop, such as:

- Posterior staphyloma with the deepest point in the papilla or in the macula
- Progressive thinning/atrophy of the choroid
- A rupture into the choriocapillaris in the Bruch's membrane (lacquer crack), with consequent retinal hemorrhages and/or choroidal neovascular membranes (Myopic CNV)
- Peripapillary atrophic crescent
- Vitreoretinal traction and myopic traction maculopathy

B. Parolini (✉) · M. Palmieri
Eyecare Clinic, Crystal Palace, Brescia, Italy

A. Finzi
Department of Ophthalmology, Istituto Clinico
S. Anna, Brescia, Italy

G. Besozzi
Department of Ophthalmology, Vito Fazzi Hospital, Lecce, Italy

R. Frisina
Department of Ophthalmology, University of Padova, Padua, Italy

Recently Ruiz-Moreno and colleagues [22] published a new classification of myopic maculopathy, with the purpose of clarifying and unifying the currently available classification systems, to improve the knowledge of the disease and its progression. The study provided a complete analysis of structural and functional changes observable and proposed the ATN classification based on three main pathological features: atrophy, traction, and neovascularization.

In this chapter we will focus our attention on the diagnosis and management of the progressive disease known as myopic traction maculopathy (MTM). First of all we will report a new classification in stages of MTM that has been recently published (Parolini et al. EJO) and then we will offer guidelines and timing of treatment customized per each stage.

23.2 Myopic Traction Maculopathy

23.2.1 Definition

Myopic traction maculopathy is a complex disease that affects high myopic eyes with posterior staphyloma. Although different studies have been published, there is no agreement on the definition, neither a complete knowledge of the natural history and the pathogenesis nor a unique classification of the disease. Moreover, the surgical treatment is still controversial.

In literature, different definitions of MTM may be found, from macular schisis-like thickening of the retina, to foveal detachment (FD), to macular foveoschisis (MF), to foveoschisis, to shallow macular detachment.

The first description of MTM was given by Phillips in 1958 [23], who reported a posterior retinal detachment, without macular hole in patients with myopic staphyloma, assuming a tractional pathogenesis of what they called "retinomacular schisis."

In 1999, Takano and Kishi first published the optical coherence tomography (OCT) characteristics and findings of "foveal retinomacular schisis" [24].

Panozzo et al. [25] first described this condition as "myopic traction maculopathy" (MTM) and established that MTM may affect patients with high myopia and posterior staphyloma in 9–34% [25].

Shimada et al. [26] described different stages of the MF, leading to a FD, through the formation of an outer lamellar hole.

Recently, Parolini et al. proposed a new classification of MTM (in press) and defined MTM as a progressive disease that first involves the innermost layers of the retina with an inner macular schisis (I-MS) and gradually progresses involving the outermost retinal layers until a macular detachment (MD) appears, while the schisis disappear. The classification is known as MTM Staging System (MSS) and differs from all other classifications already published on MTM because it provides in one Table (MSS Table) information of nomenclature, pathogenesis, and prognosis of MTM. Furthermore, for the first time, the MTM classification is presented as a Staging System to highlight the evolving dynamic nature of the disease.

23.2.2 Epidemiology

MTM is thought to affect 9% of high myopic eyes [27]. About 50% of patients affected progresses to major complications such as FTMH or MD within 2 years [28].

Panozzo et al. reported that 9–34% of high myopic eyes with posterior staphyloma may be affected by MTM [25].

23.2.3 Pathogenesis: The Game of Forces

The pathogenesis of MTM is deemed to be multifactorial and it is still not fully understood. The rigidity of ILM, the progression of the staphyloma, and the anteroposterior traction caused by epiretinal affections seem to contribute to the evolution of MTM.

Anatomically, the retina is a multilayered multicellular structure which is held together, as

a unique tissue, by *tangential centripetal* forces, mainly exerted by the Muller cells and by the external and internal limiting membranes.

In PM, different *centrifugal* forces tend to modify the shape and the location of the retina and the fovea from the ideal one, racing against the unique centripetal intraretinal force. These centrifugal forces may be exerted by the vitreous and the sclera, with two main different directions: tangential or perpendicular to the retinal tissue.

The progressive deformation of the sclera due to staphyloma induces an increasing stretching of the choroid-RPE-retina complex toward lateral and posterior orbit. The vitreous, as well as the sclera, may also generate both tangential and perpendicular centrifugal force, the latter toward the vitreous cavity.

This "Game of Forces" leads to different clinical pictures and to a combination of inner macular schisis, outer macular schisis, inner LMH, outer LMH, foveal to macular detachment, macular detachment with a FTMH, FTMH on flat retina. Figure 23.1 describes the interaction of the different forces exerted on the retina in PM.

Early stages of MTM seem to involve first the innermost retinal layers and presenting as an I-MS. Then the progression of the disease depends on the prevalent centrifugal forces exerted on the retina.

If the prevalent centrifugal forces are perpendicular (Figs. 23.2, 23.3, 23.4, and 23.5), I-MS progresses and involves the outer layers becoming an IO-MS, then an O-MS until a MD appears. While the outer component further progresses to

arrow color	type of force	direction of vector	exerted by	action
white	centripetal	to the fovea	intraretinal structure	holds the retina together
line black	centrifugal	to the anterior segment	vitreous	pull the retina anteriorly
dark grey	centrifugal	to the lateral orbit	vitreous	stretch and open the fovea
dotted grey	centrifugal	to the lateral orbit	lateral sclera	stretch and open the fovea
dashed black	centrifugal	to the posterior orbit	posterior sclera	pull the retina posteriorly

Fig. 23.1 Schematic representation of the different forces exerted on the retina in an eye with pathologic myopia

One centripetal force (white) maintains the shape and attachment of the retina

Different centrifugal forces tend to detach or stretch the retina
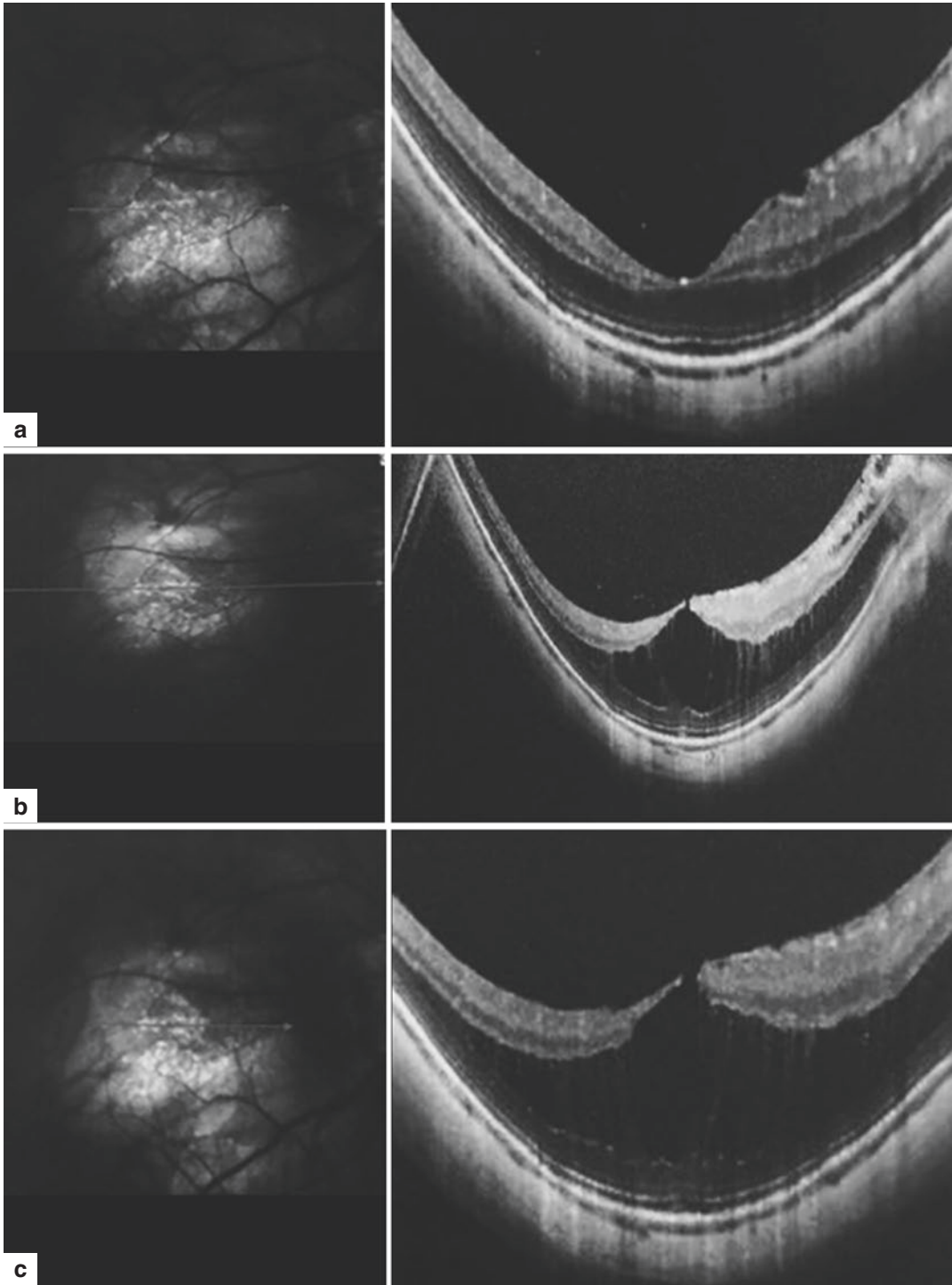
Fig. 23.2 Example of natural progression of MTM due to combined perpendicular and tangential forces. (**a**) OCT taken at age 36 shows an initial thickening of the nasal side of the inner macula (stage 1a). (**b**) Progression to MTM Stage 2b+ 4 years later, with a prevalent O-MS and an initial I-LMH. (**c**) OCT taken at age 43. Widening of the O-MS with releasing of I-MS. The stage is now 2b+. (**d**) OCT taken at age 48, showing further progression of O-MS with both I-LMH and O-LMH (Stage 2bO+)
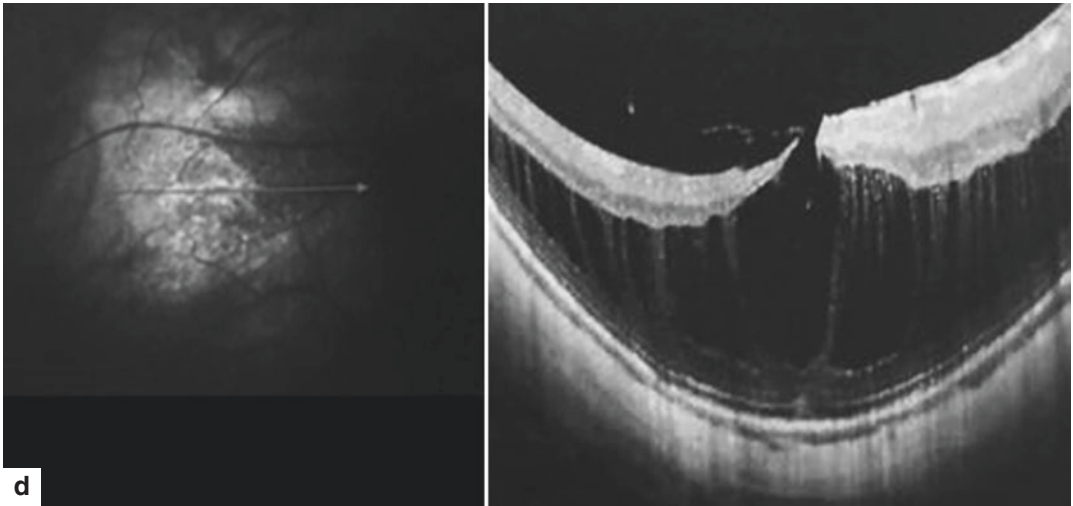
Fig. 23.2 (continued)
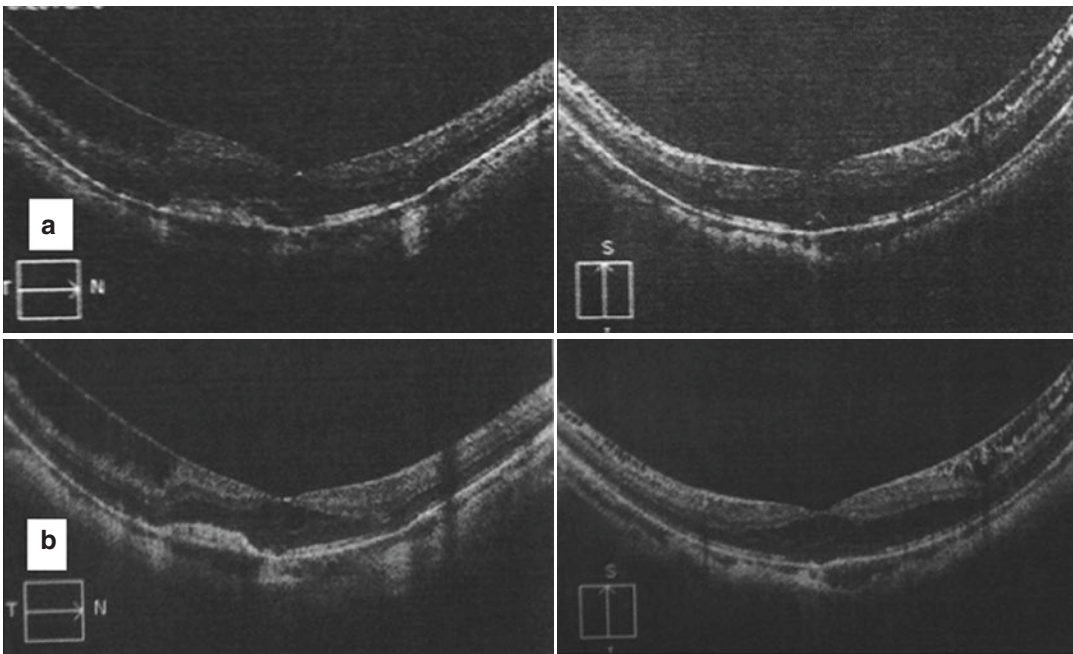
Fig. 23.3 Example of natural evolution of perpendicular forces in MTM in a male. (**a**) Horizontal and vertical OCT taken at the age of 44, showing a Stage 1a MTM and juxtafoveal CNV with mild serous foveal detachment. BCVA was 0.3 Decimal. Notice how in the horizontal scan the schisis is less evident over the CNV. (**b**) Horizontal and vertical OCT taken at the age of 46, showing a Stage 1a MTM and a juxtafoveal CNV treated with an intravitreal injection of ranibizumab. BCVA was 0.4 Decimal. The CNV is inactive and the serous neurosensory detachment is no longer visible. Notice how in the horizontal scan, the schisis is less evident over the CNV. (**c**) Horizontal and vertical OCT taken at the age of 49, showing a Stage 2a MTM and inactive juxtafoveal CNV. BCVA was 0.5 Decimal. Notice how in the horizontal scan, the schisis is less evident over the CNV. (**d**) Horizontal and vertical OCT taken at the age of 50, showing a Stage 3a MTM and inactive juxtafoveal CNV. BCVA was 0.2 Decimal
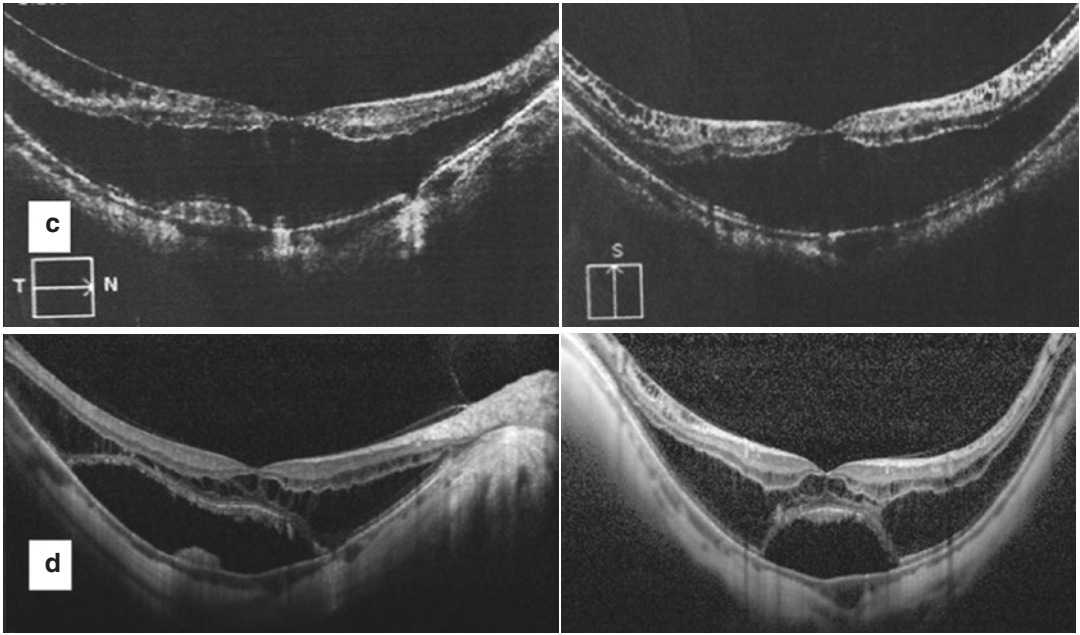
Fig. 23.3 (continued)
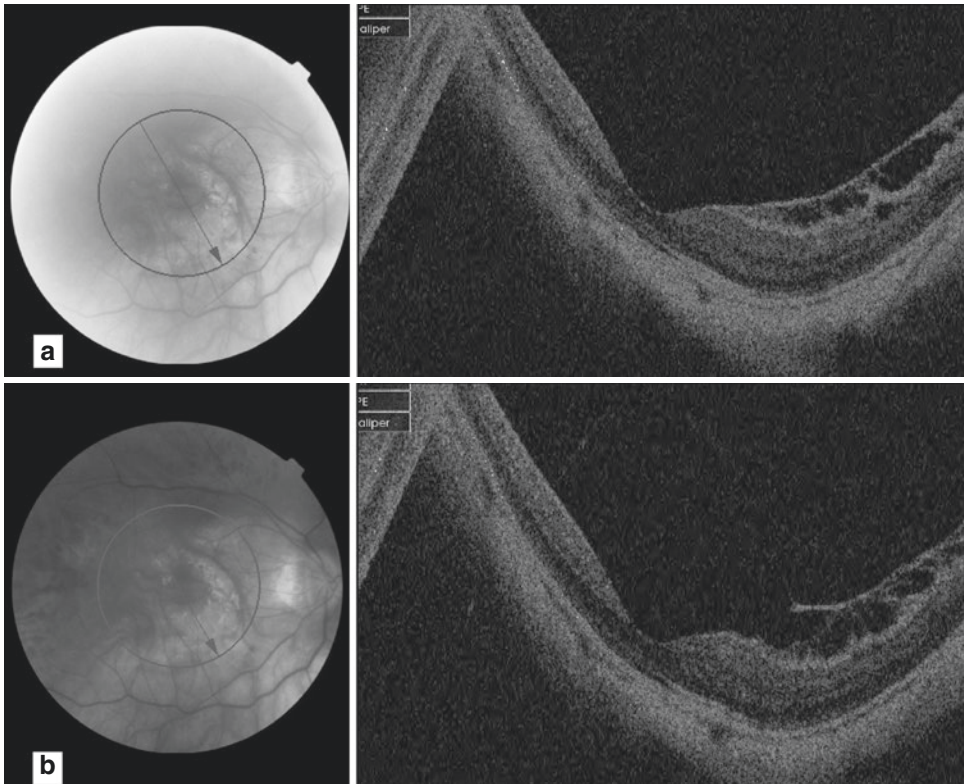
Fig. 23.4 Example of natural evolution of perpendicular forces in MTM. (**a**) OCT showing an inner macular schisis MTM stage 1a, in a female patient at the age of 45. BCVA was 0.8. (**b**) Slight progression of the inner macular schisis, which is now Stage 1a+, one year later. (**c**) OCT taken 4 years later, showing the progression to stage 2a+. BCVA was 0.7
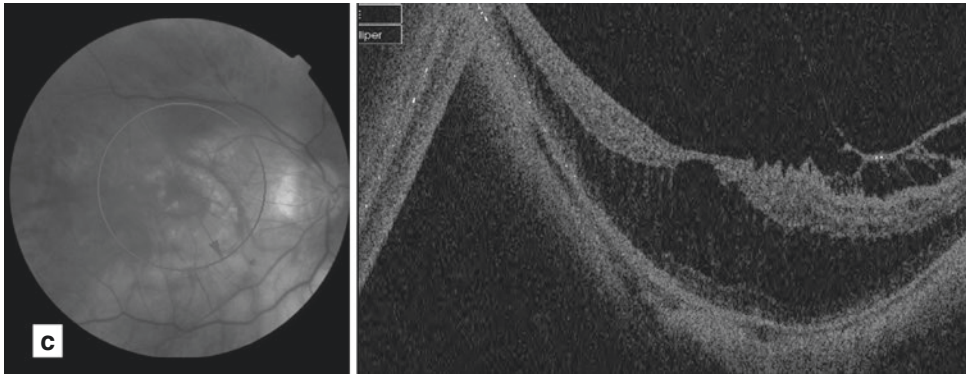
Fig. 23.4 (continued)
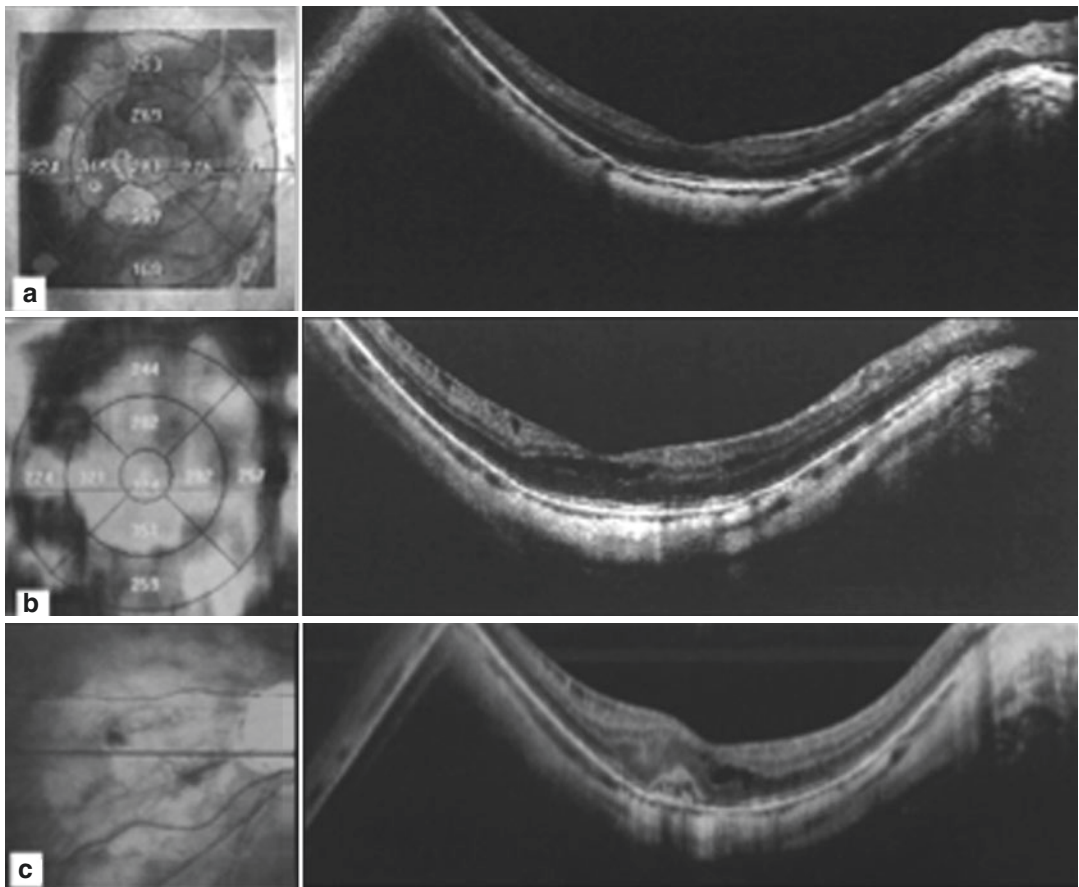
Fig. 23.5 Example of natural progression of MTM due to perpendicular forces. (**a**) OCT taken at the age of 43, in a female patient, showing no signs of MTM. (**b**) Progression to inner macula schisis, 1 year later. (**c**) One year later, at the age of 45, the patient develops a juxtafoveal CNV. The CNV exerts a pushing effect that reduces the schisis in that area. (**d**, **e**) Progressive deepening of the O-MS and releasing of the I-MS (stage 2a)
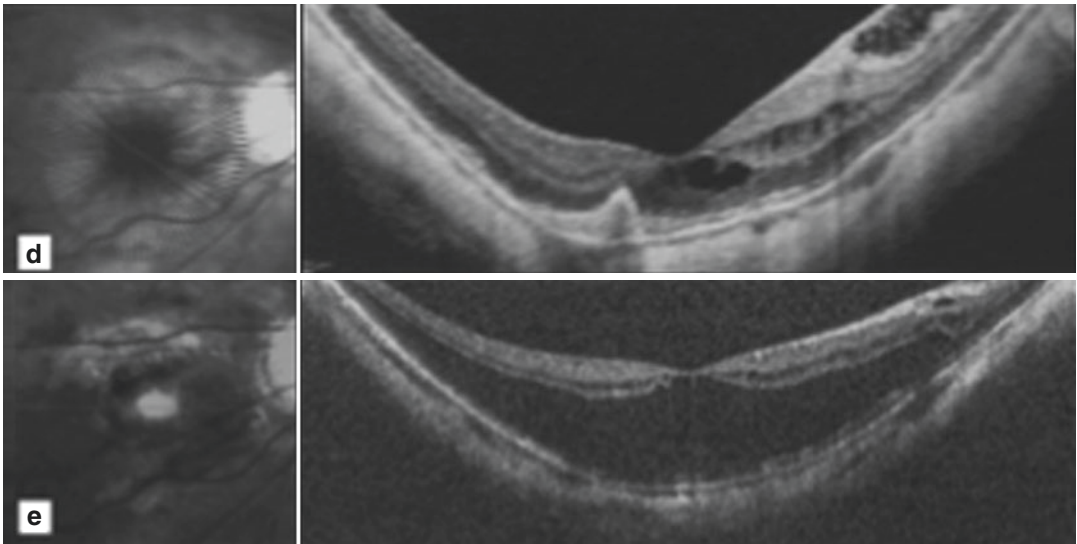
Fig. 23.5 (continued)

MD, the inner component of schisis is progressively relieved, because the intraretinal force becomes progressively prevalent when the retina detaches from the RPE.

Once the macula is detached, a disruption and splitting of the ellipsoid zone band might occur generating an O-LMH.

On the other hand, if the prevalent centrifugal forces are tangential, the patient will develop an I-LMH and eventually a FTMH (Figs. 23.6 and 23.7). The delamination of the retinal layers can be asymmetric in the different macular quadrants and the I-LMH may show different shapes based on the direction of the main vector of traction. The observation that a myopic LMH evolves into a FTMH was already made [29, 30].

When both the perpendicular and the tangential forces act together, a MD with either lamellar (Fig. 23.8) or FTMH (Fig. 23.9) will appear.

Parolini et al. (submitted for publication) hypothesized that the perpendicular evolution might manifest more significantly than the tangential evolution because of the conformation of the orbit. On the contrary, the tangential evolution is slower and more limited.

The forces exerted by the vitreous and by the sclera might act independently from each other. As well as the vitreous can pull the retina in the absence of scleral deformation (as it happens in vitreomacular traction syndromes, in non-myopic eyes), the sclera can act in the absence of vitreous, in vitrectomized eyes, or in eyes that already showed a spontaneous vitreous detachment, by exerting a centrifugal perpendicular force and a pulling effect in contrast with the rigidity of the retina.

Epiretinal abnormalities such us epiretinal membranes or vitreoretinal tractions may also be associated to every manifestation of MTM and contribute to the disease progression.

The natural course is not completely well known due to the limited number of study about it. Some patients remain stable for year while others progress. MTM spontaneous resolution has been reported. However, it seems clear the progressive nature of the disease as a consequence of its pathogenesis [31].

23.2.4 Clinical Manifestations and Diagnosis

The onset of MTM may vary among patients. PM usually begins in childhood, but the progression of MTM depends more on the age of presentation than on the age of patients**.**

Fig. 23.6 Example of natural evolution of tangential forces in MTM in a female. (**a**) OCT taken at the age of 43, showing a Stage 1b+ MTM. BCVA was 0.7 Decimal. (**b**) OCT taken at the age of 48, showing a Stage 1b+ MTM. BCVA was 0.4 Decimal. (**c**) OCT taken at the age of 53, showing a Stage 2c+MTM. BCVA was 0.1 Decimal
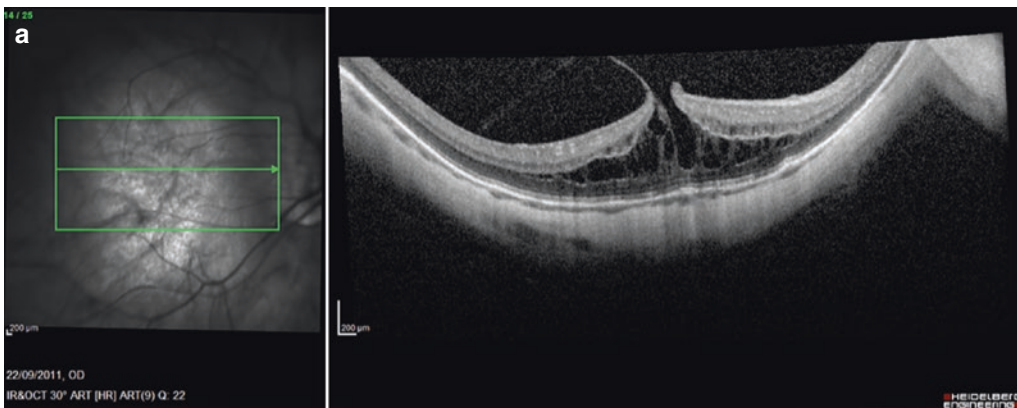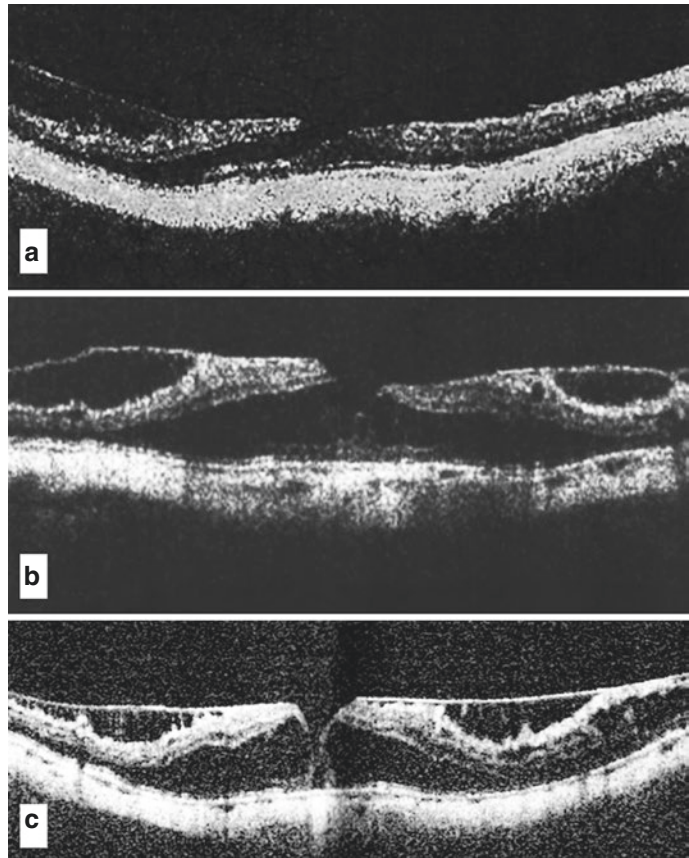
Fig. 23.7 Example of natural progression of MTM due to tangential forces. (**a**) OCT taken at the age of 42, showing an O-MS and an I-LMH with VMT (MTM Stage 2b+). (**b**) Three years later, the OCT shows a progression to a FTMH with predominantly O-MS and no evident epiretinal abnormalities (MTM Stage 2c)
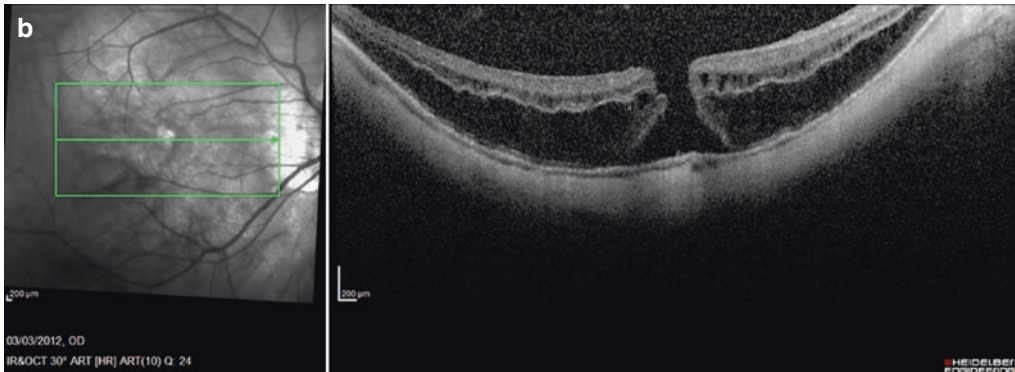
Fig. 23.7 (continued)
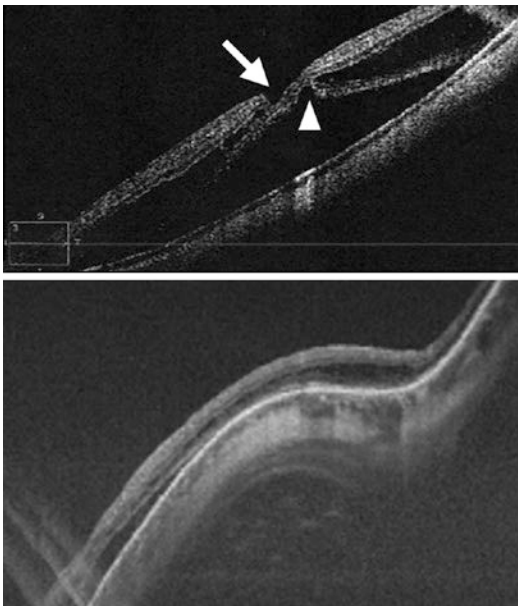
Fig. 23.8 Eye affected by MTM Stage 3bO in a 45-year-old male. (**a**) Preoperative OCT showing the schisis, the foveal detachment and an I-LMH (white arrow) and an O-LMH (white arrowhead). (**b**) OCT scan 6 months after MB, showing the resolution of the O-LMH, of the foveal detachment and of the schisis. The indentation is convex. The only available scan is not on the fovea and therefore a judgment on the I-LMH cannot be expressed

MTM may be totally asymptomatic especially in early stages [32, 33]. As a consequence of the lack of symptoms, the knowledge of the natural history is not easily predictable [34] and the disease could be underestimated. The symptoms usually reported by patients are blurred vision, reduce visual acuity, central scotoma, and metamorphopsia [25].

Indirect ophthalmoscopy and biomicroscopy are limited in detecting signs of MTM, because of the extreme retinal thinning and transparency, and the chorioretinal changes [24]. However typical changes of PM may be revealed: chorioretinal atrophy, peripapillary atrophy, staphyloma, lacquer cracks, myopic CNV.

OCT is the key instrument to diagnose this disease [35]. However the OCT 2D B-scan has limitations. This is demonstrated by the fact that the vertical and horizontal scan of these eyes can be completely different (Fig. 23.10). We should figure the posterior pole of the eye with PM as a three-dimensional concave structure, with an inner side, consisting of the vitreous cavity, and an outer side consisting of the sclera. Thus, a 3D OCT reconstruction better images the posterior pole of myopic eyes and it is more appropriate to study MTM.

MF is described as a separation of outer retinal layers, between the outer plexiform (OPL) and the outer nuclear layer (ONL). Intraretinal separations have also been observed at the level of the inner plexiform layer (INL) or at the inner limiting membrane (ILM) [36, 38]. The splitting of retinal layers appears as high reflective multiple columnar structures, with a hyporeflective space between these structures [38].

Posterior retinal detachment or, according to other definitions, FD can be another common
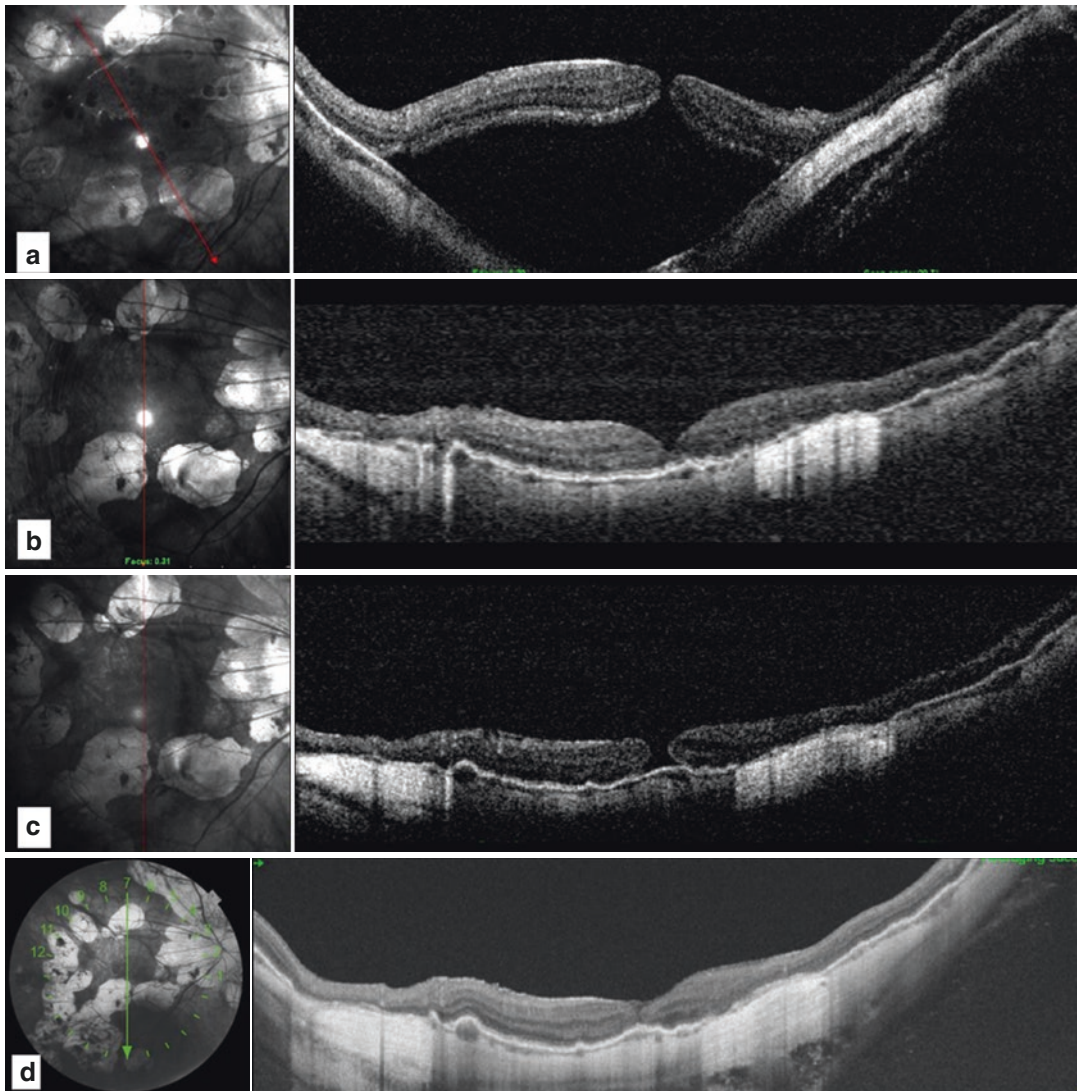
Fig. 23.9 Eye affected by MTM Stage 4c in a 51-year-old female. (**a**) Preoperative OCT showing the macular detachment with a FTMH. (**b**) OCT scan 1 year after MB, showing the resolution of the detachment. The FTMH appears closed. The indentation is flat. (**c**) OCT scan, 3 years after MB. The eye developed a reopening of the FTMH due to residual tangential traction. (**d**) OCT 1 month after PPV and ILM peeling to solve the FTMH

aspect of MTM [31]. FD is a separation between the RPE and photoreceptors layers [33, 37], usually limited to the posterior pole, and may be associated with a FTMH. Many authors confirm that FD occurs after the formation of the MF and may precede the formation of a macular hole [39].

OCT might also show the presence of an outer lamellar hole as a disruption of the ellipsoid zone band on a detached fovea.

Epimacular abnormalities may usually be detected as the hyper-reflective lines overlying the inner macular schisis and seem to be important contributors to the separation of the inner layers of the neural retina, which in turns leads to macular schisis [36].

Defects in the photoreceptors inner and outer segment may contribute to visual loss associated to MTM and may have predictive value for the postoperative visual recovery [40].
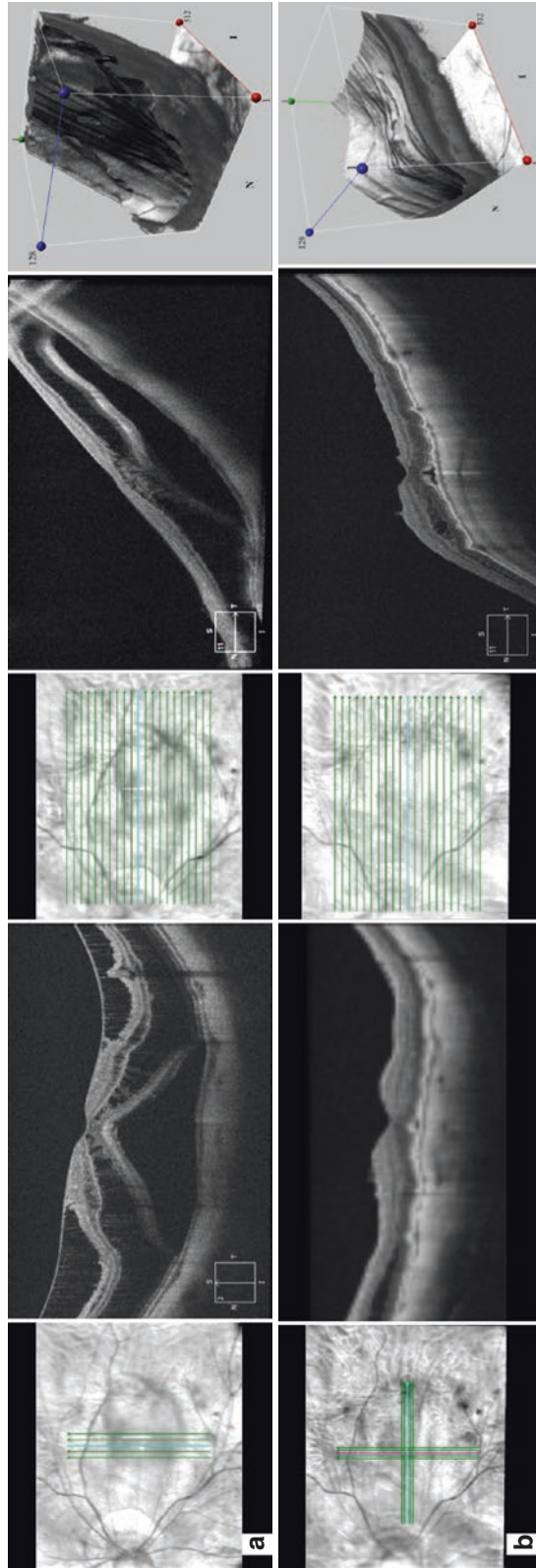
Fig. 23.10 Eye affected by MTM Stage 3a+. (**a**) Preoperative OCT scans showing a macular schisis-detachment with epiretinal abnormalities. Note the difference between the vertical and the horizontal scan. (**b**) Postoperative OCT scans after MB surgery. The profile of the sclera is flattened by the MB with an almost complete resolution of the O-MS, still visible in the nasal sector where there is no indentation by the MB. The fovea profile was restored by PPV

The use of microperimetry should also be considered to analyze foveal functionality [41].

23.2.5 Management

One of the most critical aspects of MTM is the management. This can be explained by the lack of knowledge of the natural history of the disease and by the small numbers of studies published. The current approach to MTM is to follow up patients and surgery is recommended in case of serious visual impairment and evolved macular detachment with macular holes. This management limits the functional outcomes of surgery.

Asymptomatic patients should be followed with observation every 12–18 months, since BCVA in this group is still good and the progression is slow. However, patients with epiretinal abnormalities suffering a vision loss or a worsening of metamorphopsia should undergo PPV. The presence of both a symptomatic I-LMH and a FTMH also represents an indication to surgery with PPV and maneuvers on the ILM. Similarly, patients affected by macular detachment should be directed to surgery without waiting for the formation of a macular hole.

23.2.6 Surgery

The first surgical approaches to MTM were directed to solve the most severe and final stage of MTM, the retinal detachment associated to a macular hole. The aims of these interventions were to restore anatomy and did not guarantee an acceptable functional recovery.

The idea of preventing axial elongation and scleral growth by the placement of material over the posterior part of the eye was proposed by surgeons many years before the description of MTM. Shevelev [42] first proposed, in 1930, the transplantation of fascia lata for scleral reinforcement.

Another technique proposed was a transscleral diathermy around the macular hole (Arruga 1952, Dellaporta 1953, Madroszkiewicz 1958) or the exposure of the retina to ultraviolet light associated to the injection of hypertonic saline in the sub-Tenon space, in order to induce a chorioretinitis.

The injection of gas was counseled in the cases in which the detachment persisted (Strampelli 1957) [43].

In 1957, Schepens Okamura and Brockhurst described the macular buckling procedures [44].

Borley and Snyder [45] and separately Curtin [46] described a technique for the placement of grafts of donor sclera.

In 1972, Snyder and Thompson [47] published their experiences with a modified scleral reinforcement technique. Momose [48] introduced Lyodura, derived from processed cadaver dura mater, for scleral reinforcement in 1983. After years of experience with their own variations of scleral reinforcement, both Thompson and Pruett [49], in 1990 and 1995, expressed satisfaction with the efficacy and safety of their series of cases. Curtin and Whitmore [50] in 1987 had, on the other hand, negative conclusions on the outcomes for their reinforcement techniques.

From 1957 to the 1980s, the gold standard for the treatment of macular detachment with macular hole was definitely the macular buckle (MB) [43, 44, 51–58].

The first article that considered pars plana vitrectomy (PPV) for the MHMD goes back to 1982 [59] by Gonvers. Many authors published afterwards [60, 61]. Since then, PPV has been proposed as the intervention of choice, with the rationale of eliminating the tangential tractions, allowing the retina to relax. Therefore, MB was abandoned for a while, mainly due to the challenges and complications linked to the surgical technique.

However, PPV had a limited efficacy. Indirectly this lack of success was revealed by the list of papers proposing different approaches with different tamponades. PPV with gas was linked to a high rate of failure or relapse. In 1999, Wolfensberger et al. [62] proposed the use of silicone oil associated to the laser treatment of the hole and obtained 92% of retinal reattachment, but, as expected, poor increase in vision.

The increasing use of peeling the ILM improved the range of success of PPV, as demonstrated in 2001 by Kadonoso et al. [63].

Thereafter, Lu et al. [64] in 2002 compared various methods of PPV, associating the injection of gas, with and without laser treatment of the macular hole, and injection of silicone oil without laser treatment, demonstrating the superiority of the first method, with the results of 93%, 58%, and 57%, respectively, giving a key role to laser treatment for anatomic success. It must be highlighted, however, that functional results were very poor.

Kuhn [65] in 2003 made, first, the consideration that the retinal detachment preceded the formation of the macular hole in these eyes just because, by comparison with emmetropic eyes, macular hole never causes retinal detachment. In the same year, Kanda [66] presented two patients with retinomacular schisis and retinal detachment without macular hole. The two cases were treated with 20G PPV, peeling of the ILM to the vascular arcades after staining with ICG and tamponade with 13–14% perfluoropropane (C3F8), plus facedown positioning for 7–10 days.

In 2004, Ikuno et al. [67] treated eyes with macular schisis without macular hole. A resolution of retinal detachment was noticed only in five eyes (83%) and, in the remaining eyes, only a significant reduction of retinal detachment.

Scholda et al. [68] in 2005 presented a series of 11 eyes that had not been implemented with perifoveal photocoagulation and demonstrated a retinal reattachment in 100% of cases with a good visual recovery. However the follow-up was short.

In 2006, Chen [69] reported retinal reattachment success rate, in 50–60% after PPV and gas injection.

Panozzo et al. [35], in 2007, carried out the first large-scale work on MTM. The study consisted of 24 eyes (including 5 with FD and 19 with MF), followed for 5 years, and treated with the sole purpose of removing the vitreous-retinal traction without using tamponade. The authors reported that 95.8% of the eyes had complete resolution of MTM stable in time. Four of the five eyes with macular detachment and one eye

with retinomacular schisis developed, however, a macular hole that did not hesitated in a new macular detachment and an eye remained unchanged. As for the visual recovery, 70% improved, 30% remained unchanged.

Kokame and Yamamoto [70] in 2004 pointed that the bubbles of silicone were not able to recreate the foveal depression and that the formation of an interface between the fovea and the tamponade medium was always visible.

Different authors [71, 72] presented promising results with the use of heavy silicone oil (HSO) in the treatment of eyes with persistence of idiopathic macular hole after PPV and gas injection. However, after removal of HSO, retinal detachment was reported.

In 2011, Mete et al. [73] compared the results of standard silicone oil 1000 cSt and heavy silicone oil in the ability of reattaching the retina and closing the hole in 42 cases of MHMD. The anatomic results were similar, with a macular reattachment rate of 76.5% and 81.8% for SO and HSO, respectively. The frequent relapses of macular detachment in both groups were always linked to reopening of the hole. Mete et al. concluded that there was a high recurrence rate of retinal detachment and an unsatisfactory final BCVA with both tamponades.

The success of PPV in high myopia remained limited with any tamponade, mainly because of high rate of retinal detachment recurrence, failure to close the hole in MHMD, and risk to induce an iatrogenic macular hole in MTM.

The unsatisfactory results of PPV left open the way to a new course of publications on buckling the macula, which started again, after 20 years, in 2000 with Sasoh [74].

In 2001 Ripandelli [75], and later in 2005 Theodassiadis [76], described MB success with a sponge and with a solid silicone exoplant, respectively. Although the reattachment rate with macular buckling was reported to be very high, the rate of hole closure was unknown because of lack of study with OCT.

The point was that surgeons dealing with MHMD realized the limitation of PPV. However, MB, although more efficient, remained difficult and linked to complications.

Some authors started to find a way to make the macular buckling technique easier, first of all with different buckle design.

Tanaka, Ando, and Usui [77] published in 2005 the successful approach of a new semirigid rod-exoplant in MHMD recurrences after PPV. The exoplant consisted of a T-shaped semirigid silicone rubber rod internally reinforced with titanium wires and an indenting head at one end.

In 2009, Parolini presented the 2 years results of a new design of MB, at the Heatam meeting in Amsterdam. The idea was to propose an L-shaped buckle, made with a titanium stent inserted into a silicone sleeve, with the aim to obtain a macular indentation but allowing an anterior suture. The shape resembled the Ando plomb with the difference of using a titanium stent (MRI compatible), not stainless steel wire, and soft silicone sponge, not solid silicone, to indent the macula.

In 2009, B. Ward et al. [78] examined the buckling of the posterior pole, with sclera reinforcement, as a tool for myopia control and followed the course of untreated fellow eyes. The buckled (treated) and control (untreated) eyes had axial lengths ranging from 27.8 to 34.6 mm, and myopic refractive errors ranging from −9.00 to −22.00 D. Ward concluded that the experience with 59 cases showed effective axial myopia control and an acceptable safety profile for posterior pole buckling. No case of visual acuity loss occurred with the procedure.

In 2012, Tian J et al. [79] applied the technique of macular buckling in five cases of MHMD after initial failure of pars plana PPV with ILM peeling and silicone oil tamponade. In this study, the retina was reattached after buckling. However, visual acuity did not improve and anatomical macular holes only closed in two patients. This could be related to extensive and long-term and marked atrophy of the RPE/choriocapillaris complex in the macular area.

More recent literature [80, 81] added to PPV the technique of inverted ILM flaps reporting a higher success rate to close the holes [82].

Alkabes [83] recently published a 16-year review on MB for MTM and compared the results with PPV. She clearly confirms that MB was the first technique considered to treat MHMD.

The published studies had several limitations:

1. The follow-up was generally short.
2. Macular buckle was generally proposed for end-stage MTM.
3. Surgical reports on MTM did not distinguish the result of surgery in relation to the MTM stage.
4. The analysis of cases failed after PPV was not reported.
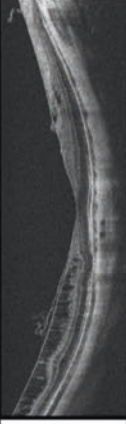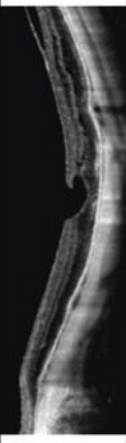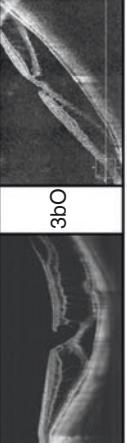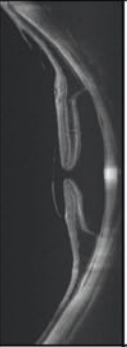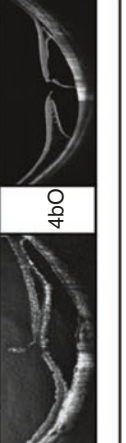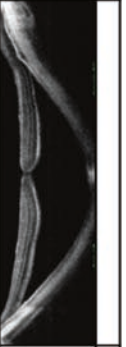
23.2.7 Guidelines to MTM Treatment

The surgical treatment of MTM is still controversial. The goals of surgery need to be anatomical and functional. The anatomical goals should be retinal attachment, hole closure, and atrophy prevention. The functional goals should be to improve or maintain central vision and the central visual field. However, in eyes with PM we should ideally aim not only to treat but also to prevent the outset or the progression of MTM, since PM is a degenerative and progressive disease.

Parolini et al. (EJO, in press) recently proposed new management guidelines of MTM (Fig. 23.11), based on the new MTM Staging System (MSS). Figure 23.12 summarizes the MTM MANAGEMENT GUIDELINES TABLE (MSS-MAN). The aim of their study was to clarify how to choose among four options of management: observation, PPV, MB, or combined surgery (MB + PPV).

The choice of treatment was made by looking at the forces exerted on the retina (Fig. 23.1), with the intension to counteract the centrifugal forces that tend to detach the retina from the eyewall, perpendicularly, and/or tend to split the retina, tangentially, in the macula. In their study, the authors used PPV, MB, or combined surgery to treat 157 eyes affected by different stages of MTM.

Observing the anatomical results of the different treatments, they concluded that PPV better addressed the tangential tractions on the inner retinal surface, i.e., the modulation of the foveal pattern, while the MB addressed the perpendicular tractions on the retina induced by scleral elongation, i.e., the modulation of the retinal pattern.

Fig. 23.11 MTM Staging System. The table describes the classification of MTM in stages offering data on pathogenesis (the perpendicular and tangential evolution) and prognosis

The PLUS sign "+" indicates epiretinal abnormalities and can be present in each stage

	STAGE	PERPENDICULAR EVOLUTION	STAGE	TANGENTIAL EVOLUTION IN LMH	STAGE	TANGENTIAL EVOLUTION IN FTMH
Inner-Outer Macular Schisis	1a	12-15 months	1b	12-15 months	1c	12-15 months
		Observation		PPV (if symptomatic)		PPV
Predominantly Outer Macular Schisis	2a	12-15 months	2b	12-15 months	2c	12-15 months
		Observation		2bO		MB +PPV
Macular Schisis-Detechment	3a	6-12 months	3b	MB + postpened PPV (if symptomatic) 6 months	3c	1-3 months
		3aO		3bO		
		MB		MB + postpened PPV (if symptomatic)		MB +PPV
Macular Detechment	4a	3 months	4b	1-3 months	4c	less than1 months
		4aO		4bO		MB+PPV
		MB		MB. Late PPV MB+PPV		

The PLUS sign "+" indicates epiretinal abnormalities and can be present in each stage

Fig. 23.12 MISS-MAN table. The table offers guidelines for the management of MTM based on stages

Treating a prevalent tangential traction with a MB brings to potential complications as well as treating a prevalent perpendicular traction with PPV. If only one component of traction is treated, the opposite component will manifest itself in time. Thus, whenever a combination of perpendicular and tangential forces is treated only with a MB, the perpendicular component is solved and the retinal pattern will improve, but the tangential force inducing alteration of the foveal pattern remains unchanged and might even worsen.

For example, if a patient affected by a mild and extrafoveal I-MS with mild ERM and without preoperative I-LMH undergoes MB, the tangential tractions induced by the buckle, pushing the retina vertically and anteriorly, lead to an iatrogenic splitting of the fovea (Figs. 23.13 and 23.22b).

In the same way, when O-MS or an FD is treated only with PPV (Fig. 23.14), the schisis and detachment have a low chance to resolve or end up in iatrogenic macular hole.

Parolini assessed that inner and outer schisis should be followed with observation every 12–18 months, since BCVA in these group is still good and the progression is slow, unless epiretinal abnormalities are associated. The symptomatic cases should be treated like cases of ERM without MTM. A high rate of anatomical success could be reached when PPV was used for schisis associated to lamellar of full thickness macular hole.

MB should be considered and evaluated case by case when outer schisis is associated to a macular hole. It can only be speculated that MB could prevent the progression to atrophy by stopping the elongation of the eye. Further studies are needed to proof this concept. MB and late PPV revealed particularly useful in cases of macular schisis and lamellar macular hole, even in eyes with macular atrophy, obtaining a gain in visual function when the schisis and the I-LMH were resolved.

The recommendation by Parolini is to treat the schisis\detachment first, with MB, and then to treat the foveal pattern with PPV, only if required by lack of recovery of visual acuity or by progression of the I-LMH.

The final anatomical resolution of the schisis is slower with MB alone, compared with combined MB + PPV.

The final restoration of the foveal profile in the presence of lamellar of FTMH was achievable only when PPV was added. However, even in these cases, PPV can be added in a later time only if needed, thus avoiding the possible side effects of PPV and restoring the foveal profile on an attached retina not affected by schisis nor detachment.

Macular detachments should be treated immediately with a MB alone. PPV might be added later on and only if needed.

Macular detachments associated to a macular hole (MHMD) should be immediately treated with combined MB + PPV in order to treat simultaneously the outer retina and the macular hole.

Both MB and combined surgery resolve the schisis. While the result of buckle is slow, progressive and visible in months, the result of subsequent or combined PPV is visible within 1–2 weeks. The surgeon should choose, case by case, whether a quick result is better than a slow result, which allows to avoid the consequences of PPV.

Some cases of MHMD were initially treated successfully only with MB and gas injection, obtaining both the retinal attachment and the complete hole closure. However, years after the first surgery, the authors observed an opening/reopening of FTMH (Figs. 23.9 and 23.15) due to the progression of the tangential traction.

In conclusion, the surgical treatment of MTM should be customized surgery per each patients depending on the stage of the disease.

23.2.8 Role of ILM Peeling

In literature there is no agreement on the role of ILM peeling. On one hand, it was shown that ILM peeling with ILM flap increased the chance of anatomical success of MHMD [80, 82]. However, it was also well shown that ILM peeling increased the risk of iatrogenic FTMH [84] when cases of MD without FTMH were treated. Therefore, the removal of the inelastic ILM should be postponed
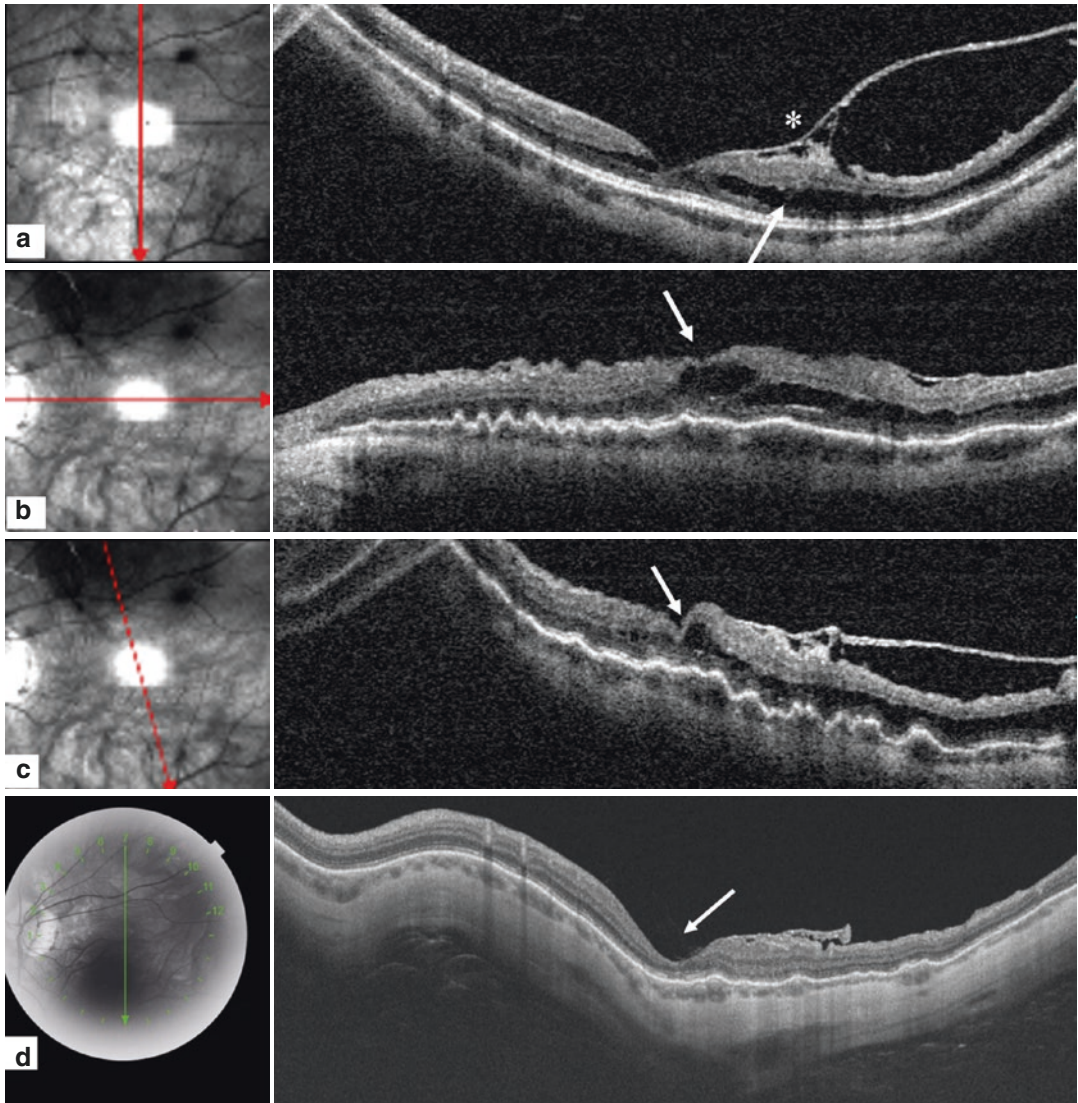
Fig. 23.13 Eye affected by MTM Stage 1a+ in a 54-year-old female. (**a**) Preoperative vertical OCT showing mild IO-MS, located only in the inferior temporal quadrant of the posterior pole and hemi-foveal involvement and epiretinal abnormalities (star). (**b**) Horizontal OCT scan 1 month after MB surgery, showing the development a temporary I-foveal schisis (arrow). A mild O-MS is still visible. The line of the RPE is wrinkled and the scleral profile is flat as a result of the MB. (**c**) Vertical oblique OCT scan 1 month after MB surgery, showing the traction exerted by the epiretinal abnormality (arrow). The O-MS is more visible where the epiretinal traction is present. The line of the RPE is wrinkled and the scleral profile is flat as a result of the MB. It appears that the pushing effect of the MB, in correspondence with the epiretinal traction, has induced an exacerbation of the schisis and tangential traction. (**d**) OCT, 2 years after MB. The schisis has disappeared. The epiretinal abnormality is less visible

to obtaining an attached macula by implanting a MB, in order to reduce this risk. Once the macula is flat, surgeons may perform PPV with or without ILM flap to release the tangential traction exerted by the ILM and to treat the FTMH, when present.
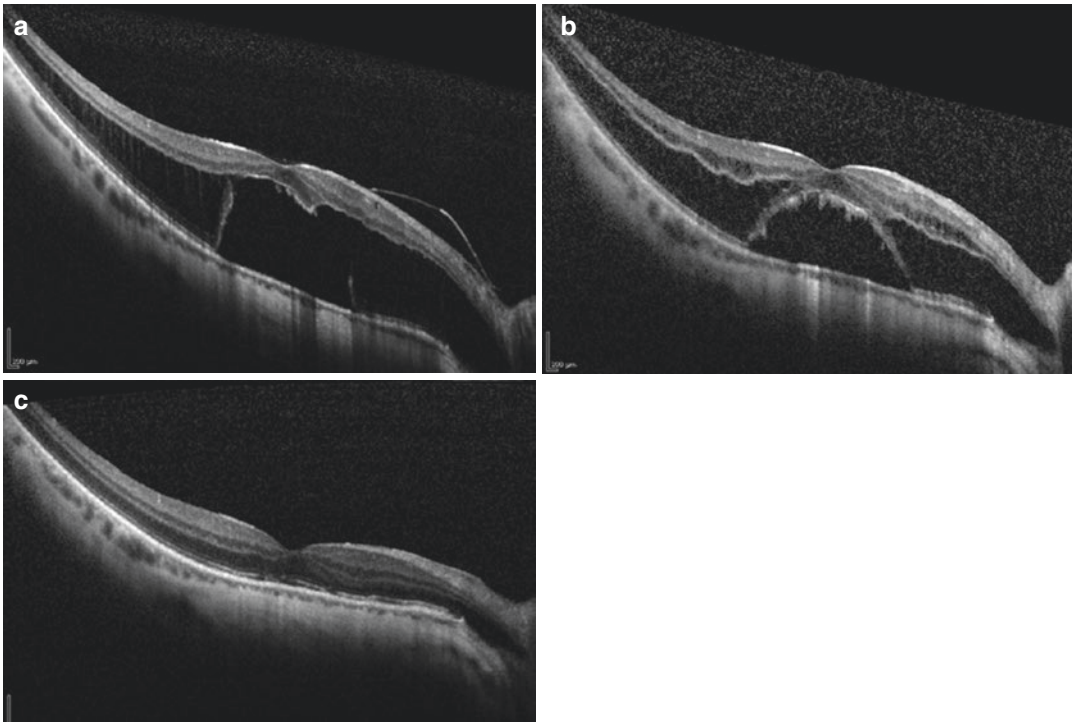
Fig. 23.14 Eye affected by MTM Stage 3aO+ in a 55-year-old male. (**a**) Preoperative OCT showing the schisis and the foveal detachment with an O-LMH. (**b**) OCT scan 8 months after PPV surgery, showing the resolution of the O-LMH and the persistence of the foveal detachment and the schisis. (**c**) OCT scan, 2 weeks after MB. The O-MS and the foveal detachment are solved

23.3 The Macular Buckle

23.3.1 Preoperative Assessment of the Eye and Patient

Complete slit lamp examination is mandatory.

BCVA and microperimetry are useful methods to follow the postoperative functional change.

Refraction should be checked in the treatment eye and in the fellow eye. An average 2.0 diopters hyperopic shift should be expected when implanting properly the MB. If the eye is still phakic, it is preferable to implant the buckle first and then to proceed with the lens removal if needed. In cases of severe cataract compromising the intraoperative view, a choice can be made either to leave the eye aphakic and proceed with a secondary implant later or preferably to implant and IOL with a myopic residual target refraction. Any previous surgery linked to a change in refraction in the treated or fellow eye should be known, in order to plan the final refractive target.

Axial length should be measured preoperatively and periodically after MB.

Any previous surgery should be known. A previous episcleral surgery or episcleral devices such as glaucoma valves could interfere with the implantation of the buckle.

Motility of the eye and diplopia should be assessed before surgery, in order to better judge if possible postoperative limitation in the eye movement were induced by the buckle or were present preoperatively and in order to adequately manage them.

Preoperative MRI is not necessary. Collecting data on the original shape of the entire eye and the staphyloma could be helpful in a clinical

Fig. 23.15 Eye affected by MTM Stage 3aO+ in a 39-year-old female. (**a**) Preoperative OCT showing the schisis and the foveal detachment with an O-LMH. (**b**) OCT scan 1 year after MB, showing the resolution of the O-LMH, of the foveal detachment and of the schisis. The indentation is flat. (**c**) OCT scan, 3 years after MB. The eye developed a FTMH due to residual tangential traction. (**d**) OCT 1 month after PPV and ILM peeling to solve the FTMH
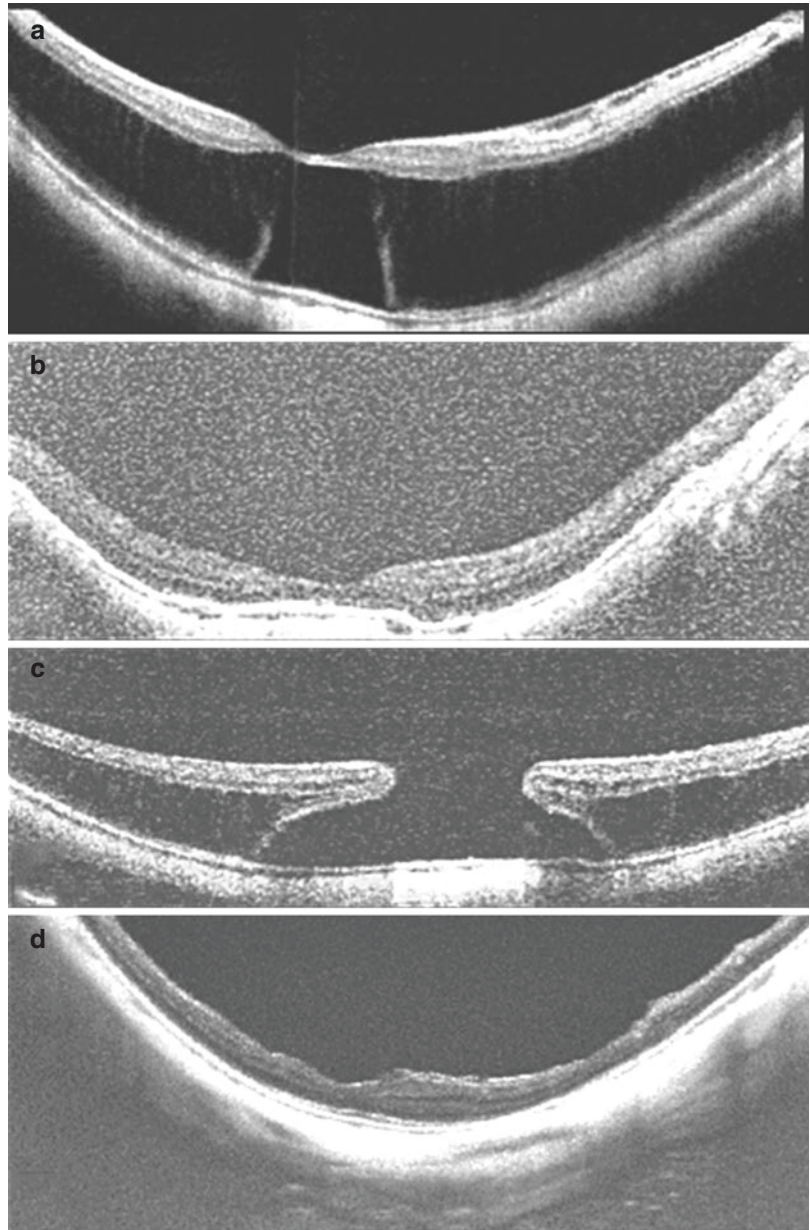
study setting and postoperatively in order to verify the position of the buckle in relation to the optic nerve (Fig. 23.16).

The category of myopic maculopathy according to the International Photographic Classification and grading system [85] should be noted, to better understand the potential postoperative gain in visual function, based on the amount and location of atrophic areas. Suspect signs of CNV should be noted in order to promptly allow

proper treatment. Wide-field fundus photo offers an easier and more accurate classification of the staphyloma [86] (Fig. 23.17).

OCT is the gold-standard exam and the main guide to MTM management. Vertical and horizontal OCT scans (at least 9 mm wide) and 3D reconstruction, when available, are useful in understanding the change in shape of the posterior pole, not only from the preop to the postoperative time, but also during the follow-up.
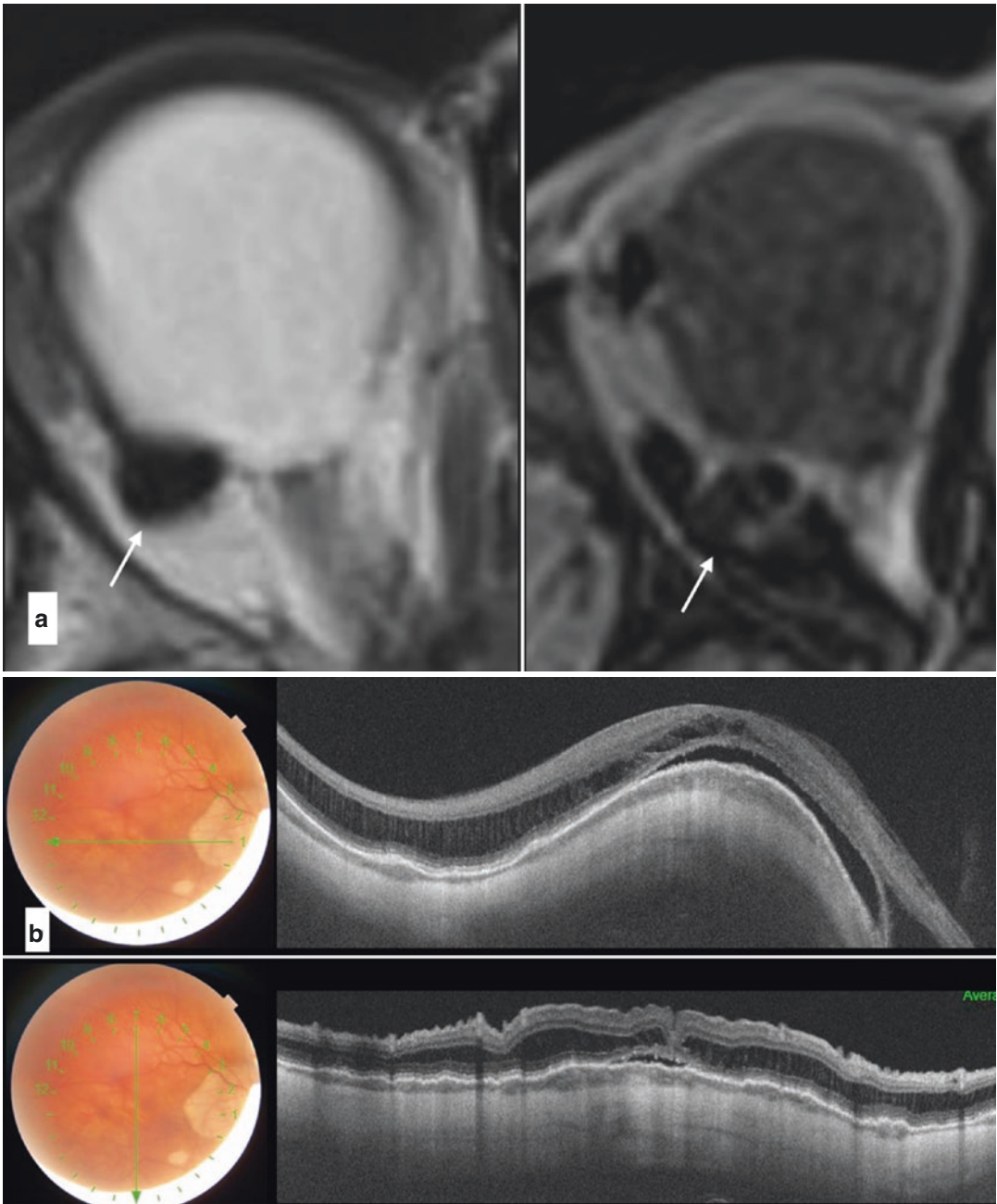
Fig. 23.16 Multimodal imaging of a patient operated with macular buckle. (**a**) MRI showing the macular buckle (white arrows) placed beneath the posterior pole. (**b**) Horizontal and vertical post-op OCT scans. The indentation of the buckle appears on the horizontal scan because the buckle was inserted from 12 to 6 o'clock in the superotemporal quadrant. The vertical scan, lying all along on the buckle is flat. (**c**) 3D OCT showing the macular profile inverted by the macular buckle
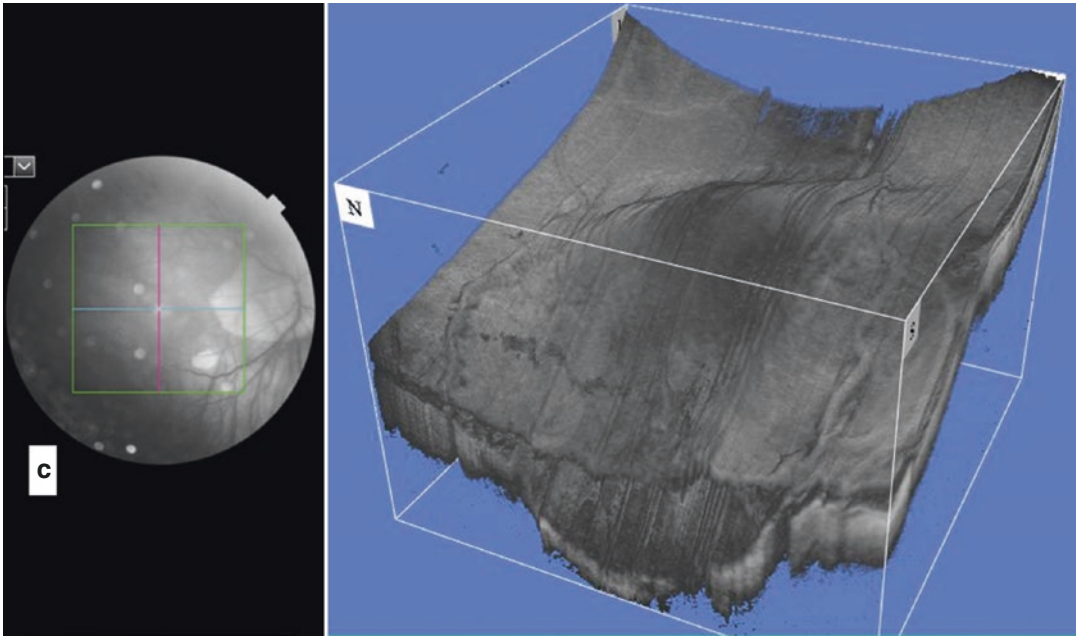
Fig. 23.16 (continued)
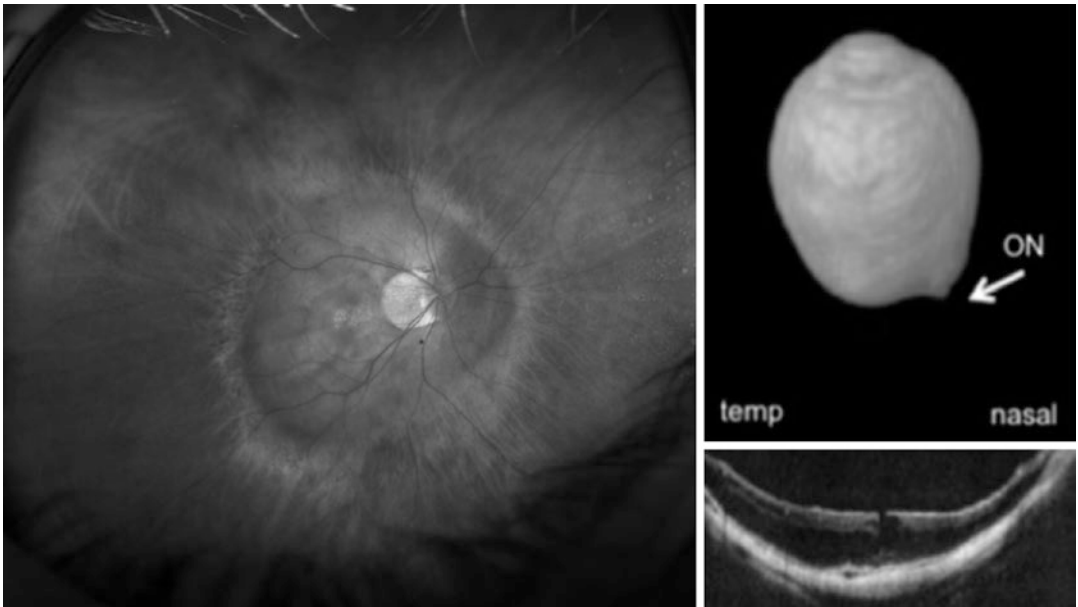
Fig. 23.17 Eye affected by MTM Stage 2b+. (**a**) Wide-field IR image showing a Type 1 Staphyloma involving the posterior pole. (**b**) MRI imaging showing the whole shape of the eyeball. The white arrow indicates the optic nerve (ON). (**c**) OCT scan showing the MTM stage 3b+ with predominantly outer schisis associated to an I-LMH

The indication for the management and choice of treatment are offered in the MTM Management Tables (Fig. 23.12) as previously reported.

23.3.2 Anesthesia

MB surgery can be performed under general anesthesia but also under local anesthesia and sedation. In case of local anesthesia in high myopic eyes, sub-Tenon with blunt cannulas is preferable over peribulbar with needle, to lower the risk of scleral perforation.

23.3.3 Types of Buckle Available

At the moment, limited types of buckles are available in the market. A self-made buckle can be used such as the one later described in this chapter.

23.3.4 Postoperative Care

Postoperative care resembles the one of any episcleral surgery. The eye is red and swollen for at least 1 week. Steroid and antibiotic drops should be advised for the first 2 weeks. The follow-up should be scheduled at least at 1 day, 1 week, 1 month, 3–6–12–18–24 months, and then every year.

23.3.5 Complications of the Macular Buckle and Their Management

Some degree of diplopia (particularly in the temporal gaze on the side of the MB location) may occur in 6% of patients in the first postoperative weeks. It is advisable to counsel the patient to move the eye in different directions for 10 min, 3–4 times every day for the first month, in order to lower the chance of formation of fibrotic membranes around the buckle and around the

muscles, Tenon's and conjunctival complex. This advice will lower the chance of postoperative diplopia.

Pain is limited and easily treatable in the first week with proper therapy.

Diplopia and pain were mostly linked to the excessive size of the first models of MB.

Exposure of the lateral arm of the buckle through the conjunctiva might occur months or years after surgery. Minimal exposure can be treated by covering the lateral arm with pericardium or donor sclera. In case of recurrent exposure, the buckle can be removed safely.

23.3.6 Effect of Macular Buckle over Time and Effect of Buckle Removal

If the buckle is removed within 3 months after surgery, the MTM could relapse with sudden vision loss (Fig. 23.18). When the buckle is removed years after surgery, the anatomical benefit remains although the indentation becomes less pronounced (Fig. 23.19). We advise not to remove the buckle whenever possible or to for at least 6 months.

The buckling effect over time seems to remain unchanged in most of the cases when the buckle is not removed.

23.3.7 Evolution of the Surgical Technique

Different models of macular buckle have been proposed in the years. The first technique consisted of suturing a sponge to the sclera behind the macula. This technique has been abandoned because it is too difficult and link to a high rate of complications. The complications mainly were derived by the need to detach the muscles to rotate the globe and mostly to the step of suturing the buckle behind the macula with difficulty in localizing the fovea and high risk of scleral
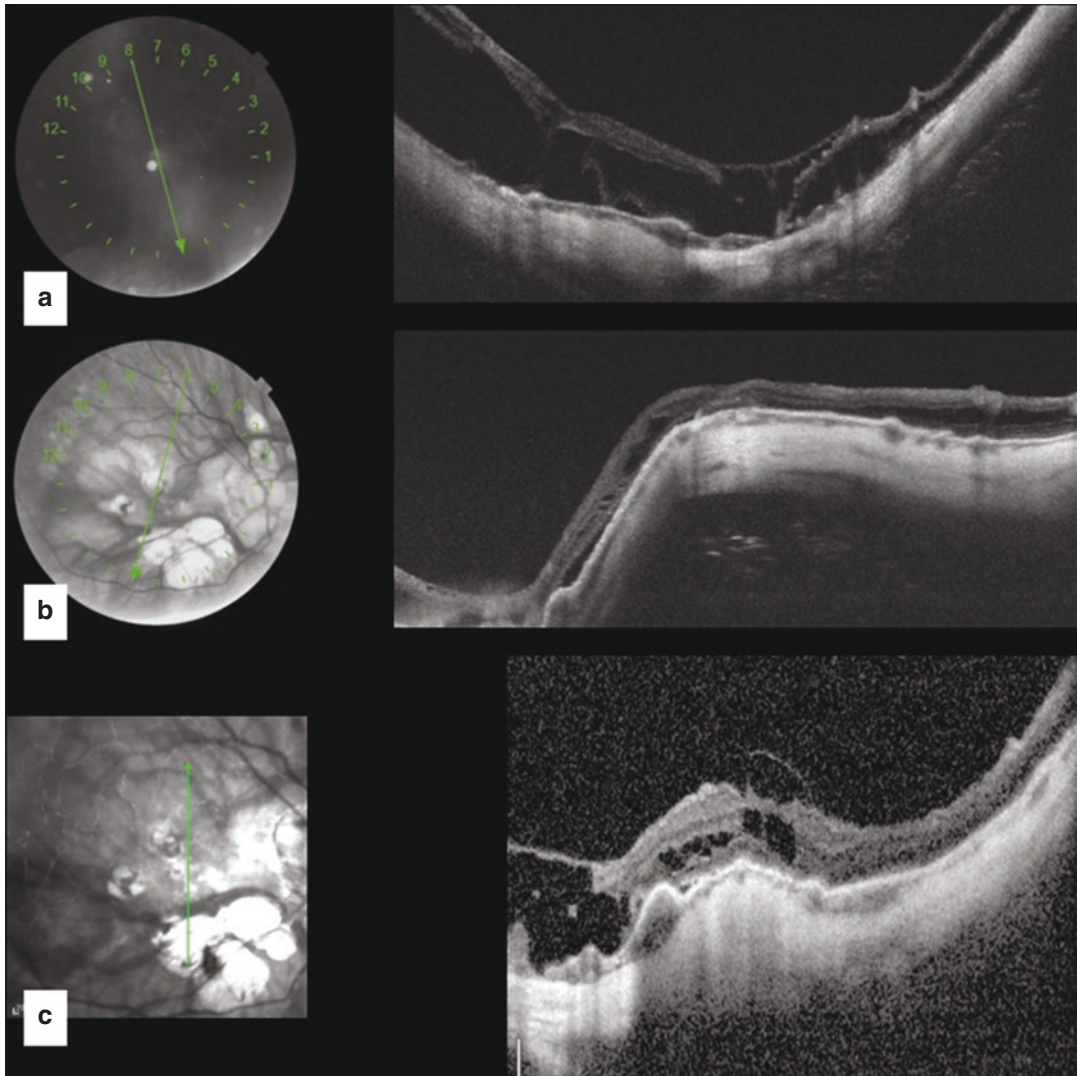
Fig. 23.18 Eye affected by MTM Stage 3aO. (**a**) Preoperative OCT showing a schisis with areas of MD and an O-LMH. (**b**) Postoperative OCT after combined MB + PPV surgery without ILM peeling showing a suc-cessful resolution of the schisis and the O-LMH. The shape is now convex over the buckle. (**c**) Recurrence of MTM, immediately after MB removal, due to pain. The MB had been implanted only 2 months before removal

perforation, retinal perforation, and internal bleeding.

Different models have been proposed to overcome this difficulty such as the model of Devine, Ando, and Landolfo [87].

The idea was to be able to move the sutures anteriorly in a safer and more accessible location.

The first model of MB proposed by Parolini (Fig. 23.20a) was created by inserting a stainless steel wire into a silicone sponge, 7 mm wide and 5 mm thick (507 Labtician). The sponge could be bent to an L-shape, with a short side, called head, to buckle the macula, and a long side, called arm, to allow an anterior suture. The MB was inserted
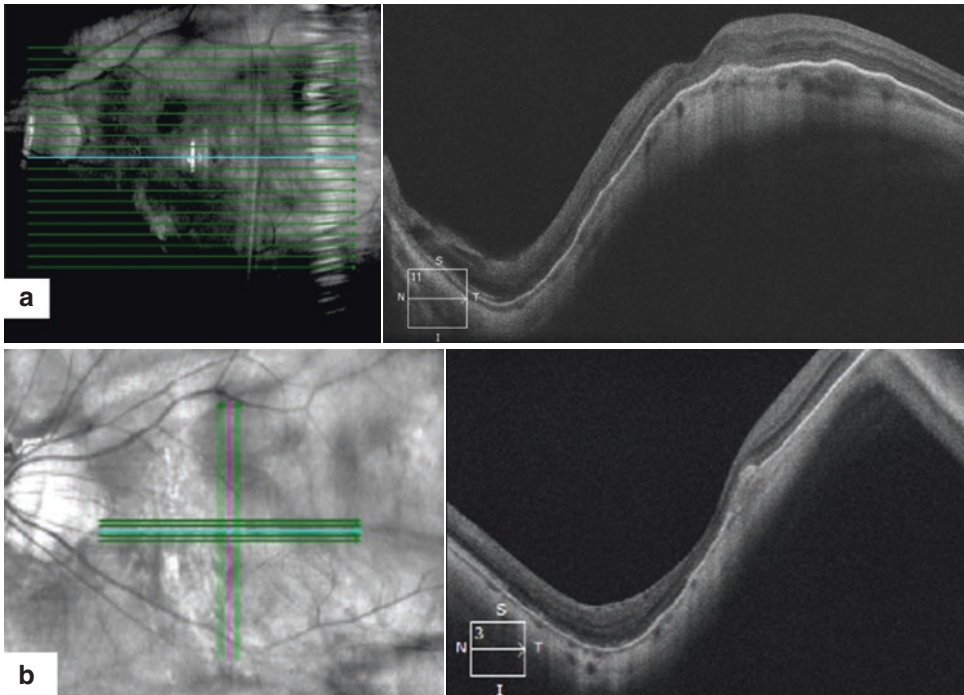
Fig. 23.19 (**a**) Postoperative OCT showing the convex shape of the posterior pole, 4 years after MB implantation. (**b**) OCT scan 2 months after MB removal. The shape of the posterior pole is convex and the fovea and choroid appear thinner. The juxtafoveal CNV occurred 1 year after MB implantation
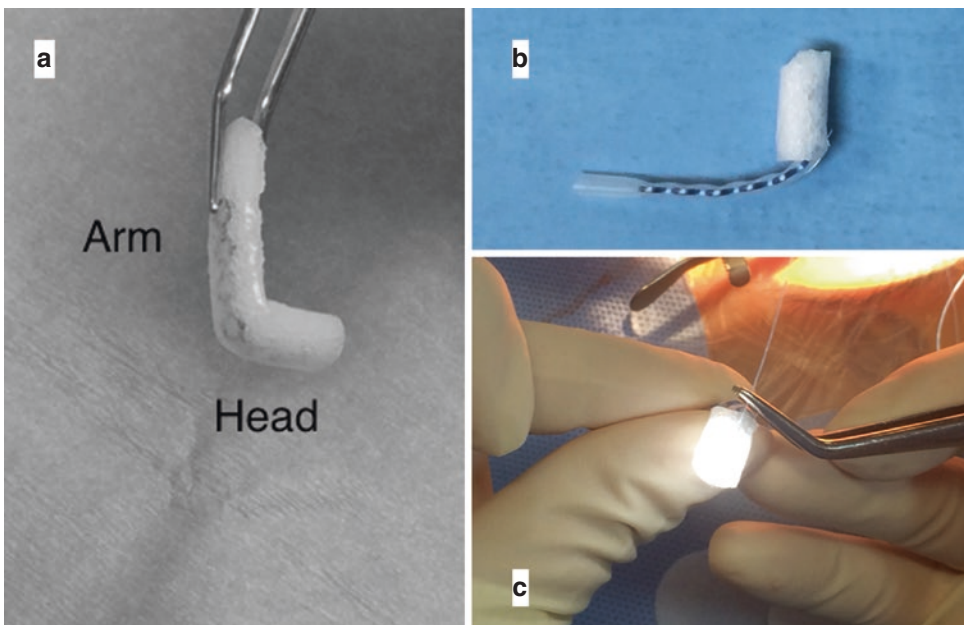
Fig. 23.20 Example of macular buckles used by the author. (**a**) First model of MB used. This MB was created with a stainless steel wire inserted into a silicon sponge. (**b**) Second model of MB. A titanium stent was covered by a silicon sleeve in the arm of the MB, while the head was covered by a silicon sponge. (**c**) Second model of MB with a fiber optic light inside the head, to control the final position of the buckle using scleral transillumination

by pushing the head behind the macular sclera, through the superotemporal quadrant, leaving the arm parallel to lateral without need of detaching any muscles. The sutures needed to stabilize the arm were placed anteriorly at the level of the insertion of the lateral rectus muscle. The first results were presented at the EVRS meeting in 2009 and at the Heatam meeting in 2009. Later, in 2011, the model was modified (Fig. 23.20b) by substituting the stainless steel stent with a titanium stent covered by a silicone sleeve (70 Labtician), in order to avoid the extrusion induced by the sponge. The solid silicone covering the head of the buckle was replaced with a soft sponge, with the aim to avoid atrophy of the RPE induced by acute angles of solid silicone. Moreover, to assess the final position of the MB, the use of a panoramic microscope and two optic fibers positioned into the pars plana and into the head of the buckle was adopted (Fig. 23.20c). The scleral transillumination helps the surgeon to manage the exact position of the buckle and center it underneath the fovea and in particular underneath the macular hole, if present. The size of the head of the buckle should be 7 mm by 8–10 mm to avoid the risk of inducing pain, diplopia, or limitations to eye movement.

The MB is positioned in the superotemporal quadrant with the lateral arm parallel either to the lateral or to the superior rectus muscle. The first option leads to buckle the macula from the temporal side to the nasal side. The second option leads to buckle the macula from 12 o'clock to 6 o'clock and parallel to the optic nerve. This position reduces the risk of optic nerve touch, extrusion, and diplopia.

The final shape of the posterior sclera should be as horizontal as possible, resembling the normal posterior pole. An excessive change in the shape of the macula, with a final convex profile, could induce metamorphopsia, unwanted tangential or excessive refractive modifications. Therefore, the most suitable shape for the head of the buckle is a flat one, in order to reach a flat scleral surface.

23.4 Personal Conclusions

Since 2000, I have extensively studied the complications of PM and MTM in particular. The unsatisfactory results obtained with PPV (both with and without peeling, and with any type of tamponade) by myself [73] and by other authors, as observed in the literature, convinced me of the idea that, only by treating the excessive elongation of the posterior scleral wall, it was possible to stop the complications of MTM.

The deformation of the sclera in PM reminded me the deformation of the ectasia of cornea in keratoconus. The posterior staphyloma could be defined as "scleroconus," since a modification in the scleral collagen is likely to produce the ectasia.

Taken to the limit, we could say that "it is the sclera that tends to detach from the retina and not the opposite."

We need to treat the sclera first and then, or simultaneously, the retina. Therefore, I felt induced to further explore the feasibility of macular buckling technique. My aim was to investigate a new model of MB, which could be easy to implant, to allow a wider use of the technique [58].

I have implanted, since 2004, more than 300 buckles, both alone and in combination with PPV, for all the complications of PM, macular hole macular detachment (MHMD), macular detachment without macular hole (MD), macular schisis (MS), and macular atrophy.

I have tried different models of buckling techniques, such as rubber bands, sutured at the insertion of the inferior and superior rectus muscle, passing through the inferior oblique muscle, or even pediatric Foley balloons, inflated with air or viscoelastic substances.

I could observe that the idea of buckling the macula was definitely successful to reach the anatomical goal. However, functional results were limited by the fact that I was operating with buckle only late cases that were failure of prior

vitrectomies and had already undergone many surgeries. Most of them had a large open macular hole and glaucoma secondary to the use of silicone oil. Moreover, surgery was still awkward and complicated.

The analysis of all my cases allowed me to notice that PPV, and recently PPV associated with ILM flap, addressed excellently the tangential vitreoretinal traction on the foveal profile induced by ERM and/or anomalous adherences between the vitreous and the ILM. MB addressed the perpendicular tractions and the retinal deformations, induced by scleral elongation.

> THE DEBATE "BUCKLE VERSUS VITRECTOMY" HAS NO MEANING

The frequently assisted debate "better buckle or vitrectomy" for MTM, in different scientific meetings, is not supported by evidence. The two techniques simply address two different problems and should be selected case by case or combined when necessary.

The target of treatment is double: the foveal profile and the retina with the sclera. The foveal profile should be treated with PPV and the retina with the sclera should be treated with MB.

If we had an ideal perfect model of MB, then we should propose MB to each patient with PM, not only to treat but also to prevent the well-known tractional and also atrophic consequences.

I am also convinced that one day, the changes in the structure of the sclera will be unraveled at a molecular level. At that time, we will be able to perform a crosslinking of the sclera.

Glossary and Terminology[1]

Inner Lamellar macular hole Inner lamellar macular hole (I-LMH) is a splitting of the foveal layers, developing from the internal limiting membrane (Fig. 23.21). The depth and width of the I-LMH may vary significantly but was not analyzed in the present study.

Inner Retinoschisis Inner retinoschisis (I-RS) is a splitting of the inner retinal layers, at different levels, from the inner nuclear layer to the ILM (Fig. 23.22). The ILM can be detached from the nerve fibers layer and connected to it with a column-like structure.

Macular detachment (MD) We defined macular detachment (MD), cases with neurosensory detachment (Fig. 23.23) with separation of the photoreceptors from the retinal pigment epithelium (RPE).

Outer Lamellar Macular Hole (O-LMH) Central splitting of the photoreceptors (Fig. 23.24). The width of the O-LMH may vary significantly but was not analyzed in the present study.

Outer RetinoSchisis Outer retinoschisis (O-RS) is a splitting of the outer retinal layers (Fig. 23.25), from the outer plexiform layer, that changes in a column-like structure, to the outer nuclear layer to the external limiting membrane.

Schisis Splitting of the neurosensory retina. Since, in most cases, the schisis interested the whole macula and not just the fovea, and since it could be found not only in the fovea but also (or only) in the extrafoveal area (Fig. 23.22), we avoided the term foveomacular schisis or foveoschisis and selected to use retinoschisis.

[1]We followed the definitions of retinoschisis suggested by Benhamou et al. [38]. We hereby provide the choices of glossary and terminology that were made in this study, in order to avoid any possible misinterpretation.
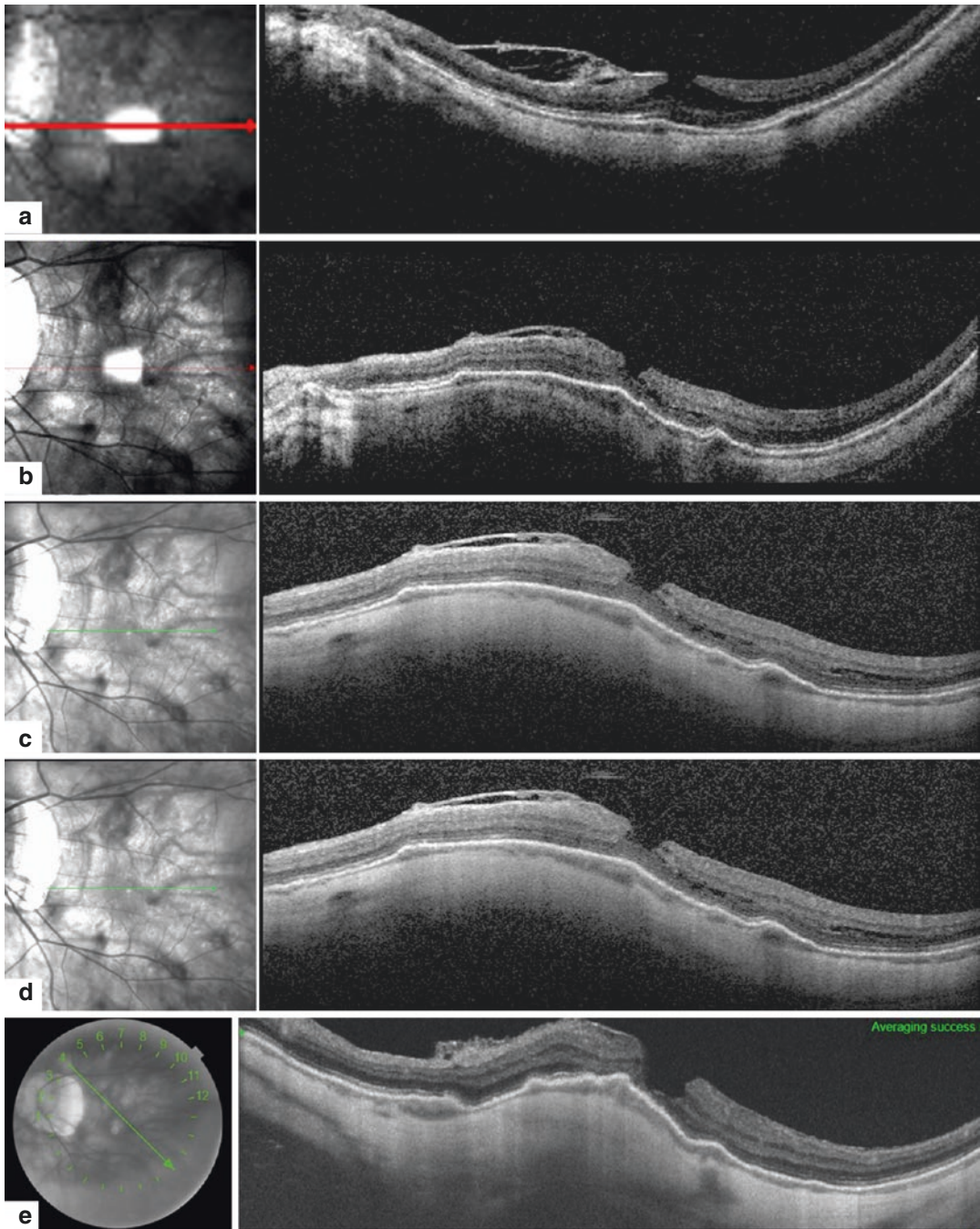
Fig. 23.21 Eye affected by MTM Stage 1a+ in a 50-year-old female. (**a**) Preoperative horizontal OCT shows inner macular schisis in the temporal extrafoveal area and epiretinal abnormalities with adhesions on one edge of the I-LMH. BCVA is 0.2 Snellen. (**b**) OCT, 1 month after MB. The inner schisis is no longer visible. The I-LMH size is smaller. The epiretinal abnormality is still well shown. (**c**) OCT, 6 months after MB. The inner schisis is no longer visible. The I-LMH is still well visible as well as the epiretinal abnormality. (**d**) OCT, 12 months after MB. The I-LMH is deeper. The epiretinal abnormality is less visible. (**e**) OCT, 18 months after MB. Slight progression of the I-LMH. BCVA is still 0.6. The Patient refused further surgery
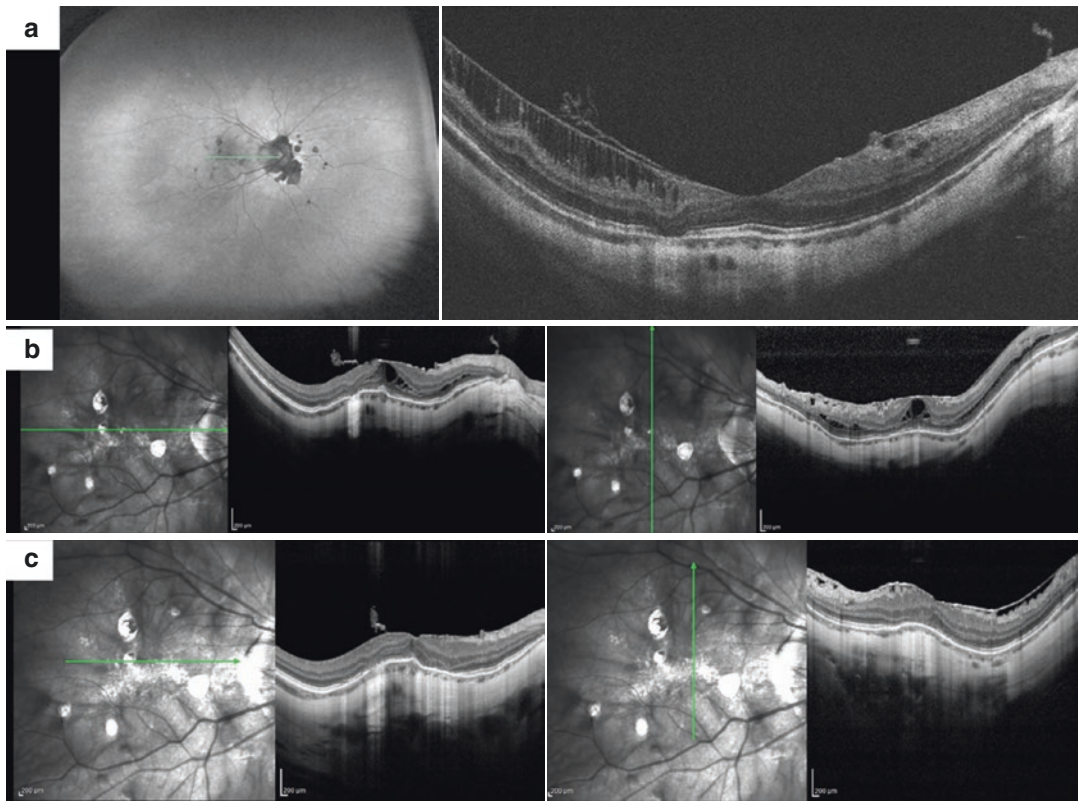
Fig. 23.22 Eye affected by MTM Stage 1a+ in a 44-year-old female. (**a**) Autofluorescence image, which shows a patchy atrophy pattern Category 3 according to the International Photographic Classification and Grading System. The OCT shows inner macular schisis in the temporal extrafoveal area with epiretinal abnormalities. (**b**) Horizontal and vertical OCT, 1 month after MB. The temporal inner schisis is no longer visible, although some schisis is still present in the nasal and inferior macula. An inner schisis, which was not present preoperatively, is visible now in the fovea. The epiretinal abnormality is still well shown in the horizontal scan with a different angle to the retina, due to the convex effect induced by the buckle. (**c**) Horizontal and vertical OCT, 1 year after MB. The schisis is no longer visible. The epiretinal abnormality is still well shown, but not inducing traction
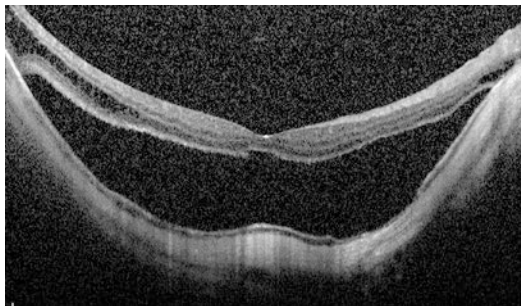
Fig. 23.23 Eye affected by MTM Stage 4a in a 65-year-old female. The macula is involved with a detachment and no schisis is visible except for the extreme temporal edge of the macula
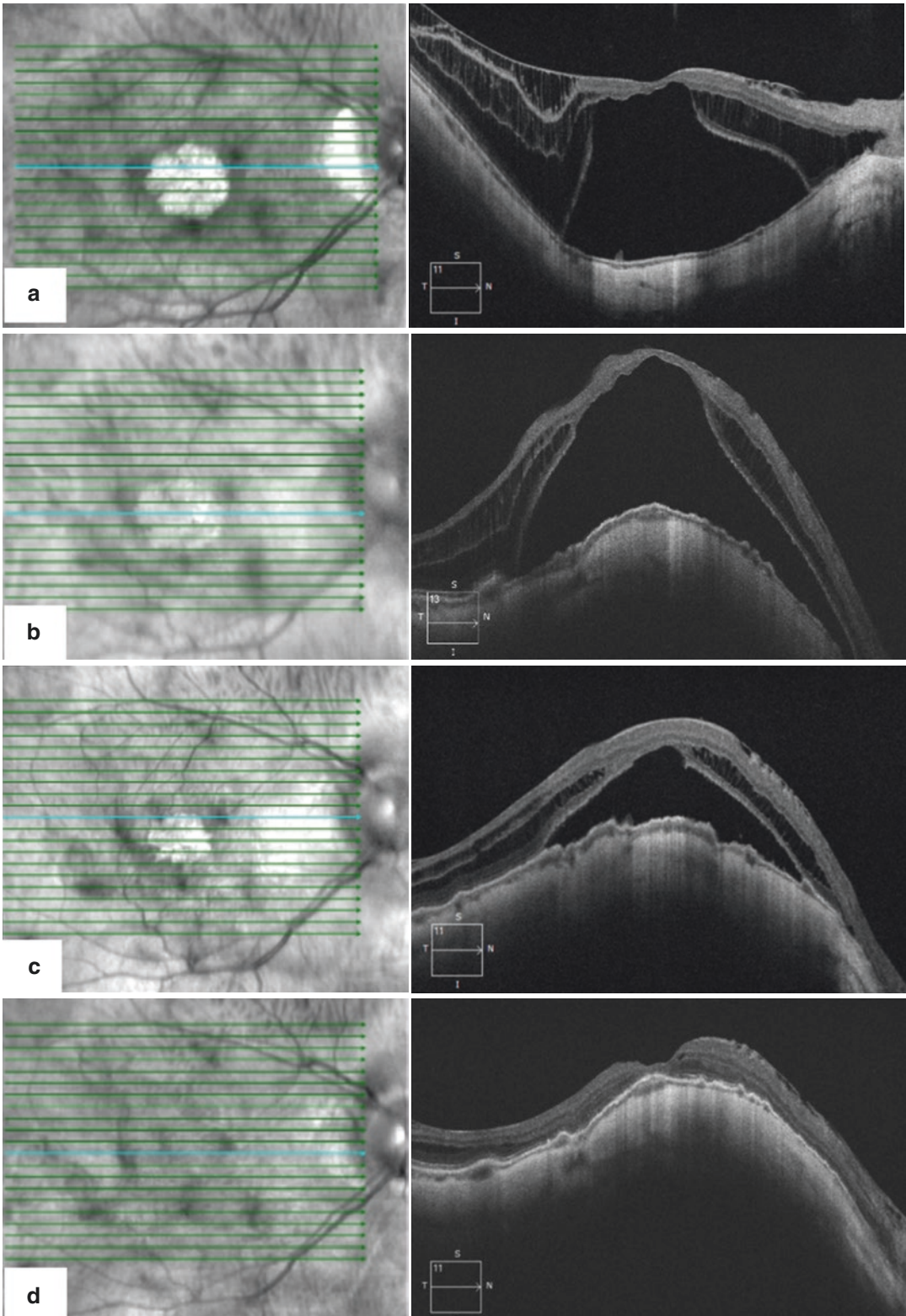
Fig. 23.24 Eye affected by MTM stage 3aO+. (**a**) Preoperative OCT showing the macular schisis and detachment associated with an O-LMH and mild epireti-nal abnormalities. (**b–e**) Progressive resolution of the disease after MB, 1, 3, 6, and 12 months, respectively. The profile of the sclera is inverted by the MB
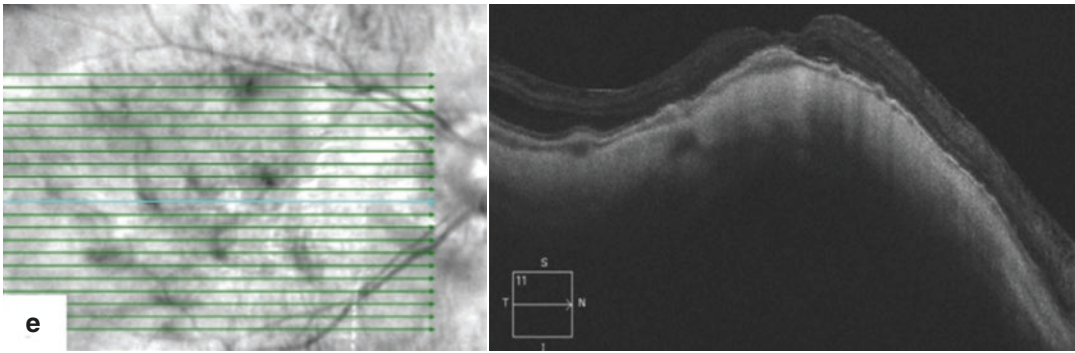
Fig. 23.24 (continued)
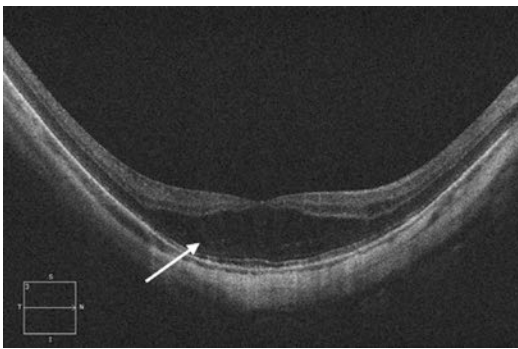
Fig. 23.25 Eye affected by MTM Stage 2a in a 48-year-old female. OCT scan showing schisis in the outer layers of the retina in the fovea

References

1. Resnikoff S, Pascolini D, Mariotti SP, Pokharel GP. Global magnitude of visual impairment caused by uncorrected refractive errors in 2004. Bull World Health Organ. 2008;86(1):63–70.

2. Pan C-W, Ramamurthy D, Saw S-M. Worldwide prevalence and risk factors for myopia. Ophthalmic Physiol Opt. 2012;32(1):3–16. https://doi.org/10.1111/j.1475-1313.2011.00884.x.

3. Tron E. Über die optischen Grundlagen der Ametropie. Albr von Græfes Arch für Ophthalmol. 1934;132(2):182–223. https://doi.org/10.1007/BF01853824.

4. Silva R. Myopic maculopathy: a review. Ophthalmologica. 2012;228(4):197–213. https://doi.org/10.1159/000339893.

5. Wolf S, Balciuniene VJ, Laganovska G, et al. RADIANCE: a randomized controlled study of ranibizumab in patients with choroidal neovascularization secondary to pathologic myopia. Ophthalmology. 2014;121:682–92.

6. Hayashi K, Ohno-Matsui K, Shimada N, et al. Long-term pattern of progression of myopic maculopathy: a natural history study. Ophthalmology. 2010;117(8):1595–611, 1611.e1–4. https://doi.org/10.1016/j.ophtha.2009.11.003.

7. Sawada A, Tomidokoro A, Araie M, Iwase A, Yamamoto T. Refractive errors in an elderly Japanese population: the Tajimi study. Ophthalmology. 2008;115(2):363–70. e3. https://doi.org/10.1016/j.ophtha.2007.03.075.

8. Pi L-H, Chen L, Liu Q, et al. Prevalence of eye diseases and causes of visual impairment in school-aged children in Western China. J Epidemiol. 2012;22(1):37–44.

9. Attebo K, Ivers RQ, Mitchell P. Refractive errors in an older population: the Blue Mountains Eye Study. Ophthalmology. 1999;106(6):1066–72. https://doi.org/10.1016/S0161-6420(99)90251-8.

10. Mitchell P, Hourihan F, Sandbach J, Wang JJ. The relationship between glaucoma and myopia: the Blue Mountains Eye Study. Ophthalmology. 1999;106(10):2010–5.

11. Vongphanit J, Mitchell P, Wang JJ. Prevalence and progression of myopic retinopathy in an older population. Ophthalmology. 2002;109(4):704–11.

12. Hu DN. Prevalence and mode of inheritance of major genetic eye diseases in China. J Med Genet. 1987;24(10):584–8.

13. Liu HH, Xu L, Wang YX, Wang S, You QS, Jonas JB. Prevalence and progression of myopic retinopathy in Chinese adults: the Beijing Eye Study. Ophthalmology. 2010;117(9):1763–8. https://doi.org/10.1016/j.ophtha.2010.01.020.

14. Gao LQ, Liu W, Liang YB, et al. Prevalence and characteristics of myopic retinopathy in a rural Chinese adult population: the Handan Eye Study. Arch Ophthalmol. 2011;129(9):1199–204. https://doi.org/10.1001/archophthalmol.2011.230.

15. Asakuma T, Yasuda M, Ninomiya T, et al. Prevalence and risk factors for myopic retinopathy in a Japanese population: the Hisayama Study. Ophthalmology. 2012;119(9):1760–5. https://doi.org/10.1016/j.ophtha.2012.02.034.

16. Cedrone C, Nucci C, Scuderi G, Ricci F, Cerulli A, Culasso F. Prevalence of blindness and low vision in an Italian population: a comparison with other European studies. Eye (Lond). 2006;20(6):661–7. https://doi.org/10.1038/sj.eye.6701934.

17. Klaver CC, Wolfs RC, Vingerling JR, Hofman A, de Jong PT. Age-specific prevalence and causes of blindness and visual impairment in an older population: the Rotterdam Study. Arch Ophthalmol. 1998;116(5):653–8.

18. Cotter SA, Varma R, Ying-Lai M, Azen SP, Klein R. Causes of low vision and blindness in adult Latinos: the Los Angeles Latino Eye Study. Ophthalmology. 2006;113(9):1574–82. https://doi.org/10.1016/j.ophtha.2006.05.002.

19. Montero JA, Ruiz-Moreno JM. Treatment of choroidal neovascularization in high myopia. Curr Drug Targets. 2010;11(5):630–44.

20. Daubs J. Environmental factors in the epidemiology of malignant myopia. Am J Optom Physiol Optic. 1982;59(3):271–7.

21. Daubs JG. Some geographic, environmental and nutritive concomitants of malignant myopia. Ophthalmic Physiol Opt. 1984;4(2):143–9.

22. Ruiz-Medrano J, Montero JA, Flores-Moreno I, Arias L, García-Layana A, Ruiz-Moreno JM. Myopic maculopathy: current status and proposal for a new classification and grading system (ATN). Prog Retin Eye Res. 2018;69:80. https://doi.org/10.1016/j.preteyeres.2018.10.005.

23. Phillips C. Retinal detachment at the posterior pole. Br J Ophthalmol. 1958;42:749–53.

24. Takano M, Kishi S. Foveal retinoschisis and retinal detachment in severely myopic eyes with posterior staphyloma. Am J Ophthalmol. 1999;128(4):472–6.

25. Panozzo G, Mercanti A. Optical coherence tomography findings in myopic traction maculopathy. Arch Ophthalmol. 2004;122(10):1455–60. https://doi.org/10.1001/archopht.122.10.1455.

26. Shimada N, Yoshida T, Sugamoto Y, et al. Progression from macular retinoschisis to retinal detachment in highly myopic eyes is associated with outer lamellar hole formation. Br J Ophthalmol. 2008;92(6):762–4. https://doi.org/10.1136/bjo.2007.131359.

27. Wallman J. Myopia and the control of eye growth. Introduction. Ciba Found Symp. 1990.

28. Tkatchenko TV, Shen Y, Tkatchenko AV. Mouse experimental myopia has features of primate myopia. Investig Ophthalmol Vis Sci. 2010;51:1297. https://doi.org/10.1167/iovs.09-4153.

29. Dell'Omo R, Virgili G, Bottoni F, et al. Lamellar macular holes in the eyes with pathological myopia. Graefes Arch Clin Exp Ophthalmol. 2018;256:1281. https://doi.org/10.1007/s00417-018-3995-8.

30. Zampedri E, Romanelli F, Semeraro F, Parolini B, Frisina R. Spectral-domain optical coherence tomography findings in idiopathic lamellar macular hole. Graefes Arch Clin Exp Ophthalmol. 2017;255(4):699–707. https://doi.org/10.1007/s00417-016-3545-1.

31. Shimada N, Tanaka Y, Tokoro T, Ohno-Matsui K. Natural course of myopic traction maculopathy and factors associated with progression or resolution. Am J Ophthalmol. 2013;156(5):948–57.e1. https://doi.org/10.1016/j.ajo.2013.06.031.

32. Road R, Province H, Province H. Diagnosis and maculopathy treatment of myopic traction. 2012. https://doi.org/10.3980/j.issn.2222-3959.2012.06.19.

33. Gaucher D, Haouchine B, Tadayoni R, et al. Long-term follow-up of high myopic foveoschisis: natural course and surgical outcome. Am J Ophthalmol. 2007;143(3):455–62. https://doi.org/10.1016/j.ajo.2006.10.053.

34. Ichibe M, Baba E, Funaki S, Yoshizawa T, Abe H. Retinoschisis in a highly myopic eye without vision impairment. Retina. 2004;24(2):331–3.

35. Panozzo G, Mercanti A. Vitrectomy for myopic traction maculopathy. Arch Ophthalmol. 2007;125(6):767–72. https://doi.org/10.1001/archopht.125.6.767.

36. Fujimoto M, Hangai M, Suda K, Yoshimura N. Features associated with foveal retinal detachment in myopic macular retinoschisis. Am J Ophthalmol. 2010;150(6):863–70. https://doi.org/10.1016/j.ajo.2010.06.023.

37. Fang X, Weng Y, Xu S, et al. Optical coherence tomographic characteristics and surgical outcome of eyes with myopic foveoschisis. Eye (Lond). 2009;23(6):1336–42. https://doi.org/10.1038/eye.2008.291.

38. Benhamou N, Massin P, Haouchine B, Erginay A, Gaudric A. Macular retinoschisis in highly myopic eyes. Am J Ophthalmol. 2002;133(6):794–800.

39. Sun CB, Liu Z, Xue AQ, Yao K. Natural evolution from macular retinoschisis to full-thickness macular hole in highly myopic eyes. Eye (Lond). 2010;24(12):1787–91. https://doi.org/10.1038/eye.2010.123.

40. Sayanagi K, Ikuno Y, Soga K, Tano Y. Photoreceptor inner and outer segment defects in myopic foveoschisis. Am J Ophthalmol. 2008;145(5):902–8. https://doi.org/10.1016/j.ajo.2008.01.011.

41. Ripandelli G, Rossi T, Scarinci F, Scassa C, Parisi V, Stirpe M. Macular vitreoretinal interface abnormalities in highly myopic eyes with posterior staphyloma: 5-year follow-up. Retina. 2012;32(8):1531–8. https://doi.org/10.1097/IAE.0b013e318255062c.

42. Shevelev M. Operation against high myopia and scleralectasia with aid of the transplantation of fascia lata on thinned sclera. Russ Oftalmol J. 1930;11(1):107–10.

43. Siam AL. Management of central retinal detachment due to a macular hole. Br J Ophthalmol. 1973;57(5):351–4.

44. Schepens CL, Okamura ID, Brockhurst RJ. The scleral buckling procedures. I. Surgical techniques and management. AMA Arch Ophthalmol. 1957;58(6):797–811.

45. Borley WE, Snyder AA. Surgical treatment of degenerative myopia; the combined lamellar scleral resection with scleral reinforcement using donor eye. Trans Pac Coast Otoophthalmol Soc Annu Meet. 1958;39:275–91; discussion 292–4.

46. Curtin B. Surgical support of the posterior sclera: part II. Clinical results. Am J Ophthalmol. 1961;52:253.

47. Snyder AA, Thompson FB. A simplified technique for surgical treatment of degenerative myopia. Am J Ophthalmol. 1972;74(2):273–7.

48. Momose A. Surgical treatment of myopia—with special references to posterior scleral support operation and radial keratotomy. Indian J Ophthalmol. 1983;31(6):759–67.

49. Pruett R. Chapter 121: Myopia (posterior segment). In: Master techniques in ophthalmic surgery. Williams & Wilkins; 1995.

50. Curtin BJ, Whitmore WG. Long-term results of scleral reinforcement surgery. Am J Ophthalmol. 1987;103(4):544–8.

51. Calabria GA, Pruett RC, Refojo MF, Schepens CL. Sutureless scleral buckling. An experimental technique. Arch Ophthalmol. 1970;83(5):613–8.

52. Theodossiadis GP, Theodossiadis PG. Optical coherence tomography in optic disk pit maculopathy treated by the macular buckling procedure. Am J Ophthalmol. 2001;132(2):184–90.

53. Theodossiadis GP, Sasoh M. Macular buckling for retinal detachment due to macular hole in highly myopic eyes with posterior staphyloma. Retina. 2002;22(1):129.

54. Rosengren B. The silver plomb method in amotio retinae: clinical experience and results. Bibl Ophthalmol. 1966;70:253–6.

55. Klöti R. Silver clip for central retinal detachments with macular hole. Mod Probl Ophthalmol. 1974;12:330–6.

56. Maćkowiak A. Retinal detachment surgery for giant tear or macular hole. The oblique encircling silastic band without evacuation of subretinal flui. Jpn J Ophthalmol. 1970;18:245.

57. Mateo C, Burés-Jelstrup A, Navarro R, Corcóstegui B. Macular buckling for eyes with myopic foveoschisis secondary to posterior staphyloma. Retina. 2012;32(6):1121–8. https://doi.org/10.1097/IAE.0b013e31822e5c32.

58. Parolini B, Frisina R, Pinackatt S, Mete M. A new L-shaped design of macular buckle to support a posterior staphyloma in high myopia. Retina. 2013;33(7):1466–70. https://doi.org/10.1097/IAE.0b013e31828e69ea.

59. Gonvers M, Machemer R. A new approach to treating retinal detachment with macular hole. Am J Ophthalmol. 1982;94(4):468–72.

60. Vallat M. Surgical treatment of retinal detachment from macular hole. Graefes Arch Clin Exp Ophthalmol. 1986;224(3):238–9.

61. Oshima Y. Complete epiretinal membrane separation in highly myopic eyes with retinal detachment resulting from a macular hole. Am J Ophthalmol. 1998;126(5):669–76.

62. Wolfensberger TJ, Gonvers M. Long-term follow-up of retinal detachment due to macular hole in myopic eyes treated by temporary silicone oil tamponade and laser photocoagulation. Ophthalmology. 1999;106(9):1786–91. https://doi.org/10.1016/S0161-6420(99)90344-5.

63. Kadonosono K, Yazama F, Itoh N, et al. Treatment of retinal detachment resulting from myopic macular hole with internal limiting membrane removal. Am J Ophthalmol. 2001;131(2):203–7.

64. Lu L, Li Y, Cai S, Yang J. Vitreous surgery in highly myopic retinal detachment resulting from a macular hole. Clin Exp Ophthalmol. 2002;30(4):261–5.

65. Kuhn F. Internal limiting membrane removal for macular detachment in highly myopic eyes. Am J Ophthalmol. 2003;135(4):547–9.

66. Kanda S, Uemura A, Sakamoto Y, Kita H. Vitrectomy with internal limiting membrane peeling for macular retinoschisis and retinal detachment without macular hole in highly myopic eyes. Am J Ophthalmol. 2003;136(1):177–80.

67. Ikuno Y, Sayanagi K, Ohji M, et al. Vitrectomy and internal limiting membrane peeling for myopic foveoschisis. Am J Ophthalmol. 2004;137(4):719–24. https://doi.org/10.1016/j.ajo.2003.10.019.

68. Scholda C. Primary silicone oil tamponade without retinopexy in highly myopic eyes with central macular hole detachments. Retina. 2005;25(2):141–6.

69. Chen Y. Treatment of retinal detachment resulting from posterior staphyloma-associated macular hole in highly myopic eyes. Retina. 2006;26(1):25–31.

70. Kokame GT, Yamamoto I. Silicone oil versus gas tamponade. Ophthalmology. 2004;111(4):851–2.

71. Rizzo S. Successful treatment of persistent macular holes using "heavy silicone oil" as intraocular tamponade. Retina. 2006;26(8):905–8.

72. Cheung B. Results of high-density silicone oil as a tamponade agent in macular hole retinal detachment in patients with high myopia. Br J Ophthalmol. 2007;91(6):719–21.

73. Mete M, Parolini B, Maggio E, Pertile G. 1000 cSt silicone oil vs heavy silicone oil as intraocular tamponade in retinal detachment associated to myopic macular hole. Graefes Arch Clin Exp Ophthalmol. 2011;249(6):821–6.

74. Sasoh M, Yoshida S, Ito Y, Matsui K, Osawa S, Uji Y. Macular buckling for retinal detachment due to macular hole in highly myopic eyes with posterior staphyloma. Retina. 2000;20(5):445–9.

75. Ripandelli G, Coppé AM, Fedeli R, Parisi V, D'Amico DJ, Stirpe M. Evaluation of primary surgical procedures for retinal detachment with macular hole in highly myopic eyes: a comparison [corrected] of vitrectomy versus posterior episcleral buckling surgery. Ophthalmology. 2001;108(12):2258–64; discussion 2265.

76. Theodossiadis GP, Theodossiadis PG. The macular buckling procedure in the treatment of retinal detachment in highly myopic eyes with macular hole and posterior staphyloma: mean follow-up of 15 years. Retina. 2005;25(3):285–9.

77. Tanaka T, Ando FUM. Episcleral macular buckling by semirigid shaped-rod exoplant for recurrent retinal detachment with macular hole in highly myopic eyes. Retina. 2005;25(2):147–51.

78. Ward B, Tarutta EP, Mayer MJ. The efficacy and safety of posterior pole buckles in the control of progressive high myopia. Eye (Lond). 2009;23(12):2169–74. https://doi.org/10.1038/eye.2008.433.

79. Tian J, Tang L-S, Guo X-J, Luo Y-H. Episcleral macular buckling for posterior retinal detachment in silicone oil filled eyes associated with myopic macular hole. Int J Ophthalmol. 2013;6(2):165–8. https://doi.org/10.3980/j.issn.2222-3959.2013.02.11.

80. Sasaki H, Shiono A, Kogo J, et al. Inverted internal limiting membrane flap technique as a useful procedure for macular hole-associated retinal detachment in highly myopic eyes. Eye (Lond). 2017;31(4):545–50. https://doi.org/10.1038/eye.2016.263.

81. Yuan J, Zhang L-L, Lu Y-J, Han M-Y, Yu A-H, Cai X-J. Vitrectomy with internal limiting membrane peeling versus inverted internal limiting membrane flap technique for macular hole-induced retinal detachment: a systematic review of literature and meta-analysis. BMC Ophthalmol. 2017;17(1):219. https://doi.org/10.1186/s12886-017-0619-8.

82. Kinoshita T, Onoda Y, Maeno T. Long-term surgical outcomes of the inverted internal limiting membrane flap technique in highly myopic macular hole reti-nal detachment. Graefes Arch Clin Exp Ophthalmol. 2017;255(6):1101–6. https://doi.org/10.1007/s00417-017-3614-0.

83. Alkabes M, Mateo C. Macular buckle technique in myopic traction maculopathy: a 16-year review of the literature and a comparison with vitreous surgery. Graefes Arch Clin Exp Ophthalmol. 2018;256(5):863–77. https://doi.org/10.1007/s00417-018-3947-3.

84. Figueroa MS, Ruiz-Moreno JM, Gonzalez del Valle F, et al. Long-term outcomes of 23-gauge pars plana vitrectomy with internal limiting membrane peeling and gas tamponade for myopic traction maculopathy. Retina. 2015;35(9):1836–43. https://doi.org/10.1097/IAE.0000000000000554.

85. Guo X, Xiao O, Chen Y, et al. Three-dimensional eye shape, myopic maculopathy, and visual acuity: the Zhongshan Ophthalmic Center–Brien Holden Vision Institute High Myopia Cohort Study. Ophthalmology. 2017;124(5):679–87. https://doi.org/10.1016/j.ophtha.2017.01.009.

86. Hsiang HW, Ohno-Matsui K, Shimada N, et al. Clinical characteristics of posterior staphyloma in eyes with pathologic myopia. Am J Ophthalmol. 2008;146(1):102–10. https://doi.org/10.1016/j.ajo.2008.03.010.

87. Landolfo V, Albini L, Romano A. Macular hole induced retinal detachment: treatment with an armed silicone implant. Ophthalmic Surg. 1986;17(12):810–2.

Surgery for Myopic Traction Maculopathy

24

Taku Wakabayashi

24.1 Introduction

Myopic traction maculopathy (MTM) is a macular complication associated with high myopia characterized by retinal thickening, retinoschisis, lamellar macular hole, and foveal retinal detachment (Fig. 24.1) [1–3]. The natural course of MTM is not favorable [4]. In the natural course of macular retinoschisis studied in 29 eyes, foveoschisis and visual acuity worsened in 20 (69%) eyes and a macular hole developed in 9 (31%) eyes over a 3-year follow-up [5]. Another study reported that 4 (50%) out of 8 eyes with macular retinoschisis developed macular hole or retinal detachment after 2 years [6]. The progression of MTM seems to be caused by an assembly of retinal traction from the adherent vitreous cortex, epiretinal membrane, internal limiting membrane (ILM), retinal vessels, and posterior staphyloma [7, 8]. Therefore, release of the retinal traction by surgery is theoretically effective in resolving MTM and preventing macular hole and macular hole retinal detachment.

24.1.1 Surgical Indications

Early stages of MTM without foveal detachment are relatively stable and asymptomatic (Fig. 24.2).

These cases are not indicated for vitreous surgery. Even though patients are aware of slight visual impairment, early surgery is not necessary because approximately 84% of the eyes are stable during the 3-year follow-up [9]. In addition, there is a risk of worsening of visual acuity after surgery in eyes with good visual acuity. Because surgery before macular hole formation is considered beneficial, the best indication for surgery is moderate-to-severe vision loss associated with the presence of foveal detachment.

24.2 Surgical Procedure

24.2.1 Vitreous Separation

A 25-gauge transconjunctival microincision vitrectomy system is usually used for MTM surgery [10]. Core vitrectomy followed by posterior vitreous detachment is performed. The vitreous adheres to the retinal surface in highly myopic eyes. Triamcinolone acetonide is useful in visualizing residual vitreous cortex. To remove the posterior vitreous, a vitreous cutter is usually used. A diamond-dusted membrane scraper is an alternate way to excise the thin vitreous cortex. Because the vitreous cortex adheres strongly to the fovea, the vitreous at the fovea should be excised with caution to avoid macular hole formation.

T. Wakabayashi (✉)
Department of Ophthalmology, Osaka University
Graduate School of Medicine, Osaka, Japan
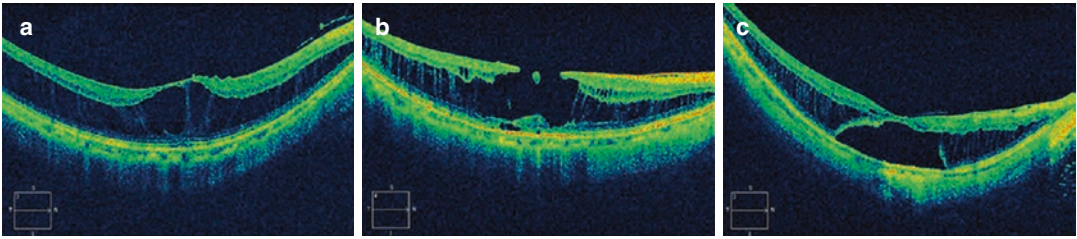
Fig. 24.1 Representative images of myopic traction maculopathy demonstrating (**a**) retinoschisis, (**b**) lamellar macular hole, and (**c**) foveal retinal detachment
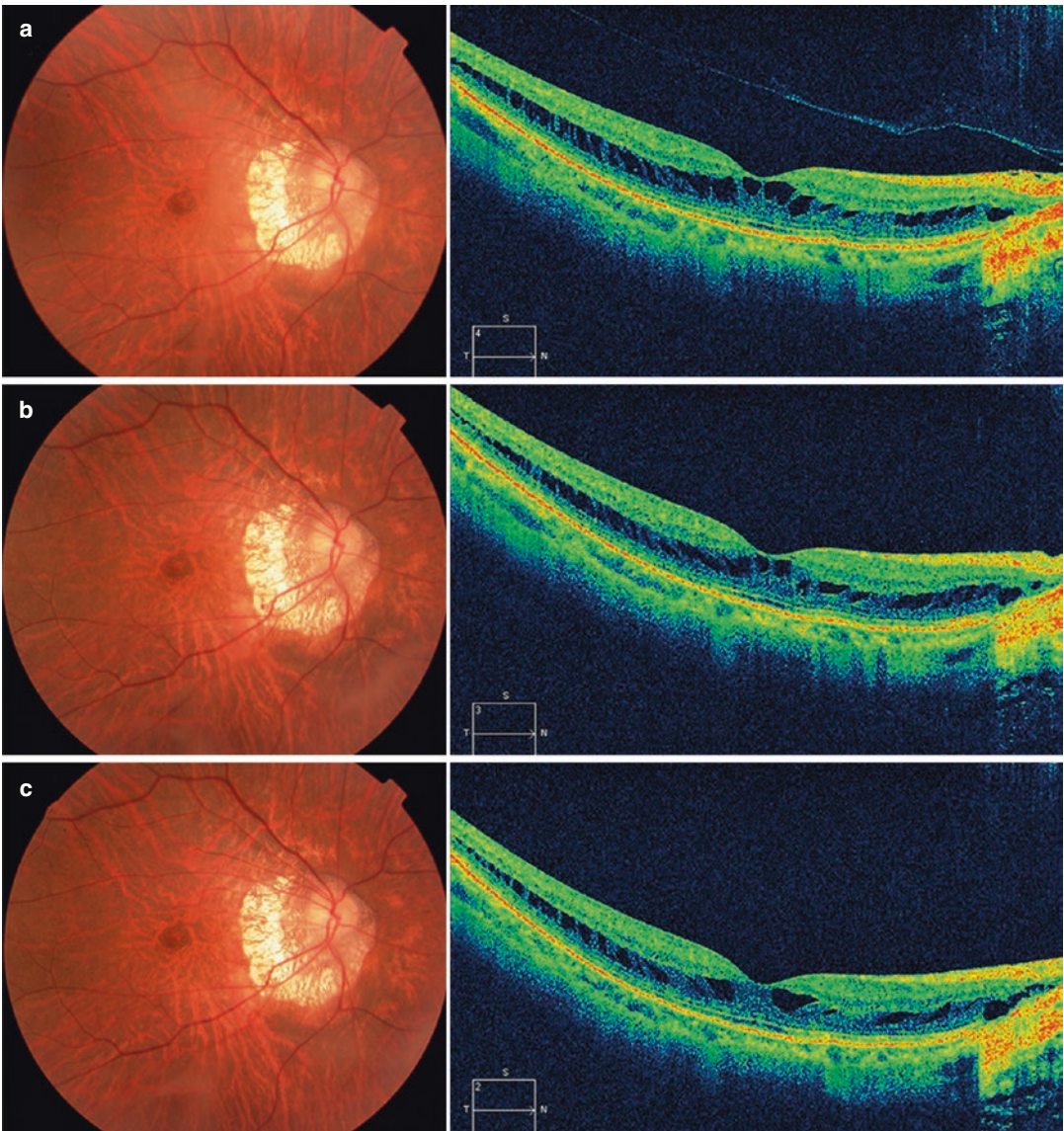
Fig. 24.2 Early stages of myopic traction maculopathy (retinoschisis) without foveal detachment. (**a**) The axial length was 28.8 mm and decimal visual acuity (VA) is 1.5. (**b**) Six months later. VA is 1.5. (**c**) One year later. VA remains 1.5

24.2.2   Internal Limiting Membrane Peeling

The necessity of ILM peeling remains controversial in MTM surgery, because some studies report that MTM can be treated by vitrectomy without ILM peeling [11, 12]. However, rigidity of the ILM seems to play a major role in the pathogenesis of MTM [13, 14]. Therefore, ILM peeling is usually performed during vitrectomy. A long-shaft forceps is used for ILM peeling. The excision of ILM can also cause removal of the residual ERM and scaffold for potential myofibroblast proliferation. Thus, indocyanine green has been used to stain the ILM; however, toxicity has been reported. Brilliant Blue G can selectively stain the ILM without toxicity.

24.2.3   Fovea-Sparing Internal Limiting Membrane Peeling

A serious complication associated with ILM peeling in MTM is the development of full-thickness macular hole postoperatively (Fig. 24.3) [15, 16]. The mechanical traction on the thinned central fovea by peeling the ILM may cause a break in the central fovea especially in eyes with foveal detachment. To avoid the development of a macular hole, fovea-sparing ILM peeling has been proposed [16, 17]. The ILM is peeled off in a circular fashion around the fovea and the ILM attached to the fovea is left intact (Fig. 24.4). In other words, the ILM is peeled from the entire macular area except the fovea. This technique can almost completely avoid the
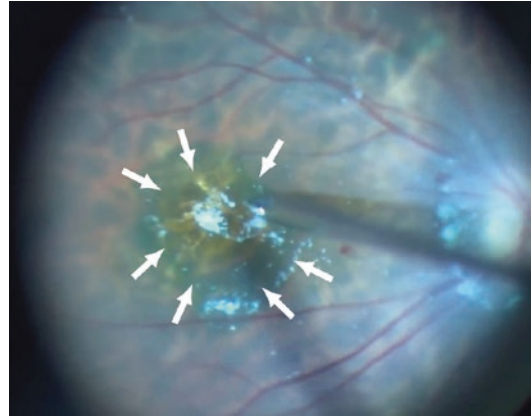
Fig. 24.4 Fovea-sparing internal limiting membrane (ILM) peeling. The ILM around the fovea was peeled off in a circular fashion, and the ILM attached to the fovea was left intact (arrowheads)

Fig. 24.3 Optical coherence tomography images depicting postoperative macular hole formation associated with internal limiting membrane (ILM) peeling. (**a**) Preoperative image shows the lamellar macular hole. (**b**) Postoperative image shows the development of macular hole after vitrectomy with standard ILM peeling
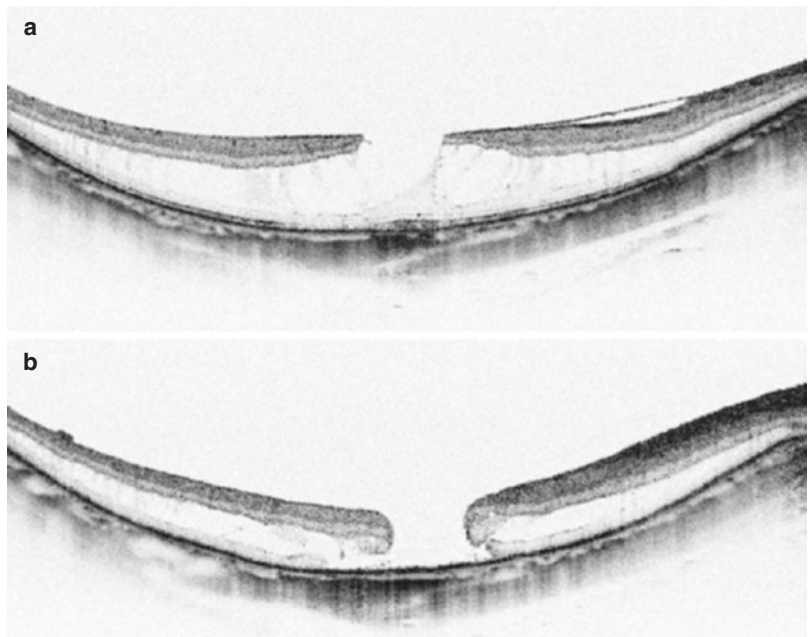
formation of a macular hole postoperatively. Shimada et al. reported that a full-thickness macular hole developed in 16% of the eyes in the complete ILM peeled group and none of the eyes in the fovea-sparing ILM group [16]. In our series, 8% of the eyes with complete ILM peeling had postoperative full-thickness macular holes, while none of the eyes that underwent fovea-sparing ILM peeling developed a macular hole postoperatively.

24.2.4 Tamponade

Air, sulfur hexafluoride (SF_6), perfluoropropane (C_3F_8), or silicone oil (SO) are used as tamponade materials to treat MTM. Zheng et al. reported faster recovery of normal retinal anatomy and significant improvement in visual acuity in eyes in which gas tamponade was used [18]. However, MTM can be treated without tamponade (only fluid) if the traction is completely removed by surgery [19]. A study comparing gas versus no-gas tamponade in the treatment of MTM found no significant differences in visual outcomes [20]. Long-lasting tamponade may prevent the development of a postoperative macular hole or macular hole retinal detachment; however, there has been no evidence to support this idea. Therefore, use of the gas tamponade is still controversial.

24.2.5 Surgical Prognosis After Vitrectomy with ILM Peeling

The retina reattaches gradually after surgery. It takes longer than 1 year in some cases. The visual outcomes after MTM surgery are favorable if no macular hole develops postoperatively (Fig. 24.5). Hattori et al. reported the surgical outcomes after vitrectomy with ILM peeling in 79 eyes with MTM [21]. The logMAR visual acuity improved significantly from 0.63 ± 0.37 to 0.51 ± 0.36 at 6 months ($P < 0.001$). The logMAR visual acuity improved significantly in retinoschisis type ($P = 0.026$) and foveal detachment type ($P = 0.013$). The lamellar MH type showed

no significant differences between pre- and postoperative visual acuity; however, visual acuity tended to be better postoperatively ($P = 0.061$). Taniguchi et al. reported the surgical outcomes after vitrectomy with ILM peeling in 61 eyes with MTM [22]. The logMAR visual acuity improved significantly from 0.67 ± 0.42 to 0.45 ± 0.36 at 12 months ($P = 0.001$). Figueroa et al. reported surgical outcomes after 23-gauge vitrectomy with ILM peeling in 30 eyes with MTM [23]. The logMAR visual acuity significantly improved from 0.66 ± 0.40 to 0.59 ± 0.53 at a mean follow-up of 33.8 ± 13 months ($P = 0.044$). Hwang JU et al. reported surgical outcomes after 23-gauge or 25-gauge vitrectomy with ILM peeling in 33 eyes with MTM [10]. The logMAR visual acuity significantly improved from 1.01 ± 0.47 to 0.76 ± 0.64 at a mean follow-up of 19.3 ± 12.8 months ($P = 0.004$). Ikuno et al. reported significant improvement in visual acuity after vitrectomy in both eyes with and without foveal detachment; however, visual gain was significantly better in eyes with foveal detachment than in eyes without foveal detachment [24]. Similarly, Kumagai et al. reported that 70% of the eyes with foveal detachment had a significant visual improvement compared with 42% of the eyes without foveal detachment [25]. The postoperative visual acuity also varies depending on the degree of chorioretinal atrophy. If the chorioretinal atrophy involves the fovea, the visual outcome is not favorable despite successful surgery.

24.2.6 Standard ILM Peeling Versus Fovea-Sparing ILM Peeling

Shimada et al. first reported the visual outcomes after fovea-sparing ILM peeling [16]. In their study, preoperative logMAR visual acuity (0.74 ± 0.50 [standard ILM peeling group], 0.65 ± 0.50 [fovea-sparing ILM peeling group]) and postoperative logMAR visual acuity (0.58 ± 0.60 [standard ILM peeling group], 0.34 ± 0.40 [fovea-sparing ILM peeling group]) did not differ significantly between standard ILM peeling and fovea-sparing ILM peeling. However, the postoperative visual acuity was significantly
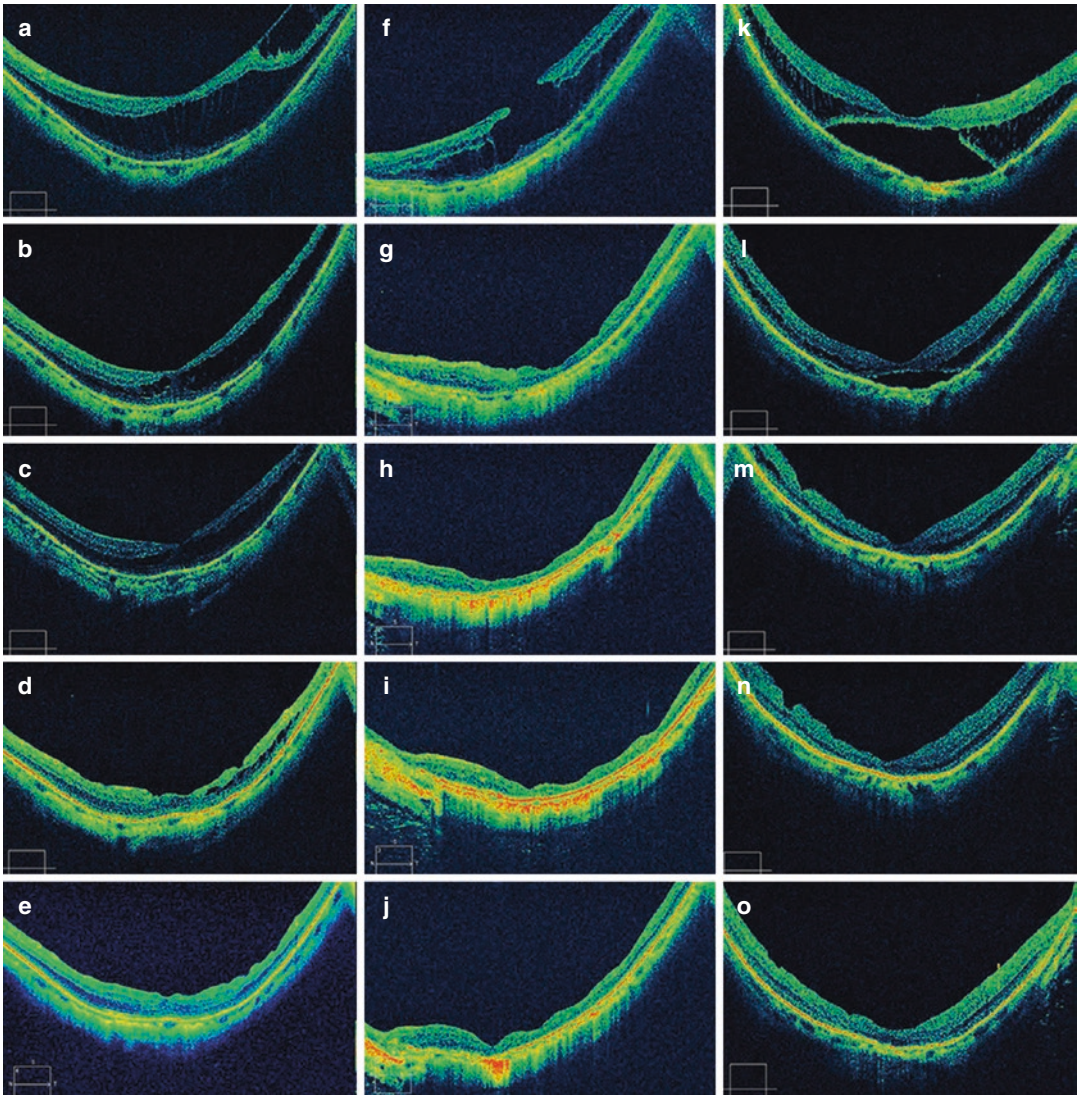
Fig. 24.5 Myopic traction maculopathy treated by vitrectomy with standard ILM peeling. (**a**) Spectral domain-optical coherence tomography (SD-OCT) image at initial presentation confirmed retinoschisis in a 65-year-old woman. The axial length was 28.1 mm, and decimal visual acuity (VA) was 0.4. (**b**) 1 month after surgery. (**c**) 3 months after surgery. (**d**) 6 months after surgery. (**e**) 12 months after surgery. The VA was 0.7. (**f**) SD-OCT image at initial presentation confirmed lamellar macular hole in a 76-year-old woman. The axial length was 31.9 mm, and decimal visual acuity (VA) was 0.3. (**g**) 1 month after surgery. (**h**) 3 months after surgery. (**i**) 6 months after surgery. (**j**) 12 months after surgery. The VA was 0.3. (**k**) SD-OCT image at initial presentation confirmed foveal detachment in a 76-year-old woman. The axial length was 27.3 mm, and decimal visual acuity (VA) was 0.4. (**l**) 1 month after surgery. (**m**) 3 months after surgery. (**n**) 6 months after surgery. (**o**) 12 months after surgery. The VA was 0.6

Table 24.1 Surgical outcomes after standard ILM peeling versus fovea-sparing ILM peeling for MTM

	Standard	FSIP	*P* value
No. of eyes	76	26	
Age (years) (mean ± SD; range)	65.5 ± 9.3 (27–83)	65.2 ± 10.8 (38–86)	0.902
Preoperative BCVA			
Landolt C acuity chart (mean; range)	0.25 (0.02–0.9)	0.25 (0.03–0.9)	
LogMAR (mean ± SD)	0.61 ± 0.39	0.60 ± 0.35	0.935
Postoperative BCVA at 12 months			
Landolt C acuity chart (mean, range)	0.43 (0.04–1.2)	0.48 (0.02–1.2)	
LogMAR (mean ± SD)	0.37 ± 0.38	0.32 ± 0.43	0.281
Visual improvement at 12 months (mean ± SD)	+0.24 ± 0.27	+0.28 ± 0.24	0.314
Postoperative macular hole formation, no (%)	6 (8)	0 (0)	0.320

BCVA best-corrected visual acuity, *FSIP* fovea-sparing internal limiting membrane peeling, *logMAR* logarithm of the minimum angle of resolution, *ILM* internal limiting membrane, *SD* standard deviation

better than the preoperative visual acuity in the fovea-sparing ILM peeling group (*P* = 0.04), but not in the standard ILM peeling group (*P* = 0.07). Ho et al. also reported the visual outcomes after fovea-sparing ILM peeling (foveolar ILM non-peeling) [26]. Although preoperative visual acuity was not significantly different between two groups (1.67 ± 0.23 [standard ILM peeling group], 1.70 ± 0.40 [fovea-sparing ILM peeling group]), the postoperative visual acuity (1.39 ± 0.33 [standard ILM peeling group], 0.89 ± 0.56 [fovea-sparing ILM peeling group]) at 52.4 ± 14.6 months was significantly better in fovea-sparing ILM peeling.

We conducted a retrospective study of consecutive series of 102 eyes with MTM who underwent primary pars plana vitrectomy at Osaka University Medical School Hospital [27]. Seventy-six eyes had conventional standard ILM peeling (standard ILM peeling group) and 26 eyes had fovea-sparing ILM peeling (FSIP group) (Table 24.1). No significant differences in baseline parameters were found between the groups, including age, gender, and preoperative visual acuity. In the standard ILM peeling group, the mean visual acuity improved significantly from 0.61 ± 0.39 before surgery to 0.37 ± 0.38 at 12-month follow-up (*P* < 0.001). In the FSIP group, the mean VA improved significantly from 0.60 ± 0.35 before surgery to

0.32 ± 0.43 at 12-month follow-up (*P* < 0.001). Postoperative visual acuity did not differ between the groups (*P* = 0.281). The mean visual improvement also did not differ significantly between the groups (*P* = 0.314). The visual acuity at the 12-month follow-up improved by 3 lines or more in 32 eyes (42%) in the standard ILM group, whereas in the FSIP group, the VA improved in 13 eyes (50%). Postoperative MH formation was developed in 6 (8%) eyes in the standard ILM peeling group but none of the eyes developed MH in FSIP group (Fig. 24.6). As a result, the VA at the 12-month follow-up deteriorated by 3 lines or more in 4 (5%) eyes in the standard ILM peeling group, whereas in the FSIP group, the VA deteriorated in 0 (0%) eyes.

24.2.7 Postoperative Complications

A postoperative complication specific to MTM is the opening of the macular hole as mentioned above, which occurs in about 5–10% of patients who undergo vitrectomy [18–23]. Cases in which ILM peeling was performed in the presence of an extremely thin fovea are at risk of developing this complication. A postoperative macular hole may occur in either type of MTM (lamellar macular hole and foveal detachment) [21].
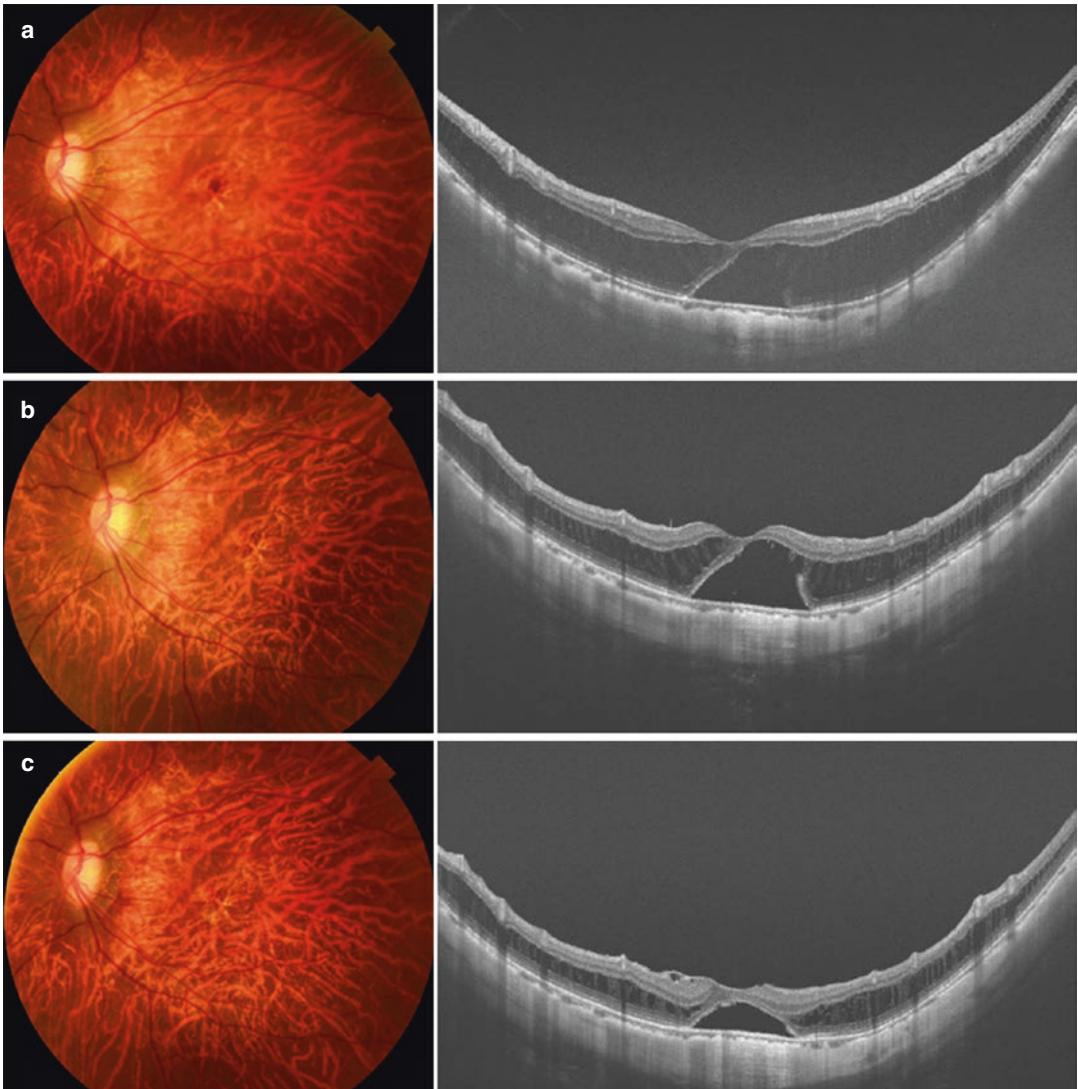
Fig. 24.6 Myopic traction maculopathy with foveal detachment in a 38-year-old woman treated by vitrectomy with fovea-sparing internal limiting membrane (ILM) peeling. (**a**) A fundus photograph and swept-source optical coherence tomography (SS-OCT) image at initial presentation confirmed foveal detachment with thin fovea. The axial length was 28.8 mm, and decimal visual acuity (VA) was 0.4. (**b**) A fundus photograph and an SS-OCT image 1 month after vitrectomy with fovea-sparing ILM peeling. The SS-OCT image revealed remaining foveal detachment. The VA was 0.4. (**c**) A fundus photograph

and an SS-OCT image 6 months after vitrectomy with fovea-sparing ILM peeling. The SS-OCT image shows a decrease in the height of the foveal detachment. The VA was 1.0. (**d**) A fundus photograph and an SS-OCT image 12 months after vitrectomy with fovea-sparing ILM peeling. The VA was 1.0. (**e**) A fundus photograph and an SS-OCT image 18 months after vitrectomy with fovea-sparing ILM peeling. The SS-OCT image shows that the retina reattached, and foveal detachment disappeared. The VA was 1.0
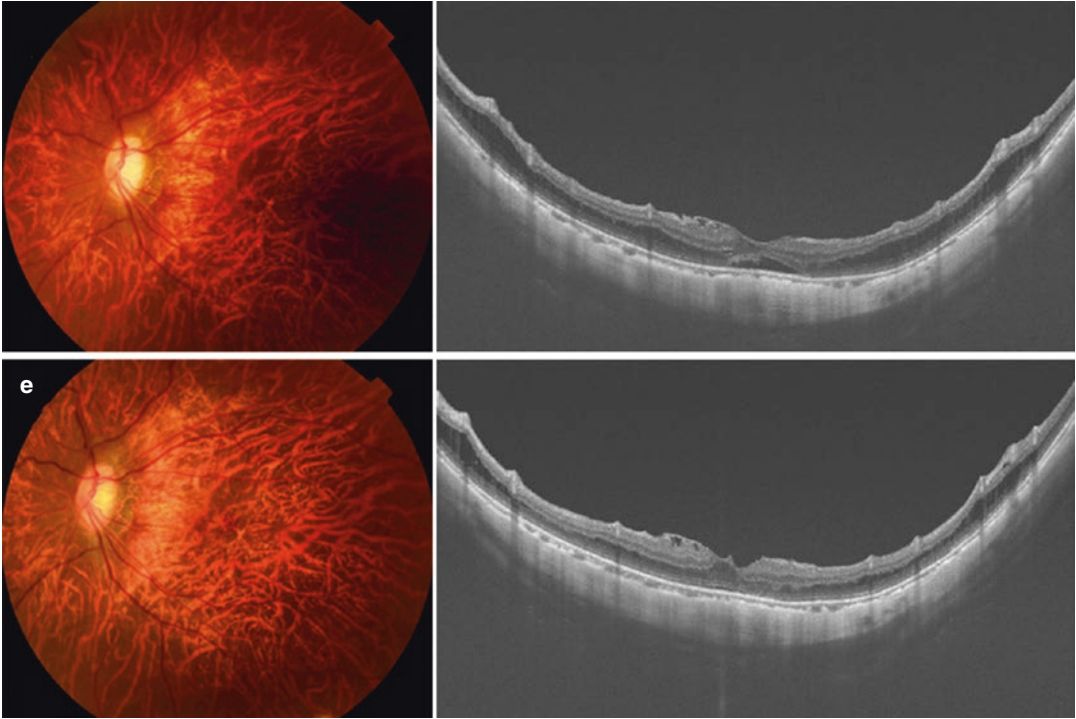
Fig. 24.6 (continued)

References

1. Phillips CI. Retinal detachment at the posterior pole. Br J Ophthalmol. 1958;42(12):749–53.
2. Takano M, Kishi S. Foveal retinoschisis and retinal detachment in severely myopic eyes with posterior staphyloma. Am J Ophthalmol. 1999;128(4):472–6.
3. Panozzo G, Mercanti A. Optical coherence tomography findings in myopic traction maculopathy. Arch Ophthalmol. 2004;122(10):1455–60.
4. Benhamou N, Massin P, Haouchine B, Erginay A, Gaudric A. Macular retinoschisis in highly myopic eyes. Am J Ophthalmol. 2002;133(6):794–800.
5. Gaucher D, Haouchine B, Tadayoni R, Massin P, Erginay A, Benhamou N, Gaudric A. Long-term follow-up of high myopic foveoschisis: natural course and surgical outcome. Am J Ophthalmol. 2007;143(3):455–62.
6. Shimada N, Ohno-Matsui K, Baba T, Futagami S, Tokoro T, Mochizuki M. Natural course of macular retinoschisis in highly myopic eyes without macular hole or retinal detachment. Am J Ophthalmol. 2006;142(3):497–500.
7. Sayanagi K, Ikuno Y, Tano Y. Tractional internal limiting membrane detachment in highly myopic eyes. Am J Ophthalmol. 2006;142(5):850–2.
8. Bando H, Ikuno Y, Choi JS, Tano Y, Yamanaka I, Ishibashi T. Ultrastructure of internal limiting membrane in myopic foveoschisis. Am J Ophthalmol. 2005;139(1):197–9.
9. Shimada N, Tanaka Y, Tokoro T, Ohno-Matsui K. Natural course of myopic traction maculopathy and factors associated with progression or resolution. Am J Ophthalmol. 2013;156(5):948–57.
10. Hwang JU, Joe SG, Lee JY, Kim JG, Yoon YH. Microincision vitrectomy surgery for myopic foveoschisis. Br J Ophthalmol. 2013;97(7):879–84.
11. Kwok AK, Lai TY, Yip WW. Vitrectomy and gas tamponade without internal limiting membrane peeling for myopic foveoschisis. Br J Ophthalmol. 2005;89(9):1180–3.
12. Yeh SI, Chang WC, Chen LJ. Vitrectomy without internal limiting membrane peeling for macular retinoschisis and foveal detachment in highly myopic eyes. Acta Ophthalmol. 2008;86(2):219–24.
13. Kobayashi H, Kishi S. Vitreous surgery for highly myopic eyes with foveal detachment and retinoschisis. Ophthalmology. 2003;110(9):1702–7.
14. Futagami S, Inoue M, Hirakata A. Removal of internal limiting membrane for recurrent myopic traction maculopathy. Clin Exp Ophthalmol. 2008;36(8):782–5.
15. Gao X, Ikuno Y, Fujimoto S, Nishida K. Risk factors for development of full-thickness macular holes after

pars plana vitrectomy for myopic foveoschisis. Am J Ophthalmol. 2013;155(6):1021–7.

16. Shimada N, Sugamoto Y, Ogawa M, Takase H, Ohno-Matsui K. Fovea-sparing internal limiting membrane peeling for myopic traction maculopathy. Am J Ophthalmol. 2012;154(4):693–701.

17. Ho TC, Chen MS, Huang JS, Shih YF, Ho H, Huang YH. Foveola nonpeeling technique in internal limiting membrane peeling of myopic foveoschisis surgery. Retina. 2012;32(3):631–4.

18. Zheng B, Chen Y, Chen Y, Zhao Z, Zhang Z, Zheng J, You Y, Wang Q, Shen L. Vitrectomy and internal limiting membrane peeling with perfluoropropane tamponade or balanced saline solution for myopic foveoschisis. Retina. 2011;31(4):692–701.

19. Lim SJ, Kwon YH, Kim SH, You YS, Kwon OW. Vitrectomy and internal limiting membrane peeling without gas tamponade for myopic foveo-schisis. Graefes Arch Clin Exp Ophthalmol. 2012;250(11):1573–7.

20. Shin JY, Yu HG. Visual prognosis and spectral-domain optical coherence tomography findings of myopic foveoschisis surgery using 25-gauge transconjunctival sutureless vitrectomy. Retina. 2012;32(3):486–92.

21. Hattori K, Kataoka K, Takeuchi J, Ito Y, Terasaki H. Predictive factors of surgical outcomes in vit-rectomy for myopic traction maculopathy. Retina. 2018;38(Suppl 1):S23–30.

22. Taniuchi S, Hirakata A, Itoh Y, Hirota K, Inoue M. Vitrectomy with or without internal limiting mem-brane peeling for each stage of myopic traction macu-lopathy. Retina. 2013;33(10):2018–25.

23. Figueroa MS, Ruiz-Moreno JM, Gonzalez del Valle F, Govetto A, de la Vega C, Plascencia RN, Contreras I, Medina JL. Long-term outcomes of 23-gauge pars plana vitrectomy with internal limit-ing membrane peeling and gas tamponade for myo-pic traction maculopathy: a prospective study. Retina. 2015;35(9):1836–43.

24. Ikuno Y, Sayanagi K, Soga K, Oshima Y, Ohji M, Tano Y. Foveal anatomical status and surgical results in vitrectomy for myopic foveoschisis. Jpn J Ophthalmol. 2008;52(4):269–76.

25. Kumagai K, Furukawa M, Ogino N, Larson E. Factors correlated with postoperative visual acuity after vit-rectomy and internal limiting membrane peeling for myopic foveoschisis. Retina. 2010;30(6):874–80.

26. Ho TC, Yang CM, Huang JS, Yang CH, Yeh PT, Chen TC, Ho A, Chen MS. Long-term outcome of foveolar internal limiting membrane nonpeeling for myopic traction maculopathy. Retina. 2014;34(9):1833–40.

27. Shiraki N, Wakabayashi T, Ikuno Y, Matsumura N, Sato S, Sakaguchi H, Nishida K. Fovea-Sparing ver-sus Standard Internal Limiting Membrane Peeling for Myopic Traction Maculopathy: A Study of 102 Consecutive Cases. Ophthalmology Retina 2020 [online ahead of print].

Practical Tips in Surgery for Myopic Maculopathy

25

Mary Ho, Andrew Chun Yue Mak, and Lawrence Pui Leung Iu

25.1 Introduction

With the dramatic increase in the prevalence of myopia worldwide, it has been estimated that one-third of the world's population will be affected by 2020 [1]. Myopic eyes are at risk of developing conditions that require vitreoretinal surgery, such as rhegmatogenous retinal detachment, myopic foveoschisis (MFS) and myopic macular holes (MHs) [2]. The incidence of high myopia and pathologic myopia in East Asia is especially high [3] and vitreoretinal surgeons in the region are increasingly operating on surgical vitreoretinal complications in highly myopic eyes. However, the intrinsic properties of highly myopic eyes, including their long axial length, posterior staphyloma, lack of scleral rigidity, peculiar vitreous anatomy and abnormal vitreoretinal adhesions, have made operations on these eyes challenging. Herein, the authors hope to provide practical tips and techniques for vitrectomy in highly myopic eyes.

M. Ho (✉) · A. C. Y. Mak · L. P. L. Iu
Department of Ophthalmology and Visual Sciences, Prince of Wales Hospital, Hospital Authority, Shatin, Hong Kong

Department of Ophthalmology and Visual Sciences, The Chinese University of Hong Kong, Shatin, Hong Kong
e-mail: maryho@cuhk.edu.hk

25.2 General Issues on Vitrectomy

25.2.1 Anaesthesia in Long Axial Length

The increased axial length and the prevalence of posterior staphyloma in highly myopic eyes present a substantial risk of inadvertent globe injury during locoregional anaesthesia. The reported rate of inadvertent globe injury in eyes of axial length above 26 mm is 1 in 140 injections with retrobulbar or peribulbar anaesthesia [4]. The authors are cautious on retrobulbar anaesthesia in eyes with axial length ≥26 mm and would generally avoid retrobulbar anaesthesia when axial length exceeds 28 mm. Peribulbar anaesthesia with prolonged ocular massage to allow intraconal spread of local anaesthetic is regarded as a safer alternative, although rare reports of globe injury with peribulbar anaesthesia do exist [5]. In eyes of extreme high myopia with axial length ≥30 mm or eyes with atypically located posterior staphyloma (e.g., inferiorly located), we recommend sub-Tenon's anaesthesia delivered through a small peritomy using a blunt-tip cannula. Surgeons should take note of the disadvantages of sub-Tenon's anaesthesia with chemosis obstructing anterior segment procedures and placement of trocars, and an occasional lack of akinesia complicating delicate surgical manoeuvres, such as membrane peeling.

25.2.2 Instrumentation in Long Axial Length

The length of the instrument is another concern while working on highly myopic eyes. Most available vitreous cutters and membrane forceps are designed for use in eyes of average sizes. Manufacturers tend not to produce ultra-long instruments because the extra length of the instrument will compromise the stiffness of the shaft, especially with modern small-gauge vitrectomy systems. When used in eyes with posterior staphyloma and long axial length, standard instruments may not reach the retinal surface at the posterior pole. This makes operations at the posterior pole challenging, including heavy liquid removal and membrane peeling steps. Some manufacturers produce long-shaft forceps for this purpose [6], but they might not be widely available.

In cases where ultra-long forceps and instruments are not available, the authors routinely insert ports at 4 mm post-limbus regardless of the lens status, which shortens the distance between the scleral wound and the posterior pole. We recommend the use of a 23-gauge vitrectomy system in cases of high axial length where surgical manoeuvres at the posterior pole are required because 23-gauge tools lack the stiffening sleeves found in the shaft of 25-gauge tools, which in turn offers an extra 1–2 mm of length to access the posterior pole. Slight indentations at ports under low infusion pressure can also provide extra reach for the posterior pole. With distortion of the anterior globe, however, corneal striae and irregular optical surface might decrease visibility. The additional advancement of instruments can also be achieved by removing the cannula and using the scleral wound for direct access. Alternatively, sclerotomy can be created by ophthalmic knives in a fashion similar to 20-gauge vitrectomy.

25.2.3 Posterior Vitreous Detachment Induction

The pathogenesis of myopia-related macular pathology involves abnormal vitreoretinal traction at the macula; thus, induction of posterior vitreous detachment (PVD) is crucial to a successful operation. Induction of PVD can be difficult in highly myopic eyes because of the tight vitreoretinal adhesion and presence of vitreoschisis. Vitreoschisis occurs with the presence of posterior vitreous cortex splitting after vitreous gel liquefaction and is associated with abnormal vitreoretinal attachment and absence of dehiscence at the vitreoretinal interface [7]. Vitreoschisis is common in myopic eyes and is present in around half of the patients with MH [8]. In the presence of vitreoschisis and strongly adhered posterior hyaloid, one may have to deal with the difficult induction of PVD, multiple layers of preretinal fibrous tissue and residual vitreous before being able to initiate internal limiting membrane (ILM) peeling.

Different adjunct agents can be employed for visualization of the vitreous cortex and facilitates induction of PVD. For example, intra-vitreal triamcinolone acetonide (IVTA) [9] or trypan blue can be injected to stain the posterior hyaloid to improve visualization. Alternatively, instruments such as intra-ocular forceps or diamond-dusted membrane scrapers (DDMS) can help to lift up the edges of the posterior hyaloid and assist induction of PVD [10].

25.2.4 Reduced Contrast for Posterior Pole or Macular-Related Surgery

Highly myopic eyes are characterized by retinal thinning and chorioretinal atrophy at the posterior pole, which leads to the increased risk of posterior pole trauma, iatrogenic retinal holes and reduced contrast during membrane peeling manoeuvres. These factors may contribute to incomplete membrane (ILM/epiretinal membrane [ERM]) removal, or paracentral iatrogenic retinal holes [11, 12]. Also, incomplete removal of ILM could result in failure of closure of MH in highly myopic eyes, which in turn results in higher risk of retinal detachment [13]. ILM peeling is recommended to start at least 1 disc diameter from the fovea and it is advisable to start at the temporal quadrant to avoid damaging the papillomacular bundle [12].

To initiate ILM peeling, surgeons must create a new ILM flap or edge to start the process. This procedure can be extremely difficult with reduced contrast and thinned retina. Several instruments may be helpful because they are designed for elevation of ILM flap, including the DDMS [14, 15] and FINESSE Flex loop [16]. However, with the use of intraoperative optical coherence tomography (OCT), evidence of surgical trauma by these instruments can be revealed. These instruments can cause micro-traumas and structural damage of the retina when compared to the direct pinch-and-peel technique [16, 17].

A myopic, tessellated fundus with generalized chorioretinal atrophy makes visualization of membranes and the ILM difficult (Fig. 25.1). Adjunctive staining tools can be employed to enhance visualization. These staining materials should be gently injected or infused to avoid iatrogenic breaks at the thinned retina. Widely available dyes include triamcinolone (vitreous staining), trypan blue, membrane blue, brilliant blue, indocyanine green (ICG) and infracyanine green. ICG was introduced in the early 2000s, but later fell out of favour because of its potential toxic effect on the outer retina and the retinal pigment epithelium (RPE).

Complete vitreous removal can be difficult in highly myopic eyes due to the presence of vitreoschisis, adherent vitreous cortex and presence of tractional pre-retinal tissue in these eyes, consisting of vitreous cortex residuals, ERM and ILM [18]. Residual vitreous membranes on the posterior pole were often commonly found even in cases with clinical vitreous detachment. Triamcinolone can be employed to assist clearing of the residual vitreous and prevent future proliferative vitreoretinopathy (PVR) development in the presence of retinal break or rhegmatogenous retinal detachment. In addition, myopic ILM is characterized by its firmly adherent, friable and sticky nature. Multiple staining and re-grasping may be required for its complete removal.

25.2.5 Avoid Dye Contact with the RPE and Related Toxic Effects

General measures are advised to avoid direct contact of dye with the RPE because of the potentially toxic effect [19]. In the presence of MH in highly myopic eyes, an extra protective layer can be employed to prevent migration of the dyes into the subretinal space. These materials include viscoelastics [20] and perfluorocarbon (PFC) [21]. In the presence of MH-related posterior pole retinal detachment, the membrane peeling procedure can be extremely difficult considering the reduced contrast, thinned retina, sticky ILM and mobile retina. In these circumstances, the subretinal fluid (SRF) can be drained first, followed by applying membrane blue stain and peeling under PFC. PFC can exert pressure onto the retina and provide a
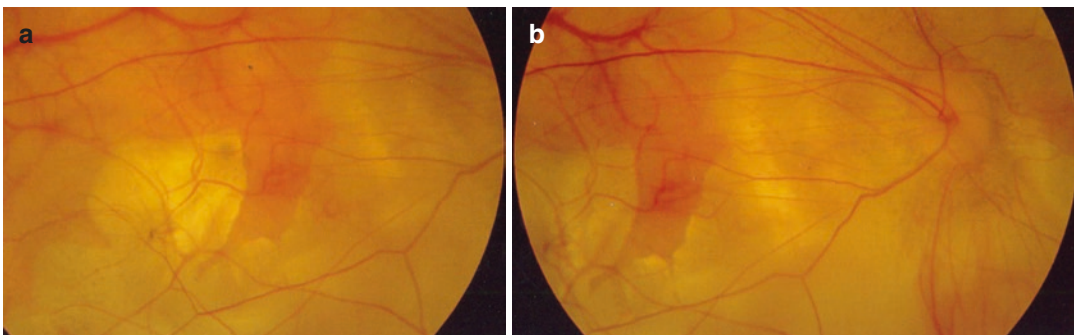
Fig. 25.1 An 83-year-old woman with pathological myopia and an extremely long eyeball (31 mm). She developed MH-related retinal detachment in both eyes consecutively. (**a**, **b**) Show the colour fundus photos illustrating the extensive chorioretinal atrophy, retinal thinning and reduced contrast, which makes membrane peeling on the posterior pole challenging

counterforce to aid membrane peeling. Dye migration to subretinal space not only causes toxic effects to the RPE, but also reduces the contrast for visualization, which makes membrane peeling even more difficult. A careful choice of different light filters may help improve tissue contrast and simultaneously reduce phototoxicity [22, 23].

Technologically speaking, intraoperative OCT and a three-dimensional (3D) viewing system can aid surgery in these challenging cases. The Ngenuity 3D viewing system (Alcon) is the preferred option for many surgeons in macular related surgeries because of its high-quality image, enhanced stereopsis perception and modified image qualities including contrast and brightness. The system allows magnification of images without much loss in image details, which can serve as a good option for highly myopic eyes [24].

Removal of ILM in highly myopic eyes can cause unavoidable trauma to the retinal nerve fibre layer. The principle of ILM peeling is to relieve its traction on the retina, which in turn creates relaxation of the retinal tissue. To allow better closure rate in MH, ILM peeling is advised to reach the retinal arcades [25–28]. However, complete ILM peeling in MFS with impending MH (Fig. 25.2) can be risky in creating a full-thickness MH. In these situations, fovea-sparing ILM peeling is advised to provide extra architectural support at the fovea and prevent formation of MHs by the separation of ILM at the central vulnerable retina [29, 30]. Other options for increasing the success rate for MH closure include autologous retinal graft, amniotic membrane and macular buckles [31–33].

25.2.6 Viewing System During Membrane Peeling

Since the 1990s, a non-contact system has been the wide-angle system of choice for many retina surgeries. However, the non-contact system does not compensate for pre-existing corneal asphericity or aberration. In highly myopic eyes, conditions for corneal asphericity are commonly encountered including previous refractive keratectomy, limbal relaxing incisions, cataract surgery, LASIK, photorefractive keratectomy or keratoconus, which adds further challenges for membrane peeling. Contact system by macular lenses provides smaller fields of view but a greater resolution that facilitates surgical manoeuvres during membrane peeling. Non-contact systems include Resight (Zeiss) and BIOM (Oculus) systems. Different objective lens can be employed for a smaller field of view, but proper posterior pole magnification. Examples include high-resolution macula lens, 90D lens or wide-field high-definition lens in the BIOM system. These objective lens in the non-contact system may hinder the angle of instrument manipulation during verticalization of instruments. Hence, the authors recommend the use of contact-type viewing systems over the non-contact type, which decreases inadvertent contact with the viewing system during manipulation. A contact-type viewing system with coupling agents will also partially alleviate optical aberrations caused by corneal folds associated with verticalization of instruments.

25.3 Pathology-Based Discussion

25.3.1 Rhegmatogenous Retinal Detachment

Retinal detachment is commonly seen in highly myopic eyes. Unlike eyes with normal axial length, retinal detachment in highly myopic eyes may be secondary to posterior para-vascular tears and MHs [34].

Several factors make retinal detachment repair in myopic eyes difficult. These eyes are characterized with abnormal vitreous, i.e. the presence of vitreoschisis, residual vitreous cortex, impossible complete PVD and abnormal vitreoretinal adhesions in different retinal regions. Many cases exhibit a 'sticky' vitreous, which is very difficult to remove. In all cases, meticulous vitreous shaving is required for complete vitreous clearing and prevention of PVR formation. Careful vitreous shaving using extra time with
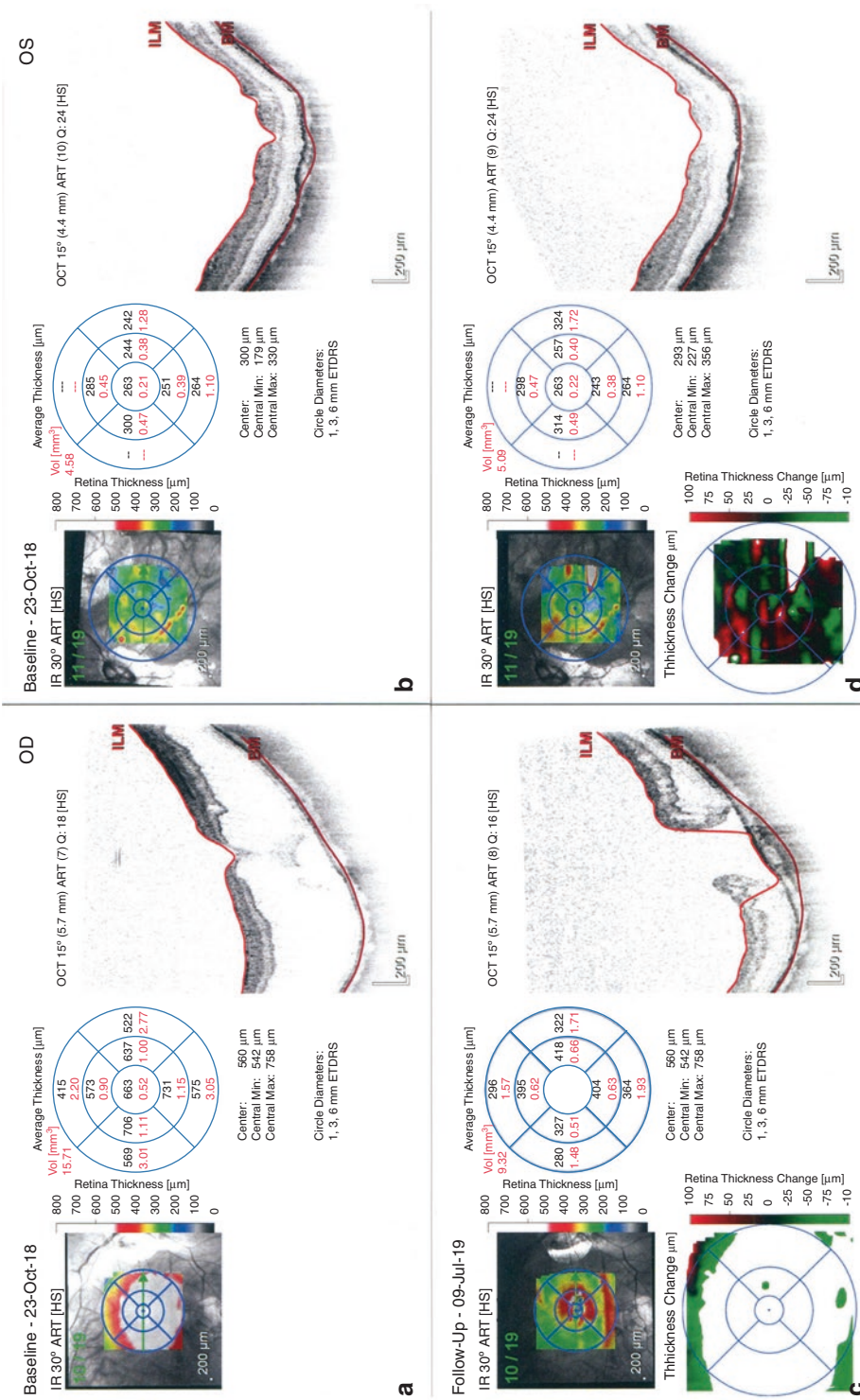
Fig. 25.2 A 63-year-old woman with bilateral pathological high myopia. Her right eye developed progressive worsening foveoschisis with fovea detachment, with a mild drop in vision to 20/80. The surgical outcome was unsatisfactory that she developed full-thickness MH after vitrectomy, membrane peeling and gas tamponade, resulting in low vision of 8/200. (**a&c**) Show the OCT scan of her right eye before and after sur-gery. She subsequently suffered from a left-eye MH-related retinal detachment with prominent posterior staphyloma. She underwent left-eye vitrectomy, membrane peel-ing and macular buckle, resulting in successfully repaired MH and stable vision of 20/120. (**b&d**) Show the OCT scan of her left eye after surgical repair. The scan shows a dome-shaped posterior sclera secondary to macular buckle indentation

the help of scleral indentation should be employed in highly myopic eyes [35–37]. Bimanual surgery with an extra light source, such as chandelier or twin light, is the choice of many surgeons in peripheral shaving with better illumination in addition to the aid of self-indentation.

Surgeons can pay attention not to forcefully induce further PVD if abnormal adhesion at the mid-periphery is noticed. In some cases, complete PVD is not possible due to the strong vitreoretinal adhesion and posterior shifting of the vitreous base [38]. If the presence of a vitreous band is noted at the equatorial region, it may give rise to proliferative vitreoretinopathy (PVR) development and a strong inward force pulling the retina inward in a ring-like fashion. There are a few ways to deal with this situation. First, one can consider adopting IVTA to enhance the vitreous contrast, which aids in the proper identification of the residual vitreous. Second, careful vitreous shaving is advised along the vitreous base, but the retina should not be damaged. Third, an external encircling band can be employed to counteract the inward force. Hence, combined pars plana vitrectomy and scleral buckle can be employed to provide a better success rate in retinal detachment surgery [38, 39]. A recent meta-analysis of studies including eyes of various axial lengths shows a higher primary reattachment rate with combined vitrectomy and encircling band. However this difference is insignificant when only pseudo-phakic eyes are analysed [40]. A supplementary encircling band would also be used in cases where complete PVD cannot be achieved or when abnormally strong vitreoretinal adhesions are present at the mid-periphery or in phakic cases when peripheral vitreous clearance is hindered. The authors advise to use scleral fixated sutures for anchoring the encircling band in highly myopic eyes because scleral tunnels should be avoided due to scleral thinning.

25.3.2 Myopic Foveoschisis

A variety of surgical techniques have been reported in the literature, ranging among gas tamponade, ILM peeling, fovea-sparing membrane peeling technique and use of macular buckles. Most reports are case series and there is no conclusive evidence on the superiority of a specific technique [41, 42].

For MFS, ILM peeling helps to ensure that all tractional forces are completely removed, including those from pre-macular glial cells and vitreous cortex [43]. It increases retinal compliance and allows the retina to better conform to the posterior staphyloma [43].

ILM peeling and gas tamponade have achieved favourable anatomical and visual outcomes in MFS cases. However, development of postoperative full-thickness MH is not uncommon and occurs in around 13–28% of patients. Thus, Shimada et al. [30] and Ho et al. [29] introduced and described the technique of fovea-sparing ILM peel in 2012. This technique advocates leaving a small piece of ILM island over the central foveolar. It is believed that preservation of foveolar ILM would preserve foveolar Müller cell integrity and therefore reduce the risk of postoperative MH development. Although studies suggested that this technique might be useful to reduce the risk of MH development and foveolar thinning [44], leaving ILM on the fovea could result in late ILM contraction and retinal thickening [30]. This technique is also more technically demanding and requires more tissue manipulation than conventional complete ILM peeling. In view of the risk of secondary MH development in patients with foveoschisis who underwent ILM peeling, a conservative treatment with regular OCT scans can be considered in patients with foveoschisis without foveal detachment.

25.3.3 Full-Thickness MHs in Highly Myopic Eyes

ILM peeling in full-thickness MH helps to reduce retinal rigidity and improve retinal compliance [45]. It also helps to reduce postoperative ERM formation and risk of MH reopening. Different meta-analyses showed that ILM peeling results in higher MH closure rate in stage 2, 3 and 4 full-thickness MH [46] and reduces the MH reopening rate from 7 to 1% [47].

There is no consensus on the optimal size of extent of ILM peeling [45]. Extended ILM peeling up to the arcade is often performed for large MH to improve retinal compliance. But longer operation time and higher risk of iatrogenic retinal trauma for extended ILM peeling may cause inadvertent retinal trauma. Dissociated optic nerve fibre layer and swelling of arcuate retinal nerve fibre layer, which can be shown on imaging modalities such as OCT and infrared fundus photographs, are two known structural changes secondary to ILM peeling [48, 49]. (Figure 25.3 shows the stepwise approach in ILM peeling for a macular hole retinal detachment.)

25.3.4 Use of Intra-ocular Tamponade

In the presence of posterior staphyloma in extreme long eyeballs, use of gas tamponades with higher buoyancy and its ability to conform to irregular scleral contours may be a better option [50, 51]. Due to the viscosity and tendency of silicone oil in forming a circular shape, a mathematical model study found that silicone oil failed to tamponade posterior protruding staphyloma [52].

There is not much debate in adopting gas tamponade in cases with full-thickness MH. For
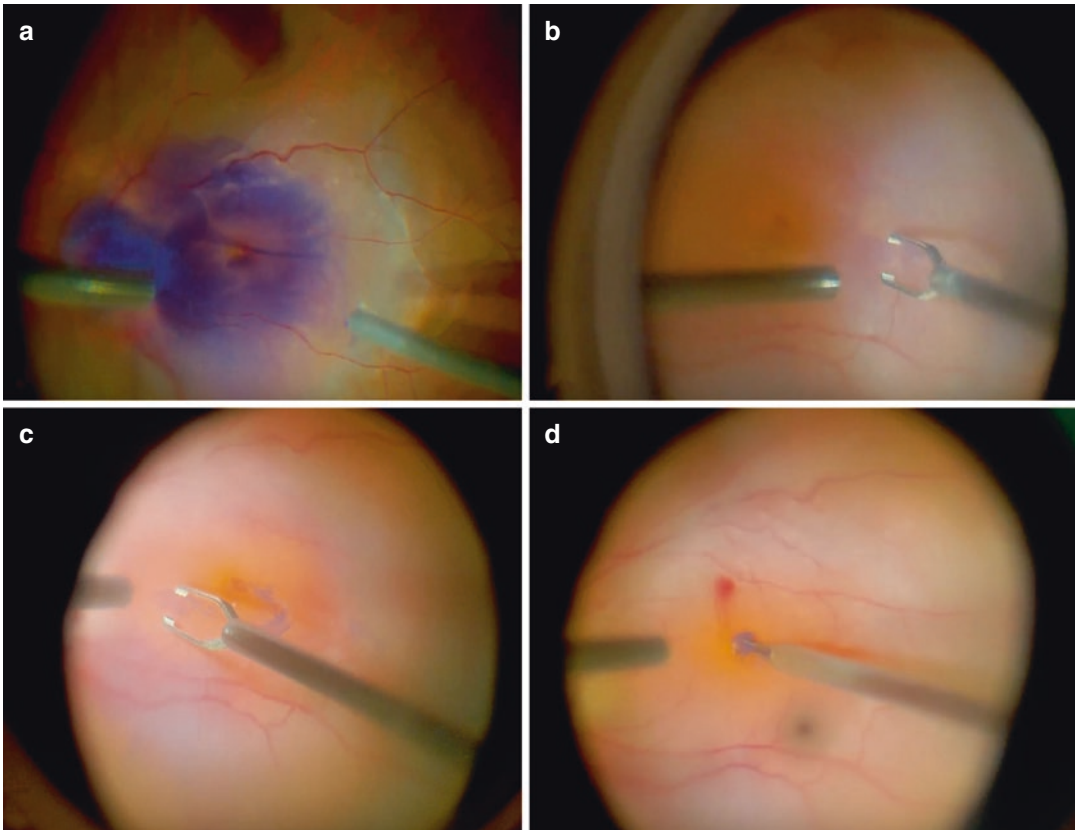
Fig. 25.3 These figures show the stepwise approach to ILM peeling in a myopic MH case. (**a**) Trypan blue staining after core vitrectomy; (**b**) ILM forceps was used to grasp and create an ILM flap temporal to the fovea; (**c**) completion of the ILM flap peeling in a circumferential fashion without complete removal of the flap at the edges of the macular hole; and (**d**) gentle application of the ILM flap into the macular hole from all sides until the ILM becomes inverted to cover the macular hole (intraoperative photos from Dr. Tsang Chi Wai)

myopic foveoschisis without MH, it is still controversial whether gas tamponade is necessary. Gas tamponade in myopic foveoschisis may help the retina in faster resolution of foveoschisis and tamponade against unnoticeable MHs [53, 54]. It also has additional benefits in displacing the SRF outside the macula towards the area with potentially healthier RPE cells, which can facilitate SRF absorption [55, 56]. However, studies have shown that gas tamponade did not have an obvious impact on functional or anatomical outcome in foveoschisis cases [43].

25.3.5 Surgical Complications Related to Leaking Sclerotomies

The 23-gauge and 25-gauge transconjunctival sutureless vitrectomy processes have gained wide popularity among vitreoretinal surgeons in the past decade [57]. While being a neat and fast way, its use in highly myopic eyes, due to the intrinsic lack of scleral rigidity, has been associated with increased incidence in sclerotomy leakage and postoperative hypotony. The sclera of high myopia cases is characterized with thinner sclera and relatively thinned nature with deranged fibre configuration [58]. Manipulation of the instrument to reach the posterior pole, excessive pressure on the sclera by the operators during peripheral shaving or posterior pole procedures may cause difficult self-sealing appositional scleral wounds. Despite the benefit of small-gauge vitrectomy with faster postoperative recovery and less patient discomfort [59], a careful decision should be made to leave the sclerotomy site un-sutured.

Sclerotomy site leakage in highly myopic eyes can lead to devastating outcomes. These complications include hypotony, suprachoroidal haemorrhage, sub-macular haemorrhage in the presence of myopic choroidal neovascularisation and retinal re-detachment due to gas leakage causing an under-filled posterior segment. Generally speaking, scleral wound leakage can be prevented by careful wound construction of bi-planar nature [60, 61], long sclerotomy tun-

nels [62], meticulous sclerotomy massage upon trocar removal and a low threshold for transconjunctival sutures.

The authors prefer 25-gauge over 23-gauge instruments in eyes lacking scleral rigidity. Theoretically, larger scleral incisions with 23-gauge (0.64 mm) will be more prone to leakage than smaller incisions with 25-gauge (0.51 mm). But surgeons must balance the relative lack of instrument stiffness and the limit of posterior pole reach as mentioned above with smaller gauge instrumentation. To further decrease the risk of leaking sclerotomies, the authors will withdraw the cannulas along the insertion trajectory and apply prolonged transconjunctival massage for a better seal [63]. If the wound integrity is in doubt, we recommend a low threshold to suture the wound with a transconjunctival absorbable suture. To avoid the foreign body sensation and post-operation inflammation secondary to the absorbable sutures, other methods, such as releasable sutures [64] or even the use of tissue glue, can be considered. Sclerotomy wound leaks should be checked for even after a single-bite suture. In the presence of abnormal scleral architecture, a small proportion of sclerotomy sites have unsatisfied wound apposition with slow leaks despite sutures. Extra-scleral wound sutures or even mattress sutures may be considered in this situation.

25.3.6 Other Complications

Post-operative complications of primary vitreoretinal surgery in highly myopic eyes included cataract progression, intra-ocular pressure (IOP) elevation, unsuccessful surgery and recurrent detachment. These fragile eyes with scleral thinning are also subjected to intraoperative complications including muscle avulsion, vortex vein damage, haemorrhage, SFR retention [65] and globe perforation.

Most studies have suggested that moderate-to-high myopia is associated with increased risk of primary open-angle glaucoma. The Beaver Dam Eye Study showed that persons with myopia were 60% more likely to have glaucoma than

those with emmetropia [66]. Hence, these patients are at risk of developing both primary and secondary glaucoma after vitrectomy operation, especially in eyes treated with silicone oil tamponade [67]. Many patients suffer from glaucomatous disc before retinal surgeries. Postvitrectomy IOP rise and higher chance of steroid responder in myopic eyes should be considered. Preventive measures such as using steroids with lower potency and less IOP effect should be considered. Also, surgeons are recommended to arrange frequent post-operation follow-up to identify the trend of IOP rise, and initiate appropriate management to avoid persistent IOP elevation causing optic nerve head damage or even wipe out.

Highly myopic eyes are often associated with zonular dehiscence and lens complications [68]. Bag dislocation due to progressive zonular dehiscence can occur many years after uneventful surgery. The risk of bag dislocation is higher in myopia case, in patients who underwent vitreoretinal surgeries or even repeated vitreoretinal surgeries including silicone oil removal. Surgeons should avoid excessive manipulation of the intra-ocular lens during combined operation or anterior chamber aspiration to avoid bag dislocation.

In cases where heavy liquid is required for intraoperative use, the authors recommend using perfluorocarbon liquids (PFCLs) of a larger volume (e.g., 7 mL kit instead of 5 mL), in view of a larger globe volume in eyes of high axial length. Occasionally, even 7 mL is insufficient for a complete fill for the posterior segment. Surgeons should pay particular attention not to overfill the globe with heavy liquid, because entrapment of heavy liquids could occur in the zonular dehiscence area around the ciliary body, leading to retained PFC. The reduced posterior pole contrast also makes visualization of heavy liquid globules difficult. PFCLs have high specific gravity, low surface tension and viscosity [65]. The surface tension of PFCLs ensures that the liquid stays relatively cohesive as globules after being injected into the vitreous cavity under fluid fill. Removal of heavy liquid can be considered under balanced salt solution (BSS)-filled eye or with the help of small amount of BSS injection under

air-filled eye. In addition, the gentle current of fluid flow using a back-flush needle may help to visualize small residual globules of heavy liquid and assist in complete removal.

Hence, preoperative careful planning, good understanding of the characteristics of highly myopic eyes and vitreoretinal surgeons' skills are equally important in reducing complications.

25.4 Conclusion

Working on highly myopic eyes with characteristics of higher axial length, posterior staphyloma, thinner and atrophic retina, degenerated vitreous and abnormal scleral fibres can be very challenging. A good understanding of the characteristics of these weak eyes helps in the operative planning. An understanding of the pathogenesis and natural history of the retinal complications of high myopia will help guide the management. Cautious pre-planning and meticulous intraoperative manipulation help to ensure success and minimize complications in these cases.

References

1. Dolgin E. The myopia boom. Nature. 2015;519(7543):276–8.
2. Ohno-Matsui K, Lai TY, Lai CC, Cheung CM. Updates of pathologic myopia. Prog Retin Eye Res. 2016;52:156–87.
3. Mak CY, Yam JC, Chen LJ, Lee SM, Young AL. Epidemiology of myopia and prevention of myopia progression in children in East Asia: a review. Hong Kong Med J. 2018;24(6):602–9.
4. Duker JS, Belmont JB, Benson WE, Brooks HL Jr, Brown GC, Federman JL, et al. Inadvertent globe perforation during retrobulbar and peribulbar anesthesia. Patient characteristics, surgical management, and visual outcome. Ophthalmology. 1991;98(4):519–26.
5. Gillow JT, Aggarwal RK, Kirkby GR. Ocular perforation during peribulbar anaesthesia. Eye (London, England). 1996;10(Pt 5):533–6.
6. Gao X, Ikuno Y, Nishida K. Long-shaft forceps for membrane peeling in highly myopic eyes. Retina (Philadelphia, PA). 2013;33(7):1475–6.
7. Sebag J. Vitreoschisis. Graefes Arch Clin Exp Ophthalmol. 2008;246(3):329–32.
8. Gupta P, Yee KM, Garcia P, Rosen RB, Parikh J, Hageman GS, et al. Vitreoschisis in macular diseases. Br J Ophthalmol. 2011;95(3):376–80.

9. Peyman GA, Cheema R, Conway MD, Fang T. Triamcinolone acetonide as an aid to visualization of the vitreous and the posterior hyaloid during pars plana vitrectomy. Retina. 2000;20(5):554–5.

10. Takeuchi M, Takayama K, Sato T, Ishikawa S, Fujii S, Sakurai Y. Non-aspiration technique to induce posterior vitreous detachment in minimum incision vitrectomy system. Br J Ophthalmol. 2012;96(11):1378–9.

11. Oie Y, Emi K, Takaoka G, Ikeda T. Effect of indocyanine green staining in peeling of internal limiting membrane for retinal detachment resulting from macular hole in myopic eyes. Ophthalmology. 2007;114(2):303–6.

12. Sandali O, El Sanharawi M, Basli E, Lecuen N, Bonnel S, Borderie V, et al. Paracentral retinal holes occurring after macular surgery: incidence, clinical features, and evolution. Graefes Arch Clin Exp Ophthalmol. 2012;250(8):1137–42.

13. Guillaubey A, Malvitte L, Lafontaine PO, Hubert I, Bron A, Berrod JP, et al. Incidence of retinal detachment after macular surgery: a retrospective study of 634 cases. Br J Ophthalmol. 2007;91(10):1327–30.

14. Kuhn F, Mester V, Berta A. The Tano Diamond Dusted Membrane Scraper: indications and contraindications. Acta Ophthalmol Scand. 1998;76(6):754–5.

15. Lewis JM, Park I, Ohji M, Saito Y, Tano Y. Diamond-dusted silicone cannula for epiretinal membrane separation during vitreous surgery. Am J Ophthalmol. 1997;124(4):552–4.

16. Uchida A, Srivastava SK, Ehlers JP. Analysis of retinal architectural changes using intraoperative OCT following surgical manipulations with membrane flex loop in the DISCOVER study. Invest Ophthalmol Vis Sci. 2017;58(9):3440–4.

17. Ehlers JP, Han J, Petkovsek D, Kaiser PK, Singh RP, Srivastava SK. Membrane peeling-induced retinal alterations on intraoperative OCT in vitreomacular interface disorders from the PIONEER study. Invest Ophthalmol Vis Sci. 2015;56(12):7324–30.

18. Sakaguchi H, Ikuno Y, Choi JS, Ohji M, Tano T. Multiple components of epiretinal tissues detected by triamcinolone and indocyanine green in macular hole and retinal detachment as a result of high myopia. Am J Ophthalmol. 2004;138(6):1079–81.

19. Maia M, Haller JA, Pieramici DJ, Margalit E, de Juan E Jr, Farah ME, et al. Retinal pigment epithelial abnormalities after internal limiting membrane peeling guided by indocyanine green staining. Retina. 2004;24(1):157–60.

20. Cacciatori M, Azzolini M, Sborgia M, Coppola M, De Molfetta V. Sodium hyaluronate 2.3% prevents contact between indocyanine green and retinal pigment epithelium during vitrectomy for highly myopic macular hole retinal detachment. Retina. 2004;24(1):160–1.

21. Facino M, Mochi B, Lai S, Terrile R. A simple way to prevent indocyanine green from entering the subretinal space during vitrectomy for retinal detachment due to myopic macular hole. Eur J Ophthalmol. 2004;14(3):269–71.

22. Chow DR. The evolution of endoillumination. Dev Ophthalmol. 2014;54:77–86.

23. Henrich PB, Valmaggia C, Lang C, Cattin PC. The price for reduced light toxicity: do endoilluminator spectral filters decrease color contrast during Brilliant Blue G-assisted chromovitrectomy? Graefes Arch Clin Exp Ophthalmol. 2014;252(3):367–74.

24. Ehlers JP, Uchida A, Srivastava SK. The integrative surgical theater: combining intraoperative optical coherence tomography and 3D digital visualization for vitreoretinal surgery in the DISCOVER study. Retina. 2018;38(Suppl 1):S88–96.

25. Bando H, Ikuno Y, Choi JS, Tano Y, Yamanaka I, Ishibashi T. Ultrastructure of internal limiting membrane in myopic foveoschisis. Am J Ophthalmol. 2005;139(1):197–9.

26. Iezzi R, Kapoor KG. No face-down positioning and broad internal limiting membrane peeling in the surgical repair of idiopathic macular holes. Ophthalmology. 2013;120(10):1998–2003.

27. Mete M, Alfano A, Guerriero M, Prigione G, Sartore M, Polito A, et al. Inverted internal limiting membrane flap technique versus complete internal limiting membrane removal in myopic macular hole surgery: a comparative study. Retina. 2017;37(10):1923–30.

28. Zhang Z, Wei Y, Jiang X, Zhang S. Pars plana vitrectomy and wide internal limiting membrane peeling with perfluoropropane tamponade for highly myopic foveoschisis-associated macular hole. Retina. 2017;37(2):274–82.

29. Ho TC, Chen MS, Huang JS, Shih YF, Ho H, Huang YH. Foveola nonpeeling technique in internal limiting membrane peeling of myopic foveoschisis surgery. Retina. 2012;32(3):631–4.

30. Shimada N, Sugamoto Y, Ogawa M, Takase H, Ohno-Matsui K. Fovea-sparing internal limiting membrane peeling for myopic traction maculopathy. Am J Ophthalmol. 2012;154(4):693–701.

31. Grewal DS, Mahmoud TH. Autologous neurosensory retinal free flap for closure of refractory myopic macular holes. JAMA Ophthalmol. 2016;134(2):229–30.

32. Rizzo S, Caporossi T, Tartaro R, Finocchio L, Franco F, Barca F, et al. A human amniotic membrane plug to promote retinal breaks repair and recurrent macular hole closure. Retina. 2019;39(Suppl 1):S95–S103.

33. Theodossiadis GP, Theodossiadis PG. The macular buckling procedure in the treatment of retinal detachment in highly myopic eyes with macular hole and posterior staphyloma: mean follow-up of 15 years. Retina. 2005;25(3):285–9.

34. Hsieh YT, Yang CM. Retinal detachment due to paravascular abnormalities-associated breaks in highly myopic eyes. Eye (Lond). 2019;33(4):572–9.

35. Chaturvedi V, Basham RP, Rezaei KA. Scleral depressed vitreous shaving, 360 laser, and perfluoropropane (C3 F8) for retinal detachment. Indian J Ophthalmol. 2014;62(7):804–8.

36. Martinez-Castillo V, Zapata MA, Boixadera A, Fonollosa A, Garcia-Arumi J. Pars plana vitrectomy, laser retinopexy, and aqueous tamponade for

pseudophakic rhegmatogenous retinal detachment. Ophthalmology. 2007;114(2):297–302.

37. Teke MY, Balikoglu-Yilmaz M, Yuksekkaya P, Citirik M, Elgin U, Kose T, et al. Surgical outcomes and incidence of retinal redetachment in cases with complicated retinal detachment after silicone oil removal: univariate and multiple risk factors analysis. Retina. 2014;34(10):1926–38.

38. Ripandelli G, Rossi T, Scarinci F, Stirpe M. Encircling scleral buckling with inferior indentation for recurrent retinal detachment in highly myopic eyes. Retina. 2015;35(3):416–22.

39. Solaiman KA, Dabour SA. Supplemental scleral buckling for inferior retinal detachment in silicone oil-filled eyes. Retina. 2014;34(6):1076–82.

40. Totsuka K, Inui H, Roggia MF, Hirasawa K, Noda Y, Ueta T. Supplemental scleral buckle in vitrectomy for the repair of rhegmatogenous retinal detachment: a systematic review of literature and meta-analysis. Retina (Philadelphia, PA). 2015;35(11):2423–31.

41. Gohil R, Sivaprasad S, Han LT, Mathew R, Kiousis G, Yang Y. Myopic foveoschisis: a clinical review. Eye (London, England). 2015;29(5):593–601.

42. Dolar-Szczasny J, Swiech-Zubilewicz A, Mackiewicz J. A review of current myopic foveoschisis management strategies. Semin Ophthalmol. 2019;34(3):146–56.

43. Meng B, Zhao L, Yin Y, Li H, Wang X, Yang X, et al. Internal limiting membrane peeling and gas tamponade for myopic foveoschisis: a systematic review and meta-analysis. BMC Ophthalmol. 2017;17(1):166.

44. Ho TC, Yang CM, Huang JS, Yang CH, Yeh PT, Chen TC, et al. Long-term outcome of foveolar internal limiting membrane nonpeeling for myopic traction maculopathy. Retina. 2014;34(9):1833–40.

45. Chatziralli IP, Theodossiadis PG, Steel DHW. Internal limiting membrane peeling in macular hole surgery; why, when, and how? Retina. 2018;38(5):870–82.

46. Spiteri Cornish K, Lois N, Scott N, Burr J, Cook J, Boachie C, et al. Vitrectomy with internal limiting membrane (ILM) peeling versus vitrectomy with no peeling for idiopathic full-thickness macular hole (FTMH). Cochrane Database Syst Rev. 2013;(6):CD009306.

47. Rahimy E, McCannel CA. Impact of internal limiting membrane peeling on macular hole reopening: a systematic review and meta-analysis. Retina. 2016;36(4):679–87.

48. Steel DH, Dinah C, Habib M, White K. ILM peeling technique influences the degree of a dissociated optic nerve fibre layer appearance after macular hole surgery. Graefes Arch Clin Exp Ophthalmol. 2015;253(5):691–8.

49. Scupola A, Grimaldi G, Abed E, Sammarco MG, Giudiceandrea A, Greco A, et al. Arcuate nerve fiber layer changes after internal limiting membrane peeling in idiopathic epiretinal membrane. Retina. 2018;38(9):1777–85.

50. Lim LS, Tsai A, Wong D, Wong E, Yeo I, Loh BK, et al. Prognostic factor analysis of vitrectomy for retinal detachment associated with myopic macular holes. Ophthalmology. 2014;121(1):305–10.

51. Mancino R, Ciuffoletti E, Martucci A, Aiello F, Cedrone C, Cerulli L, et al. Anatomical and functional results of macular hole retinal detachment surgery in patients with high myopia and posterior staphyloma treated with perfluoropropane gas or silicone oil. Retina. 2013;33(3):586–92.

52. Fawcett IM, Williams RL, Wong D. Contact angles of substances used for internal tamponade in retinal detachment surgery. Graefes Arch Clin Exp Ophthalmol. 1994;232(7):438–44.

53. Rizzo S, Giansanti F, Finocchio L, Caporossi T, Barca F, Bacherini D, et al. Vitrectomy with internal limiting membrane peeling and air tamponade for myopic foveoschisis. Retina. 2019;39(11):2125–31.

54. Kim KS, Lee SB, Lee WK. Vitrectomy and internal limiting membrane peeling with and without gas tamponade for myopic foveoschisis. Am J Ophthalmol. 2012;153(2):320–6.e1.

55. Wu TY, Yang CH, Yang CM. Gas tamponade for myopic foveoschisis with foveal detachment. Graefes Arch Clin Exp Ophthalmol. 2013;251(5):1319–24.

56. Chen FT, Yeh PT, Lin CP, Chen MS, Yang CH, Yang CM. Intravitreal gas injection for macular hole with localized retinal detachment in highly myopic patients. Acta Ophthalmol. 2011;89(2):172–8.

57. Fabian ID, Moisseiev J. Sutureless vitrectomy: evolution and current practices. Br J Ophthalmol. 2011;95(3):318–24.

58. Curtin BJ, Iwamoto T, Renaldo DP. Normal and staphylomatous sclera of high myopia. An electron microscopic study. Arch Ophthalmol. 1979;97(5):912–5.

59. Chen E. 25-Gauge transconjunctival sutureless vitrectomy. Curr Opin Ophthalmol. 2007;18(3):188–93.

60. Gutfleisch M, Dietzel M, Heimes B, Spital G, Pauleikhoff D, Lommatzsch A. Ultrasound biomicroscopic findings of conventional and sutureless sclerotomy sites after 20-, 23-, and 25-G pars plana vitrectomy. Eye (Lond). 2010;24(7):1268–72.

61. Lopez-Guajardo L, Vleming-Pinilla E, Pareja-Esteban J, Teus-Guezala MA. Ultrasound biomicroscopy study of direct and oblique 25-gauge vitrectomy sclerotomies. Am J Ophthalmol. 2007;143(5):881–3.

62. Takashina H, Watanabe A, Mitooka K, Tsuneoka H. Factors influencing self-sealing of sclerotomy performed under gas tamponade in 23-gauge transconjunctival sutureless vitrectomy. Clin Ophthalmol. 2014;8:2085–9.

63. Parolini B, Prigione G, Romanelli F, Cereda MG, Sartore M, Pertile G. Postoperative complications and intraocular pressure in 943 consecutive cases of 23-gauge transconjunctival pars plana vitrectomy with 1-year follow-up. Retina (Philadelphia, PA). 2010;30(1):107–11.

64. Lee BR, Song Y. Releasable suture technique for the prevention of incompetent wound closure in transconjunctival vitrectomy. Retina. 2008;28(8):1163–5.

65. Peyman GA, Schulman JA, Sullivan B. Perfluorocarbon liquids in ophthalmology. Surv Ophthalmol. 1995;39(5):375–95.

66. Wong TY, Klein BE, Klein R, Knudtson M, Lee KE. Refractive errors, intraocular pressure, and glaucoma in a white population. Ophthalmology. 2003;110(1):211–7.

67. Zhang T, Zhu Y, Jiang CH, Xu GZ. Long-term follow-up of vitrectomy in patients with pathologic myopic foveoschisis. Int J Ophthalmol. 2017;10(2):277–84.

68. Fernandez-Buenaga R, Alio JL, Perez-Ardoy AL, Larrosa-Quesada A, Pinilla-Cortes L, Barraquer R, et al. Late in-the-bag intraocular lens dislocation requiring explantation: risk factors and outcomes. Eye (Lond). 2013;27(7):795–801; quiz 2.

The Role of Pars Plana Vitrectomy (PPV) for the Treatment of Diabetic Macular Edema (DME)

Lekha Mukkamala, R. Joel Welch, and Lawrence S. Morse

Diabetic macular edema (DME) is a major cause of visual morbidity in the USA and developing world [1, 2]. Its prevalence continues to rise due to the expanding diabetic population [3]. The treatment of DME has evolved from focal laser to intravitreal injection of steroids and more recently anti-vascular endothelial growth factor (VEGF) [4–6]. Pars plana vitrectomy (PPV) has been considered a treatment option for DME in various circumstances. It is challenging to make definitive recommendations based on literature reports alone due to the heterogeneity of published studies and limited sample sizes. Meta-analyses attempt to pool data from smaller studies to provide more useful information. We conducted a PubMed search using the terms "pars plana vitrectomy and diabetic macular edema," "vitrectomy for macular edema," "vitrectomy and non-tractional diabetic macular edema," and "vitrectomy and refractory diabetic macular edema." The search yielded several meta-analyses and review articles [7–18], large series (>50 eyes) [19–41], and smaller series [42–79]. The summaries of the reports are presented here, accounting for variability such as morphology (i.e., with or without traction), previous treatments (laser, ste-

roids), and predisposing factors. We hope that this information can guide the recommendations of practicing clinicians, whose patients are likely equally variable.

26.1 Pathophysiology

There are several mechanisms by which PPV is thought to be beneficial for the treatment of DME [7–19, 42]. The vitreous cavity serves as a reservoir for inflammatory molecules that play an important role in the pathogenesis of DME [16]. Multiple factors damage the blood-retina barrier including loss of pericytes, increased permeability of surface membranes of RPE cells and vascular endothelial cells, and vitreoretinal traction, which allows molecules such as pro-inflammatory cytokines, advanced glycation end products (AGE), VEGF, and reactive oxygen species to gain access to the vitreous more readily [16]. Receptors for AGEs have been found on the posterior vitreous cortex, as well as footplates of Muller cells in the ELM and ILM. With activation of AGE receptors in chronic hyperglycemia, there may also be upregulation of VEGF in Muller cells and increased reactive gliosis, thereby inducing structural changes such as non-tractional intraretinal thickening. These alterations can also strengthen the vitreomacular adhesion between the posterior hyaloid and the ILM [2], leading to increased traction and edema.

L. Mukkamala · R. J. Welch · L. S. Morse (✉)
Department of Ophthalmology and Vision Science, University of California, Davis, Sacramento, CA, USA
e-mail: lekha.k.mukkamala@ucdavis.edu; lsmorse@ucdavis.edu

With removal of the vitreous, changes to this pathophysiologic process may reduce DME [16]. Pars plana vitrectomy has been reported to increase vitreous oxygenation in humans and animals, thereby reducing VEGF. In addition, the viscosity of vitreous is 300–2000 times greater than aqueous fluid, allowing molecules such as VEGF and other inflammatory cytokines to more readily diffuse away from the macula [17]. Vitrectomy can prevent the formation of strong adhesions of the posterior hyaloid face to the ILM, thereby preventing any tractional component of DME from developing [33]. In those eyes that have already developed traction, either from a taut posterior hyaloid face or from an epiretinal membrane, vitrectomy can release the mechanical component precipitating edema [16, 24]. The combination of these mechanisms makes vitrectomy a potential treatment option for DME.

26.2 Literature Review

The visual and anatomic outcomes of vitrectomy in various settings (i.e., with and without vitreomacular traction, primary vitrectomy vs. refractory to prior treatment, and with and without ILM peeling) are summarized here.

26.2.1 Eyes with DME and VMT

Multiple studies have shown that eyes with a taut posterior hyaloid membrane and evidence of vitreomacular traction (VMT) respond well to vitrectomy [20–24, 43–46]. Patients experienced resolution or improvement of macular traction and edema, as well as vision, but with eyes with macular ischemia having poorer visual prognosis [24, 45]. The DRCR.net conducted a prospective study investigating the visual and anatomic outcomes of PPV for 87 eyes with DME and VMT, as assessed clinically. All patients underwent PPV with epiretinal membrane (ERM) peeling in 61%, internal limiting membrane (ILM) peeling in 54%, pan retinal photocoagulation (PRP) in 40%, and injection of corticosteroids at the end of the procedure in 64% [22]. Eyes that under-

went cataract surgery at the time of vitrectomy were excluded.

There was a significant reduction in central subfield thickness (CST) on optical coherence tomography (OCT) at 3 and 6 months. At 6 months, there was a decrease by at least 50% of baseline in 68% of eyes, with 43% achieving CST of <250 microns. However, this did not correlate with visual acuity (VA) changes, as there was a wide range of change in VA associated with a given decrease in CST. There was an improvement of ≥10 letters from baseline in 38%, and worsening in 22%. The majority (90%) of patients had follow-up of 12 months, with few changes seen compared to the 6-month visit, despite 20 eyes (26%) undergoing additional procedures (combination of laser, steroids, and anti-VEGF agents) to treat DME, or cataract surgery (12 eyes). Based on these findings, the DRCR.net concluded that vitrectomy in eyes with DME and VMT reduced retinal thickness in most eyes but had variable visual acuity outcomes [22].

26.2.2 Eyes with DME Without VMT

26.2.2.1 Efficacy of Primary PPV in Treatment-Naïve Eyes

The role of vitrectomy as the initial treatment in eyes with DME but without evidence of traction has also been assessed to isolate the physiologic response of DME to PPV [25, 26, 33, 47–49]. A multicenter study of 120 treatment-naïve eyes without vitreomacular interface abnormalities that underwent PPV with ILM peeling was conducted to determine anatomic and visual outcomes. Visual acuity improved significantly in all eyes and remained stable for at least 24 months of follow-up ($p < 0.001$), with 43.3% and 31.7% of eyes gaining ≥5 and ≥10 letters, respectively. Central macular thickness (CMT) similarly significantly decreased and remained stable for 2 years after PPV ($p < 0.001$). The authors identified that shorter time from diagnosis to PPV was a predictor of greater visual improvement, and that for each day PPV was postponed, eyes had a 1.8% decrease in chance to improve by at least five letters by month 24. The presence of

subretinal fluid at baseline was identified as an anatomic predictor of visual improvement. However, CMT was not correlated with functional outcome [33]. None of the eyes required additional pharmacologic or laser intervention during follow-up. No eyes in this study developed visually significant cataracts requiring extraction and there was no statistically significant influence of lens status on the visual outcome ($p = 0.344$). Postoperative adverse events such as intraocular pressure (IOP) elevation, vitreous hemorrhage, and retinal detachment occurred at rates similar to larger studies [33]. The rationale for performing vitrectomy shortly after diagnosis was to take advantage of the overall effects of vitrectomy, such as decreasing concentration of VEGF and other pro-inflammatory cytokines and improving diffusion of VEGF away from the macula, before tractional components developed [33].

A similar series by of 44 eyes with treatment-naïve DME for less than 12 months demonstrated improvement in visual acuity after PPV from logMAR 1.38 (Snellen 20/448) to logMAR 0.83 (20/135) [50]. The majority of patients (60%) sustained visual gains for at least 6 months, and only four eyes had loss of visual acuity. Only three demonstrated recurrence of edema, one of which was treated with two injections of bevacizumab, with no change in vision. Similar to the authors of the previous study, Michalewska et al. [50] suggest that earlier surgical intervention before damage to the outer retinal layers portends a better visual prognosis than those eyes with recalcitrant DME that may have irreversible damage and macular ischemia. Membrane peeling and separation of the posterior hyaloid also eliminate traction that may promote the accumulation of intraretinal fluid [50].

26.2.2.2   Efficacy of PPV for Non-tractional Refractory DME

Given that more conservative measures are often attempted before pursuing surgery, most studies have investigated the outcomes of vitrectomy in eyes with a history of limited response to therapies [27, 51–55]. In a cohort of patients in Iran, eyes with refractory DME (defined as CST >300 μm after at least two intravitreal bevacizumab and one triamcinolone) but with a non-tractional epiretinal membrane underwent PPV, membrane peeling, and ILM peeling. A significant reduction in CST was noted ($p = 0.001$), but visual acuity was unchanged ($p = 0.967$) at a mean follow-up of 13.5 months [51].

Recchia et al. [55] conducted a smaller study in 2004 of 11 eyes with diffuse DME resistant to macular laser photocoagulation for at least 3 months that underwent PPV with ILM peeling. Eyes with epiretinal membrane, taut posterior hyaloid face, prior surgery, active proliferative retinopathy, and evidence of macular ischemia were excluded. Vision improved by at least one line in all eyes and by two lines in seven eyes by 3 months; the majority of these visual gains were sustained at 6 months. Macular thickness decreased by at least 20% in nine eyes and was maintained [55]. They suggested a role of surgery in eyes without vitreoretinal surface abnormalities, in which vitrectomy was not as readily considered [55]. However, this was again in the age in which steroids were the only pharmacologic agents for intravitreal injection.

26.2.2.3   PPV vs. Laser in Non-tractional Refractory DME

Jackson et al. [17] conducted a meta-analysis of randomized controlled trials comparing PPV to the standard of care (observation or macular laser) for non-tractional DME from 1946 to September 2014. Most patients in the pooled analysis demonstrated persistent DME despite macular or grid laser. Change in VA and CST for at least 6 months of follow-up was analyzed, and studies in which supplemental therapy such as intravitreal steroids or anti-VEGF injections were used during follow-up were excluded. Five trials ($n = 113$ eyes) met the inclusion criteria for their efficacy analysis, four of which compared PPV to macular laser, and one to observation. Visual acuity improvement was two letters more (logMAR 0.04) in the PPV group compared to control, but this difference was not significant ($p = 0.18$). However, when conducting additional analyses to control for the variability between studies, there was a near-significant difference in

visual acuity favoring PPV over laser at 6 months ($p = 0.05$), which reversed to favor laser at 12 months ($p = 0.07$). When assessing the response of CST, there was a significantly greater reduction in the PPV group compared to control ($p < 0.00001$) at 6 months, which also reversed by 12 months in a post hoc sub-analysis [17].

A similar meta-analysis of 11 studies ($n = 376$ eyes) by Simunovic et al. [13] demonstrated that PPV provided anatomic and visual improvement compared to natural history at 6 and 12 months in eyes that were previously treated with focal macular laser. However, when comparing concurrent treatment with macular laser versus PPV, surgery showed improved anatomic outcomes but not functional outcomes at 6 months which was not maintained at 12 months [13].

The authors therefore concluded that the visual benefits of vitrectomy for non-tractional DME were not significantly better than laser or observation. Retinal thickness reduction overall appeared to be greater in the vitrectomy groups, but results were not consistent across trials [13, 17].

26.2.2.4 PPV with vs. Without ILM Peeling

In patients that do undergo vitrectomy, the role of internal limiting membrane (ILM) peeling is controversial [13, 14, 18, 31–38, 55–67]. Gentile et al. [57] conducted a histopathologic analysis of ILM from two eyes who had undergone PPV with removal of posterior hyaloid that demonstrated a clinically taut internal limiting membrane. Analyses revealed the presence of inner monolayer of cytokeratin-positive (retinal pigment epithelial cells) and/or glial fibrillary acidic protein-positive cells with smooth muscle actin on immunostaining [57]. Removal of these contractile cells released the tangential traction and helped improve the DME in these two eyes [57]. Although these findings would advocate for ILM removal in all cases, it is unknown if these eyes benefitted specifically due to the traction clinically visible. Perhaps in eyes without this morphology, peeling of ILM would not have had as much benefit. Some authors suggest that even without clinical evidence of traction, peeling of

ILM ensures complete separation of the posterior hyaloid from the macular surface, and may play a role in the resolution of the DME [55].

A comparative study with internal control of 58 patients with 116 eyes with the same degree of non-tractional macular edema treated one eye with PPV without ILM peeling, and one with PPV with ILM peeling. Patients had failed macular laser treatments more than 3 months prior to surgery, but had not undergone intravitreal injections. All phakic eyes underwent simultaneous cataract surgery with vitrectomy. At mean follow-up exam at 80 months, the results were consistent with significantly improved visual acuity for all eyes; however, there was no difference between the cohorts with and without ILM peeling [35].

A meta-analysis of four studies yielding 672 patients by Rinaldi et al. [18] compared PPV with and without ILM peeling and found visual acuity and central macular thickness to be similar in both groups. Similarly, a meta-analysis of five studies with 741 patients similarly concluded that the visual acuity outcomes were not significantly different between patients who had PPV with or without ILM peeling. There was also no difference in central macular thickness or reduction at follow-up [14]. Although greater reduction of macular thickness after ILM peeling has been reported in several other studies, visual acuity was still similar between groups [13].

Although anatomic and visual results may be equivocal in eyes with and without ILM peeling, it is possible that the removal of the ILM may eliminate the potential scaffold for the growth of epiretinal membrane.

26.2.2.5 PPV vs. Intravitreal Steroid in Non-tractional DME

In a study of 40 eyes from 20 patients with bilateral DME, one eye was treated with PPV without ILM peeling, while the other received 4 mg of intravitreal triamcinolone [68]. Eyes in the IVT cohort showed a significant reduction in central macular thickness (CMT) at months 1 and 3 ($p < 0.0001$), which then increased almost to baseline by month 12. However, the PPV group showed a gradual decrease in CMT that was

significantly less than baseline by 12 months ($p < 0.0001$), and significantly less than the IVT cohort ($p = 0.0003$). Although visual acuity improved slightly as CMT decreased, there was no significant difference in vision between the two groups or between baseline and follow-up in either cohort. Given that each study eye was paired, systemic differences such as glucose control were not an influencing factor [68].

26.2.2.6 PPV vs. Intravitreal Anti-VEGF in Refractory Non-tractional DME

Few studies have compared the role of vitrectomy in the more recent era of treatment with anti-VEGF agents. Raizada et al. [67] conducted a comparative study of 44 eyes with refractory and non-tractional DME that were treated with either 3-monthly bevacizumab injections or PPV with ILM peeling. Patients had previously shown minimal response to laser and anti-VEGF or steroid injections, with last treatment being more than 3 months prior to enrollment. Vision significantly improved in both groups by 4 months, but was more rapid in the PPV group. Although 72.8% of patients demonstrated an improvement in vision in the bevacizumab group, compared to 59.1% in the PPV cohort, the mean change in visual acuity was similar between treatment arms (logMAR 0.20 and 0.19, respectively; $p = 0.871$). Macular thickness decreased more in the PPV group compared to bevacizumab at 4 months, but the difference was not significant ($p = 0.068$) [67]. No additional treatments were given after vitrectomy. Safety data was similar to larger scale studies [67]. The authors commented that most of their patients were pseudophakic and follow-up time of 4 months may be too short to show progression of cataract in the others. They acknowledged that although similar results in both functional and anatomic results were achieved, intravitreal injections would require multiple simple treatments, while vitrectomy involves a one-time procedure requiring more skill [67]. This study was also conducted before the use of more potent anti-VEGF agents, and prior to evidence regarding effective treatment regimens that have become available in recent years.

26.2.3 Predictors of Visual Outcome and Durability

Studies have demonstrated variable visual results after vitrectomy, regardless of anatomic success [19, 22, 33, 37–41, 53, 70–79]. In order to predict which patients would have the most visual response to PPV for DME, Chhablani et al. [70] analyzed preoperative OCTs of eyes with refractory DME. The integrity of the external limiting membrane was found to be most predictive of visual outcome ($p = 0.0277$). In their cohort of 34 eyes, each percentage increase in ELM integrity led to a 0.13 letter gain in vision. The IS/OS junction and central macular thickness were less accurate predictors of visual outcome ($p = 0.18$) [70]. Iglicki et al. [33] found that the presence of subretinal fluid at baseline was also an anatomic predictor of visual improvement. This may help in counseling patients regarding the amount of visual improvement expected after vitrectomy based on preoperative studies.

In addition, as with any systemic disease with ocular manifestation, treatment of the underlying condition is paramount to decreasing the chances of visual loss from diabetic macular edema. Yamada and coauthors [79] determined that HbA1c was the most predictive of visual and anatomic outcomes after PPV for DME. Duration of edema is also a strong factor to determine visual outcomes. As identified in treatment-naïve eyes by Iglicki et al. [33], shorter time from diagnosis to intervention was associated with visual gains.

To assess the durability of effect after vitrectomy, Navarrete-Sanchis et al. [53] conducted a year-long study assessing vision and CMT after surgery in eyes with non-tractional edema that were refractory to laser treatment. The authors noted that 45.5% of eyes met the criteria for surgical success (greater than 20% reduction in CMT, CMT of <300 μm, and no visual loss), 70% of which remained stable after 1 year [53]. Similar duration of effect was seen in the study comparing PPV to observation in treatment-naïve eyes, with effect lasting for 2 years [33]. This attests for the longevity of CMT reduction after vitrectomy, which may be important when considering the benefits of a potentially one-time

treatment of vitrectomy, compared to multiple and repeated administrations of intravitreal injections and lasers. This burden of care may influence the clinician's decision.

26.2.4 Surgical Considerations

Although patients would ideally require few additional interventions after undergoing vitrectomy, some may still necessitate future treatment with anti-VEGF. However, in a rabbit model, intravitreal retention of the drug in vitrectomies eyes was significantly less than in nonsurgical eyes [80]. Radiolabeled (I-124) bevacizumab and ranibizumab cleared significantly faster in eyes that underwent pars plana vitrectomy (2.30 ± 0.09 days and 2.13 ± 0.05 days, respectively) compared to nonsurgical controls (4.22 ± 0.07 days and 2.81 ± 0.05 days, respectively, $p < 0.0001$) [80]. Therefore, if anti-VEGF treatment is required postoperatively, the frequency may be much higher than those who have not had surgery. One potential advantage of surgery is the possible reduction of cost with a one-time intervention as patients that require prolonged courses of intravitreal injections may incur cumulatively more expense.

Surgical intervention inherently carries the risk of complications such as retinal tears, infection, and cataract progression. The studies reported here demonstrated safety data consistent with general reported standards. In the largest meta-analysis cited here, Jackson et al. [17] pooled data from 40 studies (1562 eyes) and demonstrated minimal safety concerns. The most common complications were retinal tear (7.1%), elevated intraocular pressure (5.2%), epiretinal membrane (3.3%), and vitreous hemorrhage (2.4%). Cataract formation was found in 68.6% of 121 phakic eyes. These risks must be compared to those of other treatment modalities as well. Macular laser is considered a safe treatment with minimal ocular and no systemic side effects. Intravitreal steroids carry the risk of infection as well as side effects such as IOP elevation and cataract [68]. Intravitreal anti-VEGF injections have minimal risk for endophthalmitis

(0.019–1.6%), with lower rates reported in more recent studies [81].

Key Points
- Pars plana vitrectomy is thought to be beneficial for diabetic macular edema by improving diffusion of molecules such as VEGF and other pro-inflammatory cytokines away from the macula, improving the oxygen tension in the vitreous cavity, and relieving any clinical or subclinical traction. However, the retention of anti-VEGF medications in the vitreous may be less after vitrectomy.
- Eyes with evidence of traction from taut hyaloid face or epiretinal membrane have anatomic benefit from PPV by relieving the tractional component of the DME, but visual gains do not often correlate.
- Treatment-naïve eyes that undergo vitrectomy may have a significant and sustained decrease in macular thickness and improvement in vision without additional treatment. Vision is more likely to improve in eyes with shorter duration of DME.
- Eyes that have been refractory to laser treatment may achieve anatomic but not visual results when treated with vitrectomy compared to natural history or additional laser therapy.
- ILM peeling does not definitively improve anatomic or visual outcomes; however, based on histopathology, the removal of contractile cells and the scaffold for regrowth of epiretinal membrane may provide better long-term results.
- PPV may provide longer term reduction in macular thickness compared to intravitreal steroids, but visual acuity may not be different between groups.
- PPV may have similar reduction of macular thickness and improvement in vision compared to multiple intravitreal bevacizumab injections.
- Post-PPV eyes with intact ELM on OCT may have better visual prognosis.
- Shorter duration of DME and better glycemic control may be indicative of better anatomic and visual outcomes after PPV.

- Safety data demonstrates standard risks of PPV associated with retinal surgery.
- Further study with a larger randomized trial is necessary to further elucidate the role of vitrectomy in diabetic macular edema, particularly in comparison to treatment with anti-VEGF injections.

References

Background

1. Guariguata L, Whiting DR, Hambleton I, et al. Global estimates of diabetes prevalence for 2013 and projections for 2035. Diabetes Res Clin Pract. 2014;103(2):137–49.
2. Bhagat N, Grigorian RA, Tutela A, Zarbin MA. Diabetic macular edema: pathogenesis and treatment. Surv Ophthalmol. 2009;54(1):1–32.
3. Zhang X, Saaddine JB, Chou C, et al. Prevalence of diabetic retinopathy in the United States, 2005-2008. JAMA. 2010;304(6):649–56.
4. Photocoagulation for diabetic macular edema. Early treatment diabetic retinopathy study report number 1. Early diabetic retinopathy study research group. Arch Ophthalmol. 1985;103(12):1796–806.
5. Ip MS, Bressler SB, Antonszyk AN, et al. A randomized trial comparing intravitreal triamcinolone and focal/grid photocoagulation for diabetic macular edema: baseline features. Retina. 2008;28(7):919–30.
6. Nguyen QD, Brown DM, Marcus DM, et al. Ranibizumab for diabetic macular edema: results from 2 phase II randomized trials: RISE and RIDE. Ophthalmology. 2012;119(4):789–801.

Meta-analyses and Reviews

7. Ho T, Smiddy WE, Flynn HW Jr. Vitrectomy in the management of diabetic eye disease. Surv Ophthalmol. 1992;37(3):190–202.
8. Lewis H. The role of vitrectomy in the treatment of diabetic macular edema. Am J Ophthalmol. 2001;131(1):123–5.
9. Christoforidis JB, D'Amico DJ. Surgical and other treatments of diabetic macular edema: an update. Int Ophthalmol Clin. 2004;44(1):139–60.
10. Laidlaw DA. Vitrectomy for diabetic macular oedema. Eye (Lond). 2008;22(10):1337–41.
11. Smiddy WE. Clinical applications of cost analysis of diabetic macular edema treatments. Ophthalmology. 2012;119(12):2558–62.
12. Golan S, Loewenstein A. Surgical treatment for macular edema. Semin Ophthalmol. 2014;29(4):242–56.
13. Simunovic MP, Hunyor AP, Ho IV. Vitrectomy for diabetic macular edema: a systematic review and meta-analysis. Can J Ophthalmol. 2014;49(2):188–95.
14. Nakajima T, Roggia MF, Noda Y, Ueta T. Effect of internal limiting membrane peeling during vitrectomy for diabetic macular edema: systematic review and meta-analysis. Retina. 2015;35(9):1719–25.
15. Talcott KE, Modjtahedi BS, Eliott D. Surgical management of diabetic macular edema. Int Ophthalmol Clin. 2015;55(4):123–36.
16. Crim N, Velez-Montoya R, Morales-Canton V. Surgical versus medical treatment for diabetic macular edema: a review. Med Hypothesis Discov Innov Ophthalmol. 2017;6(5):136–42.
17. Jackson TL, Nicod E, Angelis A, et al. Pars plana vitrectomy for diabetic macular edema: a systematic review, meta-analysis, and synthesis of safety literature. Retina. 2017;37(5):886–95.
18. Rinaldi M, dell'Omo R, Morescalchi F, et al. ILM peeling in nontractional diabetic macular edema: review and metanalysis. Int Ophthalmol. 2018;38(6):2709–14.

Large Series

19. Murakami T, Nishijima K, Akagi T, et al. Segmentational analysis of retinal thickness after vitrectomy in diabetic macular edema. Invest Ophthalmol Vis Sci. 2012;53(10):6668–74.
20. Bonnin S, Sandali O, Bonnel S, Monin C, El Sanharawi M. Vitrectomy with interal limiting membrane peeling for tractional and nontractional diabetic macular edema: long-term results of a comparative study. Retina. 2015;35(5):921–8.
21. Browning DJ, Lee C, Stewart MW, Landers MB 3rd. Vitrectomy for center-involved diabetic macular edema. Clin Ophthalmol. 2016;10:735–42.
22. DRCR.net Writing Committee, Haller JA, Qin H, et al. Vitrectomy outcomes in eyes with diabetic macular edema and vitreomacular traction. Ophthalmology. 2010;117(6):1087–93.
23. Flaxel CJ, Edwards AR, Aiello LP, et al. Factors associated with visual acuity outcomes after vitrectomy for diabetic macular edema: diabetic retinopathy clinical research network. Retina. 2010;30(9):1488–95.
24. Pendergast SD, Hassan TS, Williams GA, et al. Vitrectomy for diffuse diabetic macular edema associated with a taut premacular posterior hyaloid. Am J Ophthalmol. 2000;130(2):178–86.
25. Kumagai K, Furukawa M, Ogino N, et al. Long-term follow-up of vitrectomy for diffuse nontractional diabetic macular edema. Retina. 2009;29(4):464–72.
26. Yamamoto T, Takeuchi S, Sato Y, Yamashita H. Long-term follow-up results of pars plana vitrectomy for diabetic macular edema. Jpn J Ophthalmol. 2007;51(4):285–91.
27. Ikeda T, Sato K, Katano T, Hayashi Y. Improved visual acuity following pars plana vitrectomy for dia-

betic cystoid macular edema and detached posterior hyaloid. Retina. 2000;20(2):220–2.

28. Kralinger MT, Pedri M, Kralinger F, Troger J, Kieselbach GF. Long-term outcome after vitrectomy for diabetic macular edema. Ophthalmologica. 2006;220(3):147–52.

29. Romano MR, Roman V, Vallejo-Garcia JL, et al. Macular hypotrophy after internal limiting membrane removal for diabetic macular edema. Retina. 2014;34(6):1182–9.

30. Stolba U, Binder S, Gruber D, Krebs I, Aggerman T, Neumaier B. Vitrectomy for persistent diffuse diabetic macular edema. Am J Ophthalmol. 2005;140(2):295–301.

31. Asahina Y, Tachi N, Asahina Y, et al. Six-month postoperative outcomes of intraoperative OCT-guided surgical cystotomy for refractory cystoid macular edema in diabetic eyes. Clin Ophthalmol. 2017;11:2099–105. eCollection 2017.

32. Bahadir M, Ertan A, Mertoglu O. Visual acuity comparison of vitrectomy with and without internal limiting membrane removal in the treatment of diabetic macular edema. Int Ophthalmol. 2005;26(1–2):3–8.

33. Iglicki M, Lavaque A, Ozimek M, et al. Biomarkers and predictors for functional and anatomic outcomes for small gauge pars plana vitrectomy and peeling of the internal limiting membrane in naïve diabetic macular edema: the VITAL Study. PLoS One. 2018;13(7):e0200365. eCollection 2018.

34. Kalvoda J, Duskova J, Kubena A, Povysil C, Kalvodova B. Morphometry of surgically removed internal limiting membrane during vitrectomy in diabetic macular edema. Graefes Arch Clin Exp Ophthalmol. 2009;247(10):1307–14.

35. Kumagai K, Hangai M, Ogino N, Larson E. Effect of internal limiting membrane peeling on long-term visual outcomes for diabetic macular edema. Retina. 2015;35(7):1422–8.

36. Yamakoshi T, Kachi S, Sugita J, et al. Triamcinolone-assisted removal of internal limiting membrane enhances the effect of vitrectomy for diabetic macular edema. Ophthalmic Res. 2009;41(4):203–9.

37. Yoshikawa M, Murakami T, Nishijima K, et al. Macular migration toward the optic disc after inner limiting membrane peeling for diabetic macular edema. Invest Ophthalmol Vis Sci. 2013;54(1):629–35.

38. Kogo J, Shiono A, Sasaki H, et al. Foveal microstructure analysis in eyes with diabetic macular edema treated with vitrectomy. Adv Ther. 2017;34(9):2139–49. Epub 2017 Aug 14.

39. Ichiyama Y, Sawada O, Mori T, et al. The effectiveness of vitrectomy for diffuse diabetic macular edema may depend on its preoperative optical coherence tomography pattern. Graefes Arch Clin Exp Ophthalmol. 2016;254(8):1545–51.

40. Kim J, Kang SW, Shin DH, et al. Macular ischemia and outcome of vitrectomy for diabetic macular edema. Jpn J Ophthalmol. 2015;59(5):295–304.

41. Uji A, Murakami T, Suzuma K. Influence of vitrectomy surgery on the integrity of outer retinal layers in diabetic macular edema. Retina. 2018;38(1):163–72.

Smaller Series

42. Matsunaga N, Ozeki H, Hirabayashi Y, Shimada S, Ogura Y. Histopathologic evaluation of the internal limiting membrane surgically excised from eyes with diabetic maculopathy. Retina. 2005;25(3):311–6.

43. Abdel Hadi AM. Evaluation of vitrectomy with planned foveal detachment as surgical treatment for refractory diabetic macular edema with or without vitreomacular interface abnormality. J Ophthalmol. 2018;2018:9246384. eCollection 2018.

44. Gungel H, Altan C, Baylancicek DO, et al. The effects of 23-gauge pars plana vitrectomy on orbital circulation using doppler ultrasonography in diabetic macular edema with epiretinal membrane and taut posterior hyaloid. Curr Eye Res. 2017;42(1):118–24.

45. Lewis H, Abrams GW, Blumenkranz MS, Campo RV. Vitrectomy for diabetic macular traction and edema associated with posterior hyaloid traction. Ophthalmology. 1992;99(5):753–9.

46. Yamamoto T, Akabane N, Takeuchi S. Vitrectomy for diabetic macular edema: the role of posterior vitreous detachment and epimacular membrane. Am J Ophthalmol. 2001;132(3):369–77.

47. Patel JI, Hykin PG, Schadt M, Luong V, Fitzke F, Gregor ZJ. Pars plana vitrectomy for diabetic macular oedema: OCT and functional correlations. Eye (Lond). 2006;20(6):674–80.

48. Yoshizumi Y, Ohara Z, Tabuchi H, et al. Effects of kallidinogenase in patients undergoing vitrectomy for diabetic macular edema. Int Ophthalmol. 2018;39(6):1307–13.

49. Figueroa MS, Contreras I, Noval S. Surgical and anatomical outcomes of pars plana vitrectomy for diffuse nontractional diabetic macular edema. Retina. 2008;28(3):420–6.

50. Michalewska Z, Stewart MW, Lander MB 3rd, et al. Vitrectomy in the management of diabetic macular edema in treatment-naïve patients. Can J Ophthalmol. 2018;53(4):402–7.

51. Ghassemi F, Bazvand F, Roohipoor R, et al. Outcomes of vitrectomy, membranectomy and internal limiting membrane peeling in patients with refractory diabetic macular edema and non-tractional epiretinal membrane. J Curr Ophthalmol. 2016;28(4):199–205.

52. Ikeda T, Sato K, Katano T, Hayashi Y. Vitrectomy for cystoid macular oedema with attached posterior hyaloid membrane in patients with diabetes. Br J Ophthalmol. 1999;83(1):12–4.

53. Navarrete-Sanchis J, Zarco-Bosquets J, Tomas-Torrent JM, Diago T, Ortega-Evangelio L. Long-term effectiveness of vitrectomy in diabetic cystoid

macular edema. Graefes Arch Clin Exp Ophthalmol. 2015;253(5):713–9.

54. Rosenblatt BJ, Shah GK, Sharma S, Bakal J. Pars plana vitrectomy with internal limiting membranectomy for refractory diabetic macular edema without a taut posterior hyaloid. Graefes Arch Clin Exp Ophthalmol. 2005;243(1):20–5.

55. Recchia FM, Ruby AJ, Carvalho Recchia CA. Pars plana vitrectomy with removal of the internal limiting membrane in the treatment of persistent diabetic macular edema. Am J Ophthalmol. 2005;139(3):447–54.

56. Yanyali A, Horozoglu F, Celik E, Ercalik Y, Nohutcu AF. Pars plana vitrectomy and removal of the internal limiting membrane in diabetic macular edema unresponsive to grid laser photocoagulation. Eur J Ophthalmol. 2006;16(4):573–81.

57. Gentile RC, Milman T, Eliott D, Romero JM, McCormick SA. Taut internal limiting membrane causing diffuse diabetic macular edema after vitrectomy: clinicopathological correlation. Ophthalmologica. 2011;226(2):64–70.

58. Hartely KL, Smiddey WE, Flynn HW Jr, Murray TG. Pars plana vitrectomy with internal limiting membrane peeling for diabetic macular edema. Retina. 2008;28(3):410–9.

59. Hoerauf H, Bruggeman A, Muecke M, et al. Pars plana vitrectomy for diabetic macular edema. Internal limiting membrane delamination vs posterior hyaloid removal. A prospective randomized trial. Graefes Arch Clin Exp Ophthalmol. 2011;249(7):997–1108.

60. Jahn CE, Topfner von Schutz K, Richter J, Boller J, Kron M. Improvement of visual acuity in eyes with diabetic macular edema after treatment with pars plana vitrectomy. Ophthalmologica. 2004;218(6):378–84.

61. Kimura T, Kiryu J, Nishiwaki H, Oh H, Suzuma K, Watanabe D, Kurimoto M, Takagi H. Efficacy of surgical removal of the internal limiting membrane in diabetic cystoid macular edema. Retina. 2005;25(4):454–61.

62. Patel JI, Hykin PG, Schadt M, Luong V, Fitzke F, Gregor ZJ. Pars plana vitrectomy with and without peeling of the inner limiting membrane for diabetic macular edema. Retina. 2006;26(1):5–13.

63. Tamura K, Yokoyama T, Ebihara N, Murakami A. Histopathologic analysis of the internal limiting membrane surgically peeled from eyes with diffuse diabetic macular edema. Jpn J Ophthalmol. 2012;56(3):280–7.

64. Yamamoto T, Hitani K, Sato Y, Yamashita H, Takeuchi S. Vitrectomy for diabetic macular edema with and without internal limiting membrane removal. Ophthalmologica. 2005;219(4):206–13.

65. Yanyali A, Horozoglu F, Celik E, Nohutcu AF. Long-term outcomes of pars plana vitrectomy with internal limiting membrane removal in diabetic macular edema. Retina. 2007;27(5):557–66.

66. Yoshitake S, Murakami T, Uji A, et al. Association between cystoid spaces on indocyanine green hyperfluorescence and optical coherence tomography after vitrectomy for diabetic macular oedema. Eye (Lond). 2014;28(4):439–48.

67. Raizada S, Al Kandari J, Al Diab F, et al. Pars plana vitrectomy versus three intravitreal injections of bevacizumab for nontractional diabetic macular edema. A prospective, randomized comparative study. Indian J Ophthalmol. 2015;63(6):504–10.

68. Doi N, Sakamoto T, Sonoda Y, et al. Comparative study of vitrectomy versus intravitreous triamcinolone for diabetic macular edema on randomized paired-eyes. Graefes Arch Clin Exp Ophthalmol. 2012;250(1):71–8.

69. Higuchi A, Ogata N, Jo N, Wada M, Matsumura M. Pars plana vitrectomy with removal of posterior hyaloid face in treatment of refractory diabetic macular edema resistant to triamcinolone acetonide. Jpn J Ophthalmol. 2006;50(6):529–31.

70. Chhablani JK, Kim JS, Cheng L, Kozak I, Freeman WV. External limiting membrane as a predictor of visual improvement in diabetic macular edema after pars plana vitrectomy. Graefes Arch Clin Exp Ophthalmol. 2012;250(10):1415–20.

71. Giovannini A, Amato G, Mariotti C, Scassellati-Sforzolini B. Optical coherence tomography findings in diabetic macular edema before and after vitrectomy. Ophthalmic Surg Lasers. 2000;31(3):187–91.

72. Hatano N, Mizota A, Tanaka M. Vitreous surgery for diabetic macular edema—its prognosis and correlation between preoperative systemic and ocular conditions and visual outcome. Ann Ophthalmol (Skokie). 2007;39(3):222–7.

73. Ma J, Yao K, Jiang J, Wu D, Gao R, Yin J, Fang X. Assessment of macular function by multifocal electroretinogram in diabetic macular edema before and after vitrectomy. Doc Ophthalmol. 2004;109(2):131–7.

74. Nishijima K, Murakami T, Hirashima T, et al. Hyperreflective foci in outer retina predictive of photoreceptor damage and poor vision after vitrectomy for diabetic macular edema. Retina. 2014;34(4):732–40.

75. Park JH, Woo SJ, Ha YJ, Yu H. Effect of vitrectomy of macular microcirculation in patients with diffuse diabetic macular edema. Graefes Arch Clin Exp Ophthalmol. 2009;247(8):1009–17.

76. Shah SP, Patel M, Thomas D, Aldington S, Laidlaw DA. Factors predicting outcome of vitrectomy for diabetic macular oedema: results of a prospective study. Br J Ophthalmol. 2006;90(1):33–6.

77. Teresaki H, Kojima T, Niwa H, Piao CH, Ueno S, Kondo M, Ito Y, Miyake Y. Changes in focal macular electroretinograms and foveal thickness after

vitrectomy for diabetic macular edema. Invest Ophthalmol Vis Sci. 2003;44(10):4465–72.

78. Wakabayashi Y, Kimura K, Muramatsu D, et al. Axial length as a factor associated with visual outcome after vitrectomy for diabetic macular edema. Invest Ophthalmol Vis Sci. 2013;54(10):6834–40.

79. Yamada Y, Suzuma K, Ryu M, et al. Systemic factors influence the prognosis of diabetic macular edema after pars plana vitrectomy with internal limiting membrane peeling. Curr Eye Res. 2013;38(12):1261–5.

Other

80. Christoforidis JB, Williams MM, Wang J, et al. Anatomic and pharmacokinetic properties of intravitreal bevacizumab and ranibizumab after vitrectomy and lensectomy. Retina. 2013;33(5):946–52.

81. Falavarjani KG, Nguyen QD. Adverse events and complications associated with intravitreal injection of anti-VEGF agents: a review of literature. Eye (Lond). 2013;27(7):787–94.

Retinal Endovascular Surgery

27

Kazuaki Kadonosono

27.1 Introduction

Most of the retinal diseases are associated with occlusion of retinal vessels. However, we have not established surgical approach for retinal vessels yet because of its extremely small size. Retinal endovascular surgery (REV) is an exciting new avenue for retinal surgeons, and researchers are making efforts to develop effective REV techniques. An experimental study of REV was started during the 1990s. In the late 1990s, REV treatment first began as an insertion of a microcannula into branches of the retinal vasculature with injection of pharmacologic agents such as t-PA for eyes with central retinal vein occlusion [1, 2]. Some previous reports on visual acuity in CRVO patients suggested that REV can lead to recovery of vision; however, other reports showed little benefit [3, 4]. One thing that was the most challenging for REV was the retinal endovascular procedure itself. In this capture, the principle, a surgical procedure, and results of REV we have developed are noted.

27.2 Development of Endovascular Surgery with a Microneedle

Endovascular surgery involves three main variables: which instruments are used; how the vessels are pierced; and where the needle is placed. A micropipette had been used for a long time for retinal endovascular surgery manually, and it had been pierced into the central retinal vein.

However, we developed a technique for endovascular surgery which involves using a special needle to pierce the central retinal vein, and bimanually inject tPA at 2014 [5] (Fig. 27.1). We feel that the microneedle we have developed is an important instrument for cannulation. In recent years, microneedles have been fabricated
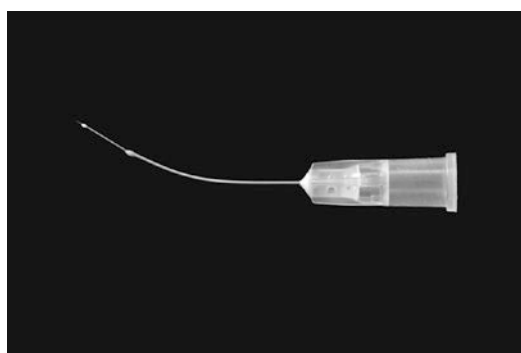
Fig. 27.1 A picture of a microneedle which is made of stainless steel; its outer diameter is 50 microns and inner diameter is 20 microns

K. Kadonosono (✉)
Department of Ophthalmology and Micro-technology, Yokohama City University, Yokohama, Japan
e-mail: kado@med.yokohama-cu.ac.jp

based on tools from the microelectronics industry, and they have been assessed as effective devices to facilitate administration delivery [6]. Fabricated microneedles are sharp and rigid, making them capable of serving as tools for microvascular surgery [6, 7]. We compared the capabilities of microneedles and conventional micropipettes for use in a microvascular procedure in porcine eyes and assessed the performance of microneedles as tools for retinal endovascular surgery [5]. As a result, we confirmed that microneedles are more feasible than micropipettes.

27.3 Surgical Indication of Endovascular Surgical Procedure

CRVO is an important cause of vision loss [8, 9]. The only proven treatment for CRVO in the past was the central vein occlusion study which showed neither improvement with grid laser treatment for macular edema nor prophylactic effect of panretinal photocoagulation [10]. Recently the use of ranibizumab was also reported in a prospective, randomized study to improve visual acuity for eyes with macular edema due to CRVO [11]. When considering the pathogenesis of CRVO, the inciting event is thought to be thrombosis within the central retinal vein, which was supported by a previous pathological study [12]. Occlusion of the major outflow channel for retinal circulation obviously increases venous pressure, resulting in the macular edema and hemorrhages typical of the disease. These persistent macular edema and/or hemorrhages have irreversible adverse effects on essential retinal cells including photoreceptors. If the eye simultaneously has closure of a substantial proportion of the perifoveal capillaries, vision is severely impaired. One pathological study showed that the venous thrombus was present at the level of the lamina cribrosa in eyes with CRVO.

We consider that eyes with CRVO are well indicated for REV and its timing should be an earliest intervention to avoid macular structure infarction. And also, eyes with refractory macular edema after many injections of anti-VEGF drug are also indicated for REV in which a cannulation procedure is the only method to improve refractory macular edema.

27.4 Surgical Procedure

All surgical procedures were performed using a 25-gauge microincisional vitrectomy system with the Constellation Vision System (Alcon Laboratories, Fort Worth, Texas). After displacement of the conjunctiva, a total of four trocars were inserted, with one trochanter used for chandelier illumination with a light source (Brightstar, DORC Company, Holland). After a core vitrectomy, both the posterior hyaloidal membrane and the internal limiting membrane around the macular region were removed. To pierce the dilated retinal vein, a microneedle with an outer diameter of 50 μm was used (Fig. 27.2). This instrument, which has been developed and manufactured solely for retinal endovascular surgery, is sharp and stiff enough to perform piercing procedures in very small vessels. The needle was connected to a 10 cc syringe containing tissue plasminogen activator (tPA) (Criactor, Eisai pharmaceutical com., Japan) with balanced saline solution (BSS plus, Alcon Laboratories, Fort Worth, Texas) (Fig. 27.3). The concentration of tPA is 43 μg/ mL which is prepared just before cannulation in an operating room. The volume of BSS with tPA injected was in proportion with the pressure of the syringe connected to the viscous fluid control system, which was controlled by the surgeon using a pedal. To manage any sudden hemorrhages during the piercing, a bimanual procedure was used, with the surgeon holding the microneedle in the right hand, and a flute needle for the suction of possible bleeding in the left hand. When accurately piercing the dilated retinal vein close to the optic nerve in an eye with CRVO, a slight sensation of loss of resistance occurs, indicating that BSS can be slowly
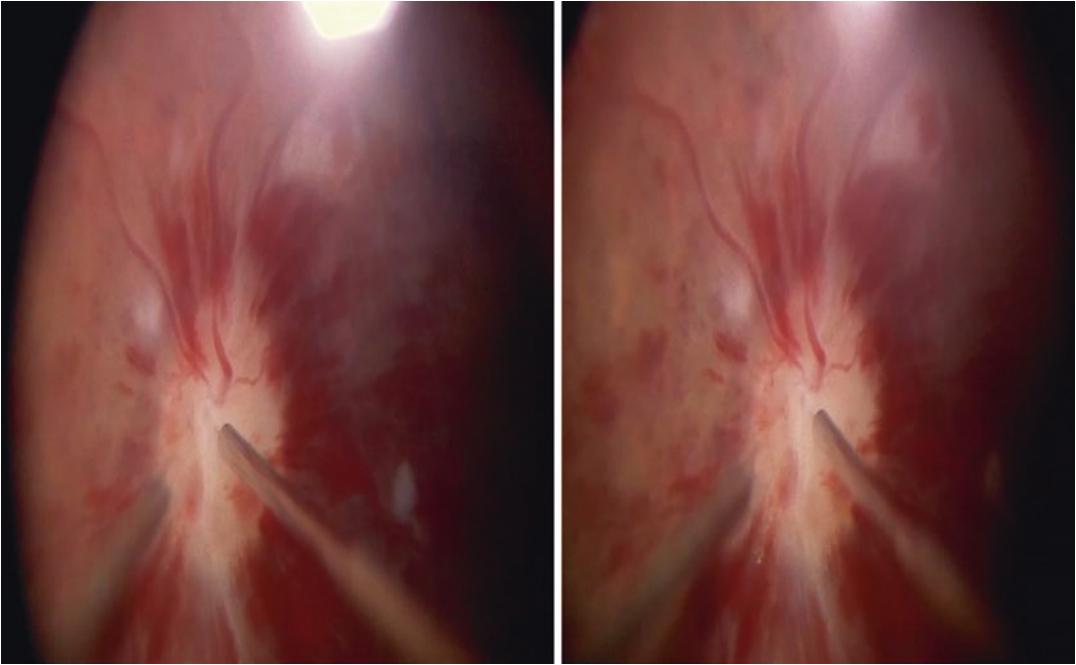
Fig. 27.2 A picture of retinal vein cannulation. The microneedle is pierced into the central retinal vein using a 3D system

injected into the retinal vein with a pressure of about 4 psi. After confirming that the vessel has turned white, the pressure is elevated to 40 psi. The time of injection is roughly 3 min, and during this period the flow of BSS in the retinal vessel can be clearly observed as a streamline. After removal of the microneedle, the vessel is checked for any bleeding.

27.4.1 Surgical Results

We reported the study published [13]. In this study, the BCVA of 9 of 12 patients had improved by more than 15 letters at 24 weeks after surgery compared with the baseline value. The mean VA had improved by 14.1 letters at 6 weeks, by 15.3 letters at 12 weeks, by 15.3 letters at 18 weeks, and by 16.3 letters at 24 weeks. The preoperative mean BCVA of 29.6 letters (20/250) had improved to 45.9 letters (20/125) at 24 weeks after surgery, and the mean decrease in central foveal thickness was 271.1 μm.

27.4.2 Complications

In our report published, no neovascular glaucoma was observed in any of the patients when examined at 24 weeks. All surgical procedures were successful, as confirmed by the streamlined flow during the injection. Intraoperative complications developed in two patients and consisted of a mild vitreous hemorrhage in one eye and a small subretinal hemorrhage in one eye, neither of which impaired VA. No occurrences of retinal tears, endophthalmitis, retinal detachment, severe vitreous hemorrhage, or recurrence of macular edema were observed during the 24-week follow-up period.

However, we should carefully follow up patients with ischemic CRVO which has a relatively high risk of developing neovascular glaucoma with performing panretinal photocoagulation. The occurrence rate of macular edema is not so high; however when we see macular edema which usually occurs about a month after cannulation, we routinely inject steroid into a sub-Tenon's space.

Fig. 27.3 A picture of retinal endovascular surgery. A surgeon holds a microneedle in the right hand to get inside an eye for injection while holding a soft-tip cannula with the left hand (**a**). A cannula is connected with 10 cc syringe, which is controlled by a foot switch in a vitrectomy machine (**b**)
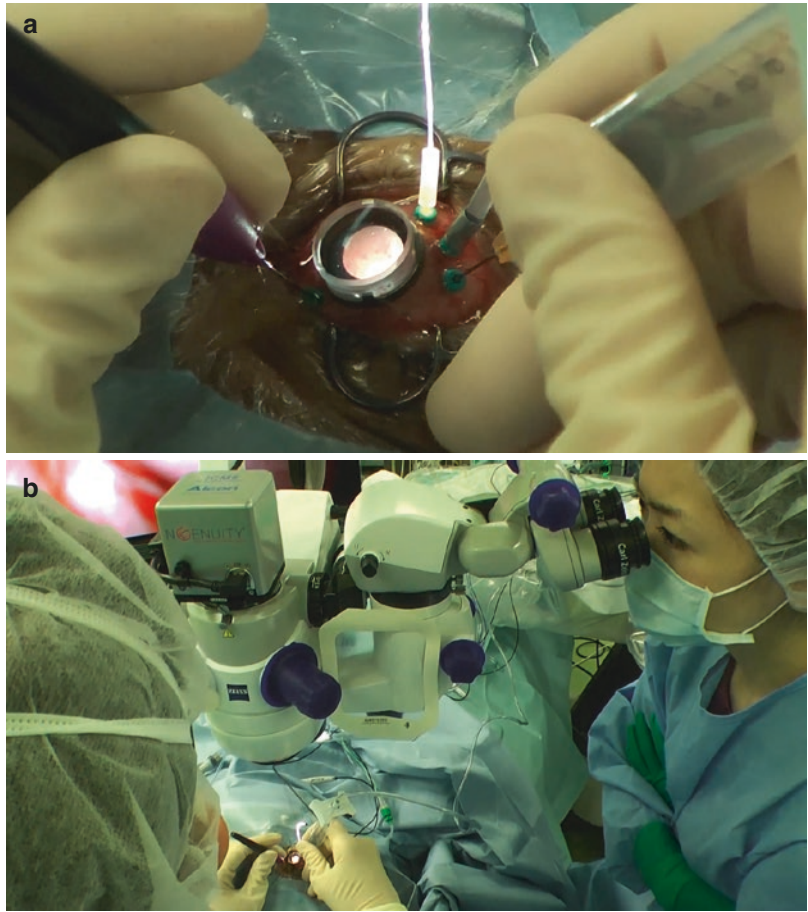
27.5 Recent Development of Cannulation for CRAO

Central retinal artery occlusion (CRAO) is caused by a thrombus or embolism in the central retinal artery. Mainly occurring in the optic nerve head, it is an ophthalmological emergency often resulting in blindness due to the resulting inner retinal ischemia [14]. If the embolism is resolved in an eye with CRAO by retinal endovascular surgery, we are able to confirm significant improvement of occluded blood flow, resulting in improved vision of a patient with CRAO. We routinely perform eyes with CRAO within 72 h or less after the onset. Patients with heart or brain problems are excluded. Surgical procedure is same as that in CRVO (Fig. 27.4). The one point different from REV for CRVO is to pierce central retinal artery. It is sometimes difficult to distinguish which vessels are arterial because the diameter of vessels is quite different from the normal one. The risk of sudden bleeding from the pierced site is much lower than expected because an arterial vessel in an eye with CRAO is essentially occluded. If the bleeding happens in an artery during cannulation, it is a good sign demonstrating recanalization of vessels. In cases with sudden bleeding in cannulation, we passively aspirate the bleeding with a soft-tip cannula in the left hand.
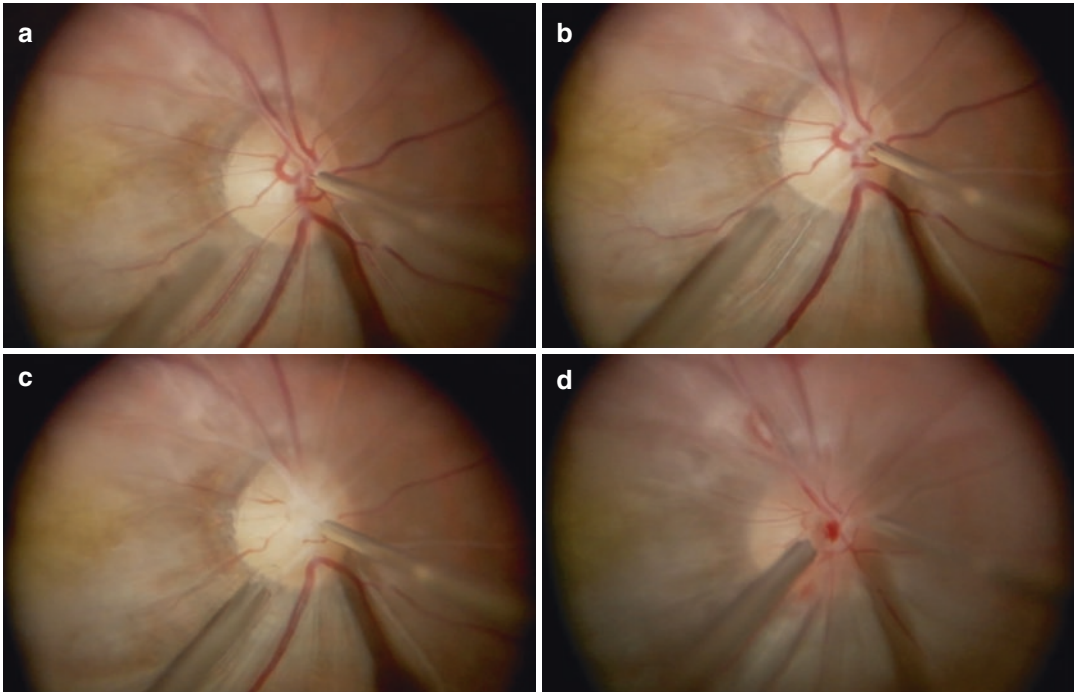
Fig. 27.4 A cannulation for an eye with CRAO. A cannula is pierced into a central retinal artery (**a**), and then tPA is injected into a vessel (**b**). The pressure of injection is maximized (80 psi) (**c**). A needle is removed to simultaneously aspirate bleedings. (**d**) Any bleedings are aspirated with a soft-tip cannula

27.5.1 Results

Overall, results are good with an average rate of improvement of visual acuity which is approximately 80% in our initial study [15]. And also, a visual field with successful REV improves but relative central scotoma remains. The result showed that there is a significant association between improvement of visual acuity and severity of CRAO. For example, it is not expected that there is significant improvement of visual acuity in eyes with complete CRAO.

27.5.2 Complications

A small number of eyes can develop vitreous hemorrhages after REV, but there is low risk of severe surgical complications such as retinal detachment, endophthalmitis, and brain infarction.

27.6   Discussion

We demonstrated retinal endovascular surgery for eyes with CRVO as well as CRAO. The results obtained were quite good, leading to significant improvements in visual acuity. This surgical technique still has some inherent difficulties; it is a challenging procedure and requires a steep learning curve to master. However, recent advances in technology such as digitally assisted vitreoretinal surgery (3D) are able to assist surgeons in performing this procedure. Moreover, robotic surgery might provide further support to surgeons performing these types of surgeries in the future [16, 17].

In conclusion endovascular surgery is one of the latest techniques in the field of ophthalmology and has garnered significant interest from vitreoretinal surgeons since pioneers started to study this kind of surgery a decade ago. The combination of excellent skills as a surgeon, sci-

ence, objective clinical evidence, and cutting-edge technology will improve this surgical technique.

References

1. Allf BE, de Juan E Jr. In vivo cannulation of retinal vessels. Graefes Arch Clin Exp Ophthalmol. 1987;225(3):221–5.
2. Tameesh MK, Lakhanpal RR, Fujii GY, Javaheri M, Shelley TH, et al. Retinal vein cannulation with prolonged infusion of tissue plasminogen activator (t-PA) for the treatment of experimental retinal vein occlusion in dogs. Am J Ophthalmol. 2004;138:829–39.
3. Weiss JN, T. E. D. C. S. Group, Green W, Chan C, Hutchins G, Terry J, Vine A, Samama M, Allf B, de Juan E, Steinkamp G, Hattenbach L, Scharrer I, Ohrloff C. Treatment of central retinal vein occlusion by injection of tissue plasminogen activator into a retinal vein. Am J Ophthalmol. 1998;126:142–4.
4. Bynoe LA, Huchins RK, Lazarus HS, Friedberg MA. Retinal endovascular surgery for central retinal vein occlusion. Retina. 2005;25:625–32.
5. Kadonosono K, Arakawa A, Yamane S, Uchio E, Yanagi Y. An experimental study of retinal endovascular surgery with a microfabricated needle. Invest Ophthalmol Vis Sci. 2011;52:5790–3.
6. Prausnitz MR. Microneedles for transdermal drug delivery. Adv Drug Deliv Rev. 2004;56:581–7.
7. McAllister DV, Wang PM, Davis SP. Microfabricated needles for transdermal delivery of macromolecules and nanoparticles: fabrication methods and transport studies. Proc Natl Acad Sci U S A. 2003;100:13755–60.
8. Orth DH, Patz A. Retinal branch vein occlusion. Surv Ophthalmol. 1978;22(6):357–76.
9. Klein R, Moss SE, Meuer SM, Klein BE. The 15-year cumulative incidence of retinal vein occlusion: the Beaver Dam Eye Study. Arch Ophthalmol. 2008;126(4):513–8.
10. Central Vein Occlusion Study Group. A randomized clinical trial of early panretinal photocoagulation for ischemic central vein occlusion: the Central Vein Occlusion Study Group N report. Ophthalmology. 1995;102(10):1434–44.
11. Larsen M, Waldstein SM, Boscia F, Gerding H, Monés J, Tadayoni R, Priglinger S, Wenzel A, Barnes E, Pilz S, Stubbings W, Pearce I, CRYSTAL Study Group. Individualized ranibizumab regimen driven by stabilization criteria for central retinal vein occlusion: twelve-month results of the CRYSTAL study. Ophthalmology. 2016;123(5):1101–11.
12. Green WR, Chan CC, Hutchins GM, Terry JM. Central retinal vein occlusion: a prospective histopathologic study of 29 eyes in 28 cases. Trans Am Ophthalmol Soc. 1981;79:371–4227.
13. Kadonosono K, et al. Endovascular cannulation with a microneedle for central retinal vein occlusion. JAMA Ophthalmol. 2013;131(6):783–6.
14. Hayreh SS, Zimmerman MB. Central retinal arterial occlusion: visual outcome. Am J Ophthalmol. 2005;140:376–91.
15. Kadonosono K, Yamane S, Inoue M, Yamakawa T, Uchio E. Intra-retinal arterial cannulation using a microneedle for central retinal artery occlusion. Sci Rep. 2018;8:1360.
16. Gijbels A, Smits J, Schoevaerdts L, Willekens K, Vander Poorten EB, Stalmans P, Reynaerts D. In-human robot-assisted retinal vein cannulation, A World First. Ann Biomed Eng. 2018;46:1676–685.
17. de Smet MD, Meenink TC, Janssens T, Vanheukelom V, Naus GJ, Beelen MJ, Meers C, Jonckx B, Stassen JM. Robotic assisted cannulation of occluded retinal veins. PLoS One. 2016;27:11(9).

Surgical Management of Optic Disc Pit Maculopathy

28

Ran Wan and Andrew Chang

28.1 Introduction

Optic disc pit is a rare congenital anomaly with a prevalence of around 0.01–0.19% [1–4]. Optic disc pit is thought to occur due to failure of closure of foetal fissure in embryogenesis, or as some suggested, 'atypical and minimal colobomata of the optic nerve heads' [1]. Histologically, optic disc pit is herniation of dysplastic retina through the lamina cribrosa into the subarachnoid space [5]. Unlike coloboma which typically affects inferior-nasal aspect of the optic nerve, optic disc pit typically affects the temporal neural retinal rim; however, pits in other locations have been reported including central and nasal rims [1].

In the absence of other complications, patients remain asymptomatic with normal visual acuity. The most visually debilitating complication of optic disc pit is maculopathy which can occur in the form of macular schisis and/or serous macular detachment. The percentage of patients with optic disc pit progressing to serous macular detachment is estimated to be around 25–75% [1, 6–9].

28.2 Pathogenesis

Optic disc pit maculopathy typically occurs in the third and fourth decades of life. Traditionally, it is thought that vitreous traction plays a significant role in the pathogenesis of optic disc pit maculopathy. Release of vitreous traction with various surgical procedures such as vitrectomy with induction of posterior vitreous detachment or macular buckling seems to resolve maculopathy [10, 11]. In addition, vitreous abnormalities, such as posterior hyaloid strands tightly attached to the optic disc [12] or condensed Cloquet's canal [13], have been reported in patients with optic disc pit maculopathy. The traction on the optic disc pit was postulated to contribute to the development of maculopathy.

The source of intra- and subretinal fluid is unclear. Vitreous and cerebrospinal fluid (CSF) has been both proposed to be the source of the fluid [14–17]. The main evidence to support the role of CSF in optic disc pit maculopathy comes from optic coherence tomography (OCT) studies which demonstrated micro-communication between the schitic cavity/subretinal space and the optic disc pit [14, 18], however not in those without maculopathy. Furthermore, one study showed that the composition of subretinal fluid was comparable to that of CSF [19]. It has been proposed that the pressure gradients resulting from normal variations in intracranial pressure observed in normal population are essential in the

R. Wan · A. Chang (✉)
Sydney Retina Clinic, Sydney, NSW, Australia
e-mail: achang@sydneyretina.com.au

accumulation of subretinal fluid in patients with optic disc pits [20, 21].

Histological evidence which suggests vitreous as the main source of intra- and subretinal fluid includes migration of different dyes between the optic disc pits and vitreous cavities [16, 22]. Furthermore, intravitreal silicone oil and intraocular gas used in vitreoretinal surgeries had been found in subretinal space in patients with optic disc pits [20, 23]. The vitreous fluid and intravitreal substance can also subsequently migrate to the disc cavitation [6, 20, 24, 25].

28.3   Diagnosis and Investigations

Patients with optic disc pits usually remain asymptomatic until developing maculopathy. The symptoms of optic disc pit-associated maculopathy are usually non-specific. Patients typically present with blurred vision, micropsia and metamorphopsia in their 30s–40s after developing maculopathy [7]. With careful clinical examination, optic disc pit could be noted. Optic disc pit usually presents unilaterally; however it can be bilateral in 10–15% of cases [7, 17, 26].

OCT has become the principal diagnostic tool in this condition. In some cases, a hypo-reflective area within the optic disc excavation is visible, which may reflect accumulated fluid underneath the optic nerve head [27]. Communication between the optic nerve margin and intraretinal and/or subretinal space can be observed on OCT. On OCT, macular schisis and separation between the neural retina and RPE are typically seen extending from the pit to the macular area. It has been reported that around 40% of patients with optic disc pit-associated maculopathy have intraretinal fluid only [28], and patients with subretinal fluid are more likely to have deteriorating vision compared to those who had intraretinal fluid only [28, 29].

Fluorescein angiogram is of limited value in diagnosing optic disc pit-associated maculopathy. Fluorescein angiogram in these cases does not show leakage of intravascular fluid into the subretinal space or schitic cavity [30]. However, in cases where the cause of maculopathy is difficult to discern, it may help to exclude other causes of maculopathy such as central serous chorioretinopathy, and choroidal neovascularisa-tion. In addition to these conditions, diseases such as myopic foveoschisis and vitreomacular traction syndrome with similar macular changes should be considered and excluded.

28.4   Treatment

There is no consensus in the treatment of optic disc pit-associated maculopathy. Cases of spontaneous resolution of optic disc-associated maculopathy have been reported [31–33]. However, this rarely occurs and it has also been observed that the final visual outcomes in these eyes on average were worse [6, 17, 34]. The following treatment modalities are commonly used in managing this condition, which include various combinations of laser photocoagulation, vitrectomy, gas tamponade and/or ILM peeling.

28.4.1 Laser

Slit-lamp-delivered laser photocoagulation temporal to the optic disc with the aim to create a barrier to prevent fluid from entering the intraretinal space has been advocated in the past [30, 35]. In general, the barricade laser alone produced very limited results [6, 35–37]. OCT post-laser photocoagulation has shown that although it may produce an adhesion between the photoreceptors and RPE layer, it is ineffective in blocking fluid migrating from the optic disc pit through the intraretinal route, the more prominent route for fluid [37, 38]. To achieve an intraretinal barrier, it has been proposed by some authors that release of traction between the posterior vitreous and the retina and gas tamponade is required.

28.4.2 Laser and Gas

Gas tamponade has been used in conjunction with laser photocoagulation as the next attempt to treat this condition. Bonnet (1990) has recruited 25 eyes with optic disc pit maculopathy and patients were either managed conservatively, underwent laser photocoagulation of the temporal margin of the optic pit or had gas tamponade in conjunction with juxtapapillary laser photocoagulation. It was found

that laser photocoagulation alone produced limited results in the reattachment of macula. When combined with gas tamponade, either SF6 or C3F8, patients either demonstrated resolution or reduced extent of macular detachment [6]. Another study carefully selected patients with no severe vitreous traction and combined laser photocoagulation with gas tamponade. Laser photocoagulation was performed post-operatively after gas was absorbed. All studied eyes showed significant flattening of maculae and in six out of nine eyes, maculae reattached [39]. However, in this study, in addition to performing the conventional 2–5 confluent rows in juxtapapillary area, laser photocoagulation was also performed along superior and inferior margins of detached retina, which might confound the interpretation of this result.

Some surgeons used the combination of juxtapapillary laser photocoagulation with vitrectomy and gas tamponade. It is thought that by performing vitrectomy, the traction from posterior vitreous that contributes to the progression of optic disc pit-associated maculopathy would be eliminated. Furthermore, following flattening of the maculae with gas tamponade, laser could reach the neurosensory retina more effectively [40]. The success rate was reported around 70% in two case series [37, 40]. Jain and Johnson (2014) proposed that adequate laser barrier is critical in this method [38]. In this study, four or five confluent rows of well-titrated laser spots were placed circumferentially in the temporal juxtapapillary region prior to vitrectomy. It was found that 80% of patients required one surgery to achieve adequate barricade with no recurrence of maculopathy. Another case series of 17 eyes compared the combination of vitrectomy, juxtapapillary laser and gas tamponade with vitrectomy alone. Although the final visual and anatomical outcomes were similar, the average time for the resolution of subretinal fluid was significantly shorter (21 months vs. 25 months) with barricade laser [41].

28.4.3 Vitrectomy with or Without ILM Peeling

Some surgeons advocate the importance of ILM peeling in complete resolution of the vitreoretinal traction [42, 43]. It is thought that ILM imposes

additional stress to retinal layers and therefore predisposing the retinal layers to splitting [43]. Shukla et al. reported a case series of seven patients with optic disc pit-associated maculopathy who underwent vitrectomy with ILM peeling, barrage laser photocoagulation and gas tamponade [44]. It was found in this study that although 86% of patients achieved better vision postoperatively, four out of the seven patients developed full-thickness macular hole 1 month post-operation. As all traction was released with vitrectomy and ILM peeling, it is thought that the thinning of the roof of the schisis contributed to the macular hole formation [44]. In this study, as progress OCT was not performed until 1 month post-op, the authors could not exclude the possibilities that some of these macular holes were secondary to iatrogenic injuries. Similarly, Talli et al. performed vitrectomy, ILM peeling and gas or silicone tamponade on eight patients and achieved high success rate (seven out of eight) of retinal reattachment, with one patient developing post-operative macular hole [45].

The mechanism behind macular hole formation following ILM peeling in these cases is not fully understood. It has been reported that following ILM peeling for the treatment of epiretinal membrane, the incidence of macular hole was around 2–2.5% [46, 47]. Interestingly, the incidence of macular hole was reported to be around 20% in the treatment of myopic foveoschisis with vitrectomy and ILM peeling [48, 49]. It was postulated that injuries to Müller cell cone during ILM peeling caused Müller cell degeneration, which might have contributed to the post-operative macular hole formation [47, 50]. It is highly likely ILM peeling in optic disc pit maculopathy causes similar damages to Müller cell endfeet and leads to macular hole formation. However, it is also worthwhile noting that macular hole could occur as the natural course of optic disc pit-associated maculopathy and it could occur without ILM peeling [51].

To further debate the role of ILM peeling, a similar study by Hirakata et al. evaluated the outcomes of vitrectomy alone with induction of a posterior vitreous detachment at the optic disc (without gas tamponade or laser photocoagulation) for the treatment of optic disc pit-associated

maculopathy and demonstrated that it took 1 year for maculae to fully reattach; however seven out of the eight studied patients showed visual improvement post-operatively, prior to full reattachment of maculae [10].

28.4.4 Fibrin Sealants

More recently, fibrin sealant has been trialled. Fibrin sealants are used to maintain homeostasis and wound repair in various conditions. Al Sabti (2008) first used Tisseel fibrin glue (lyophilised pooled human concentrate and reconstituted bovine thrombin) in conjunction with vitrectomy, drainage of subretinal fluid and C3F8 gas. It was found that although all three patients had flattening of maculae post-surgery, one patient developed post-operative macular hole [52]. Another study reported four cases of optic disc pit-associated maculopathy, which were managed with vitrectomy, drainage of subretinal fluid through the optic disc pit, temporal juxtapapillary laser and application of Evicel fibrin sealant over the optic disc head. All four cases showed reduction of subretinal fluid level, with one case of total absorption [53]. One recent study combined fibrin glue, vitrectomy and ILM abrasion using diamond-dusted membrane scraper, as well as gas tamponade. All three patients had relatively rapid response and achieved functional and anatomical improvement within 1 month, which was maintained for years post-operation [54]. These case series all had relatively small cohort size and they used different combinations of vitrectomy, gas tamponade, ILM abrasion and/or laser photocoagulation barricade; the actual significance of fibrin sealant is difficult to determine.

28.4.5 Vitrectomy with Inner Retinal Fenestration

Induction of a partial thickness fenestration near the optic disc pit has been proposed and trialed in treating this challenging condition by Ooto et al [51]. The authors believed that the intra- and sub-retinal fluid enters the retina from the optic disc pit under pressure, rather than the vitreous. Hence, redirection of the fluid towards the vitreous cavity could be achieved by creating a partial thickness fenestration temporal to the optic disc pit. Fourteen eyes out of this cohort of 18 eyes with optic disc pit maculopathy had macular detachment. These patients underwent 23 G or 25 G pars plana vitrectomy and a 25 G bent needle was used to create a partial thickness inner fenestration temporal to the disc pit. None of these patients underwent ILM peeling or laser. Seventeen out of the 18 eyes had complete resolution of the sub-foveal fluid after the surgery, with a mean resolution time of 6.1 months. The anatomical improvement was accompanied by an average of 3-line improvement in vision. There was also no re-accumulation of fluid after a long follow up time (34.6 +/- 26.6 months). Interestingly, an earlier case report utilizing the same method showed that the fenestration closed within 3 weeks of surgery and persistent macular detachment as a result of this [55]. This technique is very promising, however there is limited literature available for this method so far.

28.4.6 Macular Buckling

In addition to the above surgical interventions targeting at vitreous and retinal directly, macular buckling has been shown to be an effective method to restore vision and anatomy. Theodossiadis et al. used a scleral sponge of 7.5×5.5 mm placed over the corresponding macular area at 6- 12 o'clock meridian in these cases, which was thought to relieve vitreous traction. However, another plausible explanation is that the indentation may mechanically create a barrier to the intraretinal passage of fluid between the disc pit and the macula. Thirteen patients who underwent macular buckling were monitored for a period of around 13 years and showed that 12 studied eyes have maintained good anatomical and functional outcomes [56]. This method is technically challenging and intraoperative B-scan is required for accurate positioning of the buckle. Therefore, this method has not been widely used for the past 20 years.

28.5 Summary

Optic disc pit-associated maculopathy is a rare condition, and thus randomised control trials of various treatment modalities are likely not feasible. Current common treatment options include various combinations of juxtapapillary laser photocoagulation, vitrectomy/PVD induction, gas tamponade and/or ILM peeling. A review of available literature suggests that vitrectomy with PVD induction is a relatively safe and effective management in this condition, at least as the first-line treatment. Surgeons should choose additional procedures based on their own expertise

and experience while balancing the current available evidence. Furthermore these patients need to be closely followed up due to the risk of macular hole formation, especially in those who undergo ILM peeling as the treatment option [57].

28.6 Illustrative Cases

28.6.1 Case 1

A 17-year-old female was found to have a temporal optic disc pit in the right eye on routine eye examination (Fig. 28.1a). OCT showed the pres-
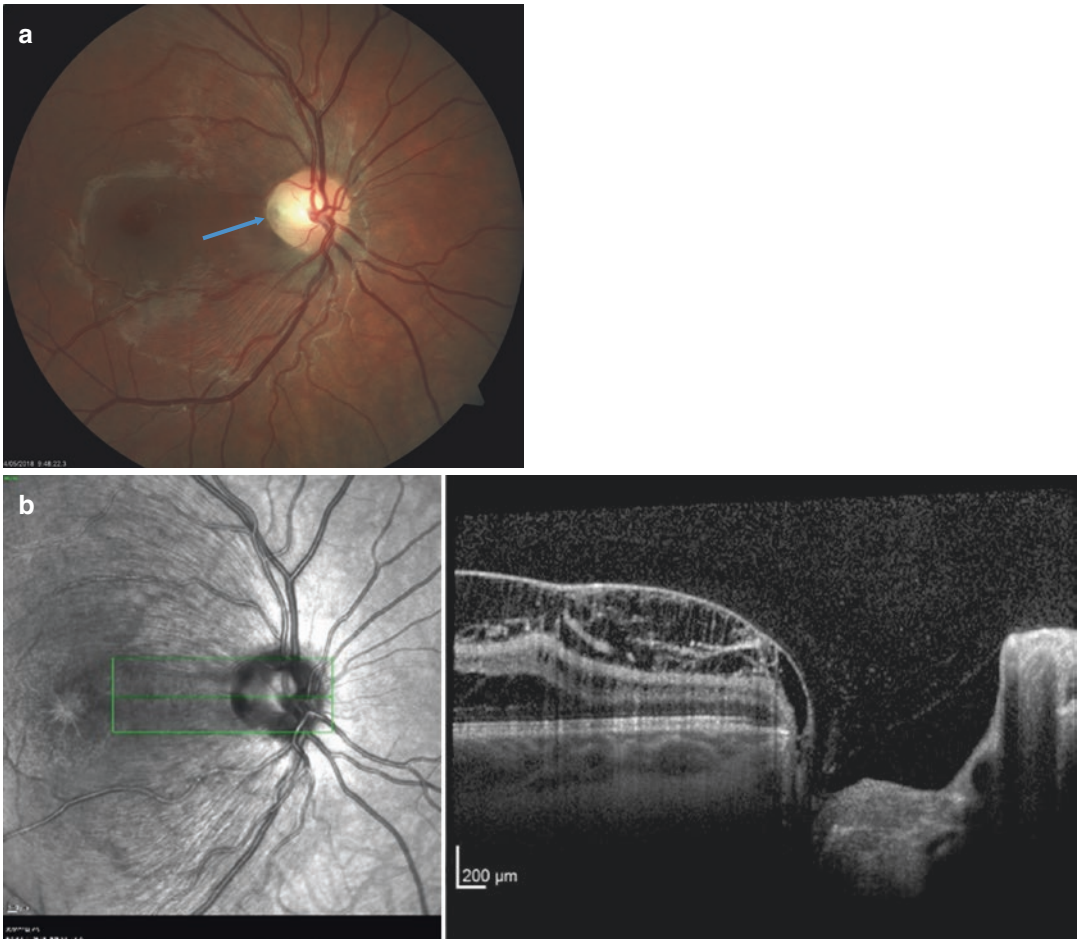
Fig. 28.1 (**a**) Fundus photograph of the right eye of a 17-year-old female with optic disc pit-associated maculopathy. A temporal optic disc pit is indicated by the arrow. (**b**) An OCT scan through the disc towards macula shows macular schisis, as well as accumulation of intra-

retinal and subretinal fluid extending from the optic disc pit to the macular area. (**c**) Progress OCT of the right macula. The macular schisis remained stable over 1-year period with no treatment
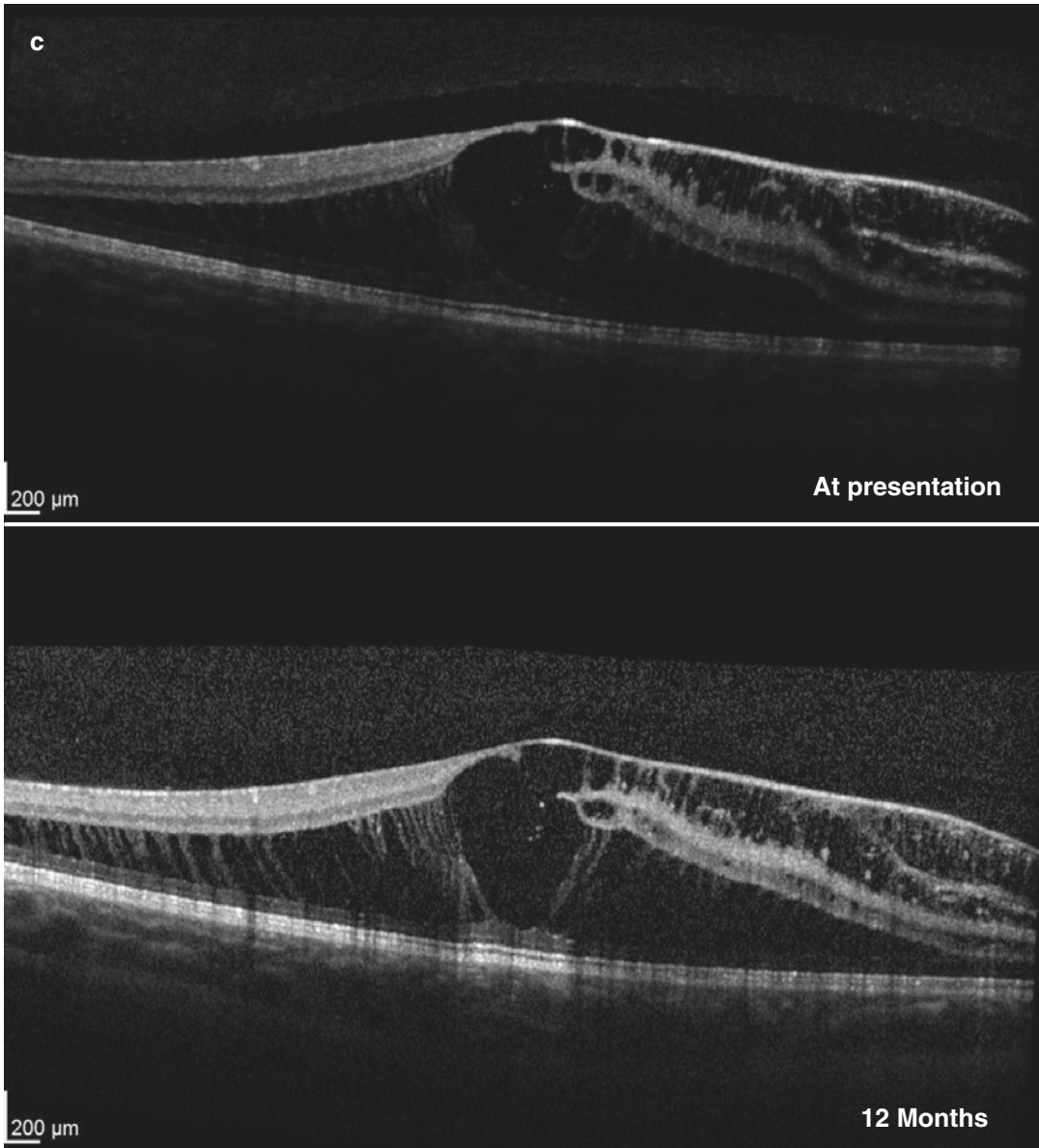
Fig. 28.1 (continued)

ence of intraretinal fluid extending to the optic disc pit (Fig. 28.1b). As the patient had minimal symptoms, she was monitored closely on a yearly basis with clinical and OCT assessment. Her visual acuity remained stable at 6/12 4 years after the initial diagnosis. The OCT finding remained stable as well (Fig. 28.1c).

28.6.2 Case 2

A 35-year-old female presented with a 2-month history of central vision loss in her right eye. At presentation, visual acuities were R: 6/60 L: 6/6. Dilated retinal examination showed a right temporal optic disc pit (Fig. 28.2a), and marked ele-

vation of macula, as highlighted by the multicolour imaging (Fig. 28.2b). OCT confirmed the macular schisis and subretinal fluid tracking from the optic disc pit, with a defect in the inner segment and outer segment junction layer at the fovea (Fig. 28.2c).

Vitrectomy with ILM peeling followed by fluid air exchange was performed (Fig. 28.2d). At 1-week post-operative visit, visual acuity in the right eye was 6/60. Progress OCT showed slight improvement of the maculopathy. However, a full-thickness macular hole developed 6 weeks after surgery (Fig. 28.2c).

She required a second vitrectomy surgery and fluid air exchange. The hole closed at 6 days after the second operation. At 6 months post-op, the macular hole remained closed with vision recovering to 6/9 (Fig. 28.2c).
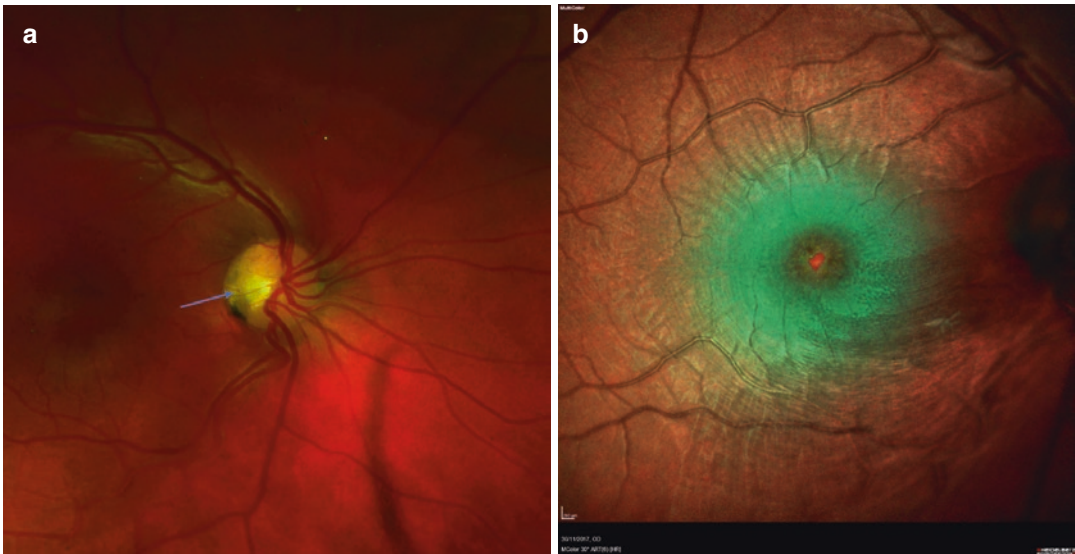
Fig. 28.2 (**a**) Retinal photo of the right optic disc. The arrow points to the temporal optic disc pit. (**b**) Multicolour imaging of the right macula. The combined pseudo-colour image enables visualisation of the maculopathy. (**c**) Pre-op and progress post-op OCT. Macular schisis and subretinal fluid extending to the optic disc pit are demonstrated on the pre-op OCT. Progress OCT showed development of macular hole 6 weeks post-operatively, which was repaired with a second vitrectomy surgery. Closure of macular hole and resolution of maculopathy were achieved after the second surgery. (**d**) Surgical still imaging. Intraoperative imaging demonstrated peeling of ILM using membrane blue dye
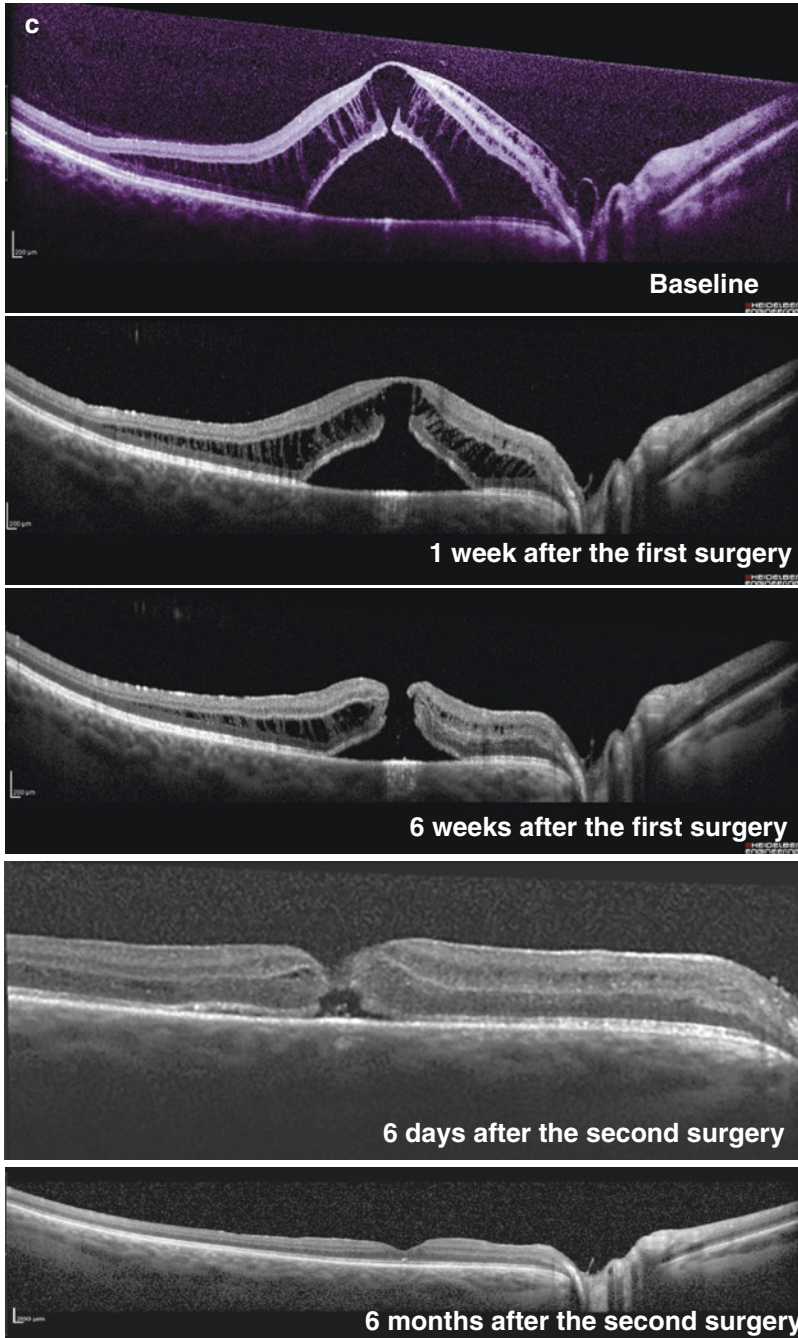
Fig. 28.2 (continued)

Fig. 28.2 (continued)
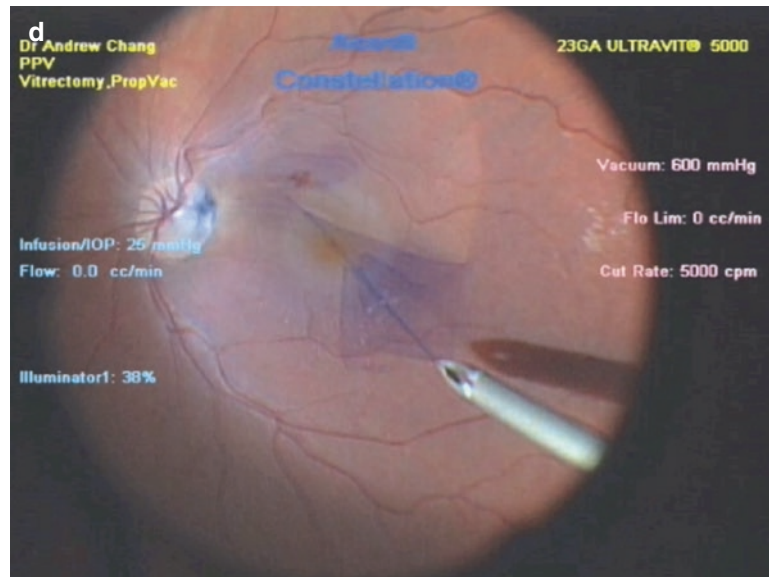
References

1. Kranenburg EW. Crater-like holes in the optic disc and central serous retinopathy. Arch Ophthalmol. 1960;64:912–24.
2. Bassi ST, George R, Sen S, Asokan R, Lingam V. Prevalence of the optic disc anomalies in the adult South Indian population. Br J Ophthalmol. 2019;103(1):94–8.
3. Wang Y, Xu L, Jonas JB. Prevalence of congenital optic disc pits in adult Chinese: the Beijing Eye Study. Eur J Ophthalmol. 2006;16(6):863–4.
4. Healey PR, Mitchell P. The prevalence of optic disc pits and their relationship to glaucoma. J Glaucoma. 2008;17(1):11–4.
5. Agarwal A. Gass' atlas of macular diseases: 2-volume set—expert consult: online and print. Elsevier Health Sciences; 2011.
6. Bonnet M. Serous macular detachment associated with optic nerve pits. Graefes Arch Clin Exp Ophthalmol. 1991;229(6):526–32.
7. Georgalas I, Ladas I, Georgopoulos G, Petrou P. Optic disc pit: a review. Graefes Arch Clin Exp Ophthalmol. 2011;249(8):1113–22.
8. Brown GC, Augsburger JJ. Congenital pits of the optic nerve head and retinochoroidal colobomas. Can J Ophthalmol. 1980;15(3):144–6.
9. Gordon R, Chatfield RK. Pits in the optic disc associated with macular degeneration. Br J Ophthalmol. 1969;53(7):481–9.
10. Hirakata A, Inoue M, Hiraoka T, McCuen BW 2nd. Vitrectomy without laser treatment or gas tamponade for macular detachment associated with an optic disc pit. Ophthalmology. 2012;119(4):810–8.
11. Theodossiadis GP, Theodossiadis PG. The macular buckling technique in the treatment of optic disk pit maculopathy. Semin Ophthalmol. 2000;15(2):108–15.
12. Hirakata A, Hida T, Wakabayashi T, Fukuda M. Unusual posterior hyaloid strand in a young child with optic disc
13. maculopathy: intraoperative and histopathological findings. Jpn J Ophthalmol. 2005;49(3):264–6.
13. Akiba J, Kakehashi A, Hikichi T, Trempe CL. Vitreous findings in cases of optic nerve pits and serous macular detachment. Am J Ophthalmol. 1993;116(1):38–41.
14. Krivoy D, Gentile R, Liebmann JM, Stegman Z, Rosen R, Walsh JB, et al. Imaging congenital optic disc pits and associated maculopathy using optical coherence tomography. Arch Ophthalmol. 1996;114(2):165–70.
15. Kuhn F, Kover F, Szabo I, Mester V. Intracranial migration of silicone oil from an eye with optic pit. Graefes Arch Clin Exp Ophthalmol. 2006;244(10):1360–2.
16. Ferry AP. Macular detachment associated with congenital pit of the optic nerve head. Pathologic findings in two cases simulating malignant melanoma of the choroid. Arch Ophthalmol. 1963;70:346–57.
17. Shah SD, Yee KK, Fortun JA, Albini T. Optic disc pit maculopathy: a review and update on imaging and treatment. Int Ophthalmol Clin. 2014;54(2):61–78.
18. Gowdar JP, Rajesh B, Giridhar A, Gopalakrishnan M, Hussain R, Thachil T. An insight into the pathogenesis of optic disc pit-associated maculopathy with enhanced depth imaging. JAMA Ophthalmol. 2015;133(4):466–9.
19. Turkcuoglu P, Taskapan C. The origin of subretinal fluid in optic disc pit maculopathy. Ophthalmic Surg Lasers Imaging Retina. 2016;47(3):294–8.
20. Johnson TM, Johnson MW. Pathogenic implications of subretinal gas migration through pits and atypical colobomas of the optic nerve. Arch Ophthalmol. 2004;122(12):1793–800.
21. Andresen M, Hadi A, Petersen LG, Juhler M. Effect of postural changes on ICP in healthy and ill subjects. Acta Neurochir (Wien). 2015;157(1):109–13.
22. Brown GC, Shields JA, Patty BE, Goldberg RE. Congenital pits of the optic nerve head. I. Experimental studies in collie dogs. Arch Ophthalmol. 1979;97(7):1341–4.
23. Dithmar S, Schuett F, Voelcker HE, Holz FG. Delayed sequential occurrence of perfluorodecalin and silicone

oil in the subretinal space following retinal detachment surgery in the presence of an optic disc pit. Arch Ophthalmol. 2004;122(3):409–11.

24. Brown GC, Shields JA, Goldberg RE. Congenital pits of the optic nerve head. II. Clinical studies in humans. Ophthalmology. 1980;87(1):51–65.

25. Ohno-Matsui K, Hirakata A, Inoue M, Akiba M, Ishibashi T. Evaluation of congenital optic disc pits and optic disc colobomas by swept-source optical coherence tomography. Invest Ophthalmol Vis Sci. 2013;54(12):7769–78.

26. Brodsky MC. Congenital optic disk anomalies. Surv Ophthalmol. 1994;39(2):89–112.

27. Michalewski J, Michalewska Z, Nawrocki J. Spectral domain optical coherence tomography morphology in optic disc pit associated maculopathy. Indian J Ophthalmol. 2014;62(7):777–81.

28. Steel DHW, Suleman J, Murphy DC, Song A, Dodds S, Rees J. Optic disc pit maculopathy: a two-year nationwide prospective population-based study. Ophthalmology. 2018;125(11):1757–64.

29. Lincoff H, Yannuzzi L, Singerman L, Kreissig I, Fisher Y. Improvement in visual function after displacement of the retinal elevations emanating from optic pits. Arch Ophthalmol. 1993;111(8):1071–9.

30. Gass JD. Serous detachment of the macula. Secondary to congenital pit of the optic nervehead. Am J Ophthalmol. 1969;67(6):821–41.

31. Gupta RR, Choudhry N. Spontaneous resolution of optic disc pit maculopathy after posterior vitreous detachment. Can J Ophthalmol. 2016;51(1):e24–7.

32. Tripathy K. Spontaneous resolution of optic disc pit maculopathy. Turk J Ophthalmol. 2017;47(3):184–5.

33. Yuen CH, Kaye SB. Spontaneous resolution of serous maculopathy associated with optic disc pit in a child: a case report. J AAPOS. 2002;6(5):330–1.

34. Sobol WM, Blodi CF, Folk JC, Weingeist TA. Long-term visual outcome in patients with optic nerve pit and serous retinal detachment of the macula. Ophthalmology. 1990;97(11):1539–42.

35. Annesley W, Brown G, Bolling J, Goldberg R, Fischer D. Treatment of retinal detachment with congenital optic pit by krypton laser photocoagulation. Graefes Arch Clin Exp Ophthalmol. 1987;225(5):311–4.

36. Theodossiadis GP, Kollia AK, Theodossiadis PG. Cilioretinal arteries in conjunction with a pit of the optic disc. Ophthalmologica. 1992;204(3):115–21.

37. Lincoff H, Lopez R, Kreissig I, Yannuzzi L, Cox M, Burton T. Retinoschisis associated with optic nerve pits. Arch Ophthalmol. 1988;106(1):61–7.

38. Jain N, Johnson MW. Pathogenesis and treatment of maculopathy associated with cavitary optic disc anomalies. Am J Ophthalmol. 2014;158(3):423–35.

39. Lei L, Li T, Ding X, Ma W, Zhu X, Atik A, et al. Gas tamponade combined with laser photocoagulation therapy for congenital optic disc pit maculopathy. Eye (Lond). 2015;29(1):106–14.

40. Postel EA, Pulido JS, McNamara JA, Johnson MW. The etiology and treatment of macular detachment associated with optic nerve pits and related anomalies. Trans Am Ophthalmol Soc. 1998;96:73–88; discussion 88–93.

41. Teke MY, Citirik M. 23 gauge vitrectomy, endolaser, and gas tamponade versus vitrectomy alone for serous macular detachment associated with optic disc pit. Am J Ophthalmol. 2015;160(4):779–85.e2.

42. Georgalas I, Papaconstantinou D, Koutsandrea C. Optic disc pit maculopathy: the value of small-gauge vitrectomy, peeling, laser treatment, and gas tamponade. Eur J Ophthalmol. 2013;23(2):275.

43. Gandorfer A, Kampik A. [Role of vitreoretinal interface in the pathogenesis and therapy of macular disease associated with optic pits]. Ophthalmologe. 2000;97(4):276–9.

44. Shukla D, Kalliath J, Tandon M, Vijayakumar B. Vitrectomy for optic disk pit with macular schisis and outer retinal dehiscence. Retina. 2012;32(7):1337–42.

45. Talli PM, Fantaguzzi PM, Bendo E, Pazzaglia A. Vitrectomy without laser treatment for macular serous detachment associated with optic disc pit: long-term outcomes. Eur J Ophthalmol. 2016;26(2):182–7.

46. Sandali O, El Sanharawi M, Basli E, Lecuen N, Bonnel S, Borderie V, et al. Paracentral retinal holes occurring after macular surgery: incidence, clinical features, and evolution. Graefes Arch Clin Exp Ophthalmol. 2012;250(8):1137–42.

47. Rush RB, Simunovic MP, Aragon AV 2nd, Ysasaga JE. Postoperative macular hole formation after vitrectomy with internal limiting membrane peeling for the treatment of epiretinal membrane. Retina. 2014;34(5):890–6.

48. Gaucher D, Haouchine B, Tadayoni R, Massin P, Erginay A, Benhamou N, et al. Long-term follow-up of high myopic foveoschisis: natural course and surgical outcome. Am J Ophthalmol. 2007;143(3):455–62.

49. Hirakata A, Hida T. Vitrectomy for myopic posterior retinoschisis or foveal detachment. Jpn J Ophthalmol. 2006;50(1):53–61.

50. Gass JD. Reappraisal of biomicroscopic classification of stages of development of a macular hole. Am J Ophthalmol. 1995;119(6):752–9.

51. Ooto S, Mittra RA, Ridley ME, Spaide RF. Vitrectomy with inner retinal fenestration for optic disc pit maculopathy. Ophthalmology. 2014;121(9):1727–33.

52. Al Sabti K, Kumar N, Chow DR, Kapusta MA. Management of optic disk pit-associated macular detachment with Tisseel fibrin sealant. Retin Cases Brief Rep. 2008;2(4):274–7.

53. de Oliveira PRC, Berger AR, Chow DR. Use of evicel fibrin sealant in optic disc pit-associated macular detachment. Ophthalmic Surg Lasers Imaging Retina. 2017;48(4):358–63.

54. Almeida DRP, Chin EK, Arjmand P, Velez G, Evans LP, Mahajan VB. Fibrin glue and internal limiting membrane abrasion for optic disc pit maculopathy. Ophthalmic Surg Lasers Imaging Retina. 2018;49(12):e271–e7.

55. Slocumb RW, Johnson MW. Premature closure of inner retinal fenestration in the treatment of optic disk pit maculopathy. Retin Cases Brief Rep. 2010;4(1):37–9.

56. Theodossiadis GP, Chatziralli IP, Theodossiadis PG. Macular buckling in optic disc pit maculopathy in association with the origin of macular elevation: 13-year mean postoperative results. Eur J Ophthalmol. 2015;25(3):241–8.

57. Wan R, Chang A. Optic disc pit maculopathy: a review of diagnosis and treatment. Clin Exp Optom. 2020;103(4):425–9.

Pediatric Macular Surgery

29

Kelley J. Bohm, Sarwar Zahid, and R. V. Paul Chan

29.1 Introduction

Pediatric eyes present unique challenges in macular surgery. Throughout this chapter, we discuss the distinct pathologies and techniques that are relevant to pediatric macular surgery, but we also must acknowledge the anatomy, surgical challenges, and complications that can render this surgical focus both challenging and rewarding. For instance, pediatric eyes are not only inherently smaller than the adult eyes we typically operate on, but they also have relatively large lenses that must be respected and/or extracted. The sclera's elasticity impacts the placement of trocars as well as wound closure. The most notable distinguishing anatomical characteristic is the vitreous form and strong adherence to the retina. Furthermore, an appreciation of each patient's disease status is critical, and amblyopia must be considered in pediatric patients.

Taking all of this into consideration, this chapter discusses the pathology and surgical techniques for traumatic macular holes, combined hamartomas of the retina and retinal pigment epithelium (RPE), macular choroidal neovascularization (CNV), posterior hyaloid contracture syndrome, and macula-involving epiretinal membranes (ERMs) in pediatric patients.

K. J. Bohm · S. Zahid · R. V. P. Chan (✉)
Illinois Eye and Ear Infirmary, University of Illinois at Chicago, Chicago, IL, USA

29.2 Surgical Indications and Techniques

29.2.1 Traumatic Macular Holes

Typical adult macular holes are thought to arise from traction both external to and within the retina—a combination of anterior-posterior parafoveal traction from the posterior hyaloid as well as tangential forces from epiretinal proliferation. They are often idiopathic, but age, gender [1], myopia, and history of inflammation or trauma are hypothesized to contribute to their development. In pediatric patients, macular holes usually result from similar forces but are nearly always induced by trauma, despite one report of an idiopathic macular hole in an 8-year-old child [2]. Traumatic holes, specifically, are often elliptical in shape and are hypothesized to result from globe compression causing retinal stress and foveal rupture [3].

Traumatic retinal holes have been described to close spontaneously, as in the patient in Fig. 29.1. Closure has been reported to occur between 8 days and 9 months following the causal injury [4–11], with the majority of closures happening between 2 and 4 months post-trauma. Reports of spontaneous closure are more common in younger patients [4–12], but the phenomenon has also been reported in adults [5]. Pathophysiologic theories behind spontaneous closure suggest that release of foveal vitreomacular traction enables
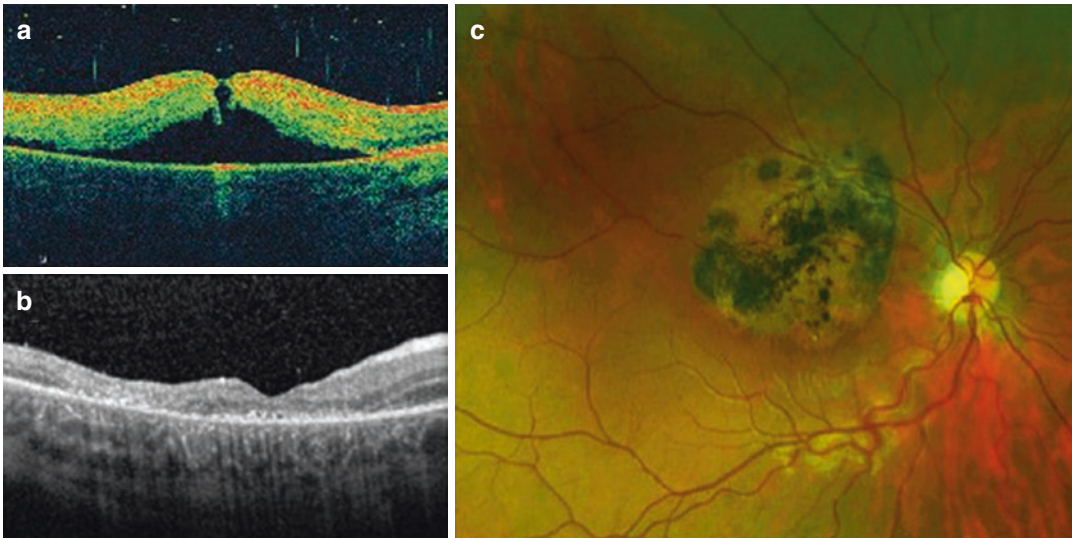
Fig. 29.1 Depicts a patient with a traumatic macular hole from blunt trauma with a soccer ball. OCT in (**a**) shows the initial macular hole, and the OCT in (**b**) was taken 2 weeks after the injury, during which time spontaneous closure of the hole occurred. Image (**c**) shows an Optos fundus photo of the macula 2 years after hole closure

hole closure [10]; however Sugiyama et al. showed, using optical coherence tomography (OCT), that some spontaneously closed holes still had posterior hyaloid attached at the edge [13]. OCTs from Sugiyama et al. also showed that in all holes that spontaneously resolved, there was a bridge of sensory retina spanning the location of the prior hole, irrespective of posterior vitreous detachment (PVD) status [13].

Macular holes requiring surgery are classically repaired in adults using pars plana vitrectomy (PPV), often peeling the internal limiting membrane (ILM) and utilizing gas endotamponade. The particularly adherent posterior hyaloid in pediatric patients poses a unique challenge in macular hole repair. Limited studies have investigated the use of ocriplasmin, a recombinant protease active against fibronectin and laminin, in cases to induce a PVD. Results suggest that ocriplasmin is tolerated well by vitrectomy patients. However, its use does not show a difference in PVD induction intraoperatively compared to placebo as reported in a study by Drenser et al. showing 50% PVD success with ocriplasmin versus 62.5% PVD success with placebo [14].

Results may skew slightly more positively when looking at the subset of macular hole patients [15]. Autologous plasmin has been described as a potential helpful adjunct for vitrectomy when administered 3 days [16] to 15–30 min [17, 18] preoperatively as well as during PPV [19]. Separately, intraoperative platelet concentrates injected into the macular hole [20] have been used with some success [20]. Overall, this evidence does not present definitive evidence for use of any one adjunct, so use of one would be up to the discretion and experience of the surgeon.

Decision for and timing of surgical intervention must also be addressed. Traumatic macular holes that closed spontaneously were small, roughly 100–200 microns [10], and thus holes that are larger are less likely to close on their own, and vitrectomy is often needed. One literature review suggests that the majority of spontaneous closures occur by 3–4 months [10], thus establishing this as a reasonable observation period prior to surgical intervention. If other factors, such as vitreous hemorrhage or retinal detachment, are present, however, sooner surgical intervention may be indicated.

29.2.2 Combined Hamartomas of the Retina and RPE

Gass et al. defined combined hamartomas of the retina and RPE (CHRRPE) in 1973 as elevated grey masses involving the RPE that cause surface contraction of the tumor and the surrounding retina toward the center of the tumor, without choroidal involvement [21]. These tumors are nearly always in the macula [22, 23], where they have a tendency to cause tractional distortion and decreased vision in 24–80% of patients due to the hamartomas' inherent contraction [22, 24]. Several studies examining OCT imaging of patients with CHRRPEs have shown common characteristics of epiretinal membranes (as seen in Fig. 29.2), inner retinal distortion, and limitation by the outer plexiform layer [23]. One study suggested that epiretinal membranes appear to extend from fibrotic membranes that originate within the CHRRPEs themselves based on OCT images [23], while others have demonstrated these membranes as being distinct from the hamartomas on OCT [25] and thus amenable for surgical removal [26, 27].

The decision to perform surgery in patients with CHRRPE is controversial. Outcomes in the literature vary—some studies report visual improvement [26–28], while others have shown that vision does not improve [29, 30], and two studies were equivocal with regard to visual outcomes [24, 31]. Most ERMs were peeled easily with full removal of the membranes, but a study by Zhang et al. noted that two of its five patients were left with residual membranes [31]. McDonald et al. found no visual improvement in their series describing two patients who were notably both older [29], and in addition to having stable vision, the postoperative imaging demonstrated persistent vascular tortuosity and cystoid macular edema. This loose correlation with age suggests that vision may not be expected to improve if macular traction and/or cystoid macular edema is long-standing, and that earlier intervention may be more successful. Close monitoring with vision testing and examination, OCT, and perhaps microperimetry [26] should be used to monitor patients for progressive traction and macular edema, which may be indications for surgery of the ERM before structural and functional macular changes become permanent.

Regarding surgical techniques, standard PPV with ERM peeling and endotamponade is typically utilized. Peeling of the ILM did not show
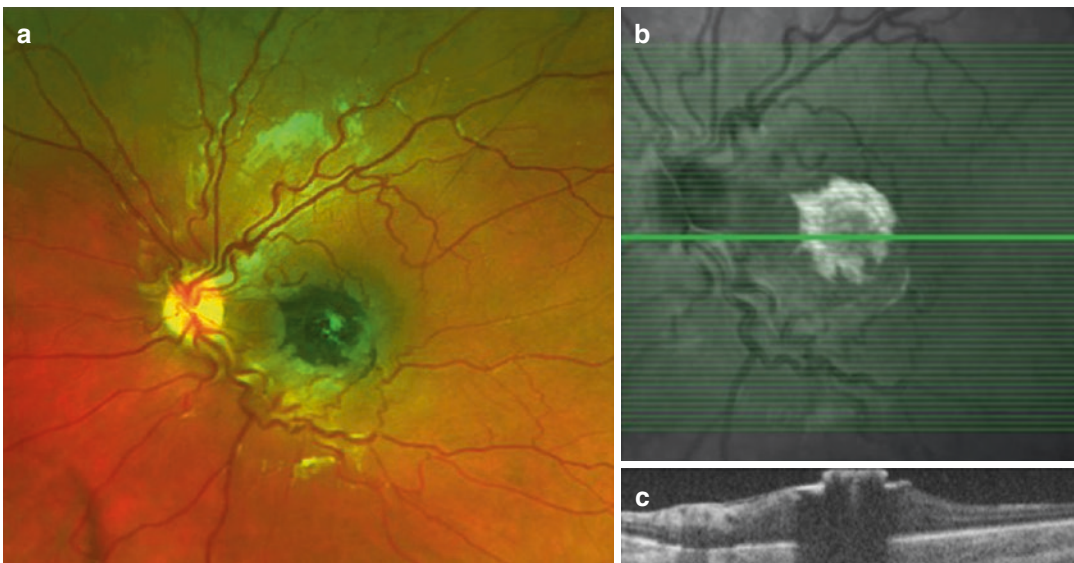
Fig. 29.2 Exhibits a 10-year-old patient with CHRRPE. Optos photo in (**a**) shows the subfoveal CHRRPE, while (**b**) and (**c**) show the OCT and raster scan which show a thin ERM over the surface of the CHRRPE

any significant visual benefit compared to no ILM peeling in one study [28]. Intraoperative OCT guidance may help further refine the peeling of ERMs away from CHRRPEs, particularly in those membranes which may be more intertwined in the CHRRPEs.

29.2.3 Macular Surgery for Choroidal Neovascularization

Macular CNV is a condition most commonly seen in adults, but can also develop in pediatric conditions such as myopic degeneration, traumatic choroidal rupture, choroidal osteoma, posterior uveitis (e.g., punctate inner choroidopathy, multifocal choroiditis), angioid streaks, hereditary macular dystrophies, and idiopathic CNV [32]. Photodynamic therapy has long been a useful treatment [33] but it has mostly been replaced by intravitreal anti-vascular endothelial growth factor (anti-VEGF) injections, which has grown in popularity as a less invasive method for treating choroidal neovascular membranes [32, 34, 35]. Surgery for macular CNV is also less commonly performed following the advent of anti-VEGF therapies. However, historically, such surgery was considered effective. Studies of surgical outcomes for pediatric macular CNV by Sears et al. and Uemura et al. found that vision improved in 72–83% with CNV recurrence in 33–35% [36, 37]. Pars plana vitrectomy, combined with excision of the choroidal neovascular membrane and air-fluid exchange, was used to excise the bulk of the membrane and flatten the macula back to its anatomical location.

29.2.4 Posterior Hyaloid Contracture Syndrome

Retinopathy of prematurity (ROP) and familial exudative vitreoretinopathy (FEVR) are pediatric diseases featuring ischemic peripheral retina that can cause both exudative and tractional retinal detachments (RDs). The tractional component of these RDs is often due to ischemia-induced proliferative vascular retinopathy predominantly affecting the periphery, but an underappreciated etiology of tractional RDs is the contraction of the posterior hyaloid interface. Because of the pediatric vitreous' particular adherence to the retina, contraction of the hyaloid can pull the retina inward, causing a broad tractional retinal detachment [38].

Surgical release of traction and repair of such detachments are difficult due to the tight adherence of the hyaloid which obscures tissue planes [38] during the membrane dissection portion of the PPV. Bimanual dissection of the hyaloid from the detached retina is necessary to achieve sufficient release of traction [38]. As discussed earlier with respect to macular holes, plasmin enzyme has also been demonstrated to dissect the interface between hyaloid and retina in pediatric posterior hyaloid contracture syndrome [38]. Its success is dependent upon the surgeon's comfort; however, because this pathology is due to this inherently strong posterior hyaloid-retina adhesion, any assistance in detaching these two planes is helpful.

29.2.5 Macula-Involving Epiretinal Membranes

Epiretinal membranes in children are distinct from those in adults—they are typically denser membranes and often translucent to opaque, as seen in Fig. 29.3, when compared to the transparent cellophane-like ERMs that occur later in life. Unlike in adults, pediatric ERMs are typically not associated with posterior vitreous detachments, but rather can be caused by inflammatory conditions such as intermediate uveitis and ocular toxocariasis, focal structural changes such as vasoproliferative tumors and CHRRPEs (previously discussed), congenital diseases such as FEVR, Coats disease, ROP, and Norrie disease, and ocular trauma [39]. Several reports of ERMs in young patients have described spontaneous membrane release with visual improvement [40, 41], so the decision to pursue macular surgery for an idiopathic ERM has been controversial. Studies from surgeons opting to perform surgery have shown that surgery in children can be
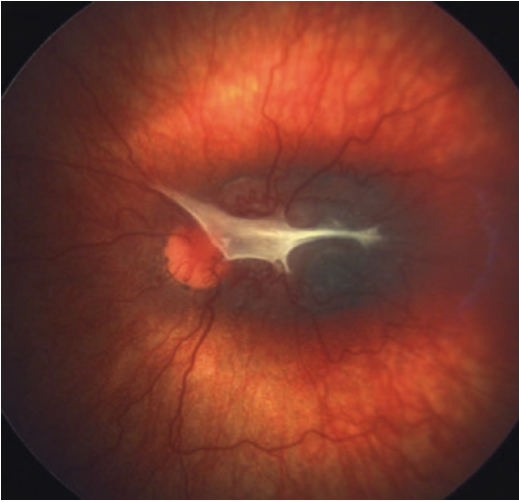
Fig. 29.3 Shows a dense, white epiretinal membrane in a 9-month-old infant with a history of retinopathy of prematurity

effective at removing the membranes and improving vision [39, 42–45] (by an average of four lines in one study [42]), with more vision improvement in patients with ERM associated with inflammation than idiopathic ERMs [42]. Postoperative visual outcomes are inversely correlated with duration of preoperative decreased vision and metamorphopsia [44], so experts have recommended early treatment for rapidly progressing symptoms. Furthermore, because of concern for amblyopia and these positive surgical outcomes, PPV with membrane peeling is often recommended in younger children to improve vision and allow complete development of the visual pathways.

29.3 Complications

Pediatric eyes can be remarkably resilient and well healing; however, they also can develop more significant inflammatory responses after surgery. Postoperative epiretinal proliferation is one such response that can cause recurrence of the preoperative ERM and worsen visual outcomes. As mentioned in the discussion on CHRRPEs, ILM peeling at the time of surgery does not statistically affect recurrence rates [28].

In patients whose ERMs are secondary to inflammation, removing the entirety of the ERM plus its ILM platform may potentially reduce the risk of recurrence in the event of postoperative inflammation. Iatrogenic retinal breaks are also always a concern during vitrectomy, particularly in these patients with a very adherent hyaloid.

Surgical Pearls
- Know the pediatric eye anatomy—large lens:eye volume ratio, scleral elasticity, adherent vitreous—and respect these parameters when planning your surgery.
- Timing can affect visual outcomes. The duration of symptoms often portends the visual outcome, and the risk of amblyopia is an important consideration.
- Sometimes less is more. For neovascular pathologies, less invasive intravitreal injections can surpass surgical intervention in cost, quality-of-life impact, and even therapeutic efficacy.

References

1. Ali FS, Stein JD, Blachley TS, Ackley S, Stewart JM. Incidence of and risk factors for developing idiopathic macular hole among a diverse group of patients throughout the United States. JAMA Ophthalmol. 2017;135(4):299–305.
2. Manayath GJ, Jain A, Ranjan R, Naik AS, Narendran V. Idiopathic full-thickness macular hole in an 8-year-old boy [published online ahead of print, 2018 Oct 9]. Retin Cases Brief Rep. 2018;10.1097/ICB.0000000000000830. https://doi.org/10.1097/ICB.0000000000000830.
3. Johnson RN, McDonald HR, Lewis H, Grand MG, Murray TG, Mieler WF, et al. Traumatic macular hole: observations, pathogenesis, and results of vitrectomy surgery. Ophthalmology. 2001;108(5):853–7.
4. Carpineto P, Ciancaglini M, Aharrh-Gnama A, Agnifili L, Cerulli AM, Cirone D, et al. Optical coherence tomography and fundus microperimetry imaging of spontaneous closure of traumatic macular hole: a case report. Eur J Ophthalmol. 2005;15(1):165–9.
5. Gonzalez-Cortes JH, Toledo-Negrete JJ, Bages-Rousselon Y, de Alba-Castilla MA, Mohamed-Hamsho J. Spontaneous closure of simultaneous idiopathic macular holes documented by spectral-

domain optical coherence tomography [published online ahead of print, 2018 May 25]. Retin Cases Brief Rep. 2018;10.1097/ICB.0000000000000749. https://doi.org/10.1097/ICB.0000000000000749.

6. Kusaka S, Fujikado T, Ikeda T, Tano Y. Spontaneous disappearance of traumatic macular holes in young patients. Am J Ophthalmol. 1997;123(6):837–9.

7. Lai MM, Joshi MM, Trese MT. Spontaneous resolution of traumatic macular hole-related retinal detachment. Am J Ophthalmol. 2006;141(6):1148–51.

8. Mitamura Y, Saito W, Ishida M, Yamamoto S, Takeuchi S. Spontaneous closure of traumatic macular hole. Retina. 2001;21(4):385–9.

9. Yamada H, Sakai A, Yamada E, Nishimura T, Matsumura M. Spontaneous closure of traumatic macular hole. Am J Ophthalmol. 2002;134(3):340–7.

10. Yamashita T, Uemara A, Uchino E, Doi N, Ohba N. Spontaneous closure of traumatic macular hole. Am J Ophthalmol. 2002;133(2):230–5.

11. Yeshurun I, Guerrero-Naranjo JL, Quiroz-Mercado H. Spontaneous closure of a large traumatic macular hole in a young patient. Am J Ophthalmol. 2002;134(4):602–3.

12. Pascual-Camps I, Barranco-Gonzalez H, Dolz-Marco R, Gallego-Pinazo R. Spontaneous closure of traumatic macular hole in a pediatric patient. J AAPOS. 2017;21(5):414–6.e1.

13. Sugiyama A, Imasawa M, Chiba T, Iijima H. Reappraisal of spontaneous closure rate of idiopathic full-thickness macular holes. Open Ophthalmol J. 2012;6:73–4.

14. Drenser K, Girach A, Capone A Jr. A randomized, placebo-controlled study of intravitreal ocriplasmin in pediatric patients scheduled for vitrectomy. Retina. 2016;36(3):565–75.

15. Stefanini FR, Maia M, Falabella P, Pfister M, Niemeyer M, Kashani AH, et al. Profile of ocriplasmin and its potential in the treatment of vitreomacular adhesion. Clin Ophthalmol. 2014;8:847–56.

16. Chuang CC, Chen SN. Induction of posterior vitreous detachment in pediatric vitrectomy by preoperative intravitreal injection of tissue plasminogen activator. J Pediatr Ophthalmol Strabismus. 2016;53(2):113–8.

17. Lee YS, Wang NK, Chen YP, Chen KJ, Hwang YS, Lai CC, et al. Plasmin enzyme-assisted vitrectomy in pediatric patients with vitreoretinal diseases. Ophthalmic Res. 2016;56(4):193–201.

18. Wu WC, Drenser KA, Trese MT, Williams GA, Capone A. Pediatric traumatic macular hole: results of autologous plasmin enzyme-assisted vitrectomy. Am J Ophthalmol. 2007;144(5):668–72.

19. Margherio AR, Margherio RR, Hartzer M, Trese MT, Williams GA, Ferrone PJ. Plasmin enzyme-assisted vitrectomy in traumatic pediatric macular holes. Ophthalmology. 1998;105(9):1617–20.

20. Wachtlin J, Jandeck C, Potthofer S, Kellner U, Foerster MH. Long-term results following pars plana vitrectomy with platelet concentrate in pediatric patients with traumatic macular hole. Am J Ophthalmol. 2003;136(1):197–9.

21. Gass JD. An unusual hamartoma of the pigment epithelium and retina simulating choroidal melanoma and retinoblastoma. Trans Am Ophthalmol Soc. 1973;71:171–83; discussions 84–5.

22. Shields CL, Shields JA, Marr BP, Sperber DE, Gass JD. Congenital simple hamartoma of the retinal pigment epithelium: a study of five cases. Ophthalmology. 2003;110(5):1005–11.

23. Chawla R, Kumar V, Tripathy K, Kumar A, Venkatesh P, Shaikh F, et al. Combined hamartoma of the retina and retinal pigment epithelium: an optical coherence tomography-based reappraisal. Am J Ophthalmol. 2017;181:88–96.

24. Schachat AP, Shields JA, Fine SL, Sanborn GE, Weingeist TA, Valenzuela RE, et al. Combined hamartomas of the retina and retinal pigment epithelium. Ophthalmology. 1984;91(12):1609–15.

25. Shields CL, Mashayekhi A, Dai VV, Materin MA, Shields JA. Optical coherence tomographic findings of combined hamartoma of the retina and retinal pigment epithelium in 11 patients. Arch Ophthalmol. 2005;123(12):1746–50.

26. Brue C, Saitta A, Nicolai M, Mariotti C, Giovannini A. Epiretinal membrane surgery for combined hamartoma of the retina and retinal pigment epithelium: role of multimodal analysis. Clin Ophthalmol. 2013;7:179–84.

27. Stallman JB. Visual improvement after pars plana vitrectomy and membrane peeling for vitreoretinal traction associated with combined hamartoma of the retina and retinal pigment epithelium. Retina. 2002;22(1):101–4.

28. Park JH, Park JM. Effects of internal limiting membrane peeling in combined hamartoma of retina and retinal pigment epithelium. J Korean Ophthalmol Soc. 2018;59(1):23–30.

29. McDonald HR, Abrams GW, Burke JM, Neuwirth J. Clinicopathologic results of vitreous surgery for epiretinal membranes in patients with combined retinal and retinal pigment epithelial hamartomas. Am J Ophthalmol. 1985;100(6):806–13.

30. Shields CL, Thangappan A, Hartzell K, Valente P, Pirondini C, Shields JA. Combined hamartoma of the retina and retinal pigment epithelium in 77 consecutive patients visual outcome based on macular versus extramacular tumor location. Ophthalmology. 2008;115(12):2246–52.e3.

31. Zhang X, Dong F, Dai R, Yu W. Surgical management of epiretinal membrane in combined hamartomas of the retina and retinal pigment epithelium. Retina. 2010;30(2):305–9.

32. Barth T, Zeman F, Helbig H, Oberacher-Velten I. Etiology and treatment of choroidal neovascularization in pediatric patients. Eur J Ophthalmol. 2016;26(5):388–93.

33. Sodi A, Murro V, Caporossi O, Passerini I, Bacci GM, Caputo R, et al. Long-term results of photodynamic therapy for choroidal neovascularization in pediatric patients with best vitelliform macular dystrophy. Ophthalmic Genet. 2015;36(2):168–74.

34. Henry CR, Sisk RA, Tzu JH, Albini TA, Davis JL, Murray TG, et al. Long-term follow-up of intravitreal bevacizumab for the treatment of pediatric retinal and choroidal diseases. J AAPOS. 2015;19(6):541–8.
35. Kohly RP, Muni RH, Kertes PJ, Lam WC. Management of pediatric choroidal neovascular membranes with intravitreal anti-VEGF agents: a retrospective consecutive case series. Can J Ophthalmol. 2011;46(1):46–50.
36. Sears J, Capone A Jr, Aaberg T Sr, Lewis H, Grossniklaus H, Sternberg P Jr, et al. Surgical management of subfoveal neovascularization in children. Ophthalmology. 1999;106(5):920–4.
37. Uemura A, Thomas MA. Visual outcome after surgical removal of choroidal neovascularization in pediatric patients. Arch Ophthalmol. 2000;118(10):1373–8.
38. Joshi MM, Ciaccia S, Trese MT, Capone A Jr. Posterior hyaloid contracture in pediatric vitreoretinopathies. Retina. 2006;26(7 Suppl):S38–41.
39. Ferrone PJ, Chaudhary KM. Macular epiretinal membrane peeling treatment outcomes in young children. Retina. 2012;32(3):530–6.
40. Mulligan TG, Daily MJ. Spontaneous peeling of an idiopathic epiretinal membrane in a young patient. Arch Ophthalmol. 1992;110(10):1367–8.
41. Desatnik H, Treister G, Moisseiev J. Spontaneous separation of an idiopathic macular pucker in a young girl. Am J Ophthalmol. 1999;127(6):729–31.
42. Benhamou N, Massin P, Spolaore R, Paques M, Gaudric A. Surgical management of epiretinal membrane in young patients. Am J Ophthalmol. 2002;133(3):358–64.
43. Bonnin S, Metge F, Guez A, Edelson C, Dureau P, Caputo G. Long-term outcome of epiretinal membrane surgery in young children. Retina. 2016;36(3):558–64.
44. Chen W, Shen X, Zhang P, Xu G, Jiang R, Huang X, et al. Clinical characteristics, long-term surgical outcomes, and prognostic factors of epiretinal membrane in young patients. Retina. 2019;39(8):1478–87.
45. Smiddy WE, Michels RG, Gilbert HD, Green WR. Clinicopathologic study of idiopathic macular pucker in children and young adults. Retina. 1992;12(3):232–6.

Part VII

Latest Surgical Advances

RPE and Choroid Transplantation in Macular Degeneration

30

Barbara Parolini, Ugo Nava, Michele Palmieri,
Angela Lucente, Alessandro Finzi, and Rino Frisina

30.1 Introduction

Age-related macular degeneration (AMD) is a chronic degenerative disease that could lead to debilitating consequences for the patient visual acuity like the development of a choroidal neo-vascularization (CNV) or atrophy of retinal pigment epithelium (RPE) cells with the associated death of overlying neuroretinal tissue, a condition better known as geographic atrophy (GA) [1, 2]. The latter is a slowly progressive complication without an available therapy; diversely CNVs could be responsible for a more rapid drop in visual acuity but could be effectively managed with medical treatment by means of repeated intravitreal injections of antibodies against vascular endothelial growth factor (VEGF) [3–5]. Those antibodies promote the regression of abnormal and leaking choroidal new vessels and, in the majority of cases, prevent the formation of a disciform scar in the macula [6].

Despite the proven efficacy of anti-VEGF, real-life data shows us that some patients do not receive intravitreal injections with the proper timing offered in the clinical trials, and some other patients progress despite meticulous treatment

[7]. For these reasons advanced AMD is not an extinguished entity but still a clinical challenge.

30.2 Background History

Before the advent of intravitreal injections, neovascular AMD end stages were a frequent finding and many efforts have been made to curb this condition; however, the role of surgery in AMD has always been controversial. In neovascular AMD, submacular surgery was conceived as an excision of CNV through a paramacular retinal incision. This approach had worse outcomes in submacular surgery trials, with the exception of cases with hemorrhagic CNV, where this type of surgery significantly reduced severe vision loss when compared to just observation [8]. These conclusions were also important to identify a subgroup of neovascular patients who could benefit from surgical intervention.

The idea of translocating the fovea from the AMD-injured site to adjacent healthier RPE was first proposed by Lindsey et al. in 1983 [9], but the procedure was performed in humans only in 1993 by Machemer and Steinhorst [10]. The technique consisted of a 360° retinotomy followed by macular rotation, although some modifications have been tried, like the limited retinal rotation that avoided the 360° retinotomy and the combined ocular counterrotation of the globe to prevent the induced cyclotropia [11, 12]. This is a

B. Parolini (✉) · U. Nava · M. Palmieri · A. Lucente
A. Finzi
Eyecare Clinic, Crystal Palace, Brescia, Italy

R. Frisina
Department of Ophthalmology, University of Padova, Padua, Italy

challenging surgical technique and its indication is limited to smaller CNVs while main complications related to this type of surgery are retinal detachment and proliferative vitreoretinopathy (PVR). Due to absence of randomized controlled trials and controversial data results, Wong et al. [13] proposed a case selection for macular relocation surgery in order to reduce the possibility of surgical complications. They observed that the highest visual gain and the lowest postoperative complications were obtained in patients with a best corrected visual acuity (BCVA) of 20/120 or worse and in particular in patients with type 2 CNV or hemorrhagic CNV.

In parallel to the advancement in macular relocation surgery, other approaches were being developed. The concept of RPE transplantation is relatively recent and has its roots in 1985 when Gouras et al. first transplanted with success human cultured RPE cells over bearded monkey Bruch's membrane [9]. The rationale for RPE transplantation in retinal diseases resided in experiments using Royal College of Surgeon rat animal model (RCS rat) where prevention of photoreceptor degeneration was achieved by pigment epithelial cell transplantation [14]. This evidence increased the attention over this topic because the graft-host integration between the donor RPE and the host photoreceptors is effectively guaranteed by spontaneous interdigitation of epithelial apical villi and photoreceptor tips restoring the anatomical-functional unit and providing curative potential for AMD. In clinical setting, Peyman et al. [15] first described a technique of autologous pedicle RPE graft after the formation of a large macular flap and removal of the submacular scar. This technique ensured visual gain from finger counting to 20/400 and restoration of fixation ability over the graft tissue at 1 year after surgery; these findings were not observed with homologous RPE cell transplantation. Consequently, autologous RPE was preferred in order to avoid immunological response, reduce immunosuppressive burden in elderly patients, and provide a lasting engraftment of the epithelium. However, even when harvested from the same eye, RPE-cell suspension technique showed worse anatomical and functional outcomes because cell suspension has insufficient adhesion to the diseased Bruch's membrane and often does not form the monolayer required for optimal RPE functioning and may undergo apoptosis. Therefore, RPE-cell suspension was progressively abandoned in favor of the free graft technique [16].

From the pedicle RPE graft approach, the surgery of RPE transplantation has evolved through different techniques. Stanga et al. [17] proved that the pigmented epithelium could be successfully translocated from the edge of neovascular lesion to a subfoveal location at the same time of the CNV removal, achieving the resumption of photoreceptor functional activities over the grafted tissue. The evidence that RPE could be effectively translocated paved the way, a couple of years later, to the development of a full-thickness patch of RPE and choroid harvested from the superior middle-peripheral retina and then engrafted through the same paramacular retinotomy used for the CNV removal [18]. This approach revealed a gain in visual function that lasted over a long-term follow-up [19–21]. The same authors used this technique in cases of submacular hemorrhage and macular RPE tear and in patients that were refractory to frequent anti-VEGF treatments and compared it to anti-VEGF intravitreal injections alone in a total of 20 patients, showing better visual gain with the RPE-choroid patch graft when surgical complications did not occur [22]. Postoperative complications encountered were recurrent retinal detachment secondary to PVR, severe hypotony, and recurrent submacular hemorrhage. To address the issue of surgical complications, Pertile and Parolini in 2007 modified the surgical procedure including a large temporal peripheral retinotomy allowing a better exposure of the macular RPE and ensuring a gentler manipulation of the full-thickness graft. In 2011 they published data from 13 cases showing no major intraocular complications and good graft stability [23]. The long-term results of RPE-choroid patch in exudative maculopathies have been recently reported [24].

Autologous RPE-choroid patch was reported in geographic atrophy cases as well [25]. The authors

reported maintenance of visual function at 3 years in two of ten operated eyes. However, long-term results of RPE-choroid patch in dry AMD, hereditary maculopathies, and exudative maculopathies other than AMD have not yet been reported.

In 2017, Parolini retrospectively reviewed the medical charts of all consecutive eyes that underwent RPE-choroid patch surgery, between 2007 and 2015, for exudative and atrophic macular degeneration by the same surgeon (BP). Collected data included demographics, best corrected visual acuity (BCVA), reading ability, retinal biomicroscopy, fixation stability based on microperimetry, as well as qualitative data from spectral domain optical coherence tomography (OCT), color fundus (CF) photography, fundus autofluorescence (FAF), fluorescein angiography (FA), and indocyanine green angiography (ICGA), in addition to surgical time and intraoperative and postoperative surgical complications.

In this chapter are reported the results of that review [26], as well as the conclusion drawn from the experience collected in 10 years of RPE-choroid patch surgery.

30.3 Graft Perfusion

Revascularization of the graft is essential to guaranteeing RPE vitality and to ensure its physiological activities. Histological observation of the process was described in pigs due to the anatomical analogy between this animal model and human choroid [27, 28]. Interestingly, the presence of intact Burch's membrane at the recipient site is not a limiting factor to the formation of vascular connections with the graft choroid because the membrane undergoes a degenerative process, mainly driven by macrophages, and disappears [29]. This phenomenon explains the technical feasibility of RPE-choroid transplantation even in dry AMD, where the Bruch's membrane is not interrupted by the passage of CNVs [30]. Vertically bridging vessels then connect the recipient bed with the graft choroid, where the majority of vessels express VEGF receptor-1 [29]. The presence of macrophages persisted for

all the follow-up duration of 3 months, suggesting a crucial role of these cells in the healing process and in angiogenesis promotion [31–33].

In clinical settings, the graft perfusion is mainly assessed with fluorescein angiography (FA) and indocyanine green angiography (ICGA). In early phase of FA, most of the signal originates from the superficial vessels because the fluorescence of the deeper vasculature is blocked by overlying melanin and fluorescein of the perfused graft [34–38]; therefore a recognizable sign of successful engraftment is observed when the graft area becomes simultaneously fluorescent with the normal choroid outside the graft area [39]. Indocyanine green angiography helps to avoid the signal blockage of the superficial melanin and enables a better visualization of vessel profile; this allows to recognize the parallel course of the vessels inside the graft area that is a typical pattern of the peripheral choroid where the graft is harvested [40, 41]. The fluorescence of this pattern allows to prove graft perfusion [39].

Although angiography provides us direct observation of vasculature filling, OCT is also useful to give some indirect signs of graft revascularization, like enlargement of vessel diameters, increase in the number of choroidal vessels, and graft thickening [42]. In fact, the technological advance in this field allows, nowadays, better choroid image quality and eye tracking to avoid movement artifacts and to ensure precise follow-up in a noninvasive way. A compromise between direct visualization of the blood flow obtained with angiography and noninvasive nature of OCT examination is OCT angiography (OCTA). This relatively recent technology allows the identification of perfusion of the graft in addition to structural OCT information [43]; the main drawback is the need of a good patient fixation during the examination in order to obtain images with proper quality. But although fixation is markedly impaired in these patients, the constant progressiveness of software updates and motion artifact improvement give reason to believe that OCTA will be a promising tool for the postoperative evaluation of RPE-choroid grafts (Fig. 30.1).
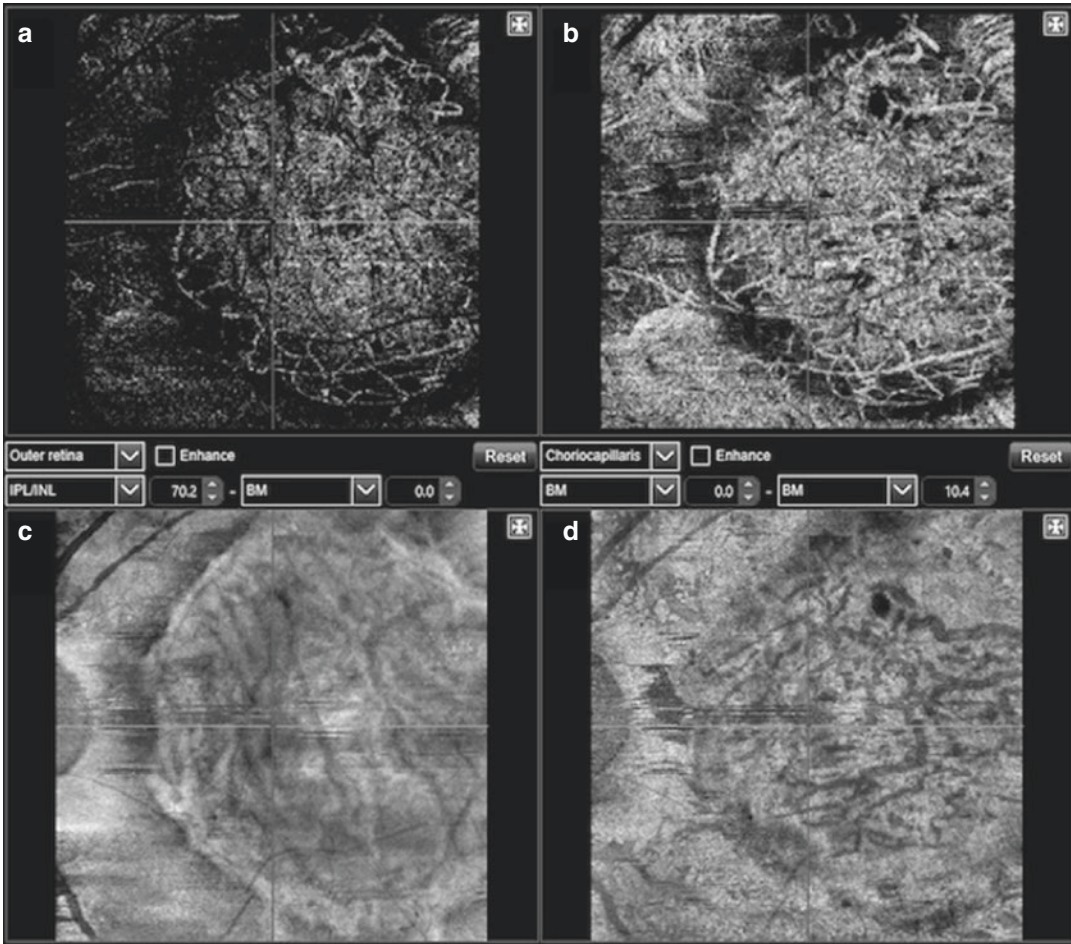
Fig. 30.1 OCT angiography (OCTA) analysis of an eye after RPE-choroid patch transplant. En face pictures of outer retina (**a**) and of the choriocapillaris (**b**) showing graphical representation of the flows inside the slabs, RPE (**c**) and choroid (**d**), En face OCT. From the flow analysis it is possible to observe the presence of patch perfusion due to the evidence of vascular network at the level of outer retina and choriocapillaris. At the choriocapillaris level, the flow inside the transplanted patch exhibits larger vessel diameters compared to the flow signal derived from the adjacent small capillary vessels

30.4 Graft Survival

Innate and adaptive immune systems are both involved in the determination of an immune privilege status of the eye. This status allows the eye to accept allografts for a longer period of time compared to a nonimmune-privileged site [44, 45].

Streilein et al. [45] have described some factors that are primarily involved in this phenomenon. First of all, blood-ocular barrier reduces the chances for the graft antigens to get in contact with the host immune system elements; secondly the limited lymphatic drainage shifts the antigen presentation in the spleen instead of the regional lymph nodes, reducing the local immune reaction. Furthermore, the inflammatory response is inhibited by a lack of antigen-presenting cells and by a relatively elevated levels of soluble molecules responsible for the onset of an immune-suppressed environment. Not least, RPE is characterized by low levels of major histocompatibility (MHC)

antigens, and even when these antigens are induced by cytokines, like interferon-γ (IFN-γ), the resulting immune system activation does not involve T-cell proliferation [46–48]. The resultant molecular ambiance determines that subretinal allograft benefits from a suppressed delayed hypersensitivity reaction making the graft resistant to immune rejection [49, 50].

Translating biological models in a pathological scenario is, unfortunately, not so obvious. In fact, choroidal neovascularization is marked by loss of vascular permeability in itself and its surgical removal determines even more the rupture of the blood-retinal barrier [51, 52] that is one of the aforementioned factors responsible for the immune privilege status of the eye. For this reason, and probably for other microenvironmental modifications still not completely understood, allogenic RPE requires immune suppression therapy that is often associated to side effects which are not always tolerated by the older age group [53]. In contrast, autologous transplantation does not suffer from the immune exposure due to blood-retinal barrier breakdown, but other issues arise. In this case, in fact, the tissue is harvested from the same eye affected by the pathology we are supposed to treat. This could be irrelevant in AMD patients, because probably the RPE alterations are limited to the posterior pole and then they do not involve the peripheral harvested cells. However, the state of health of the graft could be compromised by pathologies that extend beyond the posterior pole, like many retinal dystrophies. This concept underlines the importance of patient selection, from a clinical perspective, to offer a proper indication to surgery, but also from a statistical point of view, to obtain data from homogeneous population sampling.

Besides graft rejection, there are other factors that could lead to a graft failure. Adhesion of the RPE to the underneath Bruch's membrane is fundamental for the success of the transplantation. Choroid, RPE, and photoreceptors work as a morpho-functional unit; the bond between them is essential to the course of their metabolic activities. In exudative AMD patients the Bruch's membrane is altered by the CNV growth, fibrotic involution, persistent leakage of fluid, and cholesterol deposi-

tion [54]. In addition to this, surgical manipulation of CNV site contributes to the irregularity of the surface of the membrane with, presumably, a loss of integrins and other proteins accountable for tissue adherence. Although studies conducted with cultured fetal human RPE show that the donor epithelium could survive over exposed collagenous layers of the Bruch's membrane, the long-term engraftment is often compromised [55–57]. The impaired adhesion to the Bruch's membrane and an incomplete RPE monolayer formation are the major limits of the cell suspension transplantation technique. The choice of a free graft constituted by a patch of RPE and choroid permits to avoid the adhesion issue because the whole vascular-epithelium complex is transplanted and the morpho-functional unit is much more preserved. In this case, it is crucial that the patch is properly centered under the retina and any eventual shift of the graft should be checked and corrected before the completion of the surgery.

In reason of that, if correctly placed, autologous RPE and choroid transplantation could grant long-lasting results due to the fulfilment of two important concepts: the observance of the immune system and the respect of the morpho-functional bonds between choroid and RPE [26].

30.5 Indications to Surgery

In the study by Parolini et al. [26], from 2007 to March 2011, surgical indications were limited to exudative AMD with RPE tear and/or massive subretinal hemorrhage and to eyes with chronic active AMD refractory to frequent (six or more) injections of anti-VEGF drugs, associated with progressive visual loss. From April 2011, the inclusion criteria were further limited to eyes with same diagnosis but with significant visual loss for no longer than 1 year. The aim was to include eyes with better preoperative anatomical conditions of the external retina and relatively recent visual loss. From the same year, indications have also been extended to include eyes with neovascular maculopathies other than AMD and atrophic maculopathies, associated with retinal dystrophies.

The retrospective analysis of these cases has highlighted that only eyes with recent vision loss (within 1 year) and eyes with recent submacular hemorrhage and with outer retina still intact (i.e., with at least the external limiting membrane still visible on OCT examination) are good indications to RPE-choroidal patch surgery.

30.6   Surgical Technique in Details

Many surgical approaches have been described since the first RPE transplantation was performed. The procedure set out below is the one developed by Pertile and Parolini since 2007.

A standard three-port pars plana vitrectomy (PPV) is performed with 20-gauge (G) instrumentation. In phakic patients, PPV is routinely combined with phacoemulsification and a three-piece intraocular lens (IOL) is implanted in the capsular bag. After sclerotomy creation, posterior vitreous detachment (PVD) is induced when not already present and vitrectomy is completed in the usual manner with removal of the vitreous until reaching the anterior vitreous base, assisted by scleral indentation and triamcinolone (TA) staining. Then, the inferotemporal sclerotomy is cut perpendicularly and occupied by an illuminated infusion cannula, sutured to the sclera. The superior sclerotomies are cut tangentially to the scleral plane. Any vitreous residue that remains incarcerated into the sclerotomies is aspirated and removed with the vitrectomy probe. Since 2011 the internal limiting membrane (ILM) is peeled routinely. A retinal detachment (RD) is then induced by injecting balanced salt solution (BSS) into the subretinal space using a 41 G needle connected to the active pump of the vitrectomy machine viscous-fluid injection apparatus, set at 40 mmHg. This setting allows to obtain a steady stream during the injection into the subretinal space. RD is then extended with a fluid air exchange. Under balanced salt solution, an approximately 200° peripheral retinotomy is performed with scissors near to the ora serrata in the superior and temporal quadrant. The temporal retina is folded on the nasal retina, to expose the temporal superior and inferior subretinal space. Choroidal neovascular membrane, when present,

is removed using retinal forceps and endodiathermy is applied to the feeder vessels after CNV removal. Endodiathermy is also applied in multiple spots over macular area in all operated eyes, including those with atrophic maculopathy in the absence of a CNV, with the aim of creating micro-trauma of the choriocapillaris to enhance the revascularization of the RPE-choroid patch. The location of the harvesting site of the patch is chosen by visually selecting an area of normally appearing RPE in temporal, superior or inferior quadrants, avoiding the vortex veins. An intense diathermy is first applied around the margins of the intended patch which diameter is always approximated to three optic disc diameters. Using a 20 G vertical-cutting intraocular scissor, the combined RPE and choroidal tissue are then cut down until the clear white sclera is visible and within the margins of the diathermy burns, starting at the posterior aspect of the intended patch graft. Any encountered choroidal bleeding is mainly controlled with additional diathermy and raising the infusion pressure for several minutes. When raising the infusion pressure, the sclerotomy is kept closed by instruments to avoid retina incarceration into the sclerotomy. After dissecting the posterior part of the patch, perfluorocarbon liquid (PFCL) is injected into the subretinal space and over the isolated edges of the patch, in order to avoid the rolling or elevation of dissected edges of the RPE-choroid patch. Subsequently, the anterior half of the patch is cut and the RPE-choroid patch is transplanted using non-toothed retinal forceps, onto the submacular area under PFCL. Care is taken to flatten the border of the RPE-choroid patch with a spatula. At the harvesting site, remaining residues of choroid are removed from the sclera with aspiration and/or forceps, and the borders of incised RPE-choroid are heavily treated with endodiathermy. Perfluorocarbon liquid is progressively and slowly aspirated and subsequently reinjected in the epiretinal space in order to flatten retina on the top of the patch and to center fovea on visually healthy RPE. If the patch is not centered, then PFCL is moved again subretinally, the patch position is re-centered, and then the maneuver of moving PFCL from the subretinal to the epiretinal space is repeated. The retina is then com-

pletely reattached with PFCL and retinotomy is sealed with multiple rows of laser. Peripheral laser is applied to the retinotomy edge and extended 360°. The peripheral retina at the ora serrata anterior to the retinotomy is carefully removed with vitrectomy probe. Perfluorocarbon liquid is finally exchanged directly with 1000 centistokes (cs) silicone oil. Silicone oil is removed after at least 3 months.

Since 2017 the procedure has been safely performed with 23G instrumentation as well, although in some cases one sclerotomy needs to be enlarged in order to allow the removal of larger CNVs.

The mean surgical time was 2 h and 50 min (range 2 h 30 min–4 h 10 min) for the first 40 eyes and decreased to 1 h 40 min (range 1 h 20 min–2 h 55 min) for the subsequent cases.

30.7   What Do We Know After 10 Years of Surgery?

Which functional and anatomical realistic results can we expect from this surgery?

Which are the complications and the rate of them?

How to compare the results of this surgery with the results of anti-VEGF treatment?

If a satisfactory result is obtained, how long does it last?

All these questions were answered by the analysis of all the operated eyes since 2007 [26].

From the original cohort of 150 eyes operated between 2007 and 2018, 88 eyes (36 right and 52 left) of 84 patients (41 females and 43 males) were chosen for a detailed analysis (Table 30.1). The remaining eyes were excluded because of lack of sufficient postoperative BCVA data and a follow-up of less than 2 years, regardless of the degree of visual improvement or the presence of postoperative complications.

For the 88 eyes included in the analysis, the mean age was 71.9 ± 9.7 years (range: 42–88, median 74).

Seventy-seven eyes of 75 patients were affected by neovascular maculopathy, and 11 eyes of 9 patients by atrophic maculopathy. All 88 study eyes had a follow-up time of at least 24 months. Forty-nine (56%) eyes had a follow-up of 3–5 years, 15 (17%) eyes had a follow-up of 6–8 years, and 4 eyes (4.5%) had a follow-up of 8–9 years.

The results were divided into functional and morphological. Functional results were judged based on far BCVA, reading ability, and microperimetry, while morphological parameters were

Table 30.1 Demographic, morphological, and functional data

Demographic and functional data					
Number of patients	Age years	Gender	Eye	Pre-op BCVA treated eye logMAR	Pre-op BCVA fellow eye logMAR
Number of eyes	Mean STDV (range)	Female/male Number (%)	Right/left Number (%)	Mean STDV (range)	Mean STDV (range)
84 88	71.9 ± 9.06 (50–88)	41(48.8)/43(51.2)	36 (40.9)/52(59.1)	1.1 ± 0.2 (0.4–1.5)	0.57 ± 0.5 (0–1.5)

Maculopathy pattern subgroups					
Exudative maculopathies			Atrophic maculopathies		
Subtype	Number	%	Subtype	Number	%
AMD-CNV	48	62.3	Dry AMD	1	9.1
Hemorrhagic CNV-AMD	23	29.8	Heredo-dystrophic/atrophic maculopathies	7	63.6
Myopic CNV	2	2.6			
CNV secondary to angioid streak	1	1.3			
Idiopathic CNV	2	2.6	Pattern dystrophies	**3**	27.3
CNV secondary to laser for CSCR	1	1.3			
Total	77	100	Total	11	100

STDV standard deviation, *AMD* age-related macular degeneration, *CNV* choroidal neovascularization, *CSCR* central serous chorioretinopathy

judged by color fundus images, OCT, autofluorescence, fluorescein, and indocyanine green angiography.

30.8 Functional Parameters

30.8.1 Distance Vision and Reading Ability

BCVA was measured in Snellen notation and converted to logarithm minimum angle of resolution (logMAR) for analyses. If more than one assessment of BCVA was made during the follow-up, the BCVA demonstrating the greatest improvement from baseline was chosen. For the purpose of analysis, we classified two subgroups based on preoperative vision: the low-preoperative-BCVA group, that included eyes with preoperative BCVA <20/200 (>1 logMAR) and the high preoperative-BCVA group, that included eyes with preoperative vision ≥20/200 (≤1 logMAR). Reading ability was defined as the ability to read, at 30 cm, at least point 12 of print letters.

30.8.2 Microperimetry

For a limited number of patients and only in the postoperative time, microperimetry assessment was made, since it became available only recently. A common criticism regarding submacular surgery, and RPE-choroidal patch in particular, is the question of where the patients do fixate after surgery and if the fixation is effective over the area of retina lying on the transplant.

Macular integrity assessment device (MAIA) system was used to test the retina sensitivity and the preferred retinal locus (PRL) of fixation. A low vision test was used, consisting of 68 test loci covering the central 20°, with a 4–2 projection strategy, that changes the light intensity in 4 decibel (dB) steps, until there is a change from "not seen" to "seen" or from "seen" to "not seen." Then, the intensity changes in 2 dB steps until the stimulus is not seen again. Classification of fixation stability is represented in the MAIA by the indices P1 and P2, which are defined as the percentage of fixation points falling inside a circle of

11 and 21 radii, respectively, centered on the PRL. Eyes with P1 greater than 75% are classified as stable. If P1 is less than 75% and P2 is more than 75%, fixation is classified as relatively unstable. If both P1 and P2 are less than 75%, the pattern is described as representing unstable fixation as defined [58].

30.9 Morphological Parameters

30.9.1 Optical Coherence Tomography

Optical coherence tomography images were acquired with SD-OCT Heidelberg Spectralis (Heidelberg Engineering, GmbH, Dossenheim, Germany), Triton-Topcon (Topcon Corp, Tokyo, Japan), and Cirrus HD-OCT (Carl Zeiss Meditec, Oberkochen, Germany). Preoperatively, the integrity of the external limiting membrane (ELM) was evaluated in order to correlate the integrity of external retinal layers with the postoperative functional outcomes. Postoperatively, the OCT was used to study the RPE-choroid patch morphology and the occurrence of postoperative macular complications through qualitative analysis of the retinal and choroidal tissue morphology. We also evaluated the presence of subretinal fluid (SRF) and cystoid macular edema (CME) before and after surgery.

30.9.2 Fundus Autofluorescence

Blue light autofluorescence (BAF) obtained with HRAII Heidelberg Spectralis (Heidelberg Engineering, GmbH, Dossenheim, Germany) was used to detect the location and extension of RPE atrophy in preoperative time and to monitor RPE alterations during postoperative time. Autofluorescence is a useful tool that allows to obtain an image of the posterior pole using the fluorescence emanated from the lipofuscin material, contained in the RPE cells, during ongoing stimulation with blue light. The reflected blue light has a different wavelength from that of the autofluorescence light, so it is easy to exclude from recorded image by a proper filter. The recorded

image is reported in a scale of gray; the whiter is an area the more intense is the autofluorescence of that area. Therefore, a lack of signal is expressed as a dark area and denotes RPE atrophy or blood masking. Due to the latter condition, a color fundus photography is important to guide the operator to the proper interpretation of this exam.

30.9.3 Color Fundus Photography

Color fundus photography (Daytona, Optos, Marlborough, MA, USA) was used to document postoperative appearance of the fundus and in particular the changes of patch morphology and the amount of bleeding in the macular region and in patch harvesting site.

30.9.4 Fluorescein Angiography and Indocyanine Green Angiography

Preoperatively FA and ICGA angiography (HRAII Heidelberg Engineering, GmbH, Dossenheim, Germany) were used for the diagnosis. Postoperatively we used these test modalities to evaluate the revascularization of the RPE-choroid patch and to follow its evolution. Based on OCT, FAF, FA, and ICGA, we further categorized the study eyes into four maculopathy pattern subgroups: CNV-AMD subgroup; CNV-AMD-Hem subgroup for cases with subretinal hemorrhage; atrophy subgroup for atrophic maculopathies, and other CNV subgroup for CNV due to an etiology other than AMD.

30.10 Anatomical Results

30.10.1 Biomicroscopy and Color Fundus Photograph

For 59 eyes (67%) that did not have hazy media early postoperatively, the RPE-choroidal patch was well visible, between 1 day and 1 week, in the subfoveal area as a pigmented thick oval to
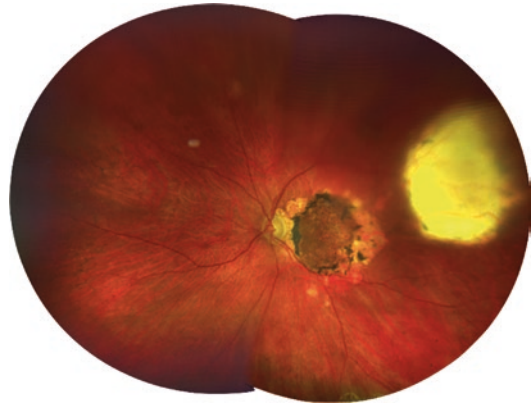
Fig. 30.2 Fundus photograph of an eye 3 months after RPE-choroid patch surgery. The patch is well visible, in the subfoveal area, as a pigmented thick oval-round tissue, with an average size of three-disc diameters. The patch results to be more pigmented than the choroid in surrounding area. In the superior-temporal quadrant, a whitish area of bare sclera identifies the harvesting site of the patch

round tissue, with an average size of three optic disc diameters (Fig. 30.2). In one peripheral quadrant (more commonly superior or temporal, seldom inferiorly), a whitish area of bare sclera was visible, identifying the harvesting site of the patch. Subretinal blood remnants at the borders of the harvesting site were a common finding and lasted for the first 4–6 weeks. Three months after surgery, the RPE-choroid patch had more defined and flat thin edges. A progressive reabsorption of blood was observed at the harvesting site.

Commonly, the patch had a darker pigmentation with respect to the surrounding tissue (Fig. 30.2). Silicone oil was removed in 78 (89%) eyes at a mean time of 5.5 months after surgery (range: 3–8 months). After silicone oil removal, the appearance of the patch and the harvesting site did not change through follow-up. In a subgroup of 39 eyes (44%), we observed a fibrotic thin scar like a whitish profile surrounding the patch. This scar extended to the harvesting site, in eyes in which the shortest distance between the edge of the patch and the harvesting site was inferior to the diameter of the harvesting site.
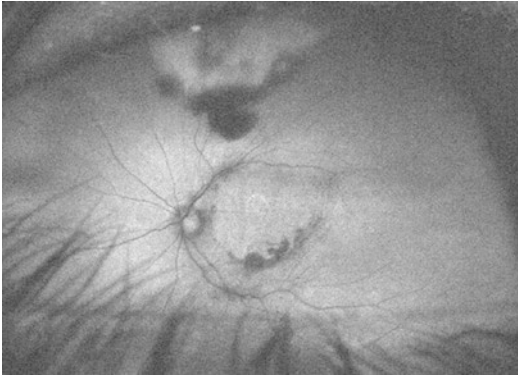
Fig. 30.3 Blue-light fundus autofluorescence (BAF) of the same eye depicted in Fig. 30.2. Over the area of the patch, BAF appeared comparable to the BAF of the surrounding choroid, although the wrinkles in the patch are visible as lines of hypo- and hyperfluorescence. Multiple areas of hypoautofluorescence are noticed at the inferior borders of the patch, where the necessary surgical manipulation was applied

30.10.2 Blue-Light Fundus Autofluorescence

For all eyes, the BAF of the patch was comparable to the BAF of the peripheral choroid. Multiple areas of hypoautofluorescence were noticed at the borders of the patch, where the necessary surgical manipulation was applied (Fig. 30.3). Fifty-nine eyes (67%) presented scattered areas of hypoautofluorescence also over the patch and in the posterior pole, around the patch, in longer follow-up.

30.10.3 Optical Coherence Tomography

The patch appeared as a subfoveal layer of RPE and choroid, with open large hyporeflective spaces corresponding to perfused choroidal vessels (Fig. 30.4). We observed the disappearance of subretinal and intraretinal fluid in the immediate postoperative follow-up in all cases that presented subretinal fluid (40%) and cystoid macular edema preoperatively (25%). The visibility of external layers of retina changed in time, being rarely visible for at least 1 month after surgery and becoming more defined in the long follow-up.

30.10.4 Fluorescein and Indocyanine Angiography

One month after surgery, FA and ICG confirmed the vascularization of the patch in all but seven eyes (7.9%). The choroidal vessels into the patch exhibited different direction as compared to the vessels of surrounding choroid (Fig. 30.4). Vascularization of the patch was homogenous in 77 (87%) eyes, while in 4 (4.5%) the patch showed a nonhomogeneous vascularization pattern, meaning that some areas of the patch were less vascularized than others and presented sectorial hypoperfusion. Figure 30.4 summarizes the multi-imaging representation of a case of hemorrhagic CNV secondary to AMD from the preoperative to the postoperative time. Figure 30.5 summarizes the evolution of one case followed from baseline and for more than 5 years with FA, ICG, OCT, FAF, and microperimetry.

30.11 Functional Results

30.11.1 Visual Outcomes

Mean baseline BCVA was 20/320 (logMar 1.2 ± 0.2) and 20/200 (logMar 0.94 ± 0.36 range: 0.4–1.5, median 1.1), respectively. By the end of follow-up time, mean BCVA improved in the whole cohort of eyes to 20/200 (logMar 0.94 ± 0.36 range: 0.2–1.3, median 1.1). The difference was statistically significant (*P* 0.009). Specifically, the statistical analysis demonstrated significant improvement of BCVA in the CNV-AMD (*P* 0.0063), CNV-AMD Hem (*P* 0.0074), and other CNV subgroups (*P* 0.0030). Visual acuity improvement was not statistically significant in the atrophy subgroup (Table 30.2). A gain in vision of at least 15 letters was obtained, respectively, in 24 (41%) eyes of the low preoperative BCVA subgroup and in 11 (37%) of the high preoperative BCVA subgroup. Forty-four (50%) eyes had BCVA of ≥20/200 after 4 years. Six (7%) eyes had BCVA of ≥20/40 after 4 years. Twenty-five eyes (28%) showed a BCVA gain between 25 and 50 letters
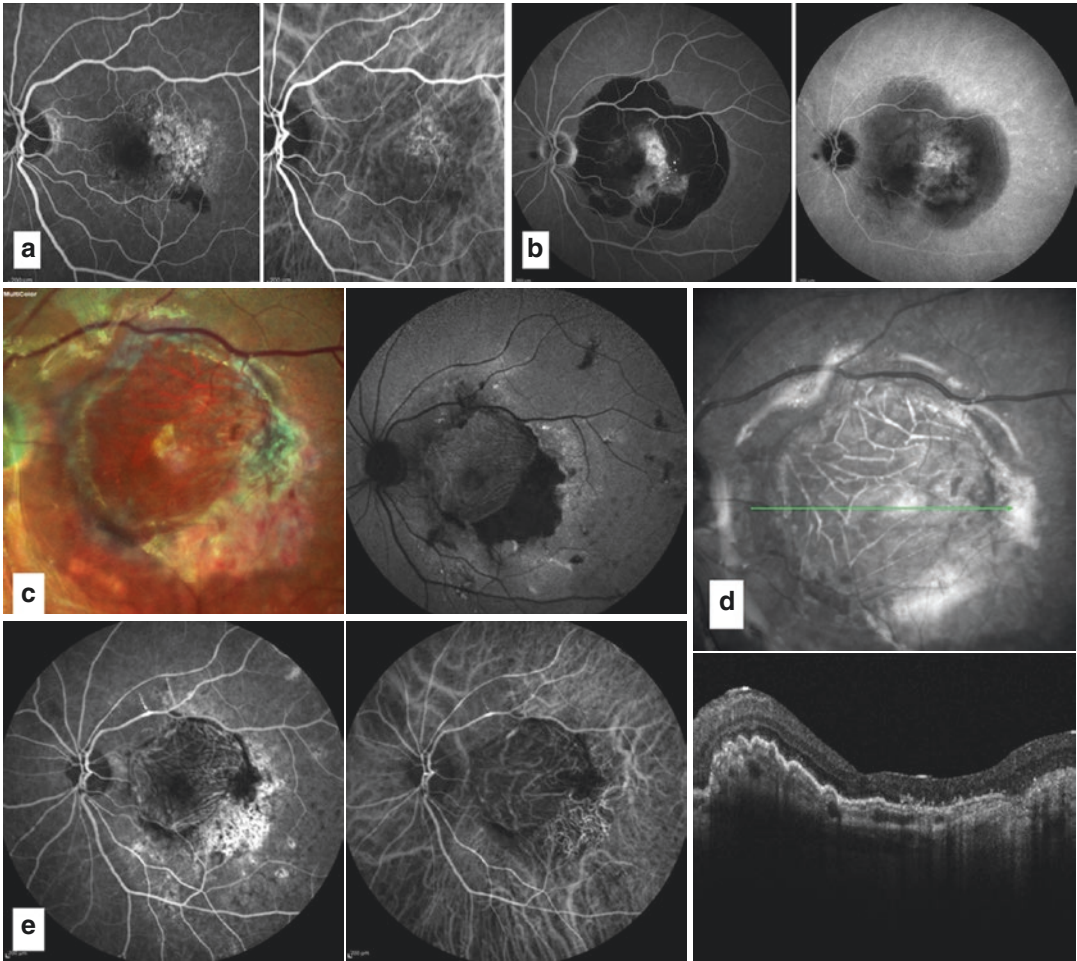
Fig. 30.4 Evolution of one eye with subfoveal CNV from 6 months preoperatively to 1-month follow-up. (**a**) FA and ICG show the subfoveal occult CNV and subretinal blood at the border, occurring 6 months prior to surgery. (**b**) FA and ICG show the subfoveal occult CNV and submacular hemorrhage, occurring 2 weeks prior to surgery. (**c**) Color fundus photo and FAF of the same eye 1 month postoperatively. (**d**) Infrared (IR) of the same eye 1 month postoperatively. (**e**) FA, ICG, and OCT of a RPE-choroid patch, 1 month postoperatively. The patch is well vascularized; BCVA is 20/40

at final measurement, after 4 years. Among the eyes with final improvement in BCVA, we observed different patterns of visual change. A progressive and fast improvement in BCVA, within 6 months after surgery, was observed in 17 eyes (20%) of patients with mean age of 64 years (range 42–64); a progressive but slow improvement in BCVA, in the first postoperative year, was observed in 14 eyes (15%) of patients with mean age of 75 years (range 65–81); a late and sudden improvement of BCVA occurred more than 1 year after surgery in 3 eyes (3.4%) of patients, who were, respectively, 66, 75, and 76 years old (mean age of 72 years). Reading ability was recovered in 43% of cases. Regarding the effect of the pattern of maculopathy on the postoperative visual acuity outcome, we found improvement of mean BCVA in the CNV-AMD (7 letters), CNV-AMD Hem (11.5 letters), and other CNV subgroups (26.7) while BCVA
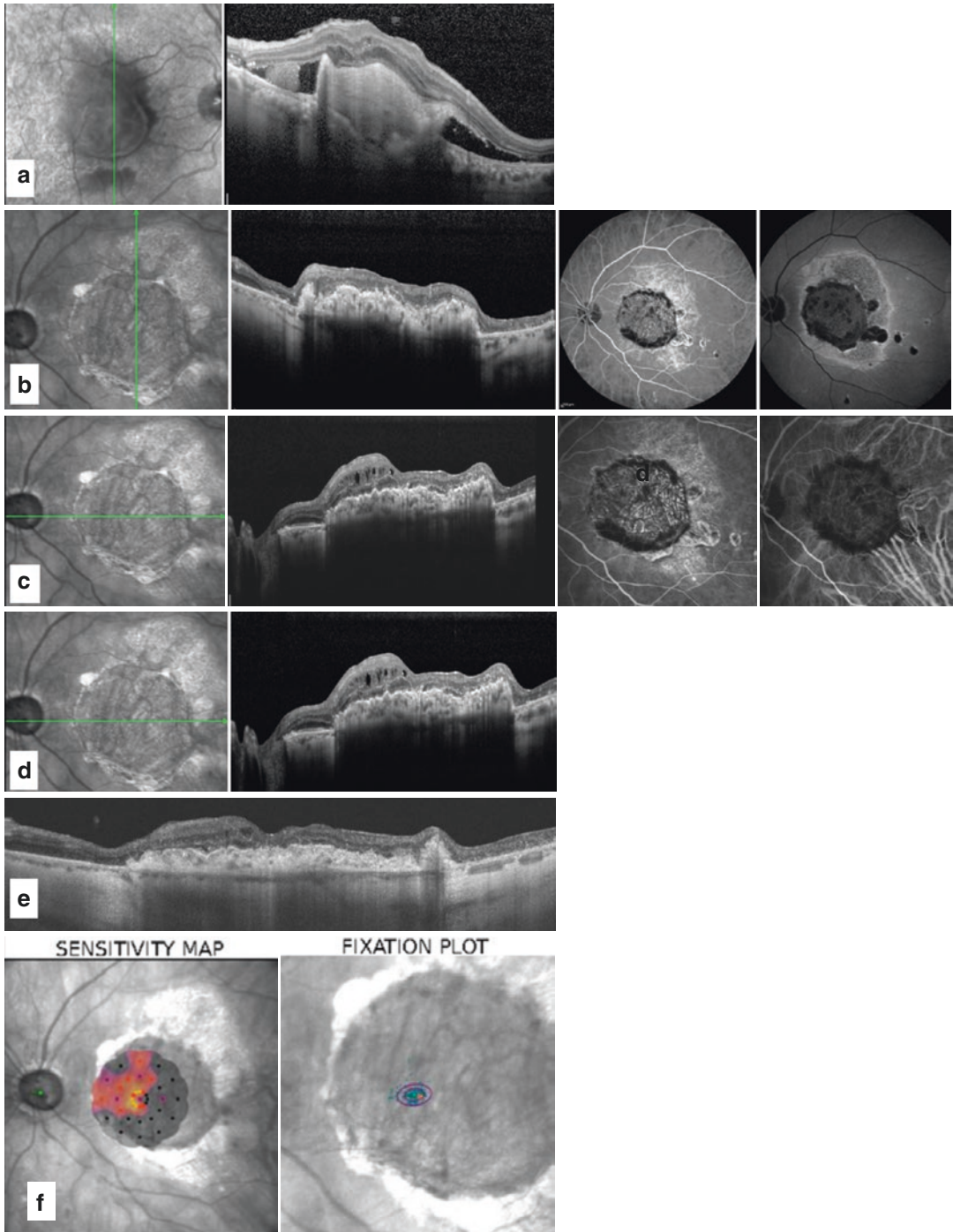
Fig. 30.5 Evolution of one eye with subfoveal CNV from 1 month preoperatively to 5-year follow-up. (**a**) OCT shows the subfoveal occult CNV and subretinal fluid and blood at the border, occurring 1 month prior to surgery. (**b**) IR, OCT, FA, and FAF show the subfoveal RPE-choroidal patch, 1 month after surgery. (**c**) IR, OCT, FA, and ICG show the subfoveal RPE-choroidal patch, 6 months after surgery. The patch is well vascularized. CME is present on the thicker side of the patch. (**d**) IR and OCT show the subfoveal RPE-choroidal patch, 1 year after surgery. CME is present on the thicker side of the patch. (**e**) OCT of a RPE-choroid patch. (**f**) Microperimetry showing the sensitivity map and fixation plot of the same eye

Table 30.2 Analysis of BCVA in whole group and in maculopathy pattern subgroups

Maculopathy pattern subgroups	Number of eyes (%)	Preoperative BCVA (logMar) Mean STDV (range)	Final BCVA (logMar) Mean STDV (range)	P value *Value < 0.05
CNV-AMD	48 (54.54)	1.1 ± 0.23 (0.6–1.5)	0.97 ± 0.39 (0.2–1.3)	*0.0063
CNV-AMD-Hem	23 (26.14)	1.2 ± 0.17 (0.7–1.5)	1 ± 0.35 (0.3–1.3)	*0.0074
Atrophy	11 (12.5)	1.0 ± 0.15 (1.0–1.3)	0.96 ± 0.336 (0.4–1.3)	0.2991
Other CNV	6 (6.82)	1.2 ± 0.27 (0.7–1.0)	0.7 ± 0.34 (0.4–1.3)	*0.0030
Whole group	88 (100)	1.1 ± 0.2 (0.4–1.5)	0.96 ± 0.37 (0.3–1.3)	*0.0090

CNV-AMD choroidal neovascular membrane-age-related macular degeneration, *CNV-AMD-Hem* choroidal neovascular membrane-age-related macular degeneration with hemorrhage, *BCVA* best corrected visual acuity, *STDV* standard deviation

Table 30.3 Gain in letter score in maculopathy pattern subgroups and functional subgroups

Maculopathy pattern subgroups	N.	Gain of at least 15 letters Number (%)	Loss of at least 15 letters Number (%)	Stable (±10 letters) Number (%)	Reading ability Number (%)
CNV-AMD	48	15 (31%)	6 (12%)	27 (56%)	18 (37%)
CNV-AMD-Hem	23	12 (52%)	1 (4%)	11 (48%)	10 (43%)
Atrophy	11	2 (18%)	2 (18%)	7 (63%)	6 (54%)
Other CNV	6	5 (83%)	0	1 (17%)	4 (66%)
Functional subgroups	N.	Gain of at least 15 letters Number (%)	Loss of at least 15 letters Number (%)	Stable (± 10 letters) Number (%)	Reading ability Number (%)
Low pre-op BCVA subgroup	58	22 (38%)	1 (2%)	35 (60%)	19 (33%)
High pre-op BCVA subgroup	30	11 (37%)	8 (27%)	11 (37%)	19 (63%)
Whole group	N.	Gain of at least 15 letters Number (%)	Loss of at least 15 letters Number (%)	Stable (±10 letters) Number (%)	Reading ability Number (%)
	88	33 (38%)	9 (10%)	46 (52%)	38 (43%)

CNV-AMD choroidal neovascular membrane-age-related macular degeneration, *CNV-AMD-Hem* choroidal neovascular membrane-age-related macular degeneration with hemorrhage, *BCVA* best corrected visual acuity, *STDV* standard deviation
Low pre-op BCVA subgroup <1 logMAR or ≤30 letters
High pre-op BCVA subgroup >1 logMAR or >30 letters

improvement was not statistically significant in the atrophy subgroup (2 letters) as compared to baseline. Table 30.3 shows the percentage of eyes gaining and losing letters of vision for each functional and maculopathy pattern subgroup. The mean time to recover the final vision was 12 months. Based on the Spearman's Rho correlation analysis, only two predictive factors were found to be associated significantly with final BCVA. The first one was the integrity of ELM (*P* 0.009, *R* 0.567): cases with ELM that appeared tomographically intact were associated with a greater final BCVA than those with non-intact ELM. The second predictive factor was the preoperative BCVA (*P* 0.001, Rho *R* 0.814). To further confirm this finding, linear regression analysis demonstrates a positive correlation between preoperative BCVA and final BCVA (*P* 0.001). Although age did not significantly correlate with final BCVA, linear regression analysis between age and gain in vision shows a tendency to a lower gain in vision with increasing age. In fact, in few patients (four eyes) between 78 and 85 years of age, we observed a significant improvement in vision between 10 and 40 letters.

30.11.2 Microperimetry

Twenty eyes, with final reading ability of at least 12 points, underwent microperimetry, which became available to us only recently. All eyes showed a central foveal fixation with average sensitivity of 10.5 dB (range 5.1–14.8 dB) and average fixation stability of P1 = 37.8% (range 10–87%) and P2 = 73.5%. Fixation was located over the patch (Figs. 30.5f and 30.6). The microperimetry grid was superimposed on the OCT B scan by matching the color fundus photographs. This allowed us to provide good correlation between the functional result in terms of retina sensitivity and the anatomical results, point by point, on the OCT scan (Fig. 30.6).

30.12 Complications

Postoperative complications were observed between 3 days and 3 months after surgery, except for RPE and choroidal atrophy which appeared later and progressively. In ten (11.4%) eyes, retinal detachment occurred and promptly underwent surgery. The detachment occurred early, within the first week (three eyes), or 3–6 weeks after the primary surgery with PVR (five eyes) or after silicone oil removal surgery (two eyes). Epiretinal membrane (ERM) developed in four eyes (4.5%). These eyes subsequently received further surgery with ERM and ILM peeling. Since internal limiting removal was performed during the primary surgical procedure, we no longer observed ERM development in the absence of retinal detachment. Four eyes (4.5%) presented postoperative subretinal hemorrhage, occurring 1 day after surgery. These eyes were in the CNV-AMD-Hem group and were undertaking anticoagulant medications, which had been stopped 15 days prior to surgery but were restarted 2–3 days after surgery. These eyes lost significant vision due to the complications with an average final vision of 20/500. Progressive atrophy of the RPE-choroidal patch occurred in six (7%) eyes, five eyes affected by exudative maculopathy, and one eye affected by atrophic maculopathy. One eye (1.1%) had no vascular-

ization in the patch and another eye showed revascularization only in one half of the patch with progressive retinal atrophy occurring only over the non-vascularized half of the patch. Gain in vision in this eye was slow and only after 3 years the patient gained BCVA of 0.2 Snellen and central fixation (Fig. 30.5f). However, atrophy could be observed even in eyes with vascularized patch. Four eyes (4.5%) operated for CNV-related maculopathy developed recurrent CNV in an extrafoveal location and were treated with anti-VEGF injections and/or focal laser. Three eyes (3%) developed cystoid macular edema and were treated with topical steroid obtaining only partial benefit (Fig. 30.5). Two eyes (2.3%) showed off-center patch which was evident 1 month after surgery. Overall ten eyes (11%) had final postoperative BCVA lower than preoperative BCVA due to complications.

30.13 Discussion

The transplantation of a full-thickness patch of RPE and choroid under the fovea is feasible and may improve the vision, in a selected group of patients affected by various types of maculopathies. Overall, the mean final vision significantly improves, when compared to the mean preoperative vision. An improvement in vision of at least 15 letters and an improvement of 25–50 letters are observed in 40% and 28% of the operated eyes, respectively, while 41% remain stable. Hence, 80% of the eyes do not experience visual loss over a long follow-up, with no further treatment, except for silicone oil removal.

The eyes that experience visual improvement not only gain far sight, but also achieve reading ability and central fixation. In fact, 43% of eyes reach the ability to read again using the area of retina over the patch, as demonstrated by microperimetry.

The course of visual acuity has been analyzed in different subgroups, based on the preoperative BCVA, the diagnosis, and the type of maculopathy. The gain in vision results to be statistically significant for eyes operated with low preoperative BCVA. However, the mean final vision is
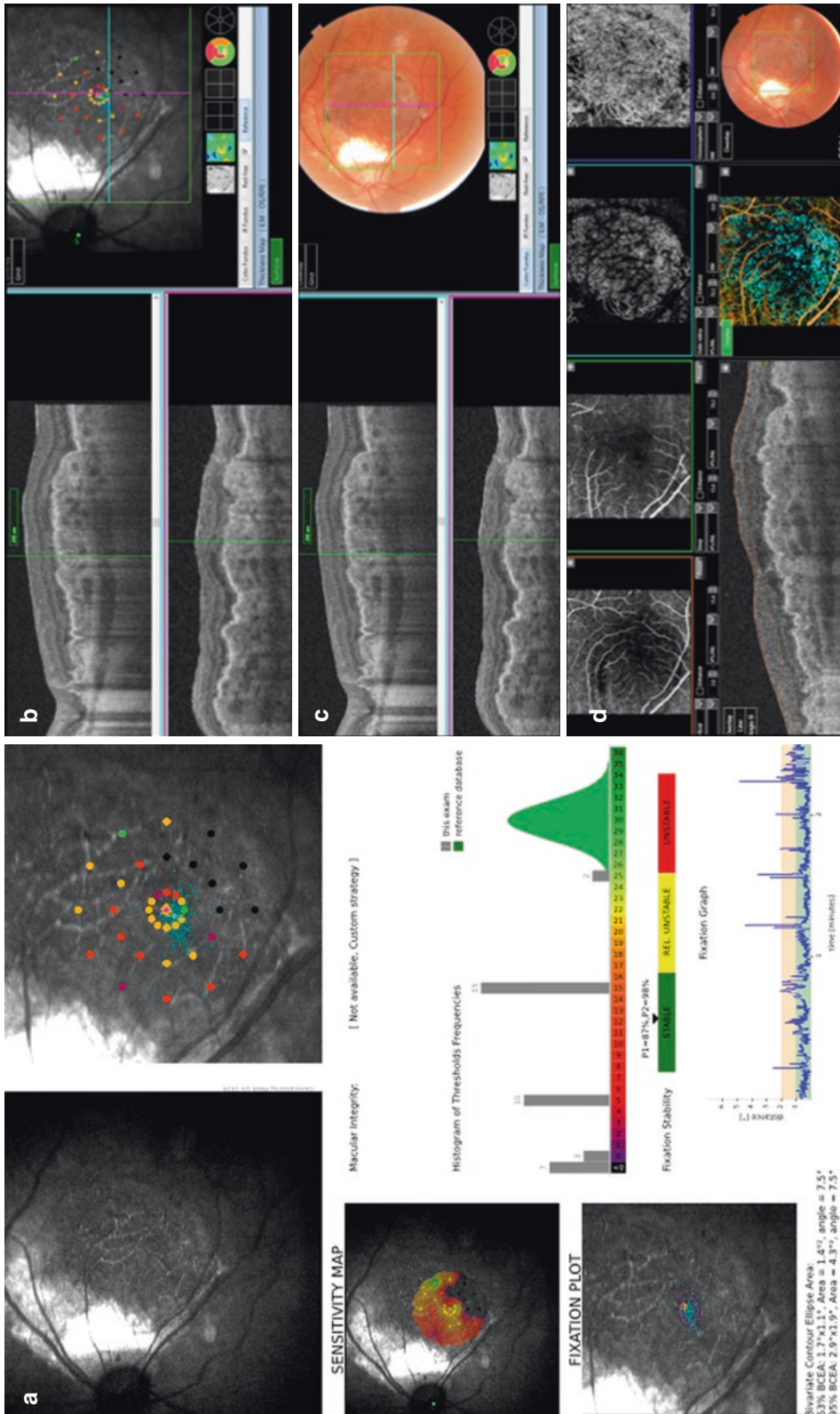
Fig. 30.6 Microperimetry analysis. (**a**) Microperimetry plot of a patient, 3 years after patch surgery. The plot shows wide areas of sensitivity corresponding to the patch, central fixation on the patch with high fixation stability: P1 = 87%, P2 = 98%. (**b**) The microperimetry grid of the same eye superimposed on the OCT B scan, by matching the color fundus photograms, to show correspondence between microperimetry and B scan shows the direct appearance of the patch. (**c**) The fundus color photo can show the direct appearance of the patch in the same spot. (**d**) Angio OCT in the same day to see correspondence with en face and flow diagram

20/200 in the low preoperative BCVA subgroup and 20/125 in high preoperative BCVA subgroup. This means that if the eye is operated when the preoperative BCVA is higher, the amount of improvement might be lower, but the absolute value of final vision will be higher. Certainly it is more difficult to decide to operate a patient with relatively good preoperative vision. However, it has been well demonstrated that if the retina is still functioning preoperatively, the amount of functional gain is higher and more stable in time.

Long-term visual gain is significant also for eyes with hemorrhagic CNV, secondary to AMD, and for CNV of other etiologies (myopia, iatrogenic, idiopathic), but not for atrophic maculopathies.

It has to be noted that the eyes that gained vision maintained it in the long term, with no further treatment.

It is difficult to compare the result of surgery with the results of intravitreal injection, because there are no comparative studies available. However, we might withdraw some conclusions by the analysis of literature. The ANCHOR study [59] reported that eyes with exudative AMD, receiving monthly injection of 0.5 mg of ranibizumab, gained 15 letters or more in 40.3% of cases after 1 year. The MARINA STUDY [3] reported a mean gain of 7.2 letters after 2 years of monthly ranibizumab injections. The VIEW study [5] reported a gain of 17.2 letters at 12 months for patients with baseline BCVA <20/200 and treated with aflibercept. However, the functional benefit obtained with monthly doses of anti-VEGF is lost over the long-term follow-up, as reported in studies describing real-life outcomes [60, 61].

With RPE-choroidal patch surgery, a gain in vision of at least 15 letters can be obtained in 40% of the low preoperative BCVA subgroup and in 37% of the high preoperative BCVA subgroup.

Ross AH et al. [62] reported that eyes treated with ranibizumab for CNV-AMD showed a change of BCVA from baseline to 1 year of +6.5, +7.5, +1.7, and −1.5 letters, respectively, for baseline VA categories of 23–35, 36–55, 56–70, and >70 letters. Furthermore, a large study con-

ducted in the UK and published in 2014 [63] reported the results of using ranibizumab for CNV-AMD in 12,951 eyes. Mean VA (letters) gain from a baseline of 55 letters was 57 (+2) letters at 1 year, 56 (+1) letters at 2 years, and 53 (−2) letters at 3 years. Overall, our results compare favorably with those obtained from anti-VEGF injection in eyes with neovascular AMD, although direct comparison may not be possible due to differences in study designs, inclusion criteria, and preoperative vision.

The visual course is different in exudative and atrophic maculopathies. Eyes affected by dry AMD show an initial improvement in vision, which remains stable for approximately 2 years. The comparison between BCVA at the end of the follow-up with the preoperative BCVA does not result statistically significant, due to the reoccurrence of choroidal atrophy 2 years post-surgery. In patients with atrophic heredo-dystrophies as well, we have seen that the disease might relapse after a few years, compromising the initial significant benefit of surgery. Nevertheless, we think that even prolonging the time of useful vision, for these patients with no other options, might be helpful while waiting for more appropriate approaches, such as genetic therapy.

The long follow-up (2–10 years) has allowed us to understand that eyes showing an improvement in vision may present different patterns of speed of visual gain, as previously reported by Van Zeeburg et al. [20] ranging from fast improvement within the first 6 months or slow and progressive visual improvement in the first year, and finally but unexpectedly presenting sudden visual improvement more than 1 year after surgery.

Although there is a trend for a lower gain in vision with increasing age, the age of the patient is not a limiting factor to reach a positive result. However, we think that there might be a relation between age and speed of visual gain after surgery: the younger patients present a possible recovery in vision within the first 6 months, while the older patients show a slow and progressive or a late but sudden improvement. The threshold age seemed to be approximately 70 years.

Indications for surgery were initially limited to CNV secondary to AMD in patients with RPE

tear and subretinal hemorrhages or patients losing vision after anti-VEGF injections. Due to the encouraging results, indications were extended after March 2011 to eyes with exudative or atrophic maculopathies affecting primarily the RPE, with a preoperative BCVA ≥20/200, and visibility of the outer retina on OCT. Having improved the selection criteria, the efficacy of surgery has improved significantly. In previous publication on patch surgery for AMD [30, 64], patients were selected based on relatively large subfoveal lesions or poorly demarcated CNVs not treatable with laser or photodynamic therapy. Leakage on fluorescein angiography plus history of recent loss of reading vision (i.e., less than 3 months) was a main requisite for surgery. Eligible eyes had BCVA corresponding to Snellen fractions ranging between 20/40 and 20/800. Based on the analysis of our patients, we think that eligible eyes should have preserved outer retinal layers, a visual acuity ranging between 20/200 and 20/80, or recent higher loss of vision due to subretinal hemorrhage or RPE tear.

Among the prognostic factors that we analyzed, only the visibility of the ELM on preoperative OCT and preoperative BCVA was statistically significant. We recommend using these parameters as good indicators for a successful result of surgery. The less damaged is the retina preoperatively, the better will be the final functional and anatomical outcome.

Patch revascularization is observed in approximately 90% of the eyes. It is not still well known which are the factors that mostly influence the revascularization. The high rate of revascularization in our study group could be due to the heavy diathermy applied to the macular choroidal surface in multiple areas before transplanting the patch of choroid, even in the absence of CNV removal, as in the atrophic cases. We think that this maneuver might create a micro-trauma to the choriocapillaris that might favor the revascularization.

The complication rate is comparable to what is reported in literature for the same subject [20, 24, 65]. Eyes with retinal detachment are reoperated and might preserve visual function. During primary surgery, an extensive and meticulous vit-

rectomy is performed and peripheral retina is carefully reviewed. Retinotomy is performed near the ora serrata, involving the superior temporal and inferior temporal quadrant. All postoperative retinal detachment cases originate from retinotomy, and are possibly due to incomplete reattachment at the time of final tamponade exchange (early detachments), or due to the occurrence of PVR at the edge of retinotomy (late detachments).

Choroidal neovascular membrane might occur at the edge of the patch and is probably due to iatrogenic intraoperative trauma to the choroid while translocating the patch under the fovea.

After the occurrence of cases of postoperative ERM, the internal limiting membrane peeling was added to the surgical technique and since then the occurrence of ERM was no longer observed. As well, we observed that ILM peeling during primary surgery preserved the macular area from PVR.

Two macular holes occurred postoperatively and two intraoperatively during the detachment of the retina with subretinal injection. It might be possible that eyes with preoperative subnormal retinal thickness are at higher risk although we were not able to statistically associate the occurrence of iatrogenic macular hole with preoperative retinal thickness. To avoid this complication, we recommend detaching retina first in the periphery and not in the submacular area. Also, when peeling the ILM, in order to avoid the postoperative occurrence of ERM on the macula, we advocate to perform a fovea-sparing ILM peeling technique, to lower the risk of developing intraoperative iatrogenic macular hole (personal observation of the surgeon). The cases that showed macular hole as postoperative complications were operated before 2015. The patients refused further surgery. In case of occurrence of macular hole at the present time, in the absence of ILM (already peeled during primary surgery), we would suggest additional procedures as recently described [66, 67].

Subretinal hemorrhages occur in patients who are undertaking anticoagulant therapy. Anticoagulant therapy should be suspended at least 20 days prior to surgery and substituted with

heparin. Patients that present severe contraindication to anticoagulant suspension should be excluded from surgery.

Off-center patch may jeopardize the result of surgery. Intraoperatively, care is taken to center the patch to the center of the fovea. However, a small patch might partially migrate in the weeks after surgery for a fibrotic involution of the edges. This is one of the complications observed in the first years of surgery. Since then, we started to isolate larger patches, at least three-disc diameters large. The large size allows easier intraoperative manipulation of the patch and compensates for the postoperative contraction and fibrosis of the edges.

The most sight-threatening complication is postoperative progressive macular atrophy. The explanation for progressive macular atrophy is not completely understood. Some of these cases of atrophy were associated with lack of patch revascularization. In other eyes, atrophy could be explained only with persistence of original pathology despite the RPE-choroid patch surgery. A recent paper [68] hypothesizes that contiguity between native and transplanted RPE could be a protective factor against the progression of patch atrophy. Therefore, a large patch could remain more protected from progressive postoperative atrophy.

The surgical technique for RPE-choroid patch graft has a steep learning curve. In fact, the operating time decreased to almost half after operating the first 50 eyes, as well as the occurrence of complications. We believe that a significant part of the success of the surgery relies on the intraoperative course, in terms of both efficacy and safety. At present a surgeon would need specific training and a learning curve of at least ten cases under the guidance of an expert tutor.

Two operations are required with the present technique because the tamponade in the first surgery is always silicone oil 1000 centistokes. Using gas as the final tamponade might be an alternative but it still needs to be proved efficient and safe. While our preference is still to use 20 G instrumentation for the surgery, the procedure could also be performed with smaller gauge instrumentation based on the surgeon preference.

This surgical technique is indicated to nearly all the eyes with diseases affecting primarily the RPE and the choroid (high myopia, idiopathic CNV, angioid streaks [69]). By inserting healthy RPE and choroid under relatively preserved photoreceptors, surgery may prolong the macular function and prevent retinal atrophy.

In conclusion, autologous RPE-choroid transplantation has shown to improve visual function in eyes with maculopathies of different etiologies, both in terms of distance vision and reading ability and in terms of central fixation. Based on our results, we recommend autologous RPE-choroid transplantation surgery only in patients with exudative maculopathies of various origins, with visible external limiting membrane and/or photoreceptors at the preoperative OCT, even when a recent subretinal hemorrhage is associated. A preoperative BCVA equal or greater than 20/200 might lead to better final functional results. Considering the possible postoperative complications with the present surgical technique, we recommend to indicate surgery only to patients with vision equal or lower than 20/100. In atrophic maculopathies, surgery might be considered only as a last resource for patients with poor vision in the other eye and a guarded outcome should be highlighted.

However, because the transplant is autologous, the availability of RPE-choroid is limited. It might be possible to obtain good functional results with a less complex surgery technique as shown in the recent literature [70]. The rationale for stem cell-derived patches, that could be implanted with an injector as an IOL, was proven by the pioneering work collected in years of autologous transplantation.

The underlying concept of RPE transplantation resembles the one of retina translocation, and resides in the idea that for maculopathies that affect primarily the choroid and RPE complex and, only in second instance the retina, by moving the fovea on top and in contact with healthy RPE, we could rescue the photoreceptor function. The implication of this idea is that surgery should be performed before the retina is irreversibly damaged by the disease.

For a long time, it was commonly thought that being a complex and risky surgery, it should be proposed to end-stage diseases and to patients with a very low visual acuity. Surgeons that tried

this technique in eyes with fibrotic atrophic CNVs and with complete loss of retinal outer segments and photoreceptors have concluded that the technique was a failure.

On the contrary, it has been demonstrated that this is a rescue therapy and therefore, in order to work, it should be offered in a phase of the disease when the preoperative visual function is still present and when the outer retina is still recognizable.

This is the weakness and the greatness of this surgery.

Brief Answers to Frequent Questions

Which functional and anatomical realistic results can we expect from this surgery?

With RPE-choroidal patch surgery, perfused and well-centered grafts were observed in more than 90% of all aforementioned cases, denoting a great and lasting engraftment success.

A gain in vision in approximately 45% of all patients.

Visual loss was recorded in the minority of cases, mainly in atrophic AMD patients.

These results were maintained over the follow-up.

Higher visual gain is achievable in patients with low preoperative BCVA but highest absolute values of letters are recorded in high preoperative BCVA group. Microperimetry helps to prove a good correlation between anatomical and functional results and fixation of the retina lying on the graft.

Which are the main positive prognostic factors?

The entity of surgical success could be expected by the observation of ELM integrity on preoperative OCT and by a better preoperative BCVA, suggesting that a healthier retina could earn better anatomical and functional results.

Which are the complications and the rate of them?

Retinal detachment (11.4%)

Progressive atrophy of the RPE-choroidal patch (7%)

Epiretinal membrane (4.5%)

Extrafoveal CNV recurrence (4.5%)

Subretinal hemorrhage (4.5%), observed only in patients with preoperative hemorrhagic CNV.

Cystoid macular edema (3%)

Off-centered patch (2.3%)

Absence of graft revascularization (1.1%)

Partial graft revascularization with atrophy of the non-perfused area (1.1%)

Overall, 11% of eyes had final postoperative BCVA lower than preoperative BCVA due to complications.

The most sight-threatening complication is postoperative progressive atrophy of the RPE-choroidal patch.

How to compare the results of this surgery with the results of anti-VEGF treatment?

There are no comparative studies available. However, comparing the results of the randomized controlled trials of anti-VEGF drugs with the one obtained from surgery data, it is possible to suppose that RPE-choroid patch surgery can provide effective and lasting results.

If a satisfactory result is obtained, how long does it last?

The cases that show a visual improvement keep improving vision for some years. The reviewed cases are obtained from data of 10 years of activity, ensuring that the achieved results are confirmed over a long-term follow-up.

Some patients may require a long time span (i.e., more than 1 year) before the visual gain is manifest.

Dry AMD and other retinal dystrophies might show a visual improvement for 2 years. After this time the progression of atrophy restarts.

References

1. Klein R, Klein BE, Linton K. Prevalence of age-related maculopathy. The Beaver Dam Eye Study. Ophthalmology. 1992;99:933–43.

2. Ferris FL 3rd, Fine SL, et al. Age-related macular degeneration and blindness due to neovascular maculopathy. Arch Ophthalmol. 1984;102:1640–2.

3. Rosenfeld PJ, Brown DM, Heier JS, et al. Ranibizumab for neovascular age-related macular degeneration. N Engl J Med. 2006;355(14):1419–31.

4. Zhang Y, Chioreso C, Schweizer ML, Abràmoff MD. Effects of aflibercept for neovascular age-related macular degeneration: a systematic review and meta-analysis of observational comparative studies. Investig Ophthalmol Vis Sci. 2017;58:5616–27. https://doi.org/10.1167/iovs.17-22471.

5. Heier JS, Brown DM, Chong V, Korobelnik JF, Kaiser PK, Nguyen QD, Kirchhof B, Ho A, Ogura Y, Yancopoulos GD, Stahl N, Vitti R, Berliner AJ, Soo Y, Anderesi M, Groetzbach G, Sommerauer B, Sandbrink R, Simader C, Schmidt-Erfurth U. Intravitreal aflibercept (VEGF trap-eye) in wet age-related macular degeneration. Ophthalmology. 2012;119:2537–48. https://doi.org/10.1016/j.ophtha.2012.09.006.

6. Avery RL, Castellarin AA, Steinle NC, Dhoot DS, Pieramici DJ, See R, Couvillion S, Nasir MA, Rabena MD, Maia M, Van Everen S, Le K, Hanley WD. Systemic pharmacokinetics and pharmacodynamics of intravitreal aflibercept, bevacizumab, and ranibizumab. Retina. 2017;37:1847–58. https://doi.org/10.1097/IAE.0000000000001493.

7. Schmidt-Erfurth U, Chong V, Loewenstein A, Larsen M, Souied E, Schlingemann R, Eldem B, Monés J, Richard G, Bandello F. Guidelines for the management of neovascular age-related macular degeneration by the European Society of Retina Specialists (EURETINA). Br J Ophthalmol. 2014;98:1144–67. https://doi.org/10.1136/bjophthalmol-2014-305702.

8. Trials WC. Surgery for hemorrhagic choroidal neovascular lesions of age-related macular degeneration: ophthalmic findings: SST report no. 13. Ophthalmology. 2004;111:1993–2006. https://doi.org/10.1016/j.ophtha.2004.07.023.

9. Gouras P, Flood MT, Kjedbye H, et al. Transplantation of cultured human retinal epithelium to Bruch's membrane of the owl monkey's eye. Curr Eye Res. 1985;4:253–65.

10. Machemer R, Steinhorst UH. Retinal separation, retinotomy, and macular relocation: II. A surgical approach for age-related macular degeneration? Graefes Arch Clin Exp Ophthalmol. 1993;231:635–41.

11. Eckardt C, Eckardt U, Conrad H. Macular rotation with and without counter-rotation of the globe in patients with age-related macular degeneration. Graefes Arch Clin Exp Ophthalmol. 1999;237:313–25.

12. Lewis H, Kaiser P, Lewis S, Estafanous M. Macular translocation for subfoveal choroidal neovascularization in age-related macular degeneration: a prospective study. Am J Ophthalmol. 1999;128:135–46.

13. Wong D, Stanga P, Briggs M, Lenfestey P, Lancaster E, Li KK, Lim KS, Groenewald C. Case selection in macular relocation surgery for age related macular degeneration. Br J Ophthalmol. 2004;88:186–90. https://doi.org/10.1136/bjo.2003.019273.

14. Li LX, Turner J. Inherited retinal dystrophy in the RCS rat: prevention of photoreceptor degeneration by pigment epithelial cell transplantation. Exp Eye Res. 1988;47:911–7.

15. Peyman GA, Blinder KJ, Paris CL, Alturki W, Nelson NC, Desai U. A technique for retinal pigment epithelium transplantation for age-related macular degeneration secondary to extensive subfoveal scarring. Ophthalmic Surg. 1991;22(2):102–8.

16. Falkner-Radler CI, Krebs I, Glittenberg C, Povazay B, Drexler W, Graf A, Binder S. Human retinal pigment epithelium (RPE) transplantation: outcome after autologous RPE-choroid sheet and RPE cell-suspension in a randomised clinical study. Br J Ophthalmol. 2010;95(3):370–5.

17. Stanga PE, Kychenthal A, Fitzke FW, et al. Retinal pigment epithelium translocation and central visual function in age related macular degeneration: preliminary results. Int Ophthalmol. 2001;23(4–6):297–307.

18. Van Meurs JC, Van Den Biesen PR. Autologous retinal pigment epithelium and choroid translocation in patients with exudative age-related macular degeneration: short-term follow-up. Am J Ophthalmol. 2003;136:688–95. https://doi.org/10.1016/S0002-9394(03)00384-2.

19. Maaijwee K, Heimann H, Missotten T, Mulder P, Joussen A, van Meurs J. Retinal pigment epithelium and choroid translocation in patients with exudative age-related macular degeneration: long-term results. Graefes Arch Clin Exp Ophthalmol. 2007;245:1681–9. https://doi.org/10.1007/s00417-007-0607-4.

20. Van Zeeburg EJT, Maaijwee KJM, Missotten TOAR, Heimann H, Van Meurs JC. A free retinal pigment epithelium-choroid graft in patients with exudative age-related macular degeneration: results up to 7 years. Am J Ophthalmol. 2012;153:120–127.e2. https://doi.org/10.1016/j.ajo.2011.06.007.

21. van Zeeburg EJT, Maaijwee KJM, van Meurs JC. Visual acuity of 20/32, 13.5 years after a retinal pigment epithelium and choroid graft transplantation. Am J Ophthalmol Case Rep. 2018;10:62–4. https://doi.org/10.1016/j.ajoc.2018.01.042.

22. Van Zeeburg EJT, Cereda MG, Amarakoon S, Van Meurs JC. Prospective, randomized intervention study comparing retinal pigment epithelium-choroid graft surgery and anti-VEGF therapy in patients with exudative age-related macular degeneration. Ophthalmologica. 2015;233:134–45. https://doi.org/10.1159/000380829.

23. Cereda MG, Parolini B, Bellesini E, Pertile G. Surgery for CNV and autologous choroidal RPE patch transplantation: exposing the submacular space. Graefes Arch Clin Exp Ophthalmol. 2010;248:37–47. https://doi.org/10.1007/s00417-009-1201-8.

24. van Romunde SHM, Polito A, Peroglio Deiro A, Guerriero M, Pertile G. Retinal pigment epithelium–choroid graft with a peripheral retinotomy for exudative age-related macular degeneration. Retina. 2019;39(2):288–95. https://doi.org/10.1097/IAE.0000000000001945.

25. Caramoy A, Liakopoulos S, Menrath E, Kirchhof B. Autologous translocation of choroid and retinal pigment epithelium in geographic atrophy: long-term functional and anatomical outcome. Br J Ophthalmol. 2010;94:1040–4. https://doi.org/10.1136/bjo.2009.161299.

26. Parolini B, Di Salvatore A, Pinackatt SJ, Baldi A, Besozzi G, Finzi A, Cardillo D, Sallam AB, Frisina R. Long-term results of autologous retinal pigment epithelium and choroid transplantation for the treatment of exudative and atrophic maculopathies. Retina. 2018;40:507. https://doi.org/10.1097/IAE.0000000000002429.

27. Simoens P, de Schaepdrijver L, Lauwers H. Morphologic and clinical study of the retinal circulation in the miniature pig. A: morphology of the retinal microvasculature. Exp Eye Res. 1992;54:965–73.

28. De Schaepdrijver L, Simoens P, Pollet L, et al. Morphologic and clinical study of the retinal circulation in the miniature pig. B: fluorescein angiography of the retina. Exp Eye Res. 1992;54:975–85.

29. Maaijwee KJM, Van Meurs JC, Kirchhof B, Mooij CM, Fischer JH, Mackiewicz J, Kobuch K, Joussen AM. Histological evidence for revascularisation of an autologous retinal pigment epithelium-choroid graft in the pig. Br J Ophthalmol. 2007;91:546–50. https://doi.org/10.1136/bjo.2006.103259.

30. Joussen AM, Heussen FMA, Joeres S, Llacer H, Prinz B, Rohrschneider K, Maaijwee KJM, van Meurs J, Kirchhof B. Autologous translocation of the choroid and retinal pigment epithelium in age-related macular degeneration. Am J Ophthalmol. 2006;142:17. https://doi.org/10.1016/j.ajo.2006.01.090.

31. Takemura R, Werb Z. Secretory products of macrophages and their physiological functions. Am J Physiol. 1984;246:C1–9.

32. Folkman J, Klagsbrun M. Angiogenic factors. Science. 1987;235:442–7.

33. Campochiaro PA, Soloway P, Ryan SJ, et al. The pathogenesis of choroidal neovascularization in patients with age-related macular degeneration. Mol Vis. 1999;5:34.

34. van den Biesen PR, Hermens WT, Slaaf D, et al. Dye extravasation and the nature of background fluorescence in sodium fluorescein angiography. Retina. 1997;17:540–6.

35. Flower RW. Choroidal fluorescent dye filling patterns. Int Ophthalmol. 1980;2:143–9.

36. Delori FC, Castany MA, Webb R. Fluorescence characteristics of sodium fluorescein in plasma and whole blood. Exp Eye Res. 1978;27:417–25.

37. Kiryu J, Shahidi M, Mori M, et al. Noninvasive visualization of the choriocapillaris and its dynamic filling. Invest Ophthalmol Vis Sci. 1994;35:3724–31.

38. van den Biesen PR, Jongsma FH, Tangelder GJ, Slaaf D. Shear rate and hematocrit dependence of fluorescence from retinal vessels in fluorescein angiography. Ann Biomed Eng. 1994;22:456–63.

39. Maaijwee K, Van Den Biesen PR, Missotten T, Van Meurs JC. Angiographic evidence for revascularization of an RPE-choroid graft in patients with age-related macular degeneration. Retina. 2008;28:498–503. https://doi.org/10.1097/IAE.0b013e318159ec24.

40. Yoneya S, Tso M. Angioarchitecture of the human choroid. Arch Ophthalmol. 1986;105:681–7.

41. Olver JM. Functional anatomy of the choroidal circulation: methyl methacrylate casting of human choroid. Eye. 1990;4:262–72.

42. van Zeeburg EJT, Cereda MG, van der Schoot J, Pertile G, van Meurs JC. Early perfusion of a free RPE-choroid graft in patients with exudative macular degeneration can be imaged with spectral domain-OCT. Investig Ophthalmol Vis Sci. 2011;52:5881–6. https://doi.org/10.1167/iovs.11-7245.

43. Veckeneer M, Augustinus C, Feron E, Schauwvlieghe PP, Ruys J, Cosemans I, Van Meurs J. OCT angiography documented reperfusion of translocated autologous full thickness RPE-choroid graft for complicated neovascular age-related macular degeneration. Eye. 2017;31:1274–83. https://doi.org/10.1038/eye.2017.137.

44. Streilein JW. Ocular immune privilege: the eye takes a dim but practical view of immunity and inflammation. J Leukoc Biol. 2003;74:179–85.

45. Streilein JW, Ksander BR, Taylor A. Immune deviation in relation to ocular immune privilege. J Immunol. 1997;158:3557–60.

46. Liversidge JM, Sewell HF, Forrester J. Human retinal pigment epithelial cells differentially express MHC class II (HLA, DP, DR and DQ) antigens in response to in vitro stimulation with lymphokine or purified IFN-gamma. Clin Exp Immunol. 1988;73:489–94.

47. Percopo CM, Hooks JJ, Shinohara T, et al. Cytokine-mediated activation of a neuronal retinal resident cell provokes antigen presentation. J Immunol. 1990;145:4101–7.

48. Sun D, Enzmann V, Lei S, et al. Retinal pigment epithelial cells activate uveitogenic T cells when they express high levels of MHC class II molecules, but inhibit T cell activation when they express restricted levels. J Neuroimmunol. 2003;144:1–8.

49. Wenkel H, Streilein J. Analysis of immune deviation elicited by antigens injected into the subretinal space. Invest Ophthalmol Vis Sci. 1998;39:1823–34.

50. Jiang L, Streilein J. Immunologic privilege evoked by histoincompatible intracameral retinal transplants. Reg Immunol. 1991;3:121–30.

51. Leonard DS, Zhang XG, Panozzo G, et al. Clinicopathologic correlation of localized retinal pigment epithelium debridement. Invest Ophthalmol Vis Sci. 1997;38:1094–109.

52. Del Priore LV, Kaplan HJ, Hornbeck R, et al. Retinal pigment epithelial debridement as a model for the

pathogenesis and treatment of macular degeneration. Am J Ophthalmol. 1996;122:629–43.

53. Del Priore LV, Kaplan HJ, Tezel TH, et al. Retinal pigment epithelial cell transplantation after subfoveal membranectomy in age-related macular degeneration: clinicopathologic correlation. Am J Ophthalmol. 2001;131:472–80.

54. Rudolf M, Curcio C. Esterified cholesterol is highly localized to Bruch's membrane, as revealed by lipid histochemistry in wholemounts of human choroid. J Histochem Cytochem. 2009;57:731–9.

55. Sugino IK, Sun Q, Wang J, et al. Comparison of FRPE and human embryonic stem cell-derived RPE behavior on aged human Bruch's membrane. Invest Ophthalmol Vis Sci. 2011;52:4979–97.

56. Gullapalli VK, Sugino IK, Van Patten Y, et al. Impaired RPE survival on aged submacular human Bruch's membrane. Exp Eye Res. 2005;80:235–48.

57. Gullapalli VK, Sugino IK, Zarbin M. Culture-induced increase in alpha integrin subunit expression in retinal pigment epithelium is important for improved resurfacing of aged human Bruch's membrane. Exp Eye Res. 2008;86:189–200.

58. Fujii GY, De Juan E, Sunness J, Humayun MS, Pieramici DJ, Chang TS. Patient selection for macular translocation surgery using the scanning laser ophthalmoscope. Ophthalmology. 2002;109:1737–44. https://doi.org/10.1016/S0161-6420(02)01120-X.

59. Brown DM, Michels M, Kaiser PK, et al. Ranibizumab versus verteporfin photodynamic therapy for neovascular age-related macular degeneration: two-year results of the ANCHOR study. Ophthalmology. 2009;116(1):57–65.e5.

60. Garweg JG, Zirpel JJ, Gerhardt C, Pfister IB. The fate of eyes with wet AMD beyond four years of anti-VEGF therapy. Graefes Arch Clin Exp Ophthalmol. 2018;256:823–31. https://doi.org/10.1007/s00417-018-3907-y.

61. Ozturk M, Harris ML, Nguyen V, Barthelmes D, Gillies MC, Mehta H. Real-world visual outcomes in patients with neovascular age-related macular degeneration receiving aflibercept at fixed intervals as per UK licence. Clin Exp Ophthalmol. 2018;46:407–11. https://doi.org/10.1111/ceo.13085.

62. Ross AH, Donachie PHJ, Sallam A, Stratton IM, Mohamed Q, Scanlon PH, Kirkpatrick JN, Johnston RL. Which visual acuity measurements define high-quality care for patients with neovascular age-related macular degeneration treated with ranibizumab? Eye. 2013;27:56–64. https://doi.org/10.1038/eye.2012.225.

63. Writing Committee for the UK Age-Related Macular Degeneration EMR Users Group. The neovascular age-related macular degeneration database: multicenter study of 92 976 ranibizumab injections: report 1: visual acuity. Ophthalmology. 2014;121(5):1092–101.

64. Heussen FMA, Fawzy NF, Joeres S, Lux A, Maaijwee K, Meurs JC, Kirchhof B, Joussen AM. Autologous translocation of the choroid and RPE in age-related macular degeneration: 1-year follow-up in 30 patients and recommendations for patient selection. Eye. 2008;22:799–807. https://doi.org/10.1038/sj.eye.6702823.

65. Van Romunde SHM, Polito A, Bertazzi L, Guerriero M, Pertile G. Long-term results of full macular translocation for choroidal neovascularization in age-related macular degeneration. Ophthalmology. 2015;122:1366–74. https://doi.org/10.1016/j.ophtha.2015.03.012.

66. Iwakawa Y, Imai H, Kaji H, Mori Y, Ono C, Otsuka K, Miki A, Oishi M. Autologous transplantation of the internal limiting membrane for refractory macular hole following ruptured retinal arterial macroaneurysm: a case report. Case Rep Ophthalmol. 2018;9:113–9. https://doi.org/10.1159/000485914.

67. Grewal DS, Mahmoud TH. Autologous neurosensory retinal free flap for closure of refractory myopic macular holes. JAMA Ophthalmol. 2016;134:229–30. https://doi.org/10.1001/jamaophthalmol.2015.5237.

68. Pertile G, Mete M, Peroglio Deiro A, Guerriero M, Sartore M, Alfano A, Polito A. New insights into the development and progression of geographic atrophy after full thickness autologous choroidal graft. Invest Ophthalmol Vis Sci. 2018;59:AMD93–AMD103. https://doi.org/10.1167/iovs.18-24229.

69. Parolini B, Alkabes M, Baldi A, Pinackatt S. Visual recovery after autologous retinal pigment epithelium and choroidal patch in a patient with choroidal neovascularization secondary to angioid streaks: long-term results. Retin Cases Brief Rep. 2016;10:368–72. https://doi.org/10.1097/ICB.0000000000000265.

70. Da Cruz L, Fynes K, Georgiadis O, Kerby J, Luo YH, Ahmado A, Vernon A, Daniels JT, Nommiste B, Hasan SM, Gooljar SB, Carr AJF, Vugler A, Ramsden CM, Bictash M, Fenster M, Steer J, Harbinson T, Wilbrey A, Tufail A, Feng G, Whitlock M, Robson AG, Holder GE, Sagoo MS, Loudon PT, Whiting P, Coffey PJ. Phase 1 clinical study of an embryonic stem cell-derived retinal pigment epithelium patch in age-related macular degeneration. Nat Biotechnol. 2018;36:1–10. https://doi.org/10.1038/nbt.4114.

Stem Cell-Derived Retinal Cells for Transplantation

31

Tai-Chi Lin, Marta Stevanovic, Leah P. Foltz, Dennis O. Clegg, and Mark S. Humayun

31.1 Introduction

Stem cell-based therapies can restore or rescue visual function in preclinical models of retinal degeneration [1–5]. While retinal degenerative diseases, such as retinitis pigmentosa (RP), age-related macular degeneration (AMD), and Stargardt disease, arise from various molecular mechanisms and affect patients of different demographics, these diseases all result in the dys-

function or death of photoreceptors and/or the RPE [1–5]. Currently, there are no effective treatments for most cases of retinal degeneration, and the retina, like other central nervous system tissues, has little regenerative potential [4, 6]. In theory, stem cell-based therapies that replace the dysfunctional or dead cells may be able to treat retinal disease.

Cell transplantation into the eye has been investigated for many years. Royo and Quay demonstrated the first intraocular transplant of fetal rat retina into the anterior chamber of the maternal parent [7]. Early work relied on transplantation of full-thickness retina, whereas later studies utilized dissociated retinal cells or cell aggregates for transplantation into the subretinal space of rats [8–13]. Silverman and Hughes were the first to isolate photoreceptor sheets from the postnatal and adult retina [14]. Their

T.-C. Lin
Department of Ophthalmology, USC Roski Eye Institute, University of Southern California, Los Angeles, CA, USA

University of Southern California Dr. Allen and Charlotte Ginsburg Institute for Biomedical Therapeutics, Los Angeles, CA, USA

Department of Ophthalmology, Taipei Veterans General Hospital, Taipei, Taiwan, Republic of China

Institute of Clinical Medicine, National Yang-Ming University, Taipei, Taiwan, Republic of China
e-mail: taichili@usc.edu

M. Stevanovic
Department of Ophthalmology, USC Roski Eye Institute, University of Southern California, Los Angeles, CA, USA

University of Southern California Dr. Allen and Charlotte Ginsburg Institute for Biomedical Therapeutics, Los Angeles, CA, USA

Center for Stem Cell Biology and Engineering, Neuroscience Research Institute, University of California, Santa Barbara, Santa Barbara, CA, USA
e-mail: mstevanovic@challiance.org

L. P. Foltz · D. O. Clegg
Center for Stem Cell Biology and Engineering, Neuroscience Research Institute, University of California, Santa Barbara, Santa Barbara, CA, USA
e-mail: leahfoltz@ucsb.edu; clegg@ucsb.edu

M. S. Humayun (✉)
Department of Ophthalmology, USC Roski Eye Institute, University of Southern California, Los Angeles, CA, USA

University of Southern California Dr. Allen and Charlotte Ginsburg Institute for Biomedical Therapeutics, Los Angeles, CA, USA
e-mail: humayun@usc.edu

method was later modified by other researchers, who eventually transplanted photoreceptor sheets and full-thickness fetal or adult retina [15–22]. These retinal transplant studies, especially those concerning fetal retinal sheet transplants, established a standard for replacement. Ethical restrictions, short-term survival after transplantation, and a lack of retinal degeneration animal models limited the utility of this method [5]. Translocation of autologous RPE sheets from the peripheral retina and transplantation of fetal human retinal/RPE sheets into the subretinal space of patients with macular degeneration were performed in the 2000s [23, 24]. In 2009, human embryonic stem cell (hESC)-derived RPE cells were transplanted into preclinical models of macular degeneration [25]. Several clinical trials have been initiated, and the long-term outcomes of these studies will be demonstrated via patient follow-up over the next several years [26–32].

The development of induced pluripotent stem cells (iPSCs) provides a new starting material for the production of retinal cells for transplantation. iPSCs are produced by reprogramming mature, differentiated cells into an immature, pluripotent state similar to that seen in ESCs [33–36]. Preclinical studies using iPSC-derived RPE cells, photoreceptors, and ganglion cells have been reported, and the iPSC-derived RPE and photoreceptors have been characterized clinically [37–39].

In this chapter, we review the development of cellular therapies for retinal disease, including methods of cell production, assessments of functional efficacy and safety in animal models, and recent progress in human clinical trials.

31.2 Sources of Stem Cells

Stem cells are characterized by their ability to self-renew, proliferate, and differentiate into many different cell types. Human ESCs were first isolated and cultured by Thomson et al. in 1998 and are a promising cell source for regenerative medicine [40]. One challenge associated with hESCs is immune rejection, which may necessitate local or systemic immunosuppression [39]. Although

intraocular spaces are immune-privileged sites, surgical trauma during the implantation of cell therapies compromises the blood-ocular barrier and subjects surrounding cells to an increased level of recognition and reaction. Moreover, a degenerated retina may no longer be immune privileged because the disease process causes a dysregulation in the microenvironment [1]. One way to address this challenge is to use patient-derived iPSCs, which have a lower risk of immune rejection [41, 42]. Other approaches include the generation of HLA-matched iPSC banks [43, 44], or genetically modified, HLA-depleted "universal" donor cells [45]. While ESCs and iPSCs are the most frequent sources for cell replacement therapy, other types of stem cells have been investigated for potential use, including undifferentiated bone marrow-derived stem cells [46] and mesenchymal stem cells [47]. The following sections describe derivation of retinal cells from hESC and iPSC.

31.2.1 Sources of RPE Cells

RPE cells play an important role in maintenaning the homeostasis of the outer retina. Their functions include transport of nutrients to the photoreceptors, phagocytosis of shed photoreceptor outer segments, and regeneration of visual photopigments [1, 48, 49]. The RPE cells absorb stray light within the eye and dissipate the heat in the retina generated by both this light and the phototransduction process. The polarized monolayer RPE cells also secrete cytokines and growth factors that are critical for maintenance of the choriocapillaris and retina. Specifically, vascular endothelial growth factor (VEGF) secreted basally is vital to the health of the choriocapillaris while pigment epithelium-derived factor (PEDF) secreted apically is essential for the microenvironment in the subretinal space [50, 51]. RPE cells are the initial site of degeneration in multiple retinal diseases, including AMD [1]. Therefore, a promising strategy to treat AMD is to generate RPE from stem cells and replace dysfunctional RPE before photoreceptors are lost.

31.2.1.1 Mammalian Embryonic Stem Cell-Derived RPE

ESCs, which are pluripotent cells harvested from the inner cell mass of a mammalian embryo at the early blastocyst stage, have unlimited self-renewal and differentiation potential [1]. Studies lead by Thomson and Sasai demonstrated that human [52] and primate [53] ESCs could generate pigmented epithelial cells. Sasai's group showed that primate ESC could differentiate into pigmented epithelial cells when cultured in the presence of a mouse cell line (PA6 stromal cells) in a differentiating media. These cells, which could be microdissected and expanded, displayed typical RPE morphology and expressed Pax-6, a gene that is important for eye development. Klimanskaya et al. reported that pigmented epithelial cells could be derived from hESCs after simply removing basic fibroblast growth factor from the media. In that study, small patches of pigmented cells appeared spontaneously after 6–8 weeks. After being microdissected and expanded, these cells expressed numerous RPE marker genes and were quite similar to native RPE [54]. Subsequent studies from additional groups have used two general strategies to generate RPE from either iPSC and hESC: the "spontaneous" method, which has been improved and refined over time, or "directed differentiation," which uses growth factors to mimic normal RPE development [55, 56]. Recently, it has been shown that a rapid, directed differentiation method was more robust than a spontaneous differentiation protocol, and both protocols resulted in similar iPSC-RPE [57]. A number of studies have demonstrated that both ESC and iPSC-derived RPE cells display RPE polarity and morphology, express typical RPE mRNAs and proteins, and carry out RPE functions such as phagocytosis and growth factor secretion in vitro. Furthermore, these cells have been shown to enhance photoreceptor survival after transplantation into the subretinal space of Royal College of Surgeons (RCS) rats [58].

31.2.1.2 Induced Pluripotent Stem Cell-Derived RPE

Takahashi et al. developed a method to create iPSCs by transducing skin fibroblasts with viral constructs expressing four transcription factors: Oct 3/4, Sox2, Klf4, and c-Myc [33–36]. This protocol allowed mature cells to return to a pluripotent state similar to that seen in hESCs. Like hESCs, iPSCs have similar morphology, gene expression, telomerase activity, proliferation, and ability to differentiate into all three germ layers [36, 59, 60]. Because iPSC can be created from a patient's own tissue, delivering autologous iPSCs or iPSC-derived cells is less likely to be hindered by immune rejection. Other advantages of iPSCs over hESCs include the presence of a variety of potential source pools from somatic cells and the avoidance of ethical concerns over the use of human embryonic tissue [61, 62]. iPSC-derived RPE cells were shown to resemble morphologic and functional properties characteristic of developing and mature RPE cells in vitro and in vivo [37, 63–65].

31.2.2 Stem Cell-Derived Photoreceptors

Patients who receive RPE transplants need to have a sufficient number of surviving, functional photoreceptor cells; otherwise replacing RPE cells will not be able to rescue vision. For patients with dysfunctional or degenerated photoreceptor cells, there is currently no therapy to repair or restore the retinal cells. Therefore, stem cell-derived photoreceptors and retinal progenitor cells (RPCs) have been proposed to replace lost photoreceptors, with or without combined hESC-RPE transplantation [66, 67]. Studies show that transplanted RPCs have a beneficial effect because the cells differentiate into functioning retinal cells in vivo and replace lost or dysfunctional elements [68, 69]. Other studies indicate that the success of RPC therapy is achieved via production of trophic factors secreted by transplanted RPC [67, 70–72]. A major challenge in incorporating photoreceptor progenitors into the retina is establishment of synaptic connections with the proximal neuronal elements [1]. Optic cups and storable stratified neural retina structures may be more likely to form synapses in vivo. Recently, differentiation of these two

types of structures from hESC was reported [73]. Furthermore, successful transplantation of embryonic and iPSC-derived 3D retinal sheets can develop a structured outer nuclear layer of fully mature photoreceptors with outer-segment structures, which may form synapses between the host bipolar cell terminals and the presynaptic terminal of graft photoreceptors [74–76]. These milestone studies highlight the new concept of regenerative medicine in retinal degeneration therapeutics, where the major emphasis would be on establishing connections between ganglion cells and optic nerve axons.

31.3 Transplantation Approaches of Stem Cell-Derived Retinal Cells

Transplantation of RPE cells has evolved since the early studies, which used autologous RPE grafts. Delivery of stem cell-derived RPE cell suspensions using intravitreal injections has been described [77, 78]. Currently, hESC- or iPSC-RPE are usually delivered into the subretinal space via one of the two methods: injection of a cell suspension or insertion of a scaffold containing a pre-generated RPE monolayer [1, 79].

In small animal models, cell suspension is usually delivered to the subretinal space via an external path. A localized peritomy is followed by the dissection of the dorsal sclera and choroid, creating a route for insertion of a needle to inject the cells into the subretinal space. Small animals have a significantly larger lens and a smaller vitreous cavity compared to their globe size; thus performing vitrectomy or retinotomy is considerably more difficult on these animals [1]. Another method to deliver cell suspensions is an internal approach involving pars plana vitrectomy, removal of the posterior hyaloid, and creation of a small retinotomy [26, 28, 54]. The cells are then injected via the retinotomy. This technique has been used in the eyes of humans and large animals [1].

To deliver RPE monolayers on a scaffold into the subretinal space, pars plana vitrectomy, removal of the posterior hyaloid, and creation of a small retinotomy are performed. To create space for the RPE monolayer implantation, a subretinal bleb is formed adjacent to the degenerated region. This bleb is hydrodissected so that it covers the degenerated area. Then, the RPE monolayer is inserted through a sclerotomy into the eye, and placed into the pocket in the subretinal space [32].

Despite the ease of performing RPE suspension injections, there are issues associated with this approach. Several in vivo studies have demonstrated that transplantation of RPE cells as a polarized monolayer leads to improved survival and better clinical outcomes [48, 58, 80]. Suspensions of hESC-RPE cells have been transplanted in human patients with dry AMD and Stargardt disease, but the extent of cell survival and restoration of vision remains uncertain [28, 31]. The maintenance of a polarized monolayer with tight junctions is important for proper RPE function. Therefore, it is essential that stem cell-derived RPE cell suspensions ultimately form a monolayer in order to perform the RPE's normal functions, such as phagocytosis of photoreceptor outer segments and formation of the outer blood-retinal barrier. An in vitro study revealed that polarized hESC-RPE cell monolayers have higher resistance to oxidative stress-induced cell death over non-polarized cultures [81]. In an animal study, the dissociated cell suspensions injected into the subretinal space appeared more vulnerable to cell death relative to the polarized RPE monolayer on a scaffold, as they survived to a lesser extent and often developed into cell aggregates or clumps [48] (Fig. 31.1). An additional concern regarding the cell suspension transplant technique is the possibility of the reflux of injected cells into the vitreous cavity, which can potentially trigger proliferative vitreoretinopathy [82].

Because of the challenges associated with RPE suspension injections, transplantation of RPE monolayers is a better alternative. One preclinical study reported that human iPSC-derived RPE cells could be cultured in sheets witout using artificial scaffold [82]. This layer of iPSC-RPE was designed for clinical use and showed no immune rejection or tumor formation
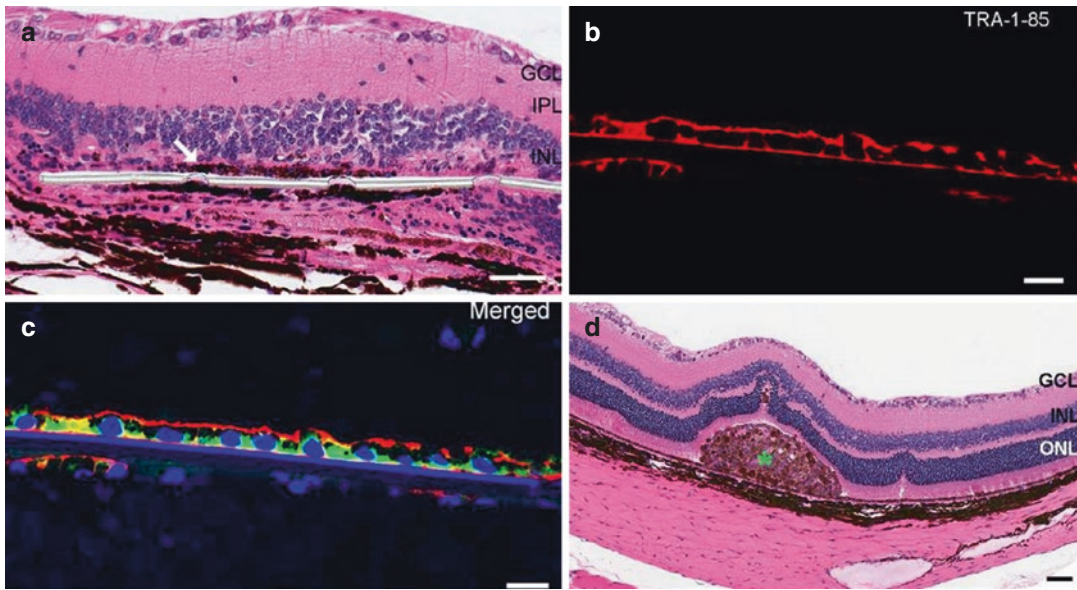
Fig. 31.1 Implanted eye with parylene C membrane in rat eye with RPE cells 12 months after surgery. Monolayer of pigmented cells (white arrow) placed in the subretinal space over the parylene membrane observed with hematoxylin and eosin staining (**a**) (scale bars: A, 50 lm.) Immunofluorescent staining for TRA-1-85 human marker ([**b**], red) was found in the transplanted cells. (**c**) Merged image of RPE65 (green), TRA-1-85 (red), and DAPI (scale bars for **b**, **c**: 10 lm.). Hematoxylin and eosin-stained section of rat eye with cell suspension injection 1 month after surgery ([**d**], scale bar: 50 lm). Aggregate of hESC-RPE cells was observed in the subretinal space

when implanted in a primate model. Based on this research, a Japanese woman with AMD became the first individual to receive a transplanted layer of autologous iPSC-RPE cells. In other studies, RPE monolayer sheets have been grown on scaffolds composed of a variety of both biodegradable and biostable materials and then implanted into the subretinal space [79, 80, 82]. Normally, the Bruch's membrane supports RPE cells; however, when it is aged and diseased, it can hinder the formation of functional RPE monolayers [83]. Artificial scaffolds can instead be used to support transplanted RPE in order to enhance their adhesion, survival, and function [1].

In general, artificial scaffolds must be biologically inert and semipermeable. In addition, they need to be flexible to facilitate delivery beneath the macula but also strong enough to preserve the cells as a monolayer [1]. Parylene is a biocompatible polymer with the highest US Pharmacopeia Class VI approval and has been used in a variety of biomedical devices. The

submicron parylene C membrane has similar characteristics to human Bruch's membrane and can function as a semipermeable membrane [29]. The membrane was designed to allow for adhesion of a polarized monolayer of RPE and diffusion of molecules, mimicking a healthy, endogenous Bruch's membrane. In vivo results from rat and Yucatan minipig studies show that transplanted hESC-derived RPE cells seeded as a monolayer on parylene C membranes can survive as an intact monolayer and improve visual function [48, 58, 84].

A phase I/IIA clinical trial of hESC-RPE is planned by Regenerative Patch Technologies (RPT) and supported by the California Institute of Technology in collaboration with researchers from University of Southern California, University of California Santa Barbara, and the City of Hope. In this trial, the composite implant, termed the California Project to Cure Blindness-Retinal Pigment Epithelium 1 (CPCB-RPE1), contains a polarized monolayer of hESC-RPE on an ultrathin, synthetic parylene
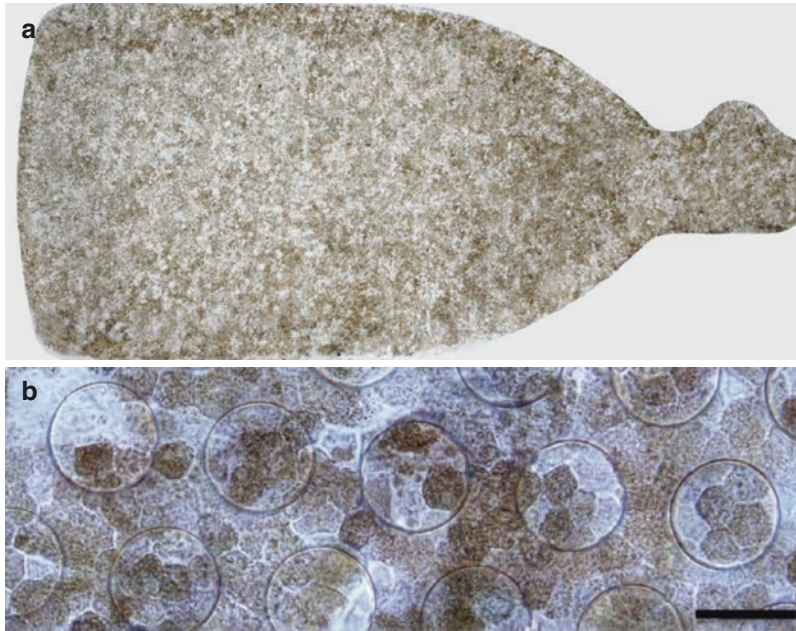
Fig. 31.2 CPCB-RPE1 implant. (**a**) Low-magnification (actual size 3.5 mm × 6.25 mm) and high-magnification (**b**) color photographs of CPCB-RPE1 (scale bar, 50 μm) The parylene membrane is 6 microns thick with submicrometer-thick circular regions and a smooth, nonporous anterior surface that promotes cell adherence. The region with tightly spaced ultrathin circular depressions has molecular exclusion characteristics similar to Bruch's membrane in order to facilitate nutrient and growth factor diffusion

substrate designed to mimic Bruch's membrane [32] (Fig. 31.2).

The London Project to Cure Blindness (LPCB) has developed a hESC-RPE cell line that can be cultured as a monolayer on a thin polyester membrane. The LPCB clinical trial was designed as a phase I, open-label, safety, and feasibility study of implantation of an hESC-RPE patch in subjects with acute wet AMD and recent rapid vision decline. The membrane that was used was a porous 10 μm thick polyethylene terephthalate sheet [85].

Because the surgical procedure for the subretinal implantation of RPE sheets can be challenging, special tools have been designed to accomplish this task [63, 86, 87] (Fig. 31.3). Custom insertion forceps were manufactured specifically for handling and delivering CPCB-RPE1. The tool consists of a handle, a thumbwheel, and a shaft that houses retractable forceps for grasping, folding, and loading the CPCB-RPE1. This tool protects the CPCB-RPE1 from damage during surgical delivery into the eye and facilitates delivery through small scleral and retinal incisions [32].

A custom-designed and manufactured device was used in the LPCB clinical trial. It consists of a handle that contains a mechanism to advance a flexible rod that passes from the wheel, through the shaft, and to the tip where the rod physically pushes the implant out of the tip of the device and into the subretinal space [85].

31.4 Efficacy of Stem Cell-Derived Retinal Cell Transplantation

31.4.1 Efficacy of RPE Transplantation

RPE rescue therapy restores vision by allowing dying photoreceptor cells to retain or regain normal physiological function. Haruta et al. originally reported successful transplanta-
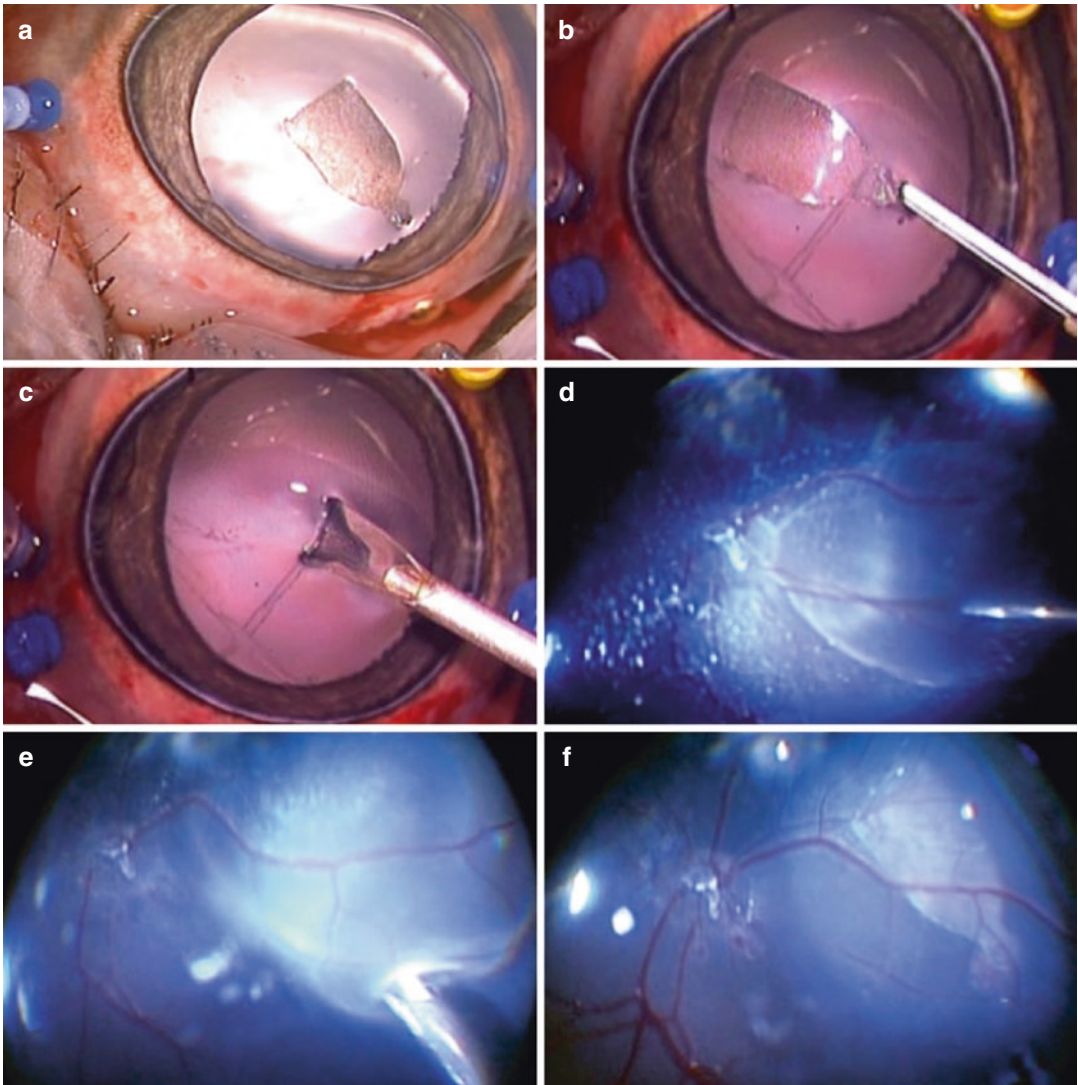
Fig. 31.3 Subretinal transplantation of an ultrathin non-absorbable substrate seeded with hESC-RPE in a Yucatan minipig eye. (**a**) Anterior segment and lens status during and after the surgical procedure. (**b**) Injector forceps hold-ing the substrate by the handle. (**c**) Injector folding the substrate. (**d**) Injection of saline in the subretinal space. (**e**) Subretinal unfolding and placement. (**f**) Posterior pole at the end of the surgical procedure

tion of primate ESC-derived RPE cells into the RCS rat subretinal space with enhanced survival of host photoreceptor cells [88]. Subretinal trans-plantation of hESC-RPE in animal models of reti-nal degeneration has been shown to rescue the degenerating photoreceptors and improve vision [25, 72, 89]. A long-term preclinical study of the injected hESC-derived RPE cells showed no tumor formation over the lifetime of immunodefi-cient mice [25]. Injected RPE cells tend to form

clusters and have limited ability to perform phago-cytosis of photoreceptor outer segments in rat models [90]. Implanted hESC-RPE monolayers survived for at least 12 months without evidence of tumor formation in immunocompromised rats [48]. Similarly, when RPE generated by directed differentiation from iPSCs were transplanted into the subretinal space of RCS rats, preserved photo-receptor morphology and optokinetic response without tumor formation were observed [90].

Promising results indicating functional and morphologic rescue were also obtained after transplantation of RPE derived from human iPSCs into the eyes of mice [37].

Transplanted RPE cells can rescue the host retina not only by replacing damaged RPE and directly interacting with overlying photoreceptors but also by releasing trophic factors [2, 5]. Lund et al. demonstrated that transplantation of human RPE cells in RCS rats could rescue some photoreceptors away from the transplant site, indicating that at least some of the rescue was due to a trophic effect [70]. Other studies also showed that pretreatment of donor retinal sheets with trophic factor-containing microspheres could significantly improve the functional effect of retinal transplants [91, 92].

31.4.2 Efficacy of Whole-Retina Transplants

Retinal transplants may establish functional synapses and directly transmit a photochemical signal to the host retina. Transsynaptic tracing studies using pseudorabies virus (PRV) provide indirect evidence of graft-host connections between transplant photoreceptors and host ganglion cells. The viruses are transferred in a retrograde direction at functional neural synapses [93]. The transfer is possible only between neurons, which are capable of assembling the viral envelope necessary for viral transfer [94]. Tracking the visual responsive sites in the superior colliculus (SC) to their corresponding location in the retina could demonstrate the presence of synaptic connections between the transplant and the host [93]. Seiler et al. conducted microinjection of PRV into the exposed surface of the SC of rats that received retinal transplants to establish PRV labeling of the retina [95]. This study demonstrated that PRV labeling mainly occurred in the retinal interneurons but rarely in the photoreceptors. Another study demonstrated that both trophic effects and synaptic connections are involved in the restoration of visual responses in the SC by retinal transplants [96].

Previous studies have shown that transplantation surgery itself could delay or arrest the degeneration of host photoreceptors and cause a transient preser-

vation of visual function. This effect caused by surgical intervention is probably related to the induction of trophic factor expression [97–99]. Neurotrophic factors are essential for developing synaptic connections in the neural retina [92]. These factors were introduced into the eye to improve functional interactions between the transplant and the host retina. Brain-derived neurotrophic factor (BDNF) and glial cell line-derived neurotrophic factor (GDNF) are known for neuroprotective effects [100–102] and for preventing photoreceptor degeneration [103–105]. Studies using retinal sheets pretreated with BDNF [91, 92] or GDNF [92] showed that the treatment effect enhanced SC responses in S334ter-line-3 transgenic rats. Furthermore, the treatment of retinal transplants with both GDNF and BDNF improved visual restoration in the SC responses, and treatment with only GDNF demonstrated greater overall restoration compared to BDNF-only pretreatment.

These and other preclinical studies paved the way for FDA approval of the first human clinical trials using hESCs to treat AMD in 2009. To date, there are a number of ongoing clinical trials testing stem cell-based replacement therapies for the treatment of macular degeneration. In July 2013, Japan's Ministry of Health approved the first clinical study using RPE derived from iPSCs for the treatment of AMD. Herein, we summarize the current major hESC-RPE and iPSC-RPE trials.

31.4.3 Ocata Therapeutics Trial Using Subretinal hESC-RPE Suspensions

Advanced Cell Technologies and investigators at University of California, Los Angeles, conducted a longitudinal prospective clinical study with a 4-year follow-up to establish the safety and tolerability of subretinal transplantation of hESC-RPE in patients with either Stargardt disease or dry AMD. In the seven patients with dry AMD, four showed improvement in best-corrected visual acuity (BCVA) at 12 months. Among the Stargardt patients, three remained stable at 12 months, while three showed improvement, and one patient's vision worsened. The authors found that 13 out of 18

patients demonstrated increased subretinal pigment after transplantation at the border of the atrophic area. Some of these areas were found to demonstrate reconstitution or thickening of the RPE layer on optical coherence tomography (OCT), possibly suggestive of successful cellular engraftment. The authors noted that these anatomic outcomes cannot be definitively ascribed to the transplanted cells in the absence of higher resolution imaging techniques, microperimetry, or specific labeling for the transplanted cells [27].

31.4.4   London Project to Cure Blindness-Subretinal hESC-RPE Sheet Implantation

The London Project to Cure Blindness (LPCB) reported successful delivery and survival of an RPE patch in two patients with severe wet AMD. The patch survived for 12 months, as assessed by biomicroscopy and OCT. These patients had a visual acuity gain of 29 and 21 letters, respectively. There was evidence of retinal function over the patch, as demonstrated by sustained or improved fixation microperimetry that showed focal sensitivity, increased visual acuity, and increased reading speed. The effect of the original choroidal neovascular membrane on function remains unknown [85].

31.4.5   RIKEN-Subretinal iPSC-RPE Sheet Implantation

Researchers at the RIKEN Center for Developmental Biology and the Center for iPS Cell Research and Application in Japan assessed the feasibility of transplanting a sheet of RPE cells differentiated from iPSCs into a 77-year-old woman with advanced wet AMD and polypoidal choroidal vasculopathy. The iPSCs were differentiated and generated from the patient's skin fibroblasts. This patient did not receive immunosuppressants and showed no signs of rejection. OCT images indicated retinal integrity over the graft at 1 year. After 1 year, the patient's BCVA had neither improved

nor decreased, although the transplanted autologous iPSC-RPE sheet remained intact with cystoid macular edema [106].

31.4.6   Regenerative Patch Technologies (RPT) Subretinal hESC-RPE Sheet Implantation

A human phase I/IIa clinical trial at the University of Southern California Eye Institute is conducted to explore the safety and efficacy of subretinal implantation of hESC-RPE monolayers seeded on an ultrathin parylene membrane (CPCB-RPE1) in patients with dry AMD and geographic atrophy (GA) involving the central fovea. The recent interim analysis reported the phase I cohort of four subjects enrolled in the study who had successfully received the composite implant. The result showed that the implant treated a large region of GA (Fig. 31.4). The overall appearance of the implant, including pigmentation, location, and size, did not change over the course of follow-up. These results indicate that the implant was stable in location and not prone to migration. OCT images showed changes consistent with hESC-RPE and host photoreceptor integration. One eye improved by 17 letters and two eyes demonstrated improved fixation. The authors suggested that CPCB-RPE1 may improve visual function in some patients with severe vision loss from advanced dry AMD [32].

31.5   Safety Studies for Stem Cell-Derived Retinal Cell Transplantation

A major consideration with stem cell therapy is that transplanted cells must not be contaminated with any undifferentiated cells. Undifferentiated pluripotent stem cells have the capacity to differentiate into all cell types of the three germ layers and, without the proper precautions, could cause tumor formation in vivo [107]. Injection of undifferentiated cells has been shown to cause development of tumors in the target area [107] (Fig. 31.5).
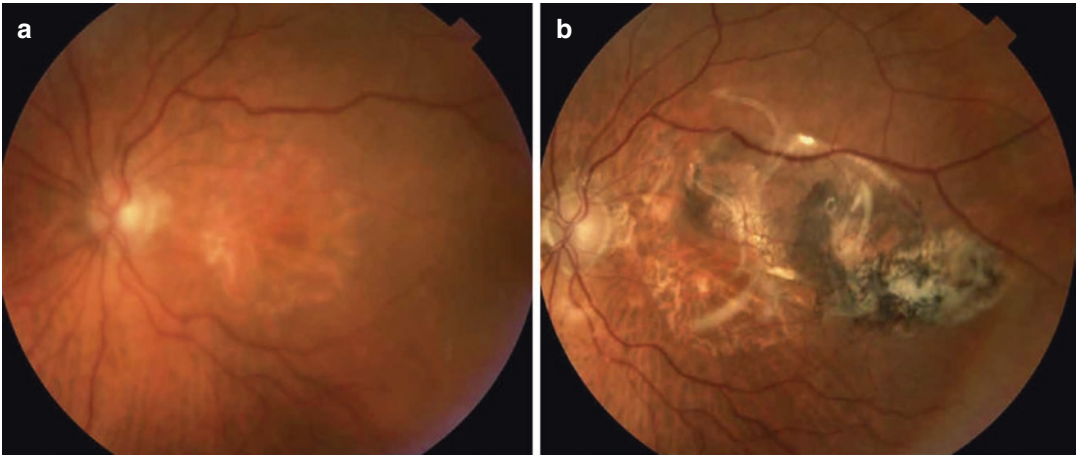
Fig. 31.4 Preoperative and postoperative color fundus photographs of the retina of a study subject. Preoperative fundus photographs (**a**) showing large areas of RPE loss, consistent with geographic atrophy. Postoperative fundus photographs at 180 days (**b**). The implant treated a large region of geographic atrophy
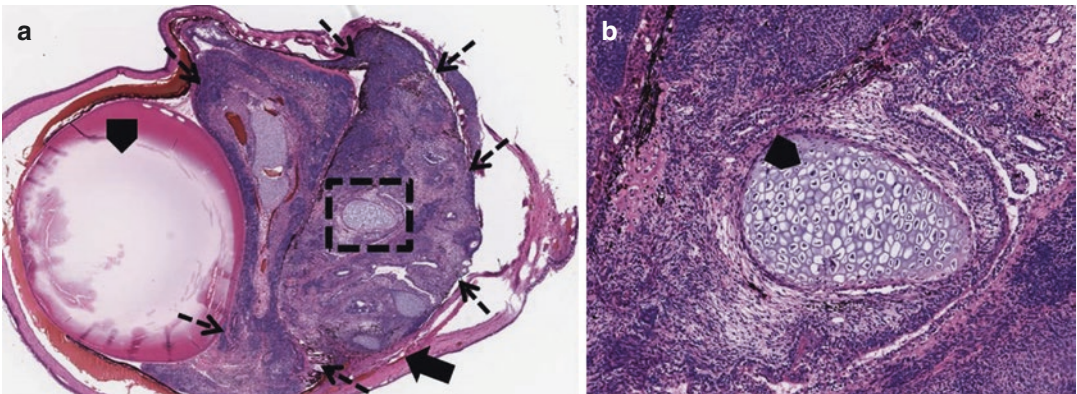
Fig. 31.5 Positive control experiments (injection of undifferentiated cells) conducted in athymic nude rats to show the development of tumors in the eye. (**a**) Teratoma formation approximately 6 weeks after injection (2 μL) of undifferentiated hESCE suspension (60,000 cells/μL) shown on H&E staining (2×) (arrowhead: lens, arrow: tumor formation originated from the subretinal space, broken arrow: the margin of the tumor). (**b**) 10× magnification of the black square from (**a**). The teratoma is composed of various cell types, including cartilage cells (arrowhead)

Stem cell-derived tissues must demonstrate the genetic and functional signature of the target cell line. Differentiation into undesired cell types is a potential threat to the success of stem cell-derived therapies. The first study that used autologous iPSC-RPE cells for therapy of AMD in Japan was halted after unexpected mutations were found in the iPSCs derived from the second patient. To overcome this issue, cord blood and samples from cord blood banks were targeted as a main source of the cells for reprogramming and a human leukocyte antigen (HLA) homozygous iPSC bank was established [108]. Before stem cell therapies are used in human subjects, extensive testing for the lack of tumor formation, absence of cell migration, and purity of stem cell derivations is necessary [109].

The importance of subjecting potential cell therapies to rigorous preclinical and animal testing is underscored by the outcomes of one clinical trial

in Florida. In this study, adipose-derived stem cells were injected into three patients based on minimal clinical evidence of safety or efficacy. The patients suffered severe bilateral vision loss after receiving the injection of autologous adipose tissue-derived stem cells. The patients' severe vision loss was related to ocular hypertension, hemorrhagic retinopathy, vitreous hemorrhage, combined traction and rhegmatogenous retinal detachment, and lens dislocation after the injection [110].

31.6 Conclusion

Stem cell-based therapies provide a novel treatment option for retinal degenerative diseases, which currently have no cure. Animal studies have demonstrated functionality, efficacy, and safety of stem-cell therapies and have provided useful data for further testing in clinical trials. Because most animal studies are relatively short-term, the long-term survival and safety of the tested therapies must be investigated in the future.

Some other issues that will need to be addressed are the absence of large prospective studies to assess visual outcomes and the undetermined optimal timing of transplantation. Coordinated efforts must integrate biomedical research, materials science, clinical application, and commercial interest to ensure success. Stem-cell based disease modeling and transplantation both require long-term, multidisciplinary approaches in order to fully develop stem cell-based therapy as a standard treatment for retinal degenerative diseases.

References

1. Nazari H, Zhang L, Zhu D, Chader GJ, Falabella P, Stefanini F, et al. Stem cell based therapies for age-related macular degeneration: the promises and the challenges. Prog Retin Eye Res. 2015;48:1–39.
2. Zarbin M. Cell-based therapy for degenerative retinal disease. Trends Mol Med. 2016;22(2):115–34.
3. Jones MK, Lu B, Girman S, Wang S. Cell-based therapeutic strategies for replacement and preservation in retinal degenerative diseases. Prog Retin Eye Res. 2017;58:1.
4. Sengillo JD, Justus S, Tsai YT, Cabral T, Tsang SH. Gene and cell-based therapies for inherited retinal disorders: an update. Am J Med Genet C Semin Med Genet. 2016;172(4):349–66.
5. Seiler MJ, Aramant RB. Cell replacement and visual restoration by retinal sheet transplants. Prog Retin Eye Res. 2012;31(6):661–87.
6. Fernandez-Nogales M, Murcia-Belmonte V, Chen HY, Herrera E. The peripheral eye: a neurogenic area with potential to treat retinal pathologies? Prog Retin Eye Res. 2019;68:110–23.
7. Royo PE, Quay WB. Retinal transplantation from fetal to maternal mammalian eye. Growth. 1959;23:313–36.
8. del Cerro M, Ison JR, Bowen GP, Lazar E, del Cerro C. Intraretinal grafting restores visual function in light-blinded rats. Neuroreport. 1991;2(9):529–32.
9. del Cerro M, Yeh HH, Marrero-Rodriguez A, Lazar E, del Cerro C. Intraocular transplantation of cell layers derived from neonatal rat retina. Brain Res. 1990;535(1):25–32.
10. Gouras P, Du J, Gelanze M, Kwun R, Kjeldbye H, Lopez R. Transplantation of photoreceptors labeled with tritiated thymidine into RCS rats. Invest Ophthalmol Vis Sci. 1991;32(5):1704–7.
11. Aramant R, Seiler M, Ehinger B, Bergstrom A, Gustavii B, Brundin P, et al. Transplantation of human embryonic retina to adult rat retina. Restor Neurol Neurosci. 1990;2(1):9–22.
12. Aramant R, Seiler M. Cryopreservation and transplantation of immature rat retina into adult rat retina. Brain Res Dev Brain Res. 1991;61(2):151–9.
13. Aramant RB, Seiler MJ. Human embryonic retinal cell transplants in athymic immunodeficient rat hosts. Cell Transplant. 1994;3(6):461–74.
14. Silverman MS, Hughes SE. Transplantation of photoreceptors to light-damaged retina. Invest Ophthalmol Vis Sci. 1989;30(8):1684–90.
15. Mohand-Said S, Hicks D, Simonutti M, Tran-Minh D, Deudon-Combe A, Dreyfus H, et al. Photoreceptor transplants increase host cone survival in the retinal degeneration (rd) mouse. Ophthalmic Res. 1997;29(5):290–7.
16. Schuschereba ST, Silverman MS. Retinal cell and photoreceptor transplantation between adult New Zealand red rabbit retinas. Exp Neurol. 1992;115(1):95–9.
17. Ghosh F, Arner K, Ehinger B. Transplant of full-thickness embryonic rabbit retina using pars plana vitrectomy. Retina (Philadelphia, PA). 1998;18(2):136–42.
18. Ghosh F, Juliusson B, Arner K, Ehinger B. Partial and full-thickness neuroretinal transplants. Exp Eye Res. 1999;68(1):67–74.
19. Wasselius J, Ghosh F. Adult rabbit retinal transplants. Invest Ophthalmol Vis Sci. 2001;42(11):2632–8.
20. Seiler MJ, Aramant RB. Intact sheets of fetal retina transplanted to restore damaged rat retinas. Invest Ophthalmol Vis Sci. 1998;39(11):2121–31.
21. Aramant RB, Seiler MJ, Ball SL. Successful cotransplantation of intact sheets of fetal retina with retinal pigment epithelium. Invest Ophthalmol Vis Sci. 1999;40(7):1557–64.

22. Aramant RB, Seiler MJ. Transplanted sheets of human retina and retinal pigment epithelium develop normally in nude rats. Exp Eye Res. 2002;75(2):115–25.

23. Fujii GY, Au Eong KG, Humayun MS, de Juan E Jr. Limited macular translocation: current concepts. Ophthalmol Clin North Am. 2002;15(4):425–36.

24. Radtke ND, Aramant RB, Petry HM, Green PT, Pidwell DJ, Seiler MJ. Vision improvement in retinal degeneration patients by implantation of retina together with retinal pigment epithelium. Am J Ophthalmol. 2008;146(2):172–82.

25. Lu B, Malcuit C, Wang S, Girman S, Francis P, Lemieux L, et al. Long-term safety and function of RPE from human embryonic stem cells in preclinical models of macular degeneration. Stem Cells (Dayton, OH). 2009;27(9):2126–35.

26. Schwartz SD, Hubschman JP, Heilwell G, Franco-Cardenas V, Pan CK, Ostrick RM, et al. Embryonic stem cell trials for macular degeneration: a preliminary report. Lancet. 2012;379(9817):713–20.

27. Schwartz SD, Tan G, Hosseini H, Nagiel A. Subretinal transplantation of embryonic stem cell-derived retinal pigment epithelium for the treatment of macular degeneration: an assessment at 4 years. Invest Ophthalmol Vis Sci. 2016;57(5):ORSFc1–9.

28. Schwartz SD, Regillo CD, Lam BL, Eliott D, Rosenfeld PJ, Gregori NZ, et al. Human embryonic stem cell-derived retinal pigment epithelium in patients with age-related macular degeneration and Stargardt's macular dystrophy: follow-up of two open-label phase 1/2 studies. Lancet. 2015;385(9967):509–16.

29. Lu B, Zhu D, Hinton D, Humayun MS, Tai YC. Mesh-supported submicron parylene-C membranes for culturing retinal pigment epithelial cells. Biomed Microdevices. 2012;14(4):659–67.

30. Lee E, MacLaren RE. Sources of retinal pigment epithelium (RPE) for replacement therapy. Br J Ophthalmol. 2011;95(4):445–9.

31. Mehat MS, Sundaram V, Ripamonti C, Robson AG, Smith AJ, Borooah S, et al. Transplantation of human embryonic stem cell-derived retinal pigment epithelial cells in macular degeneration. Ophthalmology. 2018;125(11):1765–75.

32. Kashani AH, Lebkowski JS, Rahhal FM, Avery RL, Salehi-Had H. A bioengineered retinal pigment epithelial monolayer for advanced, dry age-related macular degeneration. Sci Transl Med. 2018;10(435):eaao4097.

33. Aoi T, Yae K, Nakagawa M, Ichisaka T, Okita K, Takahashi K, et al. Generation of pluripotent stem cells from adult mouse liver and stomach cells. Science (New York, NY). 2008;321(5889):699–702.

34. Hanna J, Markoulaki S, Schorderet P, Carey BW, Beard C, Wernig M, et al. Direct reprogramming of terminally differentiated mature B lymphocytes to pluripotency. Cell. 2008;133(2):250–64.

35. Takahashi K, Okita K, Nakagawa M, Yamanaka S. Induction of pluripotent stem cells from fibroblast cultures. Nat Protoc. 2007;2(12):3081–9.

36. Takahashi K, Tanabe K, Ohnuki M, Narita M, Ichisaka T, Tomoda K, et al. Induction of pluripotent stem cells from adult human fibroblasts by defined factors. Cell. 2007;131(5):861–72.

37. Li Y, Tsai YT, Hsu CW, Erol D, Yang J, Wu WH, et al. Long-term safety and efficacy of human-induced pluripotent stem cell (iPS) grafts in a preclinical model of retinitis pigmentosa. Mol Med. 2012;18:1312–9.

38. Okamoto S, Takahashi M. Induction of retinal pigment epithelial cells from monkey iPS cells. Invest Ophthalmol Vis Sci. 2011;52(12):8785–90.

39. Garg A, Yang J, Lee W, Tsang SH. Stem cell therapies in retinal disorders. Cells. 2017;6(1):4.

40. Thomson JA, Itskovitz-Eldor J, Shapiro SS, Waknitz MA, Swiergiel JJ, Marshall VS, et al. Embryonic stem cell lines derived from human blastocysts. Science (New York, NY). 1998;282(5391):1145–7.

41. Takahashi K, Yamanaka S. Induction of pluripotent stem cells from mouse embryonic and adult fibroblast cultures by defined factors. Cell. 2006;126(4):663–76.

42. Fusaki N, Ban H, Nishiyama A, Saeki K, Hasegawa M. Efficient induction of transgene-free human pluripotent stem cells using a vector based on Sendai virus, an RNA virus that does not integrate into the host genome. Proc Jpn Acad Ser B Phys Biol Sci. 2009;85(8):348–62.

43. Taylor CJ, Peacock S, Chaudhry AN, Bradley JA, Bolton EM. Generating an iPSC bank for HLA-matched tissue transplantation based on known donor and recipient HLA types. Cell Stem Cell. 2012;11(2):147–52.

44. Morizane A, Kikuchi T. MHC matching improves engraftment of iPSC-derived neurons in non-human primates. Nat Commun. 2017;8(1):385.

45. Gornalusse GG, Hirata RK, Funk SE, Riolobos L, Lopes VS, Manske G, et al. HLA-E-expressing pluripotent stem cells escape allogeneic responses and lysis by NK cells. Nat Biotechnol. 2017;35(8):765–72.

46. Otani A, Dorrell MI, Kinder K, Moreno SK, Nusinowitz S, Banin E, et al. Rescue of retinal degeneration by intravitreally injected adult bone marrow-derived lineage-negative hematopoietic stem cells. J Clin Invest. 2004;114(6):765–74.

47. Leow SN, Luu CD, Hairul Nizam MH, Mok PL, Ruhaslizan R, Wong HS, et al. Safety and efficacy of human Wharton's jelly-derived mesenchymal stem cells therapy for retinal degeneration. PLoS One. 2015;10(6):e0128973.

48. Diniz B, Thomas P, Thomas B, Ribeiro R, Hu Y, Brant R, et al. Subretinal implantation of retinal pigment epithelial cells derived from human embryonic stem cells: improved survival when implanted as a monolayer. Invest Ophthalmol Vis Sci. 2013;54(7):5087–96.

49. Holtkamp GM, Kijlstra A, Peek R, de Vos AF. Retinal pigment epithelium-immune system interactions: cytokine production and cytokine-induced changes. Prog Retin Eye Res. 2001;20(1):29–48.

50. Zamiri P, Masli S, Streilein JW, Taylor AW. Pigment epithelial growth factor suppresses inflamma-

tion by modulating macrophage activation. Invest Ophthalmol Vis Sci. 2006;47(9):3912–8.

51. Zhu D, Deng X, Spee C, Sonoda S, Hsieh CL, Barron E, et al. Polarized secretion of PEDF from human embryonic stem cell-derived RPE promotes retinal progenitor cell survival. Invest Ophthalmol Vis Sci. 2011;52(3):1573–85.

52. Odorico JS, Kaufman DS, Thomson JA. Multilineage differentiation from human embryonic stem cell lines. Stem Cells (Dayton, OH). 2001;19(3):193–204.

53. Kawasaki H, Suemori H, Mizuseki K, Watanabe K, Urano F, Ichinose H, et al. Generation of dopaminergic neurons and pigmented epithelia from primate ES cells by stromal cell-derived inducing activity. Proc Natl Acad Sci U S A. 2002;99(3):1580–5.

54. Klimanskaya I, Hipp J, Rezai KA, West M, Atala A, Lanza R. Derivation and comparative assessment of retinal pigment epithelium from human embryonic stem cells using transcriptomics. Cloning Stem Cells. 2004;6(3):217–45.

55. Pennington BO, Clegg DO, Melkoumian ZK, Hikita ST. Defined culture of human embryonic stem cells and xeno-free derivation of retinal pigmented epithelial cells on a novel, synthetic substrate. Stem Cells Transl Med. 2015;4(2):165–77.

56. Foltz LP, Clegg DO. Patient-derived induced pluripotent stem cells for modelling genetic retinal dystrophies. Prog Retin Eye Res. 2019;68:54–66.

57. Croze RH, Thi WJ, Clegg DO. ROCK inhibition promotes attachment, proliferation, and wound closure in human embryonic stem cell-derived retinal pigmented epithelium. Transl Vis Sci Technol. 2016;5(6):7.

58. Thomas BB, Zhu D, Zhang L, Thomas PB, Hu Y, Nazari H, et al. Survival and functionality of hESC-derived retinal pigment epithelium cells cultured as a monolayer on polymer substrates transplanted in RCS rats. Invest Ophthalmol Vis Sci. 2016;57(6):2877–87.

59. Yu J, Vodyanik MA, Smuga-Otto K, Antosiewicz-Bourget J, Frane JL, Tian S, et al. Induced pluripotent stem cell lines derived from human somatic cells. Science (New York, NY). 2007;318(5858):1917–20.

60. Park IH, Zhao R, West JA, Yabuuchi A, Huo H, Ince TA, et al. Reprogramming of human somatic cells to pluripotency with defined factors. Nature. 2008;451(7175):141–6.

61. Bharti K, Rao M, Hull SC, Stroncek D, Brooks BP, Feigal E, et al. Developing cellular therapies for retinal degenerative diseases. Invest Ophthalmol Vis Sci. 2014;55(2):1191–202.

62. Hayashi R, Ishikawa Y, Ito M, Kageyama T, Takashiba K, Fujioka T, et al. Generation of corneal epithelial cells from induced pluripotent stem cells derived from human dermal fibroblast and corneal limbal epithelium. PLoS One. 2012;7(9):e45435.

63. Hu Y, Liu L, Lu B, Zhu D, Ribeiro R, Diniz B, et al. A novel approach for subretinal implantation of ultra-thin substrates containing stem cell-derived retinal pigment epithelium monolayer. Ophthalmic Res. 2012;48(4):186–91.

64. Carr AJ, Vugler A, Lawrence J, Chen LL, Ahmado A, Chen FK, et al. Molecular characterization and functional analysis of phagocytosis by human embryonic stem cell-derived RPE cells using a novel human retinal assay. Mol Vis. 2009;15:283–95.

65. Buchholz DE, Hikita ST, Rowland TJ, Friedrich AM, Hinman CR, Johnson LV, et al. Derivation of functional retinal pigmented epithelium from induced pluripotent stem cells. Stem Cells (Dayton, OH). 2009;27(10):2427–34.

66. Coles BL, Angenieux B, Inoue T, Del Rio-Tsonis K, Spence JR, McInnes RR, et al. Facile isolation and the characterization of human retinal stem cells. Proc Natl Acad Sci U S A. 2004;101(44):15772–7.

67. Luo J, Baranov P, Patel S, Ouyang H, Quach J, Wu F, et al. Human retinal progenitor cell transplantation preserves vision. J Biol Chem. 2014;289(10):6362–71.

68. Warfvinge K, Kiilgaard JF, Lavik EB, Scherfig E, Langer R, Klassen HJ, et al. Retinal progenitor cell xenografts to the pig retina: morphologic integration and cytochemical differentiation. Arch Ophthalmol (Chicago, IL: 1960). 2005;123(10):1385–93.

69. Klassen H, Kiilgaard JF, Zahir T, Ziaeian B, Kirov I, Scherfig E, et al. Progenitor cells from the porcine neural retina express photoreceptor markers after transplantation to the subretinal space of allorecipients. Stem Cells (Dayton, OH). 2007;25(5):1222–30.

70. Lund RD, Adamson P, Sauve Y, Keegan DJ, Girman SV, Wang S, et al. Subretinal transplantation of genetically modified human cell lines attenuates loss of visual function in dystrophic rats. Proc Natl Acad Sci U S A. 2001;98(17):9942–7.

71. Lund RD, Kwan AS, Keegan DJ, Sauve Y, Coffey PJ, Lawrence JM. Cell transplantation as a treatment for retinal disease. Prog Retin Eye Res. 2001;20(4):415–49.

72. Lund RD, Wang S, Lu B, Girman S, Holmes T, Sauve Y, et al. Cells isolated from umbilical cord tissue rescue photoreceptors and visual functions in a rodent model of retinal disease. Stem Cells (Dayton, OH). 2007;25(3):602–11.

73. Nakano T, Ando S, Takata N, Kawada M, Muguruma K, Sekiguchi K, et al. Self-formation of optic cups and storable stratified neural retina from human ESCs. Cell Stem Cell. 2012;10(6):771–85.

74. Assawachananont J, Mandai M, Okamoto S, Yamada C, Eiraku M, Yonemura S, et al. Transplantation of embryonic and induced pluripotent stem cell-derived 3D retinal sheets into retinal degenerative mice. Stem Cell Rep. 2014;2(5):662–74.

75. Shirai H, Mandai M, Matsushita K, Kuwahara A, Yonemura S, Nakano T, et al. Transplantation of human embryonic stem cell-derived retinal tissue in two primate models of retinal degeneration. Proc Natl Acad Sci U S A. 2016;113(1):E81–90.

76. Mandai M, Fujii M, Hashiguchi T, Sunagawa GA, Ito S, Sun J, et al. iPSC-derived retina transplants improve vision in rd1 end-stage retinal-degeneration mice. Stem Cell Rep. 2017;8(1):69–83.

77. Park SS, Bauer G, Abedi M, Pontow S, Panorgias A, Jonnal R, et al. Intravitreal autologous bone marrow CD34+ cell therapy for ischemic and degenerative retinal disorders: preliminary phase 1 clinical trial findings. Invest Ophthalmol Vis Sci. 2014;56(1):81–9.

78. Siqueira RC, Messias A, Voltarelli JC, Scott IU, Jorge R. Intravitreal injection of autologous bone marrow-derived mononuclear cells for hereditary retinal dystrophy: a phase I trial. Retina (Philadelphia, PA). 2011;31(6):1207–14.

79. Sachdeva MM, Eliott D. Stem cell-based therapy for diseases of the retinal pigment epithelium: from bench to bedside. Semin Ophthalmol. 2016;31(1–2):25–9.

80. Hynes SR, Lavik EB. A tissue-engineered approach towards retinal repair: scaffolds for cell transplantation to the subretinal space. Graefes Arch Clin Exp Ophthalmol. 2010;248(6):763–78.

81. Hsiung J, Zhu D, Hinton DR. Polarized human embryonic stem cell-derived retinal pigment epithelial cell monolayers have higher resistance to oxidative stress-induced cell death than nonpolarized cultures. Stem Cells Transl Med. 2015;4(1):10–20.

82. Kamao H, Mandai M, Okamoto S, Sakai N, Suga A, Sugita S, et al. Characterization of human induced pluripotent stem cell-derived retinal pigment epithelium cell sheets aiming for clinical application. Stem Cell Rep. 2014;2(2):205–18.

83. Sugino IK, Sun Q, Wang J, Nunes CF, Cheewatrakoolpong N, Rapista A, et al. Comparison of FRPE and human embryonic stem cell-derived RPE behavior on aged human Bruch's membrane. Invest Ophthalmol Vis Sci. 2011;52(8):4979–97.

84. Koss MJ, Falabella P, Stefanini FR, Pfister M, Thomas BB, Kashani AH, et al. Subretinal implantation of a monolayer of human embryonic stem cell-derived retinal pigment epithelium: a feasibility and safety study in Yucatan minipigs. Graefes Arch Clin Exp Ophthalmol. 2016;254(8):1553–65.

85. da Cruz L, Fynes K, Georgiadis O, Kerby J, Luo YH, Ahmado A, et al. Phase 1 clinical study of an embryonic stem cell-derived retinal pigment epithelium patch in age-related macular degeneration. Nat Biotechnol. 2018;36(4):328–37.

86. Butterwick A, Huie P, Jones BW, Marc RE, Marmor M, Palanker D. Effect of shape and coating of a subretinal prosthesis on its integration with the retina. Exp Eye Res. 2009;88(1):22–9.

87. Fernandes RAB, Stefanini FR, Falabella P, Koss MJ, Wells T, Diniz B, et al. Development of a new tissue injector for subretinal transplantation of human embryonic stem cell derived retinal pigmented epithelium. Int J Retina Vitreous. 2017;3:41.

88. Haruta M, Sasai Y, Kawasaki H, Amemiya K, Ooto S, Kitada M, et al. In vitro and in vivo characterization of pigment epithelial cells differentiated from primate embryonic stem cells. Invest Ophthalmol Vis Sci. 2004;45(3):1020–5.

89. Lund RD, Wang S, Klimanskaya I, Holmes T, Ramos-Kelsey R, Lu B, et al. Human embryonic stem cell-derived cells rescue visual function in dystrophic RCS rats. Cloning Stem Cells. 2006;8(3):189–99.

90. Carr AJ, Vugler AA, Hikita ST, Lawrence JM, Gias C, Chen LL, et al. Protective effects of human iPS-derived retinal pigment epithelium cell transplantation in the retinal dystrophic rat. PLoS One. 2009;4(12):e8152.

91. Seiler MJ, Thomas BB, Chen Z, Arai S, Chadalavada S, Mahoney MJ, et al. BDNF-treated retinal progenitor sheets transplanted to degenerate rats: improved restoration of visual function. Exp Eye Res. 2008;86(1):92–104.

92. Yang PB, Seiler MJ, Aramant RB, Yan F, Mahoney MJ, Kitzes LM, et al. Trophic factors GDNF and BDNF improve function of retinal sheet transplants. Exp Eye Res. 2010;91(5):727–38.

93. Card JP, Rinaman L, Lynn RB, Lee BH, Meade RP, Miselis RR, et al. Pseudorabies virus infection of the rat central nervous system: ultrastructural characterization of viral replication, transport, and pathogenesis. J Neurosci. 1993;13(6):2515–39.

94. Rinaman L, Levitt P, Card JP. Progressive postnatal assembly of limbic-autonomic circuits revealed by central transneuronal transport of pseudorabies virus. J Neurosci. 2000;20(7):2731–41.

95. Seiler MJ, Sagdullaev BT, Woch G, Thomas BB, Aramant RB. Transsynaptic virus tracing from host brain to subretinal transplants. Eur J Neurosci. 2005;21(1):161–72.

96. Seiler MJ, Thomas BB, Chen Z, Wu R, Sadda SR, Aramant RB. Retinal transplants restore visual responses: trans-synaptic tracing from visually responsive sites labels transplant neurons. Eur J Neurosci. 2008;28(1):208–20.

97. Humphrey MF, Chu Y, Mann K, Rakoczy P. Retinal GFAP and bFGF expression after multiple argon laser photocoagulation injuries assessed by both immunoreactivity and mRNA levels. Exp Eye Res. 1997;64(3):361–9.

98. Wen R, Song Y, Cheng T, Matthes MT, Yasumura D, LaVail MM, et al. Injury-induced upregulation of bFGF and CNTF mRNAS in the rat retina. J Neurosci. 1995;15(11):7377–85.

99. Faktorovich EG, Steinberg RH, Yasumura D, Matthes MT, LaVail MM. Basic fibroblast growth factor and local injury protect photoreceptors from light damage in the rat. J Neurosci. 1992;12(9):3554–67.

100. von Bartheld CS. Neurotrophins in the developing and regenerating visual system. Histol Histopathol. 1998;13(2):437–59.

101. Rohrer B, Korenbrot JI, LaVail MM, Reichardt LF, Xu B. Role of neurotrophin receptor TrkB in the maturation of rod photoreceptors and establishment of synaptic transmission to the inner retina. J Neurosci. 1999;19(20):8919–30.

102. Grishanin RN, Yang H, Liu X, Donohue-Rolfe K, Nune GC, Zang K, et al. Retinal TrkB receptors regulate neural development in the inner, but not outer, retina. Mol Cell Neurosci. 2008;38(3):431–43.

103. Frasson M, Picaud S, Leveillard T, Simonutti M, Mohand-Said S, Dreyfus H, et al. Glial cell line-derived neurotrophic factor induces histologic and functional protection of rod photoreceptors in the rd/rd mouse. Invest Ophthalmol Vis Sci. 1999;40(11):2724–34.

104. McGee Sanftner LH, Abel H, Hauswirth WW, Flannery JG. Glial cell line derived neurotrophic factor delays photoreceptor degeneration in a transgenic rat model of retinitis pigmentosa. Mol Ther. 2001;4(6):622–9.

105. Chaum E. Retinal neuroprotection by growth factors: a mechanistic perspective. J Cell Biochem. 2003;88(1):57–75.

106. Mandai M, Watanabe A, Kurimoto Y, Hirami Y, Morinaga C, Daimon T, et al. Autologous induced stem-cell-derived retinal cells for macular degeneration. N Engl J Med. 2017;376(11):1038–46.

107. Lin TC, Seiler MJ. Assessment of safety and functional efficacy of stem cell-based therapeutic approaches using retinal degenerative animal models. Stem Cells Int. 2017;2017:9428176.

108. Ilic D. iPSC in the past decade: the Japanese dominance. Regen Med. 2016;11(8):747–9.

109. Kuroda T, Yasuda S, Kusakawa S, Hirata N, Kanda Y, Suzuki K, et al. Highly sensitive in vitro methods for detection of residual undifferentiated cells in retinal pigment epithelial cells derived from human iPS cells. PLoS One. 2012;7(5):e37342.

110. Kuriyan AE, Albini TA, Townsend JH, Rodriguez M, Pandya HK, Leonard RE 2nd, et al. Vision loss after intravitreal injection of autologous "stem cells" for AMD. N Engl J Med. 2017;376(11):1047–53.

Submacular Surgery for Submacular Hemorrhage

32

Shumpei Obata and Masahito Ohji

32.1 Introduction

Submacular hemorrhage (SMH) is regarded as hemorrhage located in the space between the neurosensory retina and retinal pigment epithelium (RPE) at the macula. SMH occurs as a result of wet age-related macular degeneration (AMD) [1], polypoidal choroidal vasculopathy (PCV), retinal arterial macroaneurysms [1], myopic choroidal neovascularization (CNV) [2], and non-AMD causes of CNV (e.g., traumatic choroidal rupture [3] and histoplasmosis syndrome). Notably, >80% of patients exhibit SMH as a result of AMD [1]. Large size, large thickness, and extended duration of SMH result in a poor prognosis in the natural course of visual acuity [3, 4]. The natural course of untreated SMH is especially poor in patients with SMH that results from AMD [1, 3, 4]. Scupola et al. [4] described the natural course of a series of 60 patients with SMH due to AMD. Visual acuity was a mean of 20/240 (range: 20/70 to light perception) at the time of the initial examination; it worsened in 80% of eyes to reach a mean final visual acuity of 20/1250 (range: 20/100 to light perception).

Several mechanisms might cause poor prognosis in patients with SMH. First, visual dysfunc-

tion may be induced by clot formation with the disturbance of diffusion between the neurosensory retina and RPE [5–7]. In the second phase, the neurosensory retina and RPE may be damaged directly by toxic iron ions from erythrocyte degradation [5–7]. Several animal studies have shown irreversible changes in the outer retinal layers within 24 h after subretinal injection of blood (rabbit model) [8], and within 3 days of the retraction of fibrin strands (cat model) [9]. SMH prevents the exchange of nutrients, oxygen, and metabolites between the retina and choriocapillaris; in addition, iron released at hemorrhage sites is toxic to the retinal circulation, whereas the release of fibrin results in irreversible photoreceptor damage. The duration of SMH is an important factor in postoperative visual function. If surgical intervention is needed, it should be performed within 2 weeks of the onset of SMH [8, 9]. Glatt and Machemer [8] reported that in the rabbit eye, the injection of autologous blood into the subretinal space caused irreversible photoreceptor loss in <24 h; severe damage to the outer retina was observed at 7 days and the outer retina was completely absent at 2 weeks.

Therefore, rapid removal or displacement of SMH from the macula is essential to prevent irreversible damage to the retina. Several therapeutic options, including surgical and/or pharmacological interventions, have been attempted to prevent irreversible visual dysfunction due to SMH [10–17]. However, the most important decision is

S. Obata · M. Ohji (✉)
Shiga University of Medical Science,
Otsu City, Shiga, Japan
e-mail: obata326@belle.shiga-med.ac.jp; ohji@belle.shiga-med.ac.jp

whether a patient with SMH should undergo treatment or observation alone. The therapeutic strategy is determined by several factors: visual function, conditions of the fellow eye, primary disease causing SMH, duration and location of SMH, and size and thickness of SMH.

32.2 Surgical Removal of Blood and CNV

In the first surgical method used for treatment of SMH, de Juan and Machemer reported its removal through small posterior retinotomy or 180-degree retinotomy [18]. Visual acuity improved in three of four eyes and postoperative visual acuity was limited to 5/200. Three-port vitrectomy with retinotomy and removal of subretinal clot by subretinal forceps were performed in other reports in 1990–1991 [10, 19]. However, the results were disappointing, with few patients showing improvement of visual acuity.

Peyman et al. [11] first reported treatment of patients with SMH using vitrectomy with tissue plasminogen activator (tPA) as surgical adjuvant in 1991. Standard pars plana vitrectomy was performed and tPA was injected into the subretinal space. After clot dissolution, retinal hemorrhage was removed from the retinal hole via irrigation with balanced salt solution. In this report, visual outcome was disappointing in patients with AMD. In 1994, Lewis et al. [20] showed that visual outcome of vitrectomy with tPA was favorable compared with that of surgical treatment without tPA. In this prospective study, 24 consecutive eyes with recent SMH with AMD underwent vitrectomy, subretinal injection of tPA, and removal of liquefied blood. Visual acuity improved in 20 eyes (83%) after surgery and reached 20/200 or better in eight eyes. In 1995, Lim et al. [21] retrospectively reviewed the outcomes of 18 patients who underwent pars plana vitrectomy with subretinal injection of tPA; they found that visual acuity improved by 1–2 lines in 11 eyes (61%), remained unchanged in four (22%), and decreased by 1–2 lines in three (17%).

To evaluate the benefit of surgical removal of SMH, the Submacular Surgery Trials (SST) Group

B was started in 1997. This multicenter, prospective, randomized clinical trial aimed to determine whether vitrectomy to remove SMH or observation over ≥2 years resulted in better visual outcome for patients with secondary SMH due to AMD [22]. Patients who had subfoveal choroidal neovascular lesions >3.5 disk areas, comprising at least 50% blood (either blood or CNV underlying the center of the foveal avascular zone) and best-corrected visual acuity (BCVA) of 20/100 to light perception in the study eye, were included in this study. The surgical method was standard three-port pars plana vitrectomy, retinotomy, manual extraction of the blood clot to free the fovea of thick SMH, and manual extraction of CNV when possible. tPA and several types of long-acting gas tamponade were administered at the surgeon's discretion. In the SST Group B, compared with observation alone, submacular surgery did not improve or preserve visual acuity for 24 months in a greater number of eyes [22]. Surgical removal of SMH was limited to that necessary to maintain visual acuity.

32.3 Pneumatic Displacement with/Without Intravitreal tPA Injection Without Vitrectomy

In 1996, Heriot [12] described a novel, minimally invasive, outpatient procedure of intravitreal tPA and perfluoropropane (C_3F_8) gas injection for the treatment of SMH in a small clinical series. In this approach, SMH was liquefied enzymatically and then pneumatically displaced inferiorly without vitrectomy. In 1999, Hesse [23] reported the effect of intravitreal injection of tPA with gas for patients with SMH due to AMD. Eleven consecutive patients (11 eyes) with SMH involving the fovea, including elevation of the neurosensory retina, were enrolled in that study. After intravitreal injection of tPA, subretinal clots were completely or partially liquefied when treatment was initiated up to 3 days after the onset of bleeding. In another retrospective study, patients received an intravitreal injection of 30–100 μg of tPA and expansile gas (sulfur hexafluoride [SF_6] or C_3F_8) for SMH. Visual acuity was improved by ≥2 Snellen lines in 43/85 eyes (51%) at 1 week post-

operatively, in 49/77 eyes (63%) at 3 months postoperatively, and in 52/81 eyes (64%) at 12 months postoperatively. These findings suggested that intravitreal tPA with gas could improve visual acuity in most eyes with SMH [23, 24]. In case 1, pneumatic displacement was performed with intravitreal tPA injection and without vitrectomy (Fig. 32.1).

In 1998, Ohji et al. [13] reported an alternative in-office method: pneumatic displacement of

SMH without intravitreal injection of tPA. They described a small series of five patients who were treated with pure C_3F_8 gas (0.3–0.4 mL) and instructed to maintain facedown positioning; SMH was displaced completely or partially in all patients. In case 2, pneumatic displacement was performed without intravitreal tPA injection or vitrectomy (Fig. 32.2).

Other reports have demonstrated improvement of visual acuity by gas injection for sec-
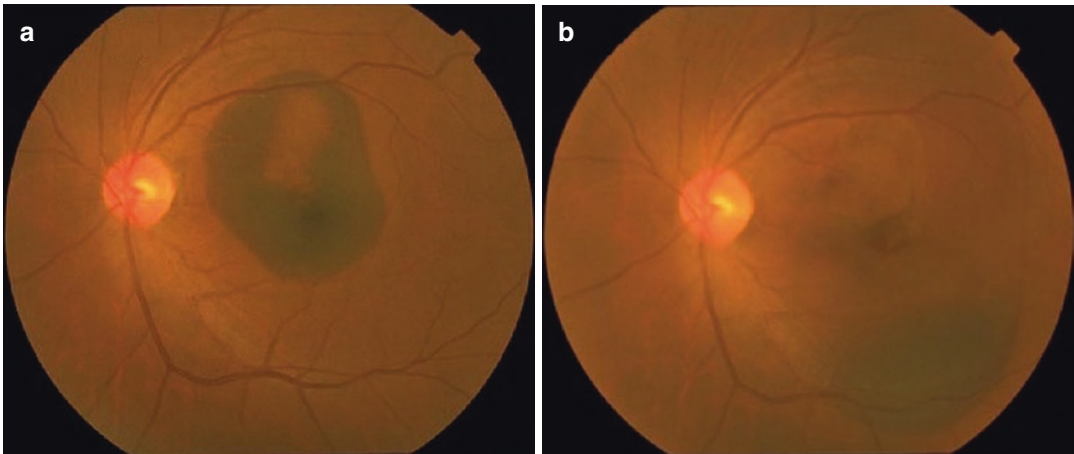
Fig. 32.1   Case 1: A 70-year-old male with submacular hemorrhage (SMH) secondary to polypoidal choroidal vasculopathy (PCV). (**a**) This patient underwent tissue plasminogen activator (tPA) and C_3F_8 injection at 14 days after the onset of SMH, (**b**) which was effective for inferior displacement of SMH. Visual acuity improved from 20/200 to 20/25
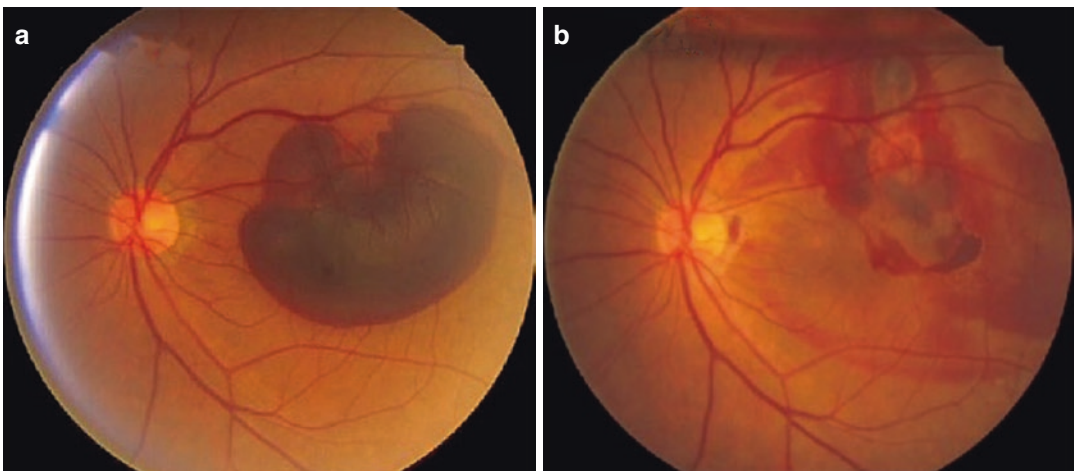
Fig. 32.2   Case 2: A 69-year-old male with submacular hemorrhage (SMH) secondary to polypoidal choroidal vasculopathy (PCV). (**a**) This patient underwent injection of C_3F_8 alone into the vitreous cavity at 5 days after sudden visual loss. (**b**) A large portion of SMH was displaced from the macula and visual acuity improved from 20/250 to 20/25 in 2 days

ondary SMH [25, 26]; this simple treatment appears safe and can improve visual acuity. To determine whether tPA is essential, Mizutani et al. [27] reported a comparison of pneumatic displacement for SMH, using gas alone and gas plus tPA. The respective incidence rates of rebleeding were 100.0% and 10% in eyes with macroaneurysms with or without tPA, whereas they were 22.2% and 33.3% in eyes with AMD treated with or without tPA. Macroaneurysms had a significantly higher risk of rebleeding when tPA was used, compared with macroaneurysms treated without tPA and AMD treated with tPA (*P* < 0.01). Fujikawa et al. [28] compared displacement of SMH between patients treated with gas alone and patients treated with gas and tPA; there were no statistically significant differences between the two groups in the mean score of displacement. Both groups had similar displacement of SMH, visual improvement, and complication rates at 1 month postoperatively. In that report, gas injection without tPA was recommended due to its production of good visual outcomes. Thus, tPA may be nonessential, but it may facilitate the displacement of SMH.

32.4   Vitrectomy with Subretinal Injection of tPA and Pneumatic Displacement

Several modified surgical treatments have been reported for the management of SMH. In 2001, Haupert et al. [14] reported an alternative technique to maximize clot lysis and displacement of SMH from the fovea while minimizing the risk of damage to the retina and RPE. They performed pars plana vitrectomy, subretinal tPA injection without clot manipulation, and fluid-gas exchange with facedown positioning for management of thick SMH. Notably, SMH was displaced from the fovea in all 11 eyes, and visual acuity was improved in 8 (73%) eyes. In 2004, Olivier et al. reported a slightly modified procedure [29]: they injected tPA with a 39G flexible translocation cannula to create a bullous

retinal detachment encompassing the entire blood clot. In 25 eyes (86%), SMH was completely displaced from the fovea. Seventeen eyes (58.6%) showed improvement of >2 lines of visual acuity, while three eyes showed loss of >2 lines of visual acuity.

In 2017, Fleissig et al. [30] described two-step pars plana vitrectomy using tPA and perfluorocarbon liquid (PFCL) tamponade. The initial vitrectomy included subretinal injection of 25 μg/0.2 mL tPA using a 41G needle; larger retinotomy and/or active blood drainage from the subretinal space were avoided. Then, PFCL (4–5 mL) was injected into the vitreous cavity to displace the hemorrhage away from the posterior pole. PFCL was maintained in the vitreous cavity for 7–17 days postoperatively; during the second vitrectomy, PFCL was removed and replaced with balanced salt solution or air. SMH was successfully displaced in six (86.7%) of seven eyes [30]. In case 3, vitrectomy was performed with subretinal injection of tPA and pneumatic displacement (Fig. 32.3).

32.5   Vitrectomy for Massive SRH (Internal Drainage vs. External Drainage)

The natural course of untreated SMH is especially poor in patients with SMH due to AMD [1, 3, 4]. Small or medium hemorrhages can be easily displaced by various pneumatic techniques, whereas massive SMH is always difficult to completely remove.

32.5.1 Vitrectomy with Internal Drainage Therapy

In patients with massive SMH, it is difficult to visualize or remove subretinal clots using conventional techniques. In 2007, Oshima et al. [15] reported a modified surgical technique comprising intravitreal injection of tPA at 12–24 h preoperatively, followed by vitrectomy to remove SMH through a peripheral small retinotomy using PFCL and long-acting gas in patients with
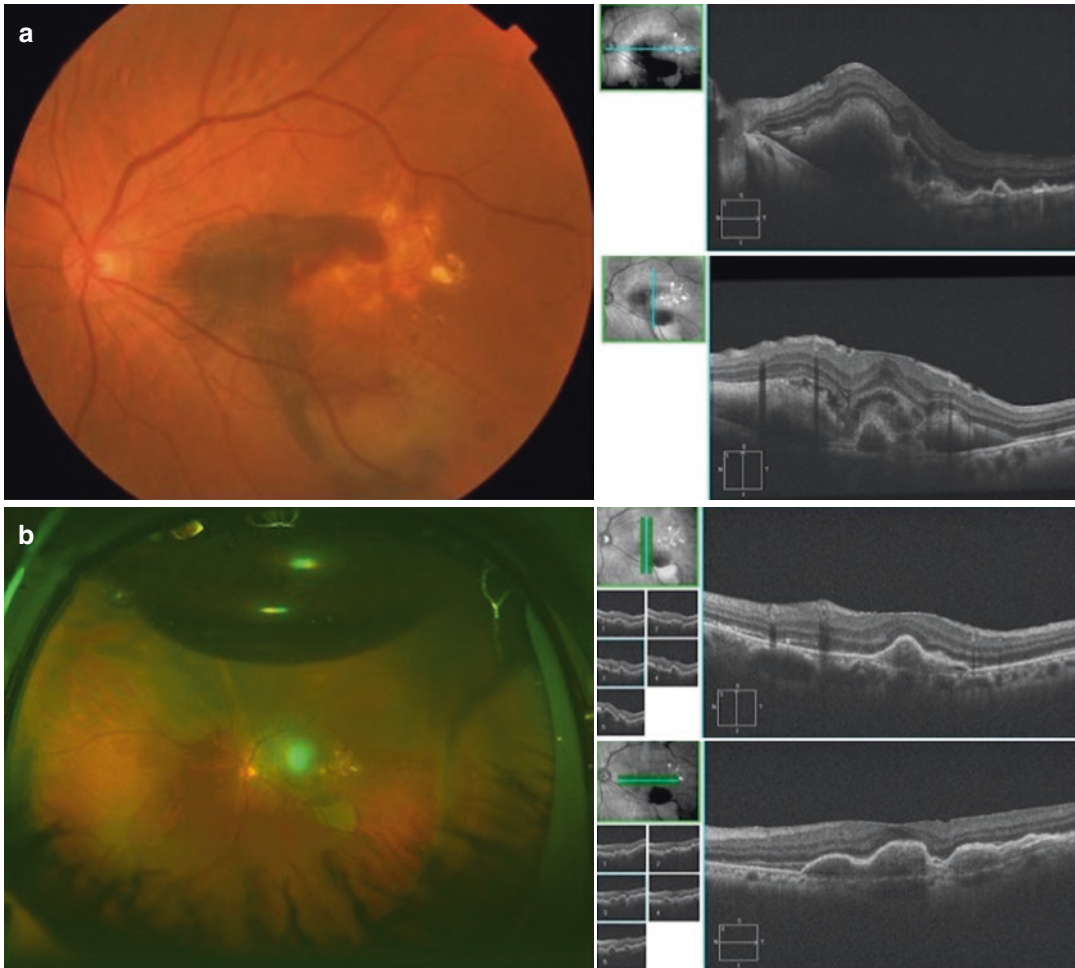
Fig. 32.3 Case 3: A 68-year-old male with submacular hemorrhage (SMH) secondary to polypoidal choroidal vasculopathy (PCV). (**a**) Initial best-corrected visual acuity was 20/133. Thus, vitrectomy with subretinal injection of tissue plasminogen activator (tPA) was performed, followed by fluid-air exchange and air tamponade. (**b**) Optical coherence tomography showed that SMH was completely displaced at 6 days postoperatively

massive SMH. The final visual acuity improved in seven of eight eyes. In case 4, vitrectomy was performed with external drainage of massive SMH and injection of tissue plasminogen activator (tPA) (Fig. 32.4).

32.5.2 Vitrectomy with External Drainage Therapy

Liu et al. [17] reported that external drainage therapy was effective for displacement of mas-

sive SMH. After cataract surgery and vitrectomy, PFCL (3–4 mL) was applied to the posterior retina; this displaced the SMH from the posterior pole to the periphery. A scleral tunnel was created by applying 30G ultrathin needles at the corresponding site to drain the SMH. BCVA improved from 20/2518 at baseline to 20/230 at 6 months postoperatively ($P = 0.043$). These findings suggest that external drainage therapy might be a useful surgical strategy in patients with massive SMH.
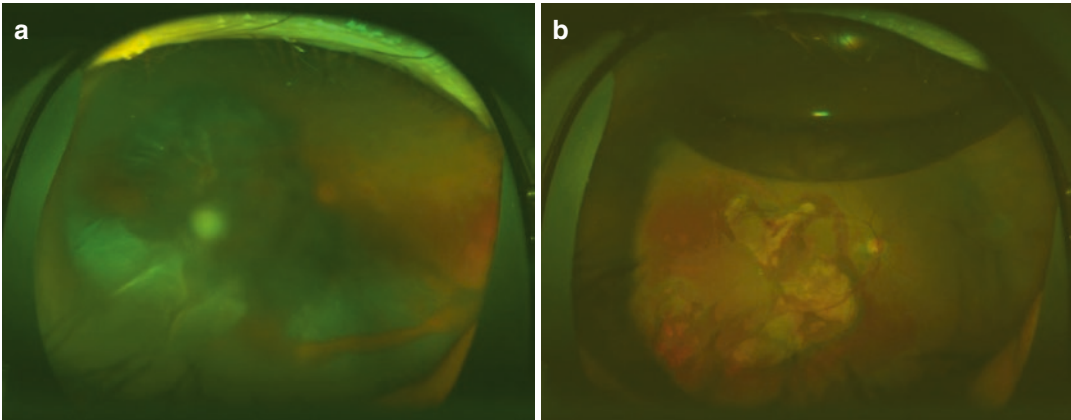
Fig. 32.4 Case 4: A 74-year-old male with submacular hemorrhage (SMH) secondary to polypoidal choroidal vasculopathy (PCV). (**a**) This patient had massive SMH and visual acuity of 20/2000. Vitrectomy was performed with external drainage of massive SMH and injection of tissue plasminogen activator (tPA); (**b**) the patient's vision subsequently improved to 20/50

32.6 Anti-vascular Endothelial Growth Factor (VEGF) Agent

In 2009, Chawla et al. [16] reported the efficacy of treatment of SMH secondary to CNV with pneumatic displacement using SF_6 gas and off-label application of intravitreal bevacizumab. In 2010, Chang et al. [31] described ranibizumab monotherapy for SMH. Predominantly hemorrhagic lesions treated with ranibizumab appeared to exhibit better visual acuity outcomes than natural history controls in submacular surgery trials. In 2013, Cho et al. [32] evaluated the effect of intravitreal anti-VEGF injections on SMH secondary to PCV. The mean visual acuity at baseline was 20/209; this improved to 20/115 at 12 months postoperatively ($P = 0.02$). Shienbaum et al. [33] reported the visual and anatomic outcomes of anti-VEGF monotherapy for management of massive SMH due to AMD. In 19 eyes, median visual acuity improved from 20/400 at baseline to 20/250 + 1 at 3 months of follow-up. In 2015, Cho et al. [34] reported the efficacy of intravitreal ranibizumab with and without pneumatic displacement for the treatment of SMH secondary to neovascular AMD. The logMAR BCVA of the ranibizumab monotherapy group improved from 20/303 at baseline to 20/182 at 12 months postoperatively ($P = 0.008$), whereas the BCVA of the combined treated group improved from 20/317 at baseline to 20/178 at 12 months postoperatively ($P = 0.003$). The mean central foveal thickness of the ranibizumab monotherapy group improved significantly, from 473 μm at baseline to 279 μm ($P < 0.001$) at 12 months postoperatively; moreover, the mean central foveal thickness of the combined treated group improved significantly, from 466 μm at baseline to 249 μm ($P < 0.001$) at 12 months postoperatively. Those findings indicated that ranibizumab monotherapy or ranibizumab therapy combined with pneumatic displacement may provide minimally invasive effective treatment for SMH. In case 5, aflibercept injections alone were performed without surgical intervention (Fig. 32.5).

To determine which patients with SMH should be treated with pneumatic displacement or intravitreal anti-VEGF monotherapy without pneumatic displacement, Shin et al. [35] assessed a combination of pneumatic displacement and intravitreal anti-VEGF therapy, compared with anti-VEGF monotherapy. In eyes with thick SMH (>450 mm), visual outcome at 6 months was better in the combination therapy group than in the monotherapy group ($P = 0.021$), whereas BCVA showed no significant difference between groups in eyes with thin SMH (<450 mm) ($P = 0.930$). The findings of that report indicated that anti-VEGF monotherapy was effective in eyes with thin SMH, whereas additional surgical treatment was needed in eyes with thick SMH.
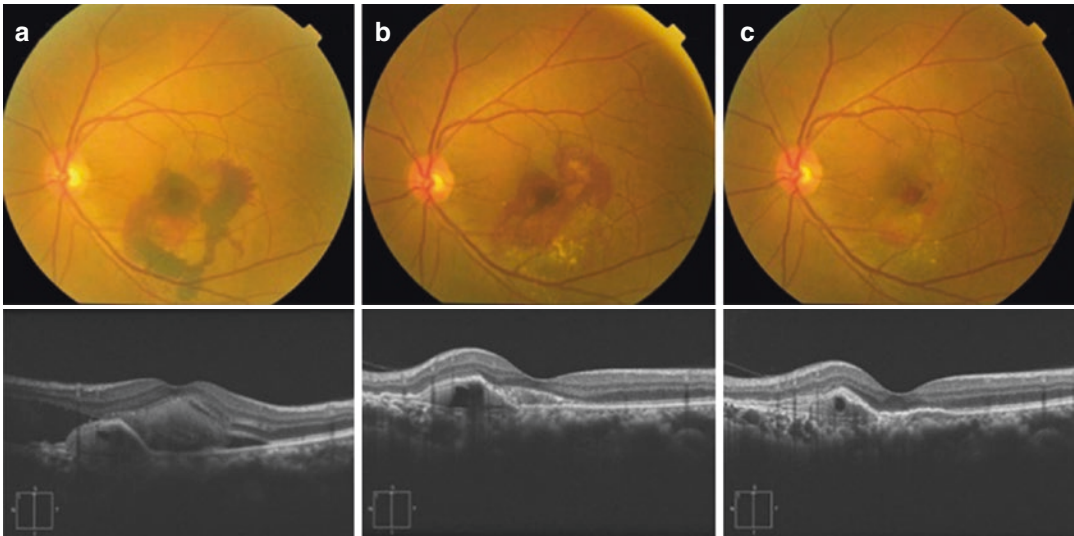
Fig. 32.5 Case 5: A 73-year-old male with submacular hemorrhage (SMH) secondary to polypoidal choroidal vasculopathy (PCV). (**a**) Visual acuity decreased to 20/200. The area of SMH at the fovea was moderate and the SMH thickness was mild. Aflibercept injections alone were performed without surgical interventions. (**b**) At 1 month after treatment, SMH decreased in size and thickness; (**c**) at 3 months after treatment, SMH completely disappeared and visual acuity improved to 20/28

In 2016, Kitagawa et al. [26] investigated the efficacy of intravitreal injection of recombinant tPA, ranibizumab, and gas without vitrectomy for treatment of SMH. Complete displacement of SMH was achieved in 17 of 20 eyes (85%), while partial displacement was achieved in the remaining 3 eyes (15%). Snellen BCVA improved from 20/139 at baseline to 20/65 at 6 months postoperatively ($P = 0.0061$). The findings suggested that SMH treatment using intravitreal injection of tPA, ranibizumab, and gas could be useful for displacement of SMH.

32.7 Conclusion

Treatment for patients with SMH should be determined on the basis of several factors: visual potential; state of the fellow eye; primary disease; and duration, location, size, and thickness of SMH. In patients who require surgery, surgical intervention should be performed within 2 weeks of the onset of SMH. In patients with thin SMH, anti-VEGF monotherapy might be effective and result in fewer complications. In patients with medium-to-large SMH, pneumatic displacement might be effective, with or without tPA and/or vitrectomy. In patients with massive SMH, tPA injection should be performed, in combination with one or more modified surgical strategies.

References

1. Ibanez HE, Williams DF, Thomas MA, et al. Surgical management of submacular hemorrhage. A series of 47 consecutive cases. Arch Ophthalmol. 1995;113:62–9.
2. Hayasaka S, Uchida M, Setogawa T. Subretinal hemorrhages with or without choroidal neovascularization in the maculas of patients with pathologic myopia. Graefes Arch Clin Exp Ophthalmol. 1990;228:277–80.
3. Bennett SR, Folk JC, Blodi CF, Klugman M. Factors prognostic of visual outcome in patients with subretinal hemorrhage. Am J Ophthalmol. 1990;109:33–7.
4. Scupola A, Coscas G, Soubrane G, Balestrazzi E. Natural history of macular subretinal hemorrhage in age-related macular degeneration. Ophthalmologica. 1999;213:97–102.
5. Cibis PA, Yamashita T. Experimental aspects of ocular siderosis and hemosiderosis. Am J Ophthalmol. 1959;48(5 Pt2):465–80.

6. Johnson MW, Olsen KR, Hernandez E. Tissue plasminogen activator treatment of experimental subretinal hemorrhage. Retina. 1991;11:250–8.

7. Lewis H, Resnick SC, Flannery JG, Straatsma BR. Tissue plasminogen activator treatment of experimental subretinal hemorrhage. Am J Ophthalmol. 1991;111:197–204.

8. Glatt H, Machemer R. Experimental subretinal hemorrhage in rabbits. Am J Ophthalmol. 1982;94:762–73.

9. Toth CA, Morse LS, Hjelmeland LM, Landers MB 3rd. Fibrin directs early retinal damage after experimental subretinal hemorrhage. Arch Ophthalmol. 1991;109:723–9.

10. Wade EC, Flynn HW Jr, Olsen KR, Blumenkranz MS, Nicholson DH. Subretinal hemorrhage management by pars plana vitrectomy and internal drainage. Arch Ophthalmol. 1990;108:973–8.

11. Peyman GA, Nelson NC Jr, Alturki W, et al. Tissue plasminogen activating factor assisted removal of subretinal hemorrhage. Ophthalmic Surg. 1991;22:575–82.

12. Heriot W. Intravitreal gas and tPA: an outpatient procedure for subretinal haemorrhage. In: Vail vitrectomy meeting 1996; Vail, CO.

13. Ohji M, Saito Y, Hayashi A, Lewis J, Tano Y. Pneumatic displacement of subretinal hemorrhage without tissue plasminogen activator. Arch Ophthalmol. 1998;116:1326–32.

14. Haupert CL, McCuen BW 2nd, Jaffe GJ, et al. Pars plana vitrectomy, subretinal injection of tissue plasminogen activator, and fluid-gas exchange for displacement of thick submacular hemorrhage in age-related macular degeneration. Am J Ophthalmol. 2001;131:208–15.

15. Oshima Y, Ohji M, Tano Y. Pars plana vitrectomy with peripheral retinotomy after injection of preoperative intravitreal tissue plasminogen activator: a modified procedure to drain massive subretinal haemorrhage. Br J Ophthalmol. 2007;91:193–8.

16. Chawla S, Misra V, Khemchandani M. Pneumatic displacement and intravitreal bevacizumab: a new approach for management of submacular hemorrhage in choroidal neovascular membrane. Indian J Ophthalmol. 2009;57:155–7.

17. Liu H, Zhang LY, Li XX, Wu MQ. 23-Gauge vitrectomy with external drainage therapy as a novel procedure to displace massive submacular hemorrhage secondary to polypoidal choroidal vasculopathy. Medicine (Baltimore). 2016;95:e4192.

18. Juan DE, Machemer R. Vitreous surgery for hemorrhagic and fibrous complications of age-related macular degeneration. Am J Ophthalmol. 1988;105:25–9.

19. Vander JF. Tissue plasminogen activator irrigation to facilitate removal of subretinal hemorrhage during vitrectomy. Ophthalmic Surg. 1992;23:361–3.

20. Lewis H. Intraoperative fibrinolysis of submacular hemorrhage with tissue plasminogen activator and surgical drainage. Am J Ophthalmol. 1994;118:559–68.

21. Lim JI, Drews-Botsch C, Sternberg P Jr, Capone A Jr, Aaberg TM Sr. Submacular hemorrhage removal. Ophthalmology. 1995;102:1393–9.

22. Bressler NM, Bressler SB, Childs AL, et al. Surgery for hemorrhagic choroidal neovascular lesions of age-related macular degeneration: ophthalmic findings: SST report no. 13. Ophthalmology. 2004;111:1993–2006.

23. Hesse L, Schmidt J, Kroll P. Management of acute submacular hemorrhage using recombinant tissue plasminogen activator and gas. Graefes Arch Clin Exp Ophthalmol. 1999;237:273–7.

24. Chen CY, Hooper C, Chiu D, Chamberlain M, Karia N, Heriot WJ. Management of submacular hemorrhage with intravitreal injection of tissue plasminogen activator and expansile gas. Retina. 2007;27:321–8.

25. Ron Y, Ehrlich R, Axer-Siegel R, Rosenblatt I, Weinberger D. Pneumatic displacement of submacular hemorrhage due to age-related macular degeneration. Ophthalmologica. 2007;221:57–61.

26. Kitagawa Y, Shimada H, Mori R, Tanaka K, Yuzawa M. Intravitreal tissue plasminogen activator, ranibizumab, and gas injection for submacular hemorrhage in polypoidal choroidal vasculopathy. Ophthalmology. 2016;123:1278–86.

27. Mizutani T, Yasukawa T, Ito Y, et al. Pneumatic displacement of submacular hemorrhage with or without tissue plasminogen activator. Graefes Arch Clin Exp Ophthalmol. 2011;249:1153–7.

28. Fujikawa M, Sawada O, Miyake T, et al. Comparison of pneumatic displacement for submacular hemorrhages with gas alone and gas plus tissue plasminogen activator. Retina. 2013;33:1908–14.

29. Olivier S, Chow DR, Packo KH, MacCumber MW, Awh CC. Subretinal recombinant tissue plasminogen activator injection and pneumatic displacement of thick submacular hemorrhage in Age-Related macular degeneration. Ophthalmology. 2004;111:1201–8.

30. Fleissig E, Barak A, Goldstein M, Loewenstein A, Schwartz S. Massive subretinal and subretinal pigment epithelial hemorrhage displacement with perfluorocarbon liquid using a two-step vitrectomy technique. Graefes Arch Clin Exp Ophthalmol. 2017;255:1341–7.

31. Chang MA, Do DV, Bressler SB, Cassard SD, Gower EW, Bressler NM. Prospective one-year study of ranibizumab for predominantly hemorrhagic choroidal neovascular lesions in age-related macular degeneration. Retina. 2010;30:1171–6.

32. Cho HJ, Koh KM, Kim HS, Lee TG, Kim CG, Kim JW. Anti-vascular endothelial growth factor monotherapy in the treatment of submacular hemorrhage secondary to polypoidal choroidal vasculopathy. Am J Ophthalmol. 2013;156:524–531.e1.

33. Shienbaum G, Garcia Filho CA, Flynn HW Jr, Nunes RP, Smiddy WE, Rosenfeld PJ. Management

of submacular hemorrhage secondary to neovascular age-related macular degeneration with anti-vascular endothelial growth factor monotherapy. Am J Ophthalmol. 2013;155:1009–13.

34. Cho HJ, Koh KM, Kim JH, et al. Intravitreal ranibizumab injections with and without pneumatic displacement for treating submacular hemorrhage secondary to neovascular age-related macular degeneration. Retina. 2015;35:205–12.

35. Shin JY, Lee JM, Byeon SH. Anti-vascular endothelial growth factor with or without pneumatic displacement for submacular hemorrhage. Am J Ophthalmol. 2015;159:904–14.e1.

Development and Experimental Basis for the Future of Prosthetic Vision

33

Penelope J. Allen and Lauren N. Ayton

33.1 Introduction

Despite dramatic advances in modern medicine over the past 100 years, there still remain many causes of severe visual loss which are not amenable to treatment. Since the 1950s, attempts have been made to provide some form of functional vision to the blind, usually by electrically stimulating the components of the visual pathway that have retained function [1]. Neurobionics, the field of direct interfacing electrical devices with sensory neurons, offers hope for patients with profound vision loss. Since the early days of this research field, technology has advanced significantly, and there have now been three regulatory-approved retinal prostheses. In addi-

tion, over 40 groups are currently actively developing and/or commercialising vision prosthesis technology (Fig. 33.1).

The general concept of a vision prosthesis, known colloquially as a "bionic eye", is that it utilises electrical stimulation to replace the function of damaged parts of the visual pathway. This can be via direct electrical stimulation using microelectrode arrays, or via light activation of photodiodes. In the case of the former, the visual scene is captured by a camera, which is usually set on a pair of spectacle frames. The video input can then be edited and filtered to improve patient outcomes [2]. The resulting video stream is converted to electrical signals which are sent either via implanted wires or wirelessly to the implanted microelectrode arrays. Activation of these electrodes causes stimulation of the remaining visual pathway, and the patient will perceive "phosphenes", or spots of light. In the case of photovoltaic arrays, the device is stimulated by direct light energy (either natural light [3] or infrared light [4]). A number of literature reviews have previously covered the differences in these approaches in detail [3, 5–8].

The phosphenes perceived by patients with these implants are not like normal human vision. Prosthetic vision is low resolution (with most available devices having less than 100 electrodes), black and white, and has inherent challenges in terms of motion perception and image fading [9, 10]. Patients who receive the devices

P. J. Allen (✉)
Centre for Eye Research Australia, Royal Victorian Eye and Ear Hospital,
East Melbourne, VIC, Australia

Department of Surgery (Ophthalmology), The University of Melbourne, Parkville, VIC, Australia
e-mail: pjallen@melbourneretina.com.au

L. N. Ayton
Centre for Eye Research Australia, Royal Victorian Eye and Ear Hospital,
East Melbourne, VIC, Australia

Department of Surgery (Ophthalmology), The University of Melbourne, Parkville, VIC, Australia

Department of Optometry and Vision Sciences, The University of Melbourne, Parkville, VIC, Australia
e-mail: layton@unimelb.edu.au
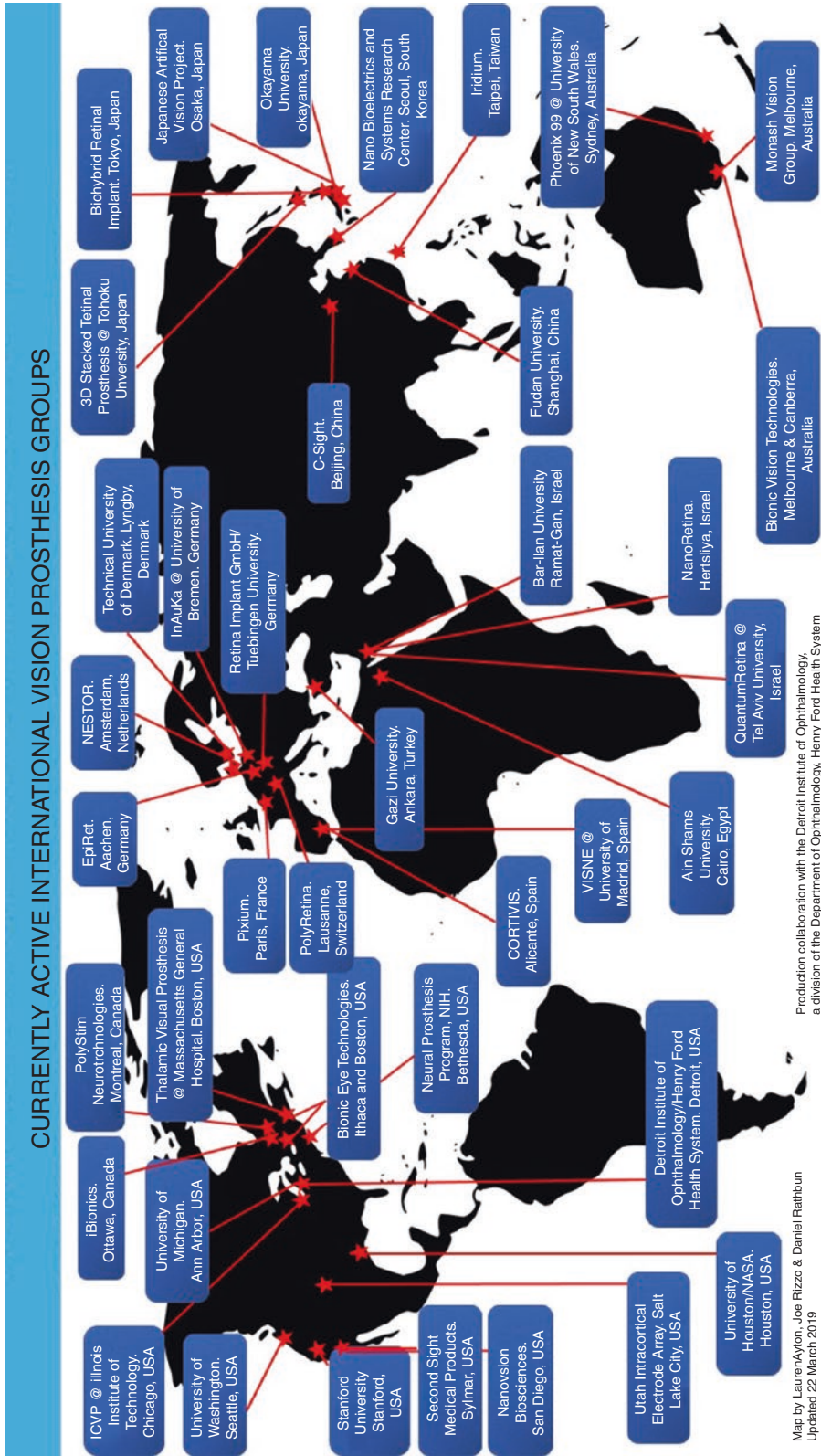
Fig. 33.1 Currently active vision prosthesis research groups, as of March 2019. Image provided by Dr. Lauren Ayton of the HOVER International Taskforce

require significant training and rehabilitation [11], and the best reported visual acuity (20/546) [12] is still well below the legal blindness level. However, despite these limitations, there is strong evidence that the devices have a beneficial effect on patient's quality of life and function [13].

There are many variations in vision prosthesis technology, but one of the major differences between devices is the surgical implantation site. If the cause of the visual loss is located within the outer retina, such as photoreceptor loss in retinal dystrophy, then the residual neuronal elements of the retina can be stimulated. For example, the most common disease to be treated with a retinal prosthesis is retinitis pigmentosa, a hereditary degenerative disease which selectively damages the outer retina whilst relatively sparing the inner retinal ganglion cells [14]. Hence, a retinal prosthesis can utilise the components of the intact visual pathway (inner retina, optic nerve) to transmit device-derived electrical impulses to the visual cortex.

Retinal prostheses can be implanted on top of (epiretinal), in between (subretinal) or behind (suprachoroidal) the neural retina (Fig. 33.2). Prostheses have also been implanted within a scleral pocket (intrascleral). Despite early fears that devices that were further away from the target retinal ganglion cells would not be able to generate perceptions for patients, this has not been the case. Clinical trials have been completed in the epiretinal [15], subretinal [16], suprachoroidal [17] and intrascleral [18] locations, and in all trials patients were able to perceive phosphenes, and showed improvement on certain visual and activity of daily living tasks.

If the eye is severely traumatised, leading to retinal ganglion cell damage or complete severance of the visual pathway, direct electrical stimulation of the optic nerve, lateral geniculate nucleus or visual cortex can be an option. These devices must be constructed from microelectrode arrays, as light cannot penetrate those locations to activate photodiodes. A strong advantage to a posterior visual pathway prosthesis, such as a cortical implant, is that the patient populations that may be helped are more broad and higher in number. Further details on patient selection are provided below. A number of groups are working on cortical devices, and patient clinical trials have commenced by the Second Sight group in the USA, who are developing a device called the Orion™.

33.2 History of Device Development

Although external electrical stimulation of the eye had been known to produce visual percepts from the eighteenth century, limitations in technology and surgical techniques prevented attempts to implant vision prostheses until the mid-twentieth century. The first known patent and published description of a retinal prosthesis was by Tassicker in 1956 [19]. Tassicker, an Australian engineer, recognised that stimulation of residual neuronal elements of the retina after damage to the photoreceptors could produce visual impulses called "phosphenes". He worked to develop a photosensitive disc coated with selenium, which was implanted subretinally in rabbits. Tassicker then collaborated with ophthalmologist Dr. John Bignell to develop the surgical technique, which was completed successfully in a human in the 1960s. Their aim was to implant the device subretinally, but the surgical plane between the choroid and retina could not be determined during surgery and so the device was placed in the suprachoroidal space. Improvements in vitreoretinal surgery techniques in the 1970s [20] allowed the development of more sophisticated retinal prostheses. Surgical procedures for different devices carry different challenges and risks, but all are testament to the skilled vitreoretinal surgeons available today.

The development of vision prosthesis devices to be implanted within the visual cortex dates from the 1920s and 1930s. Initial experiments by the German neurosurgeon Foerster used electrodes to stimulate the visual cortex, showing that the stimulation produced phosphenes which moved when different areas of the cortex were stimulated [21]. Similarly to the development of retinal prostheses, progress of cortical devices has historically been limited until the development

a Second Sight Argus II

b Retina Implant AG Alpha AMS

c Pixium Vision IRIS

IRIS® II
Epi-retinal implant

Fig. 33.2 The three currently regulatory-approved retinal prostheses: (**a**) Argus II ™ by Second Sight Medical Products, (**b**) Alpha AMS™ by Retina Implant AG and (**c**) IRIS™ by Pixium Vision. Images courtesy of the manufacturing companies

of adequate engineering solutions and neurosurgical techniques. However, it is true that cortical prostheses were the original devices in the field, with clinical trials of implantable devices occurring for a number of decades.

In the late 1960s, Brindley published work on a cortical device, which was initially developed in a baboon model [1, 22, 23]. The clinical trials of this early cortical device showed that phosphenes could be elicited with non-penetrating electrodes and that these were constant in the visual field (i.e. stimulation of a particular electrode always led to a percept in the same area of the visual field for the patient) [23]. Significant advances in the field were then made by Dobelle, who implanted 11 patients with a cortical implant [24, 25]. Whilst the results of this trial were encouraging, a number of medical and psychological side effects were noted both during and after the trial [26], which has led to greater scrutiny of trial design and patient well-being during vision prosthesis clinical trials. Currently, at least five groups around the world are working on devices to stimulate the visual cortex, from Australia, the USA, Spain and Canada.

The optic nerve [27, 28] and lateral geniculate nucleus [29, 30] have also been the focus of research attempts to develop visual prosthetic devices. These sites are inherently challenging due to surgical access considerations, and the risks of the required neurosurgical techniques. In addition, it is challenging to produce prosthetic devices with sufficient number of electrodes in a physical form that can be implanted in these inner brain structures.

33.3 Target Patient Population for Retinal Prostheses

To date, all three regulatory-approved devices (Argus II™ by Second Sight Medical Products, USA; Alpha AMS™ by Retina Implant AG, Germany; and IRIS™ by Pixium Vision, France: Fig. 33.2) are retinal prostheses for patients with retinitis pigmentosa (RP). RP is an umbrella term for a genetically heterogeneous group of diseases which are characterised by progressive photoreceptor degeneration [31]. The relative sparing of the inner retinal layers (particularly the retinal ganglion cells [14]) makes RP the key disease target for retinal prostheses, as the devices replace the function of the photoreceptors, and require the residual visual pathway to function. Other outer retinal degenerations may benefit from a retinal prosthesis, such as age-related macular degeneration, but no devices are currently approved for these conditions.

Currently it is estimated that there are 1.5 million people affected by RP worldwide [32], and there is no effective therapeutic option for these patients. RP is a complex range of diseases, which can be autosomal dominant, recessive, X-linked or simplex. Over 260 disease genes have been identified to date [33], presenting significant challenges to clinicians and researchers working in the field. The clinical phenotype of RP can vary significantly, but generally presents with early difficulties with vision in poor lighting (night-time, or dim settings), followed by progressive visual field loss. In many cases, the condition will result in eventual loss of central vision, with some patients progressing to bare or no light perception.

It is this end-stage group of patients for whom retinal prostheses may provide additional visual information to aid them in mobility, navigation and social interaction. To date, all implanted patients have had vision of worse than hand movements in both eyes. However, it is likely that this inclusion criteria will broaden as the technologies improve.

The new target population for retinal prostheses is patients with atrophic age-related macular degeneration (AMD). Currently two clinical trials are studying the use of retinal implants in people with severe central vision loss from AMD, but residual peripheral vision. The Argus II™ epiretinal implant (Second Sight Medical Products, USA) and the PRIMA™ subretinal implant (Pixium Vision, France) are both being used by patients with AMD, and results are expected in late 2019.

33.4 Target Patient Population for Optic Nerve, Lateral Geniculate or Cortical Prostheses

The use of a retinal visual prosthesis requires an intact globe and functioning retinal ganglion cells and optic nerve. Hence, any disease or injury which damages these regions of the visual pathway will prevent the retinal approach being taken. For patients with these conditions and profound vision loss, one option is to implant a device in other regions of the visual pathway, such as the optic nerve, lateral geniculate nucleus or cortex. Potential conditions that may be assisted by posterior visual pathway implants include diabetic retinopathy, glaucoma or severe ocular trauma.

In all clinical trials of vision prosthesis implants to date, it has been assumed that a developed visual cortex is required for effective stimulation. This theory states that congenital blindness cannot be treated with these devices and only patients who have had vision and lost it later in life have been included in clinical trials. However, this has not been investigated to date, and there is a possibility that neuroplasticity, which is greatest in childhood, may actually allow these devices to be used effectively in the young. Future research may consider implanting vision prostheses in children with profound vision loss, or in people with earlier stages of disease (and more residual vision), but the technology is not suitable for these patients at this time.

33.5 Functional Anatomy and Theoretical Background of Prosthetic Vision

Knowledge of the functional anatomy of the visual pathway and its processing elements is crucial for understanding the theory behind the development of prosthetic vision. With these devices, electrodes or photodiodes replace the function of damaged regions of the visual pathway. This external electrical stimulation can depolarise neurons, producing an action potential within the cell which is transmitted by the residual neuronal elements of the retina along the visual pathway to the visual cortex.

In a retinal prosthesis, stimulation of electrodes or photodiodes leads to retinotopically mapped percepts that are relatively stable and predictable [34]. This is similar to the cochleotopic organisation which utilised in the development of a cochlear implant, where stimulation of a particular area of the cochlear reproducibly produces pitch [35]. Patients can learn to interpret these phosphenes for a number of visual tasks, such as orientation in a room, object detection and simple acuity measurements [13]. These recipients of vision prostheses have not had useful vision for many years and the interpretation of prosthetic sight requires significant training. All clinical trials to date have noted improvements over time, showing the importance of this training and the potential benefits of neuroplasticity in improving patient outcomes. At this stage, the visual information provided by current generation devices is still crude and patients have not been able to give up their usual visual aids, such as guide dogs.

One of the challenges with prosthetic vision is that the devices are implanted into tissue which has been affected by the disease state. For example, in RP, histopathological studies have shown that 30% of ganglion cells and 78% of inner nuclear cells are still present in severe disease [14]. However, there is extensive remodelling of the neural retina in end-stage RP [36], which means that the neural connections are not as simple as we would hope. This remodelling occurs in three stages; Phase I is the pre-degeneration period characterised primarily by early markers of photoreceptor stress. Phase II is the period of photoreceptor loss accompanied by glial remodelling of the outer nuclear layer, leaving a glial seal between the remnant neural retina and the remnant RPE/choroid. Phase III is a protracted, life-long period of neural, glial and vascular remodelling of the survivor retina involving over 30 different modifications [36, 37]. This retinal remodelling process appears to be life-long, and may lead to unpredictable percepts when a vision prosthesis is stimulated. An additional challenge is the thinning of the choroid, which correlates

with disease duration and poorer visual acuity [38]. Geographic atrophy secondary to AMD does not produce the same degree of retinal remodelling, and hence one could assume that the responses to vision prosthesis stimulation may be more predictable.

Significant research is underway into better techniques of stimulating visual pathway neurons with prostheses, and it is likely that more targeted stimulation strategies will be possible in the future.

33.6   Epiretinal Vision Prostheses

The epiretinal approach involves attachment of the stimulating electrode or photodiode array to the surface of the retina, which allows direct stimulation of the retinal ganglion cells or axons. The surgical procedure begins with a vitrectomy, followed by an incision over the pars plana to insert the device. Current epiretinal implants are held in place over the macula using a retinal tack, such as in the Second Sight Argus II™ implant [39]. Alternative options, such as magnets, have been investigated for stabilising epiretinal devices in place [40], but these are not yet available commercially.

The percepts provided by epiretinal implants are often "streak-like", due to the direct stimulation of the arcuate retinal ganglion cell axons on the epiretinal surface. However, this is balanced by the benefits of an epiretinal location, including lower stimulation thresholds and ability to use the vitreous cavity as a heat sink, reducing the risk of thermal damage to the retina [41].

The first epiretinal prosthetic device to be implanted in a human clinical trial was Second Sight Medical Products' Argus I™, which was a 16-electrode device. The second-generation Argus II™ is a 60-electrode device and received FDA regulatory approval in 2011. Patients have been implanted with the Second Sight epiretinal devices for well over 10 years, and still are able to obtain benefit from their devices over this extended time frame [42]. Full details of the Second Sight device are outlined further in an additional chapter in this textbook.

The other notable epiretinal implant was commercialised by Pixium Vision (France), who conducted a human clinical trial of their IRIS™ device to obtain CE market approval in Europe in 2016. Their device has 150 stimulating electrodes and was developed using technology from the German EpiRet consortium [43]. Manufacture of the IRIS™ has recently been halted due to the successful pilot trial of Pixium Vision's second-generation device, the PRIMA (see below).

33.7   Subretinal Vision Prostheses

This approach also commences with a vitrectomy surgery, and then the device is implanted from an external approach to the eye, via a scleral incision. The retina is detached and the subretinal space is dissected to form a "pocket". The electrode array is then advanced in this subretinal pocket and placed beneath the fovea. Whilst the surgical techniques to implant a subretinal implant are more complicated that the epiretinal approach, the device is inherently more stable due to the location. In addition, subretinal prostheses benefit from close apposition to the neural retina (particularly the bipolar cells); hence they require lower levels of charge than more posterior implants (such as suprachoroidal and intrascleral).

The first group to implant vision prostheses in the subretinal space was Optobionics (USA), who developed the "artificial retina" silicon photodiode microchip. This device was implanted in six patients in a pilot clinical trial. Unfortunately, the natural incident light was insufficient to generate useful phosphenes [44, 45].

The leading proponents of the subretinal approach in contemporary research are Retina Implant AG (Germany), Pixium Vision (France), Bionic Eye Technologies (USA) and Iridium (Taiwan).

Retina Implant AG has developed two devices, the first-generation Alpha IMS™ and the second-generation Alpha AMS™. Both have been successful in clinical trials [16, 46–48], and have been approved through the EU regulatory processes (CE Mark). The devices use arrays of 1600

photodiodes, and significant improvements were made to length the device lifetime in between iterations. To date, the Alpha devices have only been used in patients with RP or choroideremia.

Recently, Pixium Vision has announced early results of their PRIMA photovoltaic subretinal prosthesis in patients with geographic atrophy due to age-related macular degeneration [49]. They have reported that patients were able to perceive phosphenes in their previously blind central vision (at the location of the geographic atrophy) and a best visual acuity of 20/500, which is the highest acuity reported to date [49]. Full clinical trial results are anticipated in late 2019.

One of the other founding groups of the modern era, the Boston Retinal Implant Project, started development with an epiretinal implant, but changed to a subretinal design. The group spun off to a commercial company (Bionic Eye Technologies) in 2012 and are currently completing preclinical evaluations of a subretinal implant [50]. No clinical trials of this subretinal device have occurred at this date.

Iridium, a Taiwanese company founded by Prof. Long-Sheng Fan, is also working on a subretinal implant [51], with clinical trials expected in the near future.

33.8 Suprachoroidal and Intrascleral Vision Prostheses

To date, two groups have conducted clinical trials of implants behind the choroid (the posterior blood supply of the eye). The main advantage with these locations is surgical access and device stability. The devices are held securely in pockets either between the choroid and sclera (suprachoroidal) or within the scleral tissue (intrascleral). However, this does mean that the electrodes are further away from the target retinal ganglion cells, requiring higher levels of charge to generate phosphenes.

The Japanese group in Osaka developed a 49-channel "suprachoroidal transretinal stimulation prosthesis" (STS) which is placed within a pocket dissected within the sclera. This was a second-generation device, developed from a pro-

totype nine-electrode array. The efficacy of the intrascleral devices is optimised by the fact that the sclera between the device and the choroid atrophies to a moderate degree, so that the device effectively stimulates within the suprachoroidal space. The clinical trial report of three patients (implanted for 1 year) showed improved functional vision with the device "on" compared to device "off"; however this was strongly correlated to the alignment of the device with the fovea [18]. Hence, surgical accuracy in the implantation is paramount.

Two other suprachoroidal projects currently are underway in Australia. Both originated from an Australian-wide consortium called Bionic Vision Australia, which ran from 2010 to 2016. This project resulted in the world-first trial of a suprachoroidal implant, which showed that the device was stable over a 2-year implant period, and provided functional benefit to patients [17]. After this, a commercial company spun out (Bionic Vision Technologies), which now funds work by the Centre for Eye Research Australia, the Bionics Institute, CSIRO and The University of Melbourne. This has recently led to a clinical trial of a second-generation suprachoroidal prosthesis (44 channels), which will conclude in 2020.

The other spin-off suprachoroidal device from the Bionic Vision Australia consortium was the Phoenix 99 [52], which is currently being developed at the University of New South Wales.

It still remains to be seen whether the safer surgical approaches of the suprachoroidal and intrascleral approaches are of sufficient benefit to balance the disadvantage of being further away from the residual retinal ganglion cells. However, the clinical outcomes to date are comparable, with no significant differences in patient outcomes with different device locations, showing that retinal prostheses in all locations can be of benefit.

33.9 Optic Nerve and Lateral Geniculate Nucleus

Direct stimulation of the optic nerve has been studied by several groups, with two main device designs. Firstly, the approach of a "cuff" elec-

trode consists of a series of planar electrodes which are wrapped around the nerve. Secondly, some devices have penetrating microelectrodes, which are inserted into the centre of the nerve. Optic nerve approaches have been tested in both preclinical animal models [53] and human patients [28, 54]. The surgery to implant an optic nerve prosthesis is technically difficult, due to the small size of the optic nerve and the distribution of retinal ganglion cell axons. Initial surgical approaches were to implant the devices in the intracranial portion of the nerve, which obviously has the risk profile of intracranial surgery. More recently, a surgical approach via the medial orbit has been successful and seems more prudent.

Not unexpectedly, stimulation of a "cuff" device produces activation of multiple axons and larger phosphenes, whilst stimulation with penetrating microelectrodes results in more targeted and discrete percepts. Despite these restrictions, preliminary results of the "cuff" device demonstrate that patients are able to achieve object localisation, discrimination and grasping using this device [55].

The lateral geniculate nucleus of the thalamus is the site of the synapse between the retinal ganglion cell axons and neurons that project to the primary visual cortex [56]. As it consists of six layers of cells with almost one-to-one anatomical mapping from the retina, it is considered as a possible site for a visual prosthesis [30]. Electrical stimulation of the LGN in primates has been completed [29], but human clinical trials have not yet occurred.

33.10 The Cortical Approach

There are four main groups working on cortical visual prostheses, located in the USA, Australia, Spain and Canada. To date, the only contemporary clinical trial of a cortical prosthesis is being completed by Second Sight Medical Products (USA), using the Orion™ implant.

The attraction of the cortical approach is that it could be a solution for the many severely visually impaired patients who have no functional eye or optic nerve. This patient population could include victims of severe ocular trauma (e.g. explosive or war injuries) and patients with end-stage glaucoma. In general, the cortical approach consists of a device which stimulates the occipital cortex, which is usually controlled and powered transcutaneously by an extracorporeal transmitter placed outside the head. In contrast to the historical work of Brindley and Dobelle (1960s and 1970s, respectively), current devices incorporate penetrating microelectrodes which enable much lower currents to stimulate the cortical tissue. However, the implantation of penetrating cortical electrode arrays is a major neurosurgical procedure. As with any surgery involving the opening of the skull and intradural space, there is a demonstrable risk of acute and longer term complications, which can result in a poor surgical and clinical outcome. These risks include, but are not limited to, postoperative haemorrhage, swelling, tissue infarction, infection, seizures and neurological deficits [57]. Hence, as with all vision prostheses, patient selection needs to be rigorous and informed consent thoroughly performed.

The Illinois Intracortical Visual Prosthesis (IIVP) is a device being developed by the Laboratory of Neural Prosthetic Research at the Illinois Institute of Technology, USA. Technical advances by the team have included the development of a multichannel device [58], development of specialised surgical tools [59] and generation of algorithms to encoding the artificial visual information input specifically for the cortex [58]. This team plan to implant their devices as a series of small discs containing 16 electrodes within a 5 mm disc, to tile to a total of 600–650 electrodes.

Second Sight Medical Products (USA) is currently undertaking clinical trials of a cortical prosthesis called the Orion™. The first Orion™ surgery was completed in 2018, and results are expected to be reported during the second half of 2019.

Monash Vision Group (MVG) is an Australian collaborative partnership between Monash University, Grey Innovation, MiniFAB and Alfred Health. MVG is developing a cortical vision prosthesis known as the "Gennaris" bionic

vision system. The system consists of up to 11 devices or "tiles" that have been surgically implanted in the primary visual cortex of the brain. Each tile houses its own circuitry, wireless receiver and 43 hair-thin microelectrodes which will penetrate the occipital cortex. Currently the Monash Vision Group is conducting preclinical trials in an animal model with plans to commence human implantation surgery in 2019.

CORTIVIS is a European collaborative group involving six university laboratories, one technological research centre and one company with experience in biomedical devices. They are based in Alicante, Spain. The group is conducting preclinical work towards a penetrating microarray and has completed initial proof-of-concept trials in sighted volunteers (who were undergoing neurosurgery for other medical conditions).

33.11   Patient-Centred Outcomes

One of the challenges in the field of vision restoration is how to accurately measure and report patient outcomes with these emerging technologies. At this time, vision prostheses are not able to restore high-resolution vision to recipients, and hence novel and sensitive outcome measures have had to be developed. To generate consensus in this field, and ensure transparency for clinicians, scientists and patients, an international taskforce was formed in 2012. The Harmonization of Outcomes and Vision Endpoints in Vision Restoration Trials (HOVER) Taskforce consists of over 80 of the world leaders in the areas of vision prostheses, stem cells, gene therapy, low vision and functional vision, and has generated a set of guidelines [60]. These will be available freely for use by those in the field at www.artificialvision.org.

33.12   Future Directions

33.12.1   Current Steering

A significant challenge in vision prostheses is that there is a limit to how small the electrodes

can be manufactured, in order to maintain safe stimulation parameters. For example, as an electrode becomes smaller, the electrical thresholds will increase due to increased electrode impedance, hence requiring higher stimulation levels and raising safety concerns. In addition, the retinal activation resulting from each electrode is not pointlike; instead each electrode introduces a spread of retinal activation that may overlap with activations from other electrodes. With most conventional stimulation strategies this overlap leads to image blur [61, 62]. Hence, there is now significant work underway into a technique called "current steering", which is able to manipulate the current sent to different electrodes to shape the receptive fields, hence improving potential acuity outcomes [62–64].

33.12.2   Vision Processing

One of the main advantages with a camera-based vision prosthesis system is the ability to manipulate the video image to optimise outcomes. In a basic set-up, a vision prosthesis system identifies brightness in an image, such that areas on an electrode array that map to a bright region have higher stimulation (which results in a brighter phosphene). However, this is only useful if the most salient feature of the visual scene is the brightness differences. Often, the needs of the user are more complex.

Hence, another area of great interest and research is in vision processing. Using computer science and algorithms, it is possible to enhance the translation of the digital image into electrical stimulation. For example, an algorithm known as the Lanczos filter has been shown to improve light localisation for patients with a suprachoroidal retinal prosthesis [2]. Some devices now have the ability to change between modes, such as contrast enhancement or inversion of black and white. The other filter of significant interest is augmented depth, which has been shown to improve outcomes in mobility tasks [65]. Vision processing will continue to play a significant role in current and future prosthetic devices.

33.12.3   Stimulation Strategies

The phosphenes produced by vision prostheses vary in size, shape and complexity. In many devices, there is also overlap of phosphenes [34]. To add to the challenges when evaluating phosphene vision, all of these factors vary from patient to patient. There are some consistent findings in terms of stimulation protocols; increasing stimulation levels above threshold will increase phosphene intensity, change in stimulus rate (Hz) can result in alteration in the "fullness" of the phosphene, whilst varying the phase width can result in alteration of hue. Interestingly, studies of both epiretinal [66] and suprachoroidal [34, 67, 68] devices confirm these findings. Work is ongoing into determining the best stimulation strategies for different device designs, and these improvements in "software" will be able to be supplied to patients with existing implants.

An area of particular interest in stimulation strategy research is the idea of selectively targeting specific cell types with electrode stimulation. In current devices, the stimulation is applied to a relatively large area of neurons, with cells indiscriminately stimulated. Research is now focused on understanding whether it is possible to target specific cell classes within the retina (i.e. retinal ganglion cells, bipolar cells, photoreceptors). Even more specifically, it has been proposed that stimulation could be designed to selectively activate targeted retinal ganglion cell subtypes [69], of which over 30 have been reported in the mouse retina [70]. Each of these subtypes conveys a different feature of the visual world to the brain; therefore, selective activation of RGC types could refine the image perceived by retinal implant recipients. Such refinements could reasonably include better spatial and temporal contrast and full colour vision.

33.13   Conclusion

The field of vision prostheses has grown and matured significantly in the past three decades. From early pilot studies of cortical implants, we now have access to a number of more advanced devices, which can be implanted in a range of visual pathway locations. Indeed, vision prosthe-ses are currently the only regulatory-approved treatment option for people with profound vision loss from retinitis pigmentosa, with three devices having market approval.

However, the scientists are not resting on their laurels. Work continues at a rapid pace to explore and understand the best device designs, surgical techniques and implant locations, and material science. The field has come together recently to generate a consensus document on the assessment and reporting of outcomes in vision prosthesis clinical trials, which will lead to greater transparency for people with vision loss, their clinicians and the broader public.

Research programmes are now concentrating on how to improve the stimulation of vision prostheses, through strategies such as current steering, vision processing and more specific stimulation strategies. These efforts will lead to improved devices for patients in the future. It is also believed that as the technologies advance, the number of people who can be helped by these devices will also grow (as, for example, the devices become approved for age-related macular degeneration or earlier stages of vision loss).

This is a rapidly changing field, and one that practicing ophthalmologists, optometrists, orthoptists and other health professionals should be aware of. In the future, it is the hope of all of those in the field that we will find cures for the common eye diseases, and interventions for blindness will no longer be needed. Until then, vision prostheses are bringing hope to millions of people with profound vision loss.

References

1. Brindley GS, Lewin WS. The sensations produced by electrical stimulation of the visual cortex. J Physiol. 1968;196(2):479–93.
2. Barnes N, Scott AF, Lieby P, Petoe MA, McCarthy C, Stacey A, et al. Vision function testing for a suprachoroidal retinal prosthesis: effects of image filtering. J Neural Eng. 2016;13(3):036013.
3. Zrenner E. Fighting blindness with microelectronics. Sci Transl Med. 2013;5(210):210ps16.
4. Lorach H, Goetz G, Smith R, Lei X, Mandel Y, Kamins T, et al. Photovoltaic restoration of sight with high visual acuity. Nat Med. 2015;21(5):476–82.

5. Goetz GA, Palanker DV. Electronic approaches to restoration of sight. Rep Prog Phys. 2016;79(9):096701.

6. Weiland JD, Walston ST, Humayun MS. Electrical stimulation of the retina to produce artificial vision. Annu Rev Vis Sci. 2016;2:273–94.

7. Lewis PM, Ayton LN, Guymer RH, Lowery AJ, Blamey PJ, Allen PJ, et al. Advances in implantable bionic devices for blindness: a review. ANZ J Surg. 2016;86(9):654–9.

8. Brandli A, Luu CD, Guymer RH, Ayton LN. Progress in the clinical development and utilization of vision prostheses: an update. Eye Brain. 2016;8:15–25.

9. Sekhar S, Jalligampala A, Zrenner E, Rathbun DL. Tickling the retina: integration of subthreshold electrical pulses can activate retinal neurons. J Neural Eng. 2016;13(4):046004.

10. Freeman DK, Fried SI. Multiple components of ganglion cell desensitization in response to prosthetic stimulation. J Neural Eng. 2011;8(1):016008.

11. Geruschat DR, Bittner AK, Dagnelie G. Orientation and mobility assessment in retinal prosthetic clinical trials. Optom Vis Sci. 2012;89(9):1308–15.

12. Stingl K, Bartz-Schmidt KU, Gekeler F, Kusnyerik A, Sachs H, Zrenner E. Functional outcome in subretinal electronic implants depends on foveal eccentricity. Invest Ophthalmol Vis Sci. 2013;54(12):7658–65.

13. Geruschat DR, Richards TP, Arditi A, da Cruz L, Dagnelie G, Dorn JD, et al. An analysis of observer-rated functional vision in patients implanted with the Argus II Retinal Prosthesis System at three years. Clin Exp Optom. 2016;99(3):227–32.

14. Santos A, Humayun MS, de Juan E Jr, Greenburg RJ, Marsh MJ, Klock IB, et al. Preservation of the inner retina in retinitis pigmentosa. A morphometric analysis. Arch Ophthalmol. 1997;115(4):511–5.

15. Humayun MS, Dorn JD, da Cruz L, Dagnelie G, Sahel JA, Stanga PE, et al. Interim results from the international trial of Second Sight's visual prosthesis. Ophthalmology. 2012;119(4):779–88.

16. Stingl K, Bartz-Schmidt KU, Besch D, Chee CK, Cottriall CL, Gekeler F, et al. Subretinal visual implant alpha IMS—clinical trial interim report. Vis Res. 2015;111(Pt B):149–60.

17. Ayton LN, Blamey PJ, Guymer RH, Luu CD, Nayagam DAX, Sinclair NC, et al. First-in-human trial of a novel suprachoroidal retinal prosthesis. PLoS One. 2014;9(12):e115239.

18. Fujikado T, Kamei M, Sakaguchi H, Kanda H, Endo T, Hirota M, et al. One-year outcome of 49-channel suprachoroidal-transretinal stimulation prosthesis in patients with advanced retinitis pigmentosa. Invest Ophthalmol Vis Sci. 2016;57(14):6147–57.

19. Tassicker GE. Preliminary report on a retinal stimulator. Br J Physiol Opt. 1956;13(2):102–5.

20. Machemer R, Buettner H, Norton EW, Parel JM. Vitrectomy: a pars plana approach. Trans Am Acad Ophthalmol Otolaryngol. 1971;75(4):813–20.

21. Foerster O. Contributions to the pathophysiology of the visual pathway and visual sphere. J Psychol Neurol. 1929;39:435–63.

22. Brindley GS, Lewin WS. The visual sensations produced by electrical stimulation of the medial occipital cortex. J Physiol. 1968;194(2):54–P.

23. Brindley GS, Donaldson PE, Falconer MA, Rushton DN. The extent of the region of occipital cortex that when stimulated gives phosphenes fixed in the visual field. J Physiol. 1972;225(2):57P–8P.

24. Dobelle WH, Mladejovsky MG. Phosphenes produced by electrical stimulation of human occipital cortex, and their application to the development of a prosthesis for the blind. J Physiol. 1974;243(2):553–76.

25. Dobelle WH. Artificial vision for the blind by connecting a television camera to the visual cortex. ASAIO J. 2000;46(1):3–9.

26. Lane FJ. Methods and results from interviews of eleven recipients of a visual cortex implant: an analysis of their experiences. In: The Eye and the Chip: World Congress on Artificial Vision; Detroit, Michigan. 2012.

27. Brelen ME, Duret F, Gerard B, Delbeke J, Veraart C. Creating a meaningful visual perception in blind volunteers by optic nerve stimulation. J Neural Eng. 2005;2(1):S22–8.

28. Brelen ME, Vince V, Gerard B, Veraart C, Delbeke J. Measurement of evoked potentials after electrical stimulation of the human optic nerve. Invest Ophthalmol Vis Sci. 2010;51(10):5351–5.

29. Pezaris JS, Reid RC. Demonstration of artificial visual percepts generated through thalamic microstimulation. Proc Natl Acad Sci U S A. 2007;104(18):7670–5.

30. Pezaris JS, Eskandar EN. Getting signals into the brain: visual prosthetics through thalamic microstimulation. Neurosurg Focus. 2009;27(1):E6.

31. Hartong DT, Berson EL, Dryja TP. Retinitis pigmentosa. Lancet. 2006;368(9549):1795–809.

32. Bunker CH, Berson EL, Bromley WC, Hayes RP, Roderick TH. Prevalence of retinitis pigmentosa in Maine. Am J Ophthalmol. 1984;97(3):357–65.

33. Daiger SP, Sullivan LS, Bowne SJ. RetNet: Retinal Information Network. In: The University of Texas-Houston Health Science Center, editor. https://sph.uth.edu/retnet/2019.

34. Petoe MA, McCarthy CD, Shivdasani MN, Sinclair NC, Scott AF, Ayton LN, et al. Determining the contribution of retinotopic discrimination to localization performance with a suprachoroidal retinal prosthesis. Invest Ophthalmol Vis Sci. 2017;58(7):3231–9.

35. Fallon JB, Irvine DR, Shepherd RK. Cochlear implants and brain plasticity. Hear Res. 2008;238(1–2):110–7.

36. Jones BW, Pfeiffer RL, Ferrell WD, Watt CB, Marmor M, Marc RE. Retinal remodeling in human retinitis pigmentosa. Exp Eye Res. 2016;150:149–65.

37. Jones BW, Marc RE. Retinal remodeling during retinal degeneration. Exp Eye Res. 2005;81(2):123–37.

38. Ayton LN, Guymer RH, Luu CD. Choroidal thickness profiles in retinitis pigmentosa. Clin Exp Ophthalmol. 2013;41(4):396–403.

39. Humayun MS, Dorn JD, Ahuja AK, Caspi A, Filley E, Dagnelie G, et al. Preliminary 6 month results from the Argus II epiretinal prosthesis feasibility study. Conf Proc IEEE Eng Med Biol Soc. 2009;2009:4566–8.

40. Fox K, Meffin H, Burns O, Abbott CJ, Allen PJ, Opie NL, et al. Development of a magnetic attachment method for bionic eye applications. Artif Organs. 2016;40(3):E12–24.

41. Opie NL, Burkitt AN, Meffin H, Grayden DB. Heating of the eye by a retinal prosthesis: modeling, cadaver and in vivo study. IEEE Trans Biomed Eng. 2012;59(2):339–45.

42. Yue L, Falabella P, Christopher P, Wuyyuru V, Dorn J, Schor P, et al. Ten-year follow-up of a blind patient chronically implanted with epiretinal prosthesis Argus I. Ophthalmology. 2015;122(12):2545–52.e1.

43. Roessler G, Laube T, Brockmann C, Kirschkamp T, Mazinani B, Goertz M, et al. Implantation and explantation of a wireless epiretinal retina implant device: observations during the EPIRET3 prospective clinical trial. Invest Ophthalmol Vis Sci. 2009;50(6):3003–8.

44. Chow AY, Peachey N. The subretinal microphotodiode array retinal prosthesis II. Ophthalmic Res. 1999;31(3):246.

45. Chow AY, Peachey NS. The subretinal microphotodiode array retinal prosthesis. Ophthalmic Res. 1998;30(3):195–8.

46. Gekeler K, Bartz-Schmidt KU, Sachs H, MacLaren RE, Stingl K, Zrenner E, et al. Implantation, removal and replacement of subretinal electronic implants for restoration of vision in patients with retinitis pigmentosa. Curr Opin Ophthalmol. 2018;29(3):239–47.

47. Stingl K, Schippert R, Bartz-Schmidt KU, Besch D, Cottriall CL, Edwards TL, et al. Interim results of a multicenter trial with the new electronic subretinal implant alpha AMS in 15 patients blind from inherited retinal degenerations. Front Neurosci. 2017;11:445.

48. Edwards TL, Cottriall CL, Xue K, Simunovic MP, Ramsden JD, Zrenner E, et al. Assessment of the electronic retinal implant alpha AMS in restoring vision to blind patients with end-stage retinitis pigmentosa. Ophthalmology. 2018;125(3):432–43.

49. Ishaque K, Palanker DV, Sahel JA, Holz FG, editors. An update on promising results with PRIMA in advanced dry-AMD. Pixium Vision KOL Meeting; 5 March 2019; Paris. https://www.pixium-vision.com/file_bdd/dynamic_content/file_pdf_pdf_en/1554369769_KOLMeetingslides.pdf.

50. Rizzo JF 3rd, Shire DB, Kelly SK, Troyk P, Gingerich M, McKee B, et al. Overview of the Boston retinal prosthesis: challenges and opportunities to restore useful vision to the blind. Conf Proc IEEE Eng Med Biol Soc. 2011;2011:7492–5.

51. Yang F, Yang CH, Wang FM, Cheng YT, Teng CC, Lee LJ, et al. A high-density microelectrode-tissue-microelectrode sandwich platform for application of retinal circuit study. Biomed Eng Online. 2015;14:109.

52. Bareket L, Barriga-Rivera A, Zapf MP, Lovell NH, Suaning GJ. Progress in artificial vision through suprachoroidal retinal implants. J Neural Eng. 2017;14(4):045002.

53. Yan Y, Lu Y, Li M, Ma Z, Cao P, Chen Y, et al. Electrically evoked responses in the rabbit cortex induced by current steering with penetrating optic nerve electrodes. Invest Ophthalmol Vis Sci. 2016;57(14):6327–38.

54. Brelen ME, De Potter P, Gersdorff M, Cosnard G, Veraart C, Delbeke J. Intraorbital implantation of a stimulating electrode for an optic nerve visual prosthesis. Case report. J Neurosurg. 2006;104(4):593–7.

55. Duret F, Brelen ME, Lambert V, Gerard B, Delbeke J, Veraart C. Object localization, discrimination, and grasping with the optic nerve visual prosthesis. Restor Neurol Neurosci. 2006;24(1):31–40.

56. Kandel ER, Schwartz JH, Jessell TM, Siegelbaum SA, Hudspeth AJ. Principles of neural science. 5th ed. New York: McGraw-Hill; 2012.

57. Lewis PM, Ackland HM, Lowery AJ, Rosenfeld JV. Restoration of vision in blind individuals using bionic devices: a review with a focus on cortical visual prostheses. Brain Res. 2015;1595:51–73.

58. Srivastava NR, Troyk PR. Some solutions to technical hurdles for developing a practical intracortical visual prosthesis device. Conf Proc IEEE Eng Med Biol Soc. 2006;1:2936–9.

59. Tawakol O, Bredeson SD, Troyk PR. Preparation of a neural electrode implantation device for in-vivo surgical use. Conf Proc IEEE Eng Med Biol Soc. 2016;2016:4507–10.

60. Ayton LN, Rizzo JF 3rd, Bailey I, Colenbrander A, Dagnelie G, Geruschat DR, et al. The harmonization of outcomes and vision endpoints in vision restoration trials (HOVER) consensus document. Trans.Vis. Sci. Tech. 2020;9(8):25.

61. Spencer TC, Fallon JB, Shivdasani MN. Creating virtual electrodes with two-dimensional current steering. J Neural Eng. 2018;15(3):035002.

62. Spencer M, Kameneva T, Grayden DB, Meffin H, Burkitt AN. Global activity shaping strategies for a retinal implant. J Neural Eng. 2019;16(2):026008.

63. Spencer TC, Fallon JB, Shivdasani MN. Creating virtual electrodes with 2D current steering. J Neural Eng. 2018;15(3):035002.

64. Dumm G, Fallon JB, Williams CE, Shivdasani MN. Virtual electrodes by current steering in retinal prostheses. Invest Ophthalmol Vis Sci. 2014;55(12):8077–85.

65. McCarthy C, Walker JG, Lieby P, Scott A, Barnes N. Mobility and low contrast trip hazard avoidance using augmented depth. J Neural Eng. 2015;12(1):016003.

66. Davuluri NS, Nimmagadda K, Petrossians A, Humayun MS, Weiland JD. Strategies to improve

stimulation efficiency for retinal prostheses. Conf Proc IEEE Eng Med Biol Soc. 2016;2016:3133–8.

67. Shivdasani MN, Sinclair NC, Gillespie LN, Petoe MA, Titchener SA, Fallon JB, et al. Identification of characters and localization of images using direct multiple-electrode stimulation with a suprachoroidal retinal prosthesis. Invest Ophthalmol Vis Sci. 2017;58(10):3962–74.

68. Petoe MA, Shivdasani MN. Are long stimulus pulse durations the answer to improving spatial resolution in retinal prostheses? Ann Transl Med. 2016;4(21):434.

69. Rathbun DL, Ghorbani N, Shabani H, Zrenner E, Hosseinzadeh Z. Spike-triggered average electrical stimuli as input filters for bionic vision: a perspective. J Neural Eng. 2018;15(6):063002.

70. Baden T, Berens P, Franke K, Roman Roson M, Bethge M, Euler T. The functional diversity of retinal ganglion cells in the mouse. Nature. 2016;529(7586): 345–50.

Argus II Prosthetic Vision

34

Young Hee Yoon, Lan Yue, and Mark S. Humayun

34.1 Introduction

The Argus II Retinal Prosthesis (Second Sight Medical Products Inc., Sylmar, CA, USA) is the first artificial visual implant commercially approved by the U.S. Food and Drug Administration (FDA) [1]. It is indicated for patients with end-stage retinitis pigmentosa (RP) in both eyes [2]. The Argus II has also been approved in many countries in the European Union, as well as Saudi Arabia, Canada, South Korea, and Russia, and to date, nearly 300 patients worldwide have received the implants.

The Argus II when activated results in electrically elicited visual perceptions (phosphenes) in patients who otherwise have very limited vision. After implantation, the patients must then train

using the Argus II in order to maximize the ability to use the implant to help in orientation and mobility (i.e., recognize objects). Candidates for surgery must be carefully selected to ensure that they have realistic expectations of the level of vision they might gain and they must be fully committed to undergoing visual rehabilitation and training with Argus II after surgery.

This chapter mainly focuses on the Argus II retinal prosthesis in the biomedical engineering aspects and the clinical aspects, with a brief discussion of future development and perspectives.

34.2 Biomedical Engineering Aspects of Visual Prostheses

34.2.1 Background

34.2.1.1 Visual Prosthesis

Generation of light perception, interestingly, does not always involve light entering the eye. In the fifth century B.C., ancient Greeks noted in literature of visual percepts arising from mechanical pressure to the eyeball [3], later termed phosphene. Flashing forward to the eighteenth century, another light perception rendering mechanism was discovered—LeRoy created light sensation in a blind by passing electrical currents around the head. If this was considered perhaps a fortuitous finding, more systematic investigations of the susceptibility of visual cortex to electrical

Young Hee Yoon and Lan Yue contributed equally to this work.

Y. H. Yoon (✉)
Department of Ophthalmology, Asan Medical Center, University of Ulsan College of Medicine, Seoul, South Korea
e-mail: yhyoon@amc.seoul.kr

L. Yue · M. S. Humayun
Department of Ophthalmology, USC Roski Eye Institute, University of Southern California, Los Angeles, CA, USA

USC Institute for Biomedical Therapeutics, University of Southern California, Los Angeles, CA, USA
e-mail: lyue@usc.edu; humayun@usc.edu

stimulation were reported in late 1920s and early 1930s [4, 5]. It was discovered that direct application of the electrical pulses to the visual cortex elicited phosphene perceptions in both sighted and blind subjects. More specifically, these pilot works showed that point stimulation led to localized perception in the visual field, indicating that the visual cortex remained capable of generating spatially differentiated light sensations after deprivation of vision for years.

Such research paved the path for the very first prototype cortical visual prosthesis, which was implanted in 1968. This device contained an array of 80 intracranial electrodes driven by a wirelessly powered extracranial radio-frequency receiver. A 52-year-old blind woman surgically implanted with the device reported seeing phosphenes in the forms of points, spots, and bars of light upon activation of the electrodes [6]. Significance of this work is twofold: (1) it demonstrated the possibility to use a chronically implanted electrode array to restore form vision and (2) the basic architecture of the device offered the blueprint to later visual prostheses and had continued influence today. In the 1970s, a modified design incorporating a television camera was carried out, bridging the gap between stimulation and visual inputs. This device enabled a blind subject to perceive discrete phosphenes and recognize simple patterns including large letters [7].

Despite the early success, development of cortical visual prosthesis remained relatively slow in recent decades, primarily due to concerns of surgical risks and, perhaps more importantly, the difficulty to map the visual input to the electrical output, given the complex visual processing that occurs in the visual pathway upstream of the visual cortex. Rather, recent efforts have been largely focused on the development of implants that are placed in proximity to the retina for easier access, lower surgical risks, well-preserved retinotopic mapping, as well as the ability to take advantage of the remaining retinal circuitry for visual processing. Research in this area produced two commercially available visual prostheses: Argus II from the Second Sight Medical Products Inc. (USA) and the Alpha-IMS from Retina Implant AG (Germany). Argus II is an epiretinal

implant, sitting on the innermost layer of the retina whereas Alpha-IMS is a subretinal implant that is embedded between retina and RPE. Both devices have received CE Mark approval in Europe and in addition Argus II received U.S. Food and Drug Administration (FDA) market approval in 2013. It is noteworthy that based on Argus II, the same company produced the Orion I cortical visual prosthesis system that was implanted in the first patient in January, 2018, as part of a feasibility clinical study.

34.2.1.2 Development of the Argus II System

In the 1990s, Humayun et al. demonstrated that electrical stimulation delivered from a multielectrode array to retina generated phosphenes in the blind subjects. The subjects reported retinotopically consistent perceptions in their visual field and they were able to track the phosphenes as the electrode moved across the retina [8]. Corroborating with these findings, another proof-of-concept study by Rizzo et al. showed that acute stimulation at two retinal locations produced two distinguishable phosphenes [9]. These key pilot studies revealed the retinotopic mapping between the sites of stimulation and the locations of the phosphenes generated, further demonstrating the feasibility of using multi-foci stimulation of the retina to elicit visual percepts that, to some degree, reflect the stimulation pattern. These findings laid the groundwork for a series of retinal prostheses, including the Argus I and II systems.

Argus I is the first-generation epiretinal prosthesis approved for an investigational clinical trial by the FDA. Studies with the Argus I demonstrated the safety and effectiveness of long-term retinal stimulation, motivating the development of the more advanced Argus II system [10–14]. Argus I was a modified cochlear implant containing 16 electrodes in a 4-by-4 array with a center-to-center separation of 800 μm. Two electrode diameters, 250 μm and 500 μm, were used to determine how size affected impedance and perceptual threshold, i.e., the minimum current that is needed to generate light perception. Clinical studies using arrays with alternating electrode

sizes showed that size was not as important as other factors such as stimulation amplitude and frequency, and that the threshold was low enough to allow even greater reduction in electrode size [12]. As a result, a reduced electrode diameter was used in Argus II to allow for a higher electrode count in the array—Argus II contains an array of 6-by-10 electrodes of 225 μm diameter, separated by 525 μm. Compared with its precedent, Argus II not only contains a higher electrode density for increased spatial resolution, but also covers a larger retinal area to accommodate a greater visual angle of 11° by 19° as each single electrode of Argus II subtends a visual angle of approximately 0.7°. Another notable change from Argus I to II at the device-patient interface is that the extraocular electronics was displaced from temporal bone to episclera in the superotemporal quadrant, held in place by a scleral band.

Despite these differences, the principles of operation of Argus I and II remain similar (Fig. 34.1). A miniature camera is mounted on a pair of glasses above the nosepiece to capture the visual scenes. The images acquired are delivered to an external video processing unit (VPU) worn by the user for advanced pixelization and processing. The processed information is relayed to the external transceiver coil that is built into the side arm of the glasses, from where the visual information and the power are wirelessly transmitted to the implant. The extraocular components of the implant, an internal transceiver coil and a metal case-enclosed application-specific-integrated-circuit (ASIC) chip, recover the radio-frequency signals and generate electrical pulses in accordance. The electrical signals are delivered via a transscleral cable to the intraocular electrode array surgically placed on the retina for stimulation. The electrode array is tacked epiretinally to the inner surface of retina, nearby the ganglion cell layer. The benefits of this design are as follows: (1) the prosthesis is accessible from the vitreous and the vitreous cavity makes room for surgical maneuvers, reducing risks of mechanical damage to the retina; (2) besides choroidal perfusion, fluid in the vitreous cavity serves as an additional heat sink that enhances the removal of the heat generated by the implant electronics, lowering thermal risks for chronic

Fig. 34.1 Working mechanism of an Argus epiretinal prosthesis. Images are captured by a glass-mounted camera. Processed visual information is transmitted wirelessly to the implant, where it is transformed into electrical stimuli and subsequently delivered to the retina by an electrode array placed on top of the ganglion cell layer (image from https://www.artificialretina.energy.gov)
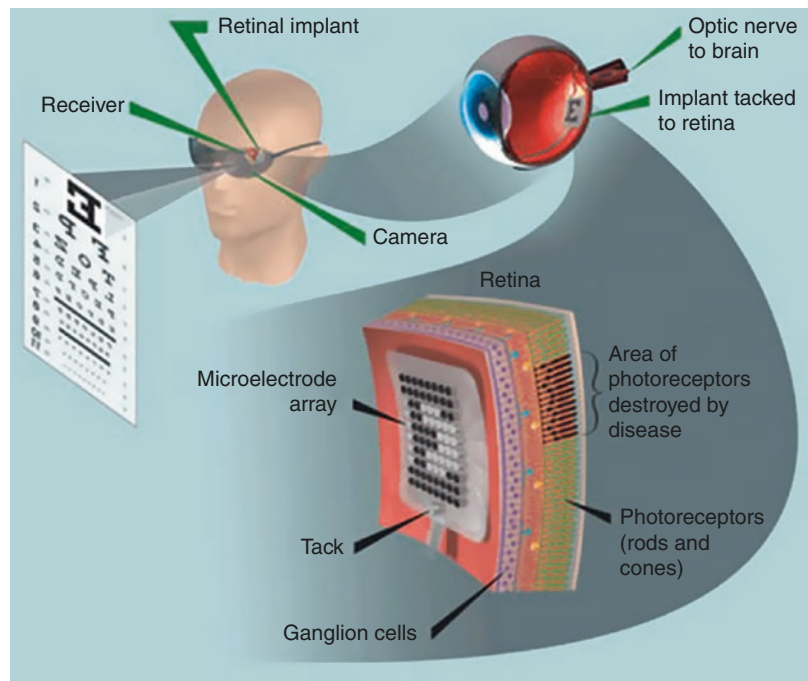
use [15]; and (3) direct stimulation of the ganglion cells is potentially useful in extensive retinal degeneration where inner retinal circuitry is altered. Presently, the epiretinal strategy faces challenges in (1) attaching the electrode array on the retina with minimal invasiveness and maintaining close proximity, and (2) avoiding perfused/distorted visual percepts from undesired activation of the axons of passage.

34.2.2 Biomedical Considerations

The entire prosthesis functions as an integral system and the design of each component carries significant biomedical implications. Oftentimes, these implications are intertwined, governed by a multitude of factors. For example, the hermetic packaging of the electronics not only determines the lifetime of the implant, but also limits the number of electrodes technically allowable; telemetry capacity and heat generation limit the data usage and power consumption, thereby affecting electrode count and ASIC layout. For the readers of this book, the discussions below will be limited to the aspects that are most directly related to the visual outcome of the prosthesis.

34.2.2.1   Visual Acuity
Visual acuity is a measure of the spatial resolution of the visual system. In sighted people, photoreceptors are capable of differentiating two points separated by as little as 1 arcmin, equivalent to 4–5 μm on retina. In pixelized prosthetic vision, it is estimated that at least ~600 pixels are needed to allow for acceptable performance of visually guided activities such as navigation and reading [16–18]. Unlike the optical stimulation, where the incident beam can be as narrow as the width of a photoreceptor, electrode-based activation is limited by the electrode layout and dimension, physical contact with the retina, and stimulation waveforms.

The best grating acuity reported with the Argus II is 20/1260, close to the theoretical limit imposed by the 525 μm electrode spacing. Smaller and denser electrodes are pursued for stimulation of higher resolution, yet technologi-

cal and physiological limitations abound. Multielectrode arrays in epiretinal prostheses typically have large electrodes arranged in a relatively sparse array, partly as a result of challenges in transscleral wiring from the stimulator chip to the electrode array. The multiphotodiode array adopted mostly by subretinal prostheses as the light sensor allows for a denser electrode placement, as the circuit and electrodes are integrated on a single substrate. At a given electrode density, electrode size is constrained, largely by the upper limit of charge injection at the electrode-tissue interface. Two primary mechanisms of charge injection occur at the electrode-electrolyte interface: the reversible charging and discharging of the double-layer capacitance/pseudocapacitance and the irreversible Faradaic reactions that onset at higher charge injection levels. The charge injection needs to be maintained sufficiently low to be fully accommodated by the reversible process and avoid the irreversible charge transfer that may degrade the electrodes and produce harmful chemical species [19, 20]. The charge density threshold that induces cellular response in the animal models was found to increase rapidly with the decrease of the electrode size [21], likely resulting in a higher risk of electrode damage. Therefore, electrode size cannot be picked arbitrarily small and it needs to satisfy safety requirements for chronic stimulation.

Spatial resolution of electrical activation is also dependent on the electrical contact between electrodes and retina. To ensure trans-retina flow of the currents, return electrodes are conventionally placed on the opposite side of retina, distant from the stimulating electrodes. In Argus II, the titanium case enclosing the extraocular electronics acts as the return. This configuration, however, does little to confine the current spread in the retina-saline system that is considered an inhomogeneous conductive medium. Various current-focusing and current-steering strategies have been explored, for example utilizing recessed electrodes and distributed return, for confined electric field and focal stimulation [22–24]. A hexagonal configuration that has one stimulating electrode surrounded by 6 "guard"

electrodes was investigated on the whole-mount rabbit retina [25]. The response threshold of the ganglion cells outside the area bound by the hex guard was found to be >2-fold higher than that inside. However, this localized stimulation comes with sacrificed efficiency—the current threshold was elevated compared with the monopolar electrode configuration as the close proximity between the stimulating and the return electrodes causes the current to be partly shorted by the more conductive physiological saline, bypassing the less conductive retina. Therefore distance between the retinal surface and the electrode is a critical determinant of the spatial resolution and stimulation efficiency. For epiretinal implants such as Argus II, the electrode array is usually 20–50 μm away from the ganglion cell layer, which may lead to exacerbated current dispersion, in comparison with subretinal implants that are in close contact with retina. New tacking strategies, for example tacking at the center of a concentric array or tacking at two opposite ends of a rectangular array, have been studied, but none have advanced to clinical prototypes. An Origami-like design of 3D spherical arrays that potentially yields better electrical contact, by maximizing array apposition to the retina, was also investigated [26].

Another limiting factor to visual acuity lies in the physiological response of the retina to electrical signals. Imaging of the calcium activity in the whole-mount retina found that the area electrically activated only scaled with the electrode diameter down to 60 μm, below which the minimum activation area did not further shrink, remaining at 150 μm diameter [27]. In addition, investigation of the retino-cortical spread function in cat cortex [28] showed that the epi- and sub-retinal thin-film electrodes of 100 μm produced a resolution of ~1–1.2° visual angle but the use of smaller fiber-cone electrodes with 20 μm base achieved only a nonlinearly improved resolution of ~0.7°. These observations suggest that both the retina and the higher visual centers in the brain interpret electrical signals differently from the normal visual inputs, possibly fundamentally limiting the spatial resolution of electrically evoked visual percepts.

34.2.2.2   Visual Field

Complementary to the visual acuity but equally important is the visual field. The normal monocular human the visual field subtends a horizontal angle of almost 180° and a vertical angle of 150°, with the macula encompassing a radius corresponding to 17° and the fovea to the central 5.2° [29]. Studies in the low-vision patients indicate that an increased visual field adds significantly to the patients' mobility and overall visual experience. Psychophysical experiments conducted in normally sighted subjects revealed that a minimum of 27°–30° of visual angle would be needed to provide adequate mobility [16, 30]. To fully restore the normal visual field, the stimulation array should cover the entire retina, with an estimated diameter of ~4 cm [31]. The actual size of the array, however, is limited, largely by surgical and mechanical factors. An epiretinal array is inserted into the intraocular space through an incision on the eyeball. The incision that can be safely made is less than 5 mm, placing a constraint on the width of the array. The array of Argus II affixed subfoveally to the retina has a dimension of 4 × 6 mm, covering a maximum visual angle of 20°. For subretinal implantation, the retina has to be detached first in order for the array to be slid underneath. Array of the Alpha IMS implant covers a visual angle of 11° and further increase in the array size risks detaching the entire retina, which is detrimental to the long-term health of the retina and the functionality of the device.

Various approaches have been taken to improve the prosthetically restored visual field. Wide-field arrays that aimed to cover a large retinal area while being surgically safe are explored. A foldable epiretinal array developed with mechanical conformity to the retinal curvature was reported to provide a visual field of 34° [32]. The concentric array, when folded, can be inserted through a 5 mm scleral incision and it will expand into a 10 mm wide array inside the vitreous cavity. Another strategy involves projecting wide-field images uncropped to a small retinal area, equivalent to converging the view. This approach, however, comes at the expense of visual acuity and image minification [33]. Conversely, image magnification can be achieved

by zooming in on the visual field. This feature was tested in Argus II and reportedly enabled a patient to read large letters [34], but the high sensitivity of image shifting to subject's head movement may compromise its appeal for daily use.

34.2.2.3   Phosphene Fading and Streaking

Visual percepts elicited by electrical currents are dependent on the types of retinal neurons stimulated. Retinal ganglion cells can be activated directly or indirectly, via synaptic transmission. The spike bursts from the indirect stimulation take advantages of neural processing by the presynaptic bipolar cells and other interneurons such as amacrine cells, better mimicking the natural spiking pattern of ganglion cells to visual stimuli. However, repeated indirect stimulation leads to exacerbated desensitization of the retinal ganglion cells [35, 36], which is believed to result in the decay in the phosphene brightness perceived by the subjects [37, 38]. Dissection of the desensitization time course in rabbit retinas revealed two components resembling the two phases of phosphene fading reported from Argus II clinical trials, one acting rapidly (hundreds of milliseconds) and the other more slowly (tens of seconds), related to interneuron inhibition [39]. In comparison with the indirect stimulation, direct activation of the ganglion cells is less prone to desensitization. Ganglion cell responses from tiger salamander retina explant closely followed direct stimulation up to 500 Hz [37]. Although direct stimulation of the ganglion cells provides superior temporal resolution, it tends to activate axons in the passage. The antidromically propagated depolarization may evoke spiking of the somata that are located further away from the electrode, causing diffused activation of the retina and producing streak-like perceptions limited in spatial resolution [13]. Elongated visual percepts were reported by both Argus I and II subjects. Such fading and distortion of the visual percepts compelled the research in selective activation between bipolar and ganglion cells and among the ganglion cell subgroups.

Interestingly, the cell population(s) activated is not only governed by its proximity to the stimulating array. Stimulus waveform is also found to tune activation selectivity between the bipolar cells and the ganglion cells [40–42]. Retinal ganglion cells are more susceptible to short-duration pulses (<150 μs) whereas inner retinal neurons favor longer pulse widths. Bipolar cells are preferentially activated by sinusoidal stimulus at 25 Hz and ganglion cells at 100 Hz. Within the ganglion cell population, specific activation of single ON and OFF parasol cells was initially accounted by Sekirnjak et al. [43], using small electrodes (9–15 μm diameter) and short-duration (0.05–0.1 ms) biphasic stimulation. Following that, localized activation of ON and OFF midget cells and bistratified retinal ganglion cells was noted, but at only ~50% of the time, due to the unwanted axonal activation [44]. Jensen and Rizzo [45] found that, in subretinal stimulation, ON and OFF cells exhibited differential thresholds for anodic-leading current pulses but not for cathodic-leading pulses, possibly unveiling another mechanism for the targeted stimulation of ON and OFF signaling pathways. It remains questionable how well these findings in the laboratory, obtained under well-controlled conditions, will translate to clinical applications, given the large variations in array-retina attachment and limitations in electrode size.

34.2.2.4   Stimulation Safety

Safety of the electrical stimulation to the retina is usually considered in two aspects—electrochemical safety and biological safety, both of which are largely determined by the stimulation parameters and the electrode characteristics.

It has been well documented that as opposed to a charge-balanced biphasic current pulse, stimulation by a monophasic current pulse of similar strength, consisting only of a cathodic or an anodic phase, created damages in tissues [46–48]. A symmetry of electrochemical processes serves to maintain the integrity of the electrodes and to avoid net charge accumulation at the electrode-tissue interface which will eventually

lead to unsafe chemical reactions [49]. Therefore, retinal implants today, including Argus II, mostly employ charge-balanced biphasic waveforms consisting of a cathodic phase for stimulation and a charge-balancing anodic phase for accelerated electrode discharge.

Despite that a voltage pulse is capable of rapid electrode discharge, voltage-controlled stimulation is less frequently used for the following reasons: (1) the electrode-electrolyte system is not entirely capacitive and thus any resistance in the electrical pathway decreases the effective stimulation current; (2) the huge capacitive current that occurs at the onset of the voltage pulse may result in uncontrolled electrode polarization; (3) stimulation efficiency peaks at the maximum current and decreases sharply during the pulse as the capacitive current is replaced by the resistive current; and (4) individual differences in the tissue resistance potentially reduce the reproducibility in the clinical use [20].

Choice of the electrode material that has high reversible charge storage capacity is crucial to the electrochemical safety. Superior to bulk platinum with a charge density limit of 0.35 mC/cm^2, advanced materials such as platinum gray (1 mC/cm^2), titanium nitride (0.9 mC/cm^2), and iridium oxide (4 mC/cm^2) [50, 51] can inject 3–10-fold higher charges. Clinically used Argus II and Alpha IMS use platinum gray and iridium oxide, respectively.

The charge storage capacity of the electrodes sets the upper limit for electrochemical safety, but the actual level of charge injection is also constrained by the safe stimulation limit of the neurons and the tissues in vicinity. Stimulation with biphasic pulse trains of 50 Hz in the rabbit eyes at various charge densities revealed evidence of structural changes in the retina when the pulse exceeded 442 μC/cm^2/phase, highlighting the importance of carefully calibrating the charge injection in the chronic stimulation of the retina [52]. It is noteworthy that increased charge density reduces the total charge that can be safely delivered to the tissue per phase, which, as mentioned earlier, places a constraint on the electrode size.

34.3 Clinical Aspects of Argus II Prosthesis

34.3.1 Indication of the Argus II Retinal Prosthesis

Argus II retinal prosthesis is indicated for patients with end-stage retinitis pigmentosa (RP) in both eyes [2]. RP is a group of hereditary outer retinal dystrophies that affects about 1 in 4,000, or more than a million people worldwide [53]. Those affected suffer from progressive visual loss that can be severe (0.5% with no light perception and 25% with ≤20/200 vision in both eyes) [54]. Postmortem histological studies of moderate-to-severe RP patients' eyes revealed that despite degeneration of all cellular layers of the retina and further cell loss as the disease progresses, the bipolar and retinal ganglion cell layers often remain relatively unaffected, with a preservation rate of 78% and 30%, respectively, even in patients with severe RP [55]. As patients with severe RP have very limited, if any, treatment options [56], they represent ideal candidates who may benefit from retinal implants.

The Argus II system includes an external set of devices worn by the patient and an electronic implant surgically installed in and around the eye (Fig. 34.2). The external equipment consists of a pair of glasses with a camera set in the center that transmits real-time video data through a wire to a video processing unit (VPU). The battery-powered VPU then converts the video data into electrical stimulation, which is sent via a wire to a transmitting coil on the side of the glasses. The implant itself consists of a receiving coil and an electronics case, which are fastened around the sclera. The transmitting coil on the glasses sends a wireless signal to the receiving coil on the eye through radio-frequency coupling, and also wirelessly supplies the implant with electric power. Once received, the electrical signal is processed by the electronics case, sent via a cable into the eye, and reaches the epiretinal microelectrode array secured onto the retina-choroid-sclera with a tack (Fig. 34.3).

Fig. 34.2 Photograph of a patient wearing the Argus II retinal prosthesis system
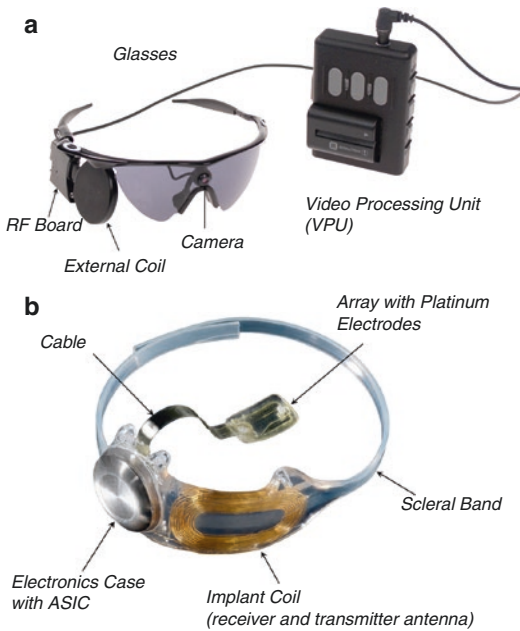
Fig. 34.3 (**a**, **b**) Illustration of the Argus II retinal prosthesis system. (**a**) The external components consisted of a glass-mounted video camera, a portable computer (the video processing unit, VPU), and an external coil. (**b**) The internal coil acts as a receiver of data from external coil, and the application-specific integrated circuit (ASIC) generates electrical pulses and sends the parameters to the microelectrode array on the macula

34.3.2 Implantation Surgery

34.3.2.1 Patient Selection

The Argus II prosthesis is indicated for patients with severe visual loss caused by advanced RP, and is intended to be implanted in one eye, preferably the worse-seeing eye. To be eligible, the patient must perceive bare light or no light in both eyes (US approval), or hand motion or less in both eyes (European and Korean approval). In addition, patients should be at least 25 years of age, have a previous history of functional vision, and have the ability to receive postimplantation clinical follow-up, device fitting, and visual rehabilitation as recommended [57, 58].

The screening process involves a standard survey, interview, and full-eye examination with biometry. The surgeon must ensure the eligibility of the patient based on criteria in the product label, absence of contraindications to implantation, and level of residual vision which must be likely to contribute to a favorable outcome. These factors are considered in addition to the patient's motivations, expectations, cognitive and communication skills, and physical abilities.

Certain ocular diseases or conditions could prevent the Argus II system from working, such as optic nerve disease, central retinal artery or vein occlusion, history of retinal detachment, trauma, severe strabismus, and amblyopia. The function of the remaining viable inner retinal layers in end-stage RP patients is first assessed with conventional means; if those fail, the evaluation can still be made by passing an electric current through the retina with transcorneal electrical stimulation [59].

Other ocular conditions, such as an extremely thin conjunctiva, axial length shorter than 20.5 mm or longer than 26.0 mm, choroidal neovascularization in the area of the intended tack location, corneal opacity, and history of strabismus surgery, should be avoided as they could prevent successful implantation surgery. Cataracts, if any, should be removed before or during implantation surgery. Patients with intolerance to general anesthesia or suggested antibiotic and steroid regimen should not be considered. Also problematic are metallic or active implantable devices in the head, such as

cochlear implants, as they may interfere with the device functioning at its full potential. Patients with an existing disease or condition that hinders understanding or communication of informed consent, fitting of the Argus II system, or postoperative follow-up, such as developmental disability or dementia, should not be considered. Depending on the patient, a preoperative psychological evaluation may need to be performed. Patients prone to eye rubbing should be advised after surgery to avoid this behavior as it can lead to postoperative complications of device exposure [58].

One of the most important, and perhaps most difficult, aspects of selecting patients is to make sure that they have realistic expectations about how the device will function. Patients should understand that the experience of seeing after surgery will be very different to how they used to see prior to sight loss. In most cases, artificial vision generated by the Argus II consists of monochromatic dark and light patterns that often shimmer. The device does not enable the perception of color. The patient must learn to interpret these patterns as objects through an arduous process analogous to learning a foreign language that requires time and patience [60].

It is also important to convey that any residual vision in the implanted eye may decline. If the patient admits to having any useful residual vision, the implant will not likely benefit the patient. The Argus II, however, could be thought of as a "safety net" against the total darkness that some patients with RP experience if their vision continues to decline.

34.3.2.2 Surgical Procedures

The surgical procedure for implanting the Argus II prosthesis incorporates many techniques familiar to the trained vitreoretinal surgeon, involving pars plana vitrectomy and scleral buckling procedures. Special precautions must be taken to avoid damaging the intricate electronic system, which is tested throughout the surgical procedure. Surgery generally takes between 1.5 and 4 h and is performed under general anesthesia [61].

For phakic patients, it is normal to begin the surgery by performing cataract extraction with or without intraocular lens implantation, as subse-

quent formation of cataracts would make it difficult to conduct clinical monitoring.

The implantation surgery itself begins with a 360-degree conjunctival peritomy to isolate all four recti muscles in preparation of placing the extraocular band carrying the receiving coil and electronics case, which are sealed in protective hermetic cases. The band is then sutured onto the sclera in the eye's supero-temporal quadrant (Fig. 34.4a). The surgeon must secure the band at the receiving coil and the application-specific integrated circuit (housed in the electronics case) in a predetermined position according to the nomogram developed by the manufacturing company (SSMP). This is important because the extraocular position of these two points determines the positioning of the array over the macula. Then, the points are stabilized by securing the rest of the band, which is positioned under each of the four recti muscles, gently tightened around the globe, and held with a Watzke's sleeve.

The next step entails a standard three-port pars plana vitrectomy, using either a 25-gauge or a 23-gauge microincision system, and must be thoroughly performed to ensure that the array is in good contact with the retinal surface. Staining the vitreous with triamcinolone is helpful to identify the adherent posterior vitreous gel on the retinal surface. Particularly, intraoperative optical coherence tomography (IO-OCT) has proven to be useful in creating a posterior vitreous detachment (PVD) and removing detached vitreous gel from the macular area (Fig. 34.4b). In addition, it is important to trim the vitreous base in the quadrant of array insertion to prevent the device from being caught within residual vitreous gel.

Once the band is in place, a 5.2 mm sclerotomy is made at the pars plana in the supero-temporal quadrant, through which the microelectrode array will be inserted into the vitreous cavity (Fig. 34.4c). The sclerotomy should be of full thickness and perpendicular to the sclera. It should be noted that choroidal detachment is possible if the array gets caught on the edge of the sclerotomy. If the extraocular band is properly positioned, the microelectrode array will rest naturally at the posterior pole of the retinal surface with minimal tension.
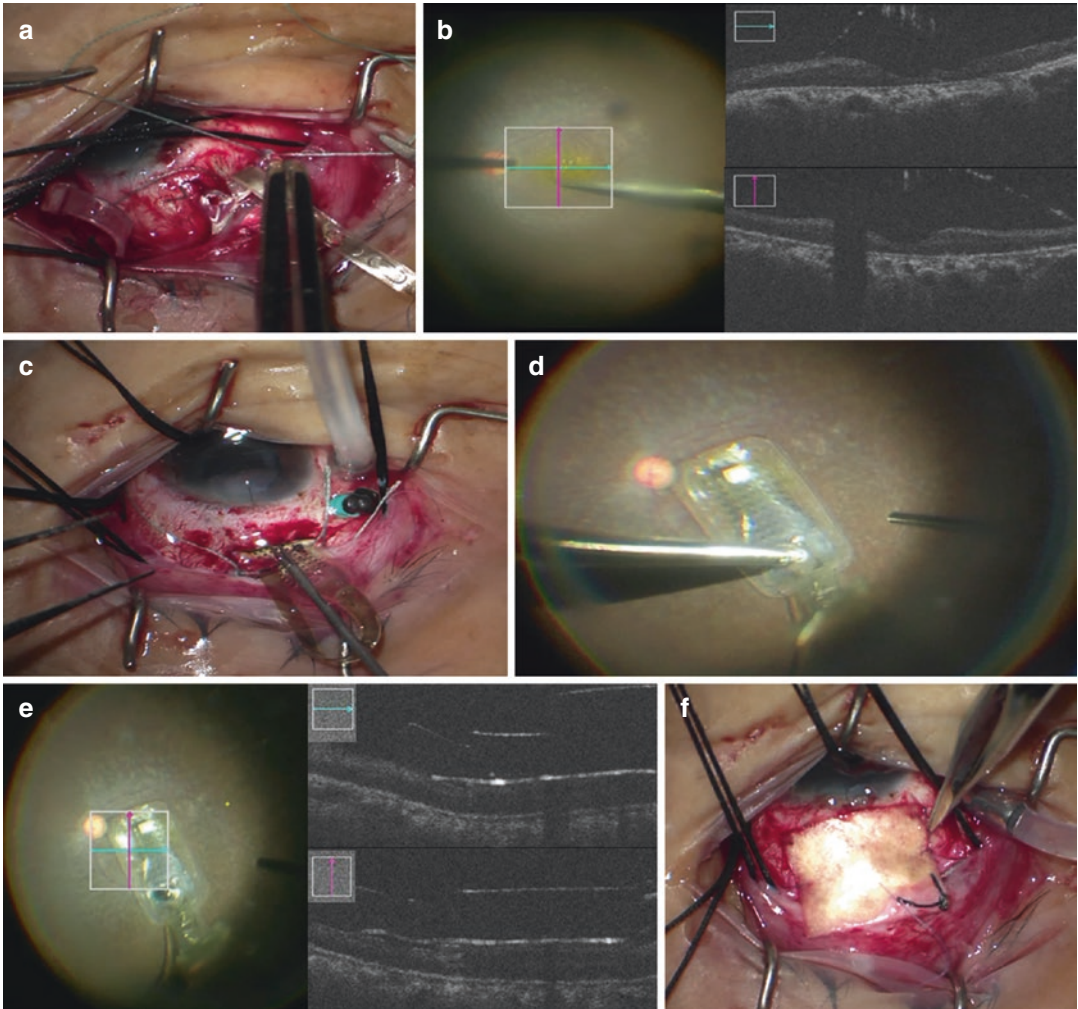
Fig. 34.4 (**a**–**f**) Intraoperative photograph of (**a**) the application-specific integrated circuit (ASIC) in hermetic casing being sutured onto sclera 5 mm from the limbus, (**b**) showing a creation of posterior vitreous detachment (PVD) under the intraoperative optical coherence tomography (OCT), (**c**) showing the insertion of the microelec- trode array into the vitreous cavity via a 5.2 mm pars plana sclerotomy, (**d**) tacking the microelectrode array to the macula, (**e**) confirming a close contact of array to the retinal surface under the intraoperative OCT, (**f**) suturing a pericardium graft over the hermetic cases and coil tabs (still image captured from surgical video)

Gentle manipulation of the array using a 19-gauge specialized tack forceps optimizes its placement in the macular region. Once a satisfac- tory array position is achieved, a single spring- tensioned, titanium tack is inserted at the base of the array, ensuring close proximity between the array and the retinal surface (Fig. 34.4d, e). Chandelier illumination may be used to allow bimanual technique to insert the tack (i.e., using

intraoperative forceps to manipulate the electrode array and using the second hand to place the tack through the tack insertion hole). For a single- handed technique one hand is used to place the tack and the second hand holds an endoillumina- tor. Surgeons may also utilize IO-OCT to gain real-time knowledge of the distance from the array and retinal surface to the array tilt, allowing imme- diate adjustments to be made if necessary [60, 62].

Fig. 34.5 On completion of surgery, a sterile OR coil which was connected to the VPU is placed parallel to the internal coil to test the integrity of the device. Impedance map of the implanted microelectrode shows that all electrodes are intact

It is crucial to meticulously close all scleral wounds to avoid scleral leakage and hypotony around the cable connecting the array to the extraocular band. The surgeon finally sutures an allograft (e.g., Tutoplast® IOP Ophthalmics, Inc., Costa Mesa, CA) or autologous fascia-lata patch over the hermetic cases and coil tabs (Fig. 34.4f). Furthermore, it is critical to close the tenon's capsule and conjunctiva to prevent the device from being exposed post-operation and avoid the risk of endophthalmitis. On completion of surgery, a sterile OR coil which was connected to the VPU is placed parallel to the internal coil to test the integrity of the device (Fig. 34.5).

34.3.2.3 Device Programming and Fitting Activation

Around 2 weeks after surgery, the patient is examined to check whether the device is properly implanted without any postoperative com-

plications (Fig. 34.6). Then, the patient is initiated into a fitting process at the clinic to optimize performance and comfort by customizing the implant's stimulation levels. The first part of the test ascertains whether electrical stimulation through each electrode results in a visual "percept," i.e., a single spot of light. Next, the threshold is measured for each electrode on the array for the minimum amount of electrical current necessary to create a percept. The test is performed using a laptop computer that directly controls the implant without input from the camera. Once the basic thresholds are measured, customized settings are created and loaded to the externally worn VPU. Then, the camera at the center of the glasses is activated for the first time, allowing the real-time video image of the world around the patient to be perceived via array stimulation. Later, additional tests are conducted to determine the effectiveness of the customized settings and the level of comfort as experienced by the patient. If the patient feels the stimulation is too bright, or not bright enough, or creates an unintended physical sensation (like a mild vibration around the eye), the settings can be readjusted until the patient feels comfortable with the stimulation (Fig. 34.7).

34.3.2.4 Rehabilitation

After the device is activated, the patient should participate rehabilitation sessions focused on assisting the patient to learn to better use the Argus II in activities of daily living. Either an occupational therapist or a low-vision optometrist is eligible to perform the rehabilitation sessions at the clinic or the patient's home (Fig. 34.8). The aim of the rehabilitation training is to equip patients with the ability to be aware of eye, head, and camera position and movements; locate small-scale light sources (micro-level scanning); locate large-scale light sources (macro-level scanning); track light; discern luminance; discriminate light sources; and recognize shapes. After four in-clinic sessions, most patients gain a basic level of control that
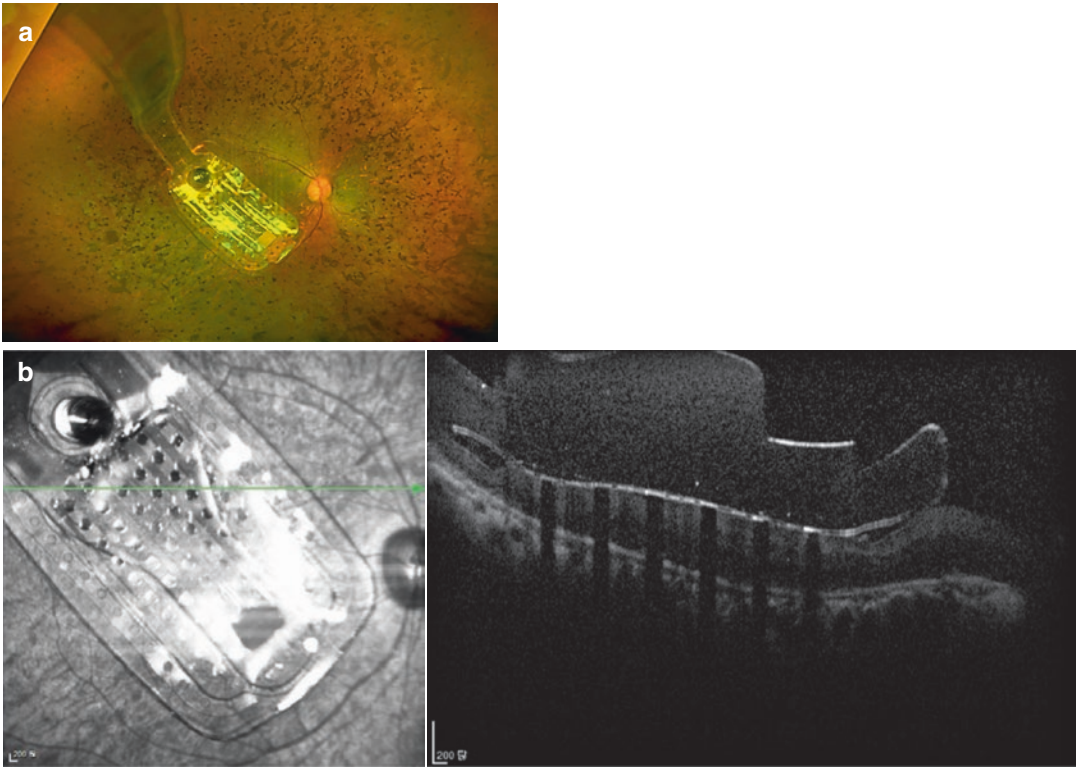
Fig. 34.6 (**a**) Wide-field fundus photograph of the micro-electrode array with 60 platinum electrodes, implanted in a patient with advanced retinitis pigmentosa. (**b**) SD-OCT image of the microelectrode array in direct contact with retinal surface. Shadows cast on the retinal image are the result of occlusion of the scanning light source by the metal electrodes

should be retested and enhanced at home as well as other indoor and exterior environments. Six additional sessions will further enhance the patient's newly acquired visual sense of orientation and mobility, and other new abilities. White canes and other mobility aids used in conjunction with the Argus help patients to improve their use of the Argus II; many report that the learning process continues for years after implantation, with their skill improving only gradually during that time [63].

Some challenges with the use of the Argus II include difficulty using an external camera for image capture due to the dissociation between the visual scene captured by the camera and the patient's eye position. In order to resolve this difficulty, patients with Argus II implants are taught to keep their gaze straight ahead at all times, so that the coil on the side of the glasses and the receiving coil on the eye may be properly aligned for signal transmission [64, 65]. This technique has also proved effective in helping patients localize objects in a three-dimensional space with higher accuracy and efficiency [66]. Another challenge is learning to use a relatively low-pixelated phosphine map to help in orientation and mobility [65].

34.3.3 Clinical Outcomes

Argus II Retinal Prosthesis Feasibility Study (ClinicalTrials.gov NCT00407602) was the pivotal clinical trial, enrolling 30 subjects between June

Fig. 34.7 (**a**, **b**) Photograph showing a patient in the process of device programming and activation. (**a**) Patient is asked to percept a spot of light and the threshold is measured for each microelectrode. (**b**) Threshold map of microelectrode array at the time of activation

2007 and August 2009, and the outcome of the study was examined at years 1, 3, and 5 [67–69].

In 2018, the retinal anatomy and the electrode array position in Argus II retinal prosthesis recipients were reported as part of the Post-Market Surveillance Studies (PMS) (ClinicalTrials.gov NCT01860092, and NCT01490827) [70].

Based on these two clinical trials and other studies, a number of reports have been published,

focusing on the device's safety, visual outcome, functional vision, and anatomic change of the macula.

34.3.3.1   Safety

Safety was one of the primary outcome measures of the pivotal feasibility trial. The cumulative number of serious adverse events (SAEs) was reported from the third to fifth years (Table 34.1).

Fig. 34.8 (**a**, **b**) Photograph showing a patient practicing visual training and rehabilitation. (**a**) Patient is looking through a clear large tube to train a head-eye position awareness and control. (**b**) Patient is taught to integrate basic visual skills into basic orientation and mobility tasks in daily lives

During an average of 6.2 ± 0.9 years (range of 5.2–7.4), 3 of the 30 enrolled patients were explanted due to recurring conjunctival erosion, and 24 of the remaining 27 patients had functional implants. The SAEs were all treatable with standard approaches, and there were no enucleations (lost eyes) during the study. Five years since implantation, 18 of the 30 patients (60%) had not experienced an SAE related to the device or surgery.

Table 34.1 Serious adverse event rates (cumulative) to 3 and 5 years after implantation

Serious adverse event type	Year 3		Year 5	
	No. (%) with serious adverse event	95% confidence interval	No. (%) with serious adverse event	95% confidence interval
Conjunctival erosion	4 (13.3)	3.1–30.7	4 (13.3)	3.1–30.7
Hypotony	4 (13.3)	3.1–30.7	4 (13.3)	3.1–30.7
Conjunctival dehiscence	3 (10.0)	2.1–26.5	3 (10.0)	2.1–26.5
Presumed endophthalmitis	3 (10.0)	2.1–26.5	3 (10.0)	2.1–26.5
Retack	2 (6.7)	0.8–22.1	2 (6.7)	0.8–22.1
Retinal detachment				
Rhegmatogenous	1 (3.3)	0.1–17.2	2 (6.7)	0.8–22.1
Tractional and serous	1 (3.3)	0.1–17.2	1 (3.3)	0.1–17.2
Retinal tear	1 (3.3)	0.1–17.2	1 (3.3)	0.1–17.2
Uveitis	1 (3.3)	0.1–17.2	1 (3.3)	0.1–17.2
Keratitis, infective	1 (3.3)	0.1–17.2	1 (3.3)	0.1–17.2
Corneal melt	1 (3.3)	0.1–17.2	1 (3.3)	0.1–17.2
Corneal opacity	1 (3.3)	0.1–17.2	1 (3.3)	0.1–17.2
Total	23		24	

Images adapted from da Cruz et al. Ophthalmology, 2016

Two of the Argus II implants had failed approximately 4 years after surgery due to the gradual loss of the ability to maintain the radio-frequency link between the transmitting and receiving coils. The implants were not removed for the duration of the clinical trial to continue collecting data for long-term safety [69].

More recently, a study by Rizzo and colleagues reported that 12 months after surgery, no major complications were detected except for a medically treated IIOP or mild choroidal detachment. These results were a marked improvement to the safety profile observed during the Argus II clinical trial phase [61]. An initial series of 11 implanted cases from Toronto in Canada also reported that there was no case of serious adverse events during a 3- to 30-month follow-up [71].

34.3.3.2 Visual Outcome

Visual function was another key measure of the pivotal trial, as determined by three computer-based tests. Because the level and nature of vision afforded by Argus II prostheses fall below the level that is normally assessed with standard visual acuity tests (e.g., logMAR/Snellen acuity and contrast sensitivity), new means of assessing Argus II-produced vision have been proposed and validated. The square localization (SL) test measures the ability to locate and touch a high-contrast white square of light on a black background on a touch-screen monitor; the direction of motion (DM) test assesses patients' ability to determine and indicate the direction of a high-contrast bar that moves across the monitor; and the grating visual acuity (GVA) test measures visual acuity using square-wave gratings of different spatial frequencies presented on a computer monitor. All three tests are performed with the Argus II turned on; off with residual vision only using both eyes for the SL and DM tests; and one eye each for the GVA test.

Patients generally perform better on the SL test with the device on than when using their residual vision only. Overall improvement is also visible in the more challenging DM test (lower mean error) with the device turned on. The GVA test, the most difficult of the three, also revealed enhanced performance with the device on. With the device turned off, all three tests were worse than 2.9 logMAR at yearly time points. With the device on, 27–48% of the patients scored at least 2.9 logMAR, depending on the time point (Fig. 34.9) [69]. In 2012, the best GVA achieved

using the Argus II was logMAR 1.8 (Snellen equivalent of 20/1262) [2].

The patients' improvements when using the system compared with their residual vision can also be observed on an individual basis, in terms of the percentage of patients who performed sig-

nificantly better with the system on than off on each assessment. Results at 1 year and 3 years were reported previously; here, results from years 3 and 5 are compared (Table 34.2) [69].

da Cruz et al. [72] investigated the ability of 21 eligible patients (among 30 Argus II feasibil-
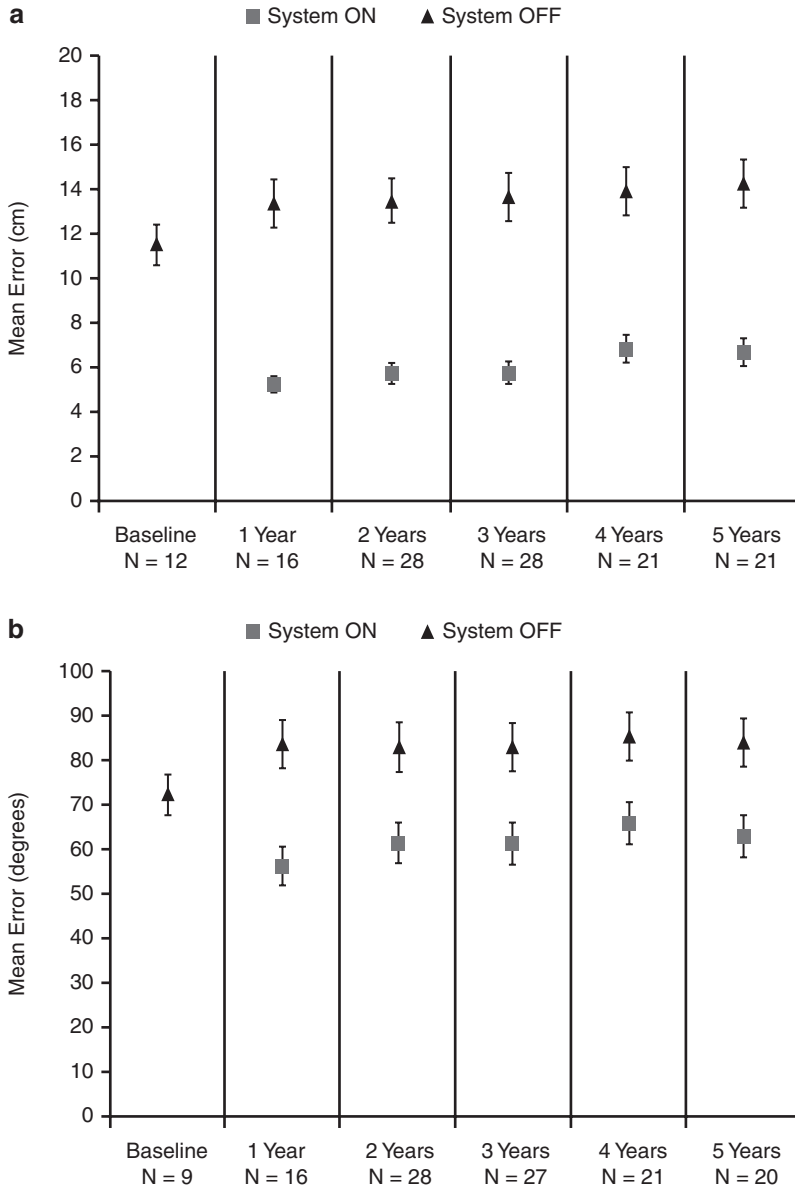
Fig. 34.9 (**a**–**c**) Graphs showing results for (**a**) square localization, (**b**) direction of motion, and (**c**) grating visual acuity at yearly time points. (**a**, **b**) Mean error with system on is shown as blue squares; mean error with the system off (with residual vision only) is shown as black diamonds. Error bars indicate standard error. (**c**) The percent of patients scoring 2.9 logarithm of the minimum angle of resolution (logMAR) or better on grating visual acuity with system on (in implanted eye) is shown at each time point. There were no patients who scored 2.9 logMAR or better with the system off in the implanted eye (images adapted from da Cruz et al.Ophthalmology, 2016)
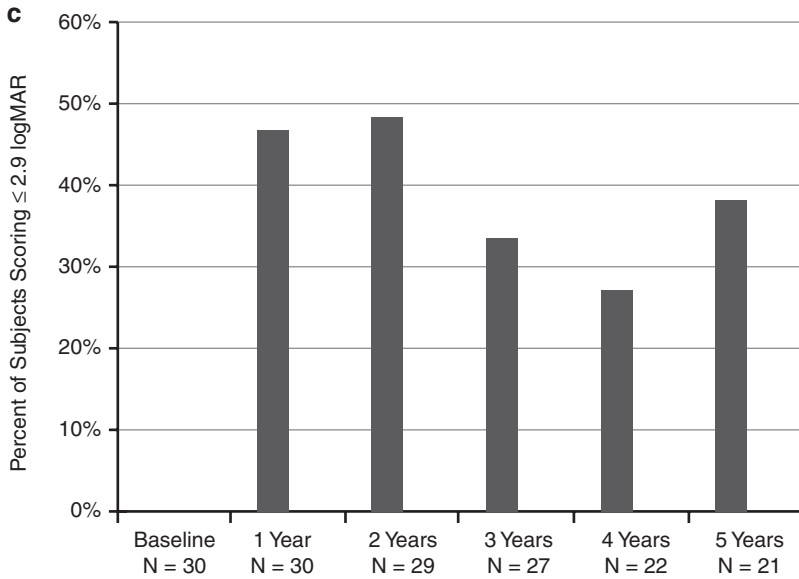
Fig. 34.9 (continued)

Table 34.2 Individual visual function assessment results

	Year 3		Year 5	
Visual function assessment	No.	Significantly better on than off (%)	No.	Significantly better on than off (%)
Square localization	28	89.3	21	80.9
Direction of motion	27	55.6	20	50
Grating visual acuity	27	33.3	21	38.1

Images adapted from da Cruz et al. Ophthalmology, 2016

ity study patients) to discriminate high-contrast, large letters presented on flat LCD screens. The letters were presented in three groups based on typographical complexity. The first group was letters with only vertical and horizontal lines; the second, letters with oblique lines or a circle; and the third, letters with an oblique and curved component. The patients identified the letters in all three groups with a significantly higher level of accuracy when the device was turned on than when it was off. The smallest letter they could identify was 1.7 inches in height (0.90 cm viewed from a 30 cm distance), which is comparable to the theoretical resolution limit of the

Argus® II device with 200 μm electrode size and inter-electrode distance (center-to-center) of 575 μm [38]. Unrehearsed, four patients were able to identify words with two to four letters using the device. Regression analyses revealed that the patient's age at the time of implantation was a statistically significant indicator of performance, as younger patients with relatively healthier residual retinas tended to show better results [72]. Other plausible indicators of superior outcomes were a greater number of activated electrodes or being diagnosed with RP at an older age in life, but these were not statistically significant.

Rizzo and colleagues reviewed the 12-month outcomes of six patients who underwent Argus II implantation surgery by a single surgeon. While four and three patients showed an improvement in SL and DM tests, all six patients showed an improvement in Goldmann perimetry a year after the surgery was performed [61]. The initial case series of 11 cases from a single center in Toronto, Canada, reported that the mean error in the SL test improved significantly with the system on, but the GVA remained the same [71].

Yoon and colleagues reported that their first Korean patient was able to read the sixth line on the ETDRS chart at a distance of 50 cm at

Fig. 34.10 (**a**, **b**) Photograph showing a patient performing letter identification test. Letters (Korean alphabet) were presented in black and white LCD screen 30 cm away from the seated patient. (**a**) The patient was able to read Korean letters, and (**b**) write simple sentences
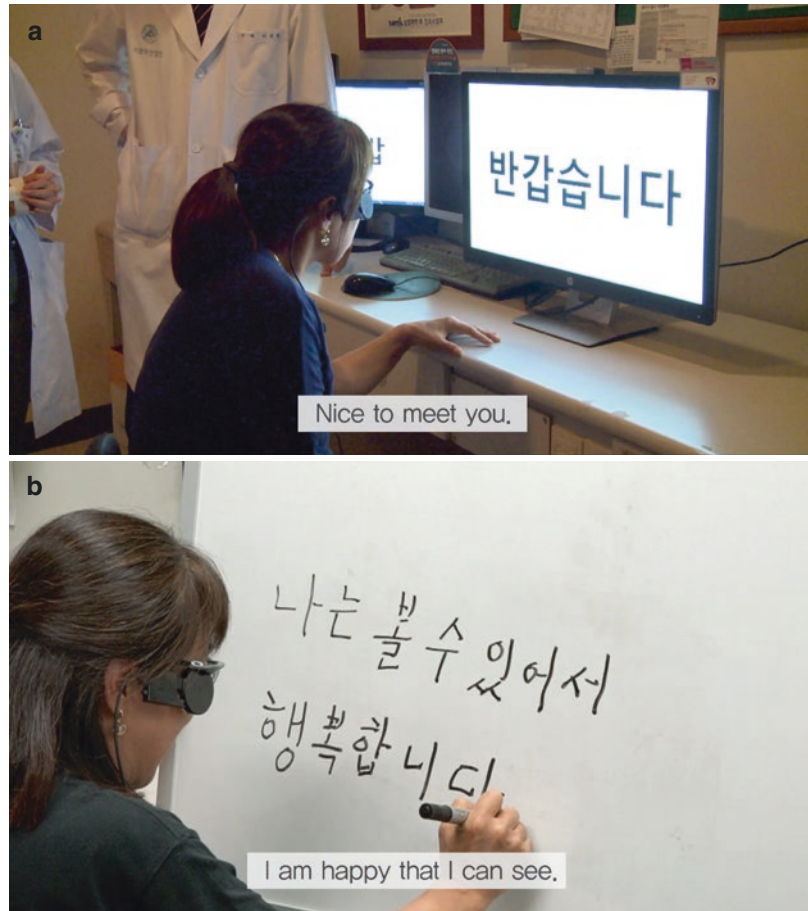
3 months. In addition, when asked to identify Korean alphabets, she was able to read Korean letters from 1.4 cm (2.66°) to 6 cm (11.4°) in height and words of 3–9 letters, and write simple sentences (Fig. 34.10) [73].

34.3.3.3   Functional Vision

The Argus II clinical trial assessed the orientation and mobility (O&M) functions by asking the patients to complete two tasks: [1] follow a 15 cm × 6 m white line marked on a dark floor, and [2] locate a dark door (1 m × 2.1 m) against a white wall from a 6 m distance. Collectively, as of 5 years after implantation, the patients demonstrated significant improvement in their performance in both tasks with the device turned on compared to when it was off

($P < 0.05$) at all time points. Figure 34.11 shows the mean percent success rates of the O&M assessments [2, 69].

The Functional Low-vision Observer Rated Assessment (FLORA) was developed to obtain an objective assessment of how a retinal prosthesis is utilized by the patient to complete a series of 35 daily activities at home. Conducted by certified low-vision specialists, the 35 tasks are divided into groups for assessing orientation, mobility, daily life, and social interaction [74].

The FLORA was completed by 26 of the 30 patients in the Argus II Retinal Prosthesis Study who had the Argus II implanted 18–44 months earlier (mean 36 months). In general, patients were able to complete 24 of 35 tasks (69%) with greater ease when the device was on, particularly

Fig. 34.11 (**a**, **b**) Graphs showing the mean percent success on (**a**) the door task and (**b**) the line task with the system on (blue squares) and off (residual vision only, black triangles). Error bars indicate standard error of the mean (images adapted from da Cruz et al. Ophthalmology, 2016)
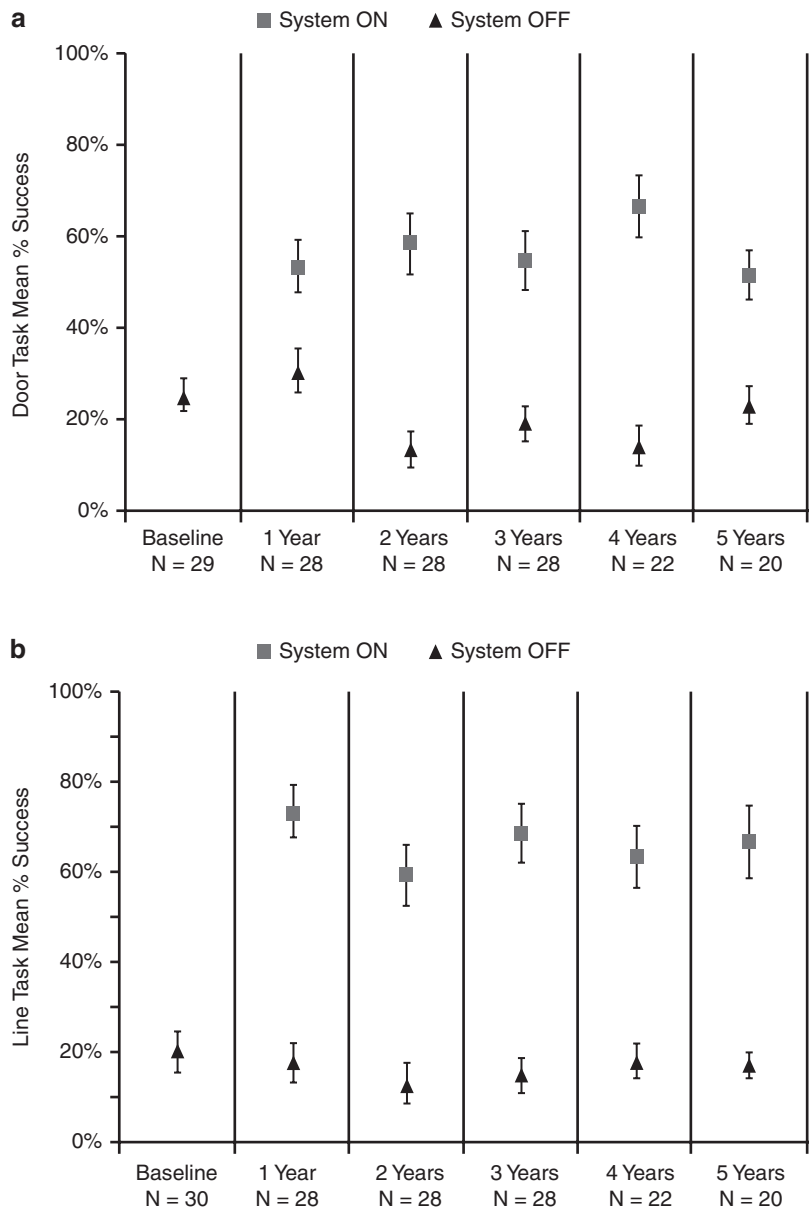
when the task required light projection and high contrast to identify an object [75].

When 28 Argus II recipients were tested on three real-world functional vision tasks (sock sorting, sidewalk tracking, and walking direction discrimination task), they performed better on all three tasks with their systems on than they did with their systems off [76].

While sighted individuals use both eye and head movements to perform visual scanning, patients using Argus II scan solely by head movements. Recent studies show that head movement coupled with an eye tracker function may increase visual stability and reduce the need for head movement. Integration of this eye tracker function in the Argus II will significantly improve

performance in orientation and mobility tasks [77, 78].

34.3.3.4   Anatomic Change

An international PMS study was conducted by Gregori and colleagues to review the postoperative macular anatomy and position of the electrode array. The team collected SD-OCT images from 33 patients at 16 surgical sites at months 0, 1, 3, 6, and 12. Despite the inconsistent quality of the OCT images, this study was able to describe the dynamic anatomy in the Argus II recipients. During the 12-month follow-up, progressive thickening of the macula under the array was commonly observed and corresponded to a narrowing of the gap between the electrode and the retinal surface over time. One year later, the array was in complete contact with the macula in about half of the postoperative eyes. Two eyes showed a hyperreflective layer representing either fibrosis or inflammatory material, but the visual function did not seem to be significantly affected [70].

34.4   Future Development and Perspectives

Overall, as the first retinal implant with regulatory approval, Argus II offers exciting opportunities to study prosthetic vision in a relatively large cohort of patients. Results from the clinical studies provide strong evidence that this epiretinal electronic implant is effective in restoring meaningful vision to patients blinded by photoreceptor degeneration.

Despite the encouraging results summarized above, the Argus II implant, containing only 60 electrodes (i.e., 60 pixels) is not able to restore high acuity vision. Further improvement in the spatial resolution demands advanced microelectronic and hermetic packaging technologies that would allow for a higher electrode density on the chip. Furthermore, improvement in the power and data management is needed to permit sufficient power supply and rapid data transmission to the implant while maintaining heat generation

under check. Additionally, novel design and implantation techniques that can hold the electrode array in closer proximity to the retina are desirable for increased stimulation efficiency.

The past decade has witnessed the rapid growth in retinal prostheses. It should be noted that, in addition to Argus II and other epiretinal implants, subretinal and suprachoroidal implants have also made tremendous progress, among which Alpha-IMS subretinal implant received CE mark approval in 2013. Different from Argus II that utilizes a video camera for image acquisition, Alpha-IMS leverages a microphotodiode array (MPDA) for light detection and current generation. Each microphotodiode in the array transforms local luminance level, in a proportional manner, into electrical pulses, stimulating the retinal neurons nearby. Under the current technology, photodiodes serving as the visible light sensor often yield low photocurrent output that is insufficient to drive neuron activation. Alpha-IMS relies on external power supply for current amplification [79], which adds to the system complexity and surgical difficulty. An alternative approach developed by Palanker et al. adopts optical amplification by converting ambient visual inputs into high-intensity near-infrared laser pulsing projected onto the subretinal photodiode array. Each pixel consists of a few photodiodes connected in series to multiply the photocurrent output [80]. This approach avoids complex electrical circuitry but its safety and efficiency await to be evaluated in humans. By addressing the low current output, MPDA was hopeful to restore high acuity vision; however, the highest visual acuity reported of the Alpha-IMS implant was 20/546 measured with the Landolt C chart, lower than the acuity of 20/200 that would be theoretically expected by 1500 pixels in the array. This observation brings us back to the earlier discussion of how the electrode density effectively shapes the visual acuity. The clinical findings so far, along with the aforementioned experimental results from the animal models, suggest that the visual acuity scales with the electrode density only to an extent beyond which other factors such as electrical properties and

processing of retina and beyond will weigh in. To truly answer this question, we need to better understand the fundamentals of the retinal processing of the electrical signals and the neural network rewiring at both the retinal and the cortical levels.

A major benefit of Alpha-IMS and other systems that similarly implant high-density light-sensing units intraocularly is that the patients can use eye movement, instead of head movement, to scan the visual field, which better mimics the natural vision. Evidence of ocular drifts and microsaccades has been noted in Alpha IMS-implanted patients [81]. These involuntary eye movements refresh the images and may contribute significantly to mitigating the phosphene fading and maintaining the perceptual stability. For implants that rely on external devices to capture images such as Argus II, miniaturized intraocularly implantable cameras that aim to similarly take advantage of eye movement were investigated. In an all-intraocular design, image output of the camera is delivered directly to the stimulator chip, driving the electrode array for stimulation. Simulation of the intraocular camera function suggests that, by controlling the field of view with eye movement, users can perform the visual tasks in a more natural manner [31]. Alternatively, an eye-tracking extraocular camera that detects the direction of gaze and captures images accordingly may offer similar benefits as an intraocular camera.

Retina is a highly diversified network of over 80 different neuronal populations that form the building blocks for about 20 circuit mosaics for parallel visual signal processing [82]. These 20 separate mosaics are interwoven over the entire retina, oftentimes with overlapping receptive fields that each extracts a distinct feature of the image flow, such as luminance, contrast, shape, color, and motion. Outputs of these mosaics are carried to the higher visual centers in the brain each via a specific ganglion cell channel, encoded by the spatiotemporal patterns of spiking [83]. In the presence of the same visual stimuli, these anatomically distinct ganglion cell types are known to exhibit differential responses that are

integrated and decoded by the cortex to generate a sense of vision. Therefore a stimulation algorithm that incorporates the firing patterns specific to each mosaic has the potential to produce retinal outputs more readily interpretable to the cortex. Such strategies are particularly appealing for highly localized stimulations with small electrodes. Due to various constraints on the electrode size, current devices only allow simultaneous activation of multiple cell populations. Technical advances in flexible electronics may someday enable implants with single-cell stimulation capabilities, demanding development of highly specified stimulation algorithm that can mimic natural ganglion cell spiking. Novel probes of retinal signal processing such as optogenetics and rapidly growing AI technologies provide interesting tools to study the spiking patterns of ganglion cells to differential image input.

At the forefront of the interdisciplinary biomedical research, Argus II and other bioelectronics retinal prostheses will continue to benefit from advancement in material sciences, electronics microfabrication, biological techniques, and emerging technologies. Future development of more advanced retinal prosthetic devices will offer the blind patients with vision that better mimics the normal for improved mobility, orientation, and object recognition. Meanwhile, the technological breakthrough will not only demand but also promote a further understanding of the retinal and cortical processing of electrical signals.

References

1. US Food and Drug Administration. Humanitarian device exemption. Accessed 27 March 2018. https://www.fda.gov/MedicalDevices/DeviceRegulationandGuidance/HowtoMarketYourDevice/PremarketSubmissions/HumanitarianDeviceExemption/.

2. Humayun MS, Dorn JD, Da Cruz L, Dagnelie G, Sahel J-A, Stanga PE, et al. Interim results from the international trial of Second Sight's visual prosthesis. Ophthalmology. 2012;119(4):779–88.

3. Grüsser OJ, Hagner M. On the history of deformation phosphenes and the idea of internal light generated in the eye for the purpose of vision. Doc Ophthalmol. 1990;74(1–2):57–85. PubMed PMID: 2209368. eng.

4. Foerster O. Beitrage zur Pathophysiologie der Sehbahn und der Sehsphare. J Psychol Neurol, Lpz. 1929;39:463.

5. Krause F, Schum H. Die epileptischen Erkrankungen. Neue Deutsche Chirurgie. 1931;49:482–6.

6. Brindley GS, Lewin W. The sensations produced by electrical stimulation of the visual cortex. J Physiol. 1968;196(2):479–93.

7. Dobelle WH, Mladejovsky M, Girvin J. Artificial vision for the blind: electrical stimulation of visual cortex offers hope for a functional prosthesis. Science. 1974;183(4123):440–4.

8. Humayun M, Propst R, de Juan E, McCormick K, Hickingbotham D. Bipolar surface electrical stimulation of the vertebrate retina. Arch Ophthalmol. 1994;112(1):110–6.

9. Rizzo JF, Wyatt J, Loewenstein J, Kelly S, Shire D. Perceptual efficacy of electrical stimulation of human retina with a microelectrode array during short-term surgical trials. Invest Ophthalmol Vis Sci. 2003;44(12):5362–9.

10. De Balthasar C, Patel S, Roy A, Freda R, Greenwald S, Horsager A, et al. Factors affecting perceptual thresholds in epiretinal prostheses. Invest Ophthalmol Vis Sci. 2008;49(6):2303–14.

11. Horsager A, Greenwald SH, Weiland JD, Humayun MS, Greenberg RJ, McMahon MJ, et al. Predicting visual sensitivity in retinal prosthesis patients. Invest Ophthalmol Vis Sci. 2009;50(4):1483–91.

12. Nanduri D, Fine I, Horsager A, Boynton GM, Humayun MS, Greenberg RJ, et al. Frequency and amplitude modulation have different effects on the percepts elicited by retinal stimulation. Invest Ophthalmol Vis Sci. 2012;53(1):205–14.

13. Nanduri D, Humayun M, Greenberg R, McMahon M, Weiland J. Retinal prosthesis phosphene shape analysis. In: Engineering in Medicine and Biology Society, 2008 EMBS 2008 30th Annual International Conference of the IEEE. IEEE; 2008.

14. Yue L, Falabella P, Christopher P, Wuyyuru V, Dorn J, Schor P, et al. Ten-year follow-up of a blind patient chronically implanted with epiretinal prosthesis Argus I. Ophthalmology. 2015;122(12):2545–52.e1.

15. Opie NL, Burkitt AN, Meffin H, Grayden DB. Heating of the eye by a retinal prosthesis: modeling, cadaver and in vivo study. IEEE Trans Biomed Eng. 2012;59(2):339–45.

16. Cha K, Horch KW, Normann RA. Mobility performance with a pixelized vision system. Vis Res. 1992;32(7):1367–72.

17. Cha K, Horch KW, Normann RA, Boman DK. Reading speed with a pixelized vision system. J Opt Soc Am A. 1992;9(5):673–7.

18. Sommerhalder J, Rappaz B, de Haller R, Fornos AP, Safran AB, Pelizzone M. Simulation of artificial vision: II. Eccentric reading of full-page text and the learning of this task. Vis Res. 2004;44(14):1693–706.

19. Cogan SF. Neural stimulation and recording electrodes. Annu Rev Biomed Eng. 2008;10:275–309.

20. Merrill DR, Bikson M, Jefferys JG. Electrical stimulation of excitable tissue: design of efficacious and safe protocols. J Neurosci Methods. 2005;141(2):171–98.

21. Sekirnjak C, Hottowy P, Sher A, Dabrowski W, Litke A, Chichilnisky E. Electrical stimulation of mammalian retinal ganglion cells with multielectrode arrays. J Neurophysiol. 2006;95(6):3311–27.

22. Suesserman MF, Spelman FA, Rubinstein JT. In vitro measurement and characterization of current density profiles produced by nonrecessed, simple recessed, and radially varying recessed stimulating electrodes. IEEE Trans Biomed Eng. 1991;38(5):401–8.

23. Wilke R, Moghadam GK, Lovell N, Suaning G, Dokos S. Electric crosstalk impairs spatial resolution of multi-electrode arrays in retinal implants. J Neural Eng. 2011;8(4):046016.

24. Palanker D, Vankov A, Huie P, Baccus S. Design of a high-resolution optoelectronic retinal prosthesis. J Neural Eng. 2005;2(1):S105.

25. Habib AG, Cameron MA, Suaning GJ, Lovell NH, Morley JW. Spatially restricted electrical activation of retinal ganglion cells in the rabbit retina by hexapolar electrode return configuration. J Neural Eng. 2013;10(3):036013.

26. Liu Y, Park J, Lang RJ, Emami-Neyestanak A, Pellegrino S, Humayun MS, et al. Parylene origami structure for intraocular implantation. In: 2013 Transducers & Eurosensors XXVII: The 17th International Conference on Solid-State Sensors, Actuators and Microsystems (TRANSDUCERS & EUROSENSORS XXVII). IEEE; 2013.

27. Behrend MR, Ahuja AK, Humayun MS, Chow RH, Weiland JD. Resolution of the epiretinal prosthesis is not limited by electrode size. IEEE Trans Neural Syst Rehabil Eng. 2011;19(4):436–42.

28. Eckhorn R, Wilms M, Schanze T, Eger M, Hesse L, Eysel UT, et al. Visual resolution with retinal implants estimated from recordings in cat visual cortex. Vis Res. 2006;46(17):2675–90.

29. Zhu J, Yang J. Subpixel eye gaze tracking. fgr. IEEE; 2002.

30. Dagnelie G, Keane P, Narla V, Yang L, Weiland J, Humayun M. Real and virtual mobility performance in simulated prosthetic vision. J Neural Eng. 2007;4(1):S92.

31. Weiland JD, Humayun MS. Retinal prosthesis. IEEE Trans Biomed Eng. 2014;61(5):1412–24.

32. Ameri H, Ratanapakorn T, Ufer S, Eckhardt H, Humayun MS, Weiland JD. Toward a wide-field retinal prosthesis. J Neural Eng. 2009;6(3):035002.

33. Hayes JS, Yin VT, Piyathaisere D, Weiland JD, Humayun MS, Dagnelie G. Visually guided performance of simple tasks using simulated prosthetic vision. Artif Organs. 2003;27(11):1016–28.

34. Sahel J, Mohand-Said S, Stanga P, Caspi A, Greenberg R. Acuboost™: enhancing the maximum acuity of the Argus II retinal prosthesis system. Invest Ophthalmol Vis Sci. 2013;54(15):1389.

35. Freeman DK, Fried SI. Multiple components of ganglion cell desensitization in response to prosthetic stimulation. J Neural Eng. 2011;8(1):016008.

36. Jensen RJ, Rizzo JF III. Responses of ganglion cells to repetitive electrical stimulation of the retina. J Neural Eng. 2007;4(1):S1.

37. Ahuja AK, Behrend MR, Kuroda M, Humayun MS, Weiland JD. An in vitro model of a retinal prosthesis. IEEE Trans Biomed Eng. 2008;55(6):1744–53.

38. Stronks HC, Dagnelie G. The functional performance of the Argus II retinal prosthesis. Expert Rev Med Devices. 2014;11(1):23–30.

39. Fornos AP, Sommerhalder J, da Cruz L, Sahel JA, Mohand-Said S, Hafezi F, et al. Temporal properties of visual perception on electrical stimulation of the retina. Invest Ophthalmol Vis Sci. 2012;53(6):2720–31.

40. Freeman DK, Eddington DK, Rizzo JF III, Fried SI. Selective activation of neuronal targets with sinusoidal electric stimulation. J Neurophysiol. 2010;104(5):2778–91.

41. Fried SI, Hsueh H-A, Werblin FS. A method for generating precise temporal patterns of retinal spiking using prosthetic stimulation. J Neurophysiol. 2006;95(2):970–8.

42. Margalit E, Thoreson WB. Inner retinal mechanisms engaged by retinal electrical stimulation. Invest Ophthalmol Vis Sci. 2006;47(6):2606–12.

43. Sekirnjak C, Hottowy P, Sher A, Dabrowski W, Litke AM, Chichilnisky E. High-resolution electrical stimulation of primate retina for epiretinal implant design. J Neurosci. 2008;28(17):4446–56.

44. Jepson LH, Hottowy P, Mathieson K, Gunning DE, Dąbrowski W, Litke AM, et al. Focal electrical stimulation of major ganglion cell types in the primate retina for the design of visual prostheses. J Neurosci. 2013;33(17):7194–205.

45. Jensen RJ, Rizzo JF III. Thresholds for activation of rabbit retinal ganglion cells with a subretinal electrode. Exp Eye Res. 2006;83(2):367–73.

46. Lilly JC, Hughes JR, Alvord EC Jr, Galkin TW. Brief, noninjurious electric waveform for stimulation of the brain. Science. 1955;121(3144):468–9.

47. Lilly JC, Austin GM, Chambers WW. Threshold movements produced by excitation of cerebral cortex and efferent fibers with some parametric regions of rectangular current pulses (cats and monkeys). J Neurophysiol. 1952;15(4):319–41.

48. Mortimer JT, Shealy CN, Wheeler C. Experimental nondestructive electrical stimulation of the brain and spinal cord. J Neurosurg. 1970;32(5):553–9.

49. Brummer S, Turner M. Electrical stimulation of the nervous system: the principle of safe charge injection with noble metal electrodes. Bioelectrochem Bioenerg. 1975;2(1):13–25.

50. Zhou DD, Dorn JD, Greenberg RJ. The Argus® II retinal prosthesis system: an overview. In: 2013 IEEE International Conference on Multimedia and Expo Workshops (ICMEW). IEEE; 2013.

51. Weiland JD, Anderson DJ, Humayun MS. In vitro electrical properties for iridium oxide versus titanium nitride stimulating electrodes. IEEE Trans Biomed Eng. 2002;49(12):1574–9.

52. Cohen E, Agrawal A, Connors M, Hansen B, Charkhkar H, Pfefer J. Optical coherence tomography imaging of retinal damage in real time under a stimulus electrode. J Neural Eng. 2011;8(5):056017.

53. Hartong DT, Berson EL, Dryja TP. Retinitis pigmentosa. Lancet. 2006;368(9549):1795–809.

54. Grover S, Fishman GA, Anderson RJ, Tozatti MS, Heckenlively JR, Weleber RG, et al. Visual acuity impairment in patients with retinitis pigmentosa at age 45 years or older. Ophthalmology. 1999;106(9):1780–5.

55. Santos A, Humayun MS, de Juan E, Greenburg RJ, Marsh MJ, Klock IB, et al. Preservation of the inner retina in retinitis pigmentosa: a morphometric analysis. Arch Ophthalmol. 1997;115(4):511–5.

56. Guadagni V, Novelli E, Piano I, Gargini C, Strettoi E. Pharmacological approaches to retinitis pigmentosa: a laboratory perspective. Prog Retin Eye Res. 2015;48:62–81.

57. Ahuja AK, Behrend MR. The Argus™ II retinal prosthesis: factors affecting patient selection for implantation. Prog Retin Eye Res. 2013;36:1–23.

58. Ghodasra DH, Chen A, Arevalo JF, Birch DG, Branham K, Coley B, et al. Worldwide Argus II implantation: recommendations to optimize patient outcomes. BMC Ophthalmol. 2016;16(1):52.

59. Xie J, Wang G-J, Yow L, Cela CJ, Humayun MS, Weiland JD, et al. Modeling and percept of transcorneal electrical stimulation in humans. IEEE Trans Biomed Eng. 2011;58(7):1932–9.

60. Finn AP, Grewal DS, Vajzovic L. Argus II retinal prosthesis system: a review of patient selection criteria, surgical considerations, and post-operative outcomes. Clin Ophthalmol (Auckland, NZ). 2018;12:1089.

61. Rizzo S, Belting C, Cinelli L, Allegrini L, Genovesi-Ebert F, Barca F, et al. The Argus II Retinal Prosthesis: 12-month outcomes from a single-study center. Am J Ophthalmol. 2014;157(6):1282–90.

62. Rachitskaya AV, Yuan A, Marino MJ, Reese J, Ehlers JP. Intraoperative OCT imaging of the Argus II retinal prosthesis system. Ophthalmic Surg Lasers Imaging Retina. 2016;47(11):999–1003.

63. Markowitz M, Rankin M, Mongy M, Patino BE, Manusow J, Devenyi RG, et al. Rehabilitation of lost functional vision with the Argus II retinal prosthesis. Can J Ophthalmol. 2018;53(1):14–22.

64. Ahuja AK, Dorn J, Caspi A, McMahon M, Dagnelie G, Stanga P, et al. Blind subjects implanted with the Argus II retinal prosthesis are able to improve performance in a spatial-motor task. Br J Ophthalmol. 2011;95(4):539–43.

65. Sabbah N, Authié CN, Sanda N, Mohand-Said S, Sahel J-A, Safran AB. Importance of eye position on spatial localization in blind subjects wearing an Argus II retinal prosthesis. Invest Ophthalmol Vis Sci. 2014;55(12):8259–66.

66. Luo YH-L, Zhong JJ, Da Cruz L. The use of Argus® II retinal prosthesis by blind subjects to achieve local-

isation and prehension of objects in 3-dimensional space. Graefes Arch Clin Exp Ophthalmol. 2015;253(11):1907–14.

67. Weiland JD, Cho AK, Humayun MS. Retinal prostheses: current clinical results and future needs. Ophthalmology. 2011;118(11):2227–37.

68. Ho AC, Humayun MS, Dorn JD, Da Cruz L, Dagnelie G, Handa J, et al. Long-term results from an epiretinal prosthesis to restore sight to the blind. Ophthalmology. 2015;122(8):1547–54.

69. da Cruz L, Dorn JD, Humayun MS, Dagnelie G, Handa J, Barale P-O, et al. Five-year safety and performance results from the Argus II retinal prosthesis system clinical trial. Ophthalmology. 2016;123(10):2248–54.

70. Gregori NZ, Callaway NF, Hoeppner C, Yuan A, Rachitskaya A, Feuer W, et al. Retinal anatomy and electrode array position in retinitis pigmentosa patients after Argus II implantation: an international study. Am J Ophthalmol. 2018;193:87–99.

71. Devenyi RG, Manusow J, Patino BE, Mongy M, Markowitz M, Markowitz SN. The Toronto experience with the Argus II retinal prosthesis: new technology, new hope for patients. Can J Ophthalmol. 2018;53(1):9–13.

72. da Cruz L, Coley BF, Dorn J, Merlini F, Filley E, Christopher P, et al. The Argus II epiretinal prosthesis system allows letter and word reading and long-term function in patients with profound vision loss. Br J Ophthalmol. 2013;97(5):632–6. https://doi.org/10.1136/bjophthalmol-2012-301525.

73. Yoon YH, Kim YJ, Humayun MS. Use of intraoperative OCT in ensuring optimal array-retina contact during argus ii implantation surgery—video presentation. American Academy of Ophthalmology 2018; 2018 October 26; McCormic Place, Chicago, IL, USA.

74. Geruschat DR, Flax M, Tanna N, Bianchi M, Fisher A, Goldschmidt M, et al. FLORA™: phase I development of a functional vision assessment for prosthetic vision users. Clin Exp Optom. 2015;98(4):342–7.

75. Geruschat DR, Richards TP, Arditi A, da Cruz L, Dagnelie G, Dorn JD, et al. An analysis of observer-rated functional vision in patients implanted with the Argus II Retinal Prosthesis System at three years. Clin Exp Optom. 2016;99(3):227–32.

76. Dagnelie G, Christopher P, Arditi A, da Cruz L, Duncan JL, Ho AC, et al. Performance of real-world functional vision tasks by blind subjects improves after implantation with the Argus® II retinal prosthesis system. Clin Exp Ophthalmol. 2017;45(2):152–9.

77. Barry MP, Dagnelie G. Use of the Argus II retinal prosthesis to improve visual guidance of fine hand movements. Invest Ophthalmol Vis Sci. 2012;53(9):5095–101.

78. Caspi A, Roy A, Wuyyuru V, Rosendall PE, Harper JW, Katyal KD, et al. Eye movement control in the Argus II retinal-prosthesis enables reduced head movement and better localization precision. Invest Ophthalmol Vis Sci. 2018;59(2):792–802.

79. Stingl K, Bartz-Schmidt KU, Besch D, Braun A, Bruckmann A, Gekeler F, et al. Artificial vision with wirelessly powered subretinal electronic implant alpha-IMS. Proc R Soc B. 2013;280(1757):20130077.

80. Wang L, Mathieson K, Kamins TI, Loudin JD, Galambos L, Goetz G, et al. Photovoltaic retinal prosthesis: implant fabrication and performance. J Neural Eng. 2012;9(4):046014.

81. Stingl K, Bartz-Schmidt KU, Besch D, Chee CK, Cottriall CL, Gekeler F, et al. Subretinal visual implant alpha IMS–clinical trial interim report. Vis Res. 2015;111:149–60.

82. Dacey DM. Physiology, morphology and spatial densities of identified ganglion cell types in primate retina. Ciba Found Symp. 1994;184:12–70. https://doi.org/10.1002/9780470514610.ch2.

83. Trenholm S, Roska B. Cell-type-specific electric stimulation for vision restoration. Neuron. 2014;83(1):1–2.

Retinal Gene Therapy

35

Mark M. Hassall and Matthew P. Simunovic

35.1 Introduction

The eye is an excellent target for gene therapy. As a 'surface' organ, the eye is easily accessible. Its small size means that correspondingly small treatment doses are required for efficacy. This fact, along with the eye's compartmentalisation, may limit the potential for systemic effects of intraocular therapies. The eye is also immunologically privileged under normal circumstances, thus limiting both intraocular inflammation and neutralising effects of the immune system on biological treatments. Its normally transparent media facilitates examination and imaging via optical means and, in the case of inherited retinal disease, the fact that it is a paired organ facilitates clinical trial design by providing an inbuilt control.

Gene therapy can be defined as the delivery of deoxyribonucleic acid (DNA) to cells as a drug to treat disease—it already offers treatment options for previously incurable inherited

eye conditions. Typically, gene therapy involves a modified viral vector carrying a functional copy of a gene into cells to replace a defective or missing copy of the same gene, thereby correcting the genetic disorder. This mechanism of action is generally described as **gene replacement** and is suitable for null mutations in autosomal and X-linked recessive disease, as well as haploinsufficiency in autosomal dominant disease. Alternative techniques include the introduction of novel genes to alter biological processes (e.g. anti-angiogenic factors in exudative ARMD) or to potentially alter cell survival or function (e.g. optogenetics). Gene therapy is different from **cell therapy**, which involves the transplantation of stem cells or differentiated cell types to replace or support diseased tissue (e.g. transplanting RPE cells as a treatment for early AMD). So too, gene therapy is distinct from **genome surgery**, which uses the CRISPR-Cas system derived from bacteria to edit the native genes with genetic mutations (e.g. to correct the *RHO;*p.P23H mutation causing autosomal dominant retinitis pigmentosa, RP). The first gene therapy for an eye disease was approved by the FDA in December 2017 [1], and there are currently over 40 active clinical trials for various gene therapies for the eye. This chapter outlines the core concepts, treatment strategies, surgical delivery techniques, and clinical trials relevant to the retinal specialist.

M. M. Hassall
Department of Ophthalmology, Flinders University, Adelaide, SA, Australia

M. P. Simunovic (✉)
Vitreoretinal Unit, Sydney Eye Hospital, Sydney, NSW, Australia

Save Sight Institute, University of Sydney, Sydney, NSW, Australia
e-mail: matthew.simunovic@sydney.edu.au

35.2 A Brief History of Gene Therapy

Watson and Crick first described the double-helix structure of DNA in 1953 [2], but it was another two decades before DNA was utilised as a potential therapy for disease. The first example of gene therapy, conducted in 1975, was undertaken in an attempt to treat systemic arginase deficiency by intravenous injection of unmodified wild-type Shope papilloma virus [3]. This first trial failed to demonstrate a treatment benefit, but nevertheless paved the way to the first approved trials using modified recombinant viruses designed and manufactured in a laboratory. One such notable trial, beginning in 1990, treated X-linked severe combined immunodeficiency (SCID-X) in children using infusions of recombinant retrovirus carrying the missing *IL2RG* gene [4].

Delivery of genes to the retina by viral vectors was first reported by Connie Cepko's group over three decades ago in experiments aimed at labelling retinal progenitor cells in newborn mice [5]. Within 10 years, experiments directed at delivering genetic payloads of wild-type genes in animal models of inherited retinal disease (IRD) [6] or retinal cell lines with genetic defects [7] were underway, and the last decade has seen rapid increase in the number of registered trials of gene therapy. In the mid-late 1990s, the identification of a large animal model of Leber congenital amaurosis (LCA) in the Briard dog in turn paved the way for translation of this technology into clinical trials in humans in the early 2000s [8].

The great early hope of gene therapy was tempered by the dual tragedies of a systemic gene therapy-related death in 1999 [9] and the first systemic gene therapy-related cancer cases in 2002 [10]. There was an appropriate slowdown in progress as the field grappled with the safety profile of modified viruses as vectors in ongoing trials.

In 2007 in London, the first human Leber congenital amaurosis (LCA) patient received a sub-retinal injection of recombinant adeno-associated virus (rAAV) carrying the *RPE65* gene as treatment [11]. This was followed very soon by a US group based in Philadelphia injecting a human LCA patient with a similar *RPE65* vector developed in parallel [12]. So began an exciting transatlantic race between groups to achieve the first FDA approval for a retinal gene therapy, culminating in the December 2017 FDA approval of voretigene neparvovec (*Luxturna*) for the US market [1]. There are currently over 40 different clinical trials underway for retinal gene therapy and the potential to cure previously untreatable diseases is immense. Before discussing some of these trials and the approaches to surgical delivery of retinal gene therapy vectors, this chapter briefly covers the fundamental principles of genetic disease and the core ideas of gene therapy.

35.3 Phenotype, Genotype, Inheritance, and the Effect on Treatment Strategy

The phenotype of a genetic disease is the physical manifestation of genetic mutations in a patient. Clear examples are the characteristic scotopic spectral sensitivity function of congenital achromatopsia or the pathognomonic vitelliform fundus appearance of Best disease. The genetic basis for the clinical phenotype is known as the genotype; yet, the genotype can arise from a number of complex genetic inheritance patterns that need to be understood when performing gene therapy.

Genetic information is stored as DNA in the cell nucleus and is formed from individual **nucleotides** (guanine, adenine, thymine, cytosine; G-A-T-C) assembled as matching pairs into a continuous double-helical molecule. A **chromosome** is a linear sequence of double-helical DNA coiled around **histone** proteins in the cell nucleus; histones support the structure and assist in modulating gene expression. Genetic material is inherited almost equally from each parent as 23 single chromosomes—including an 'X' or 'Y' sex chromosome—in the nuclei of the egg and the sperm. Thus, each offspring inherits 22 pairs of non-sex chromosomes (autosomes) and 2 sex chromosomes. Inequality of gene transfer with respect to the parental genome arises from the difference in
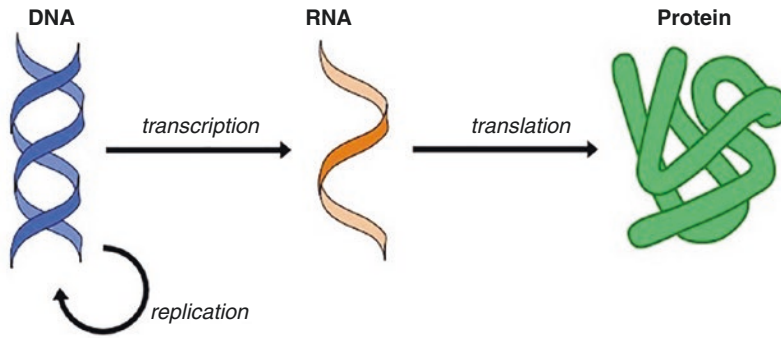
Fig. 35.1 The central dogma of molecular biology is that DNA is transcribed into RNA by polymerase enzymes in the nucleus. This messenger RNA is then translated into protein by ribosomes in the endoplasmic reticulum, thereby allowing the gene to execute a function

size of the X and Y chromosomes (in males), and the jettisoning of mitochondria (and therefore the paternal mitochondrial genome) from sperm during fertilisation of an ovum.

A gene is the basic unit of heredity and consists of a sequence of **nucleotides** that encode for a cellular function. In a simple example, a gene contains the code for a protein sequence that performs some function. With the notable exception of sex chromosome-encoded genes, one copy of each gene is inherited from each parent and this copy is located on the respective chromosome from that parent. Variations of a gene with slightly different sequences are termed **alleles** and these sequence differences are the cause of individual differences in physical traits. An individual may inherit two different alleles of the same gene. The nucleotide variation in a gene allele may change or impair the function of that gene so significantly as to cause disease.

Genes encoded by chromosomal DNA in the nucleus of the cell are **transcribed** into ribonucleic acid (RNA). This RNA is then transported out of the nucleus and **translated** into protein by ribosomes. The expression of the genetic information stored in a gene is regulated by a **promoter**, a nucleotide sequence upstream from the gene that is the initiation site for transcription. A promoter sequence may be constantly active or may only initiate transcription of a gene in certain cell types, certain stages of the cell cycle or certain cellular conditions, such as hypoxia. In genes that encode proteins, the promoter is fol-

lowed by a coding sequence made up of **introns** and **exons**. Introns are nucleotide sequences that are removed—'spliced out'—during the further processing of transcribed pre-mRNA into the final mRNA form. Thus, the previously separated exon sequences become a contiguous mRNA molecule that can then be transcribed directly into a protein sequence (Fig. 35.1).

Although most genetic information is stored as chromosomes in the nucleus, a smaller amount is inherited matrilineally as mitochondrial DNA. Mitochondria are small double-membrane-bound organelles scattered throughout the cell cytoplasm that produce ATP as an energy source for the cell. Mitochondrial DNA is inherited directly from the mother's egg and encodes for most mitochondrial functions; yet some mitochondrial genes are located in the nuclear chromosomes and the resulting proteins are transported to the mitochondria for use.

In summary, females inherit an 'X' chromosome each from their mother and father, whilst males inherit an 'X' chromosome from their mother and a 'Y' chromosome from their father. Both genders inherit 22 non-sex chromosomes (autosomes) from each parent and thus receive two alleles of each gene. If the alleles of a chromosomal gene are identical then the patient is **homozygous**, whereas a patient with two different alleles of a gene is **heterozygous**. All mitochondrial DNA is inherited from the mother and contains only one copy of each gene in each mitochondrion, although there may be many hun-

dreds or thousands of mitochondria in a single cell. A patient with identical DNA in all mitochondria is **homoplasmic**. However, an individual is said to be **heteroplasmic** if they inherit a heterogenous mixture of mitochondria containing different DNA sequences.

Thus, the phenotype of a single-gene disease is dictated by these fundamental principles of genetics. Non-disease-causing alleles are often referred to as wild-type alleles, a name introduced during early genetics research in *Drosophilia* fruit flies. Mutant alleles are inherited in an **autosomal dominant**, **autosomal recessive**, **X-linked** or **mitochondrial** pattern. The inheritance pattern of a disease must be considered when designing gene therapy treatment, as the mechanism of genetic rescue will differ.

After describing the pattern of inheritance, it is also important to consider the **penetrance** and **expressivity**. Penetrance refers to the proportion of patients carrying a certain mutant allele that also manifests the disease phenotype; in some diseases, penetrance may be incomplete due to the additional influence of factors like age, environment and epigenetics. Expressivity refers to the variation in disease phenotype along a continuous spectrum; it can only be reported in patients with penetrant mutations. Expressivity is analogous to describing the clinical severity of a disease by stages or grades.

35.3.1 Autosomal Dominant Inheritance

An autosomal dominant disease arises when one allele of a gene is able to produce the disease phenotype regardless of the sequence of the second allele; disease occurs in a heterozygous state. The mutant allele may cause disease through one of the three different mechanisms: **gain of function**, **dominant negative** or **haploinsufficiency**.

Dominant gain-of-function mutations confer novel or enhanced protein activity. This mechanism may involve conformational change of an enzymatic catalyst site, resulting in hyperactive enzyme function. For example, in autosomal dominant neovascular dominant vitreoretinopathy (ADNIV), mutations in the CAPN5 protease confer increased

protein digestion activity and lead to a constellation of signs including uveitis, ocular neovascularisation, vitreous haemorrhage, retinal degeneration and tractional retinal detachment [13].

Dominant negative mutations cause an altered protein product that impairs or disables the activity of the wild-type allele. This mechanism may involve misfolded protein aggregating with normally folded protein, creating dysfunctional aggregates. A common cause of autosomal dominant retinitis pigmentosa (RP) is the dominant-negative rhodopsin P23H mutation. Destabilised rhodopsin protein forms dysfunctional aggresomes in the cytoplasm that are marked for degradation [14] and result in rod photoreceptor death.

Dominant haploinsufficiency mutations exist on the same loss-of-function spectrum as autosomal recessive mutations. Haploinsufficiency arises when one mutant allele codes for a low-functioning or non-functioning protein; the decreased levels of normal protein are inadequate to sustain cellular functions. Retinitis pigmentosa 11 (RP11) is caused by mutations in the *PRPF31* gene that encodes an mRNA-splicing gene. The reduced rate of mRNA splicing for photoreceptor-specific genes is unable to meet the high turnover in these metabolically active cells, thereby leading to disease [15].

35.3.2 Autosomal Recessive Inheritance

Autosomal recessive mutations are loss-of-function mutations requiring two mutant alleles of the gene to cause disease. One wild-type allele of the gene is still sufficient to sustain normal cellular function, unlike in dominant haploinsufficiency. Patients must be homozygous for mutant alleles of the gene; a patient that inherits two different mutant alleles is said to be a compound heterozygote.

A prominent example in the context of the current chapter is Leber congenital amaurosis type 2 caused by bi-allelic mutations in the *RPE65* gene. RPE65 is a visual cycle enzyme expressed in retinal pigment epithelium that is

necessary for the regeneration of chromophore required for normal functioning of the rod and cone opsins. Dysfunction of the RPE65 enzyme due to mutations in both alleles of the gene results in loss of photosensitivity and so-called early-onset retinal degeneration [16].

35.3.3 X-Linked Inheritance

In males, all genes inherited on the X-chromosome are **hemizygous**—they do not have a corresponding second allele, unlike females. For this reason, a single loss-of-function allele mutation in an X-chromosome gene can cause disease in males. Females may manifest such conditions through a variety of mechanisms. First, they may inherit two mutated alleles of an X-linked gene to show a loss-of-function phenotype as described above for autosomal recessive disease. Second, some females may lack a one X-chromosome ('Turner syndrome') and may therefore exhibit disease in the hemizygous state. Finally, X-chromosomes are believed to be expressed randomly in each of the body's cells (random X-chromosome inactivation, or 'lyonisation') in females. On average, females will express 50% of maternally derived X-chromosomes and 50% of paternally derived X-chromosomes. However, expression may be skewed towards one or other of the chromosomes; through this mechanism a single mutant allele may produce disease.

X-linked retinitis pigmentosa (XLRP) is most often caused by mutations in the *RPGR* gene. RPGR plays an important role in regulating the connecting cilia of photoreceptors; RPGR mutation disrupts trafficking between the inner and outer segments, leading to retinal degeneration [17]. The disease affects men for the reasons just outlined.

35.3.4 Mitochondrial Inheritance

Mitochondrial genetic disease is inherited matrilineally. Mitochondria are responsible for producing the energy currency of the cell in the form of ATP; highly metabolically active retinal neural tissue is particularly vulnerable to ATP production deficiencies. An individual can inherit more than one population of mitochondria, thereby showing different populations of mitochondrial DNA in a single cell. This is a situation known as heteroplasmy and it influences the penetrance and expressivity of mitochondrial genetic disease.

A prominent example of mitochondrial disease in the eye is Leber hereditary optic neuropathy (LHON). First described in 1871, LHON typically manifests in the second or third decade of life resulting in bilateral and permanent loss of vision. Mutations in the mitochondrial *ND4* gene cause misfolded NADH dehydrogenase 4 protein, an important subunit of mitochondrial enzyme complex I. Efforts to treat the disease with gene therapy employ **allotropic expression**—the expression of a mitochondrial gene in the nucleus for cytoplasmic translation and transport to the mitochondria [18].

35.4 Viral Vectors for Gene Delivery

Harnessing DNA to treat genetic disease requires a transport method. DNA carries an overall negative charge due to the oxygen molecules in its phosphate backbone. This negative charge means that DNA cannot passively diffuse across cell membranes; there is no native mechanism for transmembrane DNA transportation. In cell cultures, it is possible to move DNA into cells using electroporation—subjecting cell membranes to high-voltage electric currents. However, in live animals and human patients, alternative methods are required to safely transport DNA into the target cells. The secret lies in so-called vectors; these are at present mostly recombinant viruses, though in the future other methods (such as nanoparticles) are likely to be employed more widely.

35.4.1 Expression Cassettes

Wild-type DNA viruses are adept at delivering their genomes to living cells and, indeed, are fully

Fig. 35.2 Expression cassette, which is subsequently packaged in the virus protein capsid. The coiled ends are inverted terminal repeats, palindromic nucleotide sequences required for correct packaging. CAG is a universal mammalian promoter, followed by the Kozak consensus sequence. The transgene in this instance is the CDS (exons only) of the *CNGB3* gene. The *WPRE* sequence is an example of a regulatory sequence that increases gene expression inside cells. The poly-A tail ensures that the transcribed RNA is marked as messenger RNA for translation to protein

reliant on infection for replication. Recombinant viral vectors harness this natural capacity for DNA transport whilst including modifications to improve safety and specificity. **Transduction** refers to the transfer of genetic material into a cell by a virus. To create these recombinant viruses, the gene of interest (e.g. *RPE65* for LCA type 2) is first isolated in the laboratory and then **cloned** into a custom DNA sequence called an **expression cassette**. Figure 35.2 shows an expression cassette containing—at a minimum—a **promoter**, a **Kozak consensus** sequence, a **transgene** and a **poly-A tail**.

The promoter is a nucleotide sequence that regulates the expression of a gene in different cell types and varying metabolic conditions. It is also the site at which the intracellular transcriptional machinery binds to begin transcribing DNA into RNA. The most widely used in gene therapy are universal synthetic promoters, which express transgenes in a range of cell types. The commonly used CAG promoter was formed from DNA fragments of **c**ytomegalovirus, the chicken beta-**a**ctin gene and the rabbit beta-**g**lobin gene; the CAG promoter expresses the transgene in all mammalian cell types.

Some promoters demonstrate preferential expression under certain pathological cellular conditions that may be harnesses for specific diseases. For example, the hypoxia response element (HRE) is preferentially active in hypoxic conditions and this feature can be exploited to target therapy in diseases involving hypoxic insults [19]. Other promoters—such as fragments of the cone opsin promoter—will only express genes in cone photoreceptors, which is an impor-

tant consideration in diseases such as rod monochromacy/autosomal recessive achromatopsia [20]. So too, sequences like the tetracycline-inducible promoter can be used to achieve episodic expression—by the addition or removal of tetracycline from the diet—that could be more versatile by offering modifiable expression [21].

The **Kozak consensus** sequence is six nucleotides that signify the beginning of a gene to the vertebrate intracellular transcription machinery; it plays a major role in the correct initiation of transcription. The sequence is most commonly GCCACC, followed by the ATG methionine start codon of the transgene [22].

The **transgene** refers to the gene of interest, specifically when it is artificially expressed in a cell by gene therapy. Often, only the exons of the coding sequence of a gene are used, as this is sufficient to achieve a correct protein sequence in the cytoplasm. The introns will be spliced out of the sequence during mRNA assembly. However, there is increasing recognition of the importance of (at times) including the upstream (5′UTR) and downstream (3′UTR) untranscribed regions [23]. These UTRs drive important post-transcriptional functions, such as mitochondrial localisation. The inclusion of the poly-A tail marks the transcribed RNA for translation to protein in the cell ribosome. Cellular translational machinery relies upon a repeating sequence of adenosine monophosphate to clearly identify messenger RNA.

All of these elements in the expression cassette are bound by **terminal repeats** (TRs) at each end. These palindromic nucleotide sequences remain from the wild-type virus and ensure correct packaging of the genetic sequence into the virus protein capsid [24].

The expression cassette may be further improved by **codon optimisation** of the transgene, the inclusion of **splice sites**, a **self-complementary** structure or additional post-transcriptional regulatory elements (PRE) such as the Woodchuck hepatitis virus PRE (**WPRE**).

Codon optimisation is the practice by which the codons—the 64-nucleotide triplets that code for the 20 amino acids—of a gene are modified, yet still deliver the same final protein sequence. Codon optimisation can solve issues with nucleotide sequence fidelity in repetition-rich areas [25]. Similarly, the

nucleotide sequence of mitochondrial genes delivered by allotropic expression strategies may need to be modified to avoid clashes between the mitochondrial and universal tRNA code.

Modification of a transgene to remove the introns leads to reduced mRNA levels in the cytoplasm. This may, in part, be explained by the role of splicing machinery in facilitating mRNA transport out of the nucleus [26]. Thus, transgene expression in gene therapy can be increased by the retention or reintroduction of a splice site near to the promoter; the more proximal this splice site is to the promoter, the more it increases expression [26]. However, there are clinical trials underway in which introns are not included in expression cassette, e.g. gene therapy for rod monochromacy [27].

DNA in wild-type and recombinant AAV is single stranded. After cellular transduction, the rate-limiting step towards gene expression is intracellular second-strand synthesis; only double-stranded DNA can then be transcribed and translated. This complementary strand synthesis is a slow process, but can be overcome by the design of a dimeric expression cassette containing both the sense and antisense strands of the transgene as a single continuous nucleotide sequence [28]. After transduction, the dimeric nucleotide sequence reanneals to form double-stranded DNA. Transgene expression from self-complementary vectors is more rapid and occurs at higher levels [28].

The inclusion of WPRE in the expression cassette increases the expression of the transgene protein, especially at lower doses [29]. It has been included in the current choroideraemia retinal gene therapy trial [30, 31], as well as the approved Glybera gene therapy for systemic lipoprotein lipase deficiency. WPRE can maximise gene delivery or be used to minimise the dose—and immunogenic risk—required to achieve adequate gene replacement [29].

35.4.2 Choice of Viral Vector

The expression cassette is then packaged into a virus protein capsid at high concentration, typically trillions of recombinant viral vectors per millilitre. This vector suspension can then be injected into the eye to deliver the DNA to the cells of interest. There are four main classes of recombinant viral vectors currently in use in clinical and preclinical trials: retroviruses, lentiviruses, adenoviruses (Ad) and adeno-associated viruses (AAV). Each virus type has strengths and drawbacks, although AAV—a single-stranded, non-pathogenic (save for self-limiting 'slapped cheek' syndrome in children), helper-dependent parvovirus—is the most commonly used vector in gene therapy of the eye. There are also ongoing efforts to synthesise non-viral vectors from polymers. Table 35.1 summarises each vector type, with attention to the key considerations of **genetic payload**, **immunogenicity**, **integration** and **self-replication**.

Genetic payload is the total length of DNA that can be packaged inside the virus protein capsid and is measured as the number of thousands of DNA base pairs (kilobases; kB). Immunogenicity refers to the likelihood of the vector to induce an immune response from the host; an immune response may interfere with the efficacy of treatment or, rarely, may cause serious harm or death in the case of systemic treatment [9]. Integration refers to whether the DNA delivered by the virus is incorporated into the host cell chromosomes or remains as a separate **episome** in the cell. In actively dividing cells—such as blood cells (SCID-X) or airway epithelium (cystic fibrosis)—new genetic sequences must be integrated into the chromosomal DNA in order to be vertically transmitted to new daughter cells during mitosis. In the postmitotic cells of the retina—such as photoreceptors (*rhodopsin* gene therapy*) and retinal pigment epithelium (*RPE65* gene therapy)—the new genetic material does not need to be integrated and vertically transmitted to achieve sustained expression. Integrating viruses can be oncogenic, as witnessed in the leukaemia cases of the SCID-X human trials [10].

Self-replicating viruses contain all the necessary genes in their wild-type DNA to reproduce in a cell; non-self-replicating viruses are dependent upon the genes of other viruses for propagation. Most viruses are self-replicating, but AAV is reliant upon gene sequences in adenovirus or herpes virus for replication. Without the *E1*, *E2A*, *E4* and *VA* RNA genes provided by adenovirus, AAV

Table 35.1 Types of viral vectors

Viral vector	Notable first example	Payload size (kB)	Strengths	Weaknesses
Adeno-associated virus	*RPE65* Luxturna	4.7	Low immunogenicity Non-integrating Not self-replicating	Small payload size
Adenovirus	Ornithine transcarbamylase	Up to 30	Larger payload	Higher immunogenicity Documented death from intravenous Ad infusion Self-replicating wild type
Lentivirus	*ABCA4* eye trials	Up to 10	Integrating Larger payload; current clinical trial for *ABCA4* gene that is too big for AAV	Self-replicating wild-type
Retrovirus	SCID-X (systemic)	Up to 10	Integrating; propagated in rapidly dividing cells	Potentially oncogenic; documented cases of cancer Self-replicating wild type
Non-viral vectors (polymers, lipids)	Patisiran (systemic)	Variable	Lower immunogenicity Fully customisable	New technology, still developing Harder to mass produce

cannot reproduce [32]. This gives these viruses a particularly reliable safety profile, as it is not possible for them to mutate after injection to produce an expanding viral infection in an individual or an outbreak in a population.

Recombinant adeno-associated virus (rAAV) is the commonly used virus vector in retinal gene therapy. Additional work has been performed to improve the specificity of rAAV in targeting specific cell types. Tyrosine residues in the protein capsid of the virus can be modified to improve photoreceptor or RPE targeting, as well as increase penetration through the retina after intravitreal injection [33].

35.4.3 Vector Manufacturing and Quality Control

Recombinant AAV vector is produced in the laboratory using immortalised human cells as virus assembly factories. Cells are transfected with the expression cassette DNA that contains the gene of interest, promoter and other genetic elements. The cells are also transfected with separate DNA sequences encoding for the helper proteins for virus assembly and DNA packaging into the virus inside the cell, as well as sequences for the virus capsid proteins. The transfected cells are then grown in large quantities over 1–2 weeks.

The resulting cells are then broken open to release the assembled viral particles. Pure virus is then isolated using a large centrifuge and a density gradient containing layered concentrations of a molecule like iodixanol or cesium chloride. Purified virus then undergoes quality control before human use. The capsid proteins are denatured and checked for correct size and ratios using Western blot. The number of empty virus capsids is checked using electron microscopy to ensure that the DNA cassette has been reliably packaged into the virus. The concentration of virus per microlitre is checked by qPCR titre to allow accurate dose administration in the eye. Finally, correct virus function can also be assessed by testing gene expression in human cell cultures using a variety of assays. Assembled virus is unstable at room temperature and is typically stored at −80 °C until use. Perioperative storage should be as per the manufacturer's instructions, but typically requires refrigeration. Post-operatively, remaining virus from the patient's dose may be tested on cell cultures to exclude virus dysfunction as a cause of treatment failure.

35.5   Treatment Strategies: Gene Specific

There are two core treatment strategies by which gene therapy can be used to treat gene-specific diseases: **replacement** and **silencing**. Replacement is used to treat diseases caused by autosomal recessive, dominant haploinsufficiency or X-linked loss-of-function mutations. Silencing is used to treat diseases caused by autosomal dominant gain-of-function or dominant-negative mutations.

35.5.1   Replacement

A replacement strategy reverses the genetic mechanism underlying the disease phenotype by increasing quantities of the gene and protein to restore normal cellular function. The current gene therapy trials on *CNGA3* and *CNGB3* achromatopsia are a clear example of the replacement strategy treating autosomal recessive disease. Expression of any quantity of these ion channel genes is sufficient to restore electrophysiological function in the cone photoreceptors [27]. Similarly, delivery of functional *RPGR* gene can reverse X-linked disease in rodents and is currently in phase I trials [25].

Replacement can also overcome dominant haploinsufficiency. The virus-delivered gene augments the existing functional allele of the gene. The resulting increase in wild-type protein product achieves sufficient levels for normal cellular function. *PRPH2*-associated photoreceptor degeneration is a good candidate for replacement gene therapy for haploinsufficiency, although no preclinical therapy has currently reached trials [34]. Excess replacement of the affected gene above wild-type levels can be toxic in animals and correct dosing of gene replacement is important [35].

35.5.2   Silencing

Gene therapy for dominant-negative and gain-of-function mutations requires silencing of the mutant alleles—also referred to as 'knockdown'. Silencing reduces the expression of a gene and thus minimises the damaging effect. This strategy may also require simultaneous replacement of the wild-type allele to avoid haploinsufficiency after knockdown. There are different molecular strategies used to achieve gene silencing, but most target RNA [36].

The first strategy uses short nucleotide sequences (RNA, DNA) to guide enzyme-mediated degradation of mutated RNA products. This prevents mutant protein formation and can be achieved using RNA interference (**RNAi**) or antisense oligonucleotides (**ASO**). The second strategy is to use steric-blocking RNA that impairs access of cellular machinery to pre-mRNA and mRNA, but does not cause degradation.

RNAi uses short interference RNA (**siRNA**) sequences that interact with the RNA interference silencing complex (RISC) to cleave target sequences of disease-causing mutant mRNA. RNAi is limited by the vulnerability of the siRNA to degradation, as well as the risk of off-target effects in other normal mRNAs. ASO use short sequences of single-stranded DNA that bind the mutated mRNA and target it for degradation by the RNase H enzyme. Compared to the RNAi strategy, ASO sequences can be more easily modified to reduce degradation and still be recognised by the enzyme.

Steric-blocking RNA sequences can be **translation suppressing** and target mRNA to prevent protein formation. Thus, only the normal protein is produced. Blocking RNA sequences can also be **splice switching** and target pre-mRNA to alter splicing activity; they may prevent undesirable splice variants or induce normal mRNA splicing.

Much of the existing research into gene silencing has been performed using regular infusions or injections of pure RNA constructs. Gene therapy overcomes the need to regularly deliver the RNA construct by instead transfecting the cell with a permanently functioning copy of the RNA sequence. This constant expression of the interference RNA technology achieves ongoing silencing of the mutated gene (Fig. 35.3).
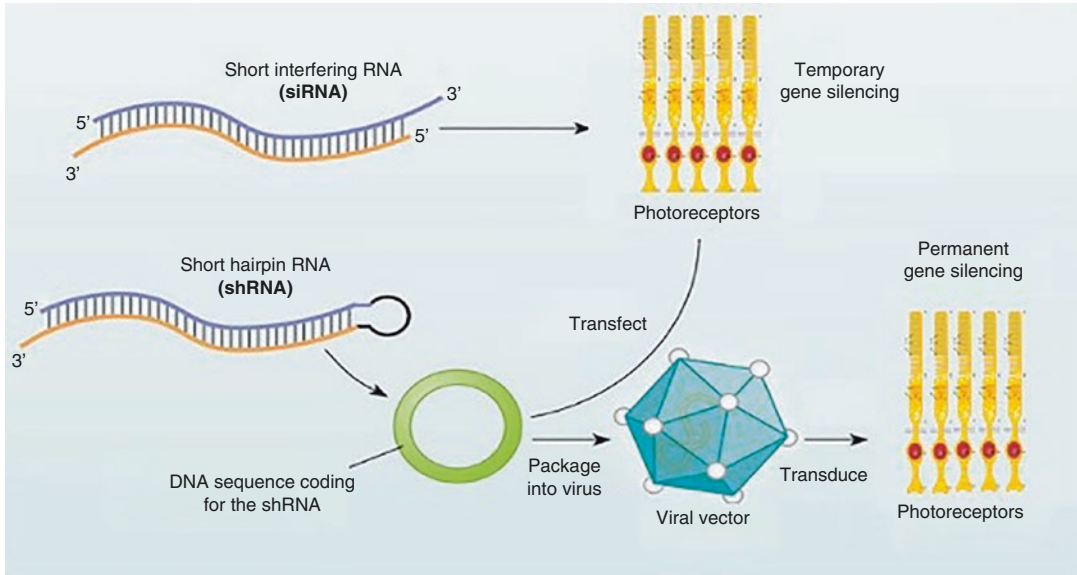
Fig. 35.3 Simple schematic of the silencing technologies and why gene therapy is more effective

35.6 Treatment Strategies: Gene Independent

There are three adjunctive methods by which gene therapy can be used to treat disease independently of the original genetic mutation: overexpression of **trophic factors**, overexpression of **anti-neovascularisation factors** and ectopic gene expression for **optogenetics**.

35.6.1 Trophic Factors

Neurotrophic factors are a family of molecules that stimulate the growth or survival of neurons. Photoreceptor survival was improved in preclinical studies overexpressing ciliary neurotrophic factor (*CNTF*) [37, 38] and brain-derived neurotrophic factor (*BDNF*) [39]. Similarly, *BDNF* gene therapy is protective to ganglion cells in rodent models of glaucoma [40]. However, neurotrophic factors have broad downstream effects on gene expression that can be difficult to predict [41] and which may prove toxic [42]. No neurotrophic factor gene therapies have reached clinical trials, but analogous human studies have used

a CNTF-releasing microcapsule inserted into the vitreous cavity. This microcapsule has been shown to be safe in RP patients and shows promise in reducing the rate of cone photoreceptor loss [43, 44], although it may be associated with more rapid progression of visual field loss. Gene therapy to express CNTF has demonstrated promise in preclinical models of IRD, and similar results might be achieved using retinal gene therapy to achieve sustained release of neurotrophic factors.

35.6.2 Anti-neovascularisation Factors

Current therapy for wet AMD involves regular intravitreal injections of monoclonal antibodies/antibody fragments or receptor decoys that bind VEGF-A +/− PDGF and suppress the activity of choroidal new vessels. There would be clear benefits to delivering a once-off intravitreal or subretinal injection of gene therapy to provide sustained expression of a gene coding an anti-angiogenic peptide. Benefits could include a reduction in costs to patients and healthcare sys-

tems and a theoretically reduced burden of endophthalmitis through a reduction in the number of intraocular interventions. Angiogenesis involves multiple steps, but two early gene therapy clinical trials focus on soluble fms-like tyrosine kinase-1 (*sFLT-1*) that has direct anti-VEGF action [45, 46]. Phase I results show good safety profile, but phase II follow-up studies have yet to be reported: at least one has failed to prove the efficacy required to proceed to pivotal trial.

35.6.3 Optogenetics

Optogenetics refers to the expression of type 1 (microbial) or type 2 (animal) opsins in secondary or tertiary neurons of the retina in order to render them light sensitive. Rarely, the technique may be used to express opsins in degenerate photoreceptors. In many respects, this approach may be considered a biological 'retinal implant'. Animal models have demonstrated a return of light sensitivity to within 2 log units of the threshold for cone activation in previously blind animals [47]. Currently, two registered clinical trials are investigating optogenetics in patients with inherited retinal degeneration (ClinicalTrials.gov Identifier: NCT02556736 & NCT03326336).

Much of the early work of optogenetics for retinal degeneration focussed on type 1 opsins. The most commonly employed is channelopsin and its derivatives; these are light-gated ion channels which alter their conformation upon photon absorption by their chromophore (all-trans retinal, which undergoes photoisomerisation to 13-*cis* retinal) which in turn leads to a change in membrane conductance. In contrast to type 2 opsins, the chromophore is not liberated: rather it photoisomerises and then relaxes back into its original conformation. The kinetics of this process are such that it is (in general) far more rapid than the normal human visual cycle.

Early work used both depolarising and hyperpolarising microbial opsins. Some studies have also targeted degenerate photoreceptors for expression of optogenetic molecules in order to re-establish their light sensitivity [48]. Subsequent preclinical studies investigated the potential for native human photosensitive opsins—melanopsin and rhodopsin—to generate light sensitivity in the inner retina [49, 50]. Further work is required before optogenetics arrives in the clinic.

We have recently performed a comprehensive review of this field, and the reader is directed to the review for an in-depth discussion of this approach [47].

35.6.4 Genome Surgery

Genome surgery is different from classical gene therapy. Rather than delivering DNA as a drug to treat disease, genome surgery edits the existing DNA of the cell to alter mutated alleles. DNA is deleted, inserted, modified or replaced at a specific location. The corrected gene then produces wild-type protein and normal function is restored. All methods involve using engineered nucleases to induce double-stranded breaks in DNA that are repaired using non-homologous end joining (NHEJ) or homology-directed repair (HDR).

Early methods in genome surgery employed zinc finger nucleases and transcription activator-like effector nuclease (TALEN). Both methods rely on the customisation of DNA-binding 'fingers' or domains within a larger protein. This limits the range of potential nucleotide sequence targets. It also makes it difficult to quickly and easily target multiple different DNA sequences during therapy development.

Genome surgery has expanded rapidly in recent years since the discovery of the CRISPR-Cas system, which improved the accuracy and efficiency of editing. This technology uses an easily modifiable guide-RNA sequence to bind and identify a nucleotide sequence for cutting by the Cas protein. It can be used to break, repair or even silence targeted genes in a cell. The CRISPR-Cas9 genes can also be delivered using modified viral vectors. There are currently no clinical trials for genome editing, although there are multiple examples of rodent models of disease being rescued using CRISPR-Cas, such as the Royal College of Surgeons/MERTK rat [51].

There have been prominent examples of researchers editing human embryos to remove

disease [52, 53]. Yet concerns remain about the off-target effects of gene editing, which could be deleterious themselves [54]. There are also ethical issues surrounding manipulation of the genome in such a way that it might be passed on to successive generations. It is important to note, however, that ocular gene therapy transgenes are not vertically transmitted.

35.7 Intraocular Delivery

The delivery of the viral vector into the eye should maximise vector transduction of the target cells and minimise trauma to the tissue. The majority of pioneering gene therapy trials have used a subretinal injection of recombinant virus vector to deliver therapy to the photoreceptors or RPE; direct contact with the target cells improves delivery. Subretinal injections carry the risk of vitrectomy surgery and iatrogenic retinal detachment and are inherently resource intensive.

Intravitreal injections of recombinant viral vectors are more effective at transducing the inner retinal cells, but in general do not achieve the same photoreceptor or RPE targeting as subretinal delivery. Intravitreal injections are less resource intensive and carry fewer risks; intravitreal delivery may require higher doses to achieve gene transfer to all cells and this may carry higher immunogenic risk. This delivery method may be more appropriate for the expression of antineovascularisation factors, neurotrophic factors or optogenetic proteins in retinal disease, or ganglion cell therapies in glaucoma.

35.7.1 Subretinal Injection

Subretinal therapy has been used in a number of clinical trials of retinal gene therapy [55]. Its principal disadvantage is that it necessitates a pars plana vitrectomy prior to subretinal injection, making the procedure accessible only to vitreoretinal surgeons, though the steps of the procedure are much the same as those used in performing subretinal injections for other indications, e.g. sub-macular haemorrhage (see
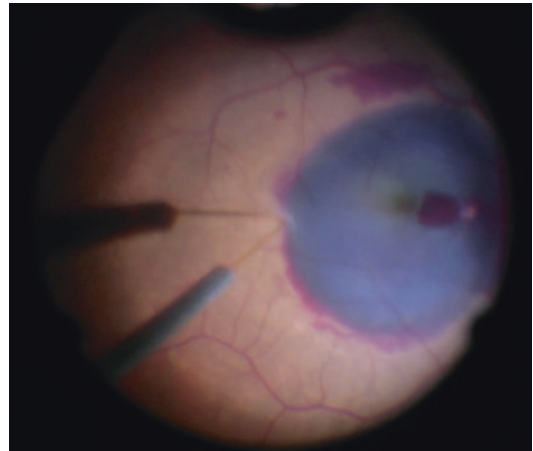
Fig. 35.4 The process of subretinal injection for gene therapy is broadly similar subretinal tPA for macular haemorrhage (shown). A 25–38 g Teflon-tipped cannula is seen here entering the subretinal space to deliver the drug under viscous fluid control

Fig. 35.4 and for a video, https://www.youtube.com/watch?v=OKYqsVz3Maw).

Briefly, a standard three-port trans-pars plana vitrectomy is performed, including core and peripheral vitrectomy with induction of a posterior vitreous detachment (unless clinically contraindicated). At this stage, subretinal injection is performed using a regular (typically 23 or 25 gauge) to fine (generally 38–41 gauge) cannula to puncture the neural retina. The surgical space between the neural retina and the retinal pigment epithelium is then 'opened' via injection of fluid, thus creating an iatrogenic retinal detachment. The retinotomy site is not subsequently subjected to retinopexy and the retina reattaches rapidly (generally within 24 h) [56].

Variations in the technique exist. For example, the surgical plane may be defined with balanced salt solution (BSS) prior to injection of the gene therapy solution (the so-called two-step technique) [57]; alternatively, the gene therapy solution itself may be used to induce retinal detachment (the so-called one-step technique) [58]. The injection itself may be performed manually (i.e. by depressing a plunger) or via the viscous fluid injection system of the vitrectomy unit. The latter allows for precise control of the pressure of injection and arguably results in greater

precision during injection. The target tissue may be detached during the injection procedure. Alternatively, injection may be performed outside of the target area and the fluid 'steamrollered' passively by the use of heavy liquid such as *n*-perfluoro-octane. Theoretical disadvantages of such an approach include the possibility of reflux via the retinotomy site and the potential for the heavy liquid to pass underneath the neural retina. Novel developments may further aid the injection, including intraoperative OCT to confirm the plane of injection and robotic surgical devices to improve the precision of injection and to minimise tissue damage [59]. Although surgery is the most commonly overlooked variable in gene therapy, we have recently described a novel qualitative and quantitative technique to track subretinally delivered drugs using fluorescein as an optical label [60].

Pars plana vitrectomy is cataractogenic [61]; furthermore it may rarely be associated with subsequent uncontrolled rhegmatogenous retinal detachment and one case of full-thickness macular hole has been reported in a patient with LCA undergoing gene therapy (though such patients have retinal thinning which may predispose to such complications) [12]. The delivery of material into the subretinal space necessitates iatrogenic detachment of the retina. Although this is generally agreed to have a deleterious effect on retinal function, studies of functional recovery following iatrogenic retinal detachment for retinal gene therapy confirm that spatial vision recovers rapidly following the procedure [56]. However, other aspects of visual function may be disturbed in the short term, including colour matching [56]. The latter finding, in combination with thinning demonstrated by optical coherence tomography (OCT), implicates loss of outer segment length in some patients [56].

35.7.2   Intravitreal

Intravitreal injection of therapeutic substances is one of the commonest procedures undertaken by eye surgeons in routine clinical practice. The procedure may be conducted in either an operating room or a suitably equipped office environment. Following local anaesthesia and preparation, the approach is to inject medications using a fine-gauge needle (e.g. 30 or 32 gauge) via a pars plana approach. Volumes of 0.05 mL are routinely injected for the management of age-related macular degeneration, and larger volumes of gas are injected for the management of retinal detachment using pneumatic retinopexy. The safest route to the vitreous cavity depends upon the patient's age and phakic status. In adults, a distance of 3.5 mm (pseudophakic) to 4.0 mm (phakic) posterior to the limbus is used. The safe approach for children may be used either from previously formulated tables informed by cadaveric studies, or empirically using transillumination [62].

The phase I trial of AAV2.sFLT01 for neovascular AMD pioneered intravitreal injections for retinal gene therapy [46]. The method varies little from existing methods for pars plana intravitreal injections in the clinic, with 0.1 mL of gene therapy solution being injected using a 30 gauge needle via a trans-pars plana approach.

Intravitreal injection has been used in phase I/II clinical trial of gene therapy for X-linked retinoschisis [63].

There are ongoing concerns regarding the immunogenicity of intravitreal injection of viral vectors [64], with the likelihood of intraocular inflammation increasing with increasing viral titres. However, advances in vector development and selection (e.g. using so-called directed evolution techniques) may help to negate or minimise the likelihood of such effects.

35.8   Post-operative Care

Alongside the normal post-operative care following vitrectomy, gene therapy patients require a few additional considerations. The first is the theoretical risk that the patient may actively shed recombinant virus vector in their tears, or other secretions, immediately following the surgery [65]. However, vector shedding studies in the choroideraemia and Leber congenital amaurosis patient cohorts have shown no detectable virus in samples after day 1 [65, 66]. Furthermore, and as

described earlier in the chapter, AAV is not self-replicating and would not pose an ongoing infection risk, even if shed.

The surgeon should also monitor the functional recovery of the macula or other retinal site(s) detached during subretinal injection. Results from the phase I/II gene therapy trials thus far have generally shown good functional recovery of the macula after deliberate iatrogenic detachment [56]. Rarely, subretinal gene therapy may be associated with macular hole [12] or rhegmatogenous retinal detachment which necessitates further surgery.

A third consideration is the use of topical or systemic immunosuppression to minimise immune response to the virus vector. Pre-existing antibodies to the virus surface proteins have been shown to reduce or prevent transgene expression; similarly, humoral immune responses to AAV have been demonstrated in non-human primates [67]. There is currently no standardised perioperative or post-operative steroid protocol for retinal gene therapy trials.

As part of the choroideraemia trial (NCT02407678), perioperative corticosteroid (oral prednisolone) was given, starting 2 days prior to surgery at 1 mg/kg for 10 days, then 0.5 mg/kg for 7 days, 0.25 mg/kg for 2 days and then 0.125 mg/kg for 2 days.

Alternatively, the London *RPE65* trial protocol administered topical steroid (dexamethasone 0.1% qds for 4 weeks), as well as oral prednisolone commencing at a dose of 0.5 mg/kg 1 week prior to administration; 1 mg/kg for the first week following administration, 0.5 mg/kg for the second week, 0.25 mg/kg for the third week and 0.125/kg for the fourth week [68].

35.9 Overcoming Amblyopia in Late Treatment of Congenital/Early Blindness

The human visual system is exquisitely sensitive to loss of afferent input in terms of its early development [69]. Patients who suffer from early deprivation of vision experience long-term aberrant neural adaptation to this deprivation (i.e.

deprivation amblyopia). Whilst this is not generally considered to be an issue for patients in whom vision does not deteriorate until after the so-called neuroplastic period of visual development, it may prove to be a key issue in treating those in whom the disease process is manifest within this period.

The effects of such deprivation may differ considerably from other forms of amblyopia, such as those resulting from image degradation due to refractive error or due to media opacification. For example, those with the latter forms of amblyopia may suffer from less severe effects on visual functions other than spatial discrimination (e.g. their sensitivity to flicker and to colour may in theory be better preserved). In patients with achromatopsia, functional MRI shows that the cortical space dedicated to foveal cones is monopolised by rod pathways and it is unclear how much of this monopoly in humans is reversible with gene therapy [70]. Work in murine models shows that dichromatic vision can be restored in models of S-cone ('blue cone') monochromacy [71]. So too, cone function can be restored in murine models of rod monochromacy after the traditional neuroplastic window [72]. Studies in simian models suggest that trichromatic colour discrimination may be acquired through gene therapy to deliver a third opsin to the retina of dichromatic adult animals, even after the so-called plastic period [73]. The mechanism for such gains of function is poorly understood and can perhaps be explained by the exploitation by the new channel of mechanisms previously devoted to extracting spectral comparisons through other means, including variations in photopigment optical density and through rod input. Whatever phenomenon underlies this observation, it is clear that current concepts of plasticity may not reflect the gains which may be made in some aspects of visual function via gene therapy. There is early evidence to suggest that gene therapy can achieve good cortical response on fMRI in LCA2 [74].

The current study designs for the clinical trials into early-onset genetic blindness—such as LCA2 and achromatopsia (Table 35.2)—aim to explore the differential rescue in younger and older patients. After initial safety cohort, the

Table 35.2 Summary of current clinical trials

Disease	Transgene	Intervention	NCT number	Phases	Enrollment (N)	Recruitment ages (years)	Completion year	Primary and secondary outcomes	Sponsor
Achromatopsia	CNGA3	Subretinal rAAV.hCNGA3	NCT02610582	I/II	9	18+	2017	Safety. Efficacy measures.	STZ Eyetrial
Achromatopsia	CNGB3	Subretinal AAV.CNGB3	NCT03001310	I/II	18	3+	2019	BCVA, QoL	MeiraGTx UK II Ltd
Achromatopsia	CNGB3	Subretinal AAV.CNGB3	NCT03278873	I/II	18	3+	2023	BCVA, QoL	MeiraGTx UK II Ltd
Achromatopsia	CNGB3	Subretinal rAAV2tYF-PR1.7-hCNGB3	NCT02599922	I/II	24	6+	2022	BCVA, colour vision	Applied Genetic Technologies Corp
Achromatopsia	CNGA3	Subretinal rAAV (AGTC-402)	NCT02935517	I/II	24	6+	2023	ADEs, BCVA, light aversion, colour vision	Applied Genetic Technologies Corp
ARMD	Endostatin and angiostatin	Subretinal retinostat (lentivirus)	NCT01301443	I	21	50+	2015	CMT on OCT	Oxford BioMedica
ARMD	Endostatin and angiostatin	Subretinal retinostat (lentivirus)	NCT01678872	I	18	50+	2029	BCVA	Oxford BioMedica
ARMD	Soluble CD59	Intravitreal AAV.CAG.sCD59	NCT03144999	I	17	50+	2019	Area of GA	Hemera Biosciences
ARMD	Soluble FLT01	Intravitreal AAV2.sFLT01	NCT01024998	I	19	50+	2018	CMT on OCT, dose tolerance	Genzyme
ARMD	Soluble FLT01	Intravitreal AAV2.sFLT01	NCT01494805	I/II	40	55+	2017	BCVA	Lions Eye Institue, Australia
ARMD	Soluble anti-VEGF monocloncal antibody fragment	Subretinal RGX-314 (AAV8)	NCT03066258	I	24	50+	2020	BCVA, CMT, area of CNV, No. anti-VEGF injections	Regenxbio

(continued)

Table 35.2 (continued)

Disease	Transgene	Intervention	NCT number	Phases	Enrollment (N)	Recruitment ages (years)	Completion year	Primary and secondary outcomes	Sponsor
ARMD	Soluble CD59	Intravitreal AAV. CAG.sCD59	NCT03585556	I	10	50+	2020	No. anti-VEGF injections, BCVA	Hemera Biosciences
Choroideremia	REP1	Subretinal AAV2. REP1	NCT03584165		100	18+	2024	BCVA, AF, OCT, microperimetry	Nightstar Therapeutics
Choroideremia	REP1	Subretinal AAV2. REP1	NCT03507686	II	15	18+	2020	BCVA, AF, OCT, microperimetry	Nightstar Therapeutics
Choroideremia	REP1	Subretinal rAAV2.REP1	NCT02077361	I/II	6	18+	2017	HVF, BCVA	Albert Innovates Health Solutions
Choroideremia	REP1	Subretinal rAAV2.REP1	NCT01461213	I/II	14	18+	2017	BCVA, microperimetry, OCT, AF	University of Oxford
Choroideremia	REP1	Subretinal AAV2. REP1	NCT02553135	II	6	18+	2018	BCVA, AF, microperimetry	University of Miami
Choroideremia	REP1	Subretinal AAV2. REP1	NCT03496012	III	140	18+	2020	BCVA, AG, OCT, microperimetry, contrast sensitivity, colour vision	Nightstar Therapeutics
Choroideremia	REP1	Subretinal AAV. REP1	NCT02407678	II	30	18-90	2021	BCVA, microperimetry, AF	University of Oxford
Choroideremia	REP1	Subretinal rAAV. REP1	NCT02671539	II	6	18+	2021	BCVA, AF, microperimetry, contrast sensitivity, colour vision	STZ Eyetrial
Choroideremia	REP1	Subretinal AAV2. hCHM	NCT02341807	I/II	15	18+	2019	Safety study only	Spark Therapeutics

Disease	Transgene	Intervention	NCT number	Phases	Enrollment (N)	Recruitment ages (years)	Completion year	Primary and secondary outcomes	Sponsor
LCA	RPE65	Subretinal rAAV2.CBSB.hRPE65	NCT00481546	I	15	8+	2026	BCVA	University of Pennsylvania
LCA	RPE65	Subretinal AAV2.hRPE65 (voretigene neparvovec-rzyl)	NCT03597399		40	1+	2028	Safety study only	Spark Therapeutics
LCA	RPE65	Subretinal AAV2.hRPE65 v2	NCT03602820		41	3+	2030	Mobility testing, BCVA, light sensitivity threshold test	Spark Therapeutics
LCA	RPE65	Subretinal AAV2.hRPE65 (voretigene neparvovec-rzyl)	NCT00999609	III	31	3+	2029	MLMT, BCVA, light sensitivity threshold test	Spark Therapeutics
LCA	RPE65	Subretinal AAV2/4.hRPE65	NCT01496040	I/II	9	6-50	2014	QoL	Nantes University Hospital
LCA	RPE65	Subretinal rAAV2.hRPE65	NCT00821340	I	3	8+	2017	BCVA	Hadassah Medical Organisation
LCA	RPE65	Subretinal AAV.RPE65	NCT02781480	I/II	27	3+	2018	BCVA, QoL, retinal function	MeiraGTx UK II Ltd
LCA	RPE65	Subretinal AAV2.hRPE65 (voretigene neparvovec-rzyl)	NCT00516477	I	12	8+	2024	BCVA	Spark Therapeutics
LCA	RPE65	Subretinal AAV2/5.OPTIRPE65	NCT02946879		27	3-100	2023	BCVA, QoL, retinal function	MeiraGTx UK II Ltd

(continued)

Table 35.2 (continued)

Disease	Transgene	Intervention	NCT number	Phases	Enrollment (N)	Recruitment ages (years)	Completion year	Primary and secondary outcomes	Sponsor
LCA	RPE65	Subretinal rAAV2/2.hRPE65	NCT00643747	I/II	12	5-30	2014	BCVA	University College London
LCA	RPE65	Subretinal rAAV2. CB.hRPE65	NCT00749957	I/II	12	6+	2017	ADEs, HVF 30-2, BCVA	Applied Genetic Technologies Corp
LCA	GUCY2D	Subretinal rAAV (SAR439483)	NCT03920007	I/II	15	6+	2021	ADEs, BCVA, ffERG	Sanofi
LHON	ND4	Intravitreal rAAV2.ND4	NCT03428178	NA	50	8-60	2020	BCVA, HVF, RNFL thickness	Huazhong University of Science and Technology
LHON	ND4	Intravitreal rAAV2.ND4	NCT03153293	II/III	40	10-65	2019	BCVA, HVF, RNFL thickness	Huazhong University of Science and Technology
LHON	ND4	Intravitreal rAAV2/2.ND4	NCT03293524	III	90	15+	2021	HVF, OCT measures, QoL, contrast sensitivity	GenSight Biologics
LHON	ND4	Intravitreal rAAV2/2.ND4	NCT02652767	III	36	18+	2019	RNFL thickness, HVF, contrast sensitivity, colour vision	GenSight Biologics
LHON	ND4	Intravitreal rAAV2/2.ND4	NCT02652780	III	36	18+	2019	RNFL thickness, HVF, contrast sensitivity, colour vision	GenSight Biologics

Disease	Transgene	Intervention	NCT number	Phases	Enrollment (N)	Recruitment ages (years)	Completion year	Primary and secondary outcomes	Sponsor
LHON	ND4	Intravitreal rAAV.ND4	NCT01267422	I	9	8-60	2015	BCVA, T-cell markers, IOP, BCVA, RNFL thickness, HVF 30-2	Huazhong University of Science and Technology
LHON	ND4	Intravitreal scAAV2-P1ND4v2	NCT02161380		30	15+	2023	Toxicity/ADEs	John Guy, University of Miami
Retinoblastoma	*Oncolytic virus*	Intravitreal replication-competent oncolytic adenovirus (VCN-01)	NCT03284268	I	13	1-12	2019	Tumour response, immune response	Foundacio Saint Joan de Deu
RP	Channelrhodopsin-2	Intravitreal RST-001	NCT02556736	I/II	21	18+	2033	Safety and dosing study	Allergan
RP	Channelrhodopsin	Intravitreal rAAV2.7m8.CAG.ChrimsonR.tdTomato	NCT03326336	I/II	18	18-75	2024	BCVA, mobility, QoL	GenSight Biologics
RP	MERTK	Subretinal rAAV2.CVMD2-hMERTK	NCT01482195	I	6	14-70	2023	BCVA	King Khaled Eye Specialist Hospital
RP	RLBP1	Subretinal AAV8.RLBP1	NCT03374657	I/II	21	18-70	2025	BCVA, HVF, contrast sensitivity, ERG, microperimetry, reading speed, mobility	
RP	PDE6B	Subretinal AAV2/5-hPDE6B	NCT03328130	I/II	12	18+	2022	BCVA, HVF, QoL	Horama S.A
X-linked retinoschisis	IRBhRS	Intravitreal AAV8-scRC/IRBPhRS	NCT02317887	I/II	24	18+	2021	BCVA, ERG, OCT measures	National Eye Institute

(continued)

Table 35.2 (continued)

Disease	Transgene	Intervention	NCT number	Phases	Enrollment (N)	Recruitment ages (years)	Completion year	Primary and secondary outcomes	Sponsor
X-linked retinoschisis	RS1	Intravitreal rAAV2tYF-CB-hRS1	NCT02416622	I/II	27	6+	2022	BCVA, schisis cavity on OCT, ERG	Applied Genetic Technologies Corp
XLRP	RPGR	Subretinal AAV.RPGR	NCT03116113	I/II	24	18+	2019	BCVA	Nightstar Therapeutics
XLRP	RPGR	Subretinal AAV.RPGR	NCT03252847	I/II	36	5+	2020	BCVA, ERG, QoL	MeiraGTx UK II Ltd
XLRP	RPGR	Subretinal rAAV2tYF-GRK1-RPGR	NCT03316560	I/II	15	6+	2024	Perimetery, BCVA, OCT, QoL	Applied Genetic Technologies Corp
Usher Syndrome	MY07A	Subretinal EIAV-CMV-MY07A (UshStat)	NCT01505062	I/II	27	6+	2020	ADEs, retinal degeneration	Sanofi
Usher syndrome	MY07A	Subretinal EIAV-CMV-MY07A (UshStat)	NCT02065011	I/II	18	18+	2035	ADEs, retinal degeneration by BCVA, perimetry, OCT	Sanofi
Stargardt disease	ABCA4	Subretinal SAR422459	NCT01736592	I/II	46	6+	2034	ADEs, retinal degeneration	Sanofi
Stargardt disease	ABCA4	Subretinal SAR422459	NCT01367444	I/II	41	6+	2019	ADEs, BCVA, IOP, OCT, ERG, FAF	Sanofi

achromatopsia trials aim to enrol patients as young as 6 years of age. The already published results from the AAV.*RPE65* trials have included patients as young as 4 years of age [1], and there is some evidence to suggest that earlier intervention may result in greater gains in terms of vision rescue [66].

35.10   Clinical Trials

35.10.1   RPE Diseases

35.10.1.1   Case Study: Luxturna and Leber Congenital Amaurosis

In December 2017, the US Food and Drug Administration approved *Luxturna* (voretigene neparvovec) as the first retinal gene therapy for human use [75]. The therapy is approved for patients with LCA type 2, an inherited retinal degeneration characterised by mutations in the *RPE65* gene. Mutations in the *RPE65* gene disrupt the normal recycling of retinal chromophore in the RPE cells, preventing phototransduction and ultimately resulting in retinal degeneration. LCA is inherited as an autosomal recessive trait and has an overall incidence of around 1 in 30,000 to 1 in 50,000 (RPE65-related LCA accounts for around 5–6% of cases). Typically, LCA2 presents in infancy with stigmata of visual loss. Although the fundus changes may be bland, there is a remarkable and global loss of autofluorescence on fundus autofluorescent imaging.

A detailed history of the *RPE65* gene discovery and *LCA2* disease genotyping is summarised elsewhere [76]. Briefly, the RPE65 protein was first described in the early 1990s, after it was discovered in the retinas of rats [77]. The following year it was mapped to the short arm of chromosome 1 in humans and, shortly thereafter, the gene was first linked to cases of LCA2 [78, 79]. An *Rpe65*$^{-/-}$ knockout mouse model was created [80], and a previously identified Briard dog model of hereditary retinal dystrophy was genotyped as *Rpe65*$^{-/-}$ model of LCA [81, 8]. Both of these animal models were crucial in the preclinical validation and optimisation of gene therapy vectors for LCA.

The first positive evidence that LCA2 could be treated was the successful electrophysiological rescue of the *Rpe65*$^{-/-}$ mouse model using oral 9-*cis*-retinal supplementation [82]. However, the rescue effect of this oral supplementation was transient and required repeated dosing. Gene therapy offered a pathway to achieve sustained restoration of normal visual function. Efforts to develop a gene therapy took a leap forward in 2001, when the Briard dog model of LCA2 was treated successfully with subretinal injections of AAV.*RPE65* [83, 84]. The rescue effect was also achieved using in utero injections of AAV.*RPE65* in the mouse model of LCA2 [85]. Around this time, there were efforts to maximise the efficacy of therapy by improving the design of the virus vector DNA components, the quality of the virus preparations and the inclusion of surfactant during injection delivery [86].

In 2007 in London, the first human LCA patient received a subretinal injection of recombinant adeno-associated virus (rAAV) carrying the *RPE65* gene as treatment [11]. This was followed very soon by a US group based in Philadelphia injecting a human LCA patient with a similar *RPE65* vector developed in parallel [12].

The phase I results demonstrated that paediatric patients had a greater response to therapy [66]. It is thought that the greater area of surviving retina and higher visual acuity at baseline, along with the amblyopic window, affect response to therapy. The phase I/II results also demonstrated the challenges of cross-species dose estimation during translation from dogs and that correct dosing—not just gene expression—is required to achieve sustained rescue [68].

The early trials also showed safety and efficacy of gene therapy when subsequently delivered to the fellow (previously untreated) eye, both in a canine model [87] and in humans [88]. These findings demonstrated that administration in the second eye was safe after previous administration of AAV2, even in those with pre-existing immunity to AAV2. This paved the way to phase 3 trials involving treatment of both eyes.

The development of the AAV.*RPE65* vectors also saw the emergence of new patient-centred primary outcome measures designed to gauge activities of daily living beyond chart-based

visual acuity, which were crucial to the demonstration of efficacy. Developed in conjunction with the FDA, the multi-luminance mobility test (MLMT) was intended to better assess the impact of small changes in contrast and luminescence sensitivity [89]. The test involves navigating a type of maze in an adjustable low-light environment and was used as the primary outcome measure of the Luxturna phase III trial. Also central to the demonstration of efficacy were measures of increment threshold sensitivity, such as microperimetry—which combines scanning laser ophthalmoscopy with perimetry—and full field stimulus threshold (FST), both of which may permit assessment of light sensitivity in patients with non-foveal fixation and nystagmus.

The Luxturna viral vector is a recombinant AAV serotype 2 vector with a cytomegalovirus (CMV) enhancer and chicken beta actin (CβA) promoter driving human *RPE65* coding sequence expression. The virus is delivered at a final dose of 1.5×10^{11} vg in a volume of 0.3 mL delivered to the subretinal space. Any patient with biallelic *RPE65* mutations causing LCA is eligible for treatment with the virus vector.

The results of the pivotal trial of Luxturna are deeply impressive. The average improvement in FST was over 100-fold (2.1 log units, or 21 dB) [1]. This translated to improved performance at the MLMT, which was correlated to overall gains in mean sensitivity assessed using FST. Nevertheless, the cost-utility treatment has recently been estimated at $643,800 per quality-adjusted life year (QALY) in the USA, and would not therefore be considered cost effective by traditional measures [90]. So-called phase IV studies of Luxturna are currently emerging and the success of the treatment in real life may prove critical in the subsequent uptake, investment and development of gene therapies.

35.10.2 Choroideraemia

Choroideraemia is an X-linked recessive chorioretinal dystrophy first described by the German ophthalmologist, Mauthner. The approximate incidence is 1 in 50,000 and symptoms typically commence in the second decade of life with nyctalopia and loss of field. Loss of central vision in general occurs late in the disease process (around the fifth decade). The structural correlates of these symptoms are centripetal chorioretinal degeneration (Fig. 35.5). The *CHM* gene encodes **R**ab **E**scort **P**rotein 1, which appears to be essential for protein trafficking within the eye.

The first clinical trial to address gene therapy for choroideraemia was reported in 2014
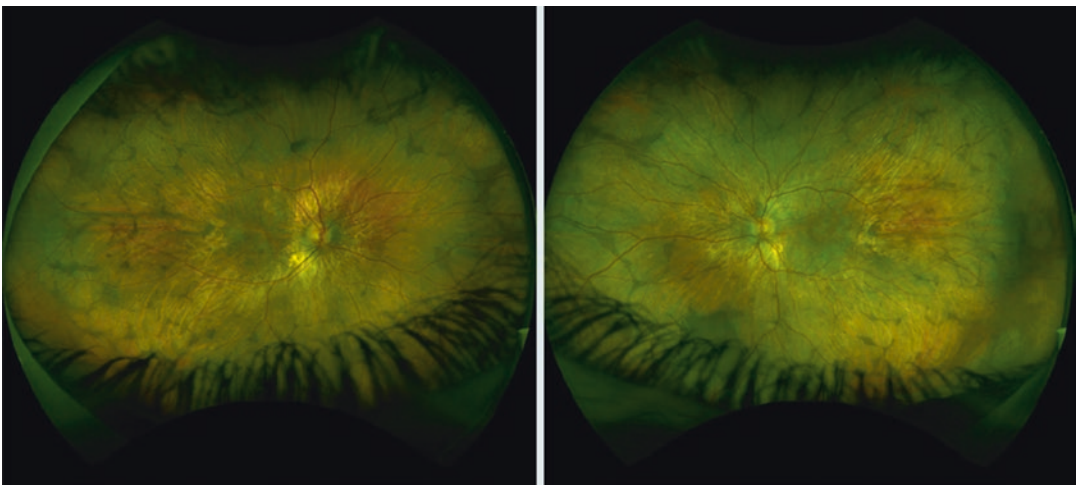
Fig. 35.5 Right and left wide-field colour fundus images of an adolescent patient with choroideraemia demonstrating loss of peripheral chorioretinal tissue with intra-retinal pigment migration; the central retina is well preserved

[31]. In this trial, gene therapy consisted of a subretinal injection of 10^{10} viral genomes as a two-step procedure which involved the macula. The treated eyes of the first six patients of the phase I/II trial were reported to have improved by about one line in visual acuity on a logMAR chart following treatment when compared to control eyes. These improvements were sustained at 2 years in the initial cohort of 6 and in the completed cohort of 14 patients treated in Oxford. One patient in one of the international treatment sites was reported to have suffered an intraretinal immune response which resulted in a loss of acuity of two lines [91]. Although the current data are limited, it appears that the principal benefit demonstrated to date is improvement in acuity rather than threshold sensitivity (in direct contrast to gene therapy for LCA secondary to RPE65 mutations) [30, 31]. The results of the phase III trial of this therapy are yet to be reported and other groups are working on similar gene therapy protocols for the condition NCT02341807.

35.10.3 Autosomal Recessive RP

The Mer-tyrosine kinase (MERTK) receptor is critical in the process of phagocytosis of shed photoreceptor outer segments. Mutations in this gene result in aberrantly long photoreceptors and accumulation of outer segment-derived debris in the subretinal space and are followed by degeneration and death. The *MERTK* gene is responsible for the retinal dystrophy observed in the Royal College of Surgeons (RCS) rat and causes autosomal recessive RP in humans. Preclinical trials using AAV [92] and adenoviral [93] vectors have demonstrated rescue of the phenotype and a phase I trial of gene therapy developed in North America has been completed in Saudi Arabia [94]. The latter delivered an AAV2 carrying the *MERTK* gene under the control of an RPE-specific promoter (VMD2 promoter). No complications secondary to the vector itself were identified and 3 of 6 patients demonstrated improvements in vision at the 12-month mark, though this was only sustained at 2 years in one subject.

35.11 Photoreceptor Disorders

35.11.1 Rod Monochromacy/ Achromatopsia

Rod monochromacy (aka 'congenital achromatopsia') is characterised by a rod-dominated or rod-exclusive visual system. The condition is inherited as an autosomal recessive trait and affects around 1 in 30,000–60,000 individuals. Patients typically present in infancy with nystagmus and photophobia. Visual acuity is typically around 6/60 and there is an absence of—or rudimentary—colour discrimination with a spectral sensitivity function corresponding to that of the normal human visual system under scotopic conditions (peak sensitivity at about 500 nm) [95]. Commonly, the fundus is clinically unremarkable except for the presence of a blunted foveal reflex. The condition primarily results from mutations to gene involved in the phototransduction cascade in the photoreceptors, including guanine nucleotide-binding protein α-transducing activity polypeptide 2 (*GNAT2*), cone photodiesterase genes (*PDE6C*, *PDE6H*) and cyclic GMP-gated cone cation channel proteins (*CNGB3*, *CNGA3*). In a minority of patients, it may also be associated with mutations in the activating transcription regulator/unfolded protein response regulator gene (*ATF6*) [96]. Gene therapy has demonstrated rescue of the phenotype in small animal models of rod monochromacy secondary to *CNGB3*, *CNGA3* and *GNAT2* mutations as well as large animal models, including a canine model of *CNGB3*-associated disease and an ovine model of *CNGA3*-associated disease. Currently there are clinical trials underway assessing gene therapy for rod monochromacy secondary to mutations in both *CNGB3* (ClinicalTrials.gov identifier NCT03001310) and *CNGA3* (ClinicalTrials.gov identifier NCT02935517) [97], with formal reporting of results awaited.

35.11.2 *GUCY2D*-Associated Leber Congenital Amaurosis

Guanylate cyclase is an intracellular second messenger involved in phototransduction; it responds

to lowered Ca+2 levels by facilitating the production of cGMP, leading to opening of cGMP-gated cation channels, which in turn results in Ca+2 elevation and a return of the photoreceptor membrane potential to its pre-excitation level. There is evidence of rescue of this phenotype via AAV-mediated gene therapy in murine models [98, 99]; although one clinical trial is registered on ClinicalTrials.gov, it is not yet actively recruiting (ClinicalTrials.gov identifier NCT03920007).

35.11.3   X-Linked RP

Mutations in the gene encoding RP GTPase regulator (*RPGR*) are the commonest cause of X-linked retinitis pigmentosa. Mutations in this gene cause nyctalopia and loss of field in young males and are thought to be expressed in the connecting cilia between inner and outer segments. The gene is prone to mutations in a highly unstable region, ORF15, which contains a 1kB purine-rich region (c.2184-3162) over which DNA polymerase 1 slippage is proposed to occur. Indeed, 70% of the errors in *RPGR*-associated RP occur in this region. One early barrier to gene therapy for this condition was unpredictable recombination during viral cloning which was successfully negotiated via codon optimisation (see above). Gene therapy employing viral vectors has demonstrated rescue in a murine model of *RPGR*-associated RP; interestingly, rescue has been demonstrated using both non-codon-optimised and codon-optimised [25] transgenes. However, it is suggested that rescue via non-codon-optimised constructs reflects differences in the murine and human models of *RPGR*-associated RP. Currently, two clinical trials of AAV-mediated gene therapy for RPGR-associated X-linked retinitis pigmentosa are underway (ClinicalTrials.gov NCT03116113, NCT03252847).

35.11.4   Usher's Syndrome

Usher's syndrome is the commonest form of combined deafness and blindness and it can be clinically classified into three different groups of disorders (Usher's I, II and III), of which there are nine genetic causes. Mutations in the gene *MYO7A* are associated with Usher's syndrome IB, which is characterised by hearing loss with vestibular dysfunction. *MYO7A* encodes a myocilin which is essential for organelle trafficking within cells. The coding sequence of the *MYO7A* is 7kB—too large for a single-AAV vector. Although dual-AAV vectors have been utilised in human cells in vitro, mice deficient in *MYO7A* [100] and porcine models, phase I/II human trials using lentiviral vectors have commenced (NCT02065011 and NCT01505062).

35.11.5   Stargardt's Disease

Stargardt's disease is an autosomal recessive macular dystrophy typified by the accumulation of retinal flecks composed of bis-retinoid, *N*-retinylidene-*N*-retinylethanolamine (A2E), followed by the development of atrophy with characteristic sparing of the peripapillary region (Fig. 35.6). The causative ABCA4 gene encodes ABCA4, a 'flippase' which translocates conjugated retinaldehyde across the outer segment cell membrane. The carrier frequency of STGD mutations is relatively high (circa 1 in 30). The cDNA of ABCA4 is 6.8 kB, which (like *MYO7A*) is too
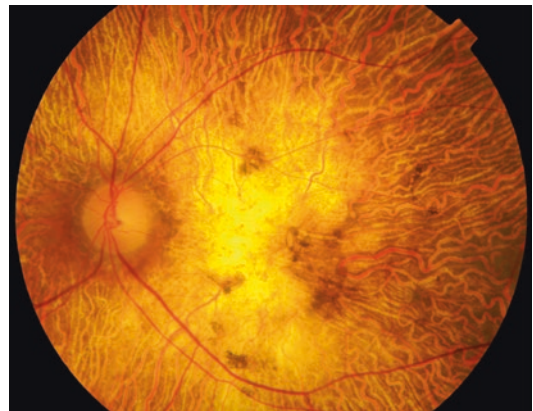
Fig. 35.6 Colour fundus photograph of a middle-aged male patient with advanced Stargardt's disease demonstrating macular atrophy and pigmentary disturbance with characteristic peripapillary sparing

large for a single-AAV vector. Lentiviral [101] as well as dual-AAV vectors [102] have been demonstrated to rescue the phenotype in murine models. Subretinal lentiviral vectors carrying *ABCA4* are currently being investigated in a phase I/II clinical trial (NCT01367444).

35.12 Inner Retinal Diseases

35.12.1 X-Linked Retinoschisis

X-linked retinoschisis is a disorder of intercellular adhesion caused by mutations to the *RS1* gene, which encodes retinoschisin. It is manifest as peripheral retinoschisis and pseudo-macular oedema that may cause a stereotypical spoke-like appearance of the macula (Fig. 35.7). Some patients develop further secondary complications including vitreous haemorrhage and retinal detachment. The condition affects around 1 in 5000 to 1 in 25,000 males and typically presents with gradual onset decline in vision in the first or second decade. A significant minority of patients may present in early childhood with strabismus or even misdiagnosed neurological deficits such as ataxia as the result of vision loss. 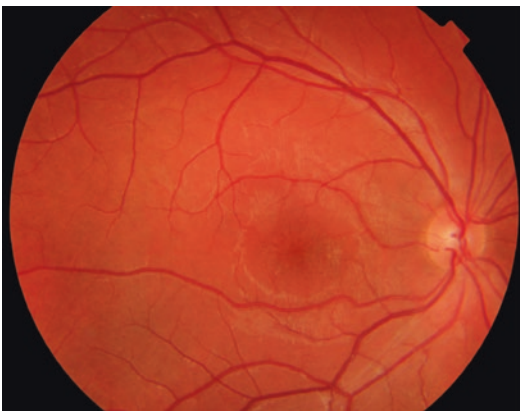Rescue of the XLRS via AAV-mediated gene replacement therapy has been demonstrated, and interestingly the use of photoreceptor-specific promoters appears

Fig. 35.7 Fundus photograph of a young adult male patient with X-linked retinoschisis demonstrating a spoke pattern at the macula

to be a more successful strategy than the use of Muller cell-specific promoters.

Currently, two trials are investigating AAV vector-mediated gene replacement delivered via intravitreal injection (NCT02317887 and NCT02416622). Early results from one of these trials have been published. One of nine patients in the trial developed significant intraocular inflammation that necessitated oral and topical steroid therapy and only one patient achieved closure of the schisis cavity, albeit transiently [63].

35.13 Multigene Disorders

35.13.1 Age-Related Macular Degeneration

The primary target for gene therapy with respect to age-related macular degeneration (ARMD) is angiogenesis in the exudative ('wet') form of the condition.

The 3-year results of a phase I/II trial of subretinal injection of an AAV vector carrying the soluble full-length VEGF receptor 1 (*sFLT1*) gene in 24 patients (plus 13 control subjects) with exudative ARMD failed to demonstrate a convincing signal of efficacy. Interestingly, patients who required fewer rescue treatments in the first year following gene therapy were also those who fared better (in terms of visual acuity and number of retreatments with anti-VEGF) over the subsequent 2 years [103]. One trial of intravitreal sFLT0 is yet to formally report its outcomes.

Subretinal injection of a lentivirus carrying transgenes for angiostatin and endostatin (RetinoStat) has been demonstrated to be safe in a cohort of patients with advanced neovascular age-related macular degeneration. There was angiographic evidence of decreased leak from neovascular membranes which correlated to the expression of the transgenes. Furthermore, sustained expression of angiostatin and endostatin was demonstrated from assays of ocular fluid at up to 4 years [104].

35.14 Summary of Current Clinical Trials in the Retina

Table 35.2 shows over 40 clinical trials currently underway for retinal gene therapy, as listed on the ClinicalTrials.gov webpage in mid-2019.

35.15 Conclusions and Future Directions

The first patient to receive AAV.*RPE65* gene therapy in normal clinical practice was a 13-year-old LCA2 patient, treated at the Massachusetts Eye and Ear Infirmary in early 2018. The substantial cost of treatment, as well as the rarity of the diseases, will be best suited by centres-of-excellence specialising in the molecular diagnostics, as well as the handling and surgical delivery of viral vectors.

The next therapies likely to enter regular clinical use are the AAV.*REP1* vector for choroideraemia undergoing a multicentre RCT led by the University of Oxford [105] and the two competing AAV.*ND4* vectors in phase III trials for Leber hereditary optic neuropathy [106, 107].

Yet there remain over 250 known genetic mutations capable of causing retinal degenerations and the current clinical trials are only replacing nine of these genes [108]. There remains substantial work to apply this revolutionary tool to the spectrum of genetic retinal diseases, especially given the preclinical pipeline required to develop and validate a vector before even commencing extensive clinical trials. Future development and clinical translation of gene therapy vectors may be streamlined by making small alterations—namely, changing the transgene to match the mutated gene—to existing virus vectors approved for safe human use. Such approaches may shorten the development pipeline.

If the full spectrum of retinal dystrophies is to be treated, the recent successful development of gene replacement strategies for recessive disease will need to be followed by clinical success with knockdown-and-replace strategies necessary to treat dominant disease.

There are ongoing efforts to develop more broadly applicable gene therapy treatments in the retina—virus vectors with effects that are mutation independent. Neuroprotective and antioxidant therapies are prominent examples. The preclinical validation of a neuroprotective brain-derived neurotrophic factor (*BDNF*) vector for ganglion cells in glaucoma is an exciting example of mutation-independent gene therapy [109].

After many decades of development and validation, gene therapy for retinal diseases has arrived and holds great promise for many previously untreatable blinding diseases.

References

1. Russell S, et al. Efficacy and safety of voretigene neparvovec (AAV2-hRPE65v2) in patients with RPE65-mediated inherited retinal dystrophy: a randomised, controlled, open-label, phase 3 trial. Lancet. 2017;390:849–60.
2. Watson JD, Crick FHC, et al. Molecular structure of nucleic acids. Nature. 1953;171:737–8.
3. Terheggen HG, Lowenthal A, Lavinha F, Colombo JP, Rogers S. Unsuccessful trial of gene replacement in arginase deficiency. Z Kinderheilkd. 1975;119:1–3.
4. Blaese RM, et al. T lymphocyte-directed gene therapy for ADA-SCID: initial trial results after 4 years. Science. 1995;270:475–80.
5. Price J, Turner D, Cepko C. Lineage analysis in the vertebrate nervous system by retrovirus-mediated gene transfer. Proc Natl Acad Sci U S A. 1987;84:156–60.
6. Lem J, et al. Retinal degeneration is rescued in transgenic rd mice by expression of the cGMP phosphodiesterase beta subunit. Proc Natl Acad Sci U S A. 1992;89:4422–6.
7. Travis GH, Groshan KR, Lloyd M, Bok D. Complete rescue of photoreceptor dysplasia and degeneration in transgenic retinal degeneration slow (rds) mice. Neuron. 1992;9:113–9.
8. Aguirre GD, et al. Congenital stationary night blindness in the dog: common mutation in the RPE65 gene indicates founder effect. Mol Vis. 1998;4:23.
9. Marshall E. Gene therapy death prompts review of adenovirus vector. Science. 1999;286:2244–5.
10. Hacein-Bey-Abina S, et al. LMO2-associated clonal T cell proliferation in two patients after gene therapy for SCID-X1. Science. 2003;302:415–9.
11. Bainbridge JWB, et al. Effect of gene therapy on visual function in Leber's congenital amaurosis. N Engl J Med. 2008;358:2231–9.
12. Maguire AM, et al. Safety and efficacy of gene transfer for Leber's congenital amaurosis. N Engl J Med. 2008;358:2240–8.

13. Wert KJ, et al. CAPN5 mutation in hereditary uveitis: the R243L mutation increases calpain catalytic activity and triggers intraocular inflammation in a mouse model. Hum Mol Genet. 2015;24:4584–98.

14. Illing ME, Rajan RS, Bence NF, Kopito RR. A rhodopsin mutant linked to autosomal dominant retinitis pigmentosa is prone to aggregate and interacts with the ubiquitin proteasome system. J Biol Chem. 2002;277:34150–60.

15. Rose AM, Bhattacharya SS. Variant haploinsufficiency and phenotypic non-penetrance in PRPF31-associated retinitis pigmentosa. Clin Genet. 2016;90:118–26.

16. Cai X, Conley SM, Naash MI. RPE65: role in the visual cycle, human retinal disease, and gene therapy. Ophthalmic Genet. 2009;30:57–62.

17. Demirci FYK, et al. X-linked cone-rod dystrophy (locus COD1): identification of mutations in RPGR exon ORF15. Am J Hum Genet. 2002;70:1049–53.

18. Feuer WJ, et al. Gene therapy for Leber hereditary optic neuropathy: initial results. Ophthalmology. 2016;123:558–70.

19. Bainbridge JWB, et al. Hypoxia-regulated transgene expression in experimental retinal and choroidal neovascularization. Gene Ther. 2003;10:1049–54.

20. Ye G-J, et al. Cone-specific promoters for gene therapy of achromatopsia and other retinal diseases. Hum Gene Ther. 2016;27:72–82.

21. McGee Sanftner LH, et al. Recombinant AAV-mediated delivery of a tet-inducible reporter gene to the rat retina. Mol Ther. 2001;3:688–96.

22. Kozak M. An analysis of 5′-noncoding sequences from 699 vertebrate messenger RNAs. Nucleic Acids Res. 1987;15:8125–48.

23. Chatterjee S, Pal JK. Role of 5′-and 3′-untranslated regions of mRNAs in human diseases. Biol Cell. 2009;101:251.

24. Ling C, et al. The adeno-associated virus genome packaging puzzle. J Mol Genet Med. 2015;9:175.

25. Fischer MD, et al. Codon-optimized RPGR improves stability and efficacy of AAV8 gene therapy in two mouse models of X-linked retinitis pigmentosa. Mol Ther. 2017;25:1854–65.

26. Furger A, O'Sullivan JM, Binnie A, Lee BA, Proudfoot NJ. Promoter proximal splice sites enhance transcription. Genes Dev. 2002;16:2792–9.

27. Hassall MM, Barnard AR, MacLaren RE. Gene therapy for color blindness. Yale J Biol Med. 2017;90:543–51.

28. McCarty DM, Monahan PE, Samulski RJ. Self-complementary recombinant adeno-associated virus (scAAV) vectors promote efficient transduction independently of DNA synthesis. Gene Ther. 2001;8:1248–54.

29. Patrício MI, Barnard AR, Orlans HO, McClements ME, MacLaren RE. Inclusion of the woodchuck hepatitis virus posttranscriptional regulatory element enhances AAV2-driven transduction of mouse and human retina. Mol Ther Nucleic Acids. 2017;6:198–208.

30. Edwards TL, et al. Visual acuity after retinal gene therapy for choroideremia. N Engl J Med. 2016;374:1996–8.

31. MacLaren RE, et al. Retinal gene therapy in patients with choroideremia: initial findings from a phase 1/2 clinical trial. Lancet. 2014;383:1129–37.

32. Matsushita T, et al. The adenovirus E1A and E1B19K genes provide a helper function for transfection-based adeno-associated virus vector production. J Gen Virol. 2004;85:2209–14.

33. Kay CN, et al. Targeting photoreceptors via intravitreal delivery using novel, capsid-mutated AAV vectors. PLoS One. 2013;8:e62097.

34. Conley SM, Naash MI. Gene therapy for PRPH2-associated ocular disease: challenges and prospects. Cold Spring Harb Perspect Med. 2014;4:a017376.

35. Mao H, Gorbatyuk MS, Rossmiller B, Hauswirth WW, Lewin AS. Long-term rescue of retinal structure and function by rhodopsin RNA replacement with a single adeno-associated viral vector in P23H RHO transgenic mice. Hum Gene Ther. 2012;23:356–66.

36. Kole R, Krainer AR, Altman S. RNA therapeutics: beyond RNA interference and antisense oligonucleotides. Nat Rev Drug Discov. 2012;11:125–40.

37. Cayouette M, Gravel C. Adenovirus-mediated gene transfer of ciliary neurotrophic factor can prevent photoreceptor degeneration in the retinal degeneration (rd) mouse. Hum Gene Ther. 1997;8:423–30.

38. Lipinski DM, et al. CNTF gene therapy confers life-long neuroprotection in a mouse model of human retinitis pigmentosa. Mol Ther. 2015;23:1308–19.

39. Daly C, et al. A brain-derived neurotrophic factor mimetic is sufficient to restore cone photoreceptor visual function in an inherited blindness model. Sci Rep. 2017;7:11320.

40. Martin KRG, et al. Gene therapy with brain-derived neurotrophic factor as a protection: retinal ganglion cells in a rat glaucoma model. Invest Ophthalmol Vis Sci. 2003;44:4357–65.

41. LeVaillant CJ, et al. Significant changes in endogenous retinal gene expression assessed 1 year after a single intraocular injection of AAV-CNTF or AAV-BDNF. Mol Ther Methods Clin Dev. 2016;3:16078.

42. Schlichtenbrede FC, et al. Intraocular gene delivery of ciliary neurotrophic factor results in significant loss of retinal function in normal mice and in the Prph2Rd2/Rd2 model of retinal degeneration. Gene Ther. 2003;10:523–7.

43. Talcott KE, et al. Longitudinal study of cone photoreceptors during retinal degeneration and in response to ciliary neurotrophic factor treatment. Invest Ophthalmol Vis Sci. 2011;52:2219–26.

44. Sieving PA, et al. Ciliary neurotrophic factor (CNTF) for human retinal degeneration: phase I trial of CNTF delivered by encapsulated cell intraocular implants. Proc Natl Acad Sci U S A. 2006;103:3896–901.

45. Rakoczy EP, et al. Gene therapy with recombinant adeno-associated vectors for neovascular age-related macular degeneration: 1 year follow-

up of a phase 1 randomised clinical trial. Lancet. 2015;386:2395–403.

46. Heier JS, et al. Intravitreous injection of AAV2-sFLT01 in patients with advanced neovascular age-related macular degeneration: a phase 1, open-label trial. Lancet. 2017;390:50–61.

47. Simunovic MP, et al. Optogenetic approaches to vision restoration. Exp Eye Res. 2019;178:15–26.

48. Busskamp V, et al. Genetic reactivation of cone photoreceptors restores visual responses in retinitis pigmentosa. Science. 2010;329:413–7.

49. Cehajic-Kapetanovic J, Milosavljevic N, Bedford RA, Lucas RJ, Bishop PN. Efficacy and safety of glycosidic enzymes for improved gene delivery to the retina following intravitreal injection in mice. Mol Ther Methods Clin Dev. 2018;9:192–202.

50. De Silva SR, et al. Long-term restoration of visual function in end-stage retinal degeneration using subretinal human melanopsin gene therapy. Proc Natl Acad Sci U S A. 2017;114(42):11211–6. https://doi.org/10.1073/pnas.1701589114. https://pubpeer.com/publications/21FE5239FB27052C876367F258AEA3?utm_source=Chrome&utm_medium=BrowserExtension&utm_campaign=Chrome.

51. Suzuki K, et al. In vivo genome editing via CRISPR/Cas9 mediated homology-independent targeted integration. Nature. 2016;540:144–9.

52. Liang P, et al. CRISPR/Cas9-mediated gene editing in human tripronuclear zygotes. Protein Cell. 2015;6:363–72.

53. Ma H, et al. Correction of a pathogenic gene mutation in human embryos. Nature. 2017;548:413–9.

54. Zhang X-H, Tee LY, Wang X-G, Huang Q-S, Yang S-H. Off-target effects in CRISPR/Cas9-mediated genome engineering. Mol Ther Nucleic Acids. 2015;4:e264.

55. Ochakovski GA, Bartz-Schmidt KU, Fischer MD. Retinal gene therapy: surgical vector delivery in the translation to clinical trials. Front Neurosci. 2017;11:174.

56. Simunovic MP, Xue K, Jolly JK, MacLaren RE. Structural and functional recovery following limited iatrogenic macular detachment for retinal gene therapy. JAMA Ophthalmol. 2017;135:234–41.

57. Xue K, Groppe M, Salvetti AP, MacLaren RE. Technique of retinal gene therapy: delivery of viral vector into the subretinal space. Eye. 2017;31:1308–16.

58. Bennett J, Chung DC, Maguire A. Gene delivery to the retina: from mouse to man. Methods Enzymol. 2012;507:255–74.

59. Xue K, et al. Robot-assisted retinal surgery: overcoming human limitations. In: Surgical retina. 2019. p. 109–14. https://doi.org/10.1007/978-981-13-6214-9_11.

60. Simunovic MP, Osaadon P, Too LK. Sodium Fluorescein as an Optical Label to Evaluate Subretinal Injection [published online ahead of print, 2020 Apr 7]. Retina. 2020;10.1097/IAE.0000000000002800. https://doi.org/10.1097/IAE.0000000000002800.

61. Do DV, Hawkins B, Gichuhi S, Vedula SS. Surgery for post-vitrectomy cataract. Cochrane Database Syst Rev. 2008;CD006366.

62. Sharma A, et al. Accuracy of scleral transillumination techniques to identify infant ciliary body for sclerostomy and intravitreal injections. Clin Exp Ophthalmol. 2019;47:478–83.

63. Cukras C, et al. Retinal AAV8-RS1 gene therapy for X-linked retinoschisis: initial findings from a phase I/IIa Trial by intravitreal delivery. Mol Ther. 2018;26:2282–94.

64. Duncan JL. Understanding ocular inflammation in eyes treated with intravitreal gene therapy. JAMA Ophthalmol. 2019;137(4):407. https://doi.org/10.1001/jamaophthalmol.2018.6915.

65. Barnard AR, Rudenko AN, MacLaren RE. Vector shedding and immunogenicity sampling for retinal gene therapy. Methods Mol Biol. 2018;1715:359–71.

66. Maguire AM, et al. Age-dependent effects of RPE65 gene therapy for Leber's congenital amaurosis: a phase 1 dose-escalation trial. Lancet. 2009;374:1597–605.

67. Reichel FF, et al. AAV8 can induce innate and adaptive immune response in the primate eye. Mol Ther. 2017;25:2648.

68. Bainbridge JWB, et al. Long-term effect of gene therapy on Leber's congenital amaurosis. N Engl J Med. 2015;372:1887–97.

69. Hensch TK, Quinlan EM. Critical periods in amblyopia. Vis Neurosci. 2018;35:E014.

70. Baseler HA, et al. Reorganization of human cortical maps caused by inherited photoreceptor abnormalities. Nat Neurosci. 2002;5:364–70.

71. Zhang Z, et al. AAV-mediated gene therapy restores cone function in a rat with an M-cone opsin deficiency, a model for blue cone monochromacy. Invest Ophthalmol Vis Sci. 2011;52:1403.

72. Carvalho LS, et al. Long-term and age-dependent restoration of visual function in a mouse model of CNGB3-associated achromatopsia following gene therapy. Hum Mol Genet. 2011;20:3161–75.

73. Mancuso K, et al. Gene therapy for red-green colour blindness in adult primates. Nature. 2009;461:784–7.

74. Ashtari M, et al. The human visual cortex responds to gene therapy-mediated recovery of retinal function. J Clin Invest. 2011;121:2160–8.

75. FDA. Press Announcements—FDA approves novel gene therapy to treat patients with a rare form of inherited vision loss. https://www.fda.gov/newsevents/newsroom/pressannouncements/ucm589467.htm. Accessed 5 Nov 2018.

76. Redmond TM, Hamel CP. [46] Genetic analysis of RPE65: from human disease to mouse model. Methods Enzymol. 2000;316:705–24. Academic.

77. Hamel CP, et al. A developmentally regulated microsomal protein specific for the pigment epithelium of the vertebrate retina. J Neurosci Res. 1993;34:414–25.

78. Marlhens F, et al. Mutations in RPE65 cause Leber's congenital amaurosis. Nat Genet. 1997;17:139–41.

79. Hamel CP, Jenkins NA, Gilbert DJ, Copeland NG, Redmond TM. The gene for the retinal pigment epithelium-specific protein RPE65 is localized to human 1p31 and mouse 3. Genomics. 1994;20:509–12.

80. Redmond TM, et al. Rpe65 is necessary for production of 11-cis-vitamin A in the retinal visual cycle. Nat Genet. 1998;20:344.

81. Wrigstad A. Hereditary dystrophy of the retina and the retinal pigment epithelium in a strain of Briard dogs: a clinical, morphological and electrophysiological study. Linköpings universitet; 1994.

82. Van Hooser JP, et al. Rapid restoration of visual pigment and function with oral retinoid in a mouse model of childhood blindness. Proc Natl Acad Sci U S A. 2000;97:8623–8.

83. Acland GM, et al. Gene therapy restores vision in a canine model of childhood blindness. Nat Genet. 2001;28:92–5.

84. Acland GM, et al. Long-term restoration of rod and cone vision by single dose rAAV-mediated gene transfer to the retina in a canine model of childhood blindness. Mol Ther. 2005;12:1072–82.

85. Dejneka NS, et al. In utero gene therapy rescues vision in a murine model of congenital blindness. Mol Ther. 2004;9:182–8.

86. Bennicelli J, et al. Reversal of blindness in animal models of leber congenital amaurosis using optimized AAV2-mediated gene transfer. Mol Ther. 2008;16:458–65.

87. Annear MJ, et al. Gene therapy in the second eye of RPE65-deficient dogs improves retinal function. Gene Ther. 2011;18:53–61.

88. Bennett J, et al. Safety and durability of effect of contralateral-eye administration of AAV2 gene therapy in patients with childhood-onset blindness caused by RPE65 mutations: a follow-on phase 1 trial. Lancet. 2016;388:661–72.

89. Chung DC, et al. Novel mobility test to assess functional vision in patients with inherited retinal dystrophies. Clin Exp Ophthalmol. 2018;46:247–59.

90. Zimmermann M, et al. Cost utility of voretigene neparvovec for biallelic RPE65-mediated inherited retinal disease. Value Health. 2019;22:161–7.

91. Dimopoulos IS, Hoang SC, Radziwon A, et al. Two-Year Results After AAV2-Mediated Gene Therapy for Choroideremia: The Alberta Experience. Am J Ophthalmol. 2018;193:130–42. https://doi.org/10.1016/j.ajo.2018.06.011.

92. LaVail MM, et al. Gene therapy for MERTK-associated retinal degenerations. Adv Exp Med Biol. 2016;854:487–93.

93. Vollrath D, et al. Correction of the retinal dystrophy phenotype of the RCS rat by viral gene transfer of Mertk. Proc Natl Acad Sci U S A. 2001;98:12584–9.

94. Ghazi NG, et al. Treatment of retinitis pigmentosa due to MERTK mutations by ocular subretinal injection of adeno-associated virus gene vector: results of a phase I trial. Hum Genet. 2016;135:327–43.

95. Simunovic MP. Colour vision deficiency. Eye. 2010;24:747–55.

96. Kohl S, Jägle H, Wissinger B, Zobor D. Achromatopsia. In: Adam MP, et al., editors. GeneReviews®. Seattle: University of Washington; 2004.

97. Kahle NA, et al. Development of methodology and study protocol: safety and efficacy of a single subretinal injection of rAAV.hCNGA3 in patients with CNGA3-linked achromatopsia investigated in an exploratory dose-escalation trial. Hum Gene Ther Clin Dev. 2018;29:121–31.

98. Boye SL, et al. AAV-mediated gene therapy in the guanylate cyclase (RetGC1/RetGC2) double knock-out mouse model of Leber congenital amaurosis. Hum Gene Ther. 2013;24:189–202.

99. Boye SE, et al. Functional and behavioral restoration of vision by gene therapy in the guanylate cyclase-1 (GC1) knockout mouse. PLoS One. 2010;5:e11306.

100. Hong D-H, Pawlyk BS, Adamian M, Sandberg MA, Li T. A single, abbreviated RPGR-ORF15 variant reconstitutes RPGR function in vivo. Invest Ophthalmol Vis Sci. 2005;46:435–41.

101. Kong J, et al. Correction of the disease phenotype in the mouse model of Stargardt disease by lentiviral gene therapy. Gene Ther. 2008;15:1311–20.

102. McClements ME, et al. An AAV dual vector strategy ameliorates the Stargardt phenotype in adult Abca4-/- mice. Hum Gene Ther. 2019;30:590–600.

103. Rakoczy EP, et al. Three-year follow-up of phase 1 and 2a rAAV.sFLT-1 subretinal gene therapy trials for exudative age-related macular degeneration. Am J Ophthalmol. 2019;204:113–23.

104. Campochiaro PA, et al. Lentiviral vector gene transfer of endostatin/angiostatin for macular degeneration (GEM) study. Hum Gene Ther. 2017;28:99–111.

105. Xue K, et al. Beneficial effects on vision in patients undergoing retinal gene therapy for choroideremia. Nat Med. 2018;24:1507–12.

106. Guy J, et al. Gene therapy for Leber hereditary optic neuropathy: low- and medium-dose visual results. Ophthalmology. 2017;124:1621–34.

107. Uretsky S, et al. Intravitreal rAAV2/2-ND4 (GS010): a gene therapy for vision loss in Leber's Hereditary Optic Neuropathy (LHON) caused by the G11778A ND4 mitochondrial mutation (S26.005). Neurology. 2017;88:S26.005.

108. RetNet—Retinal Information Network. https://sph.uth.edu/retnet/home.htm. Accessed 8 Nov 2018.

109. Osborne A, et al. Neuroprotection of retinal ganglion cells by a novel gene therapy construct that achieves sustained enhancement of brain-derived neurotrophic factor/tropomyosin-related kinase receptor-B signaling. Cell Death Dis. 2018;9:1007.

Part VIII

Combined Ophthalmic Surgical Techniques

Combined Cataract and Vitrectomy Surgery

36

Chee Wai Wong, Edmund YM Wong, Shu-Yen Lee,
Ian Yeo, Laurence Lim, Gavin S. Tan,
Quan V. Hoang, Danny Cheung, Andrew Tsai,
and Doric Wong

36.1 Introduction

Phacovitrectomy, which combines cataract surgery, intraocular lens (IOL) implantation and vitrectomy, has become a routine, safe and effective procedure in many surgical retina practices. Vision loss in many older patients may be due to the combined effects of cataract and vitreoretinal pathology. Moreover, the development of cataracts after vitreous surgery is almost invariable in phakic eyes, and the presence of significant cataract may also hinder visualisation for effective vitreous surgery.

However, the combined procedure is not without drawbacks and may not give the best outcome in all situations. There is potentially increased complexity in a combined procedure and the need for two different surgical skill sets.

C. W. Wong · E. YM Wong · S.-Y. Lee · I. Yeo
L. Lim · G. S. Tan · Q. V. Hoang · D. Cheung
A. Tsai · D. Wong (✉)
Surgical Retina Department, Singapore National
Eye Centre, Singapore, Singapore

Duke-NUS Medical School, Singapore, Singapore
e-mail: wong.chee.wai@singhealth.com.sg;
edmund.wong.y.m@singhealth.com.sg;
lee.shu.yen@singhealth.com.sg;
ian.yeo.y.s@singhealth.com.sg;
laurence.lim.s@singhealth.com.sg;
gavin.tan@singhealth.com.sg;
donny.hoang@singhealth.com.sg;
cheung.ning@singhealth.com.sg;
andrew.tsai.s.h@singhealth.com.sg;
doric.wong.w.k@singhealth.com.sg

36.2 Indications for Phacovitrectomy

Combined surgery is ideally suited for the phakic eyes of older patients with relatively uncomplicated vitreoretinal pathology which requires vitrectomy that can be completed quickly and with minimal tissue manipulation. Typical indications would include macular cases (e.g. macular holes, epiretinal membranes, vitreomacular traction, myopic macular retinoschisis) and uncomplicated vitreous haemorrhage without significant retinal traction (e.g. proliferative diabetic retinopathy with no or minimal vitreous attachments, retinal vascular disease, breakthrough vitreous haemorrhage in exudative age-related macular degeneration and polypoidal choroidal vasculopathy). A retrospective review by Demetriades et al. in the late 1990s found the top three indications to be diabetic vitreous haemorrhage, macular hole and epiretinal membrane [1].

Combined surgery has also been described in more complex pathologies including traction retinal detachment, rhegmatogenous retinal detachment and subfoveal choroidal neovascularisation. Berrocal et al. reported the use of phacovitrectomy in the management of giant retinal tear detachments [2]. Easier access to anterior structures of the eye is achieved with lens removal. Nevertheless, one must always be mindful of the possibility of increased post-operative inflammation resulting from additional procedures, imprecise IOL calcu-
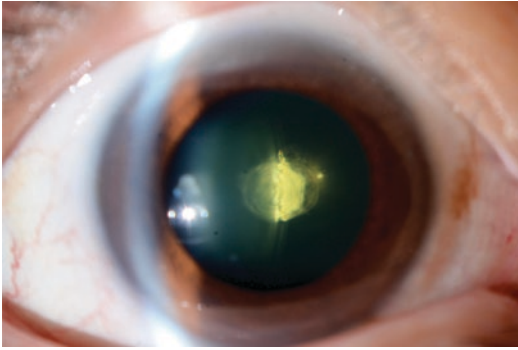
Fig. 36.1 Posterior polar cataract. Planning for a combined phacovitrectomy is prudent in these cases

lations and poor visibility due to pupillary miosis and corneal oedema should there be prolonged surgical times.

Planning for phacovitrectomy is a prudent option in the management of patients with posterior polar cataract where there is a higher risk of posterior capsular rupture and nucleus dislocation into the vitreous cavity (Fig. 36.1). The surgical team would then be prepared for quick conversion should a vitrectomy be required. In this situation, more often than not, a routine phacoemulsification proceeds without complications. However, if posterior capsule integrity is lost, the nucleus is then allowed to drop without further excessive manipulation in the anterior segment which often results in corneal oedema. Cortical clean-up and a safe, controlled posterior vitrectomy with lensectomy are carried out, and the IOL is implanted in the sulcus.

36.3 Contraindications for Phacovitrectomy

While not an absolute contraindication, there are concerns about the removal of cataract and IOL implantation in patients undergoing vitrectomy for proliferative diabetic retinopathy. Risks of anterior segment neovascularisation and neovascular glaucoma have been previously reported despite an intact posterior capsule [3, 4]. These risks can be mitigated with preoperative intravit-

real anti-vascular endothelial growth factor (anti-VEGF) injections, aggressive panretinal photocoagulation and intraoperative endophotocoagulation to the peripheral retina with wideviewing systems during vitrectomy [1]. Lahey et al. reported their experience in combined phacoemulsification and vitrectomy for 223 patients with proliferative diabetic retinopathy where only 1 patient developed post-operative neovascular glaucoma [5]. In diabetic patients, contraindications for combined surgery may include patients with pre-existing rubeosis iridis and severe traction retinal detachments [5]. Lahey et al. were of the opinion that these cases would be best treated by retaining the lens or by the complete removal of lens and anterior vitreous structures.

Other contraindications of phacovitrectomy are pathologies where removing the lens via a pars plana lensectomy would be more appropriate. These include severe anterior proliferative vitreoretinopathy where it is imperative to treat the contracted anterior vitreous and membranes, open globe injuries with or without intraocular foreign body especially where the posterior capsule may be breached, and subluxated lenses with vitreous prolapse into the anterior chamber [6].

For patients undergoing retinal detachment surgery with combined scleral buckle and pars plana vitrectomy, there is often an induced myopic shift after surgery [7]. Due to the unpredictability of IOL power calculations, cataract removal and primary IOL implantation may not be ideal unless absolutely necessary for visualisation.

36.4 Phacovitrectomy Technique

To harness the advantages and minimise the disadvantages of phacovitrectomy, a good and consistent surgical technique is required. What follows are some tips to help improve phacovitrectomy technique and outcome. For vitreoretinal surgeons less familiar with phacoemulsification and complex cataract surgery, or in practice environments where cataract surgery needs to be performed by a cataract surgeon, it would be

necessary to secure the cooperation of a cataract surgeon willing to operate in tandem on such combined cases.

36.4.1 Incision Construction for Phacoemulsification

Many surgeons are now familiar with and perform clear corneal incision phacoemulsification [8]. A corneal incision allows sparing of the conjunctiva, an advantage in patients with glaucoma or prior vitreoretinal or other conjunctiva-opening surgery. Seated superiorly for phacovitrectomy, many vitreoretinal surgeons site their phacoemulsification incisions either superiorly or displaced towards the side of their dominant hand. The incision site can be sited all the way to the horizontal meridian for either temporal or nasal corneal incisions depending on which eye is being operated on and hand dominance of the surgeon. A temporal incision avoids the difficulties associated with a prominent brow or deep-set eyes, and is also more astigmatically neutral.

However, a superior corneal incision has the advantage of being sited further away from the vitrectomy ports and is less likely to leak during vitrectomy manoeuvres. For patients with a prominent brow, slight hyperextension of the neck or slight head-down tilt (Trendelenburg position) of the surgical table will help with surgical access for superior incisions.

Alternatively, a scleral tunnel incision can be performed after a limited conjunctival peritomy (Fig. 36.2). A superior approach is usually preferred. As scleral tunnels are more distant from the cornea centre, they are less likely to impair visualisation during vitrectomy compared to corneal incisions. They can be fashioned longer, resulting in a more predictably watertight, self-sealing incision. This facilitates intraoperative scleral indentation and other manipulations of the eye without anterior chamber collapse and hypotony.

Any standard incision width from 1.8 to 3 mm can be used as dictated by the phacoemulsification set-up. Narrower incisions have been found to induce less astigmatism when combined with
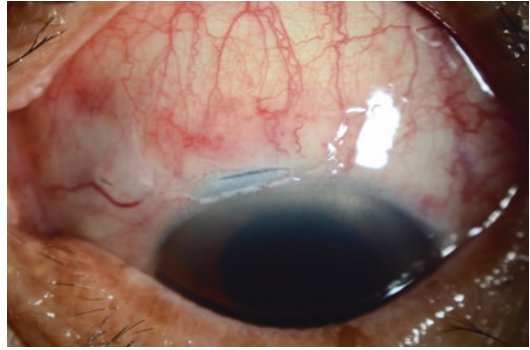
Fig. 36.2 A superior scleral tunnel incision. These incisions are less likely to impair visualisation during vitrectomy compared to corneal incisions and are predictably watertight, self-sealing incisions

23-gauge vitrectomy [9]. The length of the intracorneal or intrascleral tunnel relative to the width of the incision is the key determinant of incision integrity. "Square" or "near-square" incisions have been shown to be more stable than incisions of greater width versus length [10]. A longer intrastromal tunnel results in better wound integrity, but excessively long tunnels result in more corneal deformation during phacoemulsification, thereby possibly reducing subsequent visualisation due to corneal haze.

36.4.2 Phacoemulsification Procedure

Cataract surgery can be performed using the technique most familiar to the surgeon. A near-flawless execution of the cataract surgery is of paramount importance so as not to hinder subsequent vitrectomy. Nucleus removal should be performed with the lowest ultrasound energy, and as distant as possible from the cornea to maintain cornea clarity. All air bubbles and lens matter in the anterior chamber should be removed prior to the start of vitrectomy. Uneven fill of cohesive viscoelastic can also impair visualisation for vitrectomy. Either the viscoelastic should be completely removed or the anterior chamber is completely and evenly filled.

In eyes with a poor red reflex (typically due to dense vitreous haemorrhage) and in white mature

cataracts, trypan blue can be used to stain the anterior capsule to facilitate capsulorhexis. The size of the continuous curvilinear capsulorhexis should also be sized such that the edge overlaps the IOL optic. In general, the capsulorhexis is approximately 5 mm in diameter for a usual 6 mm optic. This reduces forward movement of the IOL after vitrectomy, especially if gas tamponade is used. A not excessively large capsulorhexis also allows for stable IOL placement in the sulcus if posterior capsule integrity is inadvertently lost. With the advent of femtosecond laser-assisted cataract surgery (FLACS), some authors have found this emerging technology to be feasible [11].

36.4.3 IOL Insertion

The IOL can be inserted towards the end of the vitrectomy, or at the usual juncture during the phacoemulsification procedure. In the former, after cortex removal, the phacoemulsification incision should be closed (see next section) and the surgeon proceeds with pars plana vitrectomy. If fluid air exchange is required, the IOL should be inserted prior to that. IOL insertion after fluid air exchange is difficult due to the positive pressure of the gas-filled vitreous chamber pushing the posterior capsule forward.

Just prior to IOL insertion, the vitrectomy infusion should be clamped, allowing the eye to soften slightly to allow for visco-expansion of the capsular bag for proper IOL placement within it. Excessive posterior infusion pressure collapses the capsular bag and shallows the anterior chamber. If the globe is too soft and the surgeon experiences difficulty with IOL injector insertion, the infusion should be unclamped momentarily to restore ocular tone, and then clamped again when inserting the IOL. The entire IOL should be completely placed within the capsular bag. Viscoelastic should be removed after the IOL haptics unfold.

The posterior capsule may be difficult to identify during vitrectomy. If a large posterior capsular rent is inadvertently created, a three-piece IOL should be placed in the ciliary sulcus.

Placing a one-piece IOL in the sulcus causes iris chafing and pigment dispersion, resulting in persistent anterior chamber inflammation and possibly secondary glaucoma.

An alternative timing of IOL insertion is during the usual juncture at the end of the phacoemulsification procedure, prior to vitrectomy. Completing the phacoemulsification portion first makes the combined surgery more convenient for some, especially when two surgeons are involved, but increases the difficulty of viewing the peripheral retina due to the IOL edge effect. Where macular surgery is concerned, our experience is that the IOL usually does not hinder the view for vitrectomy. Occasionally however, creases in the newly inserted IOL and debris or viscoelastic trapped behind the IOL can impair visualisation especially for delicate procedures like internal limiting membrane peeling.

36.4.4 Closure of Phacoemulsification Incisions

The phacoemulsification incision is commonly closed using stromal hydration for corneal incisions, or suturing with 10-0 nylon for both corneal and scleral incisions. Superior scleral tunnel incisions typically self-seal stably if well constructed and usually do not require suturing either during or at the completion of surgery. Cornea stromal hydration is performed by injecting balanced salt solution into the incision edges and roof with a 27-gauge Rycroft-style bent, blunt-tipped cannula attached to a 3 mL syringe filled with balanced salt solution. Care should be taken to avoid excessive hydration of the cornea which will hinder the view for subsequent vitrectomy. If careful hydration is insufficient to seal corneal incisions, suturing the incision with 10-0 nylon for watertight closure is preferred to overhydration and loss of intraoperative visualisation. Good incision closure results in a stable anterior chamber during trocar introduction and other intraoperative manipulations, and is critical for the stability of the IOL after surgery. To detect incision leakage, look for shallowing of the ante-

rior chamber and instability of the IOL position while the posterior infusion is turned on. Hydration or re-suturing of the phacoemulsification incision or paracentesis incision should be performed if necessary. Stability of the anterior chamber, appropriate capsulorhexis size and avoidance of excessive vitreous pressure are important in reducing IOL-related complications such as IOL capture by the pupil, anterior subluxation of the IOL and IOL-corneal touch.

36.4.5 Placement of Pars Plana Vitrectomy Ports

Phacovitrectomy is commonly performed by combining sutureless phacoemulsification and IOL implantation with sutureless, minimally invasive vitrectomy systems (23-gauge, 25-gauge or 27-gauge). The infusion port is usually placed in the infero-temporal quadrant, and the two working ports usually just above the horizontal to allow best surgical access (Fig. 36.3). We typically complete the phacoemulsification procedure before placing the pars plana ports. Others advocate placing the vitrectomy ports before phacoemulsification. Prior placement of ports circumvents the shallowing of anterior chamber and hypotony due to leakage from the phacoemulsification incision when manipulating the globe during trocar insertions. If ports are placed before phacoemulsification,
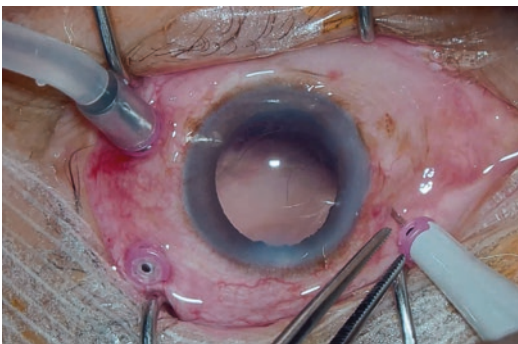
Fig. 36.3 Placement of pars plana vitrectomy ports. The infusion port is usually placed in the infero-temporal quadrant, and the two working ports usually just above the horizontal to allow best surgical access

the vitrectomy infusion should be stopped, and other cannulas plugged during phacoemulsification. If difficulty is encountered in eyes with shallow anterior chambers and high vitreous pressure, safe phacoemulsification can be facilitated by softening the eye by performing a limited vitrectomy with the vitreous cutter introduced through the preplaced ports. If the red reflex is poor as a result of vitreous opacities or haemorrhage, having a preplaced vitrectomy port will also allow for insertion of the endoillumination probe for better visualisation during capsulorhexis and cortical removal.

36.4.6 Pars Plana Vitrectomy

After cataract removal, the retina periphery can be easily accessed without worry of lens touch by vitrectomy instruments. However, care should be taken to avoid traumatising the posterior capsule which may be difficult to visualise. A more thorough anterior vitrectomy can be performed. The rest of the pars plana vitrectomy procedure is completed in the usual fashion, dictated by the pathology to be treated.

36.4.7 Completion of Combined Surgery

For phacovitrectomy where the phacoemulsification is completed before vitrectomy, surgery ends when the vitrectomy cannulas are removed. The phacoemulsification incisions are closed with hydration or suture, if necessary, as described above. The anterior chamber and IOL should both be stable. Appropriate posterior vitreous cavity pressure is important for IOL stability. After removal of vitrectomy cannulas, sclerotomy ports are checked to be self-sealing as for any vitrectomy. If there is concern about leakage, the ports can be closed with 7-0 Vicryl sutures. Leakage is possibly more common with 23-gauge systems compared to smaller gauges like 25 or 27 gauges [12]. In our experience, highly myopic eyes with thinner sclera tend to have ports which are less reliably self-sealing.

36.5   Biometry and IOL Selection

Combined phacoemulsification and IOL implantation and sutureless transconjunctival microincision small-gauge vitrectomy can provide refractive outcomes equivalent to cataract surgery alone [13] or sequential surgery [14], in cases of vitrectomy for epiretinal membranes, macular holes and diabetic retinopathy. Refractive outcomes in combined macular surgery were found to be satisfactory even with the use of a toric intraocular lens [15] although we do advise some caution in their use. Some studies have found a small myopic shift, more often in cases with gas tamponade, which may not have significant functional impact on retina patients [16]. A study by Lee et al. compared the predicted refraction by preoperative data with actual postoperative refraction in eyes undergoing vitrectomy followed by cataract surgery versus eyes undergoing cataract surgery in non-vitrectomised eyes. There was no significant difference between the predicted refraction by preoperative data and post-operative manifest refraction in both groups [17]. If refractive accuracy is deemed to be critically important to the patient, sequential surgery in which phacoemulsification and IOL implantation are deferred may be the preferred approach.

A three-piece intraocular lens is felt to sit more stably within the capsular bag with a lower incidence of lens shift and iris capture after phacovitrectomy. Recent literature, however, has found the use of single-piece or multipiece intraocular lenses to have no significant impact on the incidence of complications in combined phacovitrectomy [18].

36.6   Intraoperative Complications Specific to Phacovitrectomy

36.6.1 Pupil Miosis During Surgery

Adequate mydriasis is needed for safe vitrectomy. Maintenance of mydriasis is usually achieved through the use of topical sympathomimetic and anticholinergic agents preoperatively, and epinephrine, which is routinely added into the infusion fluid intraoperatively. In phacovitrectomy, surgical trauma may lead to miosis. The trauma stimulates prostaglandin synthesis, which together with other mediators can lead to pupillary constriction [19]. The use of topical diclofenac (1%) has been shown to prevent the onset of surgically induced miosis [20].

The use of wide-angle viewing systems allows vitreoretinal surgery to proceed in spite of suboptimal pupil dilation in many eyes. If significant miosis does occur, the pupil can often be enlarged adequately by viscoelastic injection into the anterior chamber. The pupil can also be mechanically stretched to enlarge it. More severe miosis can be overcome by the use of adjunctive devices including iris hooks and ring expanders [21].

36.6.2 Loss of Integrity of the Posterior Capsule During Surgery

Posterior capsular rupture (PCR) can occur as a complication during the cataract removal or during vitrectomy. Loss of posterior capsular integrity is usually managed no differently from any routine cataract operation [22]. Complete lens nucleus removal and cortical clean-up should be done before proceeding with vitrectomy. However, since a vitrectomy is already planned for, the nuclear and cortical clean-up can often be more effectively and less traumatically dealt with from the posterior approach via the pars plana rather than by excessive manipulation via the anterior approach. This keeps the cornea clear for vitreous surgery that follows.

In many instances, the IOL can be placed in the sulcus if anterior capsule support is adequate. IOL placement may be better delayed and performed as a secondary procedure in the presence of a PCR especially if gas or oil tamponade is required as there is a greater risk of IOL subluxation or dislocation. An appropriate method and type of secondary lens implant can be decided upon later when the retina pathology has stabilised.

36.6.3 Intraoperative Hyphaema

The presence of iris neovascularisation increases the risk of intraoperative hyphaema in cataract surgery [23] and subsequent intraocular hyphaema may impair visualisation during phacovitrectomy. The preoperative injection of intravitreal anti-VEGF a few days prior to the surgery can significantly regress iris neovascularisation and reduce the risk of hyphaema [24, 25]. Even in the absence of iris neovascularisation, hyphaema can occur as a result of hypotony during surgery, iatrogenic trauma of the iris or vigorous surgical manipulation of the eye, for example indentation of the sclera. Injection of viscoelastic into the anterior chamber of the eye to displace blood and retard its reaccumulation can help improve visualisation in these instances.

36.7 Postoperative Complications Specific to Phacovitrectomy

36.7.1 IOL Displacement and Pupil Capture

IOL displacement and pupil capture of IOL are often related to post-operative incision leakage.

Gas tamponade may sometimes push the IOL forwards, possibly contributed by inappropriate posturing after surgery, resulting in part of the IOL rim being caught anterior to the pupil edge (Fig. 36.4). As discussed earlier, care should be taken to ensure that both phacoemulsification and vitrectomy incisions are sealed at the completion of surgery. Immediate management of cases of hypotony include appropriate padding of the eye and posturing by the patient in the presence of gas tamponade. These steps can often restore the position of the IOL. What appears to be imminent pupil capture in the immediate postoperative period often resolves as gas tamponade resorbs. If repositioning of the IOL is required, this should be done early within the first few weeks of surgery typically after the gas tamponade has been resorbed [26].

36.7.2 Posterior Synechiae

Formation of posterior synechiae with adhesions of the iris to the IOL or anterior capsule is not an uncommon complication of phacovitrectomy (Fig. 36.5). This may result in decrease in visual quality, difficulties in peripheral retinal examina-
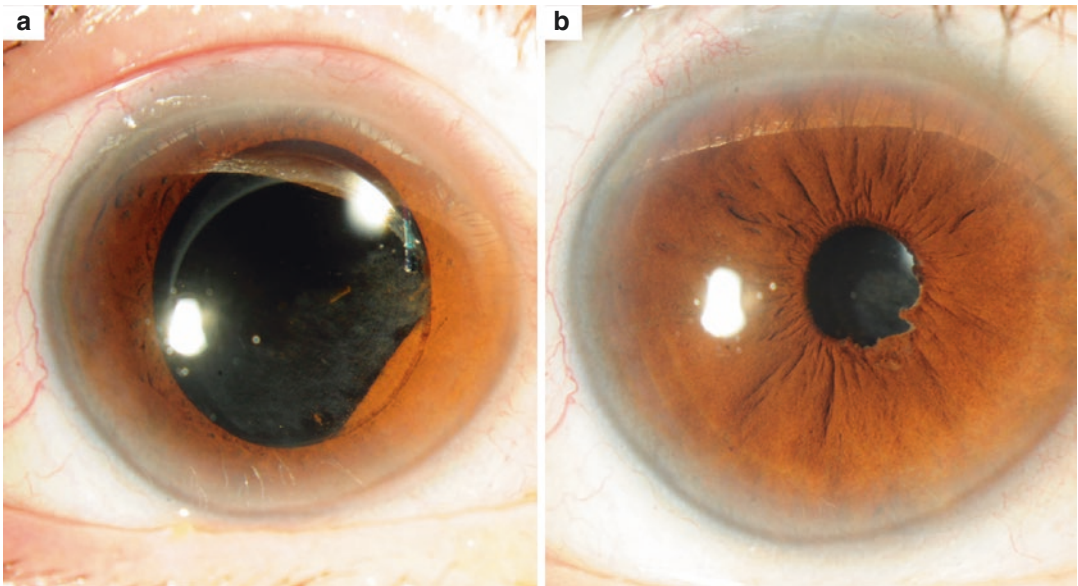
Fig. 36.4 Optic capture (**a**) in an eye after phacovitrectomy with gas tamponade. These often resolve spontaneously when the gas resorbs (**b**) but repositioning of the intraocular lens may occasionally be required
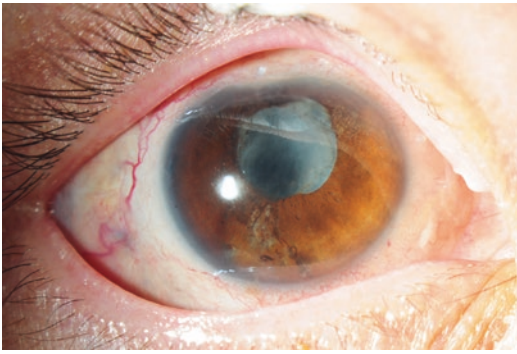
Fig. 36.5 Posterior synechiae following phacovitrectomy as a result of excessive inflammation in the early post-operative period

tion due to the impairment of pupillary movement and, rarely, secondary angle-closure glaucoma [27]. Posterior synechiae are formed from fibrous metaplasia of the inflamed iris tissue caused by early post-operative iritis [28]. C3F8 gas tamponade, oil tamponade and prolonged surgical time have been significantly associated with increased risk of developing posterior synechiae [29]. Initial management would include increased frequency of topical steroids, more intensive pharmacologic dilation of the pupil and appropriate posturing of patients in the presence of tamponade. Minor degrees of posterior synechiae are often inconsequential and can be left alone. Pupil block can be overcome with a laser peripheral iridotomy. In more severe cases, release of the posterior synechiae with the aid of viscoelastic should be performed within a few weeks once inflammation from initial surgery has abated, followed by intensive application of topical steroids.

36.8   Alternative Approaches

36.8.1 Vitrectomy First Followed by Sequential Phacoemulsification Surgery

In cases where there is adequate visualisation of the retina through the crystalline lens, vitrectomy can be performed first with sequential phaco-

emulsification surgery with IOL implant once the anatomical outcomes of the posterior segment surgery have been achieved.

There are some potential advantages to this approach. As noted earlier, vitrectomy can alter the accuracy of biometry of the eye, and reports have demonstrated a myopic shift in the refractive outcomes in phacovitrectomy [16], especially with the use of gas tamponade [30]. Biometry may also be less inaccurate in the presence of pathology such as retinal detachment [31]. Therefore, staged cataract surgery has the potential to allow more accurate refractive outcomes. This may be especially so if toric IOLs are to be implanted. However, with the advent of sutureless transconjunctival vitrectomy with smaller gauge sclerostomies, the refractive outcome in phacovitrectomy by experienced surgeons especially in straightforward macular surgery without gas can be equivalent to cataract surgery alone [13].

Performing cataract surgery later can also reduce the incidence of posterior synechiae or IOL pupil capture that can occur with combined surgery especially with gas tamponade and in eyes with inflammatory pathology [32]. In diabetic vitrectomies, there is also an increased risk of iris neovascularisation [33] that can be avoided with sequential surgery.

The major intraoperative disadvantages with this approach would be the compromised visualisation in the presence of significant cataract and the limited access to the vitreous base and anterior hyaloid in the presence of the crystalline lens.

36.8.2 Cataract Surgery First Followed by Vitrectomy

Performing cataract surgery first in eyes with visually significant cataract can improve visualisation of the posterior segment for diagnostic and management purposes. There is an advantage of this approach in patients with epiretinal membrane because of the discordance between the anatomical impact of the epiretinal membrane
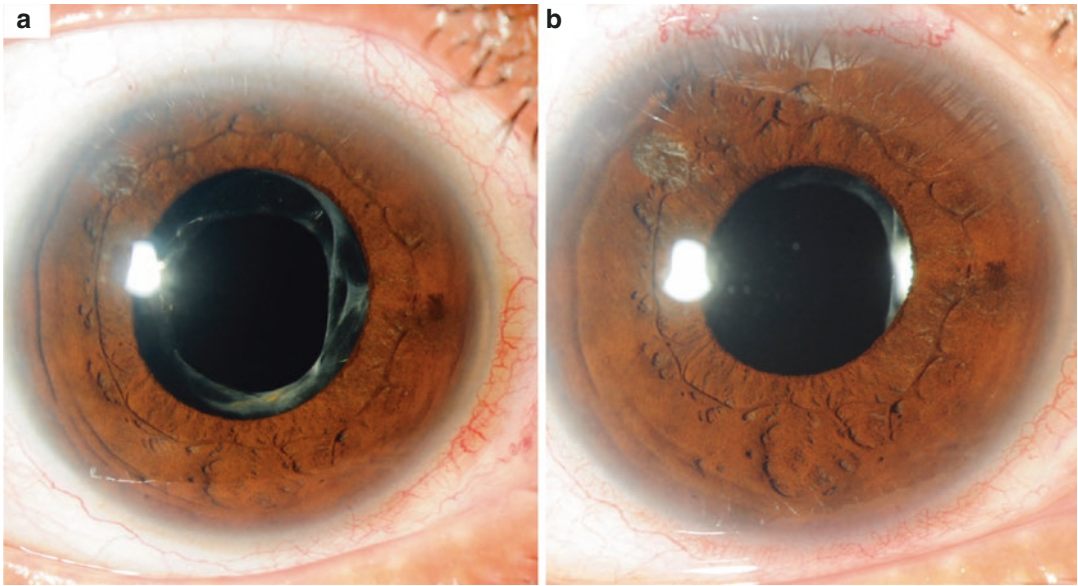
Fig. 36.6 An eye left aphakic after lensectomy with preservation of the anterior capsule rim (**a**). This allows for stable placement of intraocular lens in the sulcus (**b**) as a secondary procedure after the retinal pathology has been adequately addressed

and the functional impact on vision. In the presence of significant cataract, phacoemulsification and IOL implantation alone may be enough to address the patient's symptoms and visual loss. One study found that by performing cataract surgery first, 17% of eyes with anatomically significant epiretinal membrane did not subsequently need vitrectomy [14]. The stable in-the-bag IOL may be less likely to develop optic capture and posterior synechiae. This approach also provides the advantage of good visualisation and access to the vitreous base and anterior hyaloid in a pseudophakic vitrectomy, but may still have similar limitations with regard to biometry and postoperative refractive outcomes.

36.8.3 Primary Phacoemulsification or Lensectomy Without Lens Implantation During Vitrectomy

There are instances where removal of the crystalline lens is necessary to provide visualisation and access for adequate dissection and removal of the vitreous base and the anterior hyaloid or anterior tractional membranes. The surgeon may decide not to implant a lens during the primary surgery. These include eyes with severe proliferative vitreoretinopathy, extensive giant breaks, severe uveitis and trauma, where performing a lensectomy (or phacoemulsification) with complete removal of the lens capsule to accomplish decompartmentalisation of the eye without IOL implantation may enable the surgeon to better achieve resolution of complex vitreoretinal pathology. Preservation of the anterior capsule rim in less complicated cases may allow the surgeon to subsequently implant an IOL into the sulcus safely in a second procedure once the retinal pathology has been adequately addressed (Fig. 36.6) [34]. Although theoretically possible, leaving a vitrectomised eye aphakic but with an anterior capsular rim and an intact posterior capsule with a view to later in-the-bag IOL implantation is not a good approach. There is often rapid posterior synechia formation and posterior capsule opacification after surgery in the absence of an IOL.

36.9 Evidence Review: Safety and Efficacy of Combined Phacoemulsification and Vitrectomy

There is ample data that combined phacoemulsification and vitrectomy is a safe and effective procedure with outcomes equivalent to sequential surgery in suitable eyes [5, 14, 33, 35–38].

A large retrospective analysis of 306 eyes (145 with vitrectomy alone and 161 with combined phacovitrectomy) found that the mean visual acuity was lower in the vitrectomy-alone group. This was mainly due to cataract formation [39]. Combined surgery had similar impact on the cornea endothelium and cornea biomechanics as sequential surgery [40].

A prospective, non-randomised comparative study by Tayyab et al. [41] did suggest that in the early post-operative period, significantly more patients in the combined surgery group had anterior chamber fibrin than in the vitrectomy-only group, and there were correspondingly more patients who developed posterior synechiae in the combined surgery group.

Combined surgery does have a small risk of posterior synechiae with pupil block especially for diabetic vitrectomies. This can be relieved with a laser peripheral iridotomy [42]. There is also a risk of optic capture with or without pupil block. Historically, there has been a concern over the increased incidence of iris neovascularisation and neovascular glaucoma after combined surgery and we still advise caution in such eyes [33]. However, this has possibly become less of a concern in the anti-VEGF era. Perioperative anti-VEGF injections have been found to improve the outcomes of combined phacovitrectomy in proliferative diabetic retinopathy [43–46]. Even in cases where neovascularisation occurs, adequate post-operative vigilance with early intervention can still provide good outcomes.

36.10 Transition to Phacovitrectomy

The transition from cataract surgeon to a vitreoretinal surgeon performing combined phacoemulsification and pars plana vitrectomy typically occurs during fellowship, the ease of which depends on the acquisition of a new set of posterior segment surgical skills. Less commonly, a practising vitreoretinal surgeon trained in cataract surgery during residency must transition back to combined surgery. Oftentimes this occurs with the US-based vitreoretinal surgeons (who typically stop performing cataract surgeries after completing surgical retina fellowships) who relocate internationally. Such a transition tends to be less supervised than during fellowship, but can nonetheless be rapid, given baseline knowledge from prior training in phacoemulsification. Generally, the transition is enhanced by supportive colleagues in a facility already routinely performing combined surgeries.

There are several pearls when one is readjusting back to cataract surgery. As compared to vitrectomy, there is relatively tighter space to work in, within the anterior chamber, especially in eyes with narrow angles commonly encountered in Asia. The ergonomics therefore play an important role in terms of phacoemulsification incision placement, as discussed earlier. Moreover, both instruments are in close proximity, cross each other and interplay with one other more often in phacoemulsification than in vitrectomy when the instruments from the two ports tend to be spaced further apart. Microscope lighting for capsulorhexis, which mainly employs retroillumination, also requires some readjustment and pre-planning, versus in vitrectomy where a light-pipe incident angle and intensity are readily adjustable intraoperatively by the surgeon. Capsulorhexis, although having similarities to internal limiting membrane peeling, requires some relearning, given the variability in countertraction afforded by the zonules, capsular bag and viscoelastic fill of the anterior chamber.

36.11 Health Economics of Phacovitrectomy Versus Staged Surgery

As phacovitrectomy combines two surgeries into one, it obviates the need for patients undergoing vitrectomy to return for cataract surgery. Therefore, in addition to being safe and efficient

with good outcomes in many patients [47], another obvious benefit of this combined surgical approach is cost savings.

Cataract is commonly found in patients with an indication for vitrectomy [48]. Even among patients without visually significant cataract at the time of vitrectomy, approximately 85% of them develop a cataract that requires surgical intervention within 5 years. Therefore, it makes good sense to combine cataract surgery with vitrectomy. A cost-analysis study in the United States [49] showed that the total fees for surgeon, anaesthesiology and ambulatory surgical centre are reduced with phacovitrectomy, achieving about 17% or greater Medicare cost savings for all indications. Collectively, the data clearly shows that phacovitrectomy by a single surgeon can offer significant cost savings compared to sequential surgery. In fact, previous studies are likely to have underestimated the true cost benefit of phacovitrectomy as a result of failing to account for other factors such as post-operative visits, recovery time and time off work for patients.

References

1. Demetriades AM, Gottsch JD, Thomsen R, Azab A, Stark WJ, Campochiaro PA, et al. Combined phacoemulsification, intraocular lens implantation, and vitrectomy for eyes with coexisting cataract and vitreoretinal pathology. Am J Ophthalmol. 2003;135(3):291–6.
2. Berrocal MH, Chenworth ML, Acaba LA. Management of giant retinal tear detachments. J Ophthalmic Vis Res. 2017;12(1):93–7.
3. Mamalis N, Teske MP, Kreisler KR, Zimmerman PL, Crandall AS, Olson RJ. Phacoemulsification combined with pars plana vitrectomy. Ophthalmic Surg. 1991;22(4):194–8.
4. Scharwey K, Pavlovic S, Jacobi KW. Combined clear corneal phacoemulsification, vitreoretinal surgery, and intraocular lens implantation. J Cataract Refract Surg. 1999;25(5):693–8.
5. Lahey JM, Francis RR, Kearney JJ. Combining phacoemulsification with pars plana vitrectomy in patients with proliferative diabetic retinopathy: a series of 223 cases. Ophthalmology. 2003;110(7):1335–9.
6. Blecher MH, Kirk MR. Surgical strategies for the management of zonular compromise. Curr Opin Ophthalmol. 2008;19(1):31–5.
7. Wong CW, Ang M, Tsai A, Phua V, Lee SY. A prospective study of biometric stability after scleral buckling surgery. Am J Ophthalmol. 2016;165:47–53.
8. Leaming DV. Practice styles and preferences of ASCRS members—2003 survey. J Cataract Refract Surg. 2004;30(4):892–900.
9. Kim YK, Kim YW, Woo SJ, Park KH. Comparison of surgically-induced astigmatism after combined phacoemulsification and 23-gauge vitrectomy: 2.2-mm vs. 2.75-mm cataract surgery. Korean J Ophthalmol. 2014;28(2):130–7.
10. Masket S, Belani S. Proper wound construction to prevent short-term ocular hypotony after clear corneal incision cataract surgery. J Cataract Refract Surg. 2007;33(3):383–6.
11. de Queiroz Alves B, Brasil OFM, Espinhosa CT, Japiassu RM, Goncalves MB, Junior OM, et al. Combined femtosecond laser-assisted cataract surgery and small-gauge pars plana vitrectomy using different devices: a new trend for vitreoretinal surgery? Ophthalmic Surg Lasers Imaging Retina. 2018;49(5):374–9.
12. Kim M, Park YS, Lee DH, Koh HJ, Lee SC, Kim SS. Comparison of surgical outcome of 23-gauge and 25-gauge microincision vitrectomy surgery for management of idiopathic epiretinal membrane in pseudophakic eyes. Retina. 2015;35(10):2115–20.
13. Shi L, Chang JS, Suh LH, Chang S. Differences in refractive outcomes between phacoemulsification for cataract alone and combined phacoemulsification and vitrectomy for epiretinal membrane. Retina. 2019;39(7):1410–5.
14. Hamoudi H, Correll Christensen U, La Cour M. Epiretinal membrane surgery: an analysis of 2-step sequential- or combined phacovitrectomy surgery on refraction and macular anatomy in a prospective trial. Acta Ophthalmol. 2018;96(3):243–50.
15. Nakano Y, Nomoto H, Fukuda K, Yamaji H, Fujita T, Inoue Y, et al. Combined 25-gauge vitrectomy and cataract surgery with toric intraocular lens with idiopathic epiretinal membrane. J Cataract Refract Surg. 2013;39(5):686–93.
16. Hamoudi H, La Cour M. Refractive changes after vitrectomy and phacovitrectomy for macular hole and epiretinal membrane. J Cataract Refract Surg. 2013;39(6):942–7.
17. Lee NY, Park SH, Joo CK. Refractive outcomes of phacoemulsification and intraocular lens implantation after pars plana vitrectomy. Retina. 2009;29(4):487–91.
18. Leiderman YI, Andreoli MT, Sun B, Dawood S. Pars plana vitrectomy combined with cataract extraction: a comparison of surgical outcomes using single-piece and multipiece foldable intraocular lenses. Retina. 2015;35(6):1059–64.
19. Cole DF, Unger WG. Prostaglandins as mediators for the responses of the eye to trauma. Exp Eye Res. 1973;17(4):357–68.
20. Mirshahi A, Djalilian A, Rafiee F, Namavari A. Topical administration of diclofenac (1%) in the prevention of miosis during vitrectomy. Retina. 2008;28(9):1215–20.
21. Goldman JM, Karp CL. Adjunct devices for managing challenging cases in cataract surgery: pupil expan-

sion and stabilization of the capsular bag. Curr Opin Ophthalmol. 2007;18(1):44–51.

22. Hong AR, Sheybani A, Huang AJ. Intraoperative management of posterior capsular rupture. Curr Opin Ophthalmol. 2015;26(1):16–21.

23. Kuchle M, Handel A, Naumann GO. Cataract extraction in eyes with diabetic iris neovascularization. Ophthalmic Surg Lasers. 1998;29(1):28–32.

24. Rizzo S, Genovesi-Ebert F, Di Bartolo E, Vento A, Miniaci S, Williams G. Injection of intravitreal bevacizumab (Avastin) as a preoperative adjunct before vitrectomy surgery in the treatment of severe proliferative diabetic retinopathy (PDR). Graefes Arch Clin Exp Ophthalmol. 2008;246(6):837–42.

25. Chalam KV, Gupta SK, Grover S, Brar VS, Agarwal S. Intracameral avastin dramatically resolves iris neovascularization and reverses neovascular glaucoma. Eur J Ophthalmol. 2008;18(2):255–62.

26. Obstbaum SA, To K. Posterior chamber intraocular lens dislocations and malpositions. Aust N Z J Ophthalmol. 1989;17(3):265–71.

27. Makhzoum O, Crosby NJ, Hero M. Secondary angle-closure glaucoma due to posterior synechiae formation following phacovitrectomy. Int Ophthalmol. 2011;31(6):481–2.

28. Yeo JH, Jakobiec FA, Pokorny K, Iwamoto T, Pisacano A. The ultrastructure of an IOL "cocoon membrane". Ophthalmology. 1983;90(4):410–9.

29. Oh J-H, Na J, Kim S-W, Oh J, Huh K. Risk factors for posterior synechiae of the iris after 23-gauge phacovitrectomy. Int J Ophthalmol. 2014;7(5):843–9.

30. Suzuki Y, Sakuraba T, Mizutani H, Matsuhashi H, Nakazawa M. Postoperative refractive error after simultaneous vitrectomy and cataract surgery. Ophthalmic Surg Lasers. 2000;31(4):271–5.

31. Kim YK, Woo SJ, Hyon JY, Ahn J, Park KH. Refractive outcomes of combined phacovitrectomy and delayed cataract surgery in retinal detachment. Can J Ophthalmol. 2015;50(5):360–6.

32. Smith M, Raman SV, Pappas G, Simcock P, Ling R, Shaw S. Phacovitrectomy for primary retinal detachment repair in presbyopes. Retina. 2007;27(4):462–7.

33. Chung TY, Chung H, Lee JH. Combined surgery and sequential surgery comprising phacoemulsification, pars plana vitrectomy, and intraocular lens implantation: comparison of clinical outcomes. J Cataract Refract Surg. 2002;28(11):2001–5.

34. MacCumber MW, Packo KH, Civantos JM, Greenberg JB. Preservation of anterior capsule during vitrectomy and lensectomy for retinal detachment with proliferative vitreoretinopathy. Ophthalmology. 2002;109(2):329–33.

35. Yang Y, Zhang J, Yan H. Comparison of combined and sequential surgery for proliferative diabetic retinopathy: a single surgeon study. PLoS One. 2014;9(9):e108933.

36. Silva PS, Diala PA, Hamam RN, Arrigg PG, Shah ST, Murtha TL, et al. Visual outcomes from pars plana vitrectomy versus combined pars plana vitrectomy, phacoemulsification, and intraocular lens implantation in patients with diabetes. Retina (Philadelphia, PA). 2014;34(10):1960–8.

37. Dugas B, Ouled-Moussa R, Lafontaine PO, Guillaubey A, Berrod JP, Hubert I, et al. Idiopathic epiretinal macular membrane and cataract extraction: combined versus consecutive surgery. Am J Ophthalmol. 2010;149(2):302–6.

38. Treumer F, Bunse A, Rudolf M, Roider J. Pars plana vitrectomy, phacoemulsification and intraocular lens implantation. Comparison of clinical complications in a combined versus two-step surgical approach. Graefes Arch Clin Exp Ophthalmol. 2006;244(7):808–15.

39. Arikan Yorgun M, Toklu Y, Mutlu M, Ozen U. Clinical outcomes of 25-gauge vitrectomy surgery for vitreoretinal diseases: comparison of vitrectomy alone and phaco-vitrectomy. Int J Ophthalmol. 2016;9(8):1163–9.

40. Hamoudi H, Christensen UC, La Cour M. Corneal endothelial cell loss and corneal biomechanical characteristics after two-step sequential or combined phaco-vitrectomy surgery for idiopathic epiretinal membrane. Acta Ophthalmol. 2017;95(5):493–7.

41. Tayyab H, Khan AA, Javaid RMM. Clinical outcome of 23g Trans-Conjunctival pars plana vitrectomy—a prospective comparison of Phaco-Vitrectomy with only vitrectomy in phakic eyes. Pak J Med Sci. 2017;33(5):1123–7.

42. Raj P, Kumar K, Chandnani N, Agarwal A, Agarwal A. Secondary angle-closure glaucoma due to posterior synechiae of iris following combined phacoemulsification and 23-gauge transconjunctival vitrectomy. Semin Ophthalmol. 2017;32(5):537–42.

43. Oli A, Balakrishnan D, Rani PK. Preoperative bevacizumab administration in proliferative diabetic retinopathy patients undergoing vitrectomy: a randomized and controlled trial comparing interval variation. Am J Ophthalmol. 2018;187:168–9.

44. Zhao XY, Xia S, Wang EQ, Chen YX. Efficacy of intravitreal injection of bevacizumab in vitrectomy for patients with proliferative vitreoretinopathy retinal detachment: a meta-analysis of prospective studies. Retina. 2018;38(3):462–70.

45. Castillo J, Aleman I, Rush SW, Rush RB. Preoperative bevacizumab administration in proliferative diabetic retinopathy patients undergoing vitrectomy: a randomized and controlled trial comparing interval variation. Am J Ophthalmol. 2017;183:1–10.

46. Hsu YJ, Hsieh YT, Yeh PT, Huang JY, Yang CM. Combined tractional and rhegmatogenous retinal detachment in proliferative diabetic retinopathy in the anti-VEGF era. J Ophthalmol. 2014;2014:917375.

47. Lahey JM, Francis RR, Fong DS, Kearney JJ, Tanaka S. Combining phacoemulsification with vitrectomy for treatment of macular holes. Br J Ophthalmol. 2002;86(8):876–8.

48. Jackson TL, Donachie PH, Sparrow JM, Johnston RL. United Kingdom National Ophthalmology Database study of vitreoretinal surgery: report 1; case mix, complications, and cataract. Eye (Lond). 2013;27(5):644–51.

49. Seider MI, Michael Lahey J, Fellenbaum PS. Cost of phacovitrectomy versus vitrectomy and sequential phacoemulsification. Retina. 2014;34(6):1112–5.

Choice and Implications of Intraocular Lens in Retinal Surgery

Erica Darian-Smith, Steven G. Safran, Dan Ohman, and Minas Theodore Coroneo

37.1 Introduction

Arguably, every patient undergoing cataract surgery should be considered a potential candidate for subsequent surgery—including retinal, corneal, glaucoma, strabismus and even oculoplastic procedures. While the risks of subsequent retinal surgery are now considered relatively low, wisdom would dictate avoidance of a third procedure to replace a damaged intraocular lens (IOL), if possible. In a study with data collected on 5878 consecutive cataract operations, there was a 0.18% risk of retinal detachment 2 years after the initial surgery (high-risk cases excluded). In the same cohort it was found that the relative risk of detachment increased following YAG laser capsulotomy (4.9), with increasing age (0.94 for each added year of patient age) and increasing axial length (1.3 with an increase in the axial length of 1 mm) [1].

The evolution of IOL design has been relatively rapid and continues. This process has been described as a "stimulus-response relationship between science, technology and medicine" which has "fuelled the search for different and better materials for lens design" [2]. With advances in both retinal and corneal surgery, the relationship between IOL material and fluids used in these surgeries provides another stimulus to further improve IOL design. The term pseudophakic cataract will be used to refer to IOL opacification, whether induced by adjunctive materials or spontaneously.

Sir Harold Ridley was the pioneer of the modern-day intraocular lenses and, during WWII, developed artificial acrylic plastic lenses, made of polymethyl methacrylate (PMMA) as a replacement for the crystalline lens. However, suboptimal results caused by a combination of factors including inadequate surgical techniques, poor lens design, heavy lens weight and lack of manufacturing technology provided stimulus for further development [3]. In 1967, Charles Kelman developed phacoemulsification (which revolutionised cataract surgery) by enabling the procedure to be performed micro-invasively, through a

E. Darian-Smith (✉)
Department of Ophthalmology, Prince of Wales Hospital, Sydney, NSW, Australia

School of Medicine, The University of Sydney, Sydney, NSW, Australia

Department of Ophthalmology, University of New South Wales at Prince of Wales Hospital, Sydney, NSW, Australia

S. G. Safran
Capital Health System, New Jersey Surgery Centre, Pennington, NJ, USA
e-mail: safran12@comcast.net

D. Ohman
Ophthalmic Surgical Division, Eye Clinic, Orebro University Hospital, Orebro, Sweden
e-mail: dan.ohman@telia.com

M. T. Coroneo
Department of Ophthalmology, University of New South Wales at Prince of Wales Hospital, Sydney, NSW, Australia

small incision. However, with existing IOLs, wound size subsequently had to be enlarged for IOL insertion [4].

Prior to this, during the 1950s, another revolution had commenced in plastics. Otto Wichterle developed hydrophilic gels, based on polyhydroxyethylmethacrylate (pHEMA) with the aim of improved biocompatibility, for devices in permanent contact with living tissues [5]. Known as the father of soft contact lenses, some of Wichterle's early work was on IOLs [6]. A soft and therefore foldable IOL made from hydrogel could be implanted in a semi-hydrated state through a small incision, expanding in the eye when fully hydrated. These early "intra-cameral" lenses were implanted in rabbit anterior chambers. Perhaps an invention before its time (while the development of soft contact lenses developed apace), the next phase of foldable lenses was in the 1970s.

Intraocular lens "biocompatibility" is of importance. Though difficult to define, in general terms a biocompatible substance is one that has physical, chemical and biological compatibility with the surrounding tissues and is in sync with the mechanical behaviour of these tissues. One way to categorise biocompatibility of an IOL is to measure its inflammatory response and response of the lens epithelial cells. Therefore, objective assessment is through uveal biocompatibility (measured by the inflammatory foreign-body reaction of the eye to the implant) and through capsular biocompatibility (measured by the residual lens epithelial cell response within the capsular bag to the IOL). The ideal biocompatible IOL has the following properties: no foreign-body reaction, compatibility with the surrounding tissues (specifically the capsular bag), optimisation of vision and longevity so no additional intervention is required. Features which aid in biocompatibility include lens material, optic edge design, lens surface properties and haptic-optic combination/junction. Biocompatibility of an IOL can also, to an extent, be affected by the surgeon's technique and also the predetermined characteristics of the host tissue. PMMA, one of the earliest IOL materials, demonstrated good tissue tolerance, high uveal biocompatibility (small anterior chamber response), low foreign-body inflammatory response and good optical properties given a high refractive index. However, its rigidity, un-foldable structure, high rates of pseudophakic cataract and inability to withstand high temperatures and pressures make it an unpopular choice in the modern era. Current practice dictates the use of foldable (hydrophobic and hydrophilic) IOLs and their biocompatibility properties will be discussed further below [7–10]. An apparent contradiction in terms is that while IOL "biocompatibility" is desired, IOLs should not support/facilitate the growth of remaining lenticular cells.

The first foldable silicone IOLs were implanted in human eyes in 1976 [11]. These were rapidly adopted, and foldable silicone IOLs were market leaders during the 1980s [12]. With the advent of vitreoretinal surgery, and tamponade with silicone oil in vitrectomised eyes in the early 1990s, issues became apparent with these silicone IOLs. There was adherence of the silicone oil to the silicone IOL interface causing unacceptable visual outcomes—including reduced acuity and aberrations [13, 14]. More recently developed foldable acrylic IOLs, which obtained FDA approval in December 1994, have revolutionised the market [15]. Hydrophobic acrylic counterparts were introduced in 1993 with the first Acrysof three-piece lens (Alcon, Forth Worth, Texas, USA). Their use today is widespread [15, 16].

37.2 Part A

37.2.1 The "Ideal" Intraocular Lens

The human crystalline lens is the ideal intraocular lens. In an effort to mimic the natural lens, various prosthetic IOLs have been devised. The "ideal" prosthetic IOL is biocompatible, with spectral characteristics mimicking those of the natural lens; it has no aberrations, facilitates accommodation, is associated with minimal capsular opacity and allows the retinal surgeon a clear view of the entire retina, including the

periphery. The lens should have neutral buoyancy (specific gravity of 1), to reduce inertia of the lens with the ocular material. The lens diameter should be approximately 6 mm, enabling optimal positioning in the capsular bag, allowing insertion through a small incision [17, 18]. Other potential features of the "ideal" IOL include adjustability of IOL power/astigmatism post-surgery, long-term wide-range adjustment for paediatric aphakia, adequate magnification for low vision applications, incorporation of an intraocular pressure-sensing device, variable tinting or filter capacity, incorporation of an artificial iris (if required), potential for "reverse" imaging and access to computer/internet interfaces. Some of these features, such as adequate magnification for low-vision-application IOLs, are currently being trialled and are in their infancy; others are yet to be explored and, at this stage, remain purely hypothetical [19, 20].

Since the initial inception of IOLs there has been a range of differing designs and intraocular positioning trialled, including anterior chamber-fixated IOLs, iris-fixated IOLs, posterior chamber IOLs, sulcus-fixated IOLs and, more recently, capsulorhexis-fixated IOLs [18, 21, 22]. Given that monofocal prosthetic IOLs do not accommodate, multifocal IOLs have been designed to compensate for this to some extent. The underlying principle of multifocal IOLs is that an image in which all objects at all distances are both focused and defocused is presented to the retina. The brain then determines which object is of interest and focuses on this, only suppressing the other projected images. While it is not accommodation, it does allow the patient to focus on objects at close distances. The downside is that multiple images cause a reduction in contrast sensitivity, increased aberrations and reduced colour edge definition—this is particularly problematic in patients with pre-existing retinal disease and underlying poor-quality vision [21].

As previously discussed, biocompatibility of IOL prosthetic material is also imperative. Polymers implanted into the eye must meet specific criterion to ensure biocompatibility. An "ideal" polymer is one that:

1. Can be manufactured as a pure material
2. Can be generated in the desired shape without reducing the quality of the material or limiting its effects
3. Has the desired physical and mechanical characteristics in order to function effectively
4. Can be sterilised without altering chemical structure and functionality
5. Will not have its physical, chemical or mechanical properties negatively changed by the intraocular environment
6. Resists adherence and growth of microorganisms [7, 8, 17]

Biomaterials can be separated into two overarching categories, acrylic or silicone material. Within the acrylic subgroup lenses can further be divided into non-foldable (PMMA) or foldable types (acrylic), based on flexibility of the lens. Foldable, acrylic lenses can be further separated into hydrophilic (with a high absorbable water content) and hydrophobic (largely water repellent) subtypes. All silicone lenses are flexible (foldable) in nature. With the introduction of small-incision cataract surgery techniques and ultrasound phacoemulsification there has been a rapid decline in the use of PMMA [23]. Acrylics are polymers synthesised from esters of acrylic or methacrylic acid, with a refractive index of 1.55 and temperature-dependent resistance [15]. Foldable acrylic IOLs are advantageous over their firm PMMA counterparts due to easier sterilisation, flexibility and insertability via small limbal incisions, lack of polishing compound residues and lighter weight. Lighter weight of the IOL is particularly important as it limits the risk of zonular rupture and IOL dislocation and facilitates buoyancy in the aqueous [17]. PMMA lenses are also associated with higher rates of posterior capsule opacification (PCO) [23]. Most posterior chamber IOLs currently in use are comprised of either acrylic or silicone. The different water absorbability of acrylic IOLs accounts for differing refractive indices, thickness and overall mechanical properties of the lenses [3, 15, 17].

Posterior capsular opacification is a common complication of cataract extraction and intraocular lens insertion. It occurs in approximately

50% of cases, over a period of 6 months to 5 years following surgery [24]. It is somewhat ironic that the patient who is liberated from their initial cataract now has re-opacification of their lens capsule. PCO is treated with YAG (Nd:YAG) laser capsulotomy. Given the close apposition of the IOL to the posterior capsule, during directed laser treatment damage to the IOL occurs in approximately 40% of cases. It has been postulated that damage to the IOL may lead to release of toxic substances from within the IOL into surrounding specialised intraocular tissues causing damage—although these small levels of toxicity were predominantly in lens cultures exposed to laser powers exceeding 5 mJ (much higher powers than the range commonly used for YAG capsulotomy) [24]. However, another study demonstrated that when over 100 lesions were generated by Nd-YAG laser in a PMMA IOL, damage was purely mechanical with no measurable release of monomer (from depolymerisation of the PMMA material) [25]. Although the risk of toxic substance release from damaged IOLs appears marginal, particularly in the current lower power range of intraocular YAG capsulotomy laser use, it is still imperative that the material selected in IOLs is tested carefully and that it is biocompatible with the host tissue to limit any potential damage [24, 26, 27]. The other benefit of utilising IOLs with enhanced "capsular biocompatibility" is that YAG capsulotomy rates are decreased and so too is the subsequent risk of associated retinal tears and detachment.

Surface IOL modifications have also been trialled. Methods of surface modification include surface-coating technique, surface-grafted modification, plasma surface modification, photochemical immobilisation and layer-by-layer self-assembly. There have been a variety of surface materials and molecules trialled to alter the biocompatibility of IOLs including but not limited to heparin, PEG, MPC, TiO_2 and vinyl pyrrolidone. These recent surface modification trials have looked at gen-erating the "perfect IOL" (in one view) which is comprised of a hydrophilic anterior surface and a hydrophobic posterior surface—these lenses remain largely experimental and their responses to surgical liquids do not appear to have been assessed [28].

IOL implantation occurs not just used after cataract surgery; it is also used for refractive lens exchange in cases of high myopia, hyperopia and presbyopia. Given the widespread use of IOLs the need for the "perfectly biocompatible IOL" has never been so topical and important. Overall, it has been found that hydrophilic IOLs are associated with better uveal biocompatibility, whereas their hydrophobic counterparts are associated with better capsule biocompatibility [7, 28]. Foldable IOLs have enabled smaller corneal incisions reducing the likelihood of post-operative astigmatism, wound leak and infection. Multifocal IOLs provide an option for substituting accommodative effects, but rely on a requisite level of underlying visual function. Aside from the crystalline lens, there is no "ideal" prosthetic IOL; rather, there is a selection of lenses which are considered ideal for differing patient characteristics and surgeon techniques and preferences [21].

37.3 Part B

37.3.1 Factors to Consider for IOL Selection Preceding Vitreoretinal Surgery

Outline

1. Intraocular lens opacification after gas insertion
2. Should intraocular lenses block blue light?
3. Do some intraocular lenses allow a better view of the peripheral retina?
4. Are some intraocular lenses more prone to causing capsule phimosis and eventual subluxation?
5. Dysphotopsias and glistenings

37.4 Intraocular Lens Opacification After Gas Insertion

Cataract removal and intraocular lens insertion are sometimes required to improve intraocular visualisation prior to vitreoretinal surgery. The quandary that surgeons face is in determining the most appropriate lens material to insert to avoid lens opacification after gas or oil utilisation following prospective vitreoretinal surgery. It must be remembered that the patient demographic of those undergoing vitreoretinal surgery may have underlying suboptimal potential vision due to their pre-existing retinal condition including but not limited to diabetic eye disease, myopia, retinal detachment, macular hole, epiretinal membrane and macular degeneration. Any compromise in IOL design or function is thus likely to further compromise the final visual outcome.

37.4.1 Materials to Avoid

Hydrophilic acrylic lenses are associated with a higher tissue compatibility due to the their water content, associated low aqueous flare rates and a reduced amount of inflammatory cell accumulation on the lens surface [7]. Despite these advantages they should be avoided in any patient having any secondary vitreoretinal procedure as these IOLs are associated with a high rate of pseudophakic cataract, from calcification, over a short time period [29–31]. The causes of calcification in hydrophilic acrylic lenses are multifactorial and not well understood. Likely contributing factors are surgical technique, IOL packaging, manufacturing processes and patient's associated conditions. Calcification has also been linked to pars plana vitrectomy with gas and air tamponade [3, 32–34]. Hydrophilic IOLs are also associated with higher rates of anterior capsular phimosis increasing the rates of IOL dislocation—likely associated with their higher water content [35, 36]. Given this complication it is common for patients who have previously had hydrophilic acrylic in-the-bag IOLs inserted to undergo subsequent explantation of the IOL [3, 34, 37, 38] (Fig. 37.1).

Despite silicone lenses providing the best optical outcomes they should also be avoided in eyes in which subsequent vitreoretinal surgery is planned as they too can undergo post-operative calcification, particularly if the host eye has an underlying condition such as asteroid hyalosis [3, 39]. If the patient undergoes a vitreoretinal procedure requiring insertion of silicone oil—this may interact and adhere to the lens reducing the patient's vision. Silicone oil adheres to the IOL surface and this effect is enhanced in silicone optic IOL designs. For this reason silicone IOLs are not compatible with vitrectomised, silicone oil-filled eyes and therefore will not be discussed further in this chapter [7, 13, 40]. It is important to note that silicone oil is a common contaminant in many ophthalmic viscoelastic devices (OVDs). Thus, given the deleterious effects of silicone oil adherence to silicone IOLs, OVDs with a relatively low silicone oil content should be actively sought [41].

37.4.2 Materials of Choice

Hydrophobic acrylic lenses are favoured due to lower reported rates of pseudophakic cataract. For this reason these are generally the lenses of choice when performing cataract surgery prior to a secondary vitreoretinal operation. Other advantages of acrylic hydrophobic IOLs include material compatibility with a posterior sharp-edged design and reduced rates of epithelial cell overgrowth on the lens surface. While they have been associated with higher aqueous flare rates and inflammatory cell accumulation on the lens surface following insertion, these effects are not at a clinically significant level [7]. Despite the favourable outcomes of hydrophobic acrylic IOLs, it must be remembered that IOL material biocompatibility is also dependent on the clinical scenario. Therefore, IOL choices must be tailored to
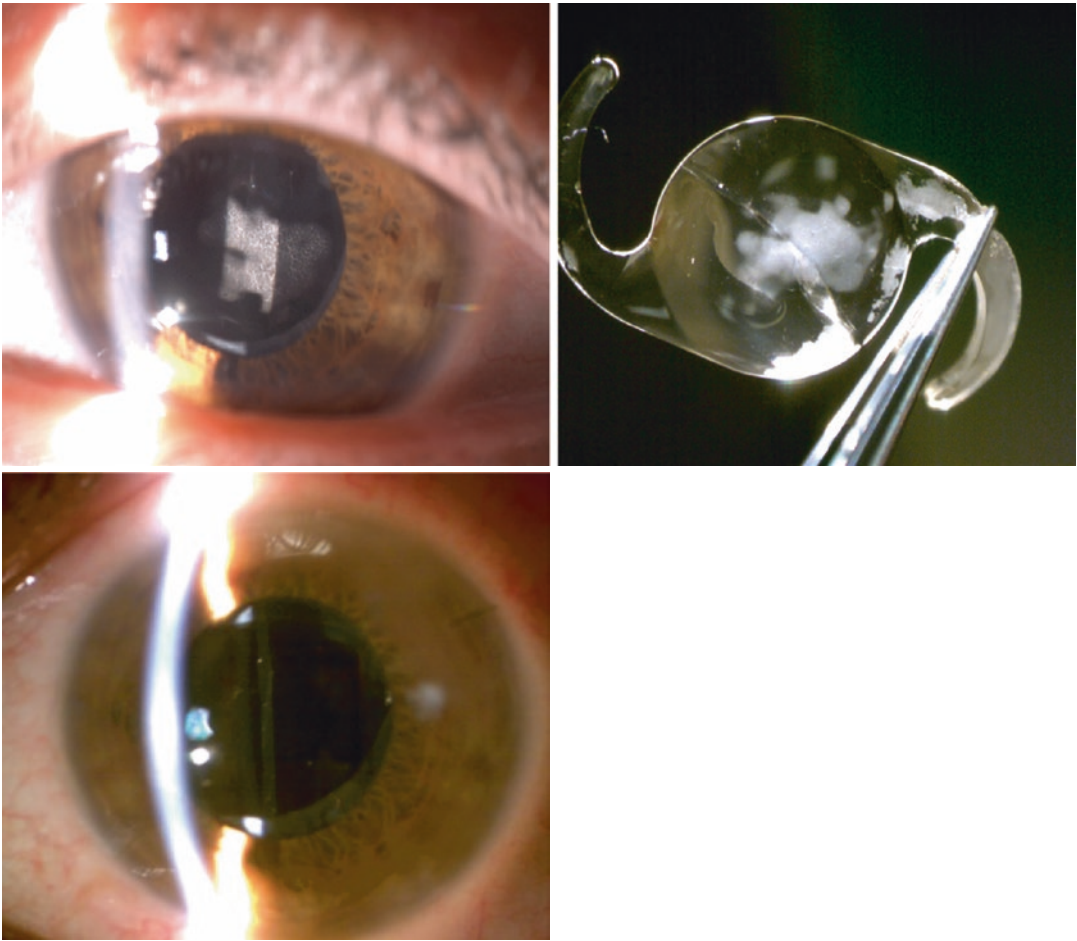
Fig. 37.1 Lenstec, single-piece, hydrophilic IOL opacification (photographs courtesy of Dr. Steven G Safran, New Jersey). Top left: Spontaneous opacification 2 years post-original cataract operation. No other procedures have been performed in the eye except a YAG laser capsulotomy. Middle left: Lenstec hydrophilic IOL following explantation from the eye—central IOL opacification present. Bottom left: Lenstec IOL exchanged for AR40e IOL, day 1 post-operative image

suit the patient's needs. For instance, hydrophobic acrylic IOLs are unsuitable for use in patients with uveitis due to their strong adherence to foreign-body cell. In such cases a hydrophilic counterpart may be preferable [28].

Currently there are four hydrophobic single-piece acrylic (SPA) IOLs in the US market (Acrysof, Envista, Hoya and Sensar) (refer to Table 37.1). The Sensar lens, Ar40, has the lowest refractive index ($n = 1.47$) compared with a range of $n = 1.54$–1.55 for the remaining IOLs. The functional optic thickness correlates with the refractive index of the lens; the lower the refractive index the thicker the lens and, generally, the smaller the functional optic. The smaller diameter optic size may increase the likelihood of dysphotopsias [10].

The following table compares the four main hydrophobic SPA IOLs on the market.

37.5 Should Intraocular Lenses Block Blue Light?

Short-wavelength, blue/ultraviolet light exposure is associated with retinal pigment epithelium damage and retinal toxicity. "Blue-blocker" IOLs typically contain yellow chromophores that

Table 37.1   Main hydrophobic SPA IOLs (US market)

Single-piece acrylic lens	Biomaterial	Haptic design and size	Refractive index
Acrysof (Alcon) [42]	Hydrophobic single-piece acrylic	STABLEFORCE haptics	1.55
Envista (Bausch and Lomb) [43]	Hydrophobic single piece acrylic	Modified C, fenestrated	1.53
Hoya (Hoya Vision) [44]	Hydrophobic single-piece acrylic	Modified C-loop	1.55
Sensar (Johnson and Johnson) [45]	Hydrophobic single-piece acrylic	ProTEC frosted, continuous 360° posterior square edge	1.47

attenuate the transmission of about half of inci-
dent short-wavelength light, depending upon
their dioptric power [46]. The rationale behind
their use is that they theoretically aid in retinal
protection and possibly slow the development
and progression of age-related macular degenera-
tion [47, 48].

A recent Cochrane review assessed the effects
of blue-light-filtering IOLs compared with non-
blue-light-filtering IOLs with respect to protect-
ing the macula and optimising retinal function. In
total, following the analysis of 51 randomised
control studies, in over 5000 eyes, the evidence
was inconclusive in terms of the effects on long-
term macular health comparing the two lens
types. There was also no clinically significant dif-
ference between the two lens types with respect
to short-term best corrected visual acuity (BCVA)
and contrast sensitivity. It remains unclear as to
whether such lenses assist in maintaining macu-
lar health and function, due to the limited
population-based epidemiological evidence sup-
porting blocking of blue ultraviolet light (UV)
IOLs [47, 48].

There have been a number of studies which
have compared the effects on circadian photoen-
trainment and sleep in patients with implanted
blue-blocking IOLs versus neutral lenses. Results
remain inconclusive [49]. More recently,
Brondsted et al. demonstrated that while blue-
blocking IOLs were shown to increase sleep effi-
ciency, nocturnal melatonin secretion was
reduced in this cohort following a year-long
period. Conclusions drawn from the study were
that while sleep quality and responsiveness of
intrinsically photosensitive (melanopsin contain-
ing) retinal ganglion cells were enhanced follow-
ing cataract surgery, no improvements were
demonstrated in circadian specific domains—

therefore, the underlying mechanism may not be
related to circadian photoentrainment [50].

37.6   Do Some Intraocular Lenses Allow a Better View of the Peripheral Retina?

It is generally believed that peripheral capsular
opacification is the main contributing factor to
reduction in the peripheral view of the retina
rather than the lens choice itself. Lens capsule
opacification, contraction and haze limit retinal
view. The smaller the optic the more difficult it is
to visualise the peripheral retina. However, with
wide-angle modern viewing systems used in vit-
reoretinal surgery (such as the BIOM (Oculus) or
RESIGHT wide-angle-viewing system (Zeiss))
the view of the retina is optimised even if the
pupil is small—therefore, in these situations the
optic size is not so critical. The Sensar three-
piece IOL (hydrophobic acrylic) has a full 6 mm
functional optic (AR40e) while the ZCB00
single-piece IOL (hydrophobic acrylic) has a
functional optic in the 5–5.5 m range with an
inert carrier ring that has no optical power. This
means that the functional optic size of the single
piece is smaller than the three piece even though
they are both physically 6 mm optics. For this
reason, the three piece may be a better choice in
eyes with larger pupils [10, 51, 52].

Apart from avoiding certain biomaterials, to
limit lens capsule opacification, there are certain
steps that should be ensured during the cataract
surgery. Routine lens epithelial cell (LEC) clean-
up is particularly important [3]. Different tech-
niques can be adopted to remove these cells
which exist underneath the capsulorhexis and
crystalline lens equator. Surgical polishing of the
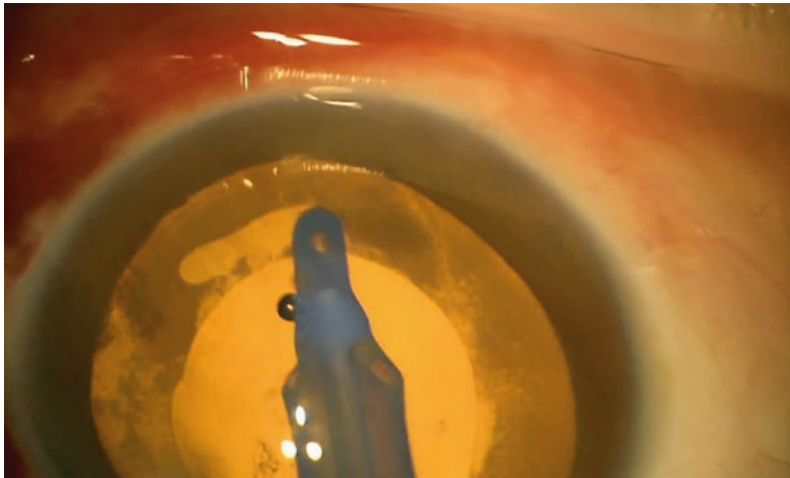
Fig. 37.2 Anterior capsule polish: The above image is a demonstration of anterior capsule polish and clean with a Bausch and Lomb CapsuleGuard handpiece to remove excess LECs from underneath the posterior surface of the anterior capsulorhexis border (image courtesy of Professor M Coroneo, Sydney)

inner surface of the anterior capsule assists in removal of the excess LECs and can safely be carried out using modern irrigation and aspiration (I/A) handpieces (Fig. 37.2). Routine removal of the LECs is important in preventing opacification, phimosis and eventual zonular degradation caused by the matrix metalloproteinase (MMPs) activation [36, 53].

In addition to making the appropriate choice of lens material, recent studies have postulated that design of the intraocular lens, independent of its material, is also important in reducing the likelihood of opacification. For instance, the Tecnis ZCB00 platform has a gunnel (a circular groove in the periphery of the IOL) and a 360-degree continuous sharp optic edge—features which aid in limiting LEC migration. Combined with LEC removal the peripheral capsule remains clear, preventing phimosis, which is advantageous for retinal surgeons. Most IOLs have a posterior square-edged design which reduces PCO rates [10, 54, 55]. Additionally, IOLs with a sharp posterior edge are less likely to have pronounced regeneratory and fibrotic PCO compared with IOLs with a round posterior edge. This is because the sharp posterior lens edge inhibits the migrating LECs. Although both silicone and acrylic sharp posterior edged lenses are associated with lower rates of PCO, anterior cap-

Table 37.2 Risk factors for increased risk of capsular contraction/IOL subluxation/dislocation [56–58]

Ocular factors	Pseudoexfoliation (PXF) >50% of cases Uveitis High myopia (increased axial length) Glaucoma (previous acute angle-closure glaucoma attack) Retinitis pigmentosa Previous vitrectomy/vitreoretinal surgery IOL factors Intraoperative zonular dehiscence
Systemic factors	Diabetes mellitus Atopic dermatitis Myotonic dystrophy/connective tissue disease (Marfan syndrome, homocystinuria, hyperlysinaemia, Ehlers-Danlos syndrome, scleroderma and Weil-Marchesani syndrome) Trauma (falls in the elderly) Aging

sular fibrosis rates were found to be higher, due to their anterior barrier effect [36].

In some instances, anterior capsular fibrosis is prominent following cataract surgery. This can result in capsular phimosis, lens subluxation and decentring of the IOL [3]. Risk factors are listed in Table 37.2.

Preventative measures also include avoidance of undersized capsulorhexis at the time of cataract surgery and prophylactic, YAG laser anterior capsule-relaxing incisions [59]. In order to improve

the view of the retina this needs to be surgically corrected during vitreoretinal surgery and removal of the anterior capsule with 25-gauge VR scissors is one of the recommended approaches.

Patients with significant retinal pathology may continue to have poor vision, despite cataract extraction. While preoperative optical coherence tomography (OCT) can often aid with diagnosis and management of patient expectations, it is sometimes only after cataract surgery that the improved view allows diagnosis and explanation as to why vision has not improved following surgery. In this setting, there are two newer types of lenses which alter the retinal image optically to try and optimise vision following cataract surgery. These have been investigated in patients with low vision from underlying age-related macular degeneration (ARMD), a condition with a 2.089% prevalence rate in the United States [60, 61].

In-eye magnifiers, such as the Scharioth Macula Lens and implantable miniature telescopes [19, 62]: The Scharioth Macula Lens has the advantage that it is a foldable one-piece IOL comprised of a mixture of hydrophilic and hydrophobic acrylic material. The patient will already have a standard IOL located in-the-bag; the Scharioth Macula Lens is implanted in addition to this lens within the ciliary sulcus. Its aspheric bifocal nature adds +10 dioptres to total the refractive power of the combined lenses. Preliminary studies demonstrate some promising outcomes with respect to reading rehabilitation following the lens implantation—however, long-term data are lacking [19, 20].

The second is an in-the-bag non-foldable IOL made of polymethyl methacrylate and comprised of Fresnel prisms. The rationale behind its use is that it displaces the central scotoma caused by ARMD (it displaces the retinal image by 1.8 mm through a Fresnel Prism IOL positioned on the back of the optic with a fixed angulation of 6°), thus negating the need for macular translocation surgery. While initial results have demonstrated successful relocation of the central scotoma, the lens is still being trialled, with preliminary results in three cases only available to date [63].

37.7 Are Some Intraocular Lenses More Prone to Causing Capsule Phimosis and Eventual Subluxation?

To prevent anterior capsule fibrosis and phimosis, the most important surgical factor is to ensure adequate removal of LECs—as demonstrated in Fig. 37.2 [3]. This is irrespective of the IOL chosen for insertion. A recent Swedish study demonstrated that the length of time the patient has been pseudophakic (up to 10 years) and phacoemulsification time were both risk factors for late in-the-bag subluxation (rather than the type of IOL itself) [64]. Ocular factors associated with longer term dislocated IOLs are included in Table 37.2 [65, 66]. Specific lens material and designs, such as silicone plate-style IOLs, are also more prone to posterior dislocation [67].

Literature supports that highly myopic patients with vitrectomised eyes are at greater risk of lens subluxation [65]. Patients with high myopia may require a specialised approach. For any patient who has significant myopia, a capsular tension ring (CTR) should be used. While not preventing subluxation, the CTR aids to assist with any subluxation surgery which may become necessary. It allows suture fixation at any meridian if subluxation were to occur. In such cases, a lens such as the Sensar Ar40 hydrophobic acrylic three-piece IOL is an option. This IOL comes in negative powers (suitable for myopes); it has longer haptics in lower powers (under 5D it is 13.5 mm), a low refractive index, full 6 mm optic and minimal glistening potential [68]. The three-piece lens will also provide a wider retinal view due to the larger optic size [10]. For patients requiring toric lens insertion a single-piece IOL will need to be inserted rather than a three-piece IOL. Combining this with a CTR in a high myope undergoing a vitrectomy may optimise results.

The majority of this chapter has focused on optimising cataract surgery and IOL choice when vitreoretinal surgery is anticipated. Combined cataract and pars plana vitrectomy is commonly performed. Gas tamponade causes a myopic shift from forward displacement of the IOL. The use

of an IOL with an angulated haptic has been shown to reduce this myopic shift and may be preferable over non-angulated subtypes during combined surgery [69]. There is the added advantage that three-piece IOLs can be optic fixated in the capsulorhexis, providing a very stable implantation strategy.

37.8 Dysphotopsias and Glistenings

When deciding on the "most appropriate" IOL lens to insert prior to vitreoretinal surgery, the aforementioned variables should be considered. The optic needs to be wide enough to provide an adequate view of the retina. Dysphotopsias are more likely when the functional optic is small [10].

Dysphotopsias are defined as unwanted optical phenomena and may be a cause of patient dissatisfaction and suboptimal vision following cataract surgery. They can be both positive and negative in nature. Positive dysphotopsias are seen by patients as bright arcs, halos or streaks whereas negative dysphotopsias are seen as a dark shadow or arc in the temporal visual field. Persisting negative dysphotopsias, in particular, can be particularly problematic for patients. The aetiology behind dysphotopsias is not well understood. There are a number of contributing factors including refractive index of the lens (increasing IOL refractive index worsens dysphotopsias), lens design (sharp versus round edge design), IOL-anterior capsule distance between the intraocular structures, patient anatomy, pupil size and location and the individual's ability to neuroadapt [70].

We have proposed that some forms of positive and negative dysphotopsias are due to a combination of a phenomenon known as peripheral light focusing and a base central prismatic effect of the IOL periphery. Our large temporal field of vision acts to collect light that is focused by the periphery of the cornea/lens onto the nasal aspect of the eye. In relation to positive dysphotopsia, the arcs are brighter than ambient light and this can only occur because of this focusing effect—readily observed clinically and confirmed by ray tracing (Fig. 37.3) [71]. The downstream consequence of this phenomenon is that it also explains negative dysphotopsia, as light is shunted away from the peripheral retina [72]. This concept offers a solution to the problem, by simply redesigning IOL peripheral optics. The peripheral IOL optic prismatic effect reduces both the view of the fundus and the patient's field of vision [73] (Fig. 37.4).

Symptoms can be visually distressing to the patient and can result in the IOL exchange if severe and persistent enough. Acrysof acrylic IOLs (MA60BM) have been linked with increased prevalence of dysphotopsias. This is in part due to their increased refractive index, unequal biconvex design of their anterior surface and square- and
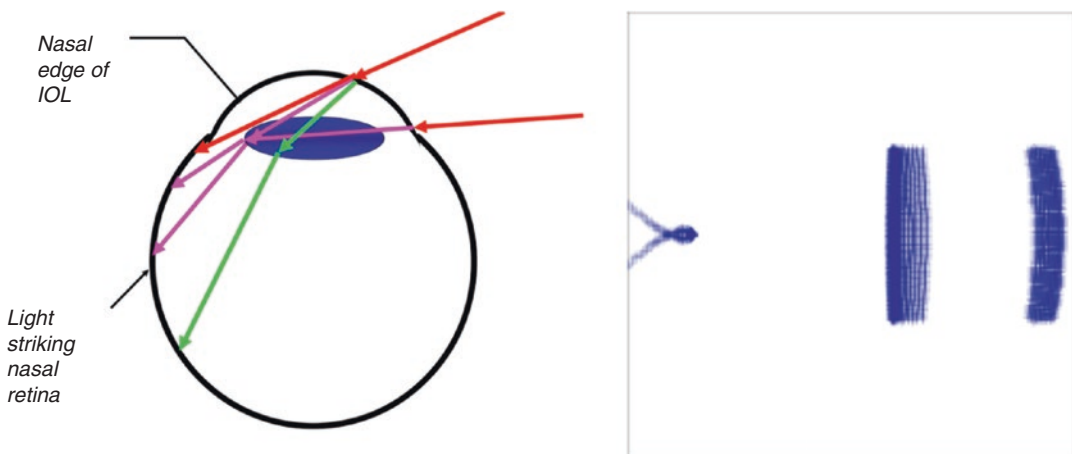
Fig. 37.3 *Ray tracing*: Pathways of peripheral light in relation to an IOL (left image). Up to three foci can be seen on the nasal retina as shown from the ray tracing (illustration courtesy of Professor M Coroneo, Sydney)
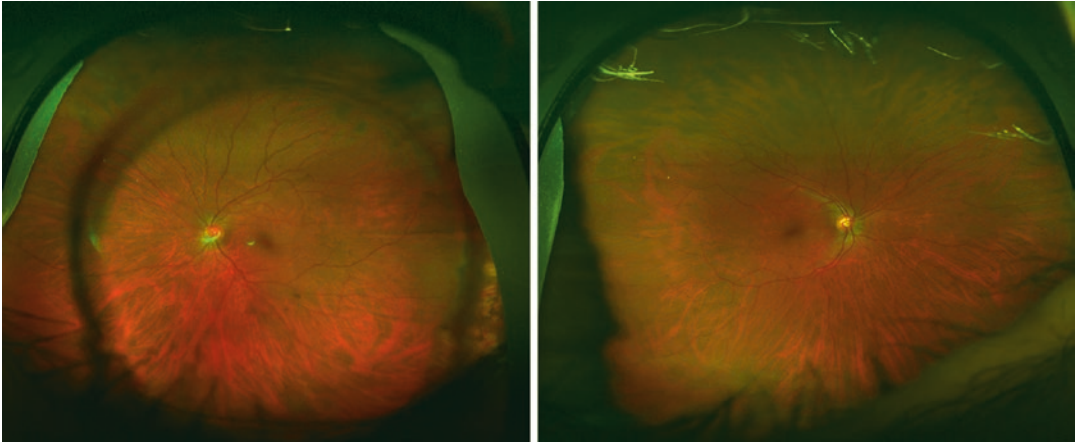
Fig. 37.4 Optos images of a pseudophakic eye (above)—implanted with AMO ZCT lens and the fellow phakic eye (below) (images courtesy of Dr. Daya Sharma, Sydney)

sharp-edged design, which is important to prevent PCO but has been linked with increased internal light scattering and subsequent dysphotopsias [74]. There is current investigation into newer IOLs which target prevention of negative dysphotopsias through specific design modifications. The Masket ND IOL (Morcher) has a peripheral groove placed anteriorly so the capsulorhexis edge is aligned in the groove, which aims to limit negative dysphotopsias. This design is based on the theory that the shadow from the capsulorhexis causes the negative dysphotopsias. This IOL received CE Mark approval in 2013 and its associated small-cohort European trial is still in its infancy [75]. Little has been published as to efficacy. The IOL design we propose is under development and apart from abolishing dysphotopsia will allow better visualisation of the peripheral retina and expanded visual field [76].

Given that a large proportion of patients undergoing vitreoretinal surgery following cataract surgery have underlying diabetic eye disease or another macular pathology which may already limit visual acuity, it is important to discuss the issue of glistenings. Glistenings and subsurface nano-glistenings (SSNGs) of the lens can severely limit the view of the retina and the functional visual acuity of patients. Light scattering on the surface of hydrophobic acrylic IOLs can ultimately lead to a white opaque appearance of the lens—the underlying hypothesis is secondary to water congregation under the IOL surface. Under an electron microscope these white opacifications appear as hydration-related vacuoles. Vacuoles with a diameter <200 μm are known as SSNGs [77]. These vacuoles occur as a result of a difference in the refractive index that occurs when the cross-links between the hydrophobic IOL copolymers are filled with fluid [7]. A case series of Alcon Acrysof (MA60BM) IOLs demonstrated the deterioration in visual function, specifically acuity, secondary to glistening and SSNGs (Fig. 37.5) [13, 78].

A method of reducing glistenings currently under experimentation is via hybrid hydrophobic IOLs. These IOLs are comprised of hydrophobic IOL material with a hydrophilic component—total water content is 4–5% and they are stored in 0.9% saline solution [7]. Preliminary studies in rabbit eyes comparing hydrophobic versus hybrid hydrophobic-hydrophilic IOLs have demonstrated lower rates of anterior cortical opacification and glistenings in the latter group [79]. It is hypothesised that the lack of glistenings in these hybrid IOLs is due to the tighter cross-links, and presence of water from the hydrophilic component which provides adequate equilibrium in the biocompatibility of the IOL material [7].

A new type of IOL, the light-adjusted lens made of flexible silicone polymer matrix and mobile, photosensitive silicone subunits (macromers), the power of which can be adjusted
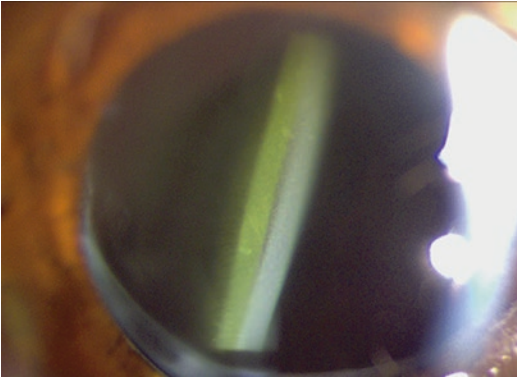
Fig. 37.5 *Acrysof IOL SSNGs*: Decreased vision and glare from severe SSNGs (photograph courtesy of Dr. Steven G Safran, New Jersey)

post-implantation with the use of ultraviolet light, is being trialled [80]. Little is known as to how this IOL will interact with intraocular gases or silicone oil.

37.9 Final Thoughts and Recommendations

Careful consideration as to the choice of intraocular lens should be made when a secondary vitreoretinal surgery is planned.

Important considerations are the following:

1. Maintaining clarity of the optic and peripheral capsule in order to maximise retinal view.
2. Avoiding lens subluxation which is exacerbated by LEC growth, MMP production and zonular degradation: Techniques should be incorporated into the surgeon's routine cataract surgery to remove LECs.
3. Ensuring biocompatibility of lens material particularly if silicone oil and/or gas tamponade will be used in future vitreoretinal surgery.
4. Taking into consideration the patient's coexisting conditions such as pseudoexfoliation, myopia, previous vitrectomy, poor vision and pre-existing zonular weakness.

Taking the above considerations into account we conclude that a hydrophobic acrylic intraocular lens should be selected. This should be used in conjunction with meticulous LEC removal and if indicated (for instance in the case of high myopes) insertion of a CTR. When a lower power lens is required, or in eyes with larger pupils, a three-piece lens can be utilised—this larger optic also provides a wider view of the retina. In cases where there is poor baseline vision from pre-existing retinal pathology then some of the newer in-eye magnifiers and scotoma-shifting IOLs may be considered following further evaluation. Ultimately, armed with this information, the surgeon needs to select the lens based on specific patient needs and a case-based risk profile.

References

1. Ninn-Pedersen K, Bauer B. Cataract patients in a defined Swedish population, 1986 to 1990. V. Postoperative retinal detachments. Arch Ophthalmol. 1996;114(4):382–6.
2. Allarakhia L, Knoll RL, Lindstrom RL. Soft intraocular lenses. J Cataract Refract Surg. 1987;13(6):607–20.
3. Nguyen J, Werner L. Intraocular lenses for cataract surgery. In: Kolb H, Fernandez E, Nelson R, editors. Webvision: the organization of the retina and visual system. Salt Lake City; 1995.
4. Pandey SK, Milverton EJ, Maloof AJ. A tribute to Charles David Kelman MD: ophthalmologist, inventor and pioneer of phacoemulsification surgery. Clin Exp Ophthalmol. 2004;32(5):529–33.
5. Wichterle O, Lim D. Hydrophilic gels for biological use. Nature. 1960;185:117–8.
6. Dreifus M, Wichterle O, Lim D. Intra-cameral lenses made of hydrocolloidal acrylates. Cesk Oftalmol. 1960;16:154–9.
7. Ozyol P, Ozyol E, Karel F. Biocompatibility of intraocular lenses. Turk J Ophthalmol. 2017;47(4):221–5.
8. Werner L. Biocompatibility of intraocular lens materials. Curr Opin Ophthalmol. 2008;19(1):41–9.
9. Amon M. Biocompatibility of intraocular lenses. J Cataract Refract Surg. 2001;27(2):178–9.
10. Dewey S. Understanding intraocular lenses: the basics of design and material. Focal Points: American Academy of Ophthalmologists. 2015; Volume XXXIII:8:1–21. Accessed: https://www.iolsafety.com/dmdocuments/understanding-intraocular-lenses-the-basics-of-design-and-material.pdf.
11. Mazzocco T, Rajacich GM, Epstein E. History of intraocular lens implant surgery. In: Inc S, editor. New Jersey; 1986.
12. Zhou KY. Silicon intraocular lenses in 50 cataract cases. Chin Med J (Engl). 1983;96(3):175–6.
13. Trivedi RH, Werner L, Apple DJ, Pandey SK, Izak AM. Post cataract-intraocular lens (IOL) surgery opacification. Eye (Lond). 2002;16(3):217–41.

14. Apple DJ, Federman JL, Krolicki TJ, Sims JC, Kent DG, Hamburger HA, et al. Irreversible silicone oil adhesion to silicone intraocular lenses. A clinicopathologic analysis. Ophthalmology. 1996;103(10):1555–61; discussion 61–2.

15. Seward HC. Folding intraocular lenses: materials and methods. Br J Ophthalmol. 1997;81(5):340–1.

16. Bellucci R. An introduction to intraocular lenses: material, optics, haptics, design and aberration. Cataract ESASO course series. Basel: Karger; 2013. p. 38–55.

17. Apple D, Kincais MC, Mamaus N, Oison RJ. Intraocular lenses—evolution, designs, complications and pathology. Baltimore Williams and Wilkins; 1989.

18. Holladay JT, Bishop JE, Prager TC, Blaker JW. The ideal intraocular lens. CLAO J. 1983;9(1):15–9.

19. Nekolova J, Rozisval P, Sin M, Jiraskova N. Scharioth macula lens: a new intraocular implant for low-vision patients with stabilized maculopathy—first experience. Biomed Pap Med Fac Univ Palacky Olomouc Czech Repub. 2017;161(2):206–9.

20. Scharioth G. New add-on intraocular lens for patients with age-related macular degeneration. J Cataract Refract Surg. 2015;41:1559–63.

21. Bolger J. What is the best intraocular lens? Br J Ophthalmol. 1994;78(4):242–3.

22. Schojai M, Schultz T, Burkhard Dick H. Capsule-fixated intraocular lens implantation in small pupil cases. J Refract Surg. 2017;33(8):568–70.

23. Hayashi K, Hayashi H, Nakao F, Hayashi F. Changes in posterior capsule opacification after poly(methyl methacrylate), silicone, and acrylic intraocular lens implantation. J Cataract Refract Surg. 2001;27:817–24.

24. Terry A, Stark WJ, Newsome DA, Maumenee AU, Pina E. Tissue toxicity of laser-damaged intraocular lens implants. Ophthalmology. 1985;92(3):414–8.

25. Scheiffarth OF, Ludwig K, Birngruber R, Gabel VP, von Meyer L. Chemical studies of intraocular lenses after experimental generation of lesions by a short-pulsed Nd-YAG laser. Graefes Arch Clin Exp Ophthalmol. 1984;222(1):43–4.

26. Chirila T, Barrett GD, Russo AV, Constable IJ, Van Saarloos PP, Russo CI. Laser-induced damage to transparent polymers: chemical effect of short-pulsed (Q-switched) Nd:YAG laser radiation on ophthalmic acrylic biomaterials. II. Study of monomer release from artificial intraocular lenses. Biomaterials. 1990;11(5):313–20.

27. Ciszewska J, Kecik T, Legec E, Mrowczynska E, Zydecki M. Chemical analysis of compounds released after damage of the intraocular lens with the Nd: YAG laser. Klin Oczna. 1996;98(3):213–6.

28. Huang Q, Cheng GP, Chiu K, Wang GQ. Surface modification of intraocular lenses. Chin Med J (Engl). 2016;129(2):206–14.

29. Barra DWL, Costa JLP, Morris C, Ribeiro T, Ventura BV, Dornelles F. Light scattering and light transmittance in a series of calcified single-piece hydrophilic acrylic intraocular lenses of the same design. J Cataract Refract Surg. 2014;40:121–8.

30. Neuhann IMWL, Izak AM, Pandey SK, Kleinmann G, Mamalis N, Neuhann TF, Apple DJ. Late postoperative opacification of a hydrophilic acrylic (hydrogel) intraocular lens: a clinicopathological analysis of 106 explants. Ophthalmology. 2004;111:2094–101.

31. Gurabardhi M, Haberle H, Aurich H, Werner L, Pham DT. Serial intraocular lens opacifications of different designs from the same manufacturer: clinical and light microscopic results of 71 explant cases. J Cataract Refract Surg. 2018;44(11):1326–32.

32. Werner L. Causes of intraocular lens opacification or discoloration. J Cataract Refract Surg. 2007;33:713–26.

33. Khurana RN, Werner L. Calcification of a hydrophilic acrylic intraocular lens after pars plana vitrectomy. Retin Cases Brief Rep. 2018;12(3):204–6.

34. Marcovich AL, Tandogan T, Bareket M, Eting E, Kaplan-Ashiri I, Bukelman A, et al. Opacification of hydrophilic intraocular lenses associated with vitrectomy and injection of intraocular gas. BMJ Open Ophthalmol. 2018;3(1):e000157.

35. Klein JP, Torun N, Berndt S, Rieck P, Bertelmann E. [Early in-the-bag spontaneous intraocular lens dislocation of hydrophilic acryl single piece lenses following uncomplicated phacoemulsification]. Ophthalmologe. 2012;109(1):54–8.

36. Sacu S, Menapace R, Buehl W, Raine G, Findl O. Effect of intraocular lens optic edge design and material on fibrotic capsule opacification and capsulorhexis contraction. J Cataract Refract Surg. 2004;30:1875–82.

37. Mamalis N, Brubaker J, David D, Espandar L, Werner L. Complications of foldable intraocular lenses requiring explantation or secondary intervention—2007 survey update. J Cataract Refract Surg. 2008;34:1584–91.

38. Werner LAD, Kaskaloglu M, Pandey SK. Dense opacification of the optical component of a hydrophilic acrylic intraocular lens: a clinicopathological analysis of 9 explanted lenses. J Cataract Refract Surg. 2001;27:1485–92.

39. Stringham J, Werner L, Monson B, Theodosis R, Mamalis N. Calcification of different designs of silicone intraocular lenses in eyes with asteroid hyalosis. Ophthalmology. 2010;117:1486–92.

40. Khawly JALR, Jaffe GJ. Intraocular lens changes after short- and long-term exposure to intraocular silicone oil. An in vivo study. Ophthalmology. 1998;105:1227–33.

41. Ohrstrom A, Svensson B, Tegenfeldt S, Celiker C, Lignell B. Silicone oil content in ophthalmic viscosurgical devices. J Cataract Refract Surg. 2004;30(6):1278–80.

42. Alcon. AcrySof® IQ Monofocal IOL Product Specifications. https://www.myalcon.com/products/surgical/acrysof-iq-iol/monofocal-iol-specifications.shtml.

43. BauschandLomb. enVista IOL. https://www.bausch.com/ecp/our-products/cataract-surgery/lens-systems/envista-iol.

44. Hoya. HOYA Vivinex™ multiSert™ (XC1-SP / XY1-SP). https://hoyasurgicaloptics.com/html/page.php?page_id=2&pid=7&pc_mode_168=details.

45. JohnsonandJohnson. SENSAR® Monofocal 1-Piece IOL. https://surgical.jnjvision.com/iols/monofocal/sensar#specifications.

46. Brockmann C, Schulz M, Laube T. Transmittance characteristics of ultraviolet and blue-light-filtering intraocular lenses. J Cataract Refract Surg. 2008;34:1161–6.

47. Sparrow J, Miller A, Zhou J. Blue light absorbing intra-ocular lens and retinal pigment epithelium protection in vitro. J Cataract Refract Surg. 2004;30(4):873–8.

48. Downie L, Busija L, Keller PR. Blue-light filtering intraocular lenses (IOLs) for protecting macular health. Cochrane Database Syst Rev. 2018;5(5):CD011977.

49. Henderson BA, Grimes KJ. Blue-blocking IOLs: a complete review of the literature. Surv Ophthalmol. 2010;55(3):284–9.

50. Brondsted AE, Haargaard B, Sander B, Lund-Andersen H, Jennum P, Kessel L. The effect of blue-blocking and neutral intraocular lenses on circadian photoentrainment and sleep one year after cataract surgery. Acta Ophthalmol. 2017;95(4):344–51.

51. Sensar. Sensar IOL with OptiEdge Design—Hydrophobic Acrylic. http://www.precisionlens.net/Websites/precisionlens/documents/AMO%20AR40%20Spec%20Sheet.pdf.

52. Tecnis. Tecnis 1-Piece Aspheric IOL—Hydrophobic Acrylic. http://www.precisionlens.net/Websites/precisionlens/documents/AMO%20ZCB00%20Spec%20Sheet.pdf.

53. Awasthi N, Wang-Su ST, Wagner BJ. Downregulation of MMP-2 and -9 by proteasome inhibition: a possible mechanism to decrease LEC migration and prevent posterior capsular opacification. Invest Ophthalmol Vis Sci. 2008;49(5):1998–2003.

54. Hartman M, Rauser M, Brucks M, Chalam KV. Evaluation of anterior capsular contraction syndrome after cataract surgery with commonly used intraocular lenses. Clin Ophthalmol. 2018;12:1399–403.

55. Emery F. Capsule opacification with 2 different IOLs: 3-year results. Ophthalmology Times. 2015; 13. Accessed: https://www.ophthalmology-times.com/view/capsule-opacification-2-different-iols-3-year-results.

56. Hayashi H, Hayashi K, Nakao F, Hayashi F. Anterior capsule contraction and intraocular lens dislocation in eyes with pseudoexfoliation syndrome. Br J Ophthalmol. 1998;82:1429–32.

57. Fernandez-Buenaga R, Alio JL, Perez-Ardoy AL, Larrosa-Quesada A, Pinilla-Cortes L, Barraquer R, et al. Late in-the-bag intraocular lens dislocation requiring explantation: risk factors and outcomes. Eye (Lond). 2013;27(7):795–801; quiz 2.

58. Ascaso F, Huerva V, Grzybowski A. Epidemiology, etiology, and prevention of late IOL-capsular bag complex dislocation: review of the literature. J Ophthalmol. 2015;2015:1–7.

59. Hayashi K, Yoshida M, Hirata A, Hayashi H. Anterior capsule relaxing incisions with neodymium:YAG laser for patients at high-risk for anterior capsule contraction. J Cataract Refract Surg. 2011;37:97–103.

60. Grzybowski A, Wasinka-Borowiec W, Alio JL, Amat-Peral P, Tabernero J. Intraocular lenses in age-related macular degeneration. Graefes Arch Clin Exp Ophthalmol. 2017;255:1687–96.

61. America PB. Age Related Macular Degeneration. http://www.visionproblemsus.org/amd/amd-map.html.

62. Gupta A, Lam J, Custis P, Munz S, Fong D, Koster M. Implantable miniature telescope (IMT) for vision loss due to end-stage age-related macular degeneration. Cochrane Database Syst Rev. 2018;5:CD011140.

63. Potgieter F, Claoue CM. Safety and efficacy of an intraocular Fresnel prism intraocular lens in patients with advanced macular disease: initial clinical experience. J Cataract Refract Surg. 2015;41(8):1559–63.

64. Dabrowska-Kloda K, Kloda T, Boudiaf S, Jakobsson G, Stenevi U. Incidence and risk factors of late in-the-bag intraocular lens dislocation: evaluation of 140 eyes between 1992 and 2012. J Cataract Refract Surg. 2015;41(7):1376–82.

65. Fenberg M. Vitrectomy as a risk factor for complicated cataract surgery. Mo Med. 2016;113(1):44–7.

66. Hayashi K, Hirata A, Hayashi H. Possible predisposing factors for in-the-bag and out-of-the-bag intraocular lens dislocation and outcomes of intraocular lens exchange surgery. Ophthalmology. 2007;114(5):969–75.

67. Gonzalez GA, Irvine AR. Posterior dislocation of plate haptic silicone lenses. Arch Ophthalmol. 1996;114(6):775–6.

68. Sensar. Sensar IOL With OptiEdge Design: Hydrophobic Acrylic. 2010. http://www.precisionlens.net/Websites/precisionlens/documents/AMO%20AR40%20Spec%20Sheet.pdf.

69. Hwang HS, Jee D. Effects of the intraocular lens type on refractive error following phacovitrectomy with gas tamponade. Curr Eye Res. 2011;36(12):1148–52.

70. Henderson B, Geneva I. Negative dysphotopsia: a perfect storm. J Cataract Refract Surg. 2015;41:2291–312.

71. Coroneo MT, Pham T, Kwok LS. Off-axis edge glare in pseudophakic dysphotopsia. J Cataract Refract Surg. 2003;29(10):1969–73.

72. Coroneo M. Cataract surgical problem: April consultation #3. J Cataract Refract Surg. 2005;31:652–3.

73. Lazarus L, Williams TD. Visual field area in phakic, aphakic, and pseudophakic individuals. Am J Optom Physiol Optic. 1988;65(7):593–7.

74. Shambhu S, Shanmuganathan VA. The effect of lens design on dysphotopsia in different acrylic IOLs. Eye. 2005;19:567–70.

75. Bhalla J, Gupta S. Dysphotopsia-unraveling the enigma. Del J Ophthalmol. 2016;27(2):97–101.

76. Coroneo M. United States Patent Application: lens design, treatment of photic disturbances in the eye. 2015. http://appft.uspto.gov/netacgi/nph-Parser?Sect1=PTO2&Sect2=HITOFF&p=1&u=%2Fnetahtml%2FPTO%2Fsearch-bool.html&r=1&f=G&l=50&co1=AND&d=PG01&s1=coroneo&s2=dysphotopsia&OS=coroneo+AND+dysphotopsia&RS=coroneo+AND+dysphotopsia.

77. Hiraoka T, Miyata K, Hayashidera T, Lida M, Takada K, Minami K, Oshika T. Influence of intraocular lens subsurface nanoglistenings on functional visual acuity. PLoS One. 2017;12(3):1–10.

78. Matsushima H, Nagata M, Katsuki Y, Ota I, Miyake K, Beiko G, Grzybowski A. Decreased visual acuity resulting from glistening and sub-surface nano-glistening formation in intraocular lenses: a retrospective analysis of 5 cases. Saudi J Ophthalmol. 2015;29:259–63.

79. Ollerton A, Werner L, Fuller SR, Kavoussi SC, McIntyre JS, Mamalis N. Evaluation of a new single-piece 4% water content hydrophobic acrylic intraocular lens in the rabbit model. J Cataract Refract Surg. 2012;38(10):1827–32.

80. Brierley L. Refractive results after implantation of a light-adjustable intraocular lens in postrefractive surgery cataract patients. Ophthalmology. 2013;120(10):1968–72.

Penetrating Keratoplasty and Macular Surgery

38

Talisa de Carlo and William F. Mieler

38.1 Introduction

Pars plana vitrectomy (PPV) is utilized to repair a variety of macular and retinal disorders. The surgery may entail removal of significant hemorrhage, retinal membrane dissection, repair of retinal detachment, removal of proliferative vitreoretinopathy (PVR), use of retinotomy and retinectomy techniques, use of intraocular tamponade agents, and placement of endolaser, along with other surgical techniques. The basic premise is the need for adequate visualization [1]. In cases with significant corneal opacification from concomitant anterior segment disease, PPV may be difficult or impossible without first managing the corneal disease. Therefore, in eyes requiring urgent retina surgery with coexisting corneal pathology that limits visualization, combined penetrating keratoplasty (PKP) and pars plana vitrectomy should be considered [2].

Other surgical options for these eyes with anterior and posterior pathology include endoscopic PPV, keratoprosthesis (KPro) and PPV, and partial-thickness keratoplasty and PPV. The use of endoscopic PPV is currently limited by its expense, and the fact that most facilities do not have this technology readily available. The surgery is more technically difficult, and some vit-

reoretinal surgeons are not yet comfortable with this technique [2]. However, when this technology is available to surgeons who are comfortable with this type of surgery, endoscopic PPV has been shown to have equivalent visual and anatomic outcomes to PKP/PPV [3]. It is also important to keep in mind however that while endoscopic PPV can help to stabilize the retinal abnormalities, there is still the corneal concerns that eventually need to be tended to.

Alternative vitreocorneal surgeries other than PKP/PPV can be utilized in select circumstances but they have their limitations. Partial-thickness keratoplasty, whether endothelial keratoplasty or anterior lamellar keratoplasty, provides suboptimal visualization during PPV due to irregularities such as swelling or folds in the grafts [1]. Further, with endothelial keratoplasty, gas tamponade is required in the anterior chamber to keep the graft in place, which can limit the utility of gas and silicone oil tamponade by the vitreoretinal surgeon [1]. These partial-thickness keratoplasties are therefore better utilized in staged surgeries where the retinal pathology does not need urgent repair and can therefore await corneal healing. KPro/PPV can be utilized in eyes that are unable to undergo PKP or have had a history of multiple prior graft failures warranting a PKP. However, the small aperture of the KPro limits the view to the retinal periphery to approximately the equator [2, 4]. Given that many of these patients have significant retinal disease

T. de Carlo · W. F. Mieler (✉)
University of Illinois at Chicago, Chicago, IL, USA
e-mail: wmieler@uic.edu

requiring close monitoring and a relatively high rate of repeat PPV, this limited view is less than ideal for both postoperative monitoring and future PPV surgery. If repeat PPV is required, either the KPro needs to be removed temporarily during the vitrectomy or significant scleral depression is needed to see past the retinal equator [4]. Please see Chap. 39 for further detail.

38.2 Indications for PKP/PPV

As previously mentioned, combined PKP/PPV is utilized in eyes requiring retinal surgery that have concomitant corneal opacification. The most common indication for combined PKP/PPV is ocular trauma, generally an open-globe injury [2]
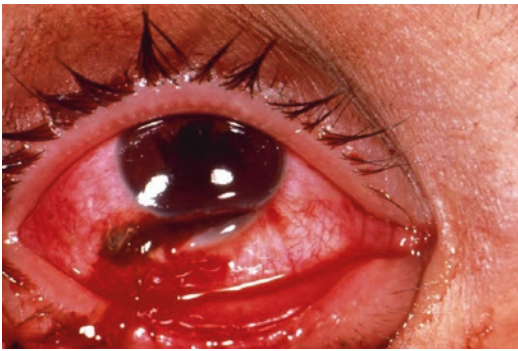
Fig. 38.1 Initial open-globe injury which led to corneal blood staining, opacification, and total retinal detachment, requiring TKP/PPV surgery

(Fig. 38.1). Posteriorly, these cases may involve retinal detachment with PVR, vitreous hemorrhage, choroidal hemorrhage or detachment, intraocular foreign body, endophthalmitis, and retinal incarceration [5]. Ocular trauma can also be complicated by corneal scar, corneal decompensation, and corneal blood staining (Fig. 38.2a, b). Nontraumatic indications for PKP/PPV are varied but include recurrent retinal detachment with corneal decompensation, endophthalmitis, glaucoma, complicated post-cataract surgery with bullous keratopathy and/or dislocated lens, silicone oil keratopathy, and uveitis [2, 6]. Etiologies of corneal opacification in either traumatic or nontraumatic cases include corneal decompensation, failed prior corneal graft, corneal scar, bullous keratopathy, persistent corneal edema, corneal blood staining, and/or corneal neovascularization [2].

38.3 Surgical Approach

The typical surgical approach to PKP/PPV starts with the vitreoretinal surgeon placing three trocars through the pars plana, and then connecting the infusion cannula, though only infusing fluid after direct visualization of the infusion cannula tip. A temporary keratoprosthesis (TKP) is awaiting (Fig. 38.3). The diseased cornea is then trephined by the corneal surgeon to a predetermined diameter (typically 6.5 mm through up to 8 mm
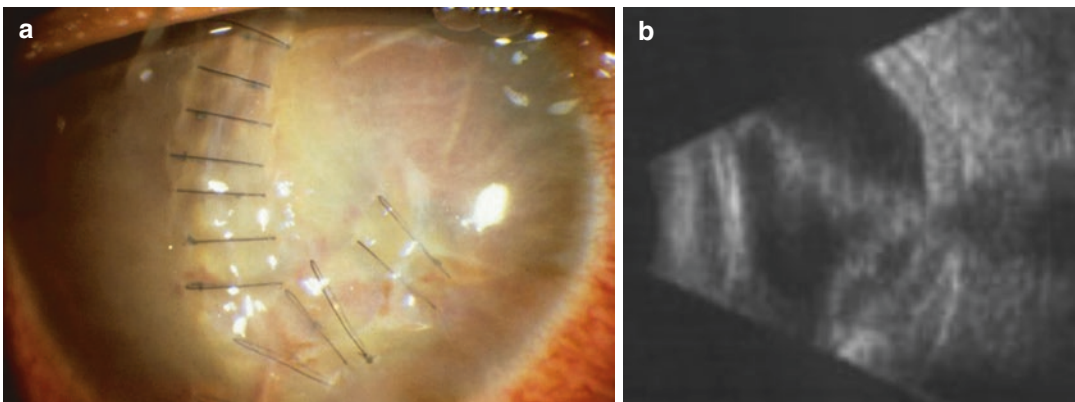
Fig. 38.2 (**a**) Corneal opacification following repair of an open-globe injury, with (**b**) echographic documentation of a total funnel-shaped retinal detachment
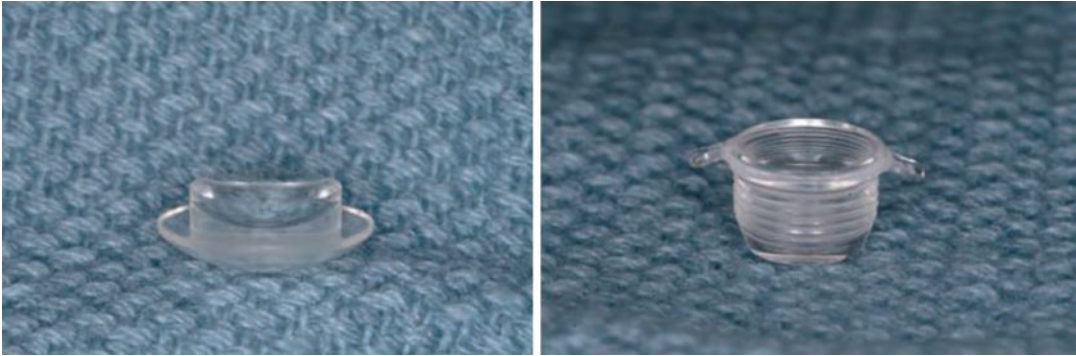
Fig. 38.3 Eckardt-style temporary keratoprosthesis (TKP) (image courtesy of Elmer Tu, MD, University of Illinois at Chicago, Chicago, IL)
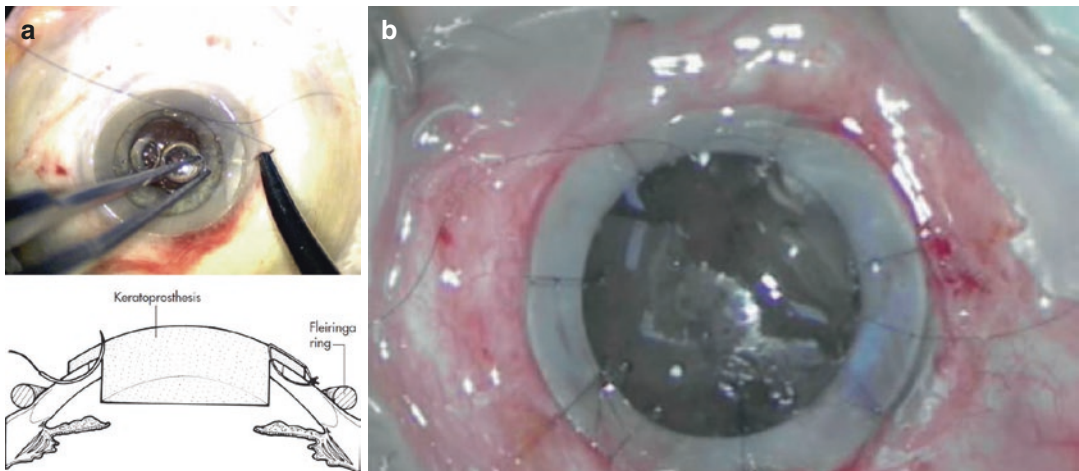
Fig. 38.4 (**a**) Initial placement of the Eckardt TKP on the host peripheral cornea, with schematic diagram, and (**b**) Eckardt TKP following completion of stabilization sutures (images courtesy of Elmer Tu, MD, University of Illinois at Chicago, Chicago, IL)

depending on the corneal pathology and stability) [1, 6]. The TKP of an equivalent size (or 0.5 mm larger) is then sutured onto the corneal opening using four to six nylon sutures (Fig. 38.4a, b). The exact technique and location of the suture placement are dependent on both the type of TKP and the health/stability of the remaining host corneal tissue [6]. PPV can then be performed by the vitreoretinal surgeon through the clear TKP including any necessary procedures such as retinal membrane dissection, repair of retinal detachment, removal of PVR, retinotomy/retinectomy, drainage of subretinal fluid, use of intraocular tamponade agents, placement of endophotocoagulation, and placement of long-term postoperative tamponade agents. After completion of the PPV, the corneal surgeon removes the TKP and sutures the PKP into place [1]. In cases requiring endotamponade, the infusion of gas or silicone oil is then performed by the vitreoretinal surgeon prior to removal of the trocars [2]. Given the complexity of many of these cases, silicone oil is often employed as it can improve rates of retina reattachment from about 36 to 60% [5] (Fig. 38.5a, b). However, as will be discussed later, silicone oil can also reduce the success of
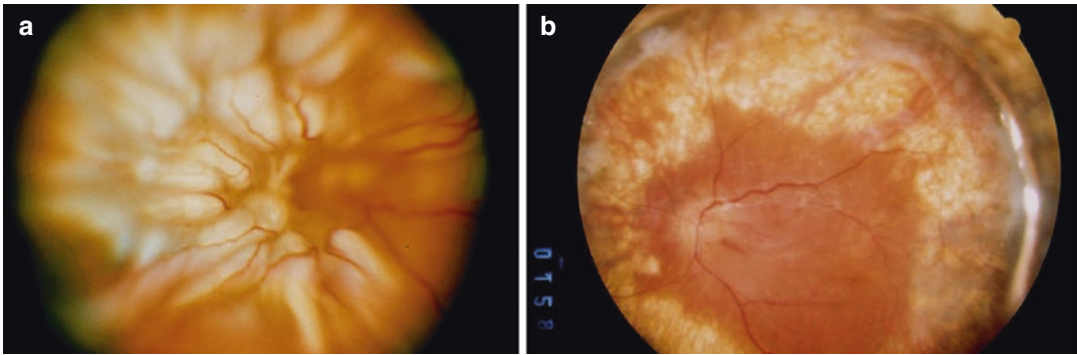
Fig. 38.5 (**a**) Preoperative total retinal detachment with PVR in a patient with an open-globe injury, (**b**) stabilization of the retina following TKP/PPV with placement of silicone oil

the corneal graft so case selection and timing of removal are important. Depending on the requirements of the case, other surgical steps such as cataract extraction, glaucoma drainage implant insertion, intraocular lens exchange, or sutured intraocular lens placement can be performed as well [1, 2].

There are multiple reasons a TKP is utilized instead of completing the entire PKP procedure prior to the PPV. This technique minimizes trauma to the PKP graft, increasing the chance of graft survival [6]. The graft would otherwise be subject to significant intraoperative manipulation and irrigation. Further, using a TKP allows for better visualization by increasing wide-field visualization and ensuring a clear surface through which the PPV can be performed. Transplant tissue is not as optically clear due to edema, stromal folds, and/or haze [6].

TKP is a relatively new tool, with the first Landers-type TKP being introduced in 1981 [7, 8]. The Landers-type TKP underwent improvements in the 1990s including adding an integrated infusion. The integrated infusion is helpful in cases with dense vitreous opacity or anterior tractional membranes where the tip of the pars plana cannula cannot be visualized, conferring a risk of subretinal infusion and iatrogenic breaks [9]. In 1987 the silicone Eckardt TKP was introduced, which is commonly used today [6]. Since the sutures are placed directly through this TKP instead of through preplaced eyelets, the surgeon has the flexibility in choosing suture location,

which is helpful in cases of trauma and endophthalmitis to avoid areas of unstable cornea. The Eckardt TKP also offers a wider optical diameter facilitating easier visualization of peripheral retina [10, 11]. Other TKP options are available though they are less commonly employed, including the silicone rubber Aachen TKP and the quartz Cobo TKP, which is mainly used in emergencies during open-sky procedures when expulsion of contents is likely. The Cobo TKP fits various trephination sizes so it does not require custom sizing and has integrated infusion port useful in certain scenarios [6]. Even wider angle keratoprostheses may be available in the near future.

38.4 Risks and Benefits

The risks of the combined PKP/PPV procedure are significant. The surgeries are often highly complex with longer surgical time and associated increased anesthesia risks [2]. It requires coordinated care with both a corneal and vitreoretinal surgeon present for the surgery. In larger academic institutions this is more easily facilitated than out in the community. In either scenario there can be significant downtime for the two surgeons during the case given that the operating surgeon switches three or four times during the case. Further, these cases have a limited visual improvement, in large part due to the severity of pathology and poor prognosis [2].

However, the benefits of the surgery are important to note. First, a combined procedure saves the patient time and can hasten postoperative recovery [2]. Staged procedures require the corneal surgery to heal before PPV can be safely performed through a stable and optically clear cornea. This delay in PPV can result in progression of the retinal disease and irreversible damage. To drive home this point, one study noted that the success rate of surgical intervention with PKP/PPV was 81.9% when performed within 1 month of injury compared with only 54.3% when surgery occurred after 1 month [12]. Therefore, in urgent retinal cases a combined procedure can salvage vision that would otherwise be lost. Most eyes that undergo PKP/PPV achieve visual stabilization and result in salvage of the eye by preventing the need for enucleation or evisceration [2, 13]. This becomes particularly important with bilateral disease where the contralateral eye may have no light perception or may have very poor visual prognosis [2].

38.5 Outcomes

Outcomes vary widely based on preoperative diagnosis and preexisting damage. Overall, multiple retrospective studies have noted visual stability or improvement in 50–70% of cases [2]. In many of these cases, the eyes have no other viable surgical option and would therefore otherwise likely progress to no light perception vision or phthisis bulbi. These cases may have early visual improvement after PKP/PPV in about 50% of patients, though only 15–20% of eyes sustain this visual improvement in the long term (6–12 months) [2]. This steep decrement in visual improvement is due to the high rate of graft failure (~58%) and recurrent retinal detachment (~33%) in the long term [2]. These cases often require additional surgeries such as repeat PKP, PPV, or glaucoma drainage implants to regain stability of the eye [14].

Certain preoperative diagnoses confer a worse prognosis. For example, eyes with endophthalmitis, in which significant preoperative permanent damage can occur in a short period of time and where for the most part only severe cases warrant PKP/PPV, the anatomic and visual prognosis is very guarded. In one series that reviewed cases of endophthalmitis that underwent PKP/PPV, early visual improvement after at least 6 months was only 46.5, and 34.8% of surgeries "failed" resulting in phthisis or evisceration [13]. In these cases, eyes with fungal endophthalmitis had the worst outcomes.

Trauma, the most common indication for PKP/PPV, can have extremely variable results that are, again, based on the degree of preoperative damage. Due to the severity of damage in many of these cases, the visual prognosis may be worse than with the general population [5, 15]. Similar to endophthalmitis, early visual improvement is seen in only 47% in traumatic eyes [5]. However late visual outcomes are similar to the overall statistics, with visual improvement in 16–20% and visual decline in 30–45% [5]. In these traumatic eyes rates of phthisis/hypotony are high at about 12–35% but graft survival is similar to the overall patient pool of 42–73% [5, 12].

Relatively common postoperative occurrences are corneal graft failure, recurrent retinal detachment, proliferative vitreoretinopathy, glaucoma, phthisis, and hypotony [1, 2, 6]. Silicone oil is typically employed in more complex retinal detachments as it improves rates of reattachment [5]. Cases that warrant silicone oil are associated with a higher likelihood of recurrent retinal detachment [2]. Further, silicone oil can induce corneal graft failure with endothelial contact especially if left in the eye for long periods of time [5]. Other factors that have been associated with corneal graft failure include postoperative hypotony, which can decrease graft clarity, and a preoperative diagnosis of trauma [2, 5]. One of the most dreaded complications of PKP/PPV is phthisis, which is seen more often in eyes that have preoperative proliferative vitreoretinopathy and/or postoperative hypotony [12]. Sympathetic ophthalmia is also a rare, though very devastating, potential complication of PKP/PPV surgery.

38.6 Summary

Combined PKP/PPV is utilized in eyes with corneal opacification that require urgent retinal surgical intervention. Advantages include the ability to repair both the anterior and posterior segment abnormalities in one surgical setting. The majority of cases are trauma related but also include endophthalmitis, complicated post-cataract surgery, and recurrent retinal detachment with corneal decompensation. A TKP facilitates the view during PPV and increases the likelihood of PKP graft survival. Overall, eyes that warrant PKP/PPV often have limited visual prognoses due to significant anterior and posterior segment damage. While substantial visual improvement is uncommon in the long term, these eyes are often otherwise inoperable and would likely result in total vision loss or phthisis bulbi without PKP/PPV. Ocular salvage and visual stability occur in 50–70% of eyes, which is the primary goal of this combined surgery. PKP/PPV is a complex but useful surgical technique that can salvage eyes with otherwise guarded visual prognoses.

References

1. Yokogawa H, Kobayashi A, Okuda T, Mori N, Masaki T, Sugiyama K. Combined keratoplasty, pars plana vitrectomy, and flanged intrascleral intraocular lens fixation to restore vision in complex eyes with coexisting anterior and posterior segment problems. Cornea. 2018;37(Suppl 1):S78–85.
2. Miller Watson R, Dawood S, Cao D, Mieler WF, Leiderman YI. Outcomes of pars plana vitrectomy in combination with penetrating keratoplasty. J VitreoRetinal Dis. 2017;1(2):116–21.
3. Chun DW, Colyer MD, Wroblewski KJ. Visual and anatomic outcomes of vitrectomy with temporary keratoprosthesis or endoscopy in ocular trauma with opaque cornea. Ophthalmic Surg Lasers Imaging. 2012;43:302–10.
4. Harissi-Dagher M, Durr GM, Biernacki K, Sebag M, Rhéaume MA. Pars plana vitrectomy through the Boston Keratoprosthesis type 1. Eye. 2013;27(6):767–9.
5. Roters S, Szurman P, Hermes S, Thumann G, Bartz-Schmidt KU, Kirchhof B. Outcome of combined penetrating keratoplasty with vitreoretinal surgery for management of severe ocular injuries. Retina. 2003;23(1):48–56.
6. Tu E, Sugar J. Temporary keratoprosthesis. In: Brightbill F, editor. Corneal surgery. 4th ed. St Louis: Mosby; 2008. p. 677–82.
7. Landers MB III, Foulks GN, Landers DM, Hickingbotham D, Hamilton RC. Temporary keratoprosthesis for use during pars plana vitrectomy. Am J Ophthalmol. 1981;91(5):615–9.
8. Koenig SB, McDonald HR, Williams GA, Abrams GW. Penetrating keratoplasty after placement of a temporary keratoprosthesis during pars plana vitrectomy. Am J Ophthalmol. 1986;102(1):45–9.
9. Benner JD, Landers MB 3rd. An infusion temporary keratoprosthesis for pars plana vitrectomy. Am J Ophthalmol. 1996;122(4):579–80.
10. Ikeda T. Pars plana vitrectomy combined with penetrating keratoplasty. Semin Ophthalmol. 2001;16(3):119–25.
11. Gross JG, Feldman S, Freeman WR. Combined penetrating keratoplasty and vitreoretinal surgery with the Eckardt temporary keratoprosthesis. Ophthalmic Surg. 1990;21:67–71.
12. Dong X, Wang W, Xie L, Chiu AC. Long-term outcome of combined penetrating keratoplasty and vitreoretinal surgery using temporary keratoprosthesis. Eye. 2006;20:59–63.
13. Dave A, Acharaya M, Agarwal M, Dave PA, Singh M, Mathur U. Outcomes of combined keratoplasty and pars plana vitrectomy for endophthalmitis with compromised corneal clarity. Clin Exp Ophthalmol. 2019;47(1):49–56.
14. Garcia-Valenzuela E, Blair NP, Shapiro MJ, et al. Outcome of vitreoretinal surgery and penetrating keratoplasty using temporary keratoprosthesis. Retina. 1999;19:424–9.
15. Gelender H, Vaiser A, Snyder WB, Fuller DG, Hutton WL. Temporary keratoprosthesis for combined penetrating keratoplasty, pars plana vitrectomy, and repair of retinal detachment. Ophthalmology. 1988;95(7):897–901.

Keratoprosthesis and Retinal Surgery

39

Lindsay Machen and William F. Mieler

39.1 Introduction

The advent of modern-day keratoprosthesis (KPro) devices began in the early 1960s at the Massachusetts Eye and Ear Infirmary, reaching governmental approval in 1992 [1]. The purpose of the KPro device is to replace the native cornea, allowing for a clear optical surface and improved visual outcome in cases of blinding and recalcitrant corneal disease. The device is primarily crafted utilizing polymethylmethacrylate (PMMA), and has undergone many iterations and alterations since its inception. While several devices have been piloted, the Boston keratoprosthesis type I and type II and the osteo-odonto keratoprosthesis remain the three primary prostheses utilized in clinical practice with an overwhelming majority of surgeons and institutions favoring type I keratoprosthesis.

39.2 Indications for Keratoprosthesis

The most common indication for KPro placement is corneal graft rejection, along with chemical injury to the cornea, autoimmune conditions such as Stevens-Johnson syndrome and mucous membrane pemphigoid, severe ocular trauma, and generalized limbal stem cell insufficiency [2, 3]. These processes lead to various forms of corneal decompensation as outlined in Fig. 39.3. For many patients, the KPro represents the final opportunity for ocular surface rehabilitation and restoration of some degree of visual function.

Initially, KPro devices were considered a last resort for visual rehabilitation and regarded as an experimental surgical intervention. However, in the past decade, the Boston KPro has gained significant popularity with increasing implementation and indication for use [4]. Current practice utilizes KPros earlier in the course of disease rather than awaiting recurrent corneal graft failure and exhaustion of all other treatment modalities.

Some practitioners view KPro as a primary treatment option for autoimmune conditions and additional blinding pathology historically unresponsive to penetrating keratoplasty (PKP). Bypassing corneal grafting for the prosthetic device may limit unnecessary procedures and has been postulated to yield better long-term anatomic and visual outcomes [3, 5]. New attitudes towards the device may result in increased utilization, though implementation remains limited by clinician comfort and expertise in the surgical procedure.

L. Machen · W. F. Mieler (✉)
University of Illinois at Chicago, Chicago, IL, USA
e-mail: wmieler@uic.edu
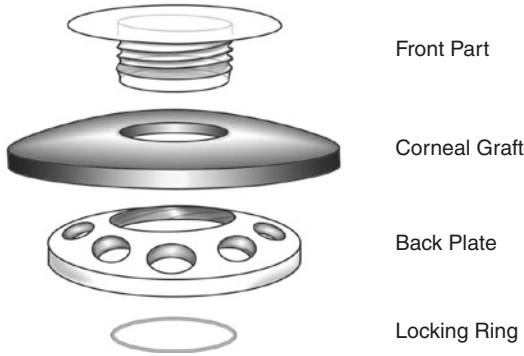
Fig. 39.1 The type 1 Boston keratoprosthesis (KPro) device, consisting of the front plate with optical stem, the donor corneal tissue, and a PMMA or titanium backplate with associated locking ring
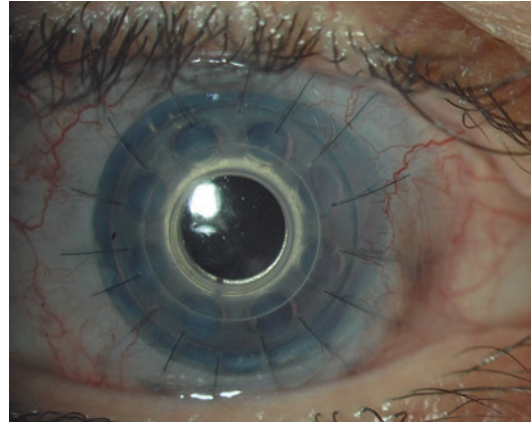
Fig. 39.2 Type 1 KPro device acutely sutured in place

39.3   Design of the KPro Device

The KPro device consists of three components, a front plate, optical stem, and a PMMA or titanium back plate, anchored by a corneal graft (Fig. 39.1). There are two types of Boston KPro devices with type I being the most popular. The type II device differs from type I with the addition of an anterior projection designed to protrude through a closed eyelid. The type II KPro is typically reserved for those patients with severely desiccated ocular surfaces, extinguished tear film, and inability to support a corneal based device [6]. Current literature focuses on type I KPro devices due to the greater prevalence of use.

Following trephine removal of the central portion of the diseased cornea, the KPro device is sutured in place with interrupted nylon sutures (Fig. 39.2). When the KPro device is being placed with the need for concurrent pars plana vitrectomy surgery, then the surgery is done through a temporary keratoprosthesis (see Chap. 38), prior to placement of the KPro device.

39.4   Postsurgical Prophylactic Treatments

Following surgical implantation, KPro patients are fitted with a bandage contact lens (BCL) and treated with antibiotic prophylaxis, typically daily topical vancomycin, though the specific antibiotic and frequency of use differ based on institutional preference. Topical corticosteroids are utilized for rejection prophylaxis [7]. Long-term retention of the device and decreased bacterial infection rates have been attributed to the combination of the BCL and prophylactic antibiotics; however, some authors attribute a concurrent and notable rise in fungal infections secondary to the use of antibiotic prophylaxis [8]. Discussion of the utility and effectivity of fungal prophylaxis is ongoing with some authors favoring monthly BCL change, regular irrigation with povidone-iodine, and/or daily antifungal, topical prophylaxis [9–11]. The incidence of fungal infection in these patients remains exquisitely low at 0.009–0.02 infections per patient year, making the financial and logistical expense of additional fungal prophylaxis a topic of great debate [9–11].

The overall success of the KPro has been directly correlated with the etiology of corneal decompensation and preexisting diagnosis necessitating transplantation (Fig. 39.3). Typically, review articles differentiate cicatrizing from non-cicatrizing conditions; cicatrizing conditions such as Stevens-Johnson syndrome (SJS), ocular cicatricial pemphigoid, and chemical burns tend to have worse outcomes with decreased graft retention and long-term success as compared to non-cicatrizing entities [12, 13]. Until recently, autoimmune conditions had been associated with greater complication rates with SJS demonstrating the worst outcomes with the highest rates of device failure and endophthalmitis [5, 6, 13]. The

	Number of Eyes (%)
Corneal Decompensation	34 (43%)
Failed Corneal Graft	17 (22%)
Traumatic Corneal Scar	16 (20%)
Bullous Keratopathy	9 (11%)
Corneal Edema	7 (9%)
Corneal Blood Staining	4 (5%)
Corneal Neovascularization	2 (3%)
Others	6 (8%)

Fig. 39.3 Corneal diagnoses leading to the need for KPro surgery (data from KPro surgical procedures at the University of Illinois at Chicago)

significant degree of persistent, systemic inflammation in SJS increases the risk for surrounding tissue damage and KPro compromise with potential development of secondary infection and posterior pole pathology such as choroidal and retinal detachment. More recent retrospective studies, however, have shown that topical vancomycin prophylaxis, aggressive control of concurrent glaucoma, and better systemic immunosuppression have altered the course of KPro survival in SJS patients and decreased the risk of failure [13]. Despite improvements in preoperative immunosuppression, surgical technique, and postoperative care, eyes affected by autoimmune and cicatrizing corneal disease remain at high risk with regard to long-term KPro survival.

39.5 Surgical Outcomes

A review of data from the University of Illinois at Chicago (UIC) has shown that in a consecutive series of 79 patients undergoing KPro surgery, 65 patients (82%) were anatomically stabilized with one surgical procedure. Of these patients, 97.5%

had undergone at least one previous surgical procedure, including 38 patients (48%) having had a previous pars plana vitrectomy, 17 patients (22%) had at least one previous PKP, and 18 patients (23%) had preexisting glaucoma. Intraoperative anatomic stability was achieved in all cases with silicone oil employed in 56% of patients.

At a mean follow-up of 26 months (minimum of 12 months, range 12–122 months), the cornea remained clear (56%) and the retina was attached in 55%. Visual results were modest with 12 patients (15%) achieving 20/400 or greater, and a similar 15% improved by >2 Snellen lines of visual acuity (Fig. 39.4). Overall, 67% of patients improved or had stable vision at the final follow-up. There were no cases of sympathetic ophthalmia.

39.6 Postoperative Complications (Risks and Benefits)

Significant modifications and improvement in KPro design and postoperative treatment over the past two decades have allowed for greater retention,

Fig. 39.4 LogMar visual acuity at the final follow-up (data from KPro surgical procedures at the University of Illinois at Chicago)

Visual Acuity(LogMAR)

2.67   2.23   2.21   2.43   2.48

PREOPERATIVE   MONTH 1   MONTH 6   1 YEAR   FINAL VISIT

Visual Acuity (LogMAR)
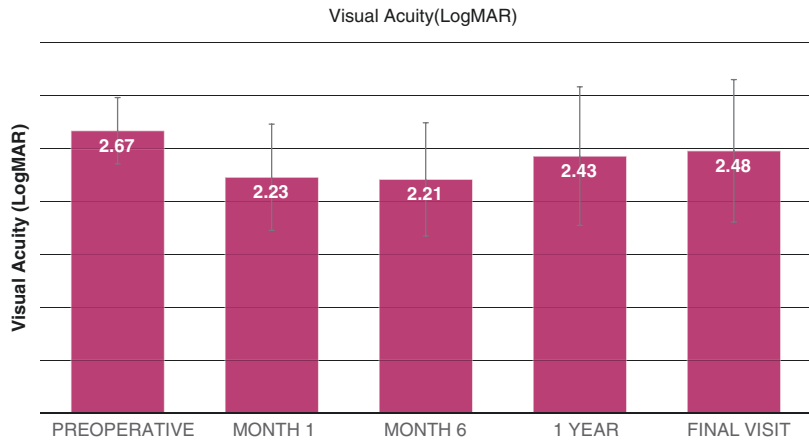
longer follow-up periods, and heightened recognition of potential retinal complications [14]. Posterior pole pathology, both concurrent and following KPro placement, can be particularly detrimental to visual potential and represent the most common causes for device failure [14, 15] (Fig. 39.5). Evaluation and treatment of KPro patients with retinal disease pose a significant challenge due to the complexity of the pathology and difficulty in complete assessment due to altered adnexal structures, narrowed view of the posterior pole, and significant loss of anatomic landmarks for surgical planning [14]. Despite the challenge, vitreoretinal surgeons must become comfortable evaluating and treating this challenging subset of patients given the increasing utilization and retention of KPro devices. The most common posterior pathology encountered includes retroprosthetic membranes, retinal detachments, endophthalmitis, sterile vitritis, and epiretinal membrane formation, which are described in greater detail below.

39.6.1 Retroprosthetic Membrane (RPM) Formation

The most common posterior segment complication is development of a retroprosthetic membrane (RPM). Though poorly defined and with an etiology as yet determined, formation of an RPM appears to represent an inflammatory response to the presence of the prosthetic KPro [16].

RPM forms in 26–65% of KPro patients with the greatest identified risk factors including infectious keratitis and stromal ingrowth [6, 14]. Additional postulated risk factors include the PMMA backplate and multiple surgical procedures at the time of KPro implantation, thus enhancing and possibly stimulating inflammation [5]. In addition to occlusion of the visual axis and impairment of best corrected visual acuity, formation of an RPM can occlude perfusion of aqueous to the donor cornea through the backplate, resulting in an increased risk of sterile keratolysis due to impeded nutrient flow [17]. In a majority of eyes with KPro and RPM, anterior segment ocular coherence tomography (OCT) has demonstrated varying degrees of increased peripheral anterior synechiae and angle closure suggesting potential for worsening glaucoma with RPM development [18]. Though contested, a decreased incidence of RPM has been noted with institution of the less inflammatory titanium backplate and with introduction of penetrating holes in the backplate medium [5, 6].

RPMs are typically identified at the slit lamp on anterior segment examination; the advent of anterior segment OCT has allowed for earlier detection of thinner, peripheral membranes providing an opportunity for earlier, less invasive intervention [18]. Not all RPMs require treatment but those that threaten corneal viability and impede central vision require intervention in the form of either Nd:YAG laser membranotomy or surgical removal [5, 16]. Earlier detection, as

	Number of Eyes (%)
History of Trauma	42 (53%)
Open Globe Injury	36 (46%; 86% of traumatized eyes)
Recurrent Retinal Detachment	24 (30%)
PVR	19 (24%; 80% of eyes with recurrent RD)
Glaucoma	18 (23%)
Prior Endophthalmitis	6 (8%)
Choroidal Hemorrhage	5 (6%)
Complicated Cataract Surgery	3 (4%)
Retinopathy of Prematurity	3 (4%)

Fig. 39.5 Underlying diagnoses leading to the use of KPro surgery (data from KPro surgical procedures at the University of Illinois at Chicago)

mentioned, may allow for more successful laser membranotomy before formation of a more vascularized and thickened membrane necessitates surgical removal [5].

39.6.2 Retinal Detachment

Retinal detachment (RD) has been reported to be as high as 18.6% in KPro patients with a combination of rhegmatogenous, tractional, and serous detachments reported [19, 20] (Fig. 39.6). Several studies have demonstrated an increased risk for postoperative RD in patients with prior intraocular surgery and systemic autoimmune disease [19, 21]. Additionally, RPM and sterile vitritis have been independently linked to an increased rate of RD [21]. Importantly, vitrectomy at the time of KPro implantation does not appear to be associated with heightened risk [21, 22]. RD in KPro patients portends poor long-term outcomes.
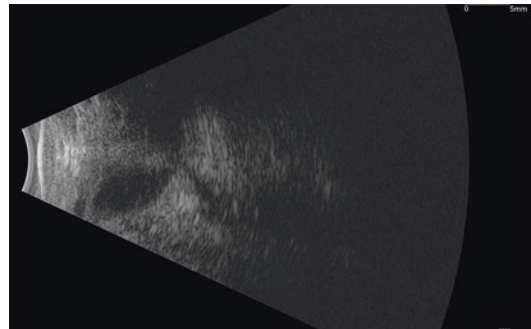
Fig. 39.6 B-scan echogram of a total RD in a patient with previous KPro surgery ×2. The detachment was repaired though with minimal visual gain

The detachments are difficult to repair, associated with significant degrees of proliferative vitreoretinopathy (PVR), and are often recalcitrant and recurrent [4]. Aggressive anterior proliferative changes emanating from the KPro and extending onto the ciliary body and pars plana

may occur, resulting in significant retinal traction and elevation with formation of subretinal fibrotic bands [4]. These tractional retinal detachments pose a significant surgical challenge with a guarded prognostic outcome [4]. Recent literature suggests the utility of small-gauge vitrectomy using valved trocars as a modern approach and technique for handling these difficult cases with significant improvement in outcome [4].

Approach to vitrectomy in a KPro patient is similar to that in patients with native corneas. Placement of trocars as close to the limbus as feasible is recommended; if the limbus is poorly defined or obscured, 9-mm marks crossing the KPro have been recommended [5]. Given the inherently pro-inflammatory nature of a KPro, use of silicone oil should be judicious and accompanied by a rigorous anti-inflammatory regimen with topical or periocular steroids [5].

39.6.3 Endophthalmitis

Endophthalmitis is a rare but visually catastrophic complication occurring after KPro placement. With the use of vancomycin prophylaxis, the rate of endophthalmitis has been measured to be as low as 0.35% per patient year; however large retrospective reviews have documented incidence as high as 12.5% [5]. The vast majority of infections show gram-positive isolates though fungal pathogens, specifically Candida species, have begun to emerge with speculation suggesting chronic treatment with antibiotics such as vancomycin and perpetual steroid requirement to be etiologic [5, 14]. The most common pathogens isolated include *Streptococcus* species, *Staphylococcus* species, *Propionibacterium acnes,* and *Candida* [15]. Studies disagree on whether bandage contact lenses (BCL) contribute to the development of fungal endophthalmitis; while recognized as beneficial for device retention, BCLs may contribute to proliferation of disease-causing organisms on the corneal surface. Device extrusion has decreased since institution of BCL therapy; however, fungal endophthalmitis rates increased during the same time frame leading to a poorly defined and contested correlation.

Endophthalmitis onset is typically explosive and associated with significant ocular pain and decreased vision. Treatment revolves around identification and adequate treatment of the offending agent either through vitreous culture and injection of intravitreal antibiotics and antifungals, surgical intervention with vitrectomy, and injection of similar anti-infective agents, or rarely systemic anti-infective agents. Several risk factors for the development of endophthalmitis have been identified including autoimmune etiologies predating KPro implantation, postoperative infectious keratitis, glaucoma drainage device exposure, and noncompliance with antibiotic prophylactic regimens [5]. Detection and prevention through routine cultures have no proven benefit and have been discredited in multiple studies. In addition, colonization of the KPro does not correlate with clinically significant infection.

39.6.4 Sterile Vitritis

When evaluating a patient with vitritis, the first consideration must go to infectious etiologies; however sterile vitritis represents a much more commonly identified condition with large-scale studies showing an incidence ranging from 0 to 10% in KPro patients [5, 14] (Fig. 39.7). Sterile vitritis is defined as varying degrees of intraocular inflammation in the absence of a detectable infectious agent and can be further differentiated from endophthalmitis by the general absence of pain or significant conjunctival or scleral injection and resolution with steroid use [5]. The reaction is felt to be inflammatory in nature and related either to the presence of the KPro foreign device or to surgical compromise of intraocular immune privilege [5]. Typical development occurs 8 months after KPro placement [14]. To date, no predisposing risk factors have been identified. Decreased vision is the predominant complaint with minimal additional symptoms. Slit-lamp examination may show mild anterior chamber cell with a described "snowflake" pattern of dense vitritis on examination of the posterior pole. Treatment centers on definitive elimination of infectious etiologies fol-
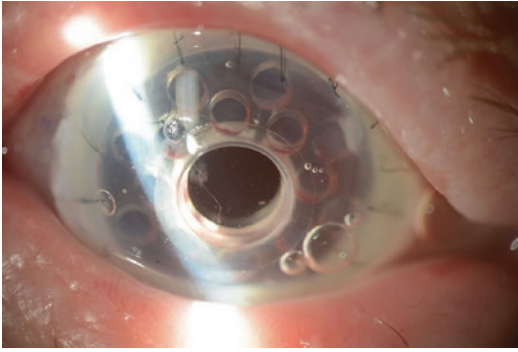
Fig. 39.7 Mild fibrin and inflammatory cell in a KPro patient 11 months following surgery. Cultures were negative and the inflammation responded to topical corticosteroid therapy

lowed by aggressive steroid management via topical, periocular, or even intravitreal pathways.

39.6.5 Epiretinal Membrane (ERM)

Another common retinal complication of KPro placement is development of an epiretinal membrane (ERM). Inflammation is speculated to play a role in ERM development in KPro patients and is noted at an increased rate in patients with silicone oil. Higher rates of ERM formation occur in those with retinal pathology predating KPro placement [14]. Effect on visual acuity is variable and rarely predictable from OCT. Attention to visual acuity and serial OCT to evaluate for vitreomacular traction and potential macular hole development is imperative. If visually significant, consideration can be given for pars plana vitrectomy (PPV) and membrane peeling.

39.7 Other Types of Keratoprosthesis

39.7.1 Osteo-Odonto Keratoprosthesis (OOKP)

Much of our discussion has focused on the Boston keratoprosthesis given its widespread utilization and prevalence; however other keratoprosthetic devices exist including the osteo-odonto keratoprosthesis (OOKP) [22]. Insertion involves a two-

stage procedure: an autologous canine tooth is harvested along with adjacent mandibular and maxillary bone. The tooth is removed with modification of the root to allow for placement of a PMMA optical cylinder within the tooth. The tooth is then implanted in the patient's cheek. The ocular surface is stripped of cornea and conjunctival epithelium with placement of a large, full-thickness buccal mucosal graft from the inner cheek. After establishing solvency, the tooth is retrieved from the cheek and implanted into the cornea through a 5 mm opening in the buccal graft. The procedure is extensive and requires the expertise of both ophthalmic and oral surgeons limiting widespread applicability.

39.7.2 Type II Boston Keratoprosthesis

Type II Boston keratoprosthesis represents another variant of the corneal prosthetic device and is utilized for patients with severely desiccated ocular surfaces not amenable to placement of a type I KPro. The type II KPro emerges from the upper lid eliminating ocular surface exposure. In type II KPro devices, the most common vitreoretinal complication was RPM formation [6].

Evaluation of KPro patients requires a combination of thorough clinical examination and imaging modalities. Use of the Optos scanning laser ophthalmoscope provides excellent visualization and identification of posterior pole pathology, though an adequate pupil aperture and relatively clear media are required for utilization [5]. B-scan ultrasonography remains a pertinent screening modality if visualization is poor, as can be the case with development of an RPM. Ocular coherence tomography can be employed to assess for cystoid macular edema and assessment of ERM.

39.8 Other Considerations and Prophylactic Measures

Surgical management of these vitreoretinal complications poses significant challenges for the surgeon due to altered anatomy, significant ocular comorbidities, and complex pathology. Different

authors advocate for different surgical approaches including suture-less small-gauge vitrectomy at the limbus with attention to potentially anteriorized retinal tissue as a result of PVR and traction [4, 14]. Several authors advocate for valved trocars due to wide fluctuations in pressure and the potential for choroidal hemorrhage and detachment [4]. In one large retrospective review, greater visualization of the posterior pole was endorsed through a contact lens system as compared to a noncontact format [23]. Favor was awarded to 23- and 25-gauge vitrectomy with preference for a closed system as open-sky approaches increased the risk of choroidal hemorrhage at the time of surgical intervention [23]. In addition, the smaller gauge intervention spares conjunctiva and addresses potential preexisting fornix foreshortening [23]. Overall, small-gauge surgery is postulated to decrease inflammation and diminish necessity for sutured sclerostomy sites. The utilization of valved trocars allows for flexibility in the location of the infusion and greater intraoperative manipulation and facility [4, 23]. Careful attention must be paid to the location of the backplate to avoid iatrogenic opacification [15]. Hemostasis throughout the procedure is essential given the inherently inflammatory nature of hemorrhage [15]. Tamponade may be required in instances of retinal detachment repair; silicone oil can be used judiciously as described and some authors suggest a therapeutic indication for perfluoro-*n*-octane for inferior retinal pathology. The potentially inflammatory nature of the perfluoro-*n*-octane, however, requires concurrent corticosteroid administration. While technically challenging, current small-gauge techniques combined with advents in the tools and expertise of vitreoretinal surgery allow for successful anatomical outcomes when specific modifications are made.

In this era of combined surgical interventions, the question of initial pars plana vitrectomy at the time of KPro placement has been heavily debated and argued with proponents supporting both positive and negative outcomes. Benefits to initial PPV include thorough assessment of the posterior pole and identification of underlying retinal pathology, elimination of inflammatory material, and removal of vitreous to allow for pars plana glaucoma drainage device insertion. The combined procedure allows for better estimation of visual prognosis and possible prevention of the development of a RPM, the most common vitreoretinal complication decreasing visual function following KPro placement. Initial vitrectomy decreases some of the challenges of postimplantation surgery and may diminish RPM formation by eliminating the necessary scaffold for formation [23].

In relatively recent retrospective reviews, authors compared eyes with KPro alone versus eyes undergoing combined PPV, glaucoma drainage tube implant, and KPro implantation [2] (Fig. 39.8). There was no statistically significant difference in the rate of intraoperative complications between eyes of each group [2]. Overall, the total number of recorded secondary

Initial Surgery Group	Baseline logMAR VA	Mean LogMAR improvement 1 year	% Eyes improved ≥ 3 lines 1 year	Mean logMAR improvement at last follow-up	% Eyes improved ≥ 3 lines last follow-up	Mean follow-up (months)
KPRO without initial PPVx (N=70)	2.47	1.17	78	0.58	58	54
KPRO combined with initial PPVx (N=55)	**2.84**	**1.15**	**72**	**1.21**	**77**	**48**
P (Fisher's exact)	**0.027**	0.512	.516	0.138	**0.036**	0.297

Fig. 39.8 Comparison of KPro surgery alone with KPro combined with PPV and tube shunt placement

procedures was greater for the KPro-alone eyes than the combination group with initial PPV; additionally, fewer eyes developed de novo PVR with retinal detachment when PPV was employed at the outset [2, 22]. Importantly, visual acuity did not differ significantly between the two groups at 1 year of follow-up, though it was better long term in the combination surgery group [2]. Given these encouraging findings, and the increasingly utilized KPro device, combination surgery with initial PPV may represent a new standard of care.

39.9 Summary

With the growing prevalence of early utilization of keratoprosthetic devices, both the anterior segment surgeon and the vitreoretinal surgeon need to be aware of the myriad of potential retinal complications, along with the special techniques required for evaluating and treating affected patients. When these devices are utilized, the key focus is the understanding of the need for various prophylactic measures including the use of a postoperative bandage contact lens and topical antibiotics. Furthermore, the possible employment of concurrent glaucoma and vitrectomy surgery at the time of placement of the keratoprosthesis possibly lessens the risk of postoperative complications, including retroprosthetic membranes, retinal detachment, endophthalmitis, vitritis, and epiretinal membranes.

While employment of artificial keratoprostheses carries substantial risks and concerns, these devices and associated surgical procedures are oftentimes the only recourse for patients with debilitating anterior segment diseases.

References

1. Salvador-Culla B, Kolovou P. Keratoprosthesis: a review of recent advances in the field. J Funct Biomater. 2016;7:13.
2. Lim J, Machen L, Areaga A, Karas F, Hyde R, Cao D, Niec M, Vajaranant T, Cortina MS. Comparison of visual and anatomical outcomes of eye undergoing Type I Boston keratoprosthesis with combination pars plana vitrectomy with eyes without combination vitrectomy. Retina. 2018;38(Suppl 1):S125–33.
3. Kang K, Karas F, Rai R, Hallak J, Kanj J, de la Cruz J, Cortina M. Five year outcomes of Boston type I keratoprosthesis as primary versus secondary penetrating corneal procedure in a matched case control study. PLoS One. 2018;13(2):1–12.
4. Petrou P, Banerjee P, Wilkins M, Singh M, Eastlake K, Limb G, Charteris D. Characteristics and vitreoretinal management of retinal detachment in eyes with Boston keratoprosthesis. Br J Ophthalmol. 2017;101:629–33.
5. Klufas M, Colby K. The Boston keratoprosthesis. Int Ophthalmol Clin. 2010;50:161–75.
6. Lee R, Khoueir Z, Tsikata E, Chodosh J, Dohlman C, Chen T. Long-term visual outcomes and complications of Boston keratoprosthesis type II implantation. Ophthalmology. 2017;124:27–35.
7. Greiner MA, Li YJ, Mannis MJ. Longer-term vision outcomes and complications with the Boston type 1 keratoprosthesis at the University of California, Davis. Ophthalmology. 2011;118:1543–50.
8. Chan C, Holland E. Infectious keratitis after Boston Type I keratoprosthesis implantation. Cornea. 2012;31:1128–34.
9. Odorcic S, Haas W, Gilmore M, et al. Fungal infections after Boston Type I keratoprosthesis implantation: literature review and in vitro antifungal activity of hypochlorous acid. Cornea. 2015;34:1599–605.
10. Odorcic S, Sabeti S, Haas W, et al. Fungal infections in Boston keratoprosthesis patients: lessons learned and novel developments on the horizon. Semin Ophthalmol. 2016;31:71–8.
11. Barnes D, Dohlman C, Durand M. Fungal colonization and infection in Boston keratoprosthesis. Cornea. 2007;26:9–15.
12. Yaghouti F, Nouri M, Abad JC, Power W, Doane M, Dohlman C. Keratoprosthesis: preoperative prognostic categories. Cornea. 2001;20:19–23.
13. Sayegh R, Ang L, Foster S, Dohlman C. The Boston keratoprosthesis in Stevens-Johnson syndrome. Am J Ophthalmol. 2007;145:438–44.
14. Pukhraj R, Rishi E, Kooundany V, Mathur G, Iyer G, Srinivasan B. Vitreoretinal complications in eyes with Boston keratoprosthesis type I. Retina. 2016;36:603–10.
15. Ray S, Khan B, Dohlman C, D'Amico D. Management of vitreoretinal complications in eyes with permanent keratoprosthesis. Arch Ophthalmol. 2002;120:559–66.
16. Rudnisky C, Belin M, Todani A, Al-Arfaj K, Ament J, Zerbe B, Ciolino J, Boston Type I Keratoprosthesis Study Group. Risk factors for the development of retroprosthetic membranes with Boston keratoprosthesis type I: multicenter study results. Ophthalmology. 2012;119:951–5.
17. Sivaraman K, Hou J, Allemann N, de la Cruz J, Cortina M. Retroprosthetic membrane and risk of sterile keratolysis in patients with type I Boston keratoprosthesis. Am J Ophthalmol. 2013;155:814–22.
18. Silva LD, Santos A, Sousa LB, Allemann N, Oliveira LA. Anterior segment optical coherence tomography findings in type I Boston keratoprosthesis. Arq Bras Oftalmol. 2018;81:42–6.

19. Goins K, Kitzmann A, Greiner M, Kwon Y, Alward W, Ledolter J, Wagoner M. Boston type I keratoprosthesis: visual outcomes, device retention, and complications. Cornea. 2016;35:1165–74.

20. Golgorsky D, Williams BK, Flynn HW. Posterior pole retinal detachment due to a macular hole in a patient with a Boston keratoprosthesis. Am J Ophthalmol Case Rep. 2017;5:56–8.

21. Jardeleza MS, Rheaume MA, Chodosh J, Lane AM, Dohlman C. Retinal detachments after Boston kerato-prosthesis: incidence, predisposing factors, and visual outcome. Digit J Ophthalmol. 2015;21:1–15.

22. Lim L, Ang C, Wong E, Wong D, Tan D. Vitreoretinal complications and vitreoretinal surgery in osteo-odonto-keratoprosthesis surgery. Am J Ophthalmol. 2014;157:349–54.

23. Kiang L, Sippe K, Starr C, Ciralsky J, Rosenblatt M, Radcliffe N, D'Amico D, Kiss S. Vitreoretinal surgery in the setting of permanent keratoprosthesis. Arch Ophthalmol. 2012;130:487–93.

Robotic Retinal Surgery

40

Ivy Zhu and William F. Mieler

40.1 Introduction

The first introduction of the word "robot" to the world had its roots not in the fields of medicine or industry, but rather in literature. Karel Capek was a Czech playwright whose 1920 play, *Rossum's Universal Robots*, used the word "robot" for the first time [1]. Capek derived the term from the Czech *robota*, meaning "forced labor," and used it to describe fictional humanoid creatures enslaved to perform mundane tasks for their human masters. In medicine, the term robot can be used to describe any machine with mechanisms capable of augmenting or replacing the capabilities of the surgeon. The most well-known example of a surgical robot is the da Vinci surgical system (Intuitive Surgical, Sunnyvale, USA), which has performed over six million surgeries worldwide since its introduction in 1999 [2]. Widespread adoption of robotic-assisted surgery in ophthalmology has been limited to date, though several machine prototypes show great promise in expanding the physical limitations of the vitreoretinal surgeon. This chapter reviews the advantages, surgical approaches, indications, limitations, and future developments of robotic-assisted surgery in the field of vitreoretinal surgery.

I. Zhu · W. F. Mieler (✉)
Department of Ophthalmology and Visual Sciences,
University of Illinois at Chicago, Chicago, IL, USA
e-mail: izhu1@uic.edu; wmieler@uic.edu

40.2 Advantages

The vitreoretinal surgeon works on the scale of microns, often at the limits of human visuospatial resolution, proprioception, and physiologic tremor. Surgeries require delicate maneuvers within a confined space that are highly dexterous with a low margin for error due to the required forces often being beyond the levels of human perception. Physiologic hand tremor has an amplitude of approximately 100 μm and can be a limiting factor with the risk of inadvertent tissue damage, particularly for the beginning or inexperienced surgeon [3]. Visualization of microstructures during surgery due to limited spatial resolution and depth perception can also present a challenge.

Robotic-assisted surgery has the potential to cancel hand tremor to provide stabilization of intraocular instruments and to automate certain steps or procedures. This in turn may limit surgeon fatigue and variability. The enhanced stability and dexterity provided by a robotic system could allow for the successful performance of certain high-risk surgical procedures, such as retinal vein cannulation, or subretinal injections. The ability of certain robotic systems to physically separate the operator and the machine also allows for the possibility of telesurgery. Ultimately, the technical potential of robotic-assisted surgery could lead to new frontiers in vitreoretinal surgery in terms of patient safety and efficacy.

40.3   Surgical Approaches

The ideal design of a robotic system should be intuitive, lightweight, and maneuverable; protect surgical entry points from instrument damage; be easily assembled by nontechnical staff; include a visualization system that matches or exceeds current surgical microscopes; and incorporate fail-safe mechanisms to prevent inadvertent injury in the event of sudden patient movements [4–6]. Three main types of surgical robots currently exist, which differ based on the complexity of the robot and the nature of human-machine interaction.

- **Conventional:** The surgeon uses a surgical microscope and microsurgical instruments to perform intraocular tasks with direct visual and proprioceptive feedback.
- **Robot-assisted tool:** The surgeon uses an optical microscope and handheld miniature robotic tool to perform intraocular tasks with visual feedback. The microsurgical tool has the ability to cancel tremor and lock depth, among other features.
- **Cooperative robotic system:** The surgeon controls the surgical tool in conjunction with the robotic system while a microscope and/or optical coherence tomography (OCT) machine provides visual feedback. The robotic system is capable of augmenting or correcting the movements of the surgeon.
- **Remote operator:** The surgeon remotely operates a joystick to direct the movements of a robot holding microsurgical tools while a surgical microscope or display provides visual feedback. This is also known as a "master-slave"-type system that was popularized by the da Vinci surgical system. Remote operator systems are the most technically complex form of surgical robots and have the potential to perform semiautomated or automated procedures with the assistance of a smart sensory feedback system.

The following subsections briefly review some published examples in the ophthalmic literature of robotic prototypes that fall under each category.

40.3.1 Robot-Assisted Tool

A robot-assisted tool, also known as a "smart" surgical tool, is an enhanced handheld instrument that is operated by the surgeon. The instrument has internal processes that allow it to augment and expand the capabilities of the surgeon. Published reports of experimental laboratory prototypes include both modified standard microsurgical tools and stand-alone devices. For example, Cutler et al. developed a 25-gauge force-sensing microforceps connected to an auditory feedback system that alerted the operator when a force exceeding 9 mN was applied during a simulated ophthalmic peeling procedure [7]. Balicki et al. attached an optical fiber to a 25-gauge microsurgical pick connected to a Fourier-domain common-path OCT that was capable of enforcing safety constraints to prevent unintentional contact with the retinal surface, scanning a surface while maintaining a constant distance, and placing the pick over a scan-identified subsurface target and penetrating the surface to reach the target [8]. Other published reports have reported similar enhancements to existing surgical tools to provide the surgeon with additional feedback [9].

In contrast to these modified existing microsurgical tools, the Micron (Fig. 40.1) is an active handheld stand-alone micromanipulator developed by Carnegie Mellon University and Johns Hopkins University capable of reducing hand tremor, detecting membrane puncture, and automatically holding a position in space [10]. When the Micron was evaluated in retinal vein cannulation of ex vivo porcine eyes, it had a 63% success rate compared to 29% using traditional tools. Importantly, the Micron is also capable of holding traditional intraocular tools. It can be further modified to include a force-pick on its tip to detect applied forces, OCT integration, a monocular camera system, or an intraocular "snake" instrument extension providing additional degrees of freedom [11–19].

Fig. 40.1 The Micron: a handheld robotic micromanipulator developed by Johns Hopkins University and Carnegie Mellon University (photo from Yang S, MacLachlan RA, Riviere CN. Manipulator design and operation of a six-degree-of-freedom handheld tremor-canceling microsurgical instrument. IEEE/ASME Trans Mechatron. 2014;20:761–72)
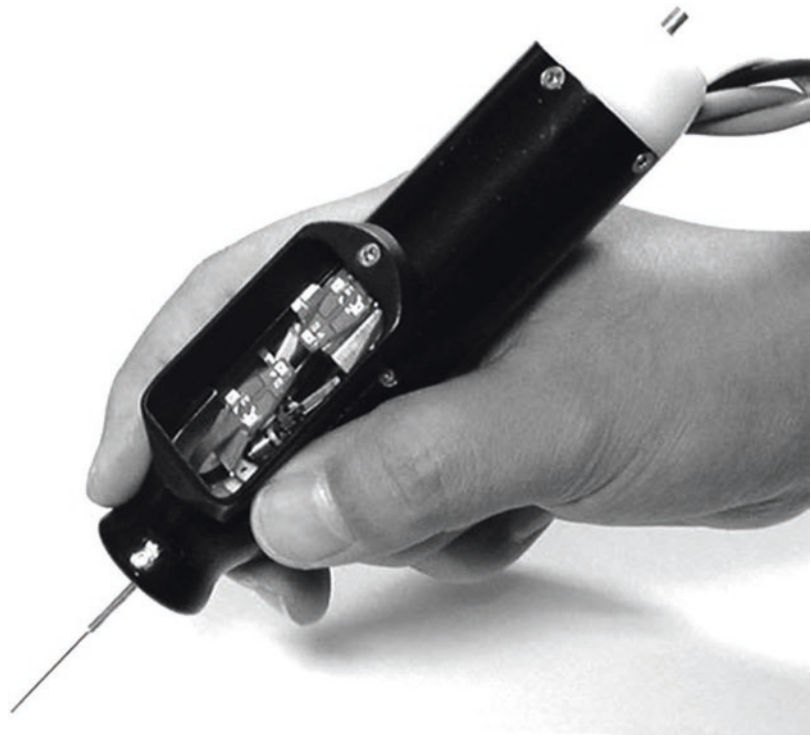
40.3.2 Cooperative Robotic System

The cooperative robotic system is configured so that the machine works simultaneously with the surgeon as co-manipulators. Instead of a remote joystick, the surgeon directly handles the arms of the robot while the robot concurrently works to smooth, cancel, or correct any operator maneuvers. The Johns Hopkins Steady-Hand Eye Robot is a surgeon-initiated robotic system with five degrees of freedom (three along the translational *x*-, *y*-, and *z*-axes and two along the rotational tilt and roll axes) [20]. The robot arm can hold either conventional or smart instruments that the surgeon then manipulates; as the surgeon directs the instrument, the robot arm increases the safety and efficiency of each movement. This device has been used in retinal vein cannulation and retinal membrane peeling in model eyes. It can also be further modified like the Micron for enhanced safety and efficiency [12, 21–23]. A similar device by the Katholieke Universiteit Leuven (KU Leuven) in Belgium was used to successfully perform retinal vein cannulation in a clinical trial of four patients with a retinal vein occlusion (Fig. 40.2) [24, 25]. Details and outcomes of the clinical trial have not yet been published.

40.3.3 Remote Operator

Remote operator systems separate the controls from the effector machine in a form of telemanipulation. The surgeon operates the controls at a workstation, often with some type of joystick, and those movements are translated by a computer processor to the machine, which then manipulates the instruments. Notable current examples include the da Vinci surgical system, PRECEYES Surgical System (Preceyes BV, Eindhoven, the Netherlands), and the Intraocular Robotic Interventional Surgical System (IRISS).

40.3.3.1 da Vinci Surgical System

The da Vinci surgical system (Fig. 40.3) was approved by the Food and Drug Administration in 2000 and is the most well-known and widely

Fig. 40.3 da Vinci Xi surgical system being used in simulated strabismus surgery (photo from Bourcier T, Chammas J, Gaucher D, et al. Robot-assisted simulated strabismus surgery. Transl Vis Sci Technol. 2019;8(3):26)

used robotic system of this type, with applications in general surgery, cardiology, urology, and gynecology among others [26]. The device consists of a separate control console and a robotic apparatus with three or four arms that hold a dual-channel endoscope and various detachable surgical tools. The endoscope relays visual input to a binocular viewfinder on the remote workstation, allowing stereoscopic viewing. Four models have been produced since its initial introduction to the market: S, Si, HD, and Xi.

Using model eyes, the da Vinci has been previously tested in the laboratory setting to evaluate its suitability for external, anterior segment, and posterior segment ocular surgery [27–34]. Extraocular surgery, such as full-thickness corneal, scleral, muscle, and amniotic membrane suturing, was found to be feasible with the da Vinci system in experimental models [27, 29–31, 34]. In particular, researchers found the wrist movements needed to manipulate instruments to be intuitive and the range of motion adequate for extraocular surgery. Recently, Bourcier et al. were able to successfully perform amniotic membrane transplantation in three human patients and pterygium surgery in one human patient using the da Vinci surgical system without intraoperative complications or conversion to conventional surgery [30, 33].

However, Bourla et al. found anterior and posterior segment surgery to be notably more difficult with the da Vinci system [28]. In their experiments, anterior segment surgery consisted of anterior chamber intraocular foreign-body removal and capsulorhexis while posterior segment surgery consisted of 25-gauge pars plana vitrectomy. There was limited maneuverability of the robotic arms intraocularly and the high center of motion of the da Vinci system (9 cm away from the eye surface) caused external stress on the surgical wounds. Visualization of intraocular structures was also difficult with the da Vinci endoscope, which could not produce the retroillumination critical to anterior segment surgery and did not have the same resolution quality as the ocular microscope. To address the high center

of motion problem with the da Vinci instrument handling, future experiments used a microrobotic Stewart platform-based parallel manipulator attached to the robotic arms [35, 36]. The combined device of the da Vinci system and Stewart platform was called the hexapod surgical system (HSS). Using automated software, the HSS was able to place the remote center of motion on the ocular surface with excellent resultant dexterity and stability; however, translational and rotational maneuvers inside the eye were limited to a 30- to 40-degree cone. More recently, Bourcier et al. attempted anterior segment cataract surgery on Kitaro model eyes with the newest da Vinci Xi model, which improved upon the previous Si model used in earlier ophthalmic investigations with a 3-D high-definition viewing system [32]. However, the limitations related to a high center of motion persisted. A second surgical assistant was also needed for manual injection of intraocular solutions and operating time was found to be increased compared to conventional surgery.

40.3.3.2   PRECEYES Surgical System

In addition to the da Vinci surgical system, the PRECEYES Surgical System (Fig. 40.4) is the only commercially available robotic surgical system and the only system specifically designed for ophthalmic surgery. The device received the CE mark from the European Union in 2019 [37]. It consists of an input joystick controlled by the surgeon and a robotic apparatus with two mechanical arms firmly secured to the temporal side of the operating table. Appropriate alignment of the robot arms and the surgical entry site is provided by an electrically driven headrest. Visual feedback is provided by a conventional operating microscope or other visualization techniques.

In the initial experimental phases, the prototype was first used to cannulate retinal veins in live, anesthetized pigs with an induced retinal vein occlusion. De Smet et al. found that the PRECEYES provided consistent cannulation of the vein for up to 20 min and that intraluminal injection of ocriplasmin proximal to the site of

Fig. 40.4 PRECEYES Surgical System: a telerobotic surgical system developed by PRECEYES BV in the Netherlands. This is the only commercially available ophthalmic robotic surgical system (photo from de Smet MD, Stassen JM, Meenink TC, Janssens T, Vanheukelom V, Naus GJ, et al. Release of experimental retinal vein occlusions by direct intraluminal injection of ocriplasmin. Br J Ophthalmol. 2016;100:1742–6)

occlusion caused clot dissolution within a few minutes [38, 39]. The size of the veins cannulated was 80 μm in diameter or more and the distal tip of the glass pipette used for cannulation was 30 μm in diameter. Using virtual surgical simulation or video monitoring, the PRECEYES Surgical System has also been compared to conventional manual surgery. Robotic-assisted surgery was found to increase procedure time, but decrease intraocular instrument movement and surgeon-inflicted tissue damage, particularly in the novice surgeon [40–42].

In 2018, the PRECEYES Surgical System was used for the first time in human patients for retinal membrane peeling and subretinal recombinant tissue plasminogen activator (tPA) injection [43]. Twelve patients were randomized to either robotic membrane peeling or manual robotic peeling with the investigators reporting equally successful surgical outcomes in both groups. No statistical difference was noted in the amount of retinal microtrauma between the two groups, though the robotic system did require a longer operating time. In evaluating subretinal injection of tPA, six patients were randomized to either manual or robotic-assisted surgery. Subretinal tPA injection was successful in all patients.

40.3.3.3 Intraocular Robotic Interventional Surgical System (IRISS)

The intraocular robotic interventional surgical system (IRISS) is a similar remote operator system designed by the Jules Stein Eye Institute and the University of California, Los Angeles, Department of Mechanical and Aerospace Engineering for ophthalmic surgery [44, 45]. The device has two controlling joysticks and two arms that hold surgical instruments with alignment of the surgical incision to the remote center of motion by low-powered lasers. It has successfully performed capsulorhexis, viscoelastic injection, hydrodissection, lens cortex removal, core vitrectomy, PVD induction, and retinal vein microcannulation in porcine eyes.

40.4 Indications

The future indications for robotic-assisted surgery are varied. Given the enhanced mechanical maneuverability and precision, delicate procedures requiring exceptionally fine movements could be consistently and safely performed such as targeted intravascular drug delivery, retinal

vessel cannulation, and subretinal injection for gene therapy [28]. The safety of existing surgical procedures could also be improved given the ability of the robotic system to potentially dampen or eliminate tremor, provide safety feedback to prevent iatrogenic retinal damage, and allow enhanced visualization and targeting of various retinal microstructures. The robot could also act as a skilled surgical assistant in certain scenarios. In areas with limited access to ophthalmic care, and specifically vitreoretinal care, remote telesurgery could be a tool to address existing healthcare gaps and disparities. Finally, robotic-assisted systems could also improve surgical training and education by providing additional sensory feedback to the beginner surgeon.

40.5   Limitations

The transition of a novel technology from bench to bedside often depends on the ability of the new technology to provide improvements over the previous or current standard of care in either safety, efficiency, cost, or outcomes. Current limitations in the widespread adoption of robotic-assisted surgical systems in ophthalmology include the lack of large-scale clinical trials, minimally significant improvement over conventional surgery, and increased cost.

At present, the PRECEYES Surgical System is the only commercially available robotic device specifically designed for ophthalmic surgery. It has been clinically trialed in nine human subjects and is only clinically approved for use in the European Union. The da Vinci surgical system has also been trialed in a handful of human subjects. While these initial reported results offer promise for the use of robotic surgical devices, they provide little insight into the safety, efficacy, and efficiency of robotic-assisted surgery in a large diverse cohort of patients.

In both clinical trials and experimental investigations of robotic-assisted surgery, the robotic-assisted device was found to provide enhanced instrument stabilization and precision at the cost of greatly increased operating time. In simulated assessments of surgeon performance, the robotic-

assisted device was found to improve surgeon instrument handling, especially in the novice surgeon, with decreased retinal microtrauma as a result. However, whether these experimental findings of reduced microtrauma can translate to the surgical setting in a meaningful way remains to be seen. In evaluating the PRECEYES Surgical System against conventional surgery in retinal membrane peeling, robotic surgery caused a statistically equivalent number of retinal microtrauma events with equivalent clinical outcomes at a significantly longer operating time [43].

The high clinical costs associated with implementation of a robotic surgical device such as the PRECEYES Surgical System are due to both direct costs related to equipment and indirect costs such as operating room time and case turnover. While costs may be lower with machines of lesser complexity such as robot-assisted tools and co-manipulator devices, their range of function is also more limited, potentially curtailing their usage and cost-effectiveness. Current success rates of vitreoretinal surgery are also very high, and the increased expense of robotic-assisted surgery may be prohibitive when weighed against potentially minimal improved clinical outcomes, especially in an increasingly cost-conscious healthcare landscape [46].

Given these limitations, the adoption of robotic-assisted surgery in the near future will likely remain restricted to technically difficult procedures with poor conventional outcomes such as retinal vein cannulation. However, these factors may change in the future as the abilities of these robotic devices continue to rapidly develop and expand.

40.6   Future Developments

The future of robotic-assisted retinal surgery is likely to include progressively greater levels of automation, potentially governed by artificial intelligence (AI) [4–6]. By coupling the surgical robot with a visual guidance system, an autonomous robotic system with the surgeon acting only in a supervisory role is possible. Using visual input from a surgical microscope or intraoperative

OCT machine, the robot could be programmed to navigate the retinal microenvironment and perform surgical steps or complete the procedure independently. This development could further be augmented and accelerated by coupling robots to AI, where deep learning methods could develop algorithms to predict, detect, and respond to various surgical situations in surgery. As with many other applications of AI, this would likely require the data input of thousands of surgeries in order to develop the algorithms necessary to correctly and reproducibly address the multifaceted decisions required in surgery.

40.7 Summary

Robotic-assisted vitreoretinal surgery is one of the next great horizons in ophthalmology and, indeed, all of surgery. The technical requirements of the vitreoretinal surgeon are becoming greater and more varied as novel interventions such as subretinal injections in gene therapy develop into reality. Future advances will likely include larger scale clinical trials, improved clinical outcomes, decreased operating times, and AI integration to achieve some degree of automation. Ultimately, robotic-assisted surgery has the potential to expand the physical capabilities of the surgeon to a superhuman level and provide even greater outcomes and safety for patients.

References

1. Lane T. A short history of robotic surgery. Ann R Coll Surg Engl. 2018;100(6 Suppl):5–7. https://doi.org/10.1308/rcsann.supp1.5.
2. Intuitive Surgical. No title. https://www.davincisurgery.com/. Published 2020. Accessed 12 Apr 2020.
3. Peral-Gutierrez F, Liao AL, Riviere CN. Static and dynamic accuracy of vitreoretinal surgeons. In: The 26th Annual International Conference of the IEEE Engineering in Medicine and Biology Society. 2004. p. 2734–7. https://doi.org/10.1109/IEMBS.2004.1403783.
4. Gerber MJ, Pettenkofer M, Hubschman JP. Advanced robotic surgical systems in ophthalmology. Eye. 2020. https://doi.org/10.1038/s41433-020-0837-9.
5. De Smet MD, Naus GJL, Faridpooya K, Mura M. Robotic-assisted surgery in ophthalmology. Curr Opin Ophthalmol. 2018;29(3):248–53. https://doi.org/10.1097/ICU.0000000000000476.
6. Channa R, Iordachita I, Handa JT. Robotic vitreoretinal surgery. Retina. 2017;37(7):1220–8. https://doi.org/10.1097/IAE.0000000000001398.
7. Cutler N, Balicki M, Finkelstein M, et al. Auditory force feedback substitution improves surgical precision during simulated ophthalmic surgery. Investig Ophthalmol Vis Sci. 2013;54(2):1316–24. https://doi.org/10.1167/iovs.12-11136.
8. Balicki M, Han J-H, Iordachita I, et al. Single fiber optical coherence tomography microsurgical instruments for computer and robot-assisted retinal surgery. Med Image Comput Comput Assist Interv. 2009;12(Pt 1):108–15. https://doi.org/10.1007/978-3-642-04268-3_14.
9. Ourak M, Smits J, Esteveny L, et al. Combined OCT distance and FBG force sensing cannulation needle for retinal vein cannulation: in vivo animal validation. Int J Comput Assist Radiol Surg. 2019;14(2):301–9. https://doi.org/10.1007/s11548-018-1829-0.
10. Maclachlan RA, Becker BC, Tabarés JC, Podnar GW, Lobes LA, Riviere CN. Micron: an actively stabilized handheld tool for microsurgery. IEEE Trans Robot. 2012;28(1):195–212. https://doi.org/10.1109/TRO.2011.2169634.
11. Mukherjee S, Yang S, Maclachlan RA, Lobes LA, Martel JN, Riviere CN. Toward monocular camera-guided retinal vein cannulation with an actively stabilized handheld robot. In: Proceedings—IEEE International Conference on Robotics and Automation. Vol. 2017. Institute of Electrical and Electronics Engineers Inc.; 2017. p. 2951–6. https://doi.org/10.1109/ICRA.2017.7989341.
12. Song J, Gonenc B, Guo J, Iordachita I. Intraocular snake integrated with the steady-hand eye robot for assisted retinal microsurgery. In: Proceedings—IEEE International Conference on Robotics and Automation. Institute of Electrical and Electronics Engineers Inc.; 2017. p. 6724–9. https://doi.org/10.1109/ICRA.2017.7989796.
13. Gonenc B, Balicki MA, Handa J, et al. Preliminary evaluation of a micro-force sensing handheld robot for vitreoretinal surgery. In: IEEE International Conference on Intelligent Robots and Systems. Vol. 2012. NIH Public Access; 2012. p. 4125–30. https://doi.org/10.1109/IROS.2012.6385715.
14. Gonenc B, Feldman E, Gehlbach P, Handa J, Taylor RH, Iordachita I. Towards robot-assisted vitreoretinal surgery: force-sensing micro-forceps integrated with a handheld micromanipulator. In: Proceedings—IEEE International Conference on Robotics and Automation. Vol. 2014. Institute of Electrical and Electronics Engineers Inc.; 2014. p. 1399–404. https://doi.org/10.1109/ICRA.2014.6907035.
15. Gonenc B, Patel N, Iordachita I. Evaluation of a force-sensing handheld robot for assisted retinal vein cannulation∗. In: Proceedings of the Annual International Conference of the IEEE Engineering in Medicine and Biology Society, EMBS. Vol. 2018. Institute

of Electrical and Electronics Engineers Inc.; 2018. p. 1–5. https://doi.org/10.1109/EMBC.2018.8513304.

16. Yang S, Balicki M, Wells TS, et al. Improvement of optical coherence tomography using active handheld micromanipulator in vitreoretinal surgery. In: Proceedings of the Annual International Conference of the IEEE Engineering in Medicine and Biology Society, EMBS. Vol. 2013. NIH Public Access; 2013. p. 5674–7. https://doi.org/10.1109/EMBC.2013.6610838.

17. He X, Van Geirt V, Gehlbach P, Taylor R, Iordachita I. IRIS: integrated robotic intraocular snake. In: Proceedings—IEEE International Conference on Robotics and Automation. Vol. 2015. Institute of Electrical and Electronics Engineers Inc.; 2015. p. 1764–9. https://doi.org/10.1109/ICRA.2015.7139426.

18. Yang S, MacLachlan RA, Martel JN, Lobes LA, Riviere CN. Comparative evaluation of handheld robot-aided intraocular laser surgery. IEEE Trans Robot. 2016;32(1):246–51. https://doi.org/10.1109/TRO.2015.2504929.

19. Yang S, MacLachlan RA, Riviere CN. Toward automated intraocular laser surgery using a handheld micromanipulator. In: IEEE International Conference on Intelligent Robots and Systems. Vol. 2014. Institute of Electrical and Electronics Engineers Inc.; 2014. p. 1302–7. https://doi.org/10.1109/IROS.2014.6942725.

20. Uneri A, Balicki MA, Handa J, Gehlbach P, Taylor RH, Iordachita I. New steady-hand eye robot with micro-force sensing for vitreoretinal surgery. Proc IEEE RAS EMBS Int Conf Biomed Robot Biomechatron. 2010;2010(26–29):814–9. https://doi.org/10.1109/BIOROB.2010.5625991.

21. Balicki M, Uneri A, Iordachita I, Handa J, Gehlbach P, Taylor R. Micro-force sensing in robot assisted membrane peeling for vitreoretinal surgery. In: Lecture Notes in Computer Science (Including Subseries Lecture Notes in Artificial Intelligence and Lecture Notes in Bioinformatics). Vol. 6363. LNCS. NIH Public Access; 2010. p. 303–10. https://doi.org/10.1007/978-3-642-15711-0_38.

22. He X, Balicki M, Gehlbach P, Handa J, Taylor R, Iordachita I. A novel dual force sensing instrument with cooperative robotic assistant for vitreoretinal surgery. In: Proceedings—IEEE International Conference on Robotics and Automation. Vol. 2013. NIH Public Access; 2013. p. 213–8. https://doi.org/10.1109/ICRA.2013.6630578.

23. He C, Patel N, Ebrahimi A, Kobilarov M, Iordachita I. Preliminary study of an RNN-based active interventional robotic system (AIRS) in retinal microsurgery. Int J Comput Assist Radiol Surg. 2019;14(6):945–54. https://doi.org/10.1007/s11548-019-01947-9.

24. Gijbels A, Smits J, Schoevaerdts L, et al. In-human robot-assisted retinal vein cannulation. A World First. Ann Biomed Eng. 2018;46(10):1676–85. https://doi.org/10.1007/s10439-018-2053-3.

25. Willekens K, Gijbels A, Schoevaerdts L, et al. Robot-assisted retinal vein cannulation in an in vivo porcine retinal vein occlusion model. Acta Ophthalmol. 2017;95(3):270–5. https://doi.org/10.1111/aos.13358.

26. George EI, Brand TC, LaPorta A, Marescaux J, Satava RM. Origins of robotic surgery: from skepticism to standard of care. JSLS J Soc Laparoendosc Surg. 2018;22(4):e2018.00039. https://doi.org/10.4293/JSLS.2018.00039.

27. Tsirbas A, Mango C, Dutson E. Robotic ocular surgery. Br J Ophthalmol. 2007;91(1):18–21. https://doi.org/10.1136/bjo.2006.096040.

28. Bourla DH, Hubschman JP, Culjat M, Tsirbas A, Gupta A, Schwartz SD. Feasibility study of intraocular robotic surgery with the da Vinci surgical system. Retina. 2008;28(1):154–8. https://doi.org/10.1097/IAE.0b013e318068de46.

29. Bourges JL, Hubschman JP, Burt B, Culjat M, Schwartz SD. Robotic microsurgery: corneal transplantation. Br J Ophthalmol. 2009;93(12):1672–5. https://doi.org/10.1136/bjo.2009.157594.

30. Bourcier T, Becmeur PH, Mutter D. Robotically assisted amniotic membrane transplant surgery. JAMA Ophthalmol. 2015;133(2):213–4. https://doi.org/10.1001/jamaophthalmol.2014.4453.

31. Bourcier T, Chammas J, Gaucher D, et al. Robot-assisted simulated strabismus surgery. Transl Vis Sci Technol. 2019;8(3):26. https://doi.org/10.1167/tvst.8.3.26.

32. Bourcier T, Chammas J, Becmeur PH, et al. Robot-assisted simulated cataract surgery. J Cataract Refract Surg. 2017;43(4):552–7. https://doi.org/10.1016/j.jcrs.2017.02.020.

33. Bourcier T, Chammas J, Becmeur P-H, et al. Robotically assisted pterygium surgery: first human case. Cornea. 2015;34(10):1329–30. https://doi.org/10.1097/ICO.0000000000000561.

34. Chammas J, Sauer A, Pizzuto J, et al. Da Vinci Xi robot–assisted penetrating keratoplasty. Transl Vis Sci Technol. 2017;6(3):21. https://doi.org/10.1167/tvst.6.3.21.

35. Mulgaonkar AP, Hubschman JP, Bourges JL, et al. A prototype surgical manipulator for robotic intraocular microsurgery. In: Studies in health technology and informatics. Vol. 142. IOS Press; 2009. p. 215–7. https://doi.org/10.3233/978-1-58603-964-6-215.

36. Bourges J-L, Hubschman J-P, Wilson J, Prince S, Tsao T-C, Schwartz S. Assessment of a hexapod surgical system for robotic micro-macro manipulations in ocular surgery. Ophthalmic Res. 2011;46(1):25–30. https://doi.org/10.1159/000314719.

37. Preceyes B.V. gains CE marking approval for its eye surgery robot. 2019. http://www.preceyes.nl/#latestnews. Accessed 13 Apr 2020.

38. De Smet MD, Stassen JM, Meenink TCM, et al. Release of experimental retinal vein occlusions by direct intraluminal injection of ocriplasmin. Br J Ophthalmol. 2016;100(12):1742–6. https://doi.org/10.1136/bjophthalmol-2016-309190.

39. De Smet MD, Meenink TCM, Janssens T, et al. Robotic assisted cannulation of occluded retinal veins. PLoS One. 2016;11(9):e0162037. https://doi.org/10.1371/journal.pone.0162037.

40. Maberley DAL, Beelen M, Smit J, et al. A comparison of robotic and manual surgery for internal limiting membrane peeling. Graefes Arch Clin Exp Ophthalmol. 2020;258(4):773–8. https://doi.org/10.1007/s00417-020-04613-y.

41. Forslund Jacobsen M, Konge L, Alberti M, la Cour M, Park YS, Thomsen ASS. Robot-assisted vitreoretinal surgery improves surgical accuracy compared with manual surgery: a randomized trial in a simulated setting. Retina. 2019. https://doi.org/10.1097/IAE.0000000000002720.

42. de Smet MD, de Jonge N, Iannetta D, et al. Human/robotic interaction: vision limits performance in simulated vitreoretinal surgery. Acta Ophthalmol. 2019;97(7):672–8. https://doi.org/10.1111/aos.14003.

43. Edwards TL, Xue K, Meenink HCM, et al. First-in-human study of the safety and viability of intraocular robotic surgery. Nat Biomed Eng. 2018;2(9):649–56. https://doi.org/10.1038/s41551-018-0248-4.

44. Rahimy E, Wilson J, Tsao TC, Schwartz S, Hubschman JP. Robot-assisted intraocular surgery: development of the IRISS and feasibility studies in an animal model. Eye. 2013;27(8):972–8. https://doi.org/10.1038/eye.2013.105.

45. Wilson JT, Gerber MJ, Prince SW, et al. Intraocular robotic interventional surgical system (IRISS): mechanical design, evaluation, and master-slave manipulation. Int J Med Robot. 2018;14(1). https://doi.org/10.1002/rcs.1842.

46. Bodner J, Augustin F, Wykypiel H, et al. The da Vinci robotic system for general surgical applications: a critical interim appraisal. Swiss Med Wkly. 2005;135(45–46):674–8. https://doi.org/10.4414/smw.2005.11022.

Part IX

Ancillary Resources for Retinal Surgery

New Ocular Drug Delivery Systems

41

Jennifer J. Kang-Mieler, Kayla M. Rudeen,
Wenqiang Liu, and William F. Mieler

41.1 Introduction

Visual impairment is a global health concern that has a significant impact on patients' physical and mental health. Leading causes of visual impairment are age-related macular degeneration (AMD), diabetic retinopathy (DR), glaucoma, eye inflammations, and retinal vein occlusion (RVO). A significant number of macular abnormalities that require surgery are also quite common in the elderly (macular holes, epiretinal membranes, vitreomacular adhesions, diabetic macular traction detachments, etc.). The number of people affected by visual problems is increasing due to an overall aging population. For example, the projected number of people with age-related macular degeneration in 2020 is 196 million, increasing to 288 million in 2040 worldwide [1]. Likewise, the number of people with DR and vision-threatening DR (VTDR) has been estimated to rise to 191.0 million and 56.3 million, respectively, by 2030 [2]. The total global economic burden of eye diseases and visual impairment was estimated at $3 trillion in 2010 and projected to increase by approximately 20% by 2020 [3].

J. J. Kang-Mieler (✉) · K. M. Rudeen · W. Liu
Illinois Institute of Technology, Chicago, IL, USA
e-mail: kang-mieler@iit.edu; kcascarilla@hawk.iit.edu; wliu43@hawk.iit.edu

W. F. Mieler
University of Illinois at Chicago, Chicago, IL, USA
e-mail: wmieler@uic.edu

With better understanding of ocular physiology and pathology, there have been numerous pharmacological agents such as dexamethasone for ocular inflammation, travoprost and bimatoprost for glaucoma, and anti-vascular endothelial growth factor (anti-VEGF) drugs for ocular neovascularization. The success of treatment not only depends on drug potency and patients' genetic response, but also relies heavily on the delivery method used, tissue barriers, and physicochemical properties of pharmacological agents involved [4]. Ocular barriers and clearance mechanisms make delivering therapeutic doses to the posterior segment of the eye challenging. These barriers include the ocular surface that causes drug loss from lacrimal fluid, lacrimal fluid-eye barriers that limit drug absorption, and blood-ocular barriers that prevent distribution of drug [5].

The eye offers multiple entry routes through which pharmacological agents can be delivered, including topical, systemic, periocular, and intraocular routes [4]. Although the optimal dose and delivery routes can usually be chosen for each drug, an issue facing most existing treatment regimen is frequent administration due to fast clearance, low bioavailability, or low stability of pharmacological agents [4, 5]. This frequent application may increase risks of complications, lower patient compliance, and cause significant socioeconomic burden on healthcare systems [4]. Therefore, designing and developing new ocular drug delivery systems (DDSs) that can achieve

controlled and extended drug release to targeted location, improve drug bioavailability, and preserve drug stability over both manufacture and release is in great demand. It was estimated that the total current market size for sustained ocular drug delivery system is worth more than $9.3 billion and continuously growing [6].

Targeted and sustained ocular drug delivery is a rapidly developing area and has great potential to achieve more effective treatment regimen for most eye diseases. This chapter presents current advancements in ocular drug delivery systems, classified into small-molecule and macromolecular biological drugs (particularly protein therapeutics). An emphasis is on systems currently in clinical studies and promising to be available on the market.

41.2 Drug Delivery Systems for Small-Molecule Drugs

Small molecules are molecules with a molecular weight less than 900 daltons [7]. Small molecules have a short half-life requiring frequent dosing and can result in poor patient compliance. Small-molecule ocular drugs, such as dexamethasone for inflammation; triamcinolone acetonide (TA) for uveitis, retinal vein occlusion (RVO), and diabetic macular edema (DME); bimatoprost for glaucoma and ocular hypertension; travoprost for glaucoma and ocular hypertension; and fluocinolone acetonide (FA) for glaucoma and ocular hypertension, are commonly prescribed to combat posterior segment diseases and symptoms.

Small-molecule drugs can be challenging to delivery to the posterior segment due to the ocular barriers and clearance mechanisms of the eye previously mentioned. Topical DDSs for small molecules, such as ophthalmic solutions and eye drops, can circumvent these challenges due to their ability to diffuse across many ocular barriers. Since they diffuse easily throughout the eye, however, small-molecule DDSs can be challenging to localize; additionally, the delivery is limited by the clearance mechanisms of the eye and administering a high initial dose to counter the clearance and diffusion of drug may become

toxic [8]. Furthermore, most treatments for posterior segment disease cannot be systemically administered since they will not reach a therapeutic dose within the eye itself [8, 9]. Intraocular injections may also be used to bypass some of these barriers, but the invasiveness of injection increases the risks of complication, such as retinal detachment, retinal hemorrhage, endophthalmitis, and increased ocular pressure [10–12]. A minimally invasive, localized, controlled, and extended release of small molecules would provide the safest and most effective DDS.

With the growing number of patients with posterior segment diseases (both medical and surgical), an increasing number of systems are being developed that allow for more effective treatment. Advances in DDSs address current issues with delivering small molecules to the posterior segment. Microneedles, hydrogels, topical treatment, injectable substances, and implants will be addressed in the following sections. Table 41.1 summarizes small-molecule DDSs currently in clinical trials or recently approved by the U.S. Food and Drug Administration (FDA).

41.2.1 Ocular Implants

One of the main benefits of solid ocular implants is that they eliminate the need for repetitive treatments by administering drug for extended periods. EyePoint Pharmaceuticals developed a solid polymer implant called Durasert™. This implant can release small molecules for up to 3 years. The implant is only 3.5 mm in length and 0.37 mm in diameter, allowing it to be injected through a needle. The Durasert™ technology has been approved by the FDA for the following products: Iluvien® (fluocinolone acetonide intravitreal implant), Retisert® (fluocinolone acetonide intravitreal implant), and Vitrasert® (ganciclovir). The properties of this system allow for the customization of release duration, linear release kinetics, and high drug loading [13, 14].

Allergan has also developed Bimatoprost SR, a biodegradable polylactic intracameral implant that releases drug for 4–6 months for the treatment of open-angle glaucoma and ocular hyper-

Table 41.1 Summary of clinical drug delivery systems for small-molecule drugs

Product name company	Target disease	Therapeutic agent(s)	Mechanism of action	Release duration	Developmental stage
Microneedle (Clearside Biomedical)	Uveitis RVO DME	Triamcinolone acetonide	Suprachoroidal injection using a microneedle	Bolus injection every 3 months	Phase 3 Phase 3 Phase 2
Bimatoprost ring (Allergan)	Open-angle glaucoma and ocular hypertension	Bimatoprost	External application of a silicone ring with an inner polypropylene structure	Up to 6 months	Completed phase 2 study that had similar results to eye drops but less adverse events
Hydrogel technology platform (Ocular Therapeutix)	Postsurgical pain and inflammation Glaucoma and ocular hypertension Retinal neovascular diseases	Dexamethasone Travoprost (PGA) Tyrosine kinase inhibitor	Bioabsorbable hydrogel plug or depot with capacity for controlling release rate of variety of drugs by modulating hydrogel pore size, and duration of hydrolysis	Up to 30 days	Dextenza® received FDA approval in 2019 Phase 1 for OTX-TIC Phase 1 for OTX-TKI
Dexycu® (EyePoint Pharmaceuticals)	Inflammation associated with cataract surgery	Dexamethasone	Intracameral injection that uses citric acid ester/Verisome® technology	21 days	FDA approval in early 2018
Bimatoprost SR (Allergan)	Open-angle glaucoma and ocular hypertension	Bimatoprost	Degradable, intracameral implant that is injected into the anterior chamber	4–6 months	NDA accepted in mid-2019
GB-102 (Graybug Vision)	nAMD, DME, RVO	Sunitinib malate	Intravitreal injection of PLGA nanoparticles	Up to 6 months	Started phase 2 trial
Durasert™ (EyePoint Pharmaceuticals)	Posterior uveitis, intermediate uveitis, panuveitis	Fluocinolone acetonide	Injectable, dexamethasone intraocular suspension	3 years	FDA approval in late 2018
ENV515 Travoprost XR (Envisia Therapeutics)	Glaucoma and ocular hypertension	Travoprost	Biodegradable intracameral implantation made from PRINT© technology	6 months	Completed phase 2 study that lowered IOP similarly to ophthalmic solution

tension. Bimatoprost SR is injected directly into the anterior chamber, allowing a much lower loading dose as compared to ophthalmic bimatoprost 0.03% solution. Furthermore, the elimination of total drug exposure improves the safety of treatment by leading to fewer adverse events. After a completed phase 3 study that showed a similar reduction in IOP by 30% as compared to daily topical treatment, the new drug application

(NDA) for Bimatoprost SR was approved in mid-2019 [15, 16].

Envisia Therapeutics created ENV515 Travoprost, another degradable polylactic intracameral implant that showed promising results as a treatment for glaucoma and ocular hypertension. A phase 2 study showed that its release of travoprost for 6 months lowers IOP similarly to ophthalmic solution [17, 18].

41.2.2 Injectable Micro/ Nanoparticles

Due to the wide availability of different materials that can be tailored for specific drugs and applications, micro/nanoparticles have also been an attractive drug delivery method for therapeutic agents. Synthetic, biodegradable polymers are commonly used to develop DDSs due to their biocompatibility, adjustable degradation, and reproducible release [19]. While intravitreal injections are more invasive than other administration routes, they allow for more direct delivery to the targeted site with well-controlled doses.

Poly(D,L-lactate-*co*-glycolide) (PLGA) has evolved into most widely used copolymer for making micro- and nanoparticles since its approval by FDA for medical and biological applications. Graybug Vision's GB-102, which recently started phase 2 clinical trials, consists of sunitinib malate-loaded poly(lactic-*co*-glycolic acid) (PLGA) microspheres that are injected into the inferior vitreous for the treatment of neovascular AMD (nAMD), diabetic macular edema (DME), and RVO. Administering by intravitreal injection allows for a localization of the microspheres, which does not disrupt vision since they are injected inferiorly. The PLGA microspheres allow for controlled, extended release of drug and high drug loading. Thus, the annual number of injections could be reduced to twice per year [20]. On the other hand, PLGA microspheres have some disadvantages such as low drug encapsulation and generation of acidic environments upon degradation [4].

Dexycu®, recently approved by the FDA, is an intracameral injection using Verisome® technology to deliver dexamethasone for 21 days for inflammation associated with cataract surgery. Developed by EyePoint Pharmaceuticals, Verisome® technology is a drug delivery system that has a wide range of applications including peptides, small molecules, and proteins. This system can be formulated into a biodegradable solid, gel, or liquid substance that provides a controlled, extended release of drug. It serves as an alternative to corticosteroid drops post-cataract surgery [21]. The Verisome® technology has application for delivery to the posterior segment.

41.2.3 Injectable Hydrogels

Hydrogels have become one of the most useful materials for biomedical applications including drug delivery, tissue-engineering scaffolds, and cell transplantation since their development in 1960s [22]. Their high water content and mild preparation conditions make them inherently good candidates as drug delivery carriers for cells and many labile therapeutic agents such as small molecules, peptides, proteins, and nucleic acids [23–25]. Some hydrogels can modulate their gelation behavior upon changes of environment, such as temperature, pH, and ionic strength [26, 27]. This makes them injectable through small-gauge needles as either aqueous solution or liquid-like form, and then they solidify into hydrogels at physiological conditions [26, 27]. These injectable hydrogels are easily fabricated and have gained significant interests as drug delivery candidate into small spaces within the body, specifically the ocular structures.

Ocular Therapeutix's hydrogel technology is a versatile platform employed to create sustained-release therapies, including OTX-TP, OTX-TIC, and OTK-TKI, that may expand treatment options across multiple ocular conditions. The easy-to-inject, bioresorbable hydrogel has an adjustable and consistent release rate [28, 29]. OTX-TP, which releases travoprost on the ocular surface for up to 90 days, is recruiting patients for its phase 3 clinical trial [30]. Similarly, OTX-TIC releases travoprost for 3–4 months for the treatment of glaucoma and ocular hypertension. Preclinical studies in beagles have demonstrated sustained intraocular pressure lowering and maintenance of drug levels in the aqueous humor [31]. Lastly, OTX-TKI is administered via intravitreal injection and releases tyrosine kinase inhibitors (TKIs) for 6 months. Preclinical studies in Dutch belted rabbits demonstrate that a therapeutic level of drug was maintained for up to 12 months with efficacy in a VEGF-induced vascular leakage model [32]. While this technology seems effective, safety and biocompatibility need to be further investigated.

Huu et al. have developed a light-responsive hydrogel that releases nintedanib-loaded nanopar-

ticles for the treatment of macular degeneration and DR for up to 30 weeks [33]. This system allows for a more controlled release of drug than bolus injections since drug release is triggered by UV exposure. Preliminary studies have shown that the light-sensitive nanoparticles are safe and biocompatible [33]. Further research must be conducted before starting clinical trials.

41.2.4 Ocular Inserts

Eye drops are commonly prescribed due to the ease of use and noninvasive qualities. Even when patients follow dosage regimens, they are less effective than other routes due to low absorbance and fast clearance within the eye. DDSs that increase the contact time of drug with the cornea allow for better delivery. Figure 41.1 shows Allergan's bimatoprost ring, an externally applied ring that releases for up to 6 months for the treatment of open-angle glaucoma and ocular hypertension. It consists of an outer silicone ring that covers a polypropylene support structure shown in Fig. 41.2. The concentration gradient allows drug to diffuse passively from the silicon matrix to the tear film. A completed phase 2 study showed similar results to eye drop treatment [15, 16]. The bimatoprost ring was able to reduce IOP with clinical relevance over less than 19 months when applied every 6 months [15, 16, 34]. A major challenge with this design is determining proper loading dose of drug and achieving a controlled drug release due to the variability of the ocular surface conditions.
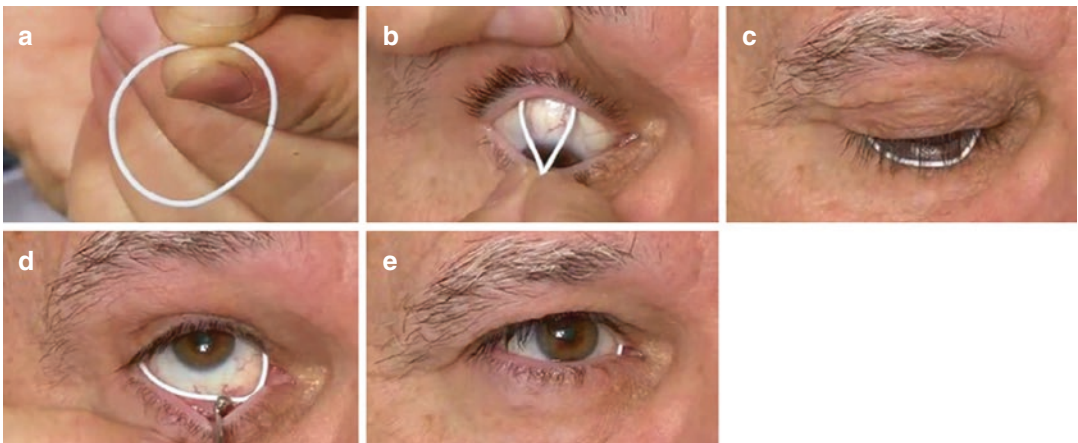
Fig. 41.1 External application of bimatoprost ring onto the upper fornix [34]

Fig. 41.2 Structure of bimatoprost ring [34]

Cross-sectional thickness = 1.0mm

24 to 29 mm Diameter

Support Structure

Silicone-Bimatoprost Matrix
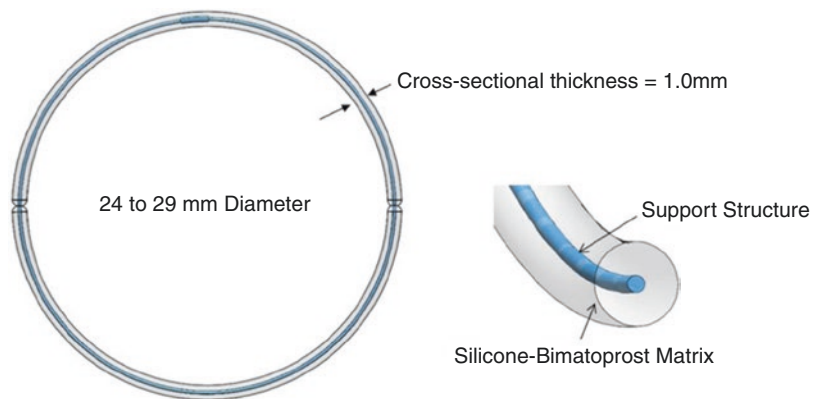
Ocular Therapeutix's resorbable hydrogel technology, as previously mentioned, is also used as an ocular insert. Dextenza® releases dexamethasone on the ocular surface for up to 30 days as a treatment for postsurgical pain and inflammation [28, 29]. It is placed in the canaliculus through the punctum, activated by moisture, and reabsorbed in the nasolacrimal system [35]. In mid-2019, the FDA accepted the resubmission of the NDA for Dextenza®.

41.2.5 Microneedles

Micron-size needles, or microneedles, enable minimally invasive delivery of free or encapsulated drug. Clearside Biomedical developed a microneedle and injector that administers a suprachoroidal injection of corticosteroid triamcinolone acetonide (CLS-TA), which is Clearside Biomedical's proprietary suspension of TA. It is used for the treatment of uveitis, RVO, and DME. The injector allows for consistent insertion of microneedle into the suprachoroidal space. Thus, this method reduces the risks commonly associated with intravitreal injections, including the potential for retinal damage [36]. Due to the small surface area of the microneedle, this system is limited to small molecules and microneedles cannot always deliver a therapeutic dose. Currently, the use of microneedles for the treatment of uveitis is undergoing a phase 3 clinical trial. Around 46.9% of patients receiving treatment had an increase in visual acuity from baseline as compared to only 15.6% of the control patients [36, 37]. As for safety, around 11.5% of treated patients had increased IOP but the control patients did not have any increases. Clearside Biomedical plans to submit a new drug application to the FDA and other regulatory agencies outside of the USA by the end of 2019 [36]. Clearside Biomedical is also conducting a phase 3 clinical trial for a combination therapy of suprachoroidal CLA-TA with one or two intravitreal injections of anti-VEGF [37]. Reported in a phase 2 study, the combination treatment group had a 61% reduction in the number of re-treatments as compared to the group treated with aflibercept alone [38].

With the increasing demand for effective treatments, there are many microneedle DDSs in preclinical stages for the delivery of small molecules. An example of microneedle in preclinical stages includes a fenestrated microneedle made from titanium deep-reactive ion etching developed by Khandan et al. [39]. The design of the fenestrated needle increases the surface area, allowing for a higher dose of drug. It may also allow for the delivery of some larger molecules [39]. Another example is a rapidly dissolving microneedles fabricated from polyvinylpyrrolidone (PVP) designed by Thakur et al. [40]. Moreover, the rapidly dissolving microneedle is less invasive than previously developed microneedles. It also has the potential to deliver macromolecules [40].

41.3   DDS for Macromolecular Biological Drugs

With the rapid progress in biotechnology in the last several decades, there has been a growing number of macromolecular biological drugs such as peptides, proteins, and nucleic acids developed for prevention, diagnosis, or treatment of a variety of diseases [41]. Ophthalmology is one field that has benefited enormously from the development of biological therapeutics. For example, the introduction of anti-VEGF therapy has revolutionized the clinical management of ocular neovascular diseases and eventually evolved into the standard of care for wet AMD and PDR [42–44]. Despite its great success, a major challenge of anti-VEGF drugs and other protein therapeutics is their fast clearance and relatively short half-life [10, 45]. Therefore, frequent and repeated intravitreal (IVT) injections (every 4–6 weeks) are required for management of chronic eye diseases. However, these repeated IVT injections usually present increased risk of potential complications including endophthalmitis, retinal detachment, intravitreal hemorrhage, and cataract [10, 12]. Additionally, the significant socioeconomic burden upon patients, families, and healthcare systems cannot be ignored. In 2017, it was estimated that there were 22.3 million IVT injections performed globally and 5.4 million injections in the

Table 41.2 Summary of clinical drug delivery systems of macromolecular biological drugs

| Product name company	Target disease	Therapeutic agents	Mechanism of action	Release duration	Developmental stage
Refillable rigid port delivery system (Genentech)	Wet AMD	Anti-VEGFs (ranibizumab)	A refillable, nonbiodegradable reservoir intravitreal implant with a diffusion-control mechanism	4–6 months, on-demand refill	Phase 2
OTX-IVT (Ocular Therapeutix and Regeneron)	Wet AMD and other serious retinal neovascular diseases	Anti-VEGFs (aflibercept)	Intravitreal injection of bioabsorbable hydrogel with capacity of controlling release by modulating hydrogel pore size and hydrolysis	4–6 months	Collaboration with Regeneron for ongoing in vitro and in vivo study
Encapsulated cell technology (Neurotech)	Retinal degenerative diseases like AMD, glaucoma, RP and MacTel	CNTF	Genetically engineered NTC-200 cell line capable of continually releasing CNTF	Over 2 years	NT-501 for treatment of MacTel in phase 2
Posterior micropump (Replenish Inc.)	Retinal diseases	Various (ranibizumab)	Wirelessly controlled micropump implant that releases drug through a one-way valve	3 months	Phase 3

USA alone [12]. Thus, a sustained DDS for protein drugs like anti-VEGF is greatly needed to reduce the frequency of IVT injections and the associated societal burdens.

Recent years have seen a variety of drug delivery systems being developed for controlled and extended delivery of anti-VEGF and other protein drugs in the form of ocular implants, cell-based systems, injectable nano/microparticles, injectable hydrogels, and composite systems [4]. However, only a limited number of systems are advancing in clinical trials. The main challenge of these DDSs is maintaining a sustained therapeutic level of protein bioactivity during both manufacture and release stages, since biological drugs like proteins rely heavily on their complex structural integrity to perform their biological activities (e.g., neutralization of a cytokine or a growth factor). Numerous stress factors during DDS fabrication, release, and degradation such as presence of catalyst, changes in temperature and pH, and polymer-induced aggregation/ adsorption [5, 46, 47] can contribute to loss of protein bioactivity. In this section, some of the most promising ocular DDSs for biological drugs, both in clinical studies and preclinical studies, are discussed. And Table 41.2 summarizes the DDSs currently in clinical studies.

41.3.1 Ocular Implants

Refillable rigid port delivery system (RPDS) is an intravitreal implant that is the size of a grain of rice (Fig. 41.3). It consists of a subconjunctival refill port outside of the eye and an intravitreal reservoir preloaded with drug. It was first developed by Forsight Vision4, and then licensed exclusively to Genentech as the platform offering ranibizumab (Lucentis®) in a sustained-release format. One of the biggest advantages of RPDS is that on-demand refills can be performed in an in-
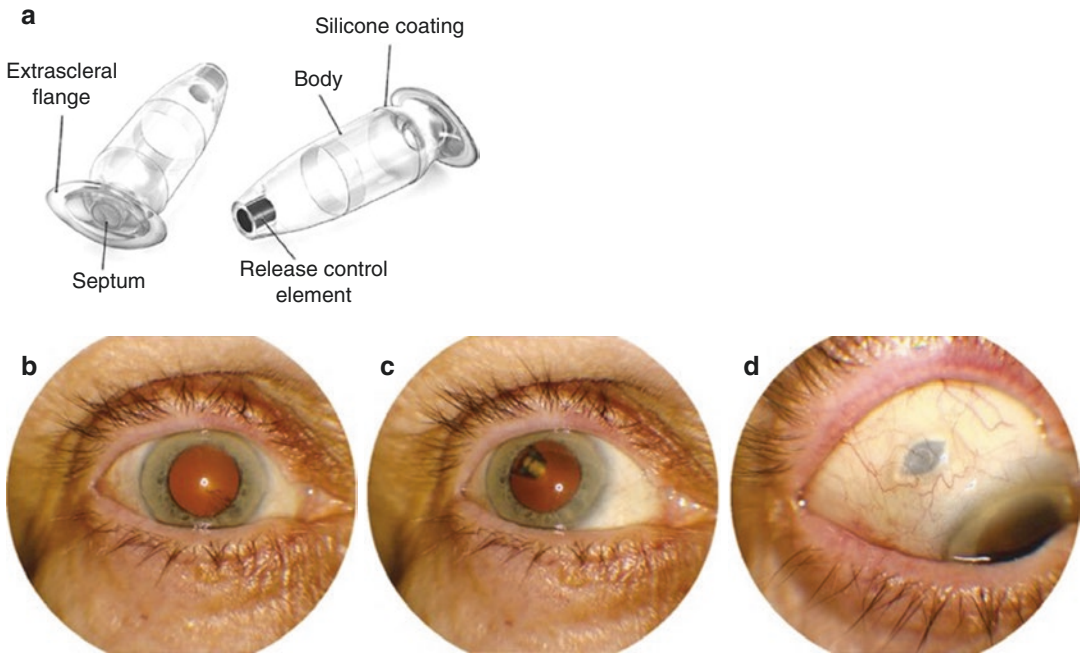
Fig. 41.3 The ranibizumab refillable port delivery system (RPDS) [49]

office procedure using a customized exchange needle. The replacement with new drug not only maintains drug potency, but also provides reproducible and predictable drug release after each refill. However, since the drug reservoir is nonbiodegradable, both surgical implantation and removal are required which may increase risks of complications [48]. Recent phase 2 data showed that the median time to refill was 8.7, 13.0, and 15.0 months in PDS 10 mg/mL, PDS 40 mg/mL, and PDS 100 mg/mL [49]. The data also demonstrated that the PDS 100 mg/mL arm had visual and anatomic outcomes comparable with monthly intravitreal ranibizumab group based on the adjusted mean BCVA [49].

Replenish Inc.'s posterior micropump (PMP) system is a mini programmable drug pump fabricated using principles of microelectromechanical system (MEMS) technology. The pumping mechanism is based on electrolysis and the pump includes a drug refill port as well as a check valve to control drug delivery [50]. Recently, the system has been investigated for safety and surgical feasibility to deliver ranibizumab for treatment of diabetic macular edema (DME) in a phase 1

study. It was reported that the PMP was safely implanted subconjunctivally in 11 diabetic patients with DME, and capable of delivering a programmable microdose of ranibizumab into the vitreous cavity for 90 days [51].

Recently, a nanoporous film device has been developed by Zordera Inc. for controlled delivery of anti-VEGF for ocular neovascularization (Fig. 41.4). This intravitreal implant consists of capsule, preloaded with drug pellet, sandwiched between a nanoporous thin film and a second impermeable thin-film layer made from biodegradable polycaprolactone (PCL). The device is only 40 μm thick, which allows intravitreal implantation through a syringe. The pore size can match the drug molecule diameter to achieve sustained, zero-order release over the course of several months before polymer complete degradation. Recent studies have established in vitro release of ranibizumab for 16 weeks, and safety and in vivo release on New Zealand rabbit model for 3 months [52].

Encapsulated cell technology (ECT) is essentially a cell-based delivery system and has been proven to be a very effective strategy for long-

Fig. 41.4 Schematic diagram showing the configuration of Zordera's nanoporous film device
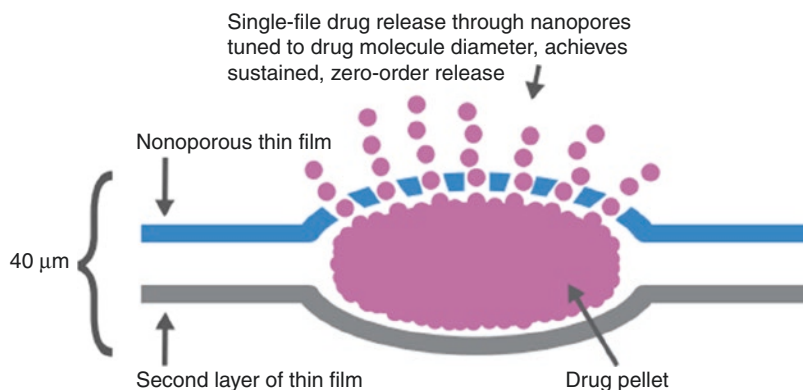
term delivery of biologically active proteins and polypeptides to both central nervous system (CNS) and retina [53]. Neurotech Pharmaceuticals, Inc. has been developing its ECT platform targeting retinal degenerative diseases like AMD, glaucoma, retinitis pigmentosa, and macular telangiectasia (MacTel). The basis of this ECT platform is the genetically engineered human retinal pigment epithelial cell line, known as NTC-200 cell line, capable of continuously secreting ciliary neurotrophic factor (CNTF). The cells are packaged into a nonbiodegradable polymeric capsule device consisting of internal scaffolding and a semipermeable exterior membrane, which allows for controlled cell growth and continuous protein production and delivery for over 2 years. Despite its invasive implantation and surgical removal procedure, this system is theoretically versatile for different cell lines and protein therapeutics with controlled, continuous, and sustained release [54]. Neurotech's NT-501 ECT for CNTF delivery is undergoing phase 2 clinical studies for the treatment of MacTel and glaucoma [55, 56].

Although the above ocular implant systems have shown promising results in preclinical studies and are currently advancing to/in clinical stages, the invasive implantation and sometimes surgical removal procedures (if nondegradable material used) required for these devices can increase risks of complications. Therefore, injectable delivery systems such as micro/nanoparticles, hydrogels, and particle-hydrogel composite systems have emerged recently as promising strategies for controlled delivery of protein drug in a minimally invasive manner.

41.3.2 Injectable Micro/Nanoparticles

Since most macromolecular biological drugs like protein are hydrophilic, they can usually be encapsulated into polymeric capsules by the solvent/evaporation method from emulsifications such as water-in-oil-in-water (w/o/w) or solid-in-oil-in-water (s/o/w) emulsions [19]. To preserve the protein stability during manufacture, additional protein stabilizers like albumin, sugars, and surfactant are commonly employed. After identifying bovine serum albumin (BSA) as a major protective agent for bevacizumab during emulsification procedure, Varshochian et al. developed an albuminated PLGA nanoparticle for sustained delivery of bevacizumab [57]. The nanoparticles were fabricated by w/o/w double emulsion using albumin as a stabilizer, with a size of ~200 nm. Their recent studies in rabbits showed that vitreous concentration of bioactive bevacizumab was maintained above 500 ng/mL for about 8 weeks after single intravitreal injection [58]. Bevacizumab-loaded PLGA microparticles were also fabricated using s/o/w method by Zhou Ye et al. [59]. The size of particles was 2–7 μm. A significantly prolonged half-life of bevacizumab in vitreous (9.6 days) and aqueous humor (10.2 days) has been achieved in New Zealand albino rabbits, compared to 3.91 days and 4.1 days for free drug, respectively [59]. However, low protein encapsulation efficiency (usually <60% for microparticles and <30% for nanoparticles, respectively), high initial bursts (20–50% of encapsulated protein in the first

24 h), incomplete release of the entrapped proteins, and loss of protein drug bioactivity during release are major challenges for PLGA particulate systems [19, 60, 61].

Among the above challenges, preserving protein drug stability and bioactivity during manufacture and release remains the biggest challenge for PLGA micro/nanoparticle systems. Protein stability is mainly affected by moisture-induced aggregation caused by initial fast water uptake, nonspecific protein adsorption to polymer surface, and covalent/non-covalent aggregation due to acidic microenvironment after polymer degradation [5, 47]. Although stabilizers are added to counter these stress factors, their primary effects are during manufacture and initial release. Significant low protein bioactivity is usually seen after 2–3 months of release [62–64]. Recent studies showed that more hydrophilic polymers such as PEG-based PLGA diblock/triblock copolymers, alginate, and polyethylene glycol-polybutylphthalate (PEG-PBT) may improve release and protein bioactivity during release [65–67]. For example, Adamson et al. investigated different formulations of their PEG-PBT microparticles (based on PEG length, PEG:PBT ratio, and water/polymer ratio) for sustained release of their newly designed anti-VEGF dual antibody [66]. It was reported that more than 50% of protein bioactivity can be maintained throughout 6 months of release in vitro. Inhibition of laser-induced choroidal neovascularization by single intravitreal injection of drug-loaded microparticles was also found in primates [66]. Despite progress in polymers, a more important concern for these injectable particulate systems is that migration of these particles after injection into the eye can cause faster clearance by phagocytes, ocular lymphatic, and vascular circulation and sometimes even lead to complications such as glaucoma and ocular inflammation [66, 68]. This movement of particles in the eye may limit their applications as sustained DDS by IVT injections.

41.3.3　Injectable Hydrogels

Ocular Therapeutix's injectable and bioresorbable hydrogel technology is recently also seeking application for sustained anti-VEGF delivery. They are collaborating with Regeneron (manufacturer for aflibercept) to investigate the feasibility of OTX-IVT for sustained delivery of aflibercept for 4–6 months targeting wet AMD and other serious retinal neovascular diseases [69].

Thermoresponsive hydrogels have been particularly attractive candidates as injectable ocular DDS in a minimally invasive manner because they used temperature change as the trigger for their gelation and changes in swelling. At room temperature, these hydrogels either are in solution form or have a fluidlike consistency. After injection into the eyes, they either in situ cross-link or solidify into a solid form upon reaching the body temperature [26, 27]. These hydrogels usually have a sharp volume phase transition temperature at ~30–33 °C, which makes them ideal candidates for localized and extended drug delivery. Recently, Kang-Mieler et al. have developed a poly(N-isopropylacrylamide) (PNIPAAm)-based thermoresponsive hydrogel by cross-linking PNIPAAm with poly(ethylene glycol) diacrylate (PEG-DA) or poly(ethylene glycol)-co-(L-lactic acid) diacrylate (PEG-PLLA-DA) through free radical polymerization [70, 71]. It was shown that this system is capable of localized release of proteins such as bevacizumab and ranibizumab for about a month and induced no long-term effects on retinal function [71, 72]. Additionally, controlled degradation and complete release from these hydrogels were achieved by incorporating biodegradable copolymer and other additives [71]. Other than PNIPAAm, thermoresponsive copolymer poly(2-ethyl-2-oxazoline)-b-poly(ε-caprolactone)-b-poly(2-ethyl-2-oxazoline) (PEOz-PCL-PEOz) was also synthesized and used to make biodegradable thermoresponsive hydrogels for extended release of bevacizumab by Wang et al. [73]. Good in vitro and in vivo biocompatibility was achieved using human retinal pigment epithelial cell line and rabbit for 2 months, respectively [73]. An extended release of bioactive bevacizumab from hydrogels for 1 month in vitro was established, although no in vivo efficacy data on animal models have been reported [73]. Poly(ethylene glycol)-poly-(serinol hexamethylene urethane), or ESHU, thermoresponsive hydrogel was developed by Rauck et al. to encapsulate and extend the

delivery of bevacizumab after IVT injection into New Zealand white rabbit eyes [74]. It was reported that the system was easily injected through a 31-gauge needle with a force required less than for a 1% solution of hyaluronic acid, a commonly injected ophthalmic material. The system was proved to be biocompatible in rabbit eyes and a significant higher bioactive bevacizumab concentration was detected in eyes receiving bevacizumab-loaded hydrogel IVT injections than those receiving the bolus injections [74].

Instead of preforming a hydrogel with phase transition properties as injectable DDS, alternative strategy is developing in situ-forming hydrogels, which usually consist of polymers in aqueous solution form and are spontaneously chemically or physically cross-linked into solid hydrogels upon physiological conditions after injection [26]. Loading with adjustable drug dosage could usually be easily achieved for these hydrogels since most protein drugs are hydrophilic and can be completely dissolved into the aqueous precursor at desirable concentrations. In addition, since usually no initiator is necessary, better protein stability and biocompatibility are anticipated [26]. Recently, a vinyl sulfone-functionalized hyaluronic acid (HA-VS)-thiolated dextran (Dex-SH) in situ-forming hydrogels have been developed by Chau et al. for controlled delivery of bevacizumab [75]. The bevacizumab-containing polymer solution was injected into rabbit eyes and then chemically cross-linked into transparent hydrogels at physiological condition. Binocular indirect ophthalmoscope (BIO) images, full-field electroretinogram (ERG), and histology showed that the hydrogels were safe for rabbit eyes after injections. It was also promising that a concentration of bioactive bevacizumab, about 10^7 times higher than bolus injection, was reportedly maintained 6 months after injection [75].

Although injectable hydrogels are very promising vehicles for use in developing new extended ocular DDSs, challenges such as (1) difficulty sterilizing, especially when biomolecules such as proteins are encapsulated [76, 77]; (2) potential for toxic effects caused by residual initiators after polymerization [78]; and (3) most-of-the-time relatively faster release of protein drugs (less than

2–3 months) due to their inherently higher water content [73–75], have limited their application as extended ocular DDS for protein therapeutics.

41.3.4 Composite DDSs

As discussed before, although injectable polymeric micro/nanoparticles usually can provide controllable and sustained drug release through adjustments made to their polymer composition, difficulties to localize them to the injection site in the eyes can be problematic for long-term release applications. Due to their either thermoresponsive or in situ gelation properties, injectable hydrogels can be good candidates as second carrier for micro/nanoparticles to obtain localized and extended drug release after injection [4]. This composite DDS may offer advantages over both particles and hydrogels alone by further extending release and reducing initial burst. In addition, both proteins and small molecules can be encapsulated into particles and hydrogels in a variety of ways to enhance delivery potential. More recently, this strategy has been validated by Kang-Mieler et al. who have combined their injectable PNIPAAm-based thermo-responsive hydrogel with PLGA microspheres to create a microsphere-hydrogel composite DDS [79–81]. Their DDS was able to encapsulate ranibizumab or aflibercept and release them in a controlled manner for ~200 days [80, 81]. In vitro bioactivity during release and in vivo efficacy in laser-induced CNV rodent model have been established [64, 82]. By controlling the amounts of microspheres suspended within the hydrogel, total amount of drug delivered to the retina can be controlled without changing the volume and injectability of the system. More recently, by introducing hydrolytically degradable polymer poly(ethylene glycol)-*co*-(L-lactic acid) diacrylate to PNIPAAm-based hydrogels, they were able to make their hydrogel also biodegradable. It was found that this microsphere-hydrogel DDS was more biocompatible and at the same time capable of releasing bioactive aflibercept for 6 months in vitro [64].

41.4   Conclusions

Due to the increased number of patients afflicted by a variety of ocular disorders, sustained DDSs providing better treatment and management of the medical and surgical diseases previously discussed in this chapter are currently in high clinical demand. Comparing to traditional methods of ocular drug delivery such as eye drops, periocular/intraocular injections, and systemic delivery, sustained DDSs are designed to encapsulate and deliver the specific therapeutic agents to the target sites for an extended period of time at a therapeutic level without any detriment to the drug. Since most of the small-molecule ophthalmic drugs are more stable than protein therapeutic drugs in terms of maintaining activity during DDS manufacture and release, there are numerous DDSs for small-molecule drugs available in the market or advancing in clinical studies. However, utilization of full clinical potential of novel sustained DDSs for protein drug (e.g., anti-VEGF) has been limited by protein instability during DDS manufacture and release. Overall, with the advancement in drug discovery and development, biomaterials, and microfabrication techniques, novel sustained DDSs for a variety of drugs targeting for ocular diseases are expected to grow fast and achieve better management and control of ocular diseases in future.

References

1. Wong WL, Su X, Li X, Cheung CM, Klein R, Cheng CY, Wong TY. Global prevalence of age-related macular degeneration and disease burden projection for 2020 and 2040: a systematic review and meta-analysis. Lancet Glob Health. 2014;2:106–16.
2. Ting DS, Cheung GC, Wong TY. Diabetic retinopathy: global prevalence, major risk factors, screening practices and public health challenges: a review. Clin Exp Ophthalmol. 2016;44:260–77.
3. Gordois A, Cutler H, Pezzullo L, Gordon K, Cruess A, Winyard S, Hamilton W, Chua K. An estimation of the worldwide economic and health burden of visual impairment. Glob Public Health. 2012;7:465–81.
4. Kang-Mieler JJ, Dosmar E, Liu W, Mieler WF. Extended ocular drug delivery systems for the anterior and posterior segments: biomaterial options and applications. Expert Opin Drug Deliv. 2017;14:611–20.
5. Radhakrishnan K, Sonali N, Moreno M, Nirmal J, Fernandez AA, Venkatraman S, Agrawal R. Protein delivery to the back of the eye: barriers, carriers and stability of anti-VEGF proteins. Drug Discov Today. 2017;22:416–23.
6. PR Newswire. Ocular drug delivery market to be worth US$18.124 billion by 2025. 2017. https://www.prnewswire.com/news-releases/ocular-drug-delivery-market-to-be-worth-us18124-billion-by-2025-manufacturers-collaborating-with-hospitals-to-bolster-positions-632232553.html. Accessed 7 Nov 2019.
7. Yang NJ, Hinner MJ. Getting across the cell membrane: an overview for small molecules, peptides, and proteins. In site-specific protein labeling. New York: Humana Press; 2015. p. 29–53.
8. Urtti A. Challenges and obstacles of ocular pharmacokinetics and drug delivery. Adv Drug Deliv Rev. 2006;58:1131–5.
9. Del Amo EM, Rimpelä AK, Heikkinen E, Kari OK, Ramsay E, Lajunen T, Schmitt M, Pelkonen L, Bhattacharya M, Richardson D, Subrizi A. Pharmacokinetic aspects of retinal drug delivery. Prog Retin Eye Res. 2017;57:134–85.
10. Peyman GA, Lad EM, Moshfeghi DM. Intravitreal injection of therapeutic agents. Retina. 2009;29:875–912.
11. Bande MF, Mansilla R, Pata MP, Fernandez M, Blanco-Teijeiro MJ, Pineiro A, Gomez-Ulla F. Intravitreal injections of anti-VEGF agents and antibiotic prophylaxis for endophthalmitis: a systemic review and meta-analysis. Sci Rep. 2017;7:18088.
12. Williams GA, Mich RO. IVT injections: health policy implications. Rev Ophthalmol. 2014. https://www.reviewofophthalmology.com/article/ivt-injections-health-policy-implications.
13. Callanan DG, Jaffe GJ, Martin DF, Pearson PA, Comstock TL. Treatment of posterior uveitis with a fluocinolone acetonide implant: three-year clinical trial results. Arch Ophthalmol. 2008;126:1191–201.
14. Haghjou N, Soheilian M, Abdekhodaie MJ. Sustained release intraocular drug delivery devices for treatment of uveitis. J Ophthalmic Vis Res. 2011;6:317–29.
15. Chen MY, Sall KN, Tepedino M, McLaurin E, Olander K, Wirta D, Flynn W, Walker G, Ling J, Yang J, Goodkin M. Patient-reported outcomes of bimatoprost ocular ring in an open-label extension study in patients with open-angle glaucoma or ocular hypertension. Invest Ophthalmol Vis Sci. 2018;59:9,1231.
16. Lee SS, Almazan A, Decker S, Zhong Y, Ghebremeskel AN, Hughes P, Robinson MR, Burke JA, Weinreb RN. Intraocular pressure effects and mechanism of action of topical versus sustained-release bimatoprost. Transl Vis Sci Technol. 2019;8:15.
17. Mansberger SL, Conley J, Verhoeven RS, Blackwell K, Depenbusch M, Knox T, Walters TR, Ahmad I, Yerxa BR, Navratil T. Interim analysis of low dose ENV515 travoprost XR with 11 month duration followed by dose escalation and 28 day efficacy evaluation of high dose ENV515. Invest Ophthalmol Vis Sci. 2017;58:2110.

18. ClinicalTrials.gov [Internet]. Bethesda (MD): National Library of Medicine (US). 2000 Feb 29. Identifier NCT02371746, safety and efficacy of ENV515 travoprost extended release (XR) in patients with bilateral ocular hypertension or primary open angle glaucoma; 2015 Feb 20 [cited 2019 Nov 5]; [about 4 screens]. https://clinicaltrials.gov/ct2/show/record/NCT02371746?term=ENV515&rank=1.

19. Herrero-Vanrell R, Bravo-Osuna I, Andres-Guerrero V, Vicario-de-la-Torre M, Molina-Martinez IT. The potential of using biodegradable microspheres in retinal diseases and other intraocular pathologies. Prog Retin Eye Res. 2014;42:27–43.

20. ClinicalTrials.gov [Internet]. Bethesda (MD): National Library of Medicine (US). 2000 Feb 29. Identifier NCT03249740, A depot formulation of sunitinib malate (GB-102) in subjects with neovascular (wet) age-related macular degeneration; 2017 Aug 2 [cited 2019 Nov 5]; [about 4 screens]. https://clinicaltrials.gov/ct2/show/record/NCT03249740?term=graybug+vision&rank=1.

21. Kiss S, Pena J. Ocular implants–a novel approach in ocular drug delivery. Rec Patents Nanomed. 2012;2:113–25.

22. Hoffman AS. Hydrogels for biomedical applications. Adv Drug Deliv Rev. 2002;54:3–12.

23. Lin CC, Anseth KS. PEG hydrogels for the controlled release of biomolecules in regenerative medicine. Pharm Res. 2009;26:631–43.

24. Peppas NA, Bures P, Leobandung W, Ichikawa H. Hydrogels in pharmaceutical formulations. Eur J Pharm Biopharm. 2000;50:27–46.

25. Peppas NA, Hilt JZ, Khademhosseini A, Langer R. Hydrogels in biology and medicine: from molecular principles to bionanotechnology. Adv Mater. 2006;18:1345–60.

26. Agrawal AK, Das M, Jain S. In situ gel systems as 'smart' carriers for sustained ocular drug delivery. Expert Opin Drug Deliv. 2012;9:383–402.

27. Klouda L. Thermoresponsive hydrogels in biomedical applications a seven-year update. Eur J Pharm Biopharm. 2015;97:338–49.

28. Talamo JH, Tyson SL, Bafna S, Joseph GP, Goldberg DF, Jones JJ, Jones MP, Kim JK, Martel JB, Nordlund ML, Piovanetti IK. Results of a phase 3, randomized, double-masked, vehicle controlled study (phase 3c) evaluating the safety and efficacy of DEXTENZA ™ (dexamethasone insert) 0.4 mg for the treatment of ocular inflammation and pain after cataract surgery. Invest Ophthalmol Vis Sci. 2017;58:1825.

29. Gira JP, Sampson R, Silverstein SM, Walters TR, Metzinger JL, Talamo JH. Evaluating the patient experience after implantation of a 0.4 mg sustained release dexamethasone intracanalicular insert (Dextenza™): results of a qualitative survey. Patient Prefer Adherence. 2017;11:487.

30. ClinicalTrials.gov [Internet]. Bethesda (MD): National Library of Medicine (US). 2000 Feb 29. Identifier NCT02914509, OTX-16-002: a phase 3 study evaluating the safety and efficacy of OTX-TP in subjects with open-angle glaucoma and ocular hypertension; 2016 Sept 21 [cited 2019 Nov 5]; [about 4 screens]. https://clinicaltrials.gov/ct2/show/study/NCT02914509?term=Ocular+Therapeutix&rank=3.

31. Driscoll A, Blizzard CD, Desai A, D'Abbraccio S, Langh J, Mangano J, Buff N, Metzinger JL, Goldstein MH, Gelormini A. Safety analysis of a sustained release travoprost intracameral hydrogel implant in beagle dogs. Invest Ophthalmol Vis Sci. 2018;59:1250.

32. Jarrett PK, Elhayek RF, Jarrett T, Lattrell Z, Kahn E, Takach S, Metzinger JL, Goldstein MH, Sawhney A. Efficacy & Tolerability of OTX-TKI, a sustained hydrogel delivery system for a tyrosine kinase inhibitor, in a VEGF induced retinal leakage model through 12 months. Invest Ophthalmol Vis Sci. 2018;59:3465.

33. Huu VA, Luo J, Zhu J, Zhu J, Patel S, Boone A, Mahmoud E, McFearin C, Olejniczak J, de Gracia Lux C, Lux J. Light-responsive nanoparticle depot to control release of a small molecule angiogenesis inhibitor in the posterior segment of the eye. J Control Release. 2015;28:71–7.

34. Brandt JD, Sall K, DuBiner H, Benza R, Alster Y, Walker G, Semba CP. Six-month intraocular pressure reduction with a topical bimatoprost ocular insert: results of a phase II randomized controlled study. Ophthalmology. 2016;123:1685–94.

35. Ocular Therapeutix. Dextenza® (dexamethasone ophthalmic insert) 0.4 mg for intraocular use. https://ocutx.com/products/dextenza. Accessed 7 Nov 2019.

36. Campochiaro P, Wykoff C, Brown D, Boyer D, Barakat M, Taraborelli D, Noronha G. Suprachoroidal triamcinolone acetonide for retinal vein occlusion: results of the tanzanite study. Retina. 2018;2:320–8.

37. ClinicalTrials.gov [Internet]. Bethesda (MD): National Library of Medicine (US). 2000 Feb 29. Identifier NCT03203447, suprachoroidal injection of triamcinolone acetonide with IVT anti-VEGF in subjects with macular edema following RVO (TOPAZ); 2017 June 28 [cited 2019 Nov 5]; [about 5 screens]. https://clinicaltrials.gov/ct2/show/study/NCT03203447?term=ocular+microneedle&rank=9.

38. Thrimawithana TR, Young S, Bunt CR, Green C, Alany RG. Drug delivery to the posterior segment of the eye. Drug Discov Today. 2011;16:270–7.

39. Khandan O, Kahook MY, Rao MP. Fenestrated microneedles for ocular drug delivery. Sensors Actuators B Chem. 2016;223:15–23.

40. Thakur R, Tekko I, Al-Shammari F, Al A, McCarthy H, Donnelly R. Rapidly dissolving polymeric microneedles for minimally invasive intraocular drug delivery. Drug Deliv Transl Res. 2016;6:800–15.

41. Zelikin AN, Ehrhardt C, Healy AM. Materials and methods for delivery of biological drugs. Nat Chem. 2016;8:997–1007.

42. Brown DM, Kaiser PK, Michels M, Soubrane G, Heier JS, Kim RY, Sy JP, Schneider S. Ranibizumab versus Verteporfin for neovascular age-related macular degeneration. N Engl J Med. 2006;355:1432–44.

43. Rosenfeld PJ, Brown DM, Heier JS, Boyer DS, Kaiser PK, Chung CY, Kim RY. Ranibizumab for neovascular age-related macular degeneration. N Engl J Med. 2006;355:1419–31.

44. Kim LA, D'Amore PA. A brief history of anti-VEGF for the treatment of ocular angiogenesis. Am J Pathol. 2012;181:376–9.

45. Park SJ, Oh J, Kim YK, Park JH, Park JY, Hong HK, Park KH, Lee JE, Kim HM, Chung JY, Woo SJ. Intraocular pharmacokinetics of intravitreal vascular endothelial growth factor-Trap in a rabbit model. Eye. 2015;29:561–8.

46. Giteau A, Venier-Julienne MC, Aubert-Pouessel A, Benoit JP. How to achieve sustained and complete protein release from PLGA-based microparticles. Int J Pharm. 2008;350:14–26.

47. Mohammadi-Samani S, Taghipour B. PLGA micro and nanoparticles in delivery of peptides and proteins; problems and approaches. Pharm Dev Technol. 2015;20:385–93.

48. Rubio RG. Long-acting anti-VEGF delivery. Retina Today. 2014;78–80. https://retinatoday.com/articles/2014-july-aug/long-acting-anti-vegf-delivery.

49. Campochiaro PA, Marcus DM, Awh CC, Regillo C, Adamis AP, Bantseev V, Chiang Y, Ehrlich JS, Erickson S, Hanley WD, Horvath J, Maass KF, Singh N, Tang F, Barteselli G. The port delivery system with ranibizumab for neovascular age-related macular degeneration: results from the randomized phase 2 LADDER clinical trial. Ophthalmology. 2019;126:1141–54.

50. Saati S, Lo R, Li PY, Meng E, Varma R, Humayun MS. Mini drug pump for ophthalmic use. Curr Eye Res. 2010;35:192–201.

51. Humayun M, Santos A, Altamirano JC, Ribeiro R, Gonzalez R, de la Rosa A, Shih J, Pang C, Jiang F, Calvilo P, et al. Implantable MicroPump for drug delivery in patients with diabetic macular edema. Transl Vis Sci Technol. 2014;3:5.

52. Lance KD, Bernards DA, Ciaccio NA, Good SD, Mendes TS, Kudisch M, Chan E, Ishikiriyama M, Bhisitkul RB, Desai TA. In vivo and in vitro sustained release of ranibizumab from a nanoporous thin-film device. Drug Deliv Transl Res. 2016;6:771–80.

53. Tao W. Application of encapsulated cell technology for retinal degenerative diseases. Expert Opin Biol Ther. 2006;6:717–26.

54. Kauper K, McGovern C, Sherman S, Heatherton P, Rapoza R, Stabilia P, Dean B, Lee A, Borges S, Bouchard B, et al. Two-year intraocular delivery of ciliary neurotrophic factor by encapsulated cell technology implants in patients with chronic retinal degenerative disease. Invest Ophthalmol Vis Sci. 2012;53:7484–91.

55. ClinicalTrials.gov [Internet]. Bethesda (MD): National Library of Medicine (US). 2000 Feb 29. Identifier NCT02862938, study of NT-501 encapsulated cell therapy for glaucoma neuroprotection and vision restoration; 2016 Aug 11 [cited 2019 Nov 4]; [1 page]. https://clinicaltrials.gov/ct2/show/NCT02862938?cond=NT-501&rank=2.

56. ClinicalTrials.gov [Internet]. Bethesda (MD): National Library of Medicine (US). 2000 Feb 29. Identifier NCT03071965, Extension study of NT-501 ciliary neurotrophic factor (CNTF) implant for macular telangiectasia (MacTel); 2017 Mar 7 [cited 2019 Nov 4]; [1 page]. https://clinicaltrials.gov/ct2/show/NCT03071965?cond=NT-501&rank=1.

57. Varshochian R, Jeddi-Tehrani M, Mahmoudi AR, Khoshayand MR, Atyabi F, Sabzevari A, Esfahani MR, Dinarvand R. The protective effect of albumin on bevacizumab activity and stability in PLGA nanoparticles intended for retinal and choroidal neovascularization treatments. Eur J Pharm Sci. 2013;50:341–52.

58. Varshochian R, Riazi-Esfahani M, Jeddi-Tehrani M, Mahmoudi AR, Aghazadeh S, Mahbod M, Movassat M, Atyabi F, Sabzevari A, Dinarvand R. Albuminated PLGA nanoparticles containing bevacizumab intended for ocular neovascularization treatment. J Biomed Mater Res A. 2015;103:3148–56.

59. Ye Z, Ji YL, Ma X, Wen JG, Wei W, Huang SM. Pharmacokinetics and distributions of bevacizumab by intravitreal injection of bevacizumab-PLGA microspheres in rabbits. Int J Ophthalmol. 2015;8:653–8.

60. Yeo Y, Park K. Control of encapsulation efficiency and initial burst in polymeric microparticle systems. Arch Pharm Res. 2004;27:1–12.

61. Manoharan C, Singh J. Insulin loaded PLGA microspheres: effect of zinc salts on encapsulation, release, and stability. J Pharm Sci. 2009;98:529–42.

62. Marquette S, Peerboom C, Yates A, Denis L, Langer I, Amighi K, Goole J. Stability study of full-length antibody (anti-TNF alpha) loaded PLGA microspheres. Int J Pharm. 2014;470:41–50.

63. Moreno MR, Tabitha TS, Nirmal J, Radhakrishnan K, Yee CH, Lim S, Venkatraman S, Agrawal R. Study of stability and biophysical characterization of ranibizumab and aflibercept. Eur J Pharm Biopharm. 2016;108:156–67.

64. Liu W, Lee BS, Mieler WF, Kang-Mieler WF. Biodegradable microsphere-hydrogel ocular drug delivery system for controlled and extended release of bioactive aflibercept in vitro. Curr Eye Res. 2019;44:264–74.

65. Zhang K, Tang X, Zhang J, Lu W, Lin X, Zhang Y, Tian B, Yang H, He H. PEG-PLGA copolymers: their structure and structure-influenced drug delivery applications. J Control Release. 2014;183:77–86.

66. Adamson P, Wilde T, Dobrzynski E, Sychterz C, Polsky R, Kurali E, Haworth R, Tang CM, Korczynska J, Cook F, et al. Single ocular injection of a sustained-release anti-VEGF delivers 6 months pharmacokinetics and efficacy in a primate laser CNV model. J Control Release. 2016;244:1–13.

67. Jay SM, Saltzman WM. Controlled delivery of VEGF via modulation of alginate microparticle ionic cross-linking. J Control Release. 2009;134:26–34.

68. Thackaberry EA, Farman C, Zhong F, Lorget F, Staflin K, Cercillieux A, Mieller AP, et al. Evaluation of the toxicity of intravitreally injected PLGA microspheres and rods in monkeys and rabbits: effects of depot size on inflammatory response. Invest Ophthalmol Vis Sci. 2017;58:4274–85.

69. Ocular Therapeutix. OTX-IVT (anti-VEGF antibody implant). https://ocutx.com/research/otx-ivt/. Accessed 7 Nov 2019.

70. Drapala PW, Brey EM, Mieler WF, Venerus DC, Kang-Derwent JJ, Perez-Luna VH. Role of thermoresponsiveness and poly(ethylene glycol) diacrylate cross-link density on protein release from poly(N-isopropylacrylamide) hydrogels. J Biomater Sci Polym Ed. 2011;22:59–75.

71. Drapala PW, Jiang B, Chiu YC, Mieler WF, Brey EM, Kang-Mieler JJ, Perez-Luna VH. The effect of glutathione as chain transfer agent in PNIPAAm-based thermo-responsive hydrogels for controlled release of proteins. Pharm Res. 2014;31:742–53.

72. Turturro SB, Guthrie MJ, Appel AA, Drapala PW, Brey EM, Perez-Luna VH, Mieler WF, Kang-Mieler JJ. The effect of cross-linked thermo-responsive PNIPAAm-based hydrogel injection on retinal function. Biomaterials. 2011;32:3620–6.

73. Wang CH, Hwang YS, Chiang PR, Shen CR, Hong WH, Hsiue GH. Extended release of bevacizumab by thermosensitive biodegradable and biocompatible hydrogel. Biomacromolecules. 2012;13:40–8.

74. Rauck BM, Friberg TR, Medina-Mendez CA, Park D, Shah V, Bilonick RA, Wang Y. Biocompatible reverse thermal gel sustains the release of intravitreal bevacizumab in vivo. Invest Ophthalmol Vis Sci. 2014;55:469–76.

75. Yu Y, Lau LC, Lo AC, Chau Y. Injectable chemically crosslinked hydrogel for the controlled release of bev-

76. Kanjickal D, Lopina S, Evancho-Chapman MM, Schmidt S, Donovan D. Effects of sterilization on poly(ethylene glycol) hydrogels. J Biomed Mater Res A. 2008;87:608–17.

77. Chang D, Park K, Famili A. Hydrogels for sustained delivery of biologics to the back of the eye. Drug Discov Today. 2019;24:1470–82.

78. Moreau MF, Chappard D, Lesourd M, Montheard JP, Basle MF. Free radicals and side products released during methylmethacrylate polymerization are cytotoxic for osteoblastic cells. J Biomed Mater Res. 1998;40:124–31.

79. Osswald CR, Kang-Mieler JJ. Controlled and extended release of a model protein from a microsphere-hydrogel drug delivery system. Ann Biomed Eng. 2015;43:2609–17.

80. Osswald CR, Kang-Mieler JJ. Controlled and extended in vitro release of bioactive anti-vascular endothelial growth factors from a microsphere-hydrogel drug delivery system. Curr Eye Res. 2016;41:1216–22.

81. Liu W, Borrell MA, Venerus DC, Mieler WF, Kang-Mieler JJ. Characterization of biodegradable microsphere-hydrogel ocular drug delivery system for controlled and extended release of ranibizumab. Transl Vis Sci Technol. 2019;8:12.

82. Osswald CR, Guthrie MJ, Avila A, Valio JA Jr, Mieler WF, Kang-Mieler JJ. In vivo efficacy of an injectable microsphere-hydrogel ocular drug delivery system. Curr Eye Res. 2017;42:1293–301.

Anaesthesia for Retinal Surgery

42

Rod J. Strykowski and Edward Matthew M. Lilley

"If there is light but no retina, does it really shine?"

42.1   Introduction

The earliest ophthalmic surgery was probably performed with no anaesthesia at all. This meant that the advent of general anaesthesia using ether was a major advance. Even with its attendant disadvantages, general anaesthesia remained the only option until cocaine was found to have useful local anaesthetic properties. Local anaesthesia using cocaine then became popular, as it allowed for the avoidance of the problems with general anaesthesia. Cocaine has significant side effects however, and its use declined with the advent of improved local anaesthetic agents such as tetracaine. Improvements in general anaesthesia also occurred at this time, and after the late 1930s there was a reduction in the use of local anaesthesia for ophthalmic surgery.

Local anaesthetic techniques grew more popular again with the development by Atkinson of an intraconal ciliary ganglion block. This came to be known as the "retrobulbar" block, and when combined with a facial nerve block, the globe anaesthesia and paresis that was achieved gave good operating conditions for a range of procedures. This led to an enormous increase in regional anaesthesia for cataract surgery in the 1950s. It allowed for smaller volumes of local

anaesthetic to be used, provided good anaesthesia and akinesia, and once the block was completed, abolition of the oculocardiac reflex was possible.

Even as local anaesthesia became more popular for anterior segment surgery, general anaesthesia remained the preferred anaesthetic for retinal surgery. However today at many institutions, even the most complex retinal surgery is routinely performed under regional anaesthesia, usually with some sedation. Improvements in regional anaesthesia and changes in surgical techniques have both contributed to this change. Scleral buckle procedures remain an important procedure, but are less common today due to the advent of vitrectomy in the 1970s, which has allowed many cases of retinal detachment to be treated without a scleral buckle.

Topical anaesthesia has reappeared as a popular technique over the last few decades. This has been associated with the development of minimally invasive cataract surgery, and is based largely on surgical preference and patient suitability.

Modern sedative drugs have facilitated the change from general anaesthesia to the various local and regional anaesthetic techniques. There are many combinations of drugs used for sedation with good results.

Although almost all ophthalmic surgeries can be performed under modern regional anaesthesia, general anaesthesia remains the first choice in

R. J. Strykowski · E. M. M. Lilley (✉)
Sydney Eye Hospital, Sydney, NSW, Australia

some cases. Examples include anaesthesia for the child, for the extremely anxious adult, for the developmentally delayed patient, as well as for some open-globe procedures. General anaesthesia is also a "rescue" for situations where regional anaesthesia proves to be inadequate, or where a patient finds themselves unable to cooperate and lay still.

Regional anaesthesia, with all its benefits, comes with associated complications and limitations. Patient assessment, and the performance of all forms of anaesthesia, should be done by a suitably trained practitioner.

42.2 Preoperative Assessment and Patient Preparation

Preoperative assessment is essential and relies on a thorough medical history and examination. This allows the anaesthesiologist to determine the best choice of anaesthetic based on the patient's comorbidities and general medical condition. Adequate facilities and equipment, as well as sufficient space and time, should be available for the assessment of each patient.

Many patients presenting for retinal surgery will be of an advanced age and are likely to suffer multiple comorbidities. Patients with known complicated medical histories will benefit from an early referral to the anaesthesiologist, with the opportunity for discussion between the surgical team and the anaesthesiologist. Such initial consultations will save significant time later and improve the quality and safety of the anaesthesia service.

In addition to the usual medical history to elicit coexisting medical conditions, factors which will be of particular interest include the patient's ability to lie flat, and whether the patient speaks the same language as those in the treating team. A recent history of a cough, and movement disorders such as Parkinson's disease, tremor, or unpredictable movements, is also of importance.

A physical examination should be performed on all patients presenting for ophthalmic surgery. This includes an airway assessment, an assessment of the peripheral pulse rate, rhythm, and

strength, along with non-invasive blood pressure measurement, pulse oximetry, and a respiratory system examination where indicated.

The number and variety of drugs patients may be taking are increasing, and some of these drugs introduce new issues. A list of the patient's current medications should be available. Drugs of particular interest include anticoagulants and medications for diabetes. The newer antiplatelet drugs and other recently introduced classes of anticoagulants add layers of complexity to decisions about which type of anaesthetic is best for a particular patient.

Whilst routine assessment of the patient by the anaesthesiologist remains essential, the *routine* ordering of preoperative testing does not. It is now well established that routine investigations should not be performed. Instead the treating medical team should order only those tests and investigations that are relevant and necessary for the individual patient. Probably the most commonly useful test will be a resting electrocardiogram (ECG). Some patients will require no preoperative testing at all.

When a local or regional anaesthetic technique is chosen for a vitreoretinal case, further discussion with the patient about the intraoperative and post-operative experience is important. The patient is instructed to lay still and not talk during these surgeries, and the instructions and advice needed may be different to that given before cataract surgery. Often in cataract surgery, the amnesia due to sedation will outlast the whole operation. Vitreoretinal surgery is frequently longer than cataract surgery, and this means sedation administered at the time of eye block may not last for the entire case. An additional factor is that magnification under a microscope means small patient movements are exaggerated and can lead to ocular morbidity.

Many vitrectomy cases, such as macular surgery, are now about 30 min in duration. However, cases of severe diabetic retinopathy, combined vitrectomy and cataract surgery including scleral sutured lenses, and vitrectomy in combination with a scleral buckle procedure can be up to several hours in duration. Discussion between anaesthesiologist and retinal surgeon will often help to iden-

tify which cases are anticipated to be prolonged (over 90 min). Our recommendation would be that if a vitreoretinal case is likely to take more than 3 h, then general anaesthesia should be considered.

Although often not appreciated by surgical teams, compared with general anaesthesia, regional anaesthesia requires a more detailed explanation to the patient of what is needed from them, and also a more detailed explanation of the likely intraoperative experience. This takes time and is an important component of the preanaesthetic assessment.

42.3 Patient Counselling by Anaesthesiologists Before Vitreoretinal Surgery

The factors discussed in the previous section indicate that during vitreoretinal surgery we are asking the patient to be cooperative, and to lay still for the entire case. This requires a clear explanation to the patient of not only the importance of this, but also what they will experience, feel, hear, and even see. In particular, this means that they will feel touching of the forehead, nose, and possibly the cheek. They are likely to hear theatre and equipment sounds, staff talking, and possibly music. Soft music played in theatre may be relaxing for patients and staff, and may improve surgical performance if chosen by the surgeon. Patients with hearing aids should be encouraged to leave at least the contralateral aid in situ to help with communication.

The patient needs to know that they can communicate their needs, particularly if uncomfortable or experiencing sharp pain or pressure. Although very uncommon during vitrectomy with modern anaesthesia, pain may still occur when the eye is akinetic. Patients need to know how to communicate this to the surgeon or anaesthesiologist (by speaking, or with hand signals), and be reassured that they will be understood. It is important to reassure patients that if any discomfort is felt, surgery will stop to allow more anaesthesia to be administered (local top-up with or without additional sedation). The ideal goal is to have a calm, relaxed, and awake patient, who

is therefore in control of their head movements. As a simple summary to non-anaesthetic staff, the patient for vitrectomy intraoperatively should be awake and cooperative, or under general anaesthesia.

Younger patients (under 40–50 years) should be told that they may retain some vision during the surgery. Patients may see shapes or colours, and occasionally experience visualisation of the instruments such as vitrector, light pipe, or forceps. Patients should be reassured that even if vision occurs, it is a common occurrence in the young, and they will almost certainly have no pain.

Special mention is warranted regarding the preoperative discussion for patients due to undergo scleral buckle operations. These cases usually take longer than vitrectomy (often about 90 min), and patients tend to be of a younger age group. As such, they are a group who are generally more anxious and less tolerant than older patients. For those that are very anxious, or not suited psychologically for a longer sedation/regional case, general anaesthesia combined with regional anaesthesia may be the best choice.

For patients undergoing scleral buckle under a sedation/regional technique, a clear and honest explanation regarding the chance of experiencing discomfort intraoperatively must occur whilst remaining sensitive to the patient's concerns. Patients having this surgery, even in the hands of experienced ophthalmic anaesthesiologists, uncommonly may experience pain that "breaks through" an otherwise dense ocular regional anaesthetic. Although it is not usually severe, this pain should be attended to immediately. This is usually achieved by a combination of further local or regional anaesthetic (topical or sub-Tenon's anaesthesia), or additional sedation. We have found that sub-Tenon's anaesthesia is not likely to be adequate as the primary technique for a scleral buckle and should be avoided if possible. Of course, sub-Tenon's will be the method of choice for top-up by the surgeon where pain occurs intraoperatively.

Scleral buckle cases are usually not performed under the microscope. As such, slight patient

movements can be tolerated by the surgeon, and do not usually present a danger to the eye. This means that sedation, particularly conscious sedation, can be safely used to a greater degree than during vitrectomy. This may be ideal for the young anxious patient, in conjunction with a peribulbar block.

We wish to address the terminology used by surgical teams and non-anaesthesiologists regarding the information provided to patients having vitreoretinal surgery. Terms such as "twilight anaesthesia" should not be used, as "twilight" is an imprecise term, and conveys different meanings to different people. Many patients may liken it to a colonoscopy which in fact is almost always a deep sedation, or in fact a spontaneously breathing general anaesthetic. This is very different from what a patient will experience during vitrectomy. Phrases such as "you will be drowsy during the case" or "you won't feel anything" are clearly misleading, and can provide patients with false expectations. This will require rectification by the anaesthesiologist taking valuable time and effort. It is preferable to explain to the patient that during vitrectomy they will be awake, but calm and comfortable. The patient should be advised to direct any more complex questions regarding sedation to the attending anaesthesiologist.

42.4 Regional Anaesthesia

Vitreoretinal surgery usually requires a formal regional anaesthetic such as a peribulbar block or sub-Tenon's block. Because many surgeons prefer an eye which is not only insensate, but also akinetic, some popular techniques for cataract surgery such as topical, intracameral, and subconjunctival local anaesthesia do not lend themselves to retinal surgery. The choice between a sharp needle or sub-Tenon's block for vitreoretinal surgery will depend on anaesthesiologist and surgeon preference and experience. Many anaesthesiologists will prefer to use sub-Tenon's blocks for patients on anticoagulants, or with large or deep-set eyes. A sharp needle block may be preferred for cases where previous pterygium surgery or other conjunctival surgery makes per-

formance of a sub-Tenon's block difficult. Prior to the development during the last decade of small-incision sutureless vitrectomy, the technique for sutured port placement during vitrectomy frequently led to adherent conjunctiva at the surgical sites, making subsequent sub-Tenon's block difficult, or impossible.

It is doubtful that any sharp needle block is purely intraconal or extraconal, because it is recognised that except near to the muscle attachments to the globe, or deep in the orbit, the muscle cone is not a complete barrier to the diffusion of local anaesthetic agents (Koornneef). Intentionally trying to place a sharp needle tip in the intraconal space became less popular after the mid- to late 1980s, when extraconal injections of local anaesthetic were named by Davis ("peribulbar"), and Bloomberg and Weiss ("periocular"). They described such injections as not only being safer, but also providing anaesthesia equal to intraconal injections. In contrast, intraconal injections have a finite increased risk. Damage is possible to vital structures that lie inside the muscle cone, such as optic nerve, ophthalmic artery and veins, or ciliary ganglion. Long needles placed in the intraconal space may reach the dural sheath surrounding the optic nerve deep near the apex of the orbit, and lead to subarachnoid injection of local anaesthetic with brainstem, or "total spinal", anaesthesia—a medical emergency. Additionally, damage to the globe itself is more likely if attempting to place a needle intraconally, particularly with longer globes, which may also have staphylomata. Such larger and myopic eyes are encountered more frequently in vitreoretinal surgery than in the general population. Therefore it is now more common to use a shorter needle (less than 32 mm, and often 25 mm), so that the tip is in the extraconal space when the local anaesthetic is injected, and deep orbital structures cannot be reached (Fig. 42.1).

The use of sub-Tenon's anaesthesia is much more common than it was a generation ago, particularly for cataract surgery. This is at least partly because of perceived improvements in safety over sharp needle blocks, and ease of teaching.

Patients presenting for vitreoretinal surgery are more likely than the general population to be myopic, and tend to have larger orbits and therefore have a possibly increased risk to globe penetration when sharp needles are used (Figs. 42.2 and 42.3).

Modern local anaesthetic agents have improved greatly since cocaine. The recent development of bupivacaine, and later ropivacaine, has allowed for rapid-onset and long-acting blocks using a single anaesthetic agent, without the use of adrenaline. Adrenaline has been used as an additive for sharp needle blocks to prolong anaesthesia but has been associated with concern about its safety in the orbit. This is primarily related to vasoconstriction of end arteries and potential tissue ischaemia.

Hyaluronidase (hyalase) is a reversible depolymerising agent that acts to weaken the hyaluronic acid connective tissue matrix, and is a commonly used additive to local anaesthetic drugs. It may facilitate faster onset of anaesthesia and a more complete block by enhancing the spread of local anaesthetic through tissue planes. It has been shown to be effective in very low concentrations, commonly from 1 to 30 units per millilitre. Concentrations higher than 75 units per millilitre may lead to more adverse allergic-type reactions. This is more likely after prior exposure, for example a previous eye block.

Allergic reactions associated with the use of hyalase are usually mild, and result in swelling and a shiny redness of the periorbital skin and eyelids. Symptoms can include a feeling of
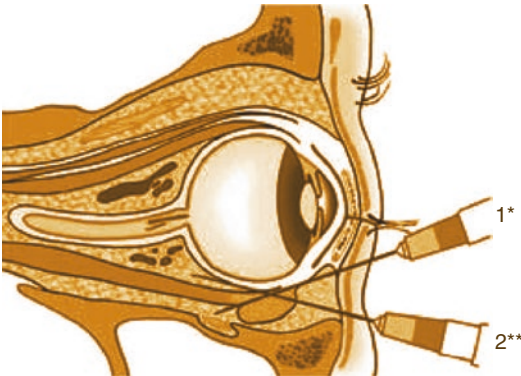
Fig. 42.1 Sharp needle blocks are often labelled as either "retrobulbar" (intraconal 2**) or "peribulbar" (extraconal 1*)
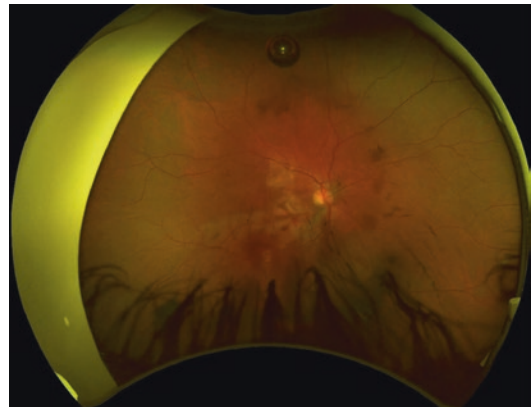
Fig. 42.2 Colour photo: shows exit wound from an injection needle through the macula
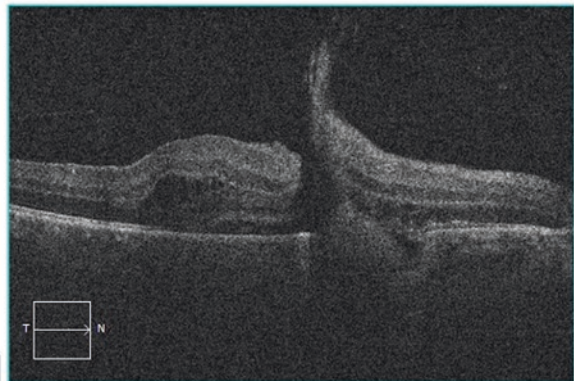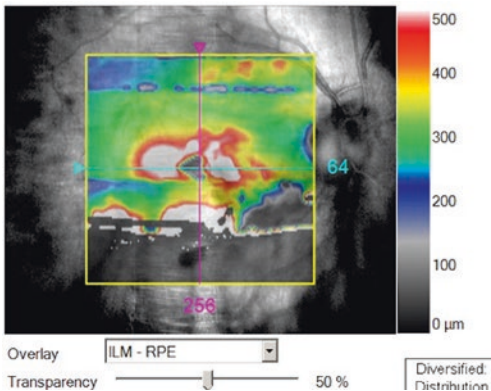
Fig. 42.3 OCT: Cross-sectional view through the macula showing a full-thickness break in the neurosensory retina

warmth or pruritis. More severe reactions can also occur, with intraorbital and periorbital oedema, and erythema similar to cellulitis (Fig. 42.4). Very rarely the orbital reaction can be so severe as to mimic an orbital tumour. Erythema and a cellulitic type appearance can spread to the contralateral eye. The more minor reactions of shiny-type redness can occur within an hour of the block, and are often revealed upon removal of the surgical eye drape post-operatively.

It is worth noting that hyaluronidase may reduce the incidence of post-operative strabismus, and has been shown to shorten the duration of anaesthesia provided by long-acting local anaesthetic agents such as bupivacaine and ropivacaine.

As a routine it is wise for an anaesthesiologist not to perform anaesthesia on a patient unless the surgeon is present. This is particularly important when sharp needle ophthalmic blocks are used, because of the risk of retrobulbar haemorrhage, a potentially sight-threatening acute complication. Treatment of this condition involves releasing the pressure behind the eye urgently by lateral can-

Fig. 42.4 Localised allergic reaction to hyaluronidase

thotomy or cantholysis. A person who can perform this procedure such as an ophthalmologist should be present, as it is expected that most anaesthesiologists will have little or no experience of performing this emergency surgical procedure.

Ultrasound-guided ophthalmic blocks have been described, and there is ongoing research in this area. It has been shown to be a valid technique, but there are concerns about the safety of the equipment and the complexity of its use. The future of this technique is still not clear.

42.5 Monitoring

Patients undergoing surgery under regional anaesthesia should be monitored with at least continuous pulse oximetry, electrocardiogram, and non-invasive blood pressure. A suitably trained practitioner should be present to observe and interpret such monitoring, and to take appropriate action when required.

42.6 Sedation

Sedation is used for patient comfort, anxiolysis, and amnesia, and to facilitate the patient lying still. It can allow brief procedures such as eye blocks that might otherwise be uncomfortable or painful, to be achieved with comfort and possibly some degree of amnesia. There are also medical indications for sedation such as the treatment of hypertension when it is caused by anxiety.

Modern sedative drugs have improved the choices available to anaesthesiologists. Commonly used drugs include midazolam, fentanyl, alfentanil, and propofol. Multiple sedation regimens are used with success and safety. The level of sedation required depends on patient and surgical preference, length of the surgery, as well as anaesthesiologist preference and usual practice.

Conscious (light) sedation allows the sedated patient to obey commands, and to communicate with the treating team. Heavier sedation may depress the patient's conscious level, allowing less clear communication, but from which state arousal can occur relatively rapidly. Further

increasing sedation may lead to general anaesthesia for short periods which should only be managed by an anaesthesiologist or anaesthetist.

Intraoperative oversedation can occur, and may be more likely in certain patient groups. This includes the elderly, those with significant medical co-morbidities, patients with a history of stroke or brain injury, or the sleep-deprived and stressed patient. Some racial groups may show increased sensitivity to sedative medication. Oversedation may be compounded by the face drapes and the darkened room during vitrectomy surgery, and may lead to snoring, intermittent airway obstruction, and unpredictable sudden patient movements. This can cause significant difficulty for the surgeon and should be avoided. Head movement of the patient poses the risk of damage to the retina during delicate manoeuvres on the surface of the macula such as surgical membrane peeling. Because of this judicious use of the lowest dose, shortest acting evanescent drugs are recommended for sedation when performing an eye block, particularly in high-risk patients. Short-term reversal of some anaesthesia drugs such as benzodiazepines and opioids is possible, and is occasionally very helpful.

For some patients the best choice is to have no sedation at all, especially for those with multiple and severe medical conditions. Non-pharmacological techniques which can also be used to manage an anxious patient include hand holding and verbal reassurance.

42.7   General Anaesthesia

Modern general anaesthetics have advanced in many ways from the days of ether. Training, techniques, equipment, and drugs have all evolved. Auxiliary drugs have also improved, a good relevant example being antiemetics.

The skills and expertise needed for general anaesthesia are used for dealing with the serious, and fortunately very rare, complications of regional anaesthesia such as brainstem anaesthesia ("total spinal") from injection of local anaesthetic agent into the cerebrospinal fluid within the optic nerve sheath.

For cases of globe rupture, and many cases of penetrating eye injury, general anaesthesia remains the method of choice. Eye blocks by their nature lead to increased pressure behind the globe, and this may result in expulsion of ocular contents. This pressure effect is also relevant during penetrating keratoplasty procedures, where the eye is completely open anteriorly for a period during the surgery, leading some surgeons to prefer general anaesthesia for such cases.

Practical matters such as arrangements of airways, depth of anaesthesia, and need for paralysis should be discussed between the surgeon and anaesthesiologist. Securing any airway device is particularly important as access to the head is often impeded during surgery.

General anaesthesia is often combined with regional anaesthesia. A regional block placed after induction of general anaesthesia will allow for a lighter plane of anaesthesia and facilitate akinesis of the eye. It will also improve patient recovery secondary to the lighter anaesthetic used, and provide post-operative analgesia. Such patients require less or more commonly no administration of potent opioid analgesia after vitrectomy surgery, and usually a minimum of such drugs postoperatively after scleral buckle surgery.

Some anaesthetic drugs have effects particularly related to ophthalmic and vitreoretinal surgery. Nitrous oxide is to be avoided in vitreoretinal surgery when a gas bubble is being instilled into the vitreous cavity. In addition, should a patient later require surgery whilst the gas is still inside the eye, the patient should be told to convey this information to the attending anaesthesiologist, so that nitrous oxide can be avoided. The rise in intraocular pressure which can otherwise result is well recognised and can threaten sight and even the viability of the eye. In this regard, and to help avoid this complication, warning wrist bands are routinely placed on patients post-operatively who have expansile gas in their eye. These bands provide information about the date and type of agent used, and contact details of the hospital where the procedure took place (Fig. 42.5).

Suxamethonium has long been known to raise intraocular pressure (IOP). This is a theoretical concern for the management of an open-eye
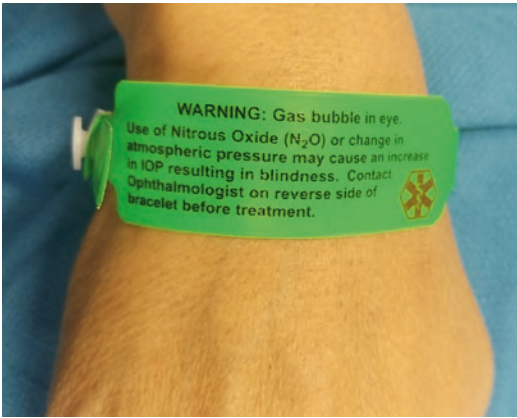
Fig. 42.5 Gas bubble wrist band

injury under general anaesthesia, but is of little significance for other eye surgery, including vitreoretinal surgery, even when high IOP precedes the surgery. Regarding an open eye, the thought is that the rise in IOP may lead to expulsion of ocular contents. This is of questionable clinical significance, as the rise in IOP is more than balanced by a similar fall in the IOP caused by the drugs that induce anaesthesia, such as propofol, and thiopentone in particular. Critically, poor muscle relaxation at the time of airway manipulation and tracheal intubation may well lead to coughing or straining with a consequent rise in IOP, risking expulsion of ocular contents. Deep-muscle relaxation with suxamethonium will avoid this. Importantly, no reports exist of such expulsion of intraocular contents due to suxamethonium itself.

The more recently introduced neuromuscular blocking agent rocuronium does not have the side effect of raising IOP, and can be used as an alternative to suxamethonium in some situations. It has the additional advantage of immediate reversibility with sugammadex. Rocuronium itself, like all drugs, has limitations, such as the current concern about anaphylaxis associated with its use.

42.8 Fasting

The introduction of routine preoperative fasting has saved lives by reducing the incidence of aspiration associated with all forms of anaesthesia. It is well advised to follow local fasting guidelines for routine cases.

The commonly used regimen of at least 6-h fasting has led to concerns regarding hydration, carbohydrate metabolism, and patient comfort. This has prompted a reduction in fasting times, particularly with regard to clear fluid. It is now widely accepted that 2–3 h is adequate fasting for clear fluids. This has advantages in regard to the factors of concern whilst actually increasing gastric emptying and demonstrating improvements in patient comfort and satisfaction.

Much retinal surgery will be performed under regional anaesthesia with a small (but defined) risk of aspiration, but may also have a degree of urgency. More urgent cases might warrant departure from fasting guidelines, and the anaesthesiologist should be consulted. Factors to be considered include the likely consequences of delaying the surgery, expected sedation required, and what and when the patient has eaten.

Pain, stress, and opioid administration can delay gastric emptying. This needs to be considered along with patient factors such as high body mass index, and coexisting diseases that may delay gastric emptying such as uraemia, autonomic neuropathy, or other gastrointestinal disorders.

42.9 Post-operative Management

Post-operative analgesia should be discussed with patients having vitreoretinal surgery. Patients can be reassured that after vitrectomy surgery post-operative pain is not a major issue. After an adequate block using 1% ropivacaine, for example, analgesia will usually last approximately 12 h. Such patients are unlikely to have significant post-operative discomfort, yet they need to know that analgesia is available if required.

It is important to note that patients after vitrectomy uncommonly require any more than paracetamol for comfort. As such, simple analgesia with paracetamol and/or nonsteroidal anti-inflammatory agents as needed with food (in consultation with the surgeon) would be suitable

for day-stay patients. Inpatients can be treated similarly. Very small doses of oxycodone (2.5–5 mg) or tapentadol (or similar) as needed, may be ordered, with or without antiemetics.

Patients undergoing scleral buckle surgery may experience pain post-operatively, and after the anaesthetic block recedes pain is likely for about 24 h. Pain in this situation can vary from mild to quite severe. Patients should be advised to take regular paracetamol, and nonsteroidal anti-inflammatory agents as needed with food (in consultation with the surgeon), and/or opioid analgesia, tramadol and tapentadol, or similar analgesia.

Various posturing may be required for patients following vitreoretinal surgery. This is a surgical requirement, and some patients may need analgesia to help achieve these positions, due to arthritis, chest wall conditions, or other pre-existing musculoskeletal or soft-tissue problems.

Management of eye surgery is a team approach, involving anaesthesiologist, surgeon, and nurses. Nowhere in eye surgery is this more evident than in vitreoretinal surgery, where complex and often long cases are commonly performed in both elective and emergency scenarios.

As discussed, communication between the patient and the team must be facilitated, and clear communication between anaesthesiologist and surgeon is crucial to deliver best patient care. This is in part because adequate anaesthesia forms the foundation for surgical success. The surgeon (and patients) need to be confident that in all cases, good-quality anaesthesia and sedation will be provided. When this falters, as will

occasionally occur, mechanisms need to be in place by the team for the timely correction of any problems identified.

Clearly, a protean degree of patient co-morbidities, surgical conditions, and psychological make-up means that individualisation of the care provided will be needed to give the best patient outcomes.

Added to these factors is the ever-increasing number of vitreoretinal surgeries carried out as day-stay procedures, allowing ambulatory care. This requires particular methods to be employed by the treating team to achieve good patient outcomes in these settings. Especially relevant is post-operative analgesia and clear and easy-to-follow patient advice, with options to receive urgent medical attention should problems develop after discharge.

Almost all patients now have a very satisfactory, safe, and effective experience for their vitreoretinal surgery in the modern medical system.

Further Reading

Gayer S. Needle base orbital regional anaesthesia for adult ophthalmic surgery. In: Kumar C, Dodds C, Gayer S, editors. OSH ophthalmic anaesthesia. From Oxford Medicine Online. © Oxford University Press; 2015. www.oxfordmedicine.com.

Johnson RW. History of ophthalmic anaesthesia. In: Kumar C, Dodds C, Gayer S, editors. OSH ophthalmic anaesthesia. From Oxford Medicine Online. © Oxford University Press; 2015. www.oxfordmedicine.com.

Kong KL, Kirkby G. Anaesthesia for vireo-retinal surgery. Curr Anaesth Crit Care. 2010;21:174–9.

Kumar CM, Dodds C. Ophthalmic regional block. Review Article. Ann Acad Med. 2006;35(3):161.

Registries in Macular Surgery

43

Rohan W. Essex

43.1 Introduction

There is a vast evidence base supporting clinical practice in ophthalmology. For most of the common diseases we can rely on randomised trials to aid us in many important treatment decisions. But where are the weaknesses in our treatments? Do our treatment decisions actually translate into improved outcomes for our patients and for the health system? Is the care we deliver as effective as that of our colleagues? How can we make ourselves better as clinicians? These real-world questions are vitally important, but relatively little attention (and even fewer resources) has historically been directed towards answering them.

Registry science is a relatively new and rapidly growing field. A clinical registry is an "… organized system that uses observational study methods to collect uniform data (clinical and other) to evaluate specified outcomes for a population defined by a particular disease, condition, or exposure …" [1]. The scope of registries is broad. A key aspect of this definition is that a registry evaluates *outcomes*: it is not simply a list of people with the condition or exposure of interest. Another key aspect of all registries is that they are designed to observe and record clinical information, but do not in themselves determine what the care will be. This is in contrast to clinical trials which mandate a particular care protocol which may be allocated randomly.

Registries have many uses:

- To monitor the incidence of disease
- To define the severity of disease
- To observe practice patterns and details of treatment administered:
- To highlight where clinical care deviates from best practice
- To define the outcomes of real-world management at this point in time, with appropriate risk adjustment for case mix:
- To highlight where outcomes might fall short:
  - For a disease
  - For a procedure
  - For a demographic group
  - For an individual clinician
- To monitor changes in outcome over time
- To report the effect of changes in practice/procedure: These changes may be a result of:
  - Advances in practice through clinical research or technology
  - Better adherence to best practice guidelines
  - Insights learned from the results of the reg-

R. W. Essex (✉)
Academic Unit of Ophthalmology, Medical School, Australian National University, Canberra, ACT, Australia

Department of Ophthalmology, Canberra Hospital, Garran, ACT, Australia

Royal Victorian Eye and Ear Hospital, Melbourne, VIC, Australia
e-mail: rohan.essex@act.gov.au

istry itself informing best practice
– A change in an individual's practice due to a targeted intervention
• To better inform patients of their prognosis using their baseline risk, as defined using the historical results of the registry
• As infrastructure to support randomised clinical trials at vastly reduced cost [2]

The feedback "loops" mentioned above are integral to the use of registries as quality improvement tools. Benchmarking at an individual or organisational level is an important quality assurance and quality improvement activity for individuals, hospitals, professional organisations and also providers of health services such as government or managed care providers.

Registries can be thought of as the "bookends" of clinical research. At the beginning they help identify and define the problem requiring further study. Research studies are then performed which result in changes to the standard of care. Then at the end the registries can monitor any changes in outcomes (and the change in practice) which result from the implementation of these changes to clinical care. Then the cycle begins again. This form of post-implementation surveillance is a reportable research outcome in itself.

43.2 Aspects of a Registry

Firstly a registry needs a reason to exist. Data collection with post hoc formulation of research questions is not only poor science, but also unlikely to result in good engagement of clinicians, patients nor funders. The reason for existence could simply be quality assurance, or might be a specific research question such as the following: "Does face-down positioning of patients following macular hole surgery result in better patient outcomes?". Having a clearly articulated purpose will help inform the appropriate design of the registry.

Secondly the disease being studied needs to have an easily and clearly defined outcome measure. Measures like visual acuity and intraocular pressure are well defined and easily measured, as

are OCT measures of macular structure such as macular thickness or presence of a macular hole. When considering macular surgery, macular hole is well suited to a registry: the outcomes of surgery can be unambiguously defined (best corrected visual acuity, hole closure), and there are published guidelines defining what is meant by hole closure [3]. In contrast epiretinal membrane surgery is less well suited: patient satisfaction following epiretinal membrane peel does not always correlate with visual acuity nor macular OCT appearance, and there is no universally adopted measure of distortion nor patient-reported outcome. Surprisingly there is no consistent definition of outcome following retinal detachment surgery. Studies require variously macular reattachment only [4, 5], retinal reattachment central to the equator without any retina affecting procedures (including epiretinal membrane peel) [6], complete retinal reattachment [7] or absence of further reattachment surgery [8, 9].

Timing of the outcome measure is also important. Some registries are designed to monitor outcomes over time for a disease, with no specific endpoint. Registries of AMD therapy are good examples of these [10, 11]. Registries of surgical interventions however tend to report outcomes at predefined time points only, or even just a single time point. If outcomes are likely to change with time following surgery then registry designers need to choose a time point for reporting carefully, balancing the desire for long-term outcomes with the likelihood of loss to follow up over time. Using macular hole surgery as an example again, it is known that macular hole closure tends to occur very early following surgery [12], and holes only rarely reopen [13]. The time point for reporting closure therefore could be relatively early following tamponade resorption (e.g. 1–2 months post-operatively). Visual acuity however progressively improves over many months post-operatively [14], but this improvement is offset by evolving lens opacity. The best time scientifically to report the outcome would be following cataract surgery, but many patients are discharged from the care of the retinal surgeon before this time, and a registry may lose the opportunity to report outcome completely if the

registry designers are too ambitious. Whichever time point[s] are chosen, it is important that all users aim to report outcomes at the same time point post-operatively. The exact duration of follow-up should also be captured to allow outcomes to be statistically adjusted appropriately. A well-considered registry will also collect safety outcome data (i.e. measures of harm) such as retinal detachment and endophthalmitis.

Risk adjustment is necessary for proper interpretation of registry data. Unlike clinical trials, clinical registries are usually defined by a single inclusion criterion, such as vitrectomy for macular hole. Inclusion criteria are therefore broad, and the vagaries of case mix are not accounted for by a randomisation process. A clinician or organisation (e.g. teaching hospital) which tends to operate on more difficult cases should not be unduly penalised in any reporting. Risk adjustment is a statistical process which aims to weight the raw outcomes of patients using the known effect of baseline risk factors on this outcome. Results should therefore be comparable between cohorts with different baseline risks. An ideal registry would collect all possible baseline features which might influence the outcome measure[s], but in reality this is impossible because the number of features may be very large, and it is certain that some predictors of outcome (e.g. genetic) are unknown. The designers of a registry must make a decision to collect all important baseline predictors, based on previously published research. Additional baseline factors can be collected so their effect can be evaluated as a research question. There is a limit however to how much can reasonably be asked of registry contributors, particularly if the data requested would not always be collected as part of routine care for a macular surgery patient (e.g. axial length). There is a risk that the more data a registry requires the less enthusiastic users are to participate, and the lower the quality of the data collected.

Methods of reporting risk-adjusted outcomes are varied and depend on whether outcomes are to be reported cross-sectionally (at a single point in time) or longitudinally over time [15]. For cross-sectional outcomes, the simplest report is

the standardised event ratio. This is the ratio of the adjusted event rate (e.g. macular hole surgery failure) divided by the expected event rate for the specific cohort operated on (based on the risk adjustment model). This should be reported with a confidence interval (e.g. 99%), which would be expected to include unity 99% of the time. Importantly, 1% of "average" surgeons will fall outside this range, so these cross-sectional point estimates of quality should be interpreted with caution, and used as flags for closer monitoring rather than any punitive regulatory response.

Another popular method for reporting cross-sectional outcomes is a risk-adjusted funnel plot (Fig. 43.1a) [16]. Funnel plots present the adjusted rate of the outcome of interest for each user/institution plotted against the number of cases operated on by the user. Superimposed on the scatterplot are 95 or 99.5% (two or three standard deviation) control limits around the overall event rate for all users. There is greater variability in estimation for small samples, hence the funnel shape of the control limits and the scatterplot, although one-sided plots are also possible (Fig. 43.1b) [17].

Plots of outcomes over time, often referred to as control charts, have their origins in the manufacturing industry. Inherent to these charts are an expected outcome and control limits, designed to signal when the system or process is "out of control". Depending on the type, control charts will detect improvement or deterioration in performance of the "system" (the surgeon, institution or health service) over time (they do not detect changes in individual patients over time). The type of plot is determined by the nature of the data (continuous, e.g. visual acuity letter score; or categorical, e.g. retinal reattachment). For success/failure outcomes the simplest approach is to present serial estimates of the standardised event ratio; however these give little indication of "drift" over time. Other plots include RACUSUM (risk-adjusted cumulative sum) [18], WEE chart (weighted estimating equation) [19], RASPR (risk-adjusted sequential probability ratio) [20, 21], RAEWMA (risk-adjusted exponentially weighted moving average) [22], RAEV (risk-adjusted exponentially weighted moving average-
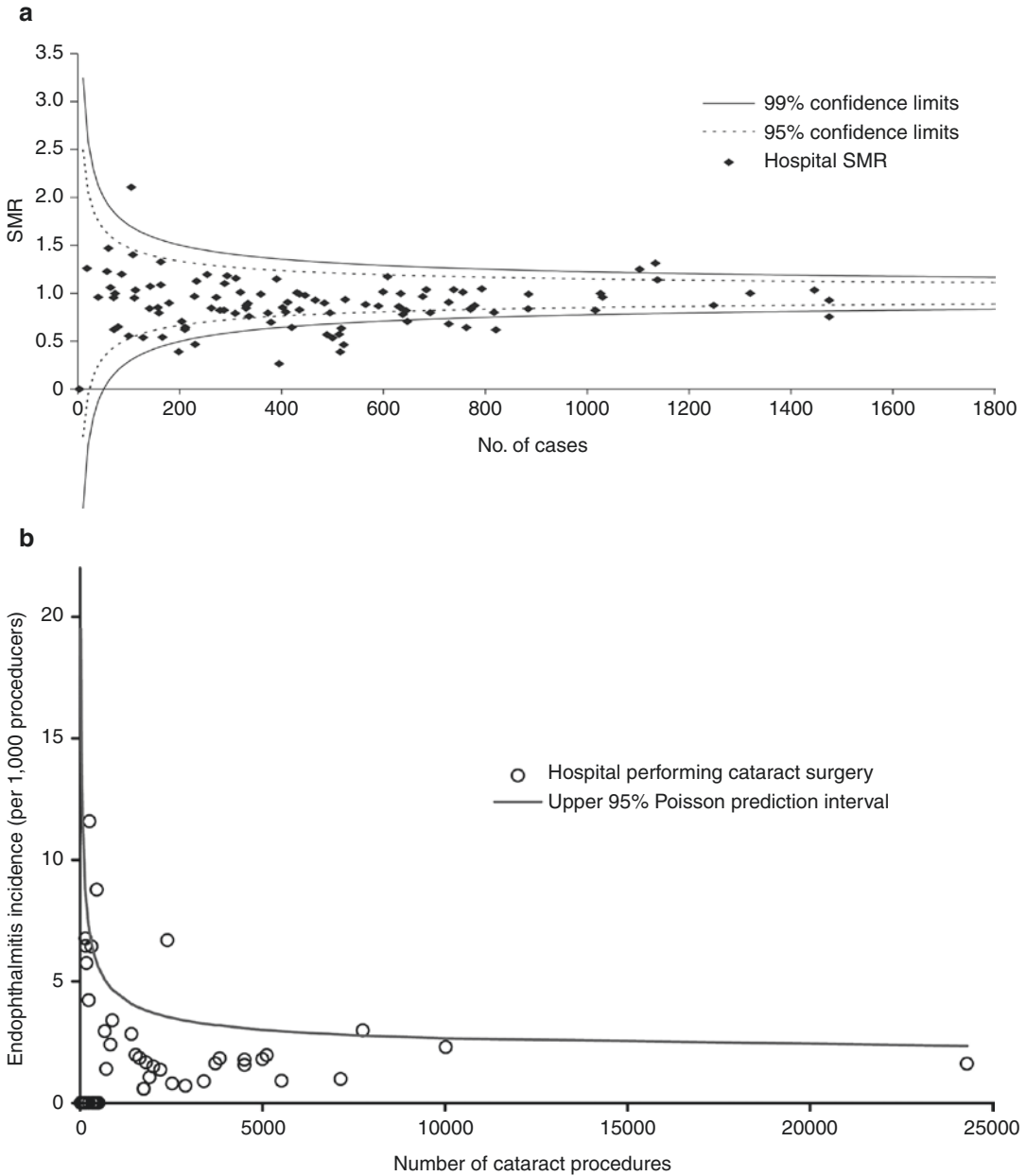
Fig. 43.1 (**a**) Two-sided risk-adjusted funnel plot. Standardised mortality ratio of intensive care patients in Australian intensive care units. (Reproduced with permission from Cook DA, Duke G, Hart GK, et al. Review of the application of risk-adjusted charts to analyse mortality outcomes in critical care. Crit Care Resusc 2008;10(3):239–51) [15]. (**b**) One-sided funnel plot. Incidence of endophthalmitis following cataract surgery. (Reproduced with permission from Ng JQ, Morlet N, Bremner AP, et al. Techniques to monitor for endophthalmitis and other cataract surgery complications. Ophthalmology 2008;115(1):3–10 [17])

VLAD) [23] and others. Exact details of these are beyond the scope of this chapter, as are the methods of risk adjustment themselves. An example of a RASPR chart is presented in Fig. 43.2 evalu-

ating excess mortality in patients seen by Dr. Harold Shipman. Dr. Shipman was a general practitioner in the UK who was convicted in January 2000 of 15 counts of murder against his
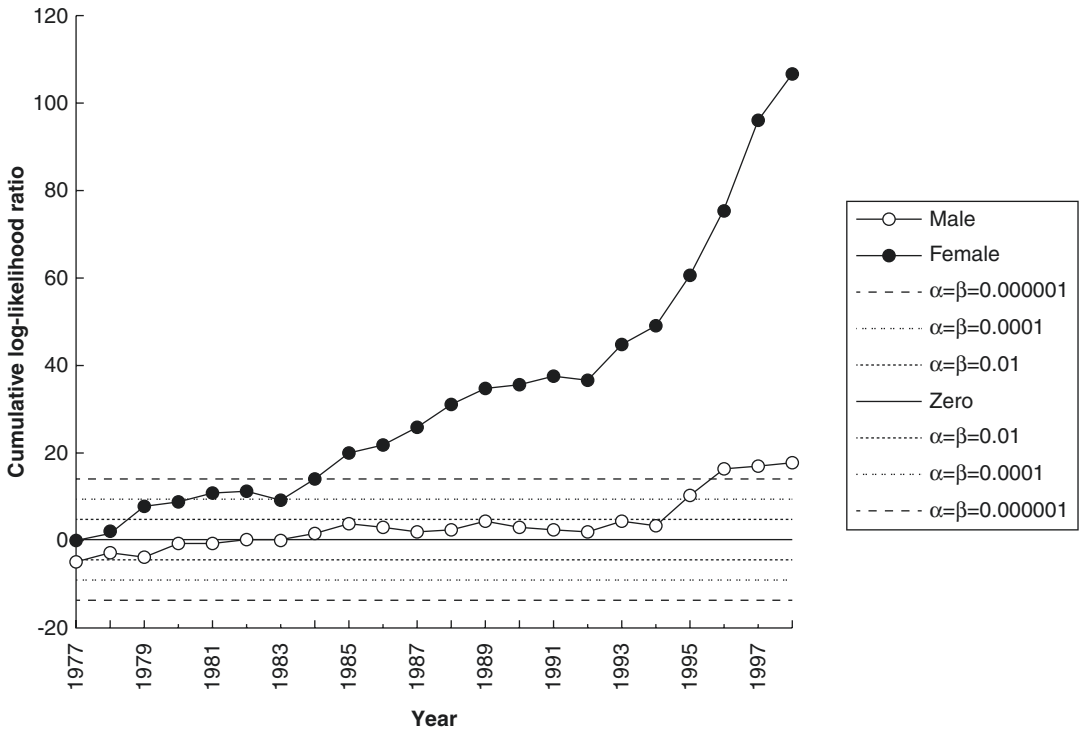
Fig. 43.2 Risk-adjusted sequential probability ratio test for detection of a doubling in mortality risk for patients of Dr. Harold Shipman: age > 64 years and death in home/practice. α = false-positive error rate; β = false-negative error rate. (Reproduced with permission from Spiegelhalter D, Grigg O, Kinsman R, Treasure T. Risk-adjusted sequential probability ratio tests: applications to Bristol, Shipman and adult cardiac surgery. Int J Qual Health Care 2003;15(1):7–13)

patients. He is thought to have killed over 200 patients, 80% of whom were elderly women [24]. He was arrested in 1998, but it can be seen from the figure that there were clear signs of excess mortality a decade earlier.

Details of the intervention performed ("the process") should also be collected. Using retinal detachment as an example, the procedure performed, choice of retinopexy and endotamponade and method of SRF drainage (if any) are all relevant (among many other factors). This information has two purposes. Firstly it allows the registry to ask research questions about the data collected (e.g. is cryo better than laser?). Secondly it allows the registry to report back to the surgeon aspects of their surgical decision-making. This allows a surgeon to compare themselves to published best practice guidelines, and supports the cycle of quality improvement ("process change"). Something that should never be

done is adjustment of outcomes based on intraoperative surgeon-dependent decisions. This could potentially adjust for poor decision-making and artifactually improve outcomes in a risk-adjusted report. An example might be adjusting for the effect of performing scleral buckling instead of vitrectomy for giant retinal tear.

Finally, there are numerous ethical issues relevant to registries in medicine. These include issues surrounding consent of the patients and also of the participating surgeons; use of identifiable, re-identifiable or unidentifiable data; ownership and storage of data; plus what to do if a registry identifies a surgeon/institution which is performing below an accepted benchmark. There are also legal implications for the sponsors/hosts/organisers of the registry regarding reporting adverse outcomes and potentially releasing data in response to a court order. These legal issues are jurisdiction specific, and several jurisdictions

have mechanisms to ensure that registry data collected in the interests of quality improvement remains privileged. Many of these issues are covered well elsewhere [25, 26].

43.3 Case Example: The Australian and New Zealand Society of Retinal Specialists (ANZSRS) Macular Hole Registry

The ANZSRS Macular Hole Registry was established in 2008 in an attempt to address the question: "Is it necessary to posture patients face down following macular hole surgery?" At that time there was a growing trend to withhold face-down positioning; however the evidence supporting non-supine positioning (NSP) was largely from small, single-centre case series with inadequate power to adequately address the question.

A non-inferiority approach was determined to be the most appropriate study design, and the study population was to be eyes with primary idiopathic macular hole (although we did include holes of all causes, plus holes undergoing revision surgery in the registry). In order to calculate the required sample size the registry was established to gather preliminary data to determine likely recruitment and also the expected success rate. All vitreoretinal surgeon members of the ANZSRS were invited to contribute cases to the registry. Ethical oversight was provided by the Royal Australian and New Zealand College of Ophthalmologists (RANZCO). Surgeons were de-identified in the database using an id number held only by the registry administrator and not by the investigators. The study administrator at times needed to contact individual surgeons to address data quality issues, and at times the contributing surgeons needed support with specific issues, therefore investigators were re-identifiable. Patients were de-identified in the dataset using a surgeon-allocated identifier, i.e. patients were also re-identifiable, but only by the contributing surgeon. The ethics committee granted an exemption to patient consent. The data

collection was initially paper based, with surgeons filling out a form at the time of surgery and posting it to the study coordinator who entered the data into an electronic database. At 3 and 12 months surgeons were sent an outcome form to complete and send back. This was later migrated into a web-based data-entry system, with system-generated outcome reminders to the surgeons (built using a grant awarded by the Ophthalmic Research Institute of Australia).

After 12 months 400 cases of primary idiopathic macular hole had been contributed. The success rate (hole closure with a single operation) was 95 and 90% of cases were being positioned face down. A 5% non-inferiority margin was felt to be appropriate. The required sample size to address the question was calculated as $n = 1810$ to demonstrate non-inferiority with a power of 90%, and type 1 error rate of 5%. A randomised trial of this size was not felt to be feasible, and the study steering committee decided to continue with the registry in an attempt to address the question. By 2015 sufficient cases had been submitted, and thanks to a last-minute recruitment drive and reminders for all surgeons to complete their follow-up we were fortunate to have more than the required number ($n = 2329$ with follow-up). The completeness of 12-month data was much worse than 3-month data ($n = 831$), and submission of 12-month data is now an optional part of the registry. The 3-month time point was felt to be a good balance to allow macular recovery following surgery but before significant lens opacity has developed.

Results have been published elsewhere [14, 27–30]. We demonstrated non-inferiority of NSP for the overall group, although we did observe a trend suggesting that NSP may have been important in larger holes. We could not conclude non-inferiority of NSP in holes larger than 400 μm. We also concluded that SF6 gas was non-inferior to longer acting gas for all hole sizes (Fig. 43.3).

Having addressed these specific research questions we were also able to explore the dataset to address other research questions. We published other baseline and surgical determinants of hole

Adjusted effect of no FDP on hole closure

Adjusted effect of SF6 gas on hole closure
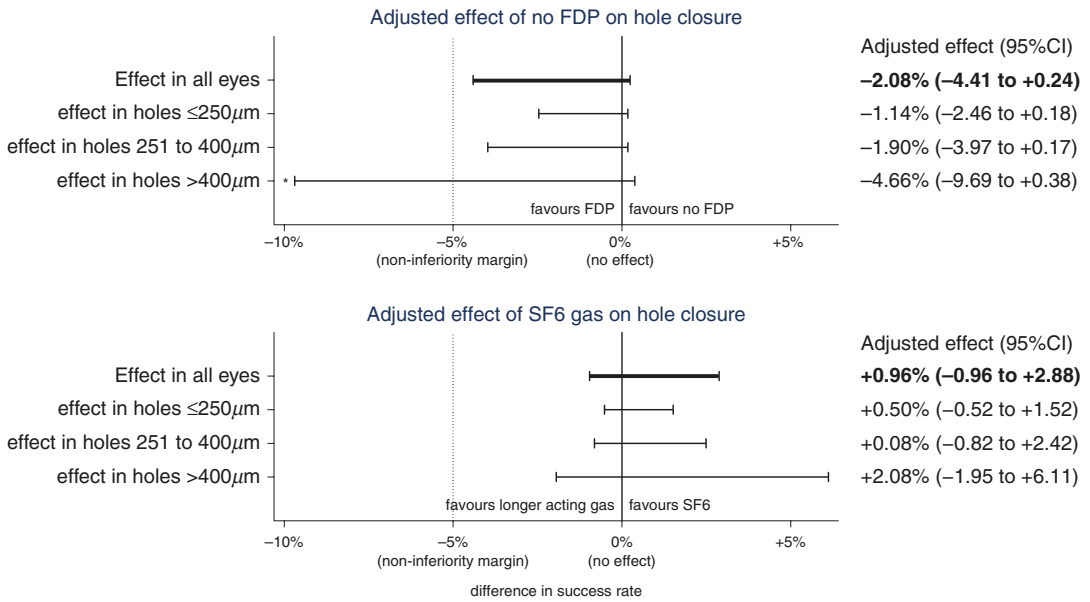
Fig. 43.3 The adjusted effects of withholding FDP and of SF6 gas use on the probability of macular hole closure. Figure shows adjusted effect for the entire study population, and the effect in the three-hole-size subgroups for each of the two interventions. (Reproduced with permission from Essex RW, Kingston ZS, Moreno-Betancur M, et al. The Effect of Postoperative Face-Down Positioning and of Long- versus Short-Acting Gas in Macular Hole Surgery: Results of a Registry-Based Study. Ophthalmology 2016;123 (5):1129–36 [27, 28].) *Non-inferiority of withholding FDP cannot be concluded in the subgroup of holes >400 μm

Table 43.1 Determinants of macular hole closure

	Odds ratio (of success)	95% CI	P value
No ILM peel	0.17	0.072–0.44	0.001*
Increasing age by 10 years	0.68	0.49–0.95	0.023*
Female gender	1.22	0.75–1.99	0.41
Left eye	1.10	0.70–1.72	0.68
Increase hole size by 100 μtm	0.74	0.67–0.81	<0.001*
Vitreous attachment to hole margin	1.20	0.74–1.93	0.46
Hole duration >9 months	0.50	0.30–0.85	0.010*
Pseudophakic lens status	1.19	0.70–2.13	0.55
Trainee surgeon	0.61	0.23–1.64	0.33
Small-gauge instruments used (23G or 25G vs. 20G)	1.47	0.53–4.09	0.46

Reproduced with permission from Essex RW, Kingston ZS, Moreno-Betancur M, et al. The Effect of Postoperative Face-Down Positioning and of Long- versus Short-Acting Gas in Macular Hole Surgery: Results of a Registry-Based Study. Ophthalmology 2016;123(5):1129–36.
CI confidence interval, *ILM* internal limiting membrane.
*$P < 0.05$

closure (Table 43.1) [27], the visual results of macular hole surgery and their determinants (Table 43.2) [14], plus the results of revision surgery for failed holes [29] and for traumatic holes [30]. The results of surgery for myopic holes are being prepared.

43.3.1 Future Plans and Challenges

Data collection for the ANZSRS Macular Hole Registry is ongoing, now as a quality assurance exercise, and in 2019 we had over 4000 macular holes in the database. As a result of the success of

Table 43.2 The effects of baseline and surgical factors on mean post-operative visual acuity at various time points

	OR of ≥ 15-letter increase in acuity at 3 months[a]	P value	OR of 15-letter increase in acuity at 12 months[a]	P value	OR of 15-letter increase in acuity at 24 months[a]	P value
Age (decades)	0.80 (0.68–0.94)	0.006	0.96 (0.74–1.24)	0.75	0.52 (0.20–1.38)	0.19
Female gender	0.84 (0.67–1.07)	0.16	0.72 (0.49–1.07)	0.10	1.08 (0.38–3.06)	0.88
Right eye	1.16 (0.94–1.45)	0.17	1.25 (0.88–1.77)	0.22	2.17 (0.78–6.04)	0.14
Duration (lag-months)	0.70 (0.60–0.81)	<0.001	0.67 (0.54–0.84)	0.001	0.79 (0.38–1.64)	0.52
Size (per hundred μm)	0.89 (0.83–0.96)	0.001	0.88 (0.79–0.99)	0.037	1.06 (0.70–1.60)	0.79
Vitreous attachment to hole margin	1.13 (0.90–1.41)	0.29	1.05 (0.73–1.52)	0.78	0.98 (0.36–2.68)	0.98
ILM peel	0.53 (0.28–1.02)	0.059	1.22 (0.41–3.69)	0.72	0.47 (0.07–3.00)	0.43
SF6 gas	1.84 (1.43–2.37)	<0.001	2.13 (1.46–3.09)	<0.001	2.08 (0.77–5.62)	0.15
Postoperative face-down positioning	1.47 (1.13–1.90)	0.004	1.33 (0.85–2.08)	0.21	0.046 (0.012–0.18)	<0.001
Trainee surgeon	0.45 (0.24–0.84)	0.013	1.33 (0.48–3.66)	0.59	0.017 (0.003–0.10)	<0.001
Small-gauge surgery (23G or 25G)	1.94 (1.05–3.58)	0.035	1.96 (0.86–4.47)	0.11	7.94 (1.52–41.6)	0.014

Eyes with successful surgery only. Results of multivariable linear regression using GEE[b]. Reproduced with permission from Essex RW, Hunyor AP, Moreno-Betancur M, et al. The Visual Outcomes of Macular Hole Surgery: A Registry-Based Study by the Australian and New Zealand Society of Retinal Specialists. Ophthalmol Retina 2018;2(11):1143–51.

ILM internal limiting membrane, *OR* odds ratio.

[a]Adjusted OR of improvement >15 letters per 1-unit increase (continuous variables) or relative to absence of factor (binary variables).

[b]Adjusted for baseline acuity, lens status, and exact timing of follow-up, in addition to other variables in the table

this project, and building on the web-based platform for the macular hole registry, we have added retinal detachment procedures to the registry, and have included a logbook function to allow users to enter all their cases to support personal research activity.

Since the specific research question has been addressed, surgeon participation has declined somewhat, underlining the importance of registries needing a reason to exist. A challenge for registry operators is to maintain user participation and enthusiasm. Regular communication to registry users and periodic activity updates have proven useful. Our registry is entirely voluntary. Most contributors are in private practice, and most do not have electronic medical record systems. Surgeons are disinclined to enter data into an electronic system more than once, and as practices transition to EMR use it is anticipated that participation may further decline.

The increasing use of EMRs internationally presents a wonderful opportunity for the collec-

tion of large clinical datasets which may be able to answer many important questions, but it also presents particular challenges. EMR systems only have rudimentary auditing ability: risk adjustment and benchmarking require centralised collection and analysis of the pooled data. Building electronic interfaces between diverse clinical systems is not always straightforward, and privacy issues and data ownership also present specific challenges. The pooled dataset is only as useful as the data the EMR systems capture. Many ophthalmic EMR systems are geared towards general ophthalmology and cataract, and retina-specific information such as retinal attachment, macular hole closure or AMD activity is seldom captured in a consistent and analysable form.

The IRIS registry (Intelligent Research in Sight) is an exciting initiative led by the American Academy of Ophthalmology which pulls de-identified clinical data from the EMR systems of over 10,000 participating ophthalmologists in the

USA [31, 32]. It reports back to physicians monthly on numerous quality measures. Many are measures of process quality (e.g. documentation of diabetic retinopathy) [33], but some are measures of clinical outcome (e.g. measures 384 [34] and 385 [35]—return to theatre and acuity improvement within 90 days of retinal detachment surgery; measure IRIS41 [36]—improvement in acuity following ERM surgery; measure IRIS46 [37] macular hole closure based on OCT), or safety of these procedures [38, 39]. We are yet to see publications based on these outcome measures.

It is likely that the future of clinical registries will depend on the integration with EMR systems. It is hoped that EMR vendors will see the benefits of improved outcome reporting driven by these registries and will build appropriate data capture measures into their systems. The ophthalmic community needs to continue to work towards standardisation of outcome measures.

References

1. Gliklich RE, Matchar D. Patient registries. In: Gliklich RE, Dreyer NA, Leavy MB, editors. Registries for evaluating patient outcomes: a user's guide, vol. 1. 3rd ed. Rockville: Agency for Healthcare Research and Quality (US); 2014.
2. Lauer MS, D'Agostino RB Sr. The randomized registry trial—the next disruptive technology in clinical research? N Engl J Med. 2013;369(17):1579–81.
3. Duker JS, Kaiser PK, Binder S, et al. The International Vitreomacular Traction Study Group classification of vitreomacular adhesion, traction, and macular hole. Ophthalmology. 2013;120(12):2611–9.
4. Azen SP, Boone DC, Barlow W, et al. Methods, statistical features, and baseline results of a standardized, multicentered ophthalmologic surgical trial: the Silicone Study. Control Clin Trials. 1991;12(3):438–55.
5. Peyman GA, Kao GW, de Corral LR. Randomized clinical trial of intraocular silicone vs. gas in the management of complicated retinal detachment and vitreous hemorrhage. Int Ophthalmol. 1987;10(4):221–34.
6. Heimann H, Hellmich M, Bornfeld N, et al. Scleral buckling versus primary vitrectomy in rhegmatogenous retinal detachment (SPR Study): design issues and implications. Graefes Arch Clin Exp Ophthalmol. 2001;239(8):567–74.
7. Joussen AM, Kirchhof B, Schrage N, et al. Heavy silicone oil versus standard silicone oil as vitreous tamponade in inferior PVR (HSO Study): design issues and implications. Acta Ophthalmol Scand. 2007;85(6):623–30.
8. Walter P, Hellmich M, Baumgarten S, et al. Vitrectomy with and without encircling band for pseudophakic retinal detachment: VIPER Study Report No 2-main results. Br J Ophthalmol. 2017;101(6):712–8.
9. Haller JA, Blair N, de Juan E Jr, et al. Multicenter trial of transscleral diode laser retinopexy in retinal detachment surgery. Trans Am Ophthalmol Soc. 1997;95:221–30.
10. Gillies MC, Walton R, Simpson JM, et al. Prospective audit of exudative age-related macular degeneration: 12-month outcomes in treatment-naive eyes. Invest Ophthalmol Vis Sci. 2013;54(8):5754–60.
11. Gillies MC, Campain A, Barthelmes D, et al. Long-term outcomes of treatment of neovascular age-related macular degeneration: data from an observational study. Ophthalmology. 2015;122(9):1837–45.
12. Eckardt C, Eckert T, Eckardt U, et al. Macular hole surgery with air tamponade and optical coherence tomography-based duration of face-down positioning. Retina. 2008;28(8):1087–96.
13. Valldeperas X, Wong D. Is it worth reoperating on macular holes? Ophthalmology. 2008;115(1):158–63.
14. Essex RW, Hunyor AP, Moreno-Betancur M, et al. The visual outcomes of macular hole surgery: a registry-based study by the Australian and New Zealand Society of Retinal Specialists. Ophthalmol Retina. 2018;2(11):1143–51.
15. Cook DA, Duke G, Hart GK, et al. Review of the application of risk-adjusted charts to analyse mortality outcomes in critical care. Crit Care Resusc. 2008;10(3):239–51.
16. Spiegelhalter DJ. Funnel plots for comparing institutional performance. Stat Med. 2005;24(8):1185–202.
17. Ng JQ, Morlet N, Bremner AP, et al. Techniques to monitor for endophthalmitis and other cataract surgery complications. Ophthalmology. 2008;115(1):3–10.
18. Steiner SH, Cook RJ, Farewell VT, Treasure T. Monitoring surgical performance using risk-adjusted cumulative sum charts. Biostatistics. 2000;1(4):441–52.
19. Steiner SH, Mackay RJ. Monitoring risk-adjusted medical outcomes allowing for changes over time. Biostatistics. 2014;15(4):665–76.
20. Grigg OA, Farewell VT, Spiegelhalter DJ. Use of risk-adjusted CUSUM and RSPRT charts for monitoring in medical contexts. Stat Methods Med Res. 2003;12(2):147–70.
21. Spiegelhalter D, Grigg O, Kinsman R, Treasure T. Risk-adjusted sequential probability ratio tests: applications to Bristol, Shipman and adult cardiac surgery. Int J Qual Health Care. 2003;15(1):7–13.
22. Grigg O, Spiegelhalter D. A simple risk-adjusted exponentially weighted moving average. J Am Stat Assoc. 2007;102(477):140–52.
23. Yue J, Lai X, Liu L, Lai PBS. A new VLAD-based control chart for detecting surgical outcomes. Stat Med. 2017;36(28):4540–7.

24. The Shipman Enquiry 2005 [2017/07/17]. Available from: https://webarchive.nationalarchives.gov.uk/20090808155005/http://www.the-shipman-inquiry.org.uk/home.asp.

25. Ahern S, Hopper I, Loh E. Qualified privilege legislation to support clinician quality assurance: balancing professional and public interests. Med J Aust. 2019;210(8):343–6.e1.

26. Adams S, DeMayo A, Howe HL, et al. Principles of registry ethics, data ownership, and privacy. In: Gliklich RE, Dreyer NA, Leavy MB, editors. Registries for evaluating patient outcomes: a user's guide, vol. 1. 3rd ed. Rockville: Agency for Healthcare Research and Quality (US); 2014.

27. Essex RW, Kingston ZS, Moreno-Betancur M, et al. The effect of postoperative face-down positioning and of long- versus short-acting gas in macular hole surgery: results of a registry-based study. Ophthalmology. 2016;123(5):1129–36.

28. Corrigendum. Ophthalmology. 2017;124(6):922–3.

29. Yek JTO, Hunyor AP, Campbell WG, et al. Outcomes of eyes with failed primary surgery for idiopathic macular hole. Ophthalmol Retina. 2018;2(8):757–64.

30. Tang YF, Chang A, Campbell WG, et al. Surgical management of traumatic macular hole: optical coherence tomography features and outcomes. Retina. 2020;40(2):290–8.

31. Parke DW 2nd, Rich WL 3rd, Sommer A, Lum F. The American Academy of Ophthalmology's IRIS((R)) registry (intelligent research in sight clinical data): a look back and a look to the future. Ophthalmology. 2017;124(11):1572–4.

32. Chiang MF, Sommer A, Rich WL, et al. The 2016 American Academy of Ophthalmology IRIS((R)) registry (intelligent research in sight) database: characteristics and methods. Ophthalmology. 2018;125(8):1143–8.

33. Rich WL, Chiang MF, Lum F, et al. Performance rates measured in the American Academy of Ophthalmology IRIS © registry (intelligent research in sight). Ophthalmology. 2018;125(5):782–4.

34. Measure 384: adult primary rhegmatogenous retinal detachment: no return to the operating room within 90 days of surgery. v. 2019.

35. Measure 385: adult primary rhegmatogenous retinal detachment surgery: visual acuity improvement within 90 days of surgery. v. 2019.

36. IRIS41: improved visual acuity after epiretinal membrane treatment within 120 days. v. 2019.

37. IRIS46: evidence of anatomic closure of macular hole within 90 days after surgery as documented by OCT. v. 2019.

38. IRIS42: return to OR or endophthalmitis within 90 days after epiretinal membrane surgical treatment v. 2019.

39. IRIS47: return to OR or endophthalmitis within 90 days after macular hole surgery. v. 2019.